SDC-91-124
November, 1991



Proceedings of the SDC Meeting held at Oak Ridge Associated Universities

Annex
SDC-91-
124

September 26-28, 1991
Oak Ridge, TN

Plenary Sessions

Thursday, September 26

Remarks by Spokesperson (including recommendation of central calorimetry)	G. Trilling(LBL)
Remarks by Technical Manager	M. Gilchriese(LBL)

Saturday, September 28

Summary of Muon Activities	R. Thun(Michigan)
9/27 SDC Calorimeter Group	D. Green(Fermilab)
Tracking Summary	W. Ford(Colorado)

LPBautz:10/14/91

AAD7872

Calorimetry

Impact of EM Calorimeter Thickness on Resolution	C. Hearty(LBL)
A Weighty Question	T. Handler(Tenn.)
Multigroove vs. Single Groove Tile-Fiber Calorimeter	V. Hagopian(FSU)

LPBautz:10/14/91

Computing and Data Acquisition

Schedule for Technical Proposal	A. Fry(SSCL)
Section 9: Online Computing - Draft	A. Fry(SSCL)
SDC Computing Section: Architectural Studies and Analysis - Draft	SDC Computing Working Group(IBM)
SDC Data Acquisition Design Requirements and Functional Specifications Version 0.99	SDC Data Acquisition Working Group
SDC Data Acquisition System Conceptual Design - Draft	E. Barsotti(Fermilab)
SDC Data Acquisition System Conceptual Design	I. Gaines(Fermilab)

LPBautz:10/29/91

Electronics

From the Front End to the Event Builder	P. Le Du(LBL&Saclay)
The Showermax Electronics	P. Le Du(LBL&Saclay)
UCLA Cosmic-Ray Test	M. Atac(UCLA)
Electron Trigger Backgrounds	M. Miller(Chicago)
SDC Trigger Design Documents	W. Smith(Wisconsin)

LPBautz:10/29/91

Muon System

Technical Proposal Chapter 7 - Outline	G. Feldman(Harvard)
Momentum Resolution, Cosmic Ray Trigger Rates	H. Iwasaki(KEK)
Octagonal Geometry Effects	J. Wiss(Illinois)
Forward Muon Chamber Rates and the Optimal Beam-Pipe/Absorber Design	A. Kulik(Protvino)
Study of the Muon Trigger Efficiency	V. Molchanov (Protvino)
Scintillation Counters for Muon Trigger System	V. Rykalin(Protvino)
Muon Scintillator R&D Activities at Michigan	R. Thun(Michigan)
Prototype of Foam Support for Muon Tubes	A. Sill(Rochester)
Finite Element Modelling of Muon Detector Module	C. Daly(Washington)
Experience with Short Drift Tubes	T. Zhao(Washington)
Forward Muon System	A. Skuja(Maryland)
Design of the Jet Cell Chamber for the SDC Muon Detector	S. Terada(KEK)
A Short Comment on Descoping of the Muon Chamber	Y. Asano(Tsukuba)
Progress in Wisconsin	D. Carlsmith (Wisconsin)
SDC Muon Simulation at Illinois	S. Errede(Illinois)
Muon Beam Tests	H. Lubatti (Washington)
Report on Beam Test Work	S. Errede(Illinois)

LPBautz:11/4/91

Tracking

Proposal for Capillary/Liquid Scintillator Tracking	L. Landsberg (Protvino)
Tracking System Design Requirements	W. Ford(Colorado)
Tracking Algorithm Overview	K. O'Shaughnessy (UC/Santa Cruz)
Segment Clustering Track Finding Method	K. O'Shaughnessy
TRF: A Track-Finding Package for Solenoidal Fields	D. Adams(Rice)
Silicon Tracker R&D and Engineering FY 92	H. Sadrozinski(UC/SC)
Silicon Detector Development in Japan	H. Miyata(Niigata)
Overview of Straw Tracking System Design	G. Hanson(Indiana)
Modular Straw Tracking Sustem	H. Ogren(Indiana)
Progress of Straw R&D at Duke U.	S. Oh(Duke)
Straw/Fiber Tracker	S. Reucroft (Northeastern)
Progress in Simulating Combined Silicon and Straw Tube Tracking System	F. Luehring(Indiana)
Pulse Attenuation in Straw Tubes	D. Rust(Indiana)
Straw Electronics and Interconnections	W. Ford(Colorado)
Overview of Fiber Tracking System Design	D. Koltick(Purdue)
Simulation Studies for a Scintillating Fiber Tracker Trigger	R. Lewis(Penn State)
VLPC Status/Plans	P. Besser(Rockwell)
Cosmic Ray Tracking Using Scintillating Fiber Ribbons and VLPCs	M. Atac(FNAL/UCLA)
Summary Report of the Fiber Tracking Group	FTG
Tracking System Requirements for the ITD	A. Sill(Rochester)
Simulation Studies of Microstrip ITD	S. Maxfield(Liverpool)
Test Results	E. Barasch(TX A&M)
Gas Microstrip Chambers - Device Status	M. Dixit(Carleton)
Layout, Material, and Tracking Length Considerations for the Intermediate Angle Region	A. Sill(Rochester)
Work on ITD	J. Dainton(Liverpool)

LPBautz:11/4/91

Outer Tracker
Mechanical Engineering Aspects

SDC Outer Tracking System: Scope of Work and Program Planning	D. Hackworth (Westinghouse)
SDC Outer Tracking-ORNL/ORDC	T. Gabriel(ORNL)
Central and Forward Tracking Subsystem	R. Swensrud (Westinghouse)
Central Tracking Chamber Assembly Proposal	D. Vandergriff(ORNL)
Radiation Length Study	R. Leitch(ORNL)

LPBautz:11/4/91

Appendix

List of Participants

Plenary Sessions

Thursday, September 26

Remarks by Spokesperson (including recommendation of central calorimetry)	G. Trilling(LBL)
Remarks by Technical Manager	M. Gilchriese(LBL)

Saturday, September 28

Summary of Muon Activities	R. Thun(Michigan)
9/27 SDC Calorimeter Group	D. Green(Fermilab)
Tracking Summary	W. Ford(Colorado)

LPBautz:10/14/91

Remarks by Spokesperson (including recommendation on central calorimetry)

G. Trilling

Presentation at Oak Ridge SDC Meeting
September 26, 1991
G. Trilling

New SDC applicants

PAC Meeting on October 3-4

SDC Technical reviews/committees

Central calorimetry technology decision



NEW COLLABORATION APPLICANTS

LAFEX (Lab de Fisica Exp. de Altas Energias)
Rio de Janeiro, Brazil

INSTITUTE OF NUCLEAR PHYSICS
Krakow, Poland

UNIVERSITE DE MONTREAL
Montreal, Canada



Dear George,

An agenda is enclosed for your October 3 meeting with the SDC subpanel of the Program Advisory Committee. We would like to focus on the following subjects:

1. The progress of the FNAL beam tests. (It might be helpful to bring with you the person in charge of the beam tests.) In addition to preliminary results, we are interested to learn what your group views as the crucial items to be tested and when they are expected to be done. Will all of the necessary results be available when the final technology choices have to be made? If not, on what will these choices be based?
2. The selection of the calorimetry technology. Was a choice made at the Oak Ridge meeting? If so, what was the basis for the choice? What are the remaining concerns about the selected technology?
3. Other technology choices. What choices have been made and what is the current schedule for making those that remain to be made?
4. Possibilities for staging the detector. Which detector components are essential for experiments at t = 0? Which can be delayed?
5. The R&D priorities. Are there still redundant efforts in any areas? Which projects are being de-emphasized? Which are being phased out? How will the FY92 funds be distributed?
6. The financial plan for living within $500M. Has there been progress on getting commitments from foreign sources of support?
7. The status of the technical design report.

We are not asking for lengthy written materials, and we ask that you limit the length of your presentations so as to leave ample time for discussion with the subcommittee.

PAC MEETING AGENDA		OCTOBER 3-4,1991
Thu. Oct. 3		
8:30 AM	Upstairs Conference Room	PAC
	Auditorium	Director's Conference Room
9:30	GEM + Luth subcommittee	SDC + Olsen subcommittee
	Upstairs Conference Room	
12:00 PM	PAC	
2:00 PM	GEM + Luth subcommittee	SDC + Olsen subcom. (if necessary)
3:00 PM	Luth subcommittee	Olsen subcommittee
5:30 PM	Adjourn	
Fri. Oct. 4	Upstairs Conference Room	Director's Conference Room
8:30 AM	PAC	
10:00 AM	GEM + Luth subcom. (if necessary)	Olsen subcommittee
11:00 AM	Luth subcommittee	
12:00 PM	PAC	
2:30 PM	Adjourn	

TECHNICAL BOARD SUMMARY STATEMENT

It is the opinion of the Technical Board that both scintillator and liquid argon technologies are viable for the SDC central calorimeter, and indeed are close in their capabilities and costs. Nevertheless, for reasons discussed below, there was a clear consensus in favor of the scintillator option. The Technical Board therefore recommends the adoption of the scintillator option, with the decision on the absorber arrangements to be made in the near future.

TECHNICAL REVIEWS/COMMITTEES

Review of Front-End Electronics Status (Sept. 9 - 11)
Review committee:
- Electronics/DAQ/Trigger Steering Committee
- Eight other experts from SDC (engineers & physicists)
- Five non-SDC experts

Muon tracking chamber review committee
- Recommend choice of muon chamber design (Feb. 1, 1992).
- Chairpersons: A. Makl, R. Thun

Hadronic absorber evaluation committee
- Evaluate calorimetric impact of various absorber configurations (November SDC meeting).
- Chairperson: J. Siegrist

Central tracking review committee
- Recommend configuration(s) contained in tech. proposal.
- Chairperson: T. Kondo

CALORIMETER CONFIGURATIONS

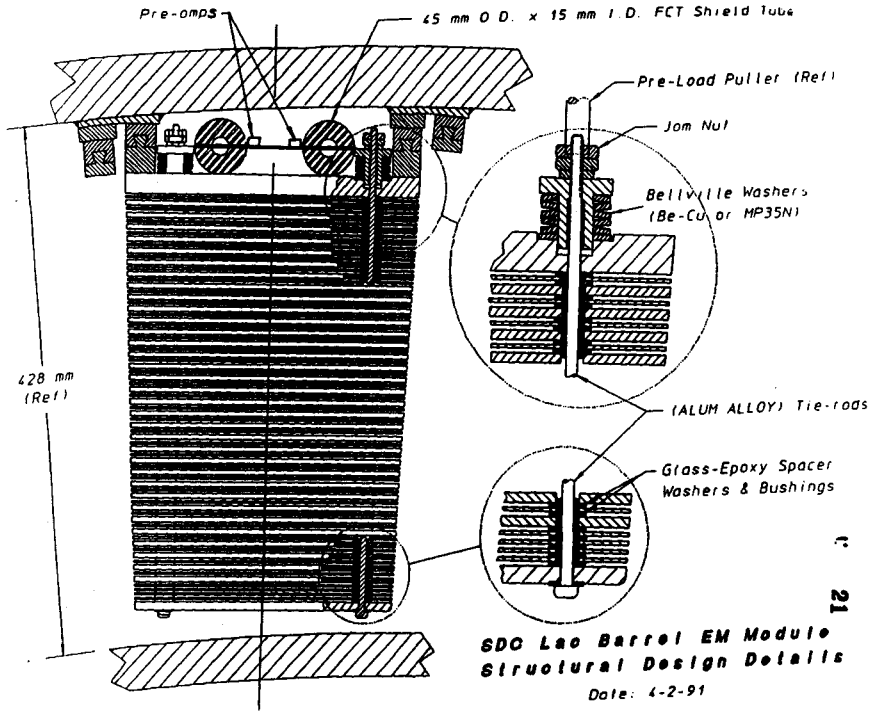
	LAR	Mod A	Mod B
Total depth (η=0)	9 λ	9 λ	9 λ
Total depth (η=3)	11 λ	11 λ	12 λ
BARREL EM			
Longitudinal segments	2	1	1
Transverse segmentation	0.05	0.05	0.05
Pb thickness (mm)	4	3.2	4
LAR/Scint thickness (mm)	4	2.5	2.5
Depth (X0)	25	22	22
BARREL HAD1			
Longitudinal segments	1	1	1
Transverse segmentation	0.05	0.05	0.1
Pb/Fe thickness (mm)	14(Pb)	25(Fe)	21(Pb)
LAR/Scint thickness (mm)	2	2.5	2.5
BARREL HAD2			
Longitudinal segments	1	1	1
Transverse segmentation	0.05	0.1	0.1
Pb/Fe thickness (mm)	14(Pb)	51(Fe)	46(Fe)
LAR/Scint thickness (mm)	2	2.5	2.5

SDC CENTRAL CALORIMETRY
History

May 1990 (EoI)	4 technological options	
November 1990 (LoI)	2 options	a) Pb/La b) Scint. tile with WLS fiber (Pb/Fe for hadronic absorb.)
August 1991	Extensive review Requirements document LA Conceptual Design Report	
September 1991	Scint. tile Conceptual Design Report	
Sept. 12-14, 1991	Technical Board Meeting Calorimeter presentations and discussion Impact on other systems, costs, integration Technical Board recommendations	
Sept. 26, 1991	Report to Collaboration	

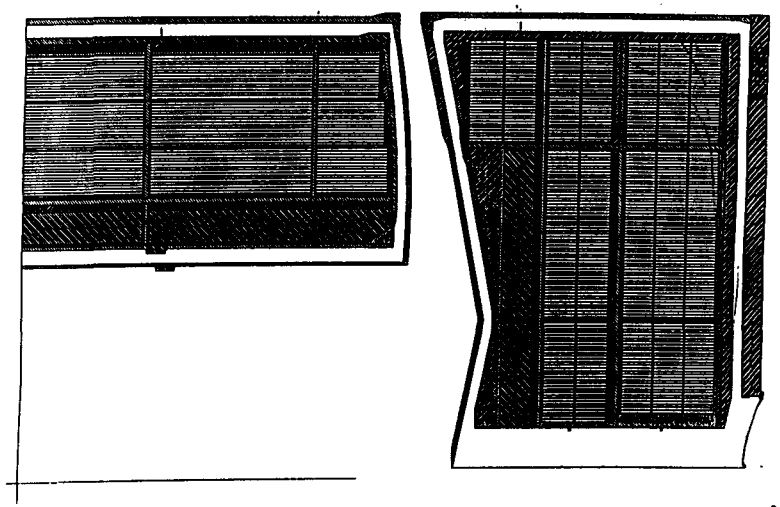
CALORIMETER CONFIGURATIONS (cont.)

	LAR	Mod A	Mod B
ENDCAP EM			
Longitudinal segments	2	2	2
Transverse segmentation	0.05	0.05	0.05
Pb thickness (mm)	4	6.3	8
LAR/Scint thickness (mm)	4	2.5	2.5
Depth (X0)	25	22	22
ENDCAP HAD1			
Longitudinal segments	1	1	1
Transverse segmentation	0.05	0.05	0.1
Pb/Fe thickness (mm)	14(Pb)	51(Fe)	31(Pb)
LAR/Scint thickness (mm)	2	2.5	2.5
ENDCAP HAD2			
Longitudinal segments	1	1	1
Transverse segmentation	0.05	0.1	0.1
Pb/Fe thickness (mm)	14(Pb)	102(Fe)	67(Fe)
LAR/Scint thickness (mm)	2	2.5	2.5
SHOWER MAX			
$\Delta\phi$ layer & $\Delta\eta$ layer	0.05/6	0.05/8	0.05/8
MASSLESS GAP	Yes	Wt layr1	Wt layr1



SDC Lac Barrel EM Module
Structural Design Details
Date: 4-2-91

Liquid Argon Calorimeter



Scintillator Calorimeter (Model A) - Iron-dominated Had 1

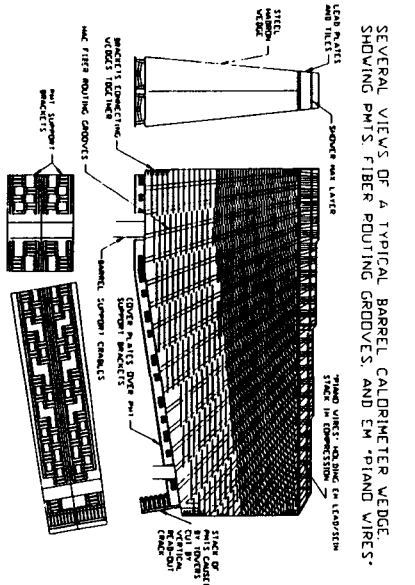
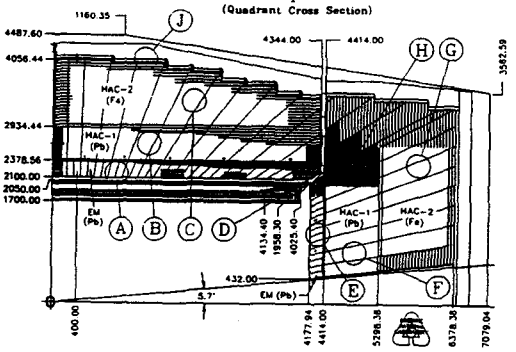


Figure 3.1(c) - Several views of a typical barrel calorimeter wedge, showing PMTs, fiber routing grooves, and EM "Piano Wires".

Scintillator Calorimeter (Model B) Lead Had 1

Tile/Fiber Descope 4 Calorimeter

(Quadrant Cross Section)



Tile/Fiber Descope 2 Calorimeter

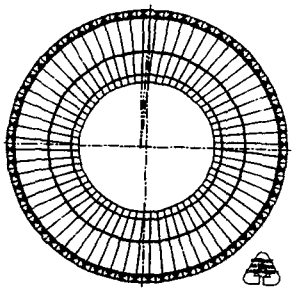


Figure 4.1 a)MODEL B Quadrant Cross section, b) End Section

Scintillator Shower Max Detector

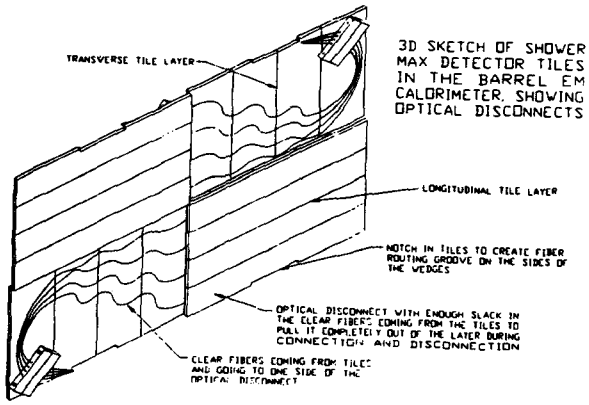
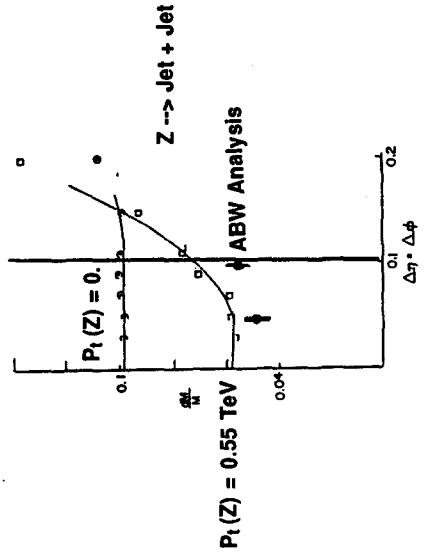
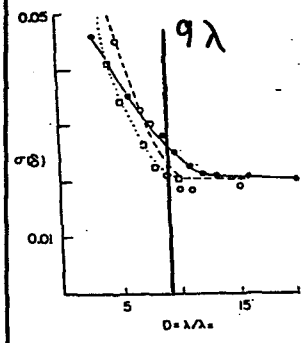


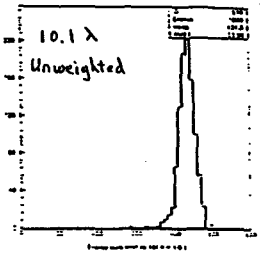
Figure 3.12 - Fiber routing in the EM shower-max assembly. The assembly contains two planes of scintillator strips for the X and Y views. The fiber routing is done between the planes. The clear readout fibers have an optical disconnect which is mounted between the planes, and canted slightly to allow the shower-max readout fibers to join the bundles for the EM calorimeter tiles.

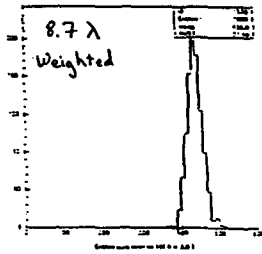
Hadron Calorimeter Transverse Granularity



Calorimeter Depth -- Di-jet Mass Resolution



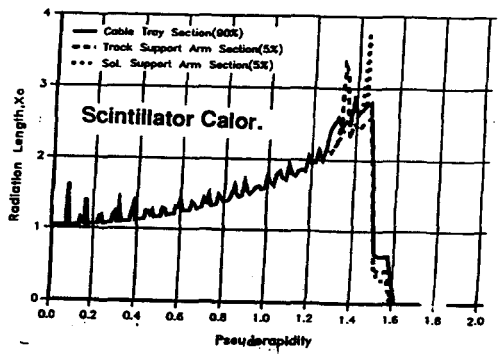


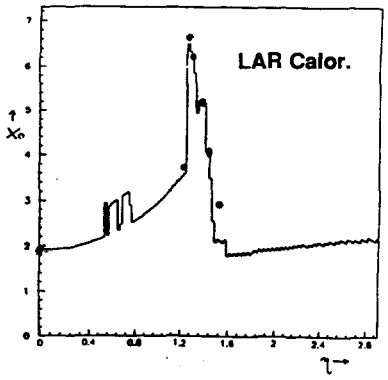


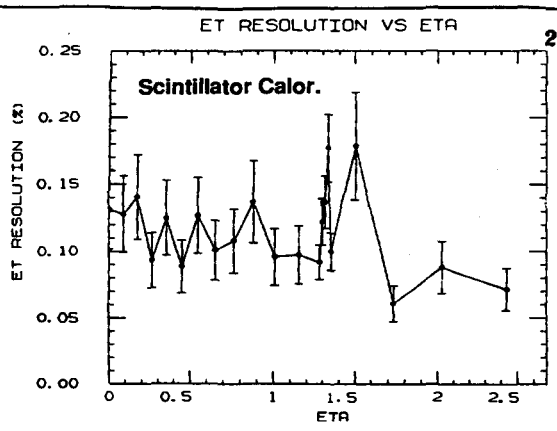
Comparison of the liquid argon (LAR) and scintillator (SCINT) calorimeter options.

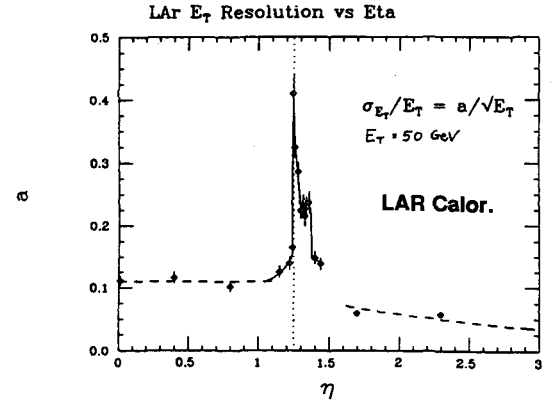
	LAR	SCINT
Electron acceptance		x
EM resolution-stochastic	very close	
EM constant term	x	
Electron, γ ID, isolation		x
Hadronic resolution-stochastic	very close	
Hadronic constant term, e/h		x
Hadronic transverse segmentation	x	
Missing E_T measurements		x
Cost (including impact on other systems)		x
Schedule	very close	
Magnetic field uniformity		x
Integration		x
Safety		x
Impact on electronics, DAQ, trigger		x
Muon system performance		x
Neutrons, albedo in cavity		x
Flexibility, upgrade		x
High $\mathcal{L}$ performance		x
Maturity of design	x	
Radiation resistance	x	
Ease of calibration	x	

Radiation Lengths V.S. Pseudorapidity









Noise/ Pileup in LAR Calor.

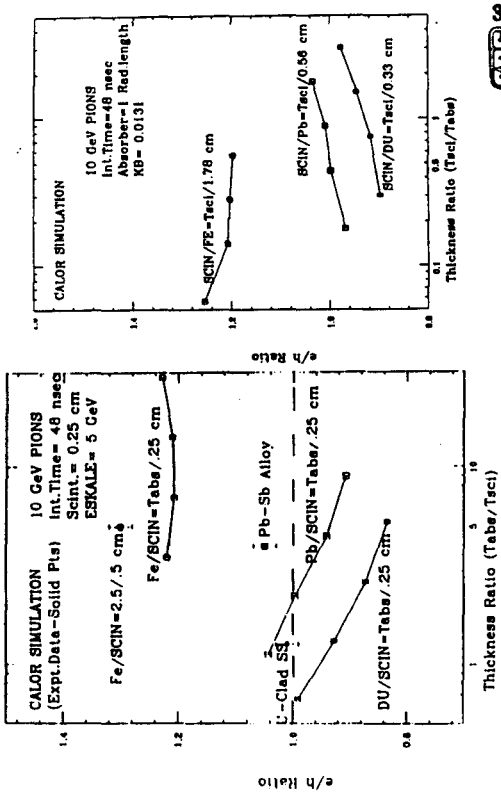
Section	N_{samp}	N_{pap}	$<r>$	C_D	C_s	C_{tot}	a	t_{peak}	per Preamp ENC	per Preamp ENE	per Preamp ENE	per Preamp Pileup	per Channel Total	per Channel Mip	per Channel Mip	σ_t
			cm	pF	pF	pF		ns	fC	MeV	MeV	MeV	MeV	MeV	S/N	ns
EM1	1	5	236	970	340	1310	5	60	1.7	27	27	30	40	32	0.8	< 1
EM2	1	26	253	3680	460	6140	11	60	4.9	75	75	54	92	161	1.7	< 1
HAD1	2	18	314	3100	1030	4130	9	100	2.8	194	274	44	278	662	6.3	2.8
								200	2.0	80	113	63	129		5.1	2.6
HAD2	2	27	387	7070	1530	8600	13	100	4.9	337	477	3	477	993	2.1	4.8
								200	3.5	139	197	4	197		5.0	3.9

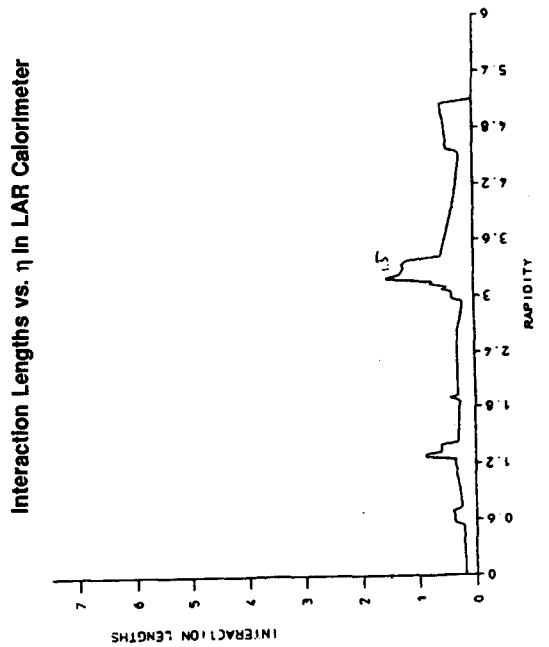
The total noise in the EM section of the calorimeter is essentially constant with peaking time in the range 60 .le. tpeak .le. 100 ns (variation is +/- 2.5%). The peaking time is selected to be 60 ns to provide better pileup supression for higher luminosity running. For a luminosity increase from 10**33 to 10**34, the total noise in EM1 plus EM2 will increase from 115 MeV to 278 MeV (i.e., proportional to Lum**0.38). This value of tpeak depends on the pileup calculation in section 7.3; a more detailed calculation will be required to finally select the shaping time. The use of variable shaping time shapers (Section 7.3.1) will enable the optimization to be based on observed backgrounds. Note, however, that a variation of +/-30% in energy deposited per crossing corresponds to a variation in the total EM noise of 10%.

SUMMARY

- Fast LAr risetime preserved by electrode structure
- $\sigma t < 4$ ns for >2 GeV in EM tower
  $\sigma t < 4$ ns for >80 GeV jet
  (both are better in endcap)
- Effect of noise and pileup on EM resolution:
  $\frac{\sigma}{Et} = \frac{0.13}{\sqrt{Et}} \oplus \frac{0.22}{Et}$ @ 10**33
- H --> $\gamma\gamma$ efficiencies
  - single γ efficiency reduced 1% [4%]
  - mass resolution worse by 5% [20%]
  - event efficiency 0.58 (fast) --> 0.56 (LAr)
    0.60 (fast) --> 0.52 (LAr)
- H --> WW --> ev + jets; isolated e- efficiency 0.92 [10**33] --> 0.72 [10**34] (tighter cuts)

e/h Ratio from Simulation





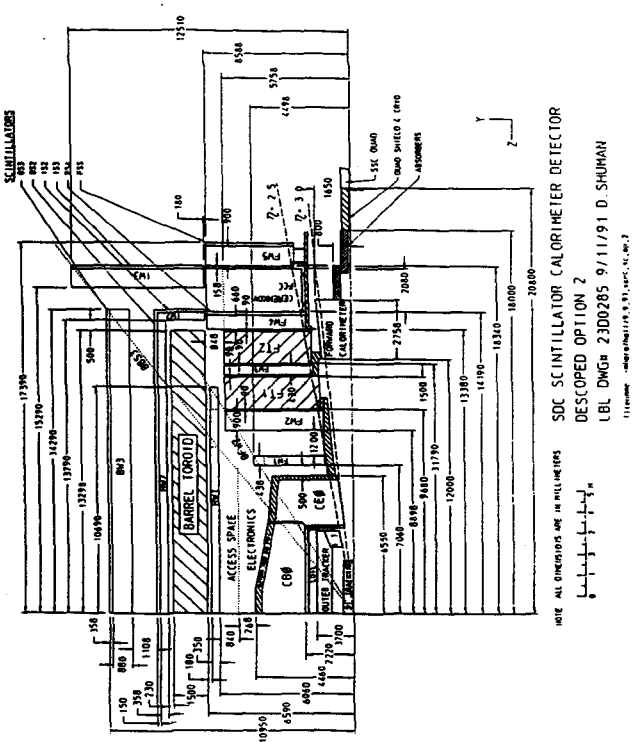
COST COMPARISON

Liquid Argon minus Scintillator

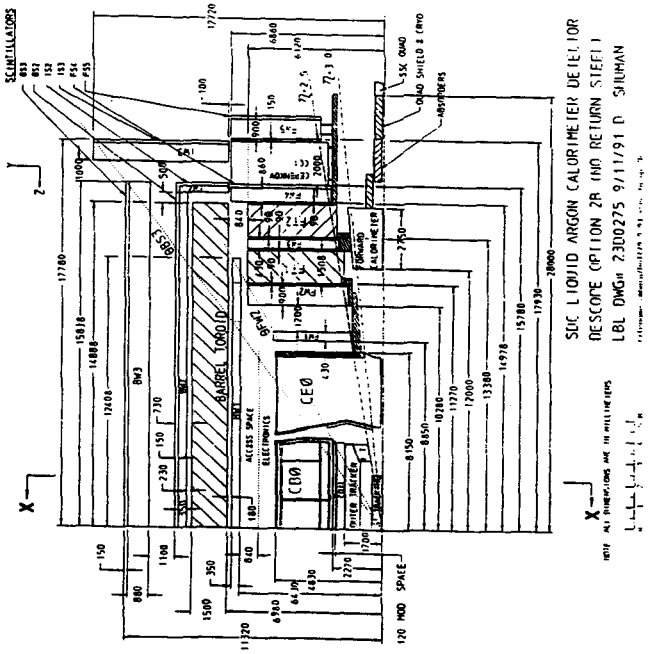
Calorimeter cost	+9 M
Electronics	+7 M
R&D	- 2 M
Prototypes	+1 M
Installation	+1 M
Underground hall	+3 M
Muon system	+10M
Total cost difference	+29 M

Giving the scintillator calorimeter 2 EM depth segments in the barrel, and 0.05x0.05 granularity in HAC1 to make it the same as the LA design would add about 14 M to the scintillator calorimeter cost.

35



36



37

(1) magnetic field contour of B_z

Type 1, (r,z/2)=(1.7m,4.0m), liquid argon

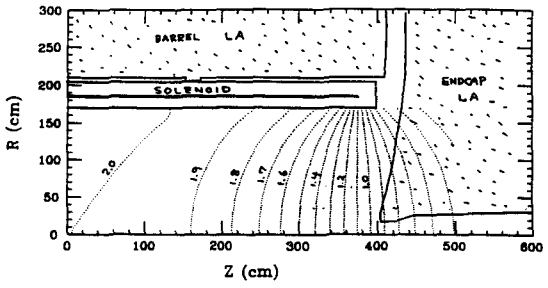


Fig. 1

(4) magnetic field contour of B_z

Type 4, (r,z/2)=(1.7m,4.0m), Tile-fiber, EM(Pb), Had(all Fe)

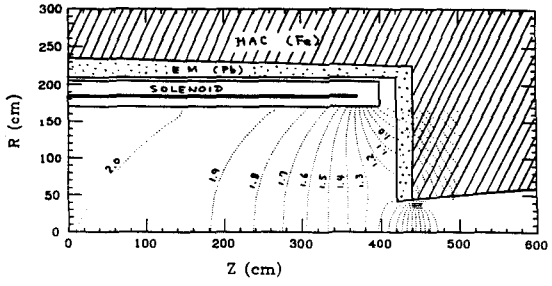


Fig. 2

38

field dependence for 1.7mx4m

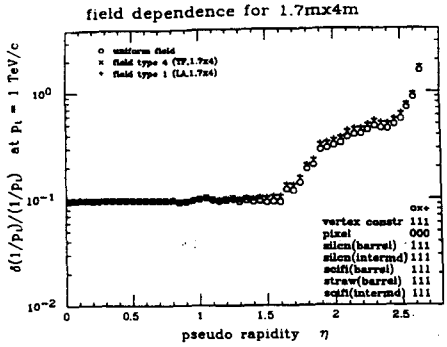


Fig. 3

field dependence for 1.7mx4m

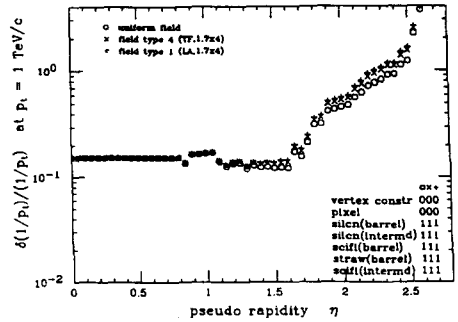


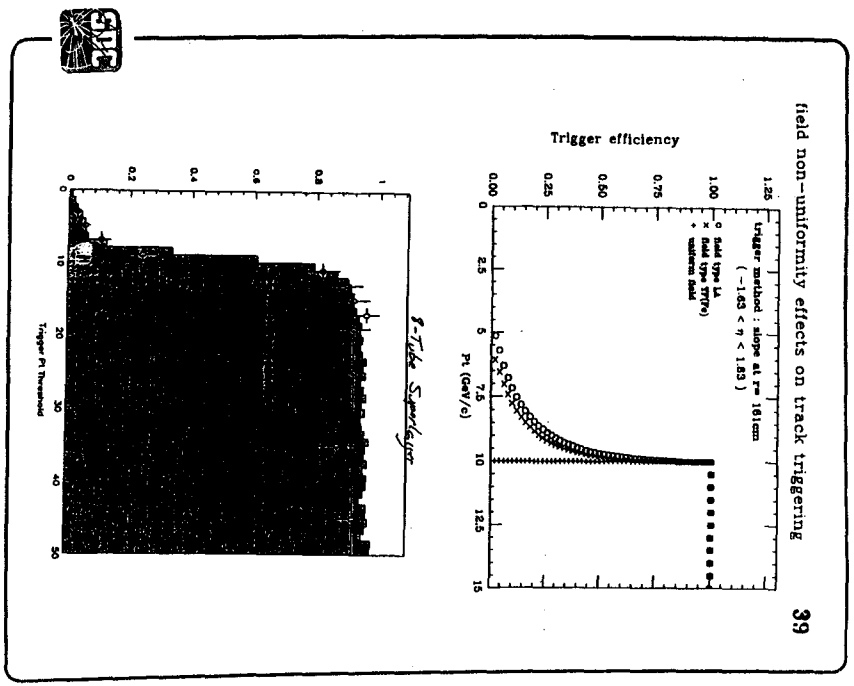
Fig. 4

IMPACT ON MAGNET

Flux return far from current sheet (Pb/LA, Pb/Scint. for HAC1).
- Large compressive stresses(~1700 tonnes) on conductor.
- Small magnetic decentering forces (< coil weight).
- Non-uniform field.

Flux return near current sheet (Fe/Scint. for HAC1, reentrant EC).
- Reduced compressive stresses.
- Larger magnetic decentering forces (> coil weight).
- More uniform field.

For the designs presented, the compressive forces varied from 1700 to 1100 tonnes. It is possible to have forces down to 100 tonnes with reentrant EC and Fe/Scint. HAC1. This requires further study to understand the impact of reentrant EM geometry.



IMPACT ON ELECTRONICS

From point of view of electronics performance, there are no significant differences between LA and Scintillator technologies.

Undesirable environmental consequences for LA:
- Detector electronics crates sit in 0.1 T magnetic field.
- Precludes commercial power supplies, fans, etc.
- Servicing and trouble-shooting more awkward.

IMPACT ON TRACKING

I. Magnetic field non-uniformity (Task Force).
(Note: Field non-uniform in all designs presented, least non-uniform in Fe/scint. hadronic calorimeter design, could be fully uniform with reentrant EM section).

1. Reduced trajectory bend angle at large z,
   Softens trigger threshold.
2. Modified time-distance relation at large z,
   Greater tolerance on synchronizer--softens threshold.
3. Pattern recognition,
   Depends on detailed pattern recognition procedure.
4. Momentum resolution,
   Very small effect for designs presented.

II. Neutron fluence in tracking cavity reduced by scintillator.
Reduction factor is 3.

43

IMPACT ON MUON SYSTEM

1. Effect of multiple scattering in calorimeter absorber on level 1 trigger threshold:

Calorimeter design	(Bend angle)/(Scattering angle)
All lead HAC (LA)	2.8
All iron HAC (Scint.)	3.9
Lead/Iron HAC (Scint.)	3.2

For fixed threshold, level 1 trigger rate is increased by Pb.

2. LA calorimeter is larger (ΔR = 0.4 m, $\Delta L/2$ = 1.6 m).
   Hence larger muon system is required,
   (included in cost comparison).

44

Radiation Hardness Test Beam Module

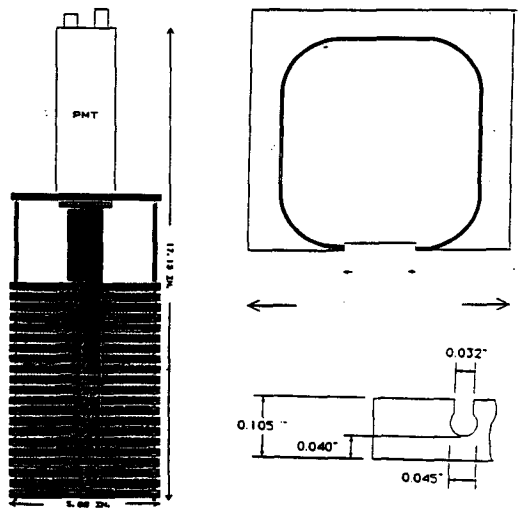


Figure 8.2 Radiation hardness test beam module.

45

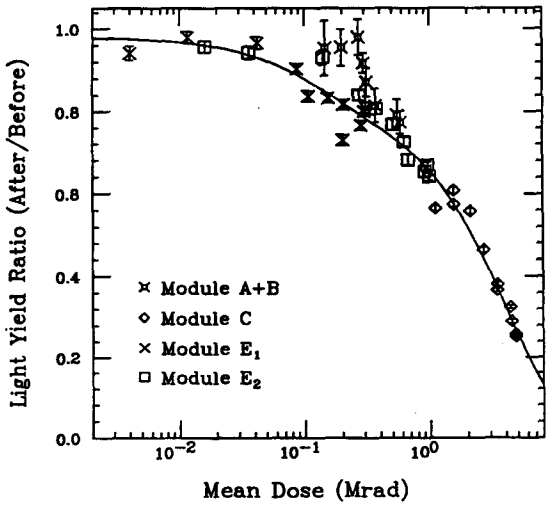


Figure 16: The 2.5-GeV electron shower induced damage as a function of the mean dose, measured with electron beam (in square-crosses) and with a ^{106}Ru source (in squares, diamonds and crosses). The curve is a fit given by Eq. (2).

46

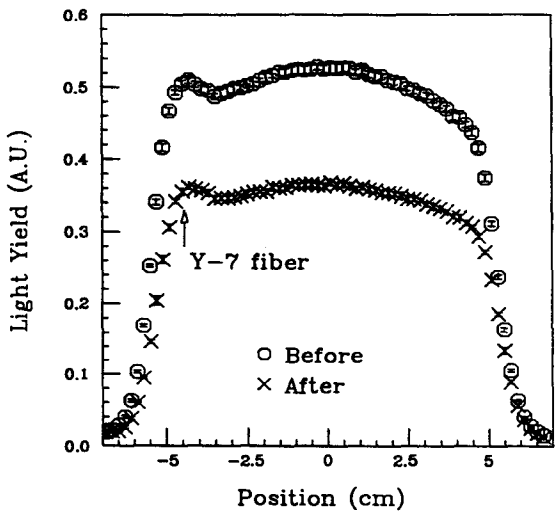


Figure 15: Response map of a tile/fiber assembly measured by scanning with a ^{106}Ru source. This assembly was non-uniformly exposed to ^{60}Co with a dose distribution of 0.62 Mrad at the center and 0.20 Mrad at the edge.

PRELIMINARY BEAM TEST RESULTS

Liquid Argon (Brookhaven)
- EM module — 6 mm Pb plates
  - $\sigma/E = 18\%/\sqrt{E}$
- Hadronic module — 12 mm Pb plates
  - $\sigma/E = 64\%/\sqrt{E}$
- From fit to e/π data, e/h = 1.23 => 3.2% constant term

Scintillator tile / fiber (Fermilab)
- ANL EM module — 5 mm Pb — 2.5 mm Scint.
  - $\sigma/E = 18\%/\sqrt{E}$
- CDF EM module — 4.8 mm Pb — 4 mm Scint.
  - σ/E = 1.6% for 100 GeV e
- CDF hadronic — 5 cm Fe — 4 mm Scint.
  - σ/E = 8% for 150 GeV π

EM Photoelectron yields scaled to SCSN81 and SDC tile/Pb
- ANL — 80 Pe/GeV
- CDF — 150 Pe/GeV
- (Uncomfortably low? — increase SDC tile to 4 mm for EM)

Remarks by Technical Manager

M. Gilchriese

Detector Drawings and Parameters

- Our goal for many months has been to "freeze" dimensions and parameters by Oct. 15 for the Technical Proposal and the cost/schedule estimate
- We are behind schedule and will remains so until more decisions are made eg. calorimeter absorber, tracking options,.....
- Nevertheless we must move as rapidly as possible to fix dimensions and parameters
- New drawing package exists - Descope 2 draft

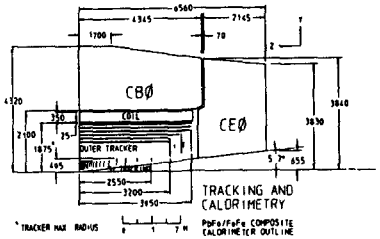
SDC Meeting

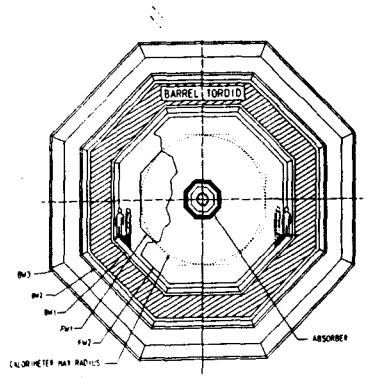
ORNL

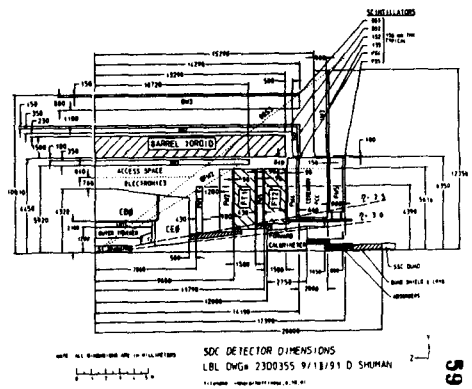
September 26, 1991

M. G. D. Gilchriese

- Milestones
- Detector dimensions and drawings
- Decisions, decisions
- Engineering integration meeting at SSCL
- Schedule for cost/schedule
- Technical Proposal
- Budget



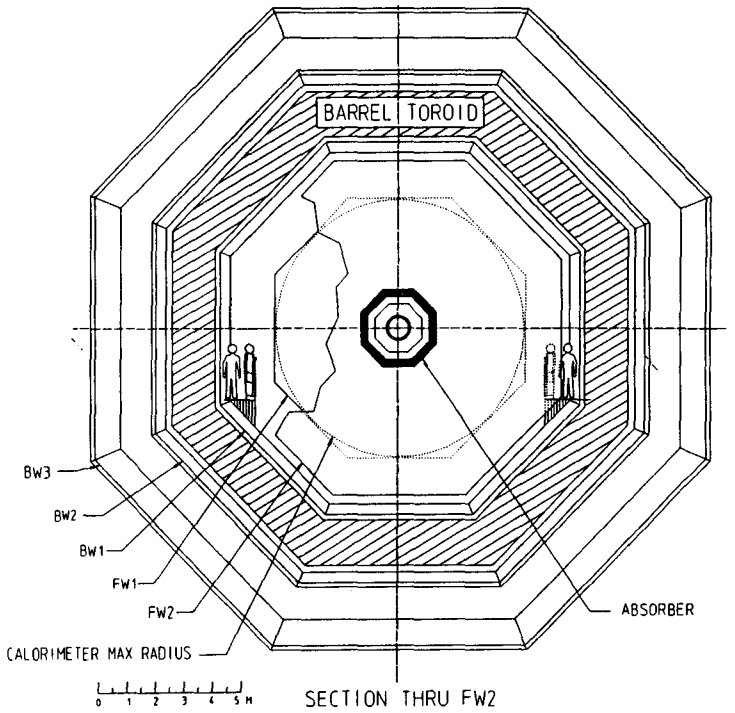




SELECTED SDC MILESTONES FY91-92†

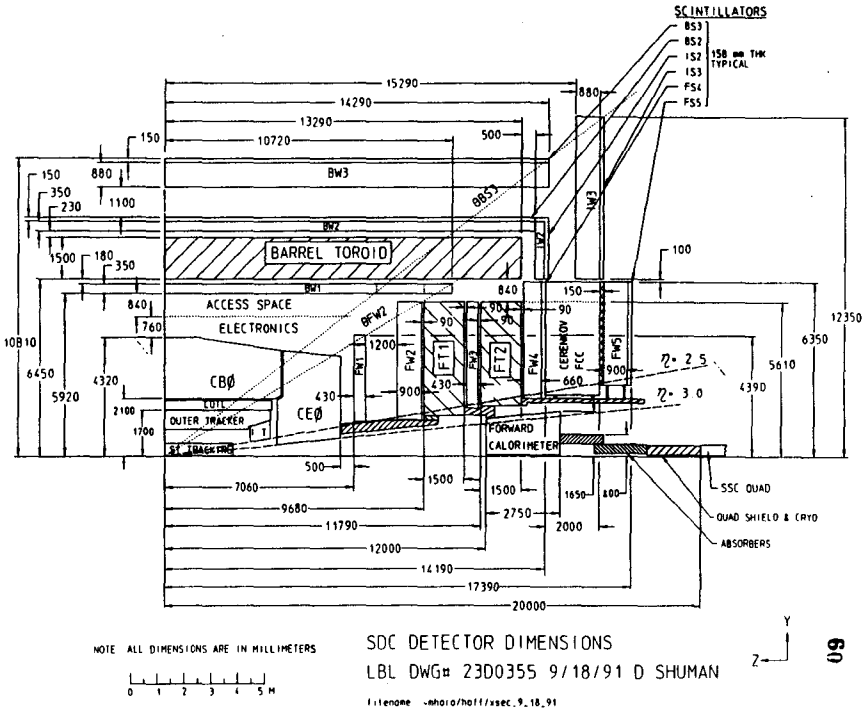
FY91 MILESTONES		FY92 MILESTONES	
Revised "baseline" design	Mar. 15	Final FY92 R&D plans	Oct. 1
1R location/hall construction type	Apr. 15	First draft of responsibility matrix	Oct. 1
Establish "baseline" for costing	May 15	SSCL/PAC meeting	Oct. 3?
Draft FY92 R&D plan	Jul. 1	Fix "baseline" for Tech. Proposal	Oct. 15
Draft R&D Management Plan	Jul. 1	Begin Title I for underground hall	Oct. 15?
Revised cost estimate	Jul. 1	Draft Management Plan	Nov. 1?
Draft construction schedule	Jul. 1	First draft of Tech. Proposal	Jan. 15
SSCL/PAC status review	Jul. 8	First draft of Cost&Schedule Book	Jan. 15
Forward cal. R&D directions	Aug. 10	Second draft of responsibility matrix	Jan. 15
Scope decision(new cost "baseline")	Aug. 10	Internal cost review	Jan. 20
Complete assignments for Tech. Proposal	Aug. 10	SSCL/PAC status review	Feb. 1?
Establish tracking "baseline"	Sep. 28	Revised Management Plan	Mar. 15?
Complete pre-Title I hall report	Sep. 30	Due date for Tech. Proposal	Apr. 1
Central calorimeter selection	Sep. 30	Due date for Cost&Schedule book	Apr. 1
		Final responsibility matrix	Apr. 1
		Begin Title II for underground hall	Apr. 15?
		SSCL/PAC review of Tech. Proposal	May 15?
		Final construction Management Plan	Jun. 1
		DOE review	Jul. 1?
		Draft agreements	Aug. 15?
		Construction start	Oct. 1

† Revised Aug. 1 1991



SECTION THRU FW2

62



NOTE ALL DIMENSIONS ARE IN MILLIMETERS

0 1 2 3 4 5 M

SDC DETECTOR DIMENSIONS
LBL DWG# 23D0355 9/18/91 D SHUMAN

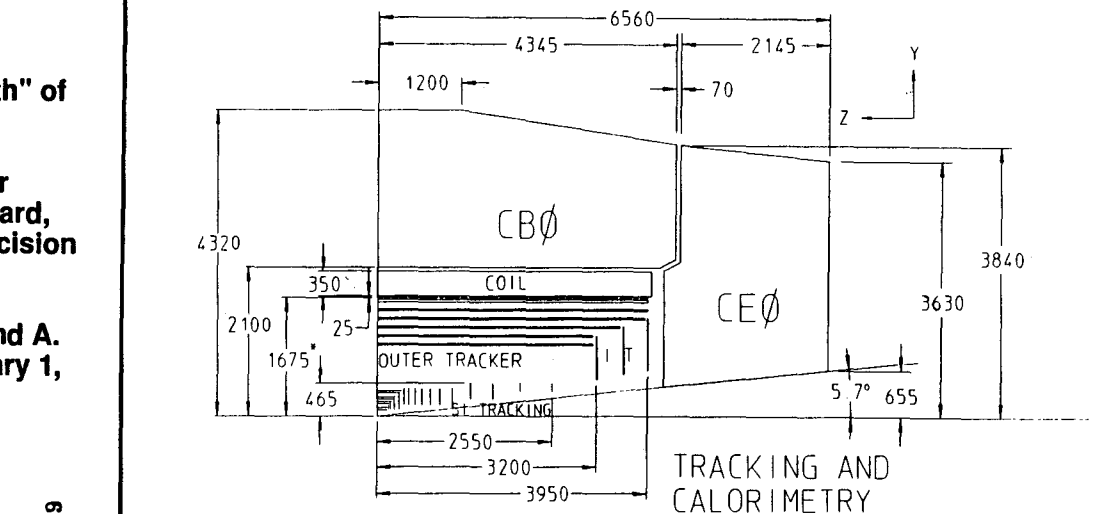
filename ~mhoto/hoff/xsec_9_18_91

60

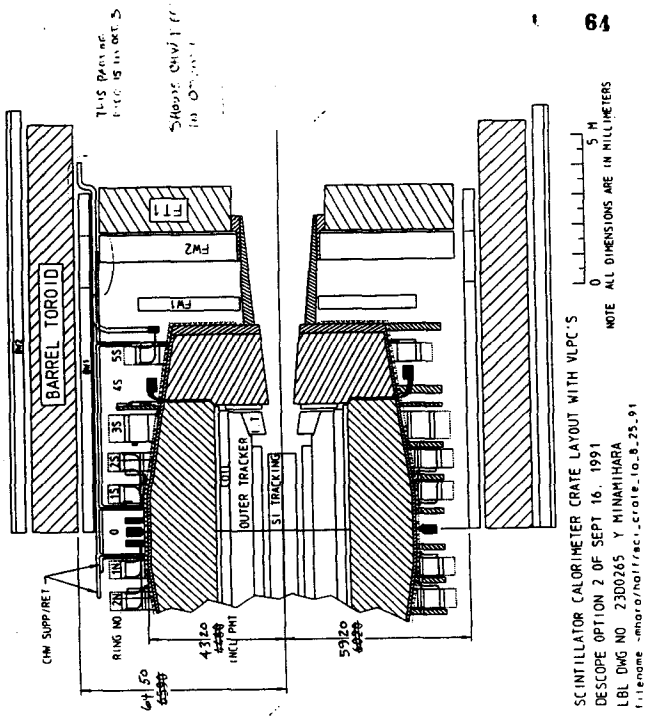
Decisions and Committees

- **Access space, radius of barrel toroid and "length" of muon system - Tech. Board this meeting**
- **Calorimeter absorber configuration - calorimeter committee(Siegrist, chair) input toTechnical Board, including impact on other systems - see list. Decision point - November 13-17 collaboration meeting**
- **Muon chamber selection committee - R. Thun and A. Maki, co-chairs. See list. Decision point - February 1, 1992**

63



61



PREAMBLE

Scintillating tile/fiber calorimetry has been selected as the choice for the central calorimeter of the SDC detector. We now have before us three basic choices for the configuration of the absorber in the hadronic section of the calorimeter: (1) a lead section(HAC1) followed by an iron section(HAC2) in both the barrel and endcap regions; (2) an iron HAC1 and HAC2 in both regions; and (3) a lead HAC1 and iron HAC2 in the barrel region with an iron HAC1 and HAC2 in the endcap region. In the case of the iron-loaded endcap, the possibility of having a reentrant endcap to provide a more uniform field must be considered. We must move as rapidly as possible to select a single absorber configuration.

CHARGE

The hadronic absorber evaluation committee is charged to evaluate the relative calorimetric performance and physics capability, as well as cost and engineering feasibility of the configurations described above. The Technical Board will make a recommendation for the optimal absorber configuration, based on the committee's evaluations and on its analysis of the impact of the absorber choice on the other detector subsystems. The committee is charged to prepare the appropriate reports and presentations for the collaboration meeting of November 13-16. If sufficient data are in hand at that time, the Technical Board will be requested to make a recommendation for the hadronic absorber configuration. If not, another date will be set to formulate a recommendation.

MEMBERSHIP OF THE COMMITTEE

Chairman.....J. Siegrist(SSCL)
Calorimeter options.....D. Green(FNAL), G. W. Foster(FNAL), L. Nodulman(ANL), J. Proudfoot(ANL)
Physics performance.....C. Hearty(LBL), M. Shapiro(LBL), ??? from Japan
Cost/schedule.....W. Edwards, D. Etherton and WSTC personnel
Engineering.....L. Bartoszek(FNAL), N. Hill(ANL), W. Pope(LBL), M. Harris/T. Thurston(SSCL, ex officio)
Others.....G. Abrams(LBL), J. Erwein(Saclay), K. Takikawa(Tsukuba),B. Wicklund(ANL)

CHARGE TO THE MUON TRACKING CHAMBER REVIEW COMMITTEE

The Muon Tracking Chamber Review Committee is charged to recommend to the Technical Board a design for the barrel muon tracking chambers. Factors to be taken into account include: performance of the chamber design, cost, schedule, alignment accuracy,ease of assembly, transportation and other engineering factors,triggering, and the impact on the overall performance of the muon system.

The Committee is requested to prepare its final recommendation by February 1, 1992. The membership of the committee is given below.

Muon Tracking Chamber Review Committee
Proposed Membership

Co-chairmen.....R. Thun*, A. Maki*

Chamber designs:
Boston dasign.....G. Feldman*
Wisconsin design...D. Carlsmith*
Washington design..H. Lubatti*
KEK design.....S. Odaka*/S. Terada*

Electronics/Trigger....Y. Arai*, J. Chapman

Engineering/Transportation/Assembly...M. Harris*, J. Pohlen*, T. Thurston*

Physics/Simulation....H. Iwasaki*, S. Willis*

Costs.....J. Bensinger*, D. Etherton*, Martin Marietta*

Others.....L. Holloway*, T. Ohsugi*/Y. Unno*, H. Ogren*, T. Fields

* accepted

- Tracking configuration(s) for Technical Proposal. T. Kondo, chair. Membership to be formulated by end of this meeting. Decision point to be determined by the end of this meeting.
- Aim towards major tracking review at Nov. 13-17 collaboration meeting with draft CDRs for tracking systems.

SDC
Engineering Meeting
SSC Laboratory
October 22-23, 1991

DRAFT AGENDA:

October 22

9:00	Introduction/Objectives	Thurston/Harris
9:30-12:30	Mechanical Integration	Thurston/Piles
	Electrical Integration	Hess
	Mechanical Assembly	Piles
	Configuration Management	Wells
1:30-5:30	Sub-System Reviews	
	Tracker Sub-System	
	Solenoid Sub-System	

October 23

9:00-12:30	Sub-System Reviews (Continued)	
	Calorimeter Sub-System	
	Muon Sub-System	
1:30-5:30	Subsystem Assembly/Installation Schedules	

Engineering Integration and Cost/Schedule

- **Regular Engineeering Integration meetings will commence on October 22-23 at SSCL**
- **See agenda(comments to Mike Harris/Tim Thurston)**
- **These meetings will be held regularly to bring together the SDC engineering team**
- **Cost/schedule "kick-off" meeting on Oct. 24 AM**
- **See schedule for production of cost/schedule book by April 1.**

Name	Sep 1991	Oct 1991	Nov 1991	Dec 1991	Jan 1992	Feb 1992	Mar 1992	Apr
SDC C/S MILESTONES WRE 9/91								
Revise C/S Procedures								
Submit Draft C/S Proc Book to SSCL								
Descoped Det Cost Kick-off Mtg								
Update Cost Estimates								
Descope Roll-up #1								
Create Prelim Draft SDC Cost Book								
Modify Cost Estimates								
Prelim Draft Cost Book Complete								
Descope Roll-up #2								
Perform Independent Cost Reviews								
Reviews Completed								
Create Final Draft SDC Cost Book								
Final Updates to Cost Estimates								
Final Draft Cost Book Complete								
Review & Finalize Revs to Cost Book								
Submit Proposal and Cost Book								
Name	Sep 1991	Oct 1991	Nov 1991	Dec 1991	Jan 1992	Feb 1992	Mar 1992	Apr

Technical Proposal Production

Overall editors: D. Groom, W. Chinowsky, G. Trilling and M. Gilchriese

The SDC Technical Proposal - Coordinating Editors

1. **Introduction - G. Trilling**
2. **Overview of the Detector - M. Gilchriese**
3. **Physics Performance - K. Einsweiler**
4. **Central Tracking System - TBA**
5. **Superconducting Solenoid - A. Yamamoto**
6. **Calorimeter System - TBA**
7. **Muon System - G. Feldman**
8. **Electronics, Data Acquisition,Trigger and Control Systems - F. Kirsten**
9. **On-line Computing - A. Fry**
10. **Off-line Computing - L. Price**
11. **Safety - J. Elias**
12. **Experimental Facilities - TBA**
13. **Installation and Commissioning - TBA**
14. **Test Beam Program - TBA**
15. **Cost and Schedule Summary - M. Gilchriese**

Budget

- Discussions with subsystem groups underway. First pass complete by mid-October.
- Revise R&D and Engineering Plan to meet final budgets by end of October.
- Append detailed agreements/budgets/MOUs by institution
- Slow process!



Other Documents Related to Technical Proposal

- Cost/schedule book. Coordinators: W. Edwards, D. Etherton.
- SDC Project Management Plan and related documents: Coordinators: T. Elioff, T. Kirk
- Preliminary hazards analysis. Coordinator: J. Elias



Technical Proposal Schedule

November 13	Detailed outline + final writing assignments and/or draft text
December 13	Zeroth draft submitted to chapter editors(and oversll editors for comments)
January 3	Submit first drsft to overall editors
January 31	Submit second drsft to oversll editors
February 21	Deliver final draft to SSCL for duplication of 150 copies
February 26-29	Review of final draft by collaboration and editors
March 23	Final printout of text with figures
March 25	Assemble, print and bind 40 copies
April 1	Submit 40 copies to SSCL

Collaboration meetings

November 13-17	SSCL
January 6-8(tentative)	Pisa
February 26-29	SSCL



Summary of Muon Activities

R. Thun

SUMMARY OF MUON ACTIVITIES - R. THUN

1.) TECHNICAL PROPOSAL

2.) "SCOPE" DISCUSSION

3.) CHAMBER REVIEW COMMITTEE

4.) PRESENTATIONS

a) H. IWASAKI .... RESOLUTION, COSMICS
b) J. WISS .... OCTAGONAL GEOMETRY EFFECTS
c) A. KULIK.... BEAM-PIPE/ABSORBER DESIGN
d) V. MOLCHANOV.... TRIGGER EFFICIENCY
e) V. RYKALIN... SCINTILLATION COUNTERS
f) R. THUN ... SCINTILLATOR R&D
g) A. SILL .... FOAM STRUCTURE
h) C. DALY .... WASH. CH. MECH. STRUCTURE
i) T. ZHAO .... WIRE DIAM., GAS MIXTURES
j) H. LUBATTI... WASHINGTON CH. R&D
K) A. SKUJA .... FORWARD MUON SYSTEM
l) S. TERADA .... JET CHAMBER
m) Y. ASANO .... DESCOPING
n) D. CARLSMITH... WISCONSIN CH. R&D
o) S. ERREDE .... SIMULATIONS, TEST BEAM
p) H. LUBATTI.... TEST BEAM

MOST IMMEDIATE "SCOPE" ISSUE:

HOW MANY LAYERS IN BW1 ?

4θ

OR 6θ

OR $4\theta + 4\phi$

OR .... ?

THICKNESS OF BW1 → TOROID I.R.

35 cm probably not enough

e.g. JET CHAMBER (6θ) : 45 cm

RESOLUTION
PATTERN RECOGNITION
TRACK LINKING

TRY TO ANSWER BY 13 NOV 91
SDC MEETING.

3

CHAMBER REVIEW COMMITTEE

1) CONTENT AND DUE DATE OF DESIGN REPORTS

DEC. (?)

2.) "SITE" VISITS:

BOSTON → WISCONSIN → WASHINGTON → KEK
2d week of JAN 92 (?)

DALLAS (DECISION)
last week of JAN 92 (?)

3.) CRITERIA
MECHANISM FOR DECISION

FELDMAN

Technical Proposal Chapter 7
Muon System

1. Introduction - Feldman
   Conceptual design
   Physics requirements - Willis
   Trigger at conceptual level
2. Scintillation counters - Thun
3. Cherenkov counters - Nauenberg
4. Central chambers - [illegible] technique
5. Forward chambers - Skuja
6. Central toroid - Cherwinka, Western
7. Forward toroid - Ditteri
8. Alignment - Eurich

Cost, schedule, assembly, electronics are probably elsewhere in the TP.

IWASAKI

I-4. Summary of σ_{P_t}/P_t

80

1. Present requirements :
   $\sigma(BW1) = \sigma(BW2, BW3) = 200\ \mu m$
   $L \equiv$ Lever arm $(BW2 - BW3) = 1.6\ m$
   seems to be overspecification.

2. $\sigma(BW1) \simeq \sigma(BW2, BW3) \times (3 \sim 4)$
   is optimum. ($L = 1.6\ m,\ 1\ m$)
   - Alignment error of BW1 relative to BW2/BW3 can be $O(\lesssim 1\ mm)$.
     (Not order of $\sim 200\ \mu m$)

3. L dependence of σ_{P_t}/P_t is small.
   - if $\sigma(BW1) = \sigma(BW2,3) = 200\ \mu m$
     even $L = 0.5\ m$ is OK (?) ←
   - if $\sigma(BW1) \simeq 1\ mm$
     $L = 1.0\ m$ is OK (?) ←

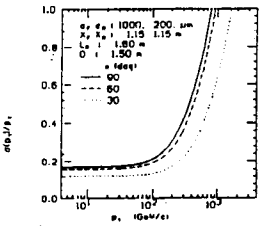
4. We need the answer to the question:
   " How much is the required σ_{P_t}/P_t for μ-ID ? "

IWASAKI

$\sigma_F = 1\ mm$, $\sigma_R = 200\ \mu m$

81

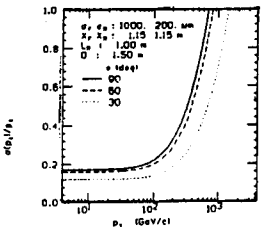
$L_R = 1.6\ m$



$$\frac{\sigma_{P_t}}{P_t} = \left[(P_t \sin\theta \cdot 1.234 \times 10^{-3})^2 + (\sqrt{\sin\theta}\ 0.1701)^2 \right]^{1/2}$$

P_t(turn) = 137.8 GeV/c @ $\theta = 90°$
148.1 60°
194.9 30°

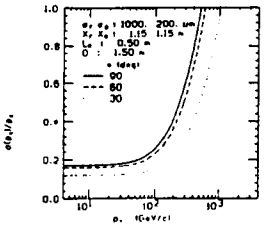
$L_R = 1.0\ m$



$$\frac{\sigma_{P_t}}{P_t} = \left[(P_t \sin\theta \cdot 1.379 \times 10^{-3})^2 + (\sqrt{\sin\theta} \cdot 0.1701)^2 \right]^{1/2}$$

P_t(turn) = 123.4 GeV/c @ $\theta = 90°$
132.6 60°
174.5 30°

$L_R = 0.5\ m$



$$\frac{\sigma_{P_t}}{P_t} = \left[(P_t \sin\theta \cdot 1.892 \times 10^{-3})^2 + (\sqrt{\sin\theta}\ 0.1701)^2 \right]^{1/2}$$

P_t(turn) = 89.9 GeV/c @ $\theta = 90°$
96.6 60°
127.2 30°

IWASAKI

II-3. Summary of the L1 trigger rates by cosmic μ

82

1. at the sea level
   - for $\Delta\alpha = 0.1$
     ($\Delta\alpha$: deflection angle cut)
     Rate ~ 2 kHz at sector "3" (top)
     0.8 kHz sector "1" (side)

2. in the underground
   - for $\Delta\alpha = 75$ mr
     Rate(sector "3") ~ 300 Hz
     " (" "1") ~ 10 Hz
     Total Rate ~ 600 Hz
   - for $\Delta\alpha = 20$ mr
     Total Rate ~ 100 Hz
   - for $\Delta\alpha = 20$ mr and $\Delta\phi = 0.1$
     Total Rate ~ 10 Hz

3. We expect (in the underground):
   Total Rate $\simeq$ 800 Hz, $\Delta\alpha = 0.1$ alone
   Total Rate $\lesssim$ 100 Hz, $\Delta\alpha = 0.1$ & $\Delta\phi = 0.1$

4. $\Delta\alpha$-cut alone is marginal.
   Rate(cosmic) $\approx$ allowable rate for μ-system ($\sim$kHz)

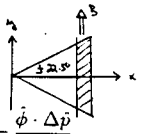
5. <u>$\Delta\alpha$-cut and $\Delta\phi$-cut</u> is a powerful discrimination for the cosmic μ.

83 WISS

Jim Wiss
September 23, 1991

Octagonal Geometry Effects

1. $\Delta\phi$ bend of toroid



(a) Bending Equations

$$\Delta\hat{p} = \frac{.3Bl}{P_\perp \cos\phi}\ \hat{p} \times \hat{b}\ , \quad \Delta\phi = \frac{\hat{\phi} \cdot \Delta\hat{p}}{\sin\theta}$$

$$\frac{\Delta\phi}{\Delta\theta} = -\ (\tan\phi)\ (\cot\theta)$$

- At $\eta = 1.5$, $\phi = 22.5°$ $\Delta\phi = -.88\ \Delta\theta$

(b) If uncorrected → magnetic ϕ smearing:

$$\sigma_\phi = \frac{200\ mrad}{P_\perp \tan\theta}$$

$\eta = 1.5$ $R\phi$ smearing at BW3

calor mcs	162 cm-Gev/$P_\perp$
toroid mag	125 cm-Gev/$P_\perp$
toroid mcs	58 cm-GeV/$P_\perp$

- Calorimeter MCS dominates ϕ smearing

KULIK

84

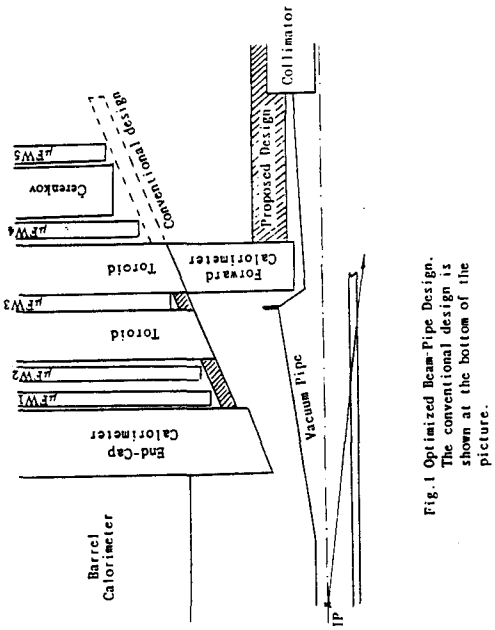


Fig.1 Optimized Beam-Pipe Design. The conventional design is shown at the bottom of the picture.

KULIK

85

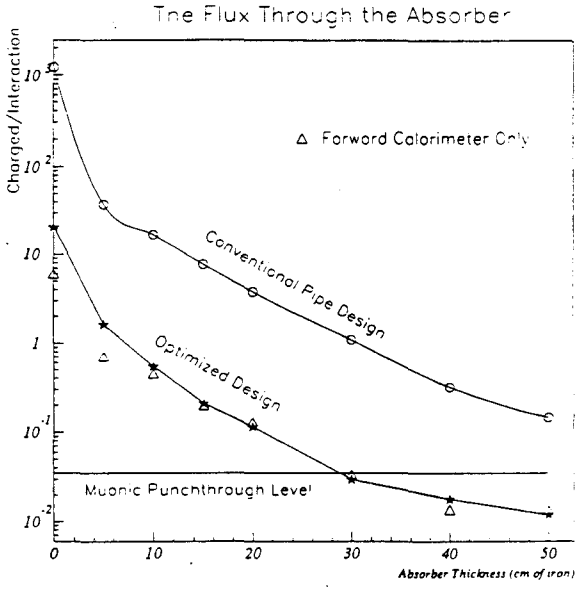


Fig.2 The Rate of Charged Punchthrough v.s. Iron Absorber Thickness. The curves "Conventional Pipe Design" and "Optimized Design" don't include the Forward Calorimeter influence. The latter is shown separately.

KULIK

86

50 cm Fe absorber

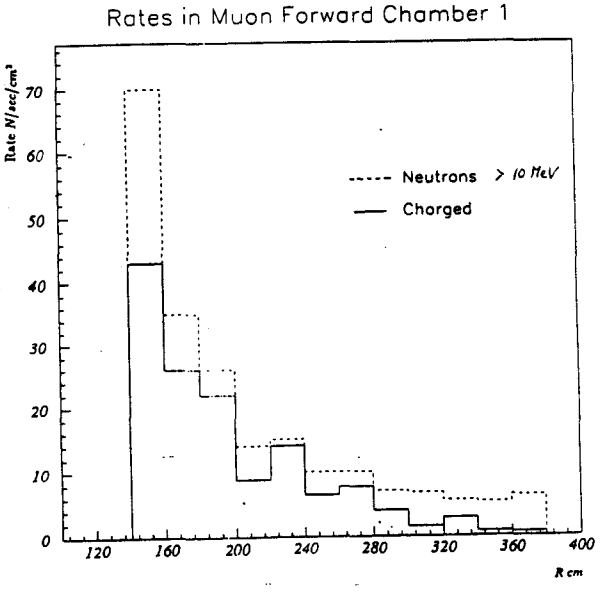


Fig.6

RYKALIN (4)

87

The sci. counters on the base of near PM with long photocathode (PMKS)

Cardinal decision of the problem is counter without light guide.

Three year ago our group began to design of the new PM with long photocathode (≤20c

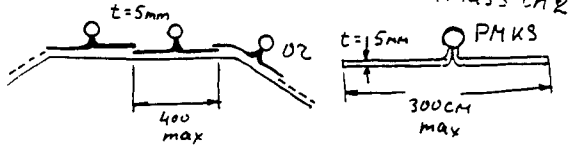
There are 8 operating samples just now.

Cross section scheme of the PMKS is shown on the Fig 4.

On Fig 5 - characteristics of the counter with PMKS

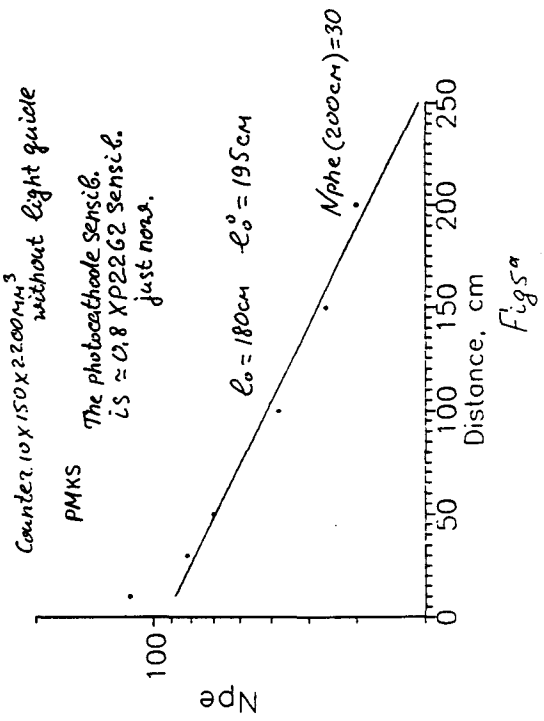
Potential advantages of the counters with PMKS

1. Absence of the light guide
2. The possibilities to decrease number of the PM in 2÷3 times and total sci. mass in 2 times.



RYKALIN

88



89 THUN

4) SUMMARY OF ACCOMPLISHMENTS TO DATE

a) We have assembled a large, three-layer cosmic-ray test stand as shown in fig. 1. Additional wire chambers and trigger scintillators will be added as required. The CAMAC-based data acquisition for this test stand is expected to be operational by the end of September, 1991. The test stand will allow the testing of large scintillation counters by triggering on cosmic-ray muons and recording their location and angle of incidence as they pass through the counters.

b) We have purchased or acquired a number of scintillation counters as listed in the following table:

Company	type		# of pieces	thickness	length	width
BICRON	BC 408	PVT	2	0.25"	117"	6.0"
			1	0.50"	117"	6.0"
			1	0.75"	117"	6.0"
KURARAY	SCSN-81	Polystyrene	2	0.6cm	270cm	15cm
			2	1.0cm	270cm	15cm
			1	2.0cm	270cm	15cm
			1	0.6cm	270cm	61cm
			1	1.0cm	270cm	61cm
NE	NE110	PVT	1	0.25"	117"	6.0"
			1	0.25"	117"	24.0"
			1	0.50"	117"	24.0"
POLYCAST	PS10	Acrylic	because of large minimum order we are negotiating an add-on to another order. We have some small pieces on hand.			

We have begun to measure the light yield and attenuation length of these scintillators with a pulse-height analyzer and the simple cosmic-ray setup shown in fig. 2. The trigger counter near the tested scintillator is 15 x 15 cm in size, and the two trigger counters are approximately 64 cm apart to insure that cosmic-ray muons enter at a reasonably normal angle of incidence. Some preliminary data are shown in figs. 3-7 which display pulse-height spectra from the scintillator as a function of distance from the phototube. The average number of detected photoelectrons <n> is also shown. (This was determined by fitting Poisson distributions to the pulse-height spectra with the constraint of a common overall scale factor that converts channel count to <n>. We have recently made some diode calibration runs which allow, in principle, a more precise determination of this scale factor since the diode data do not exhibit the long tail of the Landau distribution.) For these measurements, a RCA (Burle) 8575 phototube was attached directly to one end of the scintillator, and the other end was masked with black tape to minimize reflections from that end.

Preliminary Results:

Scintillator	Attenuation Length (cm)	Relative light yield/cm (est. error 10%)
1/2" Bicron BC408	422	0.76 (different set-up)
1/4" Bicron BC408	390	=1.00
10 mm Kuraray SCSN-81	220	0.56
6 mm Kuraray SCSN-81	160	0.50
3/8" Polycast PS10	58	0.41

90 THUN

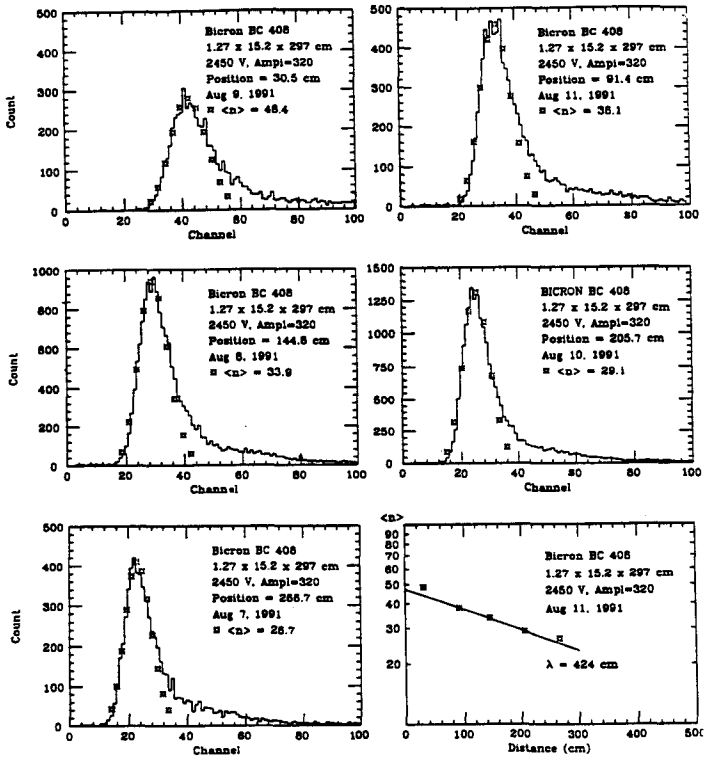


Fig. 3

91 SILL



DALY

92

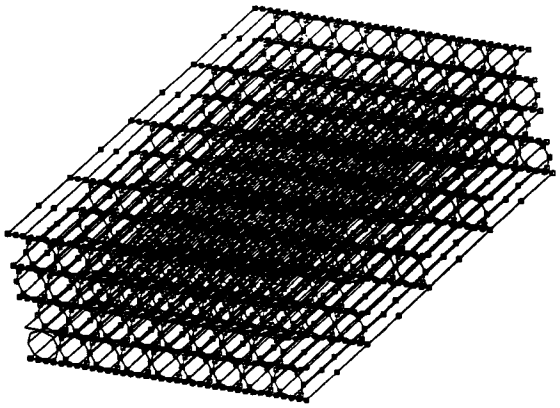


Figure 12. Detailed finite element model of a section of a 4-layer module.

ZHAO

93

increases dramatically above this point.

We have made measurements with several gases with and without the addition of alcohol. In all cases the indicated alcohol was added by flowing the gas through the alcohol which was at 3.5°C. Table I summarizes the gases tested and the operating ranges observed.

Table 1. Operating Range

Gas Mixture		Range (kV)	
	ϕ50μm	ϕ100μm	ϕ150μm
Ar-CH_4 90:10	2.4 - 2.9	2.9 - 3.35	3.4 - 3.8
Above with ethanol	2.4 - 3.5		3.4 - 4.2
Ar-C_4H_{10} 1:2	4.0 - 6.5		
Ar-CO_2 90:10	2.6 - 2.9	3.1 - 3.4	3.6 - 3.8
Above with isopropanol	2.5 - 3.0	3.0 - 3.4	3.5 - 3.8
Ar-CH_4-CO_2 90:5:5	2.7 - 3.1	3.0 - 3.4	3.5 - 3.8
Above with isopropanol			

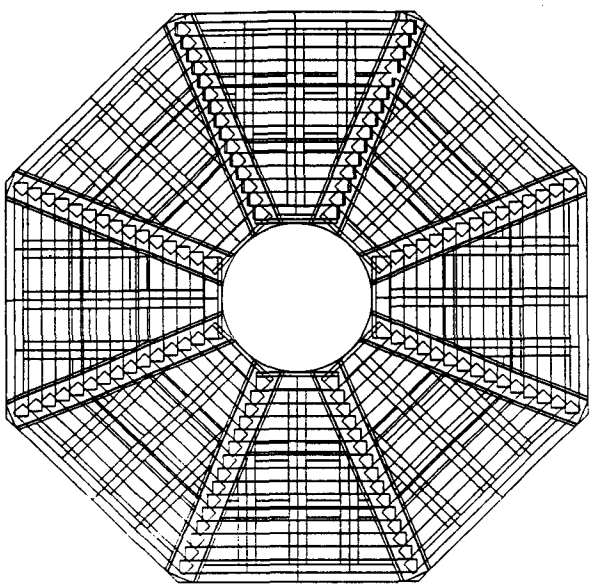
We conclude:

- The operating range of the ϕ50μm diameter wire is the largest among the three kinds of wires tested. The differences are, however, rather small.
- The operational range depends strongly on the gas mixtures. The operating range we observed for Ar/CO_2 90:10 is small. The stability is especially poor for the ϕ153μm anode. (CO_2 is known not to be a good quenching gas.)
- Alcohol surpresses the secondary streamer pulses and, therefore, makes the tube operation more stable. By adding ethanol, the operation range of the P10 gas is greatly extended and the speed of the P10 gas is not affected. The maximum drift time in both cases is 800 ns. Ethanol also helps gas mixtures containing CO_2. The effect, however, is less prominent. Isopropanol alcohol has also been tried. The results are very similar to that of the ethanol. Alcohol slows the drift speed down in the the gas mixtures containing CO_2 significantly.

We also tried Ar-CH_4 50:50. This gas is extremely fast in our tube. The maximum drift time is only about 500 ns. Another gas mixture, Ar/C_4H_{10} 1:2, has even better quenching property. The operating range is extremely large as given in the above table.

SKUJA PG6

94



μFW1 — 4θ

OCTANTS ARE STAGGERED AND ELECTRONICS ARE LOCATED ON FACES OPPOSITE WIRE MODULES

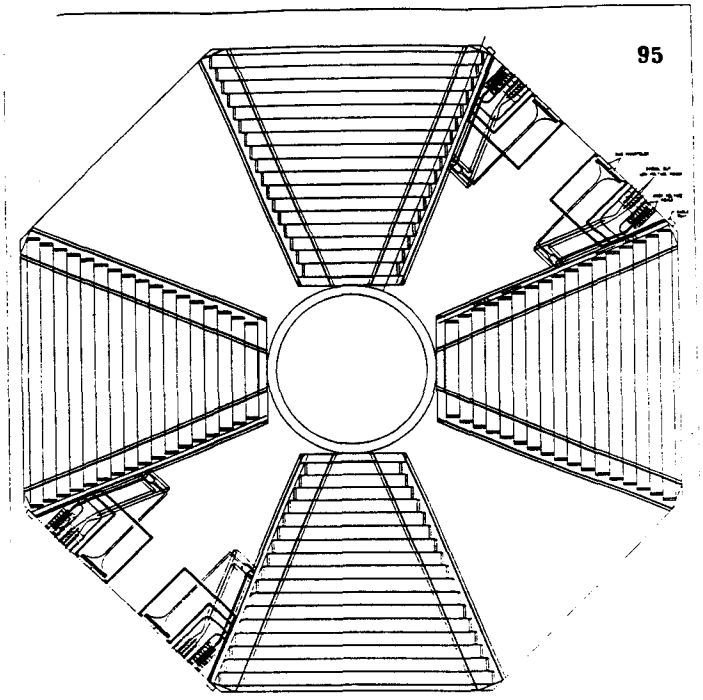
FIGURE 4

SUPER MODULE

TYPICAL

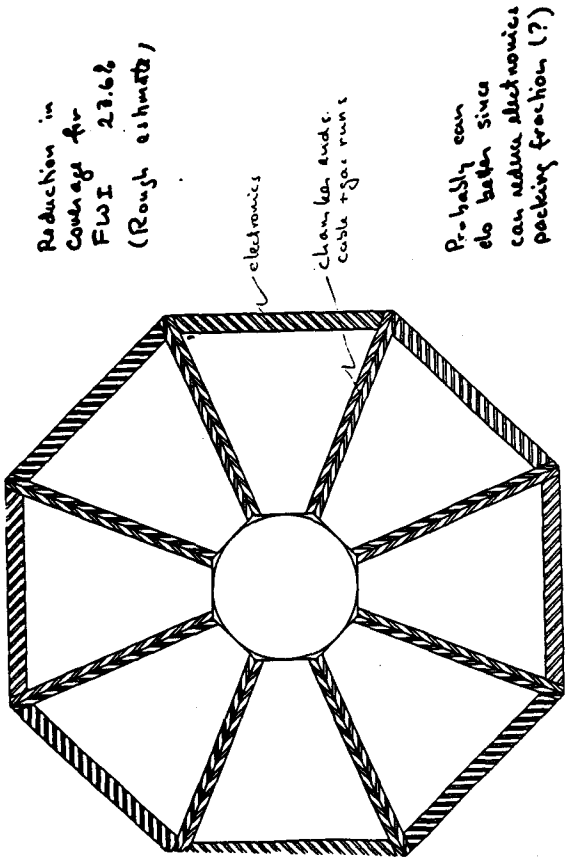
SKUJA

95



4θ FRONT LAYER

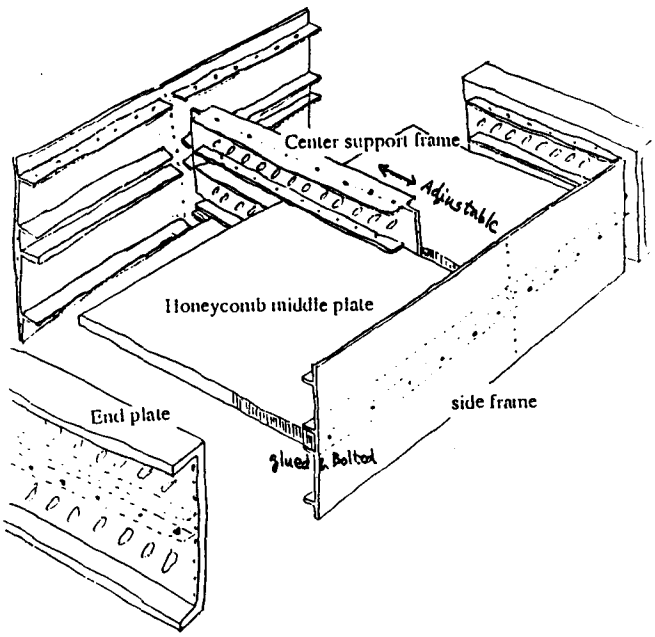
96 SKUJA



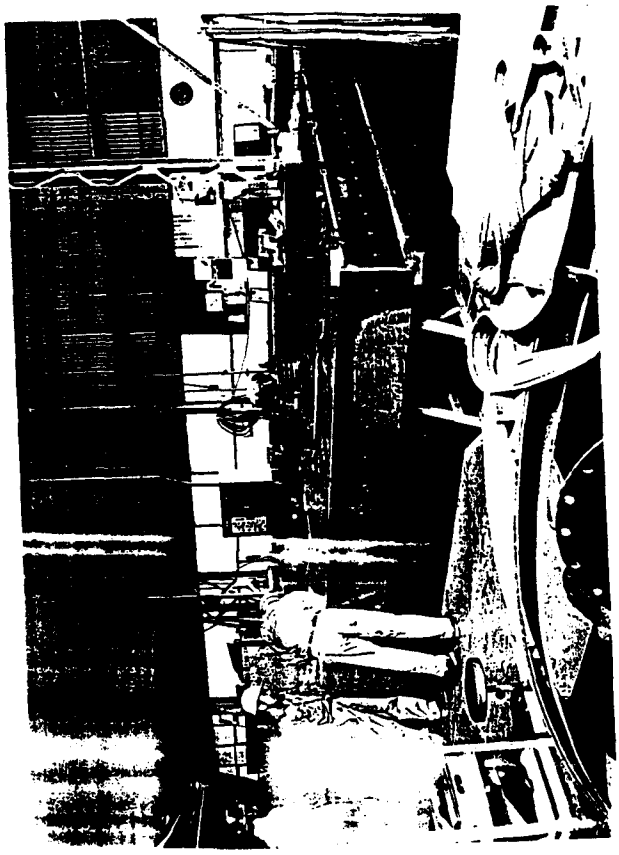
TERADA

■ Frame structure and assembly procedure:

97



98 TERADA



99

S. Odaka (KEK)
September 21, 1991
To be presented at the SDC Collab. Meeting, ORNL
Muon subgroup

Status of the Short Test Chamber

Type I ($\theta = 90°$)

Fe^{55} (5.9 keV X-ray) signal is seen.

HRS gas: Ar/CO_2/Methane (89/10/1)
$V_{anode} = V_{guard} = +1.9$ kV
$V_{cathode} = -2.8$ kV
$\Rightarrow \sim 10^5$ gas-gain

The voltages shown in my design report are too high for 50 μm^{ϕ} sense wires.
$\Rightarrow$ No problem;
Use a thicker wire (70 or 100 μm^{ϕ}).
A study of gas-gain is in progress, using thin-tube chambers.

Type II ($\theta = 30°$)

will be ready by the end of September.

100 ASANO

A short comment on the descoping of the muon-chamber

Contributed to the
muon group meeting, Sept. 1991

Yuzo Asano
Institute of Applied Physics
University of Tsukuba

Abstract

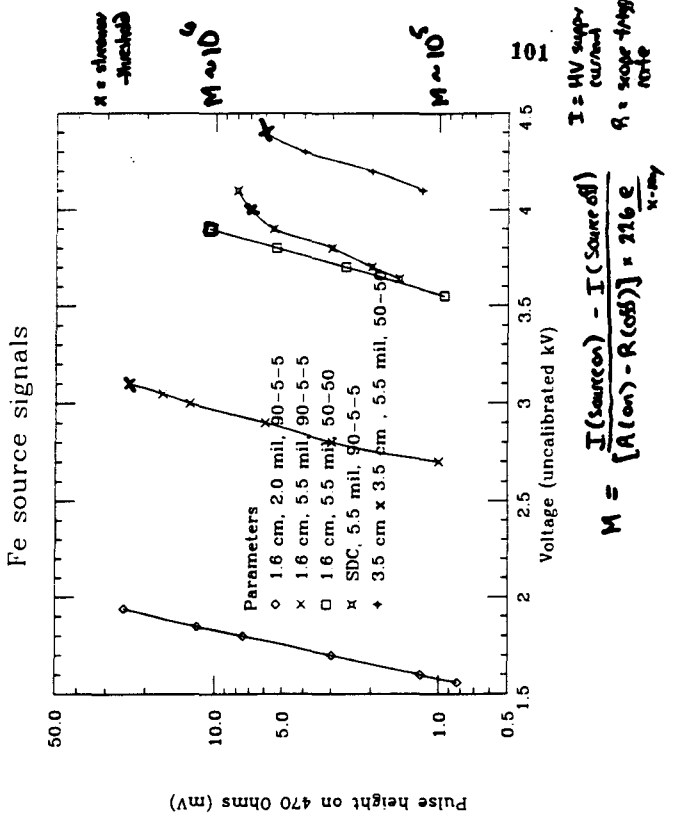
The muon cahmber seems to be one of the major target of descoping almost without limit. Unless some standard is given, the muon chamber will become the minimum set with which some known physics can be barely done, but some unpredicted physics will be lost either by the poor resolution or by the insufficient detection efficiency, or by the poor S/N ratio. Even the known physics may be lost because of insufficient luminosity (which is very likely during the first few years) and poor efficiency.
The requirement on the muon system is continuous, that is, the better the better. Chopping off every nook and corner will result in a detector which is almost of no use except for some standard phenomena which may or may not occur in nature.

Here, a small example is shown how the track-matching by extrapolating a muon track to the inner tracker is required, the efficiency of which is strongly dependent on the muon chamber performance.

The example shown here is as follows.
A possibility of matching a high Pt muon track with a high Pt pion track by mistake is examined. The requirement on the independent momentum measurement by the toroid system, and the requirement on the precision of the track determination will be recognized from the results.

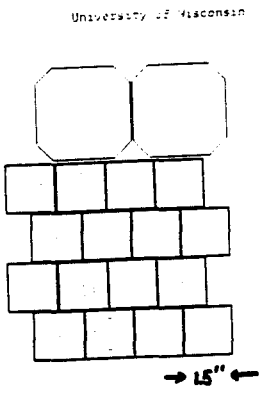
CARLSMITH

101



CARLSMITH

102



103 ERREDE

Sept. 23, 1991

SDC Muon Simulation at University of Illinois

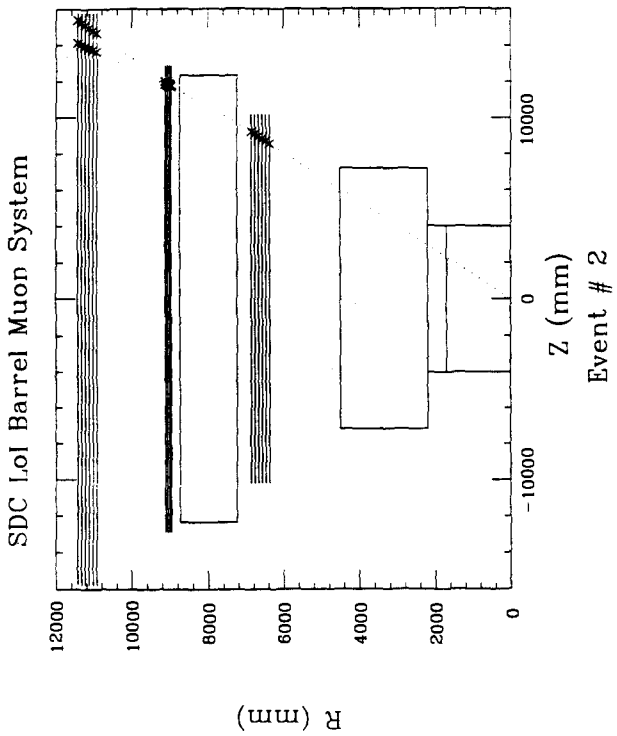
D. Errede, S. Errede, R. Gardner, M. Haney, I. Karliner D. Miller & J. Wiss

Purpose/Goals:

- In-depth studies of relative & absolute performance characteristics of candidate muon subsystem design(s):
  – barrel & intermediate regions
  - Overall drift chamber design(s) – # layers, chamber orientation (θ, ϕ, stereo)
  - Drift chamber cell configurations, shaping fields, DCH gases, etc.
  - Projective vs. non-projective cell geometries...
- In-depth studies of relative & absolute performance characteristics of candidate muon trigger design(s):
  – barrel & intermediate regions
  - HDL Verilog & VHDL trigger simulation(s)
  - Scintillator & Cherenkov counter L1 triggers
  - Muon drift chamber L1 & L2 triggers
  - Evaluate trigger efficiencies, biases, failure modes...
  - Evaluate on-line momentum resolution
  - Evaluate trigger rates
  - DACQ pipeline studies, etc.

ERREDE

104



LUBATTI

105

9-24-91 HJL

MUON BEAM TESTS

Colorado/Boulder, Fermilab, Illinois/Champaign, Maryland, Osaka City U/Japan, Rochester, Temple, Tufts, Washington, Wisconsin/Madison

GOALS

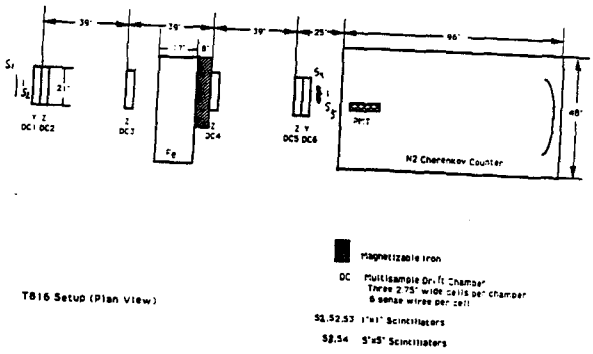
- Study number, energy and angular distribution of charged particles accompanying a muon emerging from an absorber and dependence on:
  - muon energy
  - drift chamber wall material and thickness.
- Determine efficiency of muon track reconstruction and smearing of resolution resulting from accompanying charged particles for some prototype cells.
- Čerenkov counter trigger tests

FIRST DATA RUN

- October 3, 1991
- 490 GeV muons

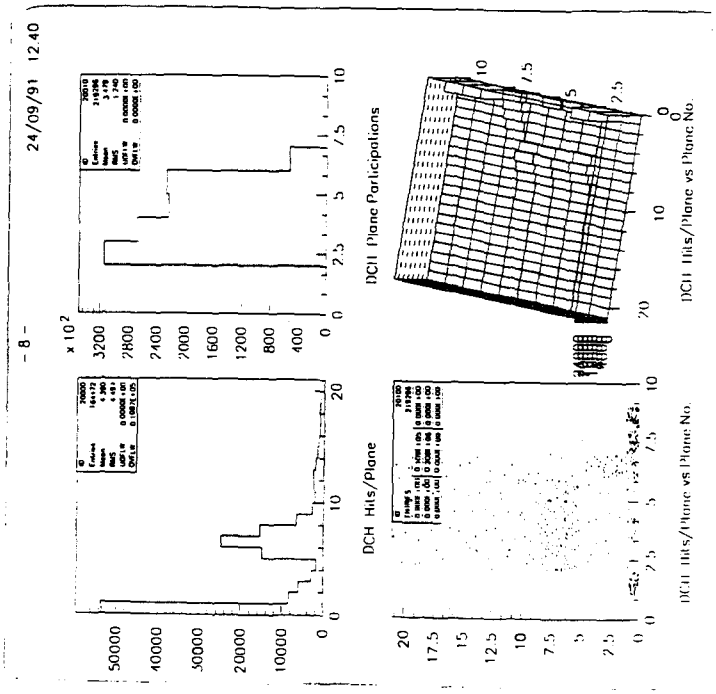
LUBATTI

106



ERREDE

107



Calorimeter Group Summary

D. Green

9/27 SDC CALORIMETER GROUP

D. GREEN

1) GREEN - SDR
TB
ETC.

109

2) CHRIS H - SIMULATIONS EM DEPTH
OANN G - MASSLESS GAPS

3) T HANDLER - ABSORBER SIMULATIONS
J REDY - OPTICS SIMULATIONS

4) V. HAGOPIAN - NEW RADDAM TEST

5) R+D:

a) OVERVIEW, SCHEDULE - DG.

b) TASKS - RADDAM.
SCINT
OPTICS
CALIB
PMT - TASKS
DELIVERABLES
ETC

SIMULATIONS - T.G.

ENGINEERING - P.M.

c) DISCUSSIONS

R+D TASKS [ASE BASE PROGRAM
USE MS - R+D FOR

110

1) RADDAM (GREEN)

a) NEW "SCREENING" - C_0

b) MODULE SHIPPING/TESTS @ BEIJING @ KEK

SMEAR DROPS - S_i

c) LONG TERM TESTS @ MICHIGAN
PROGRAM: GADOLIES
INJECTION MOLD
RED/GREEN
REDUCED PATH
SILICA

DELIVERABLES

FTE

2) SCINT (PROJ FOOT)

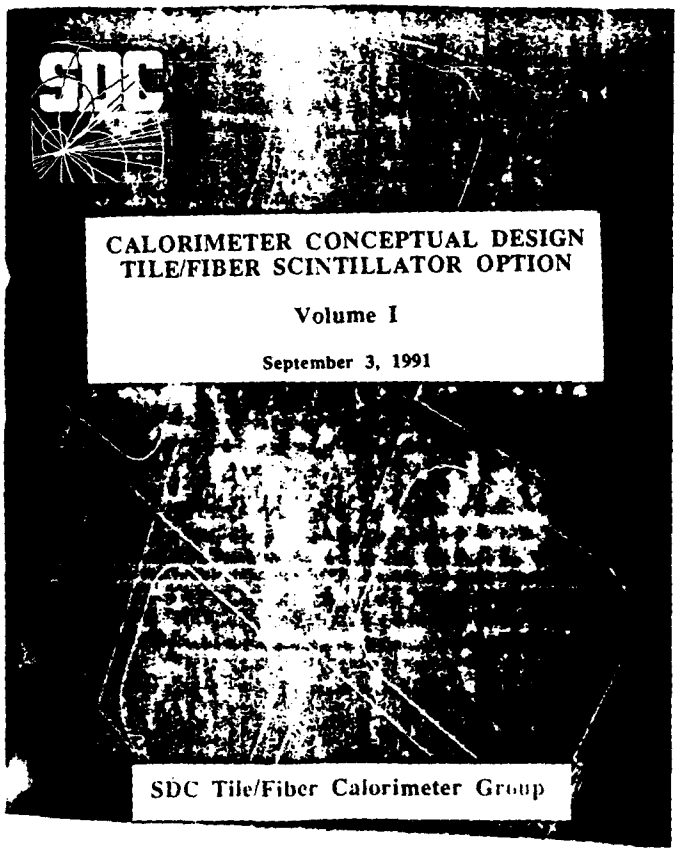
NEW RADHARD R+D

DOW, BICRON, KURARAY ... ? - TILES

SILICA + WLS, NEW FIBERS - TILE

INITIAL SCREENING?

111



112

Parameter	Requirement	Model A	Model B
EM allowed cracks	< 5 – 10%	~ 0	1.5%
holes $/\eta/ < \eta max$		1.5%	1.5%
Total electron acceptance	> .9	> 98%	> 97%
Energy Resolution			
EM stochastic term	$14\text{-}20\%/\sqrt{E_T}$	12	13.5
EM constant term	< 1 – 2%	ok	ok
HAD stochastic term	$50\text{-}75\%/\sqrt{E_T}$	65	60
HAD constant term	< 4%	< 4	2
Time stability	< 1% after correction	ok	ok
e/h response	< 1.3	< 1.2	1.0-1.05
Spatial uniformity			
EM	< 5% loss	< 2%	< 2%
HAD		< 5%	< 5%
Dynamic range			
EM	20 MeV-2 TeV	30 MeV	30 MeV
HAD	50 MeV-5 TeV	60 MeV	60 MeV
Time resolution			
EM	$\sigma \sim 5nsec, E_T > 15$	< 2nsec	< 2 nsec
HAD	$\sigma \sim 5nsec, E_T > 100$	< 2nsec	< 2 nsec
Signal peaking time	< 200 nsec	~ 10nsec	~ 10 nsec
Baseline rest.	100 nsec < τ < 6μ sec	~ 30nsec	~ 30 nsec
Noise	< 5 GeV, Δ R=.3	0	0
Pileup	< 5 GeV, Δ R=.3	ok	ok

Table 1: Critical Performance Requirements

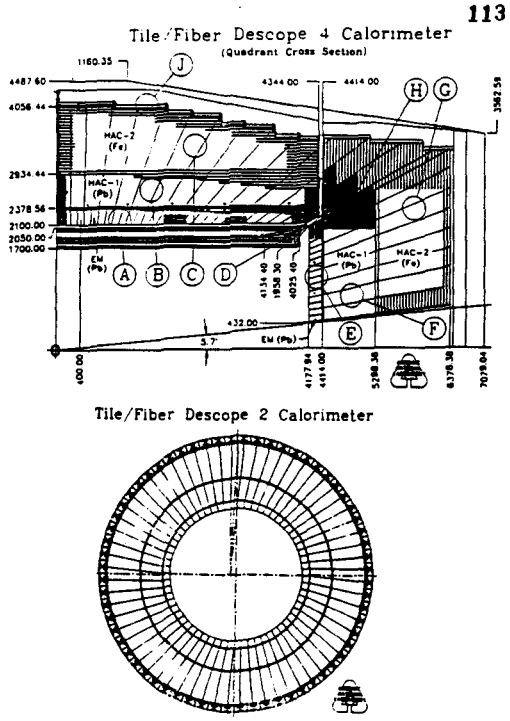


Figure 4.1 a)MODEL B Quadrant Cross section, b) End Section

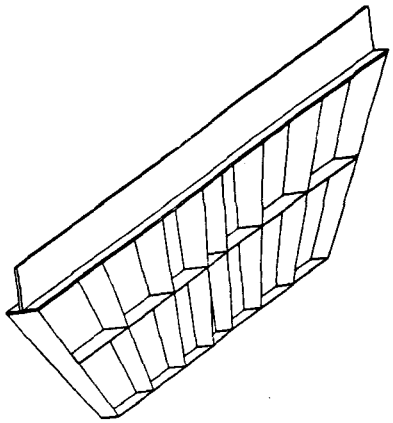


Figure 4.11 "Eggcrate" lead reinforcement concept

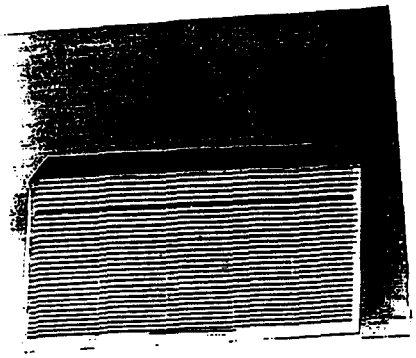


Figure 4.13 Cast lead absorber for EM Test Module 1.

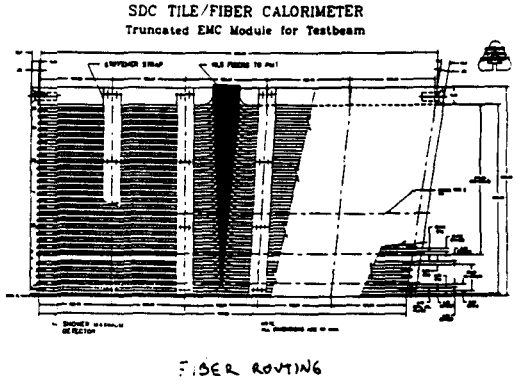
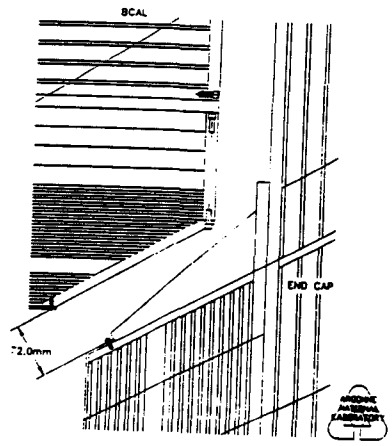


Figure 4.12 Truncated EM Test Module Design

CHIMNEY FOR SERVICES



Ⓓ Barrel/End Cap Transition

Figure 4.5 Barrel-Endcap Transition

MODEL A

HAC2 - Fe

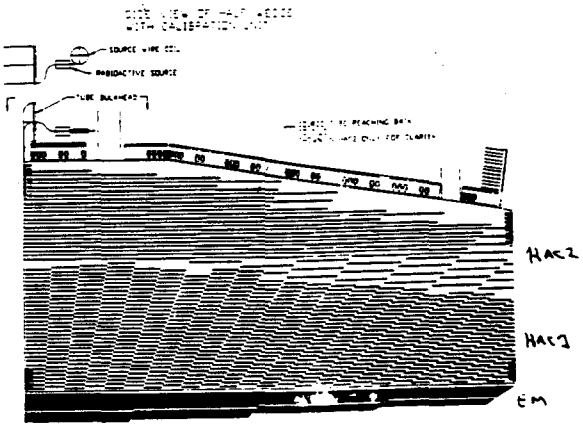
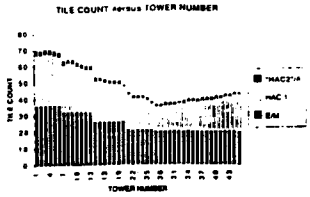


Figure 3.1(d) - Side views of a typical barrel calorimeter wedge, showing pattern of staggered slots in the iron calorimeter, PMTs, and source drives.

#



X_0



λ_0

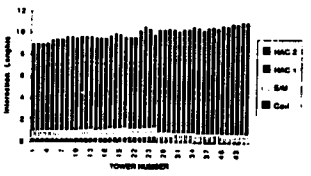
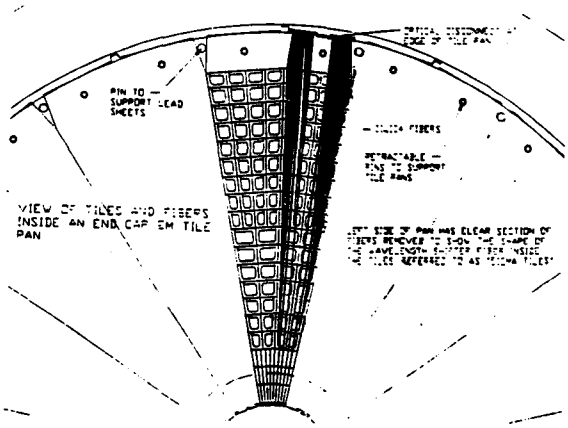


Figure 3.2 - Scintillator tile counts as a function of tower number in the iron calorimeter design. The HAC2 tile counts have been averaged over 4 towers to reflect the decreased segmentation in HAC2. Note that the majority of tiles are in the EM section.

Figure 3.3 - Calorimeter depth in radiation lengths X_0 as a function of tower number. The target for the depth for the EM calorimeter was to stay between between 22 and 25 X_0.

Figure 3.4 - Calorimeter depth in interaction lengths λ_0 as a function of tower number. The target for the depth for the full calorimeter was 9λ at 90 degrees and 11λ at 5.7 degrees.

PIZZA PIN END CAP DESIGN



INSERT?

MORE ENGINEERING

Figure 3.17 - View of tiles and fibers inside a "pizza pan" sector of the Endcap EM calorimeter. Each pan features an optical disconnect to aid in assembly. Note the "sigma tile" pattern in the outer tiles, and the high density of readout fiber in the inner tiles. The EM absorber is a series of stainless-clad lead disks supported by posts at the outer circumference.

FIBER ROUTING
EM+ HAC1

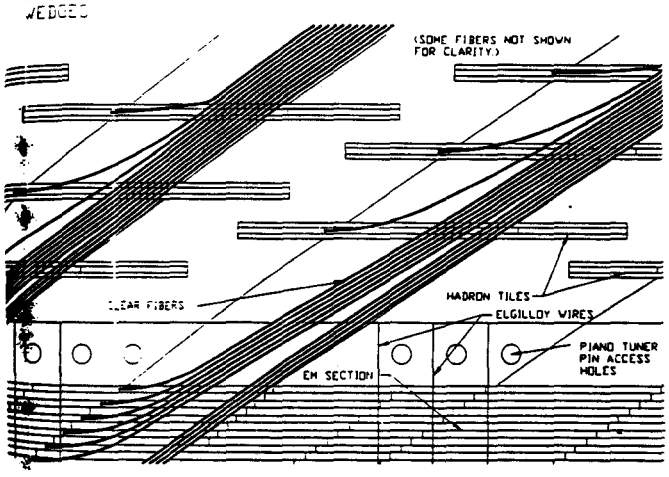
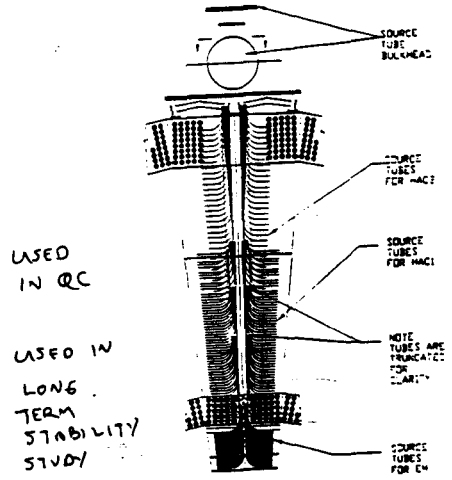


Figure 3.7 - Side view of the Barrel EM calorimeter, showing fiber routing pattern and "piano wires" for stack compression.

CALIBRATION SOURCES

FUNDAMENTAL PROBLEM



USED IN QC

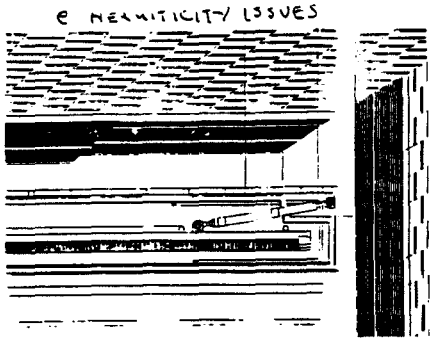
USED IN LONG TERM STABILITY STUDY

RADIATION DAMAGE PROFILE

USE TO COMPARE TO IN SITU

Figure 3.14 Calibration source tube routing in the barrel, as viewed from the 90-degree crack

e NEGATIVITY ISSUES



EGS SIMULATIONS

RE-ENTRANT PLUG?

EM RESOLUTIONS

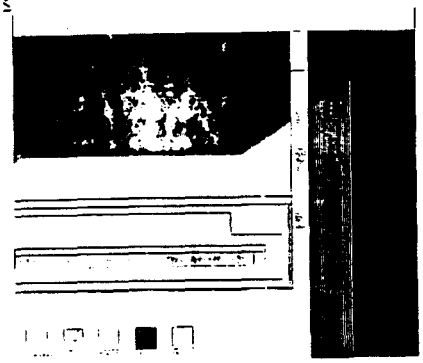


Figure 2.10 a)Solenoid drawing b) EGS model

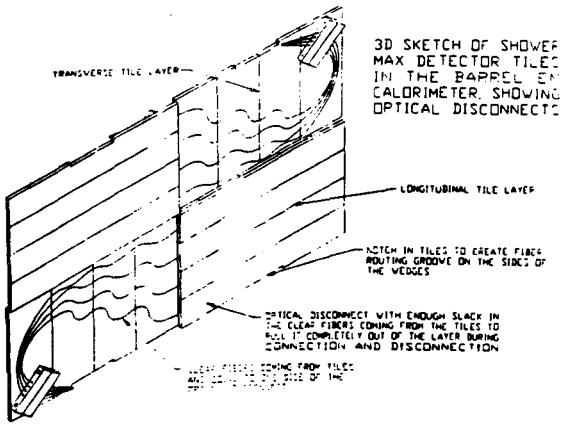


Figure 3.12 - Fiber routing in the EM shower-max assembly. The assembly contains two planes of scintillator strips for the X and Y views. The fiber routing is done between the planes. The clear readout fibers have an optical disconnect which is mounted between the planes, and canted slightly to align the shower-max readout fibers to join the bundles for the EM calorimeter tiles.

SM SIDE VIEW

VIEW OF SHOWER MAX DETECTOR IN THE BARREL EM, SHOWING OPTICAL DISCONNECTS FOR THE TWO BOTTOM LAYERS

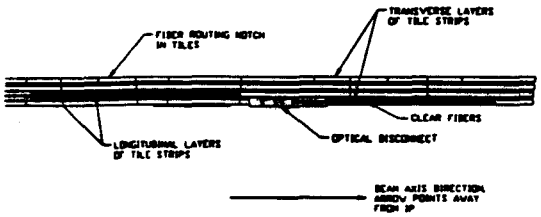


Figure 10.1 Side view of the Shower Maximum detector for the barrel . The crossed hodoscopic planes are evident, along with the optical disconnects.

PMT :

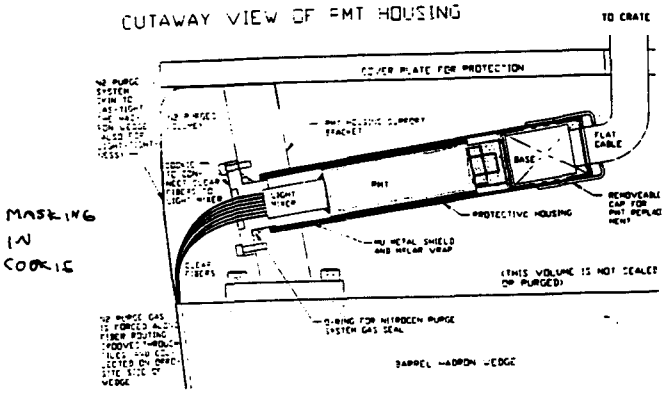
"CHARGE PUMP" BASE



Figure 7.1 Picture of a prototype PMT base showing the solid G-10 construction and the all flat cable i/o connections.

PMT MOUNT :

CUTAWAY VIEW OF PMT HOUSING



MASKING IN COOKIE

Figure 3.10 Phototube housing and support bracket at the corner of a wedge, including fiber routing, N_2 purge and light-tightness seals.

NEW BICRON PLASTIC

2.4 Mrad Co^{60}

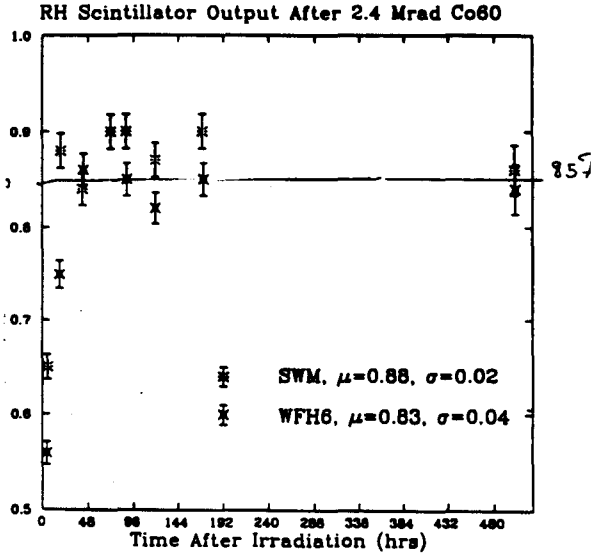
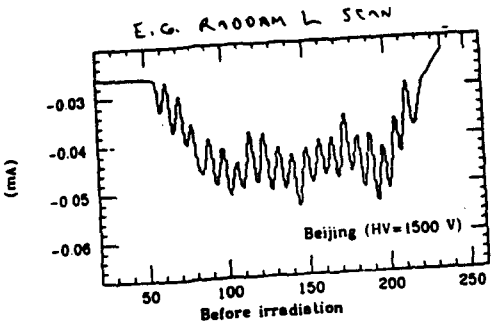


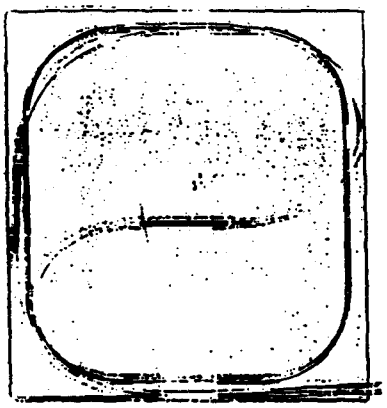
Figure 8.12 Average light output from 3 disks of 2 inches diameter read out using 2 wraps 1 mm BCF91A.

QC : ASSEMBLE MODULE
SOURCE SCAN



20 TILES

Figure 8.3 longitudinal source scan of a Beijing module.





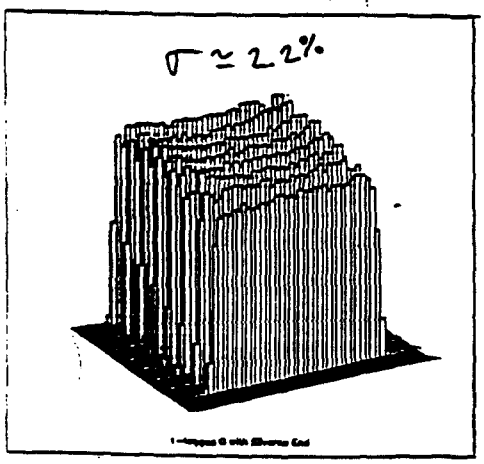
MP:OPTICS

- NO MASKING NEEDED
- "CIRCLE"

Fiber pattern chosen for our prototype. The loop of fiber in the tile can be seen as well as the external fiber routing and the steel reinforcements on the splices.

Figure 11.4 a) Fiber route within tile ("Circle") used in EM Test Module 1. b) Schematic of external fiber rout to the rear of EM Test Module 1. (all paths have a minimum bend radius of 1")

"G" TILE



NO NEED FOR ⊥ MASKING

Figure 6.11 Transverse response map for a "Sigma" tile.

LONGITUDINAL MASKING

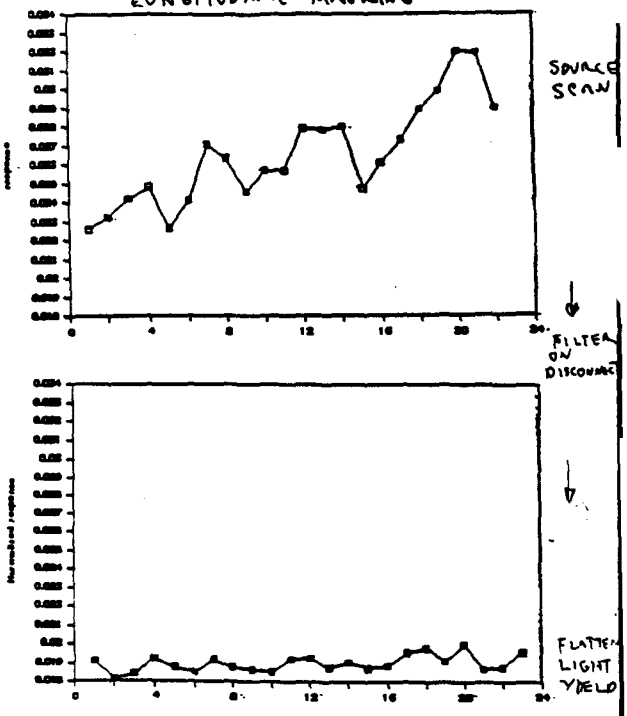


Figure 6.17 a) The longitudinal response of tiles in a tower. The horizontal scale is tile number ranging from 1 (front) to 23 (back). The vertical scale is relative light yield. The RMS variation is 11.5%.

b) The same tower as in (a), after longitudinal masking. The RMS variation is now 2.6%.

SPEC FOR ½ 7₀ CONSTANT TERM IS 27₀ LIGHT YIELD

133

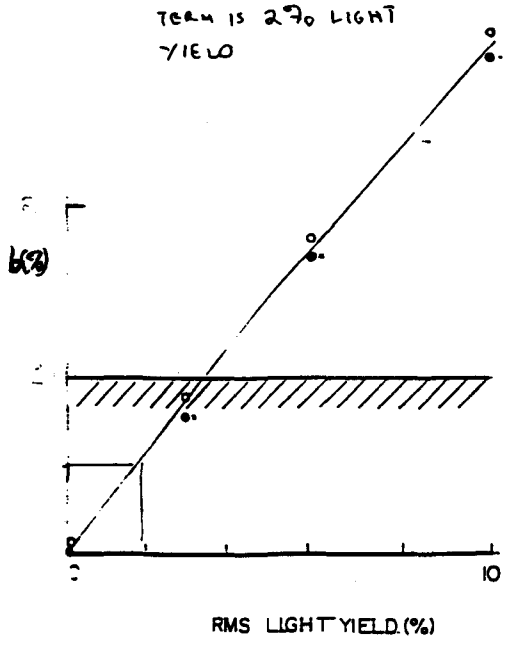


Figure 6.3 Constant term in resolution (b) vs tile-to-tile light yield variation for EGS simulated electromagnetic showers for 10 and 50 GeV electrons

SUMMARY

134

1) REQUIREMENTS → CORE → TECHNOLOGY CHOICE
CORE
⋮
IS DONE

2) MUST PRESERVE THE COLLABORATIVE GROUP OF PHYSICISTS INTERESTED IN CALORIMETRY

3) OCT 8 + – NEW FY92 R+D PLAN WITH REVISED TASKS AND PARTICIPANTS

4) NOV COLLABORATION MEETING
HAVE Pb/Fe CHOICE

⋮

5) APRIL 1 DESIGN REPORT
TEST BEAM DATA [illegible] JAN 1

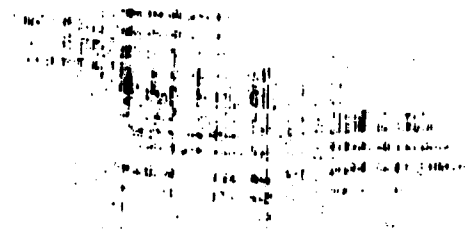
Received: from fnal.bgnet by Cnal.LBL.Gov with VMSmail ;
Fri, 20 Sep 91 10:53:32 PDT
Date: Fri, 20 Sep 91 10:53:32 PDT
From: dgroom @ fnal.bgnet
Message-Id: <9109201053332.20211a0a0@Cnal.LBL.Gov>
Subject: DRAFT task allocations for FY92 calorimeter group and task leaders. Don
To: gilg @ Cnal.LBL.Gov, pripstei @ Cnal.LBL.Gov, shur @ Cnal.LBL.Gov,
dagtesh @ Cnal.LBL.Gov, davidh @ Cnal.LBL.Gov, derek @ Cnal.LBL.Gov,
ghk @ Cnal.LBL.Gov, kadel @ Cnal.LBL.Gov, rossen @ Cnal.LBL.Gov,
wenzel @ Cnal.LBL.Gov
X-ST-Vmsmail-To: @SDC_CALOR.DIS

135

OCT 8
NEXT SSCL MEETING

| FY92 CALORIMETER GROUP BUDGET |

Dear Colleagues,
Since April there has been an effort at defining the SDC requirements for R&D in FY92. For the Calorimeter Group a strategy was adopted. At KEK we defined the maximum possible budget for SDC and thence for calorimetry. That number, 5+1M$ was the basis for a trial budget first shown at KEK. Our strategy was perhaps successful in that our Group has the largest R&D budget, while we did not have the largest request. However, our tentative allocation is only 3.8 M$ which is disheartening. In addition, it is hoped that there will be new players, now that the technology choice has been made. Indeed ALL are invited to participate in the FY92 SDC Calorimeter Group R&D proposal. Nevertheless, it must be clearly recognized that this broadening of the effort implies less support per SDC physicist.
Given that we must ramp up the engineering effort in FY92 in order to produce a Design Report and move towards a preproduction prototype, the funds for straight R&D are somewhat reduced in FY92.
Requests for funds are mismatched by a factor of about 3. I ask that those groups involved in the specific tasks contact the person indicated below and decide upon a method of reducing their collective requests to the level of reality, as defined to be the allocation within the 3.8 M$ shown below. In particular, the funds from Texas, and the efforts funded by our foreign collaborators MUST be taken into account if we are to avoid duplication.
The FY92 budget and tasks will be discussed at DPF in September. Given an expanding set of responsibilities, and a fairly flat budget we need to be as responsible as possible. There is a meeting with the SDC management on October 8, which means that a first pass budget must be in hand by the SSCL meeting. To that end, I will ask the contact people given below to present an institutional breakdown which meets the guidelines given. Thank you



Tracking Summary

W. Ford

Tracking Summary

137

w. Ford

1. Configuration (s) ("scope")
2. Performance Simulation
3. Tracking volume length
4. (Some) R&D highlights
5. Process for technical proposal

138

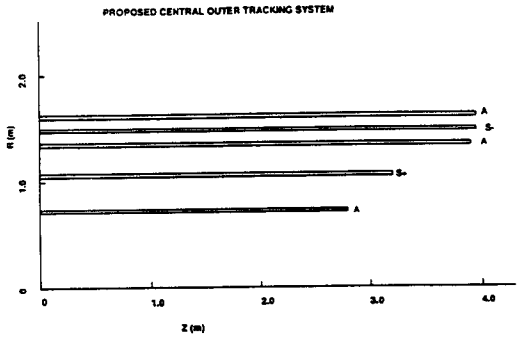


Fig. II-2. A section through one quadrant of the descoped all-straw central outer tracking system.

SAC 91-

139

Table. Central Outer Tracker Design

Superlayer	Radius (m)	Straws/Layer	Modules	Layers/Superlayer	z_{max} (m)	Stereo Angle (°)
1	0.708	1112	84	6	2.80	0
2	1.04	1640	124	6	3.20	+3
3	1.35	2120	160	8 (trigger)	3.90	0
4	1.48	2328	176	6	3.95	-3
5	1.61	2536	192	8 (trigger)	3.95	0

1.35×10^5 straws

3.5% X_0 at $\eta \sim 0$ (not including last superlayer)

Cost ~ $32M (working on detailed cost estimate)

140

Upgrade / Staging to Scintillating Fibers

Will take 2-3 years to reach design luminosity

For higher luminosity ($\sim 5 \times 10^{33}$) operation, put fibers where needed - inner superlayers

Replace inner superlayer(s) with fibers either later in design (staging) or when luminosity >> design $\mathcal{L}$ (upgrade) - when more $ available.

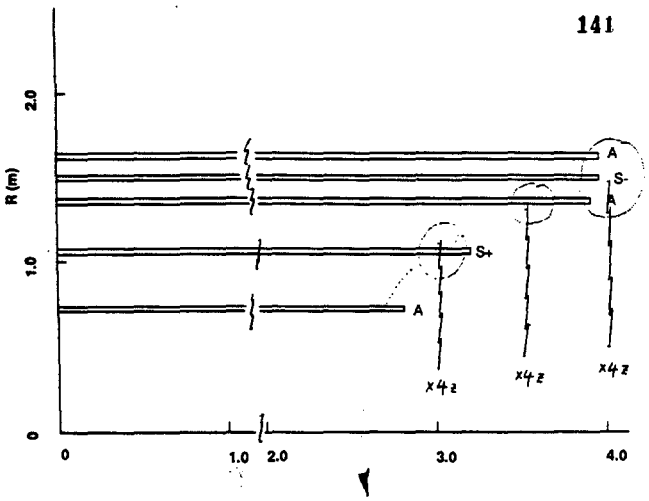
Therefore:

1) Continue fiber R&D

2) Design & engineer for staging

Microstrips in SDC ITDs - layout-status 20/9/91

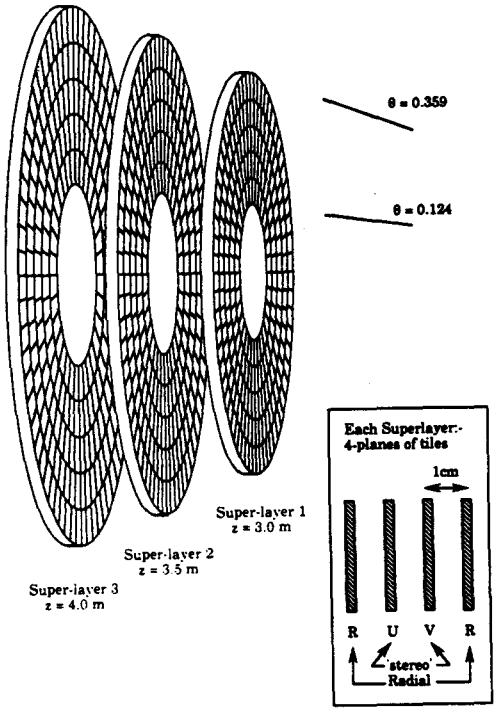
141



- outer radii and central straws ?
  - momentum resolution ? - which is better ?
  - $\perp$ strips insensitive to B inhomogeneity (Lorentz angle)
  - trigger ? - which is better ?

ITD

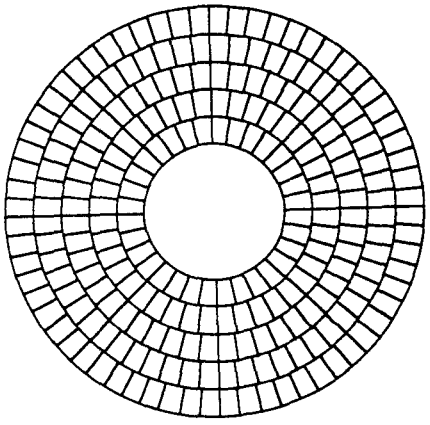
142



R-TILES at Z = ±4.0 m, ±4.03m.

143

Ring 1	0.500 - 0.700 m	32 tiles	10752 strips
Ring 2	0.700 - 0.900 m	40 tiles	12600 strips
Ring 3	0.900 - 1.100 m	48 tiles	18144 strips
Ring 4	1.100 - 1.300 m	56 tiles	18816 strips
Ring 5	1.300 - 1.500 m	64 tiles	21504 strips

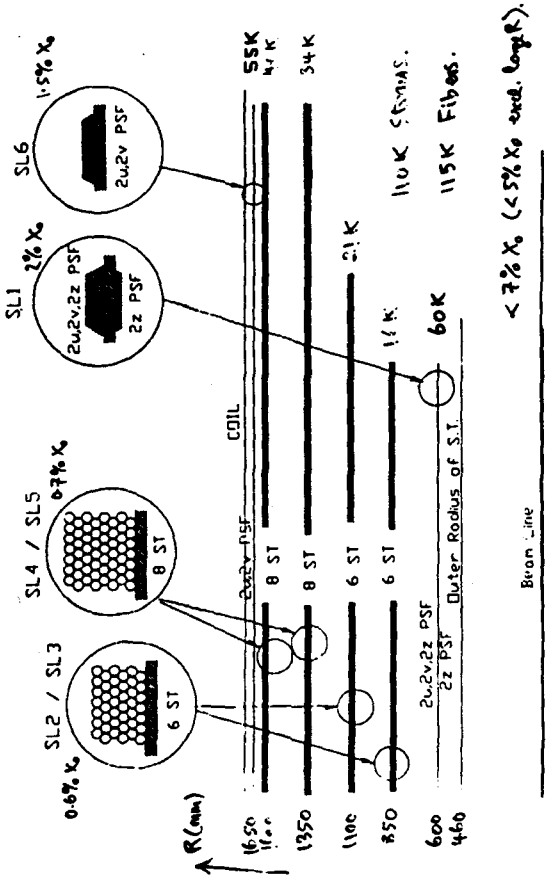


Layer Structure

144

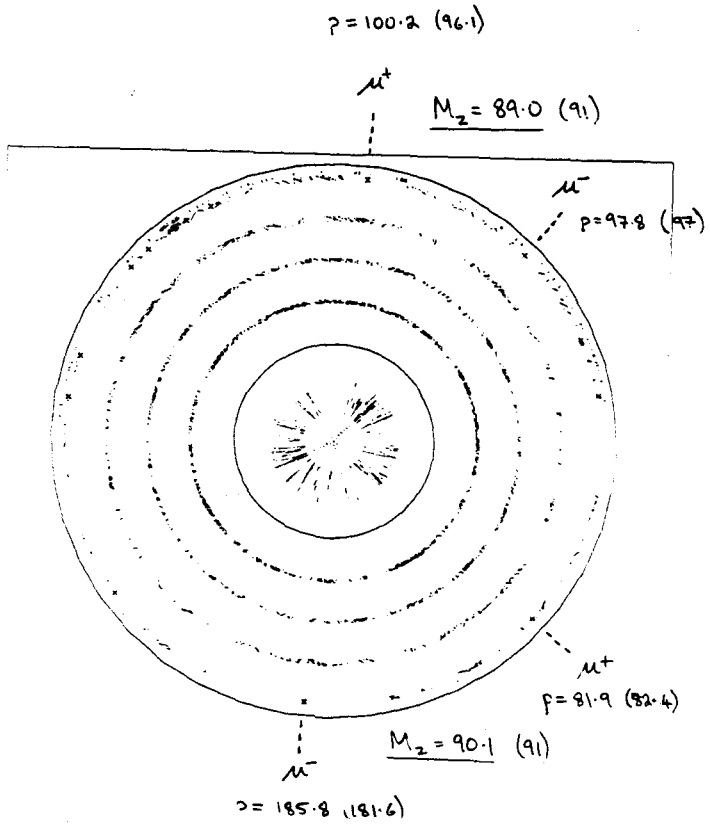
	#/Layer	Σ
4z	12.1K	48.3K
2v	11.8K	23.6K
2u	11.8K	23.6K
4z	11.8K	47.0K
2v	9.1K	18.3K
2u	9.1K	18.3K
4z	9.1K	36.5K
4z	7.0K	28.2K
4z	6.7K	26.9K
2v	4.4K	8.7K
2u	4.4K	8.7K
4z	4.3K	17.4K

145



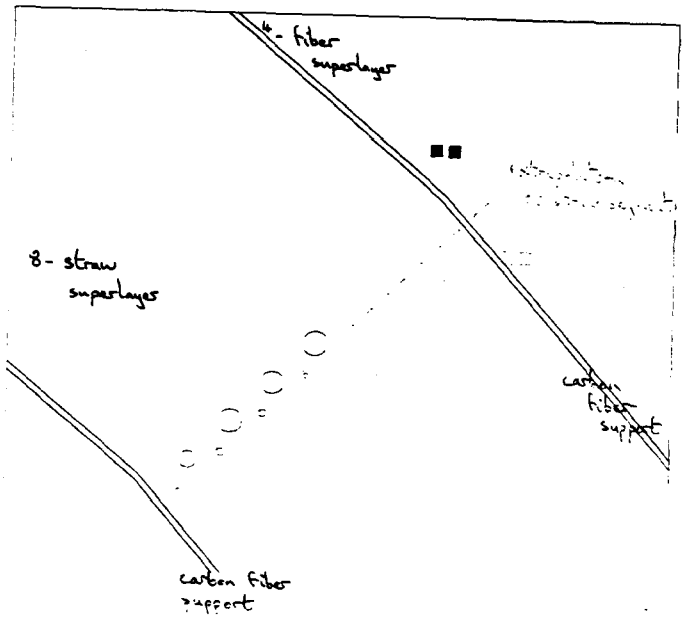
146

$M_H = 391$ (399)

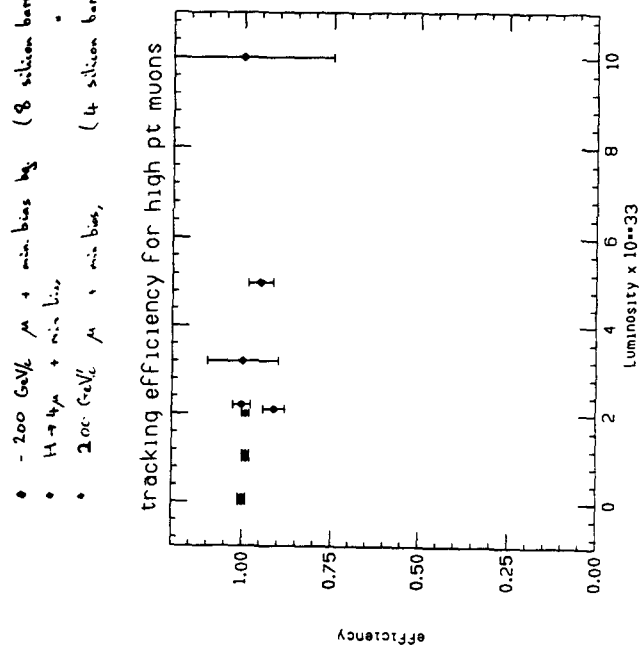


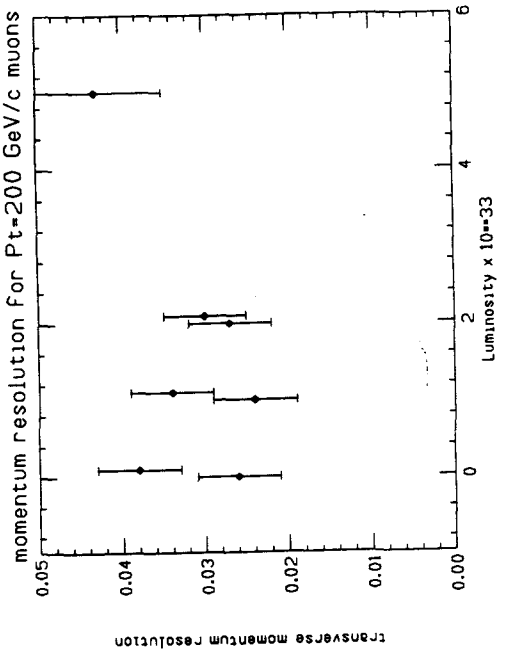
147

Hybrid Superlayer.

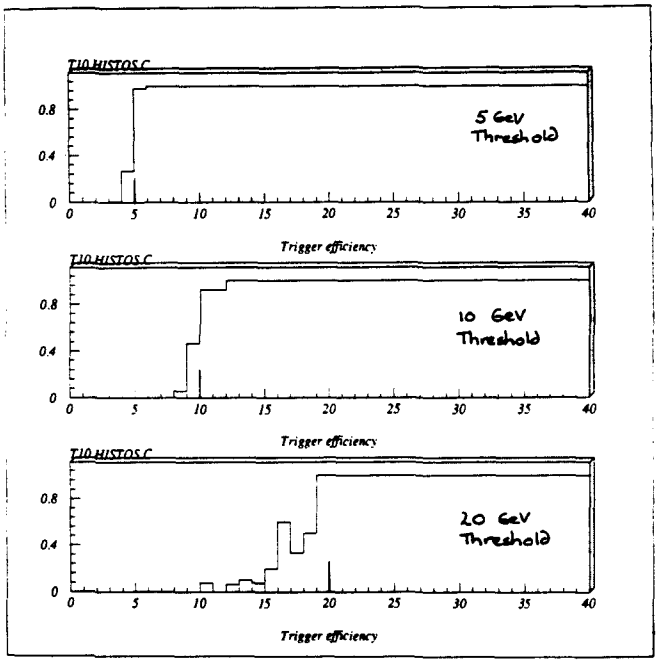


148





Broadening of trigger edge
– finite resolution in $\Delta\phi$
$\Delta p \sim \frac{1}{P_t}$



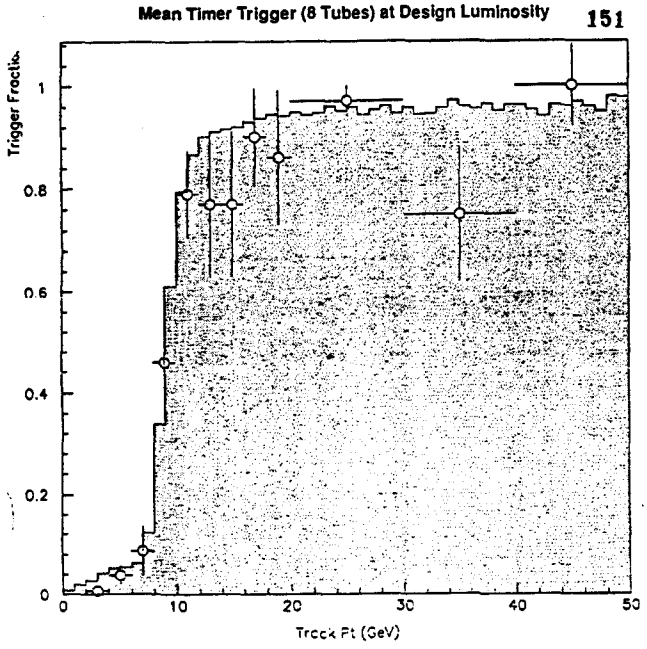


FIG. 3 The efficiency as a function of P_t for a digital mean timer based trigger operating on signals from an 8 tube deep superlayer of packed straw cells. The points are from a GEANT simulation of Higgs — ZZ events at 10^{33} luminosity and the shaded histogram is for a fast parameterized simulation tuned to match the GEANT points.

be effected) and the stiff track momentum resolution requirements (approximately 10% or

Pulse Attenuation in Straw Tubes

$\exp(-\alpha z)$ where $\alpha = R_l/2Z_0$

z is the length along the tube
α is the attenuation constant
R_l is the sum of the of the cathode and the anode resistance per unit length
Z_0 is the characteristic impedance.

ohms for a 25.4 μm wire in a 4 mm tube
" " " 38.0 " " " " " " "
" " " 51.0 " " " " " " "

ce of 25.4 μm gold plated tungsten wire is 116±4 ohms/meter.

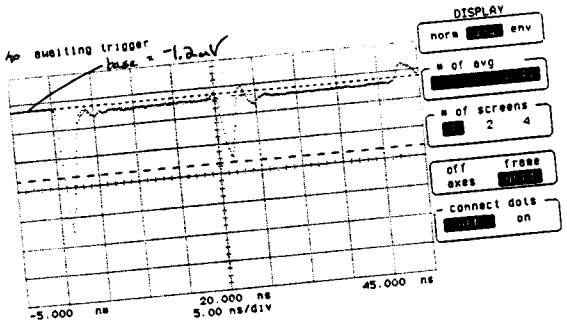
ce of 51. μm gold plated molybdenum wire is 30±1 ohms/meter

ty of 0.2-0.25 μm aluminum coating is about 0.3 ohms/square 30Ω/□.

ty of 0.15 μm copper coating is about 0.12 ohms/square 145Ω/□

6,91
+/ISO 80/20 Fe55
19 V
il 3 meter unterminated

153



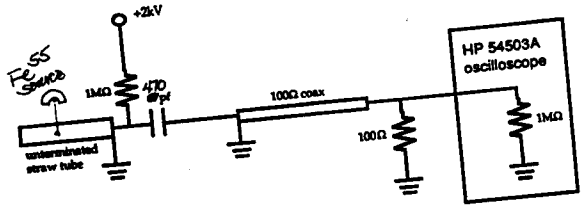


Fig. 1

154

Skin depth at 160 MHz for W/Mo is 10 μm:
No correction to the cathode resistance
~10% correction to R_1 for 25.4 μm wire
~50% " " " " 51. " " .

Measurements:

25.4 μm wire, 0.25 μm Al cathode, α=0.26/m(calc.)
=0.26/m(meas.) ±10%

51 μm wire, 0.25 μm Al cathode, α=0.14/m(calc)
=0.14/m(meas) ±10%

Estimates:

38 μm wire, 0.15 μm Cu cathode, α=0.14/m

51 μm wire, 0.15 μm Cu cathode, α=0.11/m.

Amount of material:

0.25 μm aluminum ≈ 2.8×10^{-6} R.L.
0.15 " copper ≈ 10.5×10^{-6} "
35. " mylar ≈ $122.\times10^{-6}$ "

For a total of 34 layers, copper ≈ 0.1% R.L.

Conclusion: attenuation length is 7 m; a tolerable attenuation over 4 m. (44%)

Length of the Tracking Volume

155

1. Physics (e.g., H→4ℓ) requires coverage to $|\eta| = 2.5$ with decent $\sigma(p_\perp)$ over most of the range
   ⇒ some loss for shorter tracker.

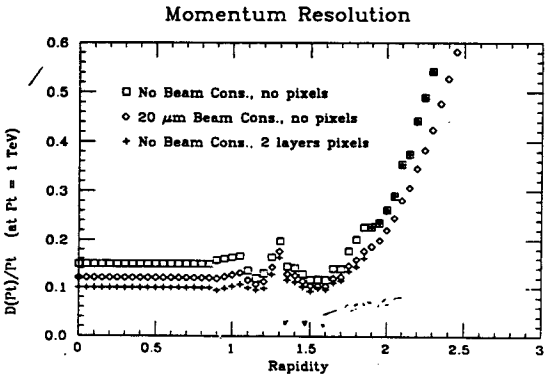
2. Magnetic field uniformity is better with a reentrant iron calorimeter. But this isn't worth the loss of coverage (-Sill, study for ITD).

3. Feasibility of a 4-m ½-long barrel
   - Latten (straws) = 5-7 m ($e^{-4/L}$ = .45-.56)
   - Latten (scifi) = 4-6 m (N_{PE} = 10(near)-4(far))
   - $\csc\theta$ = 2.6-3.1 (r = 164-136 cm)
     ⇒ Pulse height (near)/(far) = 5-6
     ⇒ Extra care w crosstalk required
   - Occupancy (4 m)/(3 m) ≈ 1.2
   - Mechanical support - OK

4. Optimal division between barrel & endcap may not be at maximal barrel length

4 m half length preferred (for tracking performance)

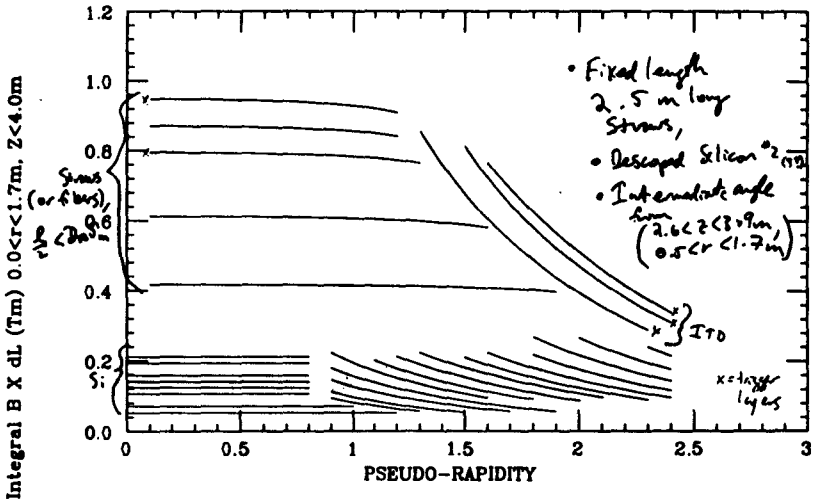
156

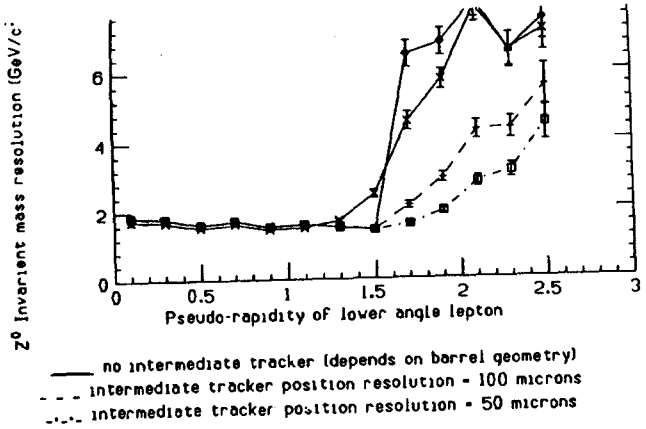


Descoped SDC detector (wires)

"LoI-like" layout

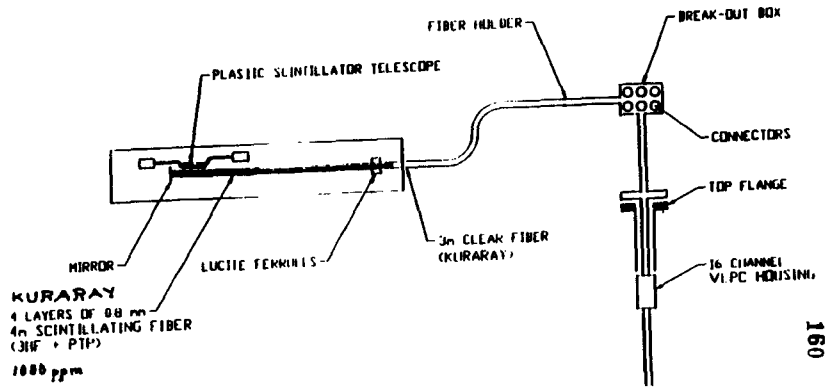
Integral Bz*dr−Br*dz normalized to ETA=0



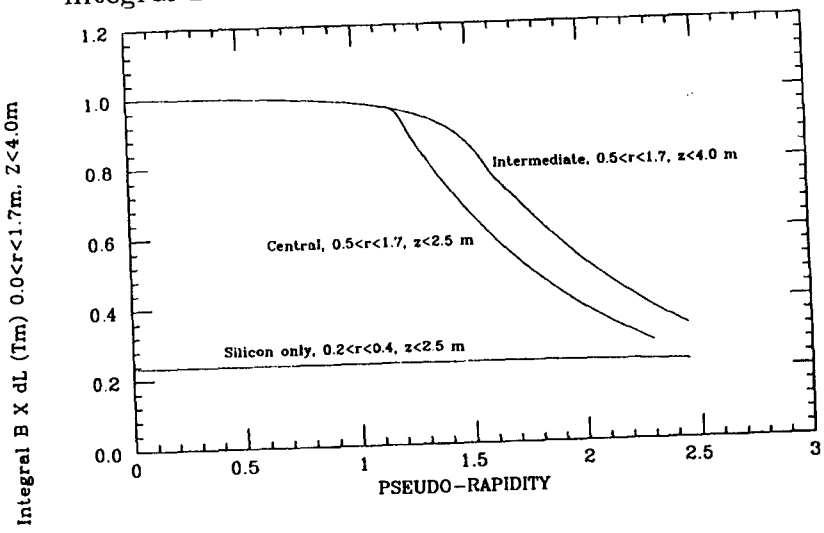


M.Atac, J. Park and D. Chrisman
UCLA
H. Fenker and K. Morgan
SSCL

UCLA COSMIC-RAY TEST

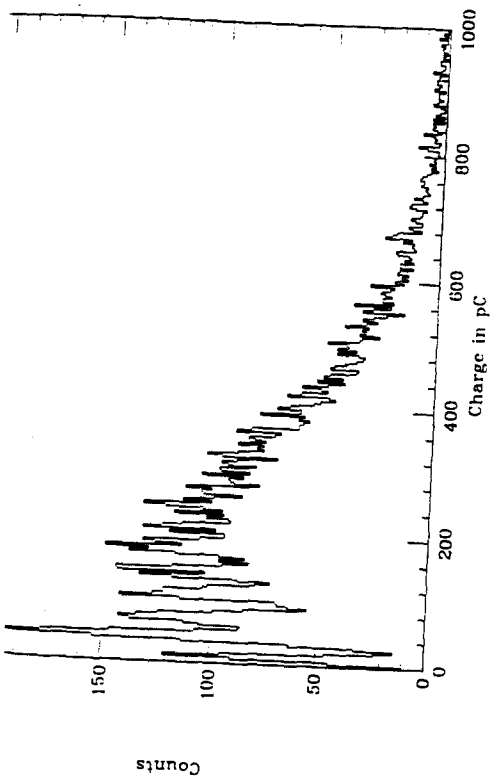


Integral Bz*dr−Br*dz normalized to ETA=0



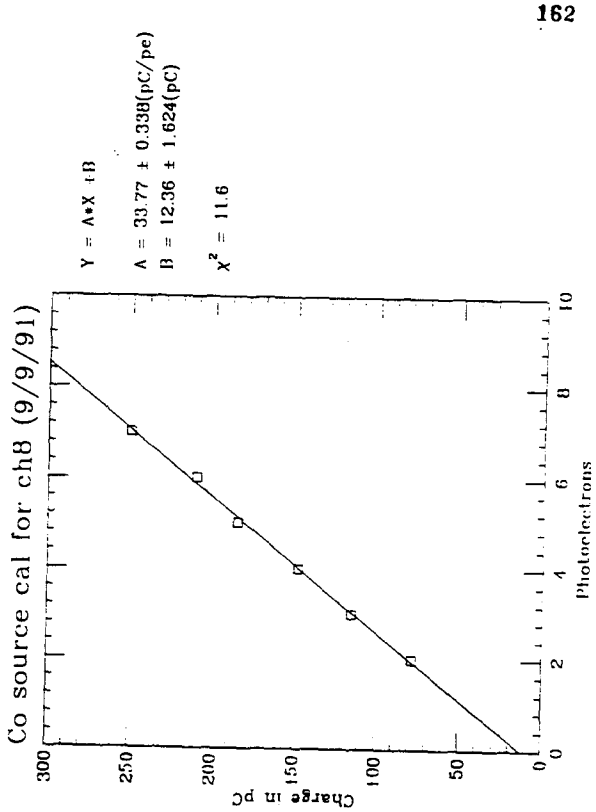
Fundamental Limits

161



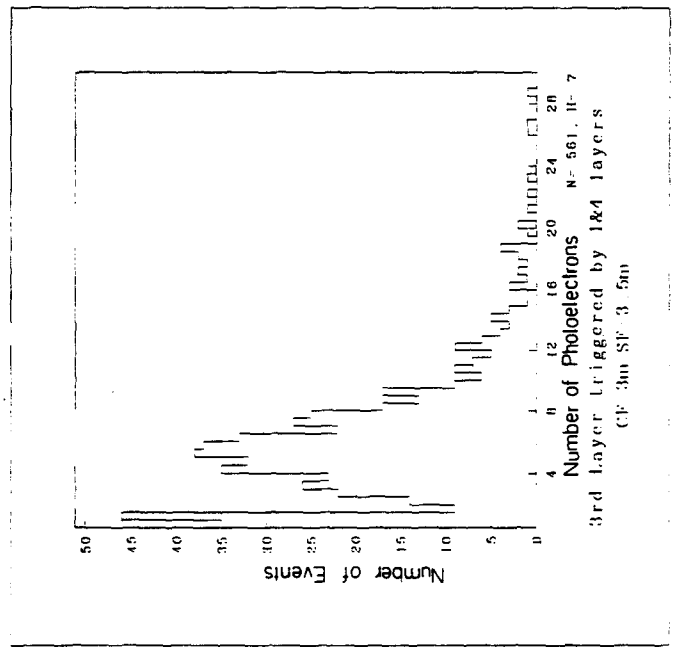
162

M. ATAC

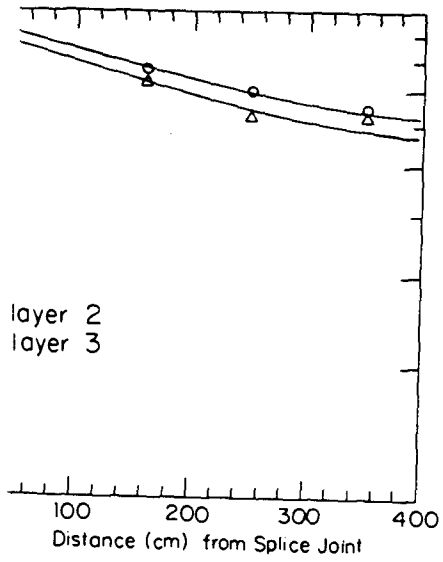


163

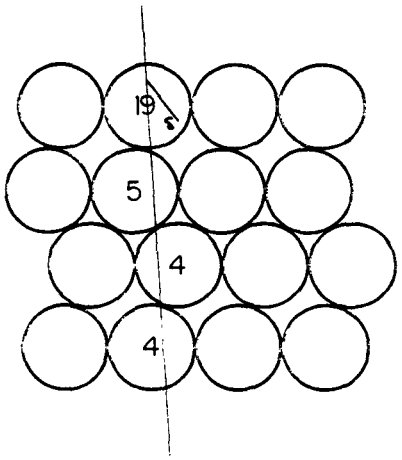
M. ATAC

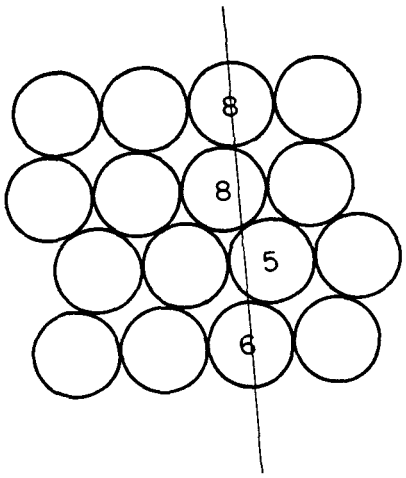


164



M. ATAC





M.ATAC

M.ATAC

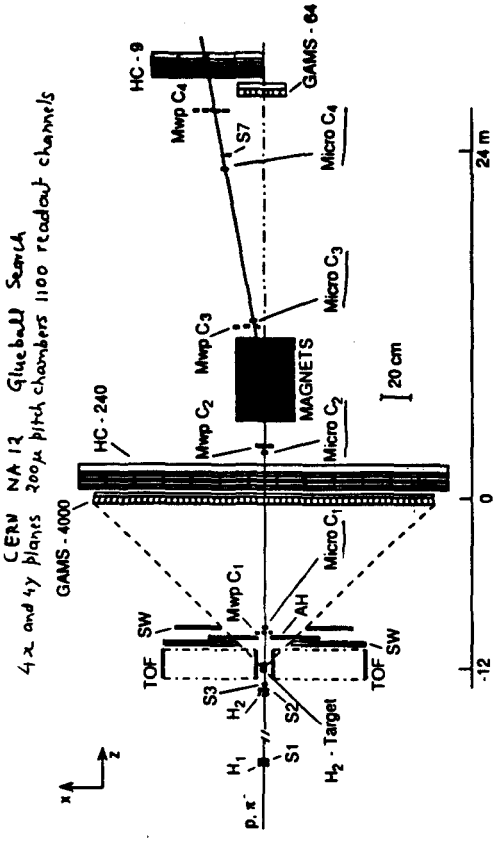


Fig.4)

Anselmi et al CERN PPE/91-122

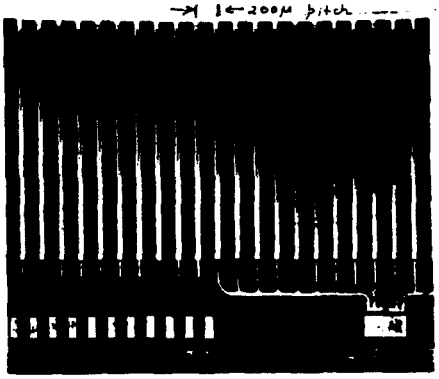


Fig.5)

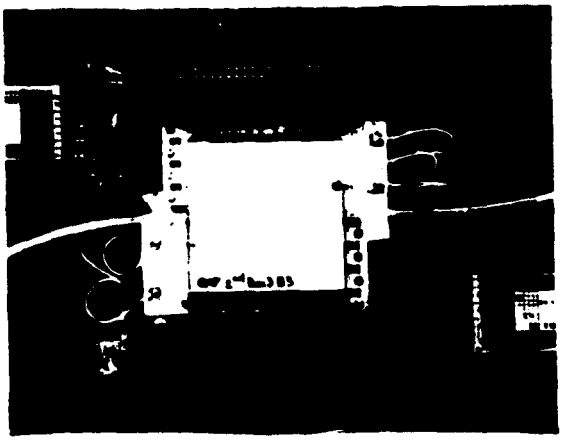


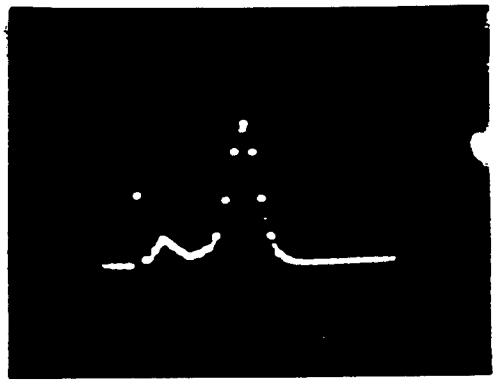
Fig.6)

Sept. 13, 1991
Ottawa, Canada

168

Tedlar 400μ chamber Fe^{55} test

Fe^{55} spectrum on Tedlar chamber



Fe^{55} Argon escape peak at 2.95 kev and at 5.9 kev are seen.

Peak	Energy, (kev)	Peak Channel Numb
Escape Peak	2.95	102
Fe^{55}	5.9	190

171

Interaction rate in tube wall = 15/sec/cm
assume 1/4 pass into the gas and deposit 1/2 the ave kinetic energy:
Integrated current = 1.2 mC/cm/yr from wall

More than half the current in outer layers from neutrons.

Limitations on the lifetime of straw tubes operated in a high radiation flux.

No problem at wire using CF_4 and isobutane.
No whisker growth; but there is a small gain change at levels of ~1mC/cm.

Possible limits of the cathode:

Ablation appears to occur at a rate not exceeding .1 μm/C/cm; or .01 μm in 10 years at 70 cm. Assumes no breakdown currents.

Measured from resistance change of an irradiated strip.

Alteration of an aluminum coating which causes breakdown.
After an extended exposure to radiation, a tube with an aluminum coating will breakdown at high gain in a high radiation flux.
Problems at the level of twice the dose, five times the gain and ten times the radiation level, for example, is a fair estimate.

170

Straw Tube Operation in High Radiation

Charged Particle Induced Integrated Current in straw tube:

Using $£ = 10^{33}/cm^2/sec$
$1 yr = 10^7$ sec
tube length = 3m
tube radius = 0.4 cm
tube gain = $2x10^4$
ionization in CF_4 = 180 e/cm

radius	Occupancy(50 ns)	Integrated Charge
69 cm	0.116	13.3 mC/cm/yr
82	0.088	10.1
95	0.070	8.0
108	0.052	6.0
122	0.040	4.6
135	0.024	2.8
148	0.018	2.1
161	0.011	1.3

Neutron Induced Intgrated Current in Straw Tube:

Using:
Neutron kinetic energy = 1MeV
Neutron fluence = $3x10^{11}/cm^2/yr$
20% isobutane in gas
5% hydrogen in straw wall
Neutron cross section = 4.5 barns on hydrogen

Interaction rate = 1.2/cm/sec in gas
Integrated current = 0.8 mC/cm/yr from gas collisions

172

Bypass the problem. Use copper coated tubes.
No breakdowns.

Besides better stability with respect to radiation they have better and more predictable conductivity.
Minor drawback: .1% R.L. vs. .03% R.L. for 34 layers.

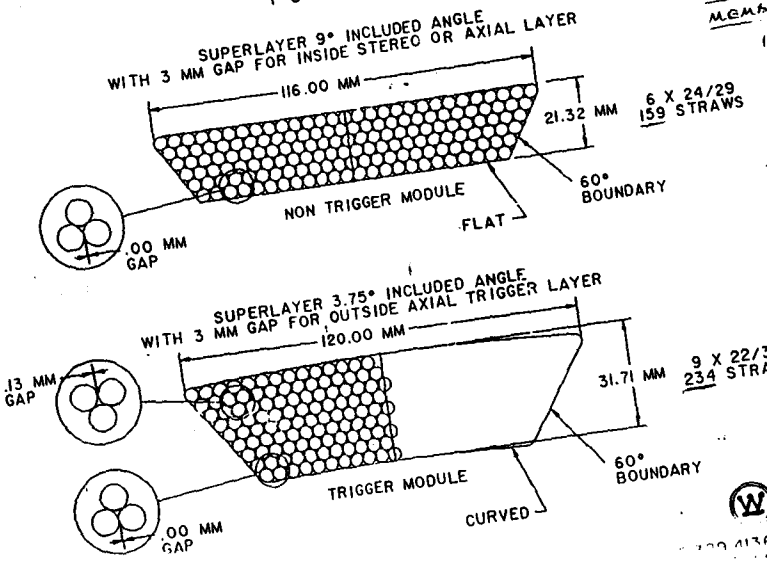
Polycarbonate base material is inferior to mylar or kapton. Dimensional stability, adhesion.

Conclusion: Straw tubes of mylar or kapton with copper coating will endure many times the radiation levels anticipated at the SSC.

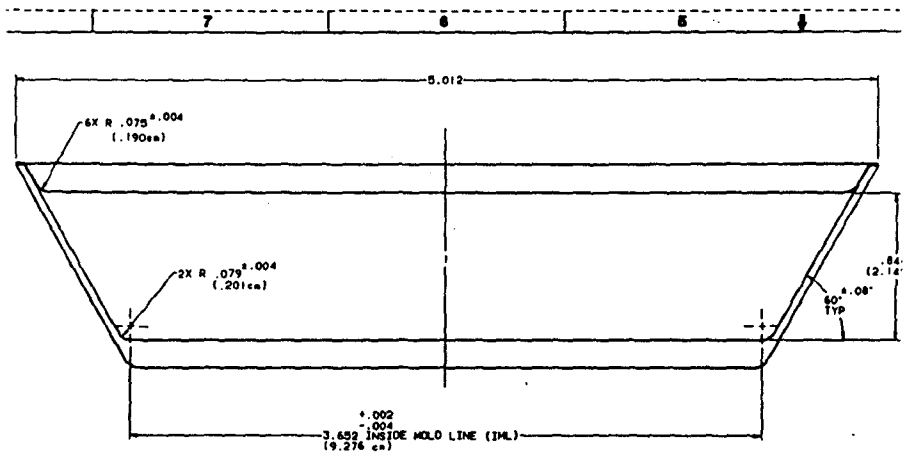
MODULAR CENTRAL TRACKING SUPERLAYER MODULES POST LOI

STRAWS ARE NOT STRUCTURAL MEMBERS

1.4 mils wall



139 4136446 R2



SHELL ASSEMBLY REFERENCE ONLY

SCALE: 4X

Conclusions on straw placement precision

Direct measurement of variation of wire supports about an ideal close packed geometry

σ= 30 microns (measurement error?)

Direct measurement of the wire positions variations from x-ray of 64 straw chamber.

σ= 25 microns

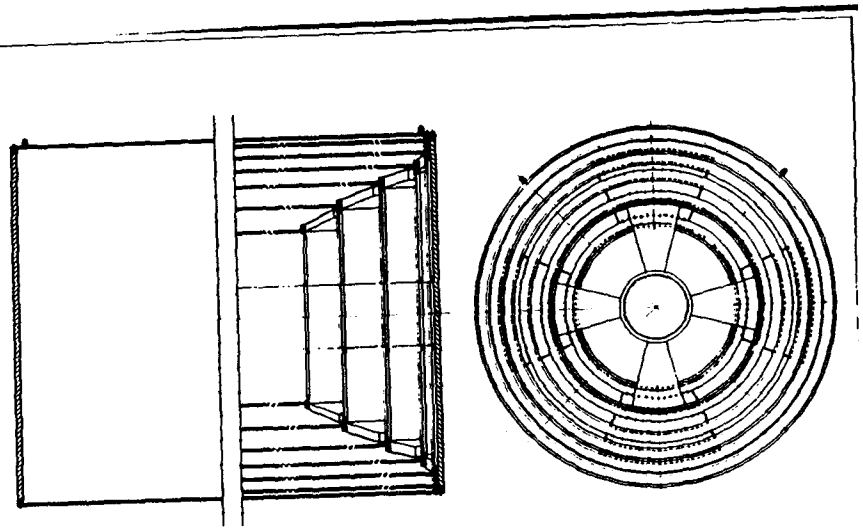
Our conclusion is that we can place the wires with an accuracy better than

σ= 30 microns

so

σ^2 superlayer=(100² + 30²)/6 + σ^2 mod int+σ^2 mod place

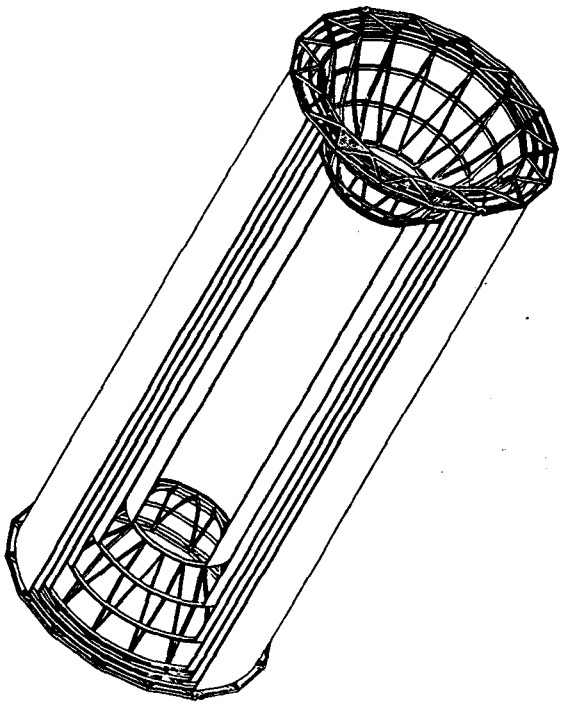
If we require 80 microns for the superlayer, then the module placement and intrinsic errors must each be about 50 microns or less.



INNER / OUTER CTC ASSEMBLY PROPOSAL

PARTIAL OVERALL ASSEMBLY

177



178

Outline of SDC Tracking Design Requirements

1. Introduction (brief)
[Purpose of this document]

2. Overview
[This section should summarize the conclusions of those that follow.]
2.1 Brief survey of physics performance considerations
2.2 Environment for the tracking system within the SDC detector
2.3 Summary of requirements: parameter tables
Angular coverage and hermiticity
p_perp resolution
phi resolution
theta resolution
impact parameter resolution
precision of pointing to the calorimeter
resolution for muon tracking
time resolution, pileup, occupancy
pattern recognition efficiency and false rate
trigger functionality
material

[The following sections should look at physics and other issues, draw conclusions about performance requirements, and justify them.]

3. Isolated charged tracks
3.1 Physics processes
3.1.1 H->4l
3.1.2 t->l-X ; 3.1.3 $Z' \to L^+L^-$
3.2 Electrons
3.2.1 Tracker material
3.2.2 Calorimeter calibration
3.3 Muons
3.4 Isolation criteria
3.4.1 b->l-X
3.4.2 c->l-X

4. Jets
4.1 Multiplicity
4.2 Shape parameters, QCD
4.3 Isolation

5. Detached vertices
5.1 Heavy quarks
5.2 Taus

6. Trigger
6.1 Level 1
6.2 Level 2

7. Problems specific to intermediate angle region
7.1 Momentum measurement
7.2 Trigger

8. Operation at greater than design luminosity

9. Practical considerations
9.1 Radiation hardness
9.2 Calibration
9.3 Computational resource usage
9.4 Access requirements
9.5 Safety
9.6 Failure modes and their management
9.7 Cost

179

Requirements for Tracking

(1) $|\eta|$ coverage out to $|\eta| \leq 2.5$, implying $H^0 \to 4$ charged lepton geometrical efficiency $\gtrsim 60\%$ for $m_H \geq 200$ GeV.

(2) Reconstruction efficiency $\geq 90\%$ (for $|\eta| < 2.5$) for $H^0 \to 4$ charged leptons, for each lepton having $P_\perp \geq 5$ GeV, at design luminosity, but assuming twice the occupancy calculated by GEANT (exclusive of lepton identification and trigger cuts).

(3) Reconstruction efficiency for same as in (2) $\geq 75\%$ at 4×10^{33} design luminosity.

(4) Reconstructed (as opposed to parametric) vertex constrained momentum resolution of $\sigma_{P_\perp/P_\perp^2} < 25\%$ (TeV^{-1}) for $|\eta| \leq 2.5$ (leaves room still for a contribution from misalignments) for $H^0 \to 4$ charged leptons.

(5) Efficiency contribution from lepton identification of $\geq 85\%$ for electrons with $P_\perp \geq 10$ GeV and $\geq 95\%$ for muons with $P_\perp \geq 10$ GeV.

(6) Position resolution at the calorimeter of ≤ 2.5 mm in $r-\phi$ or z (want error $\lesssim \sigma/2$ of calorimeter position accuracy).

(7) No special position resolution requirements at the muon system. Achievable numbers ≤ 1 cm.

(8) B single tagging efficiency $\geq 30\%$ for 125 GeV $\leq m_{top} \leq$ 250 GeV.

(8') τ tagging

180

(9) First level trigger with momentum resolution $\sigma_{P_\perp/P_\perp^2} \leq 10$ (TeV^{-1}) – implies a 10% error for a 10 GeV lepton.

(10) Second-level trigger with momentum resolution $\sigma_{P_\perp/P_\perp^2} = 2.5$ (TeV^{-1}). Gives a 10% error for a 40 GeV lepton for triggering on $Z \to e^+e^-$, $W \to e\nu$ – needed for calorimeter calibration.

(11) Discovery potential – hard to quantify. In general want maximum capabilities from detector. Based on history highest priority (other than isolated lepton of Higgs case above) would be reconstruction and impact parameter measurement of leptons within jets up to the largest jet $P_\perp$ possible (at least ≥ 500 GeV). Desired reconstruction efficiency $\geq 50\%$.

(12) Measurement of jet fragmentation at modest luminosity for QCD studies and for modelling backgrounds from jets.

(13) Survivability at standard $\mathcal{L}$ for ≥ 10 years.

(14) Allows a natural path for upgrading to a system with survivability of ≥ 10 years at $10\times$ standard $\mathcal{L}$ with emphasis (e.g. momentum resolution, pattern recognition, isolated track efficiency) to be decided based on what is learned during initial running.

Technical Proposal Milestones (Tracking)

Oct 15, '91	Draft Requirements Document
Nov. 8, '91	Final " "
Nov. 8	Draft CDR's for Si (pixels / strips) Fiber (incl. ITD) Straw Hybrid Gas ITD
Nov. 8	Preliminary cost estimates
Jan. 3	Final CDRs
Nov. 14	Kondo committee recommendation which CDR's supported for completion
Feb. 1	Kondo Comm. Recom. of baseline config. for proposal (w options if necessary).

Impact of EM Calorimeter Thickness on Resolution — C. Hearty(LBL)

A Weighty Question — T. Handler(Tenn.)

Multigroove vs. Single Groove Tile-Fiber Calorimeter — V. Hagopian(FSU)

LPBautz:10/14/91

Impact of EM Calorimeter Thickness on Resolution

C. Hearty(LBL)

Leakage from EM calorimeter worsens resolution.

Size of effect depends on
- EM calorimeter thickness
- design of first hadronic section (HAC1)

Details of EM section are less important.

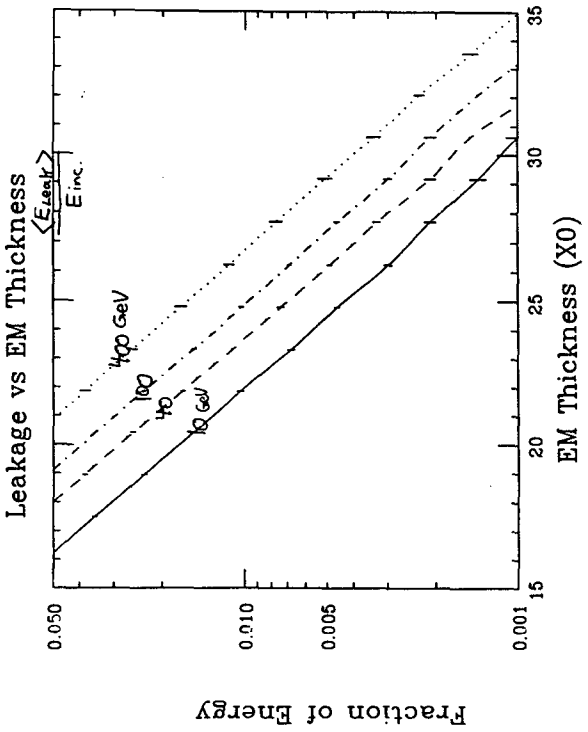
Study with EGS, 10--400 GeV e-

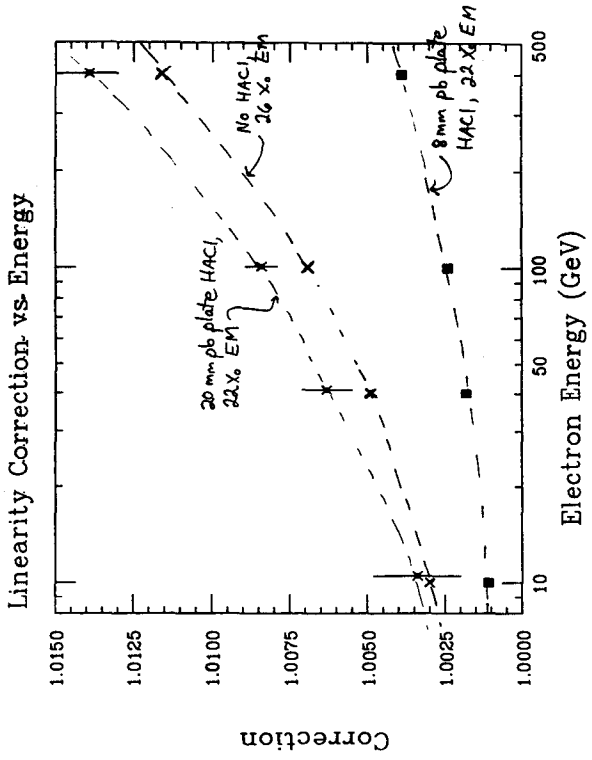
==========

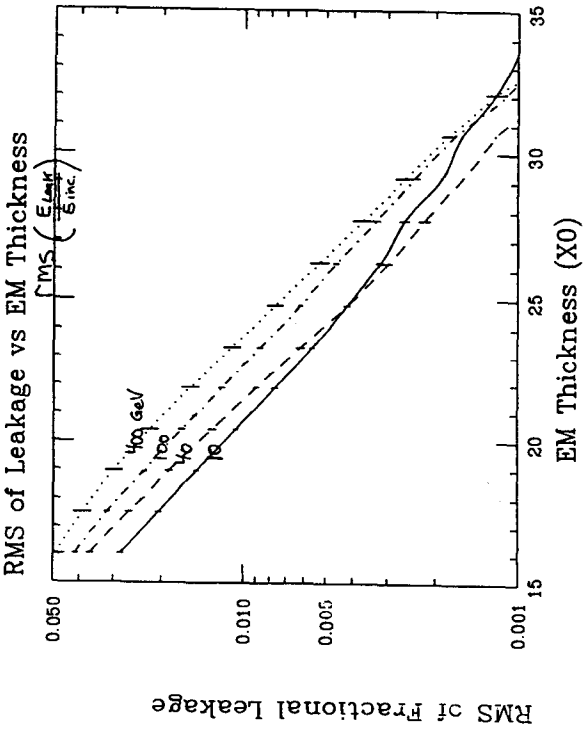
Why not have a very thick EM section?

- π conversions ==> poorer e/π separation (recover with EM2/EM1 ratio?)
- extra cost

How thin can EM section be for a desired precision?







EGS Model

- 70 layers of 4mm lead + 4mm LAr (51 X0 total)
- EM section is first 22-48 layers (16-35 X0), HAC1 is the rest.
- five HAC1 variations considered:
  - no HAC1
  - 8, 16, 20 or 32mm lead sampling (use every nth LAr gap, weight energy with value n, for n = 2, 4, 5, or 8)

Weighting EM2 or HAC1 differently does not improve resolution significantly.

Application to SDC

Three calorimeters under consideration:

LAr: 26 X0 EM, 14mm pb sampling HAC1

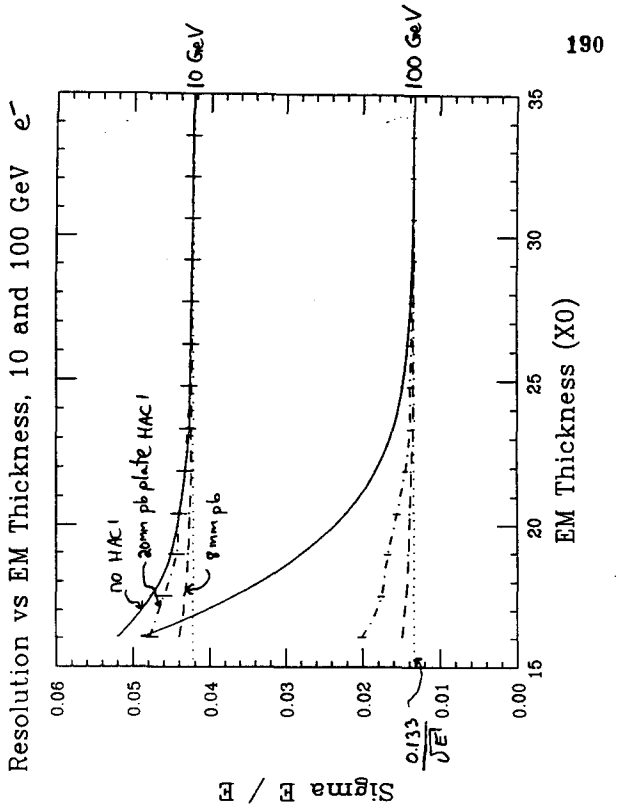
Scintillator Model A:
barrel: 1 inch Fe HAC1 (~8mm pb)
endcap: 2 inch Fe HAC1 (~16mm pb)

Scintillator Model B:
barrel: 20mm pb HAC1
endcap: 32mm pb HAC1

Scintillator EM sections are 22X0 in all cases.

LAr HAC1 noise ≈560 MeV in 0.1 by 0.1 cell
==> do not use HAC1 to measure e- energy.

HAC1 of scintillator calorimeter ≈ noiseless.



Degradation of Resolution

$\alpha \equiv \sigma_E / E_{inc}$

$\alpha_0 \equiv \sigma_E / E_{inc}$ for 51X0 EM section

$\Delta\alpha \equiv \sqrt{\alpha^{**}2 - \alpha_0^{**}2}$ quadratic increase in resolution

If HAC1 is not used, $\Delta\alpha \approx$ rms(E_{leak}) / E_{inc}

Boxes enclose three proposed SDC barrel calorimeter cases

Table I. Increase in resolution ($\sigma E/E$) as a function of EM calorimeter thickness, for various incident electron energies and five different HAD1 sections.

HAD1 Config	E (GeV)	EM Thickness (X_0) 20.4	21.8	23.3	24.8	26.2	27.7	29.2	30.8
No HAD1	10	.0117 ± .0012	.0088 ± .0011	.0061 ± .0010	.0053 ± .0009	.0043 ± .0009	.0038 ± .0007	.0034 ± .0006	.0028 ± .0006
	40	.0120 ± .0008	.0004 ± .0008	.0067 ± .0007	.0048 ± .0006	.0030 ± .0008	.0021 ± .0008	.0017 ± .0006	.0010 ± .0011
	100	.0130 ± .0005	.0088 ± .0004	.0065 ± .0004	.0050 ± .0005	.0034 ± .0005	.0022 ± .0004	.0014 ± .0004	.0007 ± .0016
	400	.0205 ± .0010	.0138 ± .0009	.0094 ± .0008	.0071 ± .0007	.0048 ± .0009	.0031 ± .0008	.0019 ± .0010	.0009 ± .0008
8 mm	10	.0052 ± .0015	.0040 ± .0024	.0032 ± .0018	.0031 ± .0010	.0019 ± .0015	.0018 ± .0009	.0010 ± .0021	.0010 ± .0015
	40	.0048 ± .0008	.0032 ± .0021	.0022 ± .0019	.0013 ± .0010	.0001 ± .0010	.0001 ± .0010	.0001 ± .0010	.0001 ± .0010
	100	.0039 ± .0003	.0030 ± .0003	.0021 ± .0004	.0018 ± .0003	.0015 ± .0004	.0013 ± .0003	.0011 ± .0003	.0011 ± .0003
	400	.0027 ± .0006	.0023 ± .0006	.0018 ± .0007	.0011 ± .0008	.0011 ± .0008	.0001 ± .0010	.0007 ± .0010	.0003 ± .0004
16 mm	10	.0090 ± .0018	.0096 ± .0013	.0064 ± .0015	.0071 ± .0011	.0041 ± .0014	.0031 ± .0010	.0022 ± .0010	.0061 ± .0004
	40	.0071 ± .0009	.0054 ± .0009	.0041 ± .0011	.0036 ± .0009	.0018 ± .0010	.0013 ± .0014	.0014 ± .0008	.0010 ± .0006
	100	.0071 ± .0003	.0042 ± .0005	.0044 ± .0004	.0025 ± .0004	.0029 ± .0003	.0013 ± .0008	.0023 ± .0003	.0007 ± .0010
	400	.0061 ± .0007	.0046 ± .0008	.0022 ± .0009	.0029 ± .0005	.0001 ± .0072	.0010 ± .0008	.0009 ± .0008	.0004 ± .0004
20 mm	10	.0121 ± .0011	.0105 ± .0011	.0071 ± .0011	.0085 ± .0013	.0070 ± .0009	.0040 ± .0013	.0024 ± .0009	.0061 ± .0006
	40	.0086 ± .0009	.0061 ± .0010	.0055 ± .0008	.0048 ± .0007	.0028 ± .0007	.0032 ± .0006	.0023 ± .0006	.0017 ± .0007
	100	.0081 ± .0004	.0087 ± .0004	.0039 ± .0004	.0037 ± .0004	.0029 ± .0005	.0025 ± .0003	.0014 ± .0006	.0009 ± .0005
	400	.0069 ± .0008	.0046 ± .0011	.0041 ± .0008	.0029 ± .0007	.0001 ± .0011	.0001 ± .0010	.0014 ± .0007	.0012 ± .0007
32 mm	10	.0152 ± .0015	.0117 ± .0014	.0075 ± .0011	.0056 ± .0009	.0079 ± .0010	.0048 ± .0007	.0013 ± .0006	.0065 ± .0006
	40	.0100 ± .0009	.0089 ± .0010	.0060 ± .0008	.0043 ± .0008	.0036 ± .0007	.0029 ± .0006	.0017 ± .0010	.0007 ± .0008
	100	.0095 ± .0004	.0074 ± .0004	.0058 ± .0004	.0038 ± .0005	.0038 ± .0004	.0027 ± .0005	.0027 ± .0003	.0011 ± .0010
	400	.0114 ± .0007	.0084 ± .0008	.0054 ± .0008	.0042 ± .0009	.0027 ± .0007	.0013 ± .0008	.0001 ± .0010	.0011 ± .0004

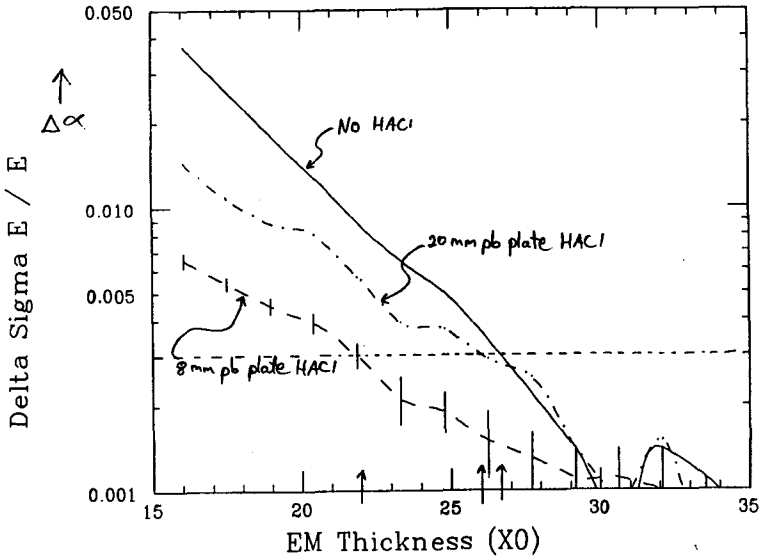
LAr

Model A barrel

Model B barrel

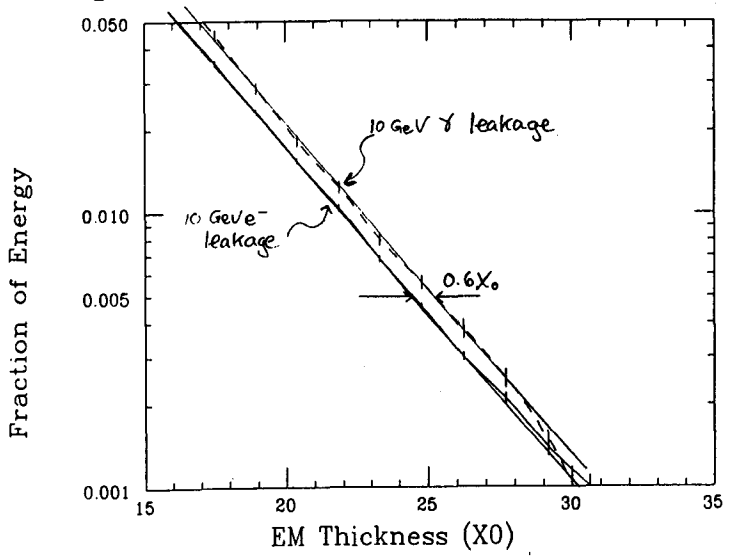
194

Increase in Res. at 100 GeV vs EM Thickness



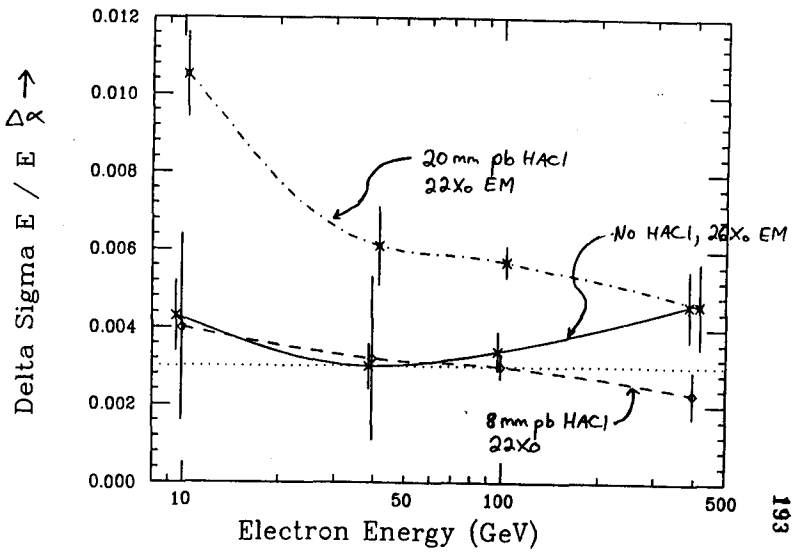
192

Leakage vs EM Thickness, 10 GeV e− and Gamma



195

Increase in Resolution vs Energy



193

Conclusions

- nonlinearity due to leakage is small and correctable

- Thickness (X0) required for increase in resolution to be less than:

Case		$\Delta\alpha$=0.003	$\Delta\alpha$=0.005
LAr (barrel & endcap) (HAC1 not used)		28	26
Model A	barrel (≈8mm pb)	22	20
	endcap (≈16mm pb)	25	22
Model B	barrel (20mm pb)	26	23
	endcap (32mm pb)	28	24

Table is applicable to more than just SDC.

- Photons require slightly thicker EM calorimeter.

A Weighty Question

T. Handler(Tenn.)

Thomas Handler
Univ of Tenn

A Weighty Question

How do you properly weight the different modules in a calorimeter

ORNL SDC Meeting
Sept 27, 1991

A Weighty Question

I) Original Weighting Scheme based on dE/dx

For a given module containing uniform cells

$$W_{mod} = \frac{\sum \rho_i \Delta x_i (dE/dx)_i}{\rho_{scint} \Delta x_{scint} (dE/dx)_{scint}}$$

II) Alternative Weighting Scheme
Minimize Resolution by adjusting module weights

Done by Maximum Likelihood Method

$$\mathcal{L} = \prod_i \frac{1}{\sqrt{2\pi}\sigma} e^{-\frac{(x_i - \bar{x})^2}{2\sigma^2}}$$

with $x_i = \sum_{j=1}^{modules} W_j x_{ij}$

Fix $\bar{x}$ and adjust W_j's and σ

Calorimeter examined

1)	10 cm Al ; 2.5 mm Scint	1 Layer
2)	1/8" Pb ; 2.5 mm Scint	38 Layers
3)	1" Al ; 0.5" Fe ; 2.5 scint	1 Layer
4)	1.0" Fe ; 2.5 mm scint	31 Layers
5)	2.0" Fe ; 2.5 mm Scint	12 Layers

pions and e⁻ at 10, 30, 75, and 125 GeV

Weights determined at each energy and applied to all energies

i.e.
4 different sets of weights generated by maximum likelihood method

use hadronic data to determine weights

Weights are

	10 GeV	30 GeV	75 GeV	125 GeV
Module 1	1.301	1.155	1.710	1.041
2	1.951	1.949	1.712	1.766
3	2.157	1.829	1.604	1.356
4	1.409	1.358	1.348	1.336
5	1.239	1.492	1.180	1.626

These are multiplied into the dE/dx weights for the different modules

Module 1	87.9418	dE/dx weights
2	9.0940	
3	52.4856	
4	59.8052	
5	118.6104	

Resolution Results

$$\frac{\sigma^2}{E^2} = \frac{a^2}{E} + b^2$$

Hadronic Resolution Fits

	a	b
dE/dx	0.664 ± 0.032	0.070 ± 0.006
10 Gev Weight	0.578 ± 0.031	0.071 ± 0.007
30 Gev Weight	0.609 ± 0.030	0.050 ± 0.007
75 Gev Weight	0.611 ± 0.029	0.049 ± 0.007
125 Gev Weight	0.589 ± 0.027	0.050 ± 0.006

EM Resolution Fits

	a	b
dE/dx	0.124 ± 0.008	0.013 ± 0.002
10 Gev Weight	0.122 ± 0.007	0.007 ± 0.002
30 Gev Weight	0.125 ± 0.008	0.007 ± 0.002
75 Gev Weight	0.133 ± 0.007	0.006 ± 0.002
125 Gev Weight	0.117 ± 0.007	0.008 ± 0.001

Linearity Questions

Hadronic Pulse Height

	10	30	75	125
dE/dx	0.61	0.68	0.69	0.70
10 Gev Weight	0.95	1.05	1.05	1.05
30 Gev Weight	0.89	0.99	1.00	1.01
75 Gev Weight	0.90	0.98	0.99	1.00
125 Gev Weight	0.87	0.97	0.98	1.00

EM Pulse Height

	10	30	75	125
dE/dx	0.67	0.65	0.65	0.65
10 Gev Weight	1.27	1.26	1.26	1.26
30 Gev Weight	1.14	1.13	1.13	1.13
75 Gev Weight	1.14	1.11	1.11	1.11
125 Gev Weight	1.15	1.14	1.14	1.13

e/h

	10	30	75	125
dE/dx	1.093	0.966	0.944	0.920
10 Gev Weight	1.344	1.206	1.197	1.195
30 Gev Weight	1.281	1.142	1.128	1.117
75 Gev Weight	1.272	1.135	1.116	1.105
125 Gev Weight	1.313	1.169	1.155	1.135

Multigroove vs. Single Groove Tile-Fiber Calorimeter

V. Hagopian(FSU)

MULTIGROOVE VS. SINGLE GROOVE

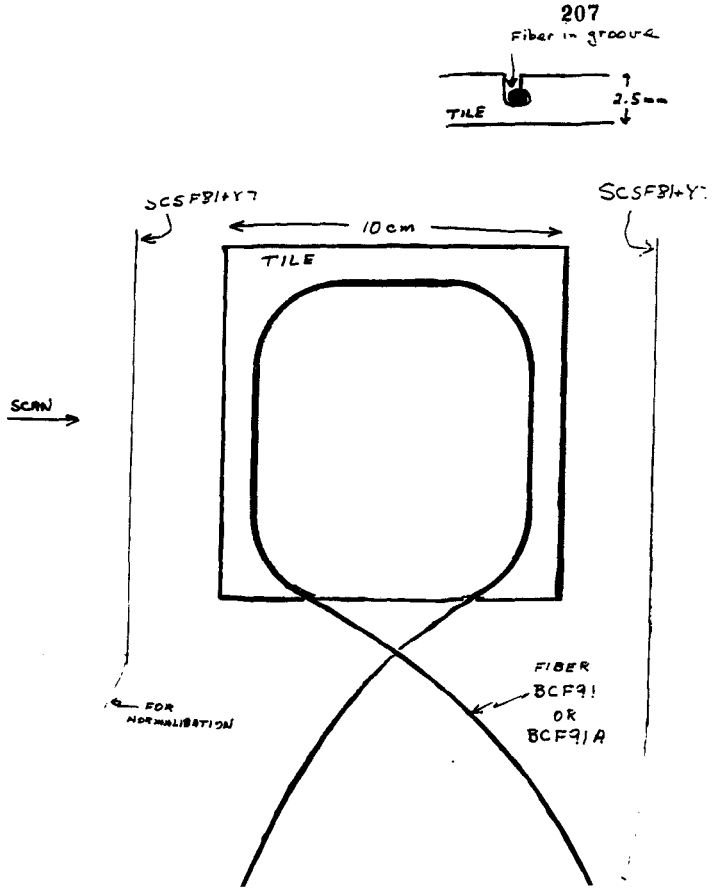
TILE-FIBER CALORIMETER

SDC Meeting
Sept 26-28, 91
Oak Ridge, Tn.

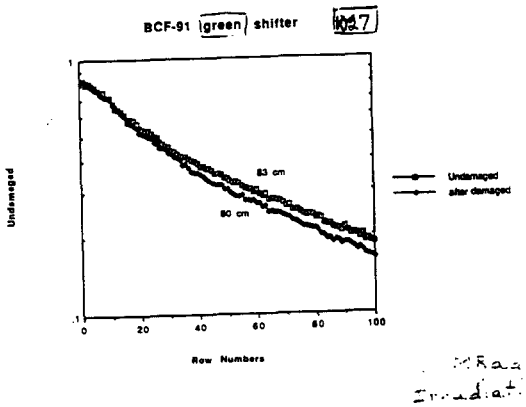
by

Vasken Hagopian
Florida State Univ.

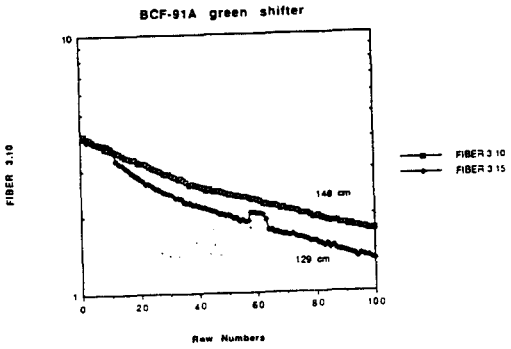
207



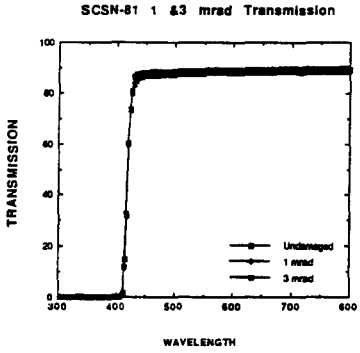
208

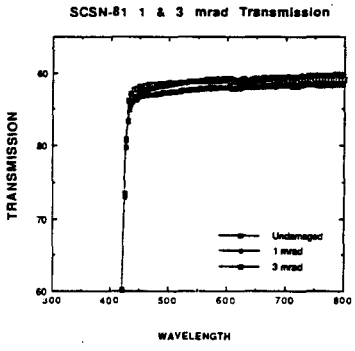


MRad Irradiation

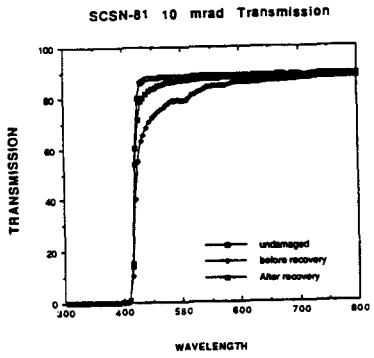


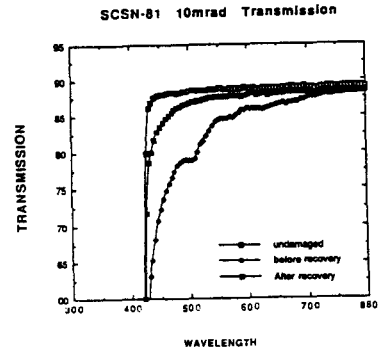
209



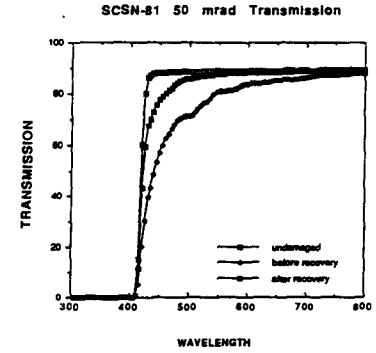


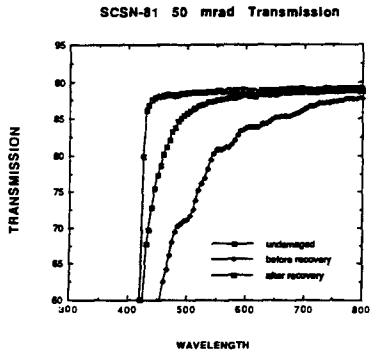
210



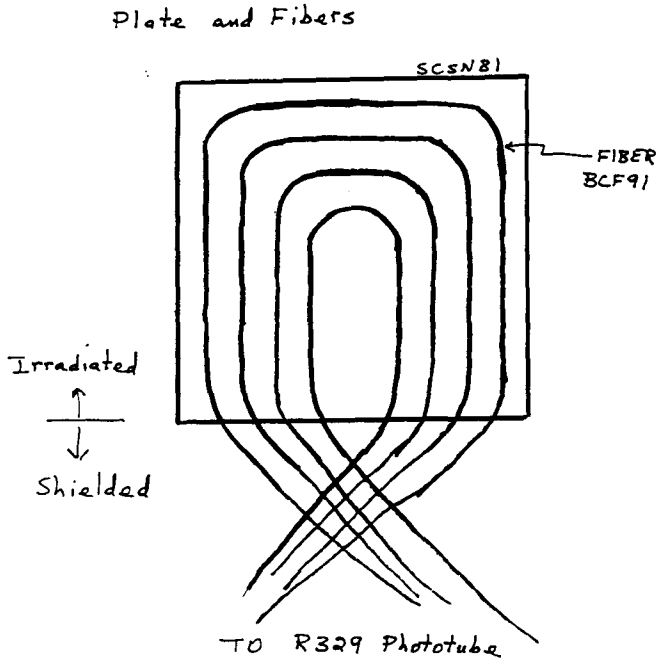


211

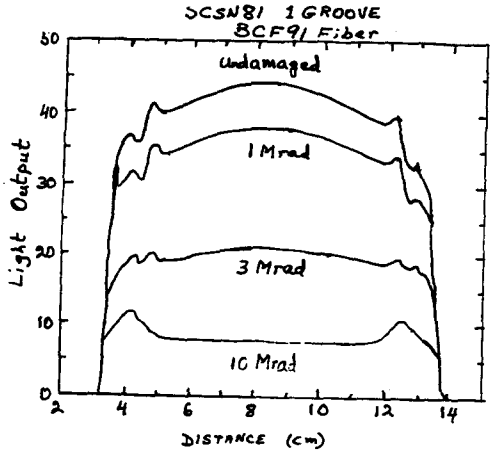




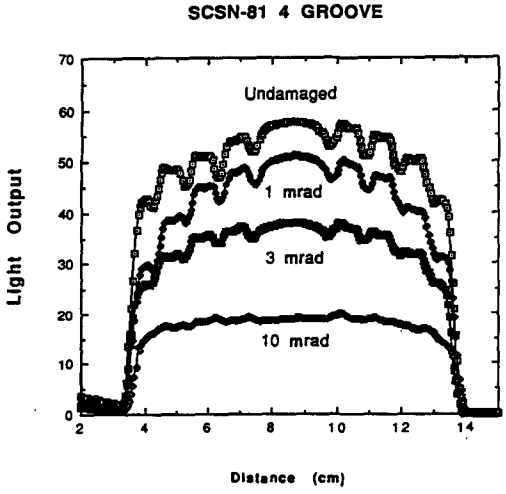
212



213



214



26 Sept 91

IRRADIATION DAMAGE

10 cm × 10 cm × 0.25 cm

SCSN81 Scintillator
BCF91 Fiber
} Both irradiated

LIGHT OUTPUT

	1 GROOVE	4 GROOVES
0	1.00	1.00
1 Mrad	0.84 ± 0.02	0.90
3 Mrad	0.48	0.67
10 Mrad	0.18	0.33

Schedule for Technical Proposal	A. Fry(SSCL)
Section 9: Online Computing - Draft	A. Fry(SSCL)
SDC Computing Section: Architectural Studies and Analysis - Draft	SDC Computing Working Group(IBM)
SDC Data Acquisition Design Requirements and Functional Specifications Version 0.99	SDC Data Acquisition Working Group
SDC Data Acquisition System Conceptual Design - Draft	E. Barsotti(Fermilab)
SDC Data Acquisition System Conceptual Design	I. Gaines(Fermilab)

LPBautz:10/29/91

Schedule for Technical Proposal

A. Fry(SSCL)

Fry 91.09.26

218

Nov 13 detailed outline of T.P.

Dec 13 0th draft

Jan 3 1st draft to overall editor

Jan 31 2nd draft to overall editor

Feb 21 Final draft 150 copies

Feb 26-29 Review by Collaborat.

Mar 23 Final Final printout

Mar 25 40 copies

Apr 1 SSCL receives 40 copies

Jan 15 1st DRAFT READY

Nov 15 Internal.

Schedule + Milestones

219

Internal draft of Tech. Prop.
Nov 10th

present T.P. to collaboration
Feb 21

Complete COST + Schedule
Nov

How do we get there?
- 1 day workshop (Nov)
Oct.

220

221

Section 9: Online Computing
DRAFT DRAFT DRAFT September 24, 1991
Address your comments to SSCVX1::FRY

9.1 Overview

The online computing system is responsible for the high level control, configuration, and monitoring of the DAQ, trigger, Level III, and slow-control subsystems of the SDC detector. It is also responsible for insuring that data from these systems is delivered on to permanent media and insuring through various monitoring functions of the data and data-taking process that data integrity is maintained. We estimate that the online system will need to be able to manage, control and record a sustained data rate of up to 100 MB/s. The online computing system also provides services, resources, and generally an environment for tasks associated with data-taking. These consist largely of standard packages and tools, which are incorporated into template programs so that the various processes necessary for data taking have a uniform structure and differ mostly in the kind of user code they contain within the standard online encapsulation.

9.2 Operational Concept

We focus on the goal of recording data on permanent media in a form in which it can be reconstructed. If data is lost or corrupted in some way, then the online system has failed. This means we must achieve a high degree of reliability and extensively monitor not only the data, but all relevant parameters and processes which affect the data taking process and ultimately the physics results of the experiment. i.e. if offline reconstruction of the data requires further information than that recorded on permanent media during data-taking, the online system is incomplete. Care must be taken to record all information necessary.

The data-taking process for the SDC detector will be highly automated. Human intervention and control will be the exception rather than the rule as the online system responds to changing accelerator conditions, physics data-taking will proceed as conditions warrant. Abnormal conditions such as can be anticipated will result in warnings to human operators and appropriate actions executed. These actions may range from requesting human intervention to invoking automatic correction procedures. Other, less automatic modes of operation, will be supported for debugging, calibrating, and in general taking of "non-physics" data.

9.3 Requirements

9.3.1 Overview

Fig. 1 shows the functional pieces of the online system which are responsible for gathering data from various sources and writing it to permanent media. These "pieces" should be viewed as processes or groups of processes which are running inside the online system CPU's. Although in many cases which CPU a process runs on may have important operational impact, it is not, in general, of overriding importance. Fig. 2 is a schematic of how the control of the data-taking process is achieved. The process labelled XPC is the primary source of experimental control. The processes labelled XPM are the sources of human control as well as the primary providers of visual data regarding the data-taking process.

9.3.2 Data logging

The online system will be capable of recording up to 100 MBytes per second of event data. This corresponds to the a maximum rate after level III processing of 100 MHz of 1 MByte events. The data will be separated into several streams (on order 20) for recording on permanent media. The streams may not be disjoint, however, there is some concern as to whether such streams will be sufficiently disjoint and whether non-disjoint streams will introduce difficulties in the physics analysis of the data. An express line stream will accept data at up to 1 Hz for immediate analysis and reduction. We estimate that after reduction it will be practical to maintain 100 GB of permanently resident data. Additionally, all other parameters necessary for offline reconstruction will be recorded as necessary to a single stream. This is data on various experimental "conditions", including the detector HV's, the magnet, various temperatures and environmental variables, and configuration parameters. We estimate that this stream will be less than 100 KBytes/sec. The monitoring of experimental conditions continues independently of data-taking both in the online system and in the slow controls system.

It will be necessary for the online system to record events from sources other than level III, not only for experimental condition data, but also for testing various parts of the system. An alternate event source will be provided to manage such data, enabling routing of test data into level III (e.g. from a tapedrive), bypassing of level III and other such tests as may be necessary. Occasionally, it will be necessary for the online system to record calibration events. These events may be much larger than physics events. The online system will be able to process events up to 20 MBytes [question: is this too big? what is the max size of a sub detector system?] in length corresponding to our best guess as to an "all channels on" situation.

9.3.3 Run Control

High level run control is the responsibility of the online system. This will be

highly automated perhaps employing an expert system to decide logical actions. The human interface for run control will be location independent, although certain actions will be permitted only from specified locations. A high level screen management package will be used to interact with the human operators so that day to day adjustments, additions, and other modifications to the human interface will be mostly confined to simple edits of particular "screens" defined using a screen/display editor. Screens should perform the function of display of online system data and interaction with human operators simultaneously. A online system programmer should be able to implement a new screen in the online system in a few hours' work. It should be possible to interact using simple command lines, point and click, function keys, and probably voice.

9.3.4 Operability and Reliability

The system must operate in a "normal" mode at least 9 out of 10 days of data taking and in this mode operation should require no more than two physicists who do not have special skills in online operation. Failure to meet this requirement will almost certainly mean failure to meet the next requirement which is that the system must have less than a 5% failure rate as measured by the ratio of time the accelerator provides beams for physics to the time the online system is recording data. This of course does not include rate dependent dead-time introduced by DAQ and Trigger systems. From time to time, it will be necessary to "re-configure" the online system. This should take no more than 5 minutes. We recognise that there will be an initial "shake-down" of the entire detector and data-taking systems where these requirements may not be met. Further to requirements of online system readiness, we believe that it should be able to be restarted in less than 10 minutes and a "cold" start requiring rebooting and loading of DAQ, Trigger, etc. parameters should be able to be accomplished in less than 30 minutes.

9.3.5 Data Monitoring

It will be necessary to monitor the data as it is acquired and written to the mass storage system. The online system must be capable of routing specified kinds of data to various "data-monitoring" processes. These processes will be capable of looking at about 1 Hz of events and the number of such processes will correspond to the number of sub-systems requiring such monitoring. Some additional processes will be required to monitor "non-event" data such as HV's and environmental conditions as well as the operation and condition of the online system itself. These processes will operate continuously, independently of the state of data-taking, however, failsafe processes should operate within the slow controls system. Some of these will operate at rates of up to 50 Hz.

9.3.6 Calibration

It will be necessary to provide software to manage calibration data and calibration sequences. Sometimes it will be necessary to log calibration data for offline processing and at other times calibrations will be processed in the online/DAQ systems and only the derived constants logged to the offline system. It will also be necessary for current calibrations to be determined as moving averages for input to reconstruction programs running both offline and in level III. The natural place for these to be calculated is probably as part of the level III processing.

9.3.7 Physics Processing

Users will have the capability of dynamically defining selection criteria to create "pools" of events which can then be shared by several users who wish to do physics analysis. The online system should be capable of supporting up to 10 "event-pool" streams with an individual rate of no more than 0.5 Hz and an integrated rate over all streams of no more than 2 Hz. There should be 5 workstations provided for interactive analysis , viewing of event-pool data, and graphical display of events.

A single stream of fully reconstructed events will be provided to a constantly running system that can dynamically allow the user to insert his own analysis subroutines into an analysis framework. This stream will be provide events as needed by the analysis routines up to a maximum rate of 1 Hz.

9.5 Relationships with and Impact on other systems

The online system contacts directly and indirectly with a number of detector subsystems. Generally, it acts as a "host" which provides services to the subsystems, like cross-compilers, configuration parameters, and file management and storage. The online system has direct and intimate contact with DAQ, Trigger, Slow Controls, and Level III. It has contact with user code from all of the various detector sub-sections. This user code may be of "offline" or other variety. It has an additional formal offline contact through the data which it writes to the mass storage system and the mass storage system itself.

Care must be taken to insure that compatible interfaces exist between these subsystems. We must strive to keep the points of contact minimal and simple so that parallel development may proceed in each of the sub-systems without excessive interdependence requiring an unrealistic degree of cooperation and organization, on the otherhand it will sometimes be advantageous to share standards across systems so that effort will not be duplicated. This philosophy extends even inside the online system software where interdependence of processes and code should be minimised. Cases where effort can be reduced are often identified naturally as

development proceeds. The points of contact must be specified at an early date so that development will not be held up and effort wasted.

We briefly summarise the relationships with other systems below:

Front-end Electronics

The online system will archive relevant parameters and be capable of supplying them to the front end on demand. It will be possible to "login" to processors in the front end from "online" computers.

Level I and II Trigger systems

The online system will archive relevant parameters and be capable of supplying them to the trigger systems on demand. It will be possible to "login" to processors in the trigger systems from "online" computers. A trigger monitor process will run in online containing user code from the trigger group. The online system is also responsible for high level trigger control and configuration. The online system can receive and log data directly from the trigger system as necessary.

Data Acquisition

The online system will archive relevant parameters and be capable of supplying them to the DAQ systems on demand. It will be possible to "login" to processors in the DAQ systems from "online" computers. A DAQ monitor process will run in online containing user code from the DAQ group. The online system is also responsible for high level DAQ control and configuration. The online system can receive and log data directly from the DAQ system as necessary.

Slow Control

The online system will archive relevant parameters and be capable of supplying them to slow control systems on demand. It will be possible to "login" to processors in the slow control systems from "online" computers. The online system will have a few condition monitoring processes which will primarily access data from slow controls concerning various environmental parameters. The online system will be able to both monitor and control HV's in the slow control system.

User Code

The online system must he able to run, control, and monitor various types of user code. These codes appear in the data monitoring processes, condition monitoring processes, configuration monitoring and control processes and other sub system control processes. The online system will provide standard templates to encapsulate user code so that externally it has an "online" appearance and functionality.

Offline Computing

The online system must provide offline with "complete" data on permanent media. It is the responsibility of online to insure that the data is complete and uncorrupted. However, occasionally problems will be detected offline which require online correction. Online will be capable of receiving messages from offline programs. It will also be capable of receiving a stream of reconstructed events for online monitoring at rate of up to 1 Hz.

9.6 Services and Tools

9.6.1 Alarms and Limits

There will be a standard error logging and detection service which can handle 10 Hz of "alarm" messages and 100 Hz of logged error messages. An alarms and limits package will provide a standard method of detecting abnormal conditions through comparisons of current conditions with historical conditions. This package will be capable of tracking the value of a variable over time and determining significant variation in a general way, such as by by comparison of a histogram to a standard histogram.

9.6.2 Database

The online system will require a database to store the details of recent configurations, brief run summaries for the duration of the experminent and full run summaries for recent runs (over the past month). We anticipate that this will require 100 GB of disk space.

9.6.3 Documentation

Effort will be required to document the online system code and operational procedures. The human interface will provide prompting and help when the user requests it. Documentation from DAQ, Trigger, etc., should also be available to and probably organised in the same way as the online documentation. It will be difficult to maintain uptodate documentation in a rapidly evolving system. We will use self-documenting code so that some documentation can be generated automatically. Documents should be managed using the code management system.

9.6.4 Software Tools and Standards

The online system will require standard software packages for code management, data management, code development, data bases, graphics, and human interfaces. Where appropriate, the same standards should be found in the offline system. Standard interfaces will be required between online processes, as well as between online processes and processes in other sub-systems. In particular, standard means of passing control messages and information, and of passing event and non-event data will be provided. These standards will be incorporated into template

programs which the user will use to execute his own user code. Extensive use of MAKE will ensure that pieces of the online system are uptodate with one another and that unecessary compilations and links are not performed.

Requirements for SDC On-Line Computing
Version 2 - Draft 91.09.24
Address comments to SSCVX1::FRY

a) Acquiring and recording data
Event data:
100 Hz of 1 MByte events to permanent storage
>20 streams of mostly disjoint (<20% overlap) events
(open question: combining non-disjoint streams for analysis)
Express line stream: 1 Hz of selected data (which is fully duplicated in other streams) goes directly to off-line analysis systems. A further 1% reduction (event selection/event compaction) reduces this 10 TB/year stream to 100GB/year permanently resident data.
*** is 100 GB enough? ********

"Non-event" (e.g. environmental) data
All data (including calibration process outputs as well as HV, magnet currents, environment, etc) goes to at least a master stream for permanent storage (looks just like an event stream). <100 KB/sec. It may also go to a database. Processes which monitor environmental conditions continue monitoring even if data-taking is stopped.

Calibration data
Maximum event size 20 MByte (all channels on)
**** what is the correct size? 20MB? 5 MB? **********
Local (subsystem) calibration requirements (for bandwidths and processing power) are spacified in DAQ and subsystem requirements.

Run Control
Run control automatically starts all required on-line processes. It can be run by 2 physicists at least 90% of the time. These physicists need not be "online" specialists.

Cold start: <30 min
Warm start: <10 min
Stop/start new run: <5 min (need to wait for pipelines/level 3 to flush)
Less than 5% downtime
Can accept and log data from other sources besides level 3, including playback from "tape" of real or simulated data, unselected data passing through level 3, data from DAQ and Trigger and condition monitoring data.
The experimental process monitor component of run control is location independent (i.e. the human interface can run anywhere).

b) Insuring data integrity
Detector performance monitoring
The processes below look at the data and log conditions as necessary. They can send alarm and error messages to request correction of abnormal conditions.
At least 1 data monitoring process for each subdetector (may be further geographical divisions)
At least 1 data monitoring process for the detector as a whole.
Each process runs at 1 Hz (higher bandwidth monitors can run in level 3 or in subsystem CPUs)
Each process will have 16 MB of data space to accumulate histograms or

tables (this implies roughly 30*16=500MB of "baseline" data available for comparison with current conditions)
Software to automatically compare data with historical conditions and flag discrepencies will be available.
A few additional data monitoring processes will be available for non-event data. These may need to run at rates of up to 50 Hz.
Parameter and configuration management
Configurations will only be changed between runs.
Normally, it is not necessary to download all configuration parameters between runs. In situations where new parameters are required only the changed parameters will be downloaded.
400 MB (10 words/channel) are required to store a configuration.
Calibration services
Error detection and alarms
Alarms can be handled at >10Hz peak rate
Errors can be logged at >100Hz
The above will be handled centrally so that it is not necessary to consult many monitors in order to find an error or alarm message.
Diagnostic services
Data base/history services
On-line data base will include recent configurations, brief run summaries for the entire experiment, and full run summaries from the last month. Total space 100 GB.

c) Physics processing
Graphical data displays
Event displays
At least 5 stations for interactive event displays
Interactive data analysis
At least 10 stations for interactive data analysis (dynamic histogram definition, etc.)
Preparation and management of streams of selected events (event pools)
Users will have the capability of defining event selection criteria that will automatically create "pools" of selected events for analysis. These pools can be shared by more than 1 user.
There can be up to 10 separate event streams, with an integrated rate of <2Hz, and no more than 0.5 Hz in any single stream.
"Full" analysis of already reconstructed
selected events in an off-line analysis framework
Dynamic linking of user routines into a constantly running full offline analysis framework will be supported. It is assumed that a selection of fully reconstructed events is available and that full analysis requires 100 Mip-sec/evt. 100 Mips are thus required to provide 1Hz capacity.

These functions will be implemented by a collection of host CPUS, workstations, consoles, subsystem CPUs, compute servers, disks, mass storage systems, networks and other peripherals sufficient to meet the needs.

d) Software Tools: The on-line system will require standard software packages for code management, data management, code development, data bases, graphics and human interfaces. These packages should be chosen so that they are appropriate for offline use as well, if possible.

The on-line systems will provides standard interfaces to the slow control system, to monitoring processes, and to data streams, as well as the variety of software tools implied in the requirements listed above for event logging,

monitoring and analysis.

Fig 91.09.26

(R&D) Questions under study

Best method to route data after level III

- routers ? ?

- SCSI II 20 Mb/sec

- S-Bus — S-bus 25 Mb/sec

Solenoidal Detector Collaboration
Computing Section

Architectural Studies and Analysis
****DRAFT DRAFT DRAFT*****

September 25, 1991

SDC Computing Working Group
IBM Federal Systems

Contents

1. SDC Driving Requirements . . . 1-1
1.1 Speeds, Feeds and Performance . . . 1-1
1.2 Risk and Cost Drivers . . . 1-1

2. Operational Concepts . . . 2-1
2.1 Computing System Overview . . . 2-1
2.1.1 Functional Division . . . 2-1
2.1.2 Geographic Distribution . . . 2-1
2.2 Interfaces . . . 2-1
2.2.1 Interfaces with Other Systems, Facilities . . . 2-1
2.2.2 Human-System Interaction . . . 2-6
2.3 Operations Scenarios . . . 2-7
2.3.1 Software Development . . . 2-7
2.3.2 Online Computing . . . 2-7
2.3.3 Offline Computing . . . 2-7
2.4 Programmatic Goals and Constraints . . . 2-10
2.5 Assumptions . . . 2-10

3. SDC System Architecture Analysis . . . 3-1
3.1 Evaluation Criteria for System Architecture Selection . . . 3-1
3.2 Problem Domain Analysis . . . 3-2
3.3 System Performance . . . 3-4
3.4 Candidate Architectures . . . 3-6
3.4.1 SDC Generic Computing Model . . . 3-6
3.4.2 Hardware Architecture Candidates . . . 3-8
3.5 Potential Architecture Selection(s) . . . 3-14

4. SDC Software Architecture Analysis . . . 4-1
4.1 Software Infrastructure . . . 4-1
4.1.1 Services . . . 4-2
4.1.2 Standards . . . 4-5
4.2 Object Oriented Analysis . . . 4-6
4.2.1 Data Storage Management (Event Topology Model) . . . 4-6

5. Performance Modeling Results . . . 5-1
5.1 Model Topology . . . 5-1
5.2 SDC SSC Computing Node . . . 5-1
5.3 Remote Centers . . . 5-1
5.4 Analysis . . . 5-1

6. Miscellaneous Support Materials . . . 6-1
6.1 Analysis Methodologies . . . 6-1
6.1.1 System Level Components . . . 6-3

1. SDC Driving Requirements

1.1 Speeds, Feeds and Performance

1.2 Risk and Cost Drivers

2. Operational Concepts

2.1 Computing System Overview

2.1.1 Functional Division

2.1.1.1 On-line Computing

2.1.1.2 Off-line Computing

2.1.1.3 Data Management

2.1.1.4 Software Development

2.1.2 Geographic Distribution

2.1.2.1 SDC Computing at the SSCL

2.1.2.2 SDC Regional Computing Centers

2.1.2.3 Participating Institutions

2.2 Interfaces

2.2.1 Interfaces with Other Systems, Facilities

2.2.1.1 SSCL Compute System

1. Data Acquisition
   FROM:
   TO:
2. Subdetector(s)
   FROM:
   TO:
3. Detector Operator
   FROM:
   TO:
4. Accelerator Control System
   FROM:
   TO:
5. Calibration System
   FROM:
   TO:

6. Physics User
   FROM:
   TO:
7. SDC Regional Computing Center
   FROM:
   TO:
8. Collaboration Control Function
   FROM:
   TO:
9. System Administrator
   FROM:
   TO:
10. Software Developer
    FROM:
    TO:

SDC COMPUTING - SSCL Compute System Interfaces

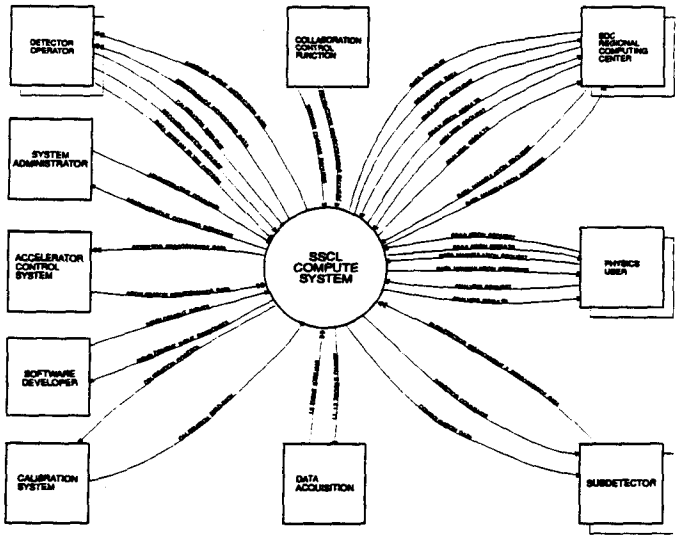


Figure 2.2-1

2.2.1.2 SDC Regional Computing Center

1. Physics User
   FROM:
   TO:
2. SSCL Compute System
   FROM:
   TO:
3. System Administrator
   FROM:
   TO:

SDC COMPUTING - SDC Regional Center Interfaces

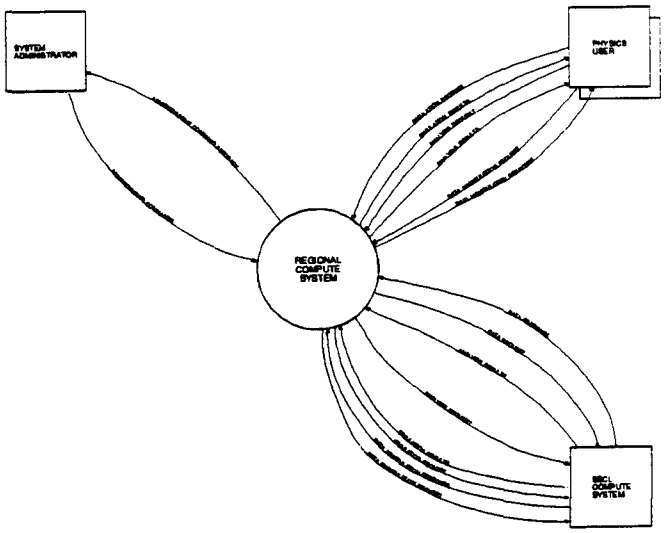


Figure 2.2-2

2.2.2 Human/System Interaction

2.2.2.1 User Interface Characteristics

2.2.2.2 User Categories

2.3 Operations Scenarios

2.3.1 Software Development

2.3.2 Online Computing

2.3.3 Offline Computing

2.3.3.1 Production

2.3.3.2 Analysis

A HIGH ENERGY PHYSICS ANALYSIS

A physicist sets out to conduct an analysis of SSC data. Whether the physicist is located at the SSC Laboratory, one of the SDC regional computing centers or at an institution participating in the SDC, the scenario will be essentially the same.

The goal of the physicist's analysis: To produce, for a selected collider run, a histogram of the distribution of invariant masses of psi meson and K + - candidates. He expects the distribution to show an enhancement at the B + - mass.

The steps the physicist follows in performing the analysis are summarized below.

The physicist:

- *Initiates a session with the SDC Computing System.*
- *Selects reconstructed data files and/or analysis product files as possible sources of data for the analysis.*
- *Reviews supporting data associated with the candidate reconstruction files and analysis product files.*
- *Makes the final selection of the data to be analyzed.*
- *Iteratively...*
  - *Specifies an analysis step that applies one or more cuts to the data.*
  - *Executes the analysis step.*
  - *Reviews the results.*
- *Histograms the results.*

The following paragraphs address these steps in greater detail.

1. *The physicist initiates a session with the SD Computing System.*

   ACTION:

   The physicist selects an available work station and initiates a "logon" process. During the logon the physicist indicates that he wants access to the system and responds to system prompts by identifying himself and supplying informatioo to authenticate his identity.

   RESULT:

   The system determines whether access for the supplied identificatioo and authenticating information has been authorized. If not, the system returns an "access denied" message to the user's workstation. If system access for this user has been authorized, a user session is initiated.

   At the initiation of a user session, the system performs the following:

   - Makes the user's personal data storage area available to the session.

     The user's personal data area supports a private database that provides the same capabilities as those provided by the SDC Computing System database. It also supports a private file system that provides the same capabilities as the SDC Computing System file system.

   - Presents an initial SD Computing System display to the user.

     The initial display complies with the user interface standards and conventions adopted by the SD Computing System and it supplies the user with the means to access the functional capabilities supplied by the SDC Computing System.

   - Notifies the user if any unacknowledged messages await his attention.

2. *The physicist selects reconstructed data files and/or analysis product files as possible sources of data for the analysis.*

   The term ***file*** is used here in a very loose sense. In this context, ***file*** is synonymous with ***"a collection of data"***. Whether the output of the reconstruction process will literally be files within the Computing System's file system or some other type of data entity (e.g., tables within a relational database, objects within an object-oriented database) is not yet known.

   ACTION:

   The physicist enters a request to the SDC data management system for a list of reconstruction files and or existing analysis products to consider for use as the basis for his planned analysis. He is likely to qualify his request by specifying one or more conditions that the files must satisfy in order to be identified as analysis input candidates.

   The analysis may be performed using:

   - Selected reconstruction files (the immediate product of the Reconstruction and Classification process),
   - Selected analysis product files (derived from previous analysis of reconstruction files)
   - A combination of the above types of files.

   The SDC database contains information about all collider runs for which reconstructed data are available. It also contains information about analysis product files derived from reconstructed data and available for use in additional analysis.

   RESULT:

   The system displays to the physicist a list of qualifying reconstruction files and or analysis product files. The list identifies the files and the runs with which they are associated. The list display also provides a means to select for display available supporting information about the candidate files.

   The supporting data associated with candidate reconstruction files consists of ancillary data for the runs which produced the raw data from which those files were made. That ancillary data includes: detector status and performance data, detector calibration data, and accelerator performance data. Supporting data for the candidate analysis product files consists of product derivation data. That derivation data describes the analysis performed to produce the given products, including: the identity of the data analyzed, the sequence of analysis steps performed, and the analysis software used.

3. *The physicist reviews supporting data associated with the candidate reconstruction files and analysis product files.*

   ACTION:

   The physicist browses the candidate list(s). He identifys files for which a look at the associated supporting data will help him to make the decision whether the given file will will not be used in the analysis. He then requests that supporting data for viewing.

RESULT:

The system presents the requested supporting information to the physicist for viewing.

4. *The physicist makes the final selection of the data to be analyzed.*

ACTION:

Having viewed the list(s) of reconstructed data and analysis products available for use in his planned analysis, and the associated supporting data, the physicist decides which data to use for his analysis and indicates his selection to the system.

RESULT:

The system acknowledges the data selection.

5. *The physicist iteratively...*

- *Specifies an analysis step that applies one or more cuts to the data.*
- *Executes the analysis step.*
- *Reviews the results.*

ACTION

The physicist proceeds with the analysis by performing a sequence of data "cuts" (a "cut" is in effect a filter which allows only data that satisfies a specified condition to pass on to the next step).

The physicist may perform a part or all of the analysis interactively if that is practical given the data volumes and amount of processing involved, or he can lay out what amounts to a job script for part or all of the analysis, then submit that script to be run in batch mode.

A representative sample of reconstructed data is available on high-speed storage for use to verify and refine the analysis procedure. p. In this scenario, the following sequence of cuts is applied:

- Reject probable cosmic ray events.

  The cut passes only those events for which the total transverse energy is less than a specified limit, say 1800 GeV.

- Reject events which do not have a primary vertex close to the center-line of the detector.

  The cut passes only those events for which the absolute value of delta-z is less than a specified limit, say 60 cm.

- Reject events that do not contain at least two muon candidates.
- Reject events for which the total transverse momentum is less than a specified threshold value.
- Reject events that do not have at least two muon candidates with differing electrical charge. - Keep only those events for which the invariant mass of the muon candidate pair falls within a specified range.

For each event remaining, look at all the charged track candidates:

- Reject tracks for which the transverse momentum is less than a specified threshold value.
- Keep only those events that satisfy detector geometry- dependent track quality cuts.

RESULT:

The computed invariant masses represent the analysis results. They now have only to be histogrammed for presentation.

6. *The physicist histograms the results.*

ACTION:

The physicist submits the computed invariant mass data to be histogrammed.

RESULT:

The historam(s) representing the analysis results.

2.3.3.3 Simulation

2.4 Programmatic Goals and Constraints

2.5 Assumptions

3. SDC System Architecture Analysis

The SDC System Architecture analysis results described in this section were produced using IBM FSD's System Architecture Development Process and Object Oriented Analysis techniques described in Section 6.1.

3.1 Evaluation Criteria for System Architecture Selection

The following are proposed evaluation criteria for system architecture selection. Weights are to be supplied.

1. Cost (Broken Out for SSCL, Regional Centers & Institutions)
   a. Hardware Life Cycle Cost
   b. Software Life Cycle Cost
      1) "Free" Software - Acquisition & Maintenance
      2) Professionally Developed - Acquisition & Maintenance
      3) COTS - Distributed Licences & Maintenance Fees
   c. Operations Cost
   d. Training Cost
2. Schedule Risk
   a. Availability of Products to Meet Evolving Standards
   b. Development Complexity Along Critical Path
   c. External Dependency Risk (e.g. free software when you need it)
   d. Availability of Critical Skills
3. Performance
   a. Meets Data Production, Storage, Reduction & Distribution Throughput Requirements
   b. Meets User Response Requirements
   c. Supports All Concurrent Activities (Live, SIM, 2nd Pass Recon,...)
4. Environment
   a. "Free" Software Maintenance Difficulty Risk
   b. Supports Portability Across Multi-Vendor Platforms
   c. Supports Interoperability Between Lab, Data Centers & Institutions
   d. Ease of Operational Use
   e. Data Base Structures Transparent to Users
   f. Ease of Changing Physics Analysis Software
   g. Stability of System Infrastructure
   h. Ease of Hardware Technology Insertion
   i. Flexibility to Grow & Evolve
   j. Technology Risk

3.2 Problem Domain Analysis

Our analysis of the SDC Proposal Computing Section requirements led us to the "Problem Domain" block diagram in Figure 3.2-1. The term "Problem Domain" means that it is an attempt at problem definition or "what" the system is intended to do (as opposed to "how" the system will be designed or built). The Problem Domain block diagram is then used as a basis for exploring candidate architectures in Section 3.4.

Figure 3.2-1 Block Diagram portrays an SDC "system boundary" as indicated by the bold line with "external interfaces" overlaying the system boundary. External interfaces are:

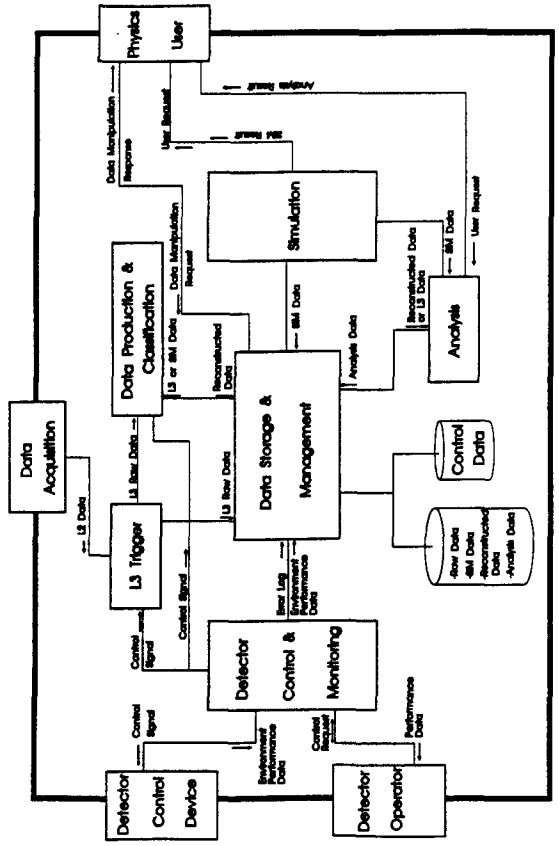
- The Level 1 and Level 2 part of Data Acquisition which feeds Level 2 data to the Level 3 part of Data Acquisition.
- Detector Control Devices which output environment performance data and receive control signals. These interfaces are with the Detector Control & Monitoring functional component.
- Detector Operators who enter control requests and receive performance data from the Detector Control & Monitoring functional component.
- Physics Users who have a number of interfaces as shown with Data Storage & Management, Simulation and Analysis functional components.

Functional Components are:

- Data Acquisition Level 3 triggering which provides Level 3 data to Data Production & Classification and to Data Storage & Management. Data Acquisition Level 3 Triggering receives control signals from Detector Operators via Detector Control & Monitoring.
- Data Production & Classification receives Level 3 data from:
  - Data Acquisition (realtime level 3 data)
  - Data Storage (playback of real level 3 data)
  - Data Storage (playback of simulated level 3 data)

  Data Production & Classification receives control signals from Detector Operators via Detector Control & Monitoring.
- Data Storage & Management receives data (for storage) from a number of sources as shown on the block diagram. Data Storage & Management in turn provides data to a number of destinations as shown.
- Simulation interacts with Physics Users and provides simulated data to Data Storage & Management and to the Analysis functional component.
- The Analysis functional component provides analysis results to Physics Users in response to their request criteria. Analysis results can also be stored via Data Storage & Management. Inputs to analysis are reconstructed data, prior analysis data, and (more rarely) level 3 data from Data Storage & Management. Simulated reconstructed data or level 3 data is also available from the Simulation functional component.

Finally a number of major categories of data are encapsulated (owned) by the the Data Management & Storage functional component. These data categories are listed in the cylinder icons on the figure.



Problem Domain Analysis Block Diagram

Figure 3.2-1

3.3 System Performance

The following SDC Proposal Computing Section requirements deal with system performance. The numbers in parenthesis are references to the May 10, 1991 version of the SDC Proposal Computing Section.

- Data Control & Monitoring Performance Requirements
  - 10 Event Streams: No more than 0.5 HZ per Stream; Integrated Rate < 2HZ (9.2.C)
  - Concurrent Sub-Detector Monitoring Processes at 1 HZ each (9.2.b)
  - Non-Event Monitoring 50 HZ (9.2.b)
  - Error Detection & Alarms > 10 HZ; Log at > 100 HZ (9.2.b)
  - Realtime Rotation on 3-D Event & Detector Viewing (10.3.2.b)

- Data Storage & Management Performance Requirements
  - Non-Event Data < 100 KByte/sec to permanent storage (9.2.a)
  - 100 HZ of 1 MByte Events to Perm. Storage; > 20 Streams (9.2.a)
  - Express Line Event Data (1HZ) Directly to Offline Analysis; 10 TByte/yr. reduced to 100 GB/yr. permanent storage (9.2.a)
  - Raw Event Size is 1 Mbyte; Processed Event Size is 2 Mbytes: Reduced Sample Size for Physics Analysis is 10**5 Bytes (10.3.5)
  - Fast, Medium, and Long Term Access (See 10.3.5)
  - Raw & Reconstructed Data Available for Analysis in < 10 Min. (10.2.1)
  - DSTs Available Within 2 Weeks of User Request (10.3.6)
  - Optimal Response for local/remote data access (10.3.1)
  - Tape Playback of Live or Sim Data (9.2.a)

- Reconstruction Performance Requirements
  - Realtime Reconstruction of 100 HZ Realtime Events; Total 10**5 Mips (10.2.1, 10.3.2.a) 10**3 Mips.Event Times 100 Events (10.3.4)
  - 2nd Pass Reconstruction of 100 HZ Events; Total 10**5 Mips (10.2.1, 10.3.2.a, 10.3.4)
  - Sim. Reconstruction; Total of 2 times 10**5 Mips (10.2.1, 10.3.4) ?Why do you need 2nd Pass on SIM data?

- Analysis Performance Requirements
  - Analysis Support for 50 Simultaneous Users at SSCL (10.3.3)
  - Local Institution; 100 Mip workstation with 10 GB local data Base or X-Terminals with Data Server (10.2.3)
  - Regional Center; 12 of 30 Users Active; 3 TB Data Base with < 1 Min. Access Time; 300 GB Fast Access; 5 Passes Requiring 10**4 Mips (10.2.2)
  - Typical Analysis Data Sample for One Analysis Station is 10**4 Events; 10**4 (100 people by 100 Mips) should be provided across the SDC for Physics Analysis (10.3.4)
  - Full Analysis Requires 100 MIPsec per Event (9.2.c)

- Network Communications Performance Requirements
  - WAN Limited to 200 Mbytes/sec (10.3.6)
  - Network Performance Data (See 10.4)
  - Optimal Response for local/remote data access (10.3.1)

- Reliability, Maintainability, Availability Performance Requirements
  - Cold Start < 30 Min.; Warm Start < 10 Min.; Stop/Start New Run < 5 Min.; < 5 Min. Downtime (9.2.a)
  - Reliability; Detector Collecting Data > 95% of Operating Time; Detector Collection Ability Uninterrupted with 20% of Channels Not Functional (9.2.e)
  - System Restart < 5 Min. By 1 Person (9.2.e)
  - System Reconfiguration < 5 Min. (9.2.e)
  - Reliability; Fix Offline Software Bugs Within 2 Weeks (10.2.6)

3.4 Candidate Architectures

3.4.1 SDC Generic Computing Model

The SDC Generic Computing Model, portrayed in Figure 3.4.1-1, is a general architecture candidate model. It features compute servers, data storage servers, and system management servers coupled together by a high speed data channel and low speed control communications LAN. It offers the following advantages:

- Separation of data communications and control communications.
- Concurrent high speed data storage and retrieval. For example, Data from the Reconstruction & Classification compute server can be stored on the Hierarchical Storage server at the same time the Analysis & Sim server is retrieving data. This could be accomplished via an intelligent HiPPI switch (100 Mbyte/sec), or a future option.
- Functionally coherent servers which would exploit present & future standard components, e.g., ISO systems management.
- Scalability of servers, communications devices and storage devices.
- Automatic hierarchical data staging and storage.
- Maximizes use of commercial off the shelf hardware and software.

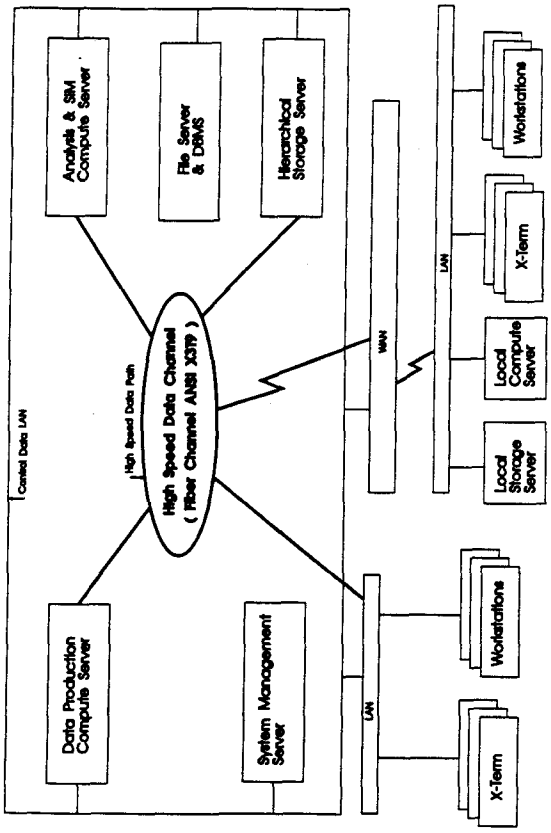


Fig 3.4.1-1

3.4.2 Hardware Architecture Candidates

3.4.2.1 Option 1

Hardware Architecture candidate option 1 is portrayed in Figure 3.4.2.1-1.

Assumptions

- 1992 Technology
- A 10 second latency in production reconstruction is acceptable
- Analysis computing resources for 50 local SSCL users must be provided. A typical analyst would require 2 to 3 jobs turned around during prime shift and 1 overnight.
- A typical analysis data retrieval for a single user will be about half of the total sample size of 10 Gigabytes (10**4 reconstructed events @ 1 Mbytes event), i.e., 5 Gigabytes. This is due to data selection criteria (metadata) and use of a data management system such as object oriented or relational. This is to say that the entire "DST" will not have to be transferred from the data base to the analysis workstation for processing.

Key Features

- Raw data at a rate of 100 MBytes/sec is routed from the Level 3 Farm via a switching and buffering system to a series of helical scan tape systems. The switch (e.g. HiPPI) would allow high speed switching to a backup drive if the current drive failed. Switching would be under control of the Systems Management function. The helical scan tape drives are high performance, high capacity emerging standard digital data (DD) tape drives which originated in the video industry. The number of drives depends upon the capacity of the drives selected. For example, a DD1 Drive can record or read 40 Mbytes/sec. with a tape capacity of up to 100 Gigabytes. A DD2 Drive records / reads at 15 Mbytes/sec with a tape capacity of 25 to 165 Gigabytes. There is also a 5 Mbyte/sec drive available from Maximum Strategies. Helical scan technology has the advantage of low cost storage. Total cost (media and recording equipment) is estimated at 0.5 cents per megabyte versus 12 to 14 cents per megabyte for optical. However, tapes have the disadvantage of requiring sequential access for retrieval versus direct access to data on an optical platter.

  In this option the Level 3 Farm would have to provide driver software to keep data flowing in a continuous stream to the helical scan drives (which do not work well with sporadic data). Also, depending on the vendor, the Systems Management software would participate in managing which drives are used for reading (from the Level 3 farm), rewinding, and writing to the reconstruction clusters. Tape storage in the archive could either be automated via robotics or manual.
- A group of small clusters handle the reconstruction processing. Each small cluster contains a small number of tightly coupled CPU's, e.g. 32 CPUs connected via a high speed backplane. Assume for 1992 each CPU can do 100 MIPs. A cluster manager schedules and controls routing of level 3 data to each CPU. There is no data communications between CPUs in the cluster. A single CPU processes a single event. Since, by requirement, 1000 MIPs are needed to process an event it will take 10 seconds to complete event processing in a CPU.

  There are enough small clusters to make a total of 1000 CPUs. Since there are 1000 CPUs the 100 HZ events will be scheduled so that all processing will occur in "realtime" but with a 10 second latency per event. As future processors become more powerful this latency would gradually decrease.

  There are two suboptions for connecting the CPU's in a small cluster. One suboption is to have the CPUs loosely coupled via a ring network (See Figure 3.4.2.1-2). Another suboption is to have the CPUs tightly coupled via a high speed switch (See Figure 3.4.2.1-3). These suboptions may not be the most cost effective or use the least amount of floor space.

- High speed switches (e.g. HiPPI channels @ 100 Mbyte/sec each) capable of routing raw data from the helical tape drives to the small clusters are included in this option. These switches, under control of Systems Management, would allow for high speed switching in case a tape drive or cluster failed.
- A data storage system consisting of 2 disk arrays. Each disk array is capable of receiving 50 Mbytes/sec for an aggregate of 100 Mbytes/sec to handle the 100 Mbytes of reconstructed data storage.
- Helical scan tape systems to receive the reconstructed data.
- An IEEE mass storage reference model standard "name server" which has knowledge of file names and directories as meta data. An object oriented or relational data base manager is co-resident with the name server. The data base manager has local storage of meta data which facilitates selected retrieval of data from the data storage system. The meta data is determined from the Object Oriented Analysis of Event Topology in Section 4.2.1. The name server, data base manager server are connected only to the low speed communication LAN because their job is primarily to direct the transfer of data to the analysis workstation.
- A set of 50 analysis work stations for local SSCL users. Each analysis workstation is 100 Mips.
- A systems management server which would comply with the ISO standard.
- A set of low cost standard tape drives, which would be used to mail analysis data to external institutions. External users would not have to purchase high cost DD2 drives.

Summary of Pros/Cons

- Pros
  - Low cost helical scan tape drives (DD2 cost is 0.5 cents per magabyte)
  - Reliability via high speed switch out of a failed tape drive or cluster.
  - Scalable
    - Add CPUs to a cluster
    - Use more powerfull CPUs
    - Upgrade HiPPI to future option
  - Exploits Industry Standards
- Cons
  - About 30 minute delay to record and playback level 3 data
  - 10 second latency to do production reconstruction
  - Tape versus optical has less direct access capabilities
  -

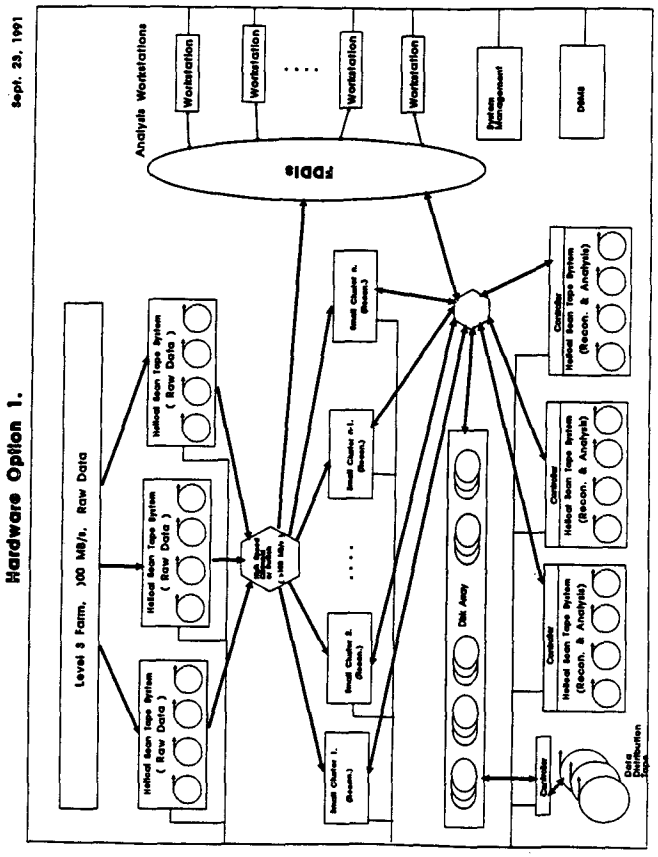


Fig 3.4.2.1-1

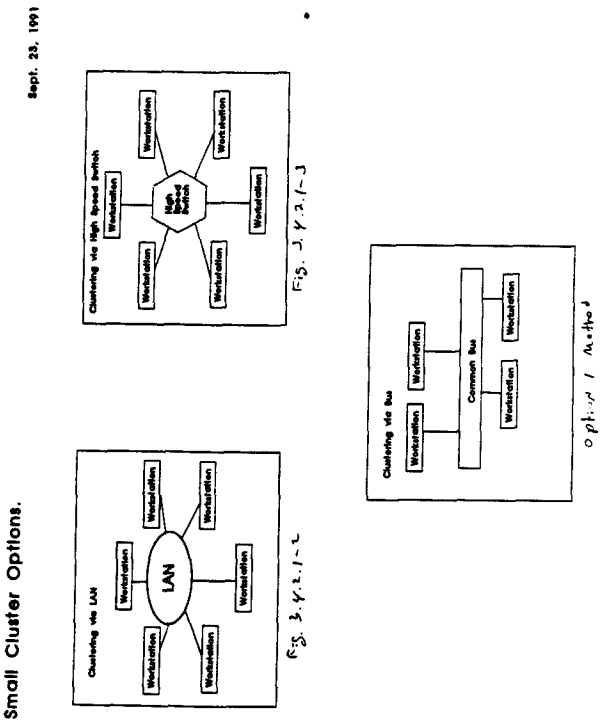


Fig. 3.4.2.1-3

Fig. 3.4.2.1-2

Fig. 3.4.2.1-1

3.4.2.2 Option 2

Hardware Architecture candidate option 2 is portrayed in Figure 3.4.2.2-1.

Assumptions

- Same as option 1

Key Features

- The only difference between option 2 and option 1 is the use of a single cluster for reconstruction. This single cluster would have to provide 100,000 MIPs (1000 Mips for 100 events sec). This single cluster might be something like the Sigma Touchstone from Intel which is to deliver between 150 and 240 GFlops sometimes in the 2nd quarter of 1992. The equivalent MIPs of the Sigma for reconstruction is unknown at this time. The Sigma will probably use an extension to the i860 processor chip which can peak at 60 MFLOPS double precision.

  Another option is the Vulcan research machines from IBM.

  All of the above (including option 1) are MIMD technologies (multiple instructions/multiple data) with either shared or distributed memory. SIMD (single instruction, single data) is not appropriate for event reconstruction because it is not a synchronous lock step type of application. For this reason, the SIMD Thinking Machines Corp's Connection Machines are not considered to be a viable option. Also, there is a possibility that the reconstruction clusters could be load balanced to do analysis processing during times when no reconstruction is being done.

Summary of Pros/Cons

- Pros
  - Cost comparison TBD.
  - General purpose RISC processors may be more appropriate than special purpose floating point processors
- Cons
  - Pushing state of art technology

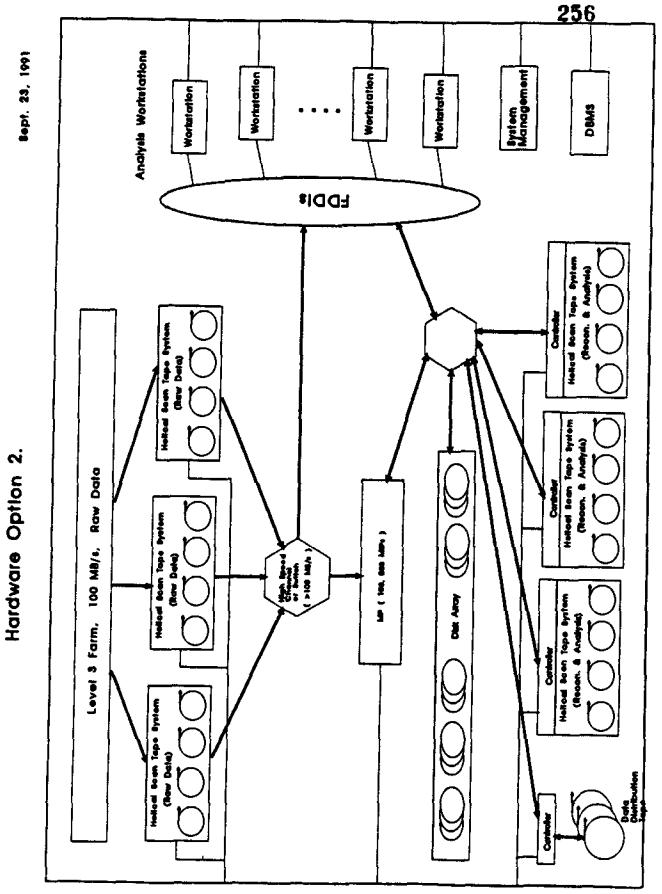


Fig. 3.4.2.2-1

3.4.2.3 Option 3

Hardware Architecture candidate option 3 is portrayed in Figure 3.4.2.3-1.

Assumptions

- Same as option 1

Key Features

- The only difference between option 3 and option 1 is the use of the disk array as a buffer input to reconstruction. In this option the level 3 data is sent to BOTH the helical scan tape system and the disk array. The level 3 data on the disk array is then routed to the reconstruction clusters via the high speed switch. Level 3 data is never routed from the tape system to the reconstruction clusters except in a contingency mode. Hence, this option has the advantage of no 30 minute delay in filling and rewinding tapes before the level 3 data goes to the reconstruction system. Also, reconstruction processing is not affected by tape drive failures.

Summary of Pros/Cons

- Pros
  - No 30 minute delay in getting level 3 data to reconstruction clusters. Reconstruction not affected by tape drive failures.
- Cons
  - TBD cost tradeoff

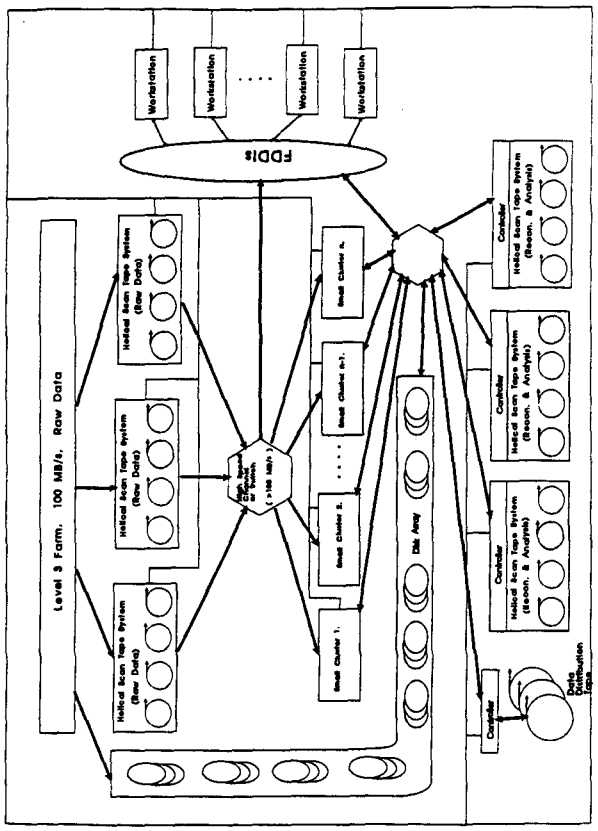


Fig 3.4.2.3-1

3.4.2.4 Option 4

Hardware Architecture candidate option 4 is portrayed in Figure 3.4.2.4-1.

Assumptions

- Same as option 1

Key Features

- Option 4 uses the disk array as in option 3 and the single reconstruction cluster as in option 2.

Summary of Pros Cons

- Pros
  - –
- Cons
  - –

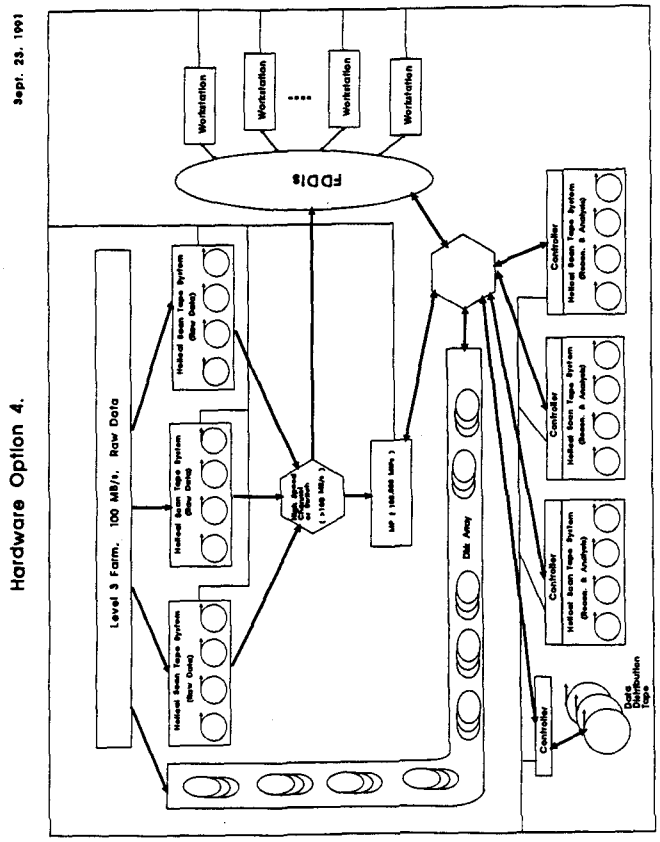


Fig 3.4.2.4-1

3.4.2.5 Option 5

Hardware Architecture candidate option 5 is portrayed in Figure 3.4.2.5-1.

Assumptions

- Same as option 1

Key Features

- Option 5 uses distributed disks attached to each cluster in lieu of disk arrays.

Summary of Pros/Cons

- Pros
  - –
- Cons
  - –

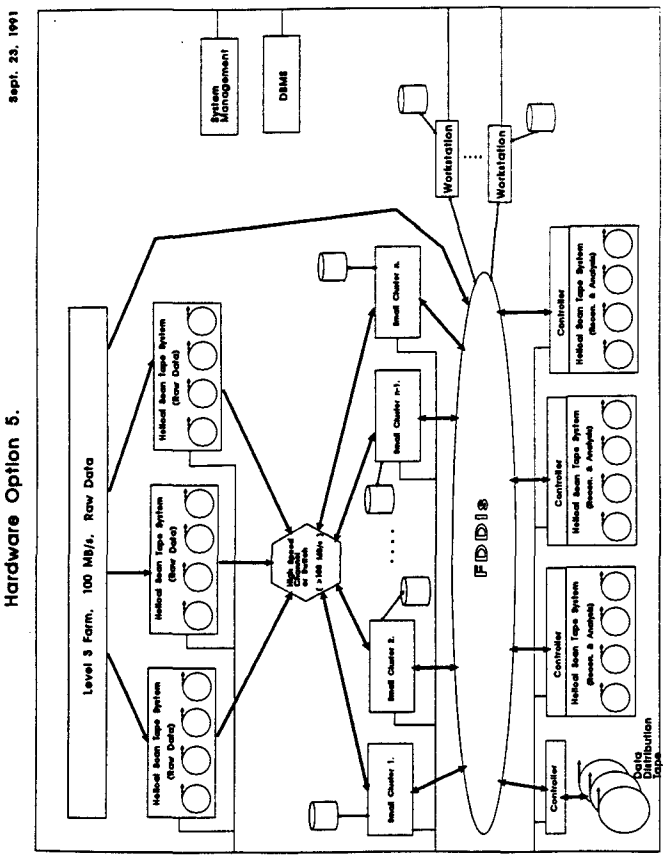


Fig. 3.4.2.5-1

4. SDC Software Architecture Analysis

The SDC Software Architecture analysis results described in this section were produced using Object Oriented Analysis techniques described in Section 6.1.

The major software architecture design goals are as follows:

- Software in general should be maintainable, efficient, reliable, understandable, reuseable and extensible.
- Software portability and interoperability should support technology upgrades and multi-vendor distributed environments.
- The user interface with the software should be standard and easy to use.
- The software architecture should provide for a software bus or infrastructure of standard services utilizing industry standard components where feasible. The goal is to incur the cost of common services "glue code" only once and to promote system integrity.
- The software architecture should provide an environment or framework which makes it easy for physists to add or modify analysis code without relink of the framework. Access to data by such analysis code should be via an easy to use object query language, i.e., knowledge of internal data structures should be transparent.
- The software architecture shall meet all performance requirements.
- Software shall be designed within budget and schedule.

The overall software architecture model is viewed as a three layer stack in Figure 4-1.

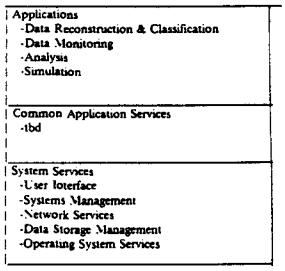


Figure 4-1

4.1 Software Infrastructure

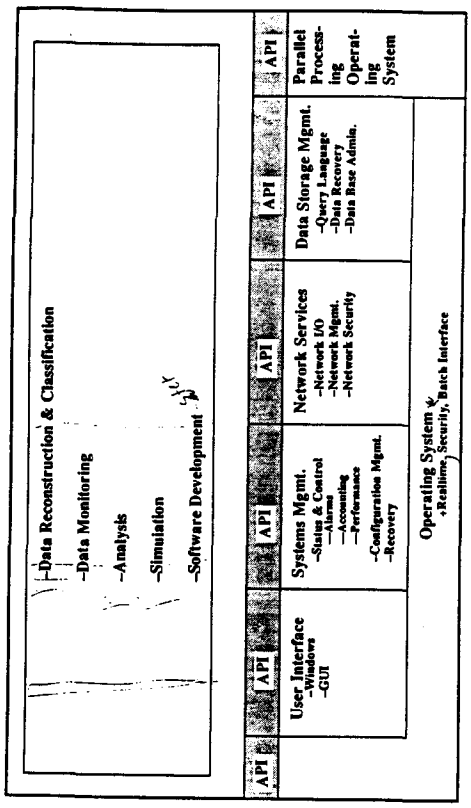
The bottom two layers of the stack portrayed in Figure 4-1 comprise the software infrastructure. The software infrastructure provides the software "glue" which binds the system together into a workable entity.

3.5 Potential Architecture Selection(s)

4.1.1 Services

The application's view of the infrastructure is via Application Program Interfaces (API) as portrayed graphically in Figure 4.1-1. The anticipated use of these API's by the applications is shown in Figure 4.1-2.

Services View of Software Architecture



Services View of Software Architecture

API Cross Reference

API Provider \ API User	Data Reconstruction & Classification	Data Monitoring	Analysis	Simulation	Software Development
Operating System +Realtime, Security, Batch	X	X	X	X	X
Parallel Proscessing OS	X				
User Interface –Windows –GUI		X	X	X	X
Systems Mgmt. –Status & Control —Alarms —Accounting —Performance –Configuration Mgmt.		X			
Network Services –Network I/O –Network Mgmt. –Network Security	X	X	X	X	X
Data Storage Mgmt. –Query Language –Data Recovery –Data Base Admin.	X	X	X	X	X

API = Application Program Interface

4.1.2 Standards

4.2 Object Oriented Analysis

4.2.1 Data Storage Management (Event Topology Model)

4.2.1.1 Event Topology Object Hierarchy

4.2.1.1.1 Overview: The Event Topology Object Hierarchy is the resulting model produced by applying Object Oriented Analysis to the problem domain of the Data Storage Management Subsystem. It can be expanded to become a full scale data base schema during the design phase of the Data Management Subsystem.

In order to effectively manage the massive amount of data and timely deliver them to the end-users, the Data Storage Management subsystem becomes the key component of the whole system. Simplicity, flexibility and expandability are the key drivers for the OOA model which will be carried over to the Data Storage Management Subsystem design phase.

There are two major inter-object relationships to interconnect and amalgamate objects into a hierarchy, the "Whole-Part" and the "Generalization-Specification" relationships (See Fig.1). The "Whole-Part" relationship is shown with a whole object at the top, and then a part object below, with a line drawn between them. A triangle marking distinguishes objects as forming a Whole-Part relationship. Each end of a Whole-Part relationship line is marked with an amount or range, indicating the number of parts that a whole may have and vice versa, at any given moment in time. In the other hand, the "Generalization-Specialization" relationship is shown with a Generalization object at the top and Specialization object below, with lines drawn between them. A semi-circle marking distinguished objects as forming a Generalization-Specialization relationship

4.2.1.1.2 Basic Data Storage Management Subsystem Accessing Scenarios: The user of the system should be able to store and retrieve the event data by querying the following objects (Fig.2)

- Event - All data related to a collision
- Tracks - Data related to a charge particle traversing the tracking chamber
- Clusters - Data related to Energy deposited on calorimeter
- Vertexes - Origin of tracks either from collision or particle decay
- Particle Candidate - Tracks and clusters made up of signature of a particle
  - Electron - one track and one EM cluster
  - Photon - No track and one EM Cluster
  - Jet (Hadronic Particle) - 0+ tracks and one hadronic cluster
  - Neutrino - Missing energy
  - Muon - Single muon track

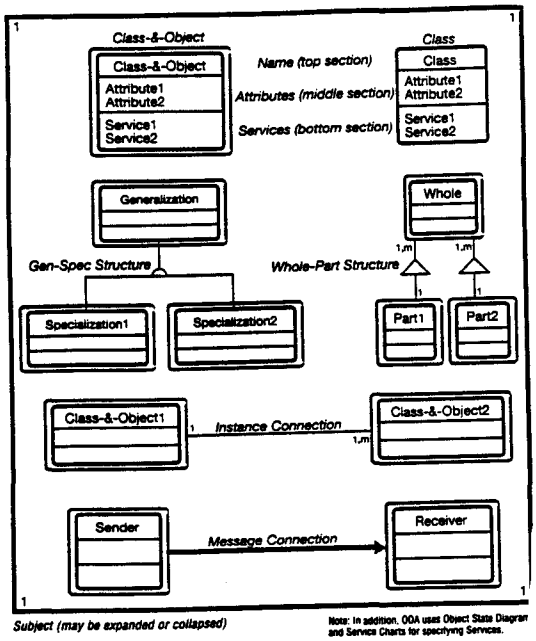


Figure A-1: OOA notations

Fig. 4.2.1-1

GTK 8-23-91

Step 2

Candidate Physics Objects Classification

Physics Object	Topology	Tracking Chamber (central, forward,...)	Calorimeter	Muon Chamber (Tracking)
Electron	Single Track	EM Cluster (Deposit Up Front, Single Tower)	No Track	
Photon	No Track	EM Cluster (Deposit Up Front, Single Tower)	No Track	
Quark/Anti-Quark (Jet)	Many Tracks ** No Tracks	Hadronic Cluster (Evenly Spread,, Multi-Tower)	No Track	
Neutrino	No Tracks	Indirect (Missing Energy)	No Track	
Muon	Single Track	Minimal Energy in Single Tower	No Track	Single Track

Fig 4.2.1-2

4.2.1.1.3 Navigating Through the Model(Fig.3) 4.2.1-3

4.2.1.1.3.1 Event Object: The Event object is the highest level object which contains all other collision related objects. The Event object is also the smallest unit which distinguish one collision from the others. The Event object contain attributes such as Event_Number, Run_Number, Trigger_Number, etc. to uniquely identify itself. It is also an aggregate of Track, Vertex, Candidate_Particle_Bucket and Cluster_Aggregate objects. An Event object is created when the first piece of the raw data is collected and is updated during the later analysis phase when more information about the event is gathered.

4.2.1.1.3.2 Topology Objects: The topology objects are those created by the reconstruction and classification algorithms. These objects are related to data which is output by the detector, or in another word, things that can be seen by the detector. There are three kind of topology objects in our current model, they are Cluster, Track and Vertex object.

- Cluster

  The Cluster object is an agregate of EM_Cluster and Hadronic_Cluster objects. This object is used to classify data which is produced by the detector calorimeter. The data related to this object is energy information. The attributes of this object are Total_Energy (sum of EM_cluster energy and Hadronic_Cluster Energy), Number_of_Towers (# of tower hit by the cluster), Shape (shape of the cluster) and Position (position vector of the cluster). The EM_Cluster and Hadronic_Cluster objects are parts of the Cluster object because the EM_Cluster is the energy detected by the Strip Chamber while the Hadronic_Cluster is the energy detected by the outer part of the Calorimeter, together they make up the Cluster.

- Track

  The Track object is used to classify data in the Tracking chamber. Tracks in the detector could be muon tracks or ordinary tracks. A track may consist of several segments. Since the track segments may not be of interests to the users who are querying the data base, we do not include them in the model. The Track object has attributes such as Algorithm_Version#, Pointed_To_Tower (the Calorimeter tower address which the track is pointing to), Position (position vector of the track), Momentum (momentum vector of the track) and Track_Type (e.g. a muon track).

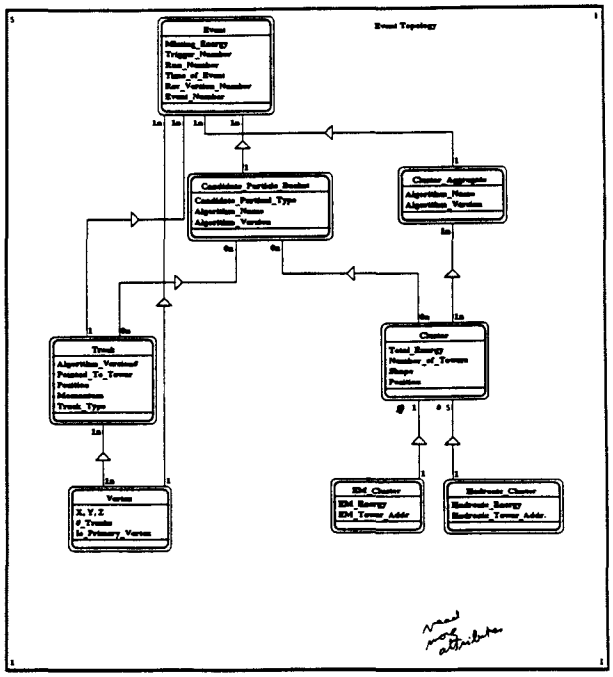
- Vertex

  The Vertex object is the kind of object that records the point where tracks are originated. There are two kind of vertexes. The primary and the secondary vertex. The primary ooe is created by a particle collision while the secondary is created by particle decay. The Vertex object has the following attributes: XYZ (coordinate in space), #_Tracks (# of track connected to this vertex) and Is_Primary_Vertex (true if this vertex is a primary vertex).

4.2.1.1.3.3 Aggregation Objects: Aggregation Objects are used to group the same type of object instances which have similar characteristics together. In our current model, there is only one aggregation object: Cluster_Aggregate. A Track_Aggregate may also be needed, but it is not clear at this point the usefulness of it. The Cluster_Aggregate object is used in this model to group all clusters which are classified by the same algorithm.

4.2.1.1.3.4 Particle Connection Object: The only type of particle connection object in our model is Candidate_Particle_Bucket. It is used to group all topology objects which have signature of a certain kind of particle. For example, an electron in the detector may have one track and one EM_Cluster. An electron finding algorithm found the track and the EM cluster, hence a Candidate_Particle _Bucket instance is created to group the track and the cluster together and give a value "Electron" to the attribute Particle_Type.

4.2.1.1.4 Summary: The OOA modeling process is an evolving one. After several iteration we have simplify it down from about 20 objects in the first cut to the current one which has only eight objects. Along the way, we have learn a lot about how a physicist do their work. A continuing perfection of the model is expected.



Track

Fig 4.2.1-3

5. Performance Modeling Results

5.1 Model Topology

5.2 SDC/SSC Computing Node

5.3 Remote Centers

5.4 Analysis

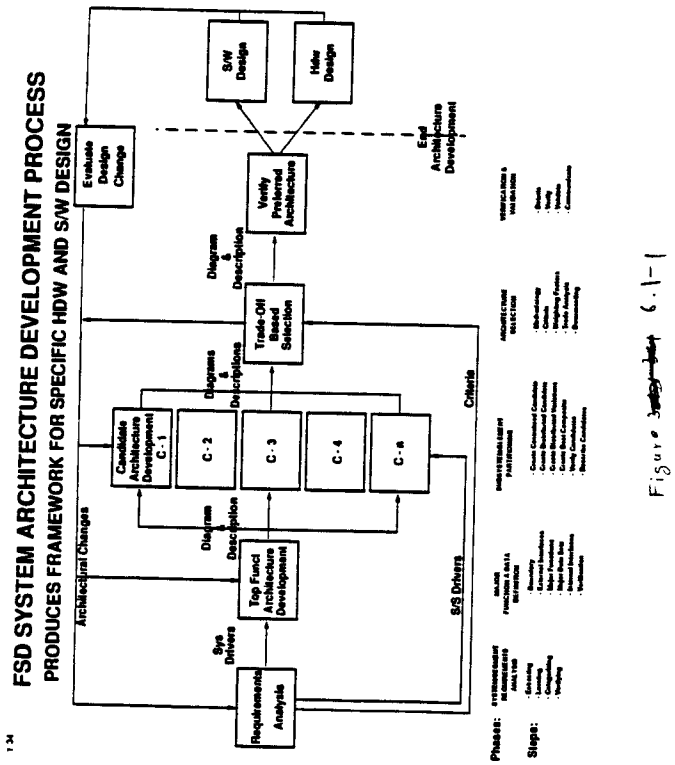


Figure 6.1-1

6. Miscellaneous Support Materials

6.1 Analysis Methodologies

The SDC System Architecture analysis results described in Section 3 were produced using IBM FSD's System Architecture Development Process as graphically portrayed in Figure 6.1-1. First, architecture evaluation criteria were developed (See Section 3.1). Next, the system requirements, in the SDC Proposal Computing Section, were analyzed and categorized into the following.

- System level components (see Section 6.1.1)
- System performance requirements (see Section 3.3).

Finally, candidate architectures were developed (see Section 3.4) and trade-off based architecture selections were made (see Section 3.5) using the evaluation criteria.

The System Architecture provides a top level view of the overall SDC online and offline system. Several other views of the architecture are needed to complete the analysis. These are provided in Section 4, Software Architecture Analysis. The software infrastructure services and standards in Section 4.1 provides a sideways view of standard services required by all application components of the SDC computing model. Section 4.2 provides an object oriented view of the Data Storage Management Domain (Event Topology) This model was developed using the method described in the book, Object Oriented Analysis, by Peter Coad and Edward Yourdon, and using the OOATool (TM) analysis tool.

6.1.1 System Level Components

6.1.1.1 Functional Domains and System Boundary

The following are proposed functional domains. Components of each functional domain are listed with references to the SDC Proposal Computing Section in parenthesis.

- Data Reconstruction & Classification
  - Run Control (9.2.a)
  - Run Setup, Config. Change Between Runs (9.2.b)
  - Recording Level 3 Output; 20 Streams + expressline (9.2.a)
  - Calibration Services (9.2.b)
  - Record Run Config., Conditions & Summary (9.2.b)
  - Preparation & Mgmt. of Event Streams, Pools (9.2.c)
  - Realtime Full Reconstruction & 2nd Pass Recon (10.2.1)
- Data Monitoring
  - Detector Performance Monitoring (9.2.b)
  - Error Detection & Alarms (9.2.b)
  - Diagnostic Services (9.2.b)
  - Event Displays; Quick Look at Express Stream (9.2.c)
  - 3-D Event & Detector Viewing With RT Rotation (10.3.2)
- Data Storage Management
  - Raw & Reconstucted Data Archive (10.2.1)
  - Random Access to SDC Data for Analysis (10.3.1)
  - Data Base Access via Keywords, Query Procedures (10.3.1)
  - Sequential Access to Any Part of Raw or Processed Data (10.3.1)
  - Distributed Data Base (10.3.1)
  - Fast, Medium & Long Term Data Storage Access (10.3.5)
  - Distribution of DST Documentation to Users (10.3.6)
  - Full Time Data Base Administration (10.3.7)
  - Data Base Manager (9.2.d, 10.5.4.1)
  - Storage Hierarchy (10.5.2.2)
  - File & Media Management (10.5.4.8)
- Analysis
  - Interactive Data Anaylsis Displays (9.2.c)
  - Desktop Analysis Workstations (10.3.3)
  - Reduced Sample for Repeated Analysis (10.2.1)
  - Full Analysis Framework (9.2.c)
  - Add User Analysis Modules Without Re-Link (10.3.2.b)

  - Regional Center Analysis (10.2.2)
  - Local Institution Analysis (10.2.3)
  - Geant Routines (10.5.3.a.1.2.5)
  - Function Fitting (10.5.4.6)
- System Services
  - Standard User Interface, X-Window, GUI (9.2.d, 10.5.4.2, 10.3.3, 10.5.4.2)
  - Recoverability (9.2.e)
  - Expert Systems for Error Analysis/Recovery (10.3.7, 10.5.2.3.3)
  - LAN Support, Standard Protocols (10.4)
  - WAN Support (10.4)
  - Communications Aids (10.4)
  - File Transfer (10.4)
  - Machine Independence (10.5.2.4)
  - Parallel Processing (10.5.4.7)
  - Kernel OS (10.5.4.3)
  - Interactive & Batch (10.5.4.4)
  - Resource Management (10.10.4.5)
- Simulation
  - Tape Playback (9.2.a)
  - Sim Data Generation (10.2.1), Geant Routines (10.5.3.a.1.2.5)
- Software Development Environment
  - Code & Library Management (9.2.d, 10.3.7, 10.5.3.e)
  - System Maintainability (9.2.e, 10.3.6)
  - Software Distribution (10.3.6)
  - 10 Years of Software Versions (10.3.6)
  - Online Help (10.3.6, 10.3.7)
  - CASE Tools (10.5.3.a.1.2.4)
  - Software Development Process (10.5.3)

The following SDC Proposal Computing Section requirements help to define the system boundary.

- Online task env. (9.1)
- Online data output to Offline analysis (9.2.a)
- Can accept and log data from source other than lv3 (9.2.a)
- Computing at SSCL (10.2.1)
- SDCSSCL analysis facilities = 4 regional centres (10.2.1)
- SDC regional centres (7) for analysis (10.2.2)

- Local institutions w low- to mid- range workstations (10.2.3)
- Software for offline computing will be distributed to user community (10.3.6)
- (-)DSTs will not be available via WAN unless... (10.3.6)
- SW distribution centralized & coordinated by SSCL.(10.3.6)
- All documentation for DSTs & offline SW available on HEP WAN.
- Offline networking include ESNET and NFSNET (10.4)
- Offline networking to foreign countries. (10.4)
- Remote X-term or workstation access for interactive file xfer...

6.1.1.2 System Data Sets

The following SDC Proposal Computing Section requirements identify system data sets.

- > 20 Streams of Event Data (100 HZ of 1 Mbyte events) to permanent storage (9.2.a)
- Express Line Event Data (1HZ) Directly to Offline Analysis; 10 TByte/yr. reduced to 100 GB yr. permanent storage (9.2.a)
- Non-Event Data < 100 KByte sec to permanent storage (9.2.a)
- Calibration Data 20 MByte + Local Cals in DAQ & Subsystems (9.2.a, 10.3.5)
- Sim Data (9.2.a)
- Simulated Data (10.2.1)
- Detector Performance Data (9.2.b)
- Configuration Data: 400 MB (10 Words/Channel) (9.2.b)
- Error Detection & Alarm Log (9.2.b)
- History of Recent Config. & Run Summaries (9.2.b)
- Raw Data Archive 10**15 Bytes/yr. (10.2.1, 10.3.1, 10.3.5)
- Reconstructed Data Archive 10**15 Bytes/yr. (10.2.1, 10.3.1, 10.3.5)
- 2nd Pass Reconstructed Data (10.2.1)
- Reduced Sample for Repeated Analysis (10.2.1, 10.3.1)
- Regional Center Data Base (10.2.2)
- Local Institution Data Base (10.2.3)
- Code Management Data Base (9.2.d, 9.2.e, 10.3.6, 10.3.7)
- Online Help for Software (10.3.6, 10.3.7)
- Documentation for DSTs (10.3.6)
- Storage Model (10.5.2.2)
- Text Editing, Graphics & Spreadsheet Data (10.5.2.3.4)
- Central Bulletin Board & Mail Service (10.5.2.3.5)
- CASE Tool Repository (10.5.3.a.1.2.4)
- File & Media Management (10.5.4.8)
- Resource Management Data (10.10.4.5)

6.1.1.3 External and User Interfaces

The following SDC Proposal Computing Section requirements identify external interfaces.

- Acquiring and recording event data (9.2.a)
- Acquiring and recording non-event data (9.2.a)
- Acquiring and recording calibration data (9.2.a)
- Tape play back of real and SIM data (9.2.a)
- Experiment process monitor is location independent (9.2.a)
- At least one data monitoring for each sub-detector (9.2.b)
- Interface & relationship with other subsystem (9.3)
- SDC regional centers (7) interfaces. (10.2.2)
- Local institutions interfaces (10.2.3)
- Offline software distributed to user community (10.3.6)
- (-)DST WAN distribution limitation (10.3.6)
- SW distribution centrolized and coordinated by SSCL (10.3.6)
- Remote X-term or workstation access to offline system (10.4)

The following SDC Proposal Computing Section requirements identify user interfaces.

- Run control can be run by two semi-skilled physicists 90% (9.2.a)
- Experiment process monitor is location independent (9.2.a)
- SW auto compare data w/ historical conditions and flag discrepencies will be available (9.2.b)
- More than 5 stations for interactive event display (9.2.c)
- More than 10 stations for interactive data display (9.2.c)
- Users define event selection criteria to create pools (9.2.c)
- Pools shared by > 1 user (9.2.c)
- Dynamic linking of user rountines into offline system (9.2.c)
- Code management, data management, GUI (9.2.d)
- Recoverbility, Operability, Maintainability (9.2.e)
- 2nd pass reconstruction (10.2.1)
- SDCSSCL analysis facilities (10.2.1)
- SDC regional centers (10.2.2)
- Local institutions (10.2.3)
- Query procedure (10.3.1)
- Support 3-D event detector reviewing with real time rotation (10.3.2
- Standard UI for all platforms (10.3.3)
- Standard GUI (10.3.3)
- Desktop w/ at least X-term functionality (10.3.3)
- Online help and documentation (10.3.6)

- Periodic revisions released (10.3.6)
- Distributed to user community (10.3.6)
- All documentations for DSTs & Offline SW available on WAN (10.3.6)
- Online help for SW (10.3.6)
- Full time DB admin team at SDC (10.3.7)
- Online help and documentation for all part nf offline (10.3.7)
- Help & consultant on call plus possible expert system.(10.3.7)
- Communication aids (10.4)
- Remote access for interactive file xfer.... (10.4)
- GUI and command line interfaces (10.5.1)
- GUI, interactive I/F, expert system, text editing, spreadsheet and central bulletin (10.5.2.3)
- Provide fIVV with access to device, tools (10.5.3.a.1.2)
- Case tools requirements (10.5.3.a.1.2)
- Utility SW (10.5.3.a.1.2)
- File & media management system (10.5.4.8)
- Resource management (10.10.4.5)

SDC Note 91-xxx
September 5, 1991

SDC DATA ACQUISITION DESIGN REQUIREMENTS AND FUNCTIONAL SPECIFICATIONS

Version 0.99

SDC Data Acquisition Working Group

1. Introduction

The goal of this document is to specify the general features of the SDC Data Acquisition (DAQ) subsystem, define the relationship between DAQ and other subsystems, and chart the course for future development of the DAQ subsystem. In developing this document, we have tried to focus on the broader design requirements and functional specifications, while avoiding detailed discussion of the implementation of these requirements and specifications. The detailed design of the DAQ is to be completed at a later stage in the DAQ design cycle (see section 8).

Design requirements for the DAQ are described in section 2. These requirements are very general in nature and state the essential requirements for the SDC DAQ without regard to implementation. The next two sections describe the functionality (section 3) and scope (section 4) assumed for the subsystems which are interfaced to the DAQ, Front End Electronics (FEE), Trigger, Online Computing, and Slow Control. A set of preliminary design parameters for the DAQ is included in section 3.5. Functional specifications for the various DAQ components and interfaces to other subsystems are described in section 5. The functional specifications, while still quite general, specify architectural choices and DAQ functionality chosen by the DAQ group to implement the design requirements in section 2. System issues that apply to the DAQ as a whole are discussed in section 6, including data integrity and partitioning requirements. Section 7 describes the functionality required for the portable DAQ, a small scale DAQ system to be used for electronics system tests, test beam, and detector subsystem commissioning. Finally, the DAQ design cycle is described in section 8.

3. DAQ Design Assumptions

The SDC DAQ is part of an integrated detector system comprised of subsystems that provide detection elements, front end electronics, trigger, DAQ, online computing, and slow control. Figure 1 shows a block diagram of the functional components of the DAQ and how they are connected to the trigger, FEE, online computing, and slow control subsystems. Before describing the functionality of the DAQ components (section 5), it is useful to first describe the assumptions made by the DAQ group regarding the functionality (sections 3.1-3.4) and scope (section 4) of the subsystems connected to the DAQ. In addition, we present a preliminary set of design parameters relevant to DAQ design in section 3.5.

3.1. Trigger

The primary function of the trigger is to select events for permanent recording that are needed for the offline physics analysis of the experiment. In addition, the trigger selects events for testing, calibration, and monitoring purposes and provides the gating logic needed to throttle the trigger to prevent data loss.

Trigger Levels

1. The trigger selection is made in 3 Levels.
2. A Level 1 accept/reject trigger decision is made for each beam crossing following a fixed latency time.
3. A Level 2 accept/reject trigger decision is made for each Level 1 accept following a variable latency time. Level 2 accept/reject decisions are issued in the same order as Level 1 accepts.
4. A Level 3 accept/reject trigger decision is made for each Level 2 accept as part of the data processing performed on data flowing through the DAQ subsystem. For events accepted by Level 3, some or all of the event data is written to permanent storage.

Trigger Inputs

5. Level 1 triggers obtain their input data directly from the FEE independent of the DAQ.
6. Level 2 triggers can either obtain their input data independent of the DAQ or use the DAQ interface with the FEE to collect data.
7. Level 3 processors receive their input from the DAQ.

Trigger Outputs

8. The trigger and/or associated gating logic will supply all fast trigger, clock, and control signals to the FEE.

9. Data blocks will be sent to the DAQ in the same sequence as Level 2 accepts are received so that data blocks in the DAQ are ordered according to crossing number.
10. Each data block will have a common format for all detector subsystems. The format will include tags that allow checking if the data is correctly associated with the event. Data blocks will have a fixed channel ordering.
11. Under normal running conditions, the size of a data block has a well defined maximum.
12. The FEE may use the DAQ data path to send data to the Level 2 trigger provided standard DAQ protocols are used.
13. A detector component may send either partial or complete event information to the trigger subsystems. For partial event transfers, the FEE must send the event data to the DAQ. For complete event transfers, the trigger subsystem may pass the event data for that component to the DAQ. These rules allow FEE designs that transfer all event data following a Level 1 accept and do not provide Level 2 buffering.
14. There will be a standardized set of control signals provided to the FEE by the DAQ and trigger subsystems.
15. Each FEE will provide the DAQ complete event data for each Level 2 accept received by the FEE. Ambiguities that would result from more than one trigger within the resolving time of a detector component will be resolved by either suppressing closely spaced triggers and/or resolving such ambiguities in the FEE (i.e., no marred events).

3.3. Online Computing

The online computing subsystem provides services, resources, and an environment for computing tasks associated with data taking.

1. The online subsystem will be capable of accepting events from a variety of sources, including the DAQ, storage media, and network connections.
2. The online subsystem will be capable of logging events to a permanent storage media at the maximum Level 3 trigger rate.
3. Calibration, monitor, control, and error information will be logged to permanent storage as needed.
4. Event dumps will be provided for monitoring, event display, and physics analysis tasks.
5. The online subsystem will provide high level run control for the experiment and allow the experiment to be controlled from various locations.

Revision History

This is the first version of the Data Acquisition Design Requirements and Functional Specifications Document to be given general circulation within SDC. Several earlier drafts were circulated to members of the data acquisition, trigger, and front end electronics groups and discussed at various data acquisition and collaboration meetings. This rather extensive review has allowed many helpful suggestions to be incorporated and led to a document which we believe represents the broad consensus of the data acquisition group. Undoubtedly, there are still many areas where further improvements could be made. It is our intention to update and ammend this document as needed to reflect ongoing progress in design and construction of the SDC data acquisition subsystem. Please send comments or suggestions for improvement to PARTRIDG@BROWNVM.

2. DAQ Design Requirements

The essential function of the DAQ is to move data from the front end electronics to permanent storage in response to an event meeting trigger conditions. In addition, the DAQ design must satisfy a number of more specific design requirements:

1. The DAQ must maintain the integrity of the data.
2. Events must not be lost or rejected by the DAQ except as a result of a triggering decision.
3. The DAQ must not lose event data except for occasional data loss in certain FEE channels with exceptionally high occupancies or as the result of a reset operation.
4. The DAQ must employ a flexible partitioning scheme to allow testing, calibration, data taking, and detector commissioning in parallel, with minimal interference.
5. Robust control and monitoring of DAQ operation must be provided.
6. The DAQ must provide for processing of the event data at well defined points in the data path.
7. The DAQ must provide a high-level human interface with a versatile, uniform, and easy to use environment for control and monitoring of DAQ operation.
8. The DAQ must be modular and have well defined interfaces and functionalities.
9. Provision must be made for substituting improved designs and or new technologies as appropriate.
10. Smooth upgrade paths must allow for the addition of channels, detector components, trigger units, and processing elements.
11. The DAQ must be scalable over a wide range of bandwidths and provide a means for increasing the DAQ bandwidth to cover the expected range of hardware trigger rates and event sizes (see section 3.5).
12. The DAQ must be testable, reliable, maintainable, and incorporate fault tolerance.
13. DAQ subsystems must be available as needed by SDC for electronic and detector system tests, test beam experiments, and commissioning of the experiment.
14. The DAQ must be efficient and cost effective.

9. **The trigger subsystem is a detector component that generates data associated with each event. Furthermore, detector subsystems that send digitised event data to the trigger may require the trigger to forward the data to the DAQ.**
10. **The trigger subsystem will send all such event data to the DAQ using standard DAQ formats and protocols.**

Trigger Gating Logic

11. The gating logic suppresses triggers when there is a DAQ or FEE condition that may lead to data loss, such as imminent buffer overflow.
12. The gating logic passes Level 1 accept and Level 2 accept/reject signals to the FEE when the experiment is alive. Deadtime is introduced by either suppressing the Level 1 accept signal or converting Level 2 accept signals to Level 2 reject signals.
13. The gating logic measures the deadtime for the experiment and no other component is permitted to independently introduce deadtime.
14. The gating logic will work with the luminosity monitor to provide the live-time gated luminosity. Note that the luminosity will vary among the machine bunches and may need to be recorded separately for each bunch.
15. The DAQ will supply the gating logic with busy signals as needed to detect conditions that may lead to data loss. Once a Level 2 accept is issued to the FEE, the event data will be sent to the selected Level 3 processor node(s) and, if accepted by the Level 3 trigger, be logged to permanent storage.
16. The gating logic may limit the number of triggers issued in a particular time interval or the number of Level 1 triggers pending a Level 2 decision to prevent buffer overflow in the front end electronics.
17. The gating logic interacts with the human interface to start and stop data taking.

3.2. Front End Electronics

The Front End Electronics (FEE) provides the DAQ with digitized detector data in response to trigger accepts.

1. Detector data relevant to a given beam crossing is stored by the FEE until the Level 1 trigger decision for that beam crossing is received.
2. Following a Level 1 accept, the FEE will continue to store such data until a Level 2 trigger decision is received.
3. Following a Level 2 accept, the FEE will send blocks of data to the DAQ that contain all data relevant to the beam crossing that generated the Level 2 accept.

6. **Monitoring packages will be provided to monitor the event data, certain non-event data such as HV, and the operation of the online subsystem.**
7. **The online subsystem will provide a variety of software tools, including various databases for calibration constants and detector parameters, graphics and histogramming packages, code management and development software, and a consistent human interface to the experiment.**

3.4. Slow Control

The slow control subsystem provides a unified monitoring and control environment for the detector.

1. The control subsystem will employ front-end instrumentation, processors, communications, and control software to monitor and control those parts of the detector not under direct control of the online or DAQ subsystems.
2. Supervisory consoles will be provided for direct access to controlled systems.
3. The control subsystem will provide the online DAQ the status of any controlled or monitored parameter on demand.
4. An interlock system based on calculated permissives will be employed to allow the online DAQ subsystem access to selected control subsystem functions.

3.5. Preliminary DAQ Design Parameters

Table 1 summarizes the currently accepted estimates of SDC design parameters relevant to the DAQ subsystem. It is expected that the DAQ design should be scalable over a range of luminosities with only minor upgrades required. Table 1 includes parameter sets for the initial design luminosity and for an upgraded DAQ operating at high luminosity. Note that these parameters have not received careful study and should be considered estimates rather than specifications.

Table 1. SDC DAQ Preliminary Design Parameters

Parameter	Design $\mathcal{L}$	High $\mathcal{L}$	Units
Maximum Luminosity	10^{33}	10^{34}	cm^2s^{-1}
Beam Crossing Rate	62.5	62.5	MHz
Maximum Interaction Rate	10^8	10^9	Hz
Level 1 Trigger Rejection Factor	$10^2 - 10^4$	$10^4 - 10^5$	
Expected Level 1 Trigger Rate	10^4	10^4	Hz
Maximum Level 1 Trigger Rate	10^5	10^5	Hz
Level 2 Trigger Rejection Factor	$10^1 - 10^2$	$10^1 - 10^2$	
Expected Level 2 Trigger Rate	10^2	10^2	Hz
Maximum Level 2 Trigger Rate	10^4	10^4	Hz
Level 3 Trigger Rejection Factor	$10^2 - 10^3$	$10^3 - 10^5$	
Expected Level 3 Trigger Rate	10^1	10^1	Hz
Maximum Level 3 Trigger Rate	10^2	10^2	Hz
Deadtime at Maximum Trigger Rate	< 10	≈ 15	%
Deadtime from DAQ Errors and Downtime	< 5	< 5	%
Level 1 Trigger Latency	2 - 4	2 - 4	μs
Maximum Level 2 Latency	100	100	μs
Average Level 2 Processing Time	< 10	< 10	μs
Time to Process an Event in Level 3	100 – 1000	100 – 1000	MIPS-sec
Farm Processing Power	$10^5 - 10^6$	$10^5 - 10^6$	MIPS
Number of Processors in Farm	500 – 5000	500 – 5000	
Average Event Size for Full Event	0.1 – 1	0.1 – 1	MB

4. Scope of the DAQ Subsystem

The scope of the DAQ subsystem is perhaps best specified by defining its boundaries with the subsystems it connects to. In the sections below, we define the boundaries between the DAQ subsystem and the trigger, front end electronics, online computing, and slow control subsystems.

4.1. Trigger

1. The Level 1 triggers obtain their input data directly from the FEE and are independent of the DAQ.
2. The Level 2 triggers receive their input data either directly from the FEE or through the DAQ.
3. The Level 3 hardware and software environment is a DAQ responsibility. Level 3 trigger algorithms are the responsibility of a Level 3 software trigger group to be established.
4. All trigger levels provide data to the DAQ and use standard DAQ protocols and data paths.
5. The gating logic and distribution of fast timing, trigger, and control signals is the responsibility of the trigger group. The Trigger, DAQ, and FEE groups will jointly define the functionality and signals needed for the gating logic.

4.2. Front End Electronics

1. An interface between the FEE and DAQ subsystems will be developed that conforms to the needs of both subsystems.
2. The FEE-DAQ interface will specify protocols for communication between the FEE and DAQ that are to be maintained across the detector.

   The FEE and trigger groups will jointly develop a mechanism for implementing calibration and test triggers. Such triggers may require special handling by the DAQ. For example, pedestal events are not zero-suppressed and may exceed normal restrictions on data block size. Calibration events may also be processed differently by processors embedded in the DAQ.

4.3. Online Computing

1. An interface between the DAQ and online subsystems will be developed that conforms to the needs of both subsystems.
2. The DAQ subsystem is responsible for the data path up to the DAQ online interface.
3. The online subsystem is responsible for logging events and any processing that is done after the Level 3 processor farm.
4. The online subsystem will provide high level run control for the experiment.

4.4. Slow Control

1. An interface between the DAQ and control subsystems will be developed that conforms to the needs of both subsystems.
2. The DAQ and control groups will jointly define the division of monitoring and control tasks.
3. A standardized package of hardware, communications, and software will be developed jointly by the DAQ and control groups that will be used where feasible.

5. DAQ Functional Specifications

This section provides functional specifications that describe architectural choices and DAQ functionality chosen by the DAQ group to implement the design requirements in section 2. The functional specifications given below are still quite general in nature and can be met in various ways; detailed implementation of the specifications will occur at a later stage in the design cycle.

The DAQ functional rompponents, principle communication paths, and connections with other subsystems are shown in figure 1. A data collection network funnels data from a large numbers of FEE and trigger inputs to a small number of high-speed data paths. This data is ordered into complete events by the event builder and sent to the processor farm, where a Level 3 trigger decision is made. Accepted events are then transferred to the online subsystem for permanent storage and further processing. DAQ control is responsible for controlling data flow in the DAQ and interacts with the trigger gating logic to suppress triggers when a busy condition exists. Interfaces are provided for the front end electronics, trigger, online computing, and slow control subsystems. The sections below define the functional specifications for each of these components.

5.1. Data Collection Network

Organization of the Data Collection Network

1. Groups of FEE channels are formed that output their data into "data funnels." The FEE channels and data collection elements that share a common funnel form a "DAQ segment."
2. A funnel has one or more layers of data collection. Each node in the first layer collects data from several FEE outputs and provides a single output to the next layer. Nodes in successive layers collect data from several outputs of the preceding layer and provide a single output to the next layer. The last layer has one data collection node that puts its output data into a "segment output buffer."
3. There can be multiple segments per detector component. Segments do not span detector component boundaries. The trigger is a detector component with one or more segments.

Data Collection Specifications

4. The output of a data collection node is a stream of data blocks with a format to be defined.
5. The FEE or data collection network will add an identification tag to the data block that uniquely identifies the event and is common to all data blocks for the event within a data collection segment.

6. **The data collection network will check the integrity of the data and report errors as part of the data block.**
7. The data collection network will provide a fixed ordering of the data block to assist pattern recognition algorithms and aid error diagnostics.
8. Every data collection node will be able to detect the beginning and end of data transfer into the node for each event.
9. Data blocks must be self-contained and unambiguous. If, for example, the bunch crossing number is needed to compute a drift time, this number must be included in the data block.
10. The data collection network will provide buffering as needed to derandomize the data flow, minimize deadtime, and avoid buffer overflow.
11. All data collection buffers will be capable of accepting downloaded data for testing and diagnostic purposes.
12. The output buffer of a data collection funnel will be able to store multiple events. It will allow non-destructive readout of an event and provide a means for flushing events. Data in the buffer should be available for test, diagnostic, and monitoring purposes via an industry standard bus.
13. A data collection node can process and change data and markers. Header information can be added to the data and redundant headers from data collection inputs can be eliminated.
14. The data collection network will provide DAQ control with the information needed to prevent buffer overflows in the FEE or data collection network.

5.2. Event Builder

Event Builder Functionality

1. The event builder makes data in the data collection output buffers available to one or more processors in the Level 3 processor farm.
2. Events accepted by the Level 3 trigger are assembled into event records containing all of the data to be permanently recorded.
3. The event builder may optionally provide a Level 3 processor with a subset of the data available in the data collection output buffers. This may be useful in cases where limited information is needed for the Level 3 decision or for monitoring and calibration tasks that need access to a subset of the data. The event builder will still be able to build complete events if accepted by the Level 3 trigger by transferring the remaining data.
4. The event builder functionality may optionally be provided as part of the farm. For example, the segment output buffers can be part of the farm, with the internal farm bus or network used to access the data. Alternatively, the event builder may be a separate component that outputs events to the appropriate processor(s).

Event Builder Specifications

5. The event builder will be able to route events to multiple destinations.
6. Routing of data through the event builder may depend on trigger type and processor availability. The event builder may use the identification tags in the data packet to determine the proper routing.
7. The assembled event records will maintain the ordering that exists in the segment output buffer. It may be useful to have a fixed ordering of such data blocks in the assembled event record.
8. The event builder may add header or trailer information to the event record.
9. All data blocks sent to the event builder will be routed to the appropriate processor(s) with no loss of data.

5.3. Processor Farm and Level 3 Trigger

Processor Farm Functionality

1. The Level 3 trigger uses software algorithms running in a farm of processing nodes to select events for logging to permanent storage media.
2. Some processing nodes may be running monitor, calibration, or spy tasks and receive their own copy of the event data.
3. Even though an event may be sent to multiple processors, only one processor will be charged with making a Level 3 trigger decision for that event.

Processor Farm Hardware Specifications

4. The processor farm should be expandable and extrapolable to take advantage of future improvements in computing technology and the potential need for increased Level 3 processing as the luminosity increases.
5. The processor farm will be able to obtain event data from the following sources: the event builder, the data logger, and network connections to the online computing system.
6. The Level 3 trigger may use special purpose processing elements such as neural networks or digital signal processors to supplement the computational capability of the general purpose farm processors.
7. The general purpose farm processors will be commercially available.
8. A mechanism will be established to prevent loss of data when the processing nodes in a given time are busy.

Processor Farm Software Specifications

9. **The Level 3 general purpose processors will be able to run most offline reconstruction code without modification.**
10. **Algorithms developed for the Level 3 trigger should generally be able to run on standard offline processors to accommodate development and testing of the code. All parts of the Level 3 trigger code that cannot run on offline processors will have routines supplied that emulate the action of such code.**
11. The processor farm is not required to perform offline processing. Nevertheless, it may be useful to provide this capability.
12. Network access will be provided to the processor farm nodes with appropriate security protection to allow downloading, control, and symbolic debugging of programs running in the farm.
13. The Level 3 algorithms may add data to the event block.
14. A mechanism will be provided to collect statistics, histograms, and other data from processors in the farm.

5.4. DAQ Control

1. DAQ control will interact with the data collection network, event builder, and processor farm to detect a "busy" condition where further triggers may lead to data loss.
2. DAQ control signals will be provided to the trigger gating logic to allow the suppression of further triggers when a busy condition exists.
3. DAQ control will determine the routing of events to processors in the farm.
4. DAQ control will provide a high-level human interface to the DAQ subsystem that allows control, configuration, and monitoring of the DAQ operation.

5.5. Interfaces

1. Well-defined interfaces will be developed for the four subsystems the DAQ is connected to: FEE, trigger, online computing, and slow control.
2. An interface may include one or more of the following: a bus standard, communications standards and protocols, a software interface, and standardized interface hardware.

   The FEE and trigger interfaces to the DAQ will be identical and include data readout, control, monitoring, and downloading capabilities.
3. The online interface will include bi-directional event transfer between the online and processor farm, and a mechanism for collecting statistics, histograms, and other data from the farm processors.

5. **The slow control interface will allow DAQ to monitor any controlled parameter allow access to selected control functions.**

6. DAQ System Issues

In this section we identify functionality and specifications that relate to the DAQ subsystem as a whole.

6.1. Partitioning and Dynamic Segment Selection

Partitioning is the act of logically dividing the detector into two or more independent subdetectors with independent control, DAQ, triggering, and deadtime. Dynamic segment selection allows partial readout of a partition depending on trigger type.

Goals for Partitioning

1. Partitioning should facilitate testing and commissioning of the detector components, FEE, trigger, and DAQ by allowing groups to work on different detector components with minimal interference.
2. Partitioning should allow calibration, diagnostic testing, monitoring, and data taking tasks to take place simultaneously and independently of one another in separate partitions. It should also be possible to combine these tasks within a partition, provided they don't interfere with one another.
3. Partitioning should reduce bandwidth requirements by suppressing readout of irrelevant data blocks. This may be particularly useful in obtaining high rates for calibration and monitoring events.

Granularity of Partitioning

4. The smallest partitionable unit is a data collection segment. A data collection segment consists of a set of FEE with common fast control signals feeding a single data collection funnel, filling the data collection output buffer.
5. Each data collection segment will be able to efficiently run at the maximum Level 2 trigger rate.
6. The granularity of data collection segments will be sufficiently fine to significantly increase the efficiency achieved by partitioning or dynamic segment selection (see below).
7. Data collection segments should divide the detector components symmetrically into geometrically similar regions. The DAQ segmentation of a given detector component should have a simple mapping to the segmentation used for other detector components.

Partitioning Specifications

8. A partition is a set of data collection segments that respond to a common gating logic. A data collection segment is a member of at most one partition.

9. **Each partition will acquire data independently of other partitions. In particular, each partition will have independent run control, independent operation of the gating logic, and independent deadtime.**
10. A partition will operate in either stand-alone or combined mode. In stand-alone mode, the partition will do its own event building, processing, and data logging. In combined mode, the partition will feed data to the event builder using the usual data links.
11. For a combined-mode partition, it is desirable to be able to assign subsets of the event builder, processing farm, and data logger to the partition so they operate independently of other partitions. The extent to which these components can be divided among partitions needs to be established.
12. Each major detector subsystem will be capable of being operated as one or more stand-alone partitions with independent gating logic, local trigger interface, event processing, human interface, and data logging components. Such a stand-alone partition is not required to operate at the trigger rates given in section 2.5.
13. The configuration of segments into partitions may be changed by software between data runs. Segments not involved in such a reconfiguration will not be significantly disturbed by reconfiguration.
14. The partitioning scheme will be simple and reliable.

Dynamic Segment Selection

15. Dynamic segment selection will allow subsets of the data collection segments in a partition to be read in response to certain trigger types.
16. The ability to dynamically select segments of the detector is motivated by the possible need for high rate calibration events that require readout of only part of the detector.
17. The trigger type is used to determine which segments are read, and the subset of segments read can change from event to event. The correspondence between trigger types and segments to be read does not change during a run.
18. The gating logic may implement dynamic segment selection by sending Level 2 reject signals to those segments that are not part of the readout. Alternatively, the unwanted segments could be discarded in the event builder or Level 3 farm, if sufficient bandwidth is available in the data collection network and event builder.
19. While the Level 2 sequence may be different for different segments, all data within a segment should have an identical Level 2 sequence number. The DAQ will add a unique event number to each segment's data block that can be used to associate data from different segments with a given event.

6.2. Data Integrity

Maintaining data integrity is one of the most important requirements for the DAQ subsystem.

Data Integrity Specifications

1. The DAQ will provide means for error detection, smooth error recovery procedures, and a high level of reliability in the DAQ subsystem.
2. Error detection and recovery should not add significantly to the overall experiment deadtime.
3. The DAQ will be able to detect and handle single errors in a data block, including corrupted pointers or word counts.
4. When event data is suppressed due to errors, error information will be added to the data block.
5. Error diagnosis will be possible in the absence of physics data.
6. Reliability for DAQ components located in areas not easily accessible will be sufficiently high as to not significantly degrade the performance of the detector. Where single component failure would seriously degrade detector performance, redundancy will be employed to minimize the risk.
7. Segmentation and DAQ topology will be chosen such that minor failures or errors do not significantly degrade the physics capabilities, alter the efficiency of triggers, or hamper monitoring.
8. The DAQ will have sufficient modularity and testability to quickly localize problems to a replaceable module.

7. The Portable DAQ

The portable DAQ is to be used for small scale detector and electronic system tests. It is anticipated that a minimal portable DAQ might be contained in a single crate, yet provide much of the functionality of the SDC DAQ. The DAQ architecture allows the operation of stand-alone partitions, with the partition consisting of at least one data collection segment. The portable DAQ would constitute such a stand-alone partition, with the local trigger interface simulating the action of the trigger and one or more processors accessing the data in the output buffers of the data collection segments. The portable DAQ will also include a human interface, a local gating logic, and the ability to log data.

The portable DAQ is also an important tool for detector integration. By providing the various detector components with portable DAQ systems, the detector groups will be prepared for integration into the SDC DAQ subsystem where they will use the same hardware and software hooks that worked with the portable DAQ.

8. DAQ Design Cycle

The DAQ design cycle will proceed in a series of clearly identifiable stages:

1. Preparation of the present document defining the SDC DAQ design requirements and functional specifications.
2. Preparation of a baseline DAQ design, schedule, cost estimate, and other matter as needed for inclusion in the SDC technical proposal.
3. Preparation of detailed rules documents that provide detailed specification of the interfaces between the DAQ subsystem and the FEE, trigger, online computing, and slow control subsystems.
4. Design studies of alternative DAQ designs, including simulation studies of various DAQ components and architectural variations, leading to selection of a DAQ design. Major design decisions will be preceded by a technical review of alternative designs by an appropriate review committee. Design decisions will be staged so that early decisions are made in those areas with long lead-time while allowing continued technical progress and commercialization where the lead-time is short.
5. Construction of a prototype hardware interface between the FEE and DAQ.
6. Development of a portable DAQ system for use in electronics and detector system tests.
7. Development of a DAQ system for use in the test beam program.
8. Final design, construction, and commissioning of the SDC DAQ subsystem.

It is expected that there will be periods of more than one of these stages at any given time and that a number of iterations will be required to achieve the goals of SDC.

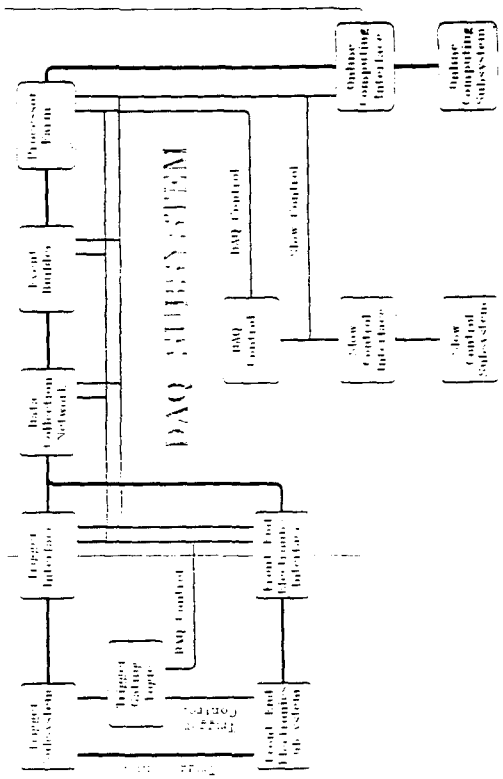


Figure 1 DAQ data flow, control, computing, and connections to other subsystems

++++++ DRAFT ++++++

SDC Data Acquisition System Conceptual Design

September 24, 1991
Ed Barsotti

The September 4, 1991 first draft of this document was reviewed by the SDC Data Acquisition Working Group at a September 5, 1991 meeting at Fermilab. Comments received at that meeting are incorporated into this document. Additional sections not yet completed have been added both as a result of the meeting and for document completeness. Drafts of these sections will be completed within a few weeks.

SDC Data Acquisition System Conceptual Design

Table Of Contents

1 Introduction 1
2 General Description 2
3 Data Acquisition System Development Infrastructure 6
4 Data Acquisition System Slow Controls Network 7
5 SDC Standard DAQ Interface Crates, Power Supplies, Backplanes, Etc. 9
5.1 Crates & Power Supplies 9
5.2 Backplanes 9
6 SDC Standard DAQ Event Data Readout & DAQ Slow Controls Interface 11
6.1 DAQ CPU Modules 11
6.2 DAQ Event Data Readout & Slow Controls Slave Interface 11
6.3 DAQ Crate Adapter/Interface Modules 11
6.4 Event Data Links 14
6.5 Event Data Link Transmitter/Receiver Test Modules 15
6.6 DAQ Slow Controls Remote Links & Repeaters 15
7 Alternative Approach To Commissioning & Readout...System Readout Crates 16
8 Event Builder Subsystem 17
8.1 Commercial Switching Network-Based Subsystem 17
8.1.1 Input Interface & Data Balancing Network 18
8.1.2 Input Queueing Network 18
8.1.3 Commercial Switching Network 19
8.1.4 Interface To The Online Processor Subsystem 19
8.1.5 Event Builder Subsystem Segmentation 20
8.2 Alternative Implementation #1...In-House-Designed Switching Network 20
8.2.1 Switching Network Implementation Details 20
8.2.2 Example Implementation 23
8.3 Alternative Implementation #2...Dual-Ported RAM-Based Subsystem 23
9 Event Data Flow Control Subsystem 24
9.1 Event Data Flow Control Unit 24
9.2 Send Event Links & Repeaters 24
10 Online Processor Subsystem 25
10.1 Processors 25
10.2 Event Request Links 25
10.3 Links To The Online Storage Subsystem 25
11 Data Acquisition System Control Computing Interface 26
11.1 Runtime User Interface 26
11.2 Control, Monitoring & Downloading User Interface 26
11.2.1 Applications Software For Supporting The Use Of Memories & Intelligent Processors 27
11.2.2 Applications Software For Supporting "Slow" (Non-Event) Data Acquisition 27
11.2.3 Applications Software For Supporting Unusual Occurrences 28
11.2.4 Applications Software For Supporting The Control & Monitoring Of Adjustable Devices 28
12 Data Acquisition System Offline Analysis Interface 29
13 Electronics Rack Protection Subsystem 30
14 System Partitioning & Dynamic Segment Aiocation 31
15 Errors, Error Detection & Error Handling 32

16 Schedule, Costs & Manpower Requirements 33
17 Possible Critical Path Items 34
18 Major Milestones 35
19 References 36

1 Introduction

The following sections contain a general description of the conceptual design of the SDC Data Acquisition System and brief descriptions of the system's major functional elements. The major functional elements described here do not represent what will actually be built, or even what will be described in the data acquisition section of the technical proposal. Rather, this writeup is merely a first attempt at a more detailed and believable Data Acquisition System for the SDC. Certain technical choices must be made in this design to allow the full system to be costed, but it is expected that these choices will all be reexamined in the light of the Data Acquisition System requirements documents that are currently being prepared.

The major (and most obvious) job of the Data Acquisition System is to collect the digital data that represents each event selected by the Trigger System and record this data on some permanent storage medium for later offline analysis. Somewhat less obvious but no less important, the Data Acquisition System must also insure the integrity of the event data stream. This involves a whole series of tasks ranging from providing calibration and monitoring services, to error handling and alarm systems, to recording various "non-event related" data streams (magnet currents, high voltages, accelerator parameters, etc.), to controlling the various processors and modules in the system, to delivering events to consumer processes for miscellaneous on-line monitoring purposes. Interfaces must also be provided to the Front-End Systems, to the Trigger Systems, to the Control System, and to the Online Computing System.

Until it is known which parts of the front-end electronics can be non-functioning and still have acceptable physics, additional required reliability/redundancy hardware and software for different components of the Data Acquisition System, specifically those on or near the detector, can not be costed in this document.

2 General Description

The general requirements of the SDC Data Acquisition System are given in Version 0.99 of the "SDC Data Acquisition Design Requirements And Functional Requirements" document dated September 5, 1991. This document was written by SDC data acquisition collaborators and has been distributed to the SDC collaboration.

Figure 1 is the data flow diagram for the SDC detector submitted as part of the SDC EoI. The figure illustrates a typical and a maximum Data Acquisition System bandwidth requirement to the online processor subsystem (Level 3) of one and ten gigabytes/second, respectively. It appears that both a descoped detector and more detailed studies of event size will result in a smaller event size and reduced data rate requirements. Perhaps 500 megabytes/second typical and 5 gigabytes/second maximum are more appropriate bandwidths to the online processor subsystem

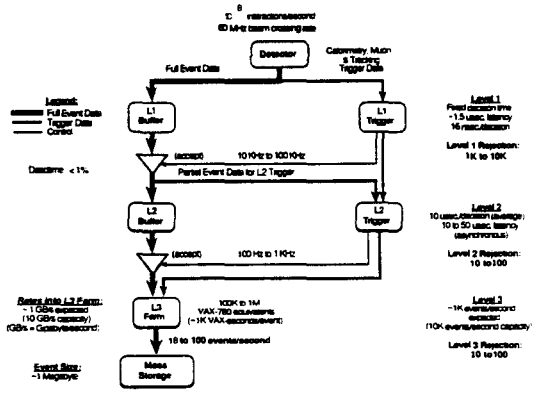


Figure 1
SDC Event Flow Diagram

Figure 2 is a WBS item-based block diagram of the SDC Data Acquisition System showing both its internal (WBS Item 5.2) interconnections and major functional components and its external connections to other SDC systems. The Electranics Rack Protection Subsystem includes all cooling and rack protection equipment for Front-End/Trigger System Data Acquisition System interface crates, the Event Builder Subsystem, the Event Data Flow Control Subsystem, the Online Processor Subsystem and the Offline Analysis Interface Subsystem.

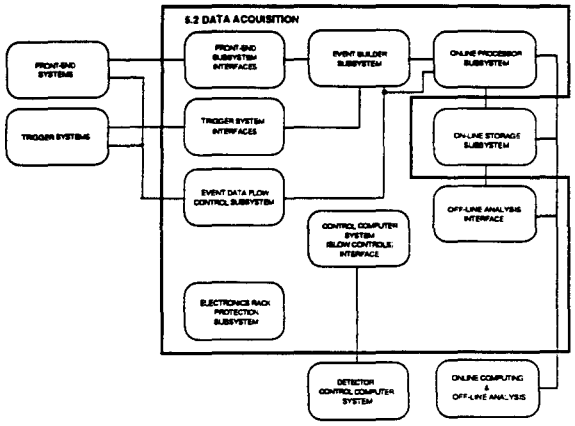


Figure 2
SDC Data Acquisition System
WBS Item-Based Block Diagram

The SDC Data Acquisition System will provide crates, power supplies, readout devices (DAQ CPUs), etc. to Front-End and Trigger Systems to ensure uniform and SDC standard interfaces to the Data Acquisition System. For each SDC Front-End and Trigger System, Table 1 lists the number of crates needing direct connection to the Data Acquisition System s downloading, monitoring, etc. (DAQ Slow Controls) link, the number of event data sources to the Data Acquisition System's Event Builder Subsystem, whether the crates will probably be SDC DAQ Standard Interface crates or special Front-End System-specific crates and the location of the crates.

To date, all crates except those of the Inner Tracking Silicon Strips and Silicon Pixels have been costed in their respective Front-End or Trigger System costs. The quantities in Table 1 are

304

"detector-descoped" quantities resulting from the last SDC Collaboration meeting and subsequent discussions. The crate types in Table 1 are presumed and thus not actually decided upon yet. A recent change in the Central Calorimeter (SCAs) and Shower Max systems resulted in removing all their counting room crates and the crates buffer module interfaces to the Data Acquisition System in favor of including DAQ CPU modules in all their "on-detector" crates. Intermediate "counting room" crates are no longer necessary as the "on-detector" crates now interface directly to the Data Acquisition System as in other front-end systems.

Front-End/Trigger System	# Crates	# Sources	Crate Type	Location
Inner Tracking Silicon Strips & Inner Tracking Silicon Pixels	10	10	SDC DAQ Std.	Counting Room
Outer Tracking Straw Tubes	16	16	SDC DAQ Std.	On Detector
Outer Tracking Scintillating Fiber & Intermediate Tracking Scintillating Fiber	14	14	Special	On Detector
Central Calorimeter (SCAs) & Central Calorimeter Shower Max	96	96	SDC DAQ Std.	On Detector
Central Calorimeter (Flash ADCs)*	96	96	Special	On Detector
Forward Calorimeter	2	2	SDC DAQ Std.	Counting Room
Muon (Wires)	48	48	SDC DAQ Std.	On Detector
Muon (Counters)	16	16	SDC DAQ Std.	On Detector
Level 1 Trigger (<= 1 KB/crate)	40	40	SDC DAQ Std.	Counting Room
Level 2 Trigger (<= 1 KB/crate)	30	30	SDC DAQ Std.	Counting Room
Totals:	272	272		

* Central Calorimeter (Flash ADCs) not counted in totals

Table 1
Descoped Quantities
Crates With DAQ CPUs & Front-End/Trigger System Event Data Sources

Figure 3 is a simplified block diagram of the event data readout components of the Data Acquisition System. Crates are used to interface all the Frant-End and Trigger Systems to the Data Acquisition System. With the Central Calorimeter (SCA) and Shower Max implementation change described above, all event data is read out by the Data Acquisition System CPU module (DAQ CPU) over the crate's bus and then sent to the Event Builder Subsystem

Event data flow is as follows. The Trigger System initiates front-end scanning via a Level 2 trigger accept message sent to front-end devices and DAQ CPUs over links not shown in Figure 3. The Event Data Flow Control Subsystem receives trigger accept and other event information from the Trigger System and event requests from processors in the Online Processor Subsystem via the Event Request Link(s). At the appropriate times, the Event Data Flow Control Subsystem initiates event data transmission from DAQ CPUs or buffer modules via a message sent over the Send Event Link(s). This message can be sent even without any requests for events from the Online Processor Subsystem because of the additional input buffering in the Event Builder Subsystem. This feature allows more efficient use of the system's buffering capabilities and thus less system deadtime. The Event Builder Subsystem also receives a similar message

305

over the Processor Ready/Send Event Link (with additional destination information) to inform it that an event can be sent through its switching network (see Section B) and onto the Online Processor Subsystem. The message sent over the Sent Event Links may be incorporated into one of the high-speed trigger cables to all front-end and trigger crates.

A link from the Event Builder Subsystem (EBS) to the Event Data Flow Control Subsystem (EDFCS) notifies the EDFCS that the EBS is running low on input buffer space and that triggers may need to be throttled or even inhibited for a short while. The Event Request Link(s) performs a similar function for the Online Processor Subsystem.

A mechanism for throttling or inhibiting triggers as a result of DAQ CPU or buffer module buffer space becoming full is also included in the Data Acquisition System. Details are not worked out yet. A special message from a DAQ CPU module or a buffer module over an Event Data Link is a possible mechanism for this trigger throttle.

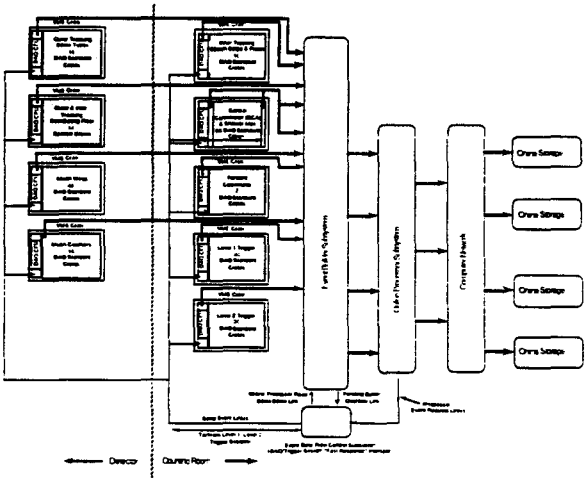


Figure 3
SDC Data Acquisition System
Event Data Flow Block Diagram

306

3 Data Acquisition System Development Infrastructure

307

This item includes specification, procurement, etc. of software and hardware items such as CASE and CAE workstations, logic state analyzers, operating systems, software licenses, etc. which are not specific to any particular Data Acquisition System component or subsystem but are general development infrastructure items used in many areas of Data Acquisition System development. Additional software and hardware items needed in addition to the above infrastructure items for the development of specific Data Acquisition System components or subsystems were costed as part of the component or subsystem costs.

Infrastructure costing assumed that, collectively, institutions working on the SDC Data Acquisition System already had roughly one half the infrastructure required for development, integration, installation and checkout of the Data Acquisition System. Examples of infrastructure items and their unit cost are given below:

Item Description	Unit Cost
- CASE workstations & software for software development	$70.0K
- CAE workstations & software for hardware development	100.0K
- PC-like workstations & software for hardware development	12.0K
- Test equipment	
- Logic state analyzer	35.0K
- Digital oscilloscope	12.0K
- Networking equipment & software	15.0K
- Additional archival equipment & software	15.0K
- Hardcopy equipment & software	15.0K

4 Data Acquisition System Slow Controls Network

The detector has an overall Control Computer System with an interconnecting network to various systems such as the Data Acquisition System. The network, called the Slow Controls Network, is used for downloading, monitoring, alarms & limits, etc. for the entire detector. This network is extended into the Data Acquisition System where it becomes the Data Acquisition (or DAQ) Slow Controls Network. Databases in various Control Computer System computers and the network bridges shown in Figure 4 segment the DAQ Slow Control Network by Front-End System and Trigger System. This segmentation allows parallelism during Data Acquisition System downloading, etc. for increased throughput, allows commissioning, debugging, etc. of each Front-End or Trigger System independent of any other system. For example, by adding the workstations as shown in Figure 4 or assigning a Control Computer System computer to a Front-End or Trigger System's "segment" of the DAQ Slow Controls Network, that part of the DAQ Slow Controls Network functions independently of the rest of the network. A secondary method for event data readout is also provided by the DAQ Slow Controls Network. Section 7 describes an alternate approach for segmenting Front-End or Trigger Systems for both commissioning and event data readout functions. DAQ Slow Controls segmentation and the workstation on the segmented network approach removes the need to have a crate through which all of a particular Front-End or Trigger System's event data passes as described in Section 7.

An Ethernet/Thinwire Ethernet DAQ Slow Controls Network was costed but the "network of choice" at the time of production ordering would actually be used in the Data Acquisition System. A serious concern yet unresolved is whether the network has high enough bandwidth such that, for example, the time it takes to download the Data Acquisition System is not excessive. Further studies are required to answer this question.

The Data Acquisition System requires that every front-end or trigger crate or component needing downloading, monitoring, etc. be interfaced to the DAQ Slow Controls Network via one of the following two methods. The first and most preferred method, requires the following:

- Electronics to be packaged in crates.
- These crates house a SDC Standard DAQ CPU module.
- The DAQ CPU module can access any other module in the crate requiring downloading, monitoring, etc.
- If no special (to the Front-End or Trigger System) backplane with an interface to the bus of the DAQ CPU module is used, all modules in the crate requiring downloading, monitoring, etc. adhere to the SDC DAQ Event Data Readout & Slow Controls Interface specifications (see Section 6.3).

The second method is generally used for connecting Front-End or Trigger System components which are on the detector and not housed in crates to the DAQ Slow Controls Network. Over the last few years, industry has emphasized using a standard such as IEEE P1197 (Test Scan) for downloading, diagnosing, monitoring, etc. ASICs. If such a standard meets our requirements (e.g., throughput), this or another similar standard serial link would be provided by the Data Acquisition System for connecting this non-crate-housed electronics to the DAQ Slow Controls Network. Details of this remote link to the DAQ Slow Controls Network are given in Section 6.6.

No other methods other than the two aforementioned methods for connecting to the DAQ Slow Controls Network would be provided.

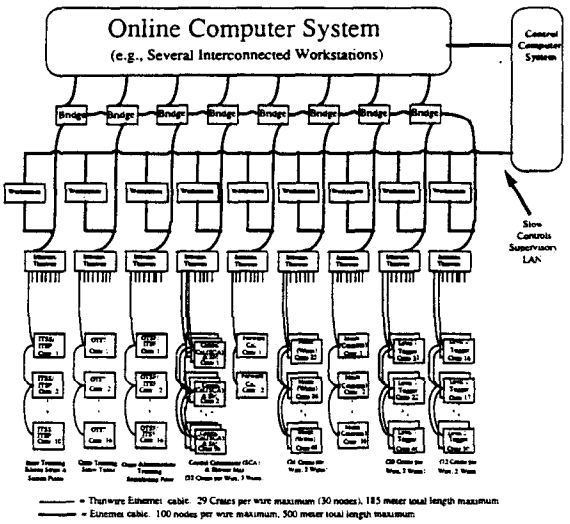


Figure 4
DAQ Slow Controls Network
Example Implementation

5 SDC Standard DAQ Interface Crates, Power Supplies, Backplanes, Etc.

5.1 Crates & Power Supplies

The Data Acquisition System implementers would provide Standard SDC DAQ Interface Crates, power supplies, a standard method to connect power to a crate and various other simple hardware "tools" such as module extenders, etc. All Front-End and Trigger System implementers will be strongly urged to use this equipment if at all possible. For example, if VMEbus was the bus of choice when production ordering occurred, powered and tested 9U x 400 crates (and/or 6U x 160 crates) would be provided. Power supplies and their technology (e.g., switching, linear, 400 cycles, etc.) are dictated by the needs of each Front-End and Trigger System. To date, all Front-End and Trigger System crates and their power, other than those for the Silicon Strips and Silicon Pixels Front-End Systems, have not been costed by the Data Acquisition System.

5.2 Backplanes

Just as for crates and power supplies, the Data Acquisition System implementers would provide standard backplanes for the Standard SDC DAQ Interface Crates.

Alternative backplane approaches not costed and needing further discussion could be provided to increase reliability and redundancy and/or to provide a Front-End or Trigger System implementer with more user space at the back of the crate for special interconnections and I/O requirements. Two data acquisition components to be described in detail in Section 6, DAQ CPU modules and DAQ Crate Adapter/Interface Modules, are mentioned below in order to help explain the alternative backplanes. The reader may wish to read about these components before continuing.

Figure 5 illustrates a VMEbus 9U x 400 crate with two high-density connector backplanes, two DAQ CPU modules and two DAQ Crate Adapter/Interface Modules. Each backplane would implement the full SDC Standard bus protocol (DAQ CPU bus interface). The two DAQ Crate Adapter/Interface Modules would allow remote control connection of either DAQ CPU (J1 and J2 connectors) to either high-density connector backplane. A dual or backup power supply system is also part of this implementation. The "user area" indicated on the figure is application specific and used generally for I/O and/or module to interconnection requirements. A single high-density connector backplane used only for increased "user area" when no additional redundancy is required would also be provided.

VMEbus was used above for example purposes only. The industry-supported bus most widely used and/or most cost effective at the time of production ordering will be used in the SDC Data Acquisition System.

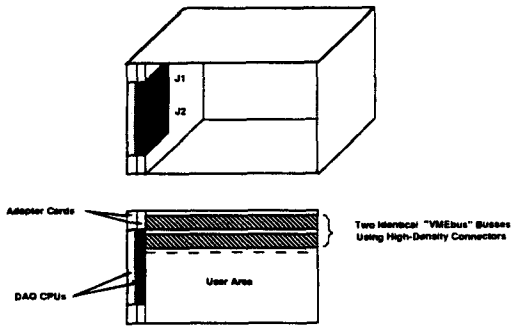


Figure 5
High-Density Connector Backplanes
For Redundancy And/Or Additional User Free Area

312

6 SDC Standard DAQ Event Data Readout & DAQ Slow Controls Interface

In order to simplify the commissioning, operation and maintenance of the SDC Data Acquisition System, the system provides a standard method by which all Front-End and Trigger Systems interface to the Data Acquisition System for both event data readout and slow controls functions. DAQ Slow Controls functions include downloading, control and monitoring of Front-End, Trigger and Data Acquisition System components. The standard SDC DAQ Event Data Readout & DAQ Slow Controls Interface components are described in the following subsections.

6.1 DAQ CPU Modules

A commercially-available microprocessor module, called the "DAQ CPU", will exist in each Front-End or Trigger System crate that connects directly to the DAQ Slow Controls Network and/or has its event data read into the Event Builder Subsystem. The DAQ CPU serves the dual role of interfacing front-end and trigger modules to both the DAQ Event Data Readout interface and the DAQ Slow Controls Network.

Event data readout and slow controls communication each have their own separate link. A mixture of Ethernet and Thinwire Ethernet was costed for the DAQ Slow Controls Network. A one gigabit/second link was costed for the Event Data Link. The network and link actually used in the final Data Acquisition System depends upon what is available commercially and cost effective at the time of production quantities of these items are being procured.

6.2 DAQ Event Data Readout & Slow Controls Slave Interface

Bus standards of today and even tomorrow leave many options for read and write accesses. To eliminate module incompatibilities, the Data Acquisition System implementers will provide a detailed design and a simulation model (including timing specifications) of the Standard SDC Event Data Readout & Slow Controls Slave Interface to the bus used in all Front-End/Trigger System interface crates. A simulation model of a bus master will also be provided to aid in complete module simulations.

All Front-End and Trigger Systems would be required to build modules using this slave interface. This guarantees both that the DAQ CPU can access these modules and that it can use SDC-standard protocols for these accesses. The only exception to this rule is the use of a special backplane bus for the Front-End or Trigger System crate's modules and an interface to the SDC Standard DAQ bus to which the DAQ CPU interfaces. The use of a special bus is highly discouraged.

6.3 DAQ Crate Adapter/Interface Modules

Using VMEbus as an example, most Front-End and Trigger System modules will probably be built using a form factor larger than that of the DAQ CPU. For example, the most popular "large VMEbus" module form factor is 9U (15.75 inches) x 400 millimeters. The DAQ CPU form factor is that of the "official VMEbus" or 6U (10.5 inches) x 160 millimeters. Commercial "adapter" modules are available providing mechanics to allow 6U x 160 modules to fit into 9U x 400 crates. The data acquisition implementers will design and develop SDC DAQ Standard Crate Adapter/Interface Modules to both provide this mechanical conversion and to house electronics for the following Data Acquisition System standard interfaces:

313

- Event Data Readout Interface: Interfaces to both Event Data Links to the Event Builder Subsystem and Send Event Links from the Event Data Flow Control Subsystem.
- DAQ Slow Controls Interface: Interface to the DAQ Slow Controls Network.
- DAQ Slow Controls Remote Link Interface: Interface to a serial link to front-end devices on or near the detector interface not able to be accessed directly by a DAQ CPU.

The Send Event port of the Event Data Readout Interface includes a fiber optic cable receiver and a connector, serial to parallel decoder logic and protocol standards. The Event Data port includes a fiber optic cable transmitter and a connector, parallel to serial encoder logic and protocol standards.

The DAQ Slow Controls Interface includes a network receiver and a connector, network transceiver and controller logic and network protocol standards.

The DAQ Slow Controls Remote Link Interface provides a port to a serial link to be used to download, monitor, control, etc. front-end devices on or near the detector which are not necessarily housed in crates. If the devices are housed in crates, these crates would not house DAQ CPU modules. This interface includes a serial link transmitter and a connector, link controller logic and link protocol standards. An IEEE serial link standard, such as IEEE P1187 (Test Scan) might be used for the remote serial link if it meets necessary requirements (speed, reliability, etc.). The Test Scan standard was specified to provide a standard method to download, test and diagnose ASICs.

These interfaces and protocols would be the only methods provided to Front-End and Trigger Systems to interface to the Data Acquisition System's event data readout system and DAQ Slow Controls network.

Figure 6 illustrates the DAQ Crate Adapter/Interface module for the VMEbus example. The two connectors on the DAQ CPU module are wired to the top two connectors on the Adapter/Interface module. If any Front-End or Trigger Systems use a standard VMEbus 6U x 160 crate, an alternative solution for interfacing their electronics to the rest of the DAQ system would use an auxiliary card as shown in Figure 7.

Figures 6 and 7 both contain a DAQ Send Event Link originating from the Event Data Flow Control Subsystem, which in turn gets its inputs from the Level 1 and Level 2 Trigger Systems and the Online Processor Subsystem. The Trigger Systems send trigger information to front-end crates via a small number of high-speed fiber optic cables. A possible alternative method for transmitting the information contained in the Send Event Link is via one of the these high-speed fiber cables. A DAQ CPU would be required to "poll" a Trigger System module contained in its crate to know when to send a particular event.

314

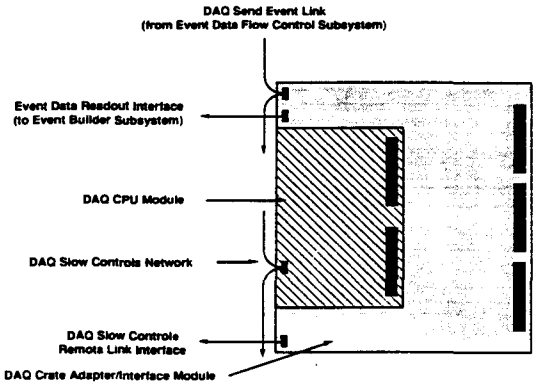


Figure 6
DAQ Crate Adapter/Interface Module

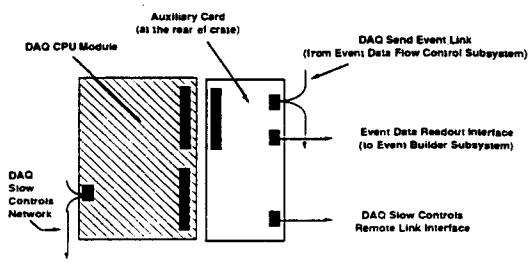


Figure 7
Alternate Implementation Using Auxiliary Card

315

Figure 8 illustrates two acceptable SDC-standard methods for interfacing Front-End or Trigger System electronics to the Data Acquisition System. In the crate on the left, modules are readout by the DAQ CPU over the crate's SDC standard bus and transmitted to the Event Builder Subsystem via the DAQ CPU.

The crate on the right illustrates a case where, for example, reading the modules over the crate's bus would not meet system throughput requirements. Originally, the buffer modules were used in the Switched Capacitor Array Calorimetry & Shower Max Front-End Systems to interface to the Data Acquisition System. Presently, buffer modules are not planned to be used by any front-end or trigger system but remain a viable alternative for event data readout if the need arises. The ports shown on these modules must adhere to the Event Data Readout Interface specifications. Event data enters these buffer modules via a serial link from non-SDC standard crates on the detector. The DAQ CPU in this second crate is only used for the DAQ Slow Controls Network.

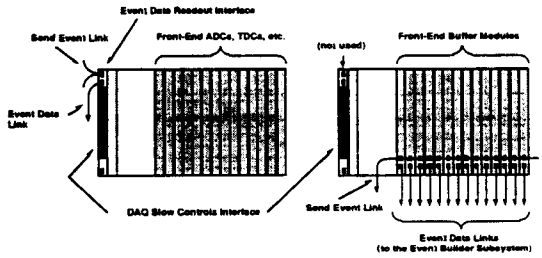


Figure 8
Two Event Data Readout Implementations

6.4 Event Data Links

Event Data Links originate from DAQ CPU modules or event data buffer modules and terminate at the inputs to the Data Acquisition System's Event Builder Subsystem. Of the 272 Event Data Links or sources (see Table 1), 178 originate from crates in the counting room and the remaining 94 originate from crates on the detector. Regardless of the amount of event data per source or the distance between the source and the Event Builder Subsystem, the Event Data Links will be identical (transmission speed, cable type, etc.). If at all possible, these links, except for transmission protocols, would be identical to those transmitting data from Front-End Systems to Trigger Systems.

The Event Data Links would be fiber optic links operating at approximately one gigabit per second. The distances from detector-mounted crates to the counting room is approximately 300 meters. This speed may require the use of 1300 nanometer laser diodes and relatively high-frequency fiberoptic cable. This relatively short distance (for fiber optic links) reduces the transmitted power requirements and the complexity of the optical receivers and may reduce the implementation cost of these devices. A link, including the cable, connectors, transmitters and

receivers and encoding and decoding logic has been costed in the low hundreds of dollars. This assumes a significant reduction in costs over those today by the time production ordering occurs.

There are a few possibilities for using IEEE/ANSI standard and industry-supported links for the Event Data Links. Two standards groups are developing fiber optic one gigabit per second standards, the Scalable Coherent Interface (SCI) group and the group which developed the copper HIPPI standard. The SCI group has just organized a committee to look into standardizing a point to point, memory to memory fiber optic link standard based on the SCI protocol. In the years to come, the high energy physics community can expect significant industry support for both of these fiber optic link standards for use primarily in the computer industry and vast industry support for the higher-speed fiber optic link standard, SONET, for use in the telecommunications industry.

What is used for both Data Acquisition System Event Data Links and Front-End to Trigger System links at production ordering time and whether the links are built by the collaboration from commercial parts or bought as a complete product will depend on availability and costs at that time.

6.5 Event Data Link Transmitter/Receiver Test Modules

The Data Acquisition System implementers will provide a self-contained module and software which allows simple testing of Event Data Links. Items such as these are extremely important during commissioning and maintenance of the various Front-End and Trigger Systems as well as the Data Acquisition System.

6.6 DAQ Slow Controls Remote Links & Repeaters

Sections 4 and 6.6 describe the DAQ Slow Controls Remote Link and its use in the Data Acquisition System. This section describes the physical characteristics of the links and a repeater system for connecting these links to detector-mounted components not having direct access (via DAQ CPU modules) to the DAQ Slow Controls network.

DAQ Slow Controls Remote (serial) Links are simple shielded twisted-pair cable. DAQ Slow Controls Remote Link Repeaters are self-contained and powered fanouts of an incoming remote link originating from a DAQ CPU module. These repeaters are required because, for example, the Silicon Strips and Silicon Pixels Front-End System has only ten Data Acquisition System interface crates and thus only ten DAQ CPU modules and DAQ Crate Adapter/Interfaces. For cable loading, cable routing, etc. reasons this Front-End System could require many more than ten sources of the DAQ Slow Controls Remote Links.

The complexity of the DAQ Slow Controls Remote Link Repeater depends upon whether messages only originate from the DAQ CPU modules or if messages can originate from detector-mounted electronics as well. It is not known at this time whether the repeater will be a commercial product or need to be developed by Data Acquisition System implementers.

316

317

7 Alternative Approach To Commissioning & Readout—System Readout Crates

318

8 Event Builder Subsystem

The proposed Event Builder Subsystem is based on a commercial switching network approach similar to networks being used in and being developed for both the telecommunications industry for high-speed parallel switching and the computer industry for interconnecting computers and peripherals at high-speed.

Two additional alternative event builder subsystems are discussed in subsections following details of the proposed commercial switching network-based Event Builder Subsystem. The first alternative is identical to the proposed Event Builder Subsystem except that the switching network is developed "in-house" by the SDC collaboration. The second alternative implements the Event Builder Subsystem with dual-ported memories rather than a switching network. This technique has practical throughput limitations which make it difficult to meet data acquisition system throughput requirements.

8.1 Commercial Switching Network-Based Subsystem

Figure 9 illustrates the components of the Event Builder Subsystem. This subsection and Sections 8.1.1 through 8.1.5 describe these components. This subsystem provides a highly-parallel, highly-efficient event data flow, high-speed and cost effective method for building physics events and transmitting these events to an Online Processor Subsystem. The Event Builder Subsystem is modular and scalable for future expansion. Note that Figure 9 does not show the (Online Processor Ready) Send Event Link input described in Section 2 and illustrated in Figure 3.

The Input Interface & Data Balancing Logic receives the event data fragments over fiber-optic cables using detector-specific protocols and performs simple static balancing (multiplexing) of small event fragments to reduce the requirements of the next stages of the Event Builder Subsystem. Table 1 of Section 2 is a list of the 272 inputs to the Event Builder Subsystem. The Input Interface & Data Balancing Logic would provide simple multiplexing of the 272 inputs into, for example, approximately 128 inputs for transmission through the other stages of the Event Builder Subsystem.

The Switching Network is preceded by an Input Queueing Network, etc. to make data flow through the Switching Network highly efficient. The function of the Input Queueing Network is to buffer and time multiplex the incoming data into fixed-length packets for synchronous transmission through the switch. With this circuitry when packets are being sent from all inputs through the switch simultaneously, no two packets have the same destination. This feature, the input data balancing logic and the multiple event buffering guarantee highly-efficient use of the throughput capability of the switch. Although both the telecommunications and multi-processor industries are presently heavily into R&D on switching networks, the Input Interface & Data Balancing Logic and the Input Queueing Network may be too physics-specific to buy commercially and thus needs to be developed by the SDC collaboration. The functions of both the Input Interface & Data Balancing Logic and the Input Queueing Network may be combined into one logic block for easier implementation.

319

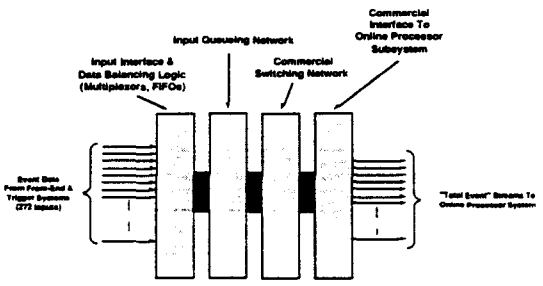


Figure 9
Switching Network-Based Event Builder Subsystem

Sending events to more than one Online Processor Subsystem processor is easily accomodated with the switch-based Event Builder Subsystem although it is felt that this and similar features should be the task of the Online Processor Subsystem.

A prototype project demonstrating the use of input queueing and a switching network for parallel event building has been successfully demonstrated at Fermilab [1],[2],[3].

8.1.1 Input Interface & Data Balancing Network

The input interface includes fiber optic receivers and serial to parallel encoder logic. The bit rate capacity on each input is approximately one gigabit per second. An "input module" would contain at least eight inputs and thus 128 to 152 inputs (8 x 16-19 islots]) could be housed in a crate. Two crates are needed to house the 272 inputs from front-end and trigger systems.

Event data fragment sizes from various front-end and trigger systems range from a few hundred bytes to several kilobytes. Event Builder Subsystem throughput is increased by providing simple static data balancing logic prior to the Input Queueing Network. This logic multiplexes FIFOs containing small event data fragments into a larger "event fragment" for input to the Input Queueing Logic. Averaged over several events, the data throughput on all inputs of succeeding stages of the Event Builder Subsystem is fairly balanced in size. This balancing reduces the complexity and size of the Event Builder Subsystem's Input Queueing and Switching Networks and increases the subsystem's throughput.

8.1.2 Input Queueing Network

The Input Queueing Network serves three purposes as follows:

- Buffers event fragments over several events so that variations in event fragment sizes, which averaged over time are relatively constant, have a negligible effect on Switching Network and thus Event Builder Subsystem throughput.
- Puts the event fragments in fixed-sized packets for transmission through the Switching Network
- Time orders the transmission of the packets such that no two packets have the same Switching Network output as their destination

It is primarily this last feature of the Input Queueing Network that allows the Switching Network and thus the Event Builder Subsystem to operate at very high bandwidths. This feature is explained in Section 8.2.

If built by the Data Acquisition System implementers, a channel of the Input Queueing Network is simply a small input FIFO fast RAM, DMA hardware and an embedded processor which is shared across as many channels as fit on a module.

8.1.3 Commercial Switching Network

Event builders, the devices used to readout event data, have evolved from simple single channel 'funnels' through a minicomputer bus, to multiple parallel channels (each with their own 'funnel' or bottleneck characteristics) feeding arrays (farms) of processors. More and more experiments are implementing event buildars with increased parallelism for higher throughput. When one considers particle beam crossing times of 16 nanoseconds and subsequent very high trigger rates, it is clear that the SDC detector data acquisition system will require the use of a totally parallel event builder with no inherent bottlenecks in addition to much larger amounts of pre-event builder buffering in order to achieve its one Megabyte per second typical and ten Megabytes per second capacity throughput requirements.

Initial discussions with industry indicate that switching networks having the size (number of inputs and outputs) and throughput needed for the SDC Data Acquisition System will be both commercially available and cost effective at the time of production ordering of data acquisition components. Interfaces to several industry-standard links (e.g., VMEbus, SONET, Fiber Channel, Fiber HIPPI, etc.) from the switching network will also be commercially available insuring a simple interface between the Event Builder Subsystem and the Online Processor Subsystem.

8.1.4 Interface To The Online Processor Subsystem

Several options exist for the interface to the Online Processor Subsystem depending upon what industry provides in both hardware and software for sending data into their large arrays of processors. If for example VMEbus is used and the Switching Network has 128 outputs each capable of transmitting data at 80 to 100 megabytes per second, the interface to the Online Processor Subsystem could be a (small) buffer/splitter such that the 80 to 100 megabytes per second of data is "split" into a few outputs. Events from each Switching Network output would be FIFO-buffered and transmitted via VME to VME links at slower speeds to the VMEbus interfaces of the Online Processor Subsystem. If industry supports transmission rates of 80 to 100 megabytes per second into large processor arrays (e.g., via standard one gigabit/second fiber links), the interface to the Online Processor Subsystem is simply an interface to the industry-supported link. Discussions with industry regarding link options to large processor arrays are ongoing. Most likely, the interface to the Online Processor Subsystem will be an industry-standard high-speed fiber optic link such as those mentioned in the previous subsection.

320

Concatenation of event fragment packets into full events can either occur in the interface to the Online Processor Subsystem or within the Online Processor Subsystem processors.

321

8.1.5 Event Builder Subsystem Segmentation

Several methods are possible for segmenting (partitioning) the Event Builder Subsystem for use during Front-End and Trigger System independent commissioning efforts, during calibrations or during a physics run. Some methods are as follows:

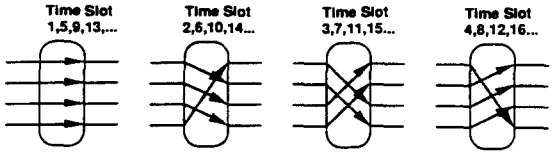
- Because the Event Builder Subsystem can operate with several independent triggers, logically "divide" the switch by the desired segmentation (e.g., by Front-End and Trigger Systems). Several barrel-shift switches operate independently of one another in this mode. Front-End or Trigger System destination processors only receive data from devices in their system
- Simply accept all the triggers at various rates and transmit only a system's data to destination processors for that system. The Switching Network rotates through all positions
- All devices receive all triggers, sending null event fragments for triggers not intended for that system. Processors get all the data and use only what they require. The Switching Network rotates through all positions.
- Physically separate the Event Builder Subsystem into several independent and smaller Event Builder Subsystems.

8.2 Alternative Implementation #1--In-House-Designed Switching Network

The Switching Network may be built by Data Acquisition System implementers or purchased commercially. Although the proposal is to buy a commercial switching network, if built the Switching Network would be based on a simple "barrel- shift" switch as detailed in the following two subsections. These two subsections should assist the reader in understanding how a commercial switching network is used to build events.

8.2.1 Switching Network Implementation Details

The operation of a barrel-shift switch and a description of a Data Acquisition System based on the use of such a switch for parallel event building have been described in detail in other documents (see References Section). Briefly, a barrel-shift switch of size N x N has N different states, state 1 connects input 1 to output 1, input 2 to output 2, etc. State 2 connects input 1 to output 2, input 2 to output 3, etc. This "shifting" continues until the state N which connects input 1 to output N, input 2 to output 1, etc. At this point the switch has "shifted" through all its N states and returns to state 1. Figure 10 illustrates the states of a 4 x 4 barrel shift switch. If input queueing logic (time division multiplexing) is used and equal packets of event data are sent through the switch at each switch state, event building at all outputs occurs in parallel producing a truely parallel event builder which is simple but capable of very high data rates



322

Figure 10
Possible Barrel Shift Configurations For A 4 X 4 Switch

Figure 11 illustrates how events are built using a barrel-shift switch. Note the different rotation sequence of the 4 x 4 switch. Any rotation sequense that sequentially rotates all inputs to all outputs is allowed. For ease of explanation, this example assumes equal fixed-sized event fragments from every event data source and that the packet size through the switch is equal to the event fragment size. The function of the Input Queueing Network in this simple example is indicated by the fixed-packet delays (packet shift registers) at the inputs of the switch.

In this example, an event consists of four equal-sized packets. Packets 1A, 1B, 1C and 1D together constitute event #1; packets 2A, 2B, 2C and 2D constitute event #2; etc. As the switch rotates through each position, all fragments of a single event are transmitted through the switch to the same output in a definite time sequence. By the second rotation of the switch, a second event is being built and sent to another output. As the switch rotates, four events are being built simultaneously at any one time and are being sent to the four different outputs.

This example is very efficient for fixed-length events but does not easily support variable event fragment and full event sizes, automatic data routing or systems with different numbers of inputs and outputs. All of these features can be provided by the addition of Input Queueing Network (in place of the fixed- packet delays). Implementation details of Queueing Networks at both the input and output of the Switching Network are given in the References Section.

In the actual Switching Network, there is no restriction that the number of inputs equal the number of outputs. Either can be larger than the other. For maximum throughput through a Switching Network with non-equal inputs and outputs, the number of inputs (outputs) times the input (output) bandwidth should equal the number of outputs (inputs) times the output (input) bandwidth

323

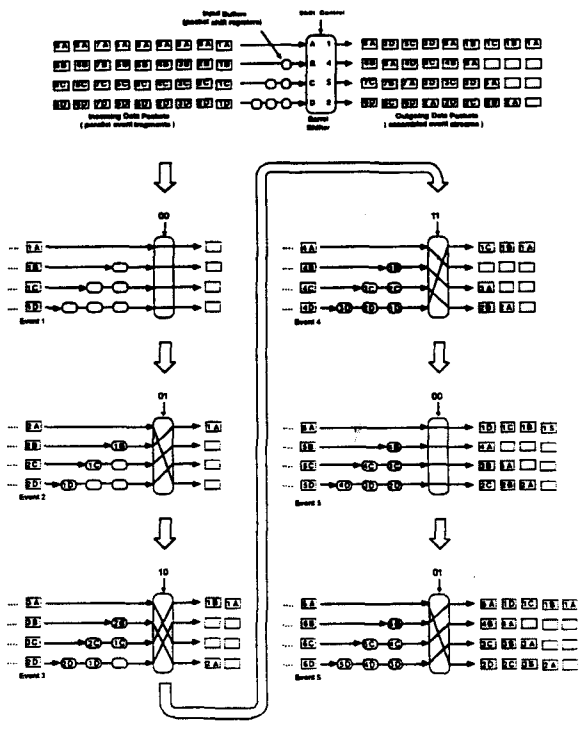


Figure 11
Simple Parallel Event Builder using a Barrel-Shift Switching Network

An in-depth conceptual design of an Event Builder Subsystem based on a switching network is presently being prepared for distribution at the November SDC Collaboration meeting [4]. This document will describe both an Event Builder Suboystem using a commercial switching network and one using a switching network developed by Data Acquisition System implementers.

8.2.2 Example Implementation

If the Event Builder Subsystem is built by data acquisition implementers and the Input Interface & Data Balancing Network reduces the number of inputs to the Input Queueing and Switching Network to 128 inputs, the following crate implementation might be built.

Twe crates each having 18 octal modules for a maximum of 288 inputs would house the Input Interface & Data Balancing Network. Two stages of one crate each would be needed to house the Input Queueing Network and Switching Network logic. The first stage crate would consist of eight 16 x 16 (dual 8 x 8) barrel-shift switch modules. The second stage would consist of sixteen 8 x 8 barrel-shift switch modules. Both module designs would be identical with only simple interconnections different. Assuming large processor array ports capable of receiving data at 80 to 100 megabytes per second, the interface to the Online Processor Suboystem would consist of one crate of sixteen octal link interface modules. Thus, the total Event Builder would be housed in five crates.

8.3 Alternative Implementation #2...Dual-Ported RAM-Based Subsystem

9 Event Data Flow Control Subsystem

9.1 Event Data Flow Control Unit

The Event Data Flow Control Subsystem is the non-event data interface of the Trigger System to the Data Acquisition System. Its function is to keep event data flowing efficiently from Front-End and Trigger Systems to tape. The features the Event Data Flow Control Unit of this system are as follows:

- Accepts Trigger System "trigger accept/reject" information.
- Accepts requests for events from the Online Processor Subsystem.
- Possibly transmits "send event" messages to DAQ CPU modules and event data buffer modules. (See Section 9.2 for another method to transmit "send event" messages)
- Transmits "destination ready; send event" messages to the Event Builder Subsystem.
- Accepts from the Event Builder Subsystem and transmits "throttle trigger" information to the Trigger System when buffers in either the Event Builder Subsystem, the Online Processor Subsystem, DAQ CPU Modules or event data buffers are almost full.

9.2 Send Event Links & Repeaters

The Send Event Links are identical in hardware to the Event Data Links (see Section 6.4). Send Event Repeaters are self-contained and powered fanouts of an incoming Send Event Link originating from the Event Data Flow Control Subsystem. Only one Front-End or Trigger System connects to a given Send Event Repeater. Several of these links originate at the Event Data Flow Control Subsystem, at least one per Front-End and Trigger System. Another method which appears to be more cost effective is use one of the Trigger System s high-speed links to front-end and trigger crates for the transmission of messages which would have been transmitted over the Send Event Links. This implementation needs further study but is included here for completeness.

10 Online Processor Subsystem

10.1 Processors

An Online Processor Suboystem with a processing power of 10^5 MIPS (VAX 780 equivalents) is assumed. Processors are a large expense item but are rapidly growing in computing power and shrinking in price. The vast majority of the 10^5 MIPS of processing power required in the Online Processor Subsystem can be ordered late in the development of the Data Acquisition System. Several companies are producing and/or developing large arrays of interconnected processors and workstations.

10.2 Event Request Links

The Event Request Links from the Online Processor Subsystem to the Event Data Flow Control Subsystem need only request new events at a typical and maximum rates of 10^3 and 10^4 events per second, respectively. Several events can be requested at a time in a single message on an Event Request Link. Thus, a small number of standard links such as Ethernet links could be used for Event Request Links.

10.3 Links To The Online Storage Subsystem

The interface from the Online Processor Subsystem to the Online Storage Suboystem has been costed by the Online Computing group as a cluster of workstations and network links with SCSI links connecting the workstations to storage media. The network links from the Online Processor Subsystem to the cluster of workstations are thus standard links such as Ethernet.

11 Data Acquisition System Control Computing Interface

The software for the data acquisition system represents a complex interplay of systems and applications programs written by the data acquisition group, the on-line computing group, the controls group, and by subsystem physicists. In general, the on-line and controls groups will provide system software, tools and templates to support applications programs; the DAQ group will provide further tools and templates (particularly relating to real-time applications) as well as certain generic applications programs (such as start-up and run control for the DAQ system and alarms and error logging applications); while the subsystem physicists will write most of the actual subsystem specific application programs for calibration, monitoring, and control, using the tools provided by the other three groups. The various software components that the DAQ group will provide are described here.

11.1 Runtime User Interface

The Runtime User Interface which includes software professional time to design, code and test runtime applications software is costed for this work. Most of the applications software items included in the Runtime User Interface are listed below:

- Run Time Control
- Control of the Online Processor & Online Storage Subsystems
- Histogramming
- Event Displays
- Calibration Database
- Consumer Processes

Many of these tools (histograms, event displays, database interface, user graphic interface, hooks for user consumer processes) will be provided by the on-line group. The DAQ group will provide additional tools specific to the real-time environment running closer to the front-end systems. In addition, the DAQ group will be responsible for application programs that start-up and control the DAQ and front-end systems (including booting, downloading, system checkout, performance monitoring, and error detection) as well as control of the on-line processor subsystem.

11.2 Control, Monitoring & Downloading User Interface

Control, monitoring and downloading are integral functions of a Data Acquisition System. A partial list of subsystems needing control and/or monitoring applications software is given below:

- Power & Grounding
- Gas
- High-Voltage
- Environmental Monitoring
- Magnet Monitoring
- Calibration Pulsers
- Cryogenic Control Systems
- Accelerator Controls Interface
- Luminosity Monitors
- Manipulators

The low-level routines that actually interact with hardware components to perform these control functions will be provided by the controls group, while subsystem groups will write the high-level routines that users will interact with. The DAQ group will provide both systems and application level support as described in the following subsections:

11.2.1 Applications Software For Supporting The Use Of Memories & Intelligent Processors

Some of the reasons for requiring this applications software are as follows:

- Downloading
- I/O (file) system services
- Terminal connections for debugging
- Network connections

The Data Acquisition System will contain a wide variety of "embedded" processors that perform various functions requiring varying degrees of intelligence. The Data Acquisition System must provide services to these processors that enables them to be booted and downloaded, allows them access to network and other I/O services, and allows programs running in these processors to be interactively debugged. A user must be able to log in to these processors to run debugging or diagnostic code. Control capabilities must be present to start up the various processors, download them with appropriate code and data for the task at hand, detect errors, restart when necessary, etc.

11.2.2 Applications Software For Supporting "Slow" (Non-Event) Data Acquisition

Some of the reasons for requiring this applications software are as follows:

- Detector parameter monitoring and logging
- Calibration data acquisition
- Data base access

Aside from the high-bandwidth event data acquisition, the system must also support the collection and recording of other types of data not specifically associated with a single interaction. These include periodic monitoring of environmental, accelerator and detector parameters (temperature, high voltages, magnet currents, luminosity, etc.).

A variety of different frequencies for this slow data acquisition must be supported. Variances with normal conditions should be detected and reported. In addition, the system must support various types of calibration data acquisition at a subsystem level where, for example, events are recorded without sparsification or pedestal subtraction, and must provide the processing power necessary to reduce this calibration data to physically meaningful quantities. Finally, the system must provide access to a data base that records the time history of both calibrations and other detector parameters.

The actual slow data acquisition will be done by low-level routines provided by the controls groups, but the DAQ group will need to provide standard slow-daq processes and templates that will allow subsystem physicists to assemble such applications quickly and easily.

11.2.3 Applications Software For Supporting Unusual Occurrences

Some of the reasons for requiring this applications software are as follows:

- (Front-End & Trigger System) diagnostic link (Test Scan-like link)
- Online diagnostics
- Alarms & limits

Given the complexity of the Data Acquisition System, faults and other error conditions must be detected automatically. This will require a diagnostic connection to various electronic components, a set of test procedures that exercise system functions at start-up and periodically thereafter, monitoring procedures that check for errors in normal data taking conditions, and a comprehensive alarm and limit system which records alarms of varying priorities and brings those alarms requiring human intervention to the immediate attention of operators.

11.2.4 Applications Software For Supporting The Control & Monitoring Of Adjustable Devices

There will be a wide variety of devices on the detector that need to be set, adjusted or manipulated remotely, ranging from voltages to pulsars. A uniform software interface to these systems must be provided that allows the experimenters to set, restore to standard conditions, record and adjust these devices.

Most of this software is provided by the controls group, but the DAQ group will provide software to present a standard user interface for these control and monitoring functions.

12 Data Acquisition System Offline Analysis Interface

The Offline Analysis Interface provides an automated method for transferring online events from the Online Storage Subsystem to the large offline computing system at the SSC Laboratory for distribution and further analysis. It is assumed that this interface consists of a commercial network such as FDDI or the HIPPI Fiber Channel. Details of the network are not known at this time.

13 Electronics Rack Protection Subsystem

The Electronics Rack Protection Subsystem includes a control chassis and the rack cooling and rack protection infrastructure (heat exchangers, plumbing, sensors, etc.). Only racks containing Front-End or Trigger System interface crates to the Data Acquisition System and racks for the Event Builder Subsystem, Online Processor Subsystem and the Event Data Flow Control Subsystem were costed.

No development of the Electronics Rack Protection Subsystem was costed. It is planned to use electronics rack protection developed by the SSC laboratory for use in other SSC systems.

14 System Partitioning & Dynamic Segment Alocation

16 Schedule, Costs & Manpower Requirements

17 Possible Critical Path Items

18 Major Milestones

19 References

[1] E. Barsotti et. al., A Proposed Scalable Parallel Open Architecture Data Acquisition System For Low to High-Rate Experiments, Test Beams and All SSC Detectors, IEEE Transactions On Nuclear Science, Vol. 37, No. 3, June 1990, pp. 1216-1221.

[2] M. Bowden, System Overview of the Scalable Parallel Open Architecture Data Acquisition System, not published, May 1990, pp. 16-25.

[3] Mark Bowden et. al., Scalable Parallel Open Architecture DAQ Prototype Project Report, not published, September, 1991.

[4] E. Barsotti, M. Bowden & Masaharu Nomachi, Event Builder Subsystem Conceptual Design, to be distributed at the November, 1991 SDC Collaboration meeting.

Note: Additional references regarding other R&D activities should be put here with accompanying text within the body of this document

SDC Data Acquisition System Conceptual Design

- Requirements
- Functional Overview
- Components
- Interfaces with other Subsystems
- Cost/Schedule
- Milestones/Technology Choices

Irwin Gaines
Sept 27, 1991

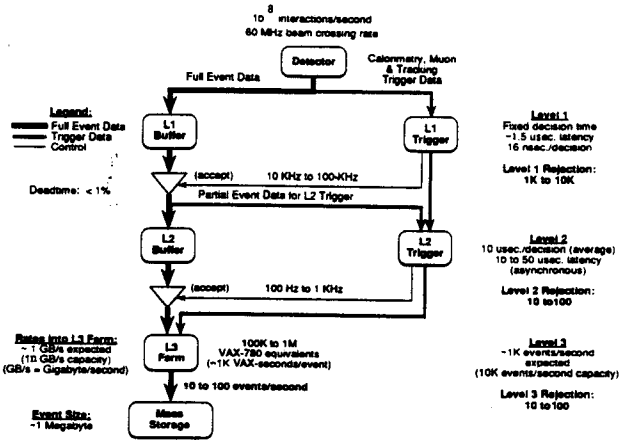
2. DAQ Design Requirements

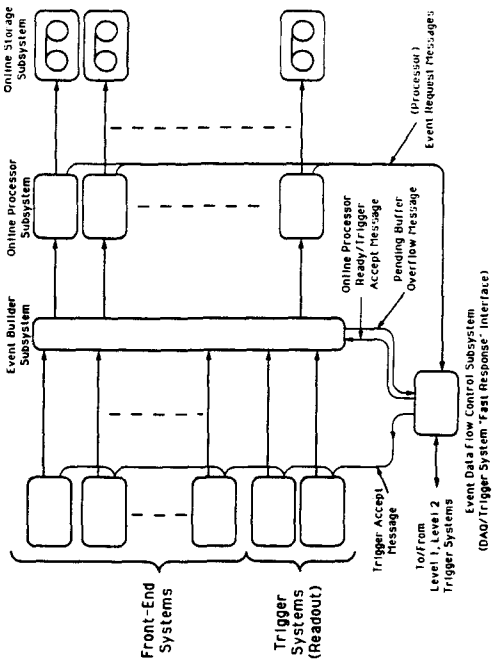
The essential function of the DAQ is to move data from the front end electronics to permanent storage in response to an event meeting trigger conditions. In addition, the DAQ design must satisfy a number of more specific design requirements:

1. The DAQ must maintain the integrity of the data.
2. Events must not be lost or rejected by the DAQ except as a result of a triggering decision.
3. The DAQ must not lose event data except for occasional data loss in certain FEE channels with exceptionally high occupancies or as the result of a reset operation.
4. The DAQ must employ a flexible partitioning scheme to allow testing, calibration, data taking, and detector commissioning in parallel, with minimal interference.
5. Robust control and monitoring of DAQ operation must be provided.
6. The DAQ must provide for processing of the event data at well defined points in the data path.
7. The DAQ must provide a high-level human interface with a versatile, uniform, and easy to use environment for control and monitoring of DAQ operation.
8. The DAQ must be modular and have well defined interfaces and functionalities.
9. Provision must be made for substituting improved designs and or new technologies as appropriate.
10. Smooth upgrade paths must allow for the addition of channels, detector components, trigger units, and processing elements.
11. The DAQ must be scalable over a wide range of bandwidths and provide a means for increasing the DAQ bandwidth to cover the expected range of hardware trigger rates and event sizes (see section 3.5).
12. The DAQ must be testable, reliable, maintainable, and incorporate fault tolerance.
13. DAQ subsystems must be available as needed by SDC for electronic and detector system tests, test beam experiments, and commissioning of the experiment.
14. The DAQ must be efficient and cost effective.

Table 1. SDC DAQ Preliminary Design Parameters

Parameter	Design $\mathcal{L}$	High $\mathcal{L}$	Units
Maximum Luminosity	10^{33}	10^{34}	$cm^{-2}s^{-1}$
Beam Crossing Rate	62.5	62.5	MHz
Maximum Interaction Rate	10^8	10^9	Hz
Level 1 Trigger Rejection Factor	$10^3 - 10^4$	$10^4 - 10^5$	
Expected Level 1 Trigger Rate	10^4	10^4	Hz
Maximum Level 1 Trigger Rate	10^5	10^5	Hz
Level 2 Trigger Rejection Factor	$10^1 - 10^2$	$10^1 - 10^2$	
Expected Level 2 Trigger Rate	10^2	10^2	Hz
Maximum Level 2 Trigger Rate	10^3	10^3	Hz
Level 3 Trigger Rejection Factor	$10^1 - 10^2$	$10^1 - 10^2$	
Expected Level 3 Trigger Rate	10^1	10^1	Hz
Maximum Level 3 Trigger Rate	10^2	10^2	Hz
Deadtime at Maximum Trigger Rates	< 10	≈ 15	%
Deadtime from DAQ Errors and Downtime	< 5	< 5	%
Level 1 Trigger Latency	2 - 4	2 - 4	μs
Maximum Level 2 Latency	100	100	μs
Average Level 2 Processing Time	< 10	< 10	μs
Time to Process an Event in Level 3	100 – 1000	100 – 1000	MIPS-sec
Farm Processing Power	$10^5 - 10^6$	$10^5 - 10^6$	MIPS
Number of Processors in Farm	500 – 5000	500 – 5000	
Average Event Size for Full Event	0.1 – 1	0.1 – 1	MB





Simplified Block Diagram
Of Costed Data Acquisition System Architecture

SDC DAQ: Major Components

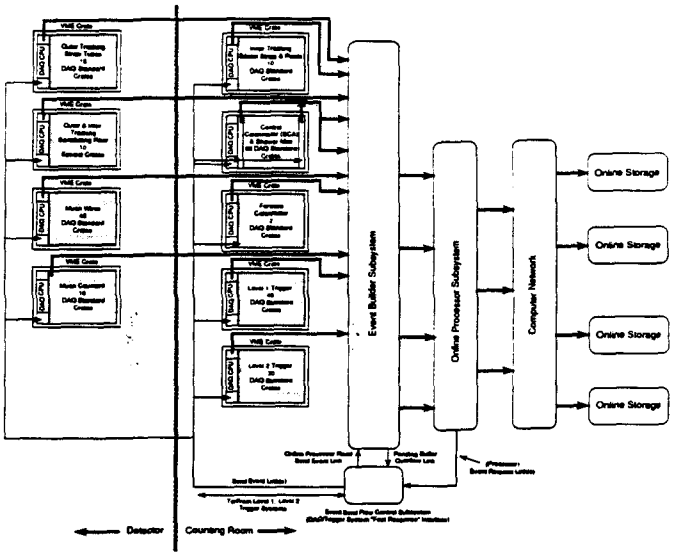
- Development Tools (5.2.1)
- Slow Controls Interface (5.2.2)
- Read-out Subsystem (5.2.3 and 5.2.4)
  Readout network for 10**6 front-end channels
- Front End and Trigger System Interfaces (5.2.5 and 5.2.6)
- Event Builder Subsystem (5.2.7)
  Switching network with 256 inputs, 256 outputs, aggregate bandwidth of 1 Gigabyte/sec
- Timing & Clock Distribution Subsystem
  High-speed dedicated links for 60Mhz clock and trigger distribution
- Data Flow Control Subsystem (5.2.8)
  Dedicated point-to-point message links to control event data flow, with message distributed to >620 destinations
- Online Processor Subsystem (5.2.9)
  Processing System with computing power of >10**5 MIPS
- Online Storage Subsystem (5.2.10)
  Mass Storage System with 100 MBytes/sec capacity
- ES&H Subsystem (5.2.11)
- DAQ Control Software (5.2.12)
  Software for control, monitoring, downloading and user interface with the DAQ system
- Offline Analysis Interface (5.2.13)
  High Performance network link (1 Gigabit/sec or greater) to offline computing system
- System Integration and Project Management (5.2.14 and 5.2.15)

DAQ Components

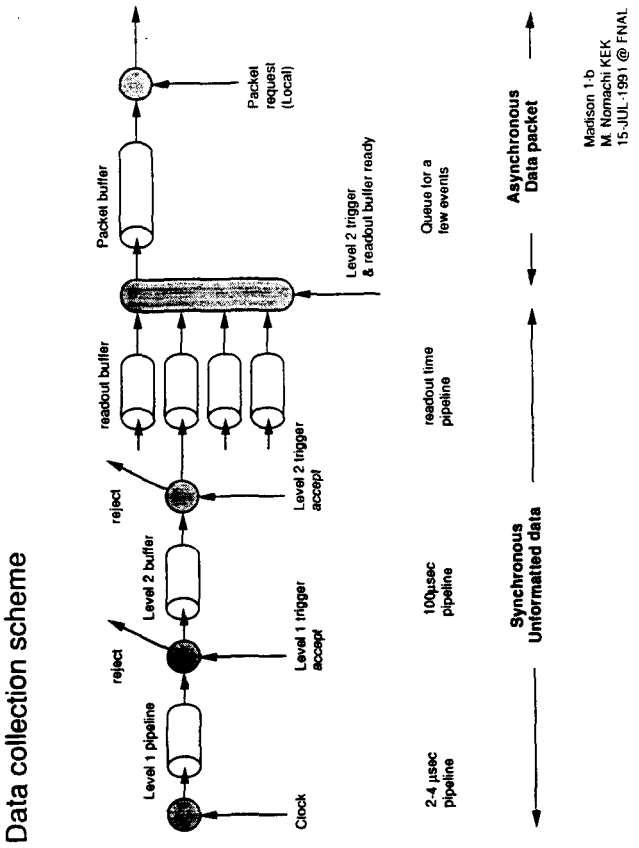
Front-End/Trigger System	# Crates	# Sources	Crate Type	Location
Inner Tracking Silicon Strips & Inner Tracking Silicon Pixels	10	10	SDC DAQ Std.	Counting Room
Outer Tracking Straw Tubes	16	16	SDC DAQ Std.	On Detector
Outer Tracking Scintillating Fiber & Intermediate Tracking Scintillating Fiber	14	14	Special	On Detector
Central Calorimeter (SCAs) & Central Calorimeter Shower Max	96	96	SDC DAQ Std.	On Detector
Central Calorimeter (Flash ADCs)*	96	96	Special	On Detector
Forward Calorimeter	2	2	SDC DAQ Std.	Counting Room
Muon (Wires)	48	48	SDC DAQ Std.	On Detector
Muon (Counters)	16	16	SDC DAQ Std.	On Detector
Level 1 Trigger (<= 1 KB/crate)	40	40	SDC DAQ Std.	Counting Room
Level 2 Trigger (<= 1 KB/crate)	30	30	SDC DAQ Std.	Counting Room
Totals:	272	272		

* Central Calorimeter (Flash ADCs) not counted in totals

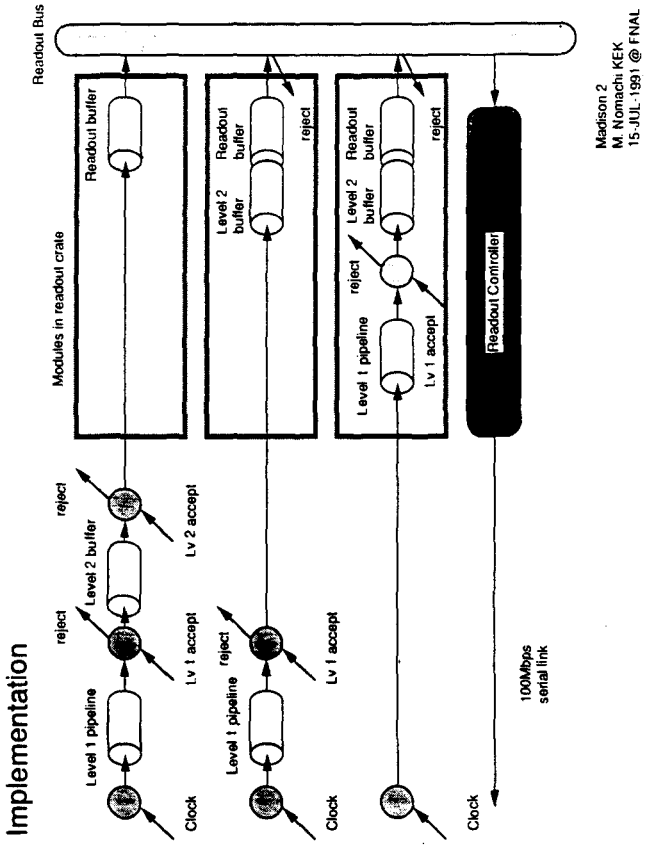
Table 1
Descoped Quantities
Crates With DAQ CPUs & Front-End/Trigger System Event Data Sources



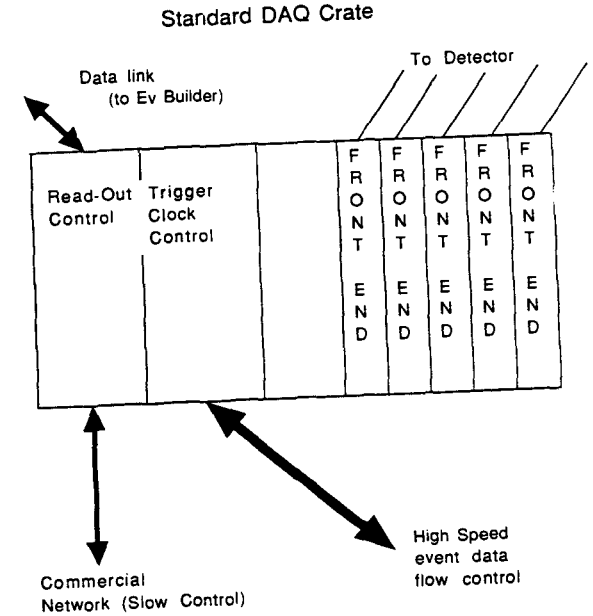
345



346



347



Standard Commercial crate and backplane
(augmented with SDC specific signals)

348

Functionality Provided By The DAQ System At The DAQ & Front-End/Trigger System Interface

In General:

- "SDC Standard" interface to the Slow Controls Network for downloading, initialization, monitoring, diagnostics, etc.
- "SDC Standard" interface to the Event Builder Subsystem & Event Data Flow Control Subsystem for event data readout
- "SDC Standard" interface to an Electronics Rack Protection chassis
- "SDC Standard" interface (module) to an industry-standard Slow Controls serial link to on-detector (non-crate-housed) PC boards

Additional If A SDC DAQ Interface Crate Is Used:

- Non-redundant (single bus) & redundant (two identical busses) crate options
- Large "user" area at crate rear for special backplane or I/O needs
- Uniform method for power supply input to the crate
- Additional & substantial software & hardware development, testing & installation support (e.g., test modules, extenders, diagnostics, etc.)
- **Less different "things" in the SDC and all the short & long-term benefits this brings**

349

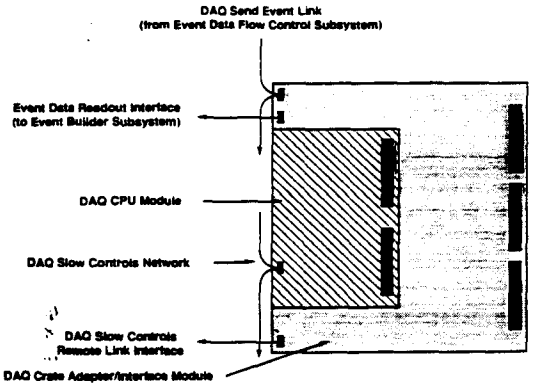


Figure 6
DAQ Crate Adapter/Interface Module

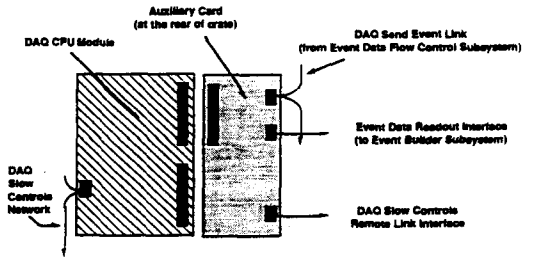
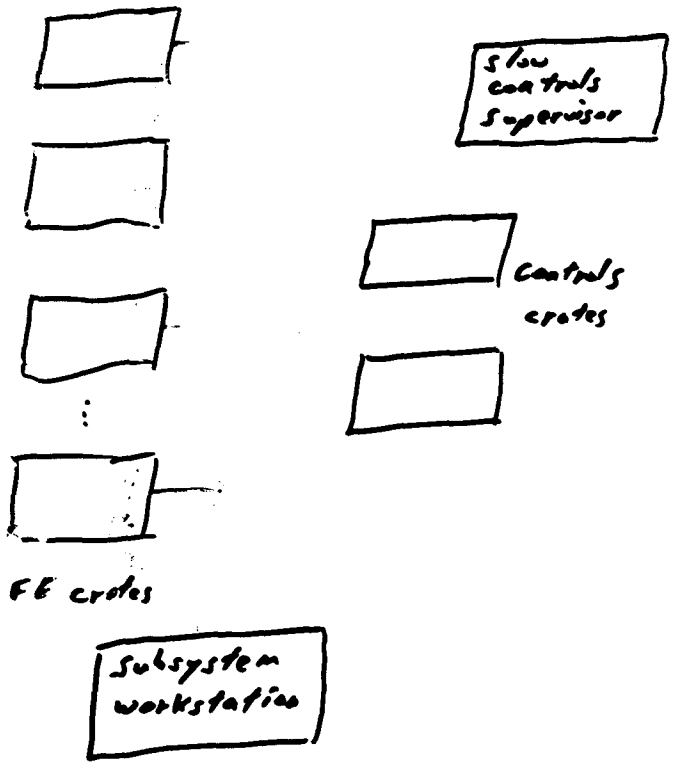


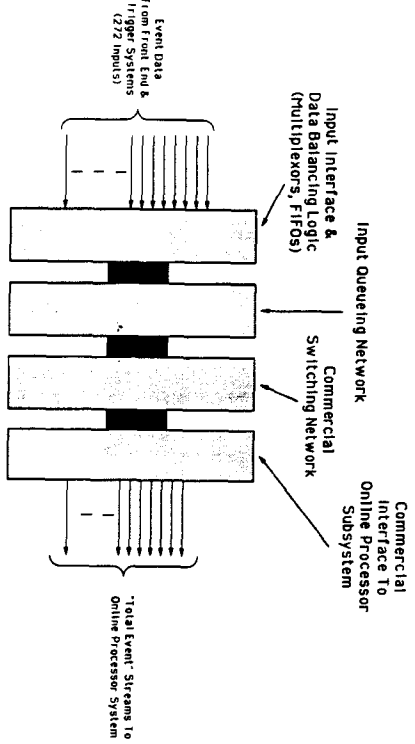
Figure 7
Alternate Implementation Using Auxiliary Card

350

For each subsystem:



351

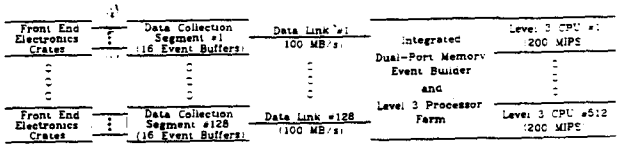


352

SUBSYSTEM CRATE

CPU	DAQ CONTROL	LOCAL TRIG	DATA COLLECT	UNUSED	UNUSED	UNUSED	UNUSED	DATA COLLECT	TRIGGER DIST	DATA COLLECT	TRIGGER DIST	DATA COLLECT	TRIGGER DIST	DATA COLLECT	TRIGGER DIST	DATA COLLECT	TRIGGER DIST	DATA COLLECT	TRIGGER DIST

353



354

Physical Location of Costed Data Acquisition System Architecture

Equipment In Counting Room	Equipment Mounted on Detector
8 Inner Tracking Silicon Strip-DAQ Standard Crates	52 Outer Tracking Straw Tube-DAQ Standard Crates
8 Inner Tracking Silicon Pixel-DAQ Standard Crates	32 Outer Tracking Scintillating Fiber-DAQ Special Crates
10 Central Calorimeter (SCA)-DAQ Standard Crates	26 Central Calorimeter (SCA)-DAQ Special Crates
2 Forward Calorimeter-DAQ Standard Crates	78 Central Calorimeter (Flash ADC)-DAQ Special Crates
30 Level 1 Trigger (<= 1KB/Crate)-DAQ Standard Crates	64 Central Calorimeter Shower Max-DAQ Special Crates
30 Level 2 Trigger (<= 1KB/Crate) DAQ Standard Crates	2 Forward Calorimeter-DAQ Special Crates
Event Builder Subsystem	54 Muon (Wires)-DAQ Standard Crates
Data Flow Control Subsystem	16 Muon (Counters)-DAQ Standard Crates
On Line Processor Subsystem	20 Intermediate Tracking Scintillating Fiber-DAQ Special Crates
ES&H Subsystem	
Off Line Analysis Subsystem	

355

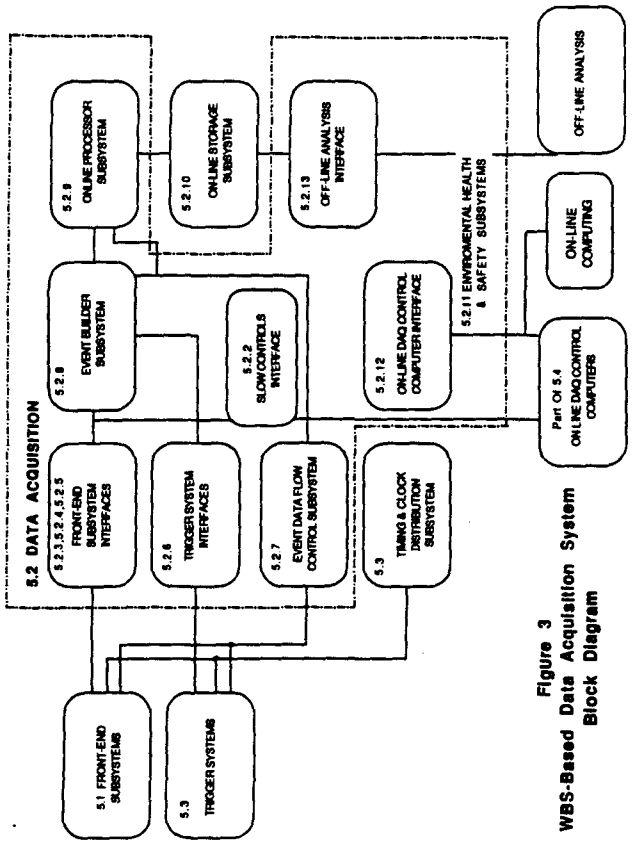


Figure 3
WBS-Based Data Acquisition System Block Diagram

356

DAQ Software

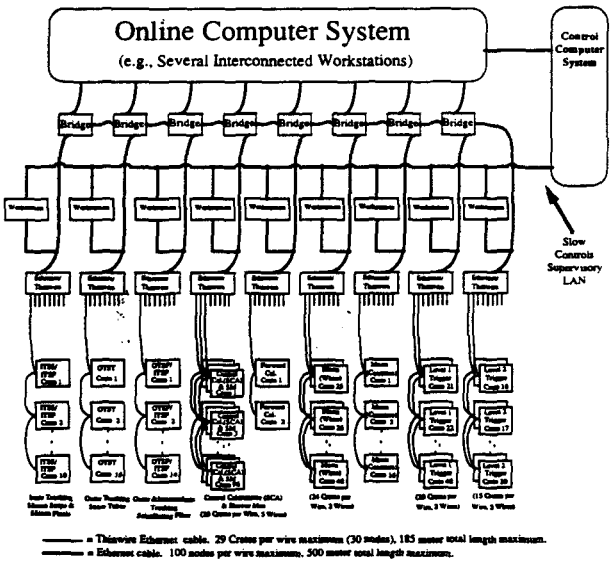
5.2.12 **Online Data Acquisition Control Computer Subsystem Interface**
(Includes network interface and links to DAQ components and all system applications software but does not include any computer system (databases, operating systems, etc.) software)
- Write interface requirements document then write interface specifications document
- Procure & develop (hardware & software) infrastructure

5.2.12.3 **Network Interface & Links To DAQ Components**

5.2.12.4 **Runtime User Interface**
(Applications software only)

5.2.12.5 **Control, Monitoring & Downloading User Interface**
(Applications software only)

1 **Applications Software For Supporting The Use Of Memories & Intelligent Processors**
2 **Applications Software For Supporting "Slow" (Non-Event) Data Acquisition**
3 **Applications Software For Supporting Unusual Occurrences**
4 **Applications Software For Supporting The Control & Monitoring Of Adjustable Devices**



SDC DAQ Timeline

1992

1993

1994

1995

1996

1997

1998

1999

Completion of DAQ requirements

Completion of DAQ system design, incl. technical choices

Completion of DAQ component design

Portable DAQ for use in test beams/labs

Prototypes of all DAQ components

Delivery of partial DAQ systems for subsystems

Installation of complete DAQ system

Certification of full, working DAQ system

Electronics

From the Front End to the Event Builder	P. Le Du(LBL&Saclay)
The Showermax Electronics	P. Le Du(LBL&Saclay)
UCLA Cosmic-Ray Test	M. Atac(UCLA)
Electron Trigger Backgrounds	M. Miller(Chicago)
SDC Trigger Design Documents	W. Smith(Wisconsin)

LPBautz:10/29/91

From the Front End to the Event Builder

P. Le Du(LBL&Saclay)

Le Du

From the front end to the event builder

1.INTRODUCTION :

Nowadays we are entering in a new epoch which is the "age of communications" where the " master-slave" relationship is replaced by the more democratic concept of "server - client" . Thus , a modern data collection system is build around a large , modular and evolving network of distributed microprocessors embedded in a multilevel structure with a high degree of parallelism and dynamic routing . Standard commercial buses, point to point connection and control network links allow the complete integration of all intelligent processing elements.

The architecture (figure 1) presents the different elements of the SDC data collection system.
The FRONT END ELECTRONICS digitizers close to the detector are organized in logical or topological partitions like subdetector branches . Local data are collected using optimized DATA LINKS to the EVENT BUILDER through a LOCAL DATA NODE performing the necessary hardware standardization and trigger synchronization. Then a series of dedicated processing FARMS performs the physics analysis from the level 3 trigger to the mass storage . The backbone of a such distributed concept consists of a dual bus connection system, one for the low speed control communication (Ethernet/Cheapernet), one for the high speed data exchanges .

The conceptual design is based on few simple rules and methodology in ordar to build and assemble a coherent and cost effective DAQ aystem .
Such concept allows to:
- SAVE money and manpower
- AVOID duplication of tasks , efforts and delays
- INCREASE the reliability and flexibility.
So , ideas like STANDARDIZATION of elements and MODULARITY of the architecture based on well accepted commercial standards which has already been succesfully experienced in some large detectors and also in aerospace/aeronautic industry , should be strongly considered as a guideline for the basic conceptual design.

a) Standardization
The SDC DAQ aystem is partitioned in a certain number of "subdetectors" branches which have the same common logical components and building blocks like front end and read out crates, interconnection data and control links , processors , interfaces , trigger synchronization.... . Overall standardization of auch basic elements is the only way to minimize cost , maintenence and evolution problems along the 15 years of the life of the experiment. Effort should be made at the beginning to define standard common features for each logical function.
The figure 2 is a tentative to identify the different elements of the read out chain and to make a selection between "dedicated" (build, test , maintain and document) and "commercial" (select and buy) devices

b) Modularity
The approch is to build a scalable MODULAR system with hardware and software elements combining top of range performance together with a user friendly integration. A coherent global design specification view must provide a smooth integration from the early test prototype to the running mode with a minimum trouble for future extensions .

2. THE FRONT END electronics
This is the interface between the detector and the digitizer. There are approximatively 300 crates located either inside the detector (central tracker, showermax, electromagnetic and hadron calorimeter) , outside (muon chambers and scintillator) or on surface (silicon, trigger ...).
Even if the front end electronics have different designs , some common features can be identified among the crate format , the Level 1 and 2 trigger distribution signals,the clock

synchronization , the gating logic ,the high speed data bus , the read out controller , the data link interface ... . Follow a brief description of these different components :
a) The CRATE :
A first study about the format shows that a 20 slots "JUMBO EURO " type crate with 9U high and 400 mm deepth could fit most of the subdetector front end space requirements. This crate must be equipped with an "high speed "data bus for "local " data read out, synchronization and timing distribution system which can be either a bus or special point to point wiring.
Reliability and remote control of such device sometime not accessible during the running operation is one of the important design goal of this crate.
b)The DIGITIZER board :
This board contains the basic read out chain from the shaper/preampli , the analog/digital pipeline, the time or amplitude converter to the first level digital buffer. Data input are acheived through a front or rear panel connector . The packaging depends on the subdetector electronics but a multiple of 16 , 32 , 64, 128 .... is strongly recommanded . Rear connectors have also the great avantage to avoid disconnecting cables when changing a card but can be limited in number of peints (maximum 192 to 256 ?) . Level 1 data sample are extractad at that level . Data output is carried out through the high speed bus connector . An "extension " bus could be useful in some case to extract digitized data sample to the level 2 trigger.
c)The "local " TRIGGER modules associated with the topology of the crate which process the level 1 (and may be 2 ?) algorithms and send out the results to the surface through optical fibres .
d) The SYNCHRONIZATION and GATING logic which distribute and control the different timing signal like the 63 MHz clock , the level 1 & 2 trigger ACCEPT/REJECT, the "local" BUSY ...
e) The READ OUT CONTROLLER which performs the entire crate data collection and first reduction
f)The INTERCONNECTION which is an interface between the "local " high speed data bus and the standard read out branch to the "Local dat Node".
g)The "dedicated" subdetector modules like monitoring and "slow control " (HV ...) .

3. THE LOCAL DATA NODE (or subsystem crate)
SDC is logically but also "sociologically" divided into a certain number (≥ 10 ?) of independent "subdetector" elements (silicon, contral tracker, intermediate tracker, showermax , electromagnetic and hadron calorimeters, muon scintillators and chambers, forward detector...etc.) with their own front end electronics and monitoring features.
Therefore there is a need for AUTONOMY during the different stages of the life of these elements from the early conception to the normal running operation which represents more than 10 years period. Testing full scale prototypes , beam calibrations , debugging during the assembly , cosmic test, on-line monitoring and control must be carried out and supported in parallel by each "subdetector" group.

Then the concept of LOCAL DATA NODE appears . This "subsystem crate" is an AUTONOMOUS and PORTABLE data acquisition system (one per subdetector for example) which inherits from the global DAQ the same principles .
They are able to perform a complete set of data collection tasks including :
a. Front end crates data read out and buffering for each detector subsystem
b. Local subevent data formatting and processing
c. Forwarding collected data to the event builder
c. Trigger synchronization which provide an interface capable of supplying trigger signals either in local mode or fanning out the signals from the global trigger and distribution to the front end crates
d. Gate synchronization which providing an interface with DAQ control and trigger gating logic to throttle the trigger when DAQ is busy and introduce event routing (dead time measurment)
f. Connection to a workstation for control, monitoring, and stand-alone operation of the subsystem (histogramming , subevent viewing, slow control (HV ...), software development

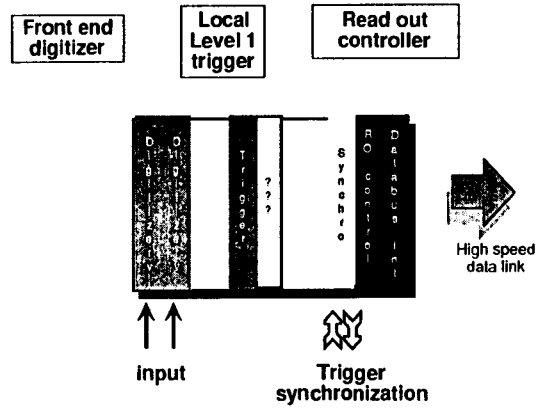
Furthermore, during the complex phase of data taking , it permits in case of nonfatal failures to remove and add dynamically a component without modifying the data acquisition structure . This is also an elegant manner to spy data in a safe non destructive way.
Evolution for the future should be easily extrapolated . It must be coherent by using commercial hardware / software as much as possible , flexible : able to acquire any kind of front end data bus or links , scalable : as the technology evolve (processor, memory ...) , portable : from the test laboratory or beam to the final implementation in the experiment . The main feature being to be directly integrated (hardware and software) in the DAQ structure allowing to each detector groups to write , test and debug their own "embedded " software into the DAQ "skeleton" and to be familiar as soon as possible with the selected experiment standards.

This is the place where the "standardization" should be completed and fully commercially supported. Today , it seems that the VME standard and its probable evolution toward the FUTUREBUS should satisfy most of the requirements .
A brief description of the role of the different "logical " components is presented in the next paragraph based on today existing devices but which can be very easily extrapoled in speed and power in the future .

a) The CRATE :
A Standard 20 slot 6U VME crate with J1 and J2 extension bus (VSB) .
b) The ACQUISITION is made via a processor which performs in parallel the read out of each front and branch or crate , the data flow being normally driven over the VSB extension bus .
c) The "Scheduler or master " processor organizes the job of acquisition oriented processors like down-line loading of data acquisition programs, synchronization of all processors and remote start/stop commands . Furthermore ,upon reception of an event acceptad by the acquisition processors, the scheduler processor can take the decision to proceed to an on-line sophisticated mathematical analysis invoking a cluster of number crunching processors .
This two first categories of processors may be the same (like MC68030/40) equipped with VME and VSB interfaces, high speed block movers, communication FIFO's and Ethernet/Cheapernet interfaces.In addition , the "scheduler" processor may be equipped with a DMA -SCSI driver for local data dump facility an like hard disk or mass storage alowing the full autonomy and portability during the first stage of operation (from the prototype to the isnstallation) .
d) The PROCESSING is made by one or more dedicated mathematical oriented processor . The main task is mainly to reduce and format the data stream. These processor should be equipped with similar(VME/VSB interfaces, communication FIFO, over the VME bus, dual port memory) as the acquisition processor , but are using RISC based architecture and large global memories in order to deliver a very large number crunching power, especially for floating point format when running large mathematical programs
The interconnection mechanisms between the different processors occur through communication FIFO's over the VME bus.
d)The Trigger and gating logic have the same functionalities described for the front end crate but in addition should be responsible for the event number, the dead time measurement .....
f) The crate interconnection system is the backbone of a distributed concept . It is the data bus in the same sense as Ethernet is the control bus. It has three major applications areas:
- it interconnects the distributed VME crates.
- it interconnects the EVENT BUILDER
- it interconnects the different on line control worskstation
The so called standard IEC821 Vertical bus (VICbus) should be taken teday as an efficient example of such connection it provides a high speed transparent connection (20 times Ethernet) over 100 meters with the avantage of having no packet/frame notion. This means optimal performance for single word transfers as well as for long DMA block transfers.
Furthermore , nice technical extra features could also be introduced like the concept of reflective memory or "broadcast" developped for application where large data buffers must be shared by several processors distributed over several VME crates, which is to create a common

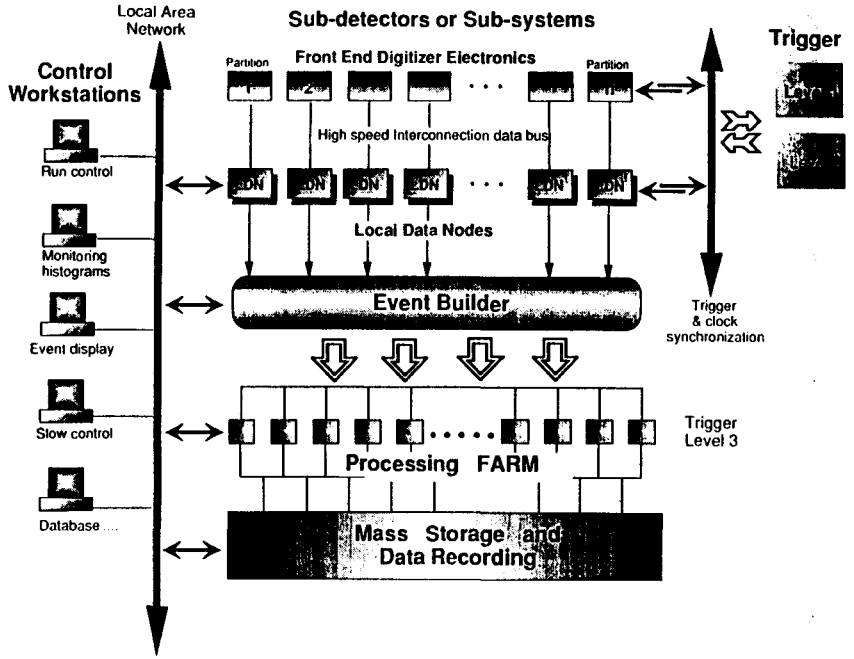
area shared between various parts of the system without any software manipulation. This means writing into a special on-board memory automatically updates the information in the memories of the other modules connected to the bus at the speed of 10 Mb/sec. When a CPU writes to a reflective memory, data are transparently broadcast all over the link and written as the same time in every memory. When a CPU reads data from the reflective memory, the cycles are kept local to the interface and do not create any activity over the link. Hence only the write cycles are transfered over the bus, saving a big deal of bandwidth.
g) The "Control WORKSTATION is the place to operate all the necessary human interface with the subdetector itself from program manipulation and storage, "local "run control and configuration,-data calibration, histogram presentation , processors terminal windows emulation , etc ..... This workstaion can also work as and intelligent spy during the data taking allowing to perform on-line fine monitoring . It should be part of the system and directly connected to the Local Data Node crate with the standard crate interconnection system.

The Front End Digitizer Crate



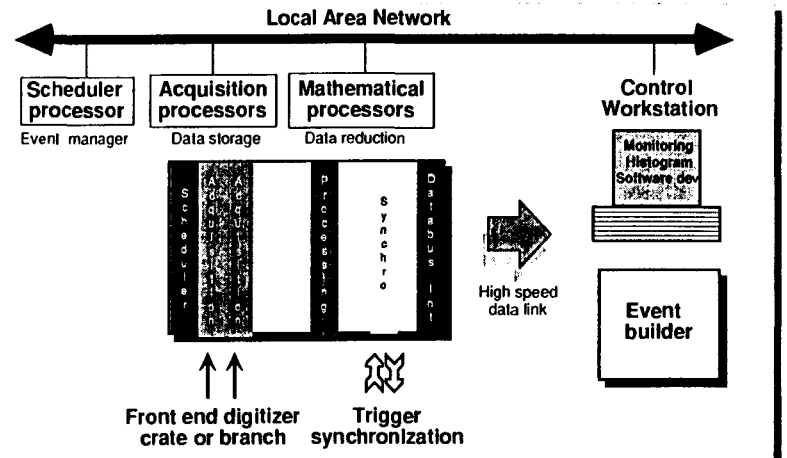
SDC DAQ 9/24/91

368



366

The Local Data Node



SDC DAQ 9/24/91

369

Components

Subdetector dedicated	Global SDC dedicated	Standard general purpose
• Front end board • Local L1T • Local L2T • Monitoring & control	• Front end crates • Syncronization (clock & Trigger) • Global L1T • Global L2T	• DAQ crates • Processors • Inteconnection links & drivers • Control worstation

- Prototype
- Test
- Document
- Duplicate
- Maintain

- Test & Select
- Integrate
- Buy

SDC DAQ 9/24/91

367

The Local Data Node

Definition:

This is a AUTONAUMOUS and PORTABLE data acquisition system (one per subdetector) which inherits from the global DAQ the same principles:

1 - Front End crate read out and buffering.
2 - Local subevent formatting and processing.
3 - Forwarding collected data to the EVENT Builder.
4 - Trigger and Gate Synchronization.
5 - Connection to the Control Workstation.

From the test

... to the Global DAQ.

The Showermax Electronics

P. Le Du(LBL&Saclay)

P. Le Dû
LBL / Saclay

Sept 91

The Showermax electronics

372

An overview of the architecture ...

From the Front End to the acquisition.

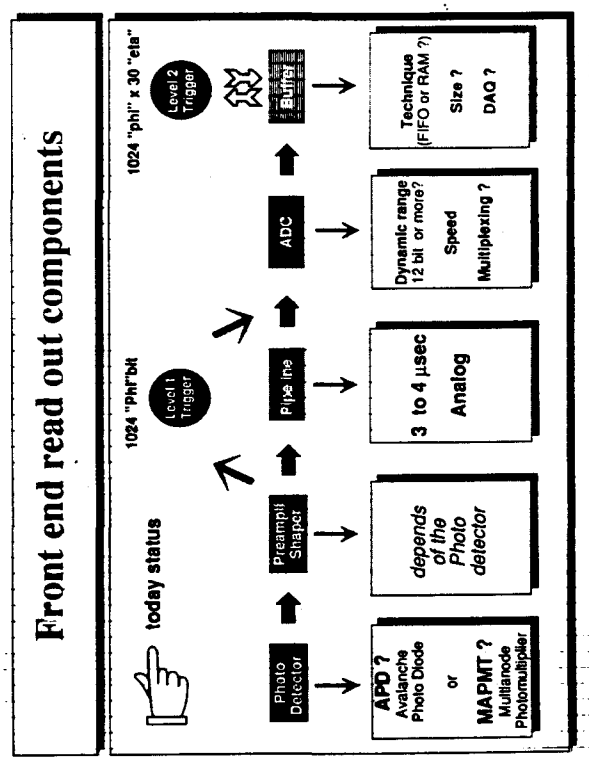
- Channels count :

  45 K + 12 K (massless gap) ⇝ 57 K

  (upgrade 1×2 towers ⟶ 102 K)

- Fully integrated with the calorimeter. el.
  - ⇝ same "building blocks" → pipeline, ADC, DAQ
  - ⇝ same FE crate
  - ⇝ common interface with L1T and L2T.
- Work on :
  - → components (ASIC's ..., connectors ....)
  - → System layout (FE board, DAQ ...)
  - → Optimization : physical - electronics segmentation reliability ...

373



9/6/91

The photodetector

374

A.P.D.

Avalanche Photo Diode

(Rockfeller - Saclay.)

General Electric Canada

- type GEC 30902 S
  - Ø 0.8 mm
  - C = 2 pF
  - Dark current ~ 50 nA
  - + special optical adapter (thin window + ball)
  - Gain ~ 200

Test ↗ Fermilab ↘ Saclay
- → Nphe / MIP ?
- → Noise ?
- → Stability ?

Compact but cost

100 → 20 $/ch.

M.A.P.M.T.

Multianode Photomultiplier

(UCLA - Saclay)

- type Philips 64ch.

Test → Fermilab
- → crosstalk ?
- → uniformity ?
- → stability .... ?

- New developments
  - → 256 ch (Philips)
  - → UCLA ...

Need space inside the detector

Volume ~ 32 Euro "6U" crates.

Front End Digitizer

375

— Ingredients —

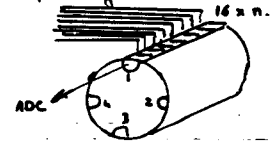
- Preampli - Shaper : (APD's)

  Parameters to optimize
  - low noise (500 e⁻ ?)
  - gain
  - frequency
  - dynamic range
  - shaping time (30 ns ?)
  - ...

- Pipeline ⟶ Analog 3 to 4 µsec

CERN-Jamon CSI Charge Integrator	LBL - CSA
1 µsec - 66 MHz. → VME card implementation	

- Analog to Digital Converter : ADC
  - ⇝ dynamic range = 12 bit should be OK
  - Search and wait for Commercial FADC 12 bit - 20 to 50 MHz.
  - multiplexing ⇝ 4 events "analog buffer" 16 x n. samples.

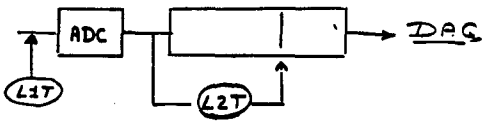


Principle.
(J.C. Buisson)

Ingredients (con't).

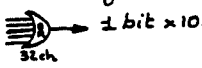
- **Digital Buffer**

  ⇝ Large Dual Port Memory which contains L1T digitized data waiting for L2T Accept to be transfered to the DAQ read out System



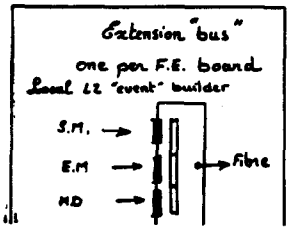
- **Level 1 Trigger :**

  The ShowerMax will be able to provide 1 bit (threshold) / channel after the preampli-shaper.



- **Level 2 Trigger :**

  Data (or sample) are extracted after the ADC

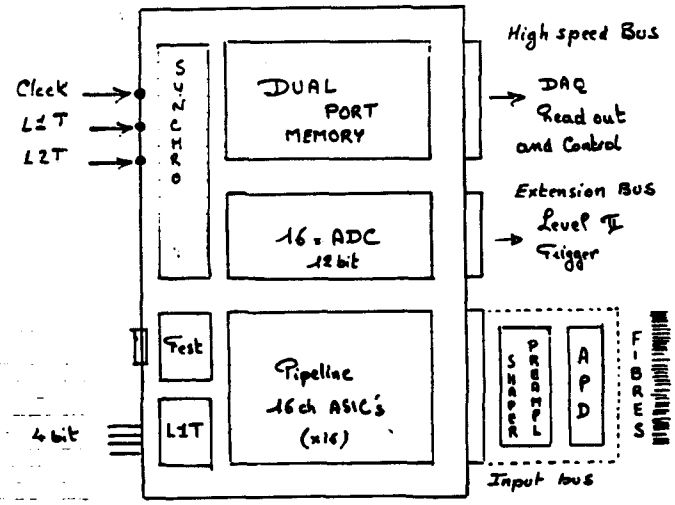


L2 Read out Controller
one per FE crate

- Distributed L2T
  - Local processing
  - Communication

The Showermax Front End Board

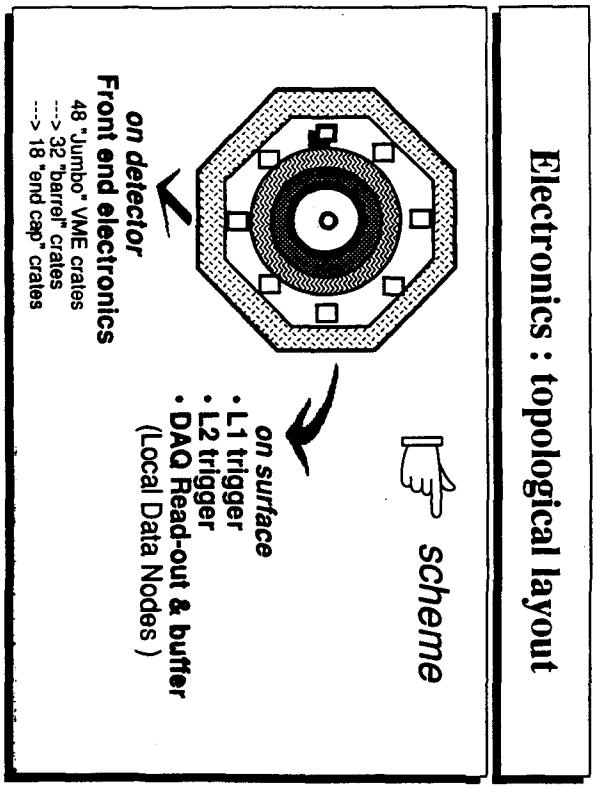
- 9U "Euro" Jumbo" crate



Problems → Layout

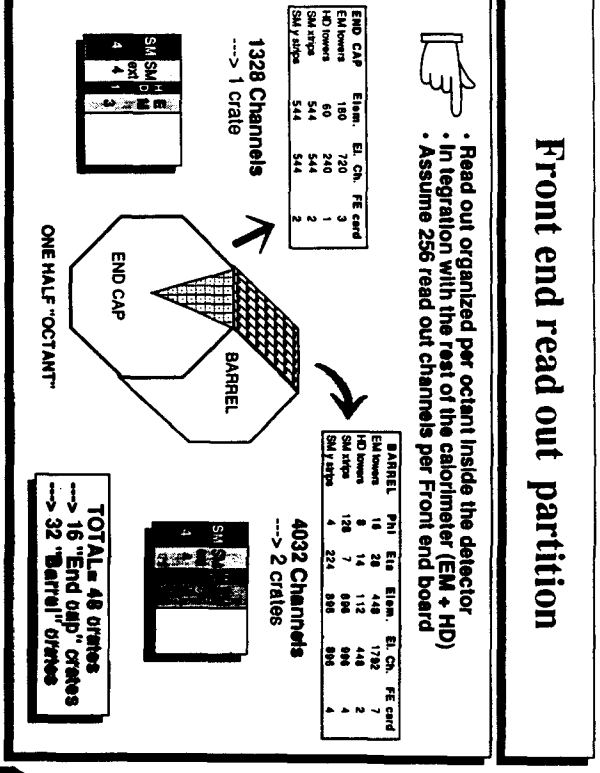
- Input connector : 256 ch ?
- Analog / digital combination ?

Electronics : topological layout



Front end read out partition

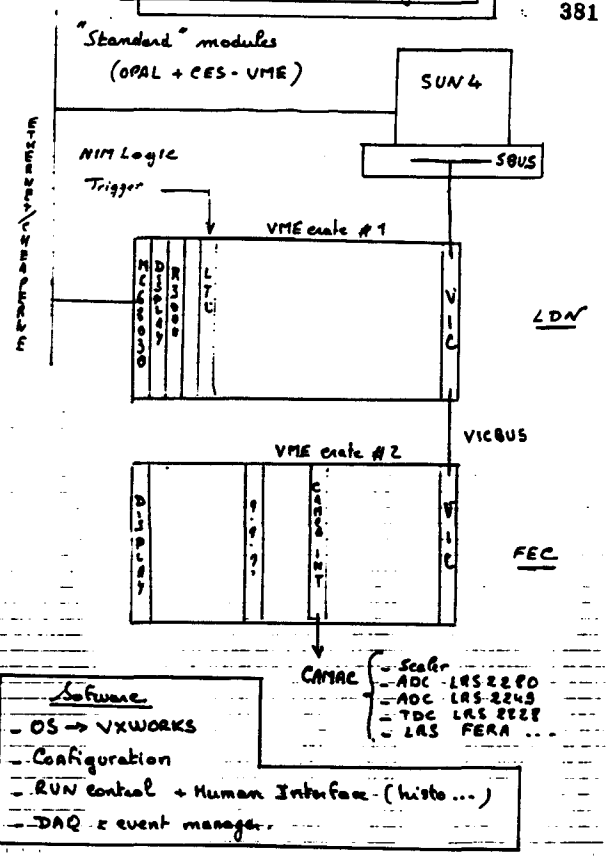
- Read out organized per octant inside the detector
- In tegration with the rest of the calorimeter (EM + HD)
- Assume 256 read out channels per Front end board



	END CAP	Elem.	El. Ch.	FE card
EM towers	180	720	3	
HD towers	60	240	1	
SM strips	544	544	2	
SM y strips	544	544	2	

	BARREL	PHI	Eta	Elem.	El. Ch.	FE card
EM towers	16	28	448	1792	7	
HD towers	8	14	112	448	2	
SM strips	128	7	896	896	4	
SM y strips	4	224	896	896	4	

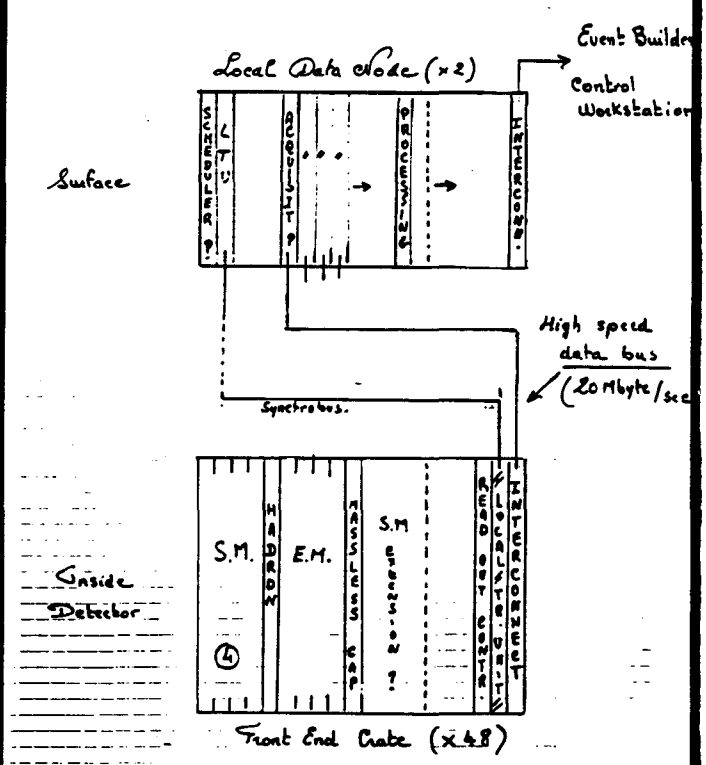
L. D. A prototype



Software

- OS → VXWORKS
- Configuration
- RUN control + Human Interface (histo ...)
- DAQ + event manager

Showermax Read out



UCLA Cosmic-Ray Test

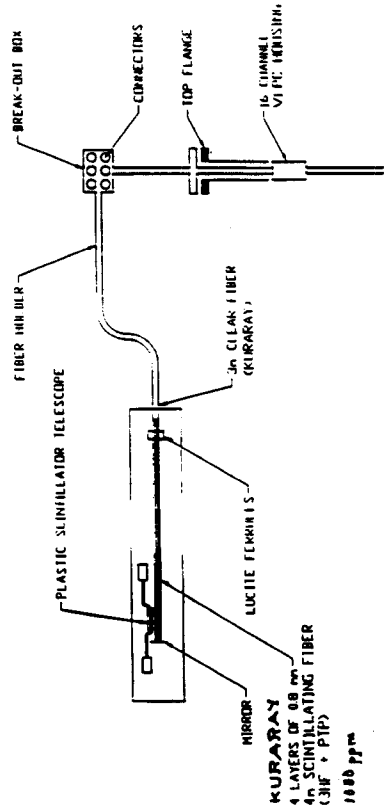
M. Atac(UCLA)

Presented by M.ATAC FNAL/UCLA

ORNL, Sept. 27, 91

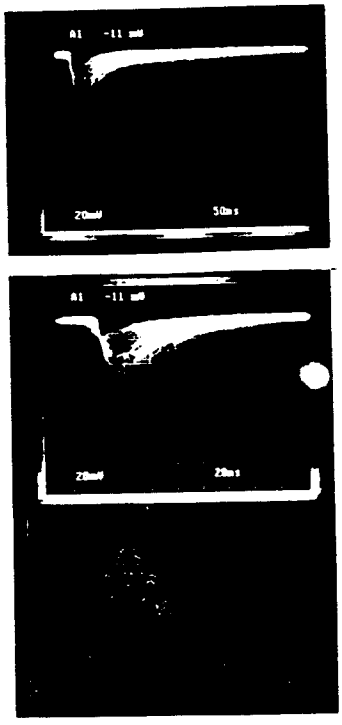
M.Atac, J. Park and D. Chrisman
UCLA
H. Fenker and K. Morgan
SSCL

UCLA COSMIC-RAY TEST



M.Petroff, M.Atac, D.Ch...
UCLA, Jan.28/1991

USING 2PA02 SILICON STRIP AMPLIFIER (By Tektronix)

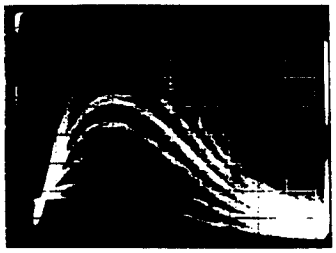


FREQUENCY

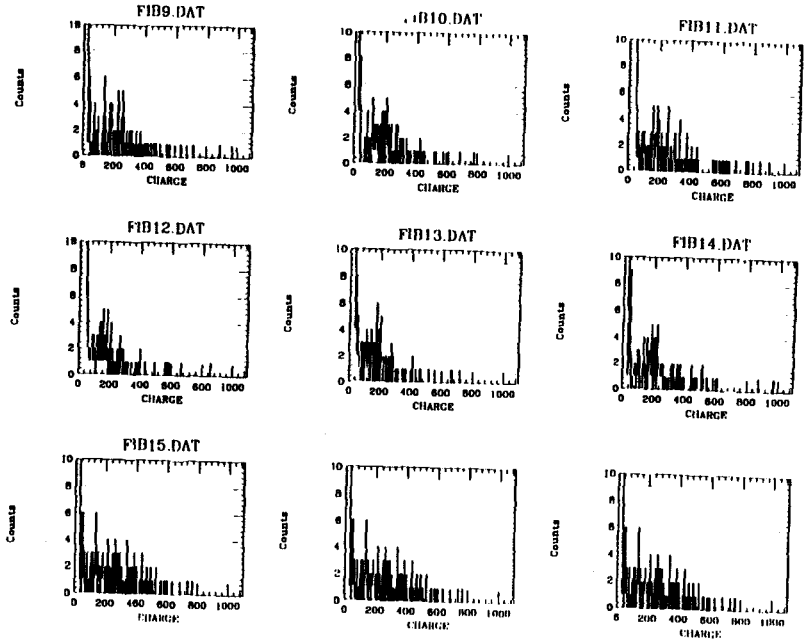
CHARGE (0.25 pC/channel)

M.ATAC

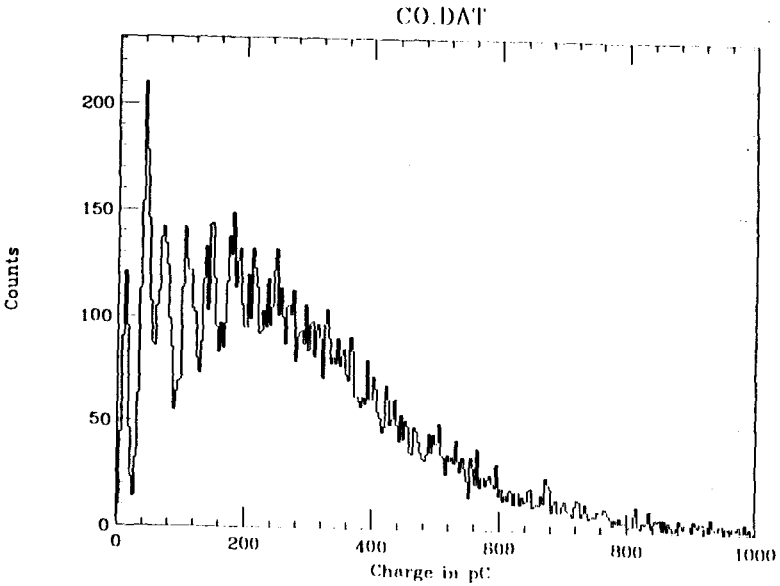
Rockwell PET ampl.



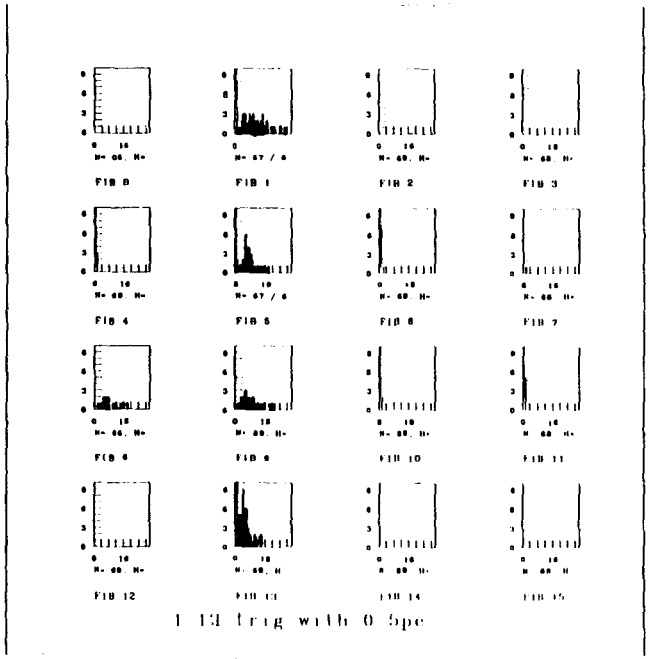
100 nsec/div 20 mV/div



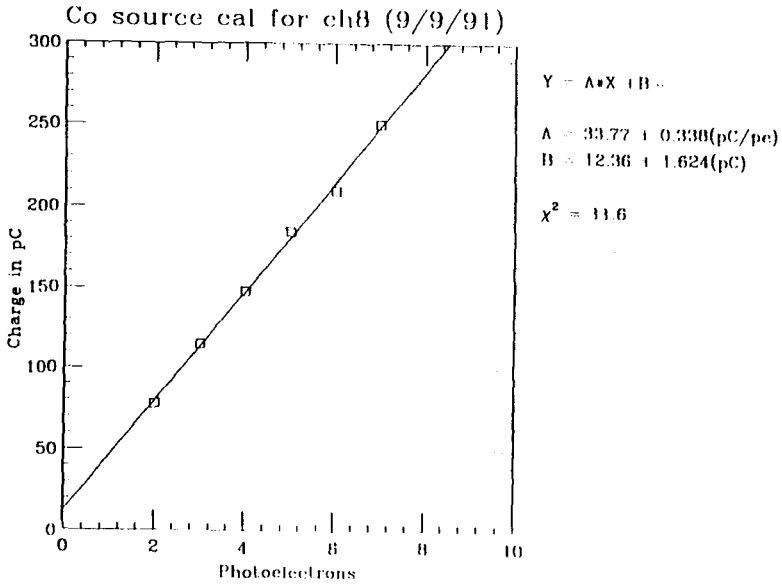
389



387

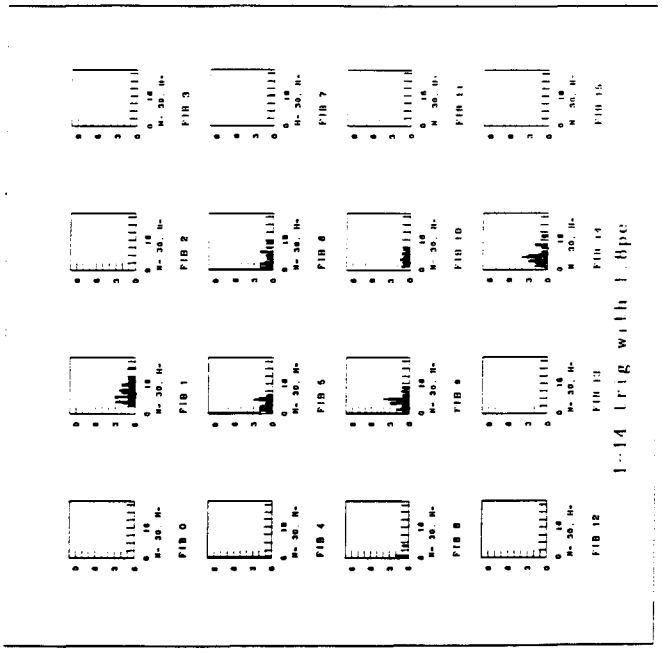


390

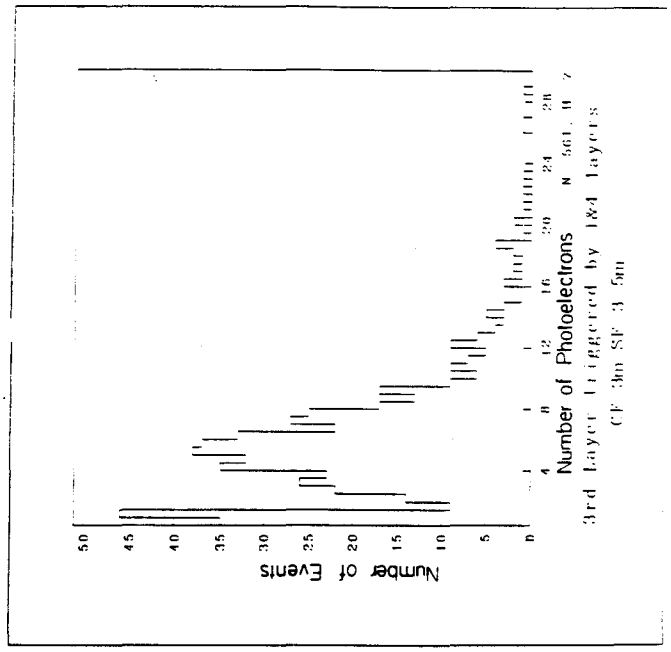


388

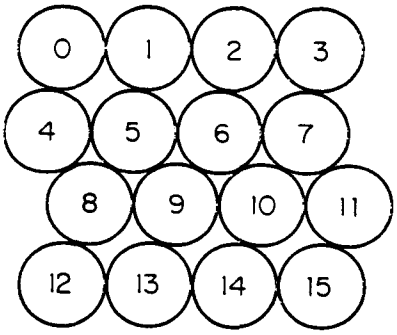
391



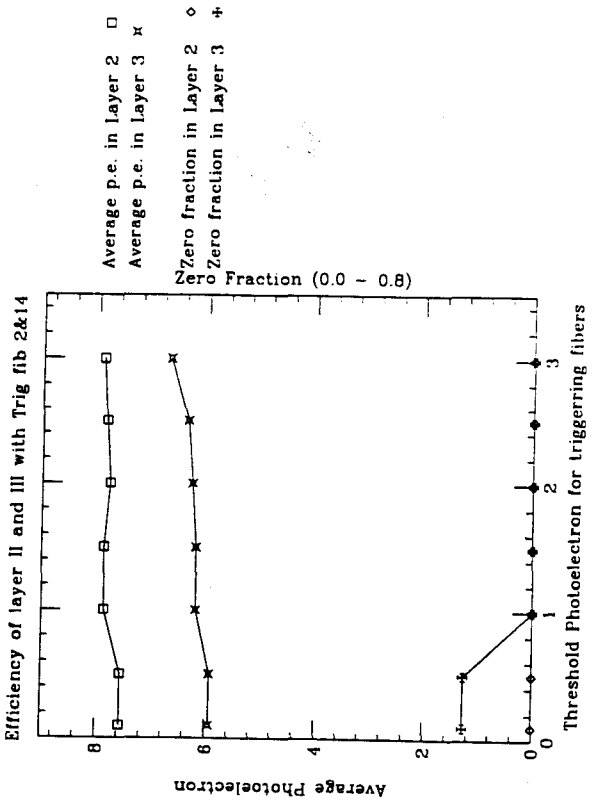
392



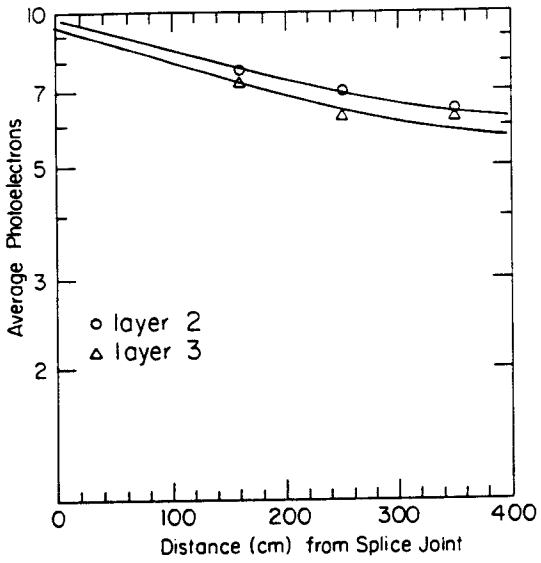
393



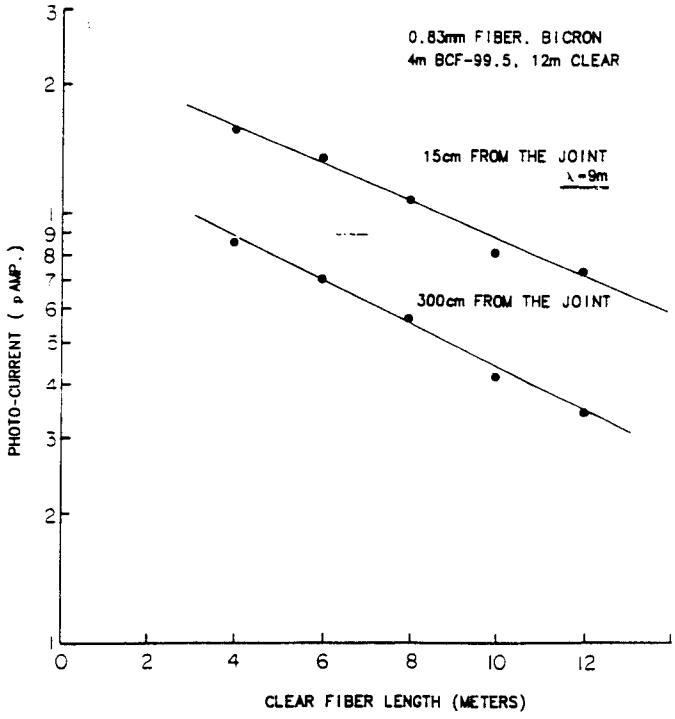
394



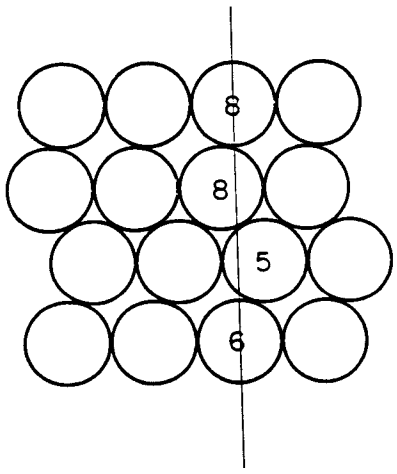
395



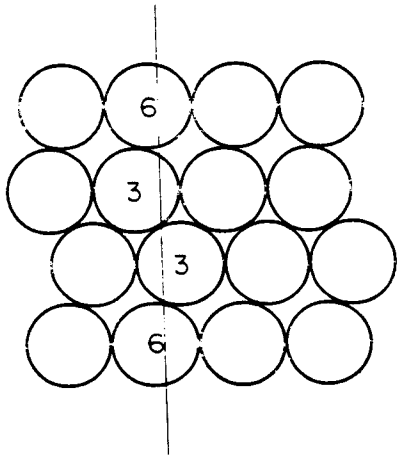
396



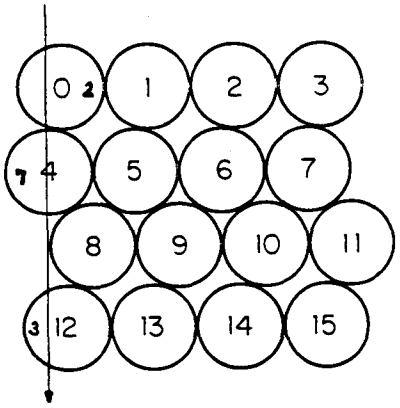
397



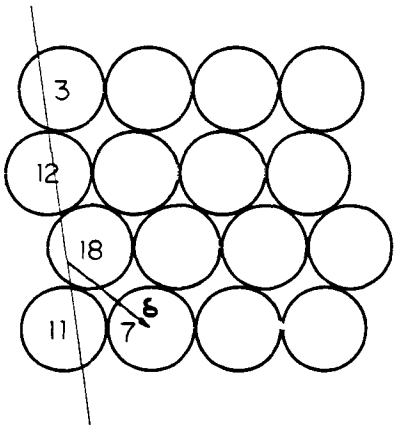
398



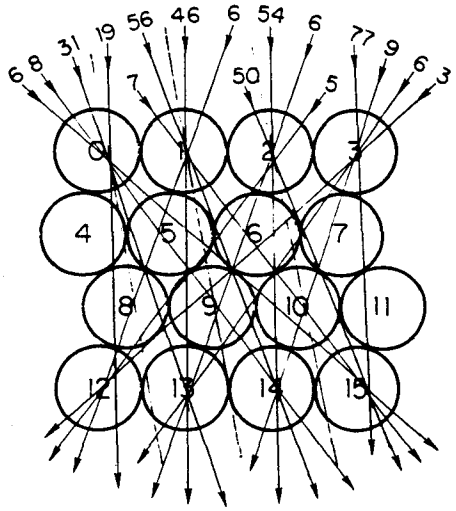
399



400

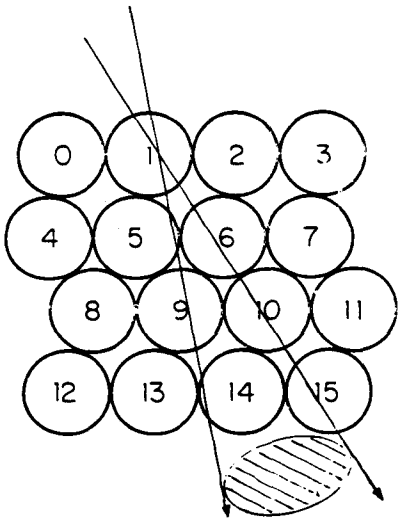


401



Number of Events Ph_{thr} = 4 p.e.

402



90% OF COSMIC-RAY TRACKS ARE WITHIN THIS SOLID ANGLE

FUTURE PLANS

- COMLETED A NEW 32 CHANNEL CRYOSTAT AND PLAN TO TAKE COSMIC-RAY DATA AT UCLA.
- HOPING TO GET IR INSENSITIVE VLPCs FROM ROCKWELL WITHIN A MONTH
- REPLACE THE VLPC I CHIPS WITH VLPC II CHIPS IN THE PRESENT CRYOSTATS AND DO BEAM TESTS HOPEFULLY AT FERMILAB. IF WE ARE LATE WE WILL DO THE TEST AT BNL.

Electron Trigger Backgrounds

M. Miller(Chicago)

405 M. Miller
U. Chicago
9/27/91

Electron Trigger Backgrounds

Purpose of Study:

Level 1, 2 electron trigger rates are dominated by background

- Overlap
- Conversions
- Early showering hadrons

If understand relative rates,
⇒ design trigger (and detector) appropriately to reduce background

Ex: Conversions

- Silicon tracker
- Reduce material

Overlap

- Shower max

SDC Note very soon

Simulation

406

Event Generation:

Minbias (ISAJET TWOJET $5 \le P_t \le 200$) overlayed on TWOJET events

Tracking:

- Propagate particles in B field to calorimeters
- 20% radiation length & no conversions, no brem
- Smear P_t w/ trigger resolution
- tracking 100% efficient
- π, K decay in flight

Calorimetry:

- Fast shower parameterization longitudinal + transverse
- Create trigger tower array for E_t

Shower max:

No simulation

Method

407

For each trigger tower store info on 4 highest Et particles entering tower and info on highest P_t track pointing to ϕ region.

E_T (P_t), η, ϕ, ID, conversion bit

Define 5 "electron" categories for clusters which pass electron cuts

Overlap (C): Tower contained γ ($P_t > 5$ GeV) but no conv. e⁻ e. Trigger-track not conv.

Showering Pion (S): Tower contained no γ, conv, or e ($P_t > 5$ GeV). Trigger-track in same tower.

Conversion (C): Conversion ($P_t > 5$ GeV) in trigger tower.

Overlap/Conv (OC): Trig track conv. and not in trigger tower

Electron (E): Electron but not conv.

Data Sets and Trigger Cuts

408

Data Sets:

ISAJET TWOJET event type

$20 < P_t < 50$ GeV 2000 events

$50 < P_t < 100$ GeV 800 events

$100 < P_t < 200$ GeV 500 events

Cuts:

Type	E_T (GeV)	Had/EM	Iso	P_t (GeV)
Loose	10	0.07	0.1	5
Tight	10	0.05	0.07	5

Separated triggers with

$E_t > 30$ GeV

$E_t < 30$ GeV

Results

All triggers :

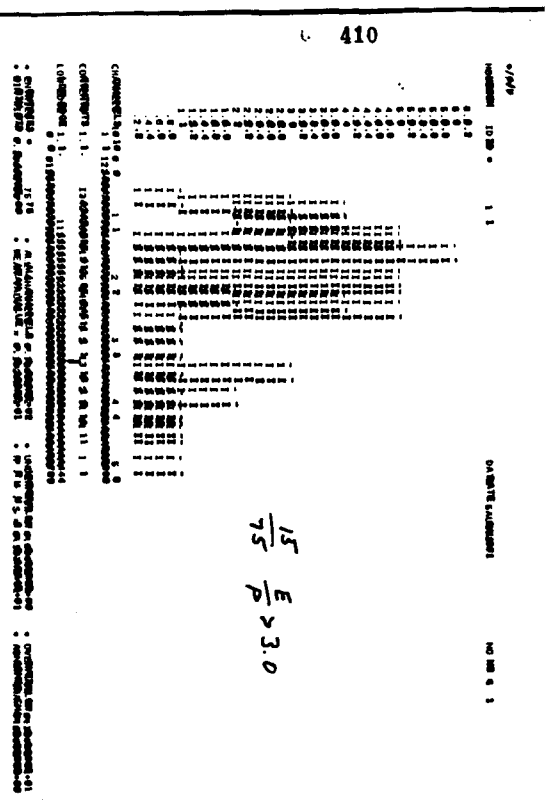
Category	Loose		Tight	
O	17	(23)	8	(16)
S	15	(20)	5	(10)
C	30	(40)	27	(55)
OC	9	(12)	6	(12)
E	4	(5)	3	(6)

$P_t > 30$ GeV

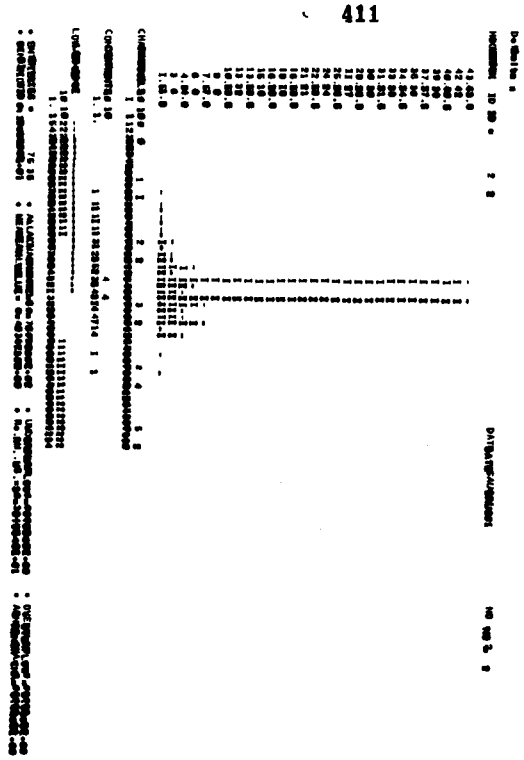
Category	Loose		Tight	
O	6	(25)	2	(13)
S	2	(8)	1	(7)
C	12	(50)	9	(60)
OC	3	(13)	2	(13)
E	1	(4)	1	(7)

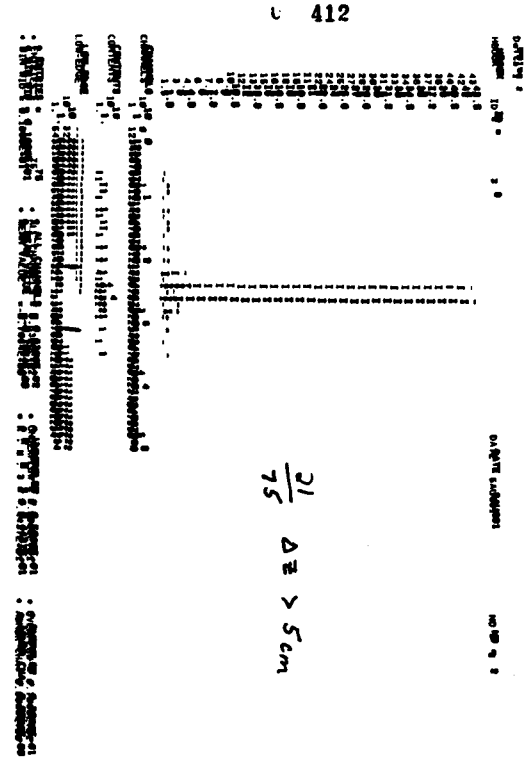
$P_t < 30$ GeV

Category	Loose		Tight	
O	11	(22)	6	(18)
S	13	(25)	4	(12)
C	18	(35)	18	(53)
OC	6	(12)	4	(12)
E	3	(6)	2	(6)



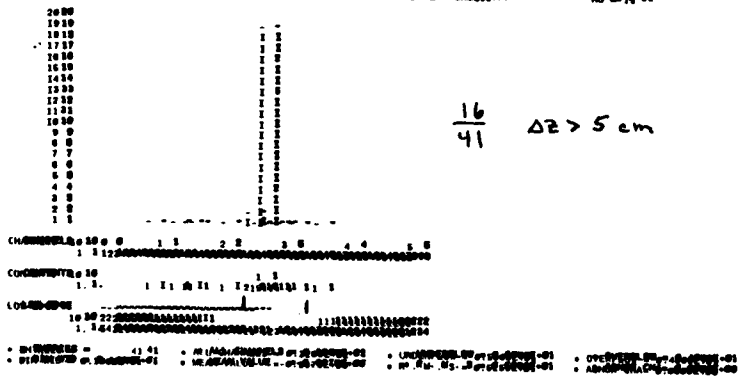
$\frac{15}{75}$ $\frac{E}{p} > 3.0$





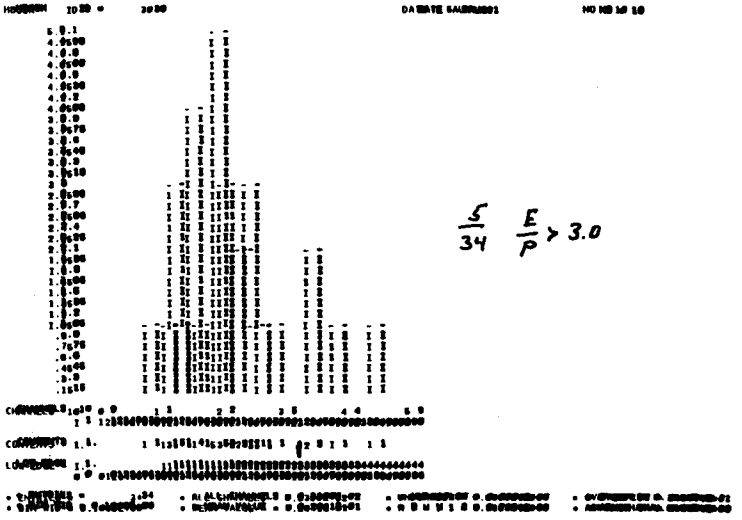
$\frac{75}{12}$ $\Delta z > 5$ cm

414



$\frac{16}{41}$ $\Delta z > 5$ cm

413



$\frac{5}{34}$ $\frac{E}{P} > 3.0$

SDC Trigger Design Documents

W. Smith(Wisconsin)

SDC Trigger Design Documents

University of Wisconsin–Madison

Contents:

D. Panescu, J. Lackey, P. Robl, W.H. Smith, *An SSC PMT Preamplifier Circuit*, SDC Note SC-91-00086, 1991.

T. Gorski, J. Lackey, W.H. Smith, W. Temple, *Isolated Electron Pattern Logic Design and Performance at the SSC*, SDC Note SDC-91-00087, 1991.

T. Gorski, J. Lackey, W.H. Smith, *Level 1 Trigger Decision Design for the SDC*, SDC Note SDC-91-00088, 1991.

W.H. Smith, T. Gorski, J. Lackey, *SDC Trigger Preliminary Conceptual Design*, SDC Note SDC-91-00090, 1991.

W.H. Smith, T. Gorski, J. Lackey, *SDC Global Level 1 Processor: Clock & Control*, SDC-91-00090, 1991.

M. Thompson, *Fiber Optic Data Transmission for the SDC Detector*, SDC Note SDC-91-00092, 1991.

SDC Note SDC-91-00086
DRAFT
September 5, 1991

An SSC Photomultiplier Tube Preamplifier Circuit

Dorin Panescu
Joe Lackey
Phil Robl
Wesley H. Smith
University of Wisconsin Madison, Physics Department
Send all the correspondence to:
Wesley H. Smith, University of Wisconsin, Madison, Physics Department, Chamberlin Hall, 1150 University Avenue, Madison, WI 53706

Abstract

This study presents the design of the front end amplifier for a calorimeter planned for the Superconducting Supercollider (SSC). The design is based on analytical computations and SPICE simulations, and is checked against tests performed on a prototyped circuit. We were looking to achieve (1) a very low droop within the 4 ns after the integration of the photomultiplier tube (PMT) signal was completed, (2) a very low noise figure for the whole amplifier in a 100 MHz bandwidth, (3) an input impedance optimized for the PMT which is actually used, (4) baseline restoration as quick as possible at the output of the clip amps, (5) no loss of information owing to the saturation at intermediary stages (e.g. integrator), and (6) an output driving 100 Ω twisted pair cables, or 50 Ω coaxial cables, in order to transmit the signal to the switched capacitor arrays.

I. Introduction

The calorimeter for an SSC detector requires good energy resolution, fast time response, fine segmentation, and a high degree of hermeticity [4]. The requirements are such that at a luminosity of 10^{33} there are 1.6 minimum bias events per beamcrossing (every 16 ns) due to 10^8 interactions/sec. For the hadron section of the calorimeter the maximal signal of any electronic channel is set at 5 TeV (assuming equal sharing of energy between the front and back sections). The minimal signal of interest in an electronic channel is determined from electron isolation and muon detection, and is defined as 30 MeV. Thus the dynamic range of this section should be $20\cdot\log\frac{5\ \text{TeV}}{30\ \text{MeV}} = 104$ dB. For the electromagnetic section of the calorimeter the maximal signal is set at 5 TeV, while the minimal signal is defined as 30 MeV, thus its dynamic range is also 104 dB. The reader is referred to [2], [11], [14], and [21], for more explanation regarding the energy bounds. The front end electronics has to be able to process the PMT output signal which has a minimum 16 ns duration and 104 dB dynamic range (in order to cover the demands of both sections). For energies of 5 TeV and 30 MeV the output current of the PMT is 50 mA and 300 nA respectively. During the time required to make a trigger decision (< 4 μs) the signal has to be stored in an analog memory at a sampling period of 16 ns.. It was found, [10], that much of the electronics development for other type of systems (e.g. ZEUS calorimeter system) was inappropriate for the very fast signals with a very high dynamic range from a scintillator calorimeter. Indeed, as presented in [3], and [8], new equipment and devices have to be used. A comparison between the performance of ZEUS calorimeter at HERA, [13], and a calorimeter for an SSC detector is given in table I. In addition to the much higher dynamic range and frequency spectrum of the input signal, the front end electronics has to deal with 10 times lower amplitude signals. This implies a better noise figure for the input amplifier, which also has to have an

acceptable signal to noise ratio (SNR) for the lowest energy level. Figure 1 presents the block diagram of the front end circuit which satisfies the general requirements derived above. In order to achieve the desired dynamic range and noise performance the most feasible solution is to split the signal into a high gain path and a low gain path. The ratio between the gains of these paths is chosen to be equal to 32. The PMT output current is conditioned by the current amplifiers, shown as (1) and (2) in fig. 1, and is integrated by the fast and low noise integrators (3) and (4).

Table I.
Comparison between significant parameters of the calorimeters for the ZEUS detector at HERA and for an SSC detector

Parameter	Calorimeter of ZEUS detector at HERA	Calorimeter for SSC detector
Minimal energy	300 MeV	30 MeV
Maximal energy	400 GeV	5 TeV
Minimal PMT output current	75 μA	300 nA
Maximal PMT output current	100 mA	50 mA
Dynamic range	62 dB	104 dB
Interval between beam collisions	96 ns	16 ns
Sampling frequency in the pipeline	96 ns	16 ns

The gain of the integration is set in accordance with the overall gain of the two paths. After the integration is completed the baseline of the signal is restored in order to avoid the loss of information. This might occur if a high energy crossing is immediately followed by a very low energy one, and subsequently one of the circuit components is close to the saturation point, where non-linearities are likely to appear. Using passive delay lines, clip amps, shown as (7) and (8) in fig. 1, restore the baseline, and transmit the signal to the cable driver stages (9) and

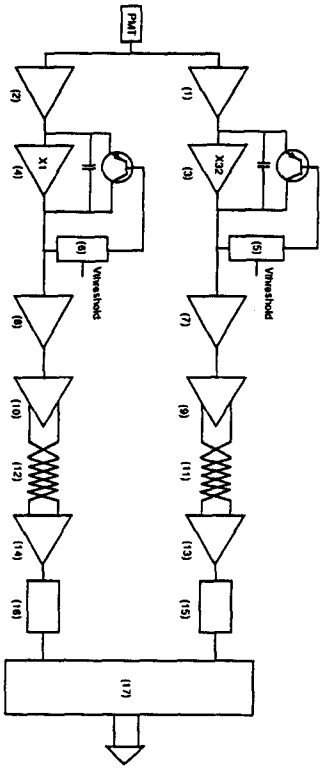


Fig. 1 The block diagram of the front end circuit

(10). The cables, shown as (11) and (12) in fig. 1, are connected to the line receivers (13) and(14) which serve as buffers for the switched capacitor arrays (15) and (16). The switched capacitor arrays (SCA) are read out after a trigger decision and digitized with a 12-bit ADC in the digital block, shown as (17) in fig. 1. Storage of the data is performed on the SCA card until the trigger determines that data should be read out. A detailed SCA presentation is provided by Kleinfelder et al., [18]. The primary function of the SCA card is to receive, process, and digitize the signal from 256 analog channels. It is physically composed of 16 SCA integrated circuits, each of them having 16 input and output channels. The SCA integrated circuit can sample and store the level of analog inputs at a 62 MHz rate. It can simultaneously store and retrieve analog samples from the different cells.To avoid large time jitter error, the integrated signal variation during the sampling process, within a 4 ns period after the integration is completed, has to be less then 1 LSB. This also means that the droop of signal at the output of the baseline restoration circuit has to be less than 1 LSB over 4 ns after the integration is completed. Under certain conditions the accomplishment of this task can bring the integrators into saturation. Thus the integrators have to be protected against the loss of information in the vicinity of the saturation point by protection circuits, shown as (5) and (6) in fig. 1, which restore the baseline at the output of the integrators just before they can saturate. The functions of the digital block are described in [15], and [16].

The goal of this study is to design the input amplifier which comprises the current amplifiers (1) and (2), the low noise and fast integrators (3) and (4), the protection against saturation circuits (5) and (6), the clip amps (7) and (8) and the cable drivers (9) and (10). The design is based on analytical computations and PSPICE, [19], simulations, and is checked against the tests performed on the real circuit. We were looking to achieve (1) a very low droop within the 4 ns after the integration of the PMT signal was completed, (2) a very low noise

figure for the whole amplifier in a 100 MHz bandwidth, (3) an input impedance optimized for the PMT which is actually used, (4) baseline restoration as quick as possible at the output of the clip amps, (5) no loss of information owing to the saturation at intermediary stages (e.g. integrator), and (6) an output driving 100 Ω twisted pair cables, or 50 Ω coaxial cables, in order to transmit the signal to the switched capacitor arrays.

II. The Design of the Input Amplifier

We consider the input amplifier to be connected to a PMT which has fast time response and low background noise, thus being suitable for high energy physics applications. Reference [20] describes the features of R580-15 which turns to be proper for these kind of applications. According to [5], and [12] the signal supplied by the PMT has exponentially shaped edges, being close to a triangle, thus within our SPICE simulations we used a piecewise linear signal which had a triangular shape. The falling and rising times were chosen to be 6 ns and 10 ns, respectively, adding to form a 16 ns overall duration pulse. The maximal output current, corresponding to 5 TeV, for this tube is 50 mA, while the minimal level, corresponding to 30 MeV, is 300 nA. In order to have proper raising and falling times at the PMT output, when the front end input amplifier is connected, a low input impedance for this stage is desired. A low value for this impedance also implies less additional noise in the input circuit, thus a better noise performance for the equipment. According to these requirements we chose the input impedance equal to 50 Ω.

A. The current amplifiers

Because the PMT output current is split between the high and low gain paths, the actual level of the lowest current which has to be integrated by the high gain path is lower than 300 nA. In order to avoid a too low SNR at the output of the integrator for this case, we chose to boost the PMT current before it is integrated. The current amplifiers, shown as (1) and (2) in fig. 1, are designed for this task. There are three main requirements which have to be satisfied by these two stages: (a) the overall input impedance has to be = 50 Ω, (b) a proper ratio between the currents going into the low gain path and into high gain path has to be provided, and (c) their current gain has to be chosen such that taking into account the gain of the next stages, the output of the front end amplifier swing need to be equal to ± 2.5 V. The diagram of the current amplifiers used for these purposes is given in fig. 2. The transistors Q1 and Q2 make up the inverting current amplifier, while the feedback coefficient is mainly given by R4 and R6. R5 is used to fix the operating point of the circuit, and the diodes D1, D2 limit its gain if the input current exceeds $= \frac{2 V_D}{R4}$. The input impedance, as it is proved below, is mainly given by R1.

The capacitors C2 and C3 compensate the transistors frequency characteristics, in order to avoid oscillations or underdamped responses.

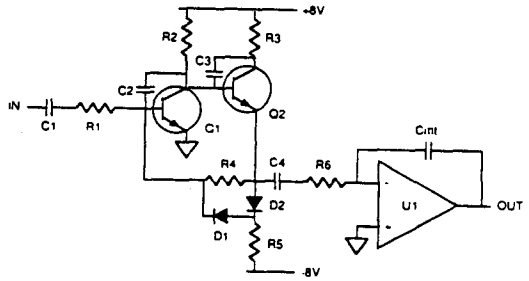


Fig. 2 The input current amplifier

The circuit has a series-shunt type of feedback, thus the gain of the amplifier without feedback is (considering the hybrid parameters model for the transistors):

$$G_I = \frac{(1+h_{21e2})\cdot R2\cdot h_{21e1}}{R1+(1+h_{21e2})\cdot(R4\|R5\|R6)} \cdot \frac{R4+R5\|R6}{R4+R5\|R6+h_{11e1}} \quad (1)$$

The feedback coefficient, β_i, is given by (2):

$$\beta_i = \frac{R5\|R6}{R4+R5\|R6} \quad (2)$$

Thus the circuit current gain with feedback is:

$$G_{if} = \frac{I_{e2}}{I_{in}} = \frac{G_I}{1+\beta_i\cdot G_I} \quad (3)$$

This gain has to be adjusted in order to find out how much of the Q2 emitter current , I_{e2} ,goes through R6 into the integrator. Because the impedance in the base of Q1 is very low, owing to the current feedback, the adjusting factor is:

$$k = \frac{I_{out}}{I_{e2}} = \frac{R5\|R4}{R6+R5\|R4} \quad (4)$$

Hence the actual current gain is:

$$G = G_{if}\cdot k \quad (5)$$

The impedance in the base of Q1 may be computed as:

$$Z'_{in} = \frac{(R4+R5\|R6)\|h_{11e1}}{1+\beta_i\cdot G_I} \quad (6)$$

And the circuit input impedance is:

$$Z_{in} = R1+Z'_{in} \quad (7)$$

In the calculations presented above the capacitors were considered to be large enough in order to be neglected. Choosing the operating collector currents for the transistors to be =1.5 mA for Q1 and =2 mA for Q2, and taking into account that the voltage developed across R2 is =8V-2·0.6V = 6.8V, and across R5 is =8V, we obtain R2 = 5.1 KΩ and R5 = 3.9 KΩ. We selected R4 and R6 as low as possible, thus it is reasonable to assume that R5≫R6 and R5≫R4, which implies R5||R6 = R6 and R5||R4 = R4. In order to have a reasonable SNR at the output of the integrator for the lowest PMT output current, and taking into account that the estimated

integrator output noise voltage is = 0.2 mV $_{rms}$, we chose the ratio between the current through the high gain path and the current through the low gain path to be = 5.5, and the gain of the current amplifiers equal to 3. Thus we obtain R4 = 330 Ω and R6 =100 Ω (for these values and an infinite G_I we would have a gain of 3.3). The transistors employed were BFR 92, for which the databook gives h_{21e} = 20, hence $h_{11e} = h_{21e}\cdot\frac{V_T}{I_C}$ = 390 Ω, G_I = -167, β_i = -0.23, k = 0.77 and G = 3.2, according to the above given formulas. The simulations by SPICE indicated a gain of 2.7, where the difference is due to neglecting the frequency characteristic of the transistors in the analytical computations presented above. Substituting the values above into eq. (6) we obtain Z'_{in} = 5 Ω, thus Z_{in} = R1. Hence, the input impedance of the whole circuit (considering both high and low gain paths) will be approximately $R_{1H}\|R_{1L}$ (the parallel combination of the input impedances of the two paths). This means that $R_{1H}\|R_{1L}$ = 50 Ω, and also we have $\frac{R_{1L}}{R_{1H}}$ = 6 (as it was found above). We conclude that R_{1H} = 56 Ω and R_{1L} = 330 Ω. The resulting input impedance (considering Z'_{in}) is = 51 Ω. In order to avoid phase shift between channels, the input time constants should be equal. $C_{1H}\cdot R_{1H} = C_{1L}\cdot R_{1L}$, which means C_{1H} = 100 nF , and C_{1L} = 18 nF. The diodes D1 and D2 are MBAL 99 ultra-fast switching diodes and they limit the gain and the output swing of the current amplifier, in order to avoid the hard saturation of the high gain path during large PMT pulses. These diodes are not used in the low gain path, and they limit the high gain when the PMT output current exceeds 4 mA.

B.The fast, low noise integrator

For the design of the fast, low noise integrator we considered several alternatives: customized IC, hybrid circuit, and the use of high speed, low noise commercial available op-amps. It turned that the quickest, and most cost effective solution was to employ high speed, and low noise op-amps, which also yielded better performance. We found that if the gain-

bandwidth product (GBWP) of the op-amp was not high enough, an overshoot occurred at the end of the integration. In order to account more exactly for this requirement on the op-amp features, we used SPICE to simulate two different cases: (1) the op-amp had a = $2.6\cdot10^8$ Hz GBWP, and (2) the op-amp had a = $2.6\cdot10^9$ Hz GBWP. Fig. 3 shows the effects of the GBWP upon the integration. It can be noticed that for a larger GBWP the overshoot is attenuated. According to these SPICE predictions we chose the AD 829 as an integrator, taking into account its 750 MHz transition frequency and its low noise performance. In order to compensate for the overshoot, not entirely eliminated, we used an AD 848 connected in a feedback network which also stabilized the d.c. output component. The outline of this integrator is presented in fig. 4, while the actual schematic is shown within the general diagram in Appendix A.

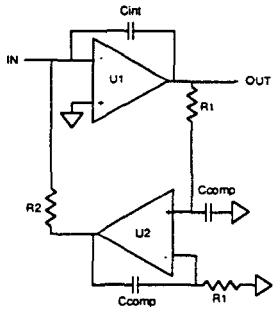


Fig. 4 The fast, low noise integrator

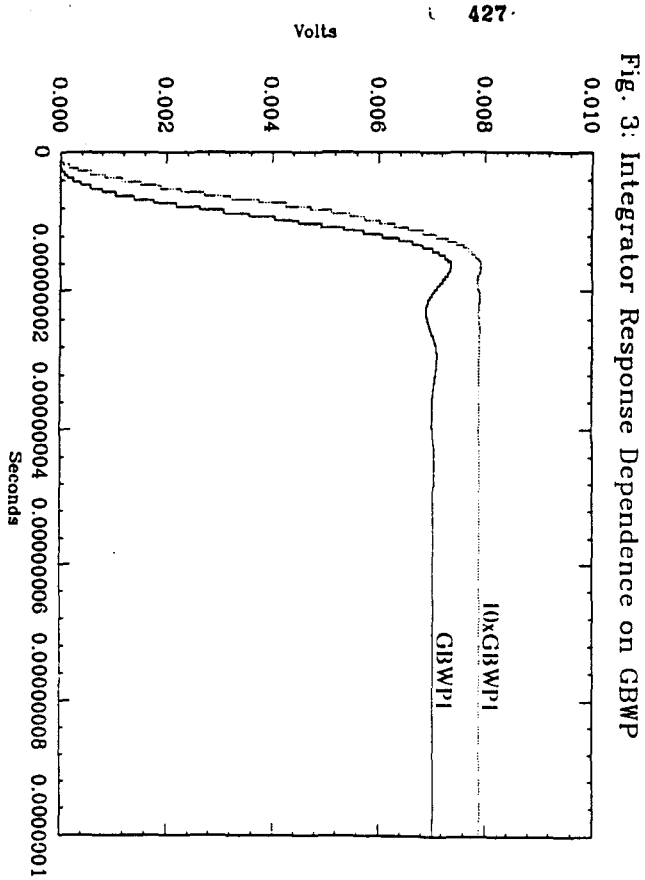


Fig. 3: Integrator Response Dependence on GBWP

Because the minimum level of the integrator output voltage is about 0.4 mV, we have to check the noise level at the integrator output in order to have it under the above mentioned value. Fig. 5 presents the basic diagram of an op-amp connected to an integrator configuration which avoids the op-amp saturation by using the bleeder resistor R. It can be demonstrated that the voltage noise RMS value at the integrator output is given by (8), [22]:

$$V_{on}^2 = e_n^2 \cdot B + i_n^2 \cdot R/(4 \cdot C) + k \cdot T/C \qquad (8)$$

Where V_{on} is the noise RMS value at the integrator output, e_n is the op-amp voltage noise spectral density, i_n is the op-amp current noise spectral density, k is Boltzman constant, T is the operating temperature in Kelvin, and B is the operating frequency range, which in this case are 300 K and 100 MHz, respectively. Considering $e_n = 2\ nV/\sqrt{Hz}$ and $i_n = 1.5\ pA/\sqrt{Hz}$ for an AD 829, according to [1], we theoretically predict V_{on} to be about 0.13 mV_{rms}, hence the noise performance satisfies 104 dB dynamic range requirements. This value corresponds to C = 10 pF, and R = 300 KΩ, a value which simulates the d.c. compensation network behavior.

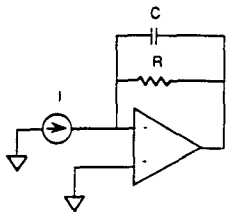


Fig. 5 The configuration for noise performance computation

For the configuration in Fig. 4 no bleeder resistor is needed because the d.c. and low frequency behavior is stabilized by the feedback network comprising R1, R2, Ccomp, and U2. The network was designed such that R2 can also compensate the overshoot which appears at the end of the integration, due to the limited GBWP of the op-amp. This solution makes the compensation easy to implement, but it has the drawback that it generates a damped low frequency oscillation at the integrator output. This oscillation does not affect the performance of the whole circuit because it is cancelled by the baseline restoration circuit. If the PMT output current pulse amplitude is equal to 300 nA, its minimal level, then, according to section A., about 254 nA will enter into the high gain path. The high gain path current amplifier amplifies this current up to about 762 nA. Considering a typical 16 ns PMT output pulse, as it was described before, this implies that the injected charge into the high gain path integrator is about 6 fC. For the integration capacitor equal to 10 pF this means an integrator output voltage of about 600 μV. Hence, this is the minimal voltage level at the integrator output. As was required it is higher than the voltage noise RMS value which was estimated to be about 130 μV. In order to have the ratio between the gains of the high and low gain paths equal to 32 the integration capacitor of the low gain path has to satisfy (5.5 is the ratio between the currents flowing into the high gain and low gain paths, respectively):

$$C_{inlg} = C_{inhg} \cdot \frac{32}{5.5} = 10\ pF \cdot \frac{32}{5.5} = 58\ pF$$

For practical reasons we chose to use 16 pF for the high gain path, and, subsequently, 91 pF for the low gain path. For these values the minimal voltage level at the integrator output is about 375 μV, which is still higher than the estimated voltage noise RMS value. Fig. 6 presents the SPICE-simulated response of the integrator to a typical 16 ns PMT output pulse. The droop, within 4 ns after the integration is completed, is about 0.1% from the peak level and it is expected to be possible to further improved it on the PCB by properly adjusting the value of R2

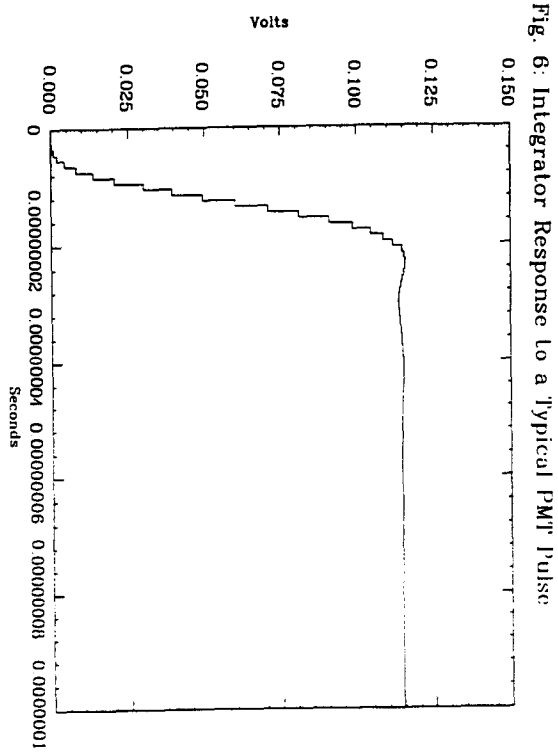


Fig. 6: Integrator Response to a Typical PMT Pulse

C. The baseline restoration circuit

If a very high energy deposit is followed by a very low energy one, the accuracy of the front end electronics may be affected because some of the devices between integrator and digital block will operate close to the saturation point, thus the information about the low energy crossing can be distorted or lost. It turns to be useful to insert a stage which has the property to restore the signal baseline, rendering the dynamic range of the circuit unaffected following a large pulse. The diagram of this circuit is presented in Fig. 7.

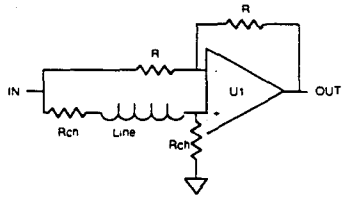


Fig. 7 The baseline restoration circuit

The signal at the non-inverting input is delayed 20 ns by the delay line. The delay can be reduced, using its 10 taps which are 2 ns apart. If a shorter delay would have been used the output signal, after the integration was completed, would not have been flat enough to avoid unsatisfactory time jitter error. As it can be seen from the diagram, the signal at the output of the stage is equal to the inverted input signal during the first 20 ns, it returns to zero in the next 20 ns, and is zero after that. Considering the PMT output pulse lasting 16 ns, this means that the

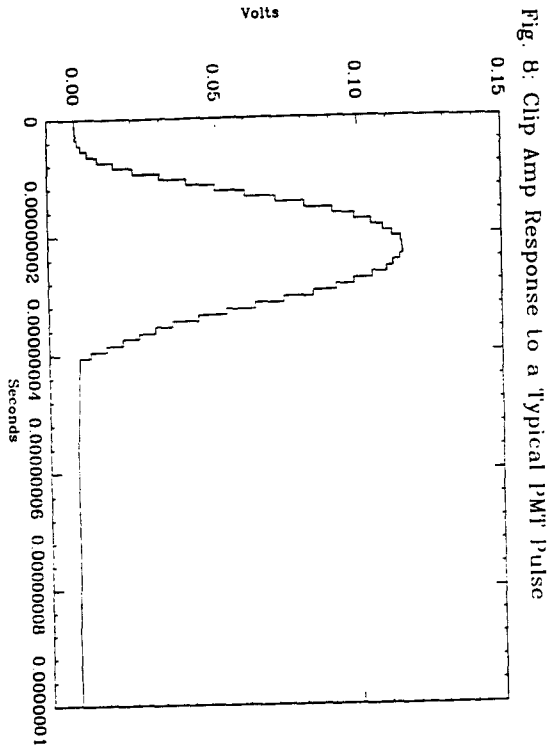


Fig. 8: Clip Amp Response to a Typical PMT Pulse

baseline is restored after 36 ns. For this application we employed CLC 400 current-feedback op-amp. There are three major reasons which justify this choice: (1) for current-feedback op-amps we have no gain bandwidth trade-off, (2) the slew rate is no longer a limiting factor, (3) and the CLC 400 has a very short propagation time and recovering quickly from saturation, [7]. For this op-amp the feedback resistor is required to be less or equal to 250 Ω, therefore we used R = 250 Ω. Because the pulse width is very short and the signal frequency spectrum very wide, in order to avoid the reflections which may appear at the ends of the delay line we terminated it with resistors, Rch, which match the line characteristic impedance at both ends. For the particular line we used (1P20, manufactured by ESC Electronics Corp.) these resistors had 100 Ω. Fig. 8 presents the SPICE-simulated response of the circuit to a typical integrator output signal.

D. The integrator protection against saturation

Even if the baseline is restored by the baseline restoration circuit, the pile-up of the signal at the output of the integrator can saturate it, causing loss of information during the actual recovery from saturation. Unfortunately this time interval may be very long due to the fact that a very low droop at integrator output was required to minimize time jitter error. The circuit presented below is designed to discharge the integration capacitor C1 when the output of the integrator U1 reaches 2V, thus avoiding the loss of information which might occur if U1 gets saturated. The first pulse for which the 2V threshold is exceeded will be normally processed, and the discharge process is delayed about 40 ns in order to permit the baseline to be restored. After this delay, the discharging of C1 is triggered and takes 40-50 ns to restore the baseline at the integrator output. In order to avoid the saturation of the SCA, which may occur during the transition generated by the discharge of C1, the output stage is provided with ultra-fast switching and clamping diodes (MBAL 99) which limit the output swing to 5V. Fig . 9 presents

the diagram of integrator protection against saturation circuit. The performance of this circuit might be affected when a high energy signal, which triggers the C1 discharge, is immediately followed by a very low energy one. If the information about the low energy crossing can not be stored in the low gain switched capacitors array and it occurs exactly during the time C1 is

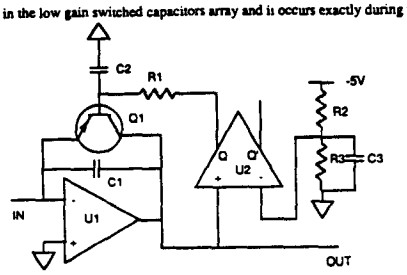


Fig. 9 Protection against saturation circuit

discharging, then the information is lost. However, the probability of an event like this is very low.The threshold which determines the triggering of the integration capacitor discharge is fixed by R2, R3 and is equal to:

$$Vthr = -5V \cdot \left(\frac{R3}{R2+R3}\right) \qquad (9)$$

This circuit has to satisfy two major requirements: (1) to switch within 40 ns after the threshold is exceeded, (2) to generate very low extra-noise at the integrator output. To satisfy the fast switching requirement we employed a very fast switching pnp transistor (2N5771) and a ultra-fast comparator (AD 96685). The comparator propagation time is about 2.5 ns while the transistor switching time is about 15 ns. R1 and C2 network adjust the delay to 40 ns. To check the second requirement we point out that most of the time the transistor Q1 is off. In the cut-off

region the transistor generates a shot-noise due to the fluctuations which appear in the collector cutoff current. The spectral density of this noise is given by, [22]:

$$i_{sn} = 4 \cdot q \cdot I_{CB0} \qquad (10)$$

where q is the electron charge, and I_{CB0} is the collector cutoff current. For the 2N5771 I_{CB0} is given to be equal to 10 nA. Substituting these values in (10) we get $i_{sn} = 6.4 \cdot 10^{-27}$ A/√Hz. In the worst case we have to add its effects upon the output voltage noise RMS value, to those of the op-amp current noise. Going back to (8) this means that we have to add $i_{sn}^2 \cdot (R/4 \cdot C)$ to the already computed squared output voltage-noise RMS. However, comparing the values of i_{sn} and i_n we found the effects of the shot-noise to be negligible compared to those of the op-amp current noise. Fig. 10 presents the SPICE simulations for the circuit behavior after the threshold was exceeded. We can see that it needs about 40 ns to recover after the capacitor was discharged, and this can cause loss of information if a very low energy crossing occurs during this period of time.

E. The cable drivers

The output stage has to be able to drive either 50 Ω coax cables or 100 Ω twisted-pair cables. The output swing, in both cases has to be equal to ± 2.5 V and in order to protect the input of the switched capacitors array this stage output has to be provided with clamping diodes (MBAL 99) which will not allow the output to exceed the mentioned swing. For this purpose we employed CLC 420 which is an 1100 V/μs slew rate, 4 nV/√Hz voltage noise and 2 pA/√Hz current noise voltage feedback op-amp. The CLC 420 is able to drive 50 Ω cables, and in order to avoid reflecuons we inserted 50 Ω resistors at the output to match the cable characteristic impedance. The diagram of the cable driver is presented in Fig. 11. The 680 pF capacitors compensate the cable frequency characteristic. The stage has a gain of 1.2 such that together

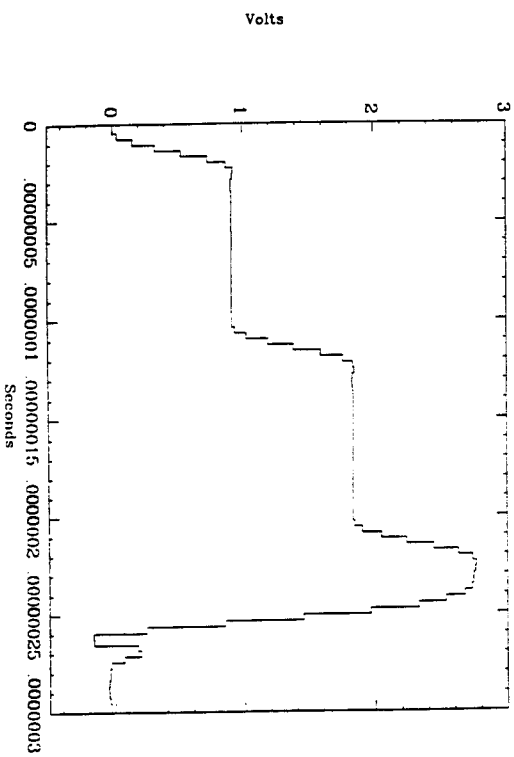


Fig. 10: Response of Saturation Protection Circuit

with the previous stages it provides the output with a ± 2.5 V swing.

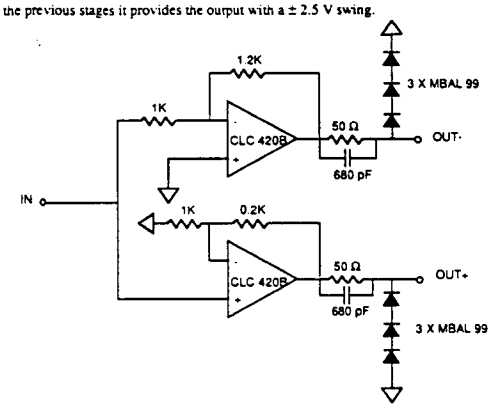


Fig. 11 The cable driver

In order to check this assertion we consider the PMT output current pulse amplitude to be equal to 50 mA. In this case the peak current flowing into the low gain path is about 7.7 mA. After it is 3 times amplified by the low gain path current amplifier it will inject about 62 pC into the low gain path integrator. For a 91 pF integration capacitor this means a 2 V integrator output voltage. Considering the 1.2 gain of the cable driver stage the front end amplifier output swing will be about 4.8 V_{p-p}, which is close to the required output swing. Similarly to eq. (8) it can be found that this stage adds about 20 uV_{rms} voltage noise to each of the front end amplifier outputs. Fig. 12 shows the SPICE simulation results for the cable driver response. It can be

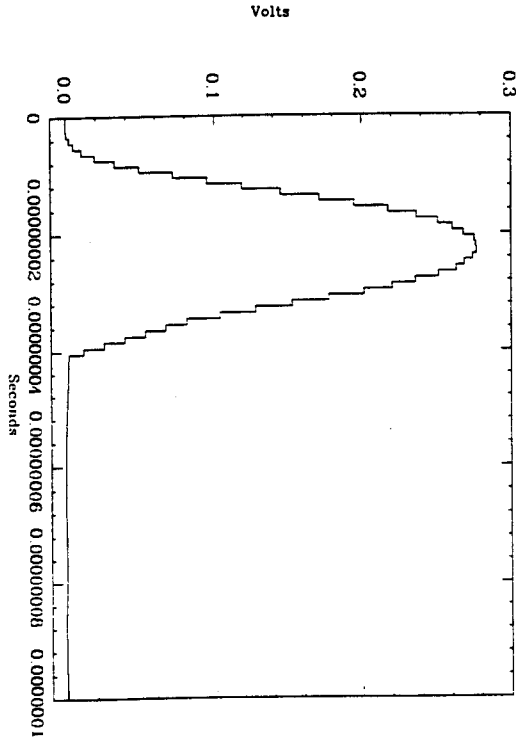


Fig. 12: Output Stage Response to a Typical PMT Pulse

concluded that, according to these simulations, the circuit meets the previously presented requirements.

III. Results

In order to test the previously presented design, we built the high gain path on a breadboard circuit. To have the current amplifier and the integrator working in the linear region for all the range of input currents we used ± 8 V voltage regulators as power supplies for this part of the amplifier. The baseline restoration stage, the protection against saturation circuit, and the cable driver were supplied from ± 5 V voltage regulators. The input signal was generated by a Hewlett Packard pulse generator which was converted into a current source by a voltage to current converter we built on the same breadboard. We used rectangular pulses in order to more easily estimate the injected charge. The results of the tests of the main parameters are summarized in table II. The measurements of the linearity with respect to the pulse width were affected by the errors introduced by the pulse generator, which could not maintain the rectangular shape of the pulses for lower width. To test the noise performance we used a Le Croy 9410 digital scope together with a low noise, 48.5 gain, and ≈ 100 MHz bandwidth voltage amplifier. The output voltage standard deviation within a 200 ms window was 11 mV, which corresponds, for the circuit itself, to 11/48.5 = 0.226 mV_{rms}. This figure is consistent with the

Table II.
Results of the tests for the breadboard circuit

Droop over 4 ns after the integration was completed	≈ 0.07 % from the peak value
Linearity with respect to the pulse width	≈ 1 % from the peak value
Output voltage noise RMS value	≈ 0.23 mV

theoretical expectation, taking into account the noise introduced by the clip-amp, and the input stage, and the fact that the test was performed on a breadboard circuit.

The front end amplifier will be built on a 6 layer 6"x4" PCB, using mostly surface mount devices. In order to avoid the undesired effects of the reflections which may occur at the ends of the delay lines, the PCB was designed such that the characteristic impedance, for the traces which connect the delay lines to the rest of the circuit, matches the 100 Ω delay line impedance. We estimate an improvement of the droop for this version of the front end amplifier due to the attenuated effects of the reflections.

IV. Conclusions

As is customary, this design involves a trade-off between the noise performance, circuit speed, and dynamic range has been made. Earlier work on front end amplifiers, [6], [9], and [17], illustrate that is difficult to achieve very good noise performance with very good speed performance for an ≈ 100 dB dynamic range. Because of the low level of the minimum input signal it is hard to achieve the needed dynamic range using only one integrator, since the noise performance is given mainly by this stage. Using only one integrator would imply a very low output voltage noise RMS value (about 30 μV). Trying to achieve a very low noise level at the output might have an undesired effect upon the circuit speed, and would make the circuit unable to distinguish crossings that are close together. Integrated versions of the front end amplifier, [9] and [17], show that a low output voltage noise level was achieved when the response time of the circuit was not fast enough to achieve a good droop performance for a typical 16 ns PMT output pulse. Also none of the solutions presented in [6], [9], and [17], reached such a low output voltage noise level to make it suitable for processing an ≈ 100 dB dynamic range input signal. Based on this reasoning we used a solution where one integrator was employed for each of the low and high gain paths. The results of the tests of the breadboard circuit show that the solution is feasible and achieves the needed requirements. The solution is also cost effective because all of the devices employed within the front end amplifier can be ordered as standard products. The circuit we presented has a droop over 4 ns, after the integration is completed, of ≈ 0.07 %, a linearity of ≈ 1 % and an output voltage noise RMS value of ≈ 0.23 mV_{rms} for an input signal dynamic range of ≈ 100 dB.

References:

[1] Analog Devices, *Linear Products Databook*, 1991.

[2] B.N.L., "Preamplifiers for Ionization Calorimeters: General Considerations," in *Front End Electronics Development for SSC Detectors*, 1990, pp. 15-19.

[3] Bicron, "Progress Report. Scintillating Plate Calorimeter Subsystem", Bicron Corporation, 1990.

[4] A. Buehring, N. Hill, M. Burke and D. Hackworth, "Mechanical Design of the Scintillating Plate Calorimeter Subsystem", Argonne National Laboratory and Westinghouse Electric Corporation, 1990.

[5] Burle Industries, *Photomultiplier Handbook*, 1980.

[6] J. Colas, "Speed of Response, Pile-up and Signal to Noise Ratio in Liquid Ionization Calorimeters," in *Proceedings of the Workshop on Calorimetry for the Supercollider*, Tuscaloosa, Alabama, R. Donaldson and M. G. D. Gilchriese, Ed., World Scientific, 1989, pp. 553-568.

[7] Comlinear Corporation, *Solutions with Speed, Databook*, 1989.

[8] H. B. Crawley and W. T. Meyer, "Flash ADC Testing", Ames Laboratory, 1990.

[9] D. DiBitonto et al., "Fast, Radiation-Hard Charge Preamplifier for Warm Liquid Calorimetry," in *Proceedings of the Workshop on Calorimetry for the Supercollider*, Tuscaloosa, Alabama, R. Donaldson and M. G. D. Gilchriese, Ed., World Scientific, 1989, pp. 583-600.

[10] C. Emoif, T. Porter, J. Dawson and T. Ekenberg, "Electronics Development", Westinghouse Electric Corporation and Argonne National Laboratory, 1990.

[11] D. Groom, "Energy Scaling of Low-Energy Neutron Yield, the e/π Ratio, and Hadronic

Response in a Calorimeter," in *Proceedings of the Workshop on Calorimetry for the Supercollider*, Tuscaloosa, Alabama, R. Donaldson and M. G. D. Gilchriese, Ed., World Scientific, 1989, pp. 59-89.

[12] T. Hayashi, "Photomultiplier Tubes for Use in High Energy Physics", Hamamatsu Photonics, 1978.

[13] L. Hervas, "The Pipelined Readout for the ZEUS Calorimeter", Facultad de Ciencias, Madrid, 1991.

[14] J. Huth, "Jet Energy Measurement," in *Proceedings of the Workshop on Calorimetry for the Supercollider*, Tuscaloosa, Alabama, R. Donaldson and M. G. D. Gilchriese, Ed., World Scientific, 1989, pp. 27-57.

[15] L.B.L., "Calorimeter Readout Electronics," in *Front End Electronics Development for SSC Detectors*, 1990, pp. 30-49.

[16] W. Smith, "A Pipelined Calorimeter First Level Trigger," in *Proceedings of the Workshop on Calorimetry for the Supercollider*, Tuscaloosa, Alabama, R. Donaldson and M. G. D. Gilchriese, Ed., World Scientific, 1989, pp. 615-630.

[17] P. M. VanPeteghem et al., "On the Design of Fully-Integrated Charge Preamplifiers for the Superconducting Supercollider," in *Proceedings of the Workshop on Calorimetry for the Supercollider*, Tuscaloosa, Alabama, R. Donaldson and M. G. D. Gilchriese, Ed., World Scientific, 1989, pp. 569-582.

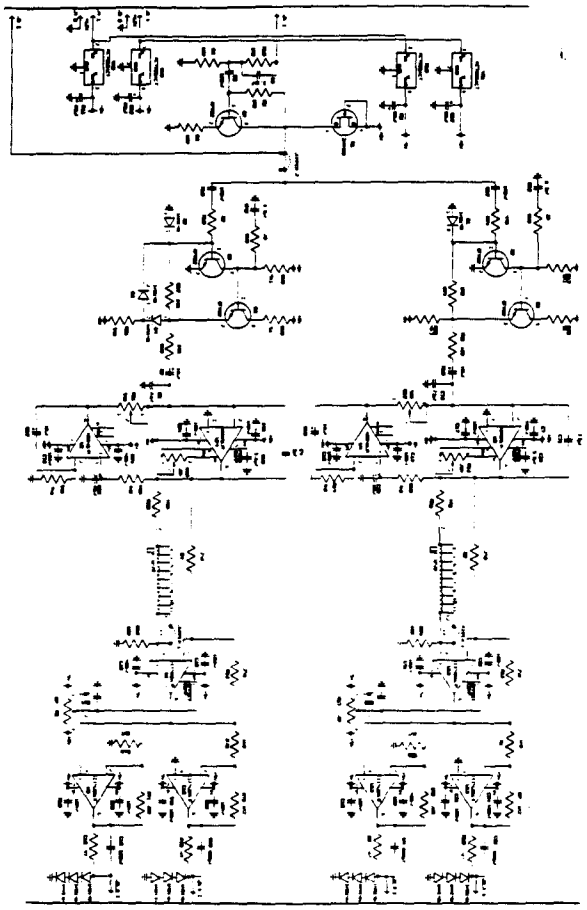
[18] S. Kleinfelder et al., "Test Results of a 90 MHz Integrated Circuit Sixteen Channel Analog Pipeline for SSC Detector Calorimetry", Lawrence Berkeley Laboratory, 1990.

[19] P. W. Tuinenga, *SPICE, A Guide to Circuit Simulations and Analysis Using PSpice*. New Jersey: Prentice Hall, 1988.

[20] Hamamatsu, "Photomultiplier tube R580-15", 1989.

[21] R. Ely et al., "Scintillating tile barrel and endcap calorimeter electronic cost estimate", 1991, Revision History.

[22] A. K. Scidmore, Linear active circuits, 1982, course notes.



SDC Note SDC-91-00087
DRAFT
September 9, 1991

Isolated Electron Pattern Logic Design and Performance at the SSC

W.H. Smith, J. Lackey, T. Gorski, W. Temple
University of Wisconsin

1 Introduction

A major requirement of the SDC First Level Trigger is the detection of electrons from inclusive W and Z production with 50% efficiency for triggering on the events that enter the detector fiducial volume. The anticipated rate of electrons from these sources is 3 KHz at the nominal SSC design luminosity of 10^{33}. However, these must be detected against a background rate of an average of 1.6 events occuring at the beam crossing frequency of 16 nsec. This input rate of 10^8 interactions every second must be reduced by a factor of at least 10^3 to 10^4 by the first level trigger. This report is a conceptual design for digital pattern logic to trigger on isolated electrons and photons in the SDC calorimeter. This logic is fully pipelined with 16 nsec clocking. This document outlines the design of this logic and presents simulation results on its performance.

The isolated electron pattern logic is part of a calorimeter trigger based on several quantities. Among these are: the total energy deposited in the calorimeter, the sum of transverse energy, missing p_T, along with the number and energies of jets and electrons ?. The trigger design presented here requires fast signal detection. The philosophy of this trigger is to collect information at the rate of the crossing frequency in order to minimize the probability of event overlap confusing the trigger. This does not imply that the full calorimeter data acquisition systems collect information at this rate. This does mean that the subset of information used by the trigger is acquired at the crossing frequency.

The calorimeter design assumes scintillator readout by some type of photomultiplier device. The calculations required for the calorimeter trigger include summing all of the energies from pulseheights recorded in the photomultipliers every 16 nsec. In addition, calculation of the transverse energy and missing p_T requires energies from pulseheights, multiplied by geometric factors. The calorimeter trigger starts with the assignment of EMC and HAC sections to trigger towers. An analog sum is made of all of a trigger tower's EMC sections and a second sum is made of all its HAC sections. These are then flash-digitized. The trigger must form the transverse energy and missing p_T sums. Given an EMC or HAC trigger tower sum of energy E, located at polar angle θ, and azimuthal angle ϕ, the sums may be formed from the quantities E, (total energy), $E_t \sin\theta$, (transverse energy) and the components $E_t \sin\theta \cos\phi$, (missing E_x) and $E_t \sin\theta \sin\phi$, (missing E_y). The digitized HAC and EMC pulseheight from each of the trigger towers is stored, multiplied by lookup tables containing these geometric factors and injected into summing networks.

The formation of jet, isolated muon and isolated electron triggers in a pipelined fashion is considerably more complicated than making sums. The detection of jets requires preservation of tower information that would be lost in a global sum. The detection of an electron requires evidence of electromagnetic energy. This is done by comparing energy deposited in the first interaction length of the calorimeter with that deposited later on a tower by tower basis. The determination of the isolation of an electron requires checking the towers bordering on the electron "candidate" tower for energy below some minimum threshold ("quiet").

The proposed design uses tables to make local tests on the amount of energy in an individual trigger tower. The ratio of HAC to EMC energy is also tested. The results of these tests are encoded and passed forward with the energy sums to a search table that looks for matches with desired patterns. Local energy sums and tests are also made.

The identification of an electron involves correlating information from the tracking and calorimeter systems. Identification of an electron in the calorimeter requires detecting isolated electromagnetic energy. The first step is to find a calorimeter trigger tower with energy in the electromagnetic compartment and little or no energy in its hadronic compartment (i.e. typically $E_{HAC} < 0.1 * E_{EMC}$). Next the towers adjacent to this tower are checked for having little or no energy in both electromagnetic and hadronic compartments. This establishes electromagnetic energy that is transversely and longitudinally isolated. Since electrons may share energy among towers, and the criteria for electron isolation needs to be relaxed for more energetic electrons, the design allows for the ratio of HAC to EMC energy to identify an electron tower to change with energy, allows for different definition of the quiet towers used in transverse isolation with different energy electron towers, and has provision for up to six energy thresholds. The latter is necessary in order to allow for different energy thresholds for single, dielenton, and multilepton events.

2 General Overview

Figure 1 shows a hardware block diagram for the Isolated Electron Trigger. Photomultiplier Tube (PMT) currents for the EMC and HAC sections of each trigger tower are digitized in a FADC to produce a value for the current. These digitized values are supplied as address to a Memory Lookup Tables (MLUs) which both convert the energy to a 12-bit linear scale for the production of jet and total missing energy sums, and also determine a state for the trigger tower, known as an Encode Tower Type (ETT) code. This code classifies a tower as electromagnetic, quiet or hadronic. The FADC and MLUs are organized in a pipeline architecture, so as to be able to sample new PMT currents and produce a new ETT code for each 16ns bunch crossing. The pipeline length will be approximately 3 crossing clocks.

The ETT codes are used to reflect the state of the trigger tower as it pertains to isolated electron triggering. The code is 3-bits wide, and thus can reflect 8 different states for the trigger tower. All of the states are programmable through the VME downloadable memory lookup tables. Two of the code values, 0 and 7, are reserved to specific states. Code 0 is reserved to indicate towers which are below all pertinent energy thresholds (i.e., "quiet"). Code 7 is reserved to indicate towers which are hadronic in energy content. The other 6

codes can be programmed to indicate that the tower are either electromagnetic or quiet in nature, at different energy levels. This capability allows for different definition of the quiet towers used in transverse isolation with different energy thresholds for electron towers. The example ETT codes below and the following discussion show a full 6-Electron threshold configuration for the ETT code. At the end of this *General Overview* section, an alternate example configuration is shown, with a second quiet threshold inserted at code 4.

ETT code definitions for 6-Electron threshold configuration:

- **Quiet.** (Code 0.) This state indicates that the energy deposition in the tower is below all electron energy thresholds.
- **E_1 Electron.** (Code 1.) This state indicates an energy deposition was detected corresponding to the passage of an electron at or above energy threshold 1.
- **E_2 Electron.** (Code 2.) This state indicates an energy deposition was detected corresponding to the passage of an electron at or above energy threshold 2.
- **E_3 Electron.** (Code 3.) This state indicates an energy deposition was detected corresponding to the passage of an electron at or above energy threshold 3.
- **E_4 Electron.** (Code 4.) This state indicates an energy deposition was detected corresponding to the passage of an electron at or above energy threshold 4.
- **E_5 Electron.** (Code 5.) This state indicates an energy deposition was detected corresponding to the passage of an electron at or above energy threshold 5.
- **E_6 Electron.** (Code 6.) This state indicates an energy deposition was detected corresponding to the passage of an electron at or above energy threshold 6.
- **Non-Electron.** (Code 7.) This state indicates an energy distribution corresponding to something other than an electron or quiet tower (hadron).

An ETT code exists for each trigger tower. The size of the trigger tower and the resulting granularity of the search grid of the isolated electron detection, in terms of η-ϕ coordinates, depends upon the summing of the PMT currents supplied to the FADC. A trigger tower size of .05 x .05 is achieved if the EMC and HAC PMT currents of each tower are digitized separately. If the currents from groups of 4 towers (in a 2x2 layout) are summed together before digitization, then the trigger tower size becomes 0.1 x 0.1. In either case, there is no effect on the structure of the ETT code, or the logic which operates upon it.

The next step in isolated electron detection is to organize the towers into 8x8 regions, for the application of their ETT data to a pattern recognition ASIC. Each 8x8 region, hereafter referred to as a "grid", has a 3-bit ETT code for each of its 64 trigger towers, for a total of 192 bits of ETT data. This data is applied via a common bus to 6 instances of a Pattern Recognition ASIC (PRA). All PRAs operate on the same ETT data simultaneously; each at a different electron threshold level. For each PRA, the electron threshold is determined by a select mask, which is under computer control. The select mask identifies the threshold level at which the PRA will identify a tower as containing an electron. Towers with ETT

codes below that threshold level will appear as quiet to the PRA for pattern recognition purposes.

Each PRA searches for isolated electron electrons at its respective threshold level in 49 possible locations within the grid. The rules for this search are described in a subsequent section. The output of the PRA is a flag word which indicates the presence of any isolated electrons within regions of the grid. These regions consist of 2x2 trigger tower geometries which are fully confined within the grid, and 1x2 or 1x1 trigger tower geometries which occupy the edges or corners of the grid. There are a total of 25 regions in an 8x8 grid: 9 confined 2x2 regions, 12 1x2 edge regions, and 4 1x1 corner regions.

Note that the logic within the PRA for decoding the ETT codes is designed in such a way that **two PRAs operating at different thresholds cannot each find an isolated electron in the same location**: the higher thresholds have priority. Each PRA can accept a new grid of ETT data every 16ns bunch crossing. The latency through the PRA to the production of the flag word is approximately 3 crossing clocks.

In addition to the PRAs, the ETT data bus is monitored by the quiet detect logic. This logic checks the raw ETT codes for the grid to detect regions which are completely quiet (all towers at ETT code 0), and produces a resulting flag word indicating which of the 25 regions is quiet. The region geometries exactly correspond to those used by the PRAs as described above.

The flag words from all of the 6 PRAs and the quiet detect logic are fed to the electron threshold decoder logic. This logic examines the flag words, and produces a 3-bit isolated electron code for each region. This code reflects the threshold at which an isolated electron was found, if the region was completely quiet, or if no isolated electron was found in the region.

For the 6-Electron threshold case, these codes are defined as follows:

- **Region Completely Quiet.** (Code 0.) This code indicates that all towers in the region were completely quiet (all had an ETT code of 0).
- **E_1 Isolated Electron.** (Code 1.) This code indicates that an isolated electron at threshold 1 was located in the region.
- **E_2 Isolated Electron.** (Code 2.) This code indicates that an isolated electron at threshold 2 was located in the region.
- **E_3 Isolated Electron.** (Code 3.) This code indicates that an isolated electron at threshold 3 was located in the region.
- **E_4 Isolated Electron.** (Code 4.) This code indicates that an isolated electron at threshold 4 was located in the region.
- **E_5 Isolated Electron.** (Code 5.) This code indicates that an isolated electron at threshold 5 was located in the region.
- **E_6 Isolated Electron.** (Code 6.) This code indicates that an isolated electron at threshold 6 was located in the region.

- **Not Isolated, Not Quiet.** (Code 7.) This code indicates that the region did not contain an isolated electron, and was also not completely quiet.

Despite the apparent similiarity, these isolated electron codes should not be confused with the ETT codes. Whereas the ETT codes refer to the raw state of individual trigger towers, the isolated electron codes refer to regions of trigger towers after an isolation cut has been performed. Code value 7 provides a good example of the difference between the two definitions. Whereas ETT code 7 refers to a trigger tower which is hadronic, isolated electron code 7 refers to a region which is not completely quiet, and did not contain an isolated electron. (As it turns out, however, a region with a tower at ETT code 7 (hadronic tower) does indeed map to isolated electron code 7 (non-quiet, non-isolated region).)

The threshold encoder logic also contains a self-test feature, in which all PRAs are set to the same threshold, and their flag words subjected to a bitwise comparison. As the PRAs are identical, their output flags should also be identical. This feature will identify a lack of total agreement between the six PRAs.

Once the isolated electron codes are generated, the final step before matching with the track and showermax data in the level 1 trigger is the combination of edge, corner partial regions of adjacent grids into 2x2 trigger tower composite regions which fall across grid boundaries. This is performed by the edge corner region checking logic described in a later section. The result produced by this logic is a map of uniform 2x2 tower regions for the entire calorimeter, each with a 3-bit isolated electron code.

As stated previously, the ETT codes 1-6 may be configured to be additional quiet states instead of electromagnetic thresholds. This is accomplished merely be reprogramming the selected ETT codes in the downloadable MLU via the VME interface to reflect the definition change for the additional quiet states. These additional quiet states will be visible as to all electron thresholds having higher ETT code values, and will not be visible to the thresholds with lower ETT code values. In addition, those PRAs which previously monitored those thresholds are disabled by the controlling processor. The result is that towers with significant energy content can be considered as quiet under certain circumstances for the purpose of detecting isolated electrons at the higher energy thresholds.

In the example below, electron threshold 4 is replaced with a second quiet threshold, resulting in the following altered ETT code definition. The gap created by the loss of a threshold is filled by the reprogramming of one or more of the remaining electron thresholds. The result is a configuration with a single quiet threshold for the bottom 3 electron thresholds, and two quiet thresholds for the top 2 electron thresholds.

- **First Quiet.** (Code 0.) This state indicates that the energy deposition in the tower is below all electron energy thresholds. This threshold is unchanged from the original definition.
- **E_1 Electron.** (Code 1.) This state indicates an energy deposition was detected corresponding to the passage of an electron at or above energy threshold 1.
- **E_2 Electron.** (Code 2.) This state indicates an energy deposition was detected corresponding to the passage of an electron at or above energy threshold 2.

- **E_3 Electron.** (Code 3.) This state indicates an energy deposition was detected corresponding to the passage of an electron at or above energy threshold 3.
- **Second Quiet Threshold** (Code 4.) This state provides an additional quiet threshold which is visible to to electron thresholds 5 and 6, but not to electron thresholds 1 through 3. This threshold is for towers which have significant energy deposition but may nonetheless be considered quiet for detecting electrons at higher energy thresholds.
- **E_5 Electron.** (Code 5.) This state indicates an energy deposition was detected corresponding to the passage of an electron at or above energy threshold 3.
- **E_6 Electron.** (Code 6.) This state indicates an energy deposition was detected corresponding to the passage of an electron at or above energy threshold 3.
- **Non-Electron.** (Code 7.) This state indicates an energy distribution corresponding to something other than an electron or quiet tower (hadron).

Continuing the example, the following isolated electron codes result. Note that code 0, *Region Completely Quiet*, is formulated exclusively from the first quiet threshold. ETT code 0. Code 5, previously occupied by isolated electrons at ETT code 4, now becomes an empty undefined state.

- **Region Completely Quiet.** (Code 0.) This code indicates that all towers in the region were completely quiet (all han an ETT code of 0).
- **E_1 Isolated Electron.** (Code 1.) This code indicates that an isolated electron at threshold 1 was located in the region
- **E_2 Isolated Electron.** (Code 2.) This code indicates that an isolated electron at threshold 2 was located in the region
- **E_3 Isolated Electron.** (Code 3.) This code indicates that an isolated electron at threshold 3 was located in the region
- **Empty/Undefined.** (Code 4.) This code is empty undefined. ETT code 4 has been reassigned to a second quiet, and the PRA operating at threshold 4 has been disabled. The encoder logic will not generate this code for any region.
- **E_5 Isolated Electron.** (Code 5.) This code indicates that an isolated electron at threshold 5 was located in the region.
- **E_6 Isolated Electron.** (Code 6.) This code indicates that an isolated electron at threshold 6 was located in the region
- **Not Isolated, Not Quiet.** (Code 7.) This code indicates that the region did not contain an isolated electron, and was also not completely quiet.

3 Memory Lookup Tables

Figure 2 shows a block diagram of the memory lookup table architecture for a single logical tower. It shows a pipeline consisting of the Flash ADCs (FADCs) that digitize the raw PMT or summed PMT signals, a fiber-optic interface to transfer the raw data off the detector, and a group of memory lookup tables, operating at the 16ns crossing clock rate. The pipeline begins with photo-multiplier tube currents of the tower EMC and HAC sections connected to a pair of FADCs. (Note that if the trigger tower size in η-ϕ coordinates is to be .05x.05, then this corresponds to a single physical tower. If the trigger tower size corresponds to .1x.1, then this corresponds to 4 physical towers in a 2x2 arrangement, with their currents summed in the analog domain.)

The output of the FADCs is a raw digital value which reflects the energy content in that section of the tower. These values are represented in the figure as being 8 bits compressed on a nonlinear scale, although it could be represented using other formats, including 8-bits mantissa with 4-bits exponent or 8-bits mantissa with 1-bit range and 1-bit overflow. The EMC and HAC digital values are transmitted together on a single optical fiber off the detector, where they are received and separated again for application to the MLUs.

There are three MLU blocks in the design. The first MLU compares the raw EMC and HAC energies to produce the ETT code. This code is used for the isolated electron detection which is subsequently described in this document. The other two MLU convert the raw EMC and HAC energies to a 12-bit linear scale, so that they can be applied to a summation tree for use in the jet threshold and total missing transverse energy triggers.

4 Pattern Recognition ASIC (PRA)

The PRA performs the task of examining the ETT codes for 8x8 trigger tower regions ("grids") to detect those trigger towers containing isolated electrons. A PRA is configured with a static threshold select under computer control to select the desired electron energy threshold. This select controls how the ETT data is decoded within the PRA. During normal operation, six PRAs, one for each electron threshold, simultaneously operate on the same ETT data for each grid in the calorimeter. During self-test mode, all PRAs operate on the same threshold, and should produce identical results.

Figure 3 shows a block diagram of the PRA. Processing within the PRA occurs in three major stages. ETT decoding to Q E bits, finding isolated electrons in the isolated electron detection blocks, and mapping the results of the isolation detection into fixed physical regions.

The first stage of processing is the ETT decoding. The top three edges of Figure 3 show the 3-bit ETT codes of 64 trigger towers (192 bits total) entering the chip. The ETT code for each trigger tower is compared to the threshold selected for the PRA. The result of this comparison is the Q and E bits. The Q bit is active if the ETT code is less than the threshold-the tower is considered quiet. The E bit is active if the

tower exactly matches the threshold-the tower is considered electromagnetic. The Q and E bits are merely a repackaging of the tower state into a format which is more convenient to the pattern recognition logic. The comparisons are performed on an individual tower basis.

In the next layer into the PRA, the Q,E bits are buffered for distribution into 49 isolated electron detection blocks. Each of these blocks examines a single 4x4 tower zone on the grid known as a "template," to determine if an isolated electron is present. The templates are placed on the grid in a 7x7 array, such that they are offset one tower horizontally and/or vertically from their neighbors. This positioning covers all of the areas on the grid where an isolated electron may occur. As stated previously, one isolated electron detection block is assigned to each template, for a total of 49. Each block produces binary flags indicating which of the trigger towers within its template contained an isolated electron.

The last step of processing in the PRA is to map the isolated electron flags for individual trigger towers from the detection blocks into 25 fixed regions. These regions correspond to 9 fully confined 2x2 trigger tower regions, 12 edge 1x2 or 2x1 trigger tower regions, and 4 corner 1x1 trigger tower regions. The result of the mapping is called the "region flag word", a 25-bit word that contains a binary flag for each region, indicating if that region contained an isolated electron or not.

The three major stages of processing are described in greater detail in subsequent subsections. To summarize, the ETT codes for an 8x8 group of 64 trigger towers are tested against the selected threshold. The results of the comparison are passed into the array of 49 isolated electron detection blocks, each located at one of the possible sites of an isolated electron, and each of which examines the state of the towers in one 4x4 template area to detect isolated electrons within that area. Each block produces binary flags for those trigger towers within its template which may contain an isolated electron. All of the individual trigger tower flags from the 49 isolated electron detection blocks are then mapped into 25 fixed regions on the grid and delivered to the output pins of the PRA.

In terms of technology, this preliminary design assumes a BiCMOS Gate Array technology, utilizing 1.0, 1.5-micron CMOS features, with a 1.5-micron bipolar commercial process. The design would require approximately 220 TTL I O pins. The chip would run at a 16ns clock rate. We have evaluated implementing this design with one vendor and have a resulting gate count of approximately 15,000 gates.

4.1 ETT Decoding to Q/E Bits

Figure 4 shows the decoding of tower ETT codes to Q E bits at all six electron thresholds. In order to be usable by the isolated electron blocks, the ETT code must first be converted into a Q and E bit for each tower. This is performed by comparing the value of each ETT code to the threshold selected for the PRA. If the ETT code is < the threshold, then the Q bit is active, and the tower is considered quiet. If the ETT code exactly matches the threshold, then the E bit is active, and the tower is electromagnetic at the correct threshold for detection by the PRA. If the ETT code is > the threshold, then neither bit is active, and the tower appears as a non-electron.

non-quiet tower to the PRA. This situation covers the cases where the tower contains a hadron or an electron at a higher threshold, in which case the isolation cut will be performed by a different PRA operating at a higher threshold. One PRA operates at each of the six thresholds.

Figure 5 contains a block diagram of the ETT decoding section in the PRA. The 64 ETT codes are received as TTL data by the input buffers. They are then converted to Q_E bits by the method described above in 64 identical decoding blocks. The Q_E bits are then passed to the first stage 16ns pipeline register at time "T1" in the design. From the pipeline registers, they are sent to fanout buffers.

4.2 Isolated Electron Detection Blocks

As stated above, there are a total of 49 isolated electron detection blocks in each PRA. Each block operates on a 4x4 section of towers known as a template. The purpose of the block is to examine the Q_E bits of the 16 towers to determine if an isolated electron is present within the bounds of the template, centered on the inner 2x2 towers.

The templates are placed on the grid in in a 7x7 array, such that they are offset one tower horizontally and/or vertically from their neighbors. The templates on the edges of the grid are placed so that one row or column of the template is actually off the grid. Towers which occupy an off-grid location are assumed to be quiet by the logic. This may result in the detection of electrons in edge towers, which are isolated on the current grid, but have not as yet passed isolation checking with adjacent towers on other grids. These electrons are mapped into edge corner regions which will undergo final isolation checking with similar regions in subsequent logic. With this placement, the templates examine all 49 possible locations for an isolated electron.

An isolated electron is present in the template if both of the following conditions are met:

1. One or more E bits is active in the inner 2x2 region. Any remaining towers in the inner 2x2 have their Q bit active.
2. All of the towers in the outer region (outside the inner 2x2) which are adjacent to active E bits in the inner 2x2 (including diagonal connections) have their Q bit active. Those towers in the outer region which are not in contact with an active E bit are considered to be "don't cares."

Note that the definition of an isolated electron allows for cases where up to 4 E-bits are set in the inner 2x2.

To determine if an isolated electron is present in a template, the detection blocks utilize a combinatorial function referred to as an Evaluation Function. This function provides a bit, called the F-value, which is active if an isolated electron is present in the template. The general case of the Evaluation Function is shown in Figure 7. The C_i through C_4 subfunctions check that any E bits set in the inner towers are adjacent to Q bits in the outer towers in the 4 corners of the template. The D subfunction is used to defer evaluation of an isolated electron candidate to the next template to the right or below. This is to avoid the condition where the same isolated electron

is detected in more than one template. (The D subfunction has special cases which apply for right-edge, bottom-edge, and bottom-right-corner templates, as indicated by the active-high signals *BOTTOM* and *RIGHT* in the definition.) The N subfunction is used to detect Non-Electron type towers or towers above the selected threshold in the inner 2x2 region.

Figure 9 contains a block diagram of the isolated electron detection section in the PRA. The Q_E bits arrive from the T1 pipeline register at the fanout buffers. These buffers distribute the Q_E bits to the 49 detection blocks. As the 49 templates overlap each other, a given tower may reside in up to 16 individual templates. As a result, a given Q_E bit may have 30 to 40 individual loads. The purpose of the buffers is to distribute this loading in the most efficient method possible. In spite of the presence of a given tower in many templates, an electron can only satisfy the isolation conditions in a single template.

Each detection block has boolean outputs, known as tower E-flags, for 2 or 4 of its inner 2x2 towers. These flags correspond to trigger tower locations in the template where an isolated electron may be assigned. When the detection block has an active F-value, it examines the E bits on the candidate towers to determine which tower contained the electron. The tower for which the E bit is active has its E-flag set active, while all other E-flags in the template are set inactive. For cases where multiple E bits are active in the template, the assignment is still only made to one tower. The E bits are examined according to a set priority, depending on the location of the template in the grid.

There are four template types, based on their location on the grid. Examples of these types are shown in Figure 8. In the examples, the tower to which the electron will be assigned is indicated with a bold outline. The template types are described below:

Non-Right, Non-Bottom Edge Templates. This group is comprised of the 36 upper-left templates on the grid. For these templates, isolated electrons will only be assigned to the left two towers of the inner 2x2 (indicies B1 and C1 in figure 7). This follows from the fact that any isolated electron within the template which does not have an E bit set in at least one of these two towers will be deferred to the template to the right. The rule for mapping in these templates is that if the E bit is set at location B1 in the template, then the electron is assigned to the tower at B1. Otherwise, if the E bit is set at location C1, then the electron is assigned to the tower at C1.

Bottom, Non-Right Edge Templates. This group is comprised of the leftmost 6 templates on the bottom edge of the grid. For the same reason as above, the assignment can again only be made to B1 and C1. However, in this case, the priority is reversed, such that C1 has higher priority over B1. This guarantees that an isolated electron on the edge of the grid that is detected in these templates will be mapped to an edge region in the region flag word.

Right, Non-Bottom Edge Templates. This group is comprised of the upper 6 templates on the right edge. For these templates, isolated electrons can be assigned to any of the inner 2x2 regions, according to the following priority. If the E bit at location B2 (upper right in the inner 2x2) is active, then the electron is assigned to the tower at B2. Otherwise, if the E bit at C2 is active, then the

electron is assigned to C2. B1 is the next tower in priority, and finally C1. The intent is to make sure that the electron is first assigned to a right edge region if possible, and then to a top edge region if the template is on the top edge, and then finally to the fully confined electron C1.

Bottom, Right Edge Template. This template is the special case at the lower right corner of the grid. The priority is the same as for the group immediately above, with the exception that the priority for B1 and C1 have been reversed. Thus, this template first attempts to assign the electron to the right edge, and then to the bottom edge, before assigning it to the confined electron B1.

The examples demonstrate how isolated electron assignment to individual towers varies with the template type. The priority is always to assign isolated electrons to towers on the edge of the grid, if possible, so that they will undergo further checking with regions from adjacent grids.

A total of 112 tower E-flags are produced by the 49 detection blocks. This includes 2 flags each from the 42 non-right edge templates (84), and 4 each from the 7 right-edge templates (28). These 112 bits are sent to the next stage 16ns pipeline register, at time "T2" in the design. From there, they will be used for region flag word generation.

4.3 Region Flag Word Generation

As stated previously, the PRA generates a region flag word for each grid of ETT data. Figure 10 shows the bit definition of the word and the mapping of the 25 regions onto the 8x8 grid of trigger towers. Note that for each region, an E-flag is defined. An E-flag is active if any of the towers in its region contains an *isolated* electron. Note that due to the nature of isolation, a maximum of one isolated electron would be found in any region. Note also the placement of the region boundaries. Those towers which are completely confined within the grid are placed in 2x2 regions. Electrons found within these regions have already been determined to be properly isolated. Those towers which are on the edge of the grid are placed in 1x2 edge or 1x1 corner partial regions. Electrons found in these regions have been determined to be isolated with respect to other towers on this grid, but require further isolation checking with towers in adjacent grids. This checking is described in a subsequent section.

The 25 region E-flags are produced from the 112 tower E-flags produced by the detection blocks using OR logic. Figure 11 contains a block diagram of the region flag word generation section in the PRA. There are 25 independent OR gates, one for each of the 25 regions. Each OR gate has 3 to 8 inputs on it, depending on the region. The number of inputs to a gate corresponds to the total number of tower E-flags from overlapping templates which map into that region. Each of the 112 tower E-flags acts as an input to the OR gate for the 2x2 region which contains that tower. The output of each OR gate is an E-flag for the region, which indicates if any tower within that region contained an isolated electron.

¿From the OR logic, the E-flags are passed to a 16nsec pipeline register at chip time "T3". ¿From there, the signals go through the output buffers of the chip, and driven as TTL data to the 25 output pins.

4.4 PRA Summary

The PRA consitues a 3-stage, 16as pipeline, which accepts a new grid of ETT data and produces a new region flag word on each clock cycle, with a latency of 2 clocks between input and output. It is optimized for six thresholds, using a 3-bit ETT code. It requires approximately 220 TTL I/O pins, plus power and ground. It will operate on a single +5V source. It will be fabricated using BiCMOS Gate-Array technology. Power consumption will be dependent in part on the density of non-quiet towers, as the more often each ETT code changes state, the more resulting switching and thus power consumption there will be inside the ASIC. Monte Carlo studies are in progress to determine the switching rates which will be seen by the ASIC. It is anticipated, however, that the switching rates will be low enough (below 10%) such that power consumption in the ASIC will be manageable.

5 Quiet Detect Logic

As shown in Figure 1, the quiet detect logic monitors the ETT data bus in parallel with the six PRAs. Its purpose is to detect 2x2 regions (using the same region geometry as is used by the PRAs as defined in Figure 10) which are completely quiet. Like the PRAs, it delivers its 25 flags ("Q-flags") to the threshold encoder logic 3 crossing clocks after sampling the ETT data. These flags will be used to help determine the isolated electron code for the region, and indirectly, through the code, can be used by the muon trigger subsystem because they identify quiet .2$\delta\eta$x.2$\delta\phi$ regions in the calorimeter.

The quiet detect logic occupies 3 pipeline stages. The first pipeline stage of the logic makes a Q-flag for each tower by NORing the 3 ETT code bits together. The result will be active Q-flags for those towers which had an ETT code of 0. The next stage ANDs together the 1, 2, or 4 tower Q-flags (depending on the region) to form region Q-flags. These Q-flags will be active only if *all towers in the region are completely quiet*. The final stage of the pipeline is merely for timing compatibility with the PRAs, so that the region Q-flags are delivered to the threshold encoder logic on the same clock cycle as the region E-flags from the PRAs.

6 Threshold Encoding

As shown in Figure 1, the electron threshold encoder logic operates on the region flag words produced by the six PRAs and the quiet detect logic. Its function is to encode the E-flags and Q-flags on a region-by-region basis to produce a 3-bit isolated electron code for each region. The isolated electron codes are described in the *General Overview* section.

The isolated electron code is defined so that each state corresponds to one of the seven flags being active. State 0 corresponds to the Q-flag from the quiet detect logic being active, states 1-6 correspond to an E-flag from the PRAs at threshold levels 1-6 respectively being active, and state code 7 is the exception, corresponding to none

of the flags being active. (Note that in programmed configurations where additional quiet states are defined, there will be empty isolated electron codes. This is due to the fact that a given PRA is disabled when its corresponding ETT code is defined as quiet, and therefore will not generate any active E-flags.) The code is produced from the Q E-flags using a variation of a common 8-to-3 priority encoder. This encoder will be implemented using commercial Programmable Logic Device (PLD) architecture, such as a 16R4, 22V10, or similiar device, which are commonly available in 20 or 24-pin packages. A total of 25 identical encoder blocks are needed for the 25 regions. These will occupy either 13 or 25 PLDs, depending on whether one or two blocks are programmed per PLD. The encode operation from the Q E-flags to the isolated electron codes should take 1 crossing clock.

Residing alongside the encoder blocks in the PLDs is the self-test logic. This self-test logic provides a quick test of the proper operation of the PRAs. The self-test must be performed while the logic off-line. During self-test mode, the six PRAs are set to the same threshold, and test ETT data is applied. If all PRAs are functioning correctly, then their E-flags should all be identical, from region to reginn (although the "correct" value for any given region is a function of the ETT test data.) The self-test logic within the PLDs checks the E-flags for the condition where there is a disagreement between the E-flags for the six PLDs. Each PLD will produce a single "Mismatch Error" signal for the one or two region encoder blocks it contains. The "Mismatch Error" signals are logged into memory and subsequently reported to the processor controlling the test via the VME interface.

Once a mismatch error has been found, the identity of the failing PRA can be determined by operating the PRAs at their normal thresholds, and examining the isolation codes produced using additional ETT test data.

7 Partial Region Resolution

Partial region resolution is term given to the task of recombining the partial 1x2 edge and 1x1 corner regions at the edges of 8x8 grids into 2x2 tower regions. It is the means by which isolation checking is performed across grid boundaries, and provides a final check of the assumption made in the PRA isolation cut that all towers just beyond the edges of the grid are quiet. The result of the recombination is a 2x2 tower region geometry of isolated electron codes across the entire calorimeter.

Figure 12 shows the mating of four adjacent grids in the calorimeter. Composite 2x2 regions are produced by pairing up adjacent 1x2 edge regions, and by grouping up quads of 1x1 corner regions. In this manner the isolated electron codes of the individual partial regions are compared against each other. The largest isolated electron code of the partial regions becomes the code for the composite 2x2 region. The reasoning for this lies in the definition of the code. A tower that contains an isolated electron at a lower threshold will appear as quiet to a higher threshold. This is demonstrated in the decoding of the ETT codes into Q E bits for the PRAs, as shown in Figure 4. The same principle applies when combining regions. A region with a lower threshold code which is adjacent to a region with an isolated electron at a higher threshold code will appear as quiet to that region, and the higher threshold code dominates over the

composite region. Note that by assigning the non-quiet, non-electron code a value of 7, this code dominates over all isolated electron codes. This is consistent with the fact that a hadronic tower could not by definition be adjacent to a tower with an isolated electron.

Figure 13 provides some examples of partial region resolution. The resolution of partial regions is performed as a final step before matching the isolated electron codes with the the hit data from the showermax and tracking subsystems. The basic logic block for this process will be a 2-to-1, 3-bit magnitude selector. This block will act as a 2-input MAX function, to deliver the larger of two input magnitudes to the output.

7.1 Partial Grids

One noteworthy feature of the PRA design is the ability to operate on reduced size grids of ETT data, and to still produce usable output results. This feature offers significant flexibility in the mapping of towers into regions in the end-cap sections of the calorimeter. Valid partial grids are formed by biasing 2x2 groups of input tower ETT codes to the PRA to the quiet state. This has the effect of relocating the edge/corner regions (and possibly deleting old regions). With some of their towers biased to quiet, 2x2 regions which used to be completely confined become 1x2 edge or even 1x1 corner regions. These partial regions can then be treated in exactly the same matter as is described above.

Towers must be biased to quiet in 2x2 groups which fall accross normal region boundaries shown in Figure 10. This rule ensures that no fully confined 2x2 regions will be adjacent to the edge of the grid. Under normal circumstances, 2x2 regions would be biased to quiet starting at one or two edges of the grid, and continuing until the desired partial grid geometry was obtained. The resulting new edge corner regions of the reduced geometry would then be matched with similiar regions from adjacent full or partial grids.

8 Design Summary

The Isolated Electron Trigger design consists of three principal sections: the MLU section, the PRA and threshold encoder section, and the edge corner resolution section. The scope of the design in these sections is at the one tower, grid (8x8 towers) and calorimeter (all towers) levels, respectively.

The MLU section has two types of memory lookups. The first type compares the energy content of the EMC and HAC sections of the trigger tower to produce an ETT code. The second type provides linearization and normalization and produces a 12-bit linear energy for both the EMC and HAC sections of the trigger tower. The architecture of the MLU section is flexible with respect to changes in format of both the input and output energies.

The PRA and threshold encoder section uses an ASIC to detect isolated electrons in 8x8 regions of towers referred to as grids. PRAs operate on the ETT codes generated by the MLU sections in a pipeline fashion to produce the region flag words. A

PRA is dedicated to each of the six mutually exclusive thresholds in the ETT code. Within a PRA, 49 overlapping 4x4 regions known as templates are examined using combinatorial logic to determine the presence of isolated electrons. For output, the grid is mapped into 25 regions as shown in Figure 10. Those regions fully confined on the grid are 2x2 towers in dimension, while those regions on the edges are 1x2, and the four corner regions are 1x1. Alongside the PRAs on the ETT data bus is the quiet detect logic, which examines the same 25 regions to determine which of those regions are completely quiet. The isolation results of the PRAs and the quiet detect logic output flags are encoded into a 3-bit isolated electron code for each of the 25 regions. This code indicates whether the region was completely quiet, contained an isolated electron at one of the six thresholds, or neither.

The edge/corner resolution section performs the final level of isolation checking across grid boundaries. It does this by forming composite 2x2 tower regions out of the 1x2 edge and 1x1 corner regions of the grids. The isolated electron code for these composite regions is simply the largest value from the component partial regions. The result of edge corner resolution is a uniform group of 3-bit isolated electron codes for all 2x2 regions in the calorimeter. During the resolution the isolated electron codes for fully combined regions are propagated alongside the partial regions, so as to maintain the proper timing relationship for matching with the tracker showermax hits.

8.1 Physical Partitioning

The SDC level 1 trigger baseline design is described in [2]. A preliminary version of the physical implementation may be found in [1].

The principal sections described above in the design summary fall neatly along possible PCB card boundaries. The first card, the "MLU card", receives the fiber-optic data for 16 trigger towers, and contains the MLUs for linearization of the energy values and generation of the ETT codes for these towers. Assuming the 16 towers represent a 4x4 region on the calorimeter, this card also contains the 12-bit adder trees for producing the bottom level of energy sums for the jet threshold and total missing energy triggers.

The next card, the "PRA card", resides in the same crate with 4 MLU cards, which deliver their ETT codes to it over the backplane. The PRA card contains the hardware necessary to process the ETT codes into isolated electron codes for one grid. This includes the six PRA ASICs, the quiet detect logic and the electron threshold decoder logic. Through its frontpanel, the PRA card delivers the 3-bit isolated electron codes for the 25 regions (75 bits total) to the edge corner resolution logic.

A single "Calorimeter" crate contains 8 MLU cards and 2 PRA cards. It also contains the additional standard cards, such as a processor, voltage monitor, and cards to interface to the clock, level 1, and level 2 subsystems. Finally, though not part of the isolated electron design, this crate could contain one or more instances of an "Energy Card", which continued the summation of energies for jet threshold and total missing energy triggers.

The edge corner recombination is performed as one of the functions of a "Match card". This card receives the tracker showermax hit data in 2x2 trigger tower resolution

format for an 8x8 tower area. It would also receive the isolated electron codes for the corresponding area. This area, however, would be offset from the PRA grid such that it recieved from 4 separate Calorimeter crates the codes necessary to resolve all partial regions within that 8x8 area. Once the partial regions are resolved, the card proceeds with the task of matching isolated electrons with tracker/showermax hits.

In conclusion, the above partitioning scheme envisions some three card types which are wholly or partially dedicated to the isolated electron pattern logic. The scheme anticipates the tight integration of this subsystem at the circuit level with the other calorimeter triggers at one end, and with the matching logic on the other. The design utilizes a feed-forward approach starting with the fiber-optic link from the detector, through the MLU cards to the PRA cards on Calorimeter crates, and finally to the matching logic.

9 Simulation Results

In order to simulate the performance of the logic, 20000 Dreil-Yan W, 60000 QCD twojet events from 20-200 GeV, and minbias events corresponding to a poisson distribution with mean 1.6 events per crossing were generated using the Monte Carlo program ISAJET. The events were integrated over three beam crossings, using a scintillator calorimeter shaping function from ZEUS. The energy deposit in the calorimeter which resulted was simulated by the program SIM3, from Greg Sullivan at the University of Chicago. The electronics as described in this document was then simulated in detail to determine how many events the proposed trigger would find. The requirement for an electron to be considered present in a tower was simply defined as the electromagnetic energy being at least ten times the hadronic energy. The requirement for a quiet tower was that the HAC energy not exceed 1 GeV, or that the EMC HAC ratio be at least ten but that the transverse energy not meet the lowest threshold. A trigger tower size of .1x.1 in η and ϕ was used for $\eta \leq 2$, and twice that for $\eta \geq 2$. All of these steps were run on Symmetric MultiProcessor Silicon Graphics Inc. 4D 380s at the Physics Detector Simulation Facility of the SSC Laboratory.

Only the $\eta \leq 3$ region of the calorimeter was simulated. The energies deposited in the calorimeter are first converted to an eight-bit logarithmic scale. For each tower, a lookup table returns the ETT code for the tower. Then the pattern logic is done for each 8x8 region of trigger towers. Finally, the isolated electron codes are put in an array so that the region matching is automatically done. Then the threshold number for the highest transverse energy isolated electron found in the barrel and endcap are returned.

The cross section for Drell-Yan W events generated by ISAJET was 1.1×10^{-1} mb. Out of these events, 63%, or $.69 \times 10^{-1}$ mb generated an electron from a W with $\eta \leq 3$. Thus a trigger looking in the $\eta \leq 3$ region of the calorimeter for electrons from W's should find no more than this cross section. In the figures following, the success at finding W events is expressed as a perrentage of the W cross section which decays to electrons which have $\eta \leq 3$. Thus 100% W efficiency corresponds to a cross section of $.69 \times 10^{-5}$ mb. For the QCD background, the rates are expressed in kHz, where 1 mb corresponds to 1000 kHz at the SSC design luminosity of 10^{33} cm^{-2} sec^{-1}.

Figure 14 shows the trigger success in finding W events plotted versus the E_t of the electron from a W in the event. Only events producing an electron with $\eta \leq 3$ were taken into consideration. A threshold of 10 GeV E_t was used. Figure 15 is the same, but for the central region of the calorimeter ($\eta \leq 1.6$). Figure 16 shows the efficiency for the endcap region of the calorimeter. We are only about 80% successful there.compared to our near 100% success in the central region.

Figure 17 shows the energy depsit of electrons from W's in their primary trigger towers in the central region. It is evident that the electron cuts in the central region could be tightened up, to requiring the EMC, HAC ratio to be 25. Figure 18, showing the energy deposits in the endcap region, shows that such tightening is not possible in the endcap. Figures 19 and 20 show the energies deposited in trigger towers immediately adjacent to the tower where a W electron hit, for the central and endcap region respectively. This demonstrates that we lose electrons in the endcap region because of adjacent minbias energy deposits.

Figures 21 and 22 show a sampling of energy deposits from twojet particles not associated with electrons or photons, which appear isolated when viewed only in the EMC section of the calorimeter. Figure 21 shows this in the central region, and Figure 22 in the endcap region. These show that the background can be reduced significantly by tightening the requirements on electron towers.

Figure 23 shows the rate of electron triggers from QCD twojet events versus the electron threshold. 1000 kHz corresponds to 1 mb. This demonstrates that if we were to use a constant threshold over all the $\eta \leq 3$ portion of the calorimeter, we would need a threshold of about 25 GeV E_t to achieve a background rate of 3kHz. Note that this is without any tracking information, and thus includes photons as well as electrons. Figure 24 shows the background rate versus W efficiency for certain combinations of thresholds in the central and endcap regions. The combinations of thresholds that produce the points shown is given in the table in Figure 25, as well as the rates for other combinations. 100% W efficiency corresponds to a cross section of $.69 * 10^{-5}$ mb, and 1000 kHz of twojet events corresponds to 1 mb of cross section.

Figures 26 and 27 show the rate of QCD triggers versus E_t threshold and W efficiency, respectively, in the central region of the calorimeter only, i.e., for $\eta \leq 1.6$. 100% W efficiency corresponds to a cross section of $.69 \times 10^{-5}$ mb, and 1000 kHz of twojet events corresponds to 1 mb of cross section. To achieve a QCD twojet rate of 2 kHz in the central region requires a threshold of 25 GeV. With this threshold, we trigger on 32% of the W cross section which decays to electrons which have $\eta \leq 3$.

Figures 28 ann 29 show the rate of QCD triggers versus E_t threshold and W efficiency, respectively, in the endcap region of the calorimeter only, i.e., for $3 \geq \eta \geq 1.6$. 100% W efficiency corresponds to a cross section of $.69 \times 10^{-5}$ mb, and 1000 kHz of twojet events corresponds to 1 mb of cross section. To achieve a QCD twojet rate of less than 1 kHz in the endcap region requires a threshold of 25 GeV. With this threshold, we trigger on 20% of the W cross section which decays to electrons which have $\eta \leq 3$.

Figure 30 shows W efficiency as a function of various combinations of thresholds in the endcap and central region. Figure 31 shows QCD background rates as a function of various combinations of thresholds as well. 100% W efficiency corresponds to a cross section of $.69 * 10^{-5}$ mb, and 1000 kHz of twojet events corresponds to 1 mb of

cross section.

In addition to simulating the electron trigger, we simulated a simple twojet trigger based on the highest E_t found in a single jet trigger tower. Figure 32 shows jet trigger rates from twojet events, assuming a jet trigger tower size of .4x.4 in η and ϕ. 1000 kHz correspoods to a cross section of 1 mb. We see that a rate of 5 kHz from single jets requires ao E_t thresbold of 175GeV.

The requirement for electron trigger performance is 50% efficiency for W's that decay to electrons in the detector fiducial volume. We therefore examine the efficiency for W's with decays to electrons for $\eta \leq 3$. With a threshold of 30 GeV in the central regioo and 20 GeV in the endcap, we achieve an efficiency of 49% for such W's with a background rate of 2.3 kHz. With a threshold of 35 GeV in the central region and 30 GeV in the endcap, we achieve an efficiency of 28% for such W's with a background rate of 0.9 kHz. With a threshold of 20 GeV in the central region and 20 GeV in the endcap, we achieve an efficiency of 65% for such W's with a background rate of 5.7 kHz. All this is done without using any information from the tracking system.

References

1. T. Gorski, J. Lackey, W.H. Smith. *Level 1 Trigger Decision Design for the SDC.* SDC Note SDC-91-00088. 1991.
2. W. H. Smith, T. Gorski, J. Lackey. *SDC Trigger Preliminary Conceptual Design.* SDC Note SDC-91-00090. 1991.

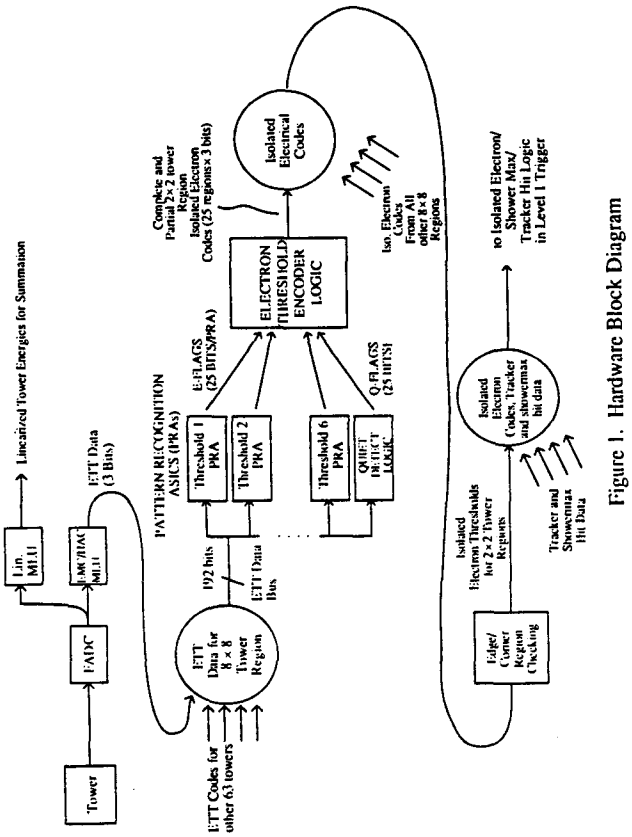


Figure 1. Hardware Block Diagram

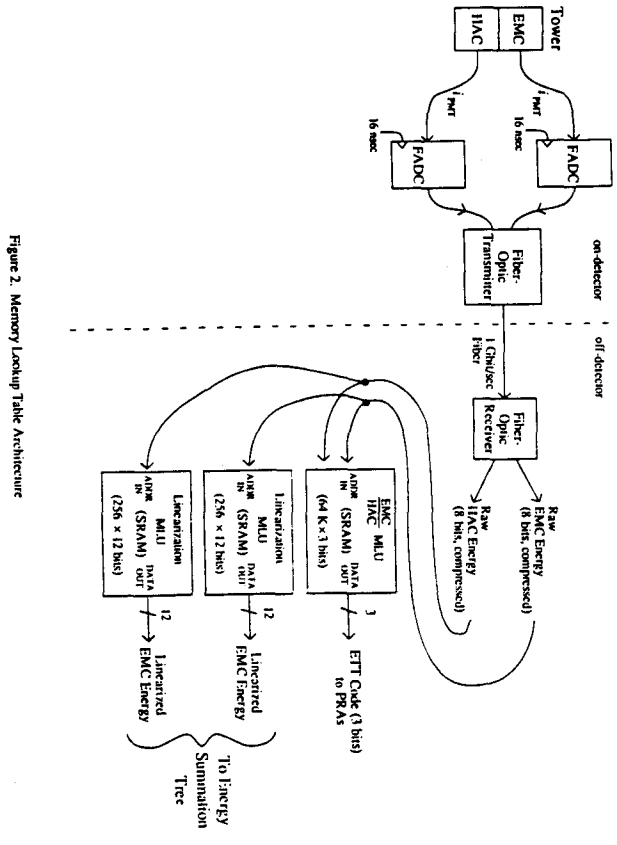


Figure 2. Memory Lookup Table Architecture

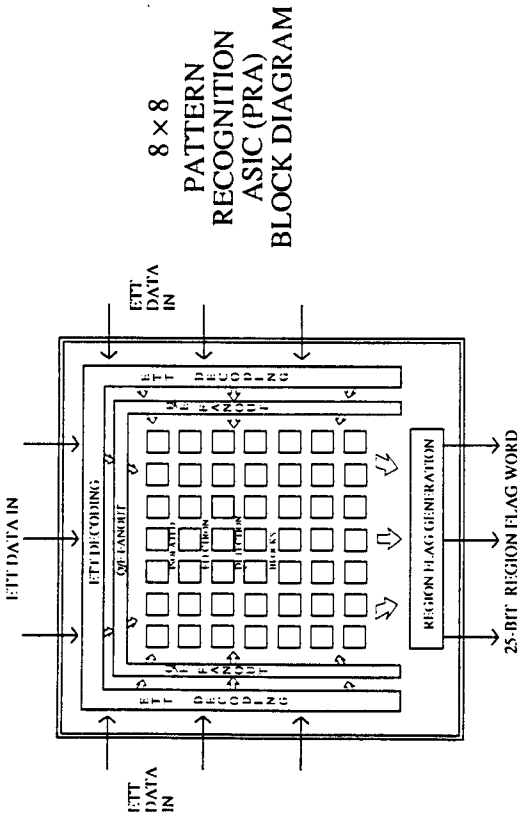


Figure 3. PRA Block Diagram

Tower ETT Code

Selected Threshold \ Q/E	0	1	2	3	4	5	6	7
1	Q	E	–	–	–	–	–	–
2	Q	Q	E	–	–	–	–	–
3	Q	Q	Q	E	–	–	–	–
4	Q	Q	Q	Q	E	–	–	–
5	Q	Q	Q	Q	Q	E	–	–
6	Q	Q	Q	Q	Q	Q	E	–

Figure 4. Decoding of ETT Codes to Q/E bits at all thresholds

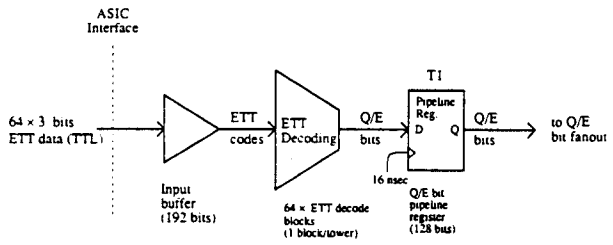


Figure 5. Block Diagram of
ETT Decoding Section of PRA

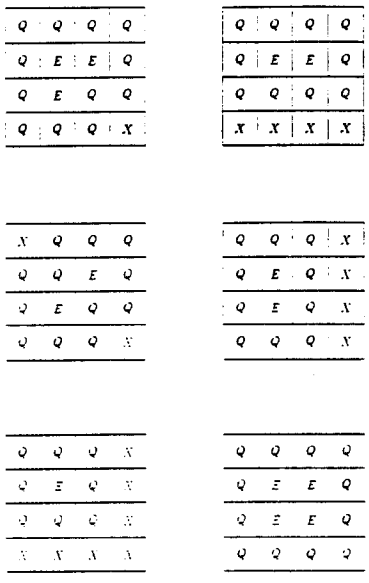
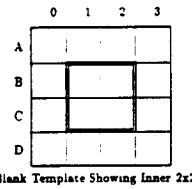


Figure 6. Examples of Isolated Electrons.
"X" denotes towers for which state is a "don't care."



Blank Template Showing Inner 2x2 Region.
Active E bits must be found in the inner 2x2 region, completely surrounded by Q bits.

Evaluation Function:

Definition: F is TRUE if the template contains an isolated electron centered within the inner 2x2 region.

$F = C_1 \cdot C_2 \cdot C_3 \cdot C_4 \cdot \overline{D} \cdot \overline{N}$, where:

$$C_1 = (Q_{A0} \cdot Q_{A1} \cdot Q_{B0}) + (\overline{E_{B1}} \cdot Q_{A1} \cdot Q_{B0}) + (\overline{E_{B1}} \cdot Q_{A1} \cdot \overline{E_{C1}}) + (\overline{E_{B1}} \cdot Q_{B0} \cdot \overline{E_{B2}}) + (\overline{E_{B1}} \cdot \overline{E_{B2}} \cdot \overline{E_{C1}})$$

$$C_2 = (Q_{D0} \cdot Q_{D1} \cdot Q_{C0}) + (\overline{E_{C1}} \cdot Q_{D1} \cdot Q_{C0}) + (\overline{E_{C1}} \cdot Q_{D1} \cdot \overline{E_{B1}}) + (\overline{E_{C1}} \cdot Q_{C0} \cdot \overline{E_{C2}}) + (\overline{E_{C1}} \cdot \overline{E_{C2}} \cdot \overline{E_{B1}})$$

$$C_3 = (Q_{D3} \cdot Q_{D2} \cdot Q_{C3}) + (\overline{E_{C2}} \cdot Q_{D2} \cdot Q_{C3}) + (\overline{E_{C2}} \cdot Q_{D2} \cdot \overline{E_{B3}}) + (\overline{E_{C2}} \cdot Q_{C3} \cdot \overline{E_{C1}}) + (\overline{E_{C2}} \cdot \overline{E_{C1}} \cdot \overline{E_{B3}})$$

$$C_4 = (Q_{A3} \cdot Q_{A2} \cdot Q_{B3}) + (\overline{E_{B2}} \cdot Q_{A2} \cdot Q_{B3}) + (\overline{E_{B2}} \cdot Q_{A2} \cdot \overline{E_{C2}}) + (\overline{E_{B2}} \cdot Q_{B3} \cdot \overline{E_{B3}}) + (\overline{E_{B2}} \cdot \overline{E_{B3}} \cdot \overline{E_{C2}})$$

$$D = (Q_{B1} \cdot Q_{C1} \cdot \overline{BOTTOM}) + (Q_{B1} \cdot Q_{B2} \cdot \overline{RIGHT}) + (Q_{B1} \cdot Q_{B2} \cdot Q_{C1} \cdot Q_{C2})$$

$$N = (\overline{E_{B1}} \cdot \overline{Q_{B1}}) + (\overline{E_{B2}} \cdot \overline{Q_{B2}}) + (\overline{E_{C1}} \cdot \overline{Q_{C1}}) + (\overline{E_{C2}} \cdot \overline{Q_{C2}})$$

Figure 7. Evaluation Function Definition
Note special conditions on the D subfunction for templates on the bottom and right edges of the grid.

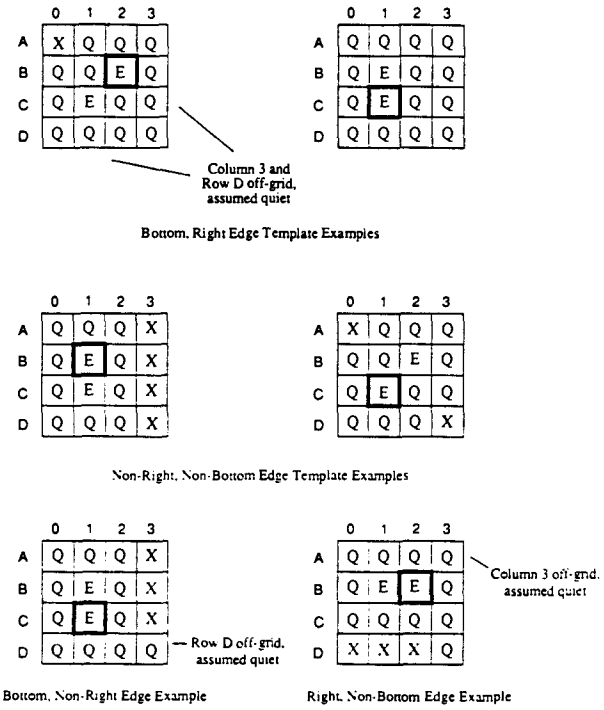


Figure 8. Examples of Isolated Electron Assignments to Towers. Isolated Electrons are assigned to Towers with bold outline.

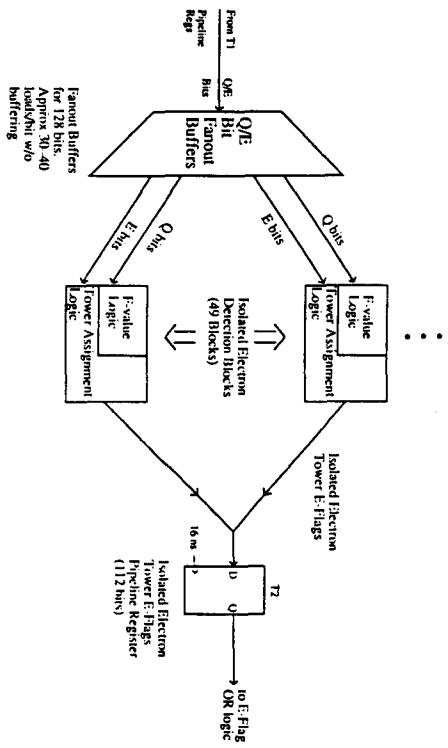


Figure 9. Block Diagram of Isolated Electron Block Section of PRA.

0	1	2	3	4
5	6	7	8	9
10	11	12	13	14
15	16	17	18	19
20	21	22	23	24

scale
= 1 tower, either $(.05)^2$ or $(.1)^2$

Bit#	Description	
0	Region 0	E-Flag
1	Region 1	E-Flag
2	Region 2	E-Flag
3	Region 3	E-Flag
4	Region 4	E-Flag
5	Region 5	E-Flag
6	Region 6	E-Flag
7	Region 7	E-Flag
8	Region 8	E-Flag
9	Region 9	E-Flag
10	Region 10	E-Flag
11	Region 11	E-Flag
12	Region 12	E-Flag
13	Region 13	E-Flag
14	Region 14	E-Flag
15	Region 15	E-Flag
16	Region 16	E-Flag
17	Region 17	E-Flag
18	Region 18	E-Flag
19	Region 19	E-Flag
20	Region 20	E-Flag
21	Region 21	E-Flag
22	Region 22	E-Flag
23	Region 23	E-Flag
24	Region 24	E-Flag

Figure 10. Region Flag Word Definition

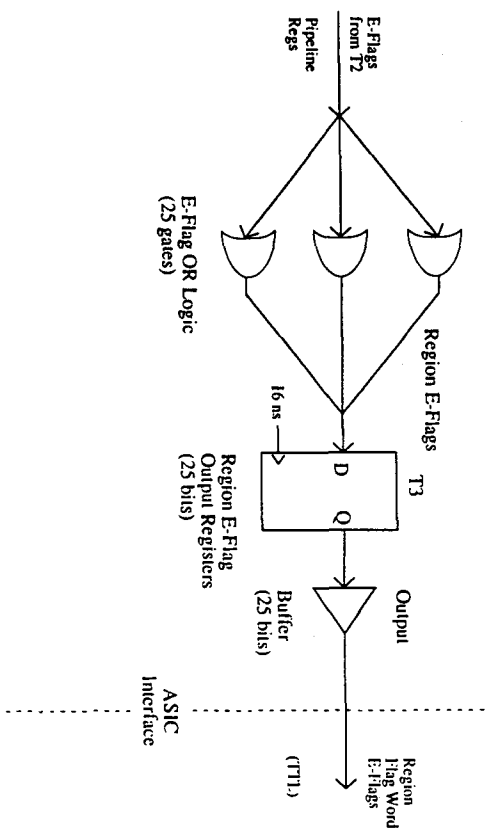


Figure 11. Block Diagram of Region Flag Word Section of PRA

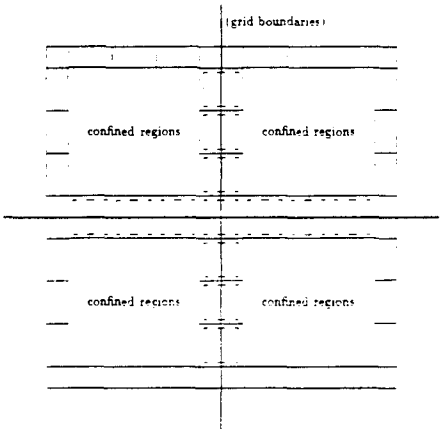


Figure 12 Four Adjacent Cards showing formation of 2x2 composite regions from edge and corner partial regions

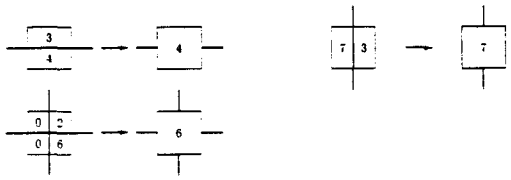


Figure 13: Examples of Partial Region Resolution
Largest subregion isolated electron code becomes the code for the composite region

probability of electron trigger 10 GeV threshold

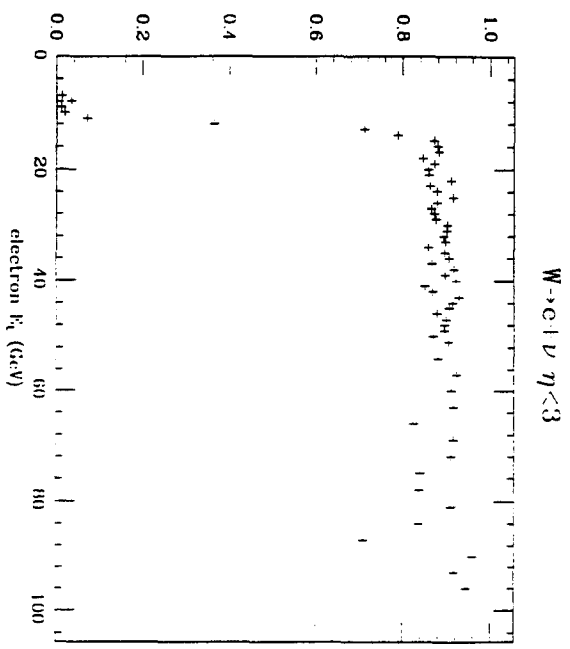


Figure 14

probability of electron trigger 10 GeV threshold

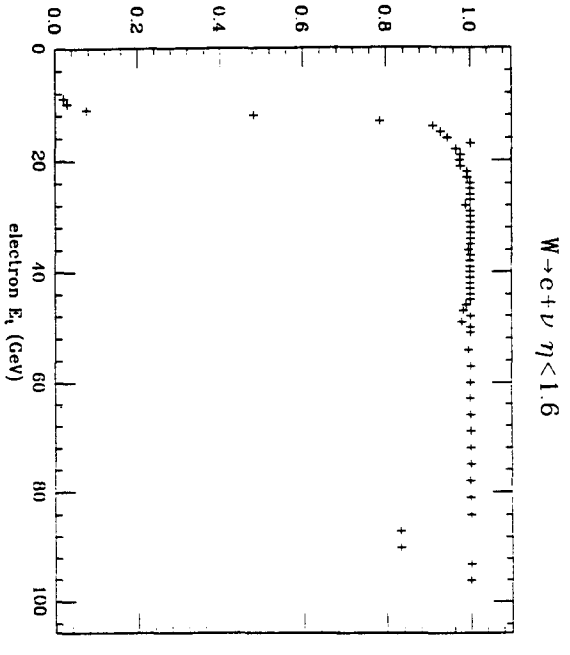


Figure 15

Figure 17

Figure 19

Figure 16

Figure 18

481

EMC isolated particles from 2-jet events

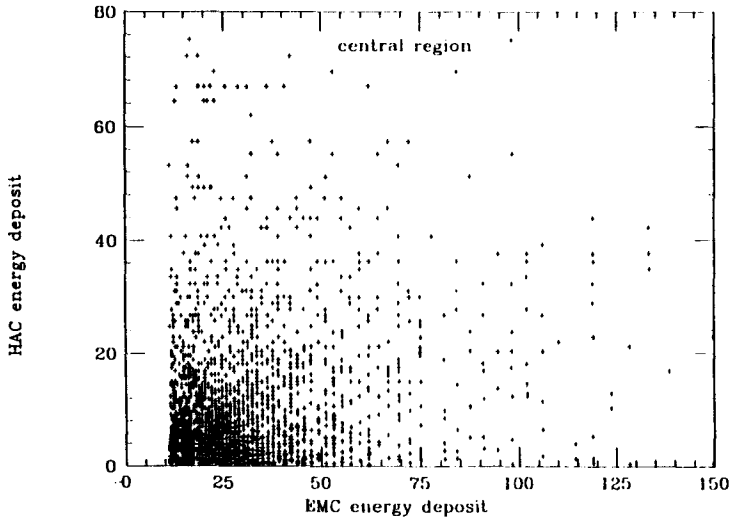


Figure 21

483

QCD 2-JET 20-200 GeV

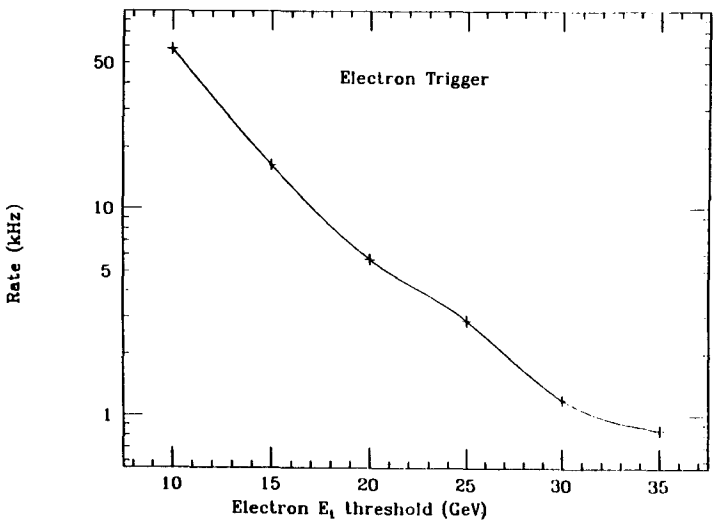


Figure 23

450

lowers adj to electrons from W $\to e\nu$ $1.6<\eta<3$

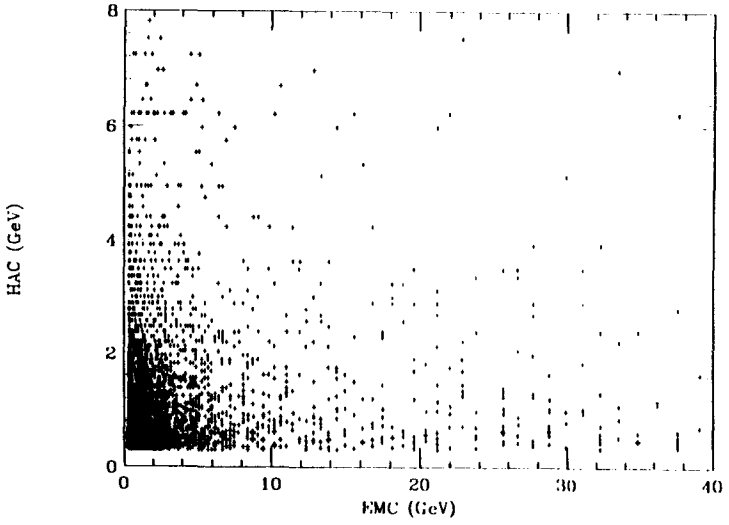


Figure 20

482

EMC isolated particles from 2-jet events

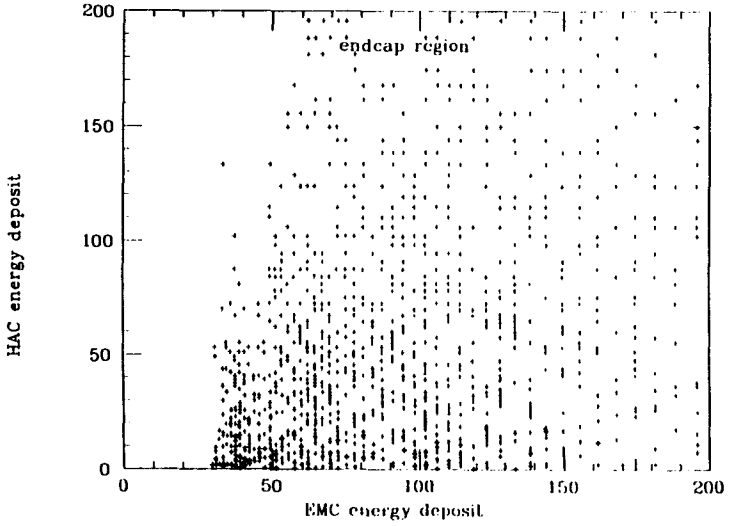
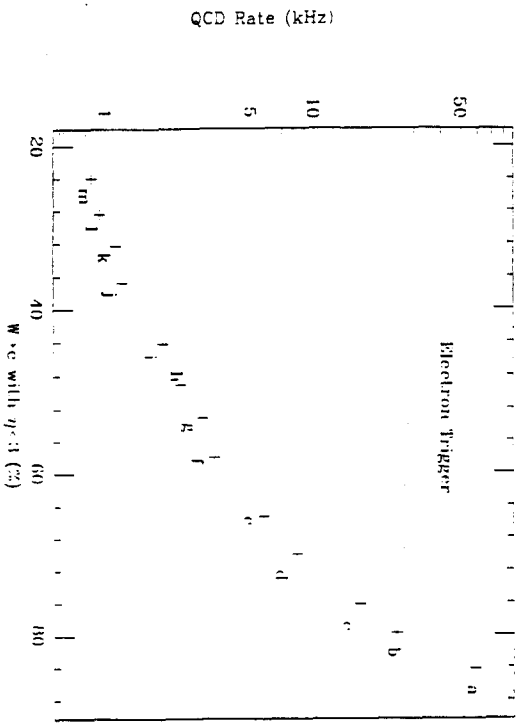


Figure 22

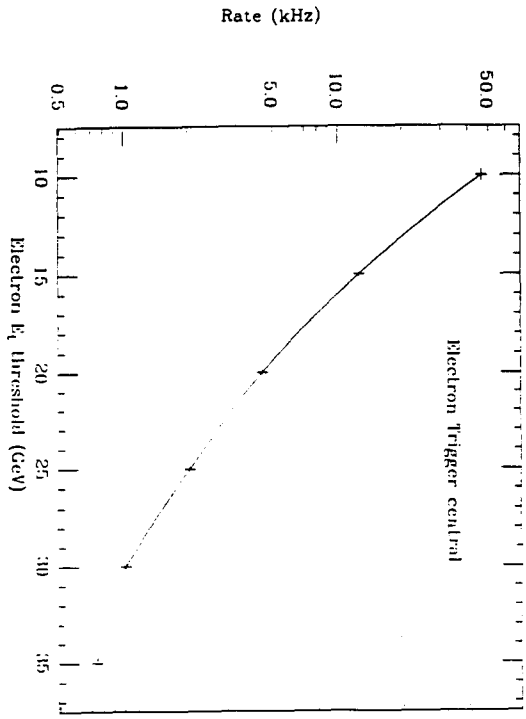


Background rate vs. W Rate

Figure 24

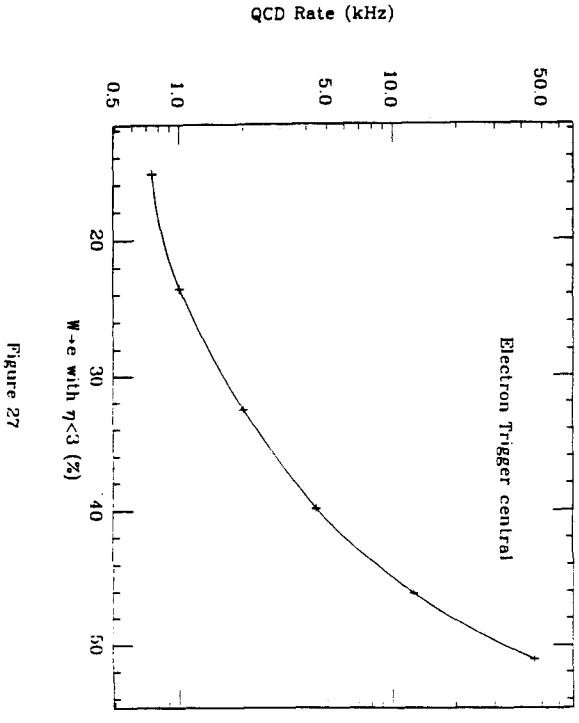
QCD rate W (%)	endcap thresholds					
central thresh	10	15	20	25	30	35
10	55.12 kHz 84.27% (a)	49.95 kHz 81.13%	47.57 kHz 76.53%	47.15 kHz 71.65%	46.50 kHz 64.34%	46.42 kHz 59.81%
15	24.54 kHz 79.75% (b)	16.32 kHz 76.19% (c)	13.91 kHz 71.60%	13.52 kHz 66.71%	12.84 kHz 59.40%	12.76 kHz 54.85%
20	16.47 kHz 73.68%	8.25 kHz 70.11% (d)	5.70 kHz 65.34% (e)	5.31 kHz 60.46%	4.63 kHz 53.15%	4.56 kHz 48.62%
25	14.05 kHz 66.43%	6.52 kHz 62.87%	3.27 kHz 58.10% (f)	2.88 kHz 53.16% (g)	2.21 kHz 45.86%	2.13 kHz 41.33%
30	13.03 kHz 57.46%	4.51 kHz 53.59%	2.26 kHz 49.13% (h)	1.87 kHz 44.19% (i)	1.19 kHz 36.84% (j)	1.12 kHz 32.31% (k)
35	12.77 kHz 49.11%	4.24 kHz 45.55%	2.00 kHz 40.78%	1.61 kHz 35.84%	0.93 kHz 28.49% (l)	0.85 kHz 23.95% (m)

Figure 25



QCD 2-JET 20 200 GeV

Figure 26



Background rate vs. W Rate

Figure 27

489

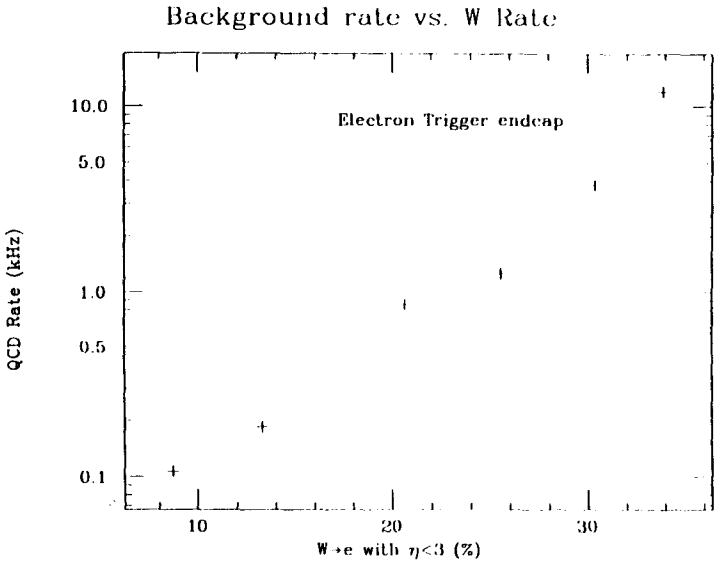


Figure 29

489

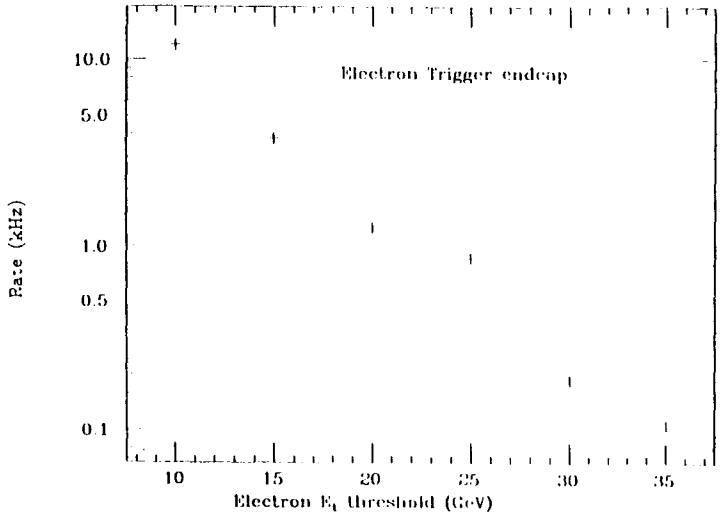


Figure 28

491

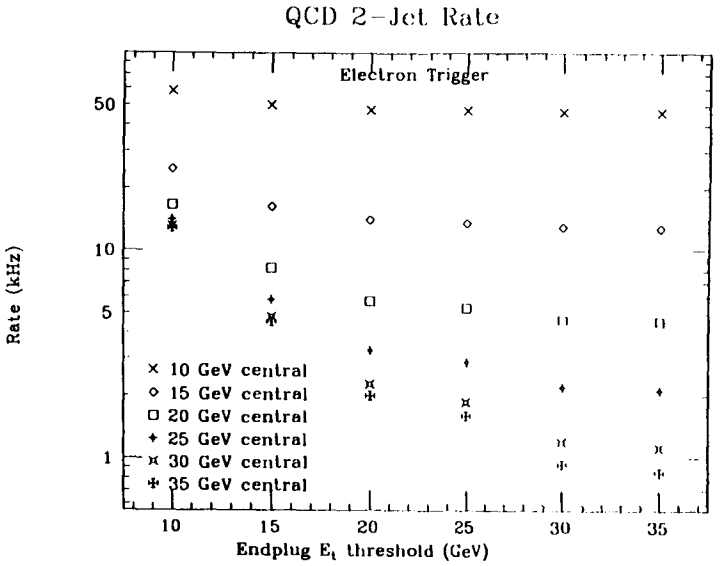


Figure 31

490

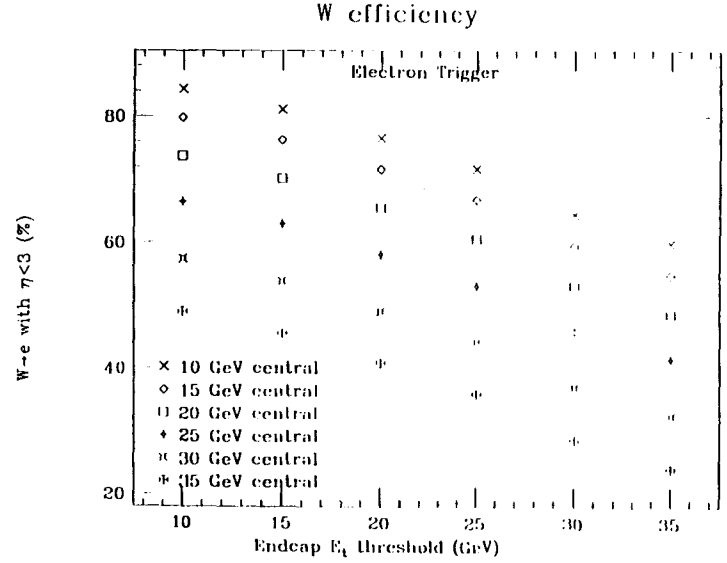


Figure 30

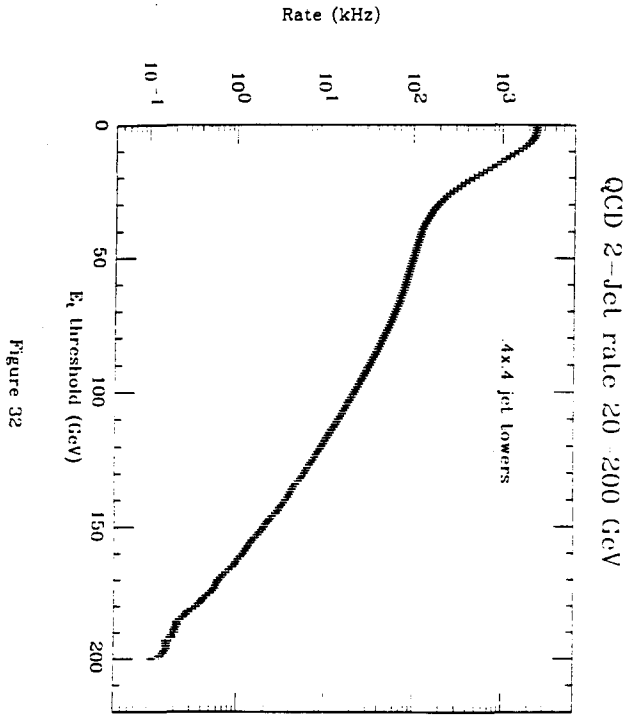


Figure 32

SDC Note SDC-91-00088
DRAFT
September 6, 1991

Level 1 Trigger Decision Design for the SDC

W.H. Smith, J. Lackey, T. Gorski.
University of Wisconsin

1 Introduction

The SDC level 1 trigger decision is based on local decisions about the presence of objects such as photons, electrons, muons, and jets, as well as global sums of E_T and missing E_T. It uses the global compilation of this information to decide whether to keep (i.e. trigger on) a particular 16 nsec beam crossing. Each of the objects, such as electrons, muons and jets, are required to pass a series of p_t or E_t thresholds, which are used in making the Level 1 Trigger Decision.

The identification of trigger objects often depends on correlations between different subsystems participating in the trigger decision. The identification of an electron involves correlating information from the tracking and calorimeter systems. Identification of an electron in the calorimeter requires detecting isolated electromagnetic energy. The first step is to find a calorimeter trigger tower with energy in the electromagnetic compartment and little or no energy in its hadronic compartment (i.e. typically $E_{HAC} < 0.1 * E_{EMC}$). Next the towers adjacent to this tower are checked for having little or no energy in both electromagnetic and hadronic compartments. This establishes electromagnetic energy that is transversely and longitudinally isolated. However, since the size of the calorimeter trigger towers (nominally .1 x .1) is coarse, this information determination is improved with information from the shower max detector. Since a photon would also deposit the same pattern in the calorimeter, but would not deposit in the tracking system, the tracking system is used to distinguish between a photon and electron.

The Level 1 Electron Trigger starts with .1 x .1 towers with energy in the electromagnetic compartment and little or no energy in the hadronic compartment surrounded by towers with little or no total energy. These isolated electron candidates are reported out on a .2 x .2 grid. In order to distinguish electrons from photons, correlation with the outer tracker is used. The shower max detector provides a local hit on .2 η x .00625 ϕ bins. The outer tracker provides tracks with a p_t on a .00625 ϕ grid. The shower max is first correlated with the tracker to produce a coincidence hit with a p_t in .2 x .2 bins (after making the coincidence on a .00625 ϕ scale for checking against the calorimeter in η ϕ, and p_t. The photons are selected without the track match, but with a shower max match and a higher energy threshold.

The Level 1 Trigger finds jets by looking for .4 x .4 calorimeter towers over a series of thresholds. It finds muons by finding muon tracks over a series of muon p_t thresholds. The muon system is not correlated with the tracking system until Level 2. It must have a

sharp enough p_t threshold to allow for a few kHz Level 1 rate while satisfying the trigger requirement above.

2 General Overview

Figure 1 shows a diagram of the Level 1 Trigger layout. Front-end crates for the calorimeter, shower max, tracking and muon subsystems are shown inside the border. Above them, off the detector, are shown the the level 1 decision processing crates. These include the Calorimeter Isolation/Summation crates, the Track/Shower Max Match crates, the Isolated Electron Match crates, the Energy Sum/Jet Threshold crate, the Muon Trigger Crates, and Final Decision crate. These crates together form a pipeline structure in which data flows off of the detector on 1 Ghit/sec optical fibers into the Calorimeter Isloation/Summation, Track/Shower Max Match and Muon Trigger crates as shown in the figure. Data is transmitted from these crates to the Isolated Electron Match and Energy Sum/Jet Threshold crates for further correlation before it is sent to the Final Decision crate. In the case of the Muon Trigger crates, their data is sent directly to the Final Decision crate. The trigger decision pipeline ends at the Final Decision crate, where a Level 1 Accept/Reject is generated and transmitted to the Global Clock/Control Crate for subsequent distribution to all DAQ and Level 1 Trigger crates.

Those crates which receive raw data directly from the front end trigger hardware on the detector contain Level 2 Interface Cards. These cards enable copies of the raw data for which Level 1 Accepts were generated to be transmitted to the Level 2 Trigger.

Each crate in the system has a backplane processor interface bus. This VME or similar-type bus is used by the DAQ Interface Processor card in each crate to program, control and monitor all of the cards in the system. This bus connection and the interface circuitry required on each card is not shown on the current card block diagrams, but is assumed to be present.

Each crate in the system also has a Level 1 Clock/Control Interface card. This card receives the level 1 clock and trigger control information from the Global Level 1 Processor and distributes it to the cards in the crate. See 3 for a further discussion of this card.

The Calorimeter Isolation/Summation crates find .1 x .1 calorimeter towers where $E_{em} \gg E_{sur}$, surrounded by quiet towers. These isolated electron candidates are reported out on a grid of .2 x .2 towers. These crates also sum up the total E_t in .4 x .4 towers, as well as the total E_x, E_y and E_t in the crate. The total .4 x .4 tower sums are tested against 8 thresholds and the number passing each is calculated.

The Track/Shower Max Match crates correlate the outer tracker hits with the shower max hits on a .00625 ϕ scale. The shower max is used to assign the track an η coordinate on a .2 scale. The p_t from the tracker is used to place the track on a 3-bit p_t scale used to match against the calorimeter E_t.

The Isolated Electron Match crates match up the shower max - outer tracker hits and the calorimeter isolated electron candidates on a .2 x .2 grid. The results are counted up in categories of track (including shower max) and calorimeter agreement on p_t, disagreement

on p_t, and shower max match only with the calorimeter (photon). For each category, the total number of matches above each of 6 E_t thresholds is accumulated. Failures to match shower max and calorimeter are also counted.

The Energy Sum Jet Threshold crate continues the global E_t, E_x, and E_y sums as well as adding up the number of .4 x .4 calorimeter towers above a series of 8 threshnlds.

The Muon Trigger Crates count up the number of muon tracks passing each of 4 programmable p_t thresholds. They also store 3 bits of p_t and the track location with a resolution of $\Delta\phi = .01$, $\Delta\eta = .05$ for use by the second level trigger.

The Final Decision Crate sums up and makes cuts on calorimeter total and missing E_t (the latter from the individual E_x and E_y sums). It sums up the total number of calorimeter .4 x .4 regions over 8 thresholds and makes cuts on this. It sums up the total number of isolated electron (and photon) candidates within the categories and p_t thresholds described above and makes cuts on these. It also sums up the total number of muons over the p_t thresholds and makes cuts on these. The resulting trigger decision is then forwarded to the level 1 clock/control logic. See 3 for a further discussion of this logic.

3 Calorimeter Isolation/Summation Crate

Figure 2 shows a Calorimeter Isolation Summation crate. There are 24 of these crates, 16 for the barrel and 8 for the intermediate regions of the detector. Each barrel crate covers 1.6 η x 0.8 ϕ. A crate contains 8 Memory Lookup cards (MLU cards), which receive the hadronic and electromagnetic energies from the .1x.1 calorimeter tower sums. The MLU cards convert the the input FADC tower sum values into E_T on a 12-bit linear scale, compute E_T, E_x, and E_y sums on the .4x.4 region of 16 trigger towers that each services, and calculate an Encoded Tower Type (ETT) code for each tower. This type is based on the amount of energy deposited in the hadronic and electromagnetic compartments. The code is 0 for any tower below the electromagnetic threshold (quiet), and 1-6 for an electron exceeding one of six thresholds, and 7 if the tower is hadronic. A further description of the ETT code and the isolated electron detection logic that uses it can be found in [1].

Each crate also contains 2 Pattern Recognition ASIC cards (PRA cards), which receive ETT codes from 4 MLU cards, corresponding to a .8x.8 region. These boards search for isolated electrons at six independent thresholds within the .8x.8 region. The result is a series of 3-bit codes indicating the absence or presence and threshold of an isolated electron. A flag exists for each .2x.2 region which is fully contained within the .8x.8 area, and for each .1x.2 or .2x.1 region which is on the edge, and for each .1x.1 region on the corners of the .8x.8 area. These isolated electron codes are transmitted to the Isolated Electron Match Crates, for further correlation with adjacent regions of the calorimeter and with data from the Tracking and Shower Max subsystems.

Each crate also contains an Energy Summation Card (Energy card). This double-width card covers a 1.6η x .8ϕ region and receives the energy sums for the .4x.4 regions from all 8 MLU cards. It computes the total E_T, E_x and E_y sums for the 1.6x.8 region. It also tests the E_T in each .4x.4 tower against 8 thresholds and calculates the number of .4x.4 towers

above each threshold. It delivers 3 bits of number above threshold for 8 thresholds, along with the 3 energy sums to the Energy Sum/Jet Thresbold Crates.

Each crate also contains a Level I Clock/Control Interface card, a Level 2 Interface card, and a DAQ Interface/Processor card.

3.1 Calorimeter Memory Lookup Card

Figure 3 shows a block diagram of the MLU card. The card operates on a .4x.4 region of the calorimeter. 16 optical fibers enter through the front panel, each carrying 8 bits of raw compressed FADC data for the EMC and HAC sections of a .1x.1 trigger tower. This data is received serially at a 1 Gbit/sec rate, and converted to a 16-bit parallel path operating at a 16ns rate, for each fiber. The output of the fiber optic receiver circuitry is received by 16 identical MLU blocks, one for each tower.

This MLU block consists of 3 separate lookup operations, all performed in parallel over a 16ns window. The first lookup operation combines the 8 bits each of raw EMC and HAC energies as address into a 64Kx3 MLU, to produce a 3-bit ETT code for the tower. This code categorizes the tower as either quiet, containing an electron at one of six thresholds, or hadronic. The last two MLUs convert the raw EMC and HAC energies to a 12-bit linear scale. The 16 ETT codes from all MLU blocks are transmitted to a PRA eard via the crate backplane. The 32 energies from the MLU blocks are summed in a 12-bit adder tree.

The adder tree is a 5-stage binary tree, 12-bits wide at all stages, that produces an E_T energy for the .4x.4 region covered by the card by suming the EMC and HAC energies from each of the 16 trigger towers. The speed at which each stage is calculated has not yet been determined. The E_T sum is converted to E_x and E_y sums in two parallel 4Kx12 MLUs. All three energies are then transmitted to the Energy card via the crate backplane.

The card also buffers the raw EMC and HAC 8-bit energies for all 16 input optical fibers for subsequent transmission to the Level 2 Interface Card after receiving a level 1 accept.

3.2 Calorimeter Pattern Recognition ASIC Card

Figure 4 shows a block diagram of the PRA card. It operates on a .8x.8 region of the calorimeter, receiving ETT data from 4 MLU cards. The 64 total 3-bit ETT codes are received on the card in a 192-bit wide register bank, and then broadcast to 6 Pattern Recognition ASICs and the quiet detect logic via a ETT data bus. Each PRA examines the entire .8x.8 region, looking for isolated electrons at a particular threshold, with each of the six PRAs selecting a different threshold. The output of each PRA is a 25-bit flag word, with a bit for each of 25 regions in the .6x.8 area indicating if that region contained an isolated electron or not at that threshold. The quiet detect logic examines the same 25 regions, and delivers 25 corresponding bits, with each bit indicating if that region was completely quiet or not. A further description of the PRA can be found in [1].

The 7 bits of raw flags, including 1 quiet flag and 6 electron flags per region, for each of the 25 regions (175 bits total) bits are delivered to the electron threshold encoder and

self-test logic. This logic examines the 7 bits for each of the 25 regions, and generates a 3-bit code, the isolated electron code. This code indicates whether the region was completely quiet, or if it contained an isolated electron, and at what level, or that neither of the above cases was true. The resulting 25x3 (75) bits of isolated electron codes are delivered to the Isolated Electron Match crates.

In self-test mode, this logic also examines the output of all 6 PRAs, which are set to the same threshold for self-test, and detects an error if the output bits of all 6 PRAs are not in agreement.

3.3 Calorimeter Energy Summation Card

Figure 5 shows the block diagram of an Energy card. This double-width card covers a 1.6η x $.8\phi$ region of the calorimeter. It receives the 8x36 (288) bits of E_T, E_x and E_y .4x.4 energy sums from the 8 MLU cards. With these energies, it performs two functions. The first function is to produce E_T, E_x and E_y energy sums for the 1.6x.8 region using 3 parallel 12-bit, 8-input adder trees. The 36 bits of total energies are then transimitted to the Energy Sum/Jet Threshold crates via the front panel.

The second function is to test the E_T .4x.4 energies against 8 thresholds and to sum the number of .4x.4 towers at each threshold. The first stage in this is to decode each 12-bit energy to none or 1 of 8 thresholds in a 4Kx8 MLU, where each output bit of the MLU corresponds to one of the 8 thresholds. This is performed simultaneously in 8 MLU blocks for each of the 8 .4x.4 E_T energies. The decoded output bits are then driven to 8 parallel 8-input adder trees, with one tree for each threshold. Each tree sums 8 binary inputs to a single 3-bit output. It references one output bit from each MLU block. The resulting 8 histogram bins of 3-bit jet towers over thresnold sums (24 bits total) are transmitted to the Energy Sum Jet Thresnold crates via the front panel.

4 Track/Shower Max Match Crate

Figure 6 shows a Track Shower Max Match crate. There are 12 of these crates: 8 for the barrel, and 4 for the intermediate regions of the detector. Each barrel crate covers 1.6 η x 1.6 ϕ. A crate contains 8 double-width Track Shower Max Hit cards (TSM cards), which receive the the raw tracker and shower max hit data for a 1.6η x 0.2ϕ region. The TSM cards correlate the track and shower max hits and deliver the results to the Isolated Electron Match Crates for further correlation with the isolated electron hits.

Each crate also contains a Level 1 Clock Control Interface card, a Level 2 Interface card, and a DAQ Interface Processor card.

4.1 Track/Shower Max Hit Card

Figure 7 shows a block diagram of the TSM card. The card operates on a 1.6 η x 0.2 ϕ region of the detector. Each card is double-width, and receives 16 optical fibers containing shower max hits and 8 optical fibers containing p_T information from the tracker. Each shower max fiber delivers 16 bits of binary hit information for a .2x.1 region, where each bit corresponds to a hit/no hit in a $.2\eta$ x 0.00625ϕ region. Each tracker fiber delivers four 4-bit bins of p_T information, where each bin corresponds to 1.6η x 0.00625ϕ, and the area covered by the data on each fiber is 1.6η x 0.025ϕ.

The data is received by the fiber optic reciever circuitry and converted to a parallel data on a 16ns clock basis. The data from both subsystems is brought together in the hit resolution sorting logic. This logic finds the largest p_T with a corresponding shower max hit in .00625 ϕ for each .2x.2 region. This is accomplished using 5-bit 32-input comparator trees.

The comparator tree finds the shower max hit with the largest p_T, or alternately, if there are no shower max hits, simply the largest p_T, as follows. At the .00625 ϕ level, the binary shower max hit/no hit bit is appended as the MSB to the corresponding p_T data, producing a 5-bit word. This is repeated for all p_Ts and shower max hits with the result being 32 5-bit values for .2 in η and .2 in ϕ. These values are delivered as unsigned data to a 32-input magnitude comparator tree, which selects the largest 5-bit value. By assigning the shower max hit bit as the MSB, the result is that all .00625 ϕ regions with shower max hits have larger values than those without, and would be selected above regions without hits. Thus, a region with a shower max hit, and with the the largest p_T will provide the value for the .2x.2 area.

A total of 8 comparator trees are used: one for each .2 in η. Each delivers a 5-bit value, where the MSB indicates if there was a shower max hit in the .2x.2 region, and the 4 other bits are the largest p_T corresponding with a shower max hit found in that region. For each region, the 4-bit p_T value is converted to a 3-bit threshold value in a 16x3 MLU block. This threshold value is selected to properly correspond with the isolated electron threshold codes generated by the Calorimeter Isolation Summation Crates. For each region, the shower max hit flag and the 3-bit p_T threshold code are transmitted to the Isolated Electron Match Crates via the front panel.

Each TSM card also buffers the raw p_T values and shower max hits received on the fiber-optic cables for subsequent transmission to the Level 2 Interface Card upon recept of a level 1 accept.

5 Isolated Electron Match Crate

Figure 8 shows an Isolated Electron Match Crate. There are 6 of these crates: 4 for the barrel and 2 for the intermediate regions of the detector. Each barrel crate covers 1.6 η x 3.2 ϕ. A crate contains 8 Region Match cards (RMC cards), each of which handles a .8x.8 region. The RMC card receives the isolated electron codes from the PRA cards, performs the last level of isolation checking on the edge corner partial regions, and then compares

the isolated electron codes against the track/shower max hit data from the TSM cards to produce a histogram summary of isolated electron - track shower max hit totals on .2x.2 regions in the .8x.8 area. There are 18 histogram bins, with each bin being 3-bits wide. The bins count the number of isolation/shower max hits with no p_T, the number with a good p_T match, and the number with a p_T mismatch, at each of the six electron thresholds. The RMCs also deliver an error flag with indicates the presence of isolated electrons without a matching shower max hit. These errors are stored for later system diagnostics.

Each crate also has 2 or 3 Isolated Electron Hit Summation cards (HSC cards). These are double-width cards which continue the histogram summation from 4 front panel input sources to a single frontpanel output. The first two cards are used to continue the summation from 4 RMC cards apiece. At this level, each HSC card covers a 1.6 η x 1.6 ϕ region. The third HSC is used to perfoem the next levels of summation using lower level HSC cards as the input source. The third HSC card position will be populated in the crates as necessary to implement the histogram summation tree.

Each crate also contains a Level 1 Clock, Control Interface card and a DAQ Interface/Proeessor card.

5.1 Region Match Card

Figure 9 shows a block diagram of the RMC card. The card operates on a .8x.8 region of the detector, which is offset .1 in η and .1 in ϕ from the .8x.8 region covered by the PRA cards. This offset is equivalent to one trigger tower in both directions. The card receives 75 bits of isolated electron codes for 25 fully confined and edge corner partial regions from 4 PRA cards. 45 of those bits represent 9 fully confined .2x.2 regions, 6 edge .1x.2 or .2x.1 regions, and a single .1x.1 corner region from from a single PRA card. 12 bits each from two other PRA cards represent 3 .1x.2 or .2x.1 edge regions and 1 .1x.1 corner region, which will be combined with corresponding edge or corner regions from the first PRA card to form composite .2x.2 regions. The last PRA card contributes 3 bits for a single .1x.1 corner region, and forms a composite .2x.2 region with the corner regions from the other 3 PRA cards.

Isolated electron codes for composite regions are generated in the partial region resolution logic. The code for a composite .2x.2 region is the largest code for any of its partial regions. The logic consists of 6 2-input 3-bit magnitude selectors, which select the larger of the 2 codes for each of the 6 edge regions, and a single 4-input magnitude selector, for the corner region. During this resolution, the codes for the confined regions are propagated along side the magnitude select logic, so that all codes stay in sync with each other in the pipeline. The output of the partial region resolution logic is 16 3 bit isolated electron codes, for each of the .2x.2 regions in the .8x.8 area. These codes are sent to the hit matching logic on the board.

The isolated electron shower max tracker hit matching logic compares the isolated electron codes to the hit data from the corresponding track and shower max sections in the detector. The track shower max data arrives from 4 different TSM cards. Each TSM card delivers a 4-bit code for each of 4 .2x.2 areas, with the total area for each card being .8 η x .2 ϕ. The code consists of a shower max hit/no hit bit, and a 3-bit code corresponding

to the p_T threshold. The logic delivers 3x6x3-bit (54) bits of histogram data, indicating the number of isolated electron/shower max hits with no p_T, the number with a good p_T match, and the number with a p_T mismatch at each of the six electron thresholds. It also delivers an error flag which indicates the presence of an isolated electron without a shower max hit. These 55 hits are delivered to the front panel, where they are transmitted to a HSC card.

The matching logic operates as follows. For each .2x.2 region, there is a 3-bit magnitude comparator and some other combinatorial logic which examines the isolated electron and p_T codes to produce 3 signals: GOOD, MISMATCH, and NOPT. GOOD is active if the p_T code is $\geq$ than the isolated electron code. MISMATCH is active if the p_T code is $<$ the electron code but not zero, and NOPT is active if the p_T code is zero. These three mutually-exclusive lines serve as enables to 3 separate 3-to-8 decoders, which all decode the electron code. Output lines 1-6 of each of the three decoders, which correspond to valid isolated electrons, are then sent as binary inputs to 18 separate 16-input adder trees. Output lines 0 and 7 of each decoder are not used. They correspond to electron codes 0 and 7, which do not indicate the presence of isolated electrons. Each tree computes the sum for one histogram bin from the 16 individual .2x.2 regions. For each region, there is also an additional combinatorial block which compares the electron code and the shower max hit bit. If the electron code is in the range 1 to 6 and the shower max hit bit is not active, then an error flag for the .2x.2 region is produced. The error flags for all 16 regions are combined in a OR tree to produce the single error flag for the entire .8x.8 area. These errors are stored on the card for subsequent diagnostic purposes.

5.2 Isolated Electron Hit Summary Card

Figure 10 shows a block diagram of the HSC card. It is the basic building block for the summation tree for the isolated electron hit histograms. At the lowest level, it operates on a 1.6x1.6 area from 4 RMC cards. At higher levels, it operates on data from up to 4 HSC cards. A HSC card is used in the Final Decision Crate to provide the histogram results for the total detector.

The HSC card is a double-width card that recieves 55 bits of electron shower max, tracker histogram and error flag data from each of 4 sources through the front panel. The logic on the card consists of 18 3-bit adder trees of 4-inputs each to sum the histograms, and a 4-input OR network to combine the error flags. The card delivers 55 bits of output data in the same format to the frontpanel, where it is delivered to the next level HSC card or the final decision logic.

6 Energy Sum/Jet Threshold Crate

Figure 11 shows an Energy Sum/Jet Threshold Crate. There is one of these crates for both the barrel and the intermediate regions of the detector. It contains 4 double-width Energy Summation Cards (ESC cards). Each card covers 1.6 η x 6.4 ϕ in the barrel region, or one end-cap in the intermediate regions of the detector. Each ESC card enmputes 12-bit E_T,

E_x and E_y energy sums from the lower level sums from 8 Energy cards.

Each crate also contains 4 Jet Threshold Summation Cards (JTSC cards). These cards cover the same area as the ESC cards. They compute the next level 5-bit Jet Threshold histograms from the lower level bins from 8 Energy cards.

Each crate also contains a Level 1 Clock/Control Interface card and a DAQ Interface/Processor card.

6.1 Energy Summation Card

Figure 12 shows a block diagram for the ESC card. This double-width card is used to compute the 12-bit E_T, E_x and E_y energy sums for the detector. At its lowest level, it covers a 1.6x6.4 area, operating on data from 8 Energy cards. A ESC card is used in the Final Decision Crate to sum up the result energies from the 4 cards in the Energy Sum/Jet Threshold crate, thus providing the total E_T, E_x and E_y energies for the detector.

The ESC card receives 3x12 bits (36 bits) of energy values from each of 8 front panel input sources. This data is driven to three identical 12-bit, 8-input adder trees–one for each energy. The three resulting 12-bit energies are then delivered to the front panel for tranmission to the next level ESC card or the final decision logic.

6.2 Jet Threshold Summation Card

Figure 13 shows a block diagram for the JTSC card. This double-width card is used to compute the jet threshold histograms for the detector. It operates in parallel with and over the same area as an ESC card. A JTSC card is also used in the Final Decision Crate to compute the final jet threshold histograms for the detector.

The JTSC card receives 6x5 bits (40 bits) of jet towers threshold from each of 8 front panel sources. This data is driven to 8 identical 5-bit, 8-input adder trees–one for each jet threshold. The eight resulting 5-bit sums are then delivered to the front panel for transmission to the next level JTSC card or the final decision logic.

7 Muon Trigger Crate

Figure 14 shows a Muon Trigger Crate. There are 6 of these crates, 4 of which cover all of ϕ and $\eta < 2.5$ in four equal sections. In addition, there are two forward muon trigger crates, one for each end. A crate contains 9 Muon Logic Cards (MLC cards). Each MLC card covers 1.2 η x 0.8 ϕ in the barrel region. A MLC card receives 12 optical fibers from the muon regional front end crates. Each of these fibers contains 3 bits of p_t and 5 bits of ϕ for the two highest p_t tracks in a .2 η x .4 ϕ region. The card buffers this raw data for transmission to the Level 2 trigger via the Level 2 Interface Card in the crate. The 24 bits of track p_t information is cooverted to one of 4 thresholds via memory lookup tables. The

OAK RIDGE NATIONAL LABORATORY
OPERATED BY MARTIN MARIETTA ENERGY SYSTEMS INC

POST OFFICE BOX 2009
OAK RIDGE TENNESSEE 37831

July 30, 1991

Distribution

Magnet and Central Tracker RRR and Interface Control Document

Attached is the latest revision to "Magnet and Central Tracker RRR and Interface Control Document", SDC Tech. Note No. SDC-91-00026. Please review and bring your comments, changes, and questions to the meeting at LBL on August 6, 1991. Please share or make copies with anyone else not on distribution which you feel should review or comment.

I am looking forward to seeing you there.

T. L. Ryan
Mechanical Technology Engineering

Attachments

Distribution

W. Miller	R. Vanberg	J. Rasson
C. Grozis	R. Swensrud	G. Alley
A. Stefanis	N. Hill	E. Zimmer-Nordorf
H. Sadrozinski	A. Goshaw	D. Koltick
H. Ogren	D. Bintinger	A. DuBois
A. Lankford	T. Moore	T. Thurston
M. Gilchriese	D. Vandergriff	B. Edwards
L. Bortoweck	J. Krebs	H. Ziock
R. Richardson	J. Elias	B. Ford
R. Rucbir	M. Harris	

8 Final Decision Crate

Figure 17 shows the Final Decision Crate. There is one crate for the Level 1 Trigger for the entire detector. This crate contains a single HSC card, ESC card, JTSC card, and MSC card. These cards perform the final level of computation for each of their respective subsystems. The HSC card computes the final histogram totals for electron/track/shower max hits. The ESC card computes final the E_T, E_x and E_y energy totals for the calorimeter. The JTSC computes the final histogram totals for jet thresholds, and the MSC card for the muon thresholds.

All four of these cards transmit their results via their front panels to the Final Decision Memory Lookup Card (FDM card). This card uses memory lookup tables and other logic to distill the input data into a trigger "vector" for each subsystem. This vector contains pertinent fields for correlation with other subsystems to produce the final trigger decision. The four vectors are transmitted to the Final Decision Logic Card (FDL card) across the backplane.

The FDL card receives the subsystem trigger vectors from the FDM card and performs the final analysis and correlation necessary to produce a level 1 accept/reject decision. It consists of a number of programmable decision blocks, each of which examines a subset of the trigger vector data to produce its decision. The decisions from all of the blocks are ORed together to produce the overall accept/reject. This decision is transmitted to the Level 1 Global Clock Control Crate for distribution throughout the detector. A further description of the Clock Control subsystem for the level 1 trigger can be found in [3].

8.1 Final Decision Memory Lookup Card

Figure 19 shows a block diagram of the FDM card. This double-width card has 4 separate memory lookup (MLU) architectures on it, one each for total and missing transverse energy triggers, jet threshold triggers, electron/track/shower max triggers, and muon triggers. Each of these architectures produces a trigger vector that is sent to the FDL card. The structure of the trigger vectors will be subsystem dependent, and reflect the general types of trigger information needed from each subsystem to serve as the basis for the final decision.

The data from each of the four subsystems enters the card through the front panel. It receives 55 bits from the HSC card, 36 bits from the ESC card, 40 bits from the JTSC card, and 12 bits from the MSC card.

The MLU architectures will have between them as necessary a limited degree of interconnections to provide a coarse correlation capability between the subsystems. This capability will permit the subsystems to tune their vector outputs with some knowledge of the state of the other subsystems, with which they will be correlated on the FDL card. An example of this is to provide the electron/track/shower max subsystem with rough knowledge of the results of the total missing transverse energy calculations, which it can then factor in when building its own vector.

8.2 Final Decision Logic Card

Figure 19 shows a block diagram of the FDL card. This double-width card receives the four subsystem trigger vectors from the FDM card via the backplane and processes them in multiple programmable trigger decision blocks to produce the accept/reject decision which is sent to the Level 1 Global Clock Control Crate.

Each programmable decision block has 3 major sections. The first section is the vector field select logic. This logic consists of reprogrammable high-density logic, such as a Field Programmable Gate Array (FPGA). A Xilinx IC is an example of this type of part. It's purpose is to select individual relevant fields from the subsystem vectors and to perform a logical correlation between them. The result of this correlation is an address to a MLU block which generates a preliminary accept signal. This preliminary accept is then passed through a programmable prescaler block. The accept signal from all of the blocks are ORed together for transmission through the front panel to the Level 1 Global Clock Control Crate.

The decision blocks all operate independently from each other on different subsets of the same vector data from the FDM card. Blocks will be allocated to different general types of triggering through dedicated connections to only certain fields of the subsystem vectors. They are thus programmable for different triggers within the scope of data available to that block. For example, one block may be dedicated to triggering conditions which involve photons and transverse energy, while another is dedicated to electron - muon conditions, each dedicated by means of the vector fields that it can access.

9 Design Summary

The level 1 decision hardware is comprised of numerous on and off-detector crates which are interconnected both electrically and optically to form multiple pipelined data streams, which come together at the Final Decision crate to generate a Level 1 Accept/Reject for the detector.

There are four major physical subsystems: the calorimeter, shower max detector, the outer tracker, and the muon subsystems. Trigger data from these physical subsystems is processed in the pipeline to form four major triggering subsystems: isolated electron/photon hits, total/missing transverse energy, jet threshold sums, and muon threshold sums.

The isolated electron/photon trigger subsystem correlates data from the calorimeter, shower max detector, and outer tracker. From the calorimeter, the raw EMC and HAC section 8-bit digitized pulseheights for .1x.1 trigger towers are transmitted to the MLU cards in the Calorimeter Isolation Summation Crates. On these cards, trigger towers are tested for transverse isolation of the energy deposition within the EMC section of the tower, and assigned to an energy threshold in the form of an ETT code. On the PRA cards, in the same crate, the trigger towers are tested for longitudinal isolation at their respective threshold on 5x8 tower regions. The result is a series of isolation codes for 2x2 trigger tower regions which are sent to the Isolated Electron Match Crates.

While this is occuring, the raw shower max and tracker hits for corresponding regions

in the detector are received by the Track Shower Max Hit Cards in the Track Shower Max Match crates. These cards receive the raw shower max hits for .2η x 0.00625ϕ regions, and correlate them with the raw p_t codes for the tracker 1.6η x 0.00625ϕ regions. The result produced by these cards is a 4-bit word for each of the .2x.2 regions corresponding to the 2x2 calorimeter trigger towers. This code contains a shower max hit flag and a threshold code corresponding to the scale of the isolation electron codes. This data is also sent to the Isolated Electron Match Crates.

Within the Isolated Electron Match Crates, the two above data streams converge. Each Region Match Card in the crate compares the results of the isolation logic with the results from the track/shower max comparison for a .8x.8 region. The result is 18 3-bit histogram bins for the area. These bins count (1) the number of isolated electrons with no p_t track (photons), (2) the number with an exact p_t track match, and (3) the number with a p_t track mismatch, at each of the six thresholds. Within these same crates, the histogram results from multiple RMC cards are summed together over increasingly larger areas in the HSC Cards. The output of the HSC cards in the individual Isolated Electron Match Crates are then sent to a final HSC card in the Final Decision Crate, where the histograms are produced for the entire detector.

The total/missing transverse energy trigger uses the same raw calorimeter trigger tower pulseheight data as the isolated electron trigger. For this subsystem, each MLU card calculates the total E_T on a 12-bit linear scale for the 4x4 region of trigger towers. It uses this value as address to two MLUs to calculate the E_x and E_y values for that region of the detector. All three values are then sent to the Energy Card in the same crate. In this card, the E_T, E_x and E_y energy values for the entire crate are calculated and from there transmitted to the Energy Sum/Jet Threshold Crate.

In the Energy Sum/Jet Threshold Crate, the regional energy sums from all of the Energy Cards are summed together in the Energy Summation Cards. Each of these cards can sum the energies from 8 Energy Cards to produce a single E_T, E_x and E_y result for the entire area. The energies from each of the ESC cards are transmitted onto the Final Decision Crate, where a single ESC card makes the final summation to produce the E_T, E_x and E_y values for the entire detector, and delivers them in turn as to the FDM cards, where the missing energy is calculated from E_x and E_y.

The jet threshold trigger also uses the calorimeter energy data. This trigger begins on the Energy Cards in the Calorimeter Isolation Summation Crates. It takes the E_T value computed for each 4x4 area of the MLU cards and compares it to one of 8 thresholds. It then sums the number of the 8 4x4 jet towers that from each MLU card which are at each threshold. This histogram result is transmitted alongside the with the E_T, E_x and E_y transverse energy calculations to the Energy Sum/Jet Threshold Crate.

In this crate, the histogram summation is continued in the Jet Threshold Summation Cards. Each of these cards can sum the histogram data from 8 Energy Cards to produce a single result consisting of 8 threshold bins with 5 bits per bin. The histogram results of each of the 4 JTSC cards are transmitted to the Final Decision Crate, where a single JTSC card computes the histogram values for the entire detector.

Finally, there is the muon trigger subsystem. Unlike the three previous trigger sub-

systems, this trigger subsystem consists of a physical subsystem which stands alone until correlation is performed in the final decision logic. Raw p_t data for the two highest p_t tracks in a .2η x .4ϕ region is transmitted from the front end in each fiber optic cable to the Muon Logic Cards. Each MLC card then compares 24 p_t tracks from 12 cables with 4 thresholds via programmable MLUs. It then sums the number of tracks at each threshold into 4 3-bit histogram bins. The histogram bins are then transmitted to a Muon Summation Card in the same crate, which produces a single set of 4 3-bit histogram bins for the entire Muon Trigger Crate. These bins are then sent to the Final Decision Crate, where a single MSC card computes the histogram values for the entire detector.

All of the subsystem trigger data pipelines converge in the Final Decision Crate at the Final Decision Memory Lookup card. This card distills the data streams down into individual trigger vectors for each subsystem, with some correlation between subsystems. The trigger vectors are then sent to the Final Decision Logic card, where the individual triggers for the detector and prescale values are programmed in. The FDL card examines the trigger vectors according to the programmed criteria and produces the Level 1 Accept/Reject for the entire detector.

10 Physical Requirements

10.1 Crate Summary

Summary of Crate Usage in the Level 1 Final Decision Logic:

Crate Type	Quantity
Calorimeter Isolation Summation	24
Track Shower Max Match	12
Isolated Electron Match	6
Energy Sum/Jet Threshold	1
Muon Trigger	6
Final Decision	1
Total Crates:	50

10.2 Card Summary

Summary of Card Usage in the Level 1 Final Decision Logic:

Card Type	Nominal per Crate Usage	Total Quantity	Comments
Calorimeter MLU	8	192	
Calorimeter PRA	2	48	
Calorimeter Energy	1	24	
Track Shower Max Match	8	96	
Isolated Electron RMC	8	48	
Isolated Electron HSC	2-3	16	incl. 1 card in Final Dec. Crate
Energy Summation	4	5	incl. 1 card in Final Dec. Crate
Jet Threshold Summation	4	5	incl. 1 card in Final Dec. Crate
Muon Logic	8	48	
Muon Summation	1	7	incl. 1 card in Final Dec. Crate
Final Decision MLU	1	1	
Final Decision Logic	1	1	
L1 Clock Control Interface	1	50	1 each in all crates
DAQ Interface Processor	1	50	1 each in all crates
L2 Trigger Interface	1	42	only in crates with L2 connection

10.3 ASIC Requirements

This section provides a preliminary assessment of custom ASICs which may need to be developed to implement the functionality described in this document. The need for an ASIC is determined by identifying those cases on the above defined cards where there is a critical need for density or speed in a functional block that cannot be met by off-the-shelf commercial devices.

The first ASIC candidate is a 12-bit adder block. This would be a fixed point 12-bit adder node with 2 or 4 inputs. It would be able to perform a summation on 2 inputs in a single 16ns crossing clock, or with 4 inputs, per two 16ns clocks in a pipeline fashion. The primary area of need for this ASIC would be on the Calorimeter MLU card and Energy cards, where it would be used to sum the large number of 12-bit E_T, E_x and E_y values present on those cards within the limited board space available to dedicate to that function.

The next ASIC candidate has already been well-defined and named as the Pattern Recognition ASIC - PRA. This ASIC has the function of performing a longitudinal isolation cut on an 8x8 array of trigger towers, at any one of six different energy thresholds. This

ASIC would utilize the high densities available with BiCMOS technology to perform its function in an board area many times smaller than what would be required with general purpose logic. Six of these ASICs will reside on each Calorimeter PRA card. For a total of 6x48, or 288 PRAs, for the detector.

The task of correlating shower max hits with track p_t values also may require an ASIC. This ASIC would be a 5-bit magnitude selector node. This node would have 2 or 4 5-bit inputs, from which it would propagate the largest value to the output. This function is required to find the largest p_t track in .2σ with a shower max hit from among the 32 tracks in .00625σ. The blocks would be stacked in a tree structure to examine the total .2σ area. This ASIC would be used on the Track Shower Max Hit cards.

Thus, there are three candidate ASICs at this time for the level 1 trigger decision logic: a 12-bit adder node, an isolation pattern recognition circuit, and a 5-bit magnitude selector.

11 Fiber Optic Cable Data Formats

This section shows the data formats for the fiber optic cables which transmit data from the front end subsystem crates to the level 1 trigger processing crates off of the detector. There are 4 format types: one each for calorimeter trigger towers, tracker p_t values, shower max hits, and muon p_t, σ bin data. A description of the fiber optic data transmission design can be found in [4].

11.1 Calorimeter EMC/HAC Energy Cable

The following chart shows the format for the data cable which transmits the EMC and HAC energies from the calorimeter front end to the MLU cards:

Bits(s)	Definition
0 to 7	EMC Energy, compressed format
8 to 15	HAC Energy, compressed format

A fiber is used to transmit the raw EMC and HAC pulseheight energies as 8-bits each of compressed data for each .1x.1 trigger tower. Each MLU card receives 16 fibers, for a total of approximately such fibers for the entire calorimeter.

11.2 Tracker p_t Cable

The following chart shows the format for the data cable which transmits the raw p_t values from the tracker:

Bits(s)	Definition
0 to 3	p_T for track 0
4 to 7	p_T for track 1
8 to 11	p_T for track 2
12 to 15	p_T for track 3

Each fiber transmits four track p_T values. Each track corresponds to a region 1.6η x .00625σ. The total region covered by a fiber is 1.6η x .025σ. Each Track Shower Max Match card receives 5 of these fibers, for a total of approximately 760 such fibers for the entire outer tracking subsystem.

11.3 Shower Max Hit Cable

The following chart shows the format for the data cable which transmits the raw flags from the shower max detector:

Bits(s)	Definition
0	hit flag for channel 0
1	hit flag for channel 1
2	hit flag for channel 2
3	hit flag for channel 3
4	hit flag for channel 4
5	hit flag for channel 5
6	hit flag for channel 6
7	hit flag for channel 7
8	hit flag for channel 8
9	hit flag for channel 9
10	hit flag for channel 10
11	hit flag for channel 11
12	hit flag for channel 12
13	hit flag for channel 13
14	hit flag for channel 14
15	hit flag for channel 15

Each fiber transmits 16 shower max hit flags. Each flag corresponds to a region .2η x .00625σ. An active flag indicates a shower max hit was detected in that region. The total region covered by a fiber is .2η x .1σ. Each Track Shower Max Match card receives 16 of these fibers, for a total of approximately 1152 such fibers for the entire shower max detector.

11.4 Muon Data Cable

The following chart shows the format for the data cable which transmits the raw p_t and σ data from the muon subsystem:

Bits(s)	Definition
0 to 2	p_t for track 0
3 to 7	σ for track 0
8 to 10	p_t for track 1
11 to 15	σ for track 1

Each fiber transmits a 3-bit p_t code and 5-bits of σ bin information for the two largest tracks in a .2η x .4σ region. The 5-bits of bin information thus provide a granularity of .00625σ. Each Muon Logic card receives 12 of these fibers, for a total of approximately 580 such fibers for the entire muon subsystem.

References

1. T. Gorski, J. Lackey, W.H. Smith, W. Temple, *Isolated Electron Pattern Logic Design and Performance at the SSC*, SDC Note SDC-91-00087, 1991.
2. W. H. Smith, T. Gorski, J. Lackey, *SDC Trigger Preliminary Conceptual Design*, SDC Note SDC-91-00090, 1991.
3. W. H. Smith, T. Gorski, J. Lackey, *SDC Global Level 1 Processor: Clock & Control*, SDC Note SDC-91-00090, 1991.
4. M. Thompson, *Fiber Optic Data Transmission for the SDC Detector*, SDC Note SDC-91-00092, 1991.

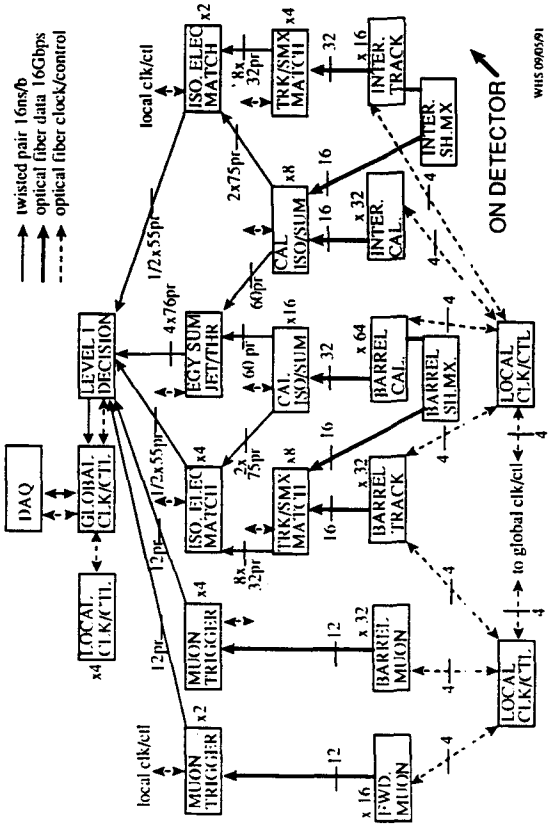


Figure 1. Level 1 Trigger Structure

512

Calorimeter Isolation/Summation Crate

Number of Crates: 16 barrel, 8 intermediate

Coverage: 1.6 η by 0.8 φ

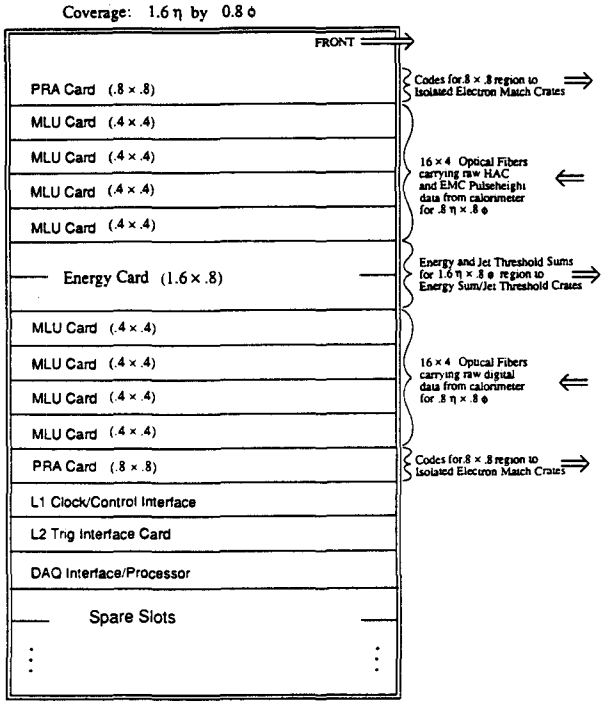


Figure 2

513

Calorimeter Memory Lookup Card
(MLU Card)

Coverage: 0.4 η × 0.4 φ

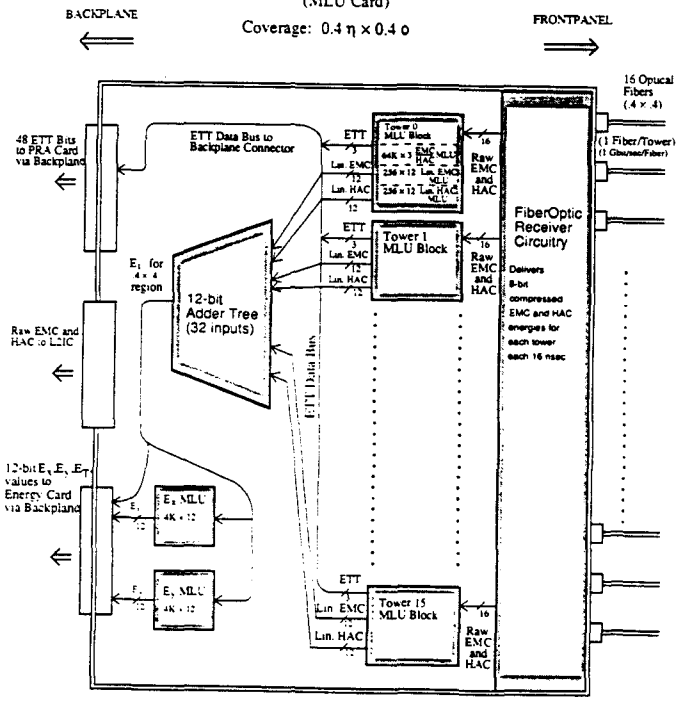


Figure 3

514

Calorimeter Pattern Recognition ASIC Card
(PRA Card)

Coverage: 0.8 η × 0.8 φ

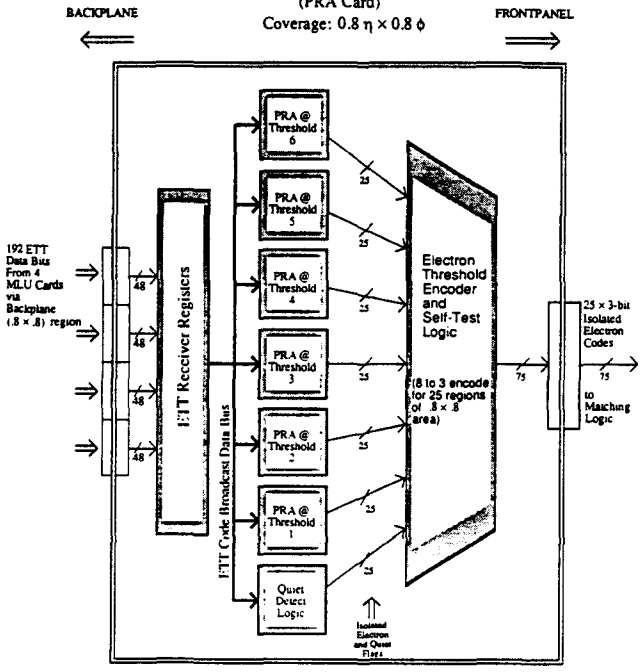


Figure 4

515

Calorimeter Energy Summation Card (Double-Width)
(Energy Card)

Coverage: 1.6 η × 0.8 φ

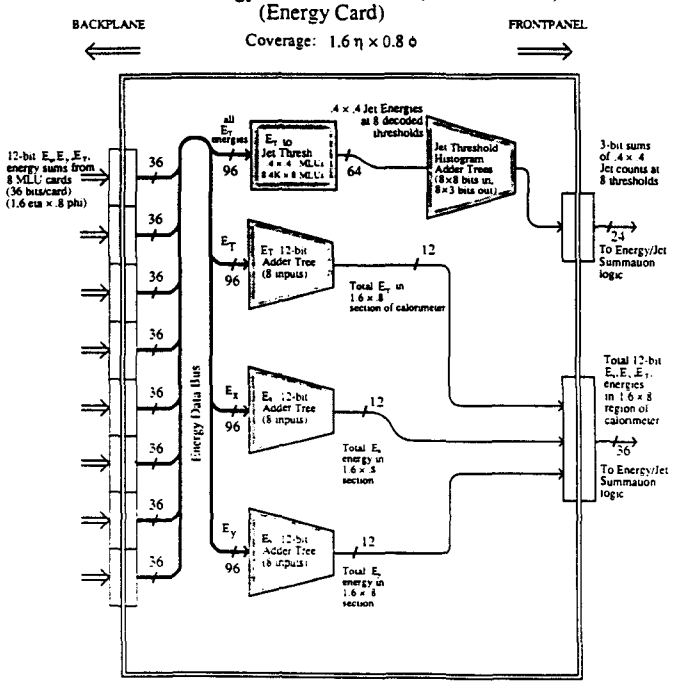


Figure 5

Track/Shower Max Match Crate

Number of Crates: 8 barrel, 4 intermediate

Coverage: 1.6 η by 0.8 ϕ

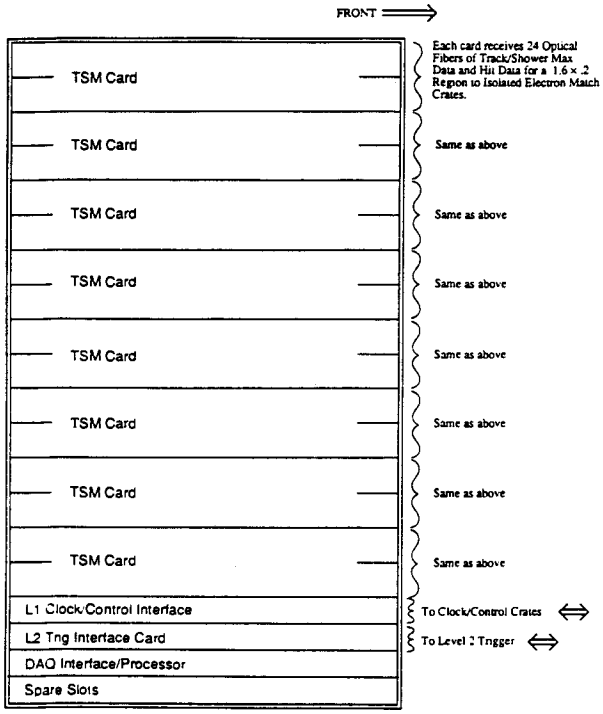


Figure 6

Tracker/Shower Max Hit Card (Double-Width Card) (TSM Card)

Coverage: 1.6 η 0.2 ϕ

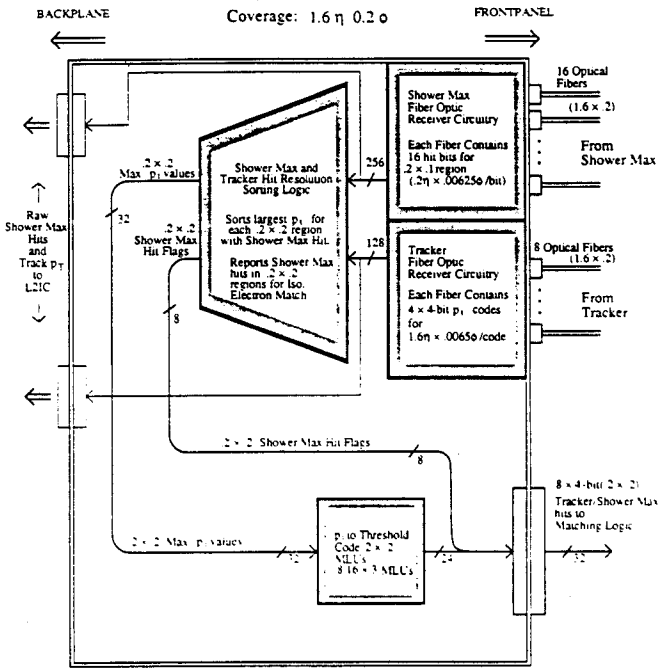


Figure 7

Isolated Electron Match Crate

Number of Crates: 4 barrel, 2 intermediate

Coverage: 1.6 η by 3.2 ϕ

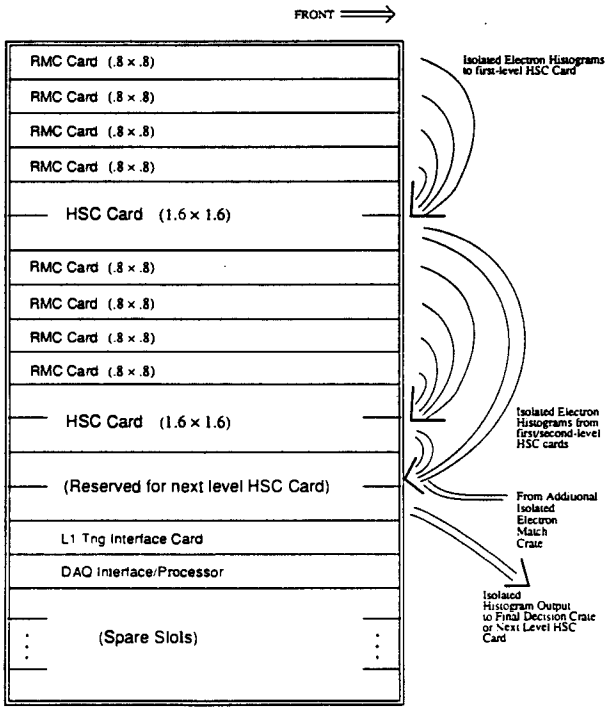


Figure 8

.2 × .2 Region Match Card (RMC Card)

Coverage: 0.8 η × 0.8 ϕ

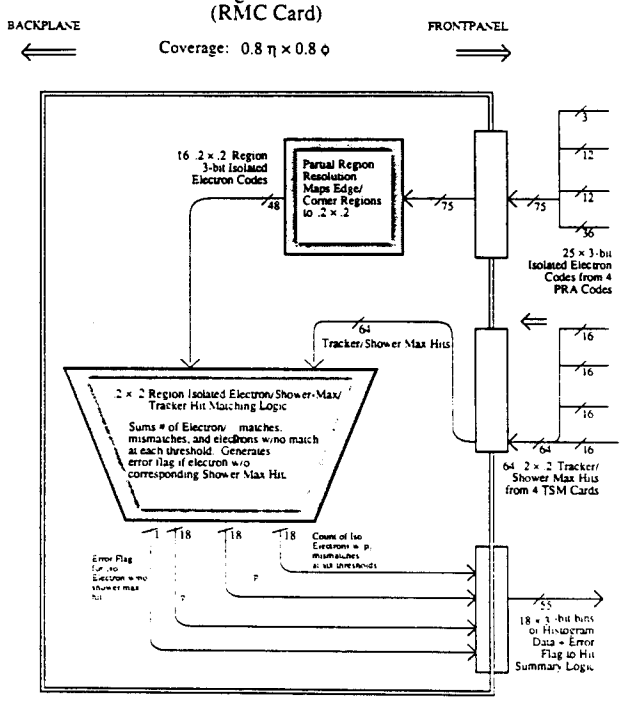


Figure 9

520

Isolated Electron Hit Summation Card (Double-Width)
(HSC Card)

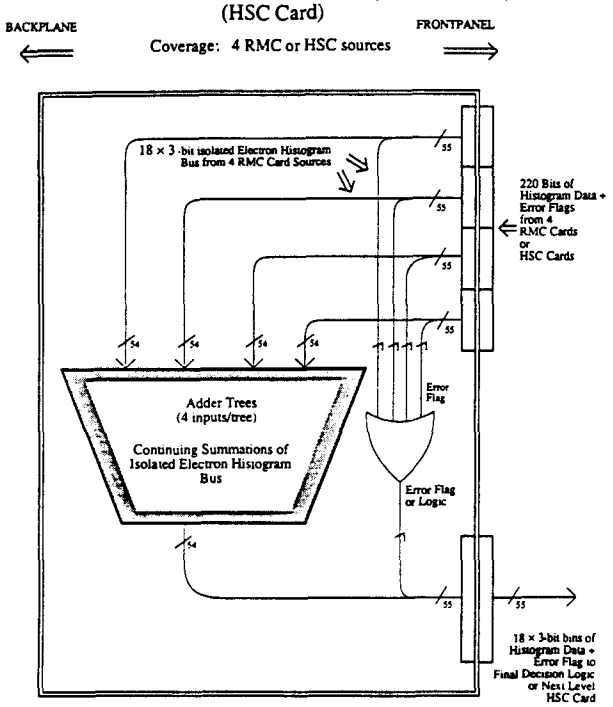


Figure 10

521

Energy Sum/Jet Threshold Crate

Number of Crates: 1 for both barrel and intermediate

Coverage: entire detector

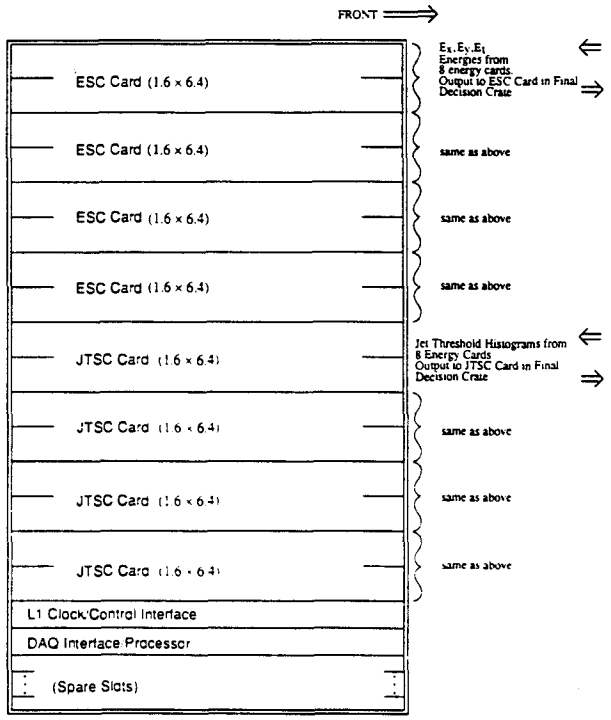


Figure 11

522

8 to 1 Energy Summation Card (Double-Width)
(ESC Card)

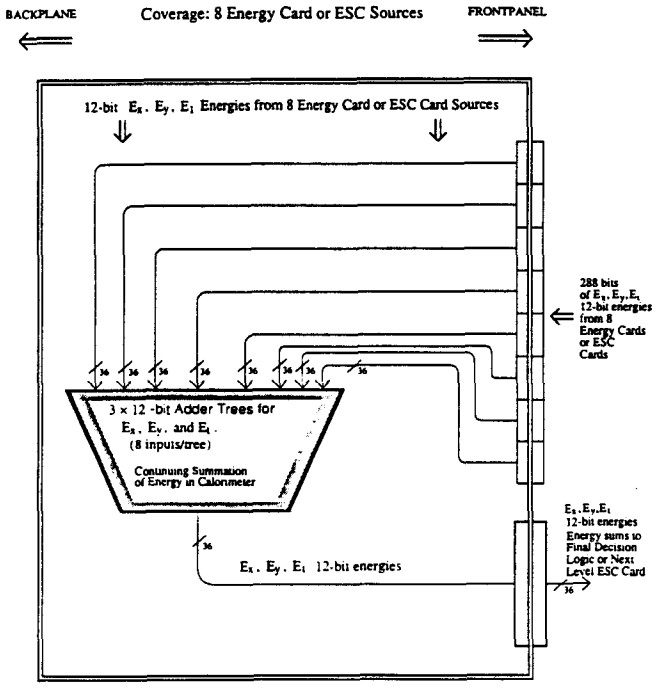


Figure 12

523

8 to 1 Jet Threshold Summation Card (Double-Width)
(JTSC Card)

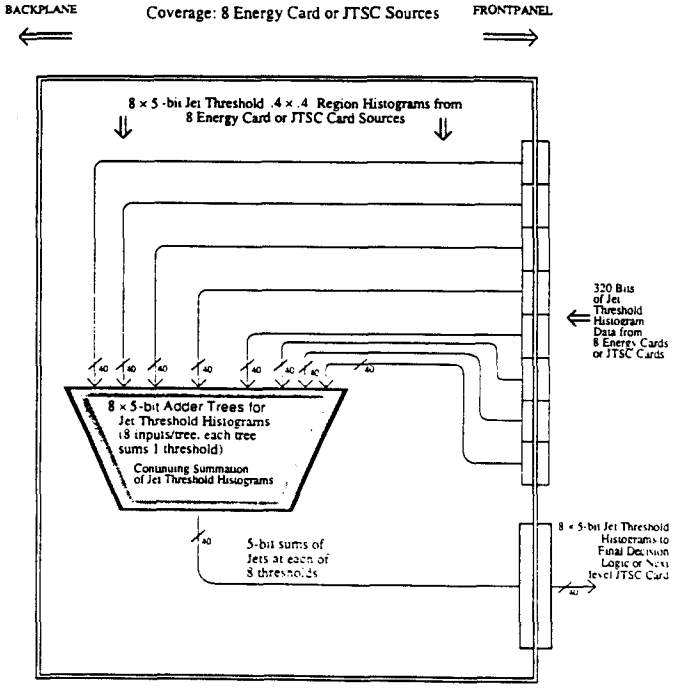


Figure 13

524

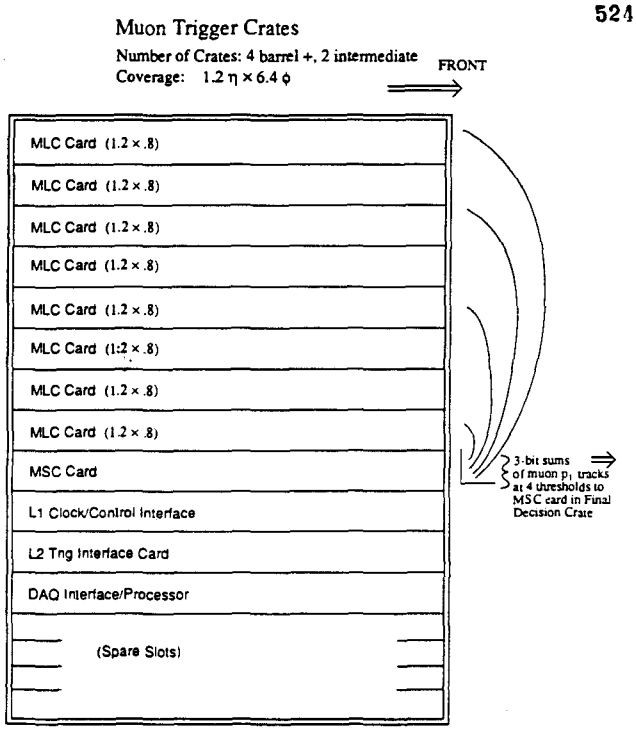


Figure 14

525

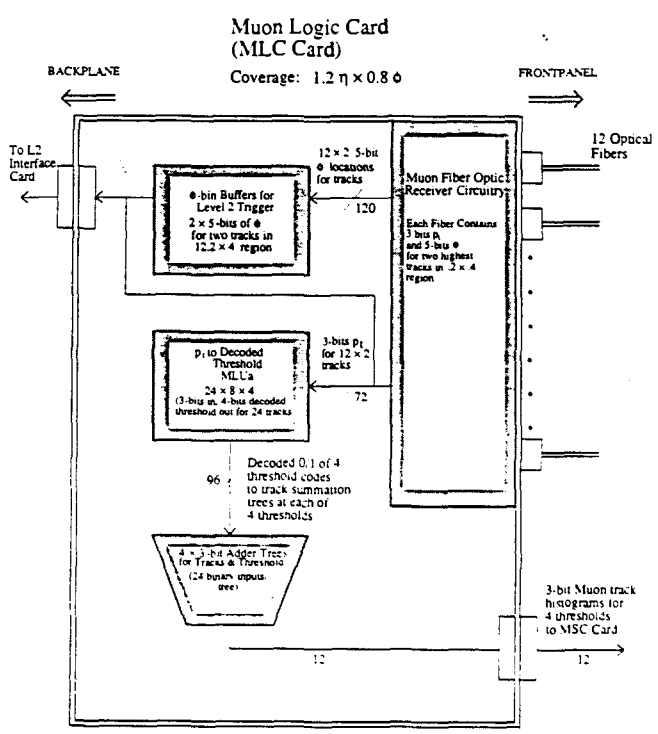


Figure 15

526

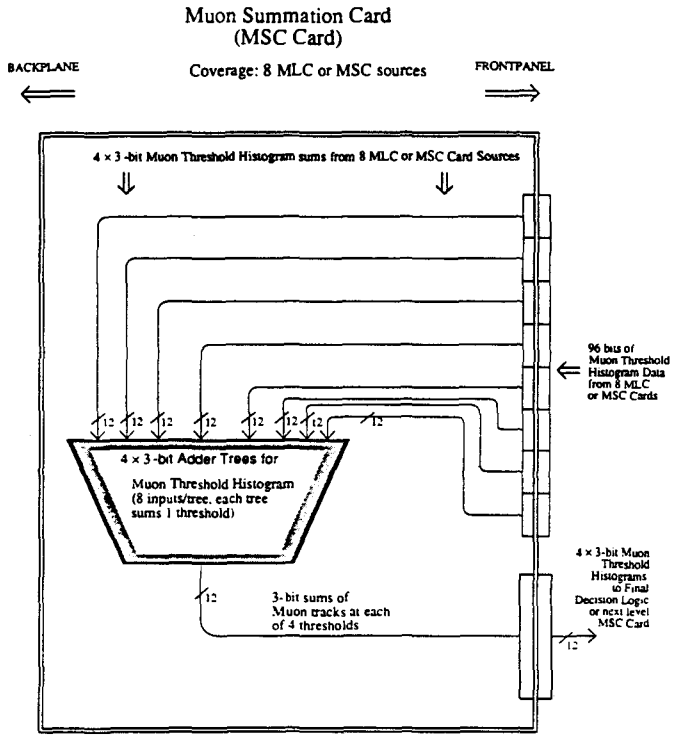


Figure 16

527

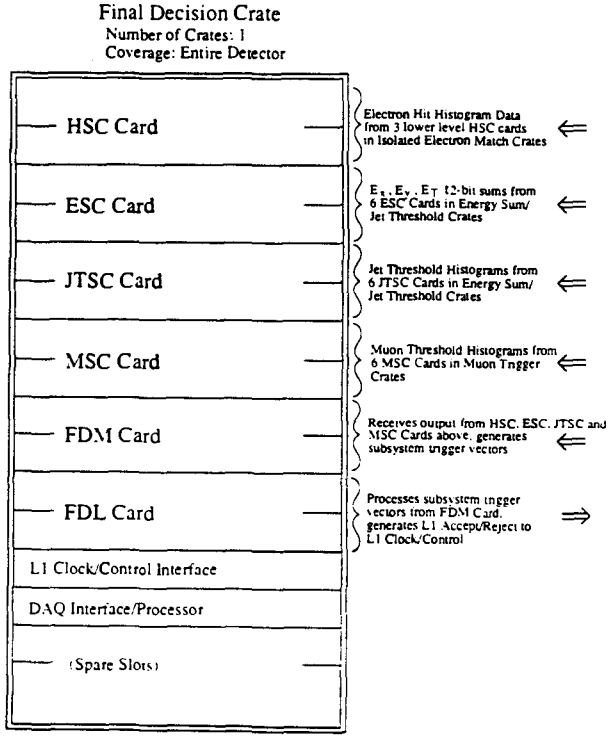


Figure 17

Final Decision Memory Lookup Card (Double-Width)
(FDM Card)

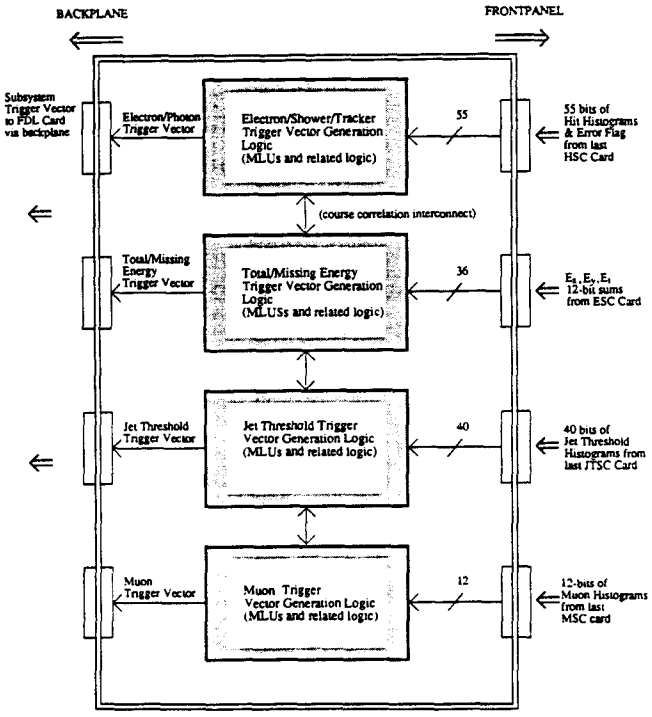


Figure 18

Final Decision Logic Card (Double-Width)
(FDL Card)

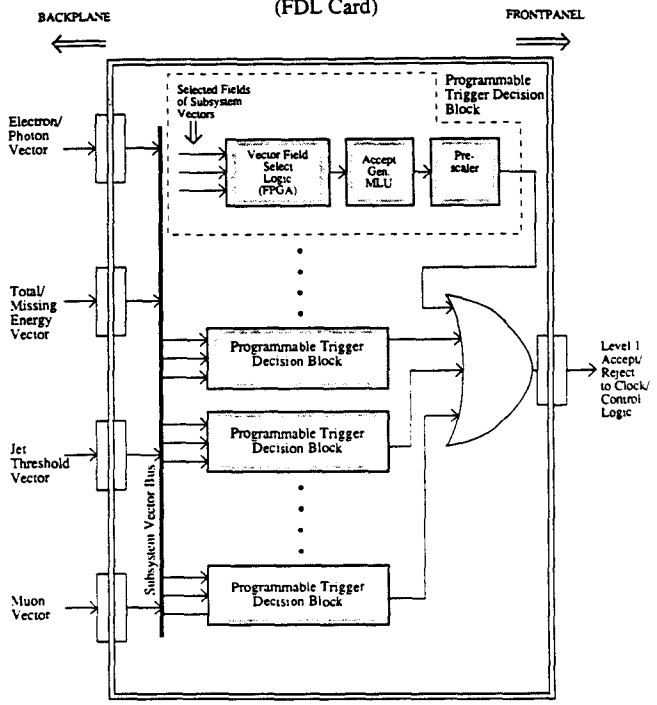


Figure 19

SDC Note SDC-91-00089
DRAFT
September 9, 1991

SDC Trigger Preliminary Conceptual Design

W. H. Smith, T. Gorski, J. Lackey
University of Wisconsin

1. Introduction

1.1. Statement of the Problem

Triggering is one of the most daunting challenges facing a modern high luminosity colliding detector such as the SDC. At the nominal SSC design luminosity of 10^{33}, an average of 1.6 events occur at the beam crossing frequency of 16 nsec. This input rate of 10^8 interactions every second must be reduced by a factor of at least 10^5 to 1 KHz, the maximum rate that can be analyzed by an online computer farm. The physical size of the SDC detector imposes constraints on signal propagation that combine with electronics technology to require more than 2 μsec for any primary decision to discard data from a particular beam crossing. The high speed of trigger decisions coupled with the volume of data produced by the unprecedented high channel counts of the SDC creates a series of technological and systems problems that surpass those previously faced by high energy physics detectors. The possibility of an increase in SSC luminosity to 10^{34}, with the accompanying order-of-magnitude increase in pileup and channel occupancy, adds to the difficulty in developing solutions. Physics at the SSC is not possible without a trigger system that operates in this environment. Inasmuch as the design of the SDC detector trigger system impacts the design of the detector, the SDC detector cannot be designed without addressing how it is triggered.

1.2. Purpose of this Document

The overall goal of this document is to present a preliminary conceptual design of the SDC trigger system as an "existence proof". This includes a summary of the trigger requirements, overall architecture and detailed design of the Level 1 and 2 trigger systems, technology of data transmission, design of clock and control systems, timing of trigger decisions, and cost selection information.

1.3. Trigger Philosophy

The key to triggering the SDC involves tracking, calorimetry and muon systems as well as the correlation of information from these systems. As described below, the Level 1 pipeline data storage time is less than 4 μsec. Since signal propagation delays are included in this pipeline time, the Level 1 trigger calculations must be done in many cases under 1 μsec. In addition, the Level 1 trigger system must be able to accept a new event every 16 nsec.

The general philosophy behind the SDC level 1 trigger system is to make local decisions about the presence of objects such as photons, electrons, muons, and jets, as well as global sums of E_T and missing E_T, and use the global compilation of this information to decide whether to keep (i.e. trigger on) a particular 16 nsec beam crossing. Each of the objects, such as electrons, muons and jets, are required to pass a series of p_t or E_t thresholds, which are used in making the Level 1 Trigger Decision.

The identification of trigger objects often depends on correlations between different subsystems participating in the trigger decision. The identification of an electron involves correlating information from the tracking and calorimeter systems. Identification of an electron in the calorimeter requires detecting isolated electromagnetic energy. The first step is to find a calorimeter trigger tower with energy in the electromagnetic compartment and little or no energy in its hadronic compartment (i.e. typically $E_{HAC} < 0.1 * E_{EMC}$). Next the towers adjacent to this tower are checked for having little or no energy in both electromagnetic and hadronic compartments. This establishes electromagnetic energy that is transversely and longitudinally isolated. However, since the size of the calorimeter trigger towers (nominally .1 x .1) is coarse, this isolation determination is improved with information from the shower max detector. Since a photon would also deposit the same pattern in the calorimeter, but would not deposit in the tracking system, the tracking system is used to distinguish between a photon and electron.

The identification of trigger objects in Level 1 must be completed within the constraints of the pipeline time and architecture. This means that correlations between some subsystems are more naturally made in the Level 2 trigger system. Since the muon trigger information is the last to arrive, processing of this information must be limited to avoid exceeding the trigger pipeline time. Therefore, while sufficient information to correlate the tracking and muon systems is available in Level 1, the correlation is done in Level 2 by reading out information stored in the Level 1 system. This is used to sharpen the muon p_t cut, which results in an important reduction in rate due to the steeply falling muon momentum spectrum.

Some of the information needed for trigger decisions is not available on the timescale of the Level 1 trigger decision. This information is then used in Level 2. An example is information from the silicon inner tracker, which provides track information in both the central and intermediate regions. The silicon tracker second level pattern recognition should be sensitive to photon conversions, which form one of the largest background to inclusive electron triggers. The second level trigger correlates information from the silicon and outer tracker to reduce the electron rate by rejecting conversions. It also uses the silicon (along with the outer tracker as mentioned above) in correlation with the muon system to sharpen the muon p_t cut.

1.4. Requirements

The trigger system must be able to trigger efficiently on these processes:

1. Electrons from inclusive W's
2. Muons from inclusive W's
3. Jets at high p_t
4. High p_t photons
5. Missing E_t
6. Low p_t Multileptons (for B physics)

The benchmark for processes 1 and 2 is 50% efficiency for W's which enter the fiducial

volume and would not be rejected by offline cuts. In other words, the trigger should get 50% of the W's it could in theory trigger on. The jet and photon p_t in processes 3 and 4 must be set such that there is a 1-2 decade overlap in jet and photon p_t data from other experiments (for example, CDF). The 50% efficiency is almost entirely due to the kinematic cut on lepton p_t. These requirements are set up to provide standards by which the trigger system performance can be assessed. They have been selected in the belief that this level of performance will provide high trigger efficiency for Higgs, t-quark, new Z', and other new phenomena. This is because the criteria listed here are established for moderate p_t single inclusive production, whereas the physics for which high efficiency is desired will feature pairs of leptons or jets or they will feature high p_t leptons or jets. These criteria are discussed in detail in Ref. 6.

1.5. Dataflow

The SDC dataflow diagram is shown in Fig. 1. The trigger and data acquisition systems have three levels. At the first level all information about the event is preserved. The first level decision is made on a subset of the total information available for the events. The deadtime at the first level is negligible. The first level decision is made at a fixed time after the interaction occurred and a first level decision is issued every 16 nsec. If the first level trigger generates an accept, the event data is moved or assigned to a buffer for the second level decision. The timing of the Level 1 decision and the time required for data storage before a Level 1 Accept is discussed below in the section on pipeline length.

The second level is defined as the decision, or series of decisions that exist between the first and third levels and is based on a subset of the total event data. A substantial part of the data may still be stored in analog form at this point. While the total processing time of the second level on an individual event may vary between 10 and 50 μsec, the second level issues a decision on the average every 10 μsec. The combined rejection factor of the first and second levels is 10^3.

After the second level trigger accept all information is digitized and read out. Full event data will be required for the third level decision. The event rate into the third level trigger is to be between 100 and 1000 Hz. Level 3 is implemented as a processing farm that is designed to achieve a rejection factor of 100, writing 10 to 100 events second to mass storage. The bandwidth of the data path to the third level farm is designed to accept up to 10K events second.

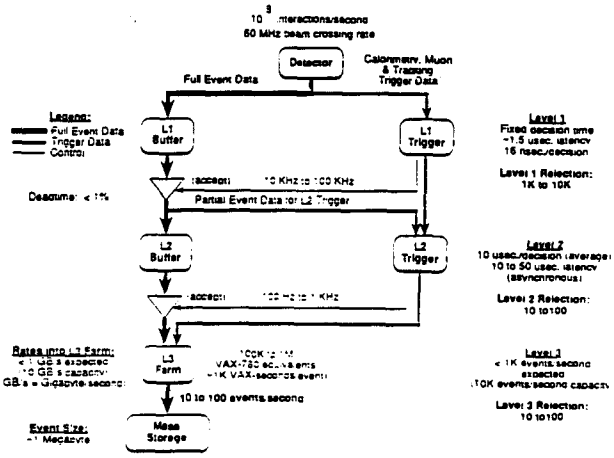


FIG. 1. Trigger and data acquisition dataflow for the SDC.

2. Level 1 Trigger

2.1. Introduction

The Level 1 Trigger finds electrons by searching for isolated electromagnetic energy in the calorimeter. It looks for .1 x .1 towers with energy in the electromagnetic compartment and little or no energy in the hadronic compartment surrounded by towers with little of no total energy. These isolated electron candidates are reported out on a .2 x .2 grid. In order to distinguish electrons from photons, correlation with the outer tracker is used. The shower max detector provides a local hit in .2 η x .00625 ϕ bins. The outer tracker provides tracks with p_t on a .00625 ϕ grid. The shower max is first correlated with the tracker to produce a coincidence hit with a p_t in .2 x .2 bins (after making the coincidence on a .00625 ϕ scale) for checking against the calorimeter in η, ϕ, and p_t. The photons are selected without the track match, but with a shower max match and a higher energy threshold. More details about these thresholds may be found in Refs. 2and 6.

The Level 1 Trigger finds jets by looking for .4 x .4 calorimeter towers over a series of thresholds. It finds muons by finding muon tracks over a series of muon p_t thresholds. The muon system is not correlated with the tracking system until Level 2. It must have a sharp enough p_t threshold to allow for a few kHz Level 1 rate while satisfying the trigger requirement above.

2.2. System Layout

Individual crates of the Level 1 Trigger logic are shown in Figure 2. The Front End Crates on the detector transmit their trigger information to the Level 1 Trigger off the detector on 1 Gbit sec optical fibers. Every 16 nsec, each fiber carries 16 bits of data to the trigger system. The same type of optical fibers carry the clock and control communication from the trigger clock and control systems to the front end electronics systems. The Level 1 Trigger Crates transmit data between themselves on short runs of twist-and-flat pair cable. Each Level 1 Trigger Crate contains a Level 2 Trigger Interface card that gathers Level 1 information buffered in the Level 1 Trigger Input Cards and transmits this information to the Level 2 after a Level 1 Accept. Each Level 1 Trigger Crate also contains a processor board, of the standard variety provided by the DAQ. Its function is to download trigger tables, monitor trigger data and provide a data path to the event builder for trigger information to be supplied with the event record to be written to tape. Each Level 1 Trigger Crate also contains a Level 1 Clock Control board that provides the 16 nsec clock and the other control functions described in the section about the interface to front end systems.

The calorimeter front end electronics crates transmit hadronic and electromagnetic compartment energies for each .1 x .1 trigger tower. The shower max detector transmits hits over threshold for 6.25 mrad ϕ by .2 η bins. The tracking detector transmits p_t bits for tracks in 6.25 mrad ϕ bins. The muon system transmits p_t bits for tracks in .2 ϕ by .25 η bins. The calorimeter isolation summation crates find isolated electrons by searching for towers with a small ratio of hadronic to electromagnetic compartment energy surrounded by quiet towers. They also sum up energy in .4 x .4 regions. These crates test the energy in the .4 x .4 towers against a series of 8 thresholds, as well as summing up the total E_t, E_x, and E_y energy found in the sum of .4 x .4 towers. The E_t, E_x, and E_y sums, as well as the number of .4 x .4 towers over each threshold are sent to the calorimeter energy sum jet threshold crates. The isolated electron information is transmitted to the calorimeter

isolated electron matching crates. These crates combine information on the boundaries of regions covered by the calorimeter isolation summation crates to find isolated electrons on region edges. They also check the electron energy against 6 thresholds.

The shower max and tracking information is sent to the track/shower max match crates. These crates match the tracks and shower max hits on a 6.25 mrad ϕ scale. The η coordinate is found from the shower max hit η value with .2 bins. The p_t value is taken from the track p_t bits. The output is a series of shower max hits, some of which are matched with tracks carrying a p_t value, and all of which are on a 6.25 mrad ϕ and .2 η scale. These hits are sent the isolated electron/photon match crates. These crates match the shower max hits with the calorimeter isolated electrons. The shower match hits which have tracks attached also check the track p_t against the calorimeter tower energy threshold, as well as matching in η and ϕ. The result is a series of calorimeter-shower max matched isolated electromagnetic hits without track matches, which are considered "photons", and a second series of calorimeter-shower max hits with track matches, which are considered "electrons". Failures to find a shower max hit to match a calorimeter isolated electrons are also reported.

The muon system transmits the muon linked segments over several p_t thresholds to the Muon Level 1 Crates. These crates count the total number of muons over p_t and forward this information to the Level 1 decision crate. The calorimeter energy sum jet threshold crates send the number of .4 x .4 towers over various thresholds as well as the total E_t, E_x, and E_y (the latter two are used to compute missing energy). The Level 1 Decision Crate then applies cuts on the energy sums and towers over threshold to form the trigger. The isolated electron/photon crates forward the number of isolated "electrons" and "photons" over various thresholds as described above. The Level 1 Decision crate then counts the total number over the thresholds to form the trigger. The Muon Level 1 crates forward the number of muons over several p_t thresholds to the Level 1 Decision crate which cuts on these to form muon triggers. The final trigger decision is converted to a Level 1 accept by the Global Clock Control crate, which transmits the decision for fanout to the local clock control crates and to the DAQ system.

2.3. Level 1 Trigger Crates

The functional descriptions of the crates in the level 1 system are presented below. More detailed descriptions of the individual boards in each of the crates, as well as the crates themselves are contained in Ref. 3.

Calorimeter Isolation Summation

These crates find .1 x .1 calorimeter towers where $E_{em} \gg E_{had}$ surrounded by quiet towers. These isolated electron candidates are reported out on a grid of .2 x .2 towers. These crates also sum up the total E_t in .4 x .4 towers, as well as the total E_t, E_x and E_y in the crate. The total .4 x .4 tower sums are tested against 8 thresholds and the number passing each is calculated.

There are 24 of these crates: 16 for the barrel and 8 for the intermediate regions of the detector. Each barrel crate covers 1.6 η by 0.9 ϕ. It contains 8 Memory Lookup Boards (MLU) that each receive the hadronic and electromagnetic compartment energies from the .1 x .1 calorimeter tower sums. Details on the techniques of electronics that can integrate a PMT signal over 16 nsec with baseline restoration are found in Ref. 1. Each MLU board receives 16 optical fibers that contain 8 bits each of hadronic and electromagnetic energy in a .1 x .1 tower from the front end calorimeter crates. The MLU boards convert

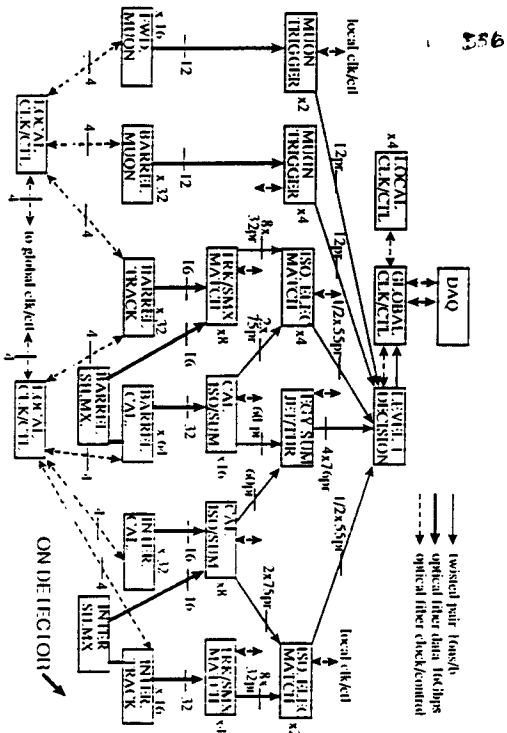


FIG. 2. Layout of Level 1 Trigger Crates.

the input FADC tower sum values into E_t on a 12 bit linear scale, compute E_t sums in the .4 x .4 region of 16 trigger towers that each services (again on a 12 bit linear scale), and calculate an Encoded Tower Type (ETT) for each tower. This type is based on the amount of energy deposited in the hadronic and electromagnetic compartments. The ETT is 0 for a tower below any electromagnetic threshold. ETT 1 through 6 indicate an electron candidate exceeding one of 6 thresholds, and 7 indicates a hadron.

Each crate also contains 2 Pattern Recognition ASIC boards (PRA), which receive the ETT bits from 4 MLU's, corresponding to a region .8 x .8. These boards perform the search for isolated electron candidates in .2 x .2 regions that are contained or on the edge (partial) of the .8 x .8 region. The result is a series of isolated electron flags, one for each .2 x .2 region that are composed of 3 bits each with 0 meaning "quiet", 1-6 meaning an isolated electron above thresholds 1-6, and 7 meaning neither quiet nor an isolated electron. There are 25 regions x 3 bits of flag = 75 bits of isolated electron information from each PRA that are transmitted to the Isolated Electron Match Crate. Of these 25 regions, 9 are contained and 16 are partial regions that need further combination with other partial regions from other Calorimeter Isolation/Summation crates to find isolated electrons. The design details of the MLU and PRA cards, along with simulation results on the performance of this isolated electron pattern logic are found in Ref. 2.

Each crate also contains a double width Energy Card. This card covers a 1.6 η by 0.8 ϕ region and receives the energy sums in .4 x .4 regions from 8 MLU's on a 12 bit scale. In addition to computing the total E_t in the .8 x .8 region, it also converts the .4 x .4 E_t sums into E_x and E_y sums and adds these up to produce the total E_x and E_y in the .8 x .8 region as well. The Energy Card also tests the E_t in each .4 x .4 tower against 8 thresholds and calculates the number of .4 x .4 towers above each threshold. Three bits of number above threshold are shipped for each of the 8 thresholds (24 bits total), along with 12 bits of E_t, E_x, and E_y (36 bits total) to the Energy Sum Jet/Threshold Crate.

Each crate also includes a Level 2 Interface Card (L2IC). After a Level 1 Accept each of the 8 MLU cards sends its stored tower electromagnetic and hadronic 8-bit FADC values over an individual differential pair on the backplane at 1 bit/16 nsec to the L2IC for subsequent transmission to the Level 2 processor. The simultaneous transmission of the 16 towers of information from each MLU takes 2.56 μsec.

Each crate also contains a Level 1 Clock Control Interface Card and a DAQ Interface Processor Board.

Track Shower Max Match

These crates correlate the outer tracker hits with the shower max hits on a .00625 ϕ scale. The shower max is used to assign the track an η coordinate on a .2 scale. The p_t from the tracker is used to place the track on a 3-bit p_t scale used to match against the calorimeter E_t.

There are 12 of these crates: 8 for the barrel and 4 for the intermediate regions of the detector. Each barrel crate covers 1.6 η by 1.6 ϕ. It contains 8 double-width Track Shower Max Hit Cards (TSMHC), each handling 1.6 η by 0.2 ϕ. The TSMHC cards each receive 16 Shower Max fiber optic cables that each cover 0.2 η by 0.1 ϕ with 16 ϕ bits at $\Delta\phi$ = 6.25 mrad apiece. They also receive 8 Tracker fiber optic cables that each cover 1.6 η by 0.025 ϕ with 4 ϕ bins of $\Delta\phi$ = 6.25 mrad with 4 bits of p_t apiece for the case of the fiber tracker and fewer bits of p_t for the case of the straw tube tracker[8]. The TSMHC matches the Shower Max and Track hits on a scale of $\Delta\phi$ = 6.25 mrad. These hits are assigned an η value from the Shower Max and a p_t value from the track. Since the Calorimeter

electrons are on a 3-bit scale, the p_t value is calculated on the same 3-bit scale. Since the calorimeter electrons are assigned to .2 x .2 regions, the output is placed in .2 x .2 bins where each bin is characterized by a four bit code. The first 3 bits are the p_t value. The fourth bit indicates whether there was a Shower Max hit. If this is zero, there has been no shower max match and the track is placed in 8 .2 x .2 bins covering the η range from 0 to 1.6, using the highest p_t track in the $\delta\phi$ = .2 region. If this is one, the 3-bit track p_t code is placed in the .2 η bin given by the shower max. The TSMHC output consists of 8 four-bit codes (32 bits) giving the track p_t and shower max hit information for a .8 η by .4 ϕ region in 8 .2 x .2 sections. This information is transmitted to the Isolated ELectron Matching Crates on 16 16-pair cables, two from each TSMHC, that each cover a .8 η by .2 ϕ region and all together cover the 1.6 η by 1.6 ϕ region.

Each crate also includes a Level 2 Interface Card (L2IC). After a Level 1 Accept each of the 8 TSMHC sends its stored shower max hits (8 η bins of 32 ϕ bits apiece = 256 bits) and track information (32 ϕ bins with 4 bits p_t = 128 bits) over an individual differential pair on the backplane at 1 bit/16 nsec to the L2IC for subsequent transmission to the Level 2 processor. The transmission of the information takes 4.22 μsec.

Each crate also contains a Level 1 Clock Control Interface Card and a DAQ Interface Processor Board.

Isolated Electron Match

These crates match up the shower max - outer tracker hits and the calorimeter isolated electron candidates on a .2 x .2 grid. The results are counted up in categories of track (including shower max) and calorimeter agreement on p_t, disagreement on p_t, and shower max match only with the calorimeter "photons". For each category, the total number of matches above each of 6 E_t thresholds is accumulated. Failures to match shower max and calorimeter are also counted.

There are 6 of these crates: 4 for the barrel and 2 for the intermediate regions of the detector. Each barrel crate covers 1.6 η by 3.2 ϕ. It contains 8 Region Match Cards (RMC), each handling 0.8 η by 0.8 ϕ. The RMC receive 75 bits from 4 different PRA cards with 25 regions giving 3 bits of isolated electron flags apiece. The RMC matches up the partial regions to complete the isolated electron pattern search. The RMC also receives 4 cables from different TSHMC that bring 4 .8 η by .2 ϕ regions with 4 .2 x .2 bins with 3 bits of track p_t and 1 bit of shower max match information to cover the .8 x .8 RMC region. The PRA and TSHMC data for each .2 x .2 region are compared for matching an isolated electron in the calorimeter with a shower max hit and a track passing the appropriate P_t threshold. The output at the front panel from these RMC's is a 3-bit count of the number of coincident calorimeter - track - shower max matches above each of 6 thresholds where there was agreement between calorimeter and track energy, plus the number of coincident matches without p_t agreement are placed above the threshold of the calorimeter value, plus the number of calorimeter - shower max matches without a track match, and finally a single bit that indicates a failure to match calorimeter and shower max information. The total information from each RMC is 55 bits and is transmitted over individual lines to the Hit Summary Card.

Each crate has 3 double-width Hit Summary Cards (HSC). The HSC is the building block for hit sums. At the lowest level, the HSC's receive data from 4 RMC's. At the higher levels additional HSC's receive and combine data from 4 HSC's at lower levels. Each half of the first two HSC's in the crate receive the match data described above from 2 RMC's, 110 bits per half HSC, covering a region 1.6 η by 0.8 ϕ, so that the two HSC's

cover a 1.6 η by 3.2 ϕ region. The HSC's sum up their input data and output this data to half of a third HSC, which is resident in half of the Isolated Electron Match Crates. The other half of the HSC receives input data from the two HSC's in another Isolated Electron Match Crate. The resulting data from the third HSC then covers a 3.2 η by 3.2 ϕ region. This data is then sent to a third HSC that resides in the Electron Match Crate that sent the data from its first two HSC's to another Electron Match Crate. The first half of this HSC then sums up the HSC data from it and the pair of Electron Match Crates to cover the 3.2 η by 6.4 ϕ barrel region. The second half performs a similar sum to cover the intermediate region. The resulting data is a 3-bit count of the number of coincident calorimeter - track - shower max matches above each of 6 thresholds where there was agreement between calorimeter and track energy, plus the number of coincident matches without p_t agreement placed above the threshold of the calorimeter value, plus the number of calorimeter - shower max matches without a track match, and finally a bit that indicates a failure to match calorimeter and shower max information. The total information from the third HSC is 55 bits and is transmitted over twisted pair cable to the Electron Match Card in the Final Decision Crate.

Each crate also contains a Level 1 Clock Control Interface Card and a DAQ Interface Processor Board.

Energy Sum/Jet Threshold

This crate continues the global E_t, E_x, and E_y sums as well as adding up the number of .4 x .4 calorimeter towers above a series of 8 thresholds.

There is one Energy Sum/Jet Threshold crate, which covers both the barrel and the intermediate regions of the detector. It contains 4 double-width Energy Sum Cards (ESC), each handling 1.6 η by 6.4 ϕ, which receive the 12-bit E_t, E_x, and E_y sums from 8 Energy Cards (each covering a region 1.6 η x .8ϕ) in 4 Calorimeter Isolation/Summation Crates. The output consists of 12-bit E_t, E_x, and E_y sums, covering 1.6 η by 6.4 ϕ, which are transmitted over a 36-pair cable to the Total Energy Summation Module in the Final Decision Crate.

This Crate also contains 4 double-width Jet Threshold Sum Cards (JTSC), each handling 1.6 η by 6.4 ϕ, which receive the 3-bit numbers of .4 x .4 towers over 8 thresholds from 8 Energy Cards (each covering a region 1.6 η x .8ϕ) in 4 Calorimeter Isolation/Summation Crates, and sums these numbers into a series of 5-bit numbers of .4 x .4 towers over 8 thresholds. These 40 bits, covering, covering 1.6 η by 6.4 ϕ, are transmitted to the Total Jet Threshold Card in the Final Decision Crate.

Each crate also contains a Level 1 Clock Control Interface Card and a DAQ Interface Processor Board.

Muon Trigger Crates

These crates count up the number of muon tracks passing each of 4 programmable p_t thresholds. They also store 3 bits of p_t and the track location with a resolution of $\Delta\phi$ = .01, $\Delta\eta$ = .05 for use by the second level trigger.

There are 6 Muon Trigger Crates. There are 4 barrel crates that cover all of ϕ and cover η < 2.5 in four equal sections. In addition, there are two forward muon trigger crates, one for each end. Each Munn Trigger Crate services 8 Muon Regional Front End Crates. There are 32 Muon Regional Front End Crates in the barrel (η < 2.5) and 8 for each forward endcap. Each regional front end crate services an octant in ϕ over its η range. In the barrel region, this represents 1/4 of an octant (divided along η). The muon

trigger relies on a scintillator signal in coincidence confirmed by a projective chamber wire pair. The trigger units are derived from the scintillator segmentation. As detailed in Ref. 4, there are two options for the scintillator layers. In the first there are two layers of scintillators that are arranged in slats sectioned to provide 32 divisions in ϕ and 156 divisions in θ. The θ divisions are composed of 96 units in the barrel region and 30 units in each of the end regions. In the second, there is one layer of scintillators, where the θ segmentation is no longer restricted by a momentum selection constraint and the differential timing of the two phototubes on each scintillator is used to enhance the ϕ binning from 32 to 128. Each barrel regional muon crate covers a region $1.2\eta \times 0.8\phi$ with 24 η bins and 4 ϕ bins (16 ϕ bins in option 2).

Each regional muon front end crate contains 14 cards, of which two are used for exchange of neighbor scintillator information, leaving 12 cards. Since isolated electrons are found in the calorimeter on a .2 x .2 grid, the muon η bins are combined into .2 η bins on each card. Therefore, each card covers a single η bins of .2 by a total ϕ range of .4, so that the 12 cards cover the $1.2\eta \times 0.8\phi$ area. This means that each card has either 2 ϕ bins (option 1) or 8 ϕ bins (option 2). In order to be compatible with either, 3 bits are needed for the value of ϕ for a track found by each card. Each track found by a card has 3 bits of p_t associated with it, corresponding to the full resolution of level 1 muon trigger system. Each card has a single 1 Gb/s optical fiber that carries the trigger information directly to a Muon Logic Card in the Muon Trigger Crates. Each card sends two tracks. Since the optical fiber bandwidth allows 8 bits per track, and the format described above uses 6 bits (3 bits of ϕ and 3 bits of p_t), an additional two bits per track are used to enhance the ϕ resolution to 5 bits. This resolution is available since there are 15,360 barrel ϕ wires arranged in 4 η sections and 4 depth layers, giving 960 ϕ bins, distributed over cards that cover half of an octant in ϕ, or 60 bins.

Each of the 6 Muon Trigger Crates contains 5 Muon Logic Cards (MLC's), each of which receives 12 optical fibers, one from each card in a single muon regional front end crate. Each optical fiber carries 3 bits of p_t and 5 bits of ϕ for the two highest p_t tracks in a $.2\ \eta \times .4\ \phi$ region. This gives each MLC a coverage of $1.2\ \eta \times 0.8\ \phi$, corresponding to one full muon regional crate. The 5 MLC's combine to give the Muon Trigger Crate coverage of a $\Delta\eta = 1.2$ slice for all ϕ.

The output of each of the MLC's is 4 2-bit numbers that indicates the number of muon tracks (none, 1, 2, 3 or more) above each of 4 programmable thresholds. Each Crate also contains a Muon Summing Module that accepts the 5 bits of tracks over thresholds from the MLC's and sums them to produce a series of 4 3-bit numbers that indicate the number of muon tracks above each of 4 programmable thresholds. These are then transmitted by a 12-pair cable to the Muon Decision Module in the Final Decision Crate.

Each crate also includes a Level 2 Interface Card (L2IC). After a Level 1 Accept each of the MLC's sends its stored 24 tracks with 3 bits p_t and 5 ϕ bits apiece, (total of 24 x 8 = 192 bits) over an individual differential pair on the backplane at 1 bit/16 nsec to the L2IC for subsequent transmission to the Level 2 processor. This transmission takes 3.1 μsec.

Each crate also contains a Level 1 Clock Control Interface Card and a DAQ Interface Processor Board.

Final Decision Crate

The Final Decision Crate sums up and makes cuts on calorimeter total and missing

E_t (the latter from the individual E_x and E_y sums). It sums up the total number of calorimeter .4 x .4 regions over 8 thresholds and makes cuts on this. Is sums up the total number of isolated electron (and photon) candidates within the categories and p_t thresholds described above and makes cuts on these. It also sums up the total number of muons over the p_t thresholds and makes cuts on these. The resulting trigger decision is then forwarded to the clock and control logic.

There is one Final Decision Crate. It contains a final HSC, which accepts the 55 bits of information from two barrel and two intermediate crate HSC's. The information from this final HSC includes a 4-bit count of the number of coincident calorimeter - track - shower max matches above each of 6 thresholds where there was agreement between calorimeter and track energy, plus the number of coincident matches without p_t agreement placed above the threshold of the calorimeter value, plus the number of calorimeter - shower max matches without a track match, and finally a bit that indicates a failure to match calorimeter and shower max information. This information is sent to the Final Decision Memory Lookup Card (FDM) describes below.

The crate also contains one Energy Sum Card (ESC). This sums the 4 input 12-bit E_t, E_x, and E_y sums, which are transmitted over 36-pair cables from one of the Energy Sum Jet Threshold Crate, the output of the ESC is also sent to the FDM.

The crate also contains one Total Jet Threshold Card which read in 4 40-pair cables carrying a series of 5-bit numbers of .4 x .4 towers over 8 thresholds for either an intermediate region or 1/2 of the barrel from the Energy Sum Jet Threshold Crates.

The crate also contains a Final Muon Card that reads in a 3-bit number of muons above a series of 4 thresholds from the 6 Muon Trigger Crates and forms a 3-bit trigger vector that is sent to the Final Decision Module.

The crate contains one Final Decision Module (FDM) card. This card has 4 separate memory lookup (MLU) architectures that on it, one each for total and missing transverse energy triggers, jet triggers, isolated electron triggers and muon triggers. Each of these MLU's produces a 3 bit code, yielding 4 3-bit codes that are sent to the Final Decision Logic Card (FDL). The energy sum MLU uses memory lookup to compute the total E_t, E_x, and E_y, uses the latter two to compute missing E_t, and then compares the total calorimeter global E_t and missing E_t sums against programmable thresholds to produce a 3-bit trigger vector that is sent to the Final Decision Logic. The jet trigger MLU compares the series of 5-bit numbers of .4 x .4 towers over 8 thresholds with a series of programmable trigger requirements to produce its 3-bit output trigger vector. The results from the electron match HSC are compared against a series of thresholds, such as one isolated electron over 20 GeV or two over 10 GeV to determine the isolated electron 3 bit output vector and a similar process is performed by the muon trigger MLU.

The Final Decision Logic (FDL) card receives this series of 4 3-bit output vectors from the Electron, Muon, Jet and Energy MLU's. The FDL contains another series of MLU's that make the final level 1 trigger decision based on programmable requirements on combinations and individual requirements on the 4 3-bit vectors. It gets its data from the FDM over the backplane. It also contains logic to prescale trigger according to downloaded factors, as well as logic to resolve triggers found in different crossings. The FDL card determines the Level 1 Decision based on physics information in the detector. If it is unable to resolve conflicting crossing information from 2 subsystems, it can issue a trigger that covers more than one crossing, along with an "ambiguity" bit to indicate the number of crossings involved. The FDL card decision is transmitted over a cable to

the the Global Clock Control Crate which turns this into a Level 1 Accept if the detector systems are able to read out the event (i.e. the DAQ is live and there are no extant errors that prevent functioning of the system).

This crate also contains a Level 1 Clock Control Interface Card and a DAQ Interface Processor Board.

Global Clock Control

The functionality of the clock and control crates is described in detail in the section on trigger interfaces, the section on communication between front end and trigger systems and in Ref. 5.

There is one Global Clock Control Crate. It contains a Machine Clock Interface Board to communicate with the interface with the accelerator RF clock. It has a Beam Pickup Interface to communicate with the beam pickup electronics. It contains a Deadtime Monitor Board that tracks the disposition of each crossing, i.e. whether accepted, rejected, or lost due to downtime of trigger and/or DAQ. There is a Final Decision Interface that connects to the FDL card in the Final Decision Crate to provide the Level 1 Accept if the DAQ is able to read out the event and there are no outstanding error conditions that prevent accepting the event (i.e. clock phase confusion, etc.). There is a Global Clock Master that provides the phase lock of the 16 nsec clock and distributes the clock to Clock Control Interface modules. There is a Global Control Master that distributes the Control signals to the Clock Control Interface Modules. Finally, there are 2 Clock Control Interface Modules that each communicate with 2 Local Clock Control Crates. The detailed function of these modules is covered in the section on communication between front end and trigger systems. This crate also contains a DAQ Interface Processor Board.

Local Clock Control

There are 4 Local Clock Control Crates. Each contains 16 Local Clock Control Boards that are connected with 4 optical fibers apiece to 4 Front End or Trigger Crates. The 4 fibers carry the Level 1 System Control, Level 1 Clock, Level 1 Control, and Level 1 Number described below in the section on the Interface to Front End Subsystems. The Crate also contains a Global Clock Control Interface Board that communicates with the Global Clock Control Crate, as well as a DAQ Interface Processor Board.

Physical Layout & Resource Requirements

The Level 1 Trigger System takes up 84 Crates. These will use 18 full-height racks with a power consumption of about 100 KW in the Counting House. There are approximately 5,000 optical fibers required to carry information from the detector to the Level 1 Trigger System.

2.4. Fiber Optic Transmission

A study of the SDC Trigger requirements by M. Thompson, U. Wisconsin, has some preliminary suggestions[11] for transmission of trigger information at 1 Gb/s on optical fibers.

1. Use signal optoelectronics with a frequency, above which a 3 dB loss of gain occurs, of 1.7 GHz to preserve the waveform of the worst case 1.125 Gbaud signal of (10101010).
2. Use multimode fiber with a core diameter of about 60 microns to allow the use of the lowest cost optoelectronics.

3. Use words of 18 bits to carry both the 16 bits of information and two bits (a,b) with b=1-a. The (a,b) bits have the purposes of delineating words and allowing slight drifts and threshold shifts to be measured. The (a) bits are from a long fixed pseudo-random sequence which has a mean time for appearing in random data of 3.68×10^{60} years.
4. Allow the information in the words of each channel to be constant, all zeroes, all ones or change with no "forbidden values".
5. Use three adjustments for each signal:
   a) a Threshold Adjustment for each receiver,
   b) a Fine delay Adjustment with steps of 125 ps and
   c) a Coarse delay Adjustment with a range of ± 14.2 ns.
6. We expect the high signal level to vary from signal to signal and to vary with time due to the use of low cost lasers and detectors and the use of imperfect optical connectors. The high signal levels and low signal levels are recorded by 2 diodes and 2 capacitors for each of the 5000 signals. The 2 voltages will be used to determine the threshold for each signal.
7. The Fine delay adjustment uses a tapped delay line with a 16:1 multiplexor and 3 fast decision circuits latching the signal just before the clock, at the clock and just after the clock. Signal transitions before and after the clock cause the charge on 2 corresponding capacitors to be incremented so that the difference of voltages on the 2 capacitors indicates the relative phase of the clock and signal transitions.
8. The Coarse delay Adjustment uses a 32 long shift register with a 32:1 multiplexor and uses 3 capacitors to collect the agreements of the signal's pattern of (a) bits with the expected pattern. During power-up or after timing errors are found, the 5-bit selection is changed until agreement of the signal and expected (a) bit patterns is found.
9. Use a multiplexing slow 8 bit or 10 bit ADC system with 128 inputs on each 9U board to read 8 analog levels produced by each of the 16 incoming Trigger Information signals. Similarly, use a multiplexing DAC to adjust the thresholds of the receiving circuits for each of the 16 signals on each 9U board.
10. Use an external computer with a 16 bit address, 16 bit data bus in sequential and slowly monitor the status of the analog voltages produced by all 5000 signals. The computer makes changes when necessary to the Threshold, Fine and Coarse adjustments. This can both permit secure word and bit alignment during power up and recovery after major disturbances.

2.5. Level 1 Pipeline Length

The proposal for the level 1 pipeline is that its length will not be less than 3.0 μsec and not more than 4.0 μsec. Representatives from Silicon, Central Tracking, Calorimeter and Muon front end electronics systems were involved in this decision. The conclusion from these systems was that while all could manage 4.0 μsec, there were significant difficulties for some to go beyond 4.0 μsec. In addition, there would be significant, but not insurmountable, difficulties for the silicon system to reach a 4.0 μsec pipeline length for some architectures. The representatives of the Tracking, Calorimeter, Muon and Global trigger systems contributed to the calculations shown below that demonstrate the necessity for a range between 3.0 and 4.0 μsec. The actual calculation results in a range from 3.1 to 3.9 μsec. The pipeline length is determined by the muon drift time. The overall

uncertainty in cable paths and electronics locations expands the range by 0.1 μsec on each side. However, it is important to add that the calculation is based on locating the central trigger decision and distribution in the counting house on the surface. If the trigger is located in the gallery, then the reduction in cable length of 40.7 m each way translates into a 0.4 μsec or 26 crossing savings.

Calculation of Level 1 Pipeline Length

The following table sums up the time for the trigger data from an interaction to reach the trigger logic and proceed through this logic to the final decision for the Level 1 Accept. The particular system chosen is the muon system, since it takes the longest and varies between 50 and 100 crossings depending on whether the muon drift time is 800 to 1600 nsec, respectively.

Muon Inputs to Global	
Propagation to Chamber	2
Drift in Chamber	50–100
Propagation along Wire	2
Segment Finder	2
Segment Linker	6
Transmission to LEVEL 1	50
LEVEL 1 Calculation	20
Total	132–182

The following table sums up the delay incurred in transmitting the Level 1 Accept signal from the Global Level 1 Logic back to the front end electronics storage pipelines.

Cause of Delay	Time (crossings)
LEVEL 1→pipeline controller (nearby)	1
Pipeline setup & synchronization	2
Pipeline Controller→Pipeline Fanout (far)	50
Local Fanout to Pipeline	10
Phase between pipeline and sample	±0.5
Pipeline overhead in sample select	1
Particle interaction→pipeline front	−5
Presamples	6
Signal shaping for sample of rise	−1
Total	64

The total pipeline length is the sum of the propagation of the trigger signals through the trigger logic to the final Level 1 Accept, which is 132 to 182 crossings for the muon system, and the propagation of the Level 1 Accept back to the front end pipelines, which is calculated to be 64 crossings. The resulting total crossings ranges between 196 and 246, or between 3.1 and 3.9 μsec. This is the range of possible Level 1 pipeline lengths, where the lower figure corresponds to a muon drift of 800 nsec and the larger a drift of 1.6 μsec.

2.6. Trigger Interfaces

Global Level 1 Processor — overall operation of the Level 1 subsystems. The Global Level 1 Processor (GL1P) receives a subset of the data from subsystems participating in the level 1 trigger. The data for each 16 nsec bunch crossing is sent by each subsystem every 16 nsec. The GL1P not only makes the final level 1 decision, but it also controls the start of any level 1 readout, disables this readout, and distributes scheduling signals for tests and calibrations. Therefore, all subsystems, even those not involved in the level 1 decision, must communicate with the GL1P.

All level 1 trigger and DAQ pipelines in the subsystems and the GL1P must be driven with a common clock synchronized to the SSC crossing frequency. This clock is distributed centrally through the GL1P. The processing of the GL1P decision is driven by this cycle.

The GL1P receives the trigger data and aligns this data in time for all the subsystems since the arrival time for the data of a particular crossing is different among the different subsystems. The particular bunch crossing number of a subsystem's data is indicated by a local bunch counter, named Bunch Phase. This Bunch Phase must accompany the trigger data from each subsystem. The subsystem also counts Level 1 triggers. This number, Level 1 ID, must also accompany the trigger data.

Level 1 Accept, Reject

After the GL1P processing, a decision is made to issue a Level 1 Accept or Reject

for each bunch crossing. This signal appears at the output of the GL1P. The Level 1 Accept/ Reject arrives at the subsystem after additional delay due to the propagation of the Level 1 Accept, Reject from the GL1P. The Level 1 Trigger Accept/Reject is a Level that strobed by the clock. This signal is accompanied by other signals such as the Bunch Phase, the Level 1 ID, and several bits of "readout type". The Level 1 ID counts Level 1 Accepts. The bits of "readout type" allow information to be sent to subsystems that may react differently to different trigger types.

Ambiguous and Overlapping Triggers

If a subsystem cannot identify data with a particular crossing, it sends the data applicable to a number of crossings with each crossing with a bit to indicate that the crossing is not identified. The GL1B has the ability to scan over several crossings, examining the data from all the subsystems, to match up data stretching over several crossings with data identifying a single crossing. This is used to identify a unique crossing for every L1 Accept. Subsystems determine the number of bunch crossings to store upon each Level 1 Accept. There is the possibility that we cannot uniquely identify a crossing from the trigger data or that we may have two Level 1 Accepts within the measurement time span of some subsystems. Following Darenbosch, Botlo, Fry and Milner (SSCL-348), we define the Level 1 Accept as a level that is high for all clock cycles to be measured. The Level 1 ID is incremented on the rising edge of the Level 1 Accept. For each overlapping trigger, the Level 1 Accept goes low for half a cycle, and when it goes high again, the Level 1 ID is incremented. To attempt to limit overlaps as much as possible, we also follow their rules for minimal spacing for Level 1 Accepts:

1. No more than 1 Level 1 Accept per 80 nsec.
2. No more than 2 Level 1 Accepts per 260 nsec.
3. No more than 3 Level 1 Accepts per 1 μsec.
4. No more than 4 Level 1 Accepts per 4 μsec.

They determine that the total cost for these rules is less than 1% at a Level 1 rate of 100 KHz and 11.5% at 500 KHz.

Trigger Control

Subsystems send trigger control information to the GL1P. This includes a busy bit to indicate that the subsystem trigger did not process the event, busy bit to indicate that the subsystem DAQ cannot read out the event, a fatal error bit to indicate that the subsystem trigger has had a fatal error and a trigger data error to indicate that the subsystem trigger data may be corrupt. An example of a trigger busy would be a reset process that had not been completed. We must allow for subsystems that cannot complete a Level 1 Reset sequence in a single 16 nsec crossing. The trigger busy bit prevents a Level 1 Accept being issued to a subsystem that must use several crossings for a reset. An example of a fatal error would be a disagreement between the Level 1 trigger number counted by the subsystem and the number sent by the GL1P. An example of a trigger data error would be either a parity check failure or another type of internal data checking failure. The control information also includes the subsystem's crossing number associated with this data. All subsystems active during a run must send this control information to the GL1P, whether or not they send data used in the Level 1 decision.

Tests

The operation and scheduling of tests during a run are controlled by the GL1P. A schedule of all tests to be run is downloaded to the GL1P before the beginning of a run by

the Central DAQ Control (CDAQC). The CDAQC also can modify this schedule during a run in response to changing detector status. The GL1P sends to all subsystems a Test Enable signal, with the type of test to be run indicated in the Test Trigger Type bits, a fixed number of crossings before the crossing when the test is to be done. This enables subsystems to prepare for the test. The tests are arranged in such a way as to allow many subsystems to do tests simultaneously. The subsystems arrange set up their tests so that the test data will be contained in the exact crossing indicated by the GL1P Test Enable Signal. The GL1P inhibits normal triggers a fixed time before the test trigger crossing so that there will be no interference. The GL1P then sends out a Level 1 Accept for the appropriate crossing to read in the test data. This Accept is accompanied by a bit in the Readout Type set to indicate that it is a test trigger.

Schematic Layout

The schematic layout of the GL1P as it interacts with a subsystem trigger is shown in Figure 3. The Clock Distribution module generates the 16 nsec clock and associated data such as the Bunch Crossing 0 and Empty Bunch Indicators from SSC accelerator clock information. It then distributes this information to the subsystems and the rest of the GL1P. This module also monitors the relative phase of the accelerator clock and the beam pickup signal, which should remain constant. The Control Interface provides all of the control signals to the subsystems and reads all of the control signals from the subsystems. All data except for the trigger data from a subsystem is brought through the Control Interface. The test scheduling and Level 1 Accept are sent to the subsystem through this module. It also monitors the subsystem deadtime and status. The trigger data from the subsystems is processed in the Trigger Logic modules. Here the data from the various regions of each subsystem are collected, counted, and placed in an appropriate format for correlation with other subsystem trigger data. This data is shipped to the Trigger Decision module, which contains the final logic to determine the Level 1 Accept. This logic also uses the output from the Control Interface to determine if the detector is able to accept the trigger and, if necessary, to determine the correct crossing to issue the trigger. Details of the interface between the GL1P and subsystems are found in Ref. 5.

2.7. Communication between Front End and Trigger Systems

Introduction

Each subsystem crate on the detector communicates with the trigger system off the detector with the cables that transmit 16 bits of data per crossing. Each of these cables could physically be an optical fiber running at 1 Gb/s. The Calorimeter, Tracking and Muon subsystems send trigger data to the Global Level 1 Trigger. They, and the Inner Tracker (Silicon Subsystem) also receive the clock from and exchange control information with the Global Level 1 Trigger.

All of the Global Level 1 Trigger Processor (GL1P) is in the counting house on the surface.

The four different optical fiber cables between Front End Systems Crates and the Trigger Crates that provide clock and control are listed below. Further details about protocols and definitions are found in Ref. 5.

Subsystem Control Cable

The Subsystem Control Cable contains several bits that inform the GL1P about the status of the subsystem and its trigger. These bits accompany the Subsystem trigger data

and refer to the status of the subsystem at the time of the crossing corresponding to the trigger data. Subsystems are not required to provide all of these bits. However, the GL1P will provide the appropriate responses if they are implemented.

The Subsystem Trigger Busy Bit is set by the subsystem if its trigger system was not active (able to process the data) during the crossing. The Subsystem Trigger Error bit is set by the subsystem if its trigger or DAQ system has an error which is not recoverable except (possibly) by a reset command. The five bits of ambiguous crossing contain the number of subsequent crossings for which the Subsystem Trigger data is valid. The Subsystem also sends 8 bits of Subsystem Crossing Number. These are the lowest 8 bits of a counter that counts the number of crossings since the last receipt of the Bunch Crossing 0.

Level 1 Clock Cable

The GL1P has three cables that go to each Subsystem Trigger. The GL1P Clock Distribution module puts its output on the Level 1 Clock cable, and the GL1P Control Interface sends out signals on the Level 1 Control and Level 1 Number cables. The GL1P Clock cable contains the 62.5 MHz clock. The Bunch Crossing 0 Indicator is set when the clock period corresponding to Bunch Crossing 0 is reached. The Empty Bunch Indicator bit is set when the crossing corresponds to an empty bunch. The 62.5 MHz clock, Bunch Crossing 0 and Empty Bunch Indicator are continuous and not interrupted.

Level 1 Control Cable

The Level 1 Control cable brings the trigger to the subsystem from the GL1P Control Interface. The Test Enable bit indicates that the GL1P has scheduled a particular test of the type indicated by the Test Trigger Type bits to take place a fixed number of crossings hence. This number of crossings is fixed for each test trigger type (and may be the same for all trigger types) at the beginning of the run and downloaned to all Subsystem trigger and DAQ systems. The three Test Trigger Type bits are set to the value given with the Test Enable bit when the Level 1 Accept is issued for the scheduled test trigger. This is done so subsystems will not have to store the Test Trigger Type bits for subsequent application when the Level 1 Accept is issued for the test event. The two bits of readout type equal 0 if the event is a normal Level 1 Accept, 1 for a Level 1 Accept not associated with a beam crossing, and 2 for a Scheduled Test Event.

The two bits of Trigger type are 0 if the event is normal Level 1 Accept, 1 for a Level 1 Accept not associated with a beam crossing, and 2 for a scheduled Test Event. The two bits of Crossing Ambiguity indicate the number of subsequent crossings that the Level 1 Accept refers to. The Level 1 Reset bit causes the the Subsystem Trigger and DAQ to be set to a well-defined empty state. The Level 1 Accept is set at the leading edge of the 62.5 MHz clock. The Level 1 Accept is a level that is high for all clock cycles to be measured.

Level 1 Number Cable

The Level 1 Number Cable comes from the GL1P Control Interface. The Level 1 ID number increases with the rising edge of each Level 1 Accept starting with 1 at the beginning of the run. The lowest order 8 bits of this number are sent to subsystems to check that the GL1P has issued the same number of Level 1 Accepts as have been received by the subsystem. The 8 bits of Bunch Crossing Number indicate which the lowest order 8 bits of the crossing number that should be taken. This number should agree with the bunch crossing number of the data at the end of the pipeline which the Level 1 Accept Rejert is referring to. If either of these checks fails, the subsystem should

request a Level 1 Reset by setting the Trigger Error bit.

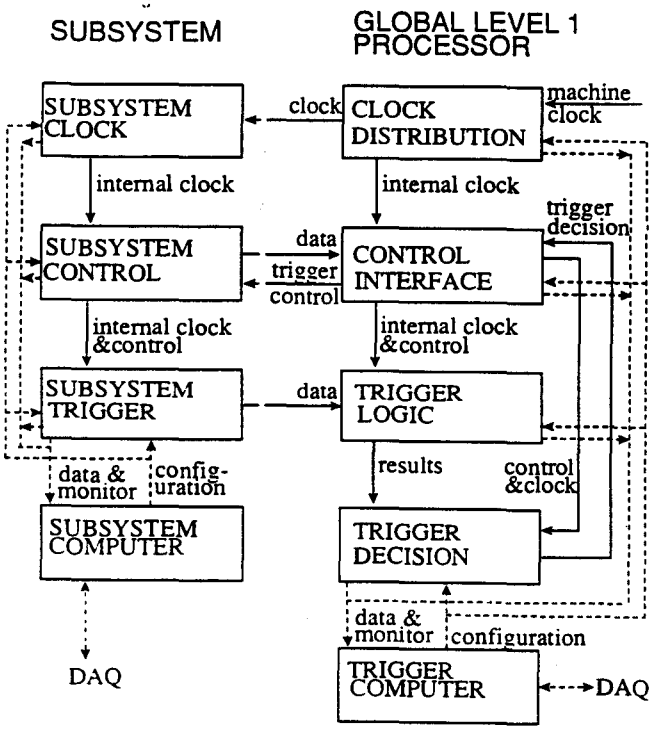


FIG. 3. Layout of the Global Level 1 Processor and Interface to Front End Systems

3. Level 2 Trigger

3.1. Introduction

The Level 2 Trigger is used to reject conversions by matching silicon tracking information with outer tracker information and calorimeter isolated electrons. The silicon tracking is also used to find secondary vertices in jets, rejecting events which have relatively low-p_t jets that passed the Level 1, and lack secondary vertices as well as any other distinguishing features. The Level 2 Trigger also uses the full shower max information to improve the electron isolation cut. The Level 2 Trigger matches tracks in the muon system with those in the tracking system to sharpen the p_t cut.

The Level 2 decision is supposed to achieve a rejection factor of between 10 and 100 in a series of pipelined steps, each of which does not exceed 10 μsec in duration and the sum of which may vary between 10 and 50 μsec in latency. On average the Level 2 issues a decision every 10 μsec. The Level 2 decision uses flexible and programmable algorithms. The basic event selection is done by jet and lepton identification and geometrical or topological correlation[8].

3.2. Level 2 Subsystems

Silicon Tracking

The Silicon Tracking Level 2 Trigger is described in detail in Ref. 7, which is summarized here. The Silicon tracker first attempts to recognise regions of interest by means of a "coarse scan". Having established areas of the two-dimensional space likely to contain high p_T tracks, it performs a second,"fine scan", in which these areas are examined with the full granularity of the silicon detector. This allows a high precision measurement of the transverse momentum of those tracks found by the pattern recognition.

In the coarse scan the data from the barrel region is tabulated in 1920 bins in ϕ, which corresponds to a distance of 0.6 mm on the circumference of the innermost silicon detector. This bin size is chosen to approximately match the ϕ granularity of the calorimeter and to keep the number of inputs to the processors to a manageable number while maintaining good resolution in transverse momentum. A two dimensional table is formed by combining these 1920 bins from 8 layers of the silicon ordered by increasing radius. In this table high transverse momentum tracks have a very small or zero variation in ϕ bin as a function of radius whereas low p_T tracks bend considerably as they pass through the eight silicon layers. The trigger processors are designed to recognize the patterns of tracks with a p_t greater than 15 GeV/c. An almost identical approach is used for the end-cap modules of the silicon detector, except that rather than filling a table of ϕ versus radius of the silicon layer, it constructs a table of ϕ against z. The same granularity in ϕ is used as for the barrel. Again, high transverse momentum tracks have a small variation in ϕ as z changes, whereas low p_T tracks curve considerably. The pattern recognition problem is therefore exactly analogous to that in the barrel once the z versus ϕ table has been constructed, so that identical trigger processors can be used.

In both the barrel and end cap modules there is a further subdivision of the data in bins of pseudorapidity η. These bins correspond in the barrel to the length of silicon wafers bonded together to form a readout unit. This is either two or three wafers. This η subdivision is somewhat coarser than that of the calorimeter, but should still allow satisfactory matching of tracking information and energy deposition.

Data from the silicon tracker in the form of a list of hit strip numbers is multiplexed from the detector to the trigger processors cards in the counting house on about 1000 optical fibers. The output of the processors will be fed to the global level 2 trigger processor, which will combine the silicon trigger data with that from other second level triggers and or with first level data if the component in question does not contribute to the second level. An interface card in each trigger processor crate will collect the trigger processor card outputs and forward them to the global level 2 system.

Tracking, Shower Max, and Calorimetry

The information for use in Level 2 from these system is described in detail in the section on Level 1 and is summarized here. The Calorimeter Level 1 Crates send their stored 8-bit electromagnetic and hadronic energy sums for the .1 x .1 trigger towers forward to the global level 2 processor after a level 1 accept. The Track Shower Max Crates send stored shower max hits (5 η bins of 32 ϕ bits apiece = 256 bits) and track information (32 ϕ bins with 4 bits p_t = 128 bits) in 64 1.6 η x 0.2ϕ regions to the second level trigger. This gives an η granularity of 1.6 for the tracker and 0.2 for the shower max, as well as a ϕ granularity of 6.25 mrad for both.

Muons

As described in the section on Level 1, the Muon Trigger Crates send the two highest p_t tracks per .2 η x .4ϕ region with 3 bits p_t and 5 ϕ bits apiece, (giving ϕ bins of .01) to the Level 2 Processor.

As described in Ref. 4, additional information from the muon system can also be used in the Level 2 decision. The θ wires in the layer inside the toroid reduce the uncertainty from the spread in the beam spot, resulting in a $\sqrt{2}$ improvement in the p_t cutoff sharpness. The information from the inner θ wires is sent up and combined with the signals from the outer layers and the result is sent to the Level 2 Processor. The muon hits can be combined with stiff tracks in the central tracker. This allows use of the p_t information from the central tracker. Due to field nonuniformities, improvement on momentum resolution beyond 20% depends on use of z information. While the muon system does provide z information, the association of a muon system θ track with a tracking system ϕ track requires significant processing that is appropriate for Level 2. Finally, the muon hit in the ϕ wires can be combined with the stiff track in the central tracker. Here the scintillator ϕ information tags the hit and provides σ information, which can be used to improve the "sagitta" measurement, and correct for z variations with z. This requires processing that is appropriate for Level 2.

3.3. Level 2 Global Processor

As described in Ref. 8, the Level 2 Processor makes a refined tracking selection based on the η, ϕ, and p_t information in the silicon, central tracker and muon systems. The shower max information is used in combination with the electromagnetic and hadronic calorimeter information to refine the isolation and E_t determination for electrons and photons. More sophisticated cluster algorithms are used to verify the E_t of jets. The silicon tracker is used to search for secondary vertices. These calculations can be performed with such devices as Digital Signal Processors, Transputers, or Massively Parallel Processors such as the Associative String Processor.

4. Cost

4.1. Methodology

The cost for the trigger system was calculated by determining the numbers of ASIC's, boards, crates, and cables. Each electronics board was costed at 2 K$, with 1.1 K$ for parts, .6 K$ for the board, and .3 K$ for assembly. Each crate was costed at 10 K$, with 2.5 K$ for hardware, 2.5 K$ for power supplies, and 5 K$ for the crate processor. Fiber optic links were costed at $ 300 per link with 35% contingency. ASIC's and boards were divided into "easy" and "hard" categories. Easy designs were estimated to take 1.5 man-years of engineering time. Hard designs were estimated to take 3 man-years of engineering time. In addition, each man-year of engineering time was assumed to also use a man-year of technician time, as well as 20 K$ of expenses for travel, supplies and computing (i.e. CAD).

4.2. Interfaces

There are a number of boundaries in the cost responsibilities between the trigger and front end electronics systems. These have been established in joint consultation with front end electronics groups. For central and muon tracking systems, the segment finding is costed with the front end electronics and the segment linking and all that follows is costed with the trigger. For calorimetry, the front end electronics costs all generation of the 8-bit hadronic and electromagnetic sums and the trigger pays for the optical link to bring the data up to the counting house. For the boundary between Level 1 and Level 2, Level 1 pays for the transmission of the data to the Level 2 Interface card (including crate and backplane), while Level 2 pays for the card. For the boundary between DAQ and trigger, the trigger pays for its crate and processor cards, while the DAQ pays for all the links that connect to the processor cards.

4.3. Summary

The following table lists the costs following the methodology and interfaces described in the previous two sections. The detailed cost breakdown is contained in Ref. 10.

Item	Cost (K$)	Conting (K$)	Total (K$)
Level 1:	16.581	5.139	21.720
Calorimeter	3.756	1.164	4.920
Muon	4.393	1.361	5.754
Track	2.592	893	3.775
Silicon	260	81	341
Global	5.290	1.640	6.930
Level 2:	5.706	1.770	7.476
Calorimeter	674	209	883
Track	264	82	346
Muon	264	82	346
Silicon	2.121	658	2.779
Global	2353	739	3.122
Total L1+L2 :	22.287	6.909	29.196

5. References

[1] D. Panescu, J. Lackey, P. Rohl, W.H. Smith, *An SSC PMT Preamplifier Circuit*, SDC Note SDC-91-00086, 1991.

[2] T. Gorski, J. Lackey, W.H. Smith, W. Temple, *Isolated Electron Pattern Logic Design and Performance at the SSC*, SDC Note SDC-91-00087, 1891.

[3] T. Gorski, J. Lackey, W.H. Smith, *Level 1 Trigger Decision Design for the SDC*, SDC Note SDC-91-00088, 1991.

[4] J. Chapman and R. Thun, *SDC Muon Trigger Preliminary Conceptual Design*, SDC Note *in preparation*, 1991.

[5] W. H. Smith, T. Gorski, J. Lackey, *SDC Global Level 1 Processor: Clock & Control*, SDC Note SDC-91-00090, 1991.

[6] M. Contreras *et al.*, *Conceptual Design of the SDC Trigger from the SDC Trigger Group*, SDC Note *in preparation*, 1991.

[7] B. Foster, G.P. Heath, R. Nickerson, *Preliminary Conceptual Design Document - Second Level trigger for the Silicon Tracker*, SDC Note *in preparation*, 1991.

[8] P. LeDu, Level 2 Trigger, Private Communication, 1991.

[9] Y. Arai, H. Ikeda, Y. Watase, *Conceptual Design of Straw Tube Readout with TMC*, 1991.

[10] W.H. Smith, T. Gorski, J. Lackey, J. LeBeck, *Cost and Schedule for the SDC Trigger*, SDC Note SDC-91-00091, 1991.

[11] M. Thompson, *Fiber Optic Data Transmission for the SDC Detector*, SDC Note SDC-91-00092, 1991.

SDC Note SDC-91-00090
DRAFT
September 9, 1991

SDC Global Level 1 Processor: Clock & Control

W.H. Smith, T. Gorski, J. Lackey
University of Wisconsin

1 Introduction

The Global Level 1 Trigger Processor is the device that collects the Level 1 Trigger data from the subsystems, distributes the Level 1 Accept and 16 nsec clock signals to all subsystems, and controls the overall operation of the Level 1 subsystems. This document describes the function of the Global Level 1 Processor, its interface to the Subsystems and its physical layout. This document outlines in specific detail the functions needed for clock and control. It also outlines the design of a module that will simulate the function of the Global Level 1 Processor for use in the development of Subsystem front end electronics. This document is preliminary in that many of the design features it is predicated on have not been officially accepted by the SDC Electronics, Trigger, and DAQ working groups. Part of the purpose of this document is to present these features to stimulate discussion leading to a determination of the design of the Level 1 Trigger system.

2 Function of the Global Level 1 Processor

2.1 Overall Data and Control Flow

The Global Level 1 Processor (GL1P) receives a subset of the data from subsystems participating in the level 1 trigger. The data for each 16 nsec bunch crossing is sent by each subsystem every 16 nsec and arrives at the input of the GL1P before 112 - 162 crossings have elapsed since the event occurred. The GL1P issues a Level 1 Trigger Accept/Reject at its output 132-182 bunch crossings after the event occurred. The timing is discussed in detail in ref 1. The GL1P not only makes the final level 1 decision, but it also controls the start of any level 1 reaction, disables this reaction, and distributes scheduling signals for tests and calibrations. Therefore, all subsystems, even those not involved in the level 1 decision, must communicate with the GL1P.

All level 1 trigger and DAQ pipelines in the subsystems and the GL1P must be driven with a common clock synchronized to the SSC crossing frequency. This clock is distributed vertically through the GL1P. This clock is phase locked to the SSC machine clock and has a 16 nsec cycle. The clock is high for ≈ 8 nsec and low for ≈ 8 nsec. The processing of the GL1P decision is driven by this cycle. For testing purposes, the GL1P operates on its own internal clock which can be varied in frequency from 70 MHz to 1 KHz.

Subsystems ship trigger data to the GL1P every 16 nsec. All of the data relevant to one crossing is shipped in one 16 nsec time period. All subsystems must send their data to the GL1P so that it arrives at the GL1P input within 2.1 - 2.6 μsec after the crossing occurred at the interaction point. Subsystems should send trigger data as soon as it is available and not delay sending trigger data for the purposes of synchronization. The subsystems must send data continuously even if they are being read out.

The GL1P receives the trigger data and aligns this data in time for all the subsystems since the arrival time for the data of a particular crossing is different among the different subsystems. The particular bunch crossing number of a subsystem's data is indicated by a local bunch counter, named Bunch Phase. This Bunch Phase must accompany the trigger data from each subsystem. The subsystem also counts Level 1 triggers. This number, Level 1 ID, must also accompany the trigger data.

2.2 Level 1 Accept/Reject

After the GL1P processing, a decision is made to issue a Level 1 Accept or Reject for each bunch crossing. The GL1P sends the Level 1 Accept/Reject to all subsystems 132 - 182 crossings after the bunch crossing. This signal appears at the output of the GL1P. The Level 1 Accept/Reject arrives at the subsystem after additional delay due to the propagation of the Level 1 Accept/Reject from the GL1P. The Level 1 Trigger Accept is a Level that is 1 for accept and 0 for reject. The Level 1 Trigger Reject is a Level that is 0 for accept and 1 for reject. These are strobed by the clock. A signal called "data valid" also accompanies the Level 1 Accept/Reject. This signal is used by some components to generate a Level 1 Strobe. Data valid is low after a Level 1 Accept for the length of the pipeline propagation time. The Level 1 Accept/Reject signal is also accompanied by additional GL1P data. This data is not necessarily propagated to all components of a subsystem, but is used as a diagnostic by the central processing of a subsystem. The data includes data valid, the Bunch Phase, the Level 1 ID, and several bits of "readout type". The Level 1 ID counts Level 1 Accepts. The bits of "readout type" allow information to be sent to subsystems that may react differently to different trigger types.

2.3 Ambiguous and Overlapping Triggers

If a subsystem cannot identify data with a particular crossing, it sends the data applicable to a number of crossings with each crossing with a bit to indicate that the crossing is not identified. The GL1P has the ability to scan over several crossings, examining the data from all the subsystems, to match up data stretching over several crossings with data identifying a single crossing. This is used to identify a unique crossing for every L1 Accept. Subsystems determine the number of bunch crossings to store upon each Level 1 Accept. There is the possibility that we cannot uniquely identify a crossing from the trigger data or that we may have two Level 1 Accepts within the measurement time span of some subsystems. Following Dorenbosch, Botto, Fry and Milner (SSCL-343), we define the Level 1 Accept as a level that is high for all clock cycles to be measured. The Level 1 ID is incremented on the rising edge of the Level 1 Accept. For each overlapping trigger, the Level 1 Accept goes low for half a cycle, and when it goes high again, the Level 1 ID is incremented. To attempt to limit overlaps as much as possible, we also follow their rules for minimal spacing for Level 1 Accepts:

- No more than 1 Level 1 Accept per 50 nsec.
- No more than 2 Level 1 Accepts per 260 nsec.
- No more than 3 Level 1 Accepts per 1 μsec.
- No more than 4 Level 1 Accepts per 4 μsec.

They determine that the total cost for these rules is less than 1% at a Level 1 rate of 100 KHz and 11.5% at 500 KHz.

2.4 Trigger Control

Subsystems send trigger control information to the GL1P. This includes a busy bit to indicate that the subsystem trigger did not process the event, busy bit to indicate that the subsystem DAQ cannot read out the event, a fatal error bit to indicate that the subsystem trigger has had a fatal error and a trigger data error to indicate that the subsystem trigger data may be corrupt. An example of a trigger busy would be a reset process that had not been completed. We must allow for subsystems that cannot complete a Level 1 Reset sequence in a single 16 nsec crossing. The trigger busy bit prevents a Level 1 Accept being issued to a subsystem that must use several crossings for a reset. An example of a fatal error would be a disagreement between the Level 1 trigger number counted by the subsystem and the number sent by the GL1P. An example of a trigger data error would be either a parity check failure or another type of internal data checking failure. The control information also includes the subsystem's crossing number associated with this data. All subsystems active during a run must send this control information to the GL1P, whether or not they send data used in the Level 1 decision.

2.5 Tests

The operation and scheduling of tests during a run are controlled by the GL1P. A schedule of all tests to be run is downloaded to the GL1P before the beginning of a run by the Central DAQ Control (CDAQC). The CDAQC also can modify this schedule during a run in response to changing detector status. The GL1P sends to all subsystems a Test Enable signal, with the type of test to be run indicated in the Test Trigger Type bits, a fixed number of crossings before the crossing when the test is to be done. This enables subsystems to prepare for the test. The tests are arranged in such a way as to allow many subsystems to do tests simultaneously. The subsystems set up their tests so that the test data will be contained in the exact crossing indicated by the GL1P Test Enable Signal. The GL1P inhibits normal triggers a fixed time before the test trigger crossing so that there will be no interference. The GL1P then sends out a Level 1 Accept for the appropriate crossing to read out the test data. This Accept is accompanied by a bit in the Readout Type set to indicate that it is a test trigger.

2.6 Schematic Layout

The functional block diagram of the GL1P as it interacts with a subsystem trigger is shown in Figure 1. The Clock Distribution block generates the 16 nsec clock and associated data such as the Bunch Crossing 0 and Empty Bunch Indicators from SSC accelerator clock information. It then distributes this information to the subsystems and the rest of the GL1P. This block also monitors the relative phase of the accelerator clock and the beam pickup signal, which should remain constant. The Control Interface provides all of the control signals to the subsystems and reads all of the control signals from the subsystems. All data except for the trigger data from a subsystem is brought through the Control Interface. The test scheduling and Level 1 Accept are sent to the subsystem through this block. It also monitors the subsystem deadtime and status. The trigger data from the subsystems is processed in the Trigger Logic block. Here the data from the various regions of each subsystem are collected, counted, and placed in an appropriate format for correlation with other subsystem trigger data. This data is shipped to the Trigger Decision Block, which contains the final logic to determine the Level 1 Accept. This logic also uses the output from the Control Interface to determine if the detector is able to accept the trigger and, if necessary, to determine the correct crossing to issue the trigger.

Table 1: CABLES FROM SUBSYSTEM TO LEVEL 1 TRIGGER:

1. Subsystem Trigger Control	
Bits	Data
1	Subsystem Trigger Busy
2	Subsystem Data Busy
3	Subsystem Trigger Error
4-8	Ambiguous Crossing
9-16	Subsystem Crossing Number
17	Timing Marker
2. Subsystem Trigger Data (There are several of these usually)	
Bits	Data
1-16	Results of Subsystem Trigger Calculation
17	Timing Marker

3 Global Level 1 Processor Subsystem Interface

3.1 Communication between the GL1P and Subsystems

Each subsystem crate on the detector communicates with the trigger system off the detector with the cables listed in Tables 1 and 2. Each cable transmits 16 bits of data per crossing. Each of these cables could physically be an optical fiber running at 1 Gb/s. If, for example, 10 fibers are required to one subsystem, then there could be one cable which would be a bundle of 10 fibers. Another implementation would be to use conventional 17-pair Ansley cable, transmitting 16 bits of data with a timing marker, or strobe, as the 17th bit. The Calorimeter, Tracking and Muon subsystems send trigger data to the Global Level 1 Trigger. They, and the Inner Tracker (Silicon Subsystem) also receive the clock from and exchange control information with the Global Level 1 Trigger. The number of crates for tracking is taken from the straws option. If we switch to the fiber tracker, then this number of crates may decrease to 78 to match the calorimeter.

All of the Global Level 1 Trigger Processor (GL1P) is off the detector, in the counting house on the surface. Table 1 lists the cables required to trigger information from the calorimeter, muon and tracking systems to the Global Level 1 Trigger Crates. Table 2 lists the cables necessary for transmission of trigger information to the calorimeter, muon, tracking, and silicon systems.

Table 2: CABLES FROM LEVEL 1 TRIGGER TO SUBSYSTEMS:

3. Level 1 Clock (from GL1P Clock Distribution)	
Bits	Data
1	62.5 MHz clock
2	Bunch Crossing 0
3	Empty Bunch Indicator
4-16	Spare
4. Level 1 Control (from GL1P Control Interface)	
Bits	Data
1	Test Enable
2-4	Test Trigger Type
5-6	Trigger Type
7-9	Readout Type
10-22	Crossing Ambiguity
23	Level 1 Reset
24	Level 1 Accept
25	Level 1 Reject
26	Data Valid
5. Level 1 Number (from GL1P Control Interface)	
Bits	Data
1-8	Level 1 ID
9-16	Bunch Phase

3.2 Subsystem Control Cable

The Subsystem Control Cable contains several bits that inform the GL1P about the status of the subsystem and its trigger. These bits accompany the Subsystem trigger data and refer to the status of the subsystem at the time of the crossing corresponding to the trigger data. Subsystems are not required to provide all of these bits. However, the GL1P will provide the appropriate responses if they are implemented.

3.2.1 Subsystem Trigger Busy

The Subsystem Trigger Busy Bit is set by the subsystem if its trigger system was not active (able to process the data) during the crossing. This could be due to a reset or more detailed initialization procedures not being complete. If this bit is set, the GL1P will not use the subsystem trigger data in making the trigger decision. The GL1P will not take undertake any action on the subsystem, such as a reset, in response to the Subsystem Trigger Busy bit being set. If the Subsystem Data Busy bit is set the Subsystem is requesting the GL1P to halt triggers. The GL1P inhibits further Level 1 Accepts until a crossing occurs where the Data Busy bit is off. This may be due to buffers becoming full. The GL1P records the number of times the Subsystem Trigger Busy and Data Busy bits are set, and the number of inhibited Level 1 Accepts.

3.2.2 Subsystem Trigger Error

The Subsystem Trigger Error bit is set by the subsystem if its trigger or DAQ system has an error which is not recoverable except possibly by a reset from the GL1P. This error could occur if an internal parity check on the subsystem data fails, or if there is an internal subsystem trigger L1ID or Bunch Phase counter disagreement. In response to this bit being set, the GL1P will issue a Level 1 Reset. In addition, the GL1P will inhibit further Level 1 Accepts until it observes the setting and release of the Subsystem Trigger Busy bit. This is because the subsystem data will no longer be valid until the reset action is completed and the data from the crossing after the reset has propagated through the Level 1 pipeline. The GL1P records the number of times the Subsystem Trigger Error bit is set and the number of inhibited Level 1 Accepts. The GL1P also informs the central data acquisition each time a Level 1 Reset is issued so that if the rate of Level 1 Resets becomes unacceptable, the run will be paused or stopped.

3.2.3 Subsystem Ambiguous Crossing

The five bits of ambiguous crossing contain the number of subsequent crossings for which the Subsystem Trigger data is valid. If a subsystem is unable to identify some data with a particular crossing, but only a range of crossings, it sets a nonzero value into the ambiguous crossing bits corresponding to the range of crossings over which the data could have occurred. When a crossing is uniquely identified, these bits are zero. The next crossing's data from the component is allowed to change. The data that is valid for several crossings only needs to be sent for the first crossing where it is valid when accompanied by a non-zero value in the ambiguity bits. The GL1P uses these bits to identify the true crossing by correlating the data found in the initial crossing with the data from other subsystems in the number of subsequent crossings given by the ambiguous crossing bits. The five bits of

ambiguous crossing give a range of up 0.5 μsec, which is sufficient for the worst conceivable time resolution.

3.2.4 Subsystem Crossing Number

The Subsystem also sends 8 bits of Subsystem Crossing Number. These are the lowest 8 bits of a counter that counts the number of crossings since the last receipt of the Bunch Crossing 0 from the GL1P. The GL1P checks this counter for sequential incrementing, except when it is reset to 0. The Subsystem Crossing Number is also used to align the various subsystems with the GL1P and other Subsystems. Each cable of Subsystem Trigger Data also carries a timing marker in the 17th bit that acts to strobe the data.

3.3 Subsystem Trigger Data Cables

The Subsystem Trigger Data cables carry 16 bits of data along with a strobe in the 17th bit to the GL1P. The GL1P uses this data to make its trigger decision. These 16 bits of data carry the results of subsystem trigger calculations. Details of this information are found in ref. 1.

3.4 Level 1 Clock Cable

The GL1P has three cables that go to each Subsystem Trigger. The GL1P Clock Distribution puts its output on the Level 1 Clock cable, and the GL1P Control Interface sends out signals on the Level 1 Control and Level 1 Number cables. The GL1P Clock cable contains the 62.5 MHz clock. This signal is a continuously on differential-ECL 16 nsec cycle signal, which is high for 8 nsec, followed by low for 8 nsec. For normal running the 62.5 MHz clock is phase locked to the machine clock. The clock is guaranteed to have the high and low phase neither shorter than 7 nsec nor longer than 9 nsec, with the sum of the two always 16 ± 0.5 nsec. This means that overall phase adjustments to the machine clock will be made in steps of less than 0.5 nsec. The phase difference between the 62.5 MHz clock and the interaction crossing time is constant. This is monitored by the GL1P using a beam pickup. The GL1P also has an independent internal clock that can be used for subsystem testing.

3.4.1 Bunch Crossing 0

The Bunch Crossing 0 Indicator is set when the clock period corresponding to Bunch Crossing 0 is reached. The Bunch Crossing 0 is defined in the time coordinates of the Level 1 Accept. This means that if the Level 1 Accept is issued by the GL1P exactly 132 crossings after the crossing where the triggering crossing occurred, Bunch Crossing 0 is issued by the GL1P exactly 132 crossings after Crossing 0 occurs at the interaction point. This signal is issued by the GL1P every 4,730 crossings, which is the approximate number of crossings the SSC beam takes to make one revolution. The phase of this signal is set up during the GL1P initialization. The Bunch Crossing 0 signal is used by the Subsystem in combination with the Level 1 Reset. Upon receipt of the Level 1 Reset, the subsystem waits until it receives the Bunch Crossing 0 Signal to release its counters and begin propagating data through its pipelines. This assures alignment after a Level 1 Reset. During the interval between Reset and Bunch Crossing 0 the Subsystem Trigger Busy bit is left on. The GL1P sends the reset a sufficient number of crossings before the Bunch Crossing 0 to assure all

Subsystems are able to become active (if functioning properly) upon receipt of Bunch Crossing 0. This number of crossing represents the time required for the Subsystem to execute the reset.

3.4.2 Empty Bunch Indicator

The Empty Bunch Indicator bit is set when the crossing corresponds to an empty bunch. The 62.5 MHz clock, Bunch Crossing 0 and Empty Bunch Indicator are continuous and not interrupted. The Empty Bunch Indicator is also defined in the time coordinates of the Level 1 Accept. As is the case for the Level 1 Accept and Bunch Crossing 0, the Empty Bunch Indicator arrives at the end of the Subsystem Level 1 pipeline just as the crossing with the empty bunch reaches it. This is because the GL1P issues the Empty Bunch Indicator exactly 128 crossings after the empty bunch passed through the interaction point. The GL1P may use the empty bunches for scheduling a test event sequence, but will do this scheduling without the Subsystem having to check the Empty Bunch Indicator. The remaining bits on the Level 1 Clock Cable are listed as spare, because no other presently conceived signals from the GL1P come from the GL1P Clock Distribution and the requirements on the quality of the 62.5 MHz clock are stringent enough to warrant not bringing many additional signals on the same cable. However, the possibility to add additional signals is admitted by designating the remaining signals as "spare".

3.5 Level 1 Control Cable

The Level 1 Control cable brings the trigger to the subsystem from the GL1P Control Interface. The Test Enable bit indicates that the GL1P has scheduled a particular test of the type indicated by the Test Trigger Type bits to take place a fixed number of crossings hence. This number of crossings is fixed for each test trigger type (and may be the same for all trigger types) at the beginning of the run and downloaded to all Subsystem trigger and DAQ systems. The three Test Trigger Type bits are set to the value given with the Test Enable bit when the Level 1 Accept is issued for the scheduled test trigger. This is done so subsystems will not have to store the Test Trigger Type bits for subsequent application when the Level 1 Accept is issued for the test event. The two bits of readout type equal 0 if the event is a normal Level 1 Accept, 1 for a Level 1 Accept not associated with a beam crossing, and 2 for a Scheduled Test Event.

3.5.1 Trigger Type

The two bits of Trigger type are 0 if the event is normal Level 1 Accept, 1 for a Level 1 Accept not associated with a beam crossing, and 2 for a scheduled Test Event. Events not associated with a beam crossing are cosmic ray triggers and other events produced by non-beam associated triggers. The 3 bits of Readout Type are specific for each Subsystem. Different Subsystems may need different readout responses for different triggers. This could mean different numbers of switched capacitors being read out, or taking earlier or later samples, or changing the way the data is processed. The Readout Type bits are meant to select a different response to a Level 1 Accept.

3.5.2 Crossing Ambiguity

The two bits of Crossing Ambiguity indicate the number of subsequent crossings that the Level 1 Accept refers to. The GL1P will attempt to correlate the various subsystems to resolve triggers to a single crossing. However, to provide the possibility that the crossing may not be resolved for a small number of triggers, the Crossing Ambiguity provides the possibility of linking together up to 5 crossings in an event from on Level 1 Accept. A nonzero value in the Ambiguity Bits indicates that that number of subsequent crossings belong to the same trigger.

3.5.3 Level 1 Reset

The Level 1 Reset bit causes the the Subsystem Trigger and DAQ to be set to a well-defined empty state. All measurement data in the DAQ and Trigger pipelines is lost. The Subsystem Bunch Phase counter is set to zero. The counter does not begin to advance from zero, nor does the Trigger system start up again until it receives the next Bunch Crossing 0 Signal. The Trigger system is active for the next crossing after the Bunch Crossing 0 Signal. The Subsystem raises its Trigger Busy until the reset is finished. After issuing a Level 1 Reset, the GL1P inhibits further Level 1 Accepts until the Subsystem raises and lowers its Trigger Busy.

3.5.4 Level 1 Accept

The Level 1 Accept is set at the leading edge of the 62.5 MHz clock, exactly 105 clocks after the event occurs at the interaction point. The Level 1 Accept is a level that is high for all clock cycles to be measured. If two triggers overlap, the Level 1 Accept goes low for half a cycle between the two of them to indicate that they are overlapping triggers. This counts as two triggers and the Level 1 ID is incremented after the half cycle low. All of the data on the Level 1 Control, Clock and Number cables is issued with the Level 1 Accept. This data is valid at the leading edge of the clock where the Level 1 Accept is set. All of these signals are synchronized with the 62.5 MHz clock. The data in Level 1 Control, Clock and Number cables should be latched with the rising clock edge and not with the Level 1 Accept.

3.6 Level 1 Number Cable

The Level 1 Number Cable comes from the GL1P Control Interface. The Level 1 ID number increases with the rising edge of each Level 1 Accept starting with 1 at the beginning of the run. The lowest order 5 bits of this number are sent to subsystems to check that the GL1P has issued the same number of Level 1 Accepts as have been received by the subsystem. The 5 bits of Bunch Crossing Number indicate which the lowest order 5 bits of the crossing number that should be taken. This number should agree with the bunch crossing number of the data at the end of the pipeline which the Level 1 Accept Reject is referring to. If either of these checks fails, the subsystem should request a Level 1 Reset by setting the Trigger Error bit.

4 Global Level 1 Processor System Layout

Individual crates of the Level 1 Trigger and Subsystem Trigger logic are shown in Figure 2.

4.1 Global Clock/Control Crate

There is one Global Clock/Control Crate. It contains a Machine Clock Interface Board to communicate with the interface with the accelerator RF clock. It has a Beam Pickup Interface to communicate with the beam pickup electronics. It contains a Deadtime Monitor Board that tracks the disposition of each crossing, i.e. whether accepted, rejected, or lost due to downtime of trigger and or DAQ. There is a Final Decision Interface that connects to the FDL card in the Final Decision Crate to provide the Level 1 Accept if the DAQ is able to read out the event and there are no outstanding error conditions that prevent accepting the event (i.e. clock phase confusion, etc.) There is a Global Clock Master that provides the phase lock of the 16 nsec clock and distributes the clock to Clock/Control Interface modules. There is a Global Control Master that distributes the Control signals to the Clock/Control Interface Modules. Finally, there are 2 Clock/Control Interface Modules that each communicate with 2 Local Clock/Control Crates. This crate also contains a DAQ Interface/Processor Board.

4.2 Local Clock/Control Crate

There are 4 Local Clock/Control Crates. Each contains 16 Local Clock/Control Boards that are connected with 4 optical fibers apiece to 4 Front End or Trigger Crates. The 4 fibers carry the Level 1 System Control, Level 1 Clock, Level 1 Control, and Level 1 Number. The Crate also contains a Global Clock/Control Interface Board that communicates with the Global Clock/Control Crate, as well as a DAQ Interface/Processor Board.

4.3 Level 1 Clock/Control Board

Every front end electronics crate, as well as every trigger system crate has a Level 1 Clock/Control Board (L1CCB). A diagram of the L1CCB is shown in Figure 3. Under normal running, this board accepts the Level 1 Clock and Control Signals from the Global Level 1 System and puts these signals out on the crate backplane for use by the other modules in the crate. These signals are the the Level 1 System Control, Level 1 Clock, Level 1 Control, and Level 1 Number. The L1CCB also receives fast error and busy signals from the other modules in the crate. The board also comunicates with the crate processor, which is the DAQ Interface Card, from which is receives other status information about busy and error states. The L1CCB is programmable by the DAQ Interface Card to return busy and error states to the Global Level 1 System depending on the local busy and error information it receives in the crate. The L1CCB is also programmed to return the correct crossing number that accompanies data from the crate that is provided for the level 1 decision. This is done by writing into a register the correct bunch crossing number to return when the bunch crossing zero signal is received.

The L1CCB also has an output for the Global Level 1 Clock and Control Signals. This is done to allow fanout of the clock to additional crates with L1CCB's downstream of this L1CCB. The L1CCB is configurable with plug-in modules to receive or send the Global

Level 1 Signals on either cables or fiber optics. The purpose of this is to avoid the more expensive fiber optic runs when the clocks are being distributed over short distances. The L1CCB output can be run on a short cable to a 1-to-4 Clock/Control Fanout Board (CCFB) for distribution of these signals. The CCFB can be configured as a 1-to-3 fanout with optical fiber in and optical fiber out, or 1-to-4 with conventional cable in and either optical fiber or cable out. This is envisioned as being done with plug-in modules.

4.3.1 Standalone Operation

The L1CCB is also operable without input signals from the GL1P. The L1CCB is able to operate in this standalone mode and generate all of the Global Level 1 Signals internally. The board has an internal oscillator and has provision for an external clock. The choice is made with a front panel switch. In standalone mode, the L1CCB is programmed and operated by the DAQ Processor Interface Card (DPIC) in the crate. It receives its instructions over the backplane. The DPIC can download a sequence of clocks with accepts, rejects, test event, and initialization and start it up with a bus command. The L1CCB is also operable with an external trigger that is enabled by command from the DPIC. The L1CCB is able to report its status back to the DPIC to identify if it is running local or GL1P triggers, if it is in an error, busy or initialize state, or what test or clock sequences it is running. The purpose of this operation is to operate the crate independently under control of local or global DAQ for calibration or test operations. The L1CCB is also able to output its internally generated clock and control signals through its front panel as it does for the signals generated by the GL1P. These signals can be sent to another L1CCB or through an CCFB fanned out to several L1CCB's. These subsequent L1CCB's will receive these clock and control signals in the same manner as they receive those from the GL1P. In this fashion, a single L1CCB can take over the clock and control function of the GL1P for a group of crates under control of the DAQ. This allows flexible partitioning of the DAQ and Trigger systems into many stand-alone groups. In the case of organization of the DAQ with subsystem crates driving the rest of the subsystem front end crates, this configuration allows the trigger distribution to be organized exactly as the DAQ.

4.3.2 L1CCB Module Design

It is expected that the L1CCB will resemble the Global Level 1 Processor Simulation Module (GL1PSM) described below. This is so that subsystems which will work with the GL1PSM will find the evolution to the final trigger system relatively straightforward in that they will replace the GL1PSM with a L1CCB, which will interact with the subsystem in a similar manner to the GL1PSM. The L1CCB will be consistent with the final SDC backplane and crate configuration and will be designed to operate with the final DAQ.

5 Global Level 1 Processor Simulation Module

5.1 Introduction

The GL1P Simulation Module (GL1PSM) emulates all of the control sequences described above for the GL1P. Its purpose is to aid in the debugging of Subsystem trigger circuits and to serve the basic functions of a trigger module for test experiments. The GL1PSM will not

have the complicated decision logic found in the GL1P. In its place, there will be a single 16-bit memory lookup table. The contents of the memory lookup table will be downloaded under VME control.

5.2 Module Design

The GL1SPM will be a double width 6 Eurocard Unit High VME module of standard depth (160 mm) with standard J1 and J2 Eurocard connectors. All input and output signals cable are differential ECL with positive logic. The positive logic is connected at the input of the drivers and output of the receivers connected to the odd pin. The negative logic side is connected to the even pin. MC10H101's are used as drivers with 390 ohm resistors on each pin tied to -5.2 V. MC10H115's are used as receivers with $\sim$ 50 ohm resistors on each pin tied to ground. The GL1PSM will have one each of the Subsystem Trigger Control and Data cables mentioned above.

5.2.1 Control and Data Cable Connections

The Subsystem Trigger Control and Subsystem Trigger Data are brought to the GL1PSM on twist-and-flat spectra-strip cable from the Subsystem according to the differential cable scheme. There will be a single 17-pair connector on the front panel of the GL1PSM for each of these. There is provision for only 16 bits of Subsystem Trigger Calculation Results. These will be fed into a 16-bit wide memory lookup table. The subsystem should send data synchronized with the timing marker in the 17th pair. The GL1PSM will latch the data with a 4 nsec delayed timing marker. The difference in timing markers between the Subsystem Trigger Control and Data cables should be less than 2 nsec.

5.2.2 Backplane Connections

The Level 1 Clock, Level 1 Control, and Level 1 Number cables are brought out through the A and C rows of the P2 backplane as described in Table 3. A high quality backplane is required with ground traces between the signal traces, such as the Bicc-Vero Microbus© backplane. All signals are brought out as single-ended ECL onto the backplane, with the exception of the 62.5 MHz clock, which uses two backplane lines driven differentially. The backplane are lines are driven with a MC10H123 (complement output) and tied to -5.2 at each end with resistors matching the backplane line impedance ($\sim$ 80 ohms, depending on load). They should be received with a MC10H101, using its complement output.

5.2.3 Clock, Accept, Reset and Test

The GL1PSM will have an internally generated 62.5 MHz clock, as well as being able to use an external ECL clock at a frequency up to 62.5 MHz. The external clock is connected through the front panel on a four pair connector that follows the differential ECL cable scheme discussed above. The other three pairs on this connector are external triggers that cause the GL1PSM to issue an Accept, initiate a test sequence, or issue a reset a certain number of clock cycles after receipt. This number of clock cycles is set by a value into one of the control registers. The selection between external and internal clock, as well as external and internal triggers, is made by two front panel switches. The module can also be reset by a third switch on the front panel.

Table 3: P2 BACKPLANE CONNECTIONS

Level 1 Clock (from GL1P Clock Distribution)	
Pins	Data
a1	GND
a2	62.5 MHz clock –
a3	62.5 MHz clock –
a4	GND
a5	Bunch Crossing 0
a6	Empty Bunch Indicator
a7,a8	Spare
Level 1 Control (from GL1P Control Interface)	
Pins	Data
a9	Test Enable
a10-12	Test Trigger Type
a13-14	Trigger Type
a15-17	Readout Type
a18-20	Crossing Ambiguity
a21	Level 1 Reset
a22	Level 1 Accept
a23	Level 1 Reset
a24	Data Valid
a25-32	Reserved for Future
Level 1 Number (from GL1P Control Interface)	
Pins	Data
[illegible]	Level 1 ID
c24-c9	Bunch Phase
c10-21	Spare
c22-32	Reserved for Future

The VME Interface design is not yet finished. It will be an A24 D16 slave.

5.3 Control Registers

Table 4 contains the Control Registers. The Test Trigger Type, Trigger Type, Readout Type, and Crossing ambiguity are set the same for all triggers based on the values written into the locations in the Trigger Register listed in Table 4. If bit 12 is set, the module will begin a test trigger sequence. If bit 13 is set, the module will start an initialization sequence. If bit 14 is set, the module is reset. Bit 14 takes precedence over bit 13, which takes precedence over bit 12. The Bunch Crossing Number for the Test Trigger is the crossing number to issue the Accept for the Test Trigger after the request for a test trigger from the external trigger or Trigger Register. The External Trigger Delay Register contains the number of crossings to delay the issuing of the Level 1 Accept after receiving an external trigger. The External Trigger Stop Register, if not set to zero, stops the sending of the 62.5 MHz clock the number of crossings entered after the receipt of the external trigger. The purpose is to "freeze" the trigger pipelines at a certain point, enabling inspection of VME-readable registers midway through the processing of triggers.

5.3.1 Mode Select Register

The Mode Select Register bit 1 enables use of an internal memory which has a pattern of Level 1 Accepts placed in it. This memory has 2^16 locations, each of which corresponds to 8 nsec of time. A 1 in a location results in the Level 1 Accept high and a 0 means low. This enables an arbitrary pattern of Level 1 Accepts over 32,768 crossings, comfortably more than one SSC cycle of 17,300 crossings. This can be used to simulate marrying of overlapping triggers in any sequence discussed. The Level 1 Reject operates as the inverse of the Level 1 Accept. The Enable External Triggers enables the use of external triggers if the front panel switch is activated (the switch exists so that you do not have to unplug cables to verify your software is not using external triggers). Bit 3 causes a reset to be issued automatically in response to a receipt of Subsystem Trigger Error. Bit 4 is used to enable a reset after timeout. Since these two features can interfere with debugging, bits 3 and 4 can turn them off.

5.3.2 Empty Bunch Location Register

The Empty Bunch Location sets the location of the first bunch of the empty bunch sequence and the Empty Bunch Length sets the length of the empty bunch sequence. The Bunch Crossing 0 register sets the length of the SSC cycle. Nominally, this is 17,300 crossings. Setting 17,300 into this register causes the Bunch Crossing 0 signal to be issued at this crossing, as well as setting the Bunch Phase and other crossing counters to zero at this point, where they resume counting. The pattern of Level 1 Accepts loaded into the internal memory is truncated at the Bunch Crossing 0 and returns to the beginning.

5.4 Status Registers

The GL1PSM has five Status Registers. The first register reports the condition of the GL1PSM. The bits in this register are denoted as follows.

Table 4: CONTROL REGISTERS

1. Trigger Register	
Bits	Data
1-3	Test Trigger Type
4-5	Trigger Type
6-8	Readout Type
9-11	Crossing Ambiguity
12	If on, start a test sequence
13	If on, start a Level 1 Reset Sequence
14	If on, reset the GL1PSM
2. Test Bunch Register	
Bits	Data
1-16	Number of Crossings from Test Enable to Accept
3. Test Setup Register	
Bits	Data
1-16	Crossing Number for Test Trigger
4. External Trigger Delay Register	
Bits	Data
1-16	Crossing Delay for External Triggers
5. External Trigger Stop Register	
Bits	Data
1-16	Stop Clock Delay for External Triggers
6. Mode Select Register	
Bits	Data
1	Enable Playback Triggers
2	Enable External Triggers (if switched on)
3	If on, issue reset after Trigger Error
4	If on, issue reset after busy on for 1 sec.
5	If on, issue reset if Subsystem Cross. disagree
7. Empty Bunch Location	
Bits	Data
1-16	First Bunch of Empty Bunches
8. Empty Bunch Length	
Bits	Data
1-16	Length of Empty Bunch Group
9. Bunch Crossing 0	
Bits	Data
1-16	Number of Crossings for Bunch Crossing 0
10. Data Valid Length	
Bits	Data
1-16	Length of Data Valid Level

- *Bit 1:* Active – If the system is operating and receiving trigger data this is set to one.
- *Bit 2:* Test – If the system is in a test trigger sequence this is set to one.
- *Bit 3:* Reset – If the system is in a reset phase this is set to one.
- *Bit 4:* Initialize – If the GL1PSM is being initialized or downloaded, this is set to one.
- *Bit 5:* Busy – If the GL1PSM has seen a busy issued by the Subsystem, this is set to one.
- *Bit 6:* Error – If the GL1PSM has seen an error issued by the Subsystem, this is set to one.
- *Bit 7:* L1ID Error – If the GL1PSM has seen a disagreement between the L1ID from the Subsystem and its internal L1ID, this is set to one.
- *Bit 8:* Crossing Error – If the GL1PSM has seen a disagreement between the crossing number from the Subsystem and its internal crossing number, this is set to one.

The error conditions mentioned above (bits 5 through 8) are only cleared by an initialize or reset command. There are 4 additional status registers. Two status registers contain the Subsystem Trigger Control and Subsystem Trigger Data that caused the last Level 1 Accept. Another two status registers contain the Level 1 Control data (bits 2 through 12), and the Level 1 Number data (all bits) sent with the last Level 1 Accept.

5.5 Generating a Level 1 Accept

There are three ways to generate a Level 1 Accept with the GL1PSM. First, an Accept is generated if the pattern in the Subsystem Trigger Data corresponds with an accepted pattern in the Trigger Data Memory Lookup Table. Second, the Accept is generated by the pattern of Level 1 Accepts loaded into the Accept Pattern Memory. Third, the Accept can be generated by the external trigger. The external trigger needs to be synchronized to the 62.5 MHz clock, and preceed it by 4 nsec in order to be latched. The choice between these trigger modes is made by the Trigger Mode Select Register, which is set by VME commands. If more than one mode is chosen, the GL1PSM will generate a trigger from either.

5.6 Generating a Test Trigger Sequence

There are two ways to initiate the Test Trigger sequence. First, use a VME command to set the Test Trigger bit (Trigger Register bit 12), with the three bits of Test Trigger Type bits (Trigger Register bits 1-3), and the Trigger Type (Trigger Register bits 4,5) set to 2. Second, set the the Test Trigger Type and Trigger Type bits as for the first case, but do not set the Test Trigger bit via VME. Then use the external trigger. This will also start the test sequence.

After the test sequence is activated, the GL1PSM will send the Test Enable with the Test Trigger Type to the Subsystem at the crossing specified in the Test Bunch Register. The GL1PSM will inhibit normal triggers for one less than the number of crossings indicated in the Test Setup Register. The GL1PSM will then send the Level 1 Accept with the Test

Readout Type that exact number of crossings indicated in the Test Setup Register after the Test Enable Signal. The GL1PSM will ignore further trigger requests until the test sequence is finished. The completion of the test sequence can be checked with bit 2 of the first status register as mentioned above. If the Subsystem Busy is on when the Level 1 Accept should be issued, the GL1PSM does not issue a Level 1 Accept and treats the situation the same as a Subsystem Trigger Error. If the Level 1 Reset sequence is begun during the test sequence, the test sequence is aborted without completion.

5.7 Generating a Reset Sequence

There are two ways to initiate the Level 1 Reset sequence. First, use a VME command to set the Reset Trigger bit (Trigger Register bit 13). Second, do not set the Reset Trigger Trigger bit via VME, but use the external reset input. This will also start the reset sequence. The GL1PSM will issue the Level 1 Reset the number of crossing indicated in the Data Valid Length Register before the Bunch Crossing 0. Since the numbering of the Bunch Crossings may be out of order before the reset, the subsystems must reset their counters to zero when they receive the Bunch Crossing 0 after receiving the Reset Signal.

The Reset is completed when the Bunch Crossing 0 Signal is received. All subsystems should be live for the next crossing. The Components will raise their Busy Bits for the Crossings where they are not able to take data due to the reset. The GL1PSM will inhibit triggers for the number of crossings in the Data Valid Length Register. The Data Valid Length Register contains the length in crossings of the Subsystem Level 1 pipeline. The GL1PSM will check that the Subsystem Busy Bits are low for the crossing after Bunch Crossing 0. If they are, the GL1PSM will issue Level 1 Accepts where appropriate for this and subsequent crossings. If the Busy does not drop, the will continue to inhibit further triggers forever, or until 1 second has passed, depending on how bit 4 of the Mode Select Register is set.

Several occurrences will also initiate a reset sequence automatically. If the Subsystem Trigger Error bit is set, all other Subsystem Trigger Data is ignored, bit 6 of the first status register will be set, and, if bit 3 of the Mode Select Register is on, the GL1PSM will begin a reset sequence as described above. If the Subsystem Crossing Number disagrees with the GL1PSM, it will set bit 5 in the first status register and depending on bit 5 of the Mode Select Register, it will begin a reset sequence as described above. In both of these cases, the GL1PSM will inhibit all Level 1 Accepts until the reset sequence is complete, whether started automatically or externally.

6 Acknowledgments

Much of this design is the result of discussions on SDC Physics and Triggering with R. Partridge, I. Gaines, J. Dorenbosch, G. Foster, M. Levi, H. Williams, A. Lankford, M. Campbell, R. van Berg, P. Sinervo, and Y. Sakai. Much of this design reflects ideas from the Zeus Trieger group, in particular, K. Tokushuku and his colleagues M. Ikeda and A. Imaeishi, from INS, University of Tokyo, L. Wiggers, Nikhef, and G. Heath, U. Bristol, as well as other members of the Wisconsin group who worked on the Zeus trigger, in particular, J. Lackey and P. Rubi.

References

[1] W.H. Smith, T. Gorski, J. Lackey, *SDC Trigger Preliminary Conceptual Design*, SDC note SDC-91-00089, 1991.

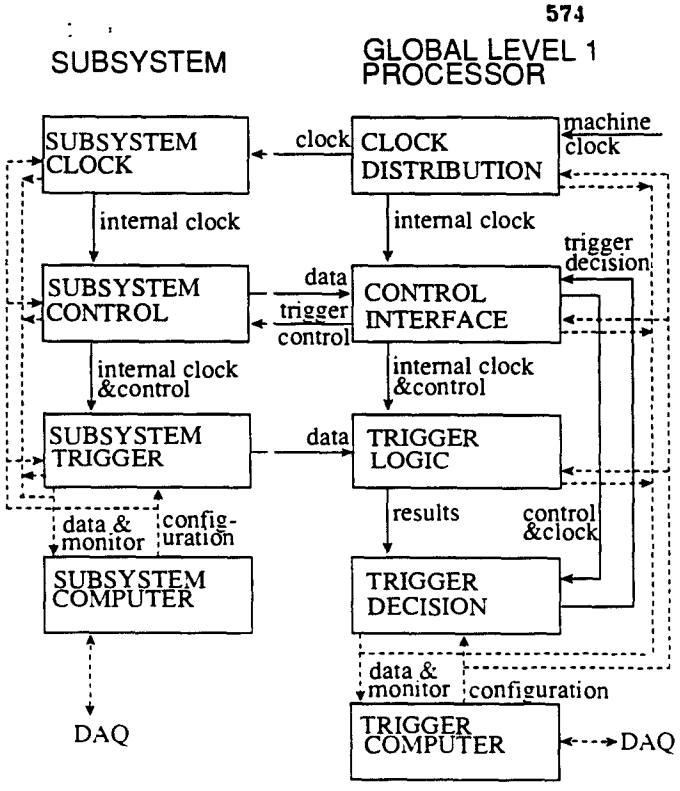


Figure 1. GL1P Functional Block Diagram

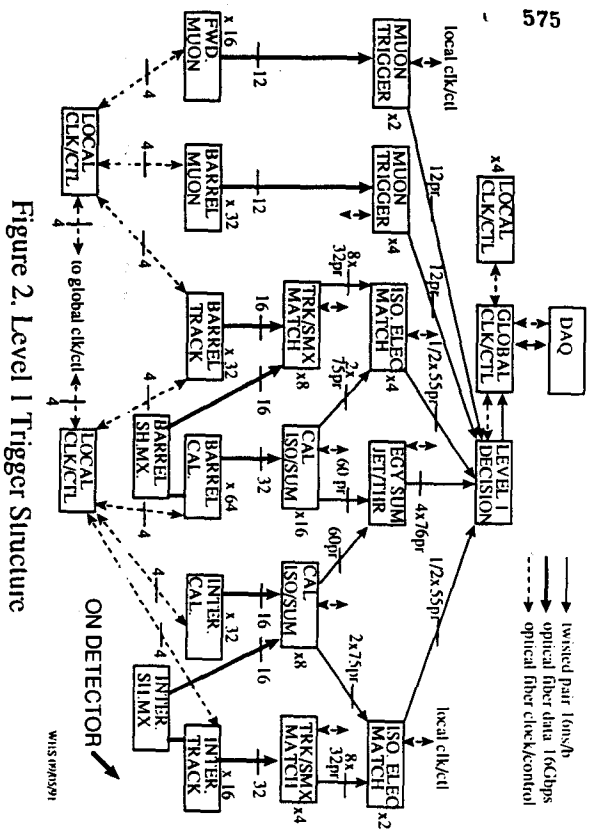


Figure 2. Level 1 Trigger Structure

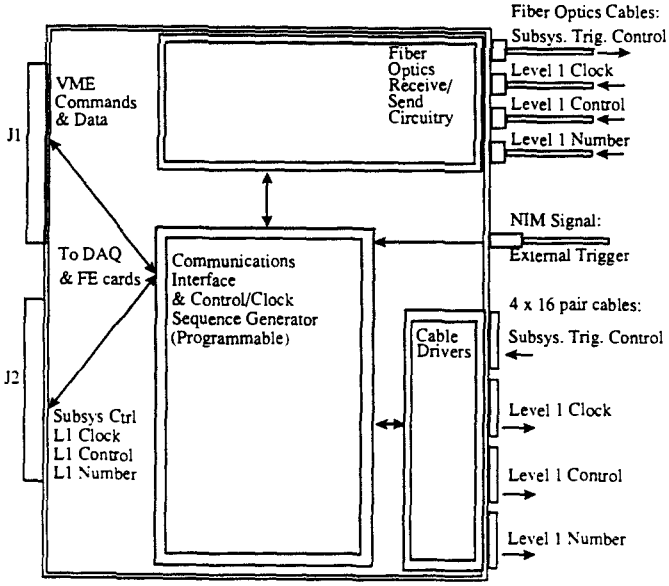


Figure 3. Level 1 Clock/Control Board

Fiber-optic Trigger Data Transmission for the SDC Detector

Murray A. Thompson
Physics Department, University of Wisconsin
1150 University Ave, Madison, Wisconsin 53706
email=thompson@PSL.wisc.edu

Preliminary Draft
September 9, 1991

1 Design Goals

1.1 Introduction

This is an early collection of thoughts on the architecture and design of the optical fiber transmission system for trigger information from the detector to the Global Level 1 Processor (GL1P).

1.2 Assumptions

The essential assumptions are

- The SDC sends a total of 5000 trigger information channels to the GL1P.
- Each Trigger Information Channel uses a single optical fiber.
- The fiber lengths are [illegible].
- Each fiber and channel [illegible] optical trigger information.
- The Trigger Information [illegible] each originate in the SDC each crossing time (16 ns).
- The primary SDC crossing clock (16 ns nominal) originates from our point of view from the SDC as a clean pulse of fixed but not exactly determined length with a nominal period of 16 ns. (The SDC may actually receive a more noisy clock and perform some clean-up functions.) The nominal 16 ns period must be fairly stable with time, temperature, pressure, aging and all potential influences. We expect that the period stays within a range of 16.0 ± 0.5 ns.

- The Trigger Information delivered to the GL1P may have a phase drift relative to the 16 ns clock used by the GL1P. We expect that the phase may be skewed within limits:
  - the short term phase fluctuations are well within ±160 ps),
  - the long term phase drifts at a rate within ±500 ps/second.
- The Trigger Information must be delivered to the GL1C Modules which have 16 ns and $\frac{16.0}{18}$ = 889 ns clocks which, except for some slight slow phase drift, are synchronous with the SDC crossing clock and are very close from GL1C Module to Module.
- the skew of each of the 5000 signals relative to the clock of the receiving logic has three parts due to a variety of causes. Some likely standard deviations in the skew of the data relative to the clock are guessed below.

Part	Cause of skew contribution	Standard deviation Contribution ns
skew of production of signal:		
	Wander of the Detector's 1.125 GHz PLL circuitry from crossing clock	$\sigma_1 = 0.115$
skew of the delivery of signal to receiving logic:		
	temperature of the fiber	$\sigma_2 =$
	delay in optoelectronics	$\sigma_3 =$
	cut length of each fiber (we assume each fiber is cut to the same length within $\pm 0.2\%$ = ±0.4 m = ±2 ns?)	$\sigma_4 = 1.120$
	electronic delays in circuitry with age and temperature	$\sigma_5 =$
	threshold drifts with age and temperature	$\sigma_6 =$
skew in the delivery of the clock to the receiving logic:		
	Wander of the GL1P's 1.125 GHz PLL circuitry from crossing clock	$\sigma_7 = 0.115$
	The distribution of the clock to the 312 receiving 9U' modules may have a ± ns variation	$\sigma_8 =$

We need to know the total standard deviation. **Until we learn differently, we will assume σ_{total} = 3.0 ns for the signal/clock skews.**

We might expect the signal clock skews to have a nearly gaussian distribution, due to the multiple partly independent effects, with a $\sigma = 3.0$ ns and about only $\frac{1}{10000}$ of

the signals to have skews beyond $\pm 3.89\ \sigma = \pm 11.7$ ns. This would imply that the 5000 signals should fit in a range of 23.4 ns.

As a result, we will aim at a range of 28.4 ns (see section 2.6 on page 11).

- the potential causes of errors will be fast random noise in the optical detectors, a low level of synchronous crosstalk on each GL1P Module board and very slow level or attenuation changes. These may cause potential bit sampling errors and word delineation errors.
- Each trigger Information word of 16 bits has 2^{16} possibilities (ie no reserved bit combinations) with the words on some fibers being constant, the words on some fibers being all 0, the words on some fibers being all 1, the words on some fibers varying slowly, the words on some fibers varying unpredictably. In other words, the fibers carry completely general 16 bit integers.
- The architecture as well as the components must be chosen to match the goals with the minimum cost. For example, if each serial path were to cost $ 500, then the overall cost of 5000 × $500 = $2,500,000 would be very serious.
- The design and first trial circuit must be ready for testing by 1995 January (3.3 years away).
- The first full working circuit must be ready by 1995 July so that orders may be placed for all components.
- The 5000 circuits must be ready by 1996 January.
- At this time, we assume that
  - the actual physics measurements will have information fed out more slowly with high reliability and independently of this trigger information.
  - A few errors in the trigger are assumed to not introduce any bias and to not effect the physics conclusions.

With this assumption, the Trigger System will not need to have parity or other error checking or encoding or [illegible]. If some of the SDC architects decide that this Trigger Information is to be also used for some physics measurements, error detection will be required. The alternative of using some error checking is briefly considered in section [illegible] on page [illegible].

1.3 A Primary Problem

The Trigger Information will be coming with a wide variation in the skews or phase drifts of the 5000 signals. We must automatically follow the drifts with time and introduce controllable delays into each of the 5000 channel paths to automatically and reliably compensate for the drifts.

1.4 Differences from long distance communications

The main differences from normal long distance communications are that:

- We can use multimode fibers (check the most suitable fibers). The short lengths of multimode fibers can deliver a greater fraction of the laser light without much increase in the signal transition times and so can reduce the expense of the receivers. The larger diameter fiber cores can reduce the alignment problems of connectors for multiple fibers.

- We need not use monochromatic lasers because the optical dispersion in the short cables due to the finite width of normal lasing diodes will cause negligible increase in the signal transition times.

- We do not need each of the 5000 signals to carry the clock frequency (since all 5000 signals will have the same exact frequency). Instead, 2 to 4 additional fibers can be used to carry a primary 1.125 GHz clock and a 16 ns crossing clock (62.5 MHz) giving the primary word delineation.

  (Normal long distance communications use encoding (such as 4b 5b or 8b/10b), line framing with data scrambling with a suitable polynomial, odd parity insertion, etc to introduce a number of transitions from which a Phase Lock Loop (PLL) can maintain a steady clock.

  The added transitions increase the total bandwidth and, usually, long distance communications employ fairly complex methods to minimize the bandwidth increase yet give protection to the clock against the expected forms of noise which may otherwise confuse the clock recognition. In long distance communications, the major costs are those of the actual long lines and so it is rational to use complex signal generation and detection.)

  For the SDC, the costs of the 5000 signal lines are small and so, when compared with long distance communications, we will
  — use a little more bandwidth as a tradeoff to
  — simplify the sending and receiving electronics.

- Each signal needs to carry phase information for its clock and word delineation relative to the primary 1.125 GHz clock and word delineation. This phase information for each signal line will change very slowly (but will have noise).

- We can tolerate a higher Bit Error Rate such as $BER = 10^{-9}$ erroneous bits but instead of the BER of 10^{-10} to 10^{-12} which long distance communications need. At this BER, 5000 channels of 16 bit words will spoil a $16 \cdot 5000 \cdot 10^{-9} = 8 \cdot 10^{-5}$ fraction of the events.

- We can use a computer to read the multiple signal levels and skews then make adjustments to the transmitters or receivers.

  (Normally, in long distance communications, only 1 or 2 lines exist and it is not economic for a computer at the receiving end to be used for the 1 or 2 lines and not practical for that computer to control the distant transmitter.)

- We can use the equivalent of signal DC coupling since we will not have intermediate amplifiers.

  (Normally, optical long distance signals pass though a number of amplifiers and have the equivalent of AC coupling.)

1.5 Differences from normal Electronics

The main differences of the optical fiber method from the normal methods using electronics to bring signals out of earlier detectors are worth listing.

Positive:

- The fibers are far more compact than coaxial cables.

- The attenuation of a 1 Gb/s signal is much less in glass fiber than in thick or thin coaxial cable.

- No noise is introduced in fibers if the detector ground is poor or the signals must be taken past extremely noisy electronics, magnetic fields or electric fields.

- Similarly, no crosstalk exists between fibers whereas, if a long low cost coaxial cable is laid as part of a dense bundle of similar cables, it is difficult to suppress all crosstalk of the synchronous transitions.

Negative:

- It is more difficult to change the routing of fibers than coaxial cables.

- The optical drivers and detectors are more expensive than equivalent electronic drivers and detectors. We note the optoelectronic costs will fall a factor of 2 each year. After rescaling some constant percentage of the 532 MBaud presented in the Fibre Channel Working Committee [illegible] we note the cost of a 1.2 Gbaud transmitter + receiver will diminish:

mid 1991	$3,000
mid 1993	$ 750
mid 1995	$ 190

  This is [illegible] the present [illegible] the projected cost using the last 3 years. The [illegible] is [illegible] a high risk in [illegible].

- The fiber optical signal levels will have more variation in generating or receiving the light levels:

  - The optical ZERO (low) level may be as much as chosen (item 11 but is usually set with some margin) to prevent the spoil in the fastest mode.
  - The optical ONE (high) level may be greater than the chosen threshold. However, due to the inability to precisely [illegible] set
    - each laser's output light level,
    - each connector's attenuation and

- each receiver's sensitivity.

  With sufficient precision, the differences between the logical ONE and the chosen threshold levels may differ by a factor of about 8. Further, as connectors are changed and lasers age, the ONE level can vary with time.

  Thus an optical signal may rise, from the low level of nearly no light, to a high level which will sometimes be about twice the threshold level and other times be about 8 times the threshold. Similarly, a signal fall may not pass the threshold until it has fallen to 6% of its ONE value. Thus, if a simple fixed threshold is used to receive the signal, then the "eye" sampling and edge detection can be badly distorted.

  (Normally, long distance systems use automatic gain control, AC coupling and polynomial scrambling to overcome this problem.)

- The use of pure serial information transmission requires a more stable clocking system than is usual in electronic systems with parallel data transfers. This stable clocking is necessary to transfer data which may have long runs of zeroes or ones without data signal transitions.

  (We hope to avoid the extra costs and bandwidth of 4b-5b or other encoding to increase the transition rates.)

  The large number of signals means that we must use a low cost simple method of compensating for clock signal skews.

- The fibers are more delicate than the coaxial cables. In order to retain the advantages of compactness, the fibers are normally protected by placing groups of 20 to 50 in strong cables.

- The fiber optoelectronics may have a lower radiation tolerance than normal electronics. This must be explored.

2 The Design

2.1 Tradeoffs

The general comments on this project compared with long distance communications and more customary electronics suggest we seek the following trade-offs:

- Use few discrete components.

- Use digital logic which can easily be placed in ASICs. This logic can be moderately complex so long as it uses few pins and little power. The ASICs also give the advantages of minimum propagation time gate and minimum cost gate.

- Use simple analog methods rather than extensive digital methods to accumulate some drift information.

- Use analog ADCs to accumulate information on the slow drifts without much cost.

- Use slow readouts with a narrow bus to monitor slowly drifting thresholds and signal delays and make adjustments in both the transmitting electronics on the SDC and the separate GLIP modules.

- Use a distant low cost computer to read the narrow bus and analyze the slow drifts and make slow changes to compensate for these. This will allow a slow bus, with few cables, to sequentially address the circuitry of each signal's transmitter and receiver to read the drifts and make compensations. Such checking could be done once per second with 200 μs being used for each signal.

- The same method would allow several milliseconds to recover any loss of word synchronization and several seconds to attain word synchronization upon powering up.

- Adjust the delay of the Trigger Information arriving at the Trigger Logic modules rather than adjust the clock used for each signal. In other words, ensure that the 16 bit integers are delivered into parallel circuitry of the trigger exactly (or at least within about ± 500 ps) when most suitable for the common word clock of the trigger circuitry.

2.2 A Possible Configuration

In the [illegible] we suggest a method [illegible] each fiber:

- ONE threshold adjustment (see section 2.4 on page [illegible]) for both a gain adjustment
- ONE fine delay adjustment (see section [illegible] on page [illegible]) to give adjustment [illegible] up to ± 3.0 ns and
- ONE coarse delay adjustment (see section 2.6 on page [illegible]) to give adjustment of up to ± 24.2 ns

The method may be integrated with a separate computer being used to measure some very slow analog levels and providing updates on the adjustments on a 200 millisecond basis. Much of the circuitry has been chosen to be suitable for ASICs to reduce the volume, reduce the number of discrete components and speed the performance. Even so, we must place emphasis on using simple principles.

The method uses the following:

1. On the SDC, receive the 16 ns period Crossing Clock and use an 18x multiplier with a phase lock loop (PLL) to generate a synchronous 1.125 GHz clock with a relative skew variation from the Crossing Clock of less than ±200 ps ($\sigma_t = \frac{100\ ps}{\sqrt{11}} = 115\ ps$).

   Use the Crossing Clock to transfer Trigger Information in parallel words. Use the 1.125 GHz clock to shift information serially.

2. send the information of each of the 5000 channels in 18 bit quantities at 1.125 Gbaud with each 16 bit integer of data followed by 2 marker bits a,b where b=1-a. In other words, ab = 01 or 10.

   The "a" bits are derived from a ROM as described on page 11.

3. For each channel, use a lasing diode with a 3 dB frequency of 1.7 GHz to give only a 3 dB drop in the optical power signal current ratio (measured in mW/mA) at the 3rd harmonic of the worst case 1.125 Gbaud signal ..0101010101010101.. We do NOT propose to search for the most economical lasers at this time.

4. transmit the light across a multimode fiber rather than single mode fiber to use the most economical receiver for each channel.

5. receive the light at the GL1P from each fiber in a PIN diode or APD of moderate sensitivity. Again, the sensitivity should have only a 3 dB drop at 1.7 GHz in the current optical power ratio (measured in mA/mW). The laser-receiver combination may thus have a 6 dB drop or a factor of 2 drop in the 1.7 GHz component of each overall signal transported out from the detector. This will imply a significant phase change in the 1.7 GHz region but will still give a fairly good "eye" signal for sampling at 1.125 Gbaud. We do NOT propose to search for the most economical receivers at this time.

6. deliver the fast analog signal into a difference amplifier which compares the signal with a threshold level (see section 2.4 on page 9). The choice of ECL, PECL or other logic levels cannot be made yet.

7. deliver the electrical signal into an analog delay line 2 ns long with 16 taps (125 ps per tap). This delay may be made part of the board by using a suitable etched or multiwire layout.

8. Select from the taps with a 16:1 multiplexor. The multiplexor is actually the first part of a decision circuit which forces the analog signal into digital states with transitions between them. The multiplexor selection is controlled by the fine delay adjustment to give an adjustment of ±1 ns. The fine delay detection and control are described in section 2.5 on page 10.

9. then feed the signal into a 32 stage shift register. The input to the shift register acts as the second part of a decision circuit. The shift register is clocked by the 1.125 GHz clock of the trigger logic circuitry and so is effectively 28.4 ns long.

   Hereafter, the signal is digital and synchronized with the clock of the trigger logic circuitry.

10. Select the signal from one of the shift register outputs by a 32:1 multiplexor with the resolution of 889 ns. The selection is controlled by the 5 bit coarse delay adjustment over a range of ±14.2 *ns*. The coarse delay detection and control are described in section 2.6 on page 11.

11. deliver the signal into an 18 bit shift register which presents 16 bits of information each 16 ns to following circuitry.

12. Pick the subset of most crucial information and send it on three fibers with the receiver having a vote circuit to give reliability. This might be useful for, say, 1% of the signals and 3% of the fibers.

2.3 Analog Voltages

Each of the 5000 signals are monitored by a multiplexing ADC system which is described later in section 2.7 on page 13. Each signal produces 7 analog levels and the threshold used for the digital decisions is an 8th analog level. The ADC system will monitor all 8 analog levels which are listed here for the *ith* signal for all 5000 signals (i = 1..5000). The generation and use of each analog voltage are described later.

1. $V_{High\ Level}(i)$
2. $V_{Low\ Level}(i)$
3. $V_{Threshold}(i)$
4. $V_{Fine\ Early}(i)$
5. $V_{Fine\ Late}(i)$
6. $V_{Coarse\ Early}(i)$
7. $V_{Coarse\ Error}(i)$
8. $V_{Coarse\ Late}(i)$

2.4 Threshold Control

The incoming signals will have a ZERO level which changes very little and, from circuit to circuit, has little variation. However, the ONE level will vary greatly.

The simplest ways are:

- to use two back to back junction diodes (or equivalent) to charge discharge a small capacitor for each signal. This circuitry uses the most positive and most negative excursions of the signal to define the mid-level which can the be used as a threshold.

- to use an multiplexing ADC to read the high and low signal levels. In this case, the signal passes two fast diodes or FET gates which produce two analog voltages $V_{High\ Level}(i)$ and $V_{Low\ Level}(i)$. The supervising computer reads these two voltages uses a multiplexing DAC to charge a capacitor with the threshold $V_{Threshold}(i)$. The computer can also read the threshold voltage $V_{Threshold}(i)$ as a check.

In each case, the capacitor is used to provide the comparison voltage or "threshold voltage" at the receiving difference amplifier. At this time, the second method seems preferable.

2.5 Fine Delay Control

16 steps of 125 ps each, range of ±1.0 ns
— TO BE EXPANDED WITH DIAGRAM —

1. The light levels for the "a" and "b" bits on each fiber will give four services for each signal:

   - give sufficient indication for any threshold (or automatic gain control) to function
   - give a clear indication of the 0 and 1 binary levels.
   - give a clear clock phase synchronization
   - give a clear word synchronization

2. Perform phase detection on the bits a,b to select the info from a tapped delay line 2 ns long.

3. Use 3 D flip-flops #1, #2 and #3, for each signal. Feed the signal in parallel to the 3 D inputs and feed the clock advanced by 0.2 ns to the Clk input of flip flop #1, the clock directly to #2 and the clock delayed by 0.2 ns to #3. The Q outputs are fed in pairs, from #1,#2 and from #2,#3 into two fast (ECL?) Exclusive ORs. The two Exclusive OR outputs are fed, via two resistors into two capacitors to produce two analog levels $V_{Fine\ Early}(i)$ and $V_{Fine\ Late}(i)$ which can be read by a slow multiplexing ADC.

   The difference between the $V_{Fine\ Early}(i)$ and $V_{Fine\ Late}(i)$ voltages on the 2 capacitors for the *ith* signal will indicate the average time between the fast *ith* signal transitions and the fast GL1P 889 ns clock transitions if these are within 0.4 ns. If the clock and *ith* signal transitions are very close, then the 2 voltages will be nearly the same for all data patterns.

   The signal is sampled in the mid-period of this clocking.

4. The 2 ADC values for each signal are read each 200 millisecond by a computer.

5. The computer considers the difference between the 2 ADC voltages as being proportional to the product $N_{TR}(i) \cdot \Delta t(i)$.

   $V_{Fine\ Early}(i) - V_{Fine\ Late}(i) \propto N_{TR}(i)\ \Delta t(i)$

   where

   - $\Delta t(i)$ is the drift skew between the ith signal and the Trigger Logic clock and

   - $N(i)$ is the average number of transitions/18 bit word in the ith signal – a number in the range between −1.75 and −18.0 because the (a,b) combination guarantees at least 7 transitions per 4 words (see later) (and guarantees at least 1 transition per word) and can have 18 transitions in words of 010101010101010101.

   Thus

   $\Delta t(i) \propto \frac{V_{Fine\ Early}(i) - V_{Fine\ Late}(i)}{N_{TR}(i)}$

   Although $N_{TR}(i)$ will vary unpredictably with i and time, the computer can assume $N = 12.0$ to make a small change without divergence and change the 4 bit selection given to the multiplexor of the fine delay from $t(i)$ to $t(i) - \Delta t(i)$.

6. By repeating the above steps, the computer can converge on the optimum value 4 bit multiplexor value which gives nearly equal values from the 2 ADCs for this signal.

2.6 Coarse Delay Control

32 steps of 889 ps each, range of ±14.2 ns
— TO BE EXPANDED WITH DIAGRAM —

1. Each of the 5000 signals leaving the SDC detector have 2 identical (a,b) bits included in each 18 bit word.

2. Each 4 words (each 64 ns), the SDC collidine detector electronics changes the 2 (a,b) bits in to give a clear word delineation. The (a,b) bits can be obtained at the detector from a simple single 256 deep ROM. The address of this ROM is incremented each 4 words (each 64 ns) with a full cycle of a pseudo-random pattern being made each 256 addresses in a time of 16.4 *us*.

   Full Cycle Time = 18 *ns word* × 16 *words /address* × 256 *addresses* = 16.4 *us*

   The "a" bits could be from a 256 deep ROM with a pseudo-random pattern so that the sequence of bits constitutes a repeating pattern which has 2^{256} possibilities. Even if the word delineation is temporarily lost, it can be recovered within a few milliseconds and is very unlikely to be tricked by random data.

   $2^{256} = 1.16 \times 10^{77}$ *years*

   The "b" bits are defined as the complement of the "a" bits so that each word has at least 1 transition and are changed only every 4 words to increase the number of transitions so that each 4 words have at least 7 transitions. All of the sending transmitters use the same ROM or use identical synchronized ROMs so that all Trigger Information words have the same (a,b) bits at the same instant, with the (a,b) bits being changed each 256 ns.

3. The word delineation selects the serial Trigger Information from a tapped shift register with 32 bits to cover the ±14.2 ns variation.

   This coarse delay has a resolution of $\frac{28.4\ ns}{32} = 889$ ps which is less than half the 2 ns full range of the fine delay so that, as a check, at least two pairs of fine and coarse delay values can be checked against each other.

The circuit is drawn as a shift register with a 32:1 multiplexor but is really a combination with simplified circuitry.

4. The word delineation is operated from a simple 5 bit register with very slow correction (see later)

5. The same ROM in the SDC also sends the (a,b) bits via a secure path to the Trigger Logic. This "secure path" has not been designed yet.

   [Alternatively, the Trigger Logic may use an identical ROM with an address counter which is synchronized with that of the SDC.]

6. Thus the Trigger Logic expects each Trigger Information word to have two bits called (x,y) which always equal the expected (a,b) bits.

   If the Trigger Information words have correct word alignment, two bits (x,y) in each word will always equal (a,b). However, during power-up or after a large disturbance, the words may not have alignment. The remainder of this section describes how alignment may be recovered.

7. Each signal has 3 binary comparitors to compare:

   - the 4 bits (w,x,y and z) of each signal word where (x,y) are in the position where the (a,b) bits are expected and
   - the 2 bits (a,b) from the ROM

   Thus, 3 comparisons are made of (w,x), (x,y) and (y,z) with (a,b).

8. Consider the values obtained by one of the Exclusive OR comparisons of the incoming supposed "a" bit of the Trigger Information with the expected "a" bit of the GLIP

   - If the words are aligned, then the comparison will give a consistent Exclusive Or output EXO=0
   - If the words are misaligned by 1 bit so that the expected "a" bit falls on the "b" bit of the data words, then the comparison will give a consistent EXO=1
   - If the words are misaligned by 1 whole word, so that the expected "a" bit falls on a random "a" bit belonging to the next or last word for 1/4 of the cases, then the comparison will give a consistent mean $m_{EXO} = 0 - \frac{0.5}{4} = \frac{1}{8} = 0.125$ and $\sigma_{EXO} = \sqrt{\frac{1}{4}0.5^2 + \frac{1}{4}0.5^2} = \frac{0.5}{\sqrt{4}}\sqrt{3-3^2} = \frac{1}{2\sqrt{8}}\sqrt{12} = 0.10825$
   - If the words are otherwise not aligned, then the comparison will give a distribution of 0's and 1's with a mean of $m_{EXO} = 0.5$ and a $\sigma_{EXO} = 0.5$

   Now consider averaging a number N of these samples and take the value of N=2500 words which would take a time of $2500 \times 16\ ns = 40\ \mu s$. Successive samples may have different averages. The distribution of the sample averages will have a mean m_{comp} with a standard deviation σ_{comp} for these four cases σ_{mean}

   - If the words are aligned, then the comparison will give a consistent sample mean $m_{comp} = 0$ and $\sigma_{comp} = 0$

   - If the words are misaligned by 1 bit so that the expected "a" bit falls on the "b" bit of the data words, then the comparison will give a consistent mean $m_{comp} = 1$ and $\sigma_{comp} = 0$
   - If the words are misaligned by 1 whole word, so that the expected "a" bit falls on a random "a" bit belonging to the next or last word for 1/4 of the cases, then the comparison will give a consistent mean $m_{comp} = 0.125$ and $\sigma_{comp} = \frac{\sigma_{EXO}}{\sqrt{N}} = \frac{0.10825}{\sqrt{2500}} = 0.002165$

     The likely hood of any sample being near 0.0 is that of being beyond $\frac{0.125}{0.002165}\sigma = 57\ \sigma$ – extremely small.

   - If the words are otherwise not aligned, then the comparisons will give a mean $m_{comp} = 0.5$ and $\sigma_{comp} = \frac{\sigma_{EXO}}{\sqrt{N}} = \frac{0.5}{\sqrt{2500}} = 0.01$ The likely hood of the average of any sample being near 0 or near 1 is that of being beyond 50 σ – extremely small.

   Thus a simple analog test on the sample average will indicate alignment or misalignment.

9. The 3 comparitors charge or discharge 3 small capacitors through resistors with an $RC \approx 1$ *millisecond* to voltages defined as $V_{Coarse\ Early}(t)$, $V_{Coarse\ Expected}(t)$ and $V_{Coarse\ Late}(t)$

12. A multiplexing ADC can read the 3 capacitor voltages. The accuracy should be sufficient to readily distinguish between $m_{comp} = 0.125$ and $m_{comp} = 0$

11. As with the Fine Delay control above, a control computer reads the ADC values each 200 milliseconds. If the words are still aligned (ie the word delineation is correct) then the (w,x), (x,y), (y,z) comparisons should be giving a maximum value for the ADC readings.

    If alignment has been lost, then realignment can be made by slowly incrementing or decrementing the 5 bit word alignment and monitoring the 3 comparison ADC readings.

    This adjustment will be very slow (seconds) and can be quite slow with 200 millisecond sampling. Allow a few seconds for normal changes within a second or two.

Of course the numbers given for the 32:1 multiplexor, 16 bits Trigger Information words, sampling periods and the 5 bit word alignment register are subject to change. However, I think the principle is fairly easy to implement. However, I think the principle is fairly easy to implement.

2.7 ADC System

A simple low cost primary ADC system and computer are used to read all analog levels and control the adjustments of receiving signals' strength in the GLIP. We assume that each of these boards has a multiplexing ADC which can read the 3 levels of $V_{Coarse\ Early}(t)$, $V_{Coarse\ Expected}(t)$ and $V_{Coarse\ Late}(t)$ for all 16 signals. The choice of the ADC or ADCs and analog multiplexing have not been made.

[We assume the time for the computer to read each value is 5 μs. Thus the total time to read all 8 levels for all 5000 signals is

Total Time = $5000 \times 8 \times 5\ \mu s = 200\ ms$.

We assume the ADCs are triggered sequentially then read sequentially so that if each measures 16 analog voltages in a staggered manner, the ADC conversion time can be as long as $\frac{200\ ms}{16} = 12.5\ ms$. Obviously, if the drifts and unexpected errors occur more frequently than once per minute, we may consider a faster readout method with a faster computer or, perhaps, several computers working in parallel and so should probably use ADCs with a conversion time less than 1 millisecond.

The accuracy of 8 bit ADCs may be sufficient and each 9U board may use 8 simple National ADC0817 8 bit 16-channel 28 pin ADCs. These have a conversion time of 100 μs. However, a more compact configuration may be found.]

2.8 Implementation

- Have 16 optical receiving circuits on half of a 9U circuit board. The other half of each board will be used by trigger circuitry.
- Use 1300 nm light since the lasers for these have the least cost.
- Require no special supply voltages

More to be added.

2.9 A Proposal for a Proof of Principle

Before any major commitment or major design effort is made, it will be important to show the elementary circuits can operate this way at 1.125 Gbaud. While the proof need not use the perfect circuitry, it is important to show

- that such 15 bit words can be easily generated and turned into a serial 1.125 Gbaud stream
- that some existing lasers can emit the signals across 200 meters of fiber
- that some existing multifiber connectors are suitable for the 200 meter fibers. We anticipate 4 to 6 connectors for each signal line
- that some existing receivers can receive the signals with a reasonably low BER
- that the use of one of the following methods is practical to allow for the variable signal size. We will compare 4 methods of stabilizing the threshold crossing
  - remotely controlling the laser output gain
  - use back to back diodes. This will require some care with junction capacitance.
  - adjustment of the threshold voltage in a receiver's difference amplifier
  - use a full DAC to provide the threshold voltage.
- that the fine delay control can work

- that the coarse delay control can work
- that some known information can be demonstrated to transferred without errors

We will plan an ASIC to compress the circuitry for several signal channels

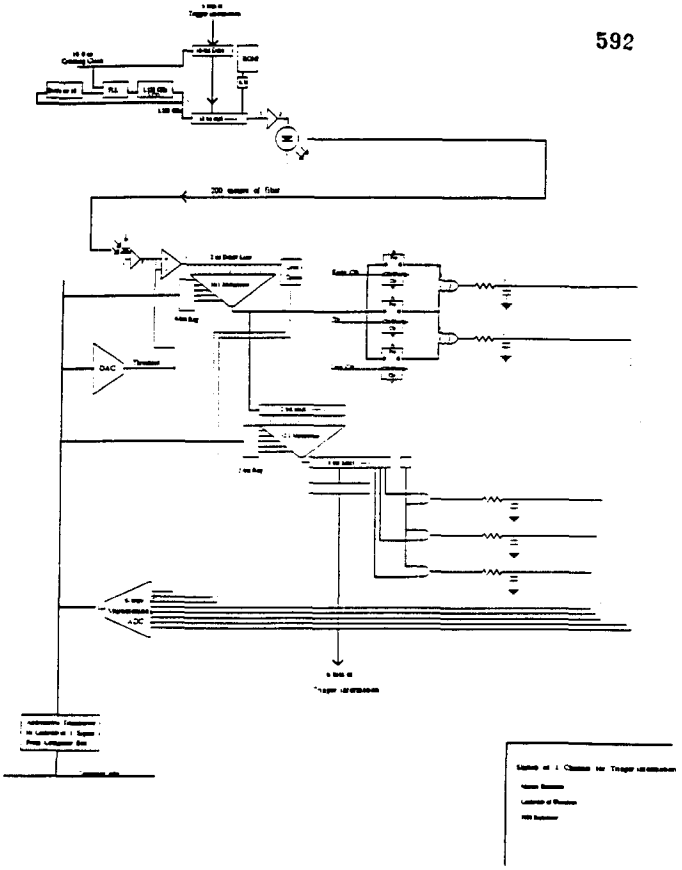
Note that this is ONLY a proof of principle — NOT a prototype!

It is at least as important to state what will NOT be done in this "Proof of Principle"

- We will NOT make any final selection of the laser
- We will NOT make any final selection of the optical receiver
- We will NOT make any ASIC yet

The reason for these omissions is that we expect considerable progress to be made in industry, under the thrust of HDTV and accelerating communication nets, during the next 2 years. We will propose a separate development in 1993 for the selection of the most suitable lasers and receivers.

If this Proof of Principle can be demonstrated with discrete components on two small circuit boards joined by a fiber, then a later step to convert it to an ASIC design (NOT proposed here) could be taken with more confidence.



2.10 Alternative with Error Detection

Although not planned now, Error Detection may be needed for two reasons.

1. In the general thrust to use low cost components at high bandwidths with marginal transmitting and receiving electronics, and the thrust to commit the use of some components which have just been created and incompletely tested, we may be forced to use components or methods which are imperfect.
2. If the "Trigger" information is to be also used for physics measurements, we will certainly need error detection.

Errors in digital systems have a different effect from the effect of errors in an analog system. A glitch in an analog system can cause an error, in say an Energy, with the size of the error in the Energy being proportional to the size of the glitch. However, a glitch in a digital system can cause an error in the Energy which is as large as half the maximum energy.

The most simple error detection method is to use byte parity which means that the bandwidth requirement is increased from 1.125 Gbaud without parity to 1.250 Gbaud with parity. Various other methods exist – for example, the 4b 5b and 8b 10b encoding methods but that of simple parity appears to have a lower cost.

Any conclusion must await further information of cost trade-offs and the likely forms of errors. For example, early questions are:

"Are double errors likely?"

"Is the extra cost to operate the lasers and receivers with 1.25 Gbaud instead of 1.125 Gbaud less than the cost saved if the circuitry for clock detection can be simplified?"

For the moment, we assume that any error detection would use 20 bit words:

```
 16 bits of data
  2 bits of odd parity
  2 bits  a,b  for word delineation
-----
  20
```

2.11 Most Important Now

At this stage I would appreciate any feedback. While the circuitry can be fun, the most important things are the initial assumptions. I would greatly appreciate any feedback on the initial assumptions.

---

file=seedfibers.txt

2.12 Summary

1. Use signal optoelectronics with a frequency, above which a 3 dB loss of gain occurs, of 1.7 GHz to preserve the waveform of the worst case 1.125 Gbaud signal of ..0101010101..
2. Use multimode fiber with a core diameter of about 60 microns to allow the use of the lowest cost optoelectronics.
3. Use words of 18 bits to carry both the 16 bits of information and two bits (a,b) with b=1-a. The (a,b) bits have the purposes of delineating words and allowing slight drifts and threshold shifts to be measured. The (a) bits are from a long fixed pseudo-random sequence which has a mean time for appearing in random data of 3.68×10^{06} years.
4. Allow the information in the words of each channel to be constant, all zeroes, all ones or change with no "forbidden values".
5. Use three adjustments for each signal:
   - a Threshold Adjustment for each receiver,
   - a Fine delay Adjustment with steps of 125 ps and
   - a Coarse delay Adjustment with a range of ±14.2 ns.
6. We expect the high signal level to vary from signal to signal and to vary with time due to the use of low cost lasers and detectors and the use of imperfect optical connectors. The high signal levels and low signal levels are recorded by 2 diodes and 2 capacitors for each of the 5000 signals. The 2 voltages will be used to determine the threshold for each signal.
7. The Fine delay Adjustment uses a tapped delay line with a 16:1 multiplexor and 3 fast decision circuits latching the signal just before the clock, at the clock and just after the clock. Signal transitions before and after the clock cause the charge on 2 corresponding capacitors to be incremented so that the difference of voltages on the 2 capacitors indicates the relative phase of the clock and signal transitions.
8. The Coarse delay Adjustment uses a 32 long shift register with a 32:1 multiplexor and uses 3 capacitors to collect the agreements of the signal's pattern of (a) bits with the expected pattern. During power-up or after timing errors are found, the 5-bit selection is changed until agreement of the signal and expected (a) bit patterns is found.
9. Use a multiplexing slow 8 bit or 10 bit ADC system with 128 inputs on each SU board to read 8 analog levels produced by each of the 16 incoming Trigger Information signals. Similarly, use a multiplexing DAC to adjust the thresholds of the receiving circuits for each of the 16 signals on each SU board.
10. Use an external computer with a 16 bit address, 16 bit data bus to sequentially and slowly monitor the status of the analog voltages produced by all 5000 signals. The computer makes changes when necessary to the Threshold, Fine and Coarse adjustments. This can both permit secure word and bit alignment during power up and recovery after major disturbances.

Muon System

Technical Proposal Chapter 7 - Outline	G. Feldman(Harvard)
Momentum Resolution, Cosmic Ray Trigger Rates	H. Iwasaki(KEK)
Octagonal Geometry Effects	J. Wiss(Illinois)
Forward Muon Chamber Rates and the Optimal Beam-Pipe/Absorber Design	A. Kulik(Protvino)
Study of the Muon Trigger Efficiency	V. Molchanov (Protvino)
Scintillation Counters for Muon Trigger System	V. Rykalin(Protvino)
Muon Scintillator R&D Activities at Michigan	R. Thun(Michigan)
Prototype of Foam Support for Muon Tubes	A. Sill(Rochester)
Finite Element Modelling of Muon Detector Module	C. Daly(Washington)
Experience with Short Drift Tubes	T. Zhao(Washington)
Forward Muon System	A. Skuja(Maryland)
Design of the Jet Cell Chamber for the SDC Muon Detector	S. Terada(KEK)
A Short Comment on Descoping of the Muon Chamber	Y. Asano(Tsukuba)
Progress in Wisconsin	D. Carlsmith (Wisconsin)
SDC Muon Simulation at Illinois	S. Errede(Illinois)
Muon Beam Tests	H. Lubatti (Washington)
Report on Beam Test Work	S. Errede(Illinois)

LPBautz:11/4/91

Technical Proposal Chapter 7 - Outline

G. Feldman(Harvard)

FELDMAN

Technical Proposal Chapter 7

Muon System

1. Introduction - Feldman
   - Conceptual design
   - Physics requirements - Willis
   - Trigger at conceptual level
2. Scintillation counters - Thun
3. Cherenkov counters - Nauenberg
4. Central chambers - based on CDR of chosen technique
5. Forward chambers - Skuja
6. Central toroid - Cherwinka, Western
7. Forward toroid - Dittert
8. Alignment - Early

Cost, schedule, assembly, electronics are probably elsewhere in the TP.

Momentum Resolution, Cosmic Ray Trigger Rates

H. Iwasaki(KEK)

Hiro Iwasaki (KEK)
SDC Collab. @ORNL
26-28/Sep/91

I. Momentum Resolution

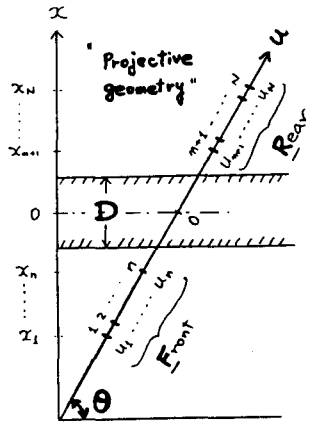
I-1. Formula of σ_{Pt}/P_t
I-2. σ_x (BW1) dependence
I-3. Lever arm (BW2 - BW3) dependence
I-4. Summary of σ_{Pt}/P_t

II. Trigger rates by Cosmic μ

II-1. L1 rate at the sea level
II-2. L1 rate in the underground
II-3. Summary of the trigger rates

II. Momentum Resolution

I-1. Formula of σ_{P_t}/P_t



$$u_i = \frac{x_i}{\sin\theta}$$

$$\frac{\sigma_{P_t}}{P_t} = \frac{P_t}{2B_0 D}\left[\sin^2\theta\,\frac{f_3}{\det(\alpha')} + \theta_s^2\left(1+\frac{D^2}{12}\left(\frac{f_4}{\det(\alpha')}\right)^2\right)\right]^{1/2}$$

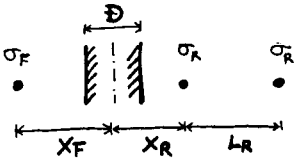
$$\theta_s = \frac{0.019}{P}\sqrt{\frac{D/\sin\theta}{X_0}}$$

$$P\theta_s = \sqrt{\sin\theta}\cdot 0.019\sqrt{\frac{D}{X_0}} \propto \sqrt{\sin\theta}$$

$$\begin{cases} \det(\alpha') = [1]_{F+R}[x^2]_F[x^2]_R - [x]_F^2[x^2]_R - [x^2]_F[x]_R \\ f_3 = [1]_{F+R}[x^2]_{F+R} - [x]_{F+R}^2 \\ f_4 = [1]_F[x^2]_F[x]_R + [1]_R[x]_F[x^2]_R - [x]_{F+R}[x]_F[x]_R \end{cases}$$

$$[f]_F = \sum_{i=1}^{n_3}\frac{1}{\sigma_i^2}f(x_i), \quad [f]_R = \sum_{i=n+1}^{n_2}\frac{1}{\sigma_i^2}f(x_i)$$

601



$$\det(\alpha') = \frac{X_F^2 L_R^2}{\sigma_F^2\sigma_R^4}$$

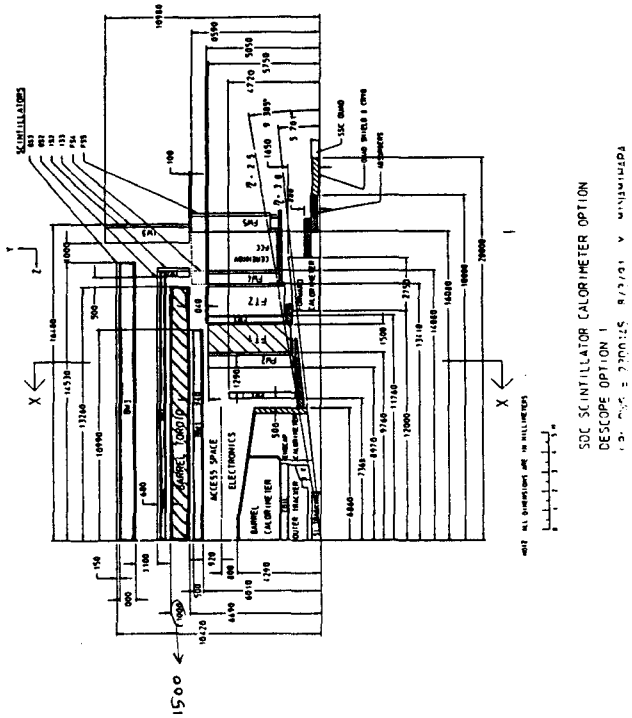
$$f_3 = \frac{L_R^2}{\sigma_R^4} + \frac{1}{\sigma_F^2\sigma_R^2}\left\{2X_F^2 + X_R^2 + (X_R+L_R)^2 + 2X_F(2X_R+L_R)\right\}$$

$$f_4 = \frac{-X_F L_R^2}{\sigma_F^2\sigma_R^4}$$

$$\frac{\sigma_{P_t}}{P_t} = \frac{P_t}{2B_0 D}\left[\sin^2\theta\,\frac{f_3}{\det(\alpha')} + \theta_s^2\left(1+\frac{D^2}{12}\left(\frac{f_4}{\det(\alpha')}\right)^2\right)\right]^{1/2}$$

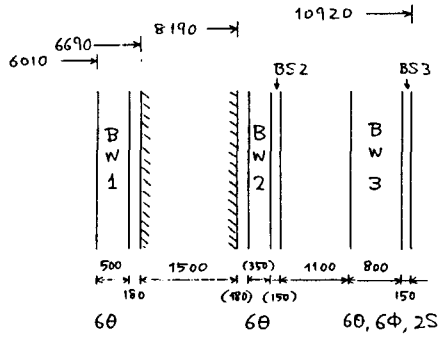
$$\begin{cases} \dfrac{f_3}{\det(\alpha')} = \dfrac{\sigma_F^2}{X_F^2} + \sigma_R^2\left(2\left(1+\dfrac{X_R}{X_F}\right)^2\dfrac{1}{L_R^2} + 2\left(1+\dfrac{X_R}{X_F}\right)\dfrac{1}{X_F L_R} + \dfrac{1}{X_F^2}\right) \\ \dfrac{f_4}{\det(\alpha')} = -\dfrac{1}{X_F} \end{cases}$$

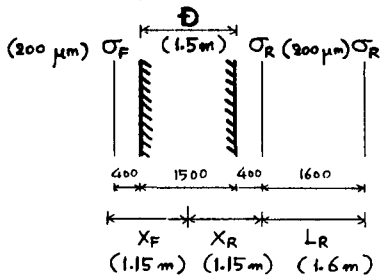
602



SDC SCINTILLATOR CALORIMETER OPTION
DESCOPE OPTION 1

603

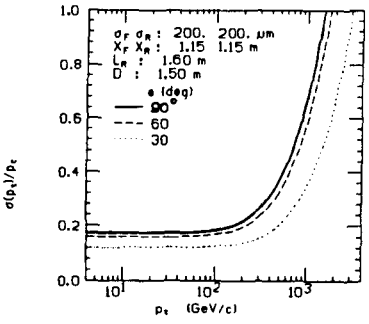




604

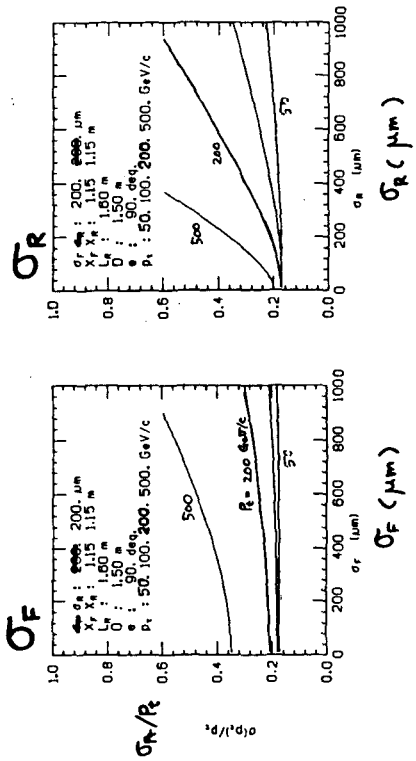
$\sigma_F = 200\,\mu m$
$L_R = 1.6\,m$

σ_{P_t}/P_t



605

I-2. σ_x (BW1) dependence



606

σ_F, σ_R

$$\frac{\sigma_t}{d\sigma/d\Omega} = \frac{\sigma_F^2}{X_F^2} + \sigma_R^2\left(2\left(1+\frac{X_R}{X_F}\right)^2\frac{1}{L_R^2} + 2\left(1+\frac{X_R}{X_F}\right)\frac{1}{X_F L_R} + \frac{1}{X_F^2}\right)$$

$$= \frac{1}{X_F^2}\left[\sigma_F^2 + \sigma_R^2\left(8\left(\frac{X_F}{L_R}\right)^2 + 4\left(\frac{X_F}{L_R}\right) + 1\right)\right]$$

$$= 0.756\left(\sigma_F^2 + \sigma_R^2 \cdot 8.0\right) \quad \left(X_F = X_R = 1.15\,m,\ L_R = 1.6\,m\right)$$

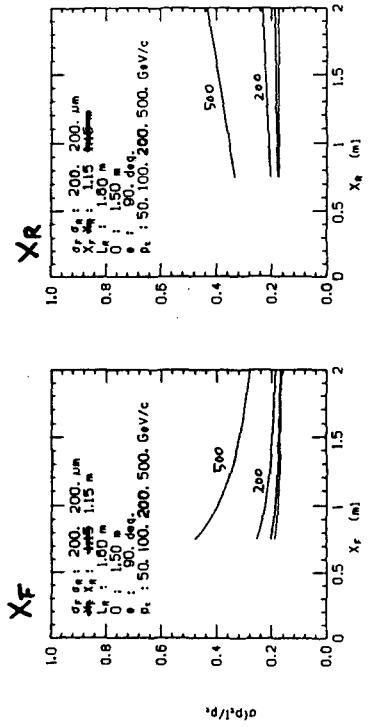
(same contribution)

$$\sigma_F \simeq 2.8\,\sigma_R$$

$$= 0.756\left(\sigma_F^2 + \sigma_R^2 \cdot 16.2\right) \quad \left(X_F = X_R = 1.15\,m,\ L_R = 1.0\,m\right)$$

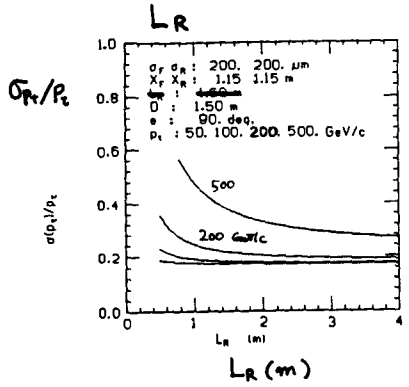
$$\sigma_F \simeq 4.0\,\sigma_R$$

607



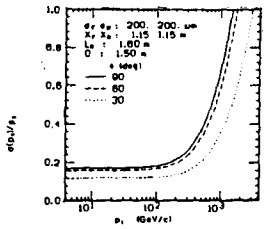
I-3. Lever arm (BW2 - BW3) dependence

10



$\sigma_F = 200\ \mu m$, $\sigma_R = 200\ \mu m$

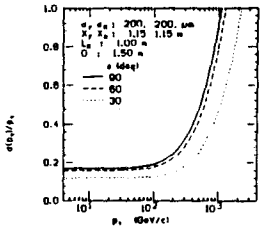
$L_R = 1.6$ m



$$\frac{\sigma_{P_t}}{P_t} = \left[(P_t \sin\theta \cdot 6.648 \times 10^{-4})^2 + (\sqrt{\sin\theta} \cdot 0.1701)^2 \right]^{1/2}$$

P_t(turn) = 263.9 GeV/c @θ = 90°
283.5 60°
373.1 30°

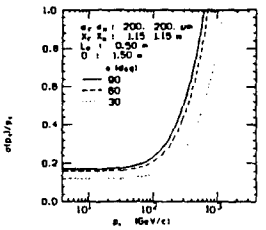
$L_R = 1.0$ m



$$\frac{\sigma_{P_t}}{P_t} = \left[(P_t \sin\theta \cdot 8.906 \times 10^{-4})^2 + (\sqrt{\sin\theta} \cdot 0.1701)^2 \right]^{1/2}$$

P_t(turn) = 191.1 GeV/c @θ = 90°
205.3 60°
270.2 30°

$L_R = 0.5$ m



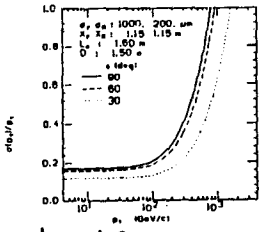
$$\frac{\sigma_{P_t}}{P_t} = \left[(P_t \sin\theta \cdot 1.572 \times 10^{-3})^2 + (\sqrt{\sin\theta} \cdot 0.1701)^2 \right]^{1/2}$$

P_t(turn) = 108.2 GeV/c @θ = 90°
116.3 60°
153.1 30°

12

$\sigma_F = 1$ mm, $\sigma_R = 200\ \mu m$

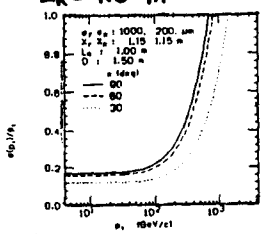
$L_R = 1.6$ m



$$\frac{\sigma_{P_t}}{P_t} = \left[(P_t \sin\theta \cdot 1.234 \times 10^{-3})^2 + (\sqrt{\sin\theta} \cdot 0.1701)^2 \right]^{1/2}$$

P_t(turn) = 137.8 GeV/c @θ = 90°
148.1 60°
194.9 30°

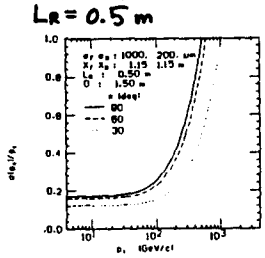
$L_R = 1.0$ m



$$\frac{\sigma_{P_t}}{P_t} = \left[(P_t \sin\theta \cdot 1.379 \times 10^{-3})^2 + (\sqrt{\sin\theta} \cdot 0.1701)^2 \right]^{1/2}$$

P_t(turn) = 123.4 GeV/c @θ = 90°
132.6 60°
174.5 30°

$L_R = 0.5$ m



$$\frac{\sigma_{P_t}}{P_t} = \left[(P_t \sin\theta \cdot 1.892 \times 10^{-3})^2 + (\sqrt{\sin\theta} \cdot 0.1701)^2 \right]^{1/2}$$

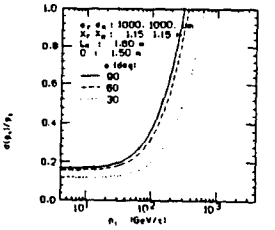
P_t(turn) = 89.9 GeV/c @θ = 90°
96.6 60°
127.2 30°

13

$\sigma_F = 1$ mm, $\sigma_R = 1$ mm

not acceptable

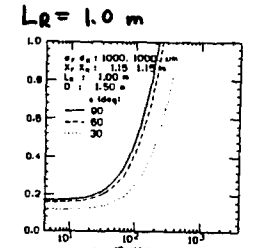
$L_R = 1.6$ m



$$\frac{\sigma_{P_t}}{P_t} = \left[(P_t \sin\theta \cdot 3.224 \times 10^{-3})^2 + (\sqrt{\sin\theta} \cdot 0.1701)^2 \right]^{1/2}$$

P_t(turn) = 52.8 GeV/c @θ = 90°
56.7 60°
74.6 30°

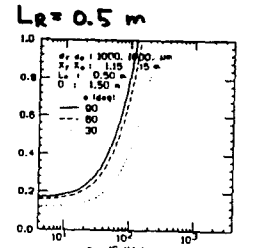
$L_R = 1.0$ m



$$\frac{\sigma_{P_t}}{P_t} = \left[(P_t \sin\theta \cdot 4.453 \times 10^{-3})^2 + (\sqrt{\sin\theta} \cdot 0.1701)^2 \right]^{1/2}$$

P_t(turn) = 38.2 GeV/c @θ = 90°
41.1 60°
54.0 30°

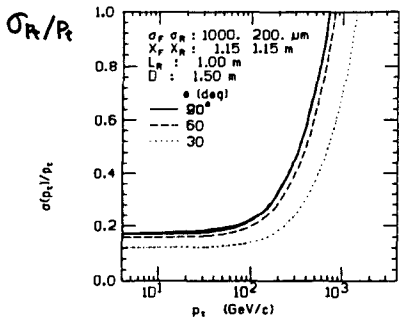
$L_R = 0.5$ m



$$\frac{\sigma_{P_t}}{P_t} = \left[(P_t \sin\theta \cdot 7.959 \times 10^{-3})^2 + (\sqrt{\sin\theta} \cdot 0.1701)^2 \right]^{1/2}$$

P_t(turn) = 21.6 GeV/c @θ = 90°
23.3 60°
30.6 30°

$\sigma_F = 1$ mm
$L_R = 1.0$ m



$$\sigma_{P_t}/P_t\left(\tfrac{1}{2}P_t\right) \simeq \sigma_{P_t}/P_t\left(P_t\right)$$

$\sigma_F = 1$ mm
$L_R = 1.0$ m

$\sigma_F = 200\,\mu$m
$L_R = 1.6$ m

I-4. Summary of σ_{P_t}/P_t

1. Present requirements :
   $\sigma(BW1) = \sigma(BW2, BW3) = 200\,\mu$m
   $L \equiv$ Lever arm (BW2 − BW3) = 1.6 m
   seems to be overspecification.

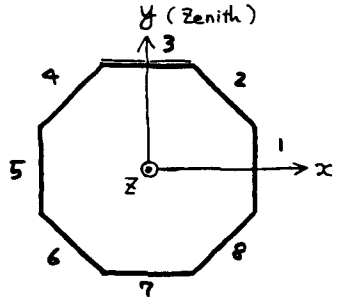
2. $\sigma(BW1) \simeq \sigma(BW2, BW3) \times (3 \sim 4)$
   is optimum. ($L = 1.6$ m, 1 m)
   - Alignment error of BW1 relative to BW2/BW3 can be $O(\lesssim 1$ mm).
     (Not order of $\sim 200\,\mu$m)

3. L dependence of σ_{P_t}/P_t is small.
   - if $\sigma(BW1) = \sigma(BW2,3) = 200\,\mu$m
     even $L = 0.5$ m is OK (?) ←
   - if $\sigma(BW1) \simeq 1$ mm
     $L = 1.0$ m is OK (?) ←

4. We need the answer to the question:
   " How much is the required σ_{P_t}/P_t for μ-IP ? "

II. Trigger rates by Cosmic μ

II-1. Level 1 Trigger rate by Cosmic μ at the sea level

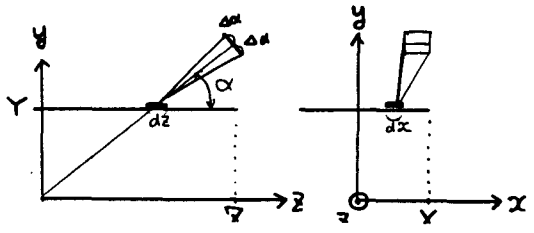


Θ : Zenith angle

$$j(\Theta) = j(0)\cos^2\Theta$$

dJ : flux crossing horizontal area, $dx\,dz$ from above

$$dJ = \int d\Omega \cdot j(\Theta)\cdot\cos\Theta\, dx\, dz$$



Cosmic Ray Fluxes

Review of Particle Properties
PL B239 (1990)

The fluxes of particles of different types depend at the ~ 10% level on the latitude, their energy, and the conditions of measurement. Some typical sea-level values[1] for charged particles are given below:

I_v flux per unit solid angle per unit horizontal area about vertical direction.
$\equiv j(\theta = 0, \phi)$ [θ = zenith angle, ϕ = azimuthal angle] ;

J_1 total flux crossing unit horizontal area from above
$\equiv \int_{\theta \le \pi/2} j(\theta,\phi)\cos\theta\, d\Omega$ [$d\Omega = \sin\theta\, d\theta\, d\phi$] ;

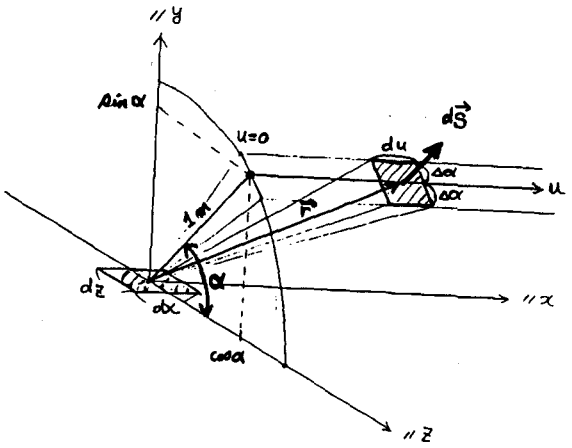
J_2 total flux from above (impinging on a sphere of unit cross-sectional area)
$\equiv \int_{\theta \le \pi/2} j(\theta,\phi)\, d\Omega$.

	Total Intensity	Hard Component	Soft Component
I_v	1.1×10^2	0.8×10^2	0.3×10^2 m^{-2} sec^{-1} sterad^{-1}
J_1	1.8×10^2	1.3×10^2	0.5×10^2 m^{-2} sec^{-1}
J_2	2.4×10^2	1.7×10^2	0.7×10^2 m^{-2} sec^{-1}

Very approximately, about 75% of all particles at sea level are penetrating, and are muons (the dominant portion of the hard component at sea level). The sea-level vertical flux ratio for protons to muons (both charges together) is about 3.5% at 1 GeV/c, decreasing to about 0.5% at 10 GeV/c.

The muon flux at sea level has a mean energy of 2 GeV and a differential spectrum falling as E^{-2}, steepening smoothly to $E^{-3.6}$ above a few TeV. The angular distribution is $\cos^2\theta$, changing to $\sec\theta$ at energies above a TeV, where θ is the zenith angle at production. The ± charge ratio is 1.25–1.30. The mean energy of muons originating in the atmosphere is roughly 300 GeV at slant depths $\gtrsim$ a few hundred meters. Beyond slant depths of ~ 10 km water-equivalent, the muons are due primarily to in-the-earth neutrino interactions (roughly 1/8 interaction ton^{-1} year^{-1} for $E_\nu > 300$ MeV, ~ constant throughout the earth).[2] Muons from this source arrive with a mean energy of 20 GeV, and have a flux of 2×10^{-9} m^{-2} sec^{-1} sterad^{-1} in the vertical direction and about twice that in the horizontal,[2] down at least as far as the deepest mines.

Sector "3" (top)



Zenith $(0, 1, 0)$

$\vec{r} = (u, \sin\alpha, \cos\alpha)$ $\qquad r = (u^2+1)^{1/2}$

$d\vec{S} = 2\Delta\alpha\, du\ (0, \sin\alpha, \cos\alpha)$

$d\Omega = \frac{1}{r^2}\frac{\vec{r}}{r}\cdot d\vec{S} = \frac{2\Delta\alpha\, du}{(u^2+1)^{3/2}}$

$\cos\Theta = (0,1,0)\cdot\frac{\vec{r}}{r} = \frac{\sin\alpha}{(u^2+1)^{1/2}}$

$$dJ = \int \frac{2\Delta\alpha\, du}{(1+u^2)^{3/2}}\ j(0)\cos^3\Theta\, dx\,dz$$

$$= 2\Delta\alpha\, j(0)\, dx\,dz \cdot \sin^3\alpha \underbrace{\int_{-\infty}^{\infty} \frac{du}{(1+u^2)^3}}_{\hookrightarrow \frac{3}{8}\pi}$$

$$\therefore dJ = \frac{3\pi}{4}\Delta\alpha\, j(0)\sin^3\alpha\, dx\,dz \quad \propto \sin^3\alpha$$

$$\sin\alpha = \frac{Y}{(Y^2+z^2)^{1/2}}$$

total flux

$$J = \int_{-X}^{X} dx \int_{-Z}^{Z} dz\ dJ$$

$$= \frac{3\pi}{4}\Delta\alpha\, j(0)\cdot 2X \underbrace{\int_{-Z}^{Z} dz\ \sin^3\alpha}_{\hookrightarrow \frac{2YZ}{(Y^2+Z^2)^{1/2}}}$$

$$\therefore J = 3\pi\,\Delta\alpha\, j(0)\frac{XYZ}{(Y^2+Z^2)^{1/2}}$$

$\begin{cases} j(0) = 0.8\times10^2\ m^{-2}s^{-1}sr^{-1} \ \text{(Hard comp.)} \\ X = (\sqrt{2}-1)Y \\ Y = 8.59\ m \\ Z = 14\ m \\ \Delta\alpha = 0.1 \end{cases}$

$\Rightarrow$ **$J \simeq 2.0$ kHz** (for sector "3" (top) at the sea level)

Sector "1" (side)

$\cos\Theta = \frac{-u}{(u^2+1)^{1/2}}$, $d\Omega = \frac{2\Delta\alpha\, du}{(u^2+1)^{3/2}}$

$$dJ = dx'dz'\, j(0)\, 2\Delta\alpha \underbrace{\int_0^{\infty} du \frac{u^3}{(u^2+1)^3}}_{\hookrightarrow \frac{1}{4}}$$

$$\therefore dJ = \frac{1}{2}\Delta\alpha\, j(0)\, dx'dz' \quad \propto \underline{\text{constant}}$$

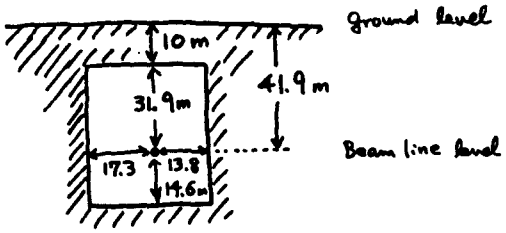
$$\therefore J = 2\Delta\alpha\, j(0)\, X\, Z$$

$\begin{cases} j(0) = 0.8\times10^2\ m^{-2}s^{-1}sr^{-1} \\ X = 3.558\ m \\ Z = 14\ m \\ \Delta\alpha = 0.1 \end{cases}$

$\Rightarrow$ **$J \simeq 0.8$ kHz** (for sector "1" (side) at the sea level)

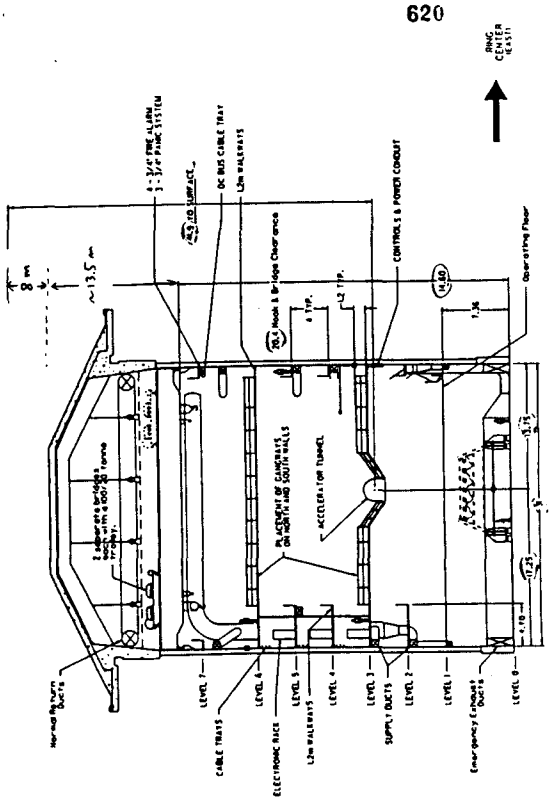
II-2. L1 rate by Cosmic μ in the underground

studied by Y. Teramoto



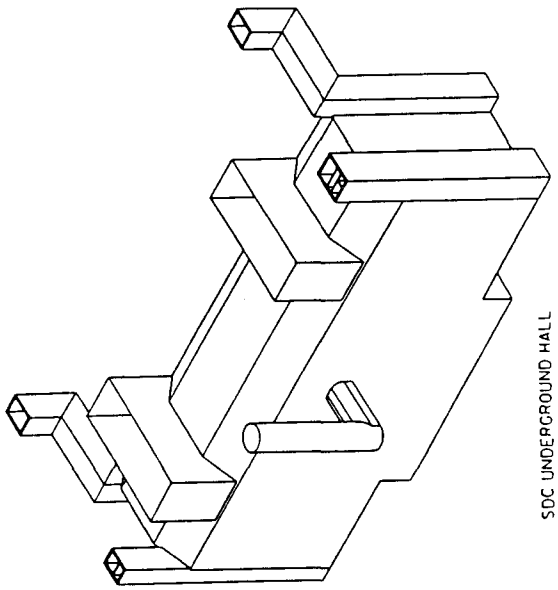
assumptions

- $\rho(\text{soil}) = 2.5\ g/cm^3$
- Exp. Hall is infinitely long along the beam line.
- $dE/dx = 2.0\ MeV/g\,cm^2$



BALL CANCHATS

FIGURE 4.1.2.4-a



SDC UNDERGROUND HALL

FIGURE 4.1.1-a

July 24, 1991

Cosmic Ray Muon Intensities at SDC

Y.Teramoto

Department of Physics, Osaka City University
3-3-138 Sugimoto, Sumiyoshi, Osaka 558, Japan

Cosmic ray muon intensities were calculated at SDC, assuming SDC locates 60 m.w.e.(meter water equivalent) depth underground. To calculate muon intensities at sea level, we used the equation[1]

$$I_\mu(P, z_0, \Theta) = A \cdot (I_{\pi\mu} + \frac{K}{\pi} \cdot I_{K\mu}) \cdot W(z_1) \qquad (1)$$

where P is the muon momentum in GeV/c, z_0 is the atmospheric depth at concero, which is 1033 g/cm^2 in this case, Θ is the zenith angle, and $\frac{K}{\pi}$ is the production ratio of kaons and pions. The muon intensities from pions, $I_{\pi\mu}$, is

$$I_{\pi\mu} = \frac{B_\pi}{1 - r_\pi^2} \cdot \left| \frac{P_1^{-\gamma}}{\gamma B_\pi + (\gamma + 1) P_1 \cos\Theta} - \frac{(P_1 / r_\pi^2)^{-\gamma}}{\gamma B_\pi + (\gamma + 1)(P_1 / r_\pi^2)\cos\Theta} \right| \qquad (2)$$

with B_π = 116 GeV/c, $r_\pi = m_\mu / m_\pi$ and the γ is the slope of the production spectra of kaons and pions. Muon intensities from kaons, $I_{K\mu}$ is expressed similarly as pions using B_K = 855 GeV, $r_K = m_\mu / m_K$. The survival probability, $W(z_1)$, is given by,

$$W(z_1) = \left[\frac{z_1}{z_0} \cdot \frac{P}{P_1} \right]^{\frac{1.662 z_1}{P \cos\Theta (1 + 1.1 P \cos\Theta / 115) z_0}} \qquad (3)$$

with the muon momentum at production, P_1,

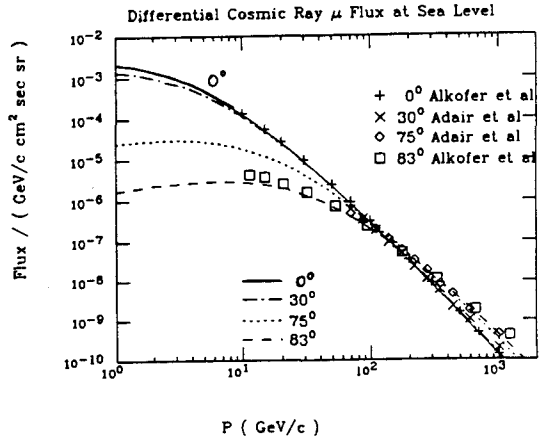
$$P_1 = P + (a + b \cdot P) \cdot (z_0 - z_1) / \cos\Theta \qquad (4)$$

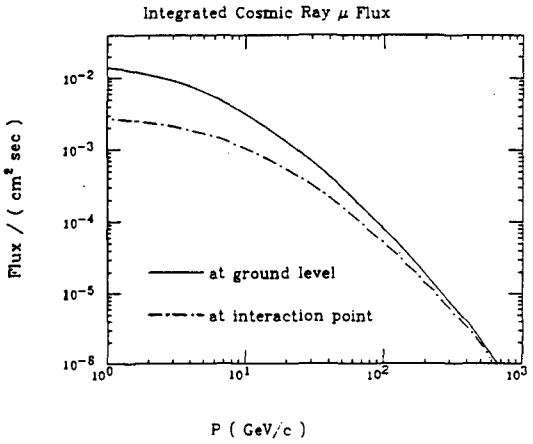
and $a = 2.5 \times 10^{-3} GeV/(g/cm^2)$ and $b = 2.78 \times 10^{-6} (g/cm^2)^{-1}$. Atmospheric depth at production, z_1, is assumed to be,

$$z_1 = 100 g/cm^2 \cdot \cos\Theta \qquad (5)$$

We used, γ = 2.75, A = 0.22 and $\frac{K}{\pi}$ = 0.3, to get a better fit to the measurements.

[1] W.D.Dau, K.Carstensen and H.Jokisch, Proc. 14th Int. Conf. on Cosmic Rays, Muochen, MN p.193, 1974. The formula in the original article were given for large zenith angles(> 79°) and used iterations to calculate the local zenith angles of the parent particles. We ignored these iterations and also tuned the parameters for small zenith angles.





~620 Hz $\Delta\alpha = \frac{15cm}{2m} = 0.075$ 75 mr

September 19, 1991

Trigger Rate in Hz. Scintillation counters only.

octant	rate(Hz) Pt > 0 GeV/c	rate(Hz) Pt > 2 GeV/c	SII (Θ < 90° ; cm² · sr)
1	0	7	1.3×10^5
2	129	88	2.5×10^5
3	314	218	2.7×10^5
4	157	106	2.5×10^5
6	11	9	1.3×10^5
Σ	620	428	10.4×10^5

~100 Hz Level 1 Trigger Rate in Hz. $\Delta\alpha = \frac{4cm}{2m}$ 20mr

octant	rate(Hz) for > Pt 0 GeV/c	2 GeV/c	3 GeV/c	6 GeV/c	10 GeV/c	SII cm² · sr
1	1.4	1.2	1.1	0.9	0.7	2.0×10^5
2	20.9	14.2	12.1	8.2	5.6	3.8×10^5
3	51.5	35.7	30.3	19.1	12.7	4.1×10^5
4	25.5	17.3	14.7	9.8	6.5	3.8×10^5
6	1.7	1.4	1.3	1.0	0.8	2.0×10^5
Σ	101.4	69.7	59.4	40.0	26.3	15.7×10^5

Trigger Rate in Hz. $\Delta\phi = 0.1$ radian case.

octant	rate(Hz) for > Pt 0 GeV/c	3 GeV/c	6 GeV/c	10 GeV/c	20 GeV/c	30 GeV/c	SII cm² · sr
1	0.0	0.0	0.0	0.0	0.01	0.00	1.3×10^5
2	0.9	0.6	0.5	0.4	0.20	0.13	2.6×10^5
3	4.1	2.4	1.6	1.0	0.42	0.23	2.6×10^5
4	1.2	0.8	0.6	0.4	0.23	0.14	2.6×10^5
6	0.0	0.0	0.0	0.0	0.01	0.00	1.3×10^5
Σ	6.2	3.8	2.7	1.8	0.87	0.51	10.2×10^5

~6 Hz



$\Delta\alpha =$ 4cm / 2m

and

$\Delta\phi = 0.1$ ($\times \frac{1}{10}$)

$\Delta\alpha = 0.1$ and $\Delta\phi = 0.1$ ⇒ ~60 Hz

$\Delta\alpha = 0.1$ alone ⇒ ~800 Hz

II-3. Summary of the L1 trigger rates by cosmic μ

1. at the sea level
   - for $\Delta\alpha = 0.1$
     ($\Delta\alpha$: deflection angle cut)
     Rate ~ 2 kHz at sector "3" (top)
     0.8 kHz sector "1" (side)

2. in the underground
   - for $\Delta\alpha = 75$ mr
     Rate(sector "3") ~ 300 Hz
     " (" "1") ~ 10 Hz
     Total Rate ~ 600 Hz
   - for $\Delta\alpha = 20$ mr
     Total Rate ~ 100 Hz
   - for $\Delta\alpha = 20$ mr and $\Delta\phi = 0.1$
     Total Rate ~ 10 Hz

3. We expect (in the underground):
   Total Rate ≃ 800 Hz, $\Delta\alpha = 0.1$ alone
   Total Rate ≲ 100 Hz, $\Delta\alpha = 0.1$ & $\Delta\phi = 0.1$

4. $\Delta\alpha$-cut alone is marginal.
   Rate(cosmic) ≈ allowable rate for μ-system (~kHz)

5. $\Delta\alpha$-cut and $\Delta\phi$-cut is a powerful discrimination for the cosmic μ.

Octagonal Geometry Effects

J. Wiss(Illinois)

Jim Wiss

September 23, 1991

Octagonal Geometry Effects

In this memo, I consider some of the complications induced by using an octagonal geometry for the barrel iron toroid and muon drift tubes in measuring muon momentum using both the θ and ϕ projections. In particular calculations will be presented on the ϕ bending created by the iron toroid and on the ϕ dependence of θ bend measurement. For the case of an octagonal geometry these effects create noticeable but not very serious degradation in momentum resolution.

1. $\Delta\theta$ and $\Delta\phi$ bends for the Toroid

We show in this section that the $\Delta\phi$ bending of the octagonal muon toroid can be comparable to the $\Delta\theta$ bends at the extreme angles in θ and ϕ. Throughout this memo we will consider the octant lying in the plane normal to the $\hat{x}$ axis.

We assume that the toroid is t meters thick, has a field strength of B which lies in the $\hat{b} = (0 \quad 1 \quad 0)$ direction. We calculate the magnetic bending on a muon which is initially directed with momentum P in the direction $\hat{p} = (S_\theta C_\phi \quad S_\theta S_\phi \quad C_\theta)$ where we find it convenient to use the notation:

$$S_\theta \equiv \sin\theta \ , \ C_\theta \equiv \cos\theta \ , \ T_\theta \equiv \tan\theta \qquad 1$$

The toroid will change the direction of the muon according to:

$$\frac{\partial\hat{p}}{\partial s} = \frac{.3\,B}{P}\ \hat{p}\times\hat{b} \qquad 2$$

where s is the total path length on which the field acts

$$\Delta s = \frac{t}{C_\phi S_\theta} \qquad 3$$

We thus have the bending relation:

$$\Delta\hat{p} = \frac{.3Bt}{P_\perp C_\phi}\ \hat{p}\times\hat{b} \qquad 4$$

We define the $\Delta\theta$ and $\Delta\phi$ bends through the Taylor expansion:

$$\Delta\hat{p} = \frac{\partial\hat{p}}{\partial\theta}\Delta\theta + \frac{\partial\hat{p}}{\partial\phi}\Delta\phi \qquad 5$$

These partial derivatives are related to orthonormal unit $\hat{\theta}$, $\hat{\phi}$ unit vectors:

$$\hat{\theta} = \frac{\partial\hat{p}}{\partial\theta} = (C_\theta C_\phi \quad C_\theta S_\phi \quad -S_\theta) \ , \ \hat{\phi} = \frac{1}{S_\theta}\frac{\partial\hat{p}}{\partial\phi} = (-S_\phi \quad C_\phi \quad 0) \qquad 6$$

Projecting out the bend angles from Eqn.(5), using the basis vectors defined by Eqn.(6), and the $\Delta\hat{p}$ expression of Eqn.(4) we have:

$$\Delta\theta = \hat{\theta}\cdot\Delta\hat{p} = \frac{.3Bt}{P_\perp C_\phi}\ \hat{\theta}\cdot\hat{p}\times\hat{b}$$

$$\Delta\phi = \frac{\hat{\phi}\cdot\Delta\hat{p}}{S_\theta} = \frac{.3Bt}{P_\perp S_\theta C_\phi}\ \hat{\phi}\cdot\hat{p}\times\hat{b} \qquad 7$$

Substituting in the explicit unit vectors (summarized in Table 2 in Section 2), it is straightforward to show:

$$\Delta\theta = -\frac{.3Bt}{P_\perp} \ , \ \frac{\Delta\phi}{\Delta\theta} = -\ (\tan\phi)\ (\cot\theta) \qquad 8$$

These calculations show that the toroid θ bend is indeed a simple expression related entirely to $P_\perp$, however as one moves away from $\phi = 0$ (the normal of the toroid) and $\eta = 0$ the toroid provides a sizeable ϕ bend as well. The octant will covers the angular range $-22.5° < \phi < 22.5°$ and (if coverage extends to $\eta = 1.5$) $25.16° < \theta \le 90°$. The largest effect occurs at $\phi = 22.5°$, $\theta = 25.16°$ where $\Delta\phi = -.88\ \Delta\theta$!

Certainly in an offline analysis, the ϕ bend due to the toroid can be corrected for in using information from any ϕ layers located outside of the toroid and no information is destroyed. It is less clear that such corrections can applied at the trigger level. Eqn.(8) tells us that the azimuthally averaged ϕ bend is zero, and that the rms ϕ bend goes as $1/P$ just as multiple coulomb scattering. At $\eta = 1.0$ the magnetic "ϕ smearing" created by a 1.5 meter toroid is 1.46 times the smearing due to the toroid's multiple coulomb ϕ scattering. At $\eta = 1.5$ the magnetic ϕ smearing becomes 2.14 times the toroid's multiple coulomb ϕ scattering. But is the magnetic effect important in the choice of which barrel muon station to place the ϕ layers?

The answer is basically no. The magnetic ϕ smearing effects will be non-existent for BW1 ϕ layers and most important for BW3 ϕ layers at the extreme value of η. For BW3, one can consider ϕ smearing due to (1) multiple scattering in the calorimeter, (2) magnetic ϕ smearing in the muon toroid, and (3) multiple scattering in the muon toroid. When weighted by their respective lever arms for muons at $\eta = 1.5$, the 1:2:3: contributions above are in the ratio 1 : 0.77 : 0.36. Hence if one could correct for magnetic ϕ smearing one would only reduce total ϕ smearing by about 20 %.

Figure 1 bears on the issue of ϕ layer placement on a possible ϕ momentum trigger and illustrates some of the points made above. We consider the best momentum resolution obtainable (using multiple coulomb scattering weighting) as a function of muon $P_\perp$ using information from a 100μ (transverse) beam constraint, the outermost two ϕ layers of the central tracker and a muon ϕ layer (modeled as a single point with 177μ resolution) placed in either BW1 (solid curve) or BW3 (dashed curve). Figure 1a is for $\eta = 0$ muons; Figure 1b is for $\eta = 1.5$ muons. The dotted curve (which differs from the dashed curve only in Figure 1b) gives the momentum resolution if one leaves out magnetic ϕ smearing.

Clearly better trigger performance in the $P_\perp$ region from 100 to 200 GeV can be obtained by placing the ϕ layer in BW1 rather than BW3. By moving the

ϕ layer radially outward, one dramatically increases the lever arm for multiple scattering from the calorimeter and toroid and thus significantly degrades the muon ϕ trigger information. The magnetic ϕ smearing effect is noticeable, but the bulk of the degradation is due to the calorimeter (modeled as a 2 m thick slab of iron) owing to large lever arm between it and the ϕ station.

2. $P_\perp$ measurement using the θ Bend

I am not aware of any proposed drift tube arrangements which solely measure $\Delta\theta$ and thus directly produce a pure measurement of $1/P_\perp$ via Eqn (8). In general, the shift in measured coordinate w (or drift time) for a given chamber is related the momentum to lowest order in $1/P_\perp$) via:

$$\delta w \propto \frac{f(\theta,\phi)}{P_\perp} \qquad 9$$

This effect is entirely correctable "off line" but serves as an extra complication at the trigger level to the extent that $f(\theta,\phi)$ exhibits significant variation. Variation of $f(\theta,\phi)$ on θ implies that one must apply a correction to momenta obtained by simple drift time subtraction which depends on the which "θ" wire is struck. It also implies that the momentum resolution becomes θ dependent. The $f(\theta,\phi = 0)$ factors are generally very easy to calculate from simple trigonometry arguments.

Variation of $f(\theta,\phi)$ on ϕ implies an additional loss of information and resolution at the trigger level if ϕ is not known. This section evaluates the severity of $f(\theta,\phi)$ variation for two proposed detector geometries. I know of no very simple argument to determine the ϕ dependence of $f(\theta,\phi)$ and have thus developed a vector calculation in Section (2b).

(2a) Detector Geometries

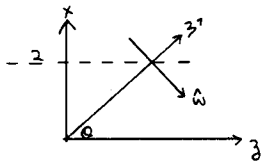
In the simplest geometry (which we will call the $\hat{z}$ geometry) the detector is in a single plane which we will put at x = 2 (we will put the toroid at x = 1 to insure a unit lever arm between toroid and detector plane). The plane reads out coordinates along the $\hat{z}$ direction. We can fully describe the detection system by

giving a point in the plane ($\vec{D}$), the detector plane normal ($\hat{\eta}$) and the readout direction ($\hat{w}$). For this simple geometry all these vectors are constants and given in Table 1 below.

By way of contrast, one can consider an idealized "projective" geometry. In this geometry, the detector is in many planes (tilted drift tubes). Each plane is orientated such that its normal points back to the origin. We assume that the centers of each drift tube lie in the plane x = 2. This geometry is sketched below and the $\vec{D}$, $\hat{\eta}$, and $\hat{w}$ vectors become the θ dependent forms summarized in the table.

Table 1 – Detector Geometries

Geometry	$\vec{D}$	$\hat{\eta}$	$\hat{w}$
$\hat{z}$	(2 0 0)	(1 0 0)	(0 0 1)
projective	$(2 \quad 0 \quad 2/T_\theta)$	$(S_\theta \quad 0 \quad C_\theta)$	$(-C_\theta \quad 0 \quad S_\theta)$



(2b) Magnetic Deflection Formula

In this section, I obtain a general expression for the change in coordinate due to magnetic bend to lowest order in $1/P_\perp$ which is used to obtain expressions for $f(\theta,\phi)$. Let $\vec{r}$ represent the intersection of a muon with the detector plane. The magnetic deflection of the measured coordinate is thus:

$$\delta w = \hat{w}_i \frac{\partial \vec{r}_i}{\partial \hat{p}_j} \Delta \hat{p}_j \quad \text{where} \quad \Delta \hat{p} \text{ is given by Eqn.(4)} \qquad 10$$

A muon which crosses the toroid midplane at point $\vec{M}$ and is directed at an angle $\hat{p}$ will intersect the detector plane at:

$$\vec{r} = \vec{M} + \frac{\ell \hat{p}}{\hat{p} \cdot \hat{\eta}} \quad \text{where} \quad \ell = \hat{\eta} \cdot \left(\vec{D} - \vec{M} \right) \qquad 11$$

Differentiating Eqn (11) we get:

$$\frac{\partial \vec{r}_i}{\partial \hat{p}_j} = \frac{\ell}{\hat{p} \cdot \hat{\eta}} \left(\hat{e}_{ij} - \frac{\hat{p}_i \hat{\eta}_j}{\hat{p} \cdot \hat{\eta}} \right) \qquad 12$$

Combining Eqn.(10), Eqn (12), and Eqn (4) we obtain:

$$\delta w = \frac{.3\, B\, t}{P_\perp} \frac{\ell}{C_\phi (\hat{p} \cdot \hat{\eta})^2} \left((\hat{p} \cdot \hat{\eta})\, \hat{w} \cdot (\hat{p} \times \hat{b}) - (\hat{w} \cdot \hat{p})\, \hat{\eta} \cdot (\hat{p} \times \hat{b}) \right) \qquad 13$$

The variable ℓ defined in Eqn (11) will generally have a polar angle dependence which can be isolated through the use of a variable ℓ:

$$\delta w = \frac{.3Bt\ell}{P_\perp} f(\theta,\phi) \text{ where } \ell = \ell(\theta = 90°, \phi = 0)$$

$$f(\theta,\phi) = \left(\frac{\ell(\theta,\phi)}{\ell} \right) \frac{1}{C_\phi (\hat{p} \cdot \hat{\eta})^2} \left((\hat{p} \cdot \hat{\eta})\, \hat{w} \cdot (\hat{p} \times \hat{b}) - (\hat{w} \cdot \hat{p})\, \hat{\eta} \cdot (\hat{p} \times \hat{b}) \right) \qquad 14$$

It straightforward to calculate the angular dependent factor $f(\theta,\phi)$ using the $\hat{p}$ and $\hat{b}$ vectors defined in Section (1) and reprised in Table 2 below and the $\vec{D}$

, $\hat{\eta}$, and $\hat{w}$ vectors defined in in the Table 1. Our normalization is to place the toroid in the plane x = 1 which makes:

$$\vec{M} = (1 \quad T_\phi \quad 1/(T_\theta C_\phi))$$

Table 2 – Compendium of Vectors

$\hat{p}$	$(S_\theta C_\phi \quad S_\theta S_\phi \quad C_\theta)$
$\hat{b}$	(0 1 0)
$\hat{p} \times \hat{b}$	$(-C_\theta \quad 0 \quad S_\theta C_\phi)$
$\vec{M}$	$(1 \quad T_\phi \quad 1/(T_\theta C_\phi))$
$\hat{\theta}$	$(C_\theta C_\phi \quad C_\theta S_\phi \quad -S_\theta)$
$\hat{\phi}$	$(-S_\phi \quad C_\phi \quad 0)$

(2r) Magnetic Deflection Results

It is straightforward to compute the $f(\theta,\phi=0)$ angular factors for both the $\hat{z}$ and projective geometry using Eqn.(4) and the vector components tabulated in Table 1 and 2. The results are:

Table 3 – Angular Factors

Geometry	$f(\theta,\phi=0)$
$\hat{z}$	$1/sin^2\,\theta$
Projective	$1/sin\,\theta$

It is also very easy to confirm the projective case from simple trigonometry for tracks in the plane $\phi = 0$. Essentially the lever arm from the toroid to a projective tube grows as $1/sin\,\theta$. The $\hat{z}$ geometry case argument is also very simple. The angular factor will very by a factor of 5.53 over the range $0 < \eta < 1.5$ for the case of the simple $\hat{z}$ geometry and by a factor of 2.35 for the case of the projective geometry. These angular factors mean that if coordinates are measured equally well over the θ range, the (non MCS contribution) to momentum resolution will

improve as $sin^2\,\theta$ (for the $\hat{z}$ geometry) and as $sin\,\theta$ for the projective geometry. The down side is that θ dependent corrections to drift time differences will be probably required at forward angles even at the trigger level.

Figure 2 is a plot of ϕ variation of the angular factor $(f(\theta,\phi)/f(\theta,\phi=0))$ for the $\hat{z}$ (Figure 2a) and projective (Figure 2b) geometry case. The solid curve is for $\eta = 0$, the dashed is for $\eta = 1.5$. If ϕ information were not available at the trigger level, the azimuthally averaged rms spread in $f(\theta,\phi)/f(\theta,\phi=0)$ would form an additional "ϕ-smearing" source of error in $\sigma P_\perp/P_\perp$ to be added in quadrature with the multiple scattering error and chamber resolution error. Figure 3 is a plot of the rms spread of $f(\theta,\phi)/f(\theta,\phi=0)$ as a function of η for the case of the $\hat{z}$ (solid) and projective (dashed) geometries. In the worse case, the additional rms smearing of about 6.5 % due to the ϕ dependence of the angular factor is quite acceptable given that the multiple scattering contribution is roughly 20 %. We note that if the geometry were in the shape of a box, the "ϕ smearing " would increase by a factor of ≈ 4 since the if ϕ range covered by a single θ wire increased by a factor of 2 withio an octant.

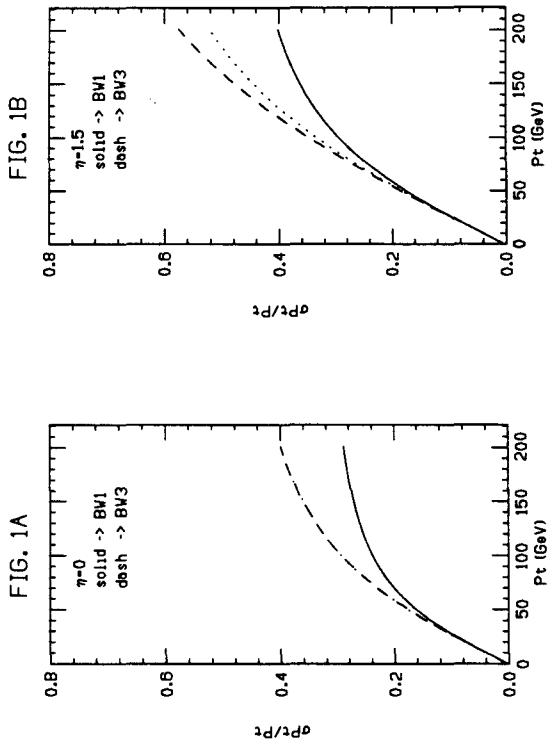
3. Summary

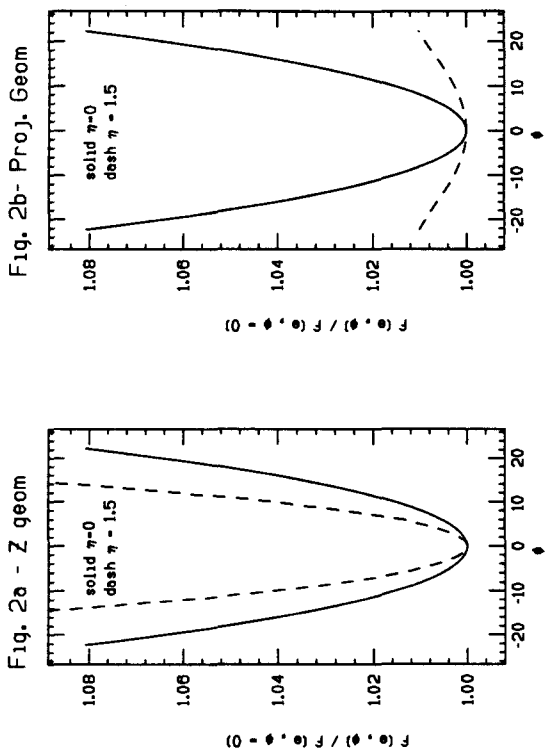
This memo studies the importance of some geometrical effects which bear on measurement of $P_\perp$ using either the ϕ or θ information from the muon chambers. For the ϕ view, the effect considered was ϕ bending owing to the octagonal muon toroid which at extreme η's is comparable to the intended θ bending of the toroid. If one does not correct for ϕ bending in the worse case ($\eta = 1.5$ for a BW3 ϕ layer) the additional magnetic ϕ smearing is at most 72 % of the existing ϕ smearing due to multiple coulomb scattering in the calorimeter and toroid. Hence correction of ϕ bending effect can only improve overall muon chamber ϕ resolution by at most 20 %. However, in the $P_\perp$ range where a second level ϕ trigger is most important, **a ϕ layer placed in BW1 will considerably out perform one placed in BW3**, because of reduced multiple scattering lever arms.

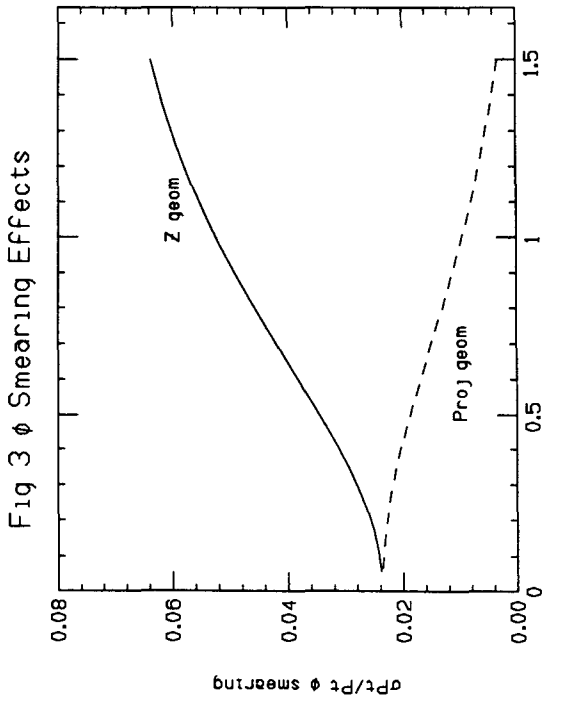
The second half of the memo investigates geometrical complications in the

measurement of $P_\perp$ using the θ layers of the muon system. Generally the change in drift time coordinates for a given θ layer will he proportional to $1/P_\perp$ but with a proportionality constant (angular factor) which depends on the polar angles of the initial muon. The θ dependence of the angular dependence is fairly simple to calculate. The angular factor is $1/sin^2\ \theta$ for a simple detector geometry which measures the $\hat{z}$ and is $1/sin\ \theta$ for the case of a projective geometry where the muon detector planes are continuously orientated to insure a projective normal. Both angular factors vary significantly over the relevant θ range, which means **some angular correction will be necessary** to momenta derived from simple drift time differences at the trigger level.

A calculational technique was developed to assess the ϕ dependence of the angular factors for the $\hat{z}$ and projective geometry. If no ϕ information is availahle at the trigger level, any ϕ dependence in the angular factors acts as an additional source of $P_\perp$ smearing. The largest ϕ angular factor variation was calculated for the $\hat{z}$ detector geometry at $\eta = 1.5$. The angular factor has a roughly parabolic dependence on ϕ and varies hy roughly 23 % from $\phi = 0 \rightarrow \phi = 22.5°$. The additional $\sigma P_\perp/P_\perp$ smearing owing to the rms ϕ variation of the angular factor is much worse for the $\hat{z}$ compared to the projective geometry and is 6.5 % in the worse case ($\hat{z}$ at $\eta = 1.5$). This additional resolution factor is unimportant compared to the dominant coulomb scattering smearing contribution.



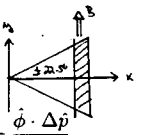




Jim Wiss
September 23, 1991

Octagonal Geometry Effects

1. $\Delta\phi$ bend of toroid



(a) Bending Equations

$$\Delta\hat{p} = \frac{.3Bt}{P_\perp cos\ \phi}\ \hat{p}\times\hat{b}\ ,\quad \Delta\phi = \frac{\hat{\phi}\cdot\Delta\hat{p}}{sin\ \theta}$$

$$\frac{\Delta\phi}{\Delta\theta} = -\ (tan\ \phi)\ (cot\ \theta)$$

- At $\eta = 1.5$, $\phi = 22.5^o$ $\Delta\phi = -.88\ \Delta\theta$

(b) If uncorrected → magnetic ϕ smearing:

$$\sigma_\phi = \frac{200\ mrad}{P_\perp\ tan\ \theta}$$

$\eta = 1.5$ $R\phi$ smearing at BW3

calor mcs	162 cm-Gev/$P_\perp$
toroid mag	125 cm-Gev/$P_\perp$
toroid mcs	58 cm-GeV/$P_\perp$

- Calorimeter MCS dominates ϕ smearing

(c) BW1 better than BW3 for ϕ trigger

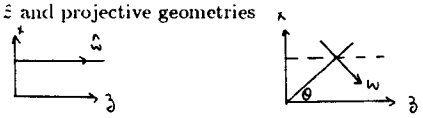
- Figure 1

2. Angular factors for $\Delta\theta$ measurement

$$\delta w \propto \frac{f(\theta,\phi)}{P_\perp}$$

- δw is measured coordinate

(a) $\hat{z}$ and projective geometries



(b) θ dependence

Geometry	$f(\theta,\phi=0)$
$\hat{z}$	$1/sin^2\ \theta$
Projective	$1/sin\ \theta$

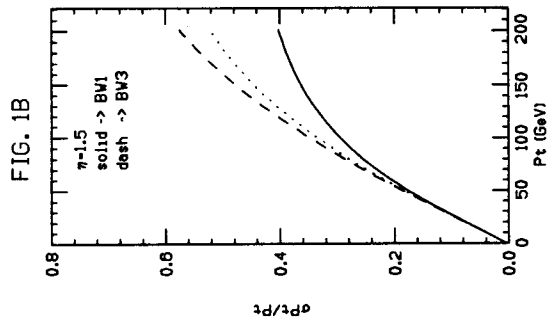
- Δw must be corrected to get $P_\perp$

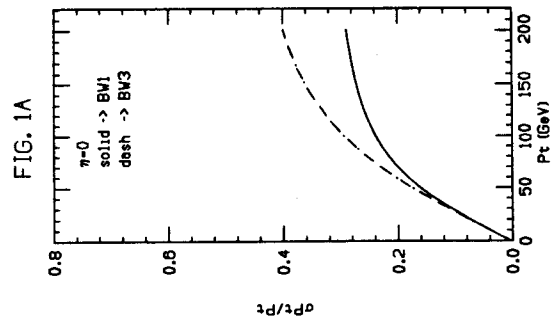
(c) ϕ variation of $f(\theta,\phi)$

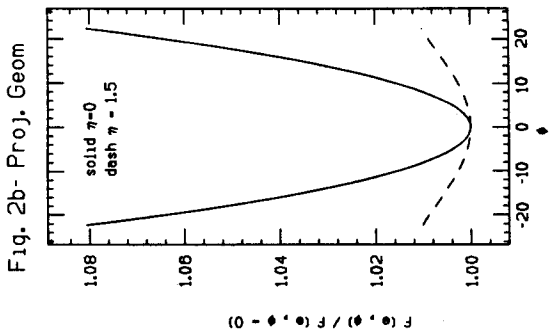
(i) Not easy to compute

(ii) $f(\theta,\phi)/f(\theta,\phi=0) \propto \phi^2$

(iii) $\sigma(P_\perp)/P_\perp$ if uncorrected is tolerable







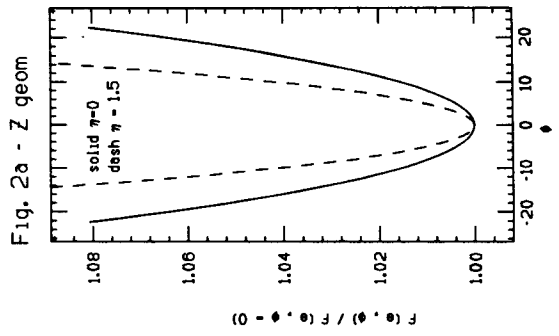
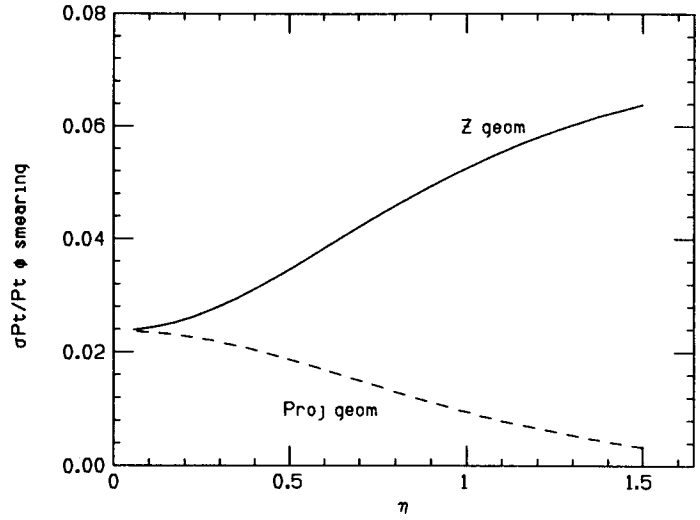


Fig 3 ϕ Smearing Effects



Forward Muon Chamber Rates and the Optimal Beam-Pipe/Absorber Design

A. Kulik(Protvino)

Alexei Kulik 08.9.91, IHEP, Protvino

SDC Forward Muon Chamber Rates and the Optimal Beam-Pipe/Absorber Design

The rates in the forward muon chambers ($1.6 < |\eta| < 3$) are calculated for various beam-pipe shapes. The influence of the beam-pipe thickness, material and the absorber thickness are also investigated. A new absorber design is proposed allowing free access to the rear chambers and saving about 150 tones of iron in each arm.

Two first chambers in the forward direction are exposed to the highest rates among all other muon chambers. There is one contribution to the rate in these chambers which is obvious: the muons hard enough to penetrate the End-Cap Calorimeter. Such muons come dominantly from the π and K-decays, their rates were estimated by Y.Sakai[1] and me[2] to be about few MHz. The contribution of any secondary interactions needs more elaborated study. Here I present a full GEANT/GHEISHA simulation although with a simplified detector model. This work continues my early study[2].

GEANT Simulation

The simulation framework wasn't chanded much since May 1991[2].

Two-jet events were simulated with the ISAJET code, $5 < jetP_t < 50$ Gev. The cross section of this process is about 100 mb.

The simplification of the detector model is as follows: calorimeters are structureless, they are just the bulky pieces of material. The material is a mixture of iron and plastic with a density of 5.5, radiation length 2.65 cm and nuclear absorbtion length 26.4 cm. May be it is not an optimal proportion, I don't know. The same approach was taken for the chambers and central tracker.

Another simplification deals with the Forward Calorimeter. Since its full simulation is time consuming (about 40 mins/event) all the

optimization of the beam-pipe design was done without it. The Forward Calorimeter influence was calculated once separately (without the beam-pipe).

The sketch of the layout (not to scale) is shown in fig.1. Dotted line shows the conventional Absorber design used in this study. The hatched piece from the Forward Calorimeter to the Collimator shows my proposal (see below). The basic dimensions are taken from the design worked out by the muon integration group 91/4/17. The inner radius of the Absorber is by 10 cm more than in the projective design. This is done to make Absorber invisible from the IP reducing by this mean secondary interactions.

In order to get a good idea of the optimal Absorber thickness the following software trick was done. The Absorber was divided to 7 layers: $4 * 5 + 3 * 10$ cm thick and rate was watched in each layer separately, as to see how fast it decreases with thickness.

Standard energy cuts for GHEISHA were applied: 10MeV for hadrons and 1Mev for electrones and gammas. The program runs on VAXSTATION 3100 as fast as about 200 events/day depending on how many users share computer.

The Beam-Pipe Shape

The conventional cylindrical design causes to enormously high rate of the secondary interactions [2]. This is due to a very small angle of a particle direction with respect to the pipe wall (see the bottom of the fig.1). So a projective-like design was proposed [2,3]. The pipe has relatively small cylindrical part of 5 cm dia, then it follows a cone downstream to the Forward Calorimeter (about 13 meters from the IP), the maximum diameter being 50 cm. Here it is attached via a flange to the second part containig a cone with a small opening angle and a short invert cone. It was assumed that the Beam Pipe is made of Aluminum, 1 mm thick at the beginnig, thickness increasing proportionally to the running diameter up to 10 mm at its end. Such design fits both the idea of projectivity and the requirements of the mechanical stability under vacuum.

Fig.2 shows the charged particles flux through the Absorber as a function of its thickness. The line marked as "Muonic Punchthrough Level" shows the irreducible rate of the muonic punchthrough. The initial flux (at zero thickness) consists mostly of electrones (note a very fast rate decrease at first 5 cm), the rest being soft hadrons and muons. As the iron Toroid was assumed to be thick enough to absorb this radiation, only its fraction hiting upstream the Toroid ($Z < 1033$ cm) was taken into account. All values here and below are normalised to one interaction in the IP.

The Forward Calorimeter

Opened triangles in fig.2 show the rates without Beam Pipe. This contains the interactions in the Forward Calorimeter, other calorimeters, air, etc... Two important notes about the Forward Calorimeter position should be done.

- Although the backsplash from the Forward Calorimeter is essential, it hits the Absorber mostly opposite the first iron Toroid. Fig.3 shows the Z-distribution of charged particles in the Absorber for the case without any Beam Pipe. Only a small fraction of this radiation hits before the Toroid and can affect the chambers' rate.
- The same is valid for the connecting flange if it is located close to the Forward Calorimeter. The simulation shows that the flange influence is negligible for 25 cm distance, while for 1 m it is comparable to the Forward Calorimeter influence.

Fig.4 shows the targets for the secondary interactions: the Vacuum Pipe, the End-Cap Calorimeter, the connecting flange and the air.

Summary of the Projective Design

Summarizing fig.2:

- Optimal design reduces secondary interactions by a factor of about 25 as compared to the conventional one.
- The contribution of the Beam Pipe to the Forward Muon Chambers rates for the optimal design does not exceed that of all other (irreducible) secondary interactions sources.
- The 30 cm thick Absorber brings the total contribution of the secondary interactions to the irreducible level of the muonic punchthrough.

Optimization Study

Fig.5 shows the rates for various pipe diameters at its end. The thickness is everywhere proportional to the current diameter starting from 1 mm at the minimal diameter of 5 cm. The steel pipe may be made thinner than the aluminum one (by a factor of about 1.4). Keeping this in our mind there is no big difference between two materials. It should be a technological choice.

The possibility was examined to reduce the pipe thickness due to the rigid outer ribs of a circular shape. Their dimensions were calculated according to the USSR standards. At the first approximation the ribs contribution vanishes the thickness gain, so there is no significant difference between this design and a "smooth" one. There is a technological choice again.

The Chambers' Rates

The rate is contributed by the muonic punchthrough and the charged particles coming out of the Absorber (fig.2). The muonic punchthrough causes to about one chamber hit per muon while some part of the flux through the Absorber doesn't hit the chambers. The total neutron and charged rates in the μFW1 chamber for the Absorber thickness of 50 cm are shown in fig.6. It is strongly dominated by the muonic punchthrough (about 90 %). The rate in the μFW2 is about the same, the rates of others being much lower. One more

possible contribution to the rates is the conversion of gammas and neutrons in chambers and in the first Toroid. Preliminary this is well below the muonic puochthrough level, detailed calculations are under the process.

The Rear Chambers and the Proposition of the New Absorber Design

The Absorber thickness of about 30 cm of iron seems to be optimal:

- Although the total flux through the Absorber (caused both by the Pipe and by the Forward Calorimeter) is about twice as high as the muonic punchthrough, its contribution to the chambers' rates still should not exceed the irreducible muonic level.
- The absolute value of the rate in fig.6 is definitely low, so there is no much danger to make the Absorber a bit thinner, in any case the rate is not likely to exceed $100/s/cm^2$

The rates of the μFW4 and μFW5 chambers is a quite different topic because it affects the first-level muon trigger. The total rate of the muonic punchthrough in this region is about 200 kHz so an optimal Pipe/Absorber design should bring all other sources down to this level or so. Preliminary comments on this are as follows. The Forward Calorimeter works like a plug: it stops the most nf incident radiation. So, mainly the Pipe interactions remain (see fig.4). It seems naturally to place an absorber just near the beam-pipe as shown in the fig.1.

The advantages of this design are:

1. The weight saving comes to 140 tones in each arm.
2. The problem of the Collimator backsplash is solved.
3. There is enough room for increasing this shielding (for example in order to absorb soft neutrons).

4. The access to the μFW4, μFW5 chambers and to the Čerenkovs is free.

The disadvantage is that this part of the Absorber can not move back together with the Forward Calorimeter and the second Toroid. It should be dismounted before.

Future Plans and Problems

Dependence on the Pipe thickness should be caleulated and compared to the fabrication dimensions tolerance to make final desicion.

The Pipe mechanical supports should be taken into account. As far as I know there is no any design to the moment.

The calculations on the new Absorber design proposed here and the simulation of the trigger seem to be the most interesting today. This requires a very powerfull computer. The longest run at VAXSTATION 3100 resulted in about 3500 events in three weeks. At least an order of magnitude more required to reach a 3 kHs level which is acceptable for the trigger. I hope for the US help.

The GEANT/GHEISHA code is not good for soft neutrons which can make the additional troubles.

References

1. Yoshihide Sakai, KEK. "Muon Trigger Rates and Momentum Resolution Calculations". SDC note.
2. A.Kulik. "Rates in the SDC Muon Chambers and Optimal Design". SDC note 91/4/28.
3. A.Kulik. "Forward Muon Rates and Shielding" EMPACT note 330 (1990).

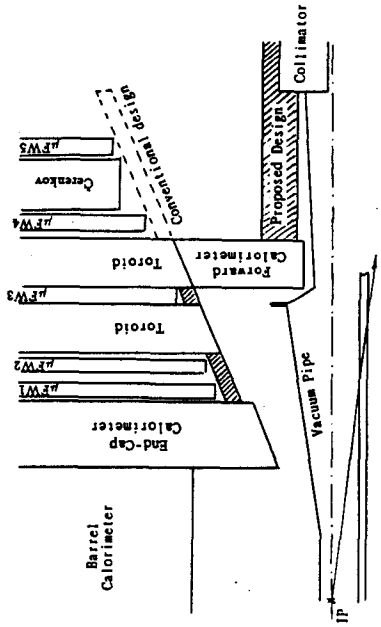


Fig.1 Optimized Beam-Pipe Design. The conventional design is shown at the bottom of the picture.

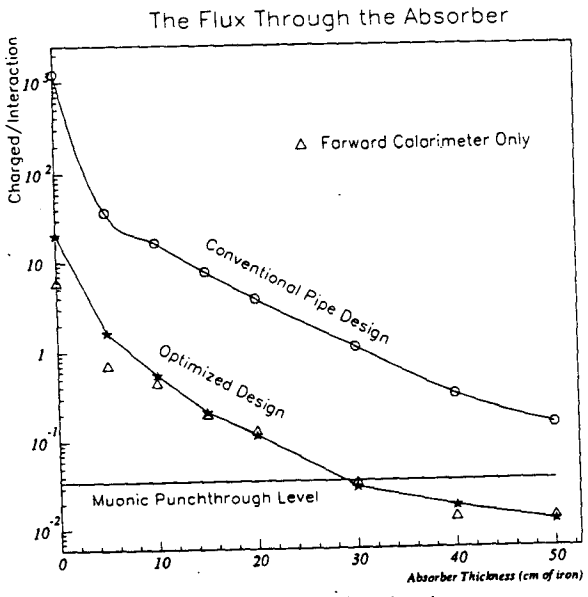


Fig.2 The Rate of Charged Punchthrough v.s. Iron Absorber Thickness. The curves "Conventional Pipe Design" and "Optimized Design" don't include the Forward Calorimeter influence. The latter is shown separately.

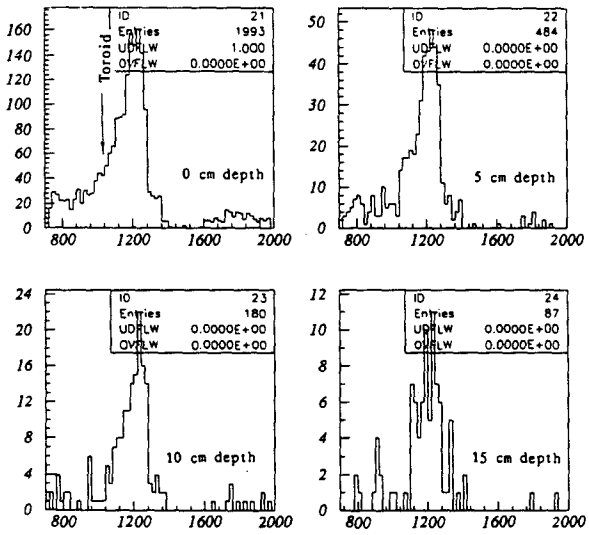


Fig.3 The distribution of charged particles along the Absorber. No Beam Pipe. Arrow shows the front face of the Toroid.

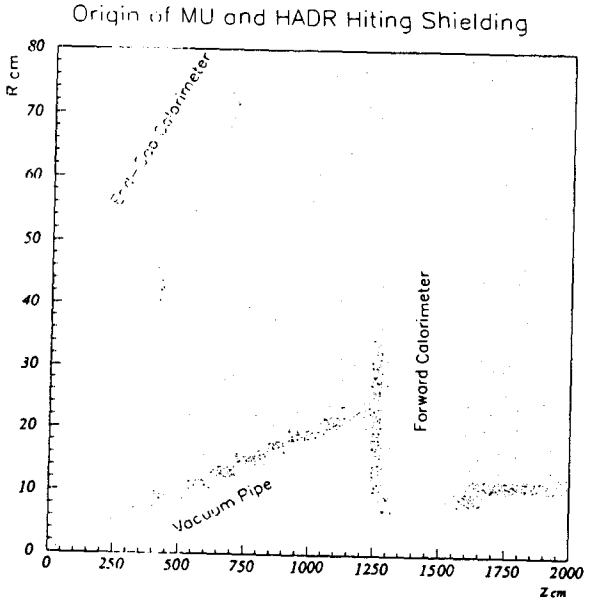


Fig.4

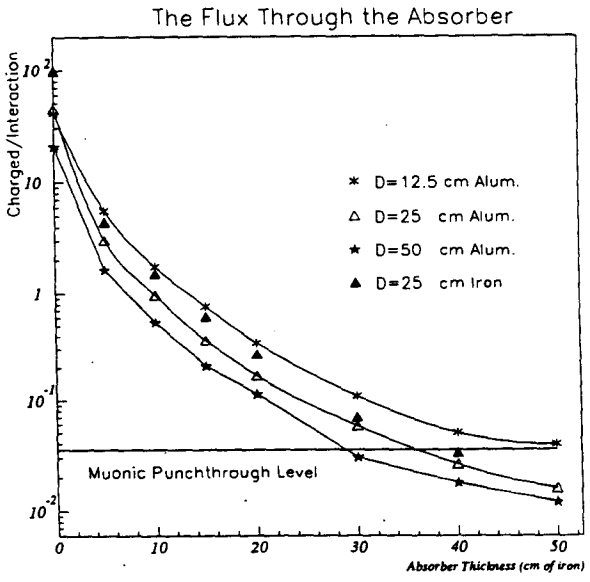


Fig.5 The Rate of Charged Punchthrough v.s. Iron Absorber Thickness. D stands for the diameter of the vacuum pipe at its big end.

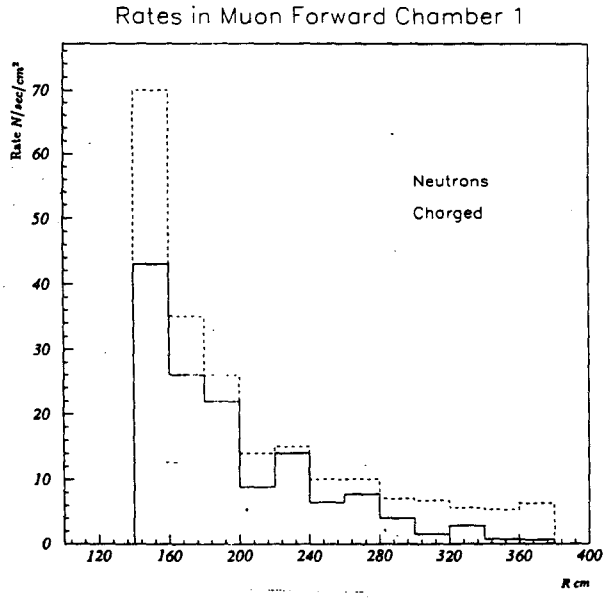

Rates in Muon Forward Chamber 1
Rate N/sec/cm²
70
60
50
40
30
20
10
0
120
160
200
240
280
320
360
400
R cm
Neutrons
Charged

Fig.6

Study of the Muon Trigger Efficiency

V. Molchanov(Protvino)

V. Molchanov
IHEP, Protvino

Study of the muon trigger efficiency

Study of the muon trigger efficiency for Higgs, Z' and t-quark production has been carried out. ISAJET was used for simulation of the Higgs and t-quark generation, PYTHIA was used for simulation of Z' and associate Higgs generation.

First geometrical efficiency was determined. It was required that all muons should be in pseudorapidity range $|\eta_\mu| < 2.5$ and all electrons should be in pseudorapidity range $|\eta_e| < 3$. Events which passed specified conditions are called reconstructible, and trigger efficiency was determined with respect to these reconstructible events. For the trigger to take place it was necessary for at least one muon with P_T more than threshold value to be in the predefined pseudorapidity range ($|\eta_\mu| < 1.0, 1.5, 2.0, 2.5$).

Results for the 400 and 800 GeV Higgs boson are shown in Fig. 1, for 150 GeV Higgs — in Fig. 2. When analyzing geometrical efficiency for associate Higgs production only muon from $W \to \mu\nu$ decay was taken into account. Results for Z' and t-quark are shown in Fig. 3. When analyzing t-quark production only the muon from $t \to b\mu\nu$ decay was taken into account. Subset of efficiencies for these processes with $|\eta| = 1.5, 2.5$ and $P_T = 15, 30$ GeV is presented in Table 1.

Some further study has been done in connection with Z' asymmetry measurement. P_T threshold does not play any role here, so question only is η range. Distribution of events over $\eta_{\mu^-} - \eta_{\mu^+}$ for 1 TeV Z' is shown in Fig. 4. Events which lie in a large square ($|\eta_\mu| < 2.5$) are reconstructible. Events which lie in four small squares ($1.5 < |\eta_\mu| < 2.5$) represent trigger inefficiency. In the same figure events which also passed additional requirements $|\eta_{Z'}| > 3$ and $|cos\theta^*| > 2/3$ (θ^* is an angle between directions of motion of μ^- and Z' in Z' rest system) are shown. Both these conditions strengthen the degree of asymmetry, but don't affect significantly trigger efficiency (see Table 2).

Distributions over $cos\theta^*$ for 1 TeV Z' with different selection criteria are shown in Fig. 5. It is clear from the last two pictures that trigger inefficiency does not change measured asymmetry value (possible change is no more than $\simeq 0.2\%$). Results for 4 TeV Z' are similar and may be found in Fig. 6-7.

Comparing trigger efficiencies in the Table 1 we can see that either reduction trigger range from $|\eta| = 2.5$ to $|\eta| = 1.5$ or increase of P_T threshold from 15 to 30 GeV has substantial effect on following processes: $H(150) \to 2\mu 2e$, associate Higgs and t-quark production, and relatively small effect on other processes. That leaves some questions which require further investigations:

- electron trigger efficiency for $H(150) \to 2\mu 2e$ process
- other possibilities for the trigger on associate Higgs production
- possible effects on the detailed determination of t-quark properties

Also it is interesting to point that while forward muon system plays a crucial role in Z' asymmetry measurement forward muon trigger makes no essential improvement.

Physical Process	Geom. Eff	$p_t > 15GeV$ $\|\eta\| < 1.5$	$p_t > 15GeV$ $\|\eta\| < 2.5$	$p_t > 30GeV$ $\|\eta\| < 1.5$	$p_t > 30GeV$ $\|\eta\| < 2.5$
$H(400) \to 4\mu$	0.621	0.980	1.000	0.974	1.000
$H(400) \to 2\mu 2e$	0.676	0.888	1.000	0.877	1.000
$H(800) \to 4\mu$	0.757	0.969	1.000	0.969	1.000
$H(800) \to 2\mu 2e$	0.813	0.864	1.000	0.861	1.000
$H(150) \to 4\mu$	0.500	0.948	1.000	0.862	1.000
$H(150) \to 2\mu 2e$	0.548	0.828	0.986	0.574	0.721
$H(150)(W \to \mu\nu)$	0.739	0.607	0.946	0.495	0.774
$Z'(1000) \to 2\mu$	0.710	0.894	1.000	0.894	1.000
$Z'(4000) \to 2\mu$	0.896	0.966	1.000	0.966	1.000
$t(150) \to b\mu\nu$	0.819	0.648	0.941	0.519	0.750
$t(250) \to b\mu\nu$	0.872	0.661	0.930	0.570	0.801

Table 1: Muon trigger efficiency (review)

Restrictions	Geom.Eff.	$\|\eta\| < 1.5$
$M_{Z'} = 1TeV$	0.710	0.894
$\|\eta_{Z'}\| > 3$	0.407	0.847
$\|cos\theta\| > 2/3$	0.210	0.943
$\|\eta_{Z'}\| > 3$ $\|cos\theta\| > 2/3$	0.099	0.974
$M_{Z'} = 4TeV$	0.896	0.966
$\|\eta_{Z'}\| > 3$	0.613	0.978
$\|cos\theta\| > 2/3$	0.318	0.939
$\|\eta_{Z'}\| > 3$ $\|cos\theta\| > 2/3$	0.209	0.963

Table 2: Muon trigger efficiency to Z'

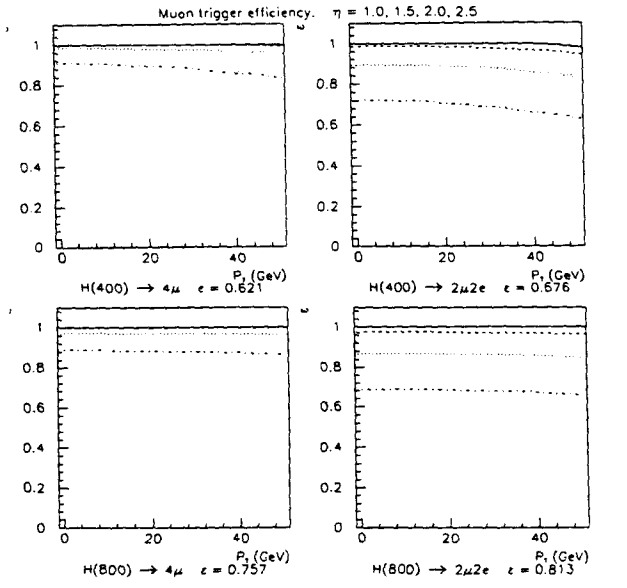


Fig 1.

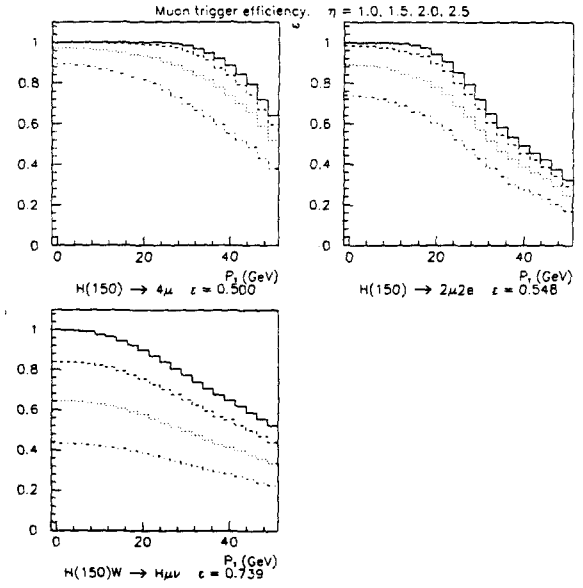


Fig. 2.

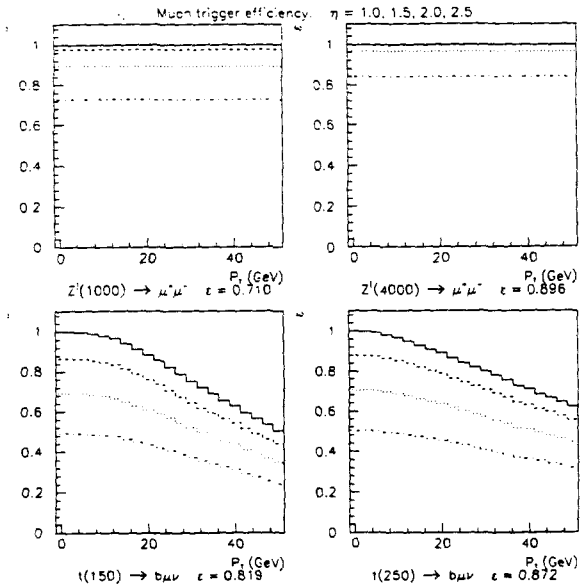


Fig. 3

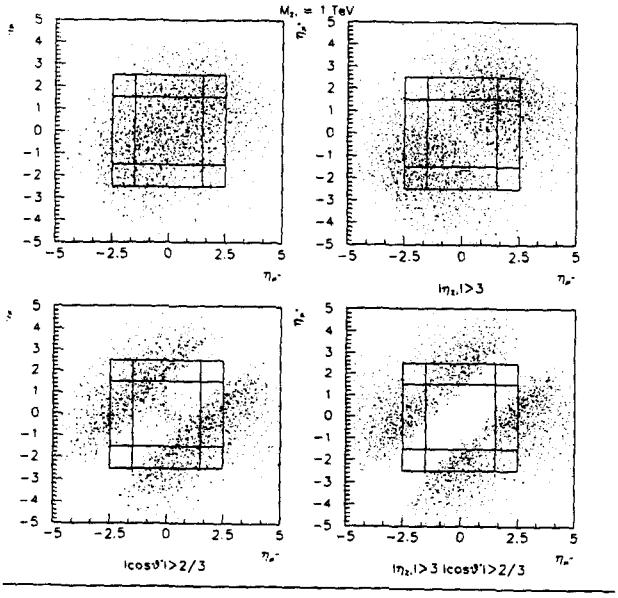


Fig. 6

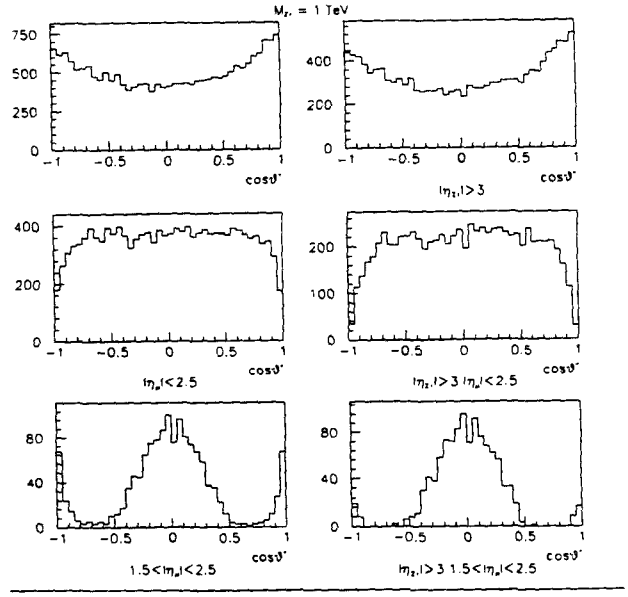
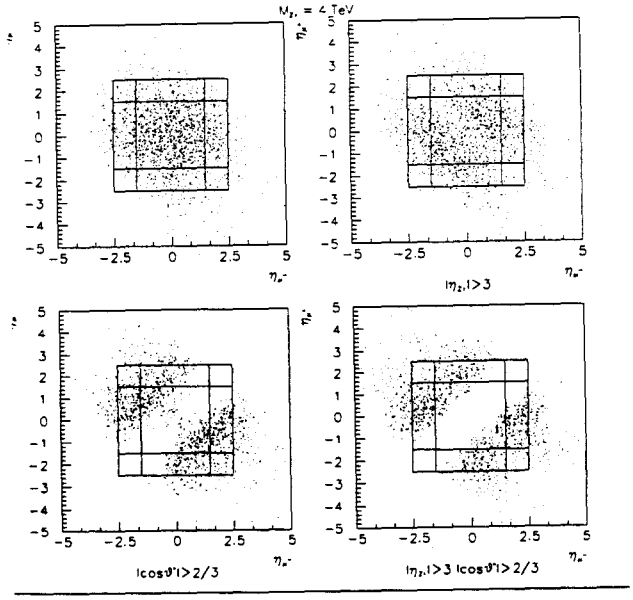
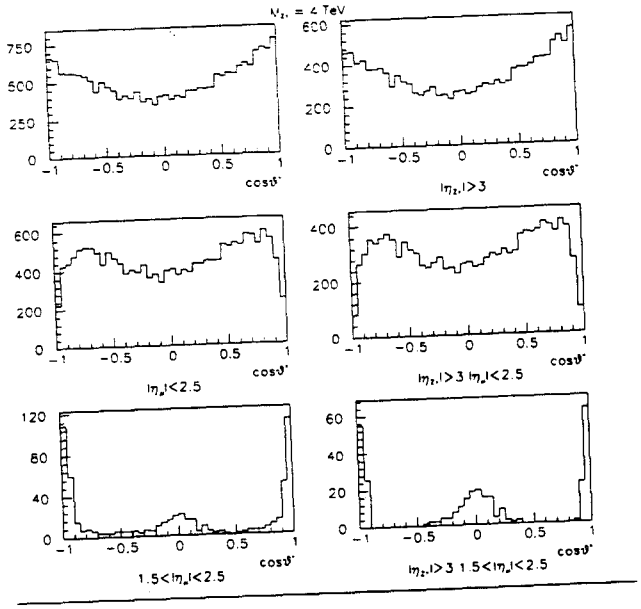


Fig. 7.

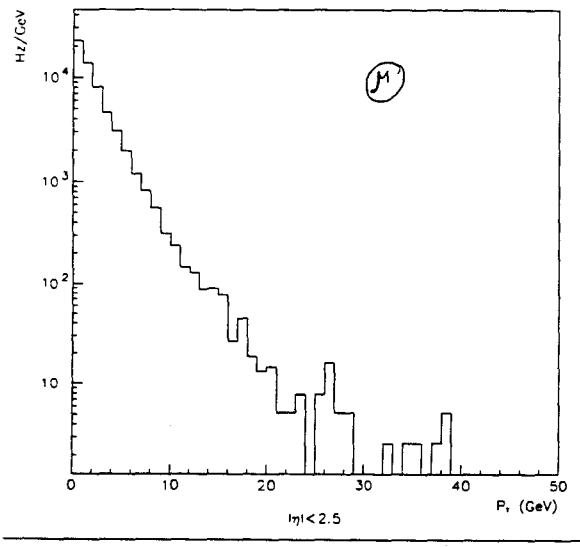
668



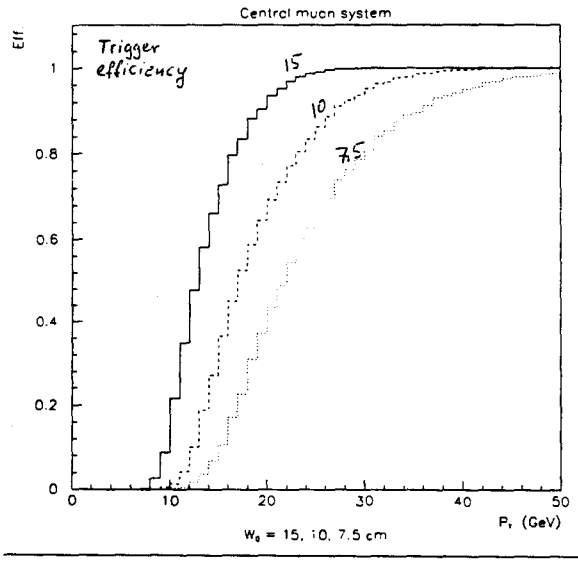
669

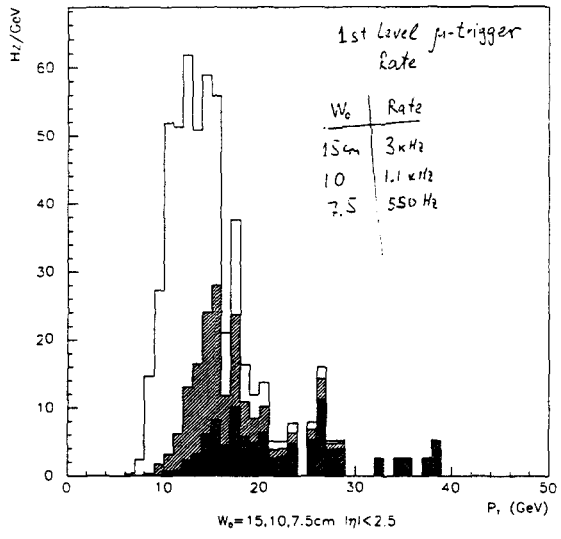


670



671




Hz/GeV
60
50
40
30
20
10
0
0
10
20
30
40
50
P_T (GeV)
1st Level μ-trigger Rate
W_o | Rate
15cm | 3 kHz
10 | 1.1 kHz
7.5 | 550 Hz
W_o=15,10,7.5cm |η|<2.5

Scintillation Counters for Muon Trigger System

V. Rykalin(Protvino)

Scintillation counters for muon trigger system

674

V. Rykalin, IHEP.

Problems: $\simeq 10^4$ counters; $2 \cdot 10^4$ PM; 60 t scintillator

Cost: $\simeq 20 \cdot 10^6$ $ ~ $20 \cdot 10^6$ Rouble (our estimation)

Counters sizes: $10 \times (150 \div 440) \times 3000_{max}$ mm^3

Number of the sci. counters is unknown precisely just now, likely number interval is $7 \cdot 10^3 \div 10^4$

Our experience

Our groupe (IHEP, Protvino, detector particle groupe, 20 scientists and engineers, 35 workman) designed and produced:

— $3 \div 4$ $\frac{\text{tons}}{\text{year}}$ of the sci. bars of the differ sizes.

— $\simeq 250$ sci. counters ($10 \times 200 \times 3000$ mm^3) for DELFI muon system.

— $\simeq 30$ sci. counters ($10 \times 200 \times 1500 \div 2500$ mm^3) for NA-12 (CERN) and GAMS (IHEP) muon systems.

675 ②

— $\simeq 60$ sci counters for NA-12 Time of flight system. ($10 \times 200 \times 1000$ mm^3).

— All scintillation and WLS elements of the NA-12 and GAMS hedron calorimeters.

— $\simeq 200$ special one dimention position sensitive PM with single photoelectron space resolution $\sigma = 1 \div 2$ mm and photocathode length $\simeq 200$ mm for sci hodoscopes, positron-emission tomographer and Ring Imaging Cerenkov Counter of the Double arm spectrometer FODS, IHEP (60 PM)

— In collaboration with INR (Moscow) designed Pb-sci-WLS fiber EM calorimeters for BNL exp. and Gluon programme on U70, IHEP.

— and so on

The sci. bars and sci counters

The sci bars are produced by extruded method from big sizes blocks of the polystyren. sci.

In main we produced sci counters with slow termal moulded light guides Its are moulded from the material of the sci. bar plate

676 ③

This technology is simplest, counter mechanical stability is very high.

Fig1 – The main characteristics of the sets of the NA-12 TOF System counter

Fig 2, 3 – Character. of the ordinary counters – prototypes for the Solenoid muon system.

Conclusion: Used light guide type is not optimal, it decreases light atten. length ($\ell_0^\circ \simeq 200$ cm, but $\ell_0 = 100 \div 120$ cm), there are the light losses on own light guide.

The light guide variants

- The twisted multibars light guides must be optimal on own losses and transparency, but its are very complicated for the multithousend production and must decrease mechanical counter stability

- Adiabatic light guide — ? on losses and transpareny of the sci bar, but must decrease mechanical stability.

677

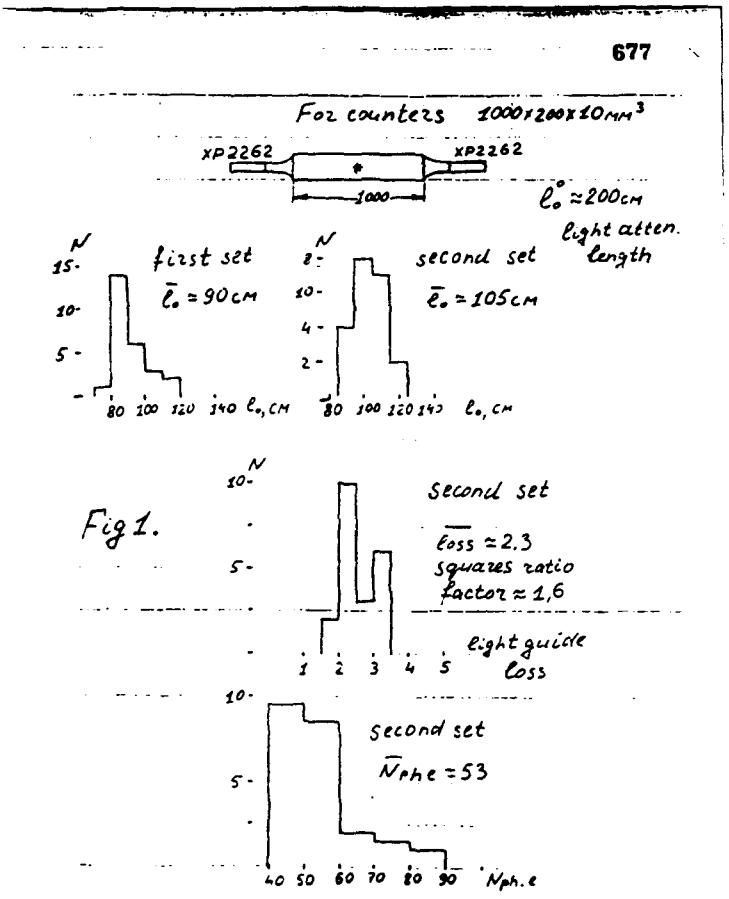


Fig 1.

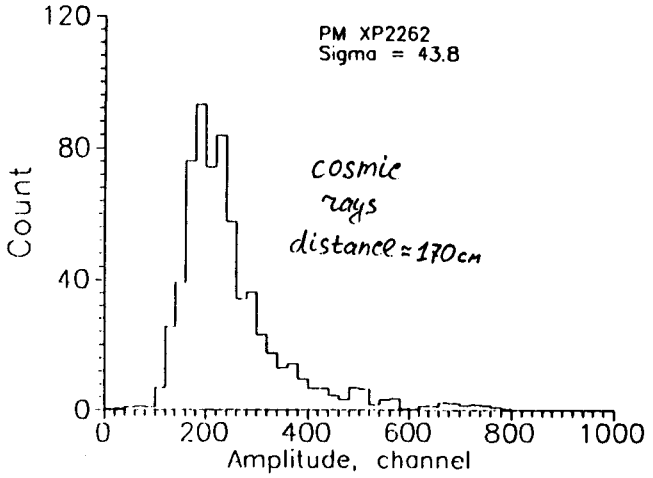


Fig 3a

680

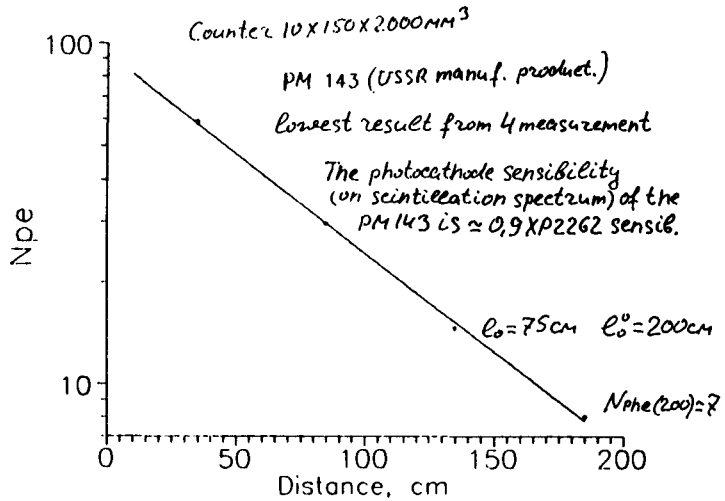
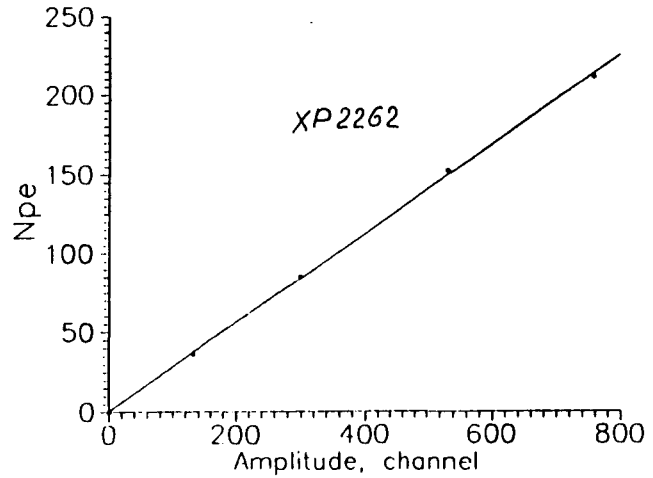


Fig 2

678

$N_{phe} = \frac{1}{\sigma^2}$; σ is MSD of the LED amplitudes distribution.



681

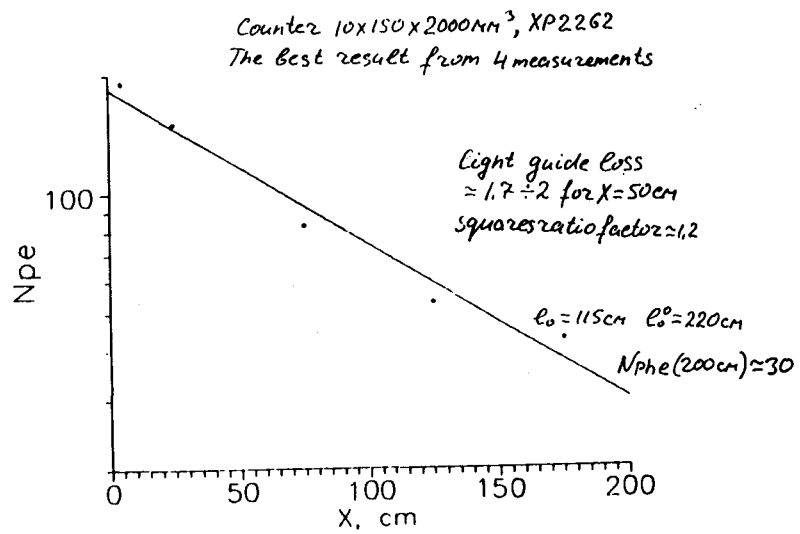


Fig 3

679

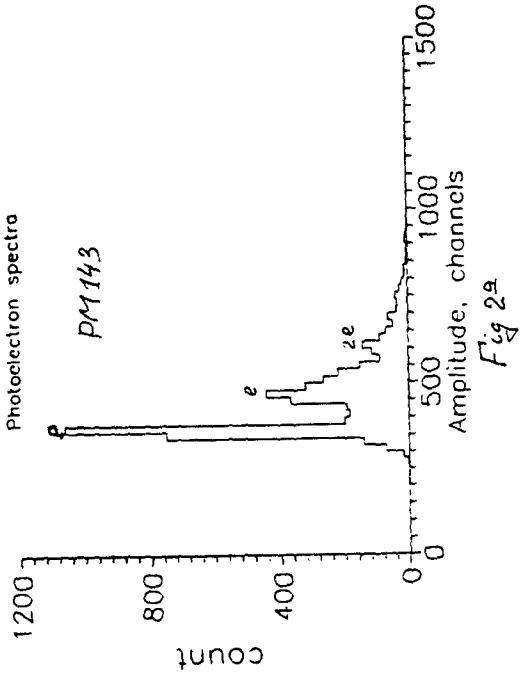


Fig 2a

The sci. counters on the base of new PM with long photocathode (PMKS)

Cardinal decision of the problem is counter without light guide.

Three year ago our group began to design of the new PM with long photocathode (≤200cm)

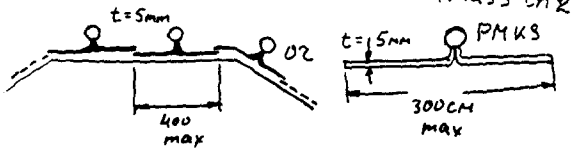
There are 8 operating samples just now.

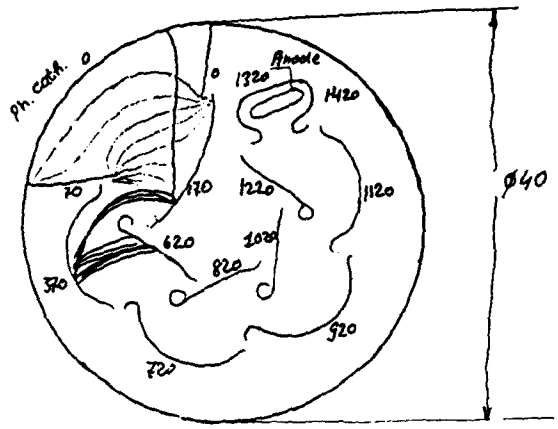
Cross section scheme of the PMKS is shown on the Fig 4.

On Fig 5 - characteristics of the counter with PMKS

Potential advantages of the counters with PMKS

1. Absence of the light guide
2. The possibilities to decrease number of the PM in 2÷3 times and total sci. mass in 2 times.





The Prototype of the dynode system was RCA-4552. This PM has massive photocathode and length dynodes ≈40mm.

PMKS $K \geq 10^6$ $U \geq 1500$; $\sigma_t \leq 1.2$ns.

$S = 50 \div 60$ MA/W ($S_{XP2262} = 70 \div 80$ MA/W)

Fig 4.

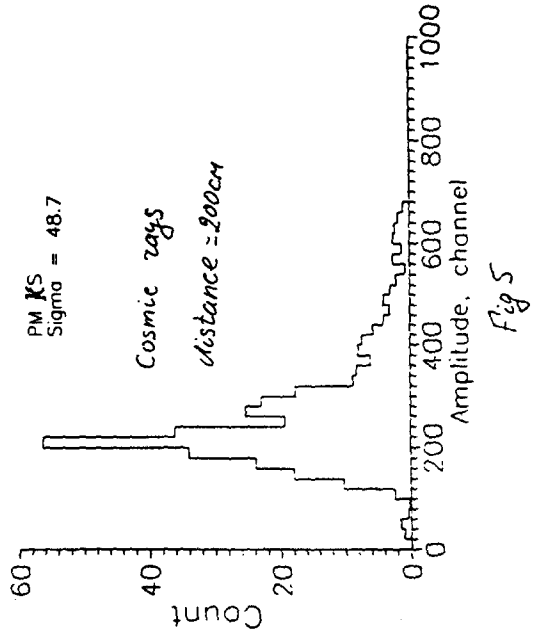
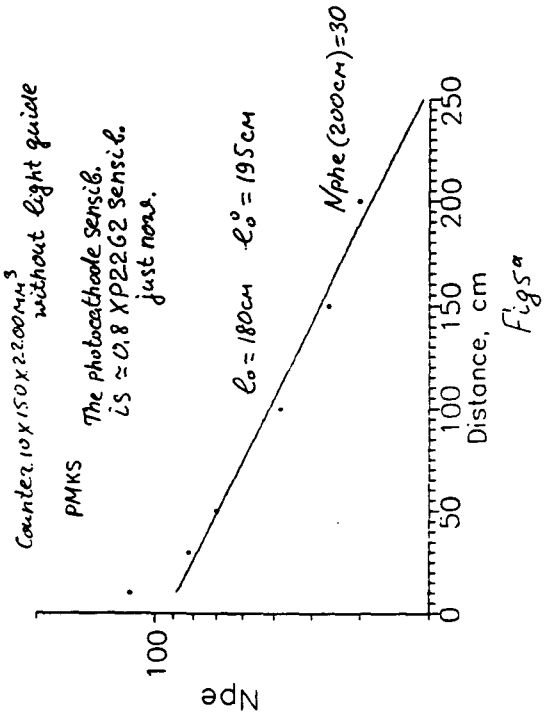


Fig 5



Figs a

- The possibilities to exchange the trigger efficiency on P_s in the case of the useing of the more narrow sci. bars and multianode PMKS (3÷5 anodes)

This was discussed in the dr Kulik communic....

The muon counters sistem cost will grow only consequently electronics cost grows practically

Muon Scintillator R&D Activities at Michigan

R. Thun(Michigan)

SDC MUON SCINTILLATOR R&D ACTIVITIES AT MICHIGAN **689**

R. Thun 16 September 1991

1) OVERVIEW

We are designing the scintillation trigger counters for the SDC muon system and are also engaged in the testing of scintillators, light guides, phototubes, and other components for this system. During the past six months, we have constructed a cosmic-ray test stand, purchased several scintillators and phototubes, and have performed a number of preliminary measurements using a simple data acquisition system.

2) SUPPORT

Support during 1991 has been obtained from several sources:

a) SSC Subsystem R&D:
Equipment funds: $ 25,500
Operating funds: $ 4,000

These funds have been committed primarily towards the purchase of scintillators, light guides, and phototubes.

b) Texas National Research Laboratory Commission (TNRLC):

The Universities of Michigan, Chicago, and Wisconsin have been awarded a joint grant to work on the SDC trigger system. Funds from this grant have been used to support personnel working on the muon scintillation trigger counters as follows:

Technician (0.8 FTE): $ 28,000
Research Fellow (3 months): $ 12,000

c) Other:

The cosmic-ray test stand and its data acquisition system have been constructed almost entirely from existing instrumentation donated by high-energy physics groups at Michigan. In addition, the University of Michigan, DoE, and NSF, are contributing to the salaries of personnel working on this project.

3) PERSONNEL:

Name	Position	Effort(FTE) /duration	Responsibilities
R. Thun	professor	50 %	supervision, data
M. Longo	professor	5 %	cosmic-ray test stand
R. Gustafson	research scientist	5 %	fiber read-out
K. De	research fellow	5 %	fiber read-out
S. Hong	research fellow	40 %	measurements
M. Marcin	research fellow	100 % /3 months	data acquisition system
C. Weaverdyck	technician	80 %	counters, equipment
E. Dodd	graduate student	25 %	measurements

Marcin and Weaverdyck are supported by the TNRLC.

4) SUMMARY OF ACCOMPLISHMENTS TO DATE **690**

a) We have assembled a large, three-layer cosmic-ray test stand, as shown in fig. 1. Additional wire chambers and trigger scintillators will be added as required. The CAMAC-based data acquisition for this test stand is expected to be operational by the end of September, 1991. The test stand will allow the testing of large scintillation counters by triggering on cosmic-ray muons and recording their location and angle of incidence as they pass through the counters.

b) We have purchased or acquired a number of scintillation counters as listed in the following table:

Company	type	# of pieces	thickness	length	width
BICRON	BC 408 PVT	2	0.25"	117"	6.0"
		1	0.50"	117"	6.0"
		1	0.75"	117"	6.0"
KURARAY	SCSN-81 Polystyrene	2	0.6cm	270cm	15cm
		2	1.0cm	270cm	15cm
		1	2.0cm	270cm	15cm
		1	0.6cm	270cm	61cm
		1	1.0cm	270cm	61cm
NE	NE110 PVT	1	0.25"	117"	6.0"
		1	0.25"	117"	24.0"
		1	0.50"	117"	24.0"
POLYCAST	PS10 Acrylic	because of large minimum order we are negotiating an add-on to another order. We have some small pieces on hand.			

We have begun to measure the light yield and attenuation length of these scintillators with a pulse-height analyzer and the simple cosmic-ray setup shown in fig. 2. The trigger counter near the tested scintillator is 15 x 15 cm in size, and the two trigger counters are approximately 64 cm apart to insure that cosmic-ray muons enter at a reasonably normal angle of incidence. Some preliminary data are shown in figs. 3-7 which display pulse-height spectra from the scintillator as a function of distance from the phototube. The average number of detected photoelectrons <n> is also shown. (This was determined by fitting Poisson distributions to the pulse-height spectra with the constraint of a common overall scale factor that converts channel count to <n>. We have recently made some diode calibration runs which allow, in principle, a more precise determination of this scale factor since the diode data do not exhibit the long tail of the Landau distribution.) For these measurements, a RCA (Burle) 8575 phototube was attached directly to one end of the scintillator, and the other end was masked with black tape to minimize reflections from that end.

Preliminary Results:

Scintillator	Attenuation Length (cm)	Relative light yield/cm (est. error 10%)
1/2" Bicron BC408	422	0.76 (different set-up)
1/4" Bicron BC408	390	=1.00
10 mm Kuraray SCSN-81	220	0.56
6 mm Kuraray SCSN-81	160	0.50
3/8" Polycast PS10	58	0.41

5) GOALS FOR THE IMMEDIATE FUTURE **691**

a) The goal with the highest priority is to make the large cosmic-ray test stand operational as soon as possible.

b) We intend to continue the program of measuring scintillator light yields and attenuation lengths.

c) We have produced several different types of light guides which we plan to test in a systematic manner. We also intend to study the feasibility of light collection schemes based on wave-shifting fibers.

692

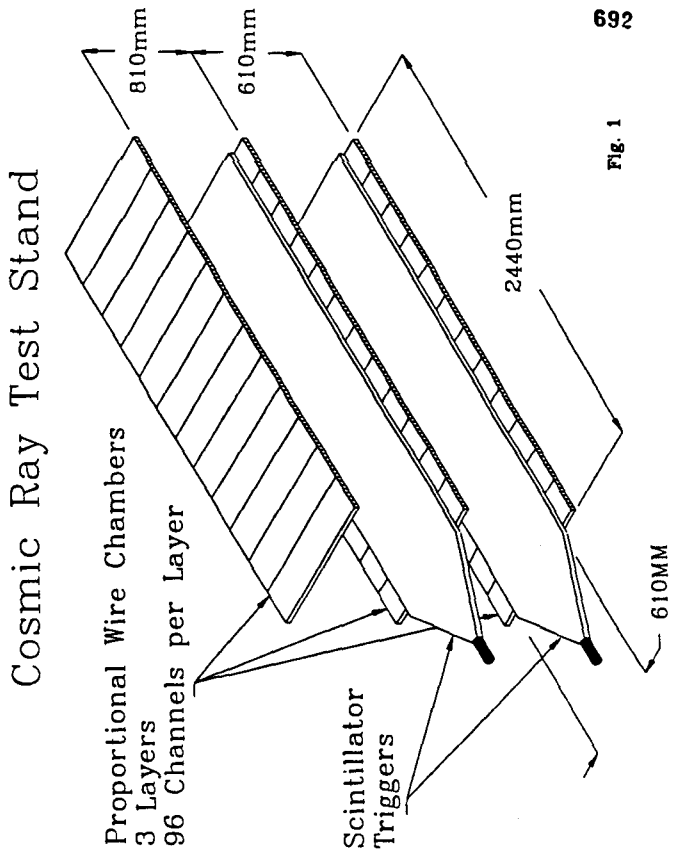


Fig. 1

693

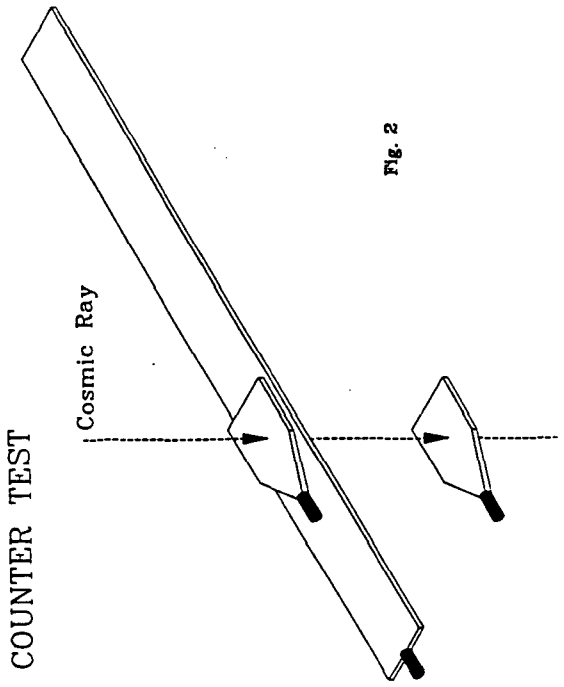


Fig. 2

694

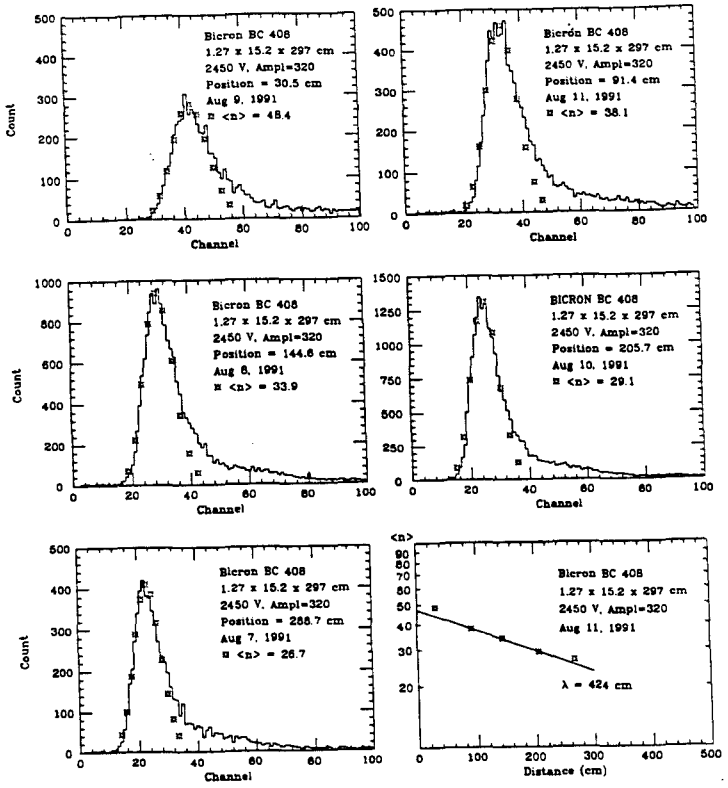


Fig. 3

695

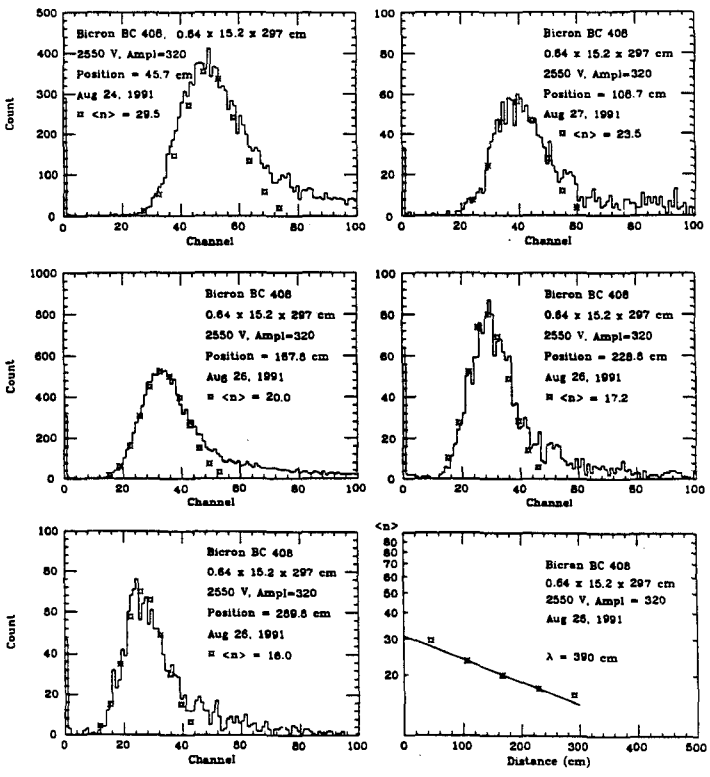


Fig. 4

696

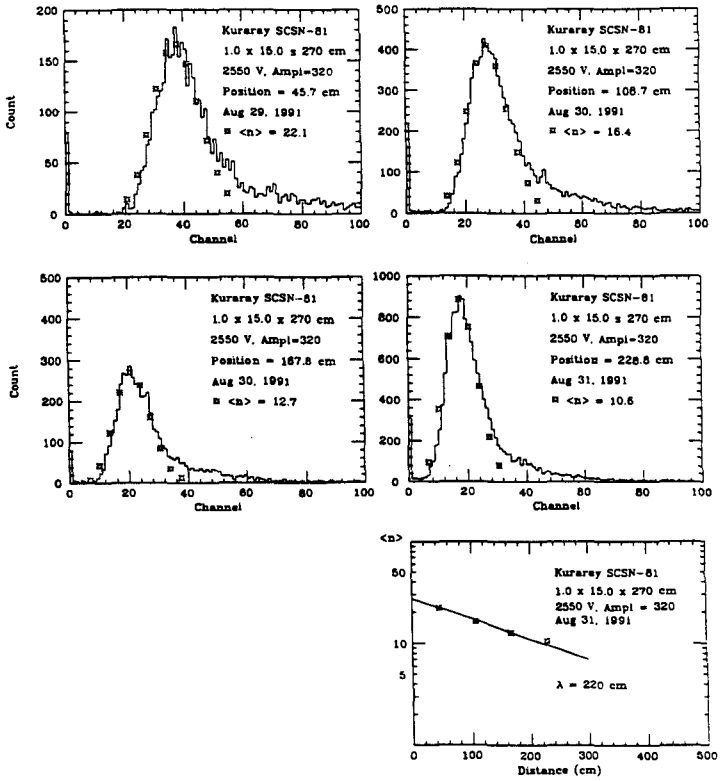


Fig. 5

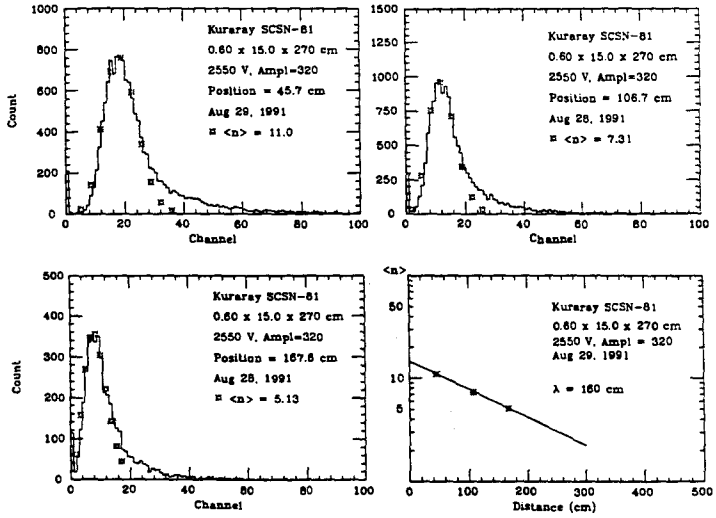

Kuraray SCSN-81
0.60 x 15.0 x 270 cm
2550 V, Ampl=320
Position = 45.7 cm
Aug 29, 1991
Σ <n> = 11.0
Kuraray SCSN-81
0.60 x 15.0 x 270 cm
2550 V, Ampl=320
Position = 106.7 cm
Aug 28, 1991
Σ <n> = 7.31
Kuraray SCSN-81
0.60 x 15.0 x 270 cm
2550 V, Ampl=320
Position = 167.6 cm
Aug 28, 1991
Σ <n> = 5.13
Kuraray SCSN-81
0.60 x 15.0 x 270 cm
2550 V, Ampl = 320
Aug 29, 1991
λ = 160 cm
Count
Channel
<n>
Distance (cm)

Fig. 6

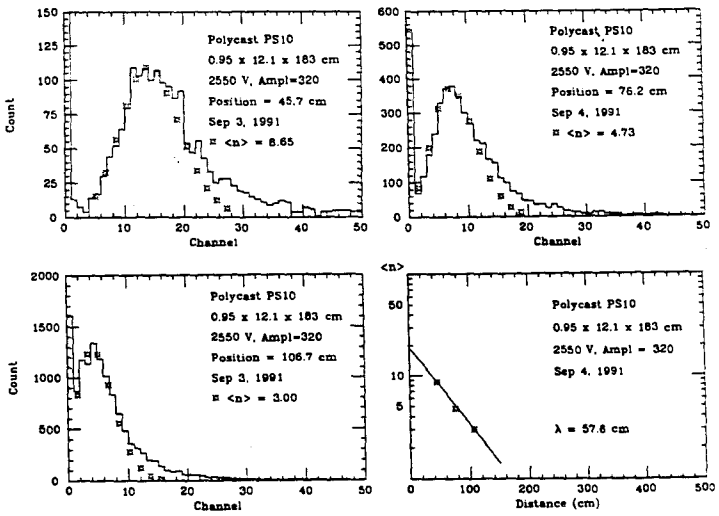

Polycast PS10
0.95 x 12.1 x 183 cm
2550 V, Ampl=320
Position = 45.7 cm
Sep 3, 1991
Σ <n> = 8.65
Polycast PS10
0.95 x 12.1 x 183 cm
2550 V, Ampl=320
Position = 76.2 cm
Sep 4, 1991
Σ <n> = 4.73
Polycast PS10
0.95 x 12.1 x 183 cm
2550 V, Ampl=320
Position = 106.7 cm
Sep 3, 1991
Σ <n> = 3.00
Polycast PS10
0.95 x 12.1 x 183 cm
2550 V, Ampl = 320
Sep 4, 1991
λ = 57.6 cm
Count
Channel
<n>
Distance (cm)

Fig. 7

Prototype of Foam Support for Muon Tubes

A. Sill(Rochester)

A. SILL

700

Progress Towards Goals:

- Have built 1 foot long (30 cm) 16 channel scale model prototype using direct injection, 1 inch tubes
- Have also built 3 each 8-layer x 4 tube arrays 1.8 m long using 3 methods (see previous transparency)
- Studied adhesion of foam to PVC plastic, aluminum, mylar, polyethylene using different approaches involving surface preparation (eg. solvent cleaning & abrasion), priming, cure time, etc.
- Measured density of foam for different filling techniques & procedures.
- more on the way

Also:

- Initiated 3-D and 2-D finite element models for simple Incarnatrons of foam & aluminum models using ANSYS for simple bars, stress-skin panels, etc. (Tubes to come later).

701

Further details (see photos):

- Mold (in progress)
- Method of filling to produce least possible pressure on tubes while foam is rising & curing
- PVC pipe used in place of resistive plastic &/or aluminum tubes for mechanical model (conservative)
- Riveting to achieve bond for templat- (intermediate Stiffener/locating guide) to aluminum sheet for top & bottom surfac
- strength both longitudinal & transverse.
-

702

Conclusion:

We have built 1-layer x 4 tube, 1.8m drift tube supports out of low mass iso-cyanurate foam, In the process, we have learned how to handle larger modules & have in progress a 16 tube, 4 layer x 9 meter long array; will measure sag & performance of this method of support in the upcoming month to 6 weeks.

☆ → It will be up to those who have proposed other methods of construction to prove that these other designs can do just as well as this one, or better (if possible).*

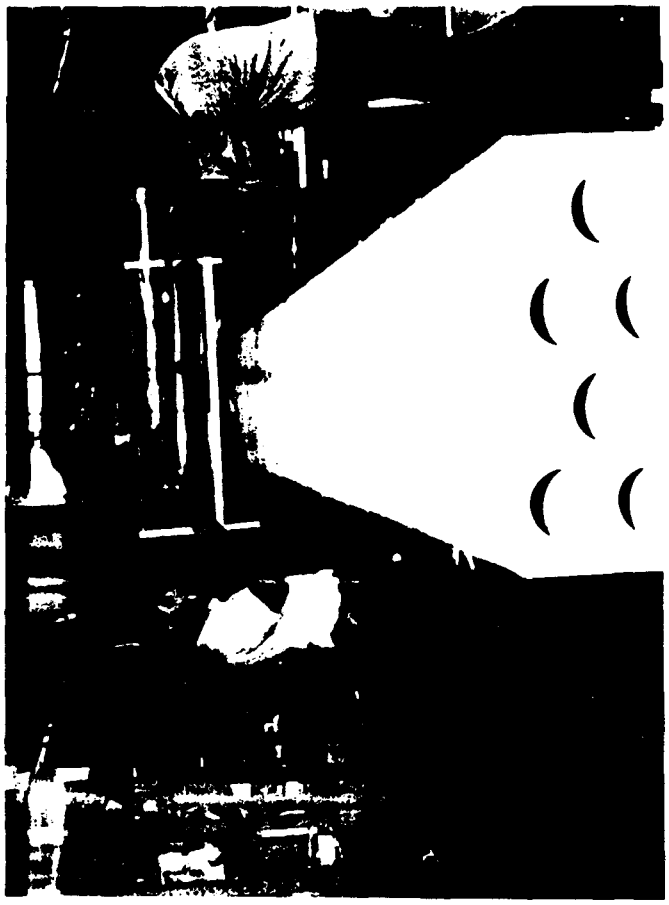
This method should prove to be a benchmark by which other ideas can be measured - as quickly as possible so that decisions can be made for FY 1992 and beyond.

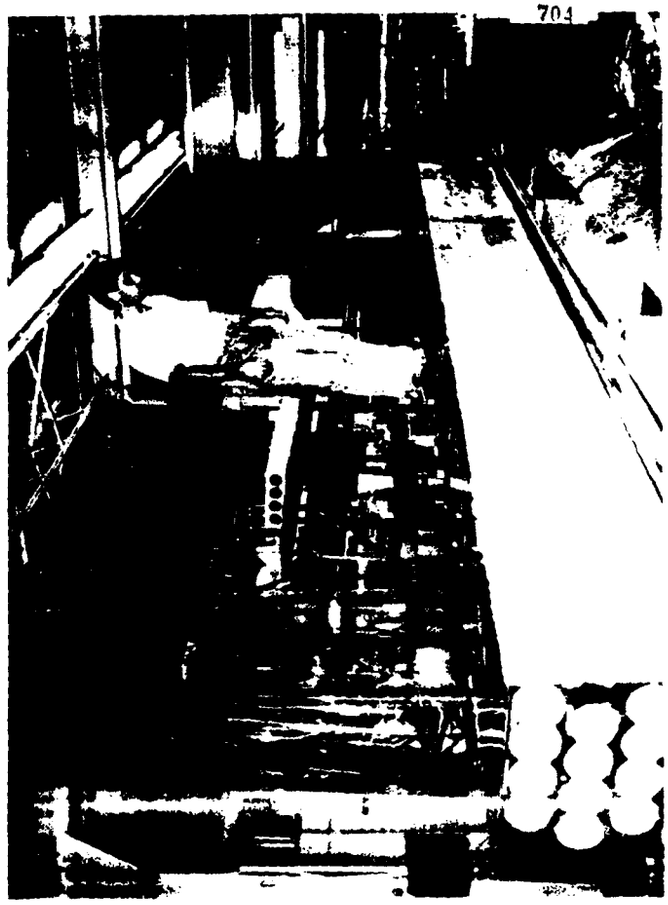
Resistive plastic inserts for field shaping prepared & ready to be tested also.

— AFS

*(in terms of sag, ease of construction, etc.)

703





Finite Element Modelling of Muon Detector Module

C. Daly(Washington)

Finite Element Modelling of Muon Detector Module Univ. of Wash. /SSC Design

C. H. Daly

Department of Mechanical Engineering, FU-10
University of Washington

September 24, 1991

The major questions to be answered by FEA of this module design are:

1. What magnitude of overall module deflection is seen for each of the modules in the three layers of the detector (BW1, BW2 and BW3)? How is this affected by support locations and the number of layers of tubes in the modules?

2. What values of shear stress are encountered in the adhesive bonding between the tubes and the plates.

The second of these questions requires a detailed model of the tube and plate structure. It is not realistic to use such a detailed model of the whole module to find overall deflections. As each module is a very large flat plate in overall shape, it is reasonable to model a module as a flat shell with just the rim of the module modeled separately. One first has to come up with equivalent properties for this shell so that it models the real structure of tubes and plates. Using data from this shell model, a small region of tubes and plates can then be modeled in detail.

In most of the analysis below, discussion is limited to a BW1 module with 4 layers of tubes in the θ direction. This is the thinnest likely module and is thus not only the simplest to model but is also the worst case for rigidity. The methods are easily extended to any other tube configuration as these are finally settled on.

A. determination of equivalent shell properties

The prototype to be built by this design team will consist of a 9 m. long section of tube and plate structure with a cross-section as shown in Figure 1. (the actual prototype will have 6 tube layers, 4 θ and 2 ϕ). The tubes are all 76.2 mm. (3.00 in.) diameter with a 1.59 mm. (0.0625 in.) wall thickness. The intermediate plates are all 1.59 mm (0.0625 in.) thick. The top and bottom plates are 6.35 mm. (0.25 in.) thick. The overall dimensions of the cross section are 630 mm. (24.8 in.) wide and 329 mm. (12.937 in.) high. The moment of Inertia I_x and area A_x of the section are then found. Together with the Young's Modulus E, the quantities EI_x and EA_x determine the properties relevant for bending and axial loading respectively. If the whole beam is simply supported at its ends, the deflection at the mid point is given by:

$$\delta_{max} = 5wL^4 / 384EI_x = 2.487 \text{ mm. } (0.0983")$$

w is the load/unit length and in this case is just the weight/unit length

As the tube/plate structure is not isotropic, we must also get similar properties in the Y-direction. In this case, the tubes would be perpendicular to the beam axis and would contribute little to the bending stiffness. Ignoring the tubes, we can then get values for I_y and A_y.

In the finite element model, the shell elements are constant thickness plates. We must choose suitable values for E and thickness t to obtain the same values for EI and EA for the model and the actual structure. It is not possible to do this for both directions at once, but as the bending stiffness will be much more important than membrane effects for this model, it is sufficient to match the values for EI_x and EI_y. One also must modify the density of the material to get the correct load/unit area for the model.

A simple test of this concept is shown in Figure 2. The 4-layer prototype is modeled as a simply supported beam using the equivalent shell elements. Analysis is done using the STIF93 8-noded quadrilateral shell element in Ansys. The maximum deflection is essentially identical to that given above.

FEA Shell model of a module.

In the Washington/SSC design, at any given layer (BW1,2,3), each face of the octagonal detector surface is made up of 3 modules. The maximum length of any given module is assumed to be one third of the axial length of the BW3 module, i.e. 9687 mm. The width is, of course different for each module. The dimensions used in the analysis described below are taken from the 8/3/91 configuration of the detector. The numbers of tube layers in each module have not been determined at the time of writing. The results given are thus tentative and can be revised easily when the final configuration is available. The configuration used here is:

BW1 module – 4 layers in θ direction
BW2 module – 4 layers in θ direction, 4-layers in ϕ direction (8 layers total)
BW3 module – 4 -layers in θ direction, 2 stereo layers (6 layers total)

All modules are supported in the radial direction at three points along the long edges (i.e. the ϕ direction). In the $\theta\phi$ plane, purely kinematic constraints are used.

Figure 3 shows a model of a 4-layer BW1 module. Because of symmetry, it is only necessary to model one quadrant of the module. The tube/plate structure is modeled by equivalent shell elements as described above. The side and end plates of the module are modeled by 19mm. (0.75 in.) thick shell elements. This module is in the top position in the barrel and is thus the worst loading case. Note that the maximum deflection of 0.37 mm. is quite acceptable. If the module is supported only at the 4 corners, the deflection is still less than 1 mm.

Figures 4–7 show results for BW1 modules on all other faces of the octagon.

Figures 8 and 9 show results for a 8-layer BW2 module and a 6-layer BW3 module respectively. The deflection of the BW2 module is acceptable but that for the the BW3 module is greater than 1.0 mm.

Discussion:

The BW1 and BW2 module configurations shown above are adequately stiff by themselves. The most important result is that a 4-layer BW1 module appears to be practical. BW1 is is adequately stiff when it mounted on either 4 or 6 supports. However, as can be seen from Figure 10, a pure kinematic, 3-point support is not practical for this module.

The 6-layer BW3 module with 6-supports shows excessive deflection. However, when BW2, BW3 and the truss spacer between are considered as a single unit, the whole structure will be very stiff indeed. The major issues to be considered will be the connections between the truss and the modules and the deflections of the whole structure due to differential thermal expansion. A model of of a supermodule composed of the BW2 and BW3 modules together with a truss composed of simple tension/compression members is shown is Figure 11.

Further work:

Truss structures such as that shown in Figure 11 will be analysed to produce a supermodule which is sufficiently rigid to be mounted on the magnet using pure kinematic supports. The effects of thermal gradients on this supermodule will be studied.

While stresses in the metal parts of the tube/plate structure are quite low (3–4 MPa from the above models), the stress on the adhesive joints also needs to be considered. For the prototype 4-layer beam, an approximate analysis gives shear stress values at the neutral axis on the order of 200–300 psi. The represents a factor of safety of about 4. In order to obtain better values for full size modules with more complex structures it will be necessary to determine the most highly loaded regions of the module from the analysis shown above and to use these conditions to load a detailed model of a small part of the whole module. Figure 12 shows such a model for part of a 4-layer module.

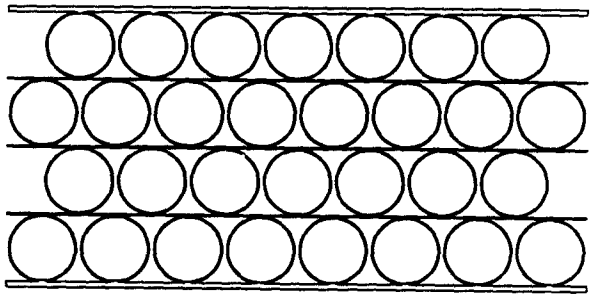


Figure 1. Cross-section of 4-layer prototype. All tubes are 1.59 mm. (0.0625 in.) wall thickness and 76.2 mm. (3.00 in.) outside diameter. The top and bottom plates are 6.35mm. (0.25 in.) thick and the intermediate plates are 1.59 mm. (0.0625 in.) thick. The whole structure is 9144 mm. (360 in.) long

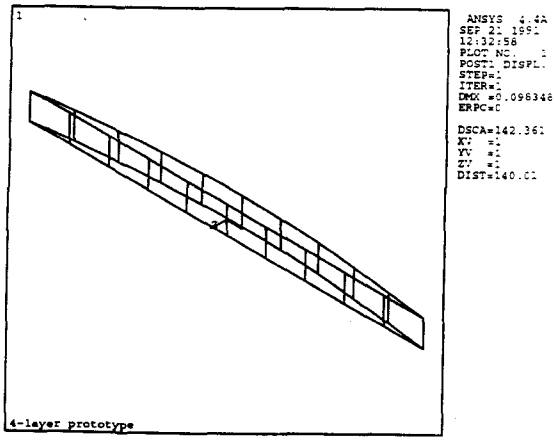


Figure 2: Test of FEA on the 4–layer prototype beam using equivalent shell elements. Note that the deflection is essentially identical to that found from classical beam theory (see text).

(In this and other Ansys output, the maximum deflection is listed as DMX. Also note that in this example, the deflection is given in inches.)

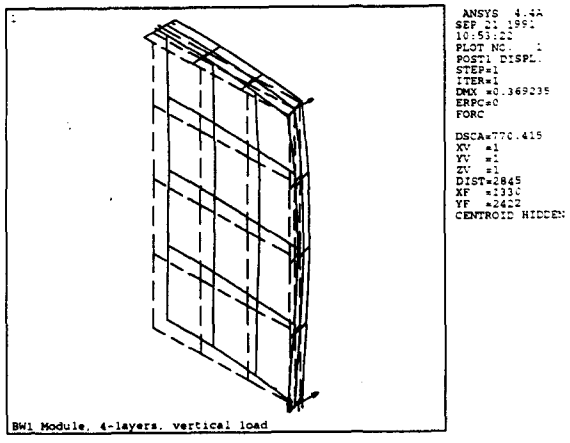


Figure 3: FEA of a 4–layer BW1 module. Only one quadrant is shown. The maximum deflection DMX is given in millimetres. This module is the one at the top position in the barrel. The overall dimensions of this module are 5186 mm. (θ–direction), 9687 mm (axial direction) and 322 mm. thick.

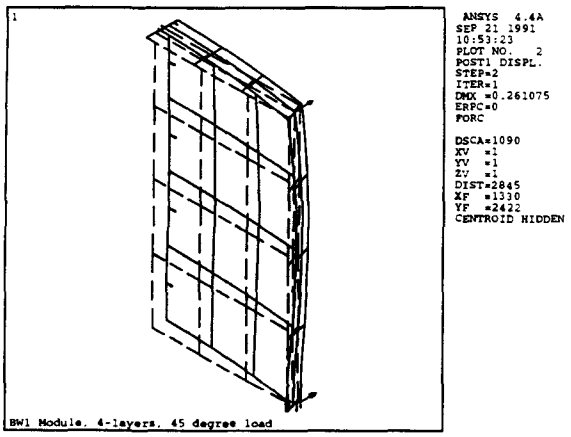


Figure 4: FEA of a 4–layer BW1 module. Only one quadrant is shown. The maximum deflection DMX is given in millimetres. This module is the one at the top, right position in the barrel.

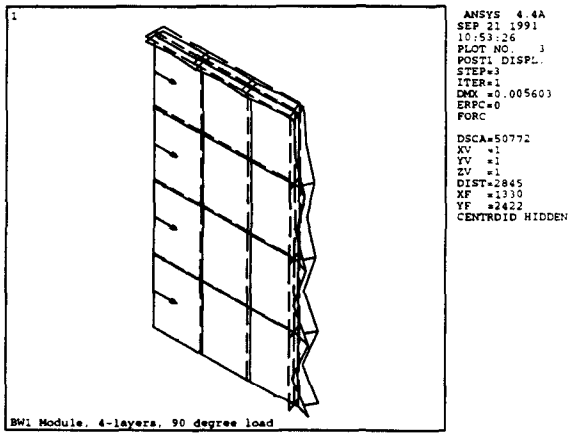


Figure 5: FEA of a 4–layer BW1 module. Only one quadrant is shown. The maximum deflection DMX is given in millimetres. This module is the one at the right side position in the barrel.

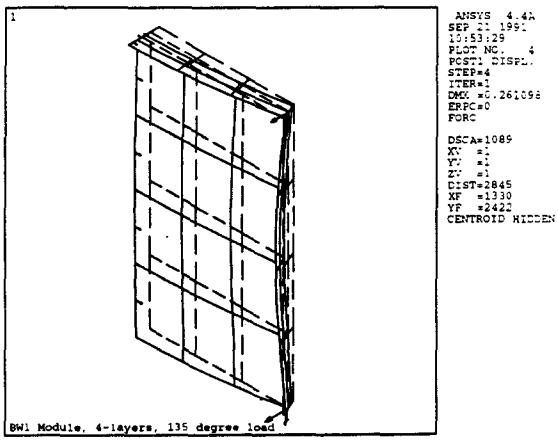


Figure 6: FEA of a 4–layer BW1 module. Only one quadrant is shown. The maximum deflection DMX is given in millimetres. This module is the one at the bottom, right position in the barrel.

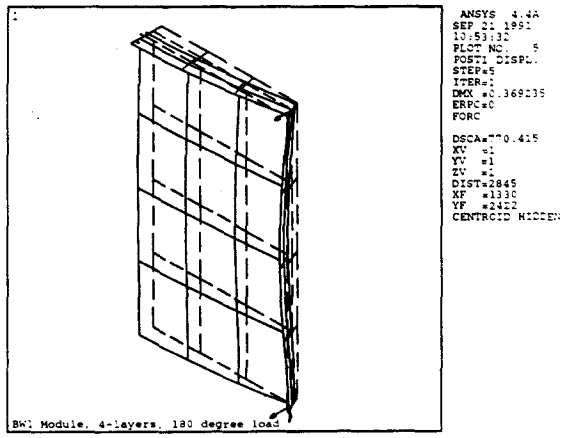


Figure 7: FEA of a 4–layer BW1 module. Only one quadrant is shown. The maximum deflection DMX is given in millimetres. This module is the one at the bottom position in the barrel.

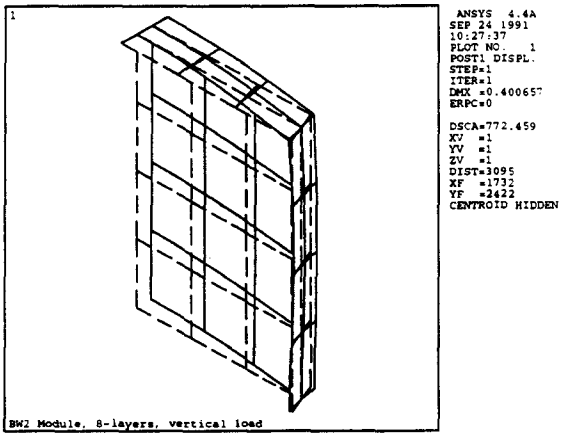


Figure 8: FEA of a 8–layer BW2 module. Only one quadrant is shown. The maximum deflection DMX is given in millimetres. This module is the one at the top position in the barrel. The overall dimensions of this module are 6664 mm. (θ–direction), 9687 mm (axial direction) and 633 mm. thick.

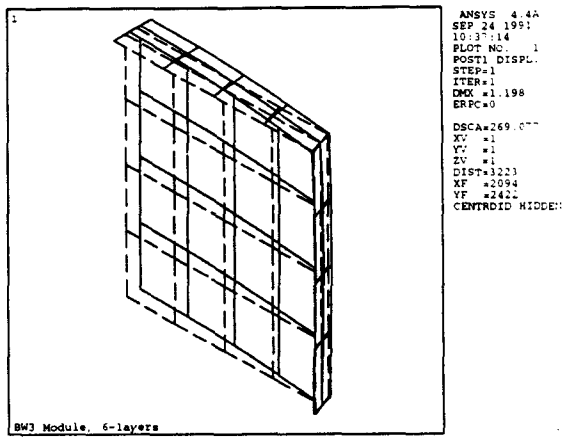


Figure 9: FEA of a 6–layer BW3 module. Only one quadrant is shown. The maximum deflection DMX is given in millimetres. This module is the one at the top position in the barrel The overall dimensions of this module are 8177 mm. (θ–direction), 9687 mm (axial direction) and 478 mm. thick..

718

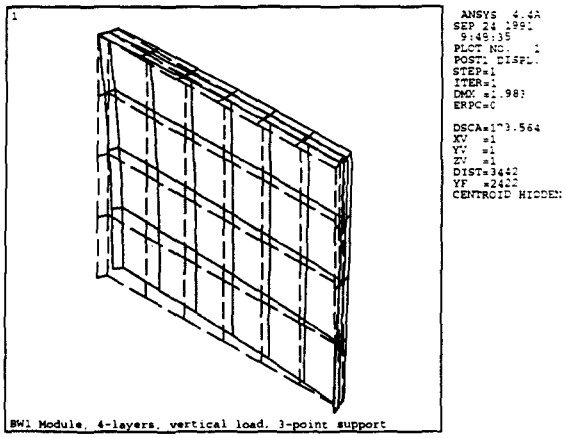


Figure 10. 4–layer BW1 module on 3 kinematic supports. Note that the maximum deflection is 1.983 mm.

13

719

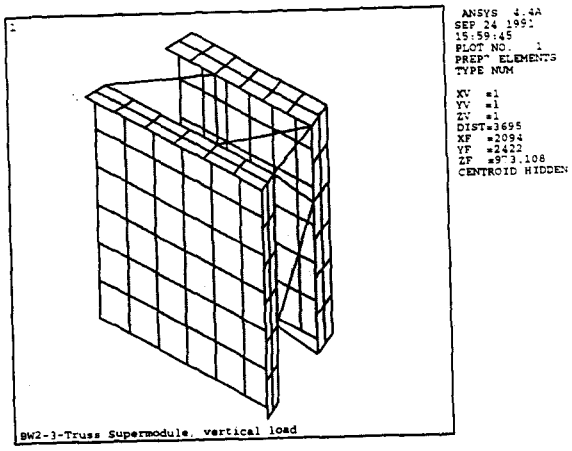


Figure 11. Supermodule composed of BW2 and BW3 modules together with their supporting truss structure. Only 1 quadrant is shown.

14

720

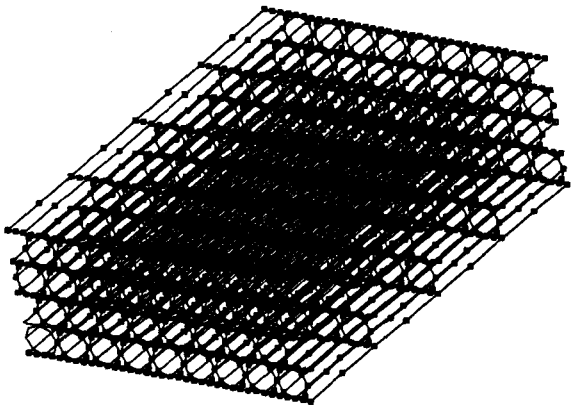
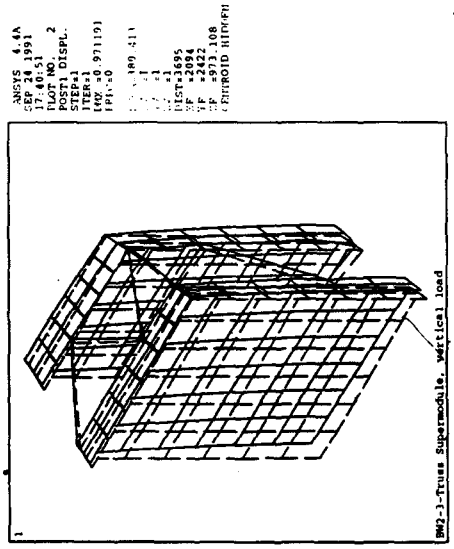


Figure 12. Detailed finite element model of a section of a 4–layer module.

15

721



722

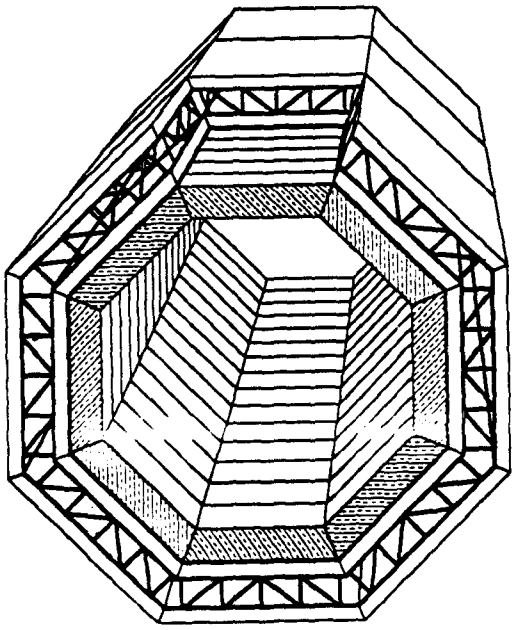
723

MUON MODULE ASSEMBLY
MEETING SSCLAB
AUGUST 28, 1991
HENRY LUBATTI

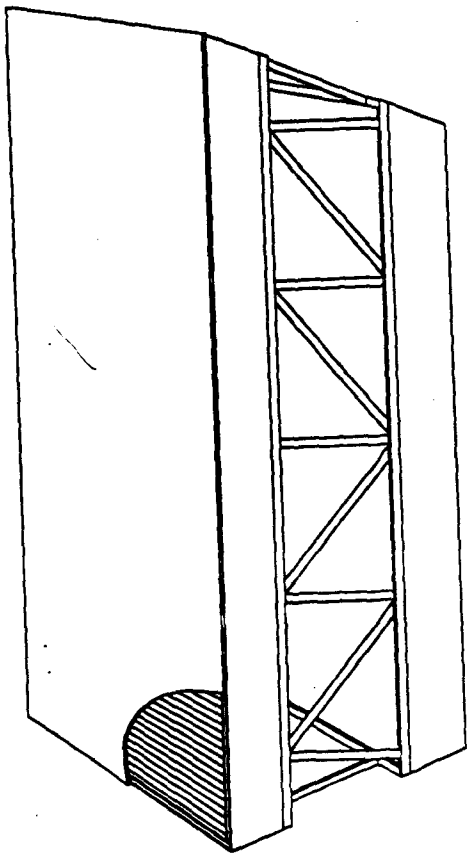
MUON DETECTOR SYSTEM

SSC-WASHINGTON APPROACH
(ROUND TUBES)

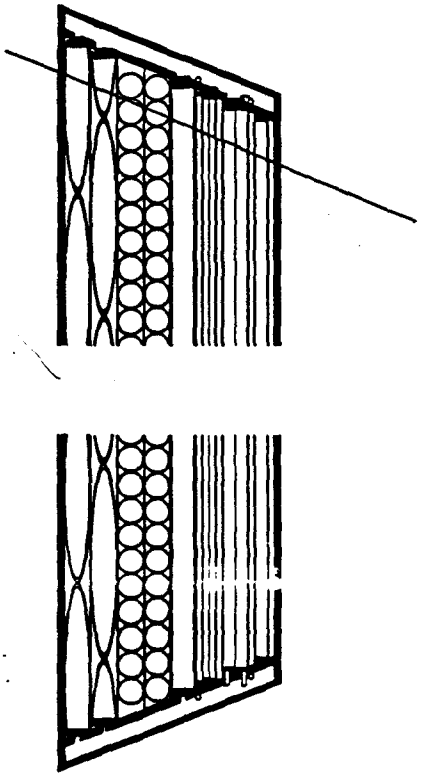
- SEPARATE THE FUNCTIONALITY OF DRIFT CELLS FROM CONSTRUCTION OF DETECTOR MODULES
- EACH DRIFT CELL IS FULLY FUNCTIONAL AND IS CONSTRUCTED AT SEVERAL DIFFERENT LABORATORIES AND UNIVERSITIES
- DRIFT TUBES ARE USED AS STRUCTURAL ELEMENTS OF THE DETECTOR MODULES
- ALIGNMENT AND ORIENTATION OF DRIFT CELLS WITHIN A MODULE IS FIXED BY DRIFT TUBE END CAPS AND MODULE END PLATES
- MODULES ARE ASSEMBLED AT THE SSC

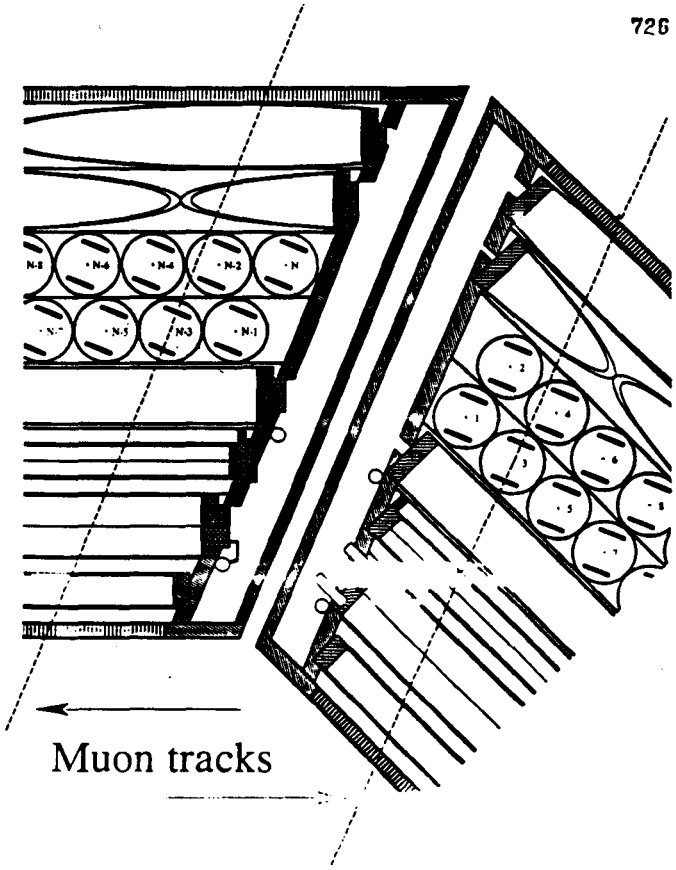


724



725




Muon tracks

Experience with Short Drift Tubes

T. Zhao(Washington)

University of Washington
Visual Techniques Laboratory
Physics Note
PHY-152

Experience With Short Drift Tubes

Tianchi Zhao
Department of Physics, FM-15
University of Washington
September 25,1991

Short 3" diameter drift tubes with three different anode wire diameters are operated with a variety of different gas mixtures. Results of these studies help us to determine the final tube design and operation conditions.

Anode Wire Diameter and Gas Mixture

There are concerns that stable proportional mode operation may not be achievable if a large diameter anode wire is used. We have compared the behavior of tubes with three different anode wires, $\phi 51\ \mu m$, $\phi 102\ \mu m$ and $\phi 153\ \mu m$ in different gas mixtures.

We directly observe the signal amplitude using a Tektronix 2465 oscilloscope. Since the proportional signal size is small, in order to enhance the visibility of signals, the oscilloscope is terminated with a 510 Ω resistor. Typical Fe^{55} source signals are given in Fig. 1.

We determine the lower limit of the operating range by demanding the signal peak to be 2mV which corresponds to $4\mu A$ maximum current. The gas amplification factor is estimated to be about 1.3×10^4. This is the gas gain we observe with our setup, not the true gas gain. Only a fraction of the total produced charges in an avalanche is observed due to the fact that the signal differentiation time constant is about 500ns.

The upper limit of the operating range is defined by observing the tube DC current. We estimate the upper limit by comparing the "dark" current and also the "source" current, the anode current when a 1mC β source is placed on top of the tube. The upper limit of the operating range is determined when the tube dark current starts to be different from zero (about 30-40nA) and the source current to be about $1\mu A$.

At a given voltage we observe indications of breakdown due to unquenched UV photon emission. This effect is clearly shown in Fig. 2. The tube dark current

increases dramatically above this point.

We have made measurements with several gases with and without the addition of alcohol. In all cases the indicated alcohol was added by flowing the gas through the alcohol which was at 3.5°C. Table 1 summarizes the gases tested and the operating ranges observed.

Table 1. Operating Range

Gas Mixture	Range (kV)		
	ø50μm	ø100μm	ø150μm
Ar-CH_4 90:10	2.4 - 2.9	2.9 - 3.35	3.4 - 3.8
Above with ethanol	2.4 - 3.5		3.4 - 4.2
Ar-C_4H_{10} 1:2	4.0 - 6.5		
Ar-CO_2 90:10	2.6 - 2.9	3.1 - 3.4	3.6 - 3.8
Above with isopropanol	2.5 - 3.0	3.0 - 3.4	3.5 - 3.8
Ar-CH_4-CO_2 90:5:5	2.7 - 3.1	3.0 - 3.4	3.5 - 3.8
Above with isopropanol			

We conclude:

- The operating range of the ø50μm diameter wire is the largest among the three kinds of wires tested. The differences are, however, rather small.
- The operational range depends strongly on the gas mixtures. The operating range we observed for Ar/CO_2 90:10 is small. The stability is especially poor for the ø153μm anode. (CO_2 is known not to be a good quenching gas.)
- Alcohol surpresses the secondary streamer pulses and, therefore, makes the tube operation more stable. By adding ethanol, the operation range of the P10 gas is greatly extended and the speed of the P10 gas is not affected. The maximum drift time in both cases is 800 ns. Ethanol also helps gas mixtures containing CO_2. The effect, however, is less prominent. Isopropanol alcohol has also been tried. The results are very similar to that of the ethanol. Alcohol slows the drift speed down in the the gas mixtures containing CO_2 significantly.

We also tried Ar-CH_4 50:50. This gas is extremely fast in our tube. The maximum drift time is only about 500 ns. Another gas mixture, Ar/C_4H_{10} 1:2, has even better quenching property. The operating range is extremely large as given in the above table.

Limited Streamer Mode

Drift tubes operating in self-quenching streamer mode are standard devices for many large muon detector systems such as CDF, ALEPH, DELPHI, ZEUS and many others. The conventional streamer mode gas mixture is argon/isobutane mixed at 30:70 ratio. This gas mixture is of course highly flammable.

Due to the safety considerations, great efforts have been devoted to finding non-flammable gas mixtures for streamer tubes [1][2][3][4][5]. So far, most of the proposed non-flammable gas mixtures contain a large portion of CO_2 and a small fraction of iso-butane or iso-pentane. Such gas mixtures, though nonflammable, require a very high electric field in order to obtain sufficiently fast drift speed. Because of this, they can only be used for tubes with small cross section. Another potentially fast nonflammable gas mixture, which the GEM muon group is investigating, is a CF4 based mixture with 8-9% of isohutane.[6] This mixture is, however, not a practical choice for the SDC muon system which has a much longer drift distance.

It is well known that gas mixtures with a small fraction of quenching gas cannot be operated in the streamer mode. We have studied in detail the behavior of gas mixtures, such as argon/CO2 90-10 and $argon/CO_2/CH_4$ 90-5-5, which are considered for SDC muon drift tubes. We have made the following observations.

- Streamer mode can occur in these gas mixtures. Clear streamer signals are shown in Fig. 3. The signal size is indeed very large and the width of the signal is very wide. The streamer signal width is independent of the time constant of the differential circuit. This is shown in Fig. 4 for 45Ω termination (45ns decay time constant) and for 500Ω (500ns time constant).
- Proportional mode and streamer mode signals coexist in these gases. Most signals do not develop into streamer mode even with the 153μm diameter anode wire running at nearly break down voltage. Both modes can be seen in Fig. 3 and 4.
- Streamer mode signals produce secondary streamers because of electrons released by the aluminum wall absorbing UV photons produced in the streamers. The time interval between the primary and secondary streamer signals is a direct measure of the total electron drift time from the wall to the wire.
- Bubbling through alcohol does help. But the streamer mode development is still far from complete.

Streamer mode does develop fully in Ar/C_4H_{10} 1:2 mixture. This is shown in Fig. 5 in which only the streamer signals are present. The signal width is much

narrower indicating strong quenching from isobutane.

In order to quantify our observation, we have attempted to measure streamer efficiency which is the fraction of signals which are streamer signals. F^{55} source spectra are taken using LeCroy QVT. The Q-mode threshold is at its minimum of 1 mV. Both proportional mode peaks and streamer mode peaks are recorded and the ratio of observed counts in both modes are measured. Typical spectra are shown in Fig. 6-10.

Streamer efficiencies as functions of high voltages for different gas mixtures and different anode wires are shown in Fig. 11.

References

[1] A. C. Benvenuti et al., "Nonflammable Gas Mixure for Plastic Streamer Tubes", NIM A2S4 (1989) 339

[2] D. M. Lee et al., "The Response of Drift Tube to Variation in Wire Diameter and Gas Filling", NIM A256 (1987) 329

[3] C. DE Clercq et al., "Drift Chambers Operated in the Limited Streamer Mode", NIM A243 (1986) 77

[4] G. Bauer et al., "Upgraded Muon Detection System for UA1 Based on Limited Streamer Tubes", NIM A253 (1987) 179

[5] J.H. Moromisato et al., "Nonflammable Gas Mixtures for Streamer Tubes", NIM A272 (1989) 177

[6] L. Orsbon, private communication.

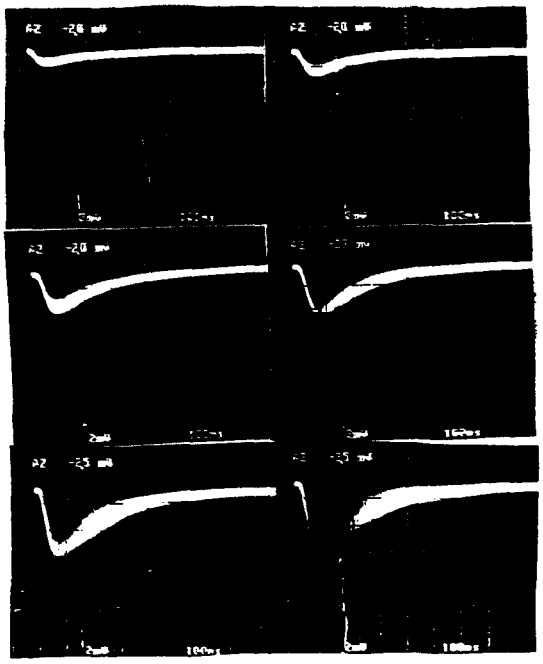
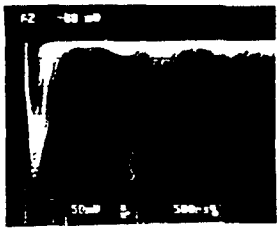


Fig. 1: P10 ϕ153μm anode, proportional mode
3.3 kV - 3.8 kV

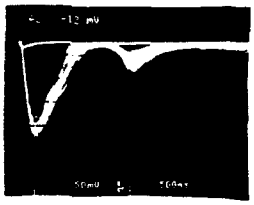


P10 ϕ100μm @ 3.6 kV

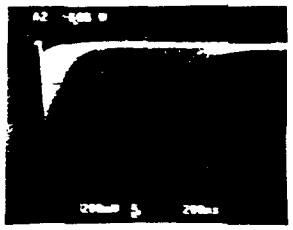
Ar-CO_2-CH_4 90:5:5 ϕ153μm @ 4.3 kV



Ar-CO_2-CH_4 90:5:5 ϕ50μm @ 3.3 kV

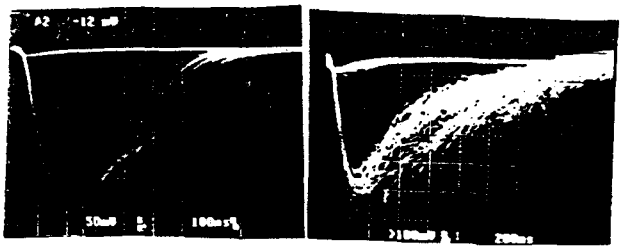


Ar-CO_2-CH_4 90:5:5 ϕ100μm @ 3.4 kV



Secondary streamers in C_4H_{10}/Ar 2:1
ϕ50μm @ 6.7 kV

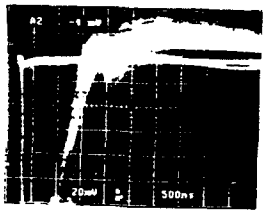
Fig. 2: Secondary streamers
(Notice the time constants)



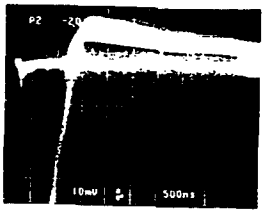
Fe^{55} @ 3.9 kV ϕ102μm

β-source @ 3.9 kV ϕ153μm

Ar-CO_2-CH_4 90:5:5

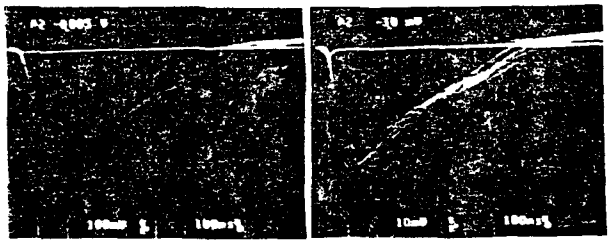


Fe^{55} @ 4.0 kV ϕ150μm
Ar-CO_2 90:10



Fe^{55} @ 3.7 kV ϕ150μm
Ar-CO_2 90:10 with ethanol @ 3.5°C

Fig. 3: Proportional mode and streamer mode signals

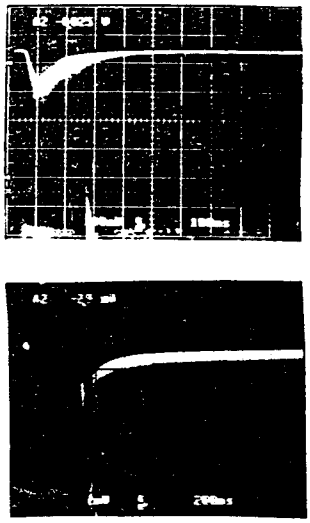


500 Ω termination

45 Ω termination

Ar-CO_2-CH_4 90:5:5
Fe^{55} ϕ160μm 4.4 kV

Fig. 4: Decay time constant of streamer mode signal does not depend on the termination resistor.

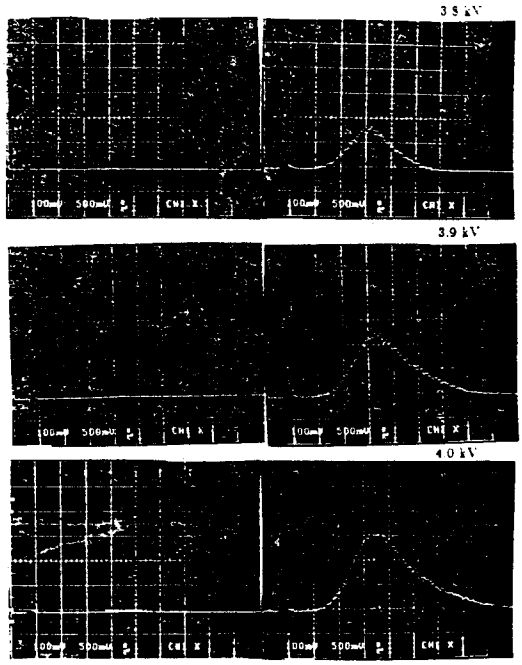


6.0 kV
ϕ100μm

5.5 kV
ϕ50μm

No proportional mode signals are visible

Fig. 5: Fully developed streamer mode Ar-C_4H_{10} 1:2

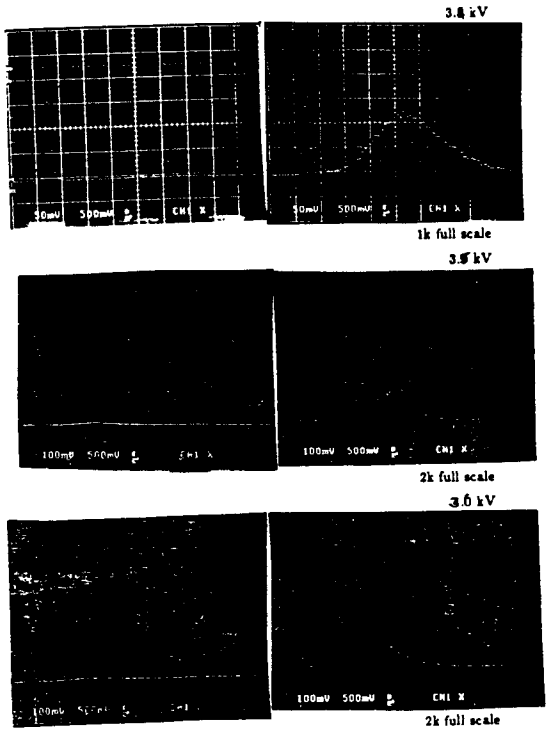


3.8 kV

3.9 kV

4.0 kV

Fig. 6: Ar-CO_2-CH_4 90:5:5
QVT spectra, Fe^{55} ϕ153μm anode
Left: 64k counts full scale
Right: 1k counts full scale



3.4 kV

1k full scale

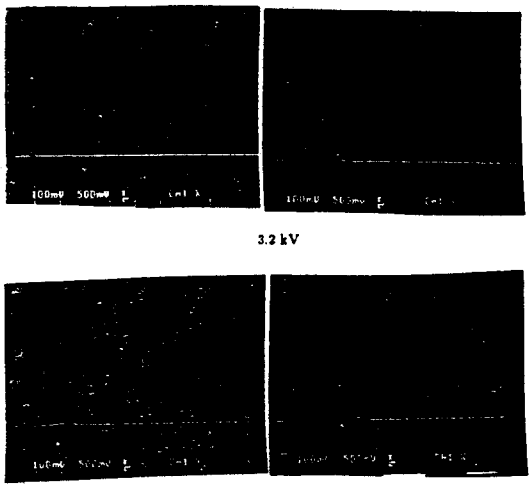
3.5 kV

2k full scale

3.6 kV

2k full scale

Fig. 7: Same as Fig. 6, but ϕ102μm anode
Left: 64k full scale



3.2 kV

3.3 kV

Fig. 8: Ar-CO_2 90:10 ϕ100μm
Left: 64k full scale
Right top: 512k full scale
Right bottom: 2k full scale

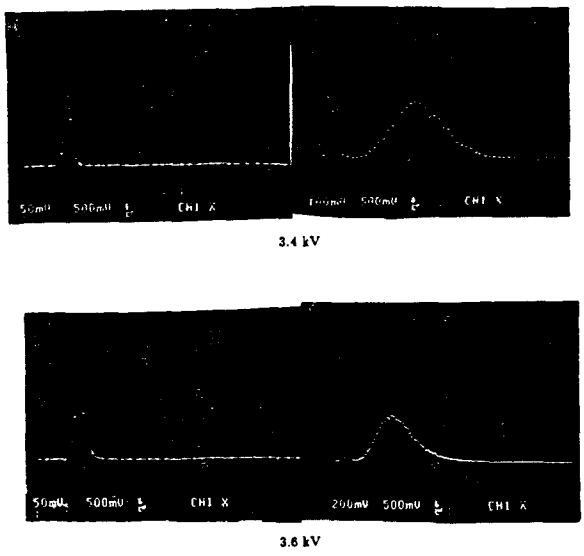


Fig. 9: P10 100μm anode
Left: 64k full scale
Right top: 512k full scale
Right bottom: 2k full scale

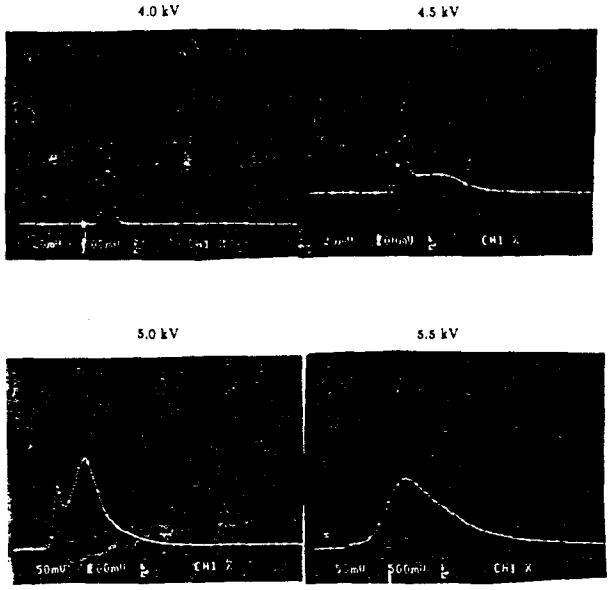


Fig. 10: Development of streamer mode in Ar-C_4H_{10} 1:2
Fe^{55} φ50μm anode

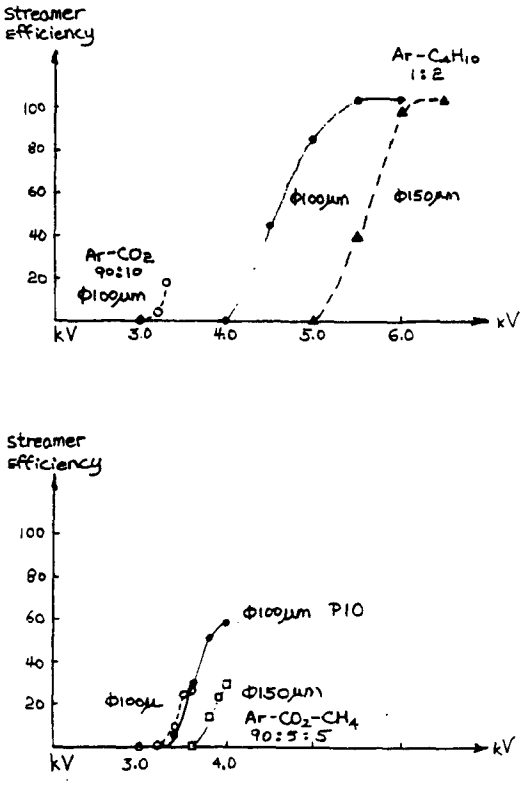


Fig. 11: Streamer efficiency plots

Forward Muon System

A. Skuja(Maryland)

744 Andris Skuja
Sept 27 /91

Forward Muon System (Univ of Maryland)

- Layout Update
  including cabling, gas lines, etc
- Length of Forward System
  "overlap" vs "no overlap" options
- First results on square drift tube
  measurements at Maryland

745

Preliminary
August 26,1991
16 pages

FORWARD DETECTOR
Rev 1

A. Skuja, M. Murbach, W. Miller, F. Desrosier, R. Bard

UNIVERSITY OF MARYLAND

Muon Chamber

Definition of components

- Chamber Module - A set of twelve(12) or sixteen(16) chambers in one extruded part. See Figure 1 extruded 12 pack.
  Est. weight(avg) 50 lbs
- Octant Module - An assembly of modules onto a trapezoidal picture frame. The modules are assembled onto both sides of the frame. See Figure 2 & Figure 3

  Est weight 3000 lbs
- Super Modules - A super module is a trussed support frame that supports eight(8) octant modules. See Figures 4,4a,4b,5 & 6.
  Est. weight 26000 lbs

The chamber module is designed with metal end caps and insulated inserts to hold the chamber wires in the center of the chamber(see figure 1). The wires are tensioned, crimped, and soldered. There are two gas ports. Gas flows into the first chamber, then into adjacent chambers via machined groves in the end caps and exits on the same end cap on the last chamber. The chambers have a circuit board on each end. One end provides a passive wire termination. The other end has an active circuit board that provides high voltage distribution, impedance matching, preamplifiers, shapers, discriminators and signal drivers. There are two connectors on the active circuit board, one for high voltage and one for low voltage and signals.
The chambers are shipped to the site in sealed shipping containers that measure 8' X 8' X 20'. They are completely tested at the point of origin.

The octant module frame is constructed from one inch thick stainless steel stock(see figure 2). There are four mounting holes. One on each corner. Each of the chamber module mounting holes are referenced to the octant module

746

mounting holes. The chamber modules are assembled from the inside, beginning on a location shelve, to the outside. The chamber modules rest upon one another and are clamped together with a tension screw on the outside chamber. Figure 3 indicates the end view of a module. At assembly, each octant is completely wired for the electronics and the gas lines.
The octant frames can be shipped to the site on pallets by commercial carrier.

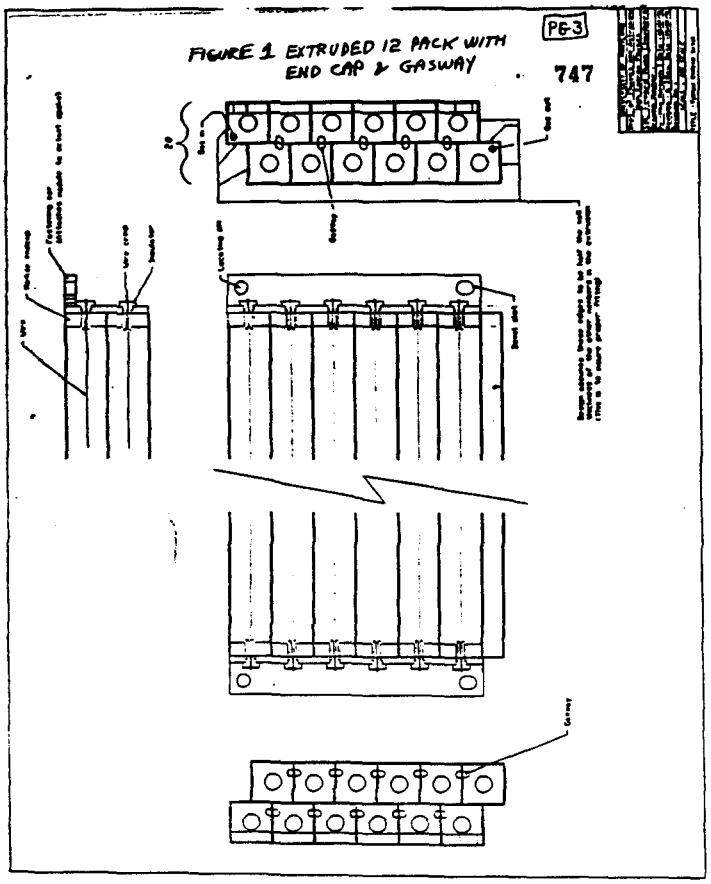
The octant modules are then installed into a super module (see fig 4,4a,4b,5,&6). The super module is held in the vertical position for the entire assembly. The cables from the chamber electronics and the gas lines are connected to electronic and gas boxes located in the outer truss sections of the super module. Each electronic box (1"X8"X12") services six(6) chamber boards. Each electonic box contains a TDC for each chamber with connectors and circuitry to allow interconnectivity between super modules to enable level 1 trigger determination. The electronics box will also provide high and low voltage distribution as well as appropriate data transmission and trigger signals. The chamber modules are connected in the boxes to allow one chamber module to be disconnected from the system. Each octant module is adjusted to be in a known position relative to the mounting points of the super module. The attachments for the super modules on the calorimeter, absorbers and the muon toroid are adjustable to allow for an exact location relative to an established reference.
The super module frame is too big to ship. It will be constructed from sections and shipped to the site for final construction.

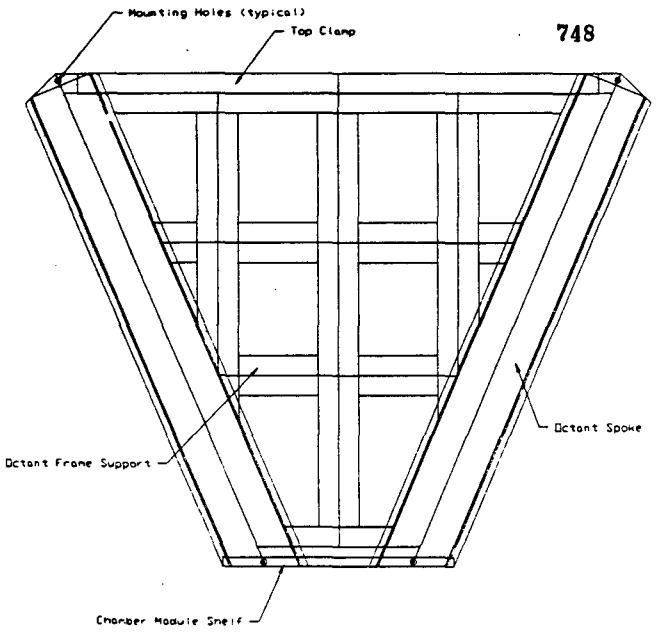
Figures 7,7a,&7b indicate the configuration of the muon chambers.

Table 1 - The total chamber count. Table 2 - The totel number of octant modules. Table 3 - The total number of super modules. Table 4 - The total number of crate boards and gas header connections.

747

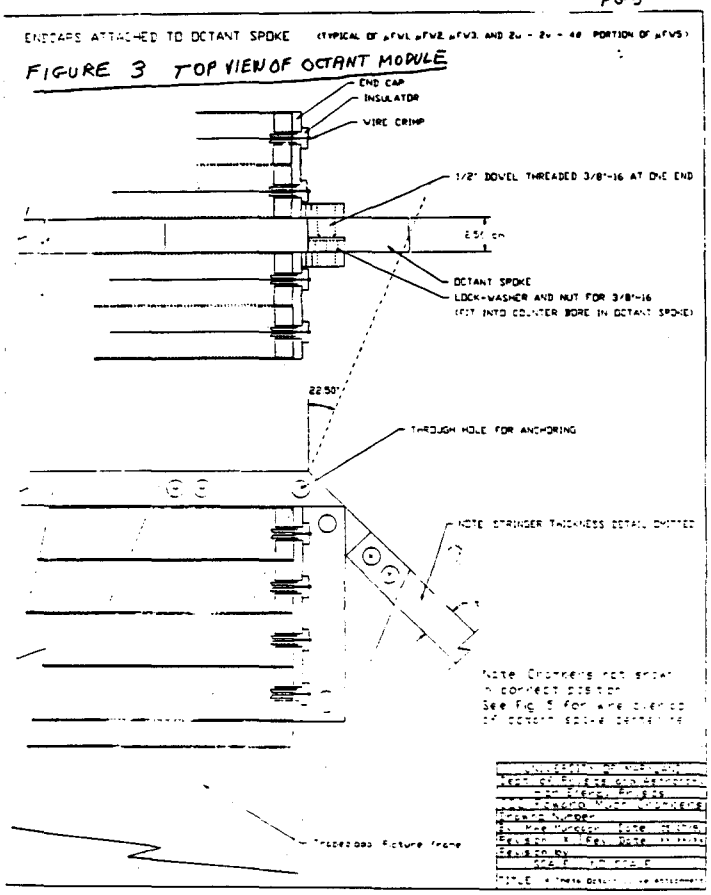
FIGURE 1 EXTRUDED 12 PACK WITH END CAP & GASWAY

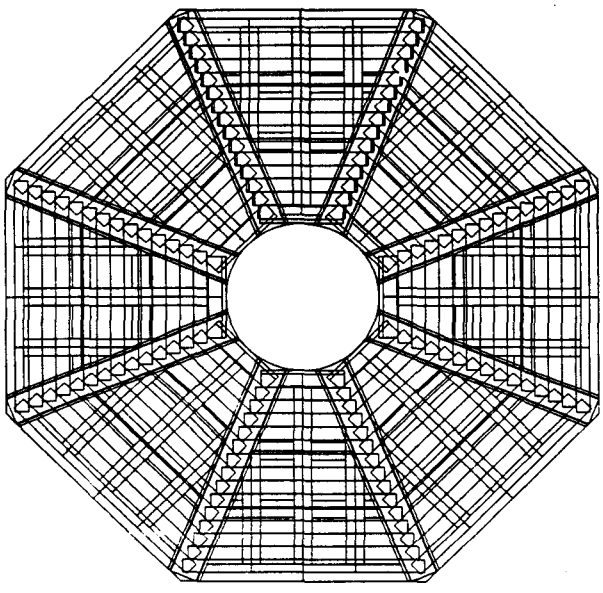




OCTANT MODULE TRAPEZOIDAL FRAME (TYPICAL)

FIGURE 2





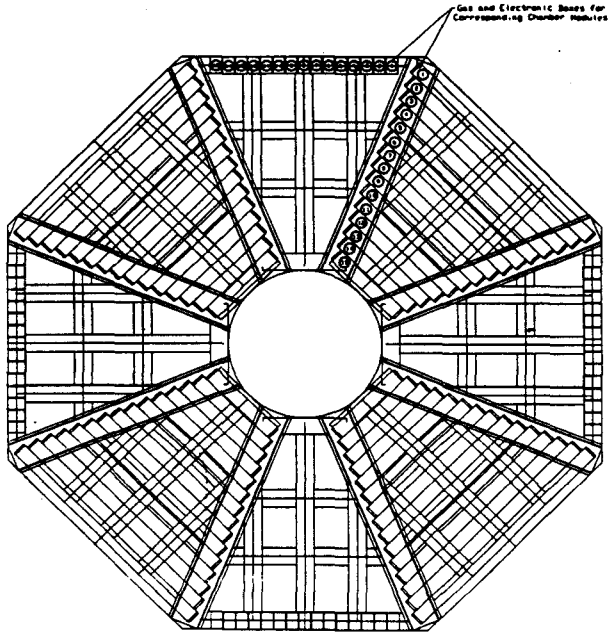
μFW1 — 4θ

OCTANTS ARE STAGGERED AND ELECTRONICS ARE LOCATED ON FACES OPPOSITE WIRE MODULES

FIGURE 4

SUPER MODULE

TYPICAL

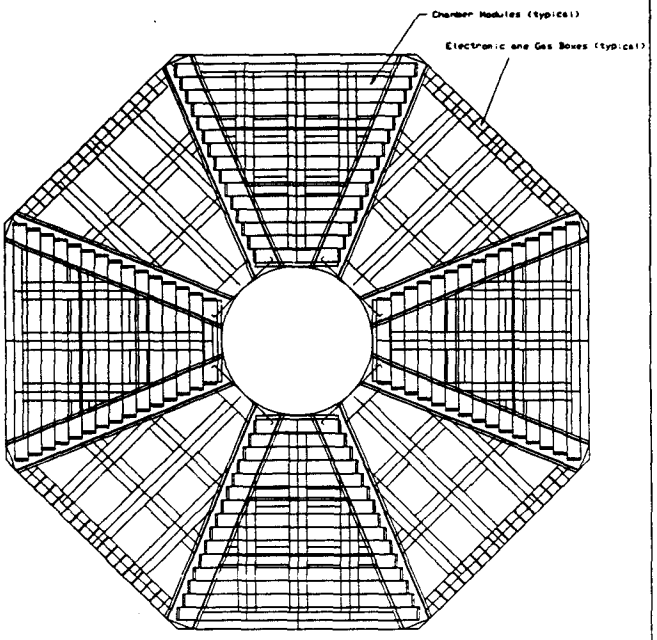


μFW1 — 4θ

FRONT LAYER OF A SUPERMODULE

FIGURE 4a

752 PG 8



μFW1 — 4θ
BACK LAYER OF A SUPERMODULE

FIGURE 4b

753 PG 9

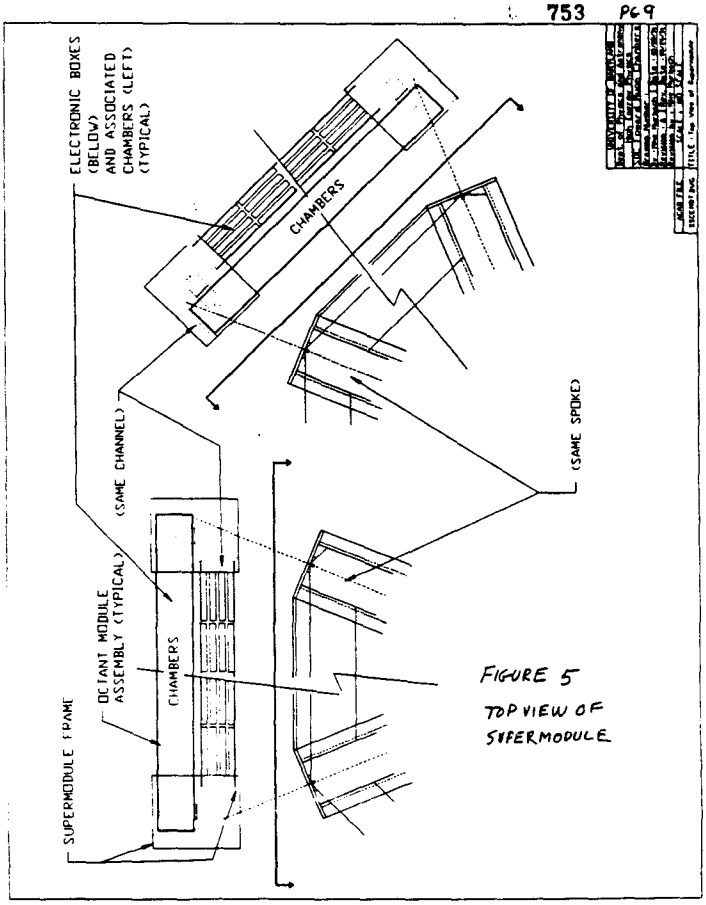
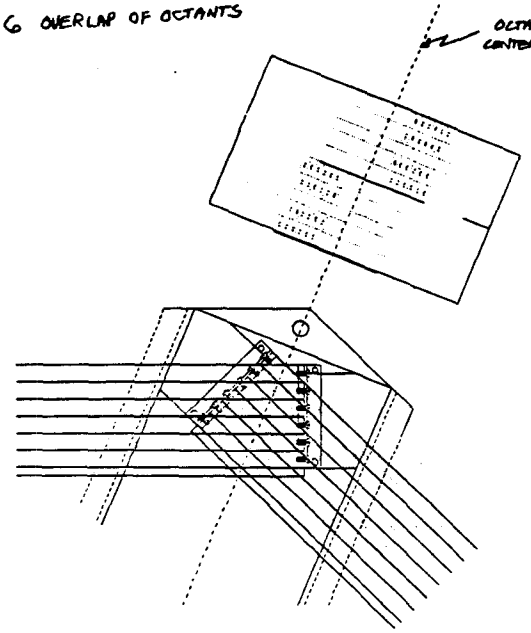


FIGURE 5
TOP VIEW OF SUPERMODULE

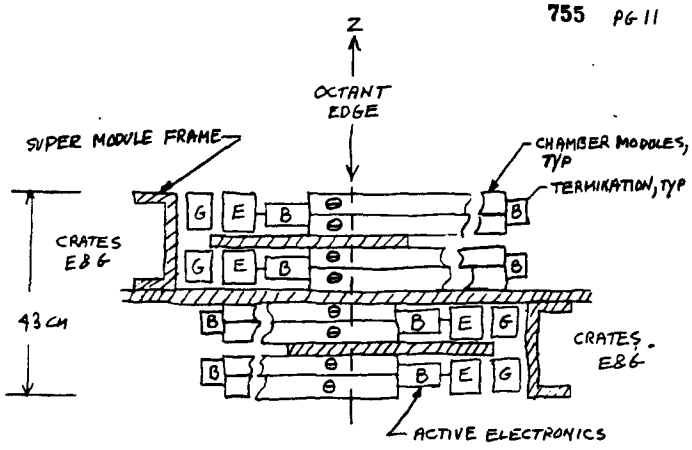
754 PG 10

FIGURE 6 OVERLAP OF OCTANTS



TYPICAL WIRE OVERLAP OF THE OCTANT SPOKE CENTERLINE

755 PG 11



B = BOARDS
E = ELEC CABLES
G = GAS LINES

FIGURE 7 — STATIONS μFW1 & μFW3
4CM CHAMBERS

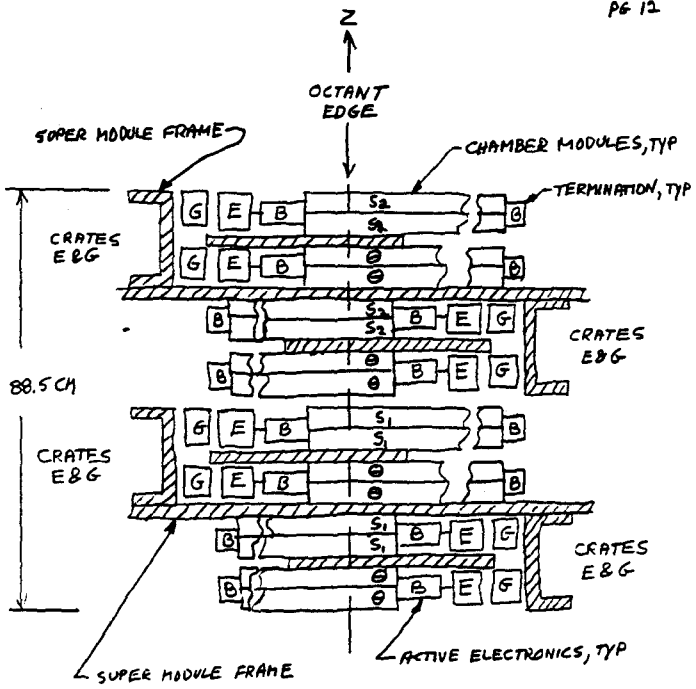
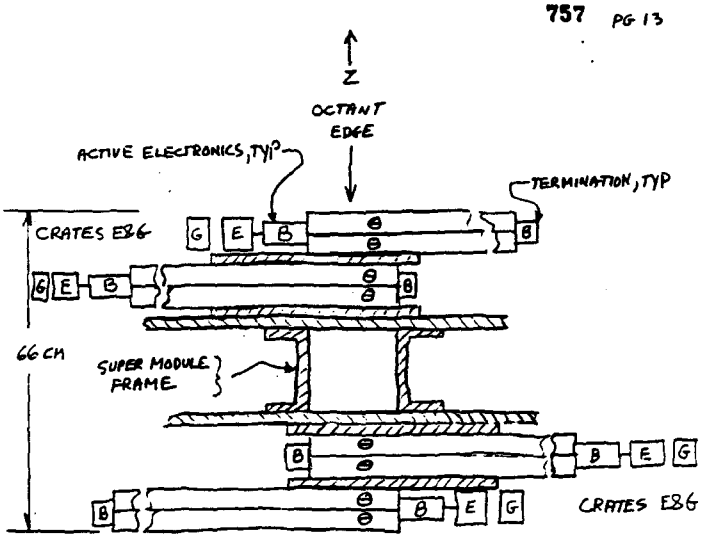


FIGURE 7a - STATIONS #1 FW1 & 5
4 CM CHAMBERS



E = BOARDS
E = ELEC CABLES
G = GAS LINES

FIGURE 7b - STATION #1 FW4
4 CM CHAMBERS

TABLE I
* CHAMBER COUNT

STATION	I	II	III	IV	V
NAME	FW1	FW2	FW3	FW4	FW5
CO-ORD	40	$\theta\theta, \theta s_1, \theta\theta, \theta s_2$	40	40	$\theta\theta, \theta s_1, \theta\theta, \theta s_2$
R (MIN) (mm)	1217	1483	1944	2216	2658
R (MAX) (mm)	4720	5750	5850	5850	6570
ΔR (mm)	3503	4267	3906	3634	3932
NO OF CHANNELS PER OCTANT $\approx \frac{\Delta R}{40}$	88	107	98	91	98
n of coord/station	4	8	4	4	8
MULTIPLICATION FACTOR = (n) X (2 ENDS) X 8 OCTANTS	64	128	64	64	128
NO OF CHANNELS ≅ MULTIPLICATION FACTOR X NO CHANNELS PER OCTANT	5632	13696	6272	5824	12544

GRAND TOTAL ≅ THE SUM OF THE NO. OF CHANNELS ≅ 43968

CHAMBER MODULES
12 PACK - 3664
16 PACK - 2748

* APPROXIMATE COUNT. NO CORRECTIONS MADE FOR LENGTHS OR PACKING FACTORS. DIMENSIONS USED FROM DE SCOPE OPTION 1 DIAGRAM - AUG 2, 1991.

8-25-91

TABLE 2
NUMBER OF OCTANT MODULES

STATION	#/OCTANT	# OF OCTANTS	SUB-TOTAL
FW1	2	8	16
FW 2	4	8	32
FW 3	2	8	16
FW 4	4	8	32
FW 5	4	8	32

TOTAL (ONE END) - 128
TOTAL (BOTH ENDS) - 256

TABLE 3
NUMBER OF SUPER MODULES

STATION	# OF SUPER MODULES	
FW1	1	
FW2	2	
FW3	1	(1 IF SPLIT TOROID, 2 IF SPLIT MODULE)
FW4	1	
FW5	2	
TOTAL (ONE END) - 7		(OR 8)
TOTAL (BOTH ENDS) - 14		(OR 16)

760

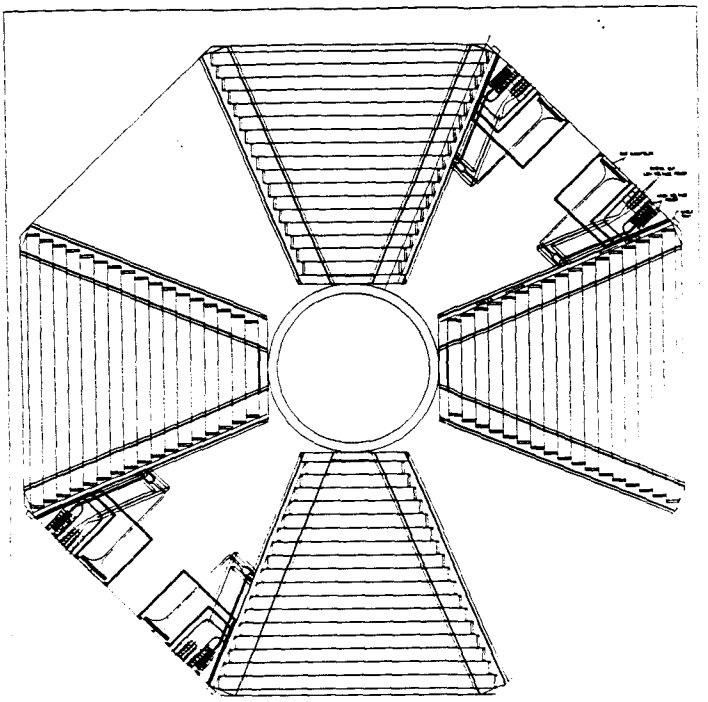
TABLE 4

TOTAL NUMBER OF ELECTRONIC BOXES AND GAS HEADER CONNECTIONS

STATION	I	II	III	IV	V
NO. OF CHANNELS (FROM TABLE 1)	5632	13696	6272	5824	12544
NO. OF ACTIVE ELECTRONIC CHAMBER BOARDS 6 CHAMBERS PER BOARD	938	2282	1045	970	2090
NO. OF ELECTRONIC BOXES, 6 CHAMBER BOARDS FOR EACH 1"x8"x12" BOX	938	2282	1045	970	2090
* NO. OF GAS HEADER CONNECTIONS FOR EACH BOX. 12 CHANNELS FOR EVERY TWO GAS LINES	469	1141	522	485	1045

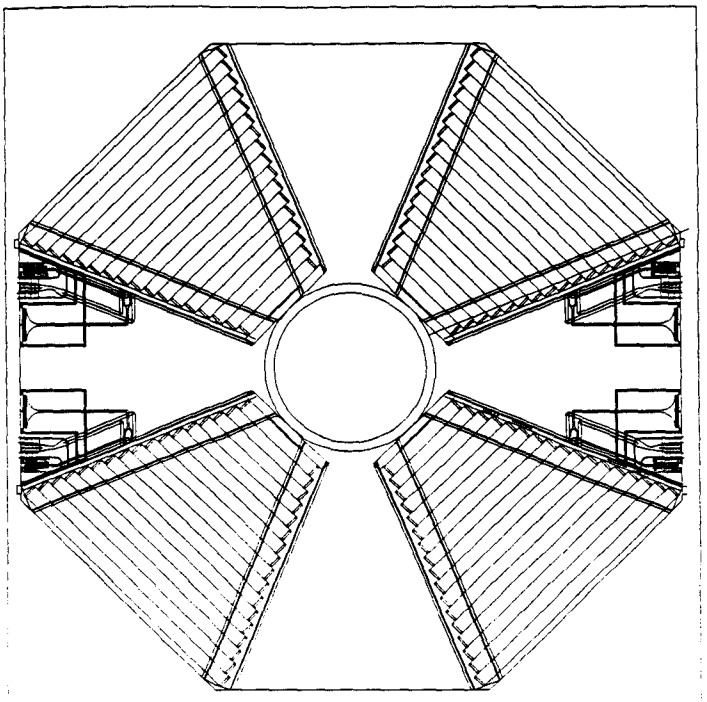
* THERE ARE ONLY TWO GAS LINES, ONE IN-ONE OUT, FOR EACH OCTANT MODULE. GAS BOXES WILL HOUSE THE HEADER CONNECTIONS FOR EACH OCTANT MODULE.

761



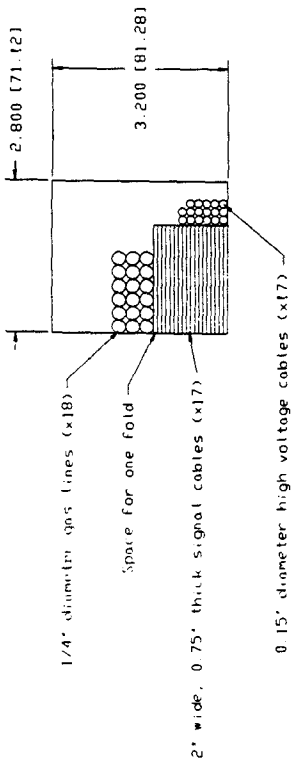
48 FRONT LAYER

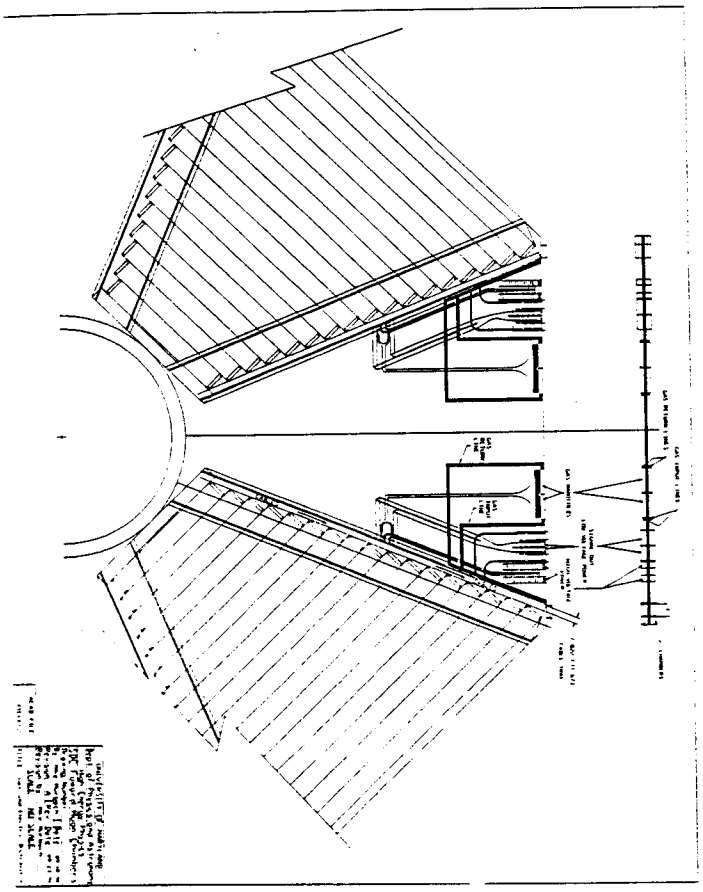
762



48 BACK LAYER

763

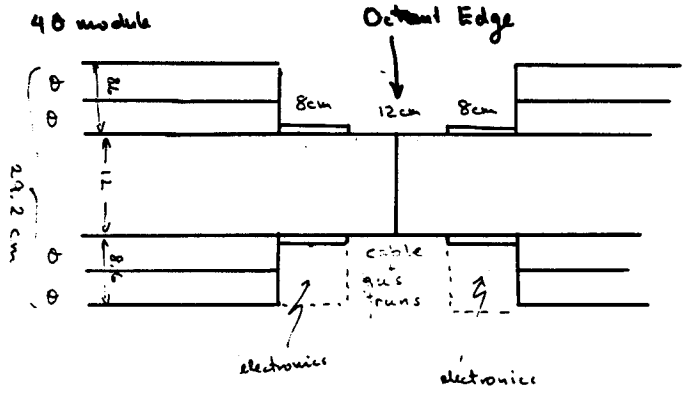




Reduction of Forward Muon System in "z"
by not-overlapping chambers

Proposed (or "raised") by integration group

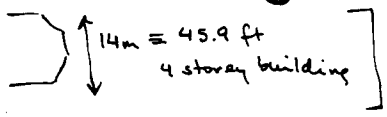
Not recommended by Maryland Group



Nominal reduction of 40 module
z-thickness by 3.8cm

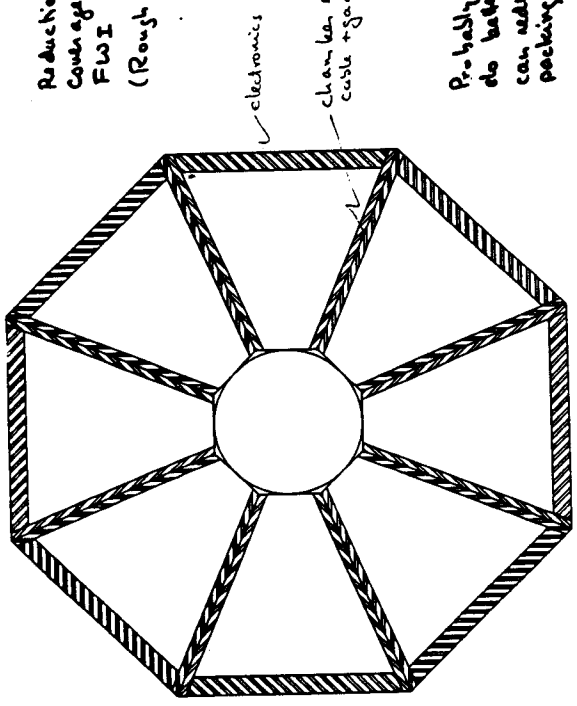
Hower do not come close to saving
6 × 13.8 cm / end ← wrong

12cm Beam

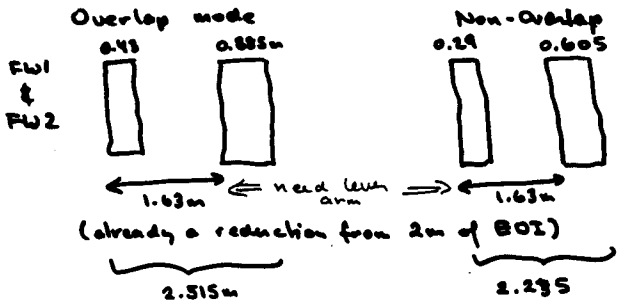


Reduction in Coverage for FW1 23.6% (Rough estimate)

Probably can do better since can reduce electronics packing fraction (?)



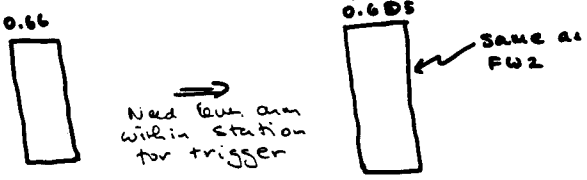
Reduction in z



Δz = 28cm

FW3 Straight reduction
Δz = 14 cm

FW4 z-thickness determined by trigger requirements



Saving: Δz = 5.5cm

FW5 Same as FW2
$\Delta z = 28$ cm

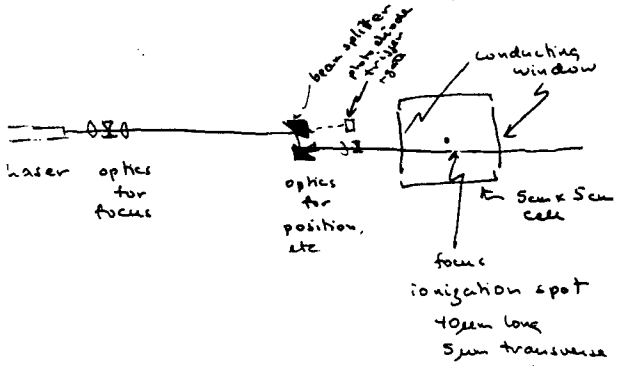
Summary –

FW1, FW2 & FW3 42 cm/end
Saves $'s

FW4 & FW5 33.5 cm/end
Does not save $'s
since outside of toroid
Does save Δz

I still cannot recommend doing this

Square Tube Measurements at Maryland
No Field-Shaping

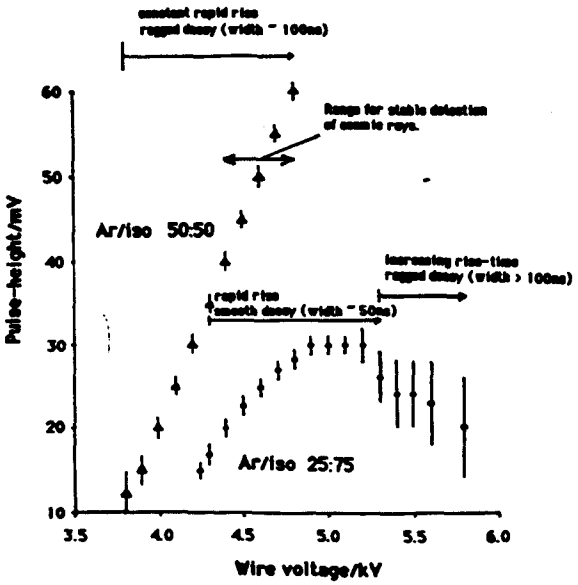


Laser NIKHEF Type 1a
100 kW
Pulsed Nitrogen laser

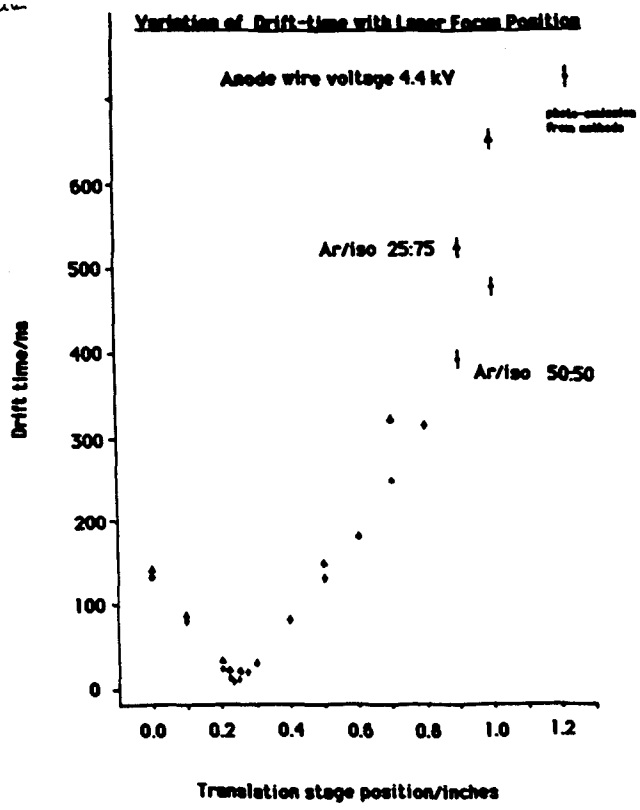
Very preliminary measurements
Easy to measure simple cells.

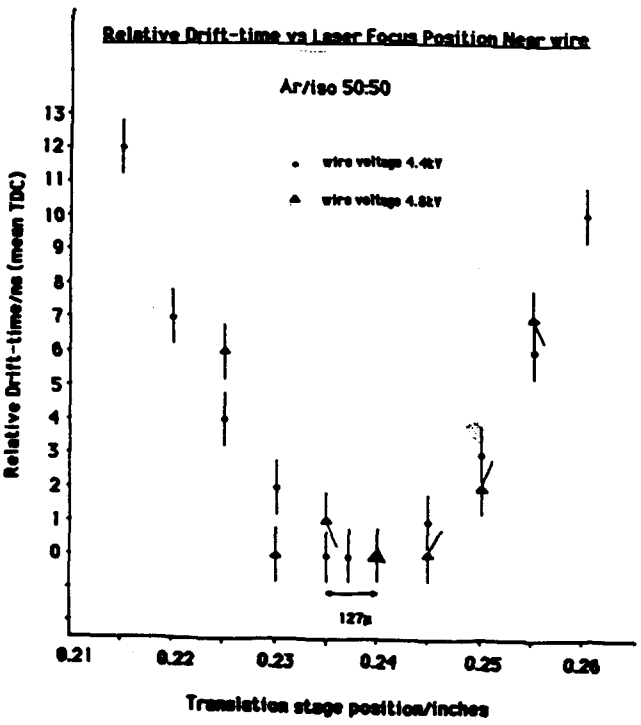
1st measurements using Argon / Isobutane (50/50)
Limited Streamer mode

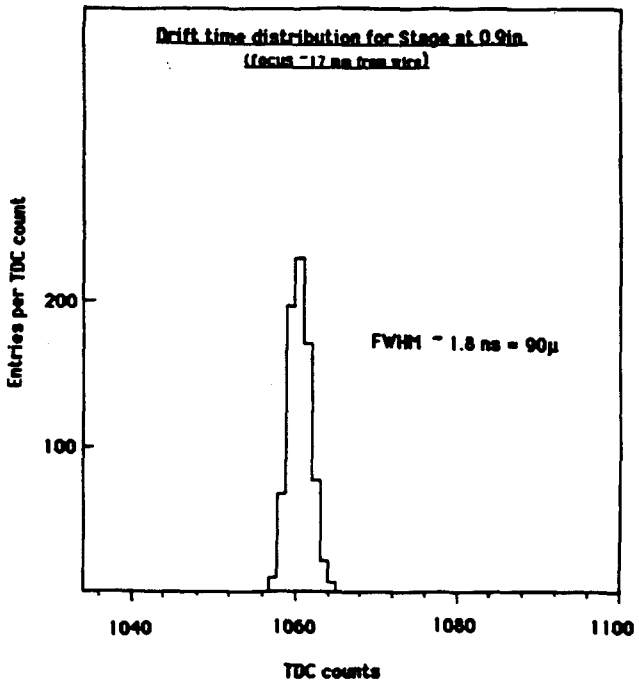
Goal: Various cells, both streamer and proportional mode
Various gases



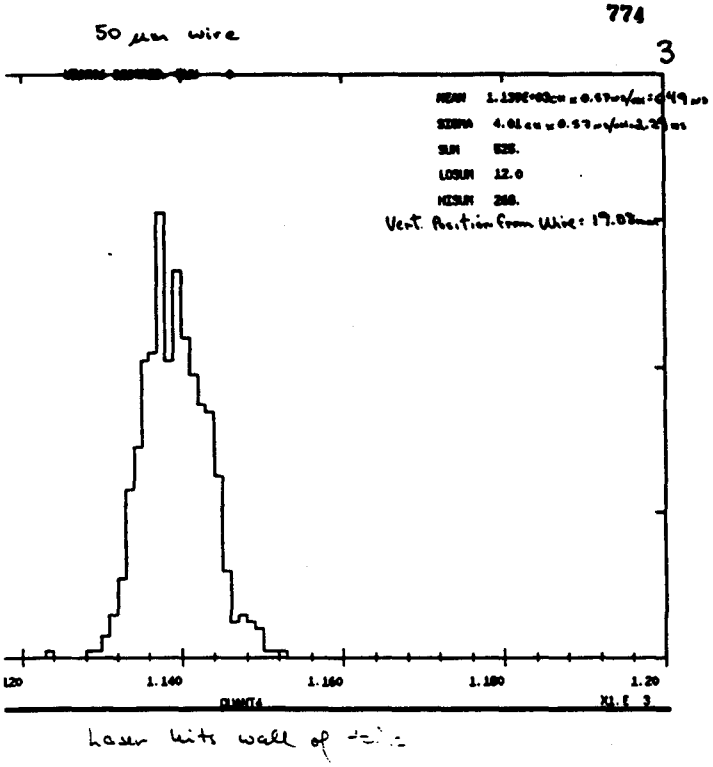
100μm





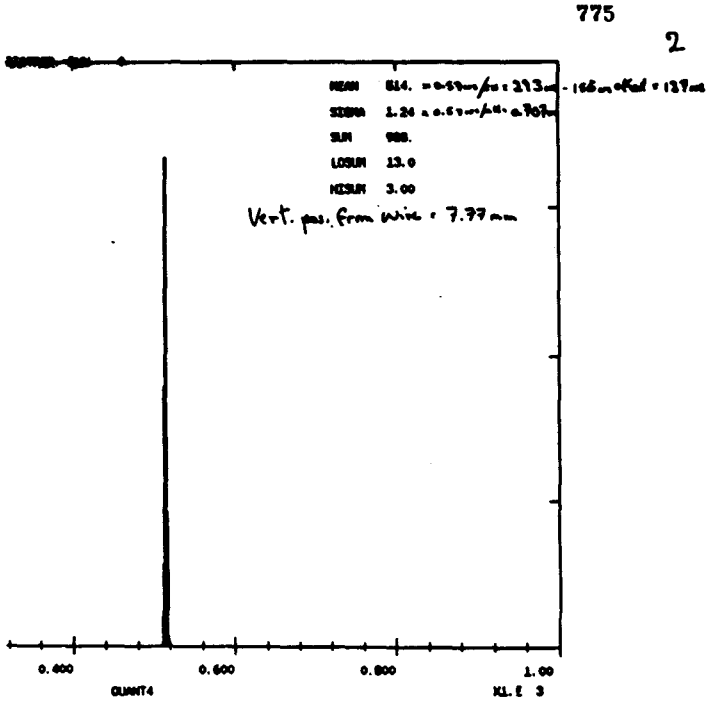


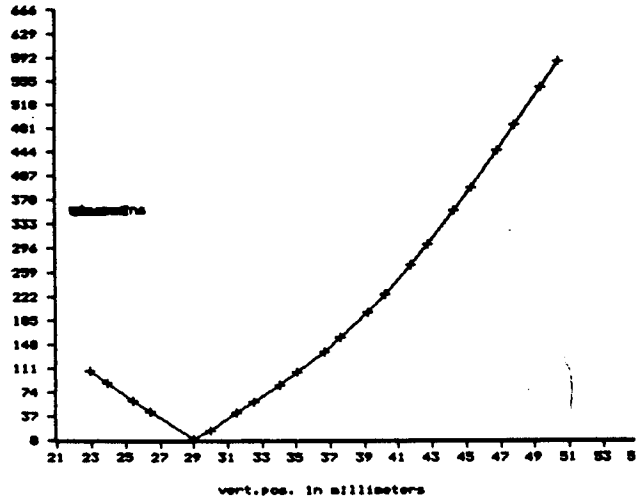
774

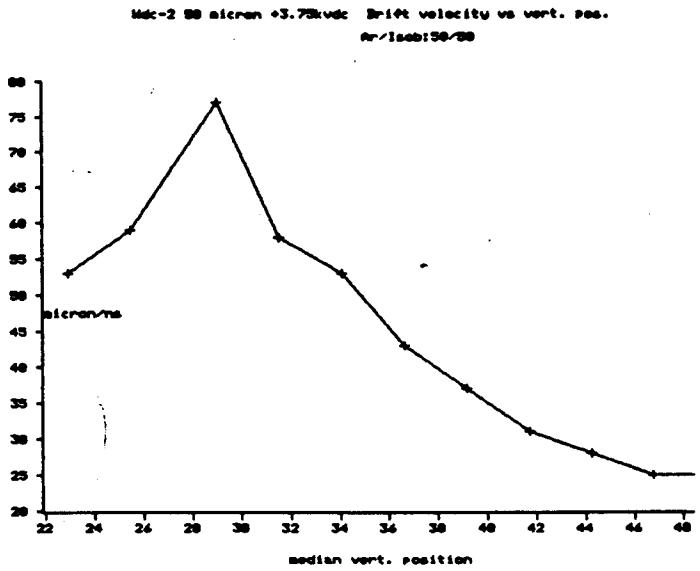


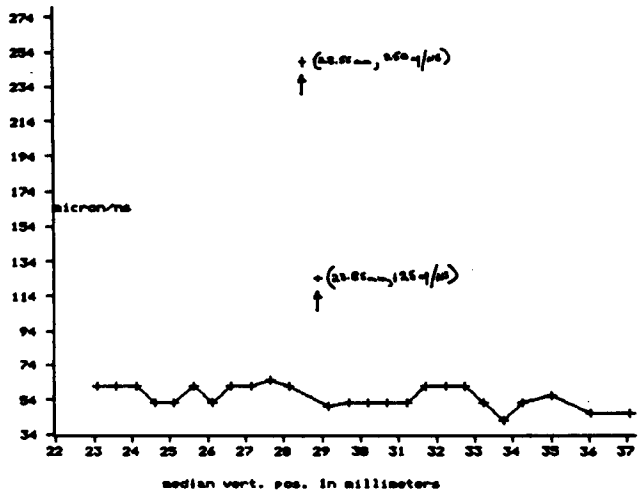
Laser hits wall of tube

775




vdc-2 90 micron +3.75kvdc Drift time vs vert. pos.
Ar/Isobl50/50
444
407
370
333
296
259
222
185
148
111
74
37
0
21 23 25 27 29 31 33 35 37 39 41 43 45 47 49 51 53
vert.pos. in millimeters


Vdc-2 90 micron +3.75kvdc Drift velocity vs vert. pos.
Ar/Isobl50/50
micron/ns
22 24 26 28 30 32 34 36 38 40 42 44 46 48
median vert. position


VDC-2 90 micron +3.75kvdc Drift vel. vs median vert. pos.
Ar/Isobl50/50
micron/ns
274
254
234
214
194
174
154
134
114
94
74
54
34
22 23 24 25 26 27 28 29 30 31 32 33 34 35 36 37
median vert. pos. in millimeters

Design of the Jet Cell Chamber for the SDC Muon Detector

S. Terada(KEK)

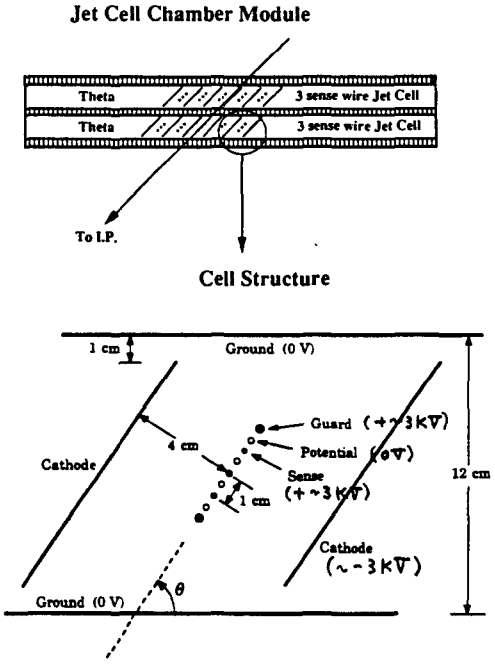
Design of the Jet Cell Chamber for the SDC Muon Detector

KEK Muon Chamber Group

Y. Funahashi, Y. Higashi, H. Iwasaki, T. Kondo, A. Maki, S. Odaka, T. Shinkawa, and S. Terada

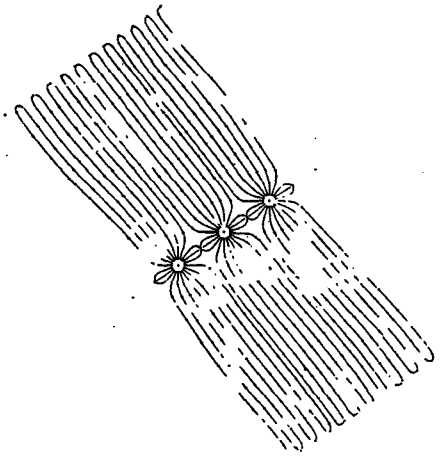
September 23,1991

Slanted Jet cell partitioned with stiff cathode plates placed in a rigid box frame

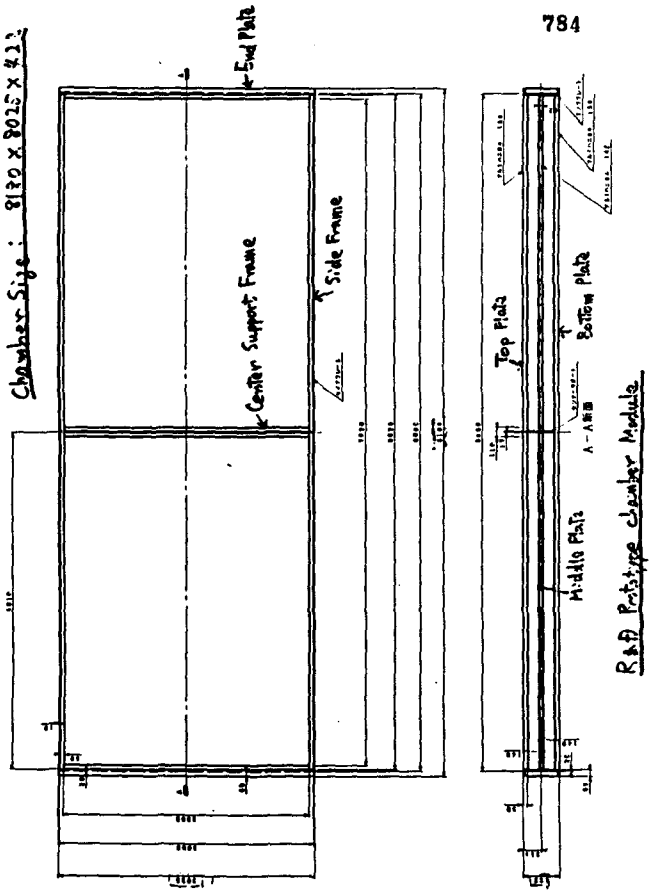


Equal Drift-time Contours

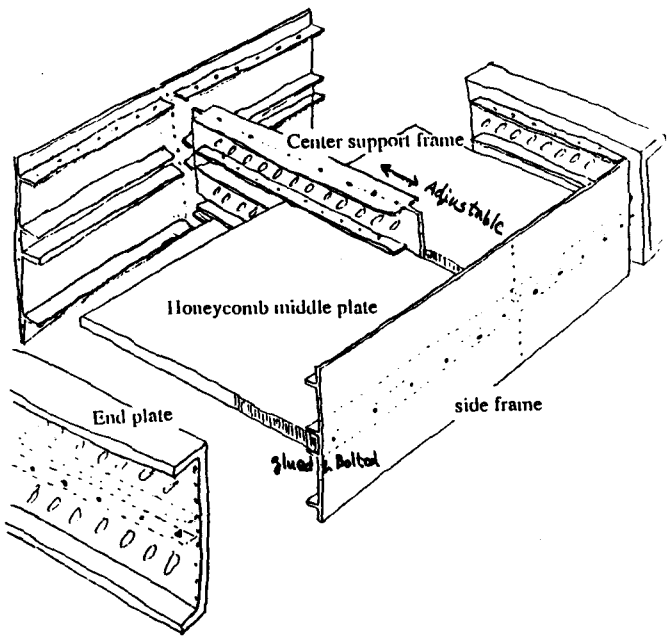
3 Sense Wires

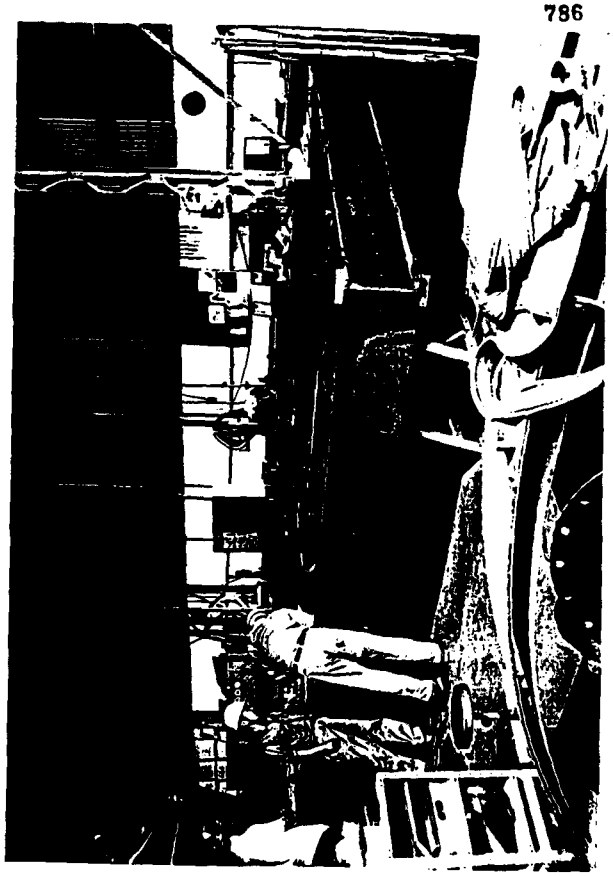


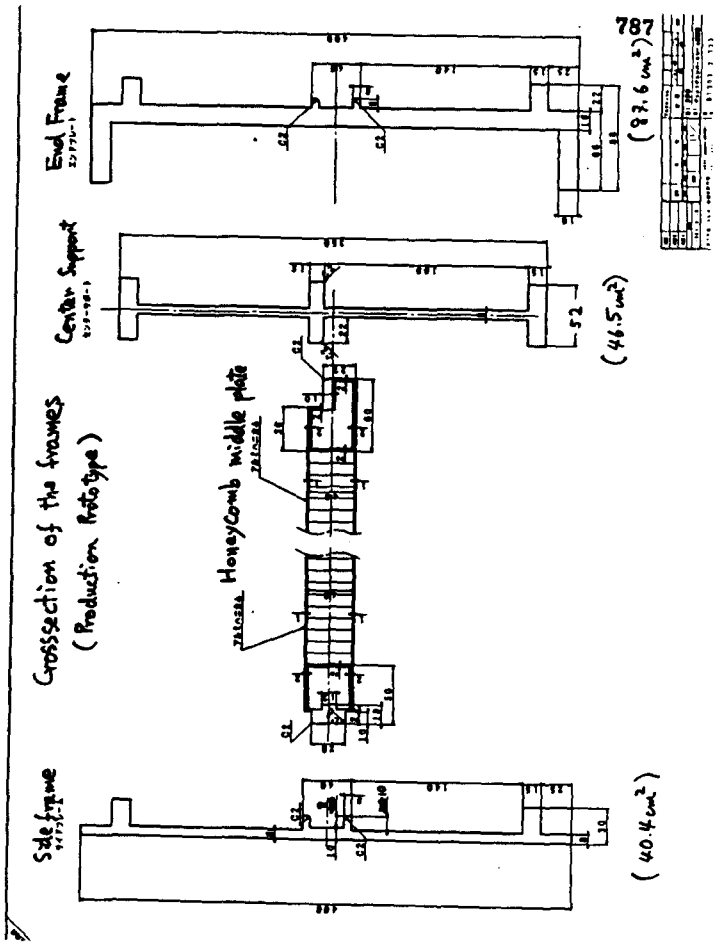
I. Large Chamber R&D



■ Frame structure and assembly procedure:







Weight of the large module 788

of 3m × 8m × 0.4m

a) Frames

i) Side frame: 87 kg/side

ii) End frame: 71 kg/end

iii) Center Support: 38 kg

iv) Middle Honeycomb: 88 kg/plate of 4m×3m

Frameweight = 530 kg/module

b) Top & Bottom plate

If we use the same honeycomb plate as the middle plate, then

$88\ \frac{kg}{plates} \times 4\ plates = 352\ kg$

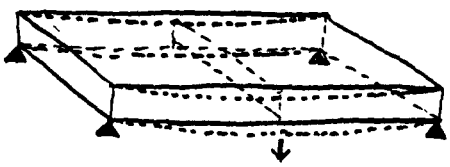
c) Cathode plate etc.

~100 kg

Grand Total = ~ 1 ton

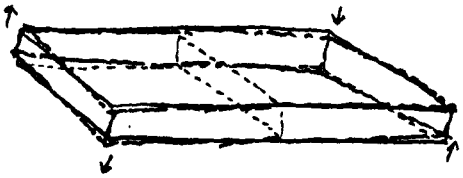
Possible deformation modes 789

a) Sag



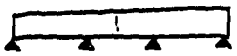
~ 1 mm by selfweight

b) Twist

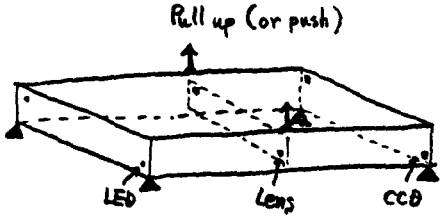


How to Compensate the deformations: 790

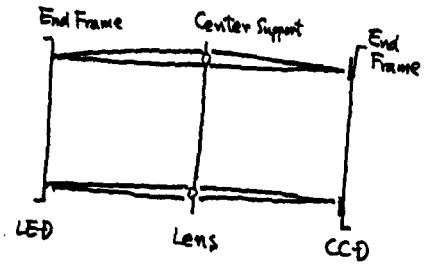
a) Multiple spport points



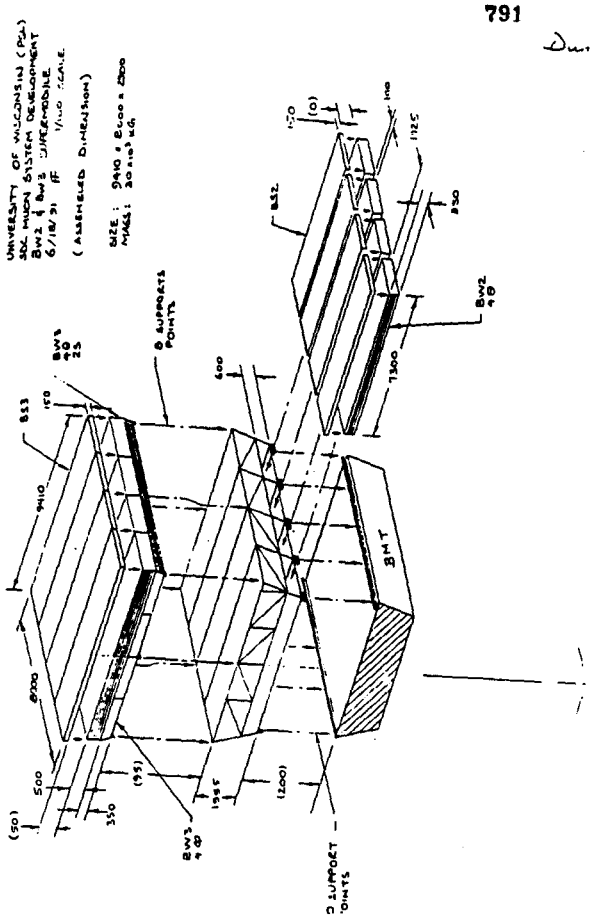
b) Adjust the frame Center



Position Measarement & Monitoring

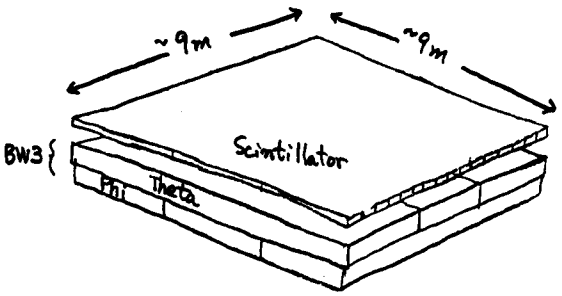


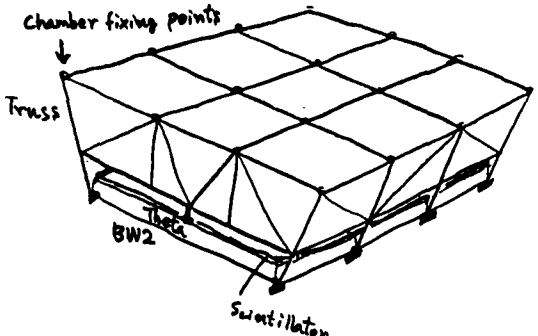
791



Supermodule assembly

Nine Modules in a supermodule





Chamber Module : ~9tons

Truss : ~5 tons ??

Tot. ~14 tons ??

S. Odaka (KEK)
September 21, 1991
To be presented at the SDC Collab. Meeting, ORNL
Muon subgroup

Status of the Short Test Chamber

Type I ($\theta = 90°$)

Fe^{55} (5.9 keV X-ray) signal is seen.

HRS gas: Ar/CO_2/Methane (89/10/1)

$V_{anode} = V_{guard} = +1.9$ kV

$V_{cathode} = -2.8$ kV

$\Rightarrow \sim 10^5$ gas-gain

The voltages shown in my design report are too high for 50 μm^{ϕ} sense wires.

$\Rightarrow$ No problem;

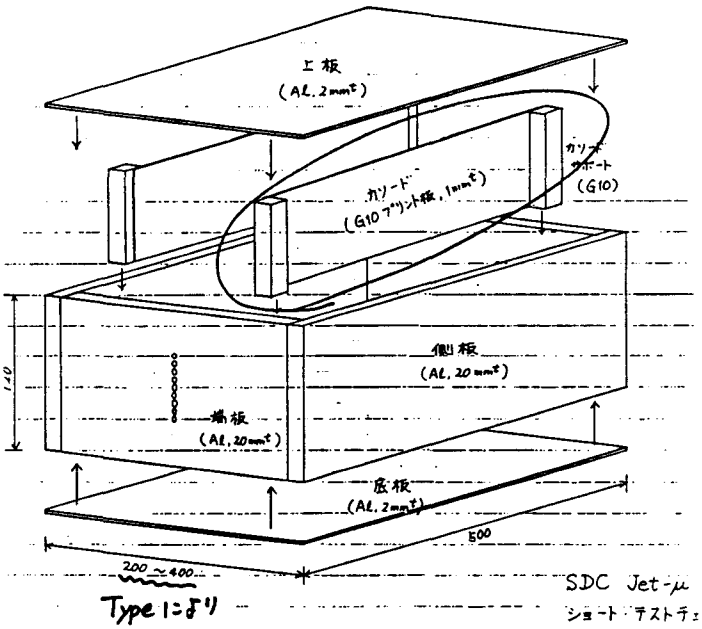
Use a thicker wire (70 or 100 μm^{ϕ}).

A study of gas-gain is in progress, using thin-tube chambers.

Type II ($\theta = 30°$)

will be ready by the end of September.

Short Jet Cell Chamber (90° type)



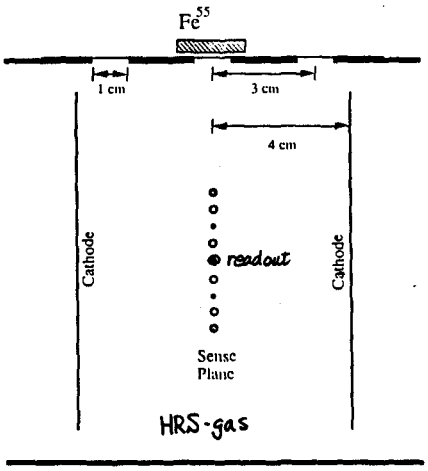
Type により異なる.

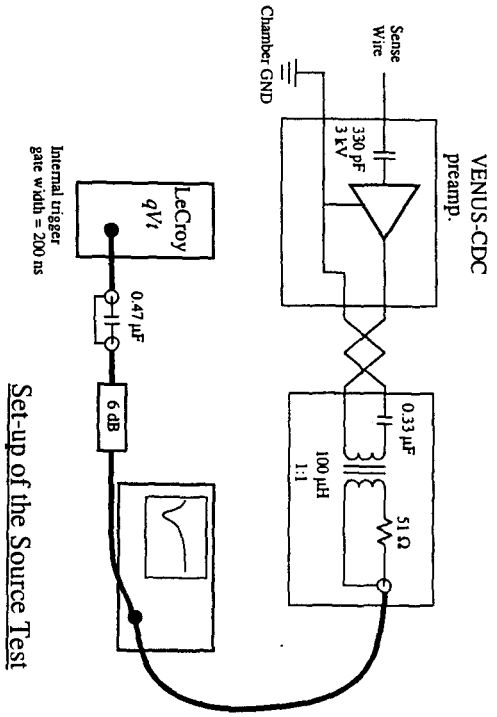
SDC Jet-μ
ショート・テストチェ
組立概念図
1991.7.2
尾高 茂
S.Odaka



Source Test

Short Chamber (Type · I)

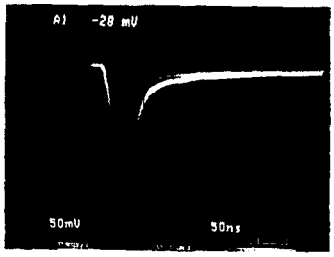




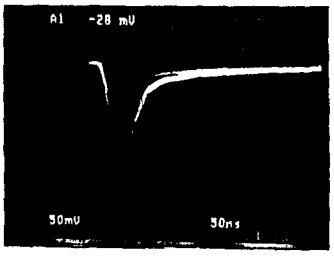
Set-up of the Source Test

Signal Shape (Fe^{55})

center

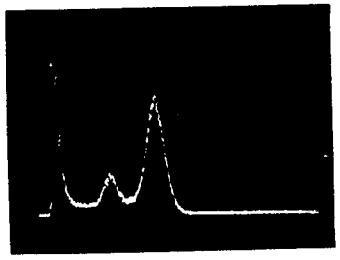


edge

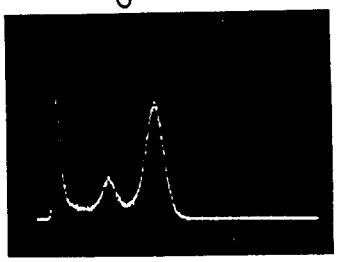


Charge (Fe^{55})

center



edge

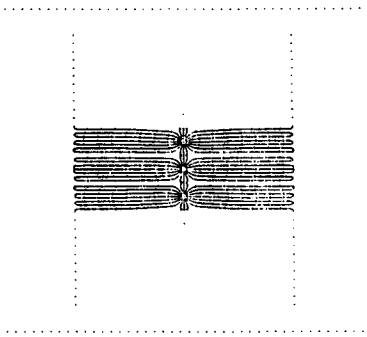


Calculation based on the present voltages

HRS gas: Ar/CO_2/Methane (89/10/1)

$V_{anode} = V_{guard} = +1.9$ kV

$V_{cathode} = -2.8$ kV



$E_{drift} \cong 800$ V/cm

$\frac{\lambda_{anode}}{2\pi\varepsilon_0} \cong 340$ V

$\frac{\lambda_{potential}}{\lambda_{anode}} \cong -0.2$

The results are different from the original design, but not bad for the HRS-gas.

A Short Comment on Descoping of the Muon Chamber

Y. Asano(Tsukuba)

A short comment on the descoping of the muon-chamber

Contributed to the
muon group meeting, Sept. 1991

Yuzo Asano
Institute of Applied Physics
University of Tsukuba

Abstract

The muon cahmber seems to be one of the major target of descoping almost without limit. Unless some standard is given, the muon chamber will become the minimum set with which some known physics can be barely done, but some unpredicted physics will be lost either by the poor resolution or by the insufficient detection efficiency, or by the poor S/N ratio. Even the known physics may be lost because of insufficient luminosity (which is very likely during the first few years) and poor efficiency.
The requirement on the muon system is continuous, that is, the better the better. Chopping off every nook and corner will result in a detector which is almost of no use except for some standard phenomena which may or may not occur in nature.

Here, a small example is shown how the track-matching by extrapolating a muon track to the inner tracker is required, the efficiency of which is strongly dependent on the muon chamber performance.

The example shown here is as follows.
A possibility of matching a high Pt muon track with a high Pt pion track by mistake is examined. The requirement on the independent momentum measurement by the toroid system, and the requirement on the precision of the track determination will be recognaized from the results.

1. Event generation

Since the number of events to be generated in a computer is limited, the condition on the event generation is such that the generated events should well represent hard collisions, so that the fraction of high Pt events is large. Events were generated by the ISAJET v.5.38 program, with a high Pt-value for the 1st level partons, as follows.

Data-set number	*1st level partons*	*Pt range of the 1st level partons (GeV/c)*	*Number of events*	*Corresponding integrated luminosity (cm^{-2})*
1	2 jets	100<Pt<2000	1000	8.7×10^{31}
2	t.t-bar	100<Pt<500	1000	3.8×10^{35}
3	b.b-bar	300<Pt<500	1000	1.7×10^{36}
4	b.b-bar	500<Pt<700	1000	1.8×10^{37}
5	b.b-bar	700<Pt<900	1000	9.7×10^{37}

The Data-set 1 was too soft, and no further analysis was made.

2. The number of muons

The number of muons with Pt>30 GeV/c in 1000 events is as follows.

No. of mu's in 1000 events	*Data set* 2	3	4	5
0	848(85%)	865(87%)	809(81%)	772(77%)
1	138(14%)	126(13%)	176(18%)	198(20%)
2	12(1.2%)	9(0.9%)	15(1%)	28(2.8%)
3	2(0.2%			2(0.2%)

An event is accompanied with 15-20% of high Pt muon. Naturally, the number of muons increases as the collision becomes harder.

3. Pions adjacent to the high Pt muons

A possibility is examined how high Pt muons are accompanied with high Pt pions, whose tracks are so close to the muon tracks

that they are confused. Since the Data Sets 2 and 3 give similar results, only Data Sets 4 and 5 are presented here.

The number of adjacent high Pt pions (within 0.1 radian from the high Pt muon) with Pt^{π}>30 GeV/c per a high Pt muon is as follows.

	30<Pt^{π}<50	50<Pt^{π}<100	100<Pt^{π}<150	150<Pt^{π}<200
DS4	2	1.6	0.5	0.2
DS5	2.8	2.5	0.6	0.3

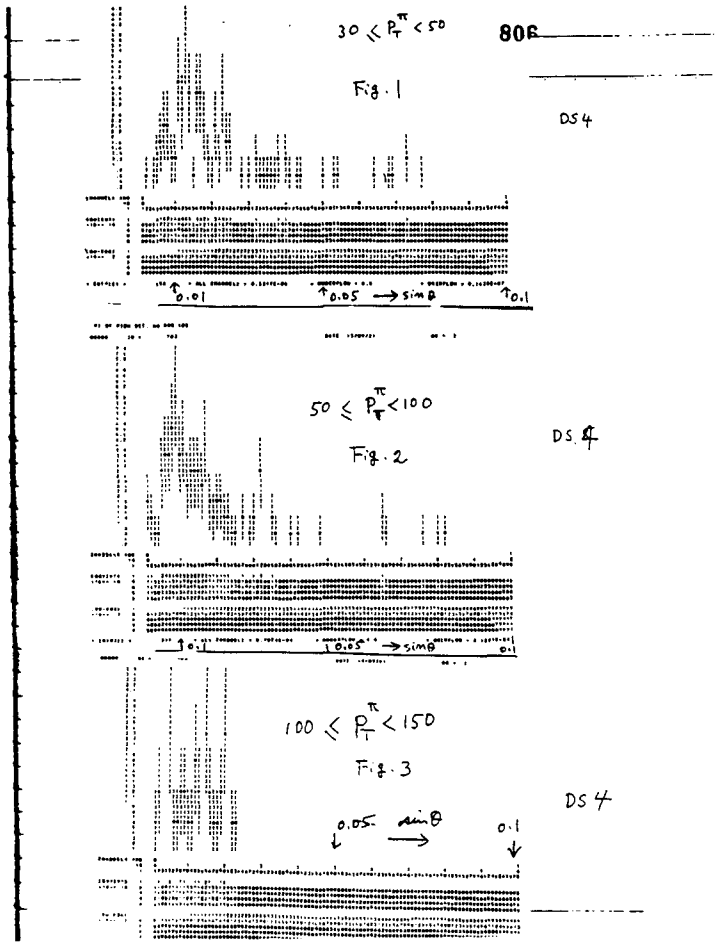
The number of pions which may be confused with the muon is sizable.

Figs.1-5 show the distribution of adjacent pions in sinθ (the angle between the muon track and the pion track) for Data-set 4. Fig.6 shows a two dimensional plot of sinθ vs (P_{π} - P_{μ}). The more confusion occurs, for the smaller sinθ and abs(P_{π} - P_{μ}). Figs.7-13 show the same distribution for Data-set 5.

We realize that the track matching of the order of 1cm is required (linear separation distance is 1cm for sinθ =0.005 if the track length is 2m), and the probability of mismatching decreases if the momentum of the muon is measured independent of the inner tracker. The matching becomes the better if the muon chamber resolution is the better.

4. conclusion

The probability of confusing a high Pt muon track with a high Pt pion track is sizable for events from hard b-bbar collisions. The more confusion will result if the resolution and the number of layers of the muon chamber become poorer. The next task we have to work on is to evaluate quantitatively how a certain physics will be affected due to mismatching of the muon tracks, and to evaluate the relation between the chamber performance and the track-matching ability. *The muon group should protect itself by making some standard of chamber quality against unlimited descoping proposals.*



807

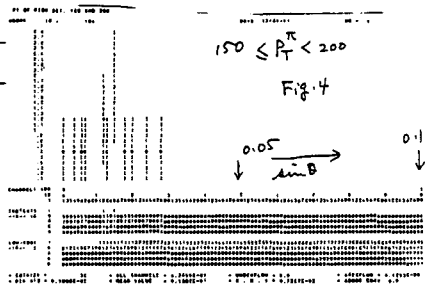


Fig. 4

DS4

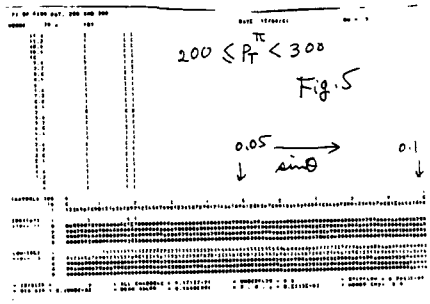
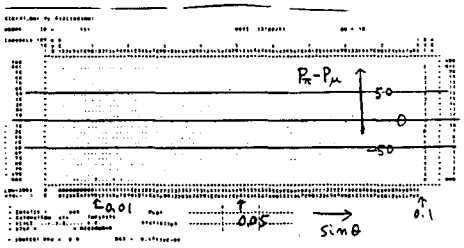


Fig. 5

DS4



DS4

Fig. 6

808

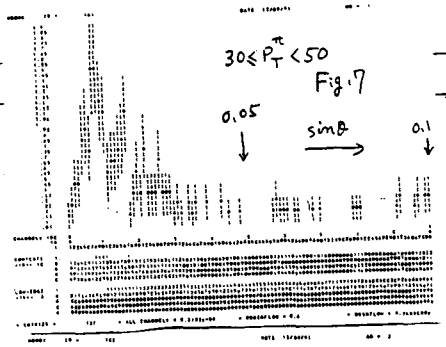


Fig. 7

DS5

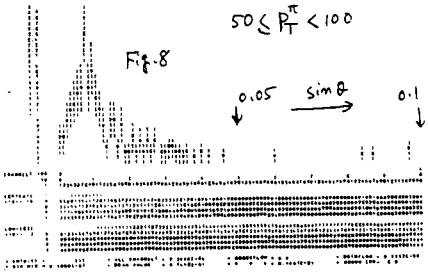


Fig. 8

DS5

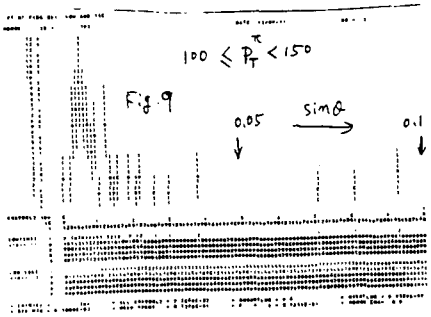


Fig. 9

DS5

809

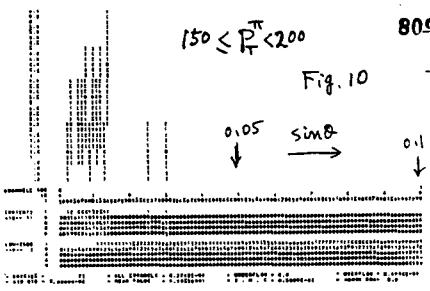


Fig. 10

DS5

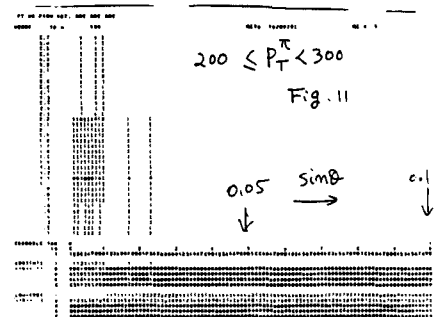


Fig. 11

DS5

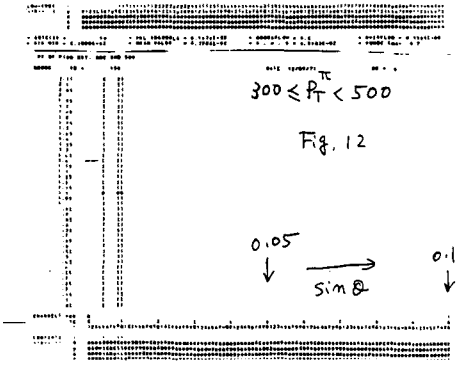
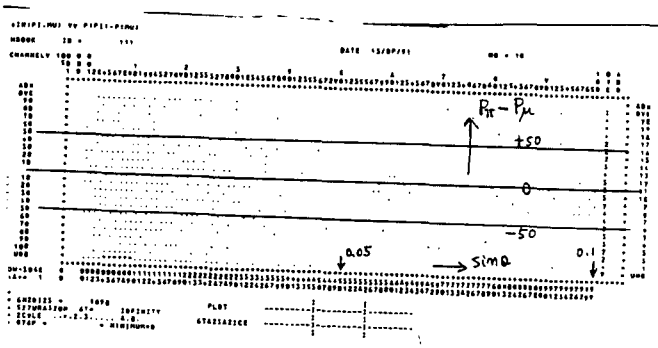


Fig. 12

DS5

810



DS 5.

Fig. 13

Progress in Wisconsin

D. Carlsmith(Wisconsin)

Progress in Wisconsin

Presented by Duncan Carlsmith

26 Sept 1991

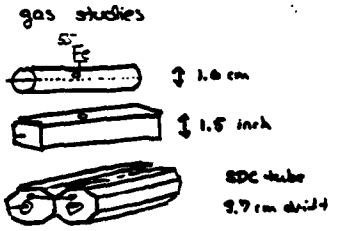
Gas studies with single tubes.

Cosmic ray tests of short samples of the Wisconsin tubes with 5.5 mil wire, $Ar(90) - CO_2(5) - Methane(5)$.

Status of large chamber.

Plans.

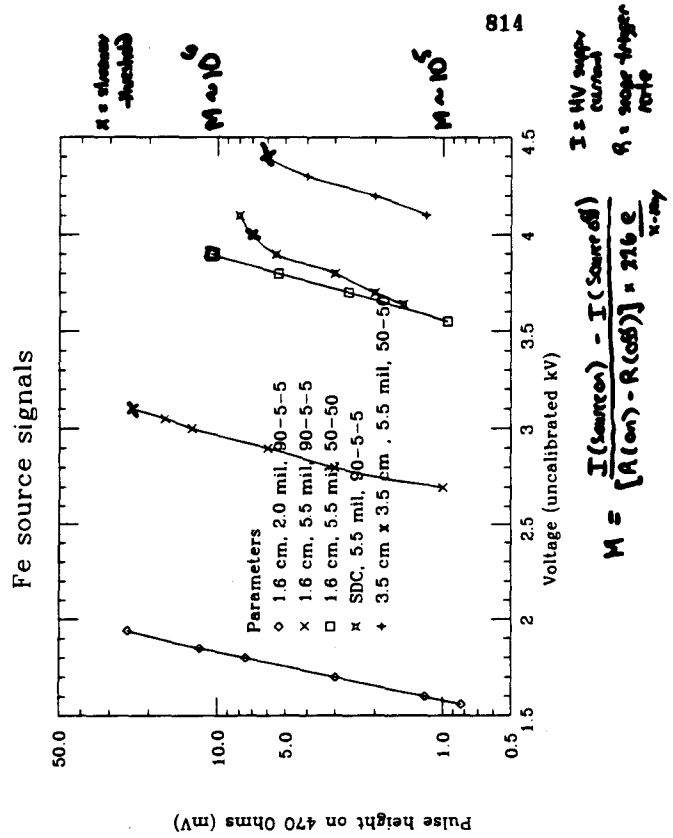
Small tube gas studies



GAS: Ar (50) / Ethane (50)
Ar (90) / CO_2 (5) / Methane (5) } premix

Wires: 2.0 mil diameter = 50 μ
5.5 mil = 140 μ

1) See sharp distribution (line) for X ray signal in proportional mode for all combinations
   ⇒ nonflammable mix is high resolution
   (see photos in notebook)
2) Surprise! Nonflammable mix has higher gain
3) No breakdown problems noticed.
4) "Streamer" mode is possible for either gas & either wire



Observations on "streamers" induced by ^{55}Fe

Ar (50) / Ethane (50) 5.5 mil wire

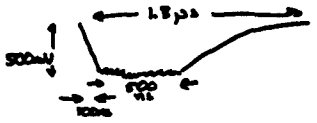
.9 cm drift brass tube ; 2 cm drift Al tube give similar results



same signal every time.

Ar (90) / CO_2 (5) / Methane (5)

.9 cm drift brass tube, 5.5 mil wire



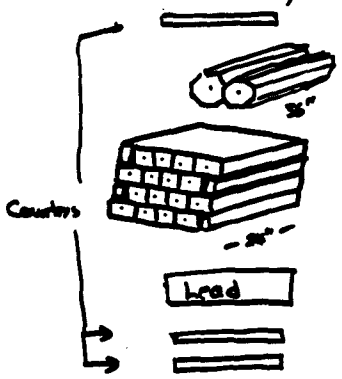
.8 cm drift Al tube, 2 mil wire



multiple saturated proportional pulses

SDC tube, 5.5 mil wire in streamer mode: Only ~ 1/3 of ^{55}Fe induced cluster convert to streamer ⇒ can't run with 100 mV threshold efficiently. What about tracks?

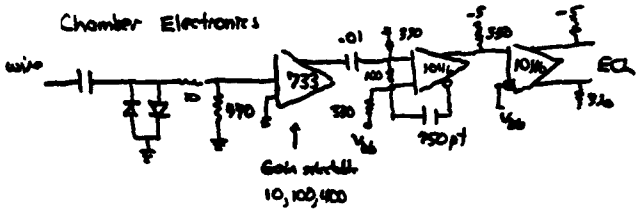
Cosmic Ray Test Setup



SDC tube
5.5 mil stainless wire
Machined test endplugs

16 channels
1.5" × 1.5" Al square tubes
NC milled endplate
5.5 mil stainless wire

Chamber Electronics



Data Acquisition

LRS CAMAC TDC's ⇒ VAX Cluster

(jumpered for 2 hit capability)

DATA ANALYSIS

Track reconstruction – fit all possibilities of tangents to circles, pick best χ^2

(Fit code cave from Asano)

MINUIT Fit to time vs distance & angle (~12 parameters) in 16 channel array by minimizing $\sum_{\text{all tracks}} \chi^2$

(ANSWER : $v_{drift} = 5 \frac{cm}{\mu s}$ constant)

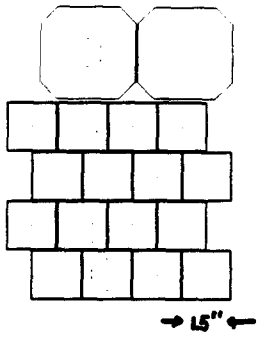
Fit also for wire positions ⇒ where they are supposed to be.

Extrapolate to 2-tube SDC chamber

Fit for location : drift velocity vs distance.

Resolution is dominated we think by multiple scattering.

University of Wisconsin

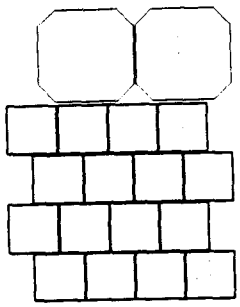


DATA

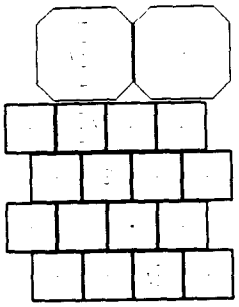
Ar (90) - CO_2 (5) - Methane (5)
140 μ wire

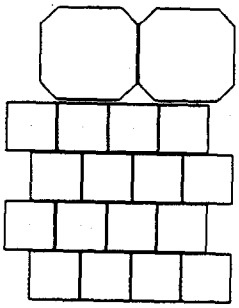
Ar (50) - Ethane (50)
140 μ wire

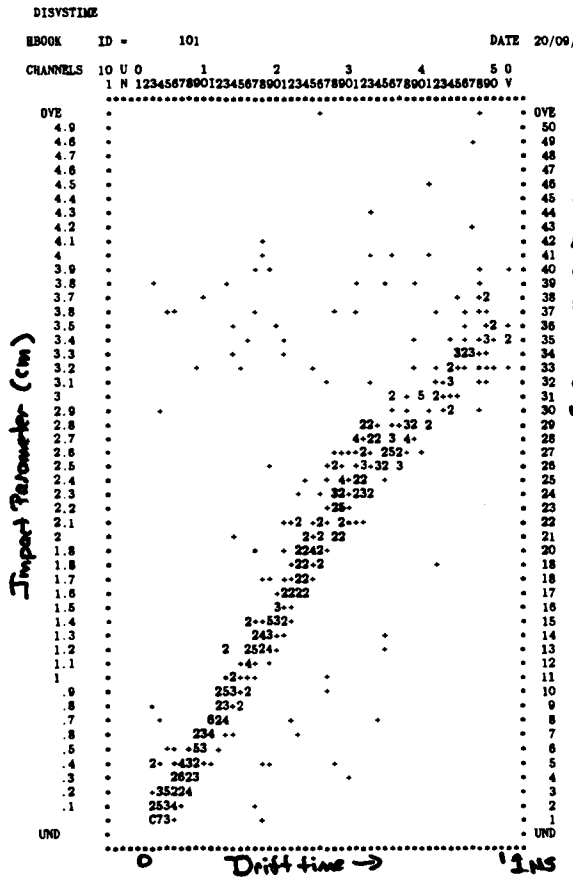
University of Wisconsin



University of Wisconsin







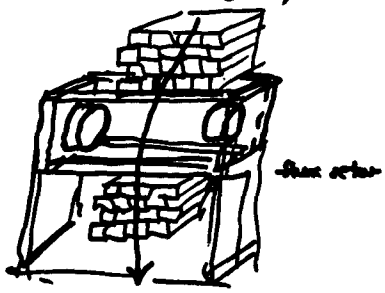
Conclusions; plans for cosmic ray tests:

1) Large wire; reclaimable mix seem fine.

2) Drift vel ∥ (small) non linearity are as anticipated.

3) To measure resolution, need to impose a p cut of ~ 2 GeV

Have found; to collect a 6 ton dipole (17" gap); p.s.; will set up in high bay



4) Wish to compare resolution for operation in streamer; proportional mode; the efficiency with actual electronics.

Other prototypes ; tests.

1) 4 tube location test (Test baseline endplug)



a) Baseline design endplugs (machined)
b) 5 mil Au-W wire
c) NC milled endplates
d) holes in tubes to view wires.

Measure actual wire locations with μscope on milling machine stage.

Preliminary result: See 160 μ deviation "containment circles" (FF)
Under investigation.

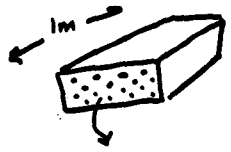
2) Long tube genes → to John Oliver ASD card



1) Look at effect of jumper schemes (for 4 chambers) on signal
2) Study transformer impedance

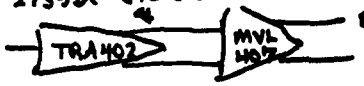
In preparation

3) Short sample beam test (TB16)



16 SDC tubes
LRS ASD card

LRS 2735DC (16 channels on a card)



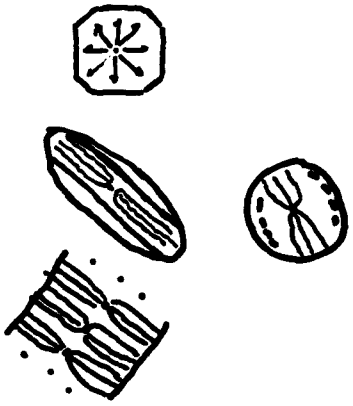
"Transistore Amp" Comparator.

Status: Have card.
Endplugs ; endplates in the shop.

Futher Goals

- Demonstrate resolution capability with large tube, nondisassemble mix
- Demonstrate mechanical strength of 4 layer "beam"
- Demonstrate we can hold tolerances to reasonable level
- Demonstrate how all pieces are made

Major Issue (Not new)



Better 2 hit resolution
Similar m.s.

Better 2hit resolution ; less m.s.

Assume mechanical problems are overcome ; each design is realized to its full potential.

Bottom line : Reconstructed muons / cost

We must have full simulation + full pattern recognition ; track reconstruction to compare muons found vs E

Status of Long Prototype

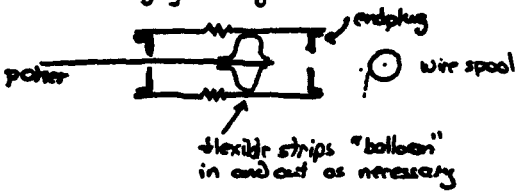
- Etched extrusion order 9.5m arrived 9/24; ~100 tubes
- Clean room ; assembly tables ; jigs are prepared
- Endplates programmed, practice piece understudy.
- Endplugs will be machined for prototype
  - injection molding is being investigated.
- 5 mil Au-W wire + 1.5 mil oversized ID stainless crimp tubes on hand

Crimp test with modified NAL crimp tool



- wire does not deform
- Breaking strength consistent with handbook values
- Need ~5% tension reproducibility

- Cherwinka stringing technique



SDC Muon Simulation at Illinois

S. Errede(Illinois)

Sept. 23, 1991

SDC Muon Simulation at University of Illinois

D. Errede, S. Errede, R. Gardner, M. Haney, I. Karliner D. Miller & J. Wiss

Purpose/Goals:

- In-depth studies of relative & absolute performance characteristics of candidate muon subsystem design(s):
  - barrel & intermediate regions
  - Overall drift chamber design(s) – # layers, chamber orientation (θ, ϕ, stereo)
  - Drift chamber cell configurations, shaping fields, DCH gases, etc.
  - Projective vs. non-projective cell geometries...
- In-depth studies of relative & absolute performance characteristics of candidate muon trigger design(s):
  - barrel & intermediate regions
  - HDL Verilog & VHDL trigger simulation(s)
  - Scintillator & Cherenkov counter L1 triggers
  - Muon drift chamber L1 & L2 triggers
  - Evaluate trigger efficiencies, biases, failure modes...
  - Evaluate on-line momentum resolution
  - Evaluate trigger rates
  - DACQ pipeline studies, etc.

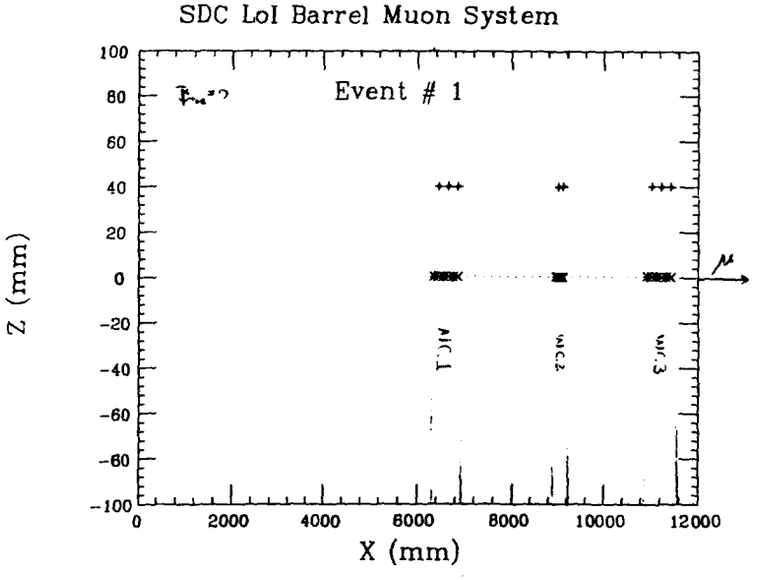
- Need realistic detailed simulation of muons in SDC
  - Event generators for input stimulus
    - Single monochromatic muons
    - Inclusive muons from $\sqrt{s} = 40\ TeV$ p-p collisions
      - prompt muons (heavy flavors, DY, W, Z^0...)
      - $\pi^{\pm}$, $K^{\pm}$ DKIF,
      - Punchthru background(s)
    - For benchmark physics processes
      - Use conventional event generators:
      - Isajet, Papageno, Herwig, CDFxxx...
  - Prompt muons & π, K, punchthru background(s)
  - Muon transport in $\vec{B}$ region(s)
  - Multiple coulomb scattering in cal & toroid(s)
  - $\delta-$ray, QED bremm and hadronic processes
  - Detailed muon detector geometries
  - Chamber resolution effects, inefficiencies, noise
  - Chamber front-end electronics, trigger electronics
  - Propagation dispersion, drift time & time-slewing effects
  - Event pileup effects
  - etc.

SDC Muon Simulation Work at UI

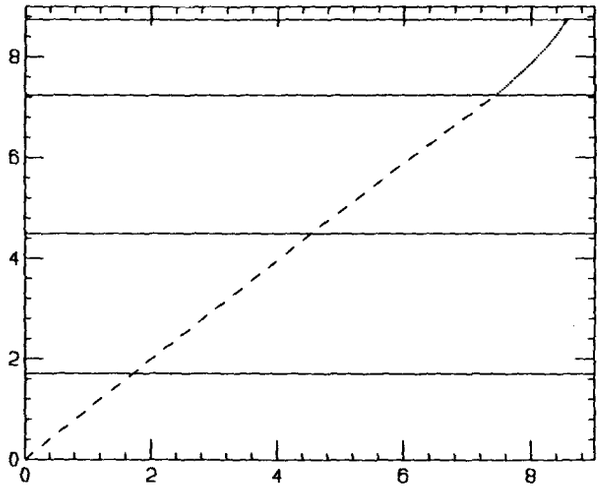
- Currently pursuing two paths:
- "Fast" simulation – to get the ball rolling...
  - Code written for muon transport, multiple coulomb scattering, $\delta-$rays, etc.
  - Code written for LoI muon geometry (Fe-scintillator calorimeter)
  - Code written for drift chamber hit simulation
  - Code written for FORTRAN → HDL I/F
  - Code written for HDL Verilog & VHDL DCH L1 barrel muon trigger simulation(s)
  - Monochromatic muon events thru L1 barrel muon trigger simulation(s) Trig effy vs Pt_{μ} curves soon
- SDCSIM GEANT-based simulation (slow...)
  - DEC 5000/200 RISC machine operational @ UI
    - SDC SHELL, SDCSIM, etc. code now running
  - SDCSIM → HDL I/F soon
  - HDL trigger simulation results from SDCSIM soon

Objectives

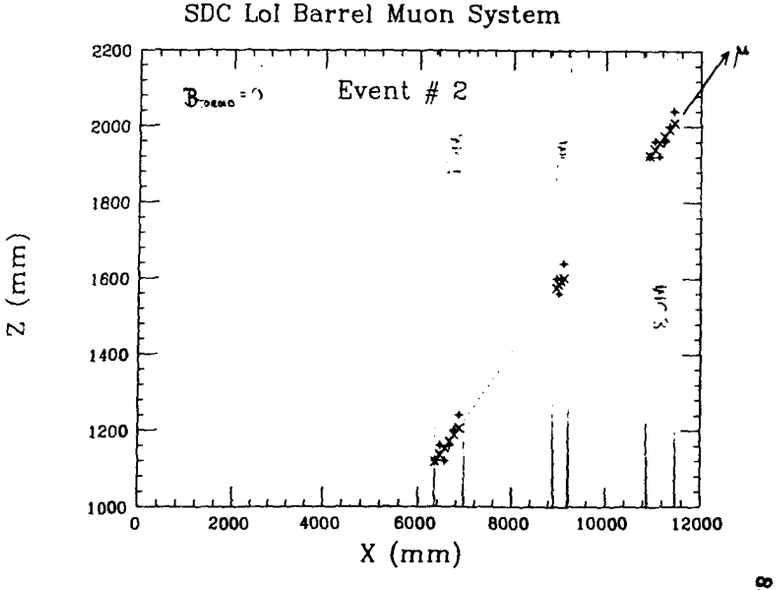
- represent trigger using hardware description language (HDL)
  - HDL will assist in engineering later: easier transition from concept to "product"
  - conventional simulation languages do not assist engineering transition; they merely confirm that an idea will work, not how to implement it
- simulate using "real" physics data
  - fast simulations that capture the essence of the physics
  - detailed GEANT, etc. simulations that contain realistic data and realistic noise...
  - collected data from test-beams; extrapolated data from other real experiments, etc.
- guide trigger design decisions
  - compare trigger alternatives
  - analyze/predict performance



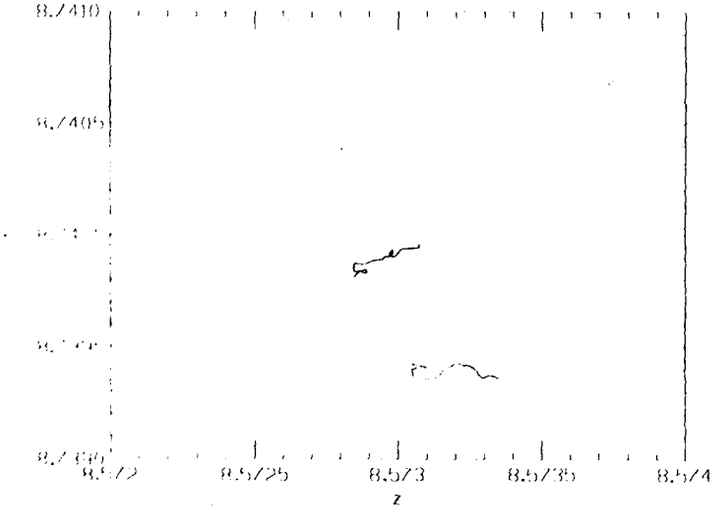
836



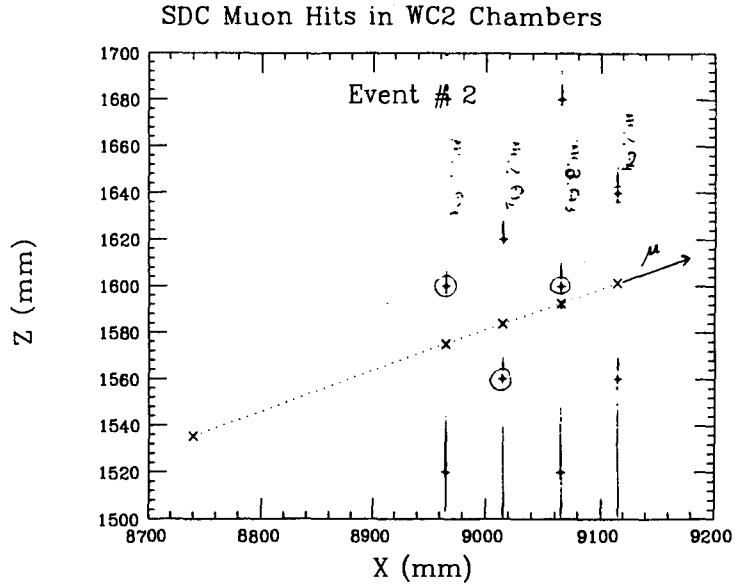
834



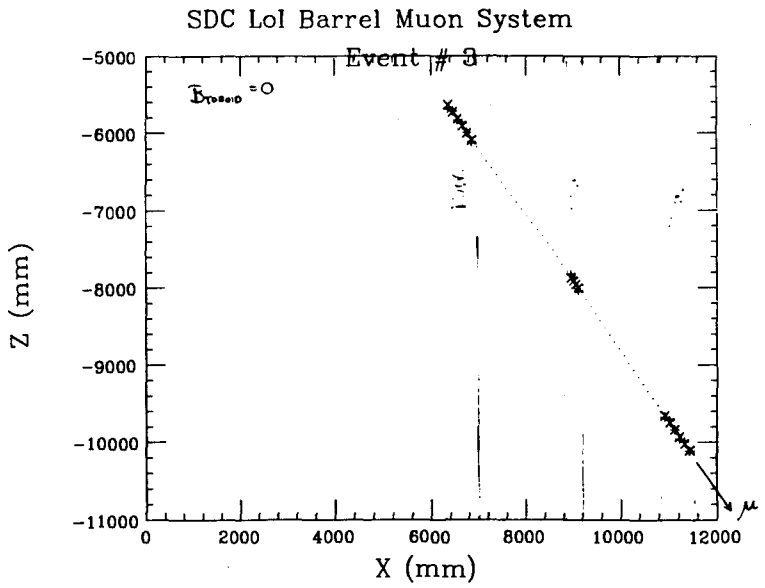
837



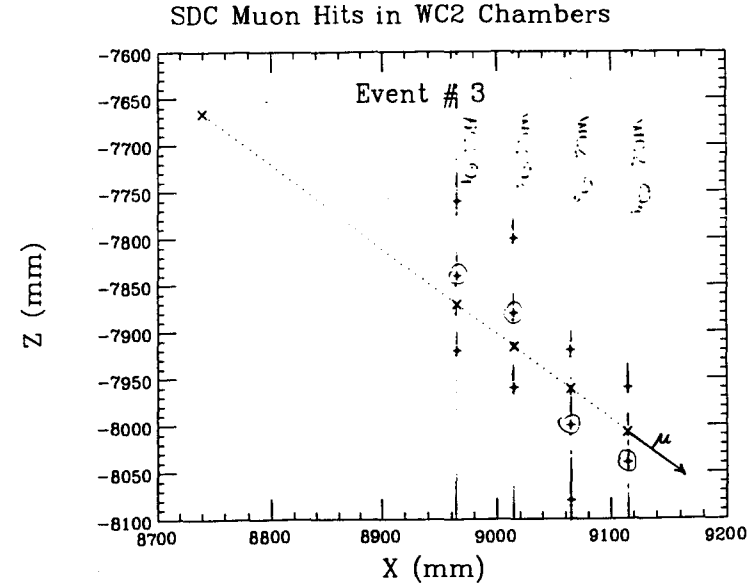
835



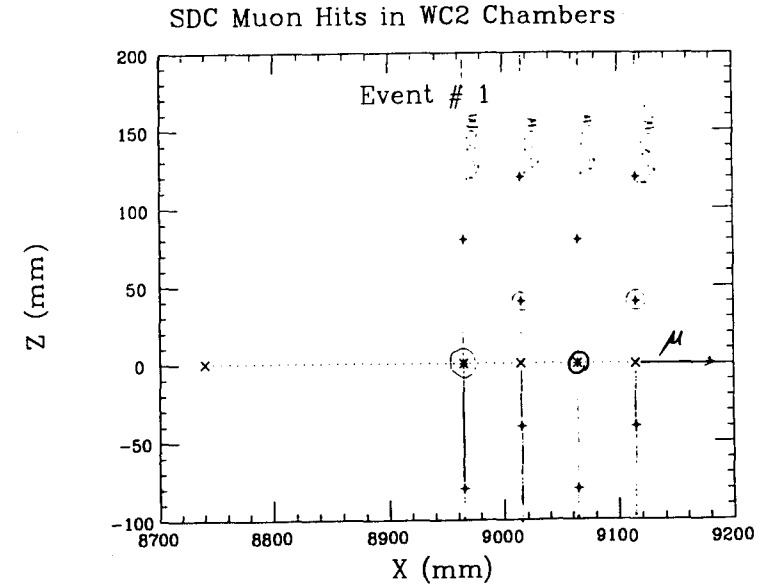
840



838

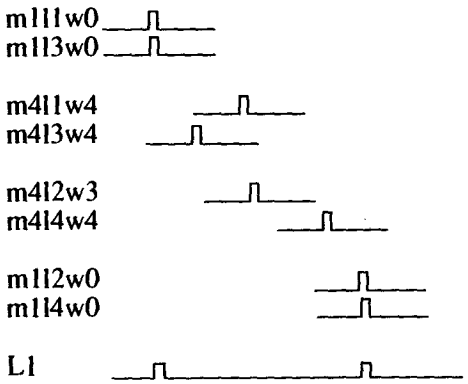


841



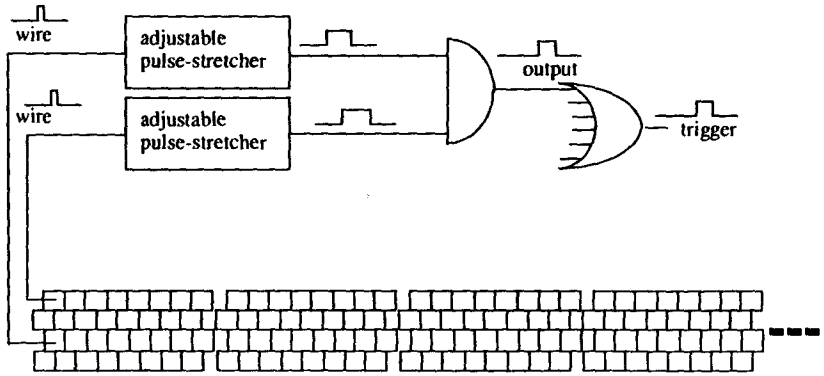
839

"Results"

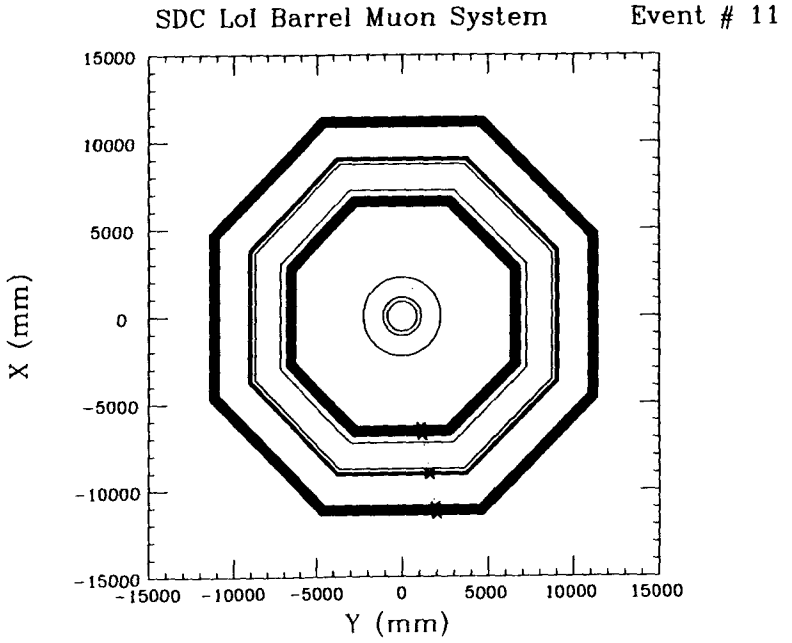


VHDL Oliver Trigger

Oliver, 11-90



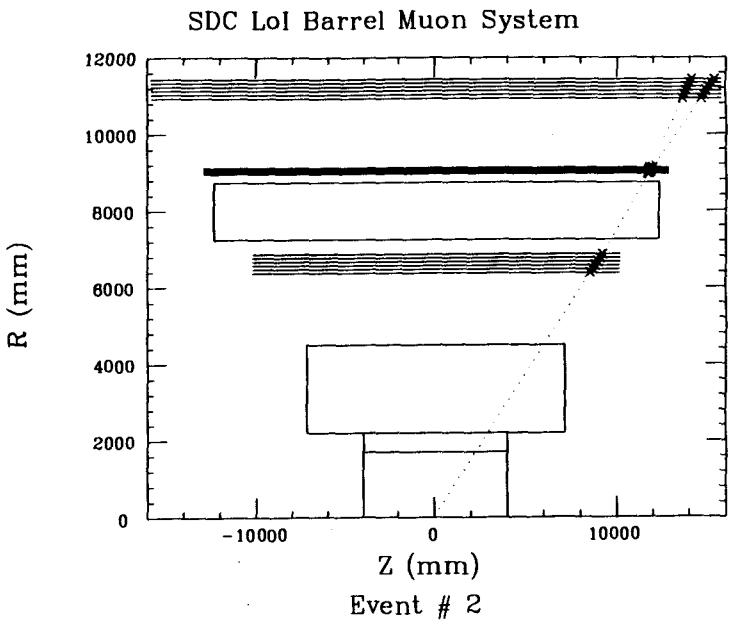
8 wires per module-layer, 4 layers (WC2), 4 modules shown...

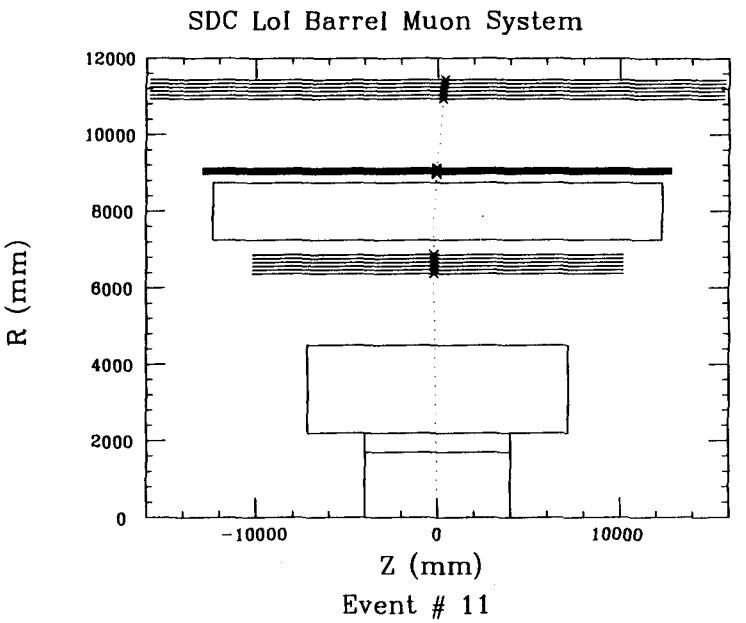


Input to the Model

time (ns)	O LL S wir	E MM
10034.70117	1202000	101
10034.75391	1206000	101
10140.35547	1206020	102
10504.10059	1202020	102
10538.95605	1204019	102
10758.48242	1208020	102
10825.54199	1208000	101
10825.59473	1204000	101
20432.49023	-1202068	202
20514.68164	-1202098	201
20591.84961	-1204098	201
20627.90039	-1204068	202
20649.34570	-1208068	202
20669.01758	-1206099	201
20746.18555	-1208099	201
20823.32031	-1206069	202
30083.30078	-1202098	301
30099.93164	-1204098	301

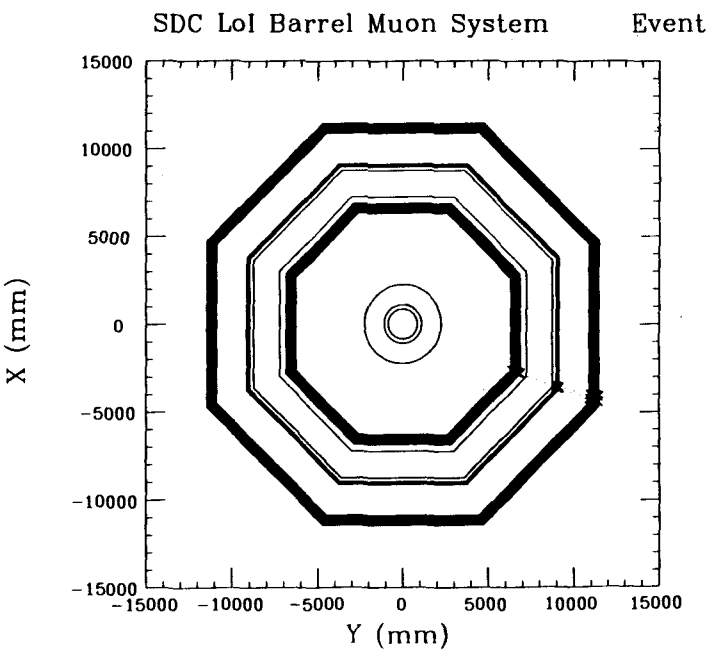
O=Octant (+/- 1..8)
S=SuperLayer (WC1,2,3)
LL=2*layer
wir=wire_number
E=event_number
MM=muon_number





What's Next

- Correct the wire chamber model for projective geometry (DONE)
- Refine the trigger model and/or look for others
- Convert from Verilog to VHDL (DONE)
- Integrate/replace the "fast" code with SDCSIM
  - have DEC 5000/200 RISC workstation
  - have copy of SHELL, etc. for ULTRIX (NOW RUNNING)
  - ~~expecting additional 2GB disk today!~~



Why VHDL

- IEEE Standard 1076
- DOD Mandate for electronics delivered to the military -> strong CAE vendor support
- supports abstract "behavioral" modeling
  - queueing models, algorithmic models, register transfer
  - not hard to get rough idea into code, and into simulation
- supports detailed "structural" modeling
  - chip by chip, wire by wire, gate by gate
  - ASICs, boards, systems can be fully (and precisely) described
- supports multi-levels
  - everything in between abstract and detailed
  - supports design evolution from abstraction to detailed implementation, with simulation all along the transition

What's next:

- use "generate" to represent more modules
- write CDF-type trigger model
- write Chapman-racetrack model for coincidence detection
- get other trigger ideas and write models
- compare triggers
- get better input data!
  - projective geometry from fast muon simulation (S. Errede)
  - interface to SDC-SHELL software development project (I. Karliner)

Why Verilog

- not a standard, but well liked by *many* electronics firms
- easier-to-write and faster-to-simulate than VHDL
- BUT:
  - has been proprietary until recently (Cadence product)
  - few tools available from anyone other than Cadence
  - VHDL is gaining ground, getting faster/easier/better every day

Verilog vs VHDL

- Verilog is still easier and faster (now)
- VHDL will be *the* language of choice in a few years
  - pressure for "one" language will squeeze the Verilog community into VHDL
- Verilog to VHDL translators are already available
- the Verilog model for the Oliver trigger presented in May, 1991 at Fermi was hand-translated into VHDL in 1.5 day (4 pages of Verilog -> 8 pages of VHDL)
- Therefore: it really does not matter which is used today...

The VHDL Oliver Trigger

- one half octant: 1/8 of phi, z>0
- all 1000 wires in each of 4 layers in WC-2
  - 8 wires in a "wire_chamber_module"
  - 125 wire_chamber_modules in a plane
  - 4 planes in a super_layer (WC-2)
- only 4 drift chamber modules were coded for simplicity
  - trivial to hand-write remaining 121
  - plan to use VHDL "generate" command instead (macro expansion facility)

Muon Beam Tests

H. Lubatti(Washington)

 M. LUBATTI

9-24-91 HJL

MUON BEAM TESTS

Colorado/Boulder, Fermilab, Illinois/Champaign, Maryland, Osaka City U/Japan, Rochester, Temple, Tufts, Washington, Wisconsin/Madison

GOALS

- Study number, energy and angular distribution of charged particles accompanying a muon emerging from an absorber and dependence on:
  - muon energy
  - drift chamber wall material and thickness.
- Determine efficiency of muon track reconstruction and smearing of resolution resulting from accompanying charged particles for some prototype cells.
- Čerenkov counter trigger tests

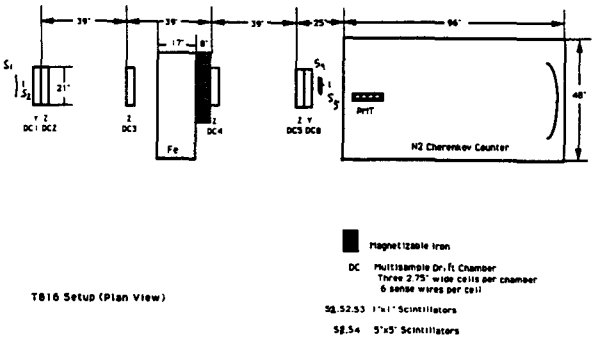
FIRST DATA RUN

- October 2, 1991
- 490 GeV muons

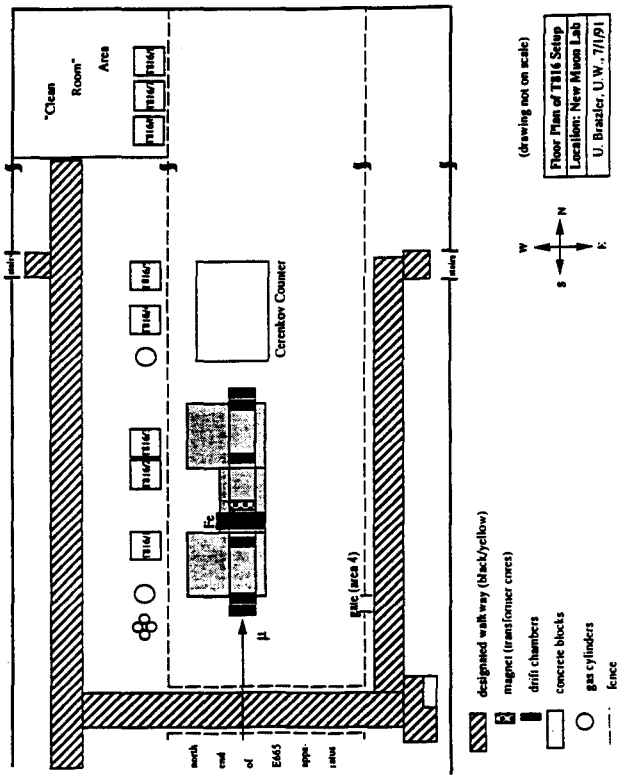
9-24-91 HJL

MUON BEAM TESTS

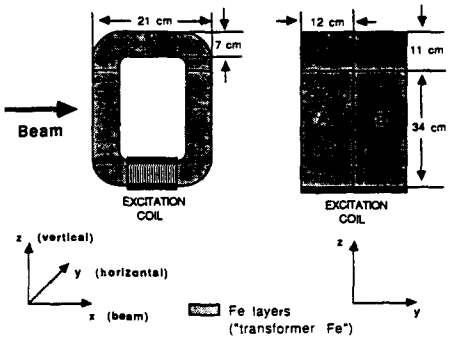
- Tevatron Muon Beam
  - Locate downstream of E665 in the New Muon Lab
  - Beam can be tuned from 100 GeV to 650 GeV with useful flux for these tests
- Apparatus
  - Scintillator trigger
  - Six multi-sampling drift chambers
    3 cells/module
    6 sense wires/cell
    Sense wire length 11 in.
    Staggered wires (0.25 mm)
    2.75 in. cell/1.375 in. drift
    Two track resolution < 3 mm
    Window 1/2 mil aluminized Kapton
  - Fe absorber (25 in.)
    Last 8 in. magnetizable
  - Čerenkov counter has 2 mirrors, each 50 cm^2
- Data Acquisition System
  - FAST BUS TDC's and ADC's
  - On-line VAX 3500
  - Log to 8 mm tape



T816 Setup (Plan View)



MAGNETIZED IRON TARGET



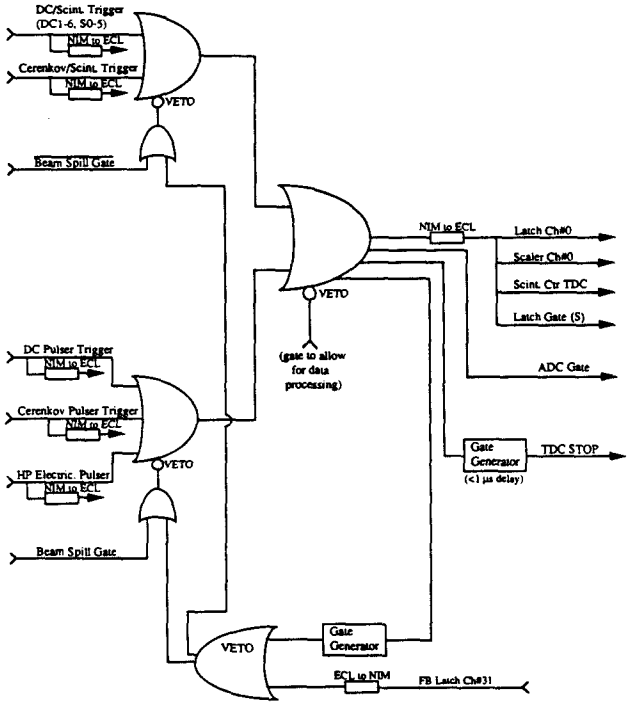
Dimensions: (see drawings)

Measured Resistance of Coils: Excitation Coil (L.ex): 4.9 ohm
Measuring Coils (L.a, L.b): 0.4 ohm
Measuring Coil (L.c): 0.6 ohm

Number of Cu Turns: L.ex: 355
L.a, L.b, L.c: 20

Diameter of Wires: L.ex: 18 gauge (40.3 mil, 156 feet/ohm) (measured: 42.5 mil)
L.a, L.b, L.c: made out of standard ribbon cable
(see sample)

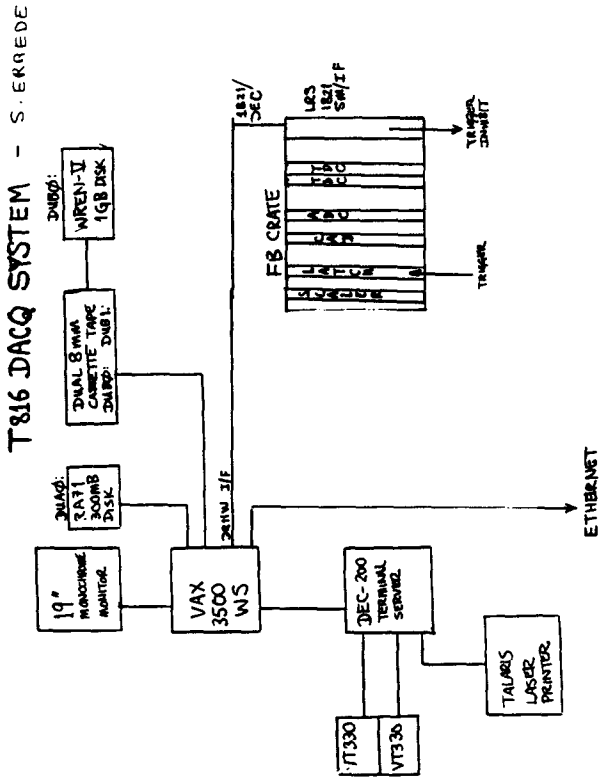
The T816 Master Trigger



MUON BEAM TEST

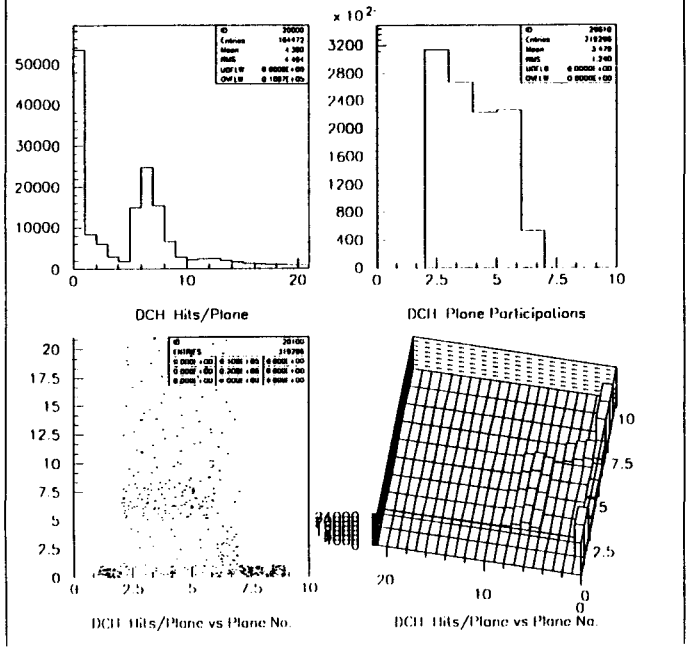
RUN OCT 3

- E_μ = 490 GeV
- DATA
  - NO MATERIAL IN FRONT OF WINDOWS
  - INTRODUCE Al, G-10, Pb ...
    upstream DC 4,5
    downstream DC 3
  - All of above w/ ≠ w/o MAGNETIC FIELD
- E665 TRIGGERS FOR MOMENTUM DISTRIBUTIONS
- TURN OFF E665 MAGNETS

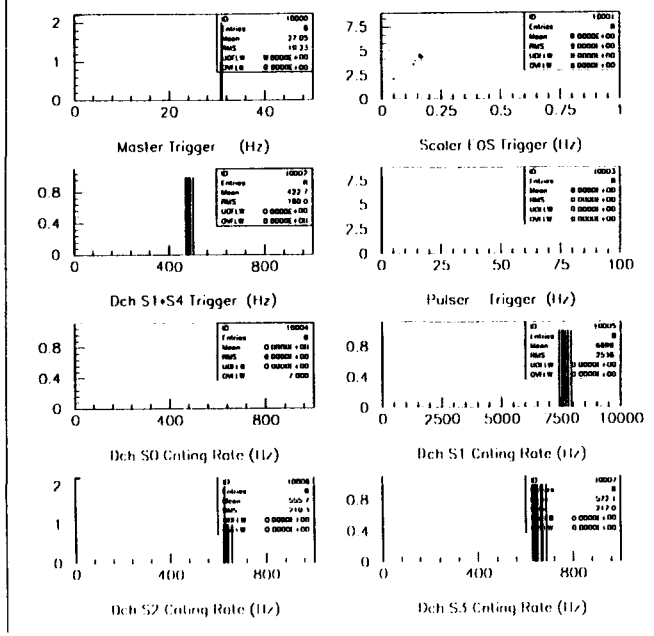


Report on Beam Test Work

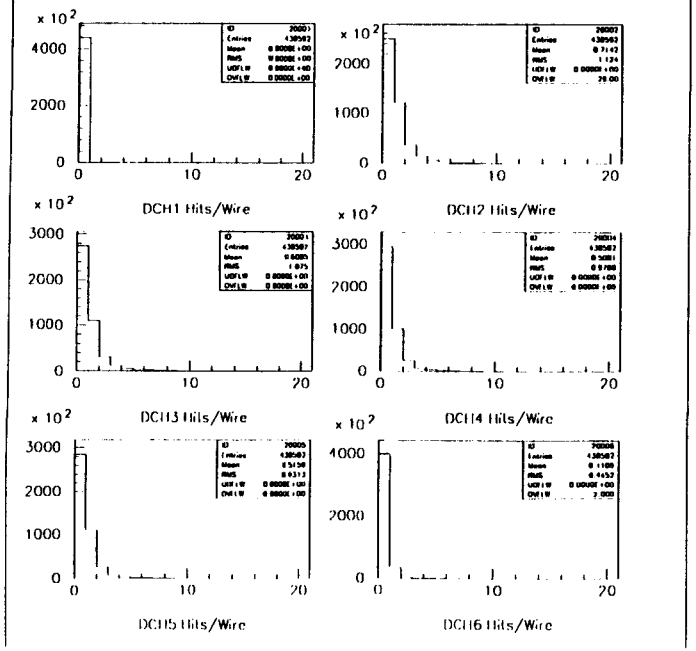
S. Errede(Illinois)



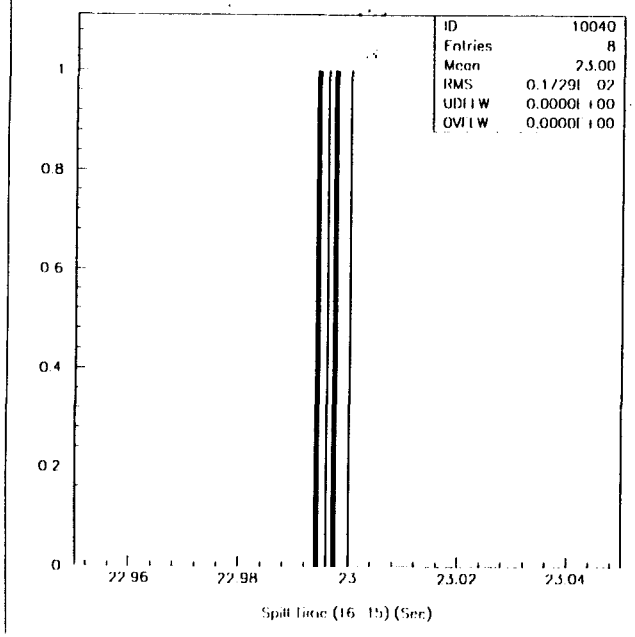
867



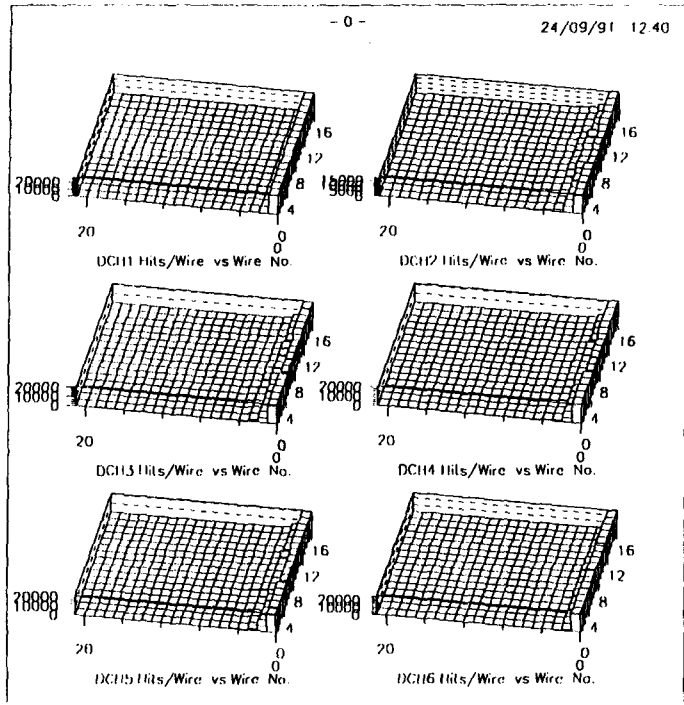
865 ל קראנד



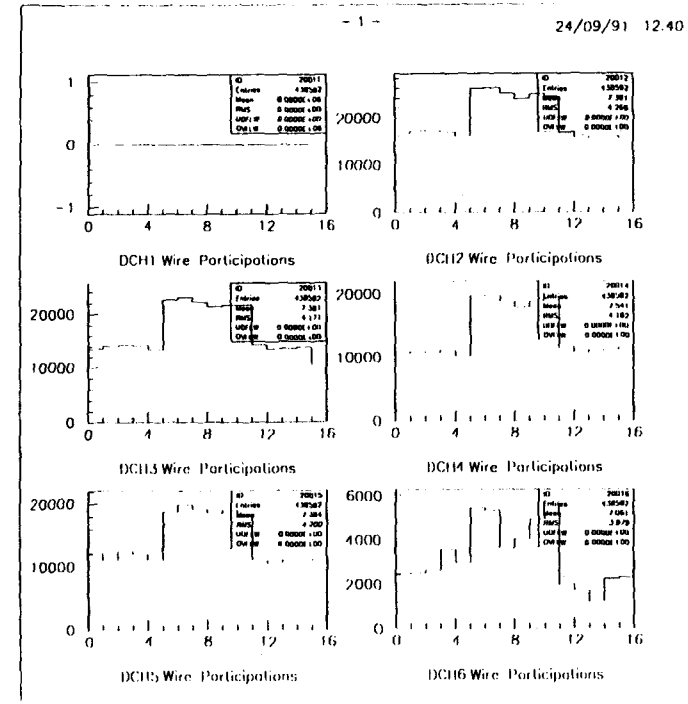
868



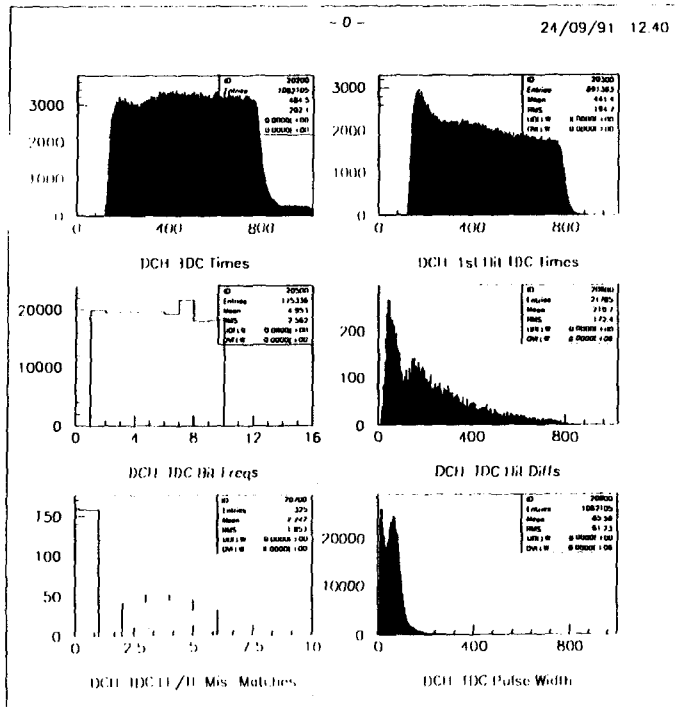
866



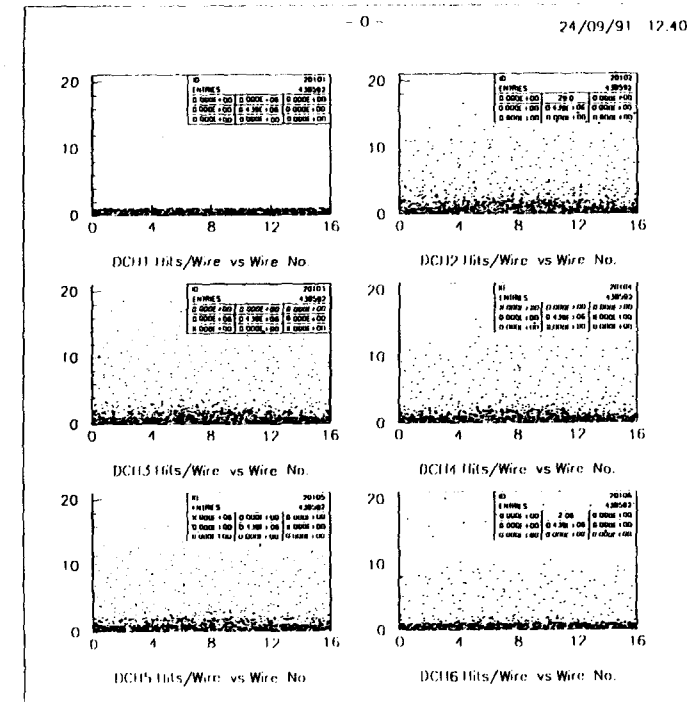
871



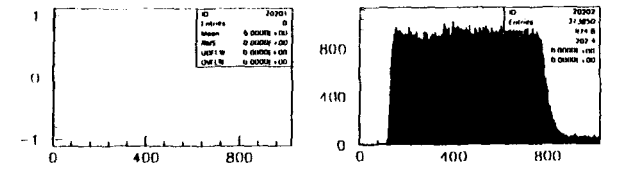
869



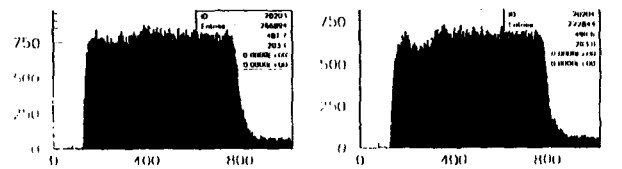
872



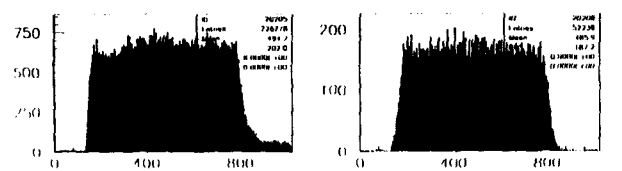
870


DCH1 TDC Times

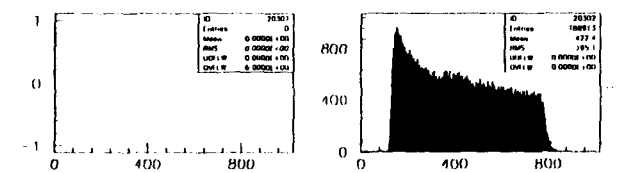
DCH2 TDC Times


DCH3 TDC Times

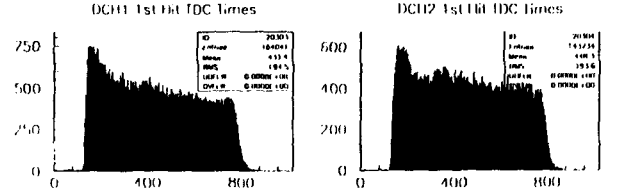
DCH4 TDC Times


DCH5 TDC Times

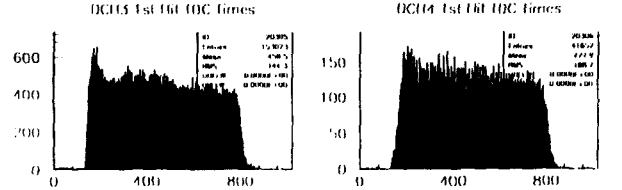
DCH6 TDC Times


DCH1 1st Hit TDC Times

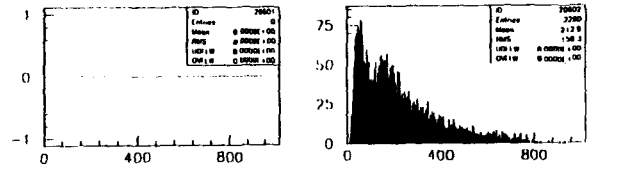
DCH2 1st Hit TDC Times


DCH3 1st Hit TDC Times

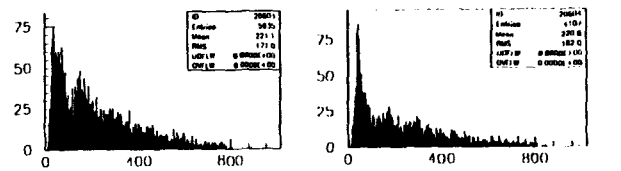
DCH4 1st Hit TDC Times


DCH5 1st Hit TDC Times

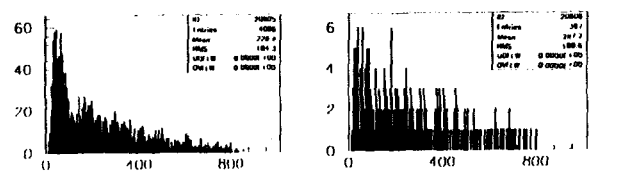
DCH6 1st Hit TDC Times


DCH1 TDC Hit Diffs

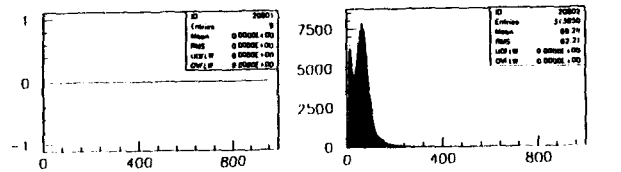
DCH2 TDC Hit Diffs


DCH3 TDC Hit Diffs

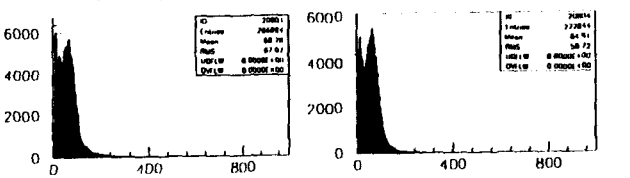
DCH4 TDC Hit Diffs


DCH5 TDC Hit Diffs

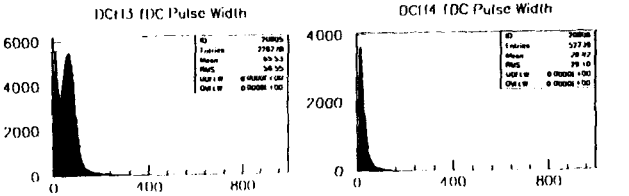
DCH6 TDC Hit Diffs


DCH1 TDC Pulse Width

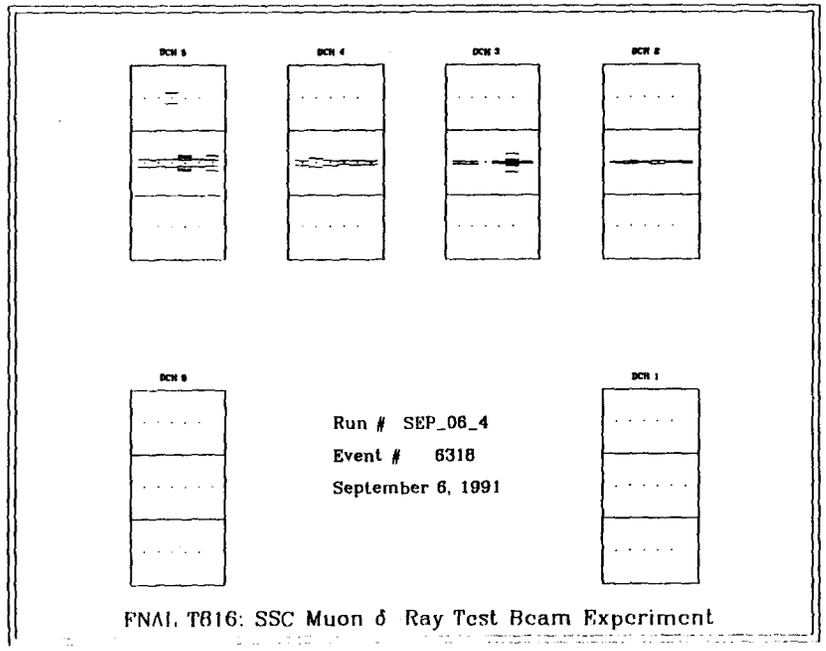
DCH2 TDC Pulse Width


DCH3 TDC Pulse Width

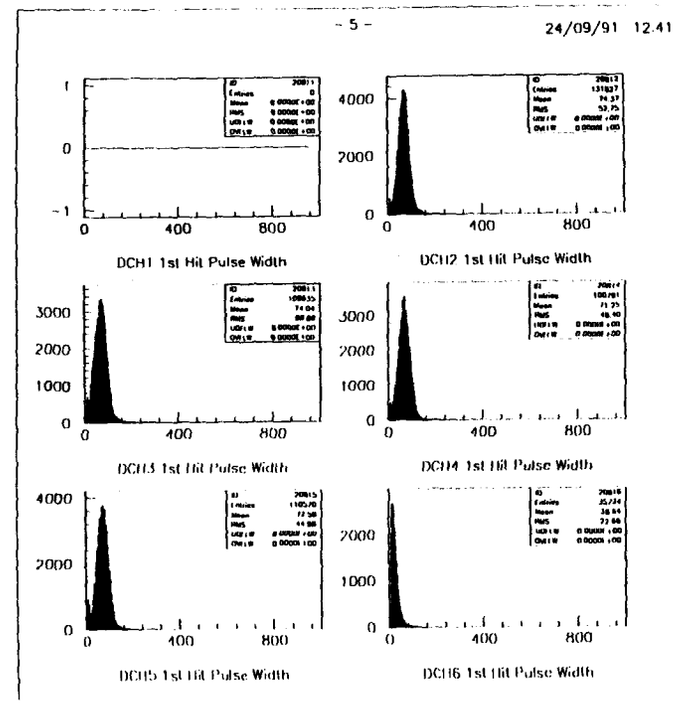
DCH4 TDC Pulse Width

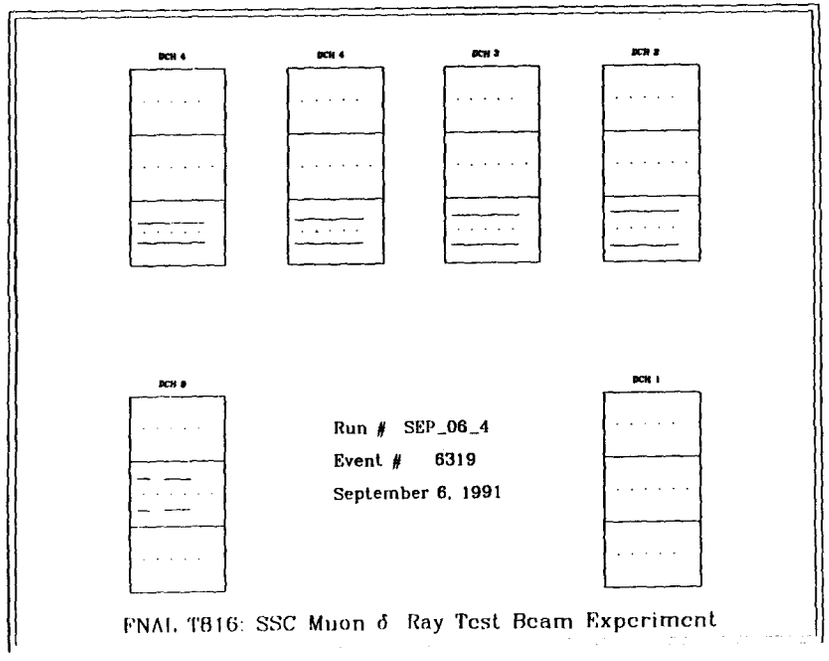

DCH5 TDC Pulse Width

DCH6 TDC Pulse Width

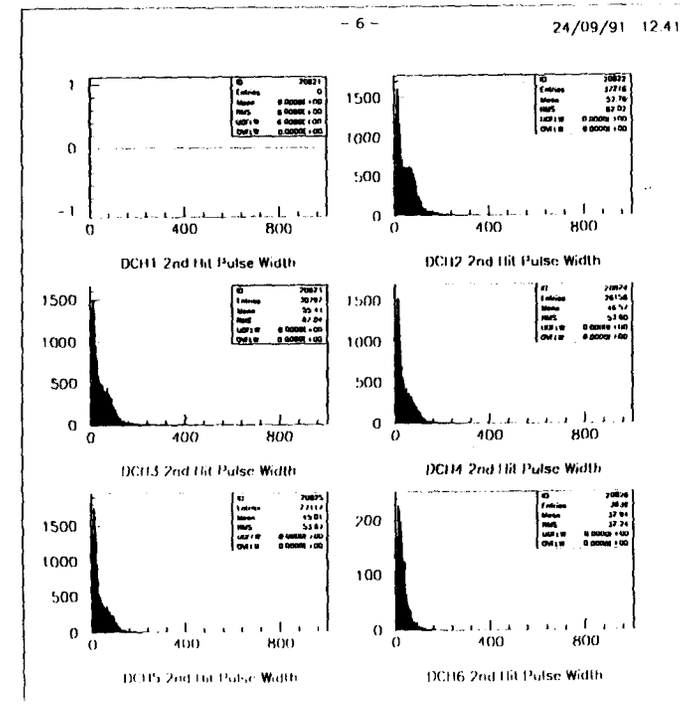


FNAL T816: SSC Muon δ Ray Test Beam Experiment

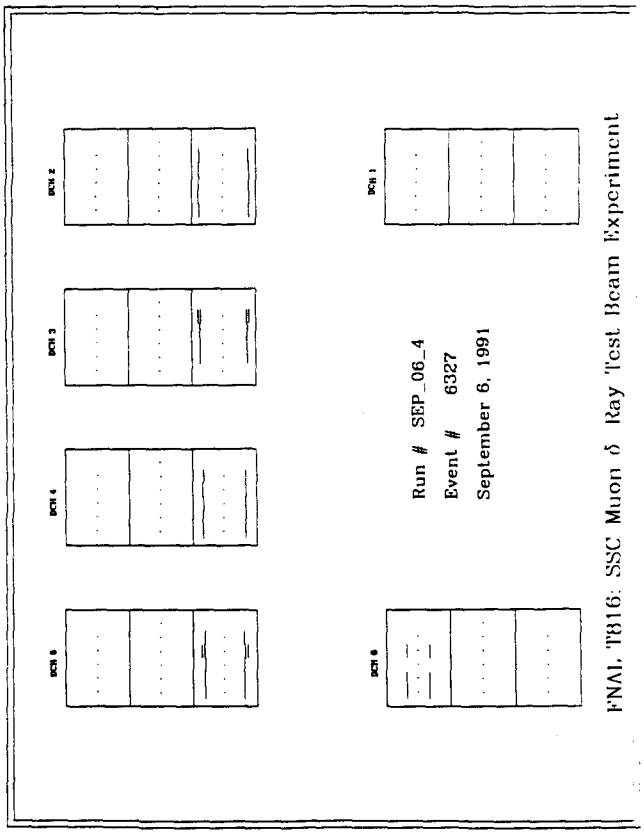




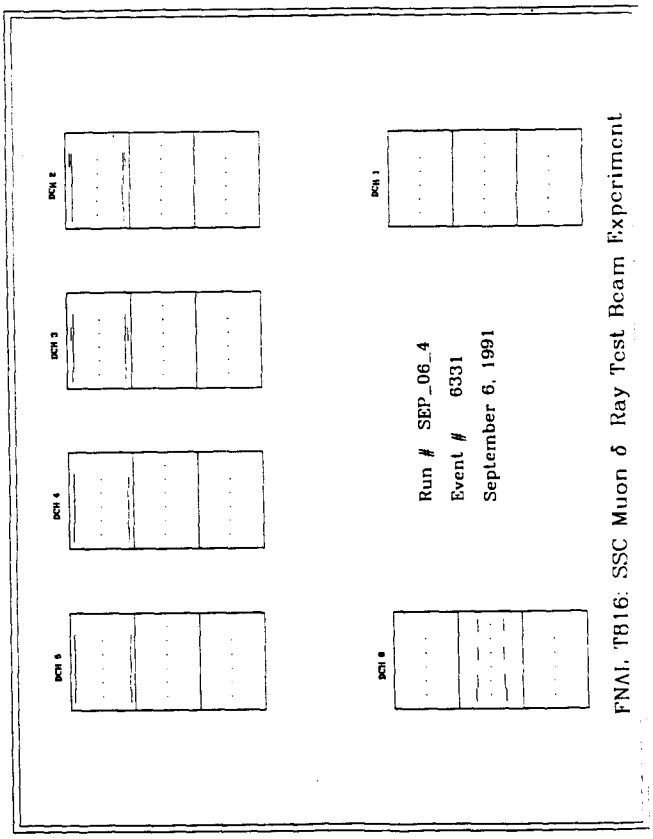
FNAL T816: SSC Muon δ Ray Test Beam Experiment



881



882



883

Steve Errede
Univ. Illinois
Sept. 23, 1991

T816 Tests of Prototype Muon Chambers

- Overall Efficiency
- Effy vs. Drift Distance
- Drift Distance vs Time - How Linear?
- Spatial Resolution
- Spatial Resolution vs. Drift Distance
- Hit Multiplicities ($\delta-$rays)
- Two/Multi-hit Spatial Resolution
- Noise Immunity/Stability/Reliability
- Angle Effect(s)
- Performance vs. Gas Type(s)
- Wire Aging vs Gas Type(s)

884

Steve Errede
Univ. Illinois
Sept. 23, 1991

T816 Tests of Prototype Muon Chambers

- People interested in bringing prototype chambers to T816 test beam need to communicate with us **ASAP/NOW** what they are planning to bring!!!
- Scale: Already spent > 1 year in setting up T816 (several man-years of work)!
- Don't come at last minute!!!
- Don't expect us to do your work!!!
- We will help you ioterface it to existing T816 DACQ system
- How many channels are to be read out?
- Plug into what? ADC/TDC? Scaler? Latch? Other???
- If TDC, what is max drift time?
- If only 2-4 channels TDC, we can provide NIM → ECL conversion for TDC's.
- If > 4 channels TDC, **YOU** provide electronics with differential ECL signals, and 34-pin twisted flat ECL cable(s) for TDC inputs.
- Bring your own HV, LV system(s)
- You bring **ALL** necessary signal, HV, LV cables
- You bring own gas system
- Want precision spatial info? - bring precision DCH holder
- i.e. Worry about geometrical reference to existing DCH's
- R.F. noise environment at TS16/FNAL ugly!
- So come early and sweat with the rest of us!

Tracking

Proposal for Capillary/Liquid Scintillator Tracking	L. Landsberg (Protvino)
Tracking System Design Requirements	W. Ford(Colorado)
Tracking Algorithm Overview	K. O'Shaughnessy (UC/Santa Cruz)
Segment Clustering Track Finding Method	K. O'Shaughnessy
TRF: A Track-Finding Package for Solenoidal Fields	D. Adams(Rice)
Silicon Tracker R&D and Engineering FY 92	H. Sadrozinski(UC/SC)
Silicon Detector Development in Japan	H. Miyata(Niigata)
Overview of Straw Tracking System Design	G. Hanson(Indiana)
Modular Straw Tracking Sustem	H. Ogren(Indiana)
Progress of Straw R&D at Duke U.	S. Oh(Duke)
Straw/Fiber Tracker	S. Reucroft (Northeastern)
Progress in Simulating Combined Silicon and Straw Tube Tracking System	F. Luehring(Indiana)
Pulse Attenuation in Straw Tubes	D. Rust(Indiana)
Straw Electronics and Interconnections	W. Ford(Colorado)
Overview of Fiber Tracking System Design	D. Koltick(Purdue)
Simulation Studies for a Scintillating Fiber Tracker Trigger	R. Lewis(Penn State)
VLPC Status/Plans	P. Besser(Rockwell)
Cosmic Ray Tracking Using Scintillating Fiber Ribbons and VLPCs	M. Atac(FNAL/UCLA)
Summary Report of the Fiber Tracking Group	FTG
Tracking System Requirements for the ITD	A. Sill(Rochester)
Simulation Studies of Microstrip ITD	S. Maxfield(Liverpool)
Test Results	E. Barasch(TX A&M)
Gas Microstrip Chambers - Device Status	M. Dixit(Carleton)
Layout, Material, and Tracking Length Considerations for the Intermediate Angle Region	A. Sill(Rochester)
Work on ITD	J. Dainton(Liverpool)

LPBautz:11/4/91

Proposal for Capillary/Liquid Scintillator Tracking

L. Landsberg(Protvino)

L.G. Landsberg, IHEP, Protvino, USSR 887

Central SDC tracking detector based on capillaries with liquid scintillator.

(proposal)

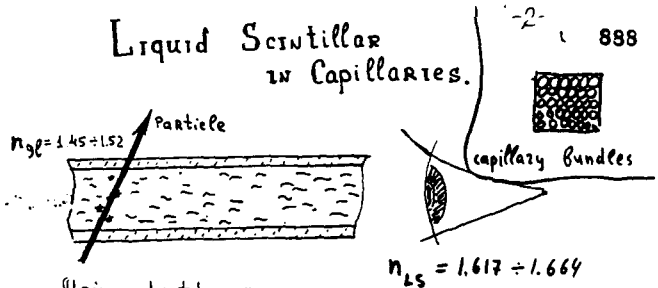
1°. Tracking detector based on capillaries with liquid scintillator (recent results IHEP-JINR group)

2°. Proposal for central SDC tracker

3°. R&D plans.

-2- 888

Liquid Scintillar in Capillaries.



Main advantages:

- high light yield (1.5-1.7 times greater than PS)
- large attenuation length in the capillaries of small diameter
  $l_{att} = 140$ cm $\phi = 110$ μm
  $l_{att} = 60$ cm $\phi = 20$ μm
- the potential for good radiation resistance ("liquid is better than solid...")
- possibility to replace LS
- scintillation decay time 3-6 ns.

$K = 0.5\left(1 - n_{gl}/n_{LS}\right)$ - trapping fraction of light

$K_{max} = 6.7\%$ (5.5% for LS = 1MN + MEMP (dyes))

-3- 889

Tracking Detector Based on Capillaries with Liquid Scintillator

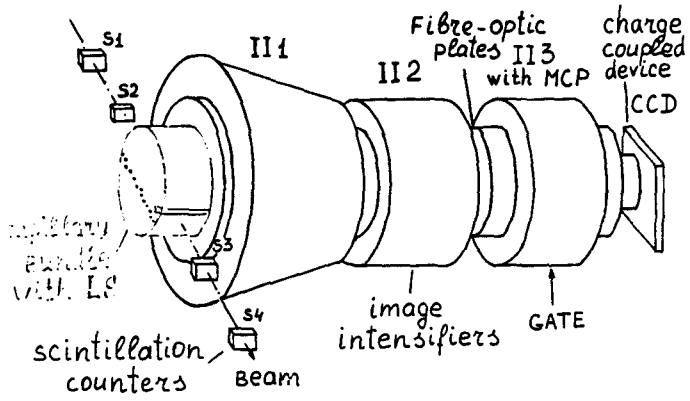
N.I. Bozhko, R.Yu. Elokhin*, S.V. Golovkin, A.M. Gorin, S.A. Korneev, E.N. Kozarenko*, V.I. Kravzov, A.E. Kushnirenko, A.M. Medvedko, A.I. Peresypkin, S.V. Petrenko, Yu.P. Petukhov*, V.E. Tyukov*, V.G. Vasil'chenko, A.A. Zaichenko.

IHEP, 142284, Protvino, Moscow region, USSR
*) JINR, 141980, Dubna, Moscow region, USSR

IHEP preprint 91-45, Protvino, 1991.

-4- 890

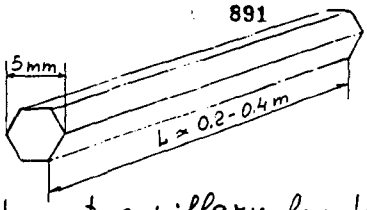
Schematic view of detector and readout system



-5-

891

Interstitial extra-mural absorber EMA



1) Hexagonal coherent capillary bundle,
capillaries of ϕ 25 μm
with centre-to-centre spacing of 32 μm
borosilicate glass with refractive index n_{cl}=1.49
Capillary bundle 0.2 m long with EMA
the active area for the bundle is 55% of the total cross-section area. → 80% possible

2) Capillary bundle without EMA:
ϕ 20 μm, centre-to-centre spacing 32 μm
L = 0.4 m

LS: 1-methylnaphthalene (1MN) based LS with a new dye MBMP (1-(2'-methoxyphenyl-3-biphenylyl-5-(4'-methoxyphenyl)-2-pyrazoline) emitting in the green region.

1MN + 0.007 mole/l MBMP

The results on measuring this LS are given in paper: Golovkin S.V. et al. - IHEP preprint 90-105
The scintillation efficiency of this LS is ≈ 1.3

-7-

893

-6-

892

The refractive index of the LS: n_{co} = 1.617

The fraction of the total light trapped by total internal reflection on the LS-glass interface: $\varepsilon \simeq 0.5\,(1-n_{cl}/n_{co})$ = 0.04

The refractive index of a LS should be as high as possible.

Attenuation curve - fig

Attenuation length:

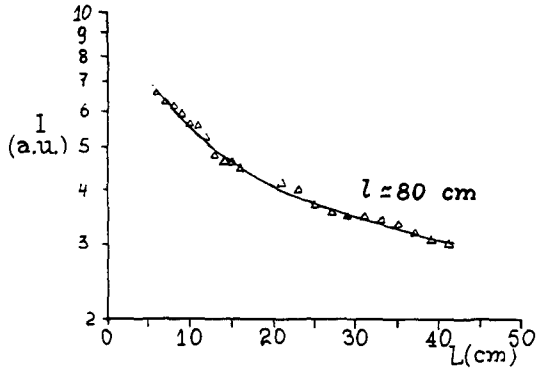
at L>10cm { l = 80 cm — bundle with EMA ϕ 25 μm
{ l = 60 cm — bundle without EMA ϕ 20 μm

This is the best result.
For capillary ϕ 100 μm we have:
l = 140 cm (at L>12cm)
fig.

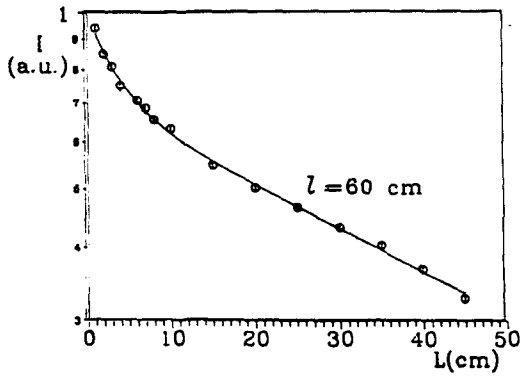
-8-

894

Light attenuation in the capillary bundle.
ϕ 25 μm, with EMA.



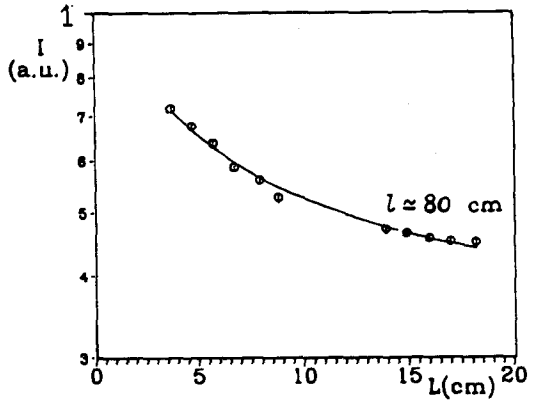
Light attenuation in the capillary bundle.
ϕ 20 μm, without EMA.



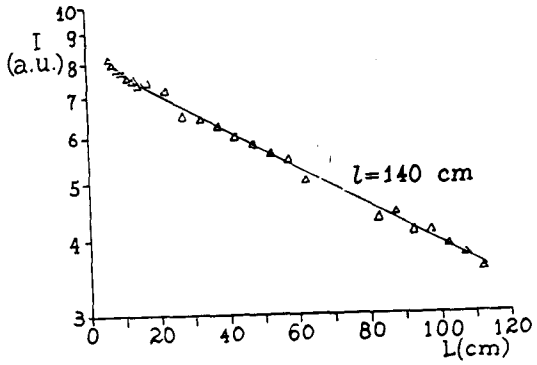
895

896

Light attenuation in the capillary bundle.
ϕ 25 μm, with EMA.



Light attenuation in the capillary
ϕ 100 μm.



897 -11-

Experimental Results on the beam

The detector was studied in a 70GeV p^+ beam. Every photoelectron from the II1 photocathod produced a spot-cluster on the CCD, for whic we analyzed:

a) pulse height in each pixel;
b) total pulse height of the cluster;
c) the coordinates (X,Y) of centre of gravit of the cluster.

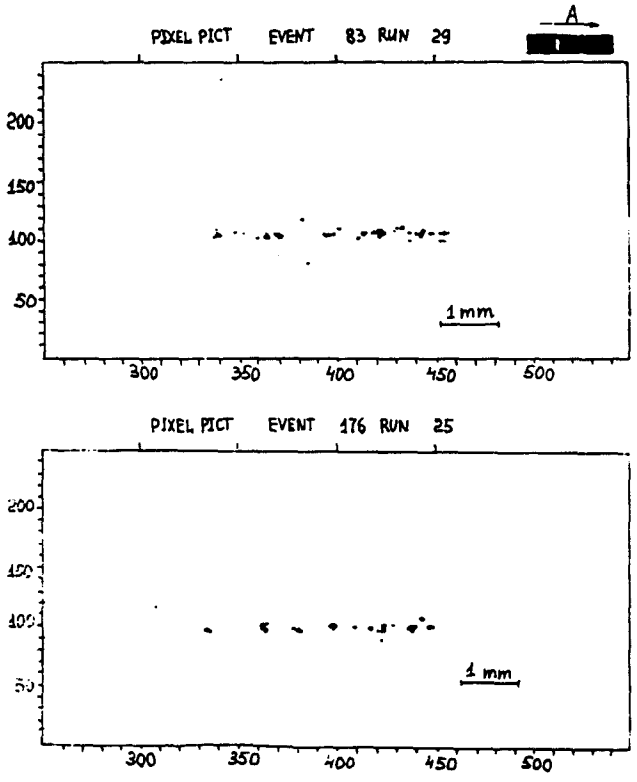
The limitation was imposed on the minimal pulse height in each pixel.
The minimal number of clusters on the track is equal to 4.

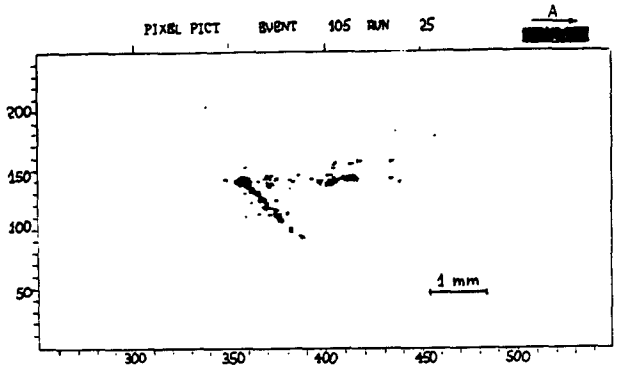
The centres of gravity of the clusters weighted by their total pulse heights were straight line fitted.

Single particle tracks were analyzed. The light pattern produced by 70GeV p^+ (Fig entering perpendicularly to the bundle wit Ei The number of clusters outside the track region is very small.
Interactions inside the bundle stand out well against background of noise fig.

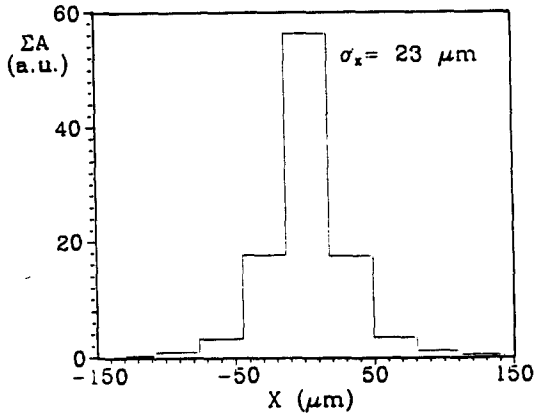
898 -12-

Image of single track produced by 70 GeV p^+ particle

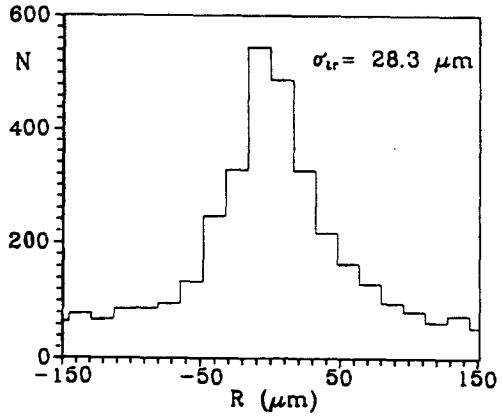




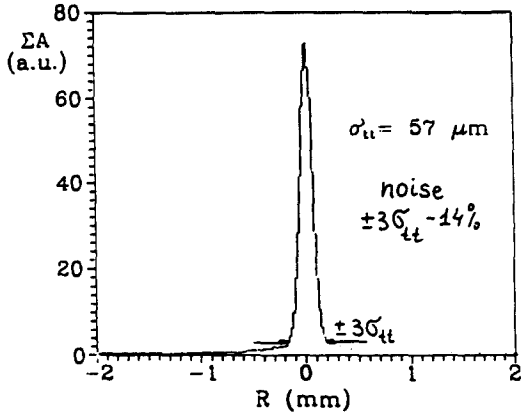
Cluster profile in X-projection.



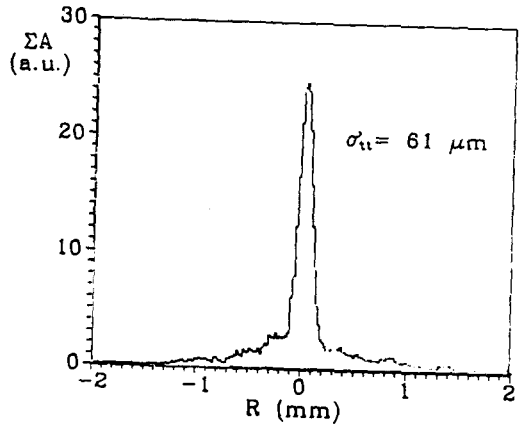
Distribution of track residuals.
bundle with EMA.



Distribution of pulse heights
transverse to track direction.
Bundle with EMA.



Distribution of pulse heights transverse to track direction.
Bundle without EMA.



Two-track Resolution

The distribution of pulse heights transverse to the fitted track direction were obtained by superimpositing 500 events. fig.

After background subtraction the distribution is Gaussian in form.

$\sigma_{tt} = 57\ \mu m$ - bundle with EMA
(30 μm - last data) $L = 155$ mm

$\sigma_{tt} = 61\ \mu m$ - without EMA

The RMS values σ_{tt} characterize the two-track resolution.

Noise

The light detected outside the track region is the noise, which makes up

outside $\pm 2\sigma_{tt}$ — **14%** (at $L = 155$ mm

of the total detected light for the bundle with EMA.

It approaches to a physical limitation of ≈10% when knock-on electrons (δ-rays) make the main contribution to the noise

For the capillary bundle without EMA:

noise — **35%** at $L = 155$ mm

20% at $L = 320$ mm

Cluster Size

The clusters were averaged with the centres of gravity superimposed.

Cluster profile - fig

$\sigma_x = 23\ \mu m$

is determined the resolution of the II-CCD system.

Here and in what follows the sizes applied to the first II input are given.

($\sigma_x = 14\ \mu m$ on the CCD surface)

Spatial Resolution

The spatial resolution of the detector was defined as residual deviations of the centers of gravity of the clusters from a straight line fitted track.

RMS residual: $\sigma_{tr} = 28\ \mu m$ (FWHM/2.36

20 μm recent data

Contributions to Resolution:

1. The main contribution is made by an insufficient high quality of treating the bundle endface.
2. The capillary cross-section size. II sy
3. Cross-talk
4. The detection of the light uncaptured in capillari

Sources of Noise

1. δ-rays on the track; - dominating one for ca with E
2. optical noise - the scintillation light uncaptured by the capillary emerges at the input of the II. - for capill without EMA
3. Cross-talk between the capillaries;
4. From II
5. From CCD

} < 3% from test measurements

Hit Density

The number of hits per unit track length (hit density) was determined from the distribution of longitudinal distances S between adjacent local maxima inside the track region(s

The distribution S was fitted by exponentia

$N \sim \exp(-S/S_{av})$

whereof S_{av} is an average longitudinal dista between LM. The hit density $n = 1/S_{av}$

$n = 4.4 \pm 0.4\ mm^{-1}$ (at $L = 155$ m

For the bundle with EMA

Using the light attenuation curve we obta n at $L = 0$:

$n_0 = 9.6\ mm^{-1}$

907 Track Impact Parameter precision

The precision with which the origin of the track can be determined (impact parameter error δ) depends on the residual σ_{tr} and the number of hits (LM) on the track – N:

$$\delta = \frac{\sigma_{tr}}{2}\sqrt{\frac{12N}{(N+1)(N+2)}}.$$

For the track 5mm long at $L = 155$ mm

$$\delta \simeq 9.7\ \mu m$$

Conclusions

A tracking detector based on capillaries with a LS exposed to the 70 GeV p^+ beam has been investigated.

Performance of the capillary detector:

Cluster size	$\sigma_x = 23\ \mu m$
Track residual	$\sigma_{tr} \simeq 30\ \mu m$ (20
Two-track resolution	$\sigma_{tt} = 57\ \mu m$ (30
Noise on image	14%
Hit density at $L = 155$ mm	$n = 4.4\ mm^{-1}$
Hit density at $L = 0$	$n_0 \simeq 9.6\ mm^{-1}$
Attenuation length	$\ell \simeq 80$ cm

-23- For capillary $\phi 100\mu m$ we have
$\ell = 140$ cm (at $L > 12$ cm) 909

$n \simeq 5.4$ at $L = 0.5$ m; $n \simeq 3.8$ at $L = 1$ m

how we make glass capillaries with the refraction index $n_{cl} = 1.44$ (fluorine-phospha glass):

$n \times 1.4$

3) More easy to make EMA for capillaries.

4) At present the radiation resistance of capillaries with an LS is under investigat. Usually, an LS has the better radiation resista. The possibility of replacing the LS will raise the radiation resistance essentially. Glass darkening caused by radiation will have a weak effect on attenuation because the scintillation light trapped in a capillary penetrates into glass a few wave lengths

preliminary result:
radiation resistance > 10 Mrad

Disadvantages:

1. Technical problems in treating the endface of bundles
2. The need in an additional small vessel with an LS connected with the bundle in case of LS leakage

Tracking detector based on capillaries with LS

Comparison capillary detectors with plastic SCIFI detectors 908

1) The scintillation efficiency of LS based on 1MN is 1.3 times higher than that of plastic scintillator.
The trapping fraction in capillaries with LS is 1.3 times larger

⇓

The best result for plastic SCIFI with small diameter ~ ϕ 30μm:

$n_0 \sim 3$–5/mm (PS + 3HF, Kyowa Gas ...
(CERN 89-10, v1, p. 176)

Capillaries with LS (1MN + MBMP)

$n_0 \sim 9.6$/mm

2) Attenuation length of plastic SCIFI with local light emission ϕ 30μm:

$\ell \simeq 45$ cm ($16 < L < 43$ cm)
PS + 3HF, Kyowa
(CERN 89-10, v1, p. 261)

Capillaries with LS ϕ 25μm:

$\ell \simeq 80$ cm ($L > 10$–20 cm)

For capillaries with LS the value of ℓ is determine primarily by the bulk transparence of LS (the reflection losses are small. $\ell_0 \sim 2_0 \cdot 10^{-5}$)

II. Proposal for central SSC tracker with capillaries with LS 910 -24-

The distinguishing features of capillaries with LS:

a) high light yeald and hit density;
b) large attenuation length for small ϕ ($\ell_a = 1.4$ m for $d = 100\mu m$);
c) the potential for good radiation resistance and a possibility to replace LC;
d) good spatial resolution.

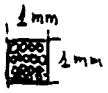
It seems quite promising to use capillaries with LS for the SSC detectors

The II + CCD readout is also promising because of small amount of channels.

But the problem of good time resolution and of the possibility to work at high luminosity (up to $10^{33}\ cm^{-2}\ sec^{-1}$) must be resolved

The main disadvantage of CCD – large readout time — may be removed by using the optoelectronic delay (for 1L trigger) and only part of CCD image zone per one event.

Capillaries with LS for central tracker.



$\Phi = 100\,\mu m$; capillary bundle active area $S = 55\%$

LS = 1MN + (0.007 mol/l) MBMP (dye)

$L_0 = 140$ cm (attenuation length)

$n_{LS} = 1.617$, $n_{ge.} = 1.49$ (Borosilicat glass) } $K = 0.5(1 - n_{ge}/n_{LS})$ - light trapping fraction

$K = 3.9\%$ } $m_0 = 9.6$ hit/mm ($L=0$) (experiment)

Plans: $n_{ge} = 1.44$ } $K = 5{,}5\%$ } $m_0 = 14$ hit/mm we use this value in all calculations

---

Reserve: 1) active area $\longrightarrow$ $S = 80\%$ } Additional increase of m_0

2) $n_{LS} = 1.664$ } $K = 6.7\%$

LS with phenylnaphthalen

General structure of central tracker

3 concentric cylindrical superlayers ($|\eta| \leq 1.92$)

R = 60 cm; 90 cm; 120 cm (up to 150 cm)

I superlayer XUVXUV (6 layers) } stereoangle X and U, V $\vartheta = \pm 10^\circ$

II " " 2×(XUVXUV) (12 layers)

III superlayer XUVXUV (6 layers)

Peanut endcap planes - up to $|\eta| \leq 2.5$

The capillary bundles are arranged in ribbons (1 mm thick; 2 ÷ 5 cm wide) and are wound onto a lightweight support cylinder. Total radiation lengths of CT at normal incidence 8.6% ... r.l.

The deviation of capillaries from parallel alignment is less then 1/5 diameter a capillary

One can consider the bundel as homogeneous mediu for particles; it is possible to measure coordinates of tracks relative to the boundary of the bundle (or may be ribbon).

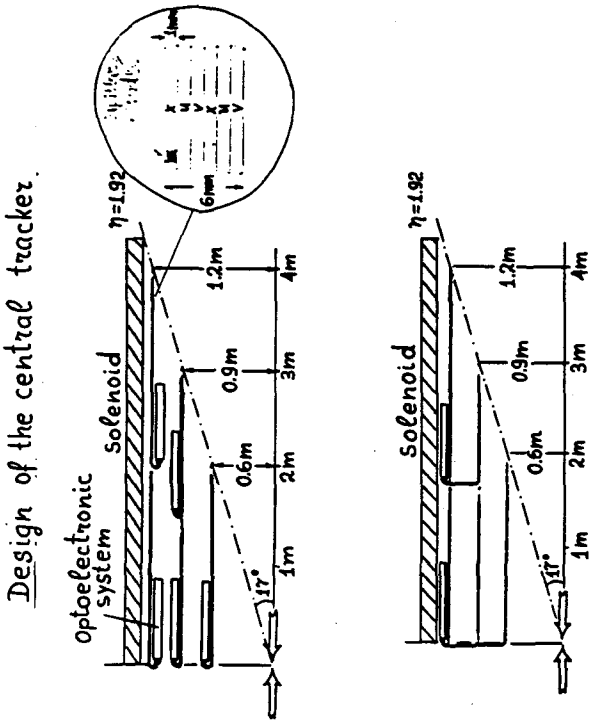
σ_{xy} /hit = 40 μm

σ_{xy} /superlayer = 5-7 μm

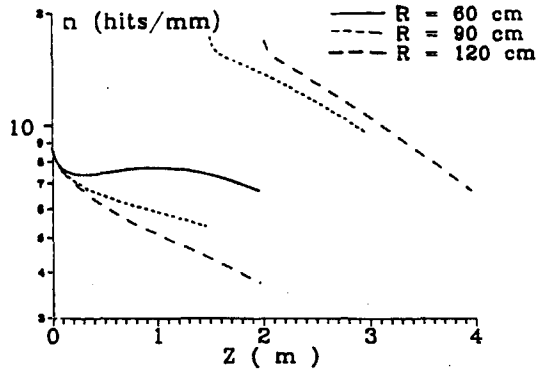
In the every superlayer we measure 3-dimensional vector.

(track segment 3 mm · $\Delta\vartheta < 10^{-2}$)

Design of the central tracker

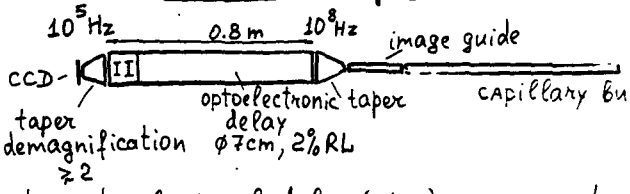


Light yield from capillary bundles in the case of central reading.



Readout system

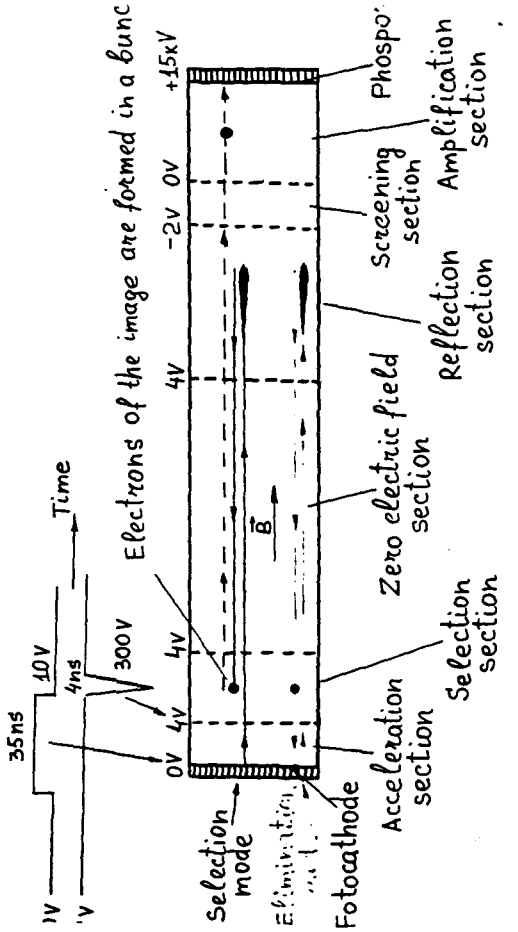
915 -29-



The optical signal delay (~1μs), necessary to produc the 1th level trigger, is realized by the optoelectron delay with image intensifier (II).
Photoelectrons drift in longitudinal magnetic fiel of central detector. For the delay prototype was obtained the resolution 25μm.
The information read out by a CCD.
Delay stores the data at an input rate of 10^5 Hz.
Assuming a rejection capability of 10^3 for the 1- level trigger → output rate 10^5 Hz (acceptable rate for CCD)

Time resolution is determined by decay time of LS (6ns) spread in the time of signal from different points of the capillary bundle (maximun ~9ns) and the time duration of the gate at the optoelectronic delay (~10ns)
Time resolution ~ 15ns
occupancy ≤ 0.7% at 10^{33} cm^{-2} s^{-1} luminosity

916 -30-



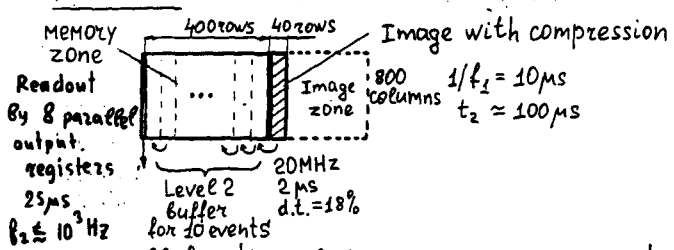
Scheme of the delay tube

CERN/LAA SF 91-3, 22 Feb. 1991.

-31-

CCD readout has a number of impo... advantages. Th...

917

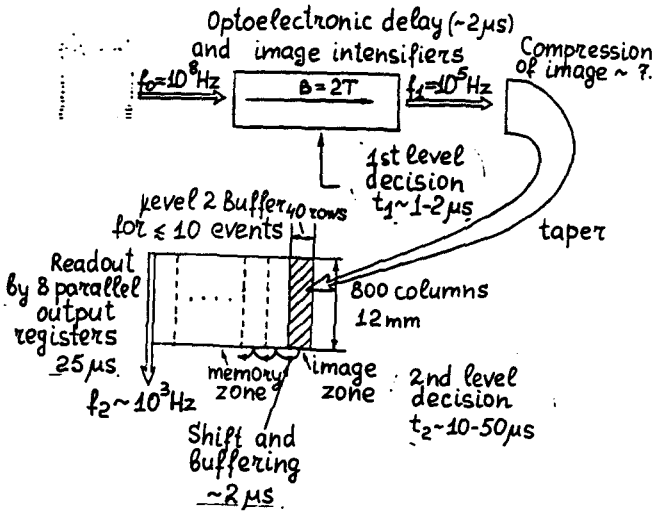


A small fraction of the image zone is used, where information is immediatly after recording sent to the memory zone, that is a buffer during the 2nd level trigger decision time (t_2) . . .

-32-

918

CCD Readout



f_1, f_2 - the rate of events passing level 1,2 trigger.

$t_1 t_2$ - decision time of level 1,2 trigger

The main disadvantage of CCD - large readout time - is removed by using the optoelectronic delay and only a part of CCD image zone per one event. One may have any level trigger buffering, which allows to reduce of electronics.

SDS trigger levels

	Level 1	Level 2	Level 3
Input rate	60 MHz	10 ÷ 100 kHz	0.1 ÷ 1 kHz
Decision time	1.5 μsec	10 ÷ 50 μsec	0.1 ÷ 1 sec
Rejection time	1K ÷ 10K	10 ÷ 100	10 ÷ 100

The worst case

$N(T_2\ L1) = 10^5\ sec^{-1}$ dead time } 18%

$N(T_2\ L2) = 10^3\ sec^{-1}$ dead time } 2.5%

} Total dead time 20% → (~10%)

The best case $N(T_2\ L1) \approx 1$ dead time several %

It is possible to reduce the dead time.

The sizes of the image zone used for a record of event (the numbers of rows equals 40) determin the total numbers of CCD (1548). It is possible to reduce the dead time if one increases the numbers of CCD and diminishes the numbers of rows

For example } 1548 CCD → 7740 CCD (5) } Total dead time is ~~4%~~

Radiation dose for outer detector ≤ 0.2 ÷ 0.5 Mrad (luminosity of $10^{34}\ cm^{-2}\ sec^{-1}$; 10 years of running)

Radiative resistance of the capillary detector >10 Mrad

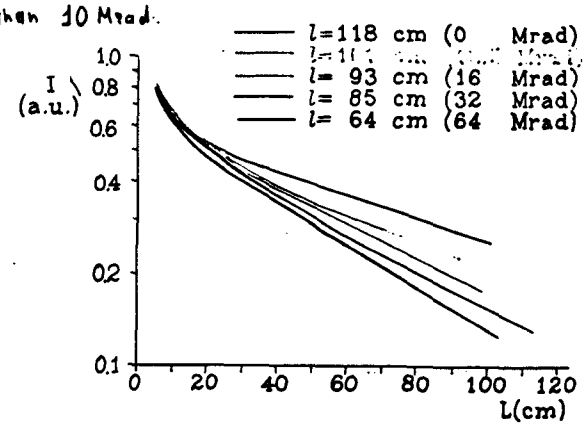
There are CCD with radiative resistance of several Mrad. Than it is possible to place CCD inside or outside the solenoid volume.

There is possibility to place readout system with CCD and part of II outside the detector volume and transmit the light signals by means of external image guide (non scintillating fibres) several meters long. After the II a light attenuation in these guides (~10-20) is not important.

Radiation resistance of the capillaries with LS

According to the first measurements it is much better than that of plastic scintillators.

Radiation resistance of the capillary detector is better than 10 Mrad.



The scintillation efficiency don't change up to 64 Mrad. In addition the replaceability of the LS singnificantly increases the radiation resistance of the detector.

At the luminosity $L = 10^{34}\ cm^{-2}\ sec^{-1}$ (SSC) for the inner shell radiation dose is equal to 0.2 ÷ 0.5 Mrad.

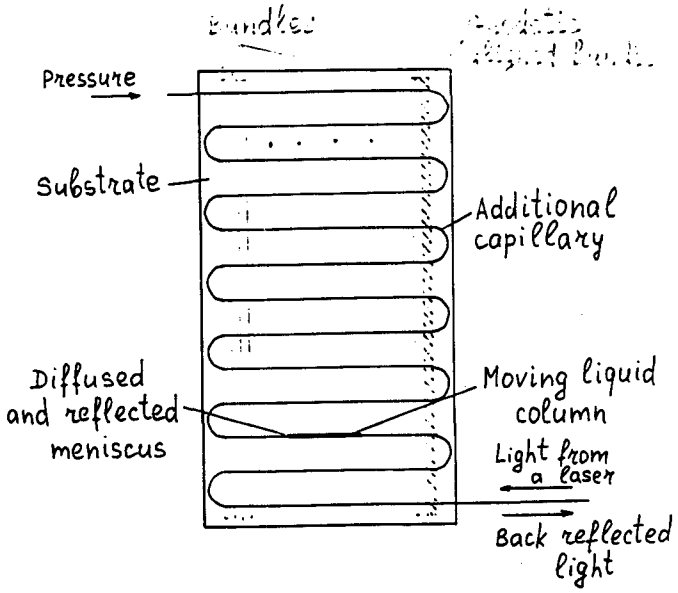
It is possible to use capillary tracking detectors for planar endcap part of tracker (at 1.7 < |η| < 2.5)

Table 2

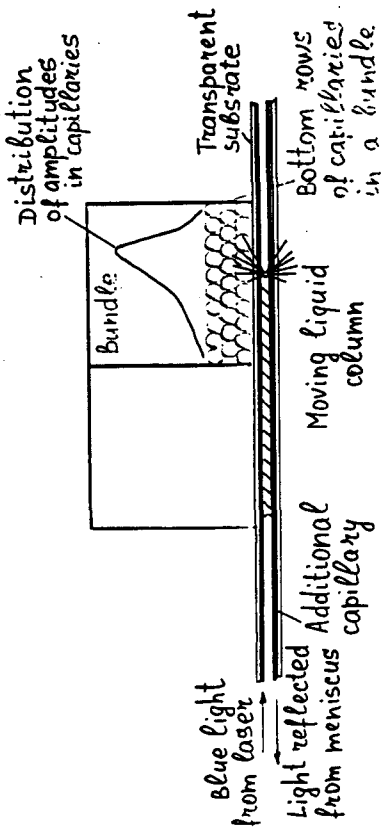
Item	Design performance	
	Proposal	SDC (LoI)
Fiber diameter	100 μm	750 μm
Outer radius	1200 mm	1600 mm
Magnetic field	2.0 T	2.0 T
Total number of elements	$0.5 \cdot 10^6$ bundles	$1 \cdot 10^6$ fibers
Number of superlayers	3	4
Number of layers in 1 superlayer	6 (12)	9 (16)
Approx. occupancy per element	10^{-3}	10^{-2}
Total radiation length at normal incidence	~8.6% *)	6.7 %
Number of channels	12400	1.000.000
Reconstruction object in superlayer	3-dimensional vector	X - vector U,V - hits
Time resolution	≈ 15 ns	
No. hits/track	≈ 150-250	
No. hits/mm	6 - 12	≈1.2
σ_{pt}/p_t (fibers only)	$30\% \cdot p_t$ (TeV/c)	$100\% \cdot p_t$(TeV/c)
σ_{xy}/hit	40 μm	
σ_{xy}/superlayer	5 - 7 μm	55 μm/measur.
σ_z/superlayer	20-50 μm	
σ_{xy} (vertex)/track	10 μm	
σ_z (vertex)/track	100 μm	
σ_φ/track	0.015 mrad	
σ_θ/track	0.10 mrad	
Two-track resolution	~100 μm	1000 μm

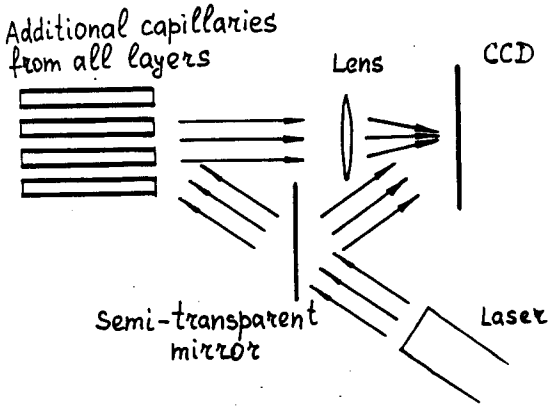
*)- for the arrangement of fig.3b. For fig.3a the optoelectronic system give an average 0.4% RL in addition.

Unwind layer on the substrate



Method of the geodetic alignment of bundles





Setup for measuring of interference picture

Summary.

The development of tracking detector for use in the SDC is proposed.
Compared to high resolution plastic scintillation fiber detectors, capillary tracker have a number of advantages.

- Owing to high scintillation and trapping efficiencies the hit density on the track is several times larger than for plastic fibers.
- Large attenuation length ($\ell = 1.4$ m for capillarys with $\phi = 100\,\mu$m) allows one to construct detector with length $\gtrsim 2$ m and spatial resolution better than 15 μm/bundel.
  $\delta(P_T)/P_T = 30\%\ P_T(\text{TeV/c})$ - good momentum resolution.
- The use of optoelectronic delay and proper choice of a small part of CCD matrix make it possible to have a fast tracking detector (with time resolution $\lesssim 15$ nsec) and with reasonably small dead time losses ($\lesssim 10\%$). The number of the channels is quite [illegible]

927

- Capillaries with LS have a record radiative resistance (better than 10 Mrad). This is quite important - and first of all for the planar endcap part of tracker (in the region of $|\eta| > 1.7$)
- The operation of this CT at high luminosity (10^{34} cm^{-2} sec^{-1}) is quite possible owing to high granularity, small occupancy high spatial resolution and good radiative resistance. At $L = 10^{34}$ cm^{-2} sec^{-1} the flux on one capillary will make up 0,013 charge partic./bunch (for inner superlayer; R = 60cm)

Disadvantages of CT with capillaries with LS

- Impossibility to use this tracker with CCD readout in the 1 and 2 levels of trigger (only in the 3 level it is possible)
- Some technical problems connected with LS.

It seems quite promising to use some hybrid system with LS with CCD readout and some part with VLPC readout for trigger capillaries with LS or plastic scintillating fibers

928

Hybrid sistems

a) Small amount of plastic fibers (φ = 750 μm) - as in LOI - with VLPS readout for trigger. All other fibers are capillaries with LS with OE + II + CCD readout.

b) Capillaries with LS with OE + II + CCD
Light signals from vacant ends of the small part of capillary bundles can be detected by VLPS and used for the trigger

c) Plastic fibres (φ = 750 μm)
Only small part of the channels - with VLPS
For all other fibres - OE + II + CCD readout

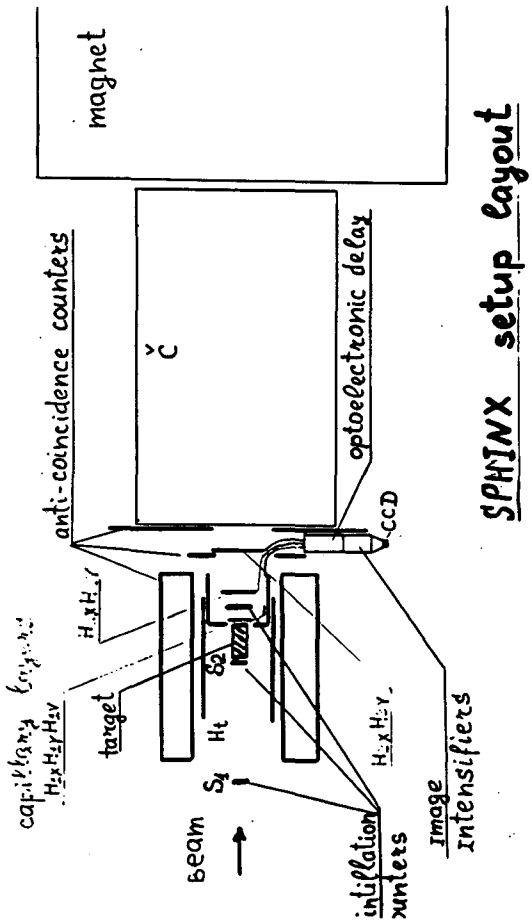
929

R&D program (up to summer of 1992)

1. Development of glass capillary bundles with low refractive index (n = 1.44) 10.1991
2. Creation and study the first prototype of optoelectronic delay tube 11.1991
3. Test of the working prototype of capillary bundles ($L \cong 1.2$ m) with optoelectronic delay 12.1991 - 3.1992
4. Development of the first working detector with 7 planes of capillaries with LS - for the use with SPHINX spectrometer
   Testing of the tracking detector
   } 5÷6 1992

Many other works with electronics, CCD, II, simulation,

930



Performance of capillary detector for SPHINX

931

Diameter of capillaries - 150μm
Length of capillaries - 0.5m
Distance between H_1 and H_3 - 200mm
Track residual/hit - 60μm
Impact parameter precision/plane - 30μm
Two-track resolution/plane - 200μm
Angular resolution/system - $3 \cdot 10^{-4}$
Output channels - 1
Time resolution - 10ns
Dead time at the event rate of 3500/s - 25%

Work sizes of planes

	H_{1X}	H_{1Y}	H_{1V}	H_{2X}	H_{2Y}	H_{3X}	H_{3V}
size	2cm	2cm	2cm	5cm	3cm	8cm	5cm

932

CENTRAL TRACKING DETECTOR BASED ON CAPILLARIES WITH LIQUID SCINTILLATOR FOR THE SDC

S.V.Golovkin, A.M.Gorin, V.I.Kravtsov, A.E.Kushnirenko, A.M.Medvedkov, A.I.Peresypkin, S.V.Petrenko, V.G.Vasil'chenko, A.A.Zaichenko

Institute for High Energy Physics (IHEP), Protvino, USSR

E.N.Kozarenko, Yu.P.Petukhov, V.E.Tyukov

Joint Institute for Nuclear Research (JINR), Dubna, USSR

R.Yu.Elokhin

Branch of Institute of Nuclear Physics (BINP), Protvino, USSR

D R A F T - corrected version of September 9, 1991

933

CENTRAL TRACKING DETECTOR BASED ON CAPILLARIES WITH LIQUID SCINTILLATOR FOR THE SDC

SUMMARY

The development of the central tracking detector for use in the SDC detector is proposed.

Compared to the high resolution plastic scintillation fiber detectors, capillary tracking detectors have a number of advantages that significantly change the situation with central tracking:

-owing to the high scintillation and trapping efficiencies the hit density on the track is several times larger than for the plastic fibers;

-large attenuation length l = 0.8 m for the capillary diameter d = 25 μm and l = 1.4 m for d = 100 μm, that exceeds several times the attenuation length for plastic fibers, allows one to construct detectors with length ≥ 2m and spatial resolution 20-40 μm.

Thanks to the large attenuation length and by reading the information from the centre of the detector, it is possible to achieve compensation of attenuation due to the tracks being inclined at the remote end of the capillaries. Central readout also relaxes the demand on the radiation resistance of the optoelectronic chain. High spatial resolution allows one to reduce the size of this detector. So it becomes possible to create the whole detector with smaller size.

Some ideas of the CCD readout at high event rates (image compression, data buffering for 2nd and 3rd levels of trigger immediately on CCD) allow to have 12400 output channels for the tracking detector.

There are possibilities to place the CCD readout system inside or outside the detector volume and also to use the optoelectronic readout system (outside the detector volume)for scintillating plastic fiber detector suggested in the LoI by the SDC.

A prototype of a tracking detector has been investigated.

934

CENTRAL TRACKING DETECTOR BASED ON THE CAPILLARIES WITH LIQUID SCINTILLATOR FOR THE SDC

The tracking detectors with scintillating fibers (SCIFI) are very promising detectors for colliding beam and fixed target experiments. A precise tracking detector with SCIFI may be about 2 m long with spatial resolution better than 20 μm, time resolution of about 10 ns and radiation resistance of > 10 Mrad.

A new type of such device is a tracking detector based on capillaries with a liquid scintillator (LS) [1,2,3,4,5,6,7]. A central tracking (CT) based on capillaries with LS is proposed for the SDC.

1.CHARACTERISTICS OF LIQUID-IN-CAPILLARY FIBER DETECTORS

The distinguishing features of such detectors are :

a) high light yield;
b) large attenuation length in the fibers of small diameter (30-100 μm);
d) the potential for good radiation resistance;
e) a possibility to replace LSs.

1.1. Light yield

In order to increase the trapping efficiency by total internal reflection on the LS-capillary interface ($K \approx 0.5 \cdot (1 - n_{gl}/n_{ls})$ one needs an LS with a high refractive index n_{ls}. An LS based on 1-methylnaphthalene (1MN, n_{ls} = 1.617) with an MDP or MBMP dyes based on pyrazoline has been obtained. This LS has high locality of light emission and scintillation efficiency 1.3-1.5 times higher than that of plastic

scintillators [3]. In addition the trapping fraction K in capillaries with LS is 1.5-2 times larger. For example, for a conventional polystyrene fiber K ≈ 3%. For the quartz capillaries (n_{gl} = 1.46) with 1MN - K ≈ 4.8% and for an LS based on phenylnaphthalene (n_{ls} = 1.664) K ≈ 6.1%.

The emission spectrum of these dyes lies in the green region, which matches the sensitivity spectrum of image intensifiers (II) used to amplify the optical signals from the detector. The green region also reduces the attenuation in the fiber and makes the radiation resistance higher [8].

A tracking detector based on the glass capillaries with n_{gl}=1.49 (25 μm in diameter and active area fraction of 55%) filled with the LS (1MN + 0.007 mol/l MBMP) was tested in a 70 GeV/c p^+ beam [6]. The signal was amplified by an II system.and information was read out by a CCD. The number of hits per unit track length obtained in the tests was n_0 ≈ 10/mm (at capillary length being L=0) which is several times larger than the hit density in plastic fibers of the same diameter [1,9]. We plan to produce glass capillaries with n_{gl}=1.44 and increase n_0 up to 14/mm. The active area fraction in the capillary bundles may be ≈ 80%.

1.2 Light attenuation in the fiber

Because of a high reflection coefficient at the LS-glass interface (1-R ≈ 4-8·10^{-5}) the attenuation in the capillary is determined by the LS bulk transparence. The attenuation length due to reflection losses (no attenuation in the LS volume, 1-R = 8·10^{-5}) is equal to l_r ≈ 1.3 m for the diameter of 30μm and l_r≈ 43 m for 1 mm diameter. The following value of the attenuation length have been obtained for the LS: 1MN+MBMP [6]: l = 0.8 m at d = 25μm (fig.1a), which exceeds several times the attenuation length for plastic fibers of a small diameter with local emission .l ≈ 0.3 - 0.5 m, d = 30 μm) [10,11]. The attenuation length 1.4 m was obtained for d = 110 μm (fig.1b).

The attenuation length of ≥ 1 m allows to construct detectors with the high spatial resolution ≥ 2 m long.

1.3 Spatial resolution

The capillary diameter and also amplification and readout systems determine the spatial resolution of the detectors based on capillary bundles with an LS. The straight-line RMS residual (σ_{tr} ≈ 30 μm) and two-track resolution σ_{tt} ≈ 60 μm was obtained in ref. [6] for the bundle of capillaries 25 μm in diameter. At present we have σ_{tr} ≈ 20 μm, σ_{tt} ≈ 30 μm for these bundles. The main contribution to the spatial resolution gave an insufficiently high quality of processing of the capillary bundle endface. The best results for capillary detector were attained in paper [7]: σ_{tt} = 15 μm. At the capillary diameter of 100 μm this size will give the main contribution to the resolution, and the track residual will be about σ_{tr} ≈ 40 μm.

1.4 Time resolution

The time resolution is determined by the LS decay time (of 3-6 ns [3,5]), the time spread of light signal propagation along the fibers and time characteristics of the optoelectronic delay required to organize the first level trigger. An optoelectronic delay of 1 μs is being designed and its prototype has been investigated [12]. It is possible to produce this delay up to 2 μs. The delay will allow one to obtain the time resolution for the detector of ≤ 15 ns.

1.5 Radiation resistance

At present the radiation resistance of the capillaries with an LS is under investigation. According to our first measurements it is much better than that of plastic scintillators, since the LS radiation resistance is higher than that of plastic scintillators. Glass darkening caused by radiation will have a weak effect on attenuation because the scintillation light, trapped in a capillary by the total internal reflection on the LS-glass interface, penetrates into

glass only a few wave lengths. Figure 2 presents the light attenuation curves versus the radiation dose. These data shows that radiation resistance of capillary detector is about of 60 Mrad. At the dose 64 Mrad the light output is fallen to approximately one half of the original value at the distance of 1 m. The scintillation efficiency don't change up to 64 Mrad. In addition the replaceability of LSs significantly increases the radiation resistance of the detectors themselves.

2.CENTRAL TRACKING DETECTOR

We propose to exploit a high spatial resolution tracking detector based on capillary bundles with an LS since it has a number of advantages:

1) fine spatial measurement accuracy;
2) high two-track resolution;
3) large attenuation length;
4) compactness;
5) high hit density on a track, we have 1 hit per 7·10^{-4} radiation length (RL) that is better than for gas chambers;
6) very high granularity;
7) fast response (signal integration time ≤ 15 ns);
8) radiation resistance;
9) replaceability;
10) flexibility: possibility to produce curved surfaces;
11) small number of output channels owing to very large scale integrated optoelectronics;
12) low cost.

2.1.General CT structure

The central tracker consists of 3 concentric cylindrical "superlayers" with axis along the beam and radii of 60, 90, 120 cm, respectively (fig.3). CT covers the rapidity range of η = 2 ÷ 1.92 (θ = 17°).Central and outer shells are divided along the axis into four parts and internal shell is divided into two parts with separate readout systems. There are two

possibilities to place readout systems: near the superlayers (fig.3a) or outside the external shell (fig.3b). The lengths of the internal and external superlayers are 2·2 m and 4·2 m, respectively. Inner and outer superlayers contains 6 layers of capillary bundles (2% RL), arranged along XUVXUV directions (X-along the beam, stereo angle between X and V, U is equal to ± 10°). Central superlayer contains 12 layers with the same structure. The thickness of layer is 1 mm. The diameter of capillaries is 100 μm. The capillary bundles in each layer have a square cross section with an area of 1 mm^2. The active packing density makes up 80%.

A peculiar feature of the superlayer is its capability to measure not only the coordinates of the passing particle, but the track vector which significantly simplifies the search for the corresponding track segment in the adjacent superlayer and reconstruction of the event. In order to improve the accuracy of the vector direction two layers are located at a distance of 3 mm.

Thanks to the large attenuation length l ≈ 140 cm and by reading the information from small η end of shells, it is possible to achieve some compensation of attenuation due to tracks being inclined at the remote end (large η end) of the capillaries (fig.4).

The capillary bundles are arranged beforehand in ribbons 1 mm thick, 2 - 5 cm wide which are wound onto a lightweight carbon fiber /epoxy support cylinder, 1 mm thick. Total radiation lengths of CT (the version fig.3b) at normal incidence is equal to 8.6% RL.

According to our preliminary data the diviation of capillaries from parallel alignment, which affects on the resolution, is less than 1/5 diameter of capillary in the capillary bundles. The parallel alignment of bundles should be of the same order. If there is no necessity to obtain the spatial resolution better than a capillary diameter d (the straight-line RMS residual σ_{tr} is not better than the contribution of capillary size to the resolution: d/3 [1]), one can consider the bundle as a homogeneous medium for the passing

particles. In this case it is not necessary to measure the geometrical position of each capillary. The sole demand is the small deviation of capillaries from parallel alignment that must be less than d/3. We measure coordinates of tracks relative to the boundary of the capillary bundle and must make the geodetic alignment of this bundle as a whole. The capillary ribbons in each layer are fixed preliminarily on the thin plastic substrate with thickness about of 0.1 mm. After that these substrates with bundles are wound onto support cylinder. We develop a new high precision method of the measurement of coordinates of the capillary bundle in each layer and positions of these layers with respect to one another (Appendix 1). This method uses the additional capillary arranged perpendicular to the bundles inside each transparent substrate as a spiral with a pitch about of 10 cm (fig.6). Coordinates of a bundle are measured by means of reemission in this bundle of the diffused blue light from the moving meniscus of a liquid column in the additional capillary lighted up by a laser. A position of the column meniscus boundaries inside the additional capillaries is determined with accuracy of ≤ 5 μm by means of interference method. Necessary precisions along ρ-coordinate (≈ 1 mm) can be make sure by mechanical construction. The final geometrical alignment of the whole detector is realized in the beam. Charged particles, recorded without magnetic field, check the mechanical alignment and the fibre coherency. It is possible to measure position of each bundle with accuracy $\rho\varphi \leq 10$ μm.

Light signals from the vacant end of the part of capillary bundles (large η end) can be detected by means, for example, fast vizible light photon counters (VLPC) and used for the 1-st level trigger.

There is a possibility to cover the rapidity range up to $|\eta| = 2.5$ by using planar endcup planes.

2.2.Readout System

The optical signal delay (~1-2 μs), necessary for the 1st level trigger decision, is realized by the gated optcelectronic

delay with image intensifier II [12,13]. Photoelectrons drift in longitudinal magnetic field produced in our case by Solénoidal magnet itself. For the delay prototype [12] the resolution was obtained to be 40 lp/mm. The dead time of this delay equals 40 ns per selected event. The information reads out by a CCD.

The length of the optoelectronic system is 80 cm, photocathode diameter is 7 cm, total diameter is 8 cm, total thickness of 2-2.5% RL. The delay tubes are arranged in such a way that particle will penetrate < 1 tube. The optoelectronic delays with IIs consist of glass tubes with photocathodes, phosphors and metal grids without any electronics. This system can be reliable and placed inside the detector volume.

At the II output the image is demagnified 6.7 times in each (ρ and φ) direction by conventional taper so that the size of the image of the capillary becomes equal to the CCD pixel size (15μm).The capillary bundles are coupled to optoelectronic systems by means of image guides ≈ 0.2-0.8 m long (fig.3) with light attenuation of 20-50%, respectively. The technology of manufacture of these tapers and image guides work up good enough. The small fiber diameter (≈ 6 μm for tapers on the CCD surface and ≤ 30 μm for image guides) and high precision of the geometrical alignment practically don't give contributions to the spatial resolution.

There is a possibility to place the CCD readout system outside the detector volume and transmit the light signals by means of image guides (non-scintillating fibers) 3 - 8 m long. After the II light attenuation in these guides (≤ 10) is not important.

Light signals amplified by the II make up of 10^4 electrons per CCD pixel, therefore the signals from passing charged particle through a CCD (≈ 10^2 electrons/pixel) and the CCD noise (≈ 10^2 electrons/pixel) lie below a threshold.

The CCD readout (fig.5. has a number of important advantages. In order to realize these advantages it is necessary to have the optoelectronic delay and a high rejection capability of the 1st level trigger so as to have $f_1 \leq 10^5$ Hz event rate at the CCD input. (At the event rate of 10^8 Hz the rejection

capability is 10^3).

The main disadvantage of CCD - large readout time - is removed by using the optoelectronic delay and only the part of CCD matrix per one event. It means that we can have 2-nd and even 3-rd trigger level data buffering immediately on CCD.

In the case of $1/f_1 \leq t_2$ (fig.5) the image is shifted and buffered for the 2nd level trigger in the memory zone of a CCD. At the worst, when the 1st trigger rejection capability is 10^3 and the event rate high enough $f_1 = 10^5$ Hz, at the shifting time of each event of 2 μs (transfer frequency 20 MHz) the dead time is equal to 18%. The sizes of the image zone used for a record of events (the number of rows equals 40) determine the total number of CCDs (1548). It is possible to reduce this dead time up to 4% if one diminishes the number of rows by a factor of 5 and increases the number of CCDs by the same factor respectively. For high rate of transfer the CCD electrodes should be made of Al, and the CCD should be illuminated from the backside of the substrate.

For the second level trigger decision time of 10-50 μs it is necessary to have the buffer in the image zone about 10 events. There is a possibility to read out the event during ≈ 25 μs (the CCD readout frequency 160 MHz, eight parallel output registers [14]) to use it in the third level trigger or to make the event buffering during the decision time of the third level trigger. At the rate of events passing level 2 trigger $f_2 = 10^3$ Hz the dead time equals 2.5%. At the worst $f_1 = 10^5$ Hz and $f_2 = 10^3$ Hz the total dead time of the readout system equals ≈ 30% or 5% at the total number of CCDs of about 1550 or 7750, respectively. At the rates $f_1 = 10^4$ Hz and $f_2 = 100$ Hz the total dead time determined by the shifting time of each event (2%) equals 2.3% at the number of CCDs of 1550.

To reduce the dead time or to relax the demands on the readout frequency of CCDs we are considering a possibility of compressing the track image in the direction perpendicular to the beam (ρ-direction) while transmitting the image into the memory zone by summing adjacent rows. Each layer divided into

several sublayers, where all pulse heights are summed up and assigned to the middle of each sublayer. The centres of gravity of obtained distributions weighted by their total pulse height are straight line fitted. As it follows from the calculations, that at reasonable number of segments (≈3-5) such compression (3.5-2) does not significantly worsen the angular and spatial accurasies(~ 20-50%).

The number of capillary bundles, optoelectronic systems and CCDs is shown in Table 1. The number of output channels (≈12400) is less then for other central trackers by many orders of magnitude. If we use additional planar superlayers in (ρ,φ)-plane (six disk arrays) to cover the rapidity range up to $|\eta| = 2.5$ the number of output channels is increased by 30%.

This gated optoelectronic readout can also be used for scintillating plastic fiber detector, suggested in the Letter of Intent by the SDC.

2,3. CT performance

The estimations of CT main parameters are summarized in Table 2. All calculation are based on parameters of capillaries that we have just now. These results are preliminary and the further development is needed.

Amount of Capillary Bundles
and Readout Channels Table 1.

Super-layer	Length m	Read-Out Section cm^2	Bundle length km	Delay tubes No.	CCDs No.	Output channels No.
Outer	4·2.0	1810	362	47	564	4512
Center	4·1.5	2710	407	70	840	6720
Inner	2·2.0	450	90	12	144	1152
Total	-	3970	859	129	1548	12384

Hit density on the track was estimated from the results $n_0 \approx 10/mm$ obtained for glass with $n_{gl} = 1.49$. The bundles of capillaries with $n_{gl} = 1.44$ are being manufactured at present. For the capillary bundles with a LS ($n_{ls} = 1.617$) we shall have $n_0 \approx 14/mm$, with an account of light attenuation in the light guide - $n_0 \approx 10/mm$. Some compensation of light attenuation is obtained, since the light yield at the remote end of the capillary bundle increases due to the track being inclined (fig.4). A reflecting surface used at the remote end of the bundle will also allow to increase the light yield. The expected hit density is 4-18/mm.

The coordinate and momentum resolution are presented in Table 2. The spatial resolution of one superlayer is $\sigma_{xy} \approx$ 4-7 μm, $\sigma_z \approx$ 30-50 μm, two-track resolution is 100 μm. The momentum resolution calculated for CT itself without any other detectors is $\sigma_{pt}/p_t \approx 30\% p_t$ (TeV/c).

Thanks to a small diameter of capillaries (100 μm) and high hit density the spatial, two-track, and momentum resolutions are much better than that of plastic fibers (750 μm in diameter), suggested in LoI by the SDC.

Time resolution is determined by the decay time of the light emission of the scintillator, spread in the time of signal from different points of the capillary bundles and the time duration of gate at the optoelectronic delay. The time resolution of the detector will be ≈15 ns; occupancy ≤ 1% at 10^{34} $cm^{-2}s^{-1}$ luminosity .

Operation of this CT at high luminosity (10^{34} $cm^{-2}s^{-1}$) is quite possible owing to high granularity, small occupancy and high spatial resolution. At the luminosity 10^{34} $cm^{-2}s^{-1}$ the flux on one capillary will make up 0.013 charged particle/bunch crossing for inner superlayer (R = 60 cm).

The density of charged particles in the centre of a 1 TeV jet will be ≈ 10/cm^2 at the distance R = 10 cm [15]. It seems possible to reconstruct all the tracks of energetic charged particles in jets with large P_t. Monte Carlo studies of the CT track performances are under way now.

Table 2

Item	Design performance	
	Proposal	SDC (LoI)
Fiber diameter	100 μm	750 μm
Outer radius	1200 mm	1600 mm
Magnetic field	2.0 T	2.0 T
Total number of elements	$0.5 \cdot 10^6$ bundles	$1 \cdot 10^6$ fibers
Number of superlayers	3	4
Number of layers in 1 superlayer	6 (12)	8 (16)
Approx. occupancy per element	10^{-3}	10^{-2}
Total radiation length at normal incidence	~8.6% *)	6.7 %
Number of channels	12400	1,000,000
Reconstruction object in superlayer	3-dimensional vector	X - vector U,V - hits
Time resolution	≈ 15 ns	
No. hits/track	≈ 150-250	
No. hits/mm	6 - 12	≈1.2
σ_{pt}/p_t (fibers only)	$30\% \cdot p_t$ (TeV/c)	$100\% \cdot p_t$(TeV/c)
σ_{xy}/hit	40 μm	
σ_{xy}/superlayer	5 - 7 μm	55 μm/measur.
σ_z /superlayer	30-50 μm	
σ_{xy} (vertex)/track	10 μm	
σ_z (vertex)/track	100 μm	
σ_φ /track	0.015 mrad	
σ_θ /track	0.10 mrad	
Two-track resolution	~100 μm	1000 μm

*)- for the arrangement of fig.3b. For fig.3a the optoelectronic system give an average 0.4% RL in addition.

Radiation doses were estimated. For the inner shell radiation dose is equal to 0.2 - 0.5 Mrad at the luminosity of 10^{34} $cm^{-2}s^{-1}$. Radiation resistance of the capillary detector is better than 10 Mrad. At present there are CCDs with the radiation resistance of several Mrad [16]. Therefore CCDs can place inside or outside the detector volume.

There is possibility to use a hybrid of this detector and the scintillating fiber detector, suggested in LoI by the SDC (like a hybrid of straw tubes and the fiber detector). Such a hybrid detector permits to reduce the number of scintillating fibers using them mainly for the first level trigger and have smaller number of output channels at higher spatial and momentum resolution.

3. COST ESTIMATION

Cost Estimation of CT (Thousands of roubles) Table 3

Liquid Scintillator	900
Capillary bundles	3000
Optoelectronic delay	7000
CCD	1500
Electronics for CCD	500
Facility	500
Total	13,300

Include Research & Development

4. OTHER APPLICATIONS OF LS-IN-CAPILLARIES

1. Vertex detector;
2. Intermediate Angle Tracker;
3. Image preconverter;
4. φ-tracker.

5. R&D PROGRAM AND ITS MILESTONES

The goal of the R&D program is creation and studying the prototypes of the tracking detector.

The R&D program milestones are as follows:

1. Investigation of LS (solvents and dyes) with high efficiency and long attenuation length. 06.1991
2. Development of glass capillaries and capillary bundles with low refractive index. 10.1991
3. Creation and studying of optoelectronic delay tubes. 11.1991
4. Development of high resolution image intensifier systems. 12.1991
5. Development of CCD readout technique with fast clear, data compression and data buffering on CCD. 12.1991
6. Electronics. 01.1992
7. Creation prototype of tracking detector. 02.1992
8. Studying of the prototype of CT in test beam. 03.1992
9. Simulation to optimize the design of CT. 12.1991

REFERENCES

1. N.S. Bamburov et al.. Nucl. Instr. and Meth. A289, 265 (1990)
2. A.G. Denisov et al.. IHEP preprint 90-96, Protvino, 1990.
3. S.V. Golovkin et al.. IHEP preprint 90-105, Protvino, 1990.
4. A. Artamonov et al.. CERN-EP/90-58.
5. R. Ruchti et el., IEEE Trans. Nucl. Sci.. NS-36, 146(1989).
6. N.I.Bozhko et al., IHEP preprint 91-45, Protvino, 1991.
7. M.Adinolfi et al., CERN-PPE/91-66.
8. S. Majevski et al., CERN 89-10, V.1, 239 (1989).
9. C. Roda, CERN/EF/Instr. 89-1.
10. C. Angelini et al.. CERN-EP/89-112.
11. C. D'Ambrosio et al.,CERN 89-10, V.1, 261 (1989).
12. T. Gys et al., CERN 89-10, V.1, p 255.
13. T. Gys et al., CERN/LAA-SF91-3.
14. Laser Focus World, July 1991, p. 188.
15. Report of the Task Force on Detector R&D for the Superconducting Super Collider. SSC-SR-1021 (1986).
16. C.P. Chang. IEEE Trans., NS-25,1454 (1978).

Figure Captions

Fig.1. Light attenuation of the bundle of capillaries 25 μm in diameter (a) and 100 μm in diameter (b) for solution 1MN + 0.007 mol/l MBMP.

Fig.2. Light attenuation in capillaries of 100 μm in diameter for solution 1MN + 0.007 mol/l MBMP at different radiation doses (preliminary results).

Fig.3. Design of the central tracker.

Fig.4. Light yield of CT.

Fig.5. CCD readout.

Fig.6. Method of the geodetic alignment of bundles.

APPENDIX 1

We develop a new high precision method of the measurement of coordinates of the capillary bundle in each layer and positions of these layers with respect to one another.

This method uses the additional capillary arranged perpendicular to the bundles inside each transparent substrate as a spiral with a pitch about of 10 cm (fig.6). A moving liquid column (with high refractive index, for example undope 1MN) in the additional capillary is lighted up by a laser along the capillary. The blue light from laser is diffused from a meniscus of a column and reemited in the neighbouring bundle in a liquid scintillator with a green dye. A position of the bundle with respect to the meniscus is determined with accuracy of $\leqslant$ 10 μm by means of the measurement of the amplitude distribution of the light picture on the output of the bundle. A position of the meniscus along the additional capillary is determined with accuracy of $\leqslant$5 μm by means of interference between back reflected light from the meniscus and part of input light from a laser.

For only one bundle in each layer on a substrate the geodetic alignment has to be performed. With respect to this bundle one can find the initial position of a meniscus in each turn of a liquid column in the spiral capillary.

Due to this capillary being placed in the transparent substrate and the meniscus of the liquid column could illuminate two layers, it is possible to measure positions of these layers with respect to one another (with accuracy of $\leqslant$ 20 μm). It is possible to determine more exactly a coordinate of the additional capillary in the direction perpendicular to this capillary (with accuracy of $\leqslant$ 50 μm).

The length of the additional capillary for the layer of the outer shell is about of 150 m. For the empty quartz capillary with polymeric cover the attenuation length is large enough to use such capillaries.

This method can be used for the geodetic alignment of the scintillating fiber detector suggested in the LoI.

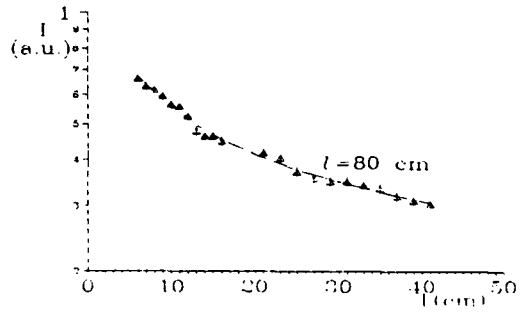


Fig.1a

951

952

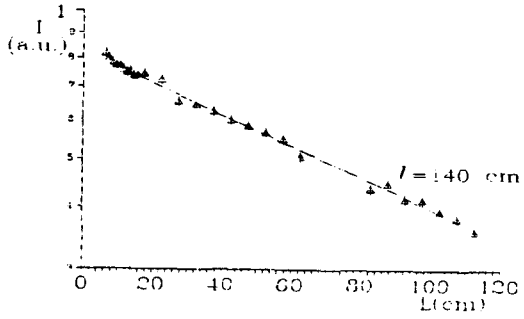


Fig 1b

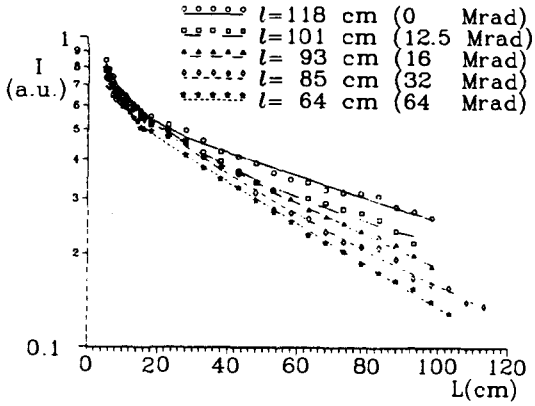


Fig.2.

953

954

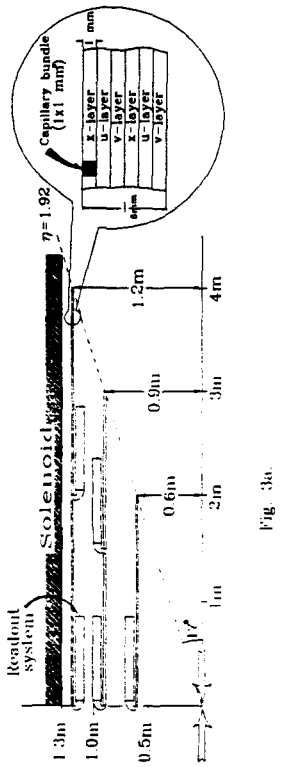


Fig. 3a.

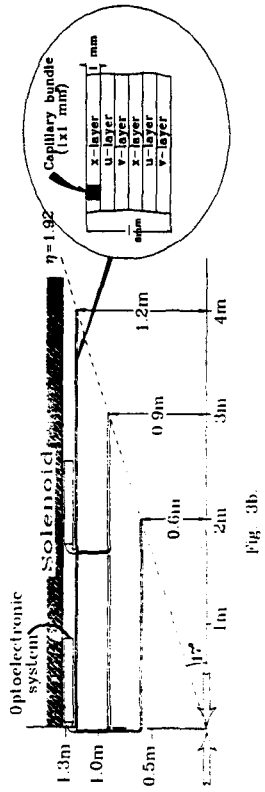


Fig. 3b.

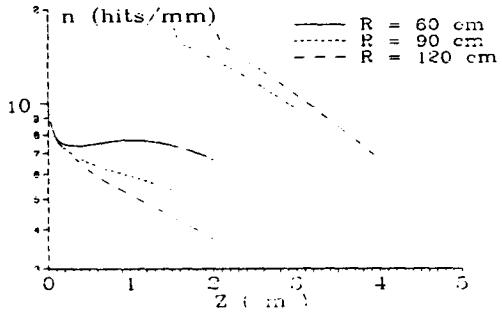


Fig.4

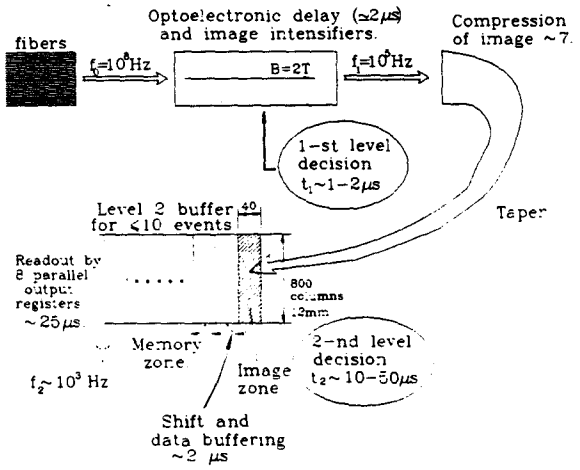
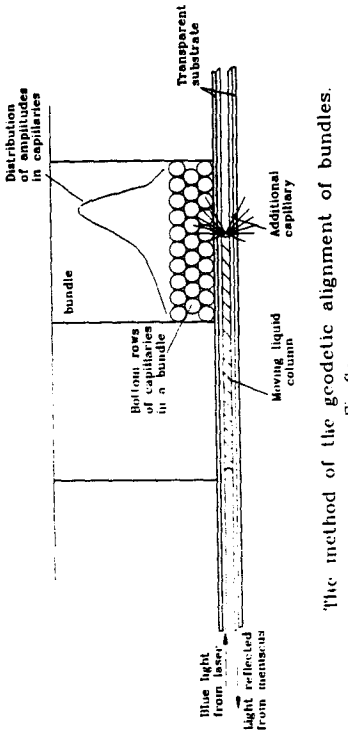


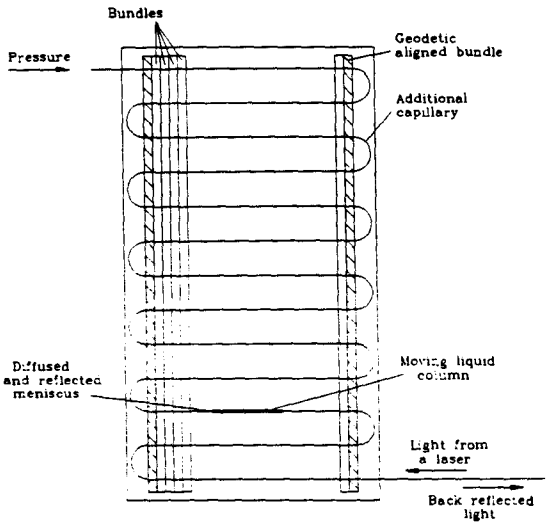
Fig 5 CCD Readout.

f_1, f_2 – the rate of events passing level 1,2 trigger

t_1, t_2 – decision time of level 1,2 trigger

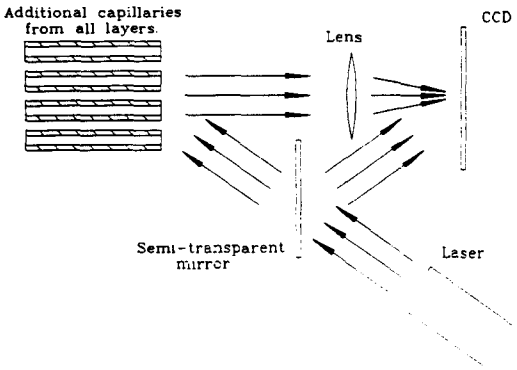


The method of the geodetic alignment of bundles.
Fig 6a



Unwind layer on the substrate

Fig 6b



Setup for measuring of
interference picture

Fig 6c

Tracking System Design Requirements

W. Ford(Colorado)

Outline of SDC Tracking Design Requirements

1. Introduction (brief)
[Purpose of this document]

2. Overview
[This section should summarize the conclusions of those that follow.]
2.1 Brief survey of physics performance considerations
2.2 Environment for the tracking system within the SDC detector
2.3 Summary of requirements; parameter tables
Angular coverage and hermiticity
p_perp resolution
phi resolution
theta resolution
impact parameter resolution
precision of pointing to the calorimeter
resolution for muon tracking
time resolution, pileup, occupancy
pattern recognition efficiency and false rate
trigger functionality
material

[The following sections should look at physics and other issues, draw conclusions about performance requirements, and justify them.]

3. Isolated charged tracks
3.1 Physics processes
3.1.1 H->4l
3.1.2 t->l+X ; 3.1.3 $Z' \to l^+l^-$
3.2 Electrons
3.2.1 Tracker material
3.2.2 Calorimeter calibration
3.3 Muons
3.4 Isolation criteria
3.4.1 b->l+X
3.4.2 c->l+X

4. Jets
4.1 Multiplicity
4.2 Shape parameters, QCD
4.3 Isolation

5. Detached vertices
5.1 Heavy quarks
5.2 Taus

6. Trigger
6.1 Level 1
6.2 Level 2

7. Problems specific to intermediate angle region
7.1 Momentum measurement
7.2 Trigger

8. Operation at greater than design luminosity

9. Practical considerations
9.1 Radiation hardness
9.2 Calibration
9.3 Computational resource usage
9.4 Access requirements
9.5 Safety
9.6 Failure modes and their management
9.7 Cost

Requirements for Tracking

(1) $|\eta|$ coverage out to $|\eta| \leq 2.5$, implying $H^0 \to 4$ charged lepton geometrical efficiency $\gtrsim 60\%$ for $m_H \geq 200$ GeV.

(2) Reconstruction efficiency $\geq 90\%$ (for $|\eta| < 2.5$) for $H^0 \to 4$ charged leptons, for each lepton having $P_\perp \geq 5$ GeV, at design luminosity, but assuming twice the occupancy calculated by GEANT (exclusive of lepton identification and trigger cuts).

(3) Reconstruction efficiency for same as in (2) $\geq 75\%$ at 4×10^{33} design luminosity.

(4) Reconstructed (as opposed to parametric) vertex constrained momentum resolution of $\sigma_{P_\perp/P_\perp^2} < 25\%$ (TeV^{-1}) for $|\eta| \leq 2$ (leaves room still for a contribution from misalignments) for $H^0 \to 4$ charged leptons.

(5) Efficiency contribution from lepton identification of $\geq 85\%$ for electrons with $P_\perp \geq 10$ GeV and $\geq 95\%$ for muons with $P_\perp \geq 10$ GeV.

(6) Position resolution at the calorimeter of ≤ 2.5 mm in $r-\phi$ or z (want error $\lesssim \sigma/2$ of calorimeter position accuracy).

(7) No special position resolution requirements at the muon system. Achievable numbers ≤ 1 cm.

(8) B single tagging efficiency $\geq 30\%$ for 125 GeV $\leq m_{top} \leq$ 250 GeV.

(8') τ tagging

(9) First level trigger with momentum resolution $\sigma_{P_\perp/P_\perp^2} \leq 10$ (TeV^{-1}) – implies a 10% error for a 10 GeV lepton.

(10) Second-level trigger with momentum resolution $\sigma_{P_\perp/P_\perp^2} = 2.5$ (TeV^{-1}). Gives a 10% error for a 40 GeV lepton for triggering on $Z \to e^+e^-$, $W \to e\nu$ – needed for calorimeter calibration.

(11) Discovery potential – hard to quantify. In general want maximum capabilities from detector. Based on history highest priority (other than isolated lepton of Higgs case above) would be reconstruction and impact parameter measurement of leptons within jets up to the largest jet $P_\perp$ possible (at least ≥ 500 GeV). Desired reconstruction efficiency $\geq 50\%$.

(12) Measurement of jet fragmentation at modest luminosity for QCD studies and for modelling backgrounds from jets.

(13) Survivability at standard $\mathcal{L}$ for ≥ 10 years.

(14) Allows a natural path for upgrading to a system with survivability of ≥ 10 years at $10\times$ standard $\mathcal{L}$ with emphasis (e.g. momentum resolution, pattern recognition, isolated track efficiency) to be decided based on what is learned during initial running.

Outline of SDC Tracking Design Requirements

1. Introduction (brief)
[Purpose of this document]

2. Overview
[This section should summarize the conclusions of those that follow.]
2.1 Brief survey of physics performance considerations
2.2 Environment for the tracking system within the SDC detector
2.3 Summary of requirements; parameter tables
Angular coverage and hermiticity
p_perp resolution
phi resolution
theta resolution
impact parameter resolution
precision of pointing to the calorimeter
resolution for muon tracking
time resolution, pileup, occupancy
pattern recognition efficiency and false rate
trigger functionality
material

[The following sections should look at physics and other issues, draw conclusions about performance requirements, and justify them.]

3. Isolated charged tracks
3.1 Physics processes
3.1.1 H->4l
3.1.2 t->l+X ; 3.1.3 $Z' \to l^+l^-$
3.2 Electrons
3.2.1 Tracker material
3.2.2 Calorimeter calibration
3.3 Muons
3.4 Isolation criteria
3.4.1 b->l+X
3.4.2 c->l+X

4. Jets
4.1 Multiplicity
4.2 Shape parameters, QCD
4.3 Isolation

5. Detached vertices
5.1 Heavy quarks
5.2 Taus

6. Trigger
6.1 Level 1
6.2 Level 2

7. Problems specific to intermediate angle region
7.1 Momentum measurement
7.2 Trigger

8. Operation at greater than design luminosity

9. Practical considerations
9.1 Radiation hardness
9.2 Calibration
9.3 Computational resource usage
9.4 Access requirements
9.5 Safety
9.6 Failure modes and their management
9.7 Cost

965

Efficiency sensitive to acceptance, esp. for smaller masses (because 4 tracks)
Einsweiler says $\varepsilon(\eta<1.5) \sim \varepsilon(\eta<2.5)/(2\text{-}2.5)$

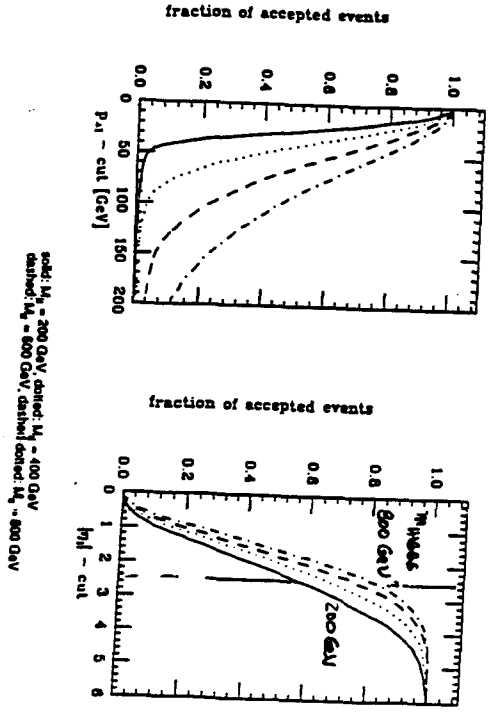
$p_\perp$ min for trigger ~ 10–15 GeV

LoI assumed 85% efficiency for e, μ tracking within the acceptance
" " $\sigma(p_\perp)/p_\perp \simeq .25$ @ 1 TeV (see figure)

Lepton isolation ($E_\perp < 5$ GeV) in $\sqrt{|\Delta\alpha|^2+|\Delta\eta|^2} < .3$
Note: outer barrel projective, ⇒ jet occupies $\Delta\Omega \simeq .6$.
⇒ Want to be able to do pattern recognition in or near jets. ($\Delta\Omega_j$ may be small).

→ $\varepsilon(H\to 4l) > 85\%$ (⇒ $|\eta| < 2.5$)
→ $\sigma(p_\perp)/p_\perp < \begin{cases} .2 & @\ 1\ TeV,\ |\eta|<1.6 \\ <1 & "\ ,\ |\eta|>1.6 \end{cases}$
→ $p_\perp$ threshold for trigger $\gtrsim$ 10 GeV

966



967

Conclusions (Einsweiler)

1) multi-lepton final states:
- removing both e + μ coverage between 1.5 and 2.5 gives:
- Factor 2–2.5 reduction in acceptance for:

$H\to ZZ^*$
$H\to ZZ$
$W+H \hookrightarrow \gamma\gamma$
$t\bar{t}+H \hookrightarrow \gamma\gamma$

Note: this is not $(.6)^4 \sim \frac{1}{8}$

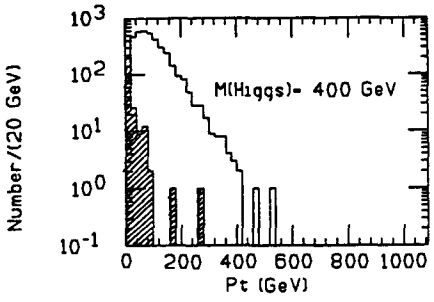
- signal and backgrounds scale

2) Z' asymmetry
- factor ~2 reduction in acceptance
- similar reduction in observed asymmetry
⇒ measurement for 1 TeV Z' seriously compromised

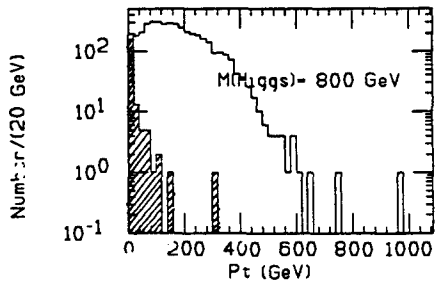
) effect for μ alone ~ ½ ...

51

968



8.2 The P_T distribution of electrons in Higgs events for $M_H = 400$ GeV. The hatched bins indicate the contribution from non-Z sources in Higgs events.

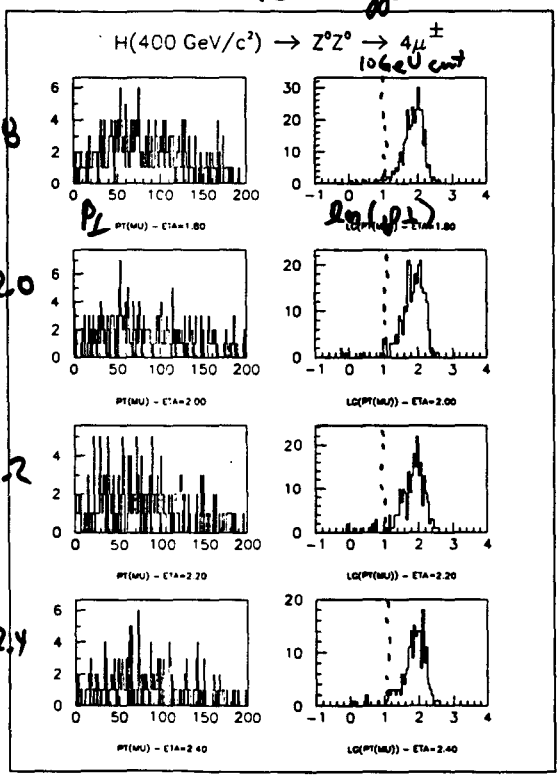


8.3 Same as 8.2 but for $M_H = 800$ GeV.

Cahn, et al.

400 GeV Higgs:

969



Trost

970

3. Isolated charged tracks
3.1 Physics processes
3.1.2 t->l+X

Measure t mass from:

$t\bar{t} \rightarrow$ iso e iso μ X

$t\bar{t} \rightarrow W^+ b\, W^- \bar{b} \rightarrow l + 4\,\text{jets} + \not{E}_T$

- tag 2 jets as b by large track impact parameters
- reconstruct W from 2 non-b jets
- " t from W + b jet

$t\bar{t} \rightarrow$ iso e non-iso μ

from $t \rightarrow W^+ b X$

$\mu^- X$

$e^+ X$

(μ at edge of a jet; could one do electron ID near jets with precise track-shower match?)

→ ε (b tag) ≳ 50% for $t \rightarrow W b$ events

→ ε ($\tau \rightarrow 3\pi$ jet detection) ≳ ?

971

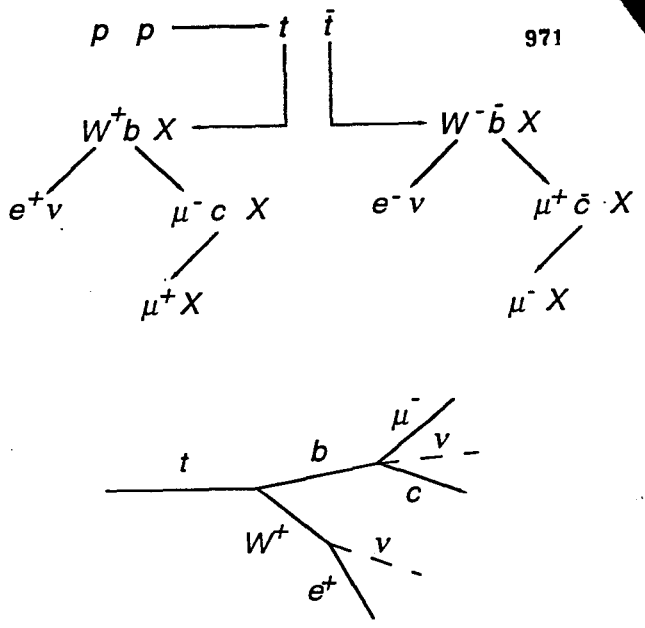
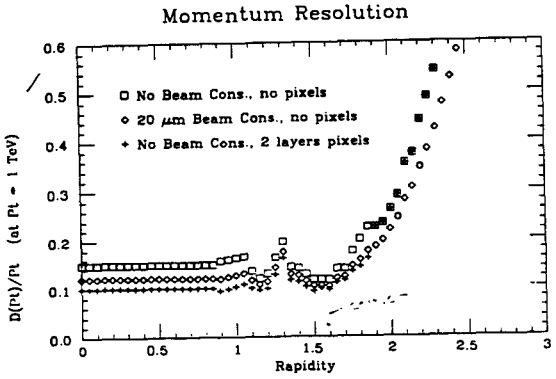


Figure 3) Schematic of top production and decay into leptons.

972



Descoped SOC detector (wires)

22 $W \to$ jet jet

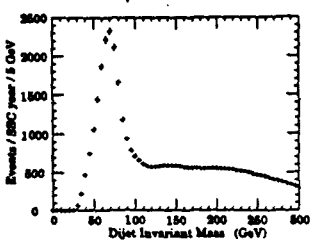


FIG. 33. The dijet invariant mass distribution for all combinations of two jets in $t\bar{t}$ events, where the dijet system was required to have $p_t > 180$ GeV/c. The events have an electron with $p_t > 40$ GeV, missing-$E_t > 30$ GeV, 4 jets with $p_t > 30$ GeV, and at least two tagged b quark jets. The tagged b jets are excluded when forming the dijet combinations.

$t \to W$ jet

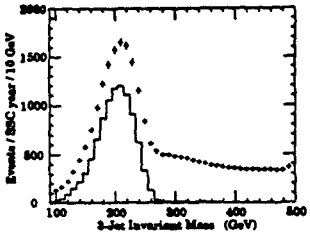


FIG. 34. The three-jet invariant mass distribution for all events with a W candidate having dijet invariant mass between 80 GeV and 96 GeV with $p_t > 180$ GeV/c, where we have only considered the three-jet systems formed from each of the tagged b jets and the W candidate. The solid curve shows only the correct combination of the W and b jets.

two from the W decay and one each from the b and $\bar{b}$ quarks. We therefore require the events to have at least four jets with $E_t > 30$ GeV and $|\eta| < 2.0$. This initial selection results in 546,000 events per SSC year for the e + *jets* final state, assuming the ISAJET $t\bar{t}$ cross section of 1.54 nb.

The primary background to this channel arises from QCD production of W bosons with associated *jets*. We reduce this background by requiring that at least two of the jets satisfying the kinematic cuts are tagged as b quark candidates using the presence of large impact-parameter tracks in the transverse plane as discussed in Ref. 61. This cut retains ~ 10% of the signal events, and leaves an estimated background from W + *jets* production that is less than 0.1% of the signal. We then take all pair combinations of the jets in the event which do not contain b quark candidates and form dijet systems from them.

The resulting invariant mass spectrum for these dijet combinations is shown in Fig. 33, where we have added the requirement that the p_t of the resulting dijet system be greater than 180 GeV/c to reduce the combinatorial background. One sees a clear W signal above a relatively small background. In this plot, there are 9500 signal events per SSC year above a combinatorial background that is less than half of the signal in the dijet invariant mass region between 80 and 96 GeV. The hard-p_t cut on the dijet system retains approximately 37% of the correctly reconstructed signal events and reduces the combinatorial background by a factor of 8.

The W mass determination depends on effects resulting from the jet clustering (loss of energy out of the cone or below the calorimeter tower threshold), and from overlap of parton showers with each other and with the underlying event. We have employed a relatively small cone size in this analysis ($R = 0.4$) to optimize the reconstruction efficiency of the two jets arising from the W decay. We have also performed the analysis using cone sizes up to $R = 0.8$ and have found that the reconstruction efficiency falls with increasing cone size with very modest improvements in the W mass resolution. We have also considered the effect of more stringent cuts on the jets (*e.g.* raising the jet E_t thresholds or reducing the η interval) and have found that they provide relatively modest improvements in the overall signal-to-noise and mass resolution with considerable reductions in signal rate.

We define a W candidate to be any dijet combination (excluding tagged b jets) that has an invariant mass between 50 and 95 GeV and $p_t > 180$ GeV/c. We pair these W candidates with each of the tagged b jets to form the three-jet invariant mass distribution shown in Fig. 34. An impressive top signal is seen above a combinatorial background that is relatively flat and slowly changing under the signal peak.

$t \to H^+ b$

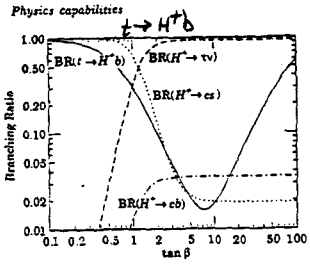


FIG. 27. Branching fractions for the reactions $t \to H^+ b$ (solid) and $H^- \to \tau\nu$, $c\bar{s}$, $c\bar{b}$ as a function of $\tan\beta$[66]. We have assumed $M_{top} = 250$ GeV and $M_{H^-} = 150$ GeV.

by requiring two tagged b-jets (from the decay of the t and $\bar{t}$) each with $p_t > 30$ GeV/c and $|\eta| < 2.0$. We used ISAJET version 6.31 to generate the $t\bar{t}$ events. The background from non-$t\bar{t}$ events is negligible.

In Method (i) we search for $t\tau$ events (*e.g.*, $t \to b\bar{b}W^+ \to b\bar{b}\ell^+\nu$, $\bar{t} \to \bar{b}H^-$ or $\bar{b}W^-$ $\to \bar{b}\tau^-\nu$) in which the τ decays to a single $\pi^\pm$ (or $K^\pm$) with $p_t > p_t^{cut}$ where $p_t^{cut} = 40$ GeV/c. The τ signature is an isolated charged hadron, where isolation for a hadron is defined in analogy with the lepton definition above. Note that this requires a good momentum measurement for the charged hadron. If t quarks only decay to W^+b, the observed number of t^-t^- events plus lepton universality in W decays allows us to compute the number of $t\tau$ events expected. If instead top quarks can also decay to H^-b, and if $BR(H^- \to \tau\nu)$ is not small, we would detect an excess of $t\tau$ events over the universality prediction.

The statistical significance of the excess in the observed number of isolated pions over the prediction from universality is given in Fig. 28. It is important to include the polarization of the τ's in Monte Carlo studies; ignoring this polarization reduces the number of standard deviations by a factor of two. After one year of SSC running, we could detect five standard deviation signals for $t \to H^-b$, $H^- \to \tau^-\nu$ for all $\tan\beta > 0.5$.

For smaller values of $\tan\beta$, where $BR(H^- \to \tau\nu)$ becomes small, we must employ the $H^- \to c\bar{s}$ decay mode (Method (ii)). For this purpose, we have extended the technique described in Ref. 66 to study

significance of observation 35

$t \to H^+ b$ branching fraction

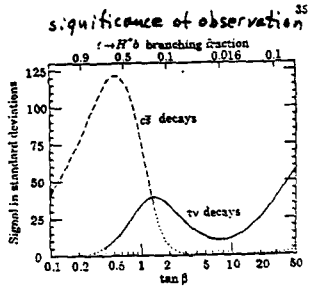


FIG. 28. The solid curve shows the statistical significance of the excess of isolated pions due to $t \to H^-b$, $H^- \to \tau\nu$, and $\tau \to \pi\nu$ relative to expectations for $t \to W^-b$ (assuming lepton universality) as a function of $\tan\beta$ (bottom labels). We require an isolated lepton with $p_t > 40$ GeV/c and an isolated pion with $p_t > 40$ GeV/c (for $p_t > 100$ GeV/c there are $\frac{1}{3}$ as many standard deviations). The dashed curve shows the statistical significance of the H^- peak in the two-non-b-jet invariant mass distribution as a function of $\tan\beta$. We assume one SSC year of running and have taken $M_{top} = 250$ GeV and $M_{H^-} = 150$ GeV. For $\tan\beta$ values where the curves become dotted, the given technique has become marginal for H^- discovery. The upper labels give the $t \to H^-b$ branching ratio, which reaches a minimum at $\tan\beta \approx 8$, see Fig. 27.

a 250 GeV top quark decaying to H^- (or W^-) with $H^-(W^-) \to u\bar{d}$ or $c\bar{s}$ (with the same lepton trigger as for Method (i)). Jets are formed by clustering final-state particles appearing in the region $|\eta| < 3.0$ within a cone of radius $R < 0.7$. The 4-momenta of these jets are then smeared with the assumed jet resolution of the SDC calorimeter.

Any two jets (excluding the tagged b jets) within $|\eta| < 2.5$ and $p_t > 20$ GeV are then used to form invariant mass combinations. The combinatorial background can be reduced by restricting the dijet invariant mass plot to the two (non-b) jets with the highest transverse momenta that in combination with either one of the tagged b jets yield a three-jet invariant mass smaller than 400 GeV. This requirement is consistent with the top quark mass of 250 GeV already measured by the methods described above. The combinatorial background is seveeely reduced

26 $t \to H^+ b$ (↳ $c\bar{s}$), $t \to W b$ (↳ jj)

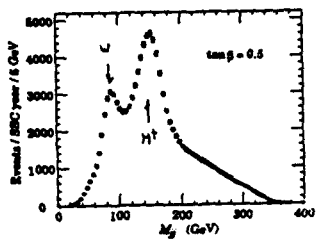


FIG. 29. Two-jet mass distribution, for the sum of the $t\bar{t} \to WWb\bar{b}$ and $t\bar{t} \to WH\bar{b}\bar{b}$ events in the case $\tan\beta = 0.5$. Only one two-jet combination per event is plotted: the combination with the two highest p_t non-b jets consistent with the t mass (see text).

by only plotting one combination per event, and this choice is usually the correct one. The resulting W^+ and H^+ peaks for $\tan\beta = 0.5$ are shown in Fig. 29.

To quantify the statistical significance of the H^+ mass peak, we again plot the number of standard deviations above background as a function of $\tan\beta$ in Fig. 28. The combinatorial background can arise from either $t\bar{t} \to WWb\bar{b}$ or $WH\bar{b}\bar{b}$. These two sources look very similar, so we can scale the combinatorial background to fit the observed data. The signal is the number of events above this scaled background in the H^- or W^+ peak. The highest $\tan\beta$ value for which we could discover the charged Higgs by this method depends critically on understanding the shape of the combinatorial background. We conservatively argue that Method (ii) is useful only for $\tan\beta < 1.5$. For $\tan\beta > 1.5$ the H^+ peak is much less distinct, though the W peak remains visible. For $\tan\beta < 0.2$, where there are very few WW decays, the W mass peak is not visible above the background, although the H^- peak may be substantial (with 1,000 or 10,000 events for $\tan\beta = 0.06$ or 0.2 respectively). The lowest value of the branching ratio $t \to H^+b$ for which we are sensitive depends on the $H^+ \to \tau\nu$ branching ratio and the $H^+ \to c\bar{s}$ branching ratio, but is roughly 2%.

Conclusions

We have described three different techniques for discovering the top quark and measuring its mass. The isolated $e\mu$ mode yields a clear signal, but a less reliable mass determination. The lepton + jets and the sequential $e\mu$ modes provide mass measurements dominated by systematic errors, which we estimate to be 3–6 GeV for the two modes for a top mass of 250 GeV and one nominal SSC year of luminosity. As the errors are overwhelmingly systematic, measurements made using a substantially smaller data sample will have only slightly larger errors.

We have also analyzed the decay properties of the top quark. The ratio of the semi-leptonic decay rate to the $q\bar{q}$ rate can be measured with a precision of 2–3%. The specific case of $t \to H^+b$ has also been studied in $t\bar{t}$ events in which the second t decays to W^+b. In the particular case of $M_{top} = 250$ GeV and $M_{H^-} = 150$ GeV, detection of the charged Higgs boson appears possible over the entire interesting range of parameter space ($t \to H^+b$ branching ratios above 2%) using either $H^+ \to \tau\nu$ decays or $H^+ \to c\bar{s}$ decays or both. These studies illustrate the importance of efficiently tagging b-quark jets and measuring charged hadron momenta to identify τ's.

4.4. Jet energy resolution

Demonstrate the jet energy resolution of your proposed detector by studying decays

- $Z \to jet + jet$
- $Z' \to jet + jet$, $M_{Z'} = 1$ TeV

We have studied the dijet invariant mass resolution from Z and Z' decays and the irreducible contributions to the dijet invariant mass resolution from physics-related sources such as clustering, jet fragmentation fluctuations and contributions from underlying events. These effects determine a minimum mass resolution that is independent of detector parameters. In addition, we have studied the effects on the mass resolution induced by the detector, particularly by calorimeter energy resolution.

Detector Independent Effects

The energy and angular resolutions of jets from Z's and Z''s depend on the production process, which determines the distribution of transverse momenta. Furthermore, the dijet mass resolution depends on the Lorentz boost of the Z's and Z''s. At low p_t we form the invariant mass of the two jets, whereas for highly boosted Z's the invariant mass of the coalesced jet provides the best estimate of the mass. At low p_t, jets are broad, with substantial tails of particles escaping from any reasonable

3. Isolated charged tracks
3.2 Electrons
3.2.1 Tracker material

976

electron bremsstrahlung → inefficiency of E_{cal} - p_{track} match for electron ID

γ conversion →
fake high $p_\perp$ track trigger
fake e signature in/near jets from $\pi^+ - \gamma$ overlap

Material at small r hurts more than at large r (except fake high $p_\perp$ trigger)

Task force: electron ID main issue

→ Require $\geq$ 10% X_0 inside 50 cm
$\geq$ 20% X_0 total

→ Track position at EM cal $< \sigma$ (shower centroid)

977

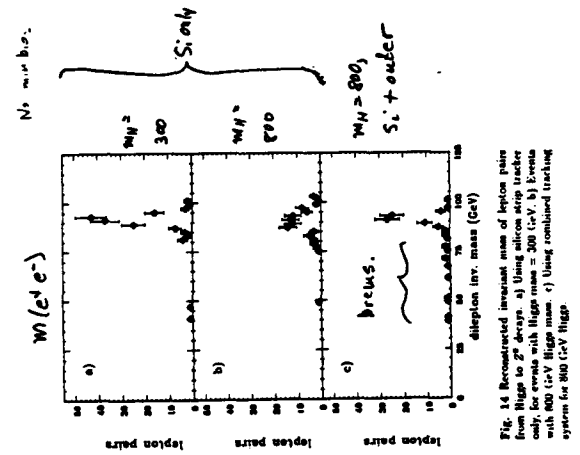


Fig. 14 Reconstructed invariant mass of lepton pairs from Higgs to Z^0 decays. a) Using silicon strip tracker only, for events with Higgs mass = 300 GeV. b) Events with 800 GeV Higgs mass. c) Using combined tracking system for 800 GeV Higgs.

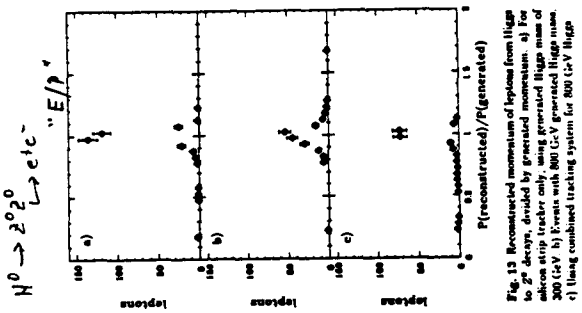


Fig. 13 Reconstructed momentum of leptons from Higgs to Z^0 decays, divided by generated momentum. a) For silicon strip tracker only, using generated Higgs mass of 300 GeV. b) Events with 800 GeV generated Higgs mass. c) Using combined tracking system for 800 GeV Higgs.

25

$H \to Z^0 \to$ 4e efficiency for Si tracker

978

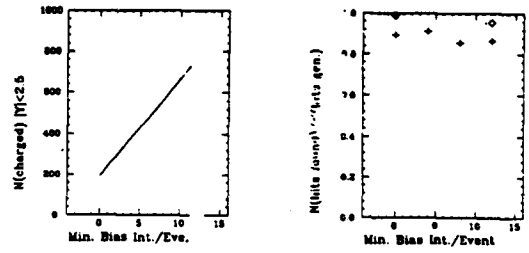


Fig. 15 Number of charged tracks ... event in fiducial regions (rapidity less t... 2.5) as a function of the number of m... mum bias interactions added to the 800 G... Higgs event.

Fig. 16 Fraction of generated track hits found by the tracking algorithm for lepton tracks from 800 GeV Higgs decays, as a function of the minimum bias background. The squares are for the silicon strip tracker alone; the crosses for stripes combined with an outer tracker.

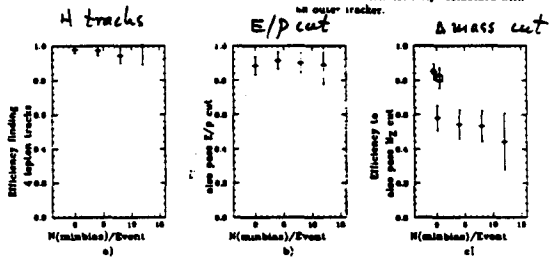


Fig. 17 Efficiency for Higgs to four leptons event reconstruction, as a function of the number of minimum bias interactions added. a) Efficiency for reconstructing all four lepton tracks. b) Efficiency for all four lepton tracks to also pass the E/p cuts. c) Efficiency for the invariant mass of both lepton pairs to also be within 5 GeV of the nominal Z^0 mass. Points plotted as crosses are for Higgs mass of 800 GeV, with the outer tracker used in the analysis. In c) the square is for Higgs to four muons. The diamond is for the case of 300 GeV Higgs, without using the outer tracker in the analysis.

32

3. Isolated charged tracks
3.2 Electrons
3.2.2 Calorimeter calibration

980

$\sigma_E/E\big|_{EMCal} \sim .12/\sqrt{E} \oplus .01$

(i.e., constant ~ .01 for $E \gtrsim 100$ GeV)

Need

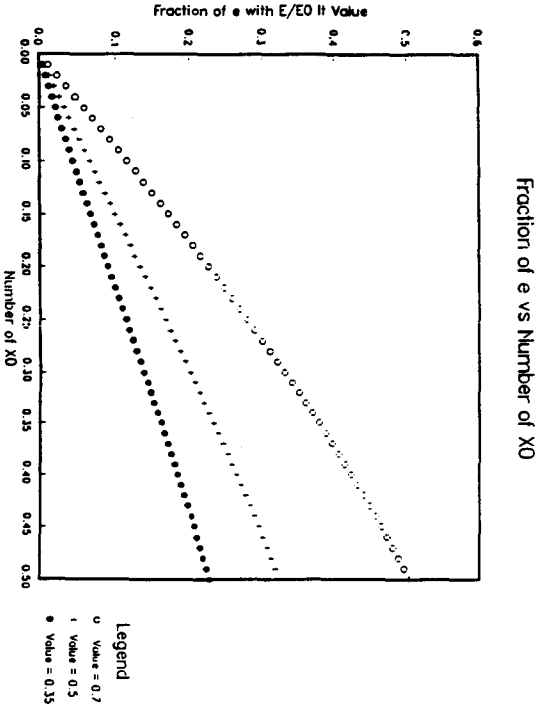
→ iso e with $\sigma_{p_\perp}/p_\perp < .01\sqrt{N_{evt}}$ @ 100 GeV

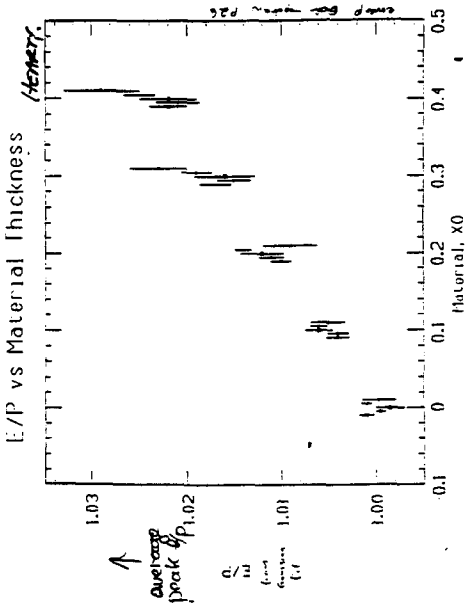
→ e from Z^0

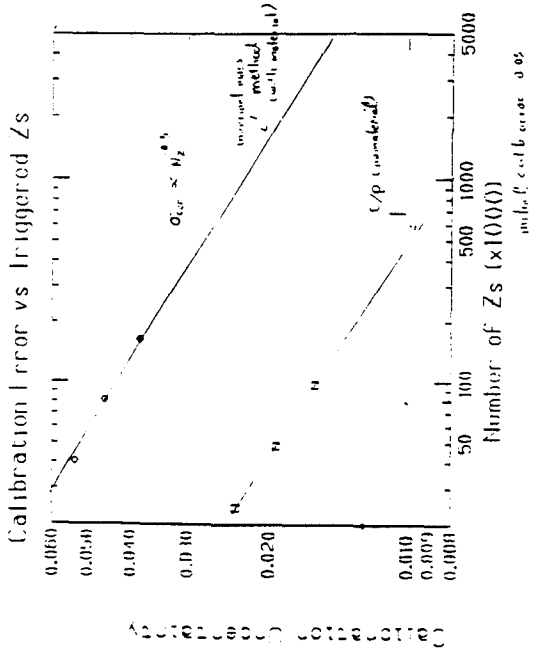
→ for $|\eta| < 2.5$ ($\sigma_{p_\perp}$ worse for $|\eta| > 2.0$)

→ < .2 X_0 material

979







38

39

3. Isolated charged tracks
3.3 Muons

983

Need $p_\perp$ for inner/outer track match
Alignment between inner/outer trackers
for improved $p_\perp$ meas.
z' mass from $\mu\mu$ decay is resolution-limited
z' asymmetry meas. needs large $|\eta|$ coverage
$p_\perp \simeq M_{z'}/2$ large, ⇒ need sign of charge to $p_\perp \sim 2$ TeV
→ $\sigma(p_\perp)/p_\perp \tilde{<} .2$ @ 1 TeV

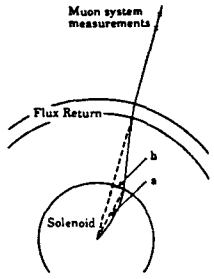


FIG. 12. Illustration of the reason for the improvement of momentum resolution coming from azimuthal measurements in the muon system. Without the muon system measurements, the sagitta is shown by a, whereas with the muon system measurements, the effective sagitta is shown by b. The curvature of a very low momentum track has been used for the purpose of illustration.

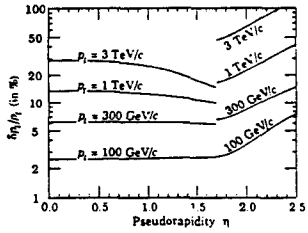


FIG. 13. Muon momentum resolution as a function of pseudorapidity for various values of transverse momentum. A resolution of 0.25 (TeV/c)$^{-1}$ from Table 1 is used to characterize the central tracking performance.

about a factor of 50 less, indicating that the muon system will remain operational at very high luminosities. The momentum resolution obtained with just the muon system and the outer superlayer of the central tracker is shown in Fig. 14.

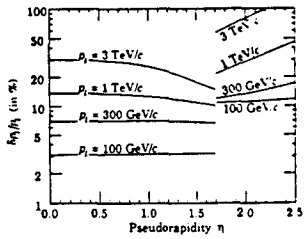


FIG. 14. Muon momentum resolution as a function of pseudorapidity for higher-than-design luminosity. For $|\eta| < 1.7$, it is assumed that the Si system and outer superlayer of the outer tracking system are operational. For $|\eta| > 1.7$, only information from the muon system is used.

Engineering progress

Work is underway on the design of the iron toroids and their assembly in the underground hall. A preliminary design, taking into account manufacturing feasibility in Japan, the United States, and the USSR will be completed and reviewed by March 1991. Detailed assembly scenarios will then be formulated by engineers at the University of Wisconsin /PSL, LBL, RTK, and the SSCL. Work has begun at Fermilab and PSL on chamber support and alignment.

Conceptual engineering design of chambers and trigger counters and their supports will be completed by July 1991. Funds to support the engineering design of the muon system are requested in this LoI.

985

nate the mass resolution for both low- and high-p_t Z and Z' production for the range of calorimeter performance under investigation by the SDC. The physics study of top quark detection through multi-jet mass reconstruction (Section 4.3) confirms this conclusion. For some conditions in which the intrinsic fluctuations are very small (low-p_t Z' for example), extreme e/h deviation from unity produces detectable degradation. We believe that the design goals given in Table 1 represent a reasonable match to the requirements suggested by the analysis described here.

4.5. Z' of mass 4 TeV

Demonstrate the acceptance and resolution (not the ability to run at extremely high luminosities) of the lepton detector by a study of a Z' with a mass of 4 TeV. Show a measurement of the mass and asymmetry for 1000 produced $Z' \to e^+e^-, \mu^+\mu^-, \tau^+\tau^-$ each.

To answer this question we assume that the Z' has the same couplings to quarks and leptons as the standard model Z. Such a Z' has a larger production cross section than the E_6 Z_η discussed in the EoI[69]. In this study we have required that 1000 events be produced in each of the $e^+e^-, \mu^+\mu^-, \tau^+\tau^-$ channels with the invariant mass of the lepton pair in the range $M_{Z'} \pm \Gamma_{Z'}$, where $\Gamma_{Z'}$ is the full width of the Z' (112 GeV in our model). The running time to collect these events at $\mathcal{L} = 10^{33}\,\mathrm{cm}^{-2}\mathrm{s}^{-1}$ would be about 10 years: therefore, such a heavy object can only be explored in detail with higher luminosity running of the SSC. To answer the question as posed, we assume the detector performance expected at the nominal SSC luminosity, as defined in Section 4.1. More details of this analysis can be found in Ref. 72.

The Z' Mass and Width Measurements

Figure 35 shows the invariant mass spectra for e^+e^- and $\mu^+\mu^-$ pairs from the Z' as well as the background from continuum Drell-Yan processes. There are no other relevant backgrounds.* The pseudorapidity coverage of the SDC detector corresponds to a geometrical acceptance of 86% for the the e^+e^- and $\mu^+\mu^-$ modes. In the e^+e^- channel, the mass resolution of the detector is less than the natural width of the Z' so that the mass and width can both be measured. For the 1000 event sample shnwn in Fig. 35(a), after deconvoluting the resolution of the detector we obtain an error on the mass of ±3 GeV and an error on the width of ±7 GeV.

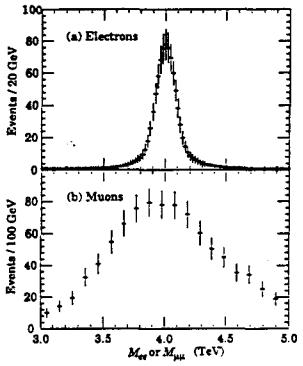


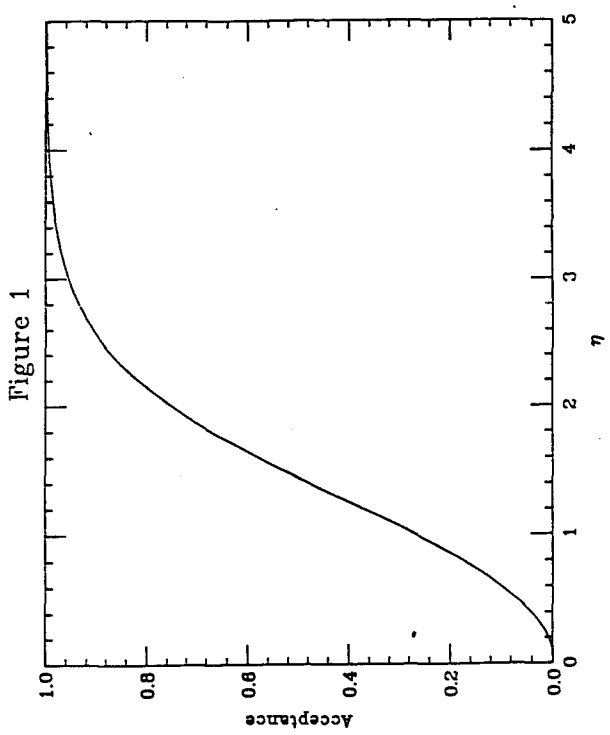
FIG. 35. The invariant mass distribution of (a) e^+e^- pairs and (b) $\mu^+\mu^-$ pairs from Z''s of mass 4 TeV, including the Drell-Yan background.

The peak in the μ channel, shown in Fig. 35(b), enables a measurement of the Z' mass with an error of ±10 GeV. The resolution in this channel is clearly not good ennugh to obtain information concerning the width. Universality is tested by comparing the event rates in the e^+e^- and $\mu^+\mu^-$ channels, corrected for the difference in resolution for the two channels. The two plots shown in Fig. 35(a) and Fig. 35(b) give 993 and 904 events in these channels respectively if we sum over dilepton masses in the range 3 TeV < M_{ll} < 5 TeV. In the absence of the Z' these values would he 38 and 41. The dominant error in this measurement of e/μ universality will be the 4.5% statistical error.

The situation is more complex for the $\tau^+\tau^-$ channel. Pairs of isolated tracks from the decays $\tau \to e\nu\nu$, $\tau \to \mu\nu\nu$, and $\tau \to \pi\nu$ can he exploited. The e^+e^- final state (hut not the $\mu^+\mu^-$ final state)

*The absence of serious backgrounds for high-p_t dileptons has been demonstrated in the UA1 [73], UA2 [74], and CDF [75] experiments. The ratin nf the Z' cross section to QCD background at the 55C is similar to the ratio of Z production to QCD at current collider energies.

986



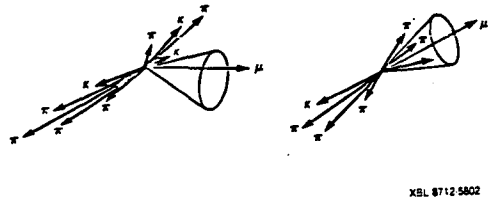
987

3. Isolated charged tracks
3.4 Isolation criteria
3.4.1 b->l+X
3.4.2 c->l+X

t mass measurement from
$t\bar{t} \to$ iso e non-iso μ

→ $\mathcal{E}$ (e or μ from b decay) > ν —

988



XBL 8712-5802

Figure 4) An example of isolated and non-isolated leptons in an event.

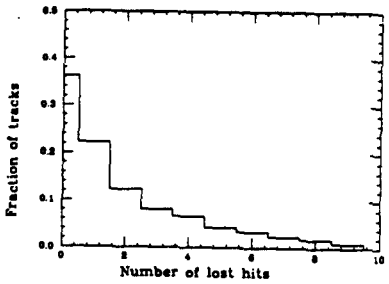


Fig. 20 Number of hits lost per track for jets with $P_\perp > 1$ TeV. The solid line is when the two hit separation is forced to be 250 microns; the dotted line is for 150 microns.

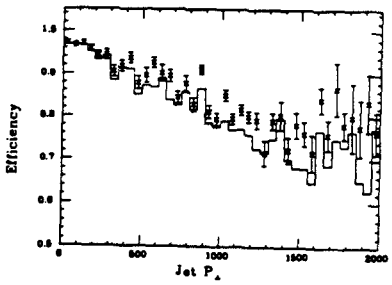


Fig. 21 Track-finding efficiency for a separation of 250 (histogram) and 150 (points) microns

4. Jets
4.1 Multiplicity

Distinguish W, Z from q, g jets

$\tau \to 3\pi$

4. Jets
4.2 Shape parameters, QCD

Tune up Monte Carlo

4. Jets
4.3 Isolation

Jet multiplicity

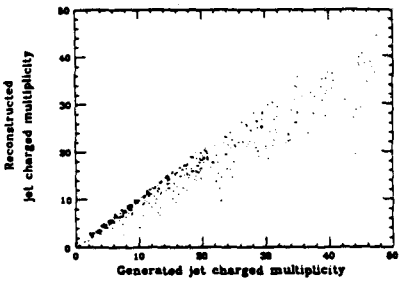


Fig. 23 Reconstructed vs. produced jet multiplicities for 1 TeV ISAJET events.

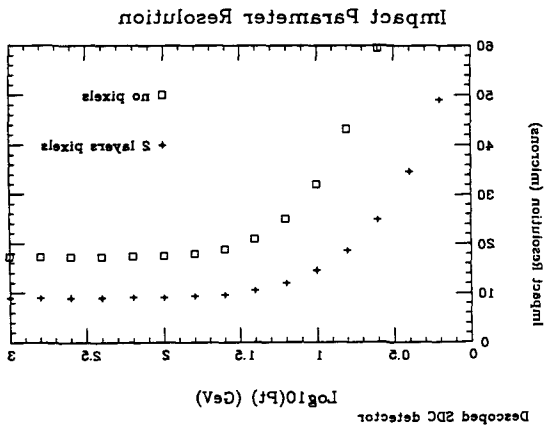
(e.g., to distinguish (W, Z) from QCD jets)

5. Detached vertices
5.1 Heavy quarks

b tagging critical for b physics

→ ε(b tag) $\gtrsim$ 50%

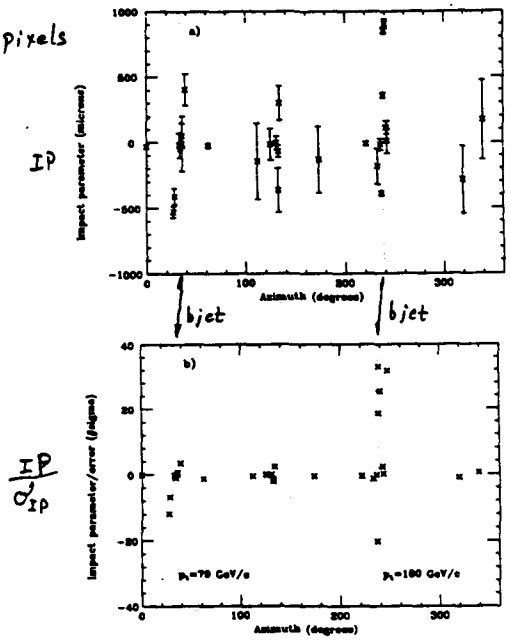
993



b tagging

Si, no pixels

994



IP

$\frac{IP}{\sigma_{IP}}$

Fig. 26 Charged tracks ($|\eta| < 2.5$, $P_\perp > 1$ GeV) in an ISAJET $t\bar{t}$ event with m_{top} = 150 GeV, for the system without a pixel vertex detector. a) Simulated impact parameter and error vs. azimuth ϕ. The two b jets are indicated by dotted lines. b) Number of sigma of impact parameter vs. azimuth ϕ. The horizontal dotted lines show 3 sigma cut.

c, b jet tagging efficiency

995

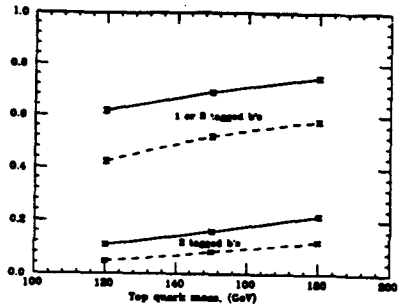


Fig. 26 Overall efficiency for single and double tags vs. m_{top} for the tracking system with (solid) and without (dashed) a pixel vertex detector.

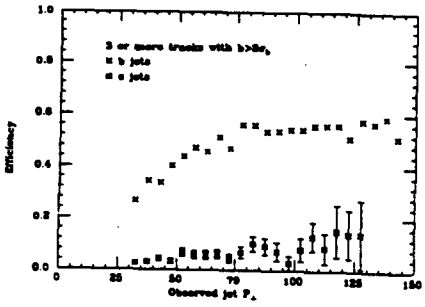


Fig. 27 Tagging efficiency for c jets compared to b jets vs. jet $P_\perp$, for the tracking system without an inner vertex detector.

5. Detached vertices
5.2 Taus

996

$W \to \tau \nu$ $\quad H^+ \to \tau \nu$

$\tau \to e \nu$
$\mu \nu$
$\rho \nu$
$(3\pi^{\pm})\nu X$
$\pi \nu$ $\quad$ (eg $t \to H^+ b$)

997

Rate without tracking for trigger on iso e or iso μ ($p_\perp > 10$ GeV) = ____

Max. allowed = ____

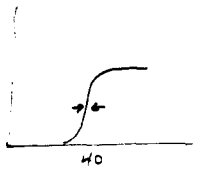
→ ⇒ Rate ($p_\perp > 10$ chg track trigger) < ____

(over $|\eta| < 2.5$?)

998

High $p_\perp$ electrons (from Z,W) for calorimeter calibration: $p_\perp \gtrsim 50$ GeV.
↖ 20

→ $\sigma_{p_\perp}/p_\perp^2 = 2.5$ TeV^{-1} at level 2



206 @ 35 (-e)
-(Bri)

999

1000

$H \to 4\ell$ for heavy H is rare:

$\rightarrow \frac{\varepsilon(4 \text{ iso } \ell)}{\varepsilon(\mu\ @\ 10^{33})} > \frac{10^{33}}{\mathcal{L}}$

$\rightarrow$ $< \$85$M (current target)

Requirements for Tracking

(1) $|\eta|$ coverage out to $|\eta| \leq 2.5$, implying $H^0 \to 4$ charged lepton geometrical efficiency $\gtrsim 60\%$ for $m_H \geq 200$ GeV.

(2) Reconstruction efficiency $\geq 90\%$ (for $|\eta| < 2.5$) for $H^0 \to 4$ charged leptons, for each lepton having $P_\perp \geq 5$ GeV, at design luminosity, but assuming twice the occupancy calculated by GEANT (exclusive of lepton identification and trigger cuts).

(3) Reconstruction efficiency for same as in (2) $\geq 75\%$ at 4×10^{33} design luminosity.

(4) Reconstructed (as opposed to parametric) vertex constrained momentum resolution of $\sigma_{P_\perp/P_\perp^2} < 25\%$ (TeV^{-1}) for $|\eta| \leq 1.8$ (leaves room still for a contribution from misalignments) for $H^0 \to 4$ charged leptons. → req'mt for $\eta > 1.8$

(5) Efficiency contribution from lepton identification of $\geq 85\%$ for electrons with $P_\perp \geq 10$ GeV and $\geq 95\%$ for muons with $P_\perp \geq 10$ GeV.

(6) Position resolution at the calorimeter of ≤ 2.5 mm in $r-\phi$ or z (want error $\lesssim \sigma/2$ of calorimeter position accuracy).

(7) No special position resolution requirements at the muon system. Achievable numbers ≤ 1 cm.

(8) B single tagging efficiency $\geq 30\%$ for 125 GeV $\leq m_{top} \leq$ 250 GeV. purity

(8') τ tagging

(9) First level trigger with momentum resolution $\sigma_{P_\perp/P_\perp^2} \leq 10$ (TeV^{-1}) – implies a 10% error for a 10 GeV lepton.

(10) Second-level trigger with momentum resolution $\sigma_{P_\perp/P_\perp^2} =$ 2.5 (TeV^{-1}). Gives a 10% error for a 40 GeV lepton for triggering on $Z \to e^+e^-$, $W \to e\nu$ – needed for calorimeter calibration.

(11) Discovery potential - hard to quantify. In general want maximum capabilities from detector. Based on history highest priority (other than isolated lepton of Higgs case above) would be reconstruction and impact parameter measurement of leptons within jets up to the largest jet $P_\perp$ possible (at least ≥ 500 GeV). Desired reconstruction efficiency $\geq 50\%$.

(12) Measurement of jet fragmentation at modest luminosity for QCD studies and for modelling backgrounds from jets.

(13) Survivability at standard $\mathcal{L}$ for ≥ 10 years.

(14) Allows a natural path for upgrading to a system with survivability of ≥ 10 years at $10\times$ standard $\mathcal{L}$ with emphasis (e.g. momentum resolution, pattern recognition, isolated track efficiency) to be decided based on what is learned during initial running.

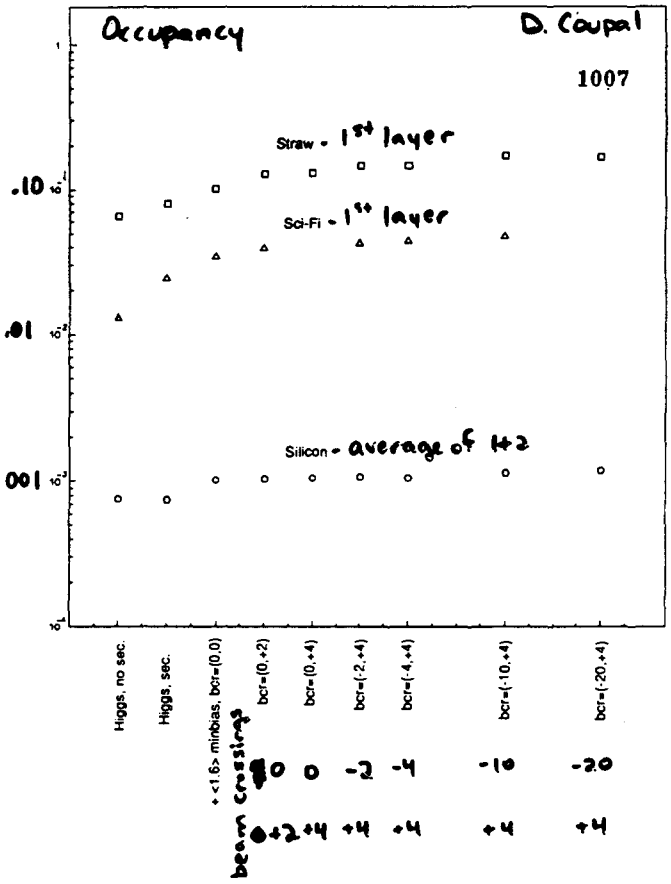
Tracking Algorithm Overview

K. O'Shaughnessy(UC/Santa Cruz)

Tracking algorithm overview

1006

- Algorithms have evolved from independent code from each technology
- Converted to work within the shell (at least for the original system)
  - common event generators
  - mechanism for minbias
  - out of time beam crossings
- Agreed on a set of conventions
  - track parameters →
  - (segment parameters) (→)
  - method of passing information



SDC conventions

1008

coordinate system:

- x out of the ring (~ west)
- y up
- ⇒ z ~ north

B field is in the $+\hat{z}$ direction

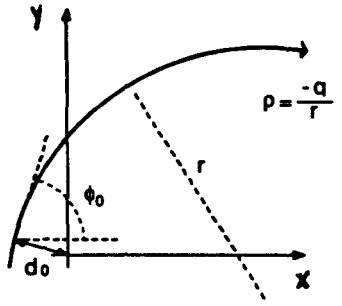
track parameters

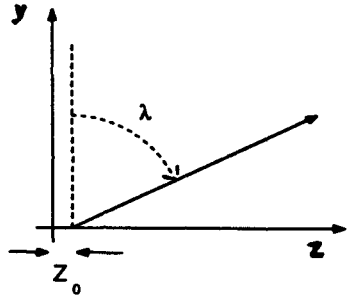
helical fit, measured at distance of closest approach to origin (DCAϕ)

- b_0 xy impact parameter
- ϕ_0 ϕ of track at DCAϕ
- $\rho \equiv -\frac{q}{r}$ $r \equiv$ radius of curvature
- z_0 z intercept at DCAϕ
- $\tan\lambda$ tangent of dip angle

Track parameters

1009



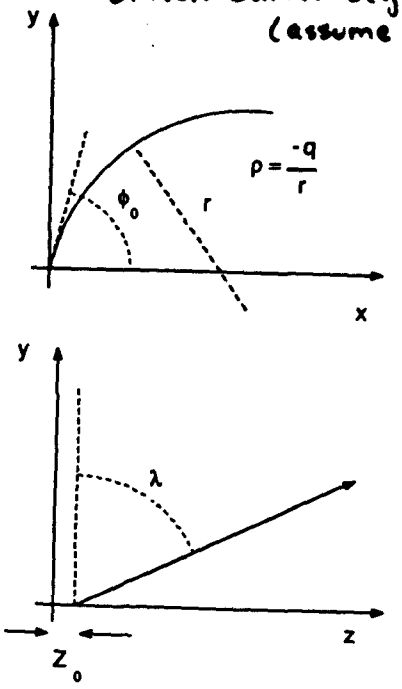


Positively charged track is shown
⇒ negative ρ

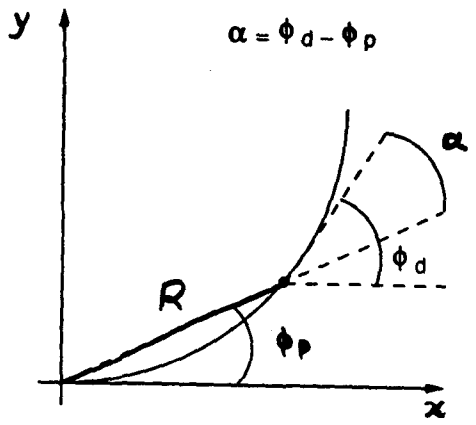
impact parameter + when origin contained inside curve.

Silicon barrel segment parameters (assume $b_0 = 0$)

1010



1011



outer barrel segment parameters

axial R, ϕ_p, α

$z, \tan\lambda$
↑ at the measurement point

1012

Conversion from outer barrel segments to silicon (ST) barrel segments

Measure and store

$R, \phi_p, \alpha, (\rho), \underbrace{z, \tan\lambda}_{\text{if have stereo information}}$

Want to calculate

$R, (b_0 = 0), \phi_0, \rho, z_0, \tan\lambda$

$$\phi_0 = \phi_p - \alpha$$

$$\rho = \frac{2}{R}(\sin\alpha)$$

$$z_0 = z - R\tan\lambda$$

($R, \tan\lambda$ are the same)

Errors:

e.g.

$$\langle \delta\phi_0^2 \rangle = \langle \delta\phi_p^2 \rangle + \langle \delta\alpha^2 \rangle - 2\langle \delta\phi \, \delta\alpha \rangle$$

1013

- caveats and other common points
  - uniform magnetic field (effect of non-uniformity on each algorithm not assessed yet) global vs. local strategy
  - material for support material smeared out/underestimated in general

→ This meeting:
thorough specification of physics processes (and conditions e.g. $\int \mathcal{L} dt$, out of time crossings etc) for comparisons between algorithms.

Segment Clustering Track Finding Method

K. O'Shaughnessy

Segment clustering
track finding method

1015

1016

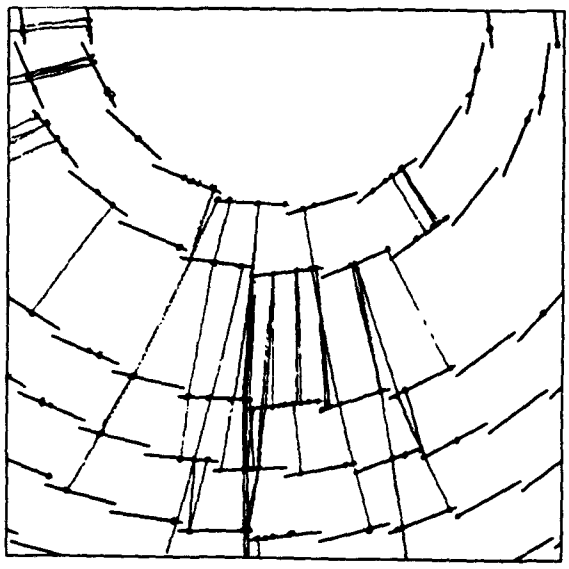
Measure local segments in the detector, characterize by parameters that are global (eg DCAϕ)

Premise: All segments from the same track should have the same parameters.

$\therefore$ can use the parameters and their errors* to make a χ^2 test to see if segments associate.

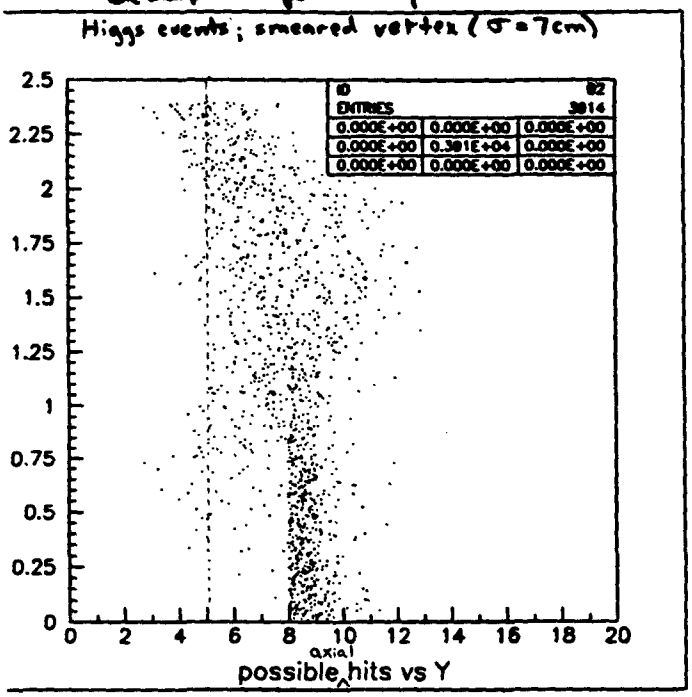
$\Rightarrow$ Result is a set of "clusters" which are candidate tracks

* account for multiple scattering by increasing error

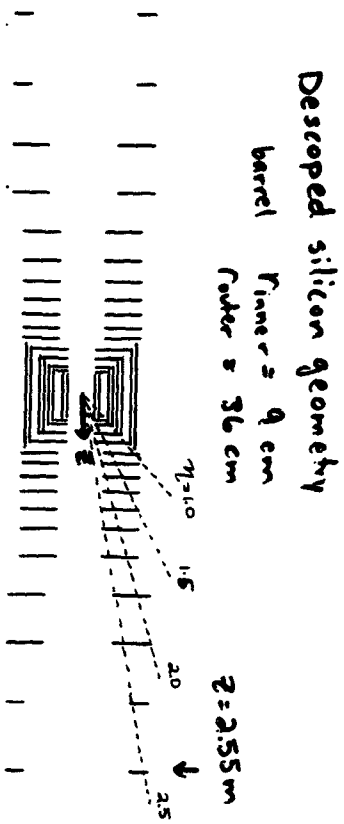


1017

Descoped geometry



1018



Track fitting

Iterative fit

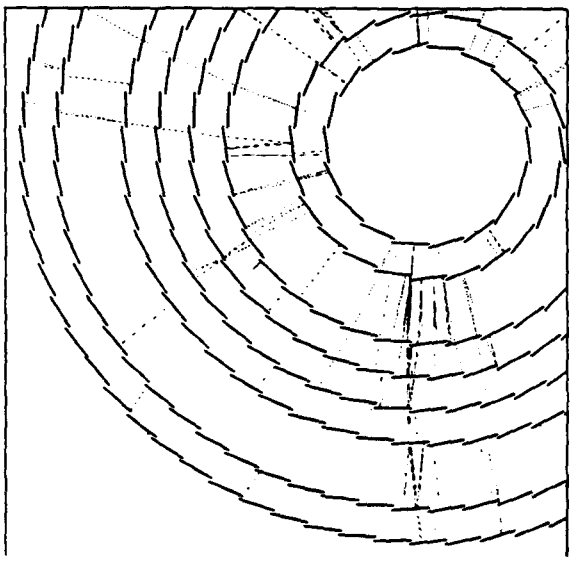
initial pass
- use segment parameters as initial guess
- prepare list of hits from segment list
- require n points to start
- iterate up to m times or until χ^2 is steady (whichever is less)

delete bad points
- if χ^2 above a cut, delete the point with the largest residual
- iterate again
- continue until up to k points have been deleted or χ^2 below cut

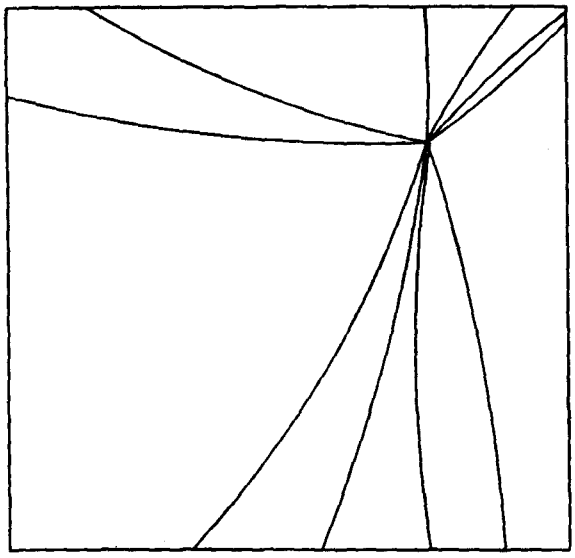
pick up missed hits
- extrapolate track parameters and pick up hits that are within a road.
- Iterate to get new track parameters.

includes multiple scattering

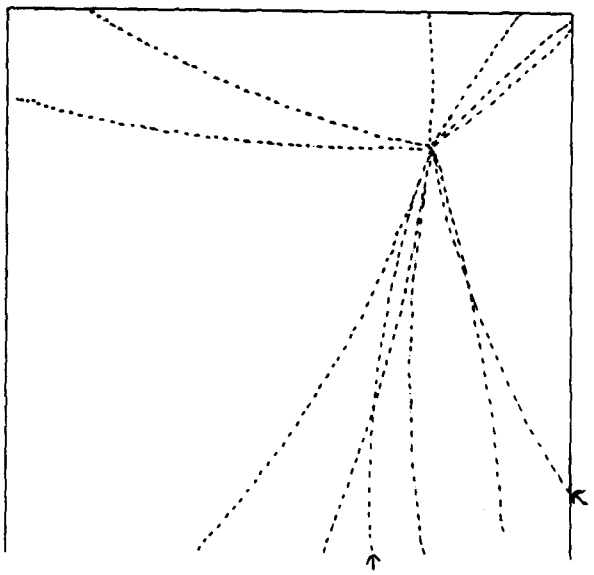
Silicon barrel (descoped version).
All segments with $-.8 < \eta < .8$

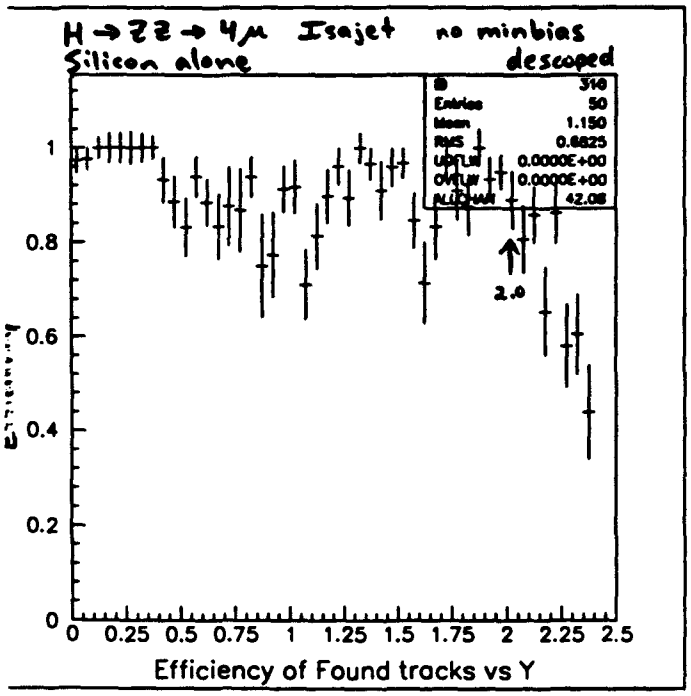


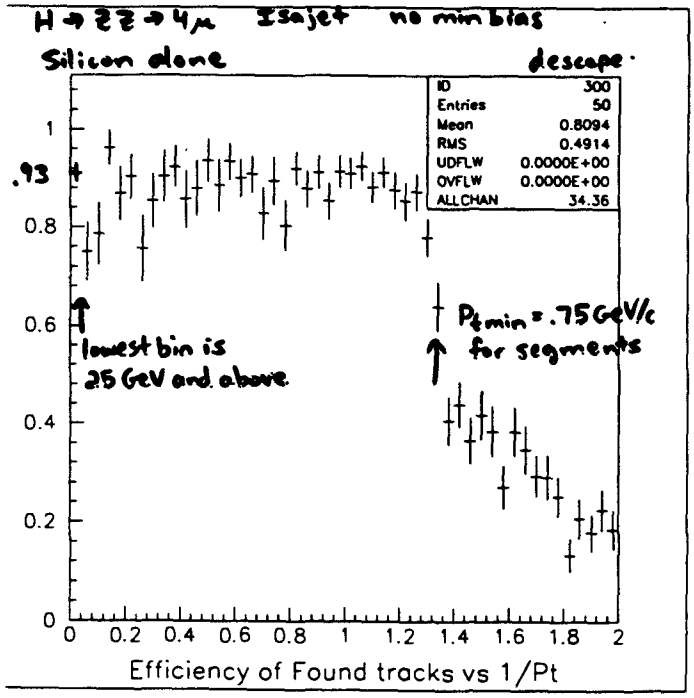
Reconstructed tracks with $-.9 < \eta < .9$
$P_t > 0.5$ GeV/c

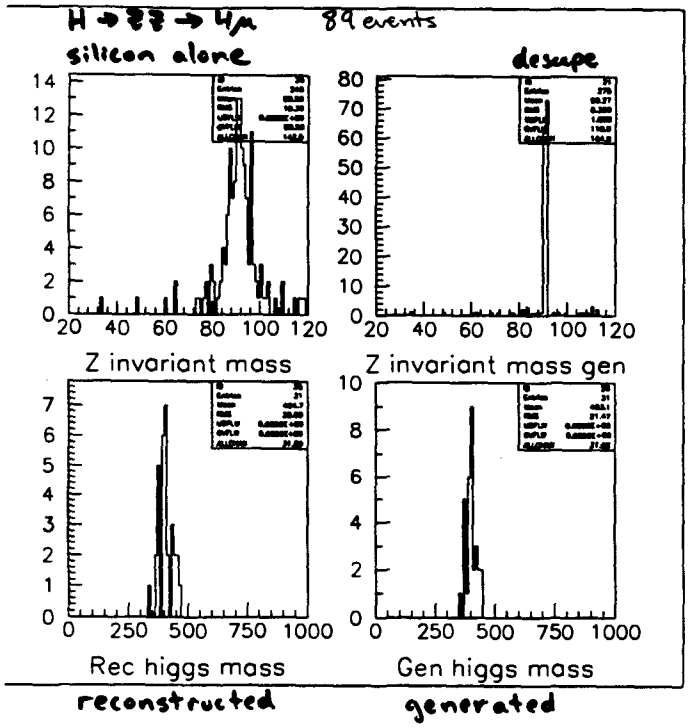


MC particles with $-.9 < \eta < .9$, $P_t > 0.5$ GeV









Status of TS package

(1) Next release (Oct. 6) will unpack and convert outer barrel segments to DCAφ parameters.

(2) Still need to work through any conversion problems for the clustering of segments from different technologies (e.g. errors, control flags)

(3) Fit can almost pick up the WR (straw) segments using the road and fit them. (Need geometry and stereo conversion)

(4) Next stage is to cluster other geometries and use hit level information in the fit.

ILWAYS Optimize finding and fitting parameters

TRF: A Track-Finding Package for Solenoidal Fields

D. Adams(Rice)

1028

TRF: A Track-Finding Package for Solenoidal Fields

D. Adams
26 SEP 91
Rice U.

1. Description
2. Program Flow
3. Example Map
4. Extending TRF
5. Status + performance

Description

1029

TRF uses a road-following technique to link space points or vectors.

- Points can be 2D or 3D
- Points are grouped on surfaces - either cylinders or disks
- Does not require direction information (vectors) but can take advantage of it.
- Can cluster scifi digitizations in 2D and 3D.

Program Flow

Initialization

1030

1. Read instructions from input file TRF.DAT
   a) set constants
   b) define superlayers: 1 or more scifi layers
      1 Si layer (coord. bank)
   c) higher level superlayer definition
      e.g. combine x,u,v ⇒ 3D supercluster
   d) road map - instructions for track-finding
2) Read scifi + Si geometry from SDC data banks

Event Analysis

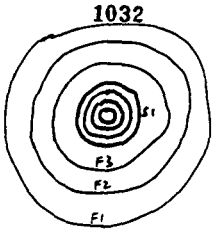
1031

1) Read in scifi digitizations
2) Cluster scifi digi's. ⇒ 2D superclusters (scl's) and coordinates (coor's)
3) Combine 2D scl's ⇒ 3D scl's + coor's.
4) Write the scifi scl's + coor's. to SDC D.S.
5) Read Si (and scifi) coor's. from SDC D.S.
6) Find tracks as instructed by map
7) [Refit tracks in optimal way] (not implemented)
8) Write tracks to the SDC D.S.

→

Example Map

1032



1. Start tracks in F1 w/ rvc (radial vertex constraint) and zvc (z vertex constraint).

   $\varphi_{SF1}, \alpha_{SF1}$ determine $T_{r\varphi}$ w/ rvc

   z_{SF1} determines T_z w/ zvc

2) Remove zvc

3) Extend tracks to F2

   $\varphi_{SF1}, \varphi_{SF2}$ determine $T_{r\varphi}$ w/ rvc ($\alpha_{SF1}, \alpha_{SF2}$ ~over C)

   z_{SF1}, z_{SF2} determine T_z

4) Extend tracks to F3

   $\varphi_{SF1}, \varphi_{SF2}, \varphi_{SF3}$ overdetermine $T_{r\varphi}$ by 1 w/ rvc

   $z_{SF1}, z_{SF2}, z_{SF3}$ overdetermine T_z by 1

5) Remove rvc

6) Extend tracks to S1

   φ_{SF1} φ_{SF2} φ_{SF3} φ_{SF4} overdetermine $T_{r\varphi}$ by 1

   z_{SF1} z_{SF2} z_{SF3} z_{SF4} overdetermine T_z by 2.

7) Extend tracks to S2

   .
   .
   .

Extending Tracks

1033

1. Propagate track to the superlayer surface (cylinder or disk)

2. Estimate scl. or coor. from the propagated track.

3. Compare each scl. or coor. w/ this estimate and identify nearby ones as candidates.

4) Define a new track for each candidate by adding the candidate scl or coor. to the existing track.

5) Refit each of the new tracks and discard those w/ χ^2 too large.

Status + Performance

1034

Recently (this week) we finished moving TRF into SDCSIM.

Plan to look at:

- single μ's, e's — ϵ $\Delta p/p$
- $H \to ZZ \to 4\mu$ — ϵ
- $Z' \to \mu\mu$ — $\Delta p/p$

Following figures show results previously obtained w/o SDCSIM for 1, 2, ... 6 QCD inelastic events in a beam xing.

- ϵ for selected tracks ~ 98%
- false track rates
- CPU time performance (IBM RS6000/530)

1035

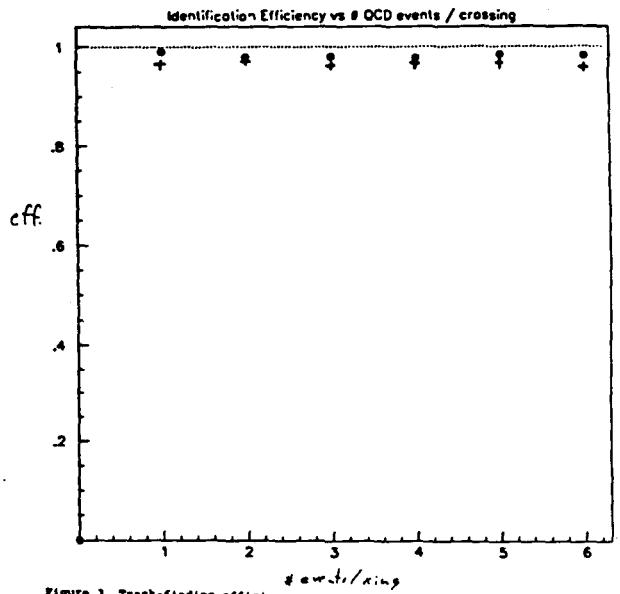


Figure 3. Track-finding efficiency vs the number of events/crossing for selected tracks (see text). The crosses are 3 degree stereo and the circles 8-10 degrees.

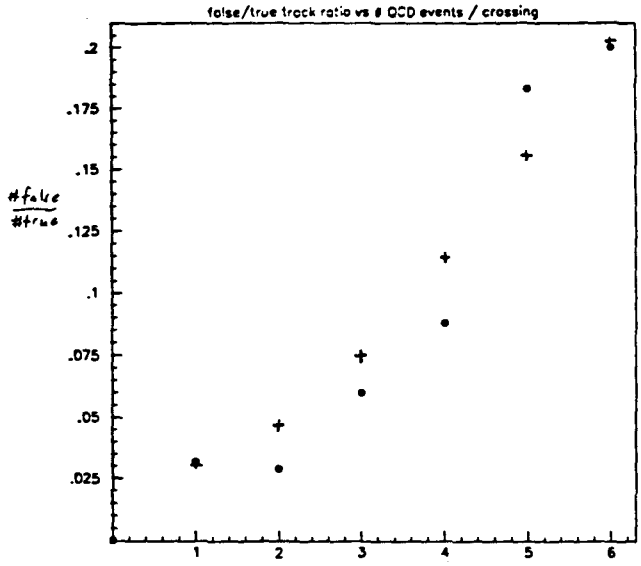


Figure 4. Ratio of false tracks to candidate tracks as a function of the number of events in a crossing. The crosses are 3 degree stereo and the circles 8-10 degrees.

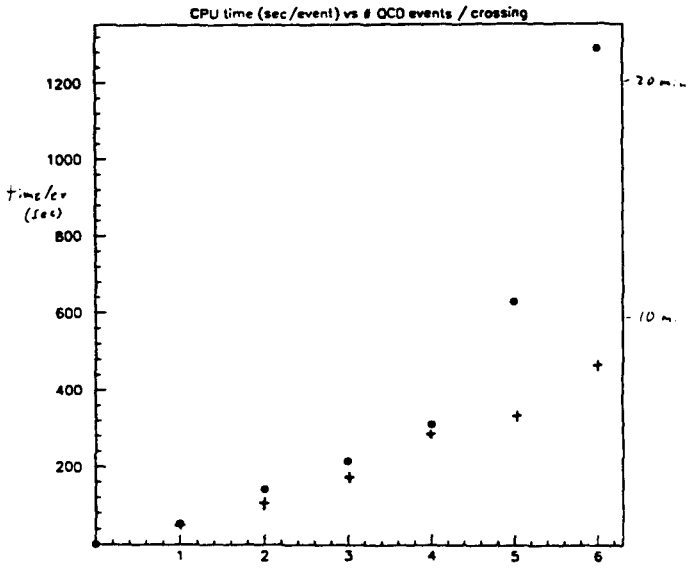


Figure 5. CPU time required to track and reconstruct a crossing vs the number of events/crossing. The CPU was an IBM RS6000 rated at 34.9 MIPS.

Silicon Tracker R&D and Engineering FY 92

H. Sadrozinski(UC/SC)

Silicon Tracker R&D and Engineering FY 1992

Overview of the Silicon Tracking System

Accomplishments in FY's 1988–91

R&D in FY 1992

Budget for FY 1992

Conclusions

Hartmut F.-W. Sadrozinski
UC Santa Cruz
9–26–91

SILICON TRACKING SUBSYSTEM

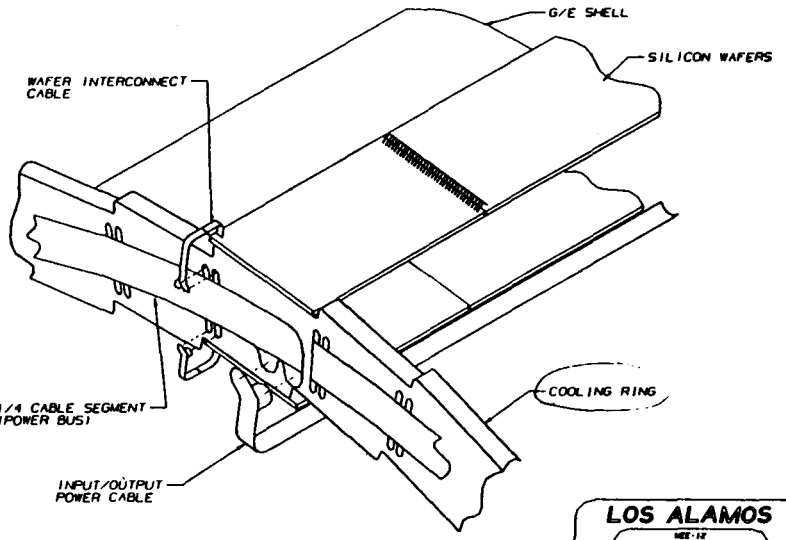
- Pattern recognition for tracking at the SSC
- Combined with the outer tracking structures, including the muon chambers, provides high precision momentum information over the full pseudo-rapidity region $|\eta| < 2.5$
- Provides high resolution vertex information
- Potential for Level 2 trigger

Critical areas of work to achieve a Silicon tracking system with adequate performance:

- low-power, low-noise, radiation-hard electronics;
- low-mass, ultra-stable, mechanical structures;
- low-mass, vibration-free, cooling systems;
- maximally radiation-hard detectors;
- development of data acquisition and triggering schemes.

1044

SILICON TRACKING SYSTEM

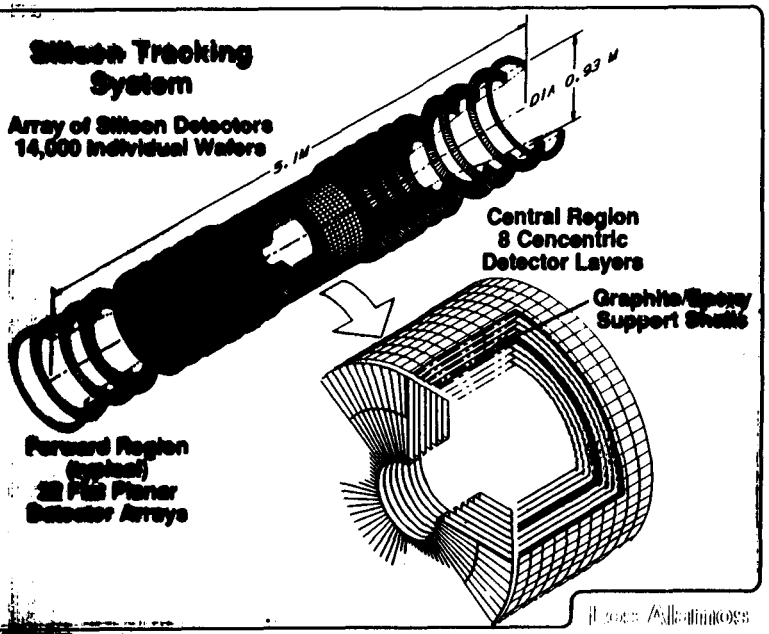


LOS ALAMOS

1046

Silicon Tracking System

Array of Silicon Detectors
14,000 Individual Wafers

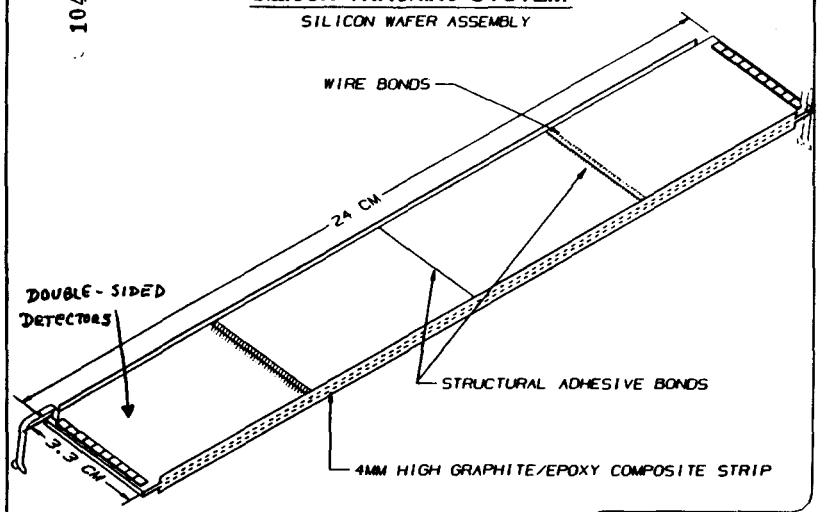


Los Alamos

1043

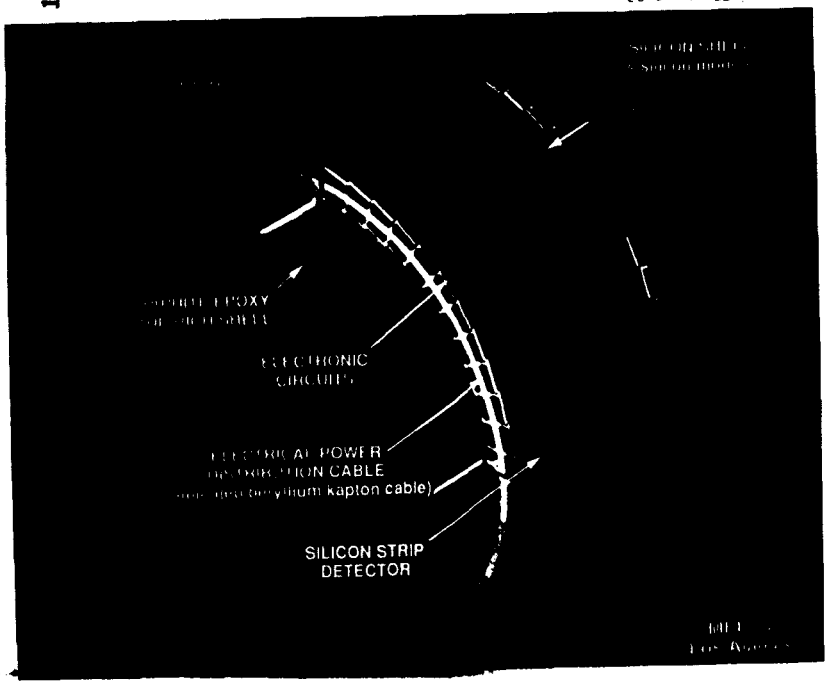
SILICON TRACKING SYSTEM

SILICON WAFER ASSEMBLY



LOS ALAMOS

1045

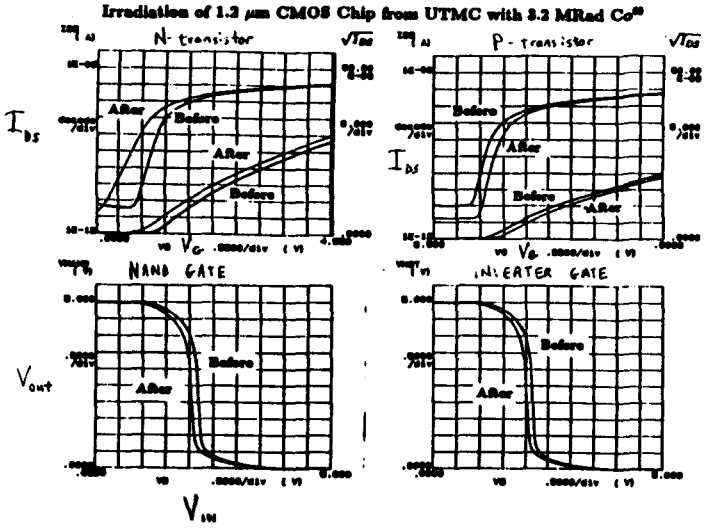


1048

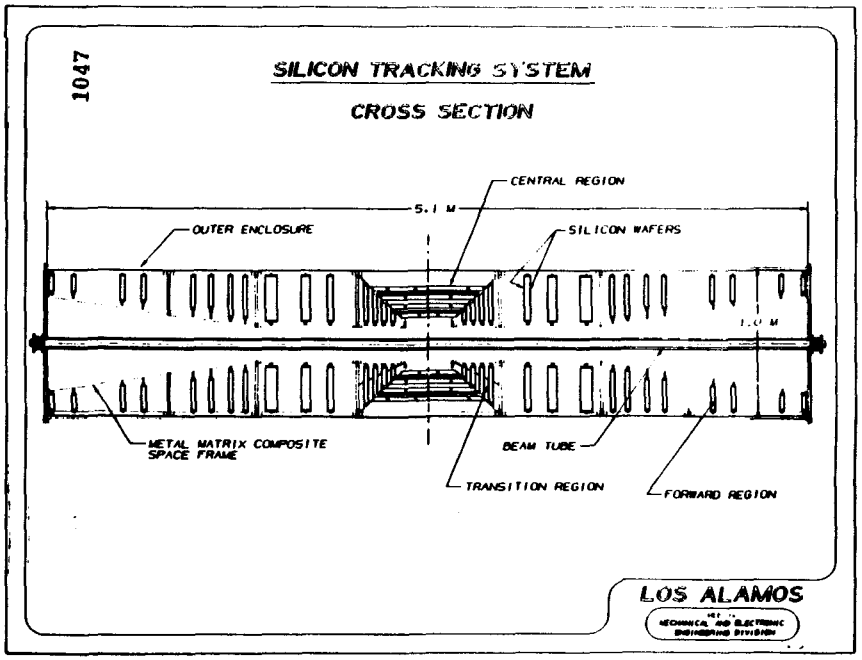
MAJOR ACCOMPLISHMENTS:

1. Demonstration that double-sided silicon detectors will function properly up to doses of 10^{14} particles cm^{-2}, implying 20 years of lifetime at a radius of 15 cm for the SSC design luminosity.
2. Demonstration that bipolar and radiation hardened CMOS electronics will function for the same fluences as listed above for the detectors.
3. Design, fabrication and testing of a fast analog front-end chip with power consumption of less than 1 mW/channel.
4. Construction of a prototype wick-cooling ring demonstrating the removal of heat for hours by a fully passive system (i.e., without pumps).
5. Finite element calculations for the major mechanical elements of the detector satisfying our dimensional tolerance goals.
6. Demonstration of the basic mechanical structure of a detector module, with sufficient rigidity and ruggedness.
7. A first critical path decision choosing 12 cm detector units with a two-chip set (bipolar preamplifier and discriminator plus CMOS data storage chip) as the basic detector module.
8. Detailed construction schedule and cost estimate for an SSC silicon tracker.
9. Distribution of work among institutions for the construction of an SDC tracker.

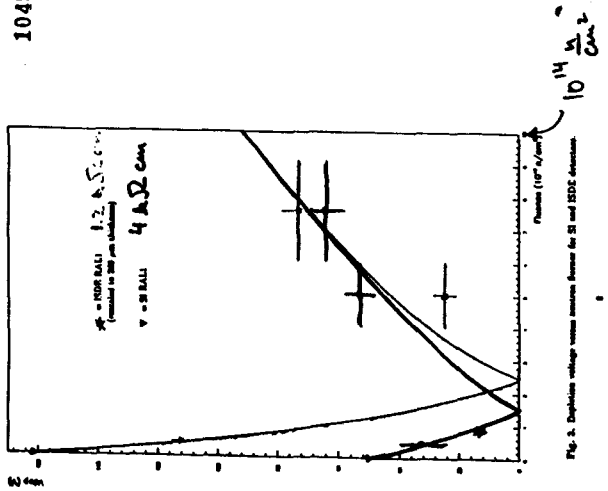
1050



1047



1049



1052

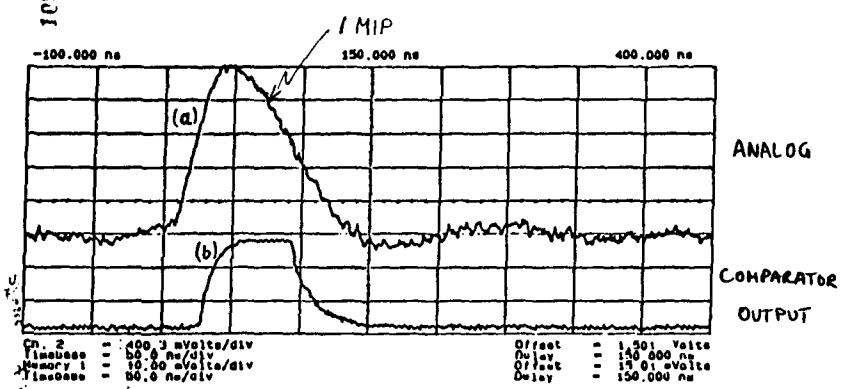
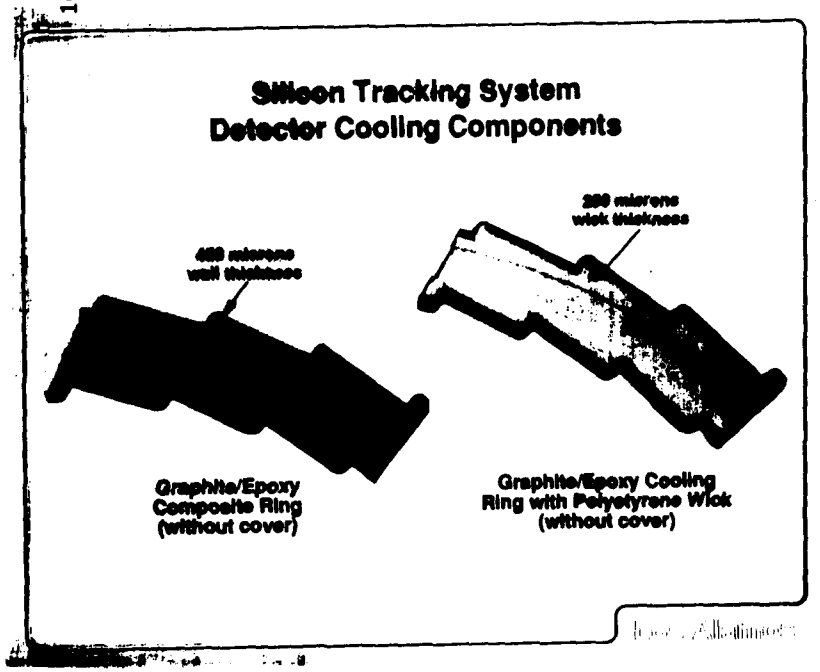


Fig.17. Records of the output signals from the BJT-JFET circuit for input charge of 4 fC and input capacitance of 10 pF; (a) preamplifier output, (b) discriminator output.

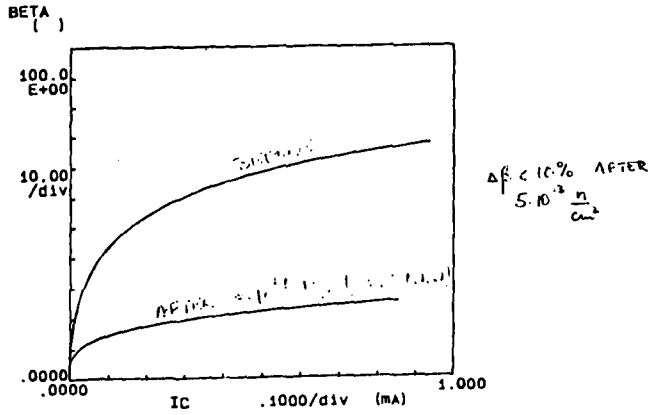
PRE-AMP + COMPARATOR < 1 mW/CH

(BIPOLAR + JFET)

105



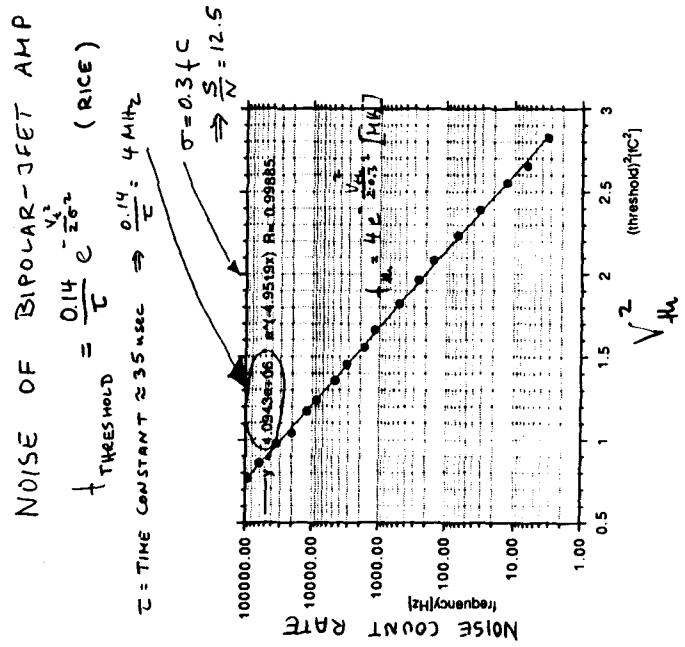
1051

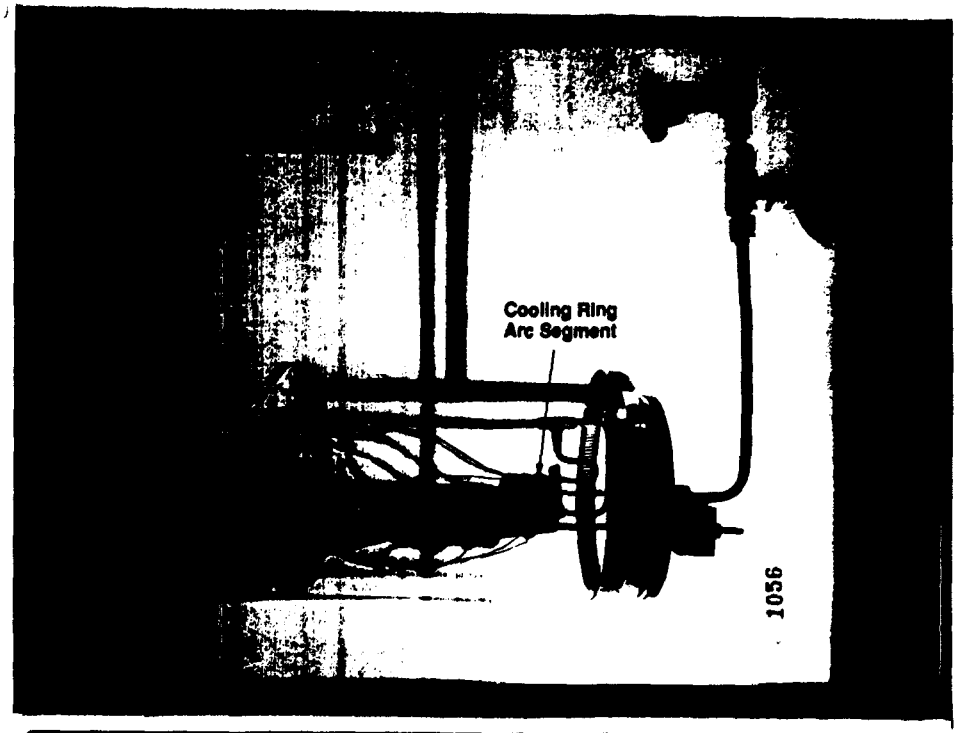


$\Delta\beta < 10\%$ AFTER $5 \cdot 10^{13}$ n/cm²

Fig. 47 β before and after irradiation

1053





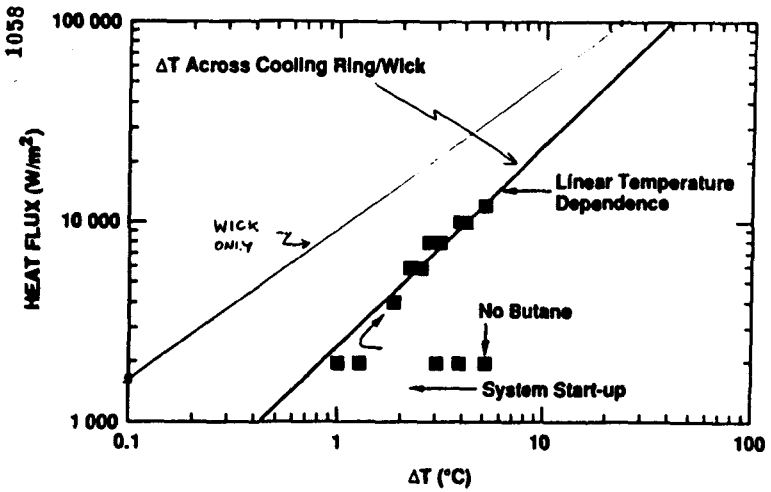
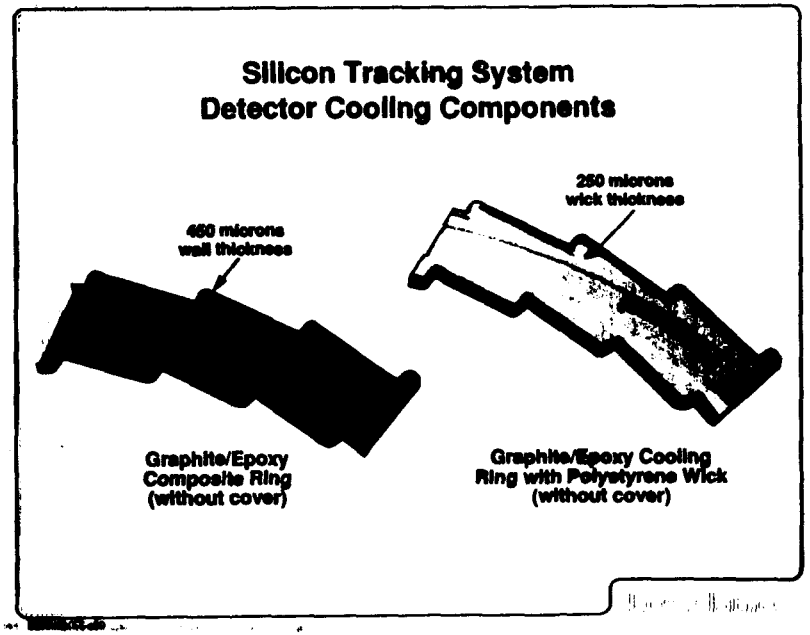
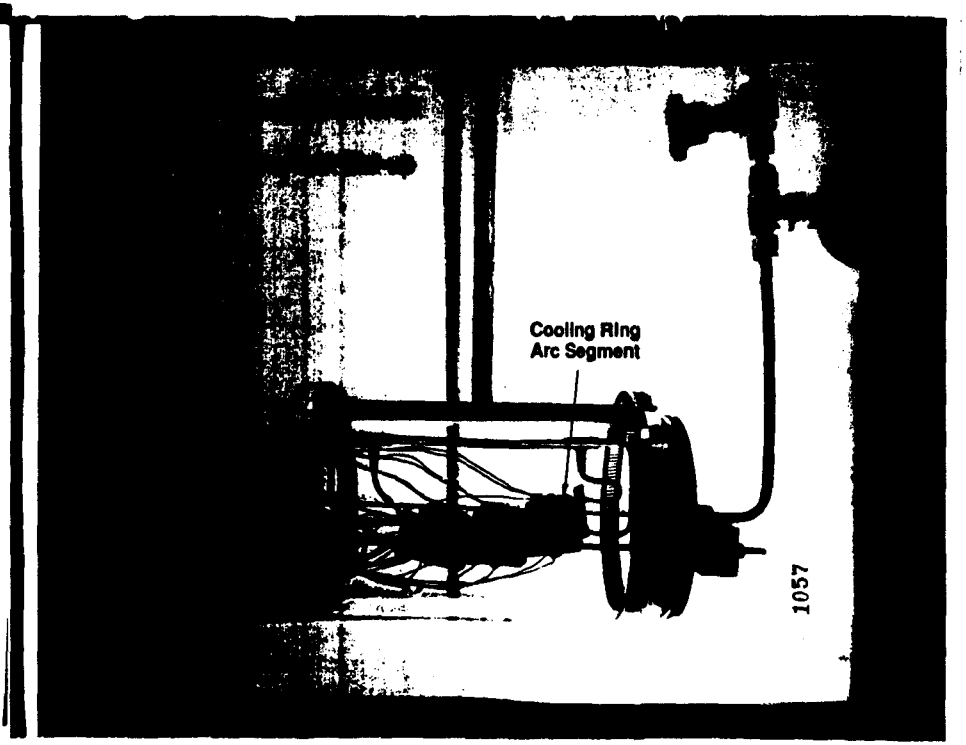


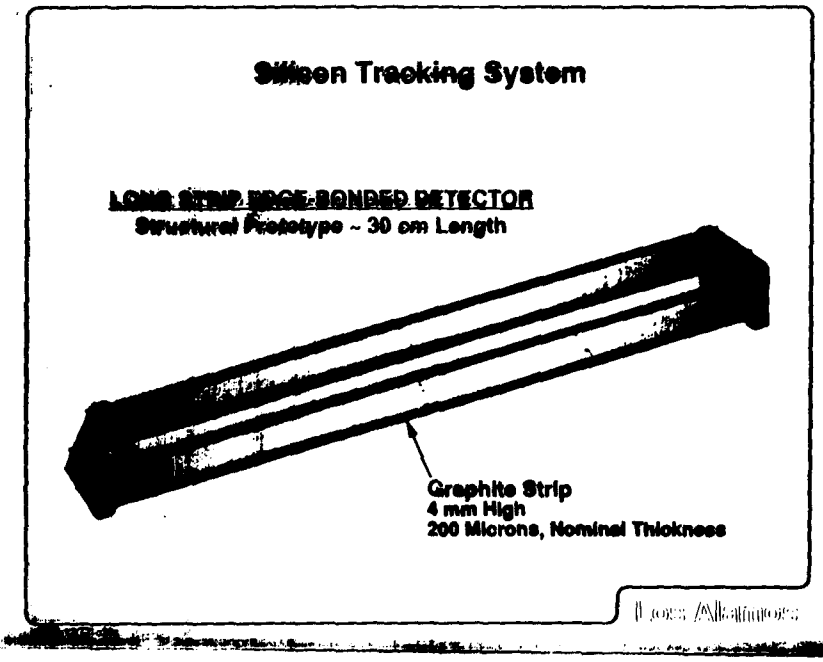
Figure 3-12. Contoured polystyrene-wick cold boundary test heat flux results expressed as a function of temperature change.

1055





1060



1059

Maximum uncorrelated positioning errors:

Silicon detector:	Circumferential	5 μm
	Radial	80 μm
	Longitudinal	250 μm
Straw superlayer:	Circumferential	35 μm
	Radial	1200 μm
	Longitudinal	250 μm

Maximum correlated system error, silicon relative to straws:

Rotational alignment:	10^{-5} radians
Radial alignment:	600 μm
Longitudinal coordinate:	250 μm
Displacement of detector centroids:	15 μm

Note, all the numbers above are meant to be standard deviations, not the edges of box shaped distributions, which span a range of ± 1.73 times the values tabulated above.

1062

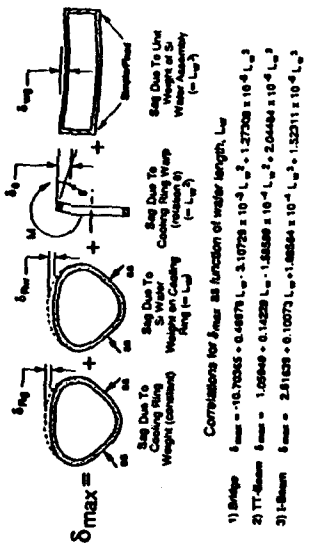
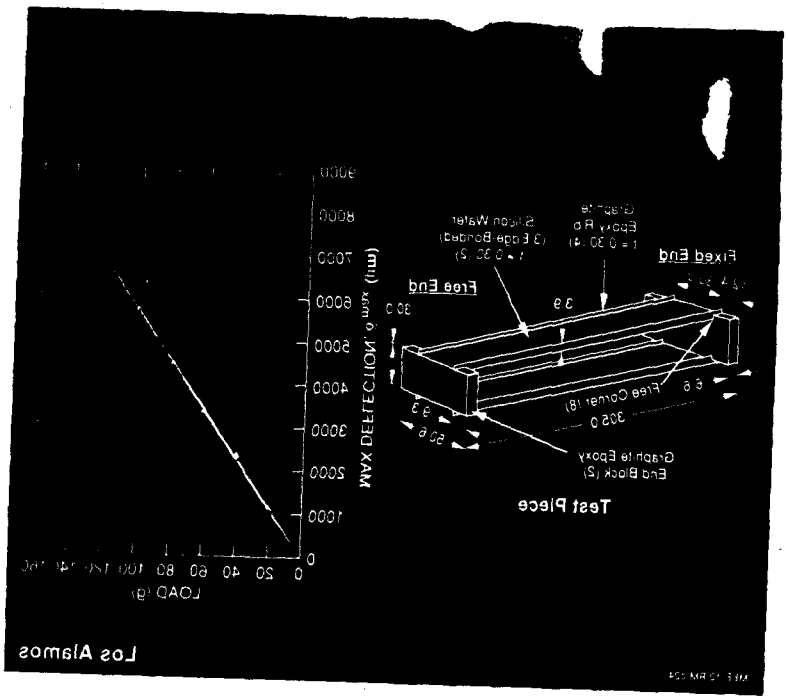


Figure 3-9. Displacement components contributing to silicon shell sag and displacement correlations expressed as a function of wafer length.

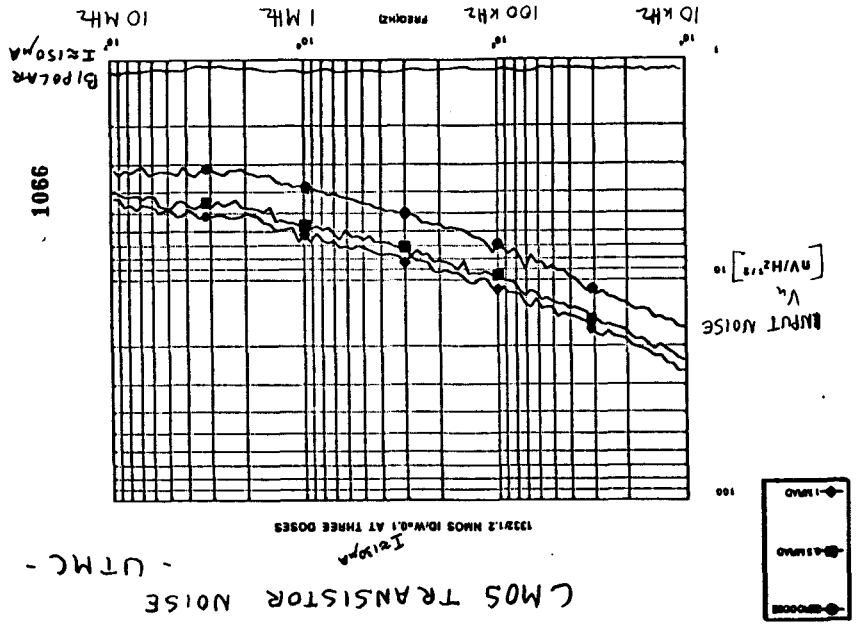
1061



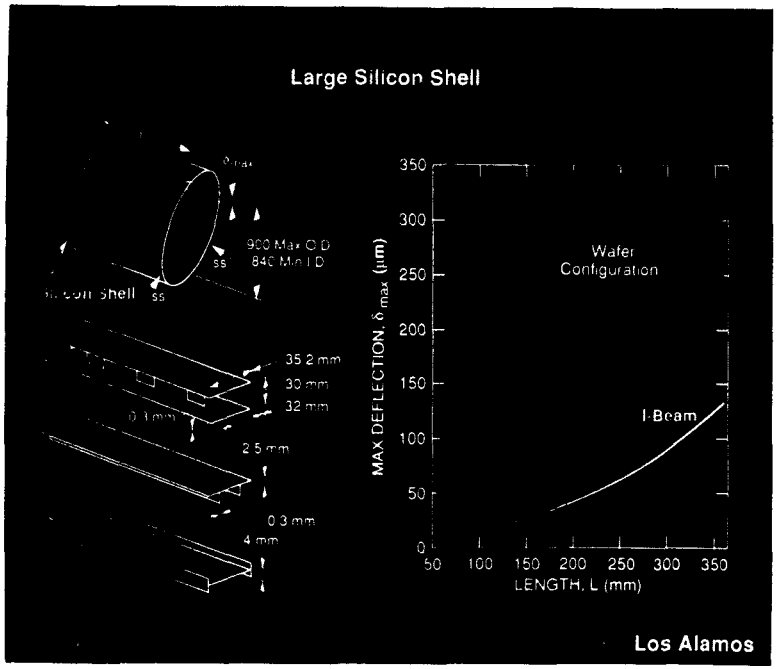
1064

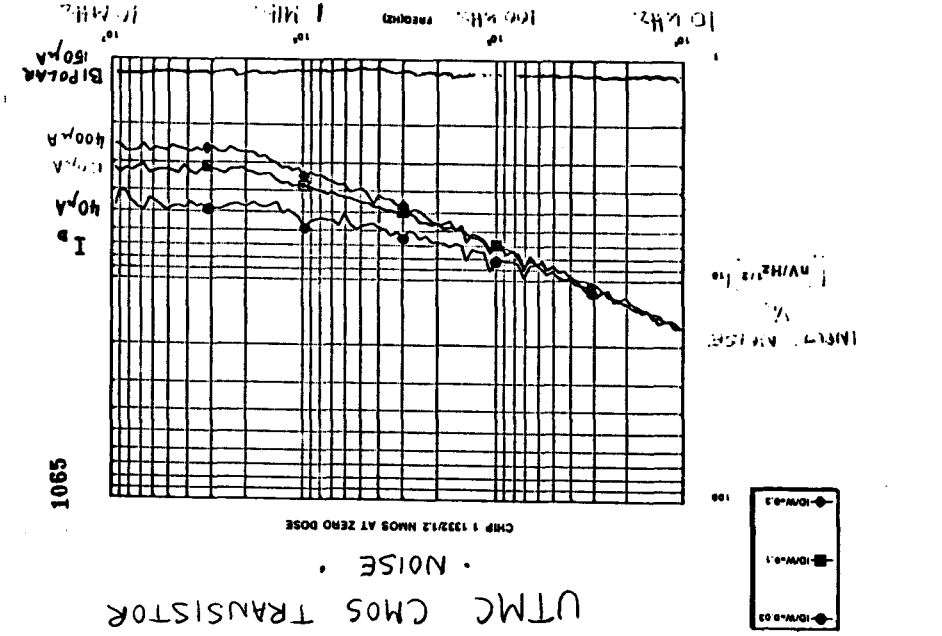
Our first critical milestone—selection of detector length and type—has been met, with the choice of 12 cm detector length and double-sided detectors. This is based on considerations of cost and material (argue for longest units) and signal-to-noise and power (argue for shorter units). It also reflects the progress in Japan on the fabrication of double-sided detectors and progress on low-power bipolar front-ends.

Our next milestone is a selection of the stereo angle for the second side of the detector. This should be selected by the end of calendar 1991 and will be based mainly on simulation results for the full tracking system.



1063





1067

TABLE 5.

Total Power of CMOS Front-Ends = $P_{AMP} + P_{COMP} + P_{DIG}$ vs. Input Noise Q_n and Strip Length L				
Strip Capacitance = 1.2 pF/cm; CR-RC Shaping Time τ = 20 ns Shunt Resistance R_p = 200 kΩ Power of Stages Following Preamplifier P_{flx} = 0.5 mW NO SHORT STRIPS Total Noise = 1.1 x Noise of Input Transistor Alone				
Φ_{max} = 10^{14} cm^{-2} Detector Leakage Current = 100 nA/cm				
Q_n [el]	Power [mW] vs. Strip Length			
	6 cm	8 cm	12 cm	18 cm
1000				
1100	4.0			
1200	2.8	6.9		
1300	2.2	4.4		
1400	1.7	3.4		
1500	1.4	2.7	8.3	
$r_\perp$ = 27 cm; 10 years at L = 10^{33} cm^{-2}s^{-1} Detector Leakage Current = 60 nA/cm				
Q_n [el]	Power [mW] vs. Strip Length			
	6 cm	8 cm	12 cm	18 cm
1000	6.1			
1100	3.5			
1200	2.6	5.6		
1300	2.1	4.0		
1400	1.6	3.1	10.7	
1500	1.3	2.5	7.1	

POWER GOAL : 1mW/CHANNEL

1068

TABLE 7.

Total Power of BJT Front Ends = $P_{AMP} + P_{COMP} + P_{DIG}$ $r_\perp$ = 27 cm; 10 Years at L = 10^{33} cm^{-2}s^{-1}								
Strip Capacitance = 1.2 pF/cm; CR-RC Shaping Time τ = 20 ns Shunt Resistance R_p = 200 kΩ; Leakage Current = 60 nA/cm								
Preamplifier Supply Voltage = 3.5 V; Current in Output Buffer = 10 μA Total Noise = 1.1 x Noise of Input Transistor Alone								
DC Current Gain of Input Transistor B = 100								
Q_n [el]	Preamplifier Current [μA] vs. Strip Length				Power per Channel [mW] vs. L_{strip} (P_{flx} = 0.5 mW)			
	6cm	8cm	12cm	18cm	6cm	8cm	12cm	18cm
1000	46	134			0.70	1.00		
1100	34	66			0.65	0.77		
1200	27	49	171		0.63	0.71	1.13	
1300	22	39	102		0.61	0.67	0.89	
1400	18	32	78		0.60	0.65	0.81	
1500	16	27	63	183	0.59	0.63	0.76	1.18
DC Current Gain of Input Transistor B = 30								
Q_n [el]	Preamplifier Current [μA] vs. Strip Length				Power per Channel [mW] vs. L_{strip} (P_{flx} = 0.5 mW)			
	6cm	8cm	12cm	18cm	6cm	8cm	12cm	18cm
1000								
1100								
1200	34				0.65			
1300	25	56			0.62	0.73		
1400	20	38			0.60	0.67		
1500	17	30			0.59	0.64		

POWER GOAL : 1mW/CHANNEL

1069



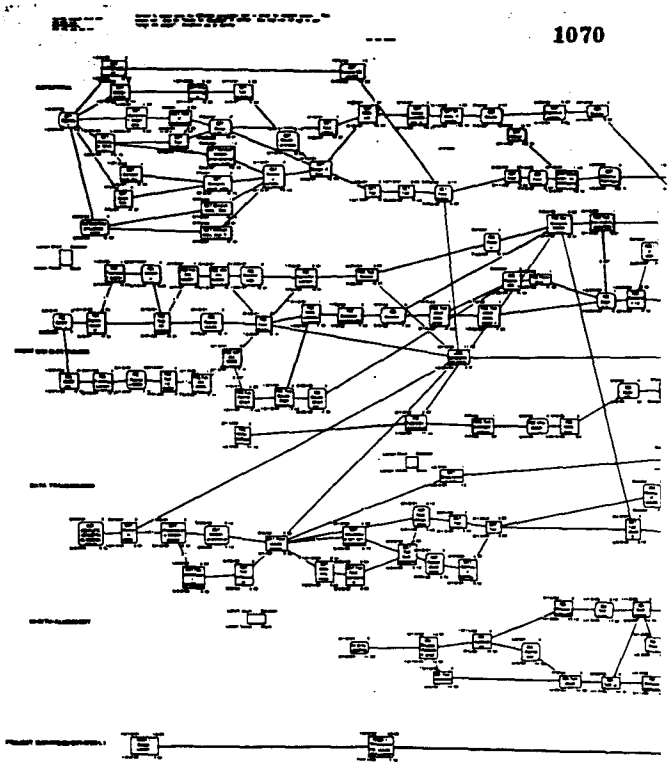
Subsystem R&D Progress Report for a Silicon Tracking System FY 1990-91

California Institute of Technology
University of California, Davis
University of California, Riverside
University of California, Santa Cruz
University of Hawaii
Johns Hopkins University
University of Pittsburgh
Fermi National Accelerator Laboratory
Lawrence Berkeley Laboratory
Los Alamos National Laboratory
University of Oklahoma
Stanford Center for Integrated Systems
Hiroshima University
Hiroshima Institute of Technology
KEK, National Laboratory for High Energy Physics
Nagoya University
Niigata University
Okayama University
Wakayama Medical College
Universities of Pisa and Sassari, and INFN-Pisa
University of Turin
University of Bristol
University of Cambridge
Imperial College
University of Oxford
Rutherford Appleton Laboratory
Krakow Institute of Nuclear Physics
Joint Institute for Nuclear Research, Dubna
Silicon Dynamics, Inc.
United Technologies Microelectronics Center
Senter for Industriforskning
EG&G Solid State Products Group
Engineering Solutions

FORWARD
DETECTORS
MECH
FEE
BARREL
DETECTORS
DAQ/
TRIGGER

Santa Cruz Institute for Particle Physics
University of California, Santa Cruz

1070



1072

WORK DISTRIBUTION AND PLAN FOR NEXT YEAR (FY 92)

Electronics

- *Front-End Electronics*

The development of front-end electronics is the responsibility of LBL with contributions from UCSC, KEK, Oxford and RAL.

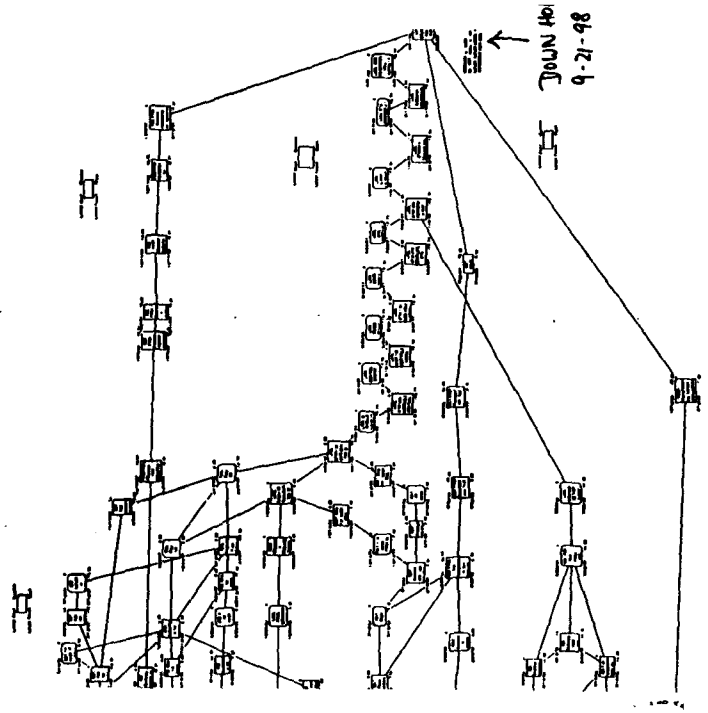
Scope

Front-end electronics for the silicon tracker includes:

1. The circuitry immediately associated with each detector, i.e., the readout chips with preamplifiers, shapers, comparators, time-stamping, data buffering, and sparse readout circuitry.
2. Bus selector chips that organize the signal flow to the output lines.

-Fiber optic drivers and associated circuitry, i.e., serialization and transceiver control are included under data acquisition.-

1071



1073

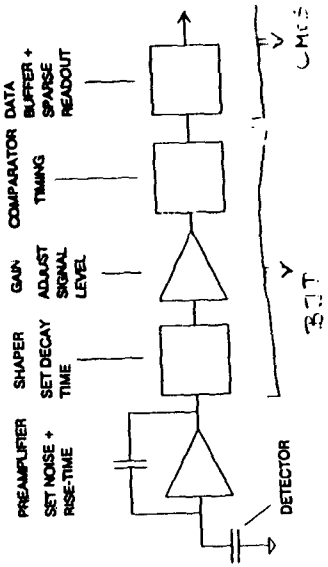


FIG. 1. BLOCK DIAGRAM OF FRONT-END SYSTEM

1074

Electronics Schedule

Mass production of electronics start summer 1994

A complete chip set representing the final design must be completed by fall of 1993.

This leaves FY92 and FY93 for the complete design cycle, which includes several iterations with interspersed tests.

A prototype front-end chain must be available by the end of FY92 to allow time for testing and subsequent iterations.

Architecture

The front-end electronics must meet the following specifications:

Noise	$Q_n < 1200$ electrons (i.e., S/N $\geq$ 20)
Timing accuracy	$t < 15$ ns for 1 fC $\leq Q_s \leq$ 8 fC
Peaking time	$\sim$ 20 ns
Power per channel	Pch < 1 mW (including data buffering and sparse scan)
Double-pulse resolution	$t_{\text{dead}} < 160$ ns
Inefficiency per channel	< 0.5% (including losses due to pile-up, circuit recovery time, finite buffer capacity, etc.)

The stages including the preamplifier through the comparator will be implemented with bipolar transistor IC's.

The time stamping and sparse readout circuitry will be implemented in radiation-hard CMOS.

• *Module Design and Cabling*

Detectors and their associated readout electronics will be combined in individually testable modules.

Critical issues are cross-talk from the readout chips to the detector and minimizing the mass.

Cabling for the silicon tracker electronics must also be of low mass and designed to provide adequate isolation, both within the bus, and between the bus and other parts of the system, especially the detectors.

Since the silicon tracker has several million channels of electronics, efficient on-chip data sparsification is crucial.

SILICON DETECTOR MODULES

READ-OUT CHIPS ON DETECTOR

DETECTORS MUST OVERLAP ELECTRONICS HYBRIDS FOR FULL COVERAGE

Electronics Tasks

Test system aspects, i.e. cabling, cross-talk and techniques that allow low-mass structures.

Produce a test system that includes all of the front-end electronics circuitry through the comparator output (bipolar transistor IC).

Produce a second prototype chip that implements time-stamping and some form of data buffering and sparse readout (rad-hard CMOS).

Details of FY92 work will be determined by the outcome of several key tests that are currently underway:

(1) Radiation tests of several commercial bipolar processes.

(2) Cross talk measurements on various detector-electronics-cable configurations.

(3) Initial circuit analysis and design of preamplifiers, shaping circuitry, and comparators

- *Data Acquisition and Triggering R&D*

This area is the responsibility of the collaboration members from the U.K., in particular the Rutherford Laboratory, Oxford and Bristol groups.

The work on data acquisition is related to fiber optic readout.

Three alternatives for the driver are under investigation (lasers, LED's and optical modulators) as well as a study of fiber radiation resistance.

Trigger studies are emphasizing the reconstruction of high transverse momentum tracks for a second-level trigger.

A specific second-level trigger scheme using hit patterns has been defined and an estimate of the number of trigger cards completed.

At lower priority, schemes for generating a contribution to the first level trigger are also under study.

IS THIS GENERIC ?

Detector Program

- *Barrel Detectors*

Development of rad-hard double-sided silicon detectors (DSSD's) is being continued by our Japanese collaborators in conjunction with Hamamatsu Photonics Company, in particular emphasizing the barrel part of the tracker.

Optimization of the DSSD's (minimize capacitance) P IMPLANTS VS FIELD PLATE ON N-SIDE

Extensive radiation damage tests will give a deeper understanding of the expected detector performance.

The schedule aims at producing barrel DSSD's in 1992 and an extensive beam test in 1993.

A consequence of the manufacturing runs in 1992 should be an understanding of the yield and cost for detector production.

Mechanical Engineering Tasks

Construction of a full-scale replica of a central region super-layer section with associated graphite support structures, kinematic supports, and an integral heat pipe cooling network.

The stability will be monitored with an external optical set-up.

Confirmation of data extracted from an internal fiber-optic optical position monitoring system which will become part of the overall detector assembly.

Demonstration of alignment/assembly concepts.

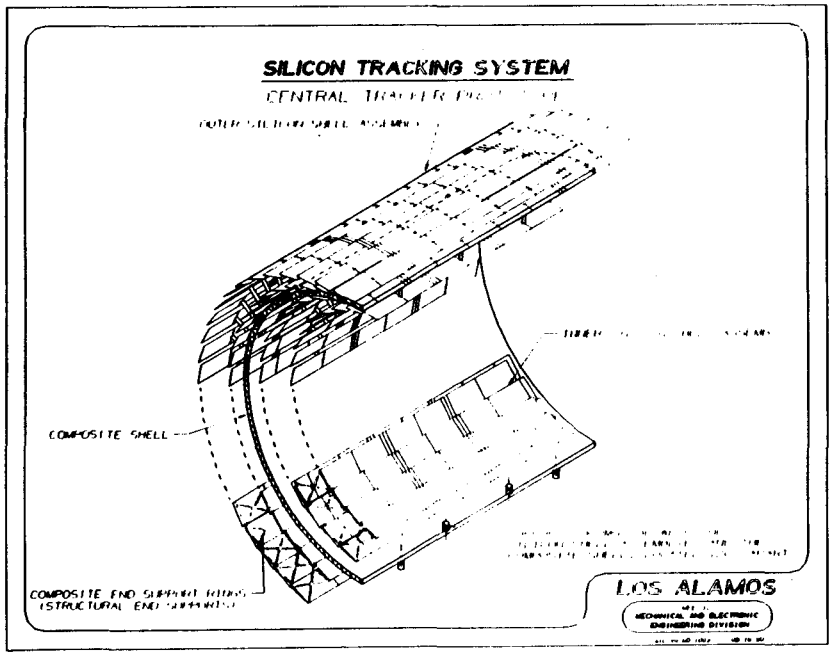
Demonstration of all steps essential to performing a highly repetitive, precision assembly operation.

Development and demonstration of opto-mechanical work stations suited to performing important elements of this task are planned.

Operational tests of the prototype central region for ES&H plans.

Compatibility tests of materials in a combined radiation and hydrocarbon environment (fully-active strip detector with associated cabling in an open butane vapor atmosphere).

1085



1086

• *Forward Detectors*

The development of the forward detectors, which are arranged in the form of disks, is being done at Lawrence Berkeley Laboratory, Johns Hopkins University, UC Riverside, University of Pittsburgh, and the University of New Mexico.

These detectors will be similar to the barrel ones in their functional design but their geometrical lay-out will vary.

As for the case of the barrel detectors, collaboration with Hamamatsu will continue. An alternative source of the forward silicon detectors is the Institute for Space Device Engineering in collaboration with the SDC collaborators from Dubna, U.S.S.R.

1083

Mechanical Engineering

The mechanical design work for the silicon tracker is being done at the Los Alamos National Laboratory.

Critical mechanical stability and cooling tests utilizing a prototype of the central region:

(1) wick development tests;

(2) design and construction of a graphite composite cooling ring;

(3) development of a mechanical support method for the silicon detectors.

1084

Silicon Tracking System

Silicon Strip Detector
- Fabricability
- Stress strain - reliability of bonded joints, stability characteristics
- Adhesives - material fluid compatibility in radiation environment

G E Structures
- Fabricability - ultralightweight, low Z cooling ring
- *Material stability - cooling fluid absorption*

Alignment Assembly
- Silicon strip detector array - repetitive placement to < 25 microns
- Silicon shell assembly alignment verification techniques
- Prototype stability demonstration by FY93

Cooling
- Wick performance characteristics
- Wick fabricability - construction defects, cost effective anufacturing techniques
- Functionality in a radiation environment

Los Alamos

1087

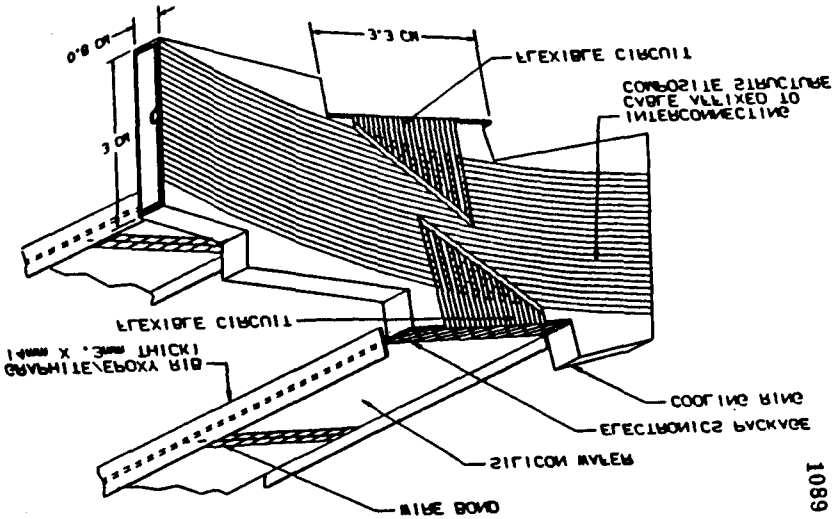
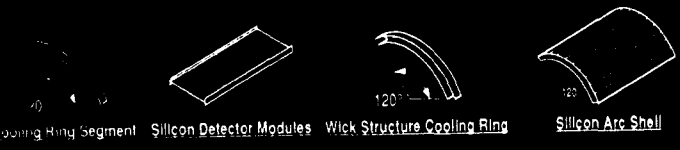


Figure 3-4. Graphite/epoxy cooling ring with silicon wafers and electronic components.

1089

Silicon Tracking System

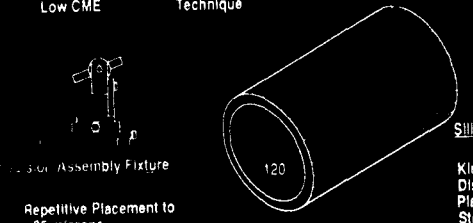


Fabricability of Ultralightweight G E Ring Materials for Stability
- High k_T
- Low CME

Fabricability
Fragility
Adhesive Materials Compatibility with Active Strip Detector Volume Assembly Technique

Optimize Performance Geometry
Investigate Transients
Fabricability Wick Structure via Molding

Ability to Structurally Withstand Thermal Cycle
Measure Temperature Gradients Under *Simulated Thermal* Loads
Precision Assembly Alignment of Silicon Detector Modules



Silicon Shell Development Unit

Kinematic Mount Demonstration
Disassembly Reassembly Precision Placement
Stability Under Static Conditions

Assembly Fixture

Repetitive Placement to < 25 microns
Alignment Inspection

Los Alamos

1088

SILICON TRACKING SYSTEM

Tasks

Enhance thermal conductivity transverse to wall
- K_T = 0.15 W/cm-K

Minimize moisture expansion
- CME < 20 ppm

Control thermal expansion
- 1 < CTE < 4 ppm/K

Tests Planned

Physical specimens

Physical tests: K, CME, CTE, and E

Material compatibility/outgas (photocarbon)

Heat pipe operation

Cooling ring

Options

Fillets - Particles
- Diamond, aperitcal
- Aluminum nitride, flakes

Shorter fibers, 80-100 microns

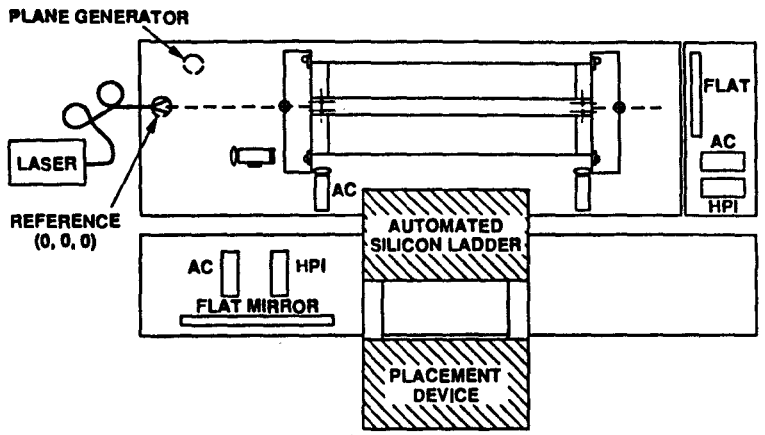
Epoxy/cyanate resin

Cyanate resin

Fiber modulus

1090

ALIGNMENT - ASSEMBLY



1093

BUDGETS AND SCHEDULE

R&D priorities for next year, have been organized in order to:

A – Establish Proof of Principle for the unique aspects of the SSC silicon tracker.

B – Complete the design to allow further costing and confidence that our contingency estimates are correct.

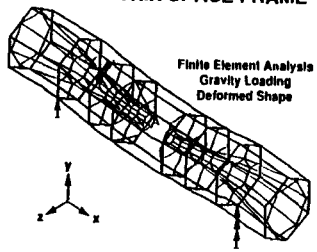
C – Remain on schedule for 1999 installation.

1094

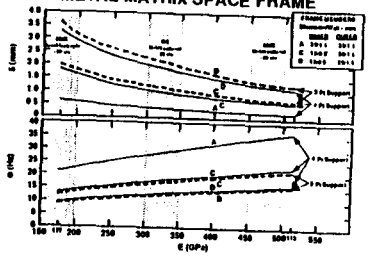
MG 53

SPACE FRAME STRUCTURE

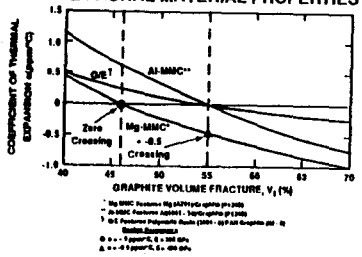
METAL MATRIX SPACE FRAME



METAL MATRIX SPACE FRAME

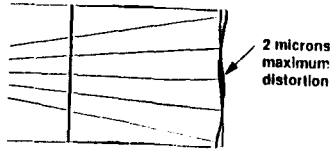


UNIDIRECTIONAL MATERIAL PROPERTIES



DETECTOR THERMAL ANALYSIS

Average CTE = -0.5 ppm/°C
ΔT = -20°C
Overall Length Expansion = 0.055 mm



Local CTE variations = ± 0.1 ppm/°C

1091

Los Alamos

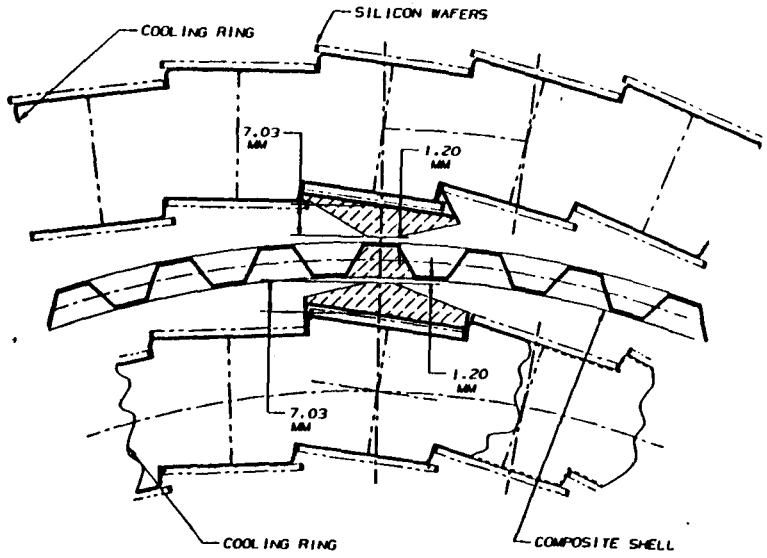


Figure 1. Three-point kinematic mounting scheme with mechanism mounting space shown in crosshatch.

1092

TABLE 2 FY 1992 SILICON TRACKER R + D COSTS

TASK (cont)	GOALS	PROTOTYPES/TESTS	COST $K LABOR	COST $K MATERIALS	TOTAL
COOLING RING PROTOTYPE DEVELOPMENT	O DEMONSTRATE FABRICABILITY WITH 120 DEG. ARC SEGMENT	O TOOLING PROTOTYPE COMPRESION MOLDS O G/E RING PROTOTYPES	$160	$95	
	O ACHIEVE THERMAL CONDUCTIVITY ENHANCEMENTS FOR ELIMINATING EXCESSIVE THERMAL GRADIENTS	O MATERIAL PHYSICAL SPECIMENS TESTS O FULL RING ASSEMBLY (120 DEG. SEGMENTS)			
	O ACHIEVE TAILORED G/E MATERIAL PROPERTIES - LOW MOISTURE ABSORPTION				
SILICON DETECTOR MODULE	O DEMONSTRATE CONSTRUCTION OF EDGE BONDED SILICON LADDER ASSEMBLY	O TOOLING PROTOTYPE VACUUM CHUCK HOLDING FIXTURE	$160	$80	
	O DEMONSTRATE STRUCTURAL INTEGRITY OF MODULE USING ROOM TEMP. CURING ADHESIVE FOR FACILITATING HIGH PRODUCTION RATES AND MINIMIZING INTERNAL RESIDUAL STRESSES	O THERMAL BEHAVIOR OF ADHESIVE UV CURING PRODUCTS O STRUCTURAL COMPONENT TEST O MODULE RADIATION/MATERIAL COMPATIBILITY TESTS			
	O DEMONSTRATE MATERIAL COMPATIBILITY USING ACTIVE STRIP DETECTOR				
	O PRODUCE SUFFICIENT MODULES FOR 120 DEG ARC SILICON SHELL AND FULL SILICON PROTOTYPE SHELL				
WICK DEVELOPMENT	O COMPLETE INVESTIGATION OF POLYSTYRENE - THERMAL RESISTANCE MEASUREMENTS - TRANSIENT BEHAVIOR	O TEST VARIOUS POLYSTYRENE WICK THICKNESSES/ GEOMETRICAL SHAPES O 120 DEG. ARC WICK SEGMENT TOOLING PROTOTYPE	$200	$80	
	O PRODUCE 120 DEG. ARC SEGMENT WICK WAIRTERY	O CONDUCT 120 DEG. ARC COOLING RING TESTS O CONDUCT 120 DEG. ARC SILICON SHELL			
	O UPGRADE WICK FACILITY TEST TO ENCOMPASS TEST OF FULL SILICON SHELL PROTOTYPES	PROTOTYPE TESTS			
ALIGNMENT/STABILITY MEASUREMENTS	O DEVELOP ALIGNMENT/ASSEMBLY CONCEPT FOR PLACEMENT/BONDING SILICON DETECTOR MODULES ONTO 120 DEG. ARC SHELL AND/OR FULL SHELL PROTOTYPE	O OPTICAL ALIGNMENT UNIT COMPATIBLE WITH OPERATOR CONTROLLED MECHANICAL ASSEMBLY	$250	$100	
	O DEVELOP MEANS OF MEASURING SILICON STRUCTURE STABILITY TO <5 MICRONS	O METROLOGY LIKE MEASUREMENTS DETERMINING STABILITY OF SILICON STRUCTURES AND COMPONENT MATERIAL PROPERTIES			
	O DEVELOP ALIGNMENT/STABILITY MEASURING TECHNIQUES SUITED TO ANY GEOMETRY, NOT "RESTRICTED TO SILICON BARREL" GEOMETRY	O ENVIRONMENTAL CONTROL CHAMBER FOR COMPONENT TESTS AND MATERIAL TESTS			

A The unique aspects, also critical for costing, are:

(1) Rad-hard electronics with sufficient speed and signal-to-noise.

(2) Simultaneous input/output system functionality; i.e., no interference between clocks and analog front ends.

(3) Double-sided detectors with capacitance/cm of $\leq$ 1.2 pF, stable under radiation. Need both rectangular and wedge-shaped shapes.

(4) Wick heat removal system.

(5) Very light mechanical system stable to 5 μm.

(6) Large system which can have assemblies removed and replaced.

C To remain on schedule:

(7) Electronics/mechanical integration.

(8) Development of large scale mechanical support structure.

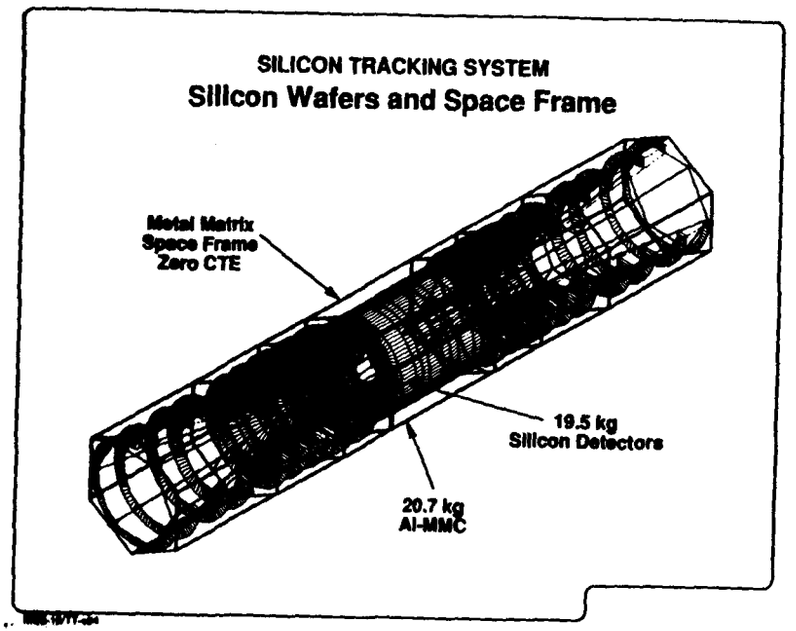
(9) Material compatibility tests.

TABLE 2 FY 1992 SILICON TRACKER R + D COSTS

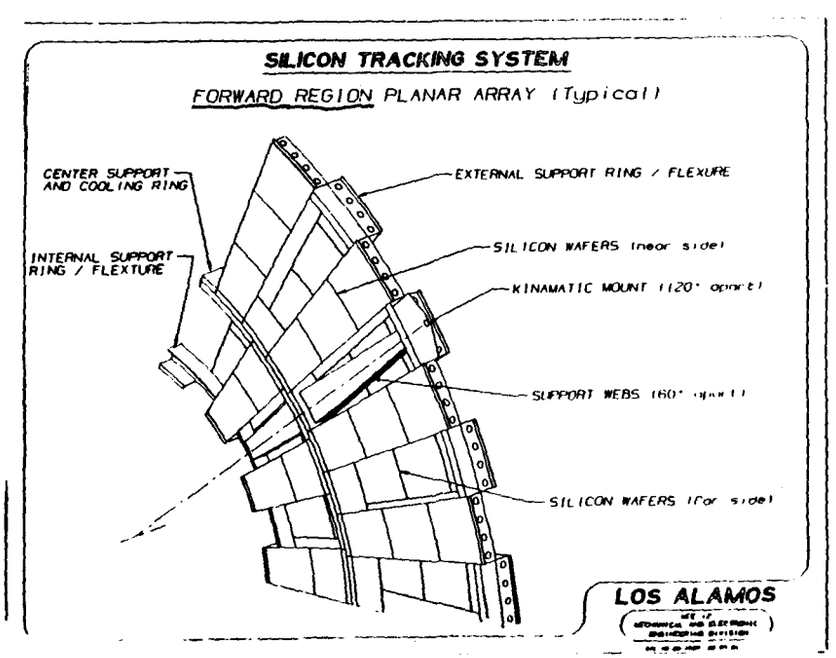
TASK (cont)	GOALS	PROTOTYPES/TESTS	COST $K LABOR	COST $K MATERIALS	TOTAL
CENTRAL REGION PROTOTYPE	O DEVELOP OPERATOR-CONTROLLED MECHANICAL ASSEMBLY UNIT FOR SILICON DETECTOR MODULE	O PROTOTYPE TESTS OF OPERATOR CONTROLLED MECHANICAL ASSEMBLY UNIT FOR SILICON MODULES	$118	$75	
	O ASSEMBLE 120 DEG. ARC SILICON SHELL UNIT	O COOLING TEST OF 120 DEG. ARC SHELL ASSEMBLY			
	O DEVELOP KINEMATIC MOUNT SUPPORT FOR COOLING RING/SILICON SHELL STRUCTURE	O PROTOTYPE LOW MASS, LOW 2 KINEMATIC MOUNT	$124	$20	
	O BUILD COMPLETE SILICON SHELL MODULE	O CONDUCT STATIC STABILITY TESTS	$130	$55	
	O DEMONSTRATE SILICON DETECTOR MODULE PLACEMENT TO 25 MICRONS	O FRAGILITY TESTS OF PARTIAL SILICON SHELL ASSEMBLY			
		SUBTOTAL (MECHANICAL)	$1,140	$515	$1,655
		GRAND TOTAL	$2,040	$905	$2,945

TABLE 2 FY 1992 SILICON TRACKER R + D COSTS

TASK	GOALS	PROTOTYPES/TESTS	LABOR	COST $K MATERIALS	TOTAL
TECHNICAL MANAGEMENT	O PREPARE PROPOSALS, BUDGETS & OVERSEE SCHEDULE	UCSC	$30	$0	
MECH ENG MANAGEMENT	O PREPARE PROPOSALS, BUDGETS & OVERSEE SCHEDULE	LANL	$60	$0	
PROPOSAL SUPPORT	O ELABORATION OF DESIGN FOR PROPOSAL	LANL	$100	$0	
		SUBTOTAL (PROJECT MANAGEMENT)	$190	$0	$190
DOUBLE SIDED DETECTOR DEVELOPEMENT	O FABRICATE DOUBLE SIDED DETECTORS WITH FIELD PLATE ISOLATION	O COMPARE CAPACITANCE & RADIATION RESISTANCE OF FIELD PLATE AND P-IMPLANT ISOLATION	$0	$60	UCSC
DETECTOR MODULE	O COMBINE DETECTORS & FRONT END ELECTRONICS TO INDIVIDUALLY TESTABLE MODULES	O TEST RADIATION HARDNESS & CROSSTALK O TEST DIFFERENT SHIELDING TECHNIQUES	$170	$50	LBL
CABLES	O DEVELOPE LOW MASS CABLES O LAY OUT CABLING PLAN	O TEST NOISE ISOLATION CABLES O TEST POWER BYPASSING	$40	$40	LBL
BIPOLAR FRONT END CHIP	O DESIGN, FABRICATE & TEST CIRCUIT BLOCKS O DESIGN, FABRICATE & TEST FULL MULTICHANNEL ARRAY	O TEST RADIATION HARDNESS, NOISE, TIME WALK, POWER CONSUMPTION, & DEAD TIME	$270	$125	LBL / UCSC
CMOS DATA STORAGE CHIP	O DESIGN, FABRICATE & TEST TEST CIRCUITS (MOSIS) O DESIGN & FABRICATE FULL SIZE RAD HARD CHIP	O TEST RADIATION HARDNESS O TEST DIGITAL TIME STAMPING & DATA BUFFERING O TEST SPARSE SCAN READOUT	$230	$115	LBL / UCSC
		SUBTOTAL (DETECTORS/FRONT END ELECTRONICS)	$710	$390	$1,100



1101



1102

Contributions other than SSC R & D Funds

- Technical Management, $90 - UCSC
- 1/2 FTE for radiation testing,$47 k (from Texas) - UCSC
- 1 1/2 Technician FTE for chip testing - UCSC
- Development of detectors with p isolation - Japan
- Development of wedge-shaped detectors (from Texas) - Johns Hopkins
- Development of fiber readout and DAQ - U.K.
- One bipolar fabrication run, $85 k (from Texas) - UCSC

1099

TASKS not included in FY92 Budget

C Electronics:

Bus Selector Chip

Transmission Protocol

C Mechanical:

Forward Region

Space Frame

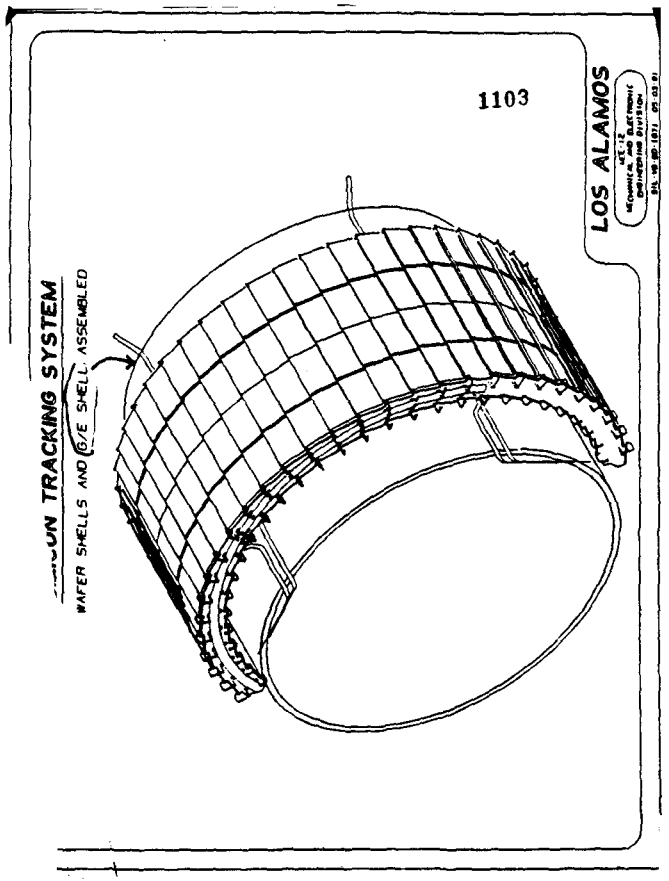
Graphite Shell

Full arc Cooling Ring

Outer Gas Enclosure

Beam Pipe

1100



1105

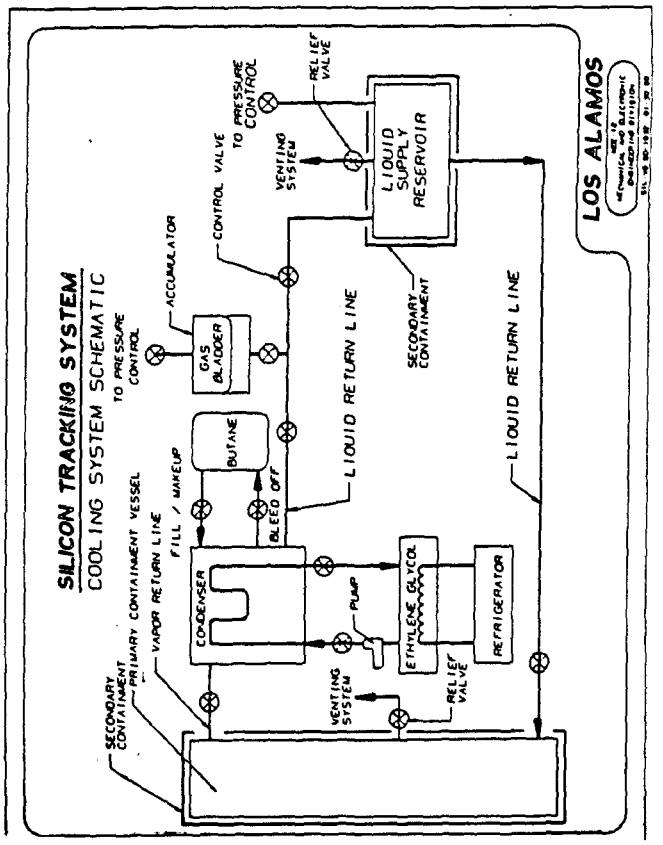


Table 1. Silicon Subsystem R&D Milestones for Next Year

Milestones and Goals	Date
1. Front-end Electronics	
Establish final design parameters	10/91
Fabricate first prototype preamplifier/shaper/comparator chip	12/91
Fabricate second prototype front-end chip	4/92
If necessary, third iteration of chip	8/92
Determine architecture for time stamping/data buffering	12/91
Fabricate prototype chips as necessary using MOSIS to test circuit concepts, followed by fabrication of rad-hard digital chip	7/92
Preliminary design of data transmission system	8/92
Complete prototype data-transmission system for initial system tests	7/92
2. R&D, Double-Sided Detectors (DSSD), Barrel Geometry	
Prototype full-length DSSD	11/91
Test prototype	2/92
Mock-up detector with LSI chip	3/92
Prototype of final DSSD	8/92
Combine detectors, chips, bussing	9/92
Beam and radiation test	9/92
3. R&D Forward Disk Detectors	
Finalize size and arrangement of disk detectors	11/91
Mask specifications for given design	1/92
Procurement of wedge detectors specific to SDC geometry	4/92
Testing, DC and signal characteristics	7/92
4. Major Mechanical R&D	
Cooling ring development complete	2/92
Cooling ring fabrication for prototype	6/92
Study of adhesives, candidates established	12/91
Prototype Si detector assemblies fabricated	2/92
Si-shell assembly tooling complete	1/92
Start component-shell final development	6/92
Precision prototype alignment test complete	6/92
Assemble shell	8/92
Forward region concept definition	3/92

Conclusions

- 1988–1991 R&D has answered many basic questions:
  Radiation hardness of detectors and electronics;
  Low-noise electronics with low power consumption;
  Evaporative cooling concepts;
  Material studies for modules, space frames, cylinders, etc.;
  F.E.A. for stability;
  Alignment / assembly concepts.
- 1992 R&D plan covers essential engineering tasks to evaluate unique aspects of the silicon tracker:
  Fabricate chips and detectors, build mechanical structures and modules, build tooling for alignment and assembly.
- Limitation in funding forces delay in engineering : forward structure, space frame, graphite shell, enclosure, chip development.
  Note that there are large non-SSC contributions: foreign countries (Japan, U.K.), Texas, Universities, unburdening of rates (LBL, LANL, UCSC).
- Schedule for 1999 turn-on is in jeopardy without increased funding.

Silicon Detector Development in Japan

H. Miyata(Niigata)

H. Miyata SDC Meeting at Oak Ridge

1108 (A)

Silicon Detector Development in Japan

T. Ohsugi and Y. Chiba (Hiroshima Univ.)
H. Ikeda, N. Ujiie, Y. Unno and M. Tanaka (KEK)
N. Tamura (Okayama Univ.)
K. Niwa and M. Nakamura (Nagoya Univ.)
H. Miyata (Niigata Univ.)
M. Daigo (Wakayama Medical)
S. Kobayashi and A. Murakami (saga Univ.)
J. Haba and Y. Nagashima (Osaka Univ.)

1109

SSD R&D Subject in Japan

I. Detector Integration
 (1) Mechanical Evaluation Samples
 (2) Microbump Bonding and Double Side Wire Bonding
 (3) Wafer Aligner

II. Double Sided Strip Detector
 (1) Capacitance Evaluation Samples
 (2) High Bias Tolerant AC Coupling Detector ($V_{Bias} \geq 100$ V)
 (3) Environmentally Robust Detector (Passivation of SiN?)
 (4) Full Size DSSD Prototype

These 2 subjects concern to Popcorn Noise.

III. Radiation Damage Study
 (1) SSD with Polysilicon Resister
 (2) Popcorn Noise and Leakage Current Increase
 (3) Effect of Bias Voltage Feed during Irradiation
 (4) Future Beam Test Plan

I. Detector Integration
 (1) Mechanical Evaluation Samples

1110

 1) For the test of mechanical mock-up
  1. SSD Alignment
  2. SSD Glueing
  3. Bonding
  4. Accuracy of the Dimension of SSD senser (Position of Fiducial mark etc.)

 2) No connection to readout electronics

 3) Samples
  1. Single Sided Samples — Available by the End of Sep.
   P side (Axial Strips) : 120 Samples — Done
   N side (Stereo Strips) : 120 Samples — Almost
  2. Double Sided Samples — Available in Oct.
   120 Samples — Need to check before final prod.
  3. Cut Samples
   For the test of Wafer Aligner
   No strip patterns
   40 Samples have been made.

(B)

1111 -1-

Specification of Mechanical Evaluation Sample

T. Ohsugi

To develop mechanical and electrical integration ideas and techniques, mockup barrel detector element (double sided strip) which has demensions of real detector should be designed and be prepared to the integration study group.

This is the first idea of the specification (geometrical) of the barrel detector element.

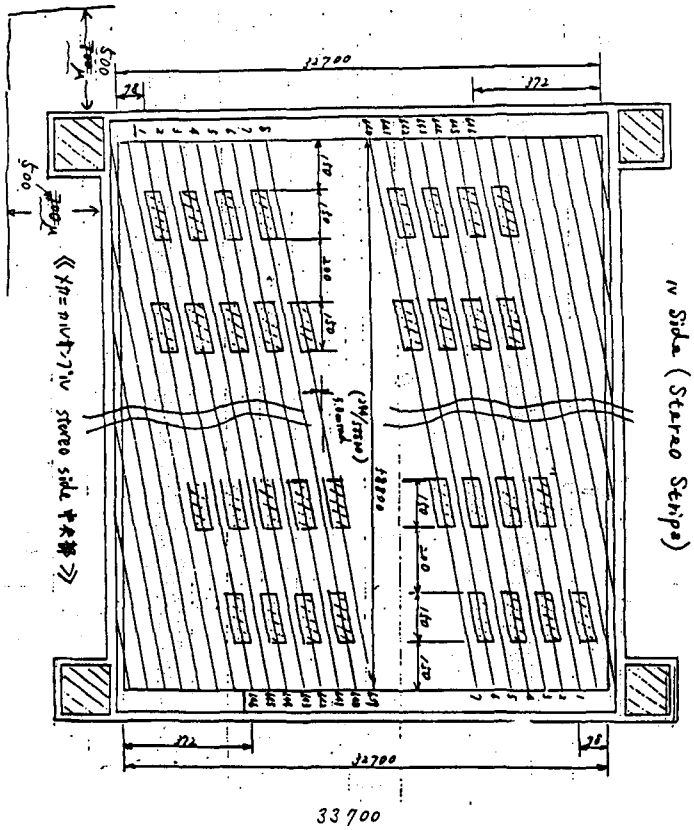
Specification:
Only Al electrode is installed.

Double sided polished substrate
size: 33.7 mm x 57.6 mm

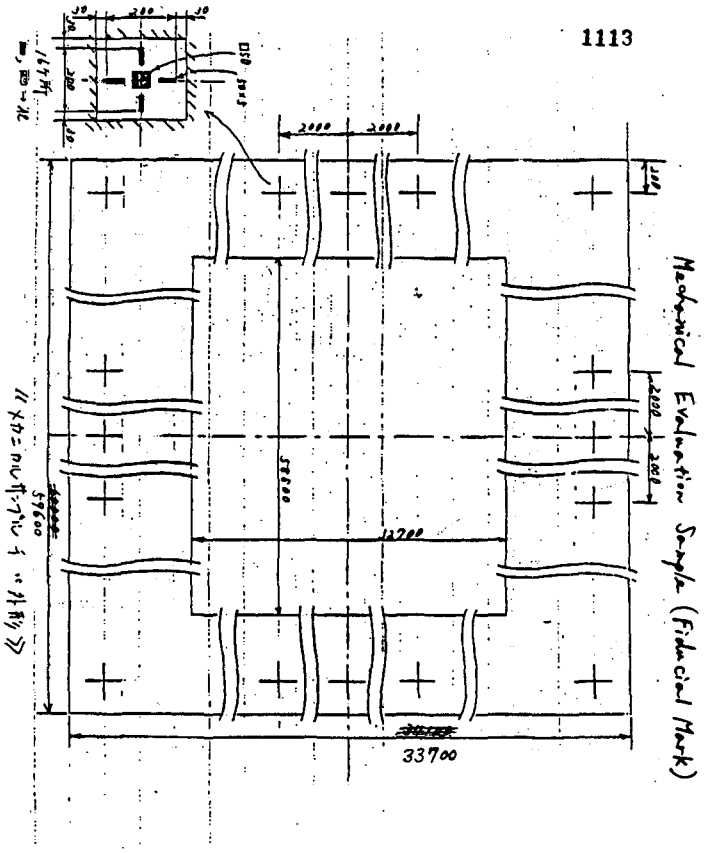
strip geometry:
normal strip side: 50 μm pitch parallel, 60 mm long.
slant strip side: 5 mradian tilted compared with normal strip (started at the same edge of normal strip, and ended at 6 advanced normal strip edge).
bonding pad: placed inside guard ring.
size -- 50 μm x 150 μm
implemented on both side
Strip number should be printed at both edge of strips.

Edge Space : 500 μm

1112



1113



(2) Microbump Bonding and Double Side Wire Bonding

1114

Microbump Bonding

Developed in 1987 by Matsushita Elec. Co.

50 μm pitch and 300 μm thick silicon bonding has no problem, except for Radiation Damage of Resin.

1) Bump

Material : Au, Indium

Diameter : 5 μm

2) Resin

Acrylic with a mixture of 8 types of resins

Cured by UV light

Dielectric constant : $\sim$3.7

Resin will be soft over 70 $\sim$ 80°C

3) Radiation Damage Test of Resin

5 kinds of resins were exposed to ^{60}Co γ up to 5 Mrad

Mechanical, Electrical Test : Looks OK

But found possible evidence of severe shrink.

This might hurt SSD.

Next test will be for Neutron.

Double Side Wire Bonding

→ Wafer Aligner

1115

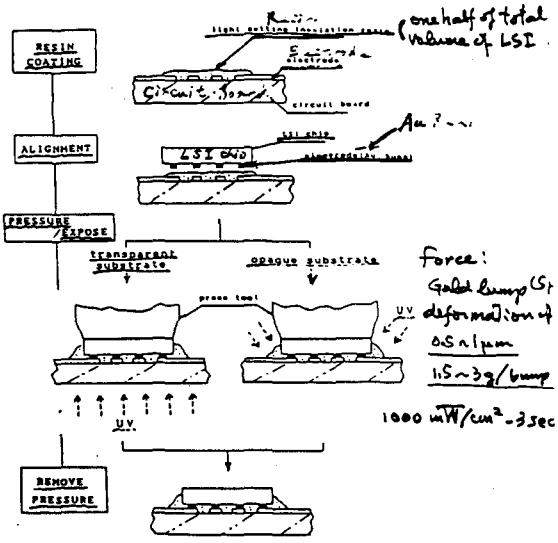


Fig. 2. Process of microbump bonding method.

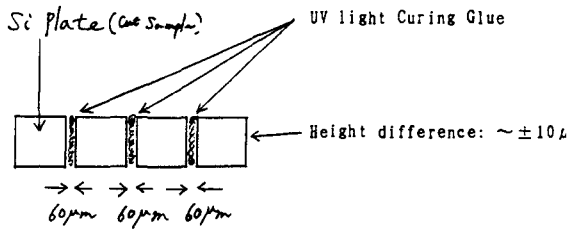
(3) Wafer Aligner

Wafer Aligner has been designed and being fabricated at KEK by Kohriki-san for development of techniques of

a) Glueing between detectors for making ladder.

b) Double sided wire bonding. — DSSD Sensor (33mm×

{Yamamoto-san (Hamamatsu) Meeting Sep. 21 (a)



This project is not for SDC proper. Budget is from different source.

II. Double Sided Strip Detector

(1) Capacitance Evaluation Samples

For the minimization of detector capacitance.
Samples will be available by the End of Nov.

1) P side samples : 20 pieces (= 5 wafers)

- P side: 4 different width of p strip on one wafer
  6, 10, 20, 30 μm
- N side: Flat plane

2) N side samples : 20 pieces (= 20 wafers)

- P side: Flat plane
- N side: All combinations of 3 different n^+ strip width x 4 different p^+ isolation channel on one wafer.

n^+ strip : 6, 10, 20 μm
p^+ isolation channel : 6, 10, 20, 24 μm

Implantation density : $\sim 10^{14} B/cm^2$

Capacitance Measurement Samples

Length:	6 cm
Pitch:	50 μm
No. of channels:	64
Width:	3.4 mm

Strip Geometry

p-side samples;

p-strip width: 6 μm, 10 μm, 20 μm, 30 μm.

n-side samples;

n-strip width: 6 μm, 10 μm, 20 μm,

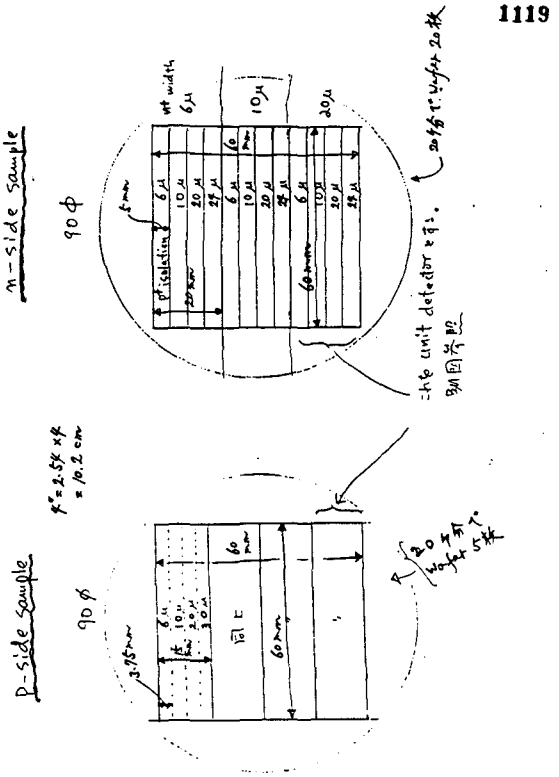
each of these is combined with following four p-isolation width: 6 μm, 10μm, 20 μm, 24 μm.

Edge Space : 300, 500, 700, 900μm

1991 ~~Oct~~ T-D

Capacitance Measurement Sample.

n-side sample



p-side sample

(4) Full Size DSSD Prototype

Additional funding ($70K) has been approved for this work by JSD Executive Board.
This prototype (Sensor) will be available by the End of April, 1992.
Goal of this work will be to measure Cosmic Rays.
(In Fall, 1992 with Ladder Detector)

1) Senser

DSSD 33 mm x 60 mm
640 channels on each side (Axial & Stereo)

2) Readout Electronics

We hope it will be supplied from LBL.

II. Radiation Damage Study

(1) SSD with Polysilicon Resister

The bias feeding resister of Polysilicon seems to be stable?

1) The voltage drop at the resister is much smaller in this case than those in the previous case with Punch-Through and Accumulation Layer.
(≲0.5V)
P side (≲30V)
N side (≲15V)

2) Isolation between strips keeps being good for the irradiation of 4 Mrad.
$R_{ss} \approx 1M\Omega$

The results will be written up as a SDC report.

P side

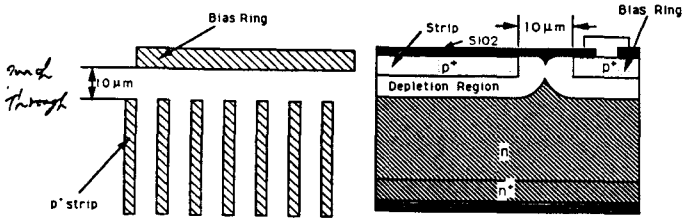


Fig. 1(a) Fig. 1(b)

N side

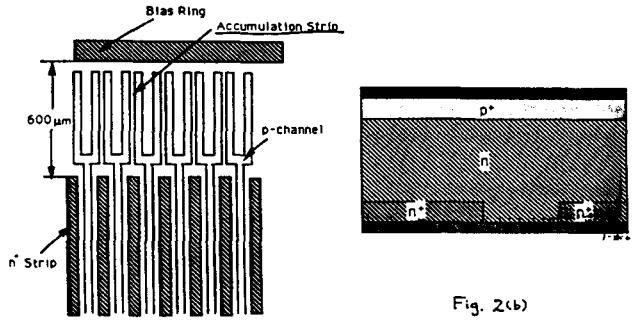
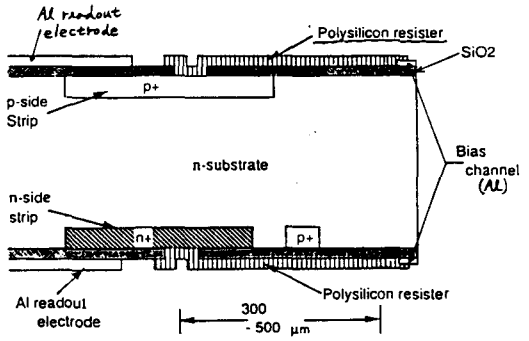


Fig. 2(a) Fig. 2(b)

Polysilicon biased DSSD

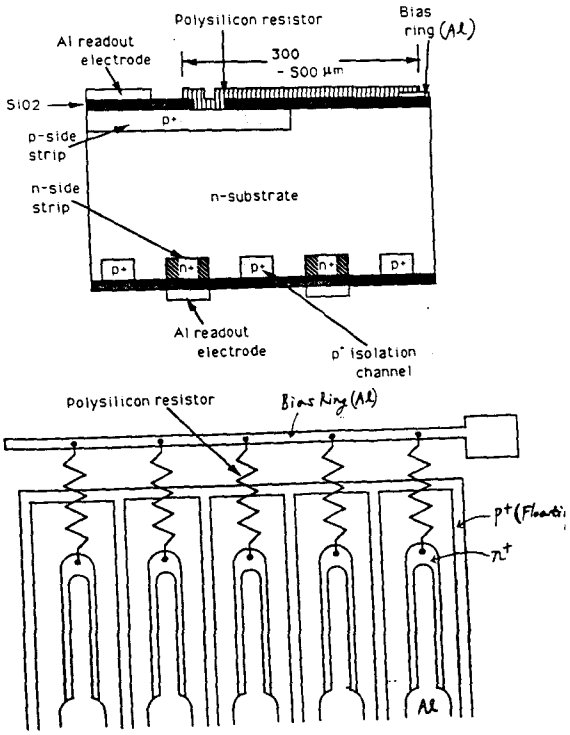


Size: Active Area of 6.4 x 6.4 mm^2
Thickness: 300μm Strip pitch: 100μm
Bulk: ~ 4 kΩ n-type
Bias Supply Resister,
p-n Junction side: — Polycrystalline Silicon (5μmW) (~400 kΩ)
n+ ohmic contact side: — Polycrystalline Silicon (5μmW) (450~ 700 kΩ)

Channel Isolation of n-side;
floating p+ surrounding n+ strip;
Two different implantation density on p+
1) 5 x 10^{12} B per cm^2 (≈ 10^{17} B per cm^3) Nb1
2) 10^{14} B per cm^2 (≈ 10^{19} B per cm^3) Nb2

Polysilicon biased DSSD

1124



3

1125

N Side

Voltage difference btwn Bias & Strip Accumulation Layer

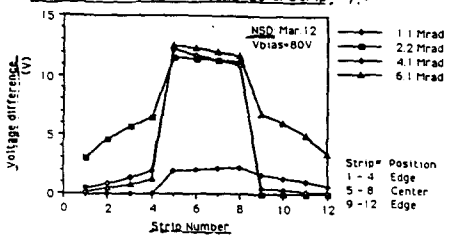


Fig. 10(a)

P Side

Voltage differnce btwn Bias & Strip punch Through

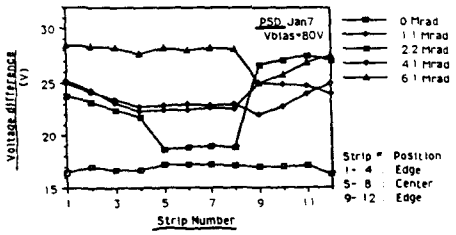


Fig. 10(b)

N Side

Voltage Drop @ Biasing Resistor Poly silicon

1126

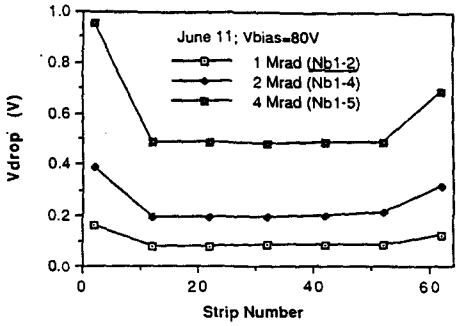


Fig. 12(a)

V Side

Voltage Drop @ Biasing Resistor Polysilicon

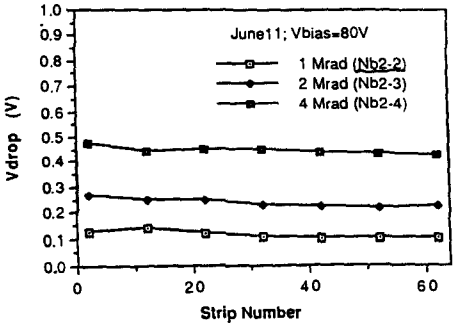


Fig. 12(b)

P Side

Inter-strip Isolation punch Through

1127

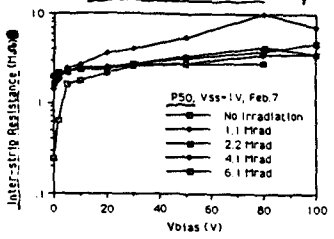


Fig. 9(a)

P Side

Interstrip Isolation Poly Silicon

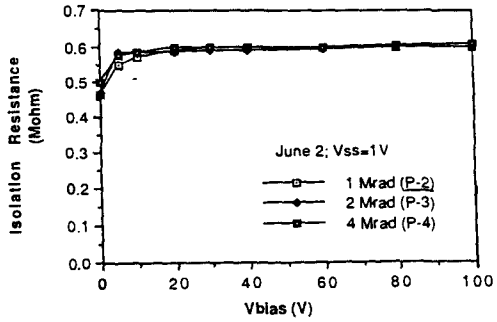


Fig. 9(b)

(2) Popcorn Noise and Leakage Current Increase

1) Preliminary Result

1128

1. DC coupling readout is better than AC coupling.
2. Floating of AC readout terminal is better than grounded.
3. Previous types of SSD which are using "Punch Through" or "Accumulation Layer" look better than SSD with polysilicon.

2) Discussion with Yamamoto-san

We had meeting with Yamamoto-san at Hamamatsu on Sep. 21 about this problem.

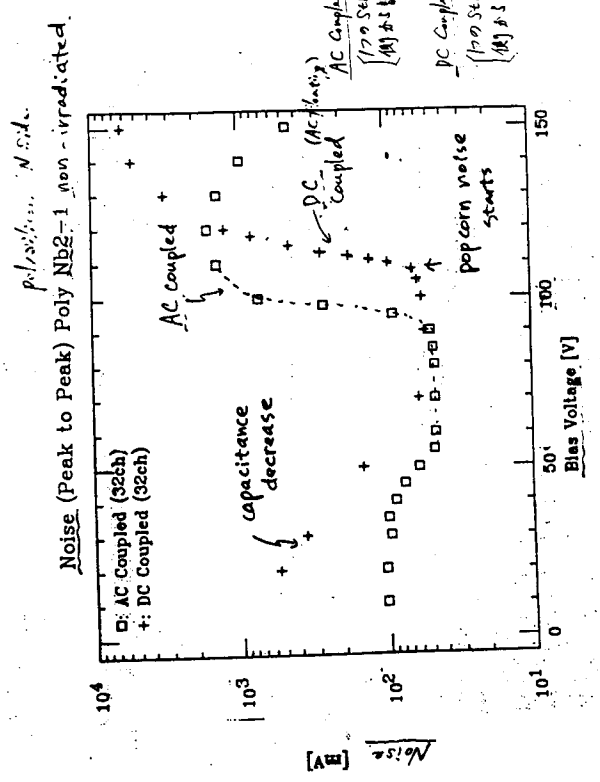
The reason of the popcorn noise and leakage current increase above ~100V is. [redacted]

These SSD's are designed to use with Bias Voltage of less than ~80V.

3) "New Polysilicon SSD"

Yamamoto-san will design "New Polysilicon SSD" which can be used with higher Bias Voltage.

1129



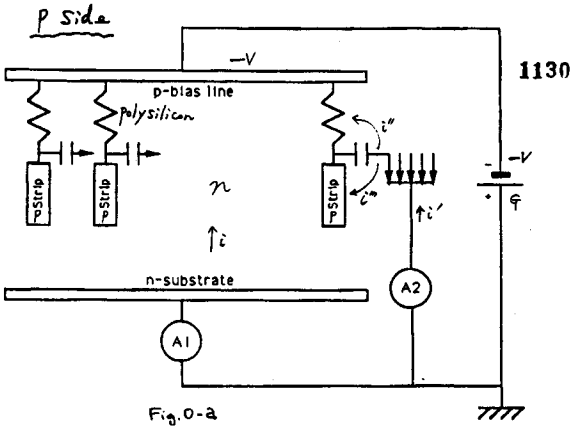
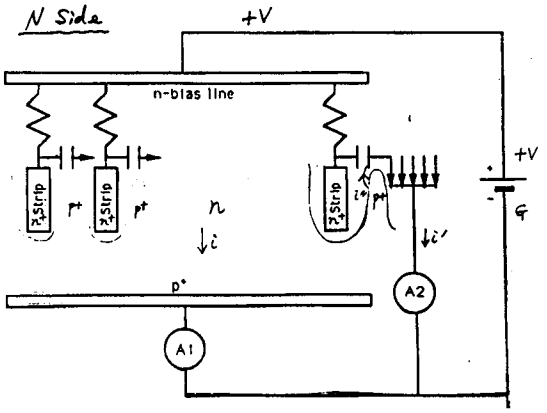


Fig.0-a

1130



1131

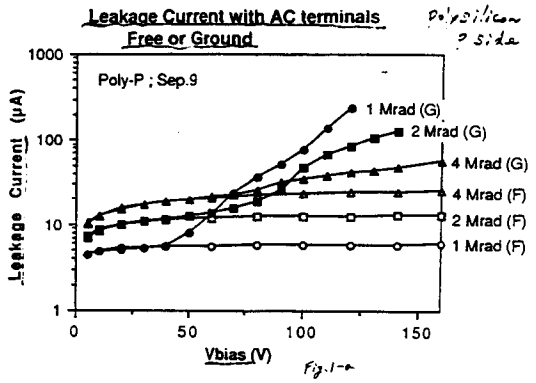


Fig.1-a

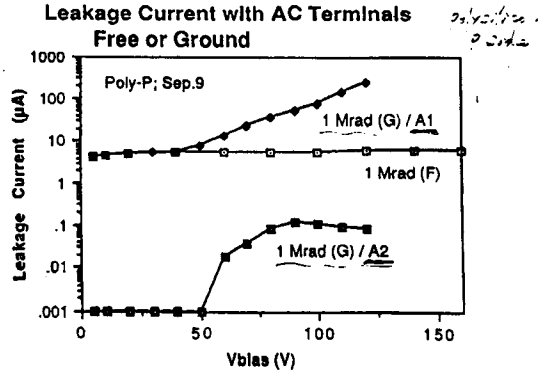


Fig.1-b

1132

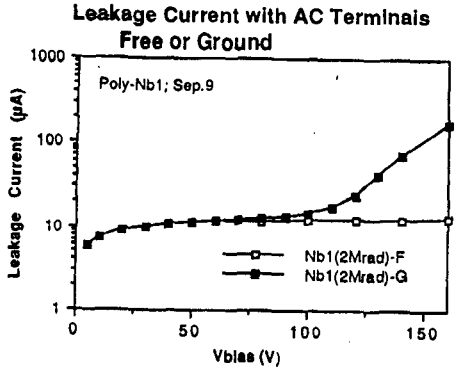


Fig.2-c

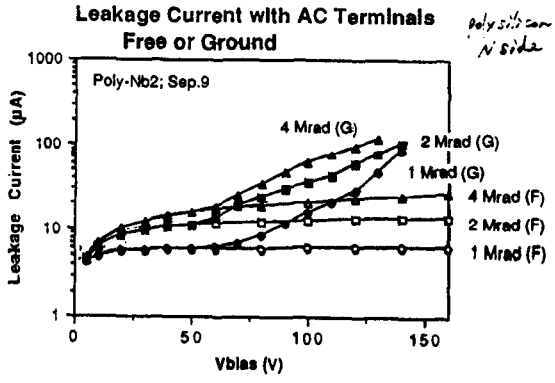
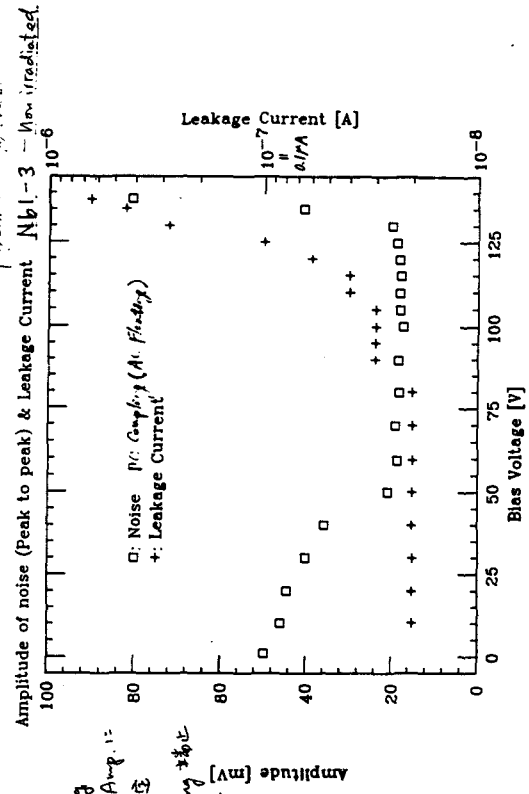
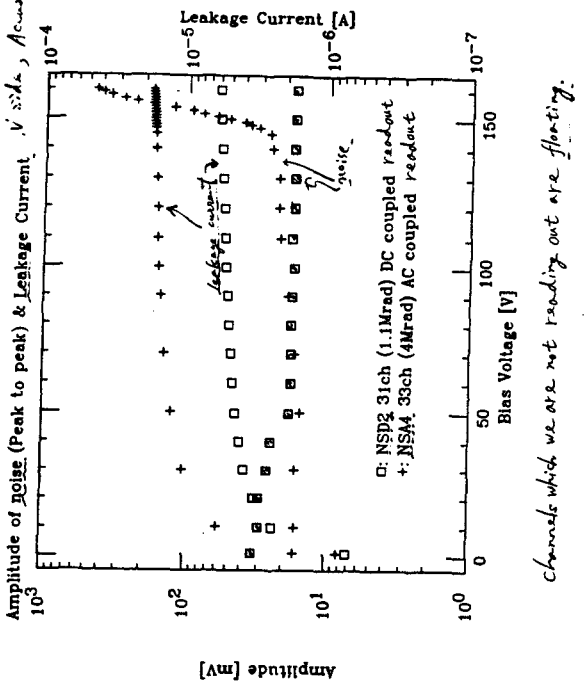


Fig.3

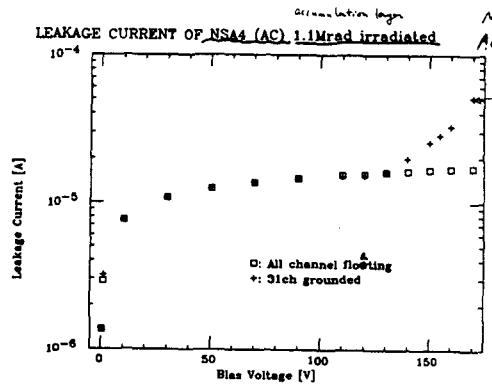
1133

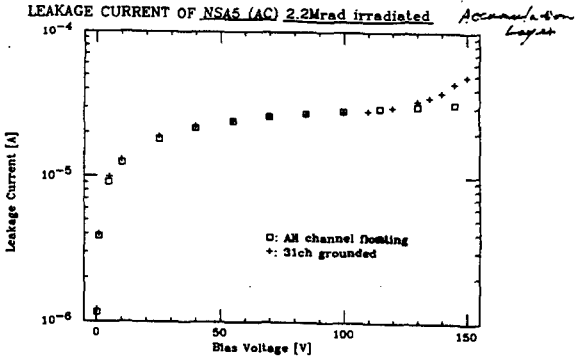


1134



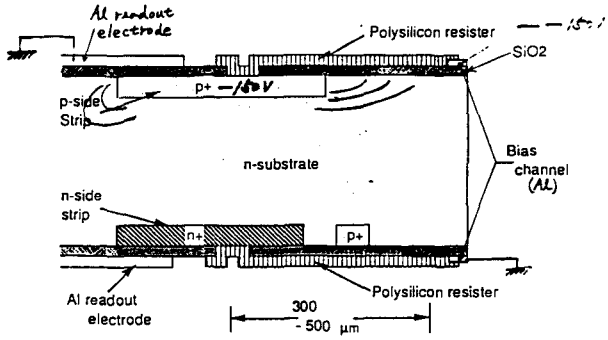
1135





Polysilicon biased DSSD

1136

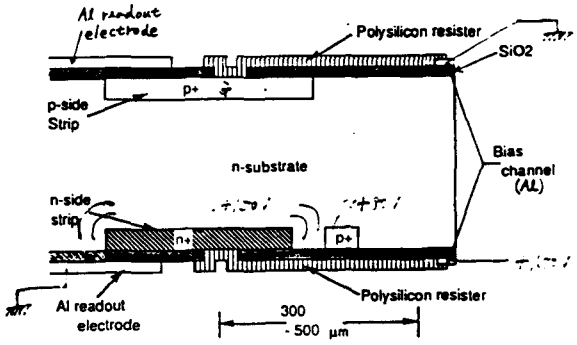


Size: Active Area of 6.4 x 6.4 mm^2
Thickness: 300μm Strip pitch: 100μm
Bulk: ~ 4 kΩ n-type
Bias Supply Resister,
p-n Junction side: — Polycrystalline Silicon (5mm)
(~400 kΩ)
n+ ohmic contact side: — Polycrystalline Silicon (5mm)
(450~ 700 kΩ)

Channel Isolation of n-side;
floating p+ surrounding n+ strip;
Two different implantation density on p+
1) 5 x 10^{12} B per cm^2 (≈ 10^{17} B per cm^3) Nb1
2) 10^{14} B per cm^2 (≈ 10^{19} B per cm^3) Nb2

Polysilicon biased DSSD

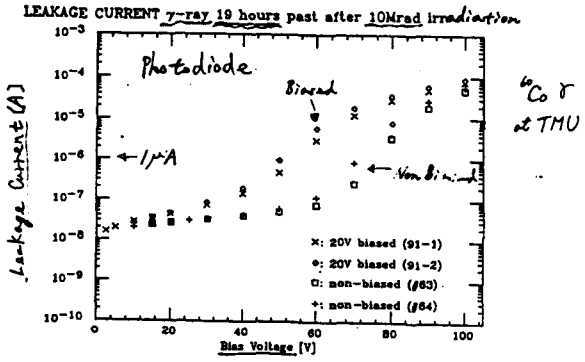
1137

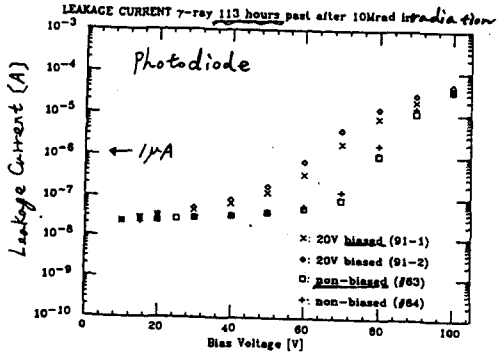


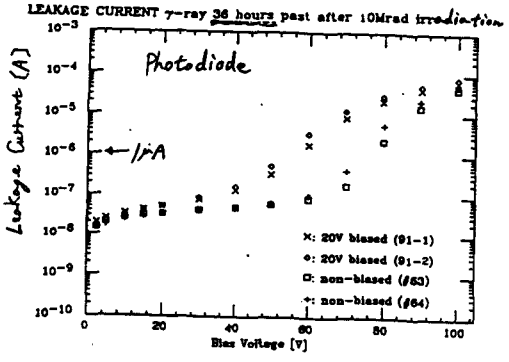
Size: Active Area of 6.4 x 6.4 mm^2
Thickness: 300μm Strip pitch: 100μm
Bulk: ~ 4 kΩ n-type
Bias Supply Resister,
p-n Junction side: — Polycrystalline Silicon (5mm)
(~400 kΩ)
n+ ohmic contact side: — Polycrystalline Silicon (5mm)
(450~ 700 kΩ)

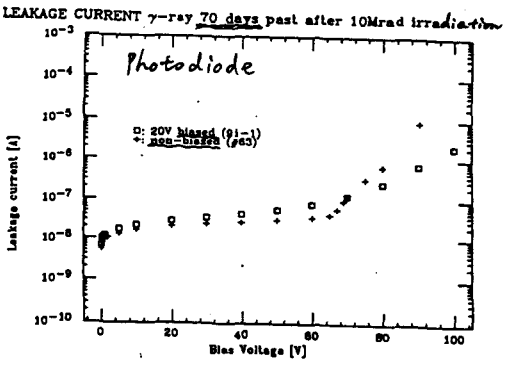
Channel Isolation of n-side;
floating p+ surrounding n+ strip;
Two different implantation density on p+
1) 5 x 10^{12} B per cm^2 (≈ 10^{17} B per cm^3) Nb1
2) 10^{14} B per cm^2 (≈ 10^{19} B per cm^3) Nb2

(3) Effect of Bias Voltage Feed during Irradiation 1138







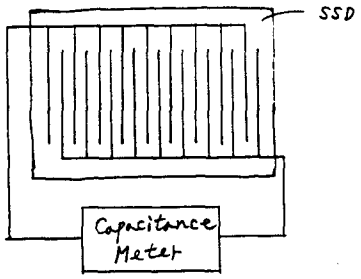


(4) Future Beam Test Plan

Beam test will be done for following samples at RCNP (Proton 65 MeV, Osaka Univ.) in March 1992.

1) Newly Desinged DSSD with Polysilicon for Higher Bias Voltage (~150V).
   6.4 mm x 6.4 mm, 100μm pitch, 64 ch AC coupling readout, With the Bias Voltage through the irradiation

2) Capacitance Measurement Sample (We have now).
   6.4 mm x 6.4 mm, 100μm pitch, 64 strips
   Strips are connected each other once in 2 strips.



Overview of Straw Tracking System Design

G. Hanson(Indiana)

OVERVIEW OF STRAW TRACKING SYSTEM DESIGN

G. Hanson
9-27-91

1143

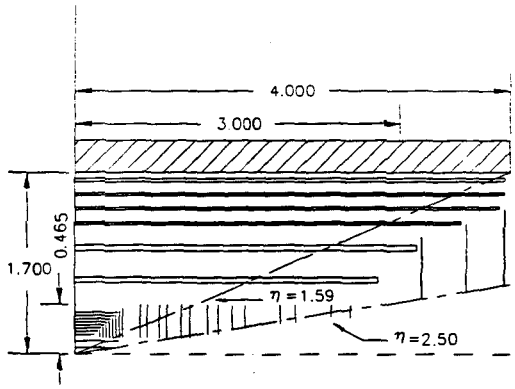


Fig. II-1. A section through one quadrant of the tracking system of the baseline design.

1144

Engineering baseline design cost ~ $ 6CM

[illegible] central tracking system

budget = $ 3.5M - includes silicon

and intermediate angle tracking

as well)

Need conceptual design for proposal

- Detailed design
- Engineering
- Simulation of performance
- Costing
- Schedule

1145

Proposed Design

(Detailed parameters to be determined from simulation)

Assume descoped silicon tracker

(Needed to identify b-jets, etc.)

How many superlayers?

Axial:

Two at large radius needed for trigger - must perform at high luminosity

One at inside radius (70cm? 1m?) to link to silicon tracker

Stereo:

Two - one at +3°, one at -3°

Would like to use outer one in Level 1 (2?) trigger → z information

1146

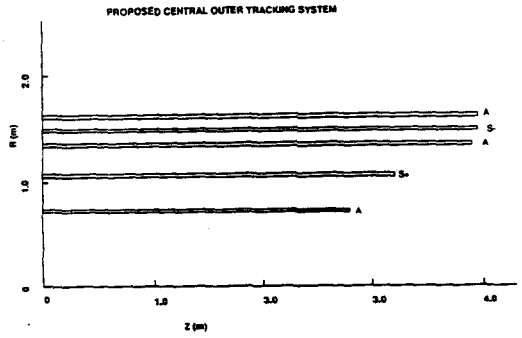


Fig. II-2. A section through one quadrant of the descoped all-straw central outer tracking system.

Table. Central Outer Tracker Design

Superlayer	Radius (m)	Straws/Layer	Modules	Layers/Superlayer	z_{max} (m)	Stereo Angle (°)
1	0.708	1112	84	6	2.80	0
2	1.04	1640	124	6	3.20	+3
3	1.35	2120	160	8 (trigger)	3.90	0
4	1.48	2328	176	6	3.95	-3
5	1.61	2536	192	8 (trigger)	3.95	0

1.35×10^5 straws

3.5% X_0 at $\eta \sim 0$ (not including last superlayer)

Cost ~ $ 32M (working on detailed cost estimate)

Performance

Performance and detailed design parameters to be determined in simulation using global pattern recognition and track fitting (Fred Luehring's talk).

This straw outer tracking system will not be sufficient without the silicon tracker (not enough redundancy for z-measurement for one thing)

Upgrade / Staging to Scintillating Fibers

Will take 2-3 years to reach design luminosity

For higher luminosity ($\sim 5 \times 10^{33}$) operation, put fibers where needed - inner superlayer(s).

Replace inner superlayer(s) with fibers either later in design (staging or when luminosity >> design) (upgrade) - when more $ available.

Therefore:

1) Continue fiber R&D

2) Design & engineer for staging

This five superlayer proposal offers a minimal outer tracking system, which, with the silicon inner tracker, provides

1) A complete tracking system for the proposal (along with an intermediate angle tracker).

2) A tracking system that meets the cost goal.

3) upgrade / staging to fibers for inner superlayer(s).

4) A conceptual design for which we can do the necessary detailed design engineering, simulation, costing, and scheduling.

Conceptual Design Report Meeting this evening
Melton Hill Suite, Garden Plaza 4th floor
"after the Banquet"

IUHEE 91-8
SDC 91-00061
August 21, 1991

PROPOSAL FOR CENTRAL OUTER TRACKING SYSTEM

G. Hanson, F. Luehring, H. Ogren and D. Rust
Indiana University

Introduction

We need to decide on a central outer tracking design for the proposal since there is a great deal of work to be done - engineering, simulation, and costing. The decision will also influence the use of the FY 1992 R&D money, which is very limited. This note describes some of the thinking behind the conceptual design proposed by Gail Hanson at the Tracking Group Meeting at the SDC Collaboration Meeting at LBL. At this meeting it was proposed that the decision on outer tracking technology be made by a panel consisting of members of the tracking groups and collaboration members outside the tracking groups. We feel that it would be much better if the tracking groups could come to a consensus first and then have the decision reviewed by the panel.

Fibers vs. Straws

Scintillating fibers offer an advantage at high luminosity because of their finer segmentation and therefore lower occupancy. However, there is still proof-of-principle R&D to be done, as well as costing information for the VLPCs. It is likely that we will not have enough information at the time the decision must be made for the proposal to be able to decide on an all-fiber outer tracker. An affordable all-fiber outer tracker may not have enough layers for adequate pattern recognition and stereo measurement. Since fibers introduce more material per superlayer, they are best used where really needed in regions of high occupancy for straws at high luminosity.

A system of both fibers and straws could offer some advantages, but the cost will undoubtedly be higher because of carrying out both technologies. The Hybrid Tracking Group claims that this is not the case; both groups are reviewing costs.

We would like to maintain the capability of upgrading to scintillating fibers for the inner superlayer(s) if needed for high luminosity, either later in the design of the detector so that we could have scintillating fibers at turn-on, or a few years after turn-on. It is expected that it will take two to three years for the SSC to reach design luminosity. Meanwhile straw inner superlayers should perform well. It seems likely that the SSC will reach a

maximum luminosity of ~ 5×10^{33} cm $^{-2}$ s^{-1} rather than 10^{34} cm $^{-2}$ s^{-1}, and in any case that will take several years. Our proposal encourages the scintillating fiber R&D to continue, with funding from several sources (SSC, HEP, TNRLC).

How Many Superlayers?

The minimum number of superlayers needed can be determined from the following requirements for the outer tracking system:

1. High-p_T track segment trigger
2. Momentum measurement in conjunction with the silicon inner tracking system
3. Sufficient pattern recognition capability to link track segments in the inner and outer tracking systems
4. Measurement of the coordinate along the beam direction (z), in conjunction with the silicon tracker.

In order to provide the high-p_T track segment trigger, we need at least one axial superlayer at the outer radius. At higher luminosities we may require two axial superlayers for the trigger. There is also the possibility of including one of the stereo superlayers so as to obtain the z-coordinate for a high-p_T track in the trigger, although we haven't included this in our proposal. *We propose two axial superlayers at large radius for the trigger.*

Momentum measurement is accomplished by using both the inner and outer tracking systems in an integrated manner. In order to do this, track segments have to be linked between the two systems. This is the main focus of the tracking simulation effort. Indications are that we will need an axial superlayer relatively close to the silicon tracker. The exact radius cannot be determined until we have progressed further with the simulation studies. This inner superlayer might be upgraded to scintillating fibers at high luminosity, if needed. *Thus we propose a third axial superlayer at a radius of about 70 cm.*

The minimum number of stereo superlayers is two, one with wires running at about +3° to the beam direction, the other at -3°. The best choice would probably be to have both of them at large radius so as to obtain the best resolution in angle and the best coordinate measurement for linking to the calorimeter and muon system. However, some information about the z-coordinate may prove useful in linking to the silicon tracker, since it also provides z information. Note that with the present very small angle stereo (1 mrad) in the silicon tracker, the resolution per measurement in z is about the same (3 mm) in the inner and outer tracking systems. The exact location of this superlayer needs to be determined from the simulation studies. *We propose two stereo superlayers, one between the outer two axial superlayers and one at an intermediate radius of about 1 m.*

The conclusion is that *five superlayers* would provide a minimal system with reasonable performance and essentially no redundancy, especially for the z measurement. It has been suggested that due to budgetary constraints four superlayers would be enough. In that case, two would be axial and two stereo. There are two possibilities: two axial superlayers at the outer radius for the trigger, or one at the outer radius and one at the inner radius to provide linking to the silicon. In the former case, linking to the silicon would probably be difficult, although more simulation studies are needed to substantiate this. In the latter case, we would not have the possibility of using two outer axial layers in the trigger, which could be needed at higher luminosities.

It has also been suggested that we reduce the number of straw layers in each superlayer, allowing more superlayers. However, this would increase the material and the cost. Most of the material is in the supports for the straws, not in the straws themselves. The cost is dominated by a fixed cost and then by a cost per superlayer. The incremental cost per channel or module is relatively small compared with these.

The Proposal

The Table lists the components of the proposed outer tracking system, which consists of five superlayers of straw tubes, three axial superlayers and two stereo. The design is also shown in the figure. The three outer superlayers are placed as in the engineering baseline design. The inner superlayer is placed at about 70 cm radius, consistent with the envelope for the outer tracking system. The second superlayer is equidistant from the inner superlayer and the three outer superlayers. The radial positions of the superlayers and the exact arrangement (axial vs. stereo) are rather arbitrary here and are the subject of simulation studies. The lengths of the superlayers are in agreement with the η coverage as in the engineering baseline design and would be adjusted to accommodate the intermediate angle tracking system. The two outer axial superlayers are trigger layers and have 8 straws per superlayer. The other superlayers have 6 straws per superlayer. The amount of material in the outer tracking system at 90° is 3.5% of a radiation length including all supports (not including the last superlayer). A preliminary cost estimate, based on the costing structure developed by Westinghouse Science and Technology Center and Indiana University, is $34.8M. The cost is being reviewed, and there is some possibility of reduction. There are a total of 1.35×10^5 straws.

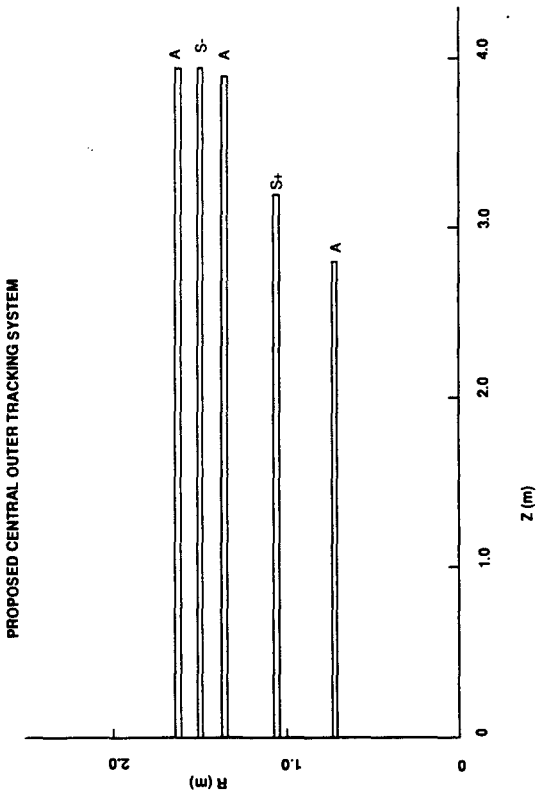
We would like to continue the scintillating fiber R&D so that the inner superlayer(s) could be upgraded to scintillating fibers if needed at higher luminosity or even by turn-on if technology progress and funds permit.

Conclusions

This proposal offers a central outer tracker that, with the silicon inner tracker, forms a complete tracking system that should perform well at luminosities up to at least the design value, which is important for presentation in the proposal. The amount of material is minimal. The cost is within the target value for the tracking system. The proposal also offers the possibility of continuing the scintillating fiber R&D for upgrading the inner superlayers, where occupancy could be a problem with straws for higher luminosity, on a time scale consistent with the foreseen turn-on schedule for the SSC. We can use this proposal to plan future R&D, carry out definite simulation studies, and do the design, engineering, and costing needed for the SDC proposal. We would like our proposal to receive serious consideration.

Table. Central Outer Tracker Design

Superlayer	Radius (m)	Straws/Layer	Modules	Layers/Superlayer	z_{max} (m)	Stereo Angle (°)
1	0.708	1112	84	6	2.80	0
2	1.04	1640	124	6	3.20	+3
3	1.35	2120	160	8 (trigger)	3.90	0
4	1.48	2328	176	6	3.95	-3
5	1.61	2536	192	8 (trigger)	3.95	0



Modular Straw Tracking Sustem

H. Ogren(Indiana)

Modular Straw Tracking System

1158

Basic Straw R&D

Performance tests with 64 straw modules

Construction Techniques

Design and building of 4 meter system

Materials consideration

engineering aspects

design of 1 meter

Schedule

Milestones

1159

Basic Straw R&D

Performance tests with 64 straw modules

Six chambers have been produced. Each has 64 straws. Now in operation at Indiana University, Colorado University, University of Michigan, University of Pennsylvania, and KEK.

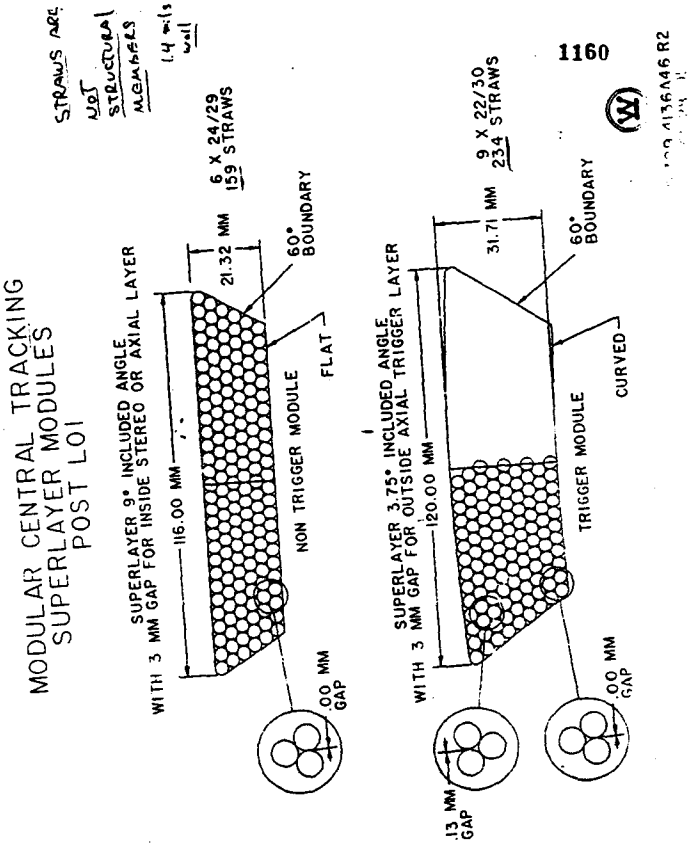
Performance tests with 64 straw modules (and longer straw prototypes)

Attenuation	(Dave Rust)
High Radiation testing	(Dave Rust)
Electronics integration	(Bill Ford)

We have developed construction techniques that will we applied to the larger and longer chambers.

Thin carbon composite skin
Wire support
Low mass end plate
Electronics interface
Data acquisition electronics
Electronics test bed for all groups

1160



1161

Alignment Requirements

The momentum precision requirements set a limit of $\sigma_{superlayer} = 80$ **microns** for the track position measurement at each superlayer.

For the modular system we can write:

$$\sigma^2_{superlayer} = (\sigma^2_{intrinsic} + \sigma^2_{wire\ placement})/6 + \sigma^2_{module\ intrinsic} + \sigma^2_{module\ placement}$$

Measurements of straw related errors:

Close packing alignment

NDT measurements of complete module

Measurements of Module related errors.

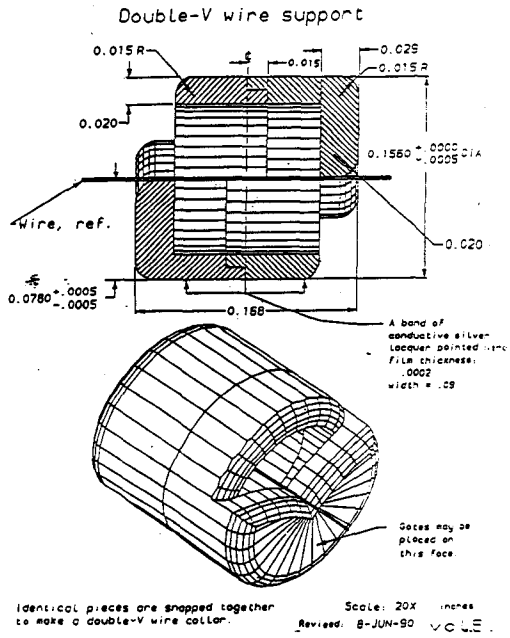
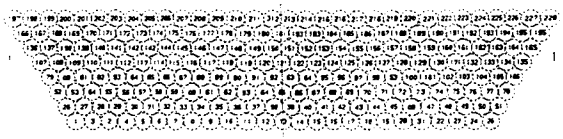


Fig. 2 Double V dimensions

Alignment of straws within a module



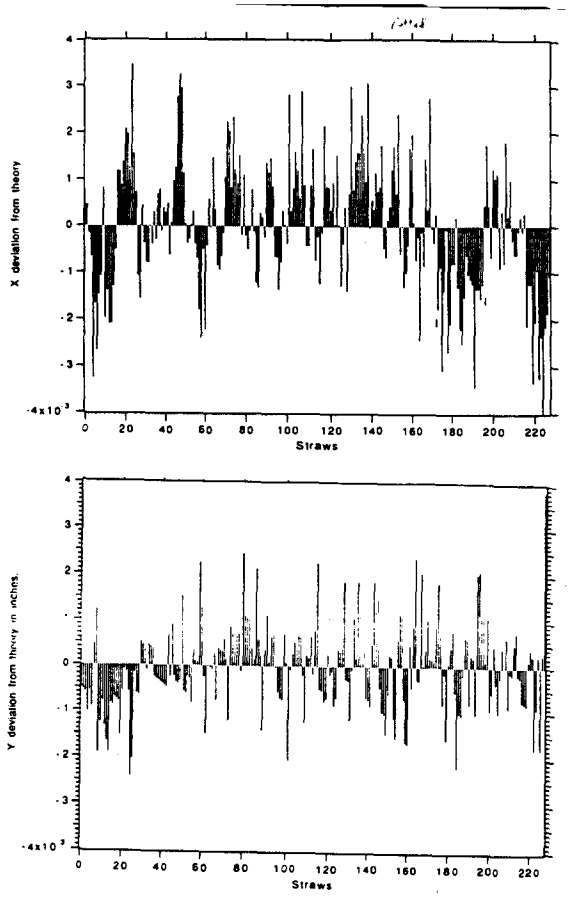
The precision is set by the position of the wires (not the straws).

The wires are held by wire supports every 80 cm. The wire supports are postioned by clamping and potting in a close-packed geometry.

Direct measure of wire supports- clamped, glued, and self supported.

Array of x- y position were fitted to an ideal close packed geometery.

Resulting deviation was found to be $\sigma = 30$ microns.



Alignment Requirements

The momentum precision requirements set a limit of $\sigma_{superlayer} = 80$ micons for the track position measurement at each superlayer.

For the modular system we can write:

$$\sigma 2_{superlayer} = (\sigma^2_{intrinsic} + \sigma^2_{wire\ placement})/6 + \sigma^2_{module\ intrinsic} + \sigma^2_{module\ placement}$$

Measurements of straw related errors:

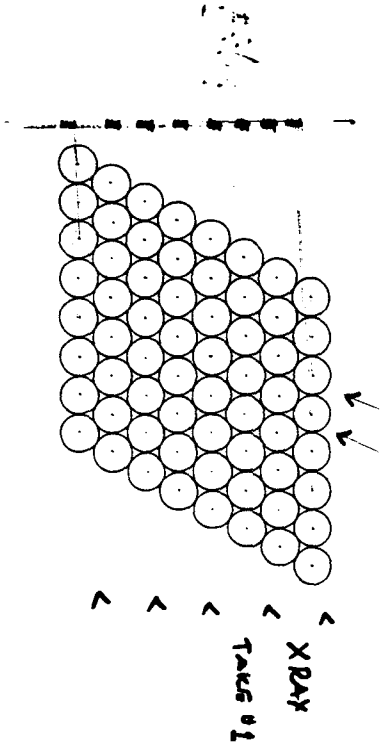
Close packing alignment

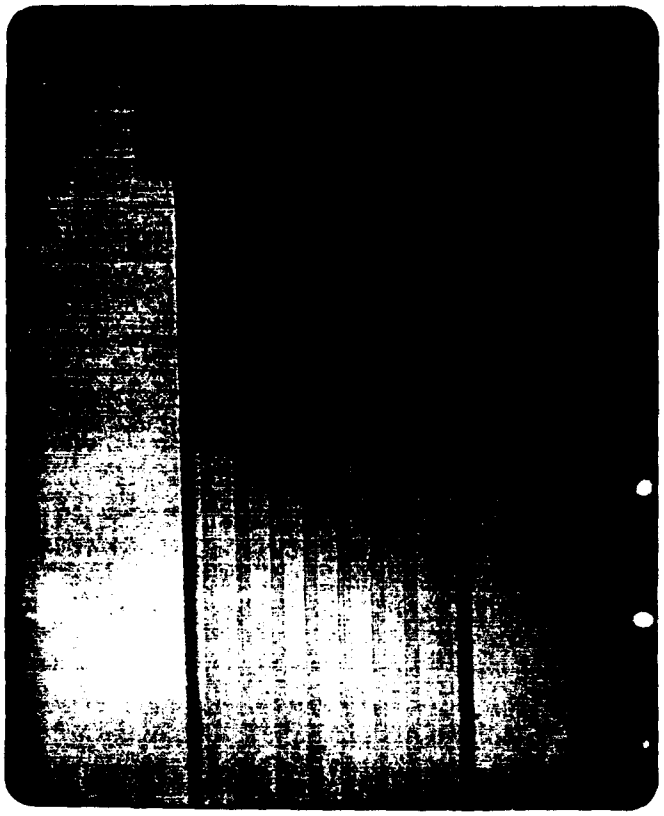
NDT measurements of complete module

Measurements of Module related errors.

Test and calibration of each module

- check gas tightness
- test module with HV
- x ray for wire positon
- cosmic ray tests
- Determine best fit to close packed geometry at each 80 cm point.





endB, take 1

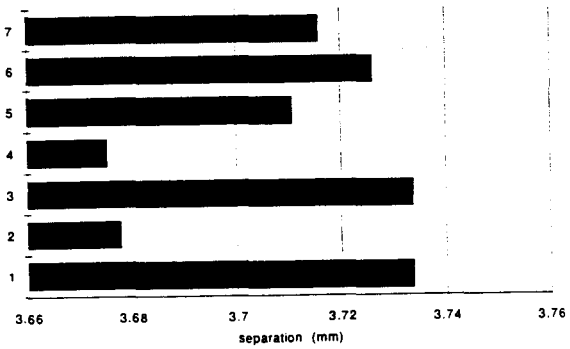
	A	B	C	D	E	F	G	H
1	38.8	25.3	9.6	6.2	23.2	40.7	58.1	76.4
2	108.2	121.4	137.7	153	171.5	190.4	206.6	222.8
3	253	266.9	283.2	300.6	318.8	336.8	354.1	369.8
4	400	414.9	430.4	447.8	464.1	484.9	500	517
5	544.7	561	578.2	595.4	613.4	630	646.6	663.3
6	690.8	707.7	724.8	743.6	761.7	778.8	792.4	808.9
7	837.5	854.4	873.5	891.1	907.8	925.3	941.5	956.8
8	983.8	1002.4	1024.3	1041.2	1058.1	1074.1	1088.9	1103.6
9								
10	147	146.7	147.3	146.8	148.3	149.7	148.5	146.4
11	144.8	145.5	145.5	147.6	147.3	146.4	147.5	147
12	147	148	147.2	147.2	145.3	148.1	145.9	147.2
13	144.7	146.1	147.8	147.6	149.3	145.1	146.6	146.3
14	146.1	146.7	146.6	148.2	148.3	148.8	145.8	145.6
15	146.7	146.7	146.7	147.5	146.1	146.5	149.1	147.9
16	146.3	148	150.8	150.1	150.3	148.8	147.4	146.8
17								
18	146.085714	146.814286	147.7	147.857143	147.842857	147.628571	147.257143	146.742857
19	0.97198863	0.92092086	1.68720676	1.07681187	1.75010204	1.65500683	1.25280637	0.73452284

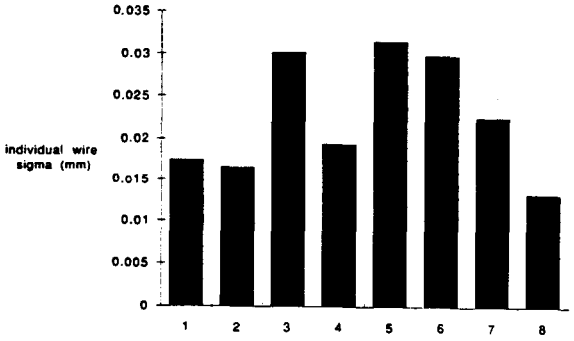
endB, take 1

	A	B	C	D	E	F	G	H
1	38.8	25.3	-9.6	6.2	23.2	40.7	58.1	76.4
2	108.2	121.4	137.7	153	171.5	190.4	206.6	222.8
3	253	266.9	283.2	300.6	318.8	336.8	354.1	369.8
4	400	414.9	430.4	447.8	464.1	484.9	500	517
5	544.7	561	578.2	595.4	613.4	630	646.6	663.3
6	690.8	707.7	724.8	743.6	761.7	778.8	792.4	808.9
7	837.5	854.4	873.5	891.1	907.8	925.3	941.5	956.8
8	983.6	1002.4	1824.3	1041.2	1058.1	1074.1	1088.9	1103.6
9								
10	147	146.7	147.3	146.8	148.3	149.7	148.5	146.4
11	144.8	145.5	145.5	147.6	147.3	146.4	147.5	147
12	147	148	147.2	147.2	145.3	148.1	145.9	147.2
13	144.7	146.1	147.8	147.6	149.3	145.1	146.6	146.3
14	146.1	146.7	146.6	148.2	148.3	148.8	145.8	145.6
15	146.7	146.7	148.7	147.5	146.1	146.5	149.1	147.9
16	146.3	148	150.8	158.1	150.3	148.8	147.4	146.8
17								
18	146.085714	146.814286	147.7	147.857143	147.842857	147.628571	147.257143	146.742857
19	0.97198863	0.92092086	1.68720676	1.07681187	1.75010204	1.65500683	1.25280637	8.73452284

Chart7

Chart6





Conclusions on straw placement precision

Direct measurement of variation of wire supports about an ideal close packed geometry

σ= 30 microns (measurement error?)

Direct measurement of the wire positions variations from x-ray of 64 straw chamber.

σ= 25 microns

Our conclusion is that we can place the wires with an accuracy better than

σ= 30 microns

so

σ^2 superlayer=$(100^2 + 30^2)/6 + \sigma^2$ mod int+σ^2 mod place

If we require 80 microns for the superlayer, then the module placement and intrinsic errors must each be about 50 microns or less.

1174

Material in modules

The material in the tracker is mainly at smaller radii. NOT IN STRAWS!

Effects of material:

- **Higher trigger rate for High Pt electrons**
- **Multiple scattering and degrades momentum resolution**
- **photons conversions confuse track finding**

1175

1176

1177

MODULES

	η=0.00	η=0.55	η=1.00	η=1.75	η=1.85	η=1.95	η=2.15
Straws Mylar et al (Xo=24 cm) Tungsten (Xo=0.35 cm)	1.36%	1.80%	3.52%	4.80%	3.33%	2.44%	1.46%
Modules Graphite Epoxy (Xo=25 cm) Rohacell Foam (Xo=875 cm)	0.87%	1.23%	2.17%	2.56%	2.12%	1.56%	0.94%
Support Cylinder Graphite Epoxy (Xo=25 cm) Rohacell Foam (Xo=875 cm)	0.37%	0.52%	0.94%	1.09%	0.89%	0.66%	0.40%
End Plates Graphite Epoxy (Xo=25 cm)	0.00%	0.00%	0.00%	4.29%	4.20%	4.17%	4.11%
Page Holder Graphite Epoxy (Xo=25 cm)	0.00%	0.00%	0.00%	4.29%	4.20%	4.17%	4.11%
Capacitor Substrate G-10 (Xo=19.4 cm)	0.00%	0.00%	0.00%	0.70%	0.69%	0.68%	0.67%
Capacitor Alumina Oxide (Xo=8.2 cm)	0.00%	0.00%	0.00%	2.18%	2.15%	2.13%	2.10%
Silicon Substrate G-10 (Xo=19.4 cm)	0.00%	0.00%	0.00%	0.70%	0.69%	0.68%	0.67%
Electronics Silicon (Xo=9.36 cm)	0.00%	0.00%	0.00%	0.41%	0.41%	0.41%	0.41%
Passivator Glass (Xo=12.7 cm)	0.00%	0.00%	0.00%	0.08%	0.08%	0.08%	0.08%
Copper (Xo=1.43 cm)	0.00%	0.00%	0.00%	0.18%	0.18%	0.18%	0.18%
Structural Supports Graphite Epoxy (Xo=25 cm)	0.00%	0.00%	0.00%	0.00%	0.30%	1.04%	0.40%
TOTAL	2.60%	3.67%	6.63%	20.42%	19.24%	18.18%	15.56%

4 LAYERS

RESULTS SUMMARY

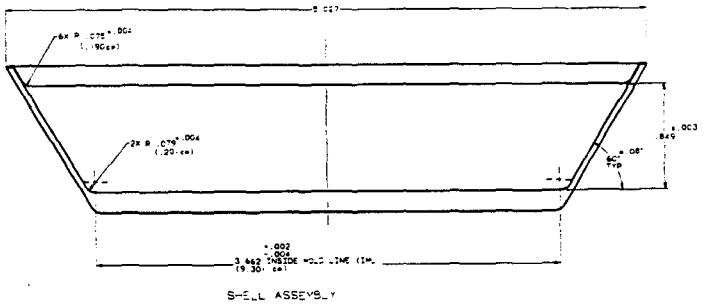
TABLE NUMBER 1
SUMMARY TABLE OF RADIATION LENGTH CALCULATIONS

TABLE #	SUPPORT CYLINDER GRAPHITE TK/LAYER INCHES	SUPPORT CYLINDER FOAM TYPE	SUPPORT CYLINDER FOAM TK INCHES	SHIM RING EFFECTS	MODULES GRAPHITE TK/LAYER INCHES	MODULES FOAM TYPE	MODULES FOAM TK INCHES	MODULE EDGE EFFECTS	PERCENT RADITION LEN/LAYR CM
2	0.0045	51WF	1	NO	0.006	51WF	0.14	NO	0.98
	0.0045	31IG	1	NO	0.006	51WF	0.14	NO	1.15
3	0.0045	31IG	1	NO	0.006	51WF	0.14	NO	0.92
4	0.0045	31IG	1	NO	0.0045	51WF	0.14	NO	0.87
5	0.0045	31IG	1	NO	0.0045	31IG	0.14	NO	0.98
6	0.0045	31IG	0.59	NO	0.0045	51WF	0.14	NO	0.82
7	0.0045	31IG	0.59	NO	0.0045	31IG	0.14	NO	0.76
8	0.0045	31IG	0.59	NO	0.0045	31IG	0.14	YES	0.78
9	0.0045	31IG	0.59	YES	0.0045	31IG	0.14	YES	0.79
9 (SAME AS ABOVE EXCEPT EDA = 1.64)									2.12
10 (SPACEFRAME END DISK SPREAD RADIATION LENGTH CALCULATION)									0.24
0.24 RAD LG IS EQUIVALANT TO 0.008 Inch Thick Aluminum Sheet)									
0.024 Inch Thick [illegible]									

.71% X_0

1178

Module construction

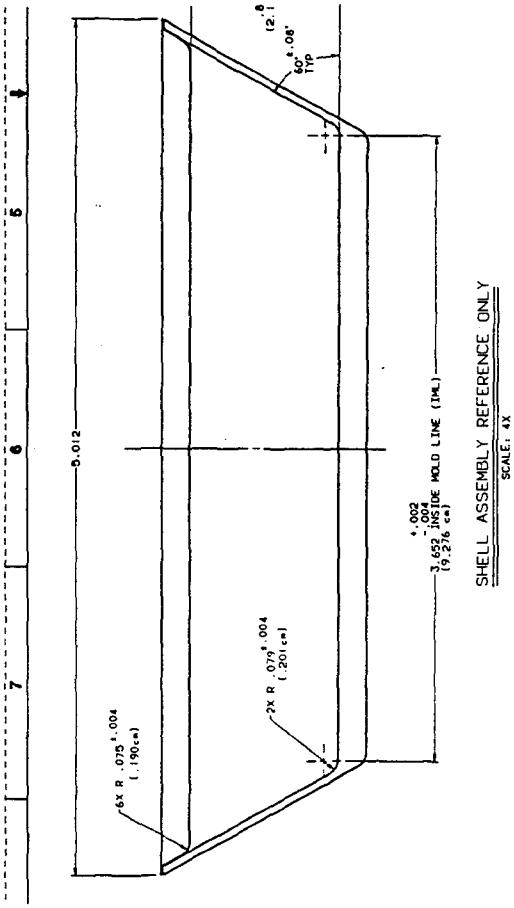


Material in 6 layers of straws= 0.23% X_0

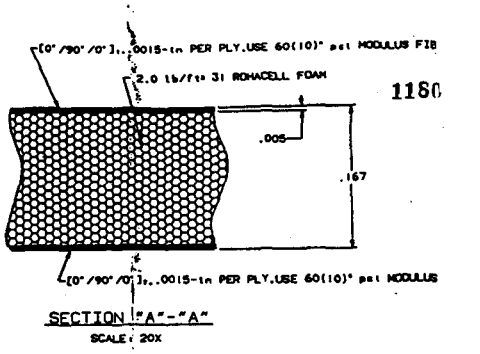
Material in lid and base (averaged over sides)= 0.301% X_0 (3 layers-0.0015 ", IG31 foam)

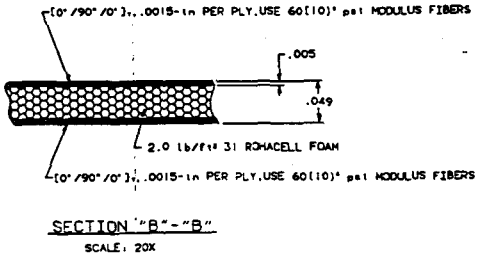
Total material = 0.53 %X_0

1179



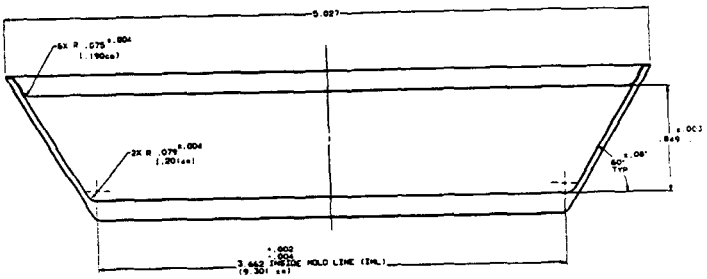
1180





1181

Module construction



Material in 6 layers of straws= 0.23% X_0

Material in lid and base (averaged over sides)= 0.301% X_0 (3 layers-0.0015 ", IG31 foam)

Total material = 0.53 %X_0

WHY WAS FOAM CONSTRUCTION USED?

1) STRENGTHEN MODULE AGAINST OUTWARD STRESS OF STRAWS

2) PREVENT WARPING OF MULTILAYER CARBON LAMINATES

3) PROVIDES MUCH LARGER SAFETY FACTOR FOR WIRE TENSION FORCES (12-15 Kg)

MATCHED MOLDS ARE REQUIRED



- THICKNESS CONTROLLED (<1 mil)
- FLATNESS OK
- ALL SURFACES PRECISION
- FIDUCIAL INSERTION EASY

1 meter prototype is under construction

Composites Horizons, Inc. , Covina, Ca.

- six shell for 64 straw modules
- 30 inch long layer trapezoidal shell
- Foam core panels for more stiffness.

First tests on panels indicate thickness variations less than 25 microns and flatness better than 35 microns for 1 meter sample.

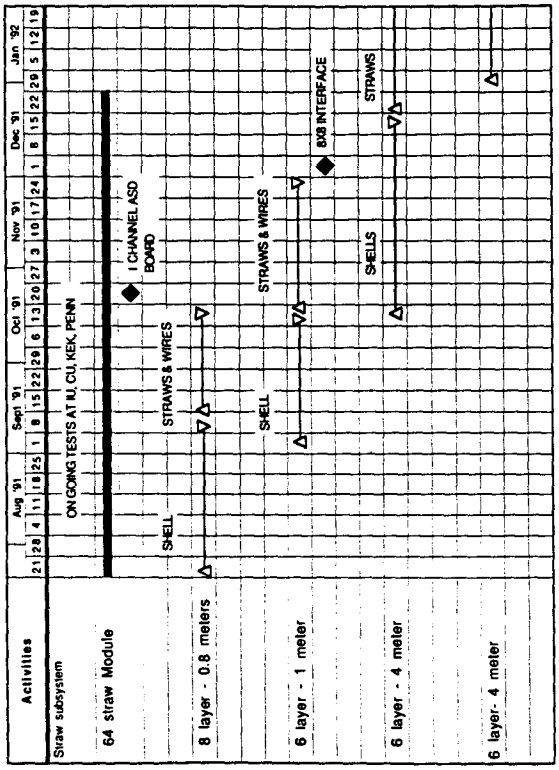
The top an bottom parts are each formed by a set of matched graphite molds. These are machined by

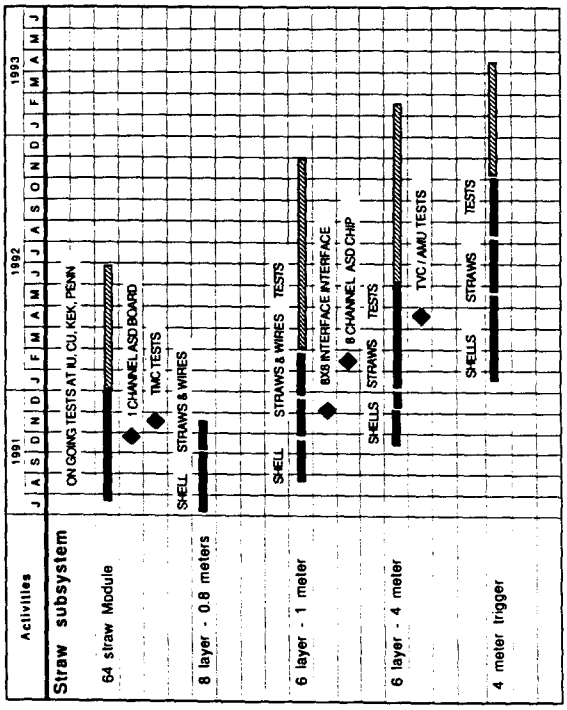
Coast Composites, Inc. , Irvine, Ca.

- 1 meter mold set , Sept. 30.

1 meter shell to be delivered October 18,1991

4 meter shell delivered December 13,1991





Summary

• Straw placement precision has been measured.We can locate the relative positions of wires in a module within σ =30 microns.

• The intrinsic module straightness must be less than s = 50 microns. Carbon composites with a foam sandwich can be formed with this precision. Delivery of 4 meter module in December will allow a direct measurement.

Engineering work on cylinder support and tracker support will set the precision we can expect module placement. 50 microns will probably not be a problem.

Progress of Straw R&D at Duke U.

S. Oh(Duke)

KEK TMC module test.

Chamber operation under SSC environment.
- Current draw.
- Resolution measurement

7 meter long working straw tube cells.
- Efficiency near wire support
- Efficiency near wire-glass-wire joint
- Do we need a terminator?

Wire position Measurement using collimated Sr90 source
- Accuracy of 50-100 microns.

First Modular super-layer construction.
- 100 channel shell-less module.

Progress of the straw placing machine.

TMC1004 32-Channel CAMAC Multi-Hit

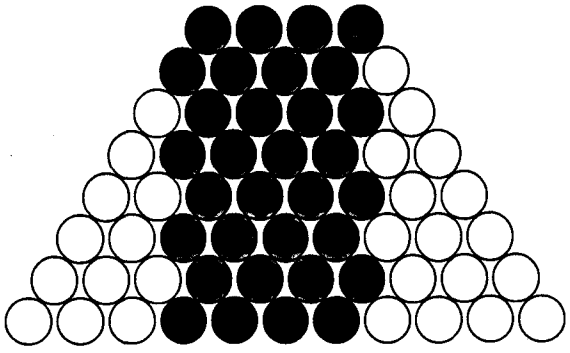
TDC Module Manual

Rev.1.0 Mar. 19, 1991

Prepared by Y. Arai
KEK, National Laboratory for High Energy Physics
1-1 Oho, Tsukuba, Ibaraki, Japan
Tel : 0298-64-1171 ex.6212
Fax : 0298-64-2580
Bitnet : ARAIY@JPNKEKVX

North-Holland

& METHODS IN PHYSICS RESEARCH



Construction and performance of a 2.7 m long straw drift tube prototype chamber for the SSC

S.H. Oh, A.T. Goshaw and W.J. Robertson
Department of Physics, Duke University, Durham, NC 27706, USA

Received 4 April 1991

We report the construction and testing of a 2.7 m long straw tube drift chamber consisting of 60 channels. The straw tubes with 2 mm radius are stacked in a pyramid shape up to eight tube layers. There are two wire supports inside each tube for electrostatic stability. 25 tubes out of 60 are instrumented for measurement of resolution, gas gain, and attenuation length. Resolution of close to 110 μm and attenuation length of 500 cm are obtained.

1. Introduction

The design of the central tracking chamber in a solenoidal detector [1] for the Superconducting Super Collider (SSC) calls for a cylindrical tracking chamber ≥ 6 m long. Using straw tubes with small radii is one of the options [2] for the tracking chamber. Due to the bunch spacing and the occupancy rate, the tube radius should not be greater than 2 mm. The central tracking chamber will likely consist of several cylindrical superlayers, with each superlayer typically made up of about eight layers of tubes. In order to cover a large tracking volume, superlayers are separated by about 10–15 cm from each other. In this chamber, track segments are found in each superlayer first and then the segments from different superlayers are linked to form a complete track.

For a feasibility study, we have constructed a 2.7 m long superlayer on a flat surface. In the prototype, 60 straw tubes with 2 mm radius are stacked in a pyramid shape up to eight tube layers. The tubes used in the prototype have a wall thickness of 50 μm of mylar on a 8 or 12 μm thick aluminum cathode. Because of the length of each cell, sense wires have to be supported and our study shows that the support is needed about every meter. Two wire supports are placed inside each tube in the prototype.

By successfully constructing and operating the prototype, we have verified that the basic design concept is sound and can be extended to a full size cylindrical central chamber. Specifically we have demonstrated the following: First, we showed that layers of tubes can be placed straight with an accuracy better than 100 μm over several meters once a flat base surface is provided. Second, a double-wall endplate designed by our group provides a simple way to supply gas, tension the sense wire and mount electronics. Third, the wires can be supported inside tubes at 1 m intervals to make a long working straw cell. Fourth, a large number of channels can be made operational simultaneously without difficulty. This is important since the expected number of channels for the final tracking chamber is about 200 000. Finally, we showed that spatial resolution of close to 110 μm can be achieved and the attenuation length is long enough that signals from the end of the detector farthest from the readout electronics are not significantly degraded.

Although using a tube for a drift cell is not new [3] and there have been efforts to use small radius straw tubes [4], our prototype is the first of its kind in terms of length, tube radius and number of channels.

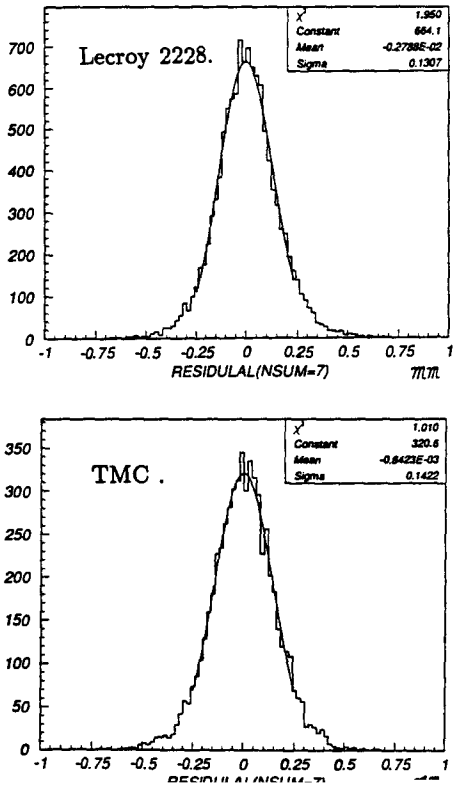
This article is organized as follows. In section 2 we present results of an electrostatic stability study. We measured the position of the sense wire inside a 2 mm radius tube as a function of high voltage with different tension in the wire and different initial displacement. In section 3, we discuss a design of a wire support. Section 4 contains details of the design and construction of the 2.7 m prototype. In section 5, we present the results of tests to measure the gain, attenuation length and resolution of the prototype. We present our conclusions in section 6.

2. Electrostatic stability

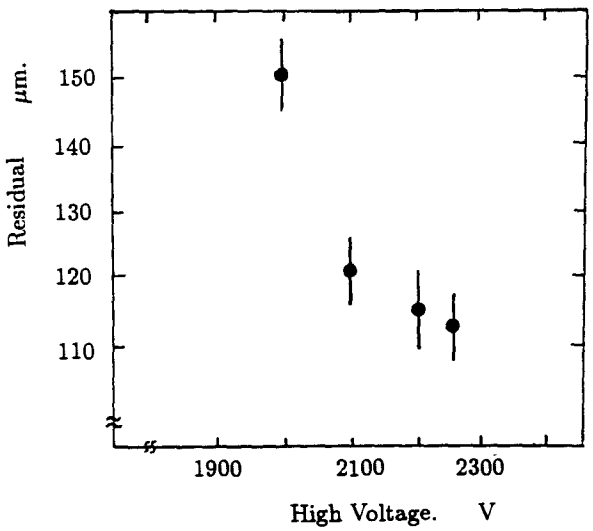
The design for the central tracking chamber in a solenoidal detector at the SSC uses 2 mm radius straw tube detector elements. The sense wire would be oper

0168-9002/91/$03.50 © 1991 – Elsevier Science Publishers B.V. All rights reserved

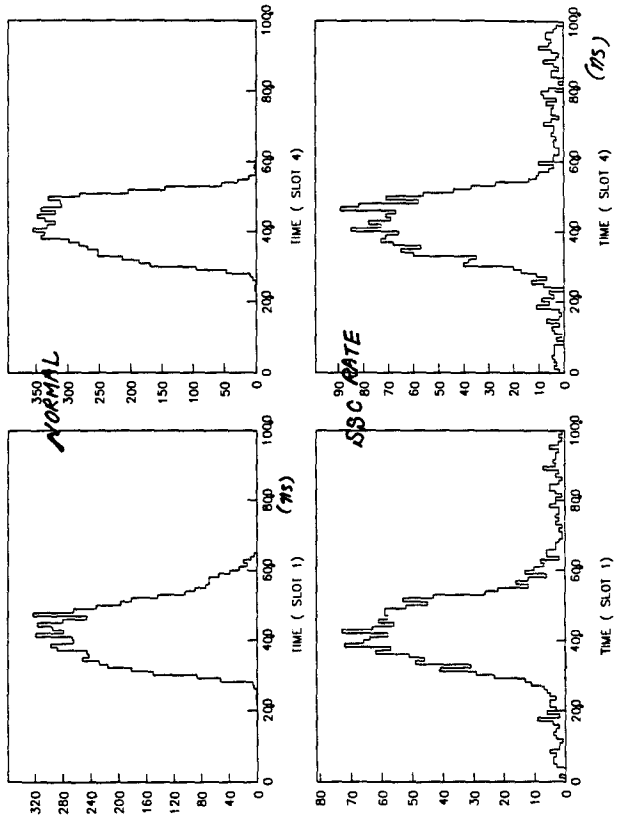
1193



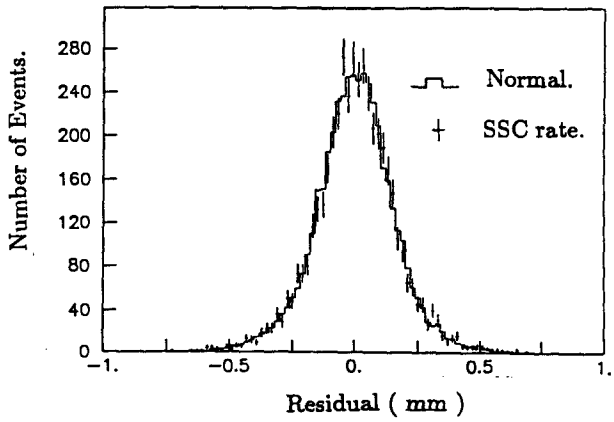
1194



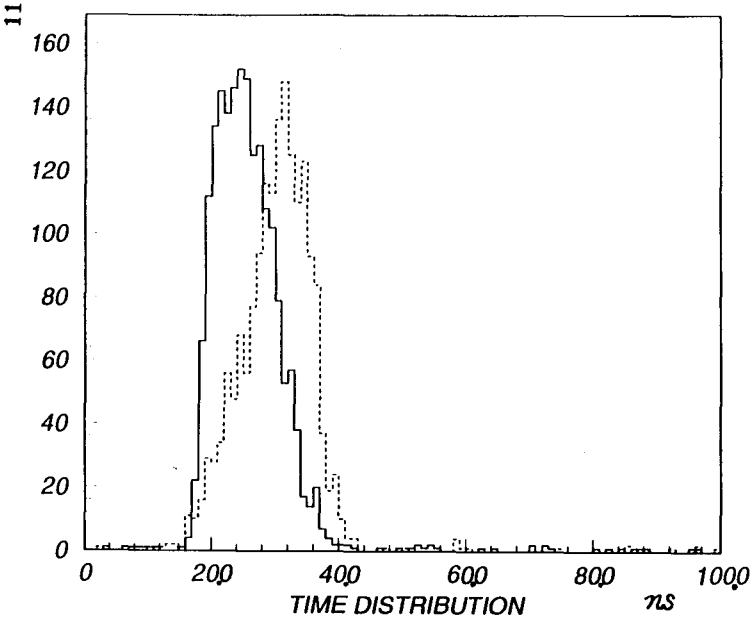
1195



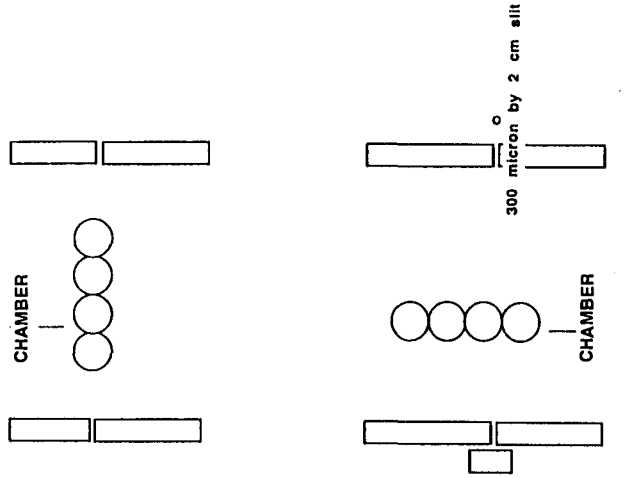
1196



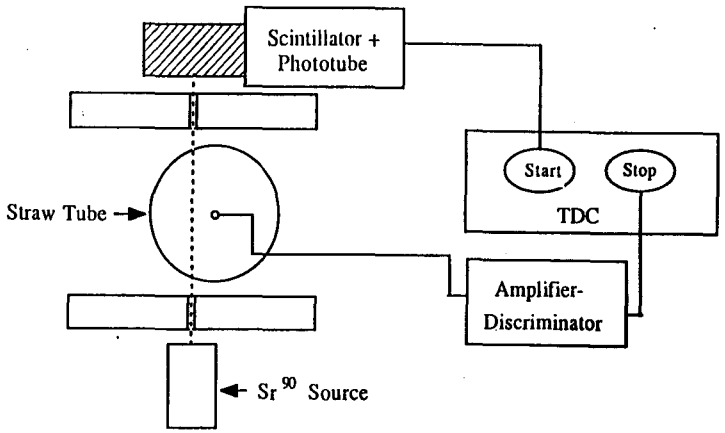
1198



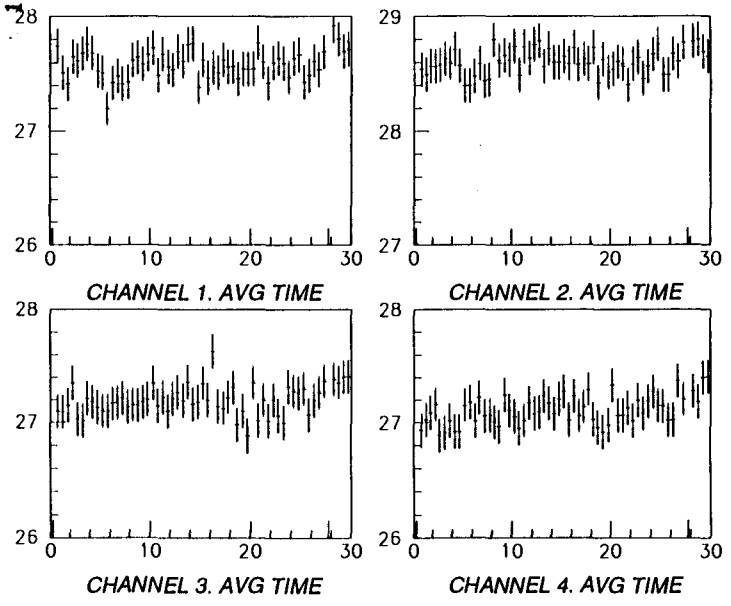
1200



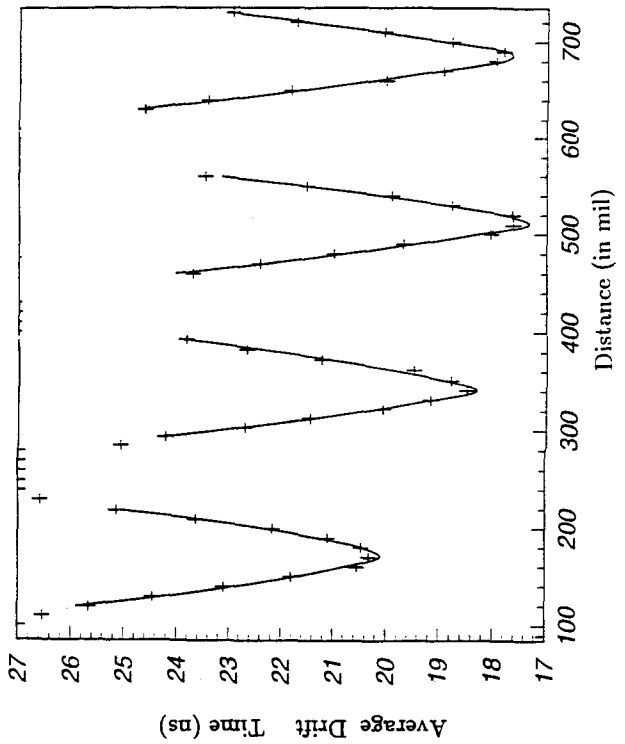
1197



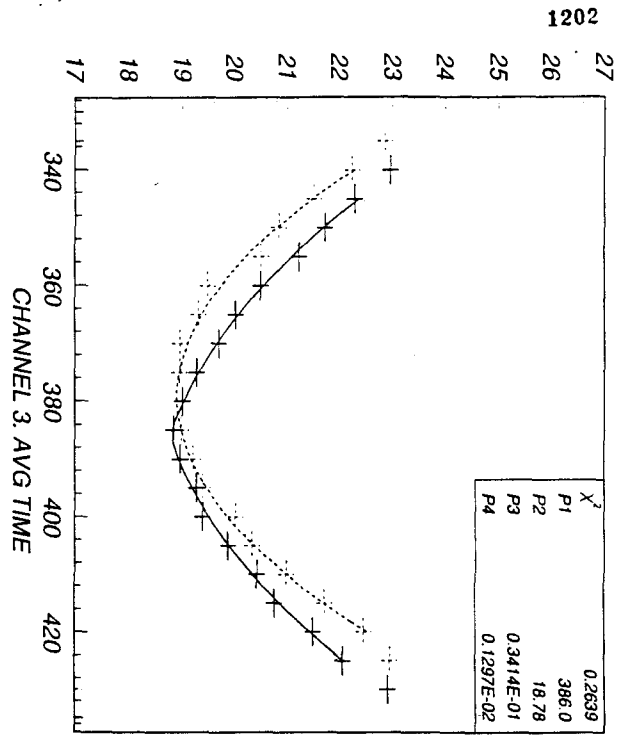
1199



1201



1202



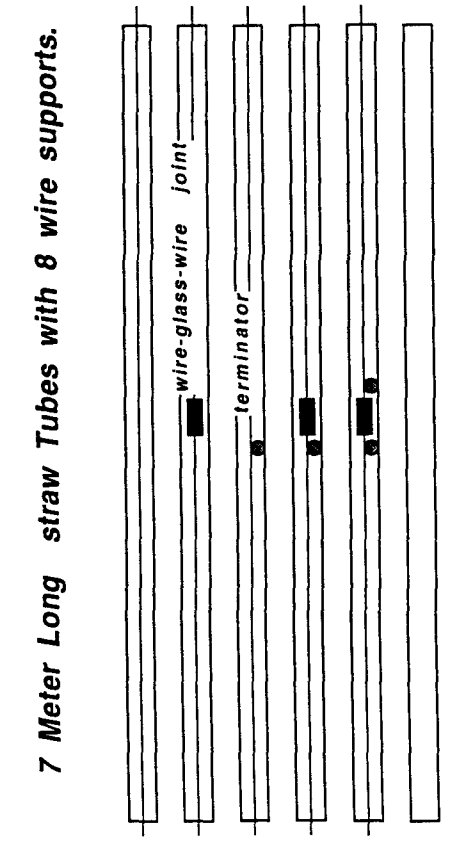
1203

Straw Placing Machine.

One of the design concept of the tracking detector is to place single straws on a cylindrical base made of carbon fiber (rather than placing modules on the base).

This concept requires a straw placing machine.
Duke has been designing the machine.
The necessary parts are in order and the construction should start within a month.

1204



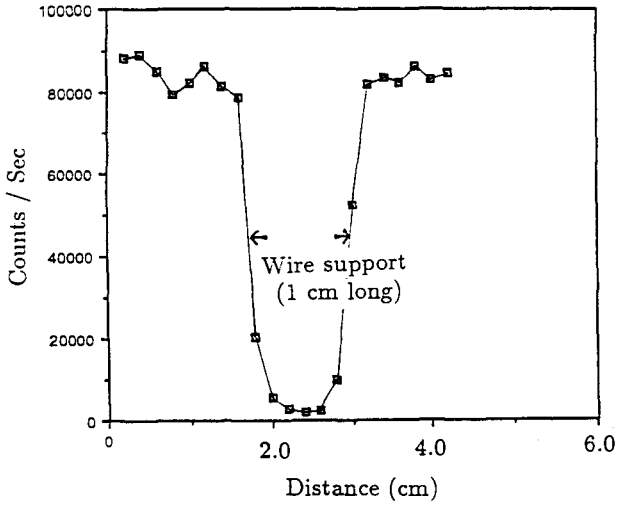


Fig. 1.12 Straw tube detection efficiency near the wire support.

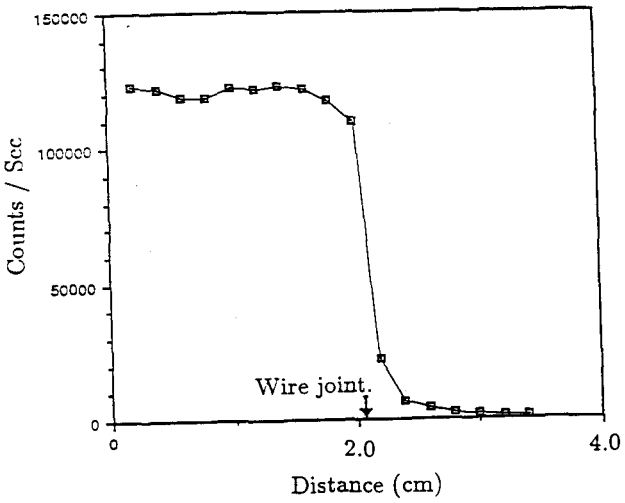


Fig. 1.13 Straw tube detection efficiency near the wire break.

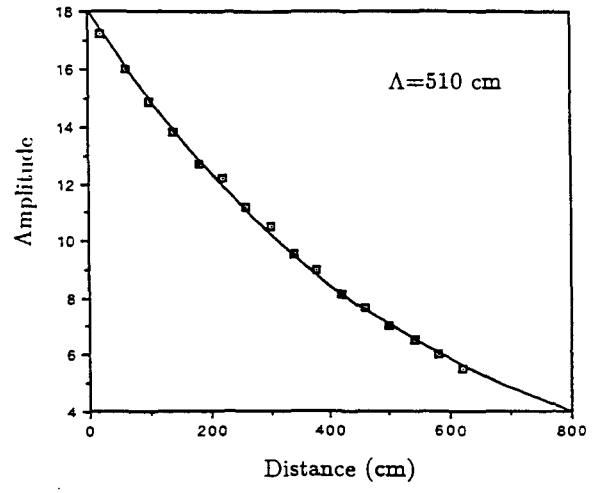
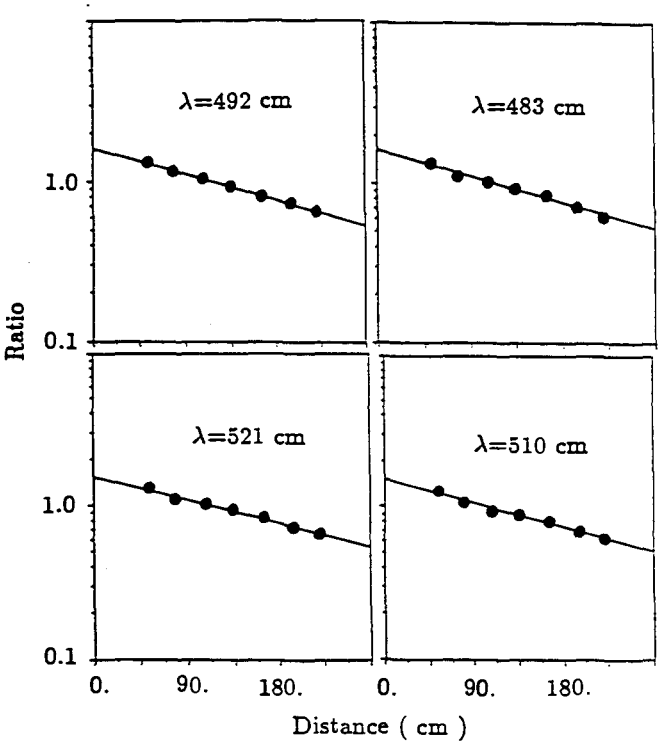
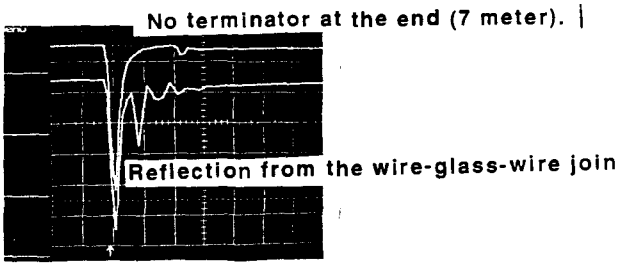
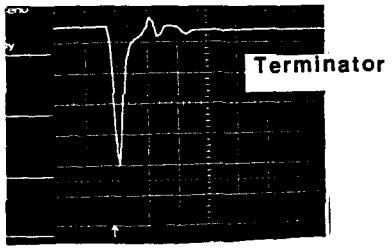


Fig. 1.14 Straw tube attenuation length measurement (7 m straw tubes).



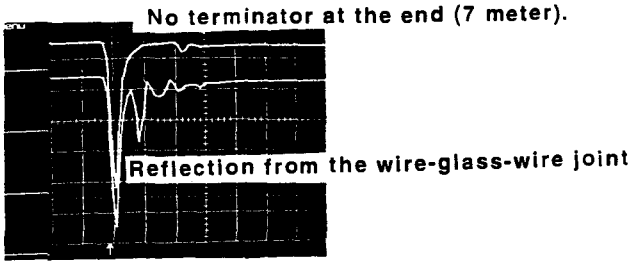
Source (Fe55) 30cm from the readout end.

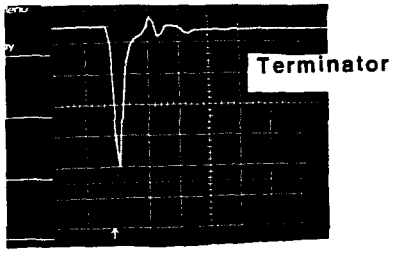




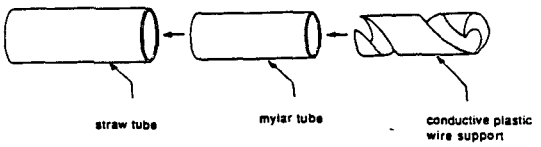
20ns/div

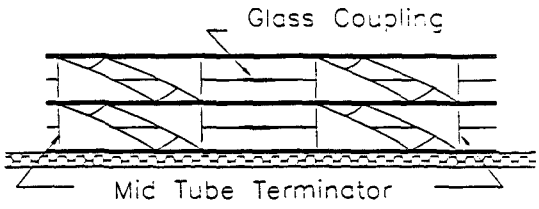
Source (Fe55) 30cm from the readout end.





20ns/div





Terminator.

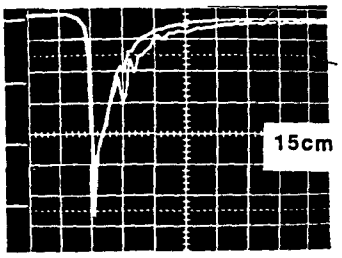
For : Without the terminator the dead time of the cell is increased due to the reflected pulses. The reflected pulse may interfere with another pulse and distort its timing.

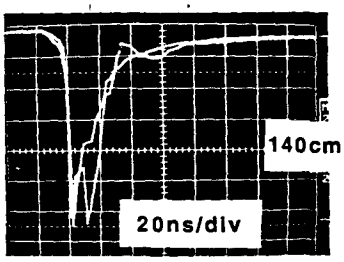
Against: One more assembly procedure.
More material.
More electronic noise due to the resistor.

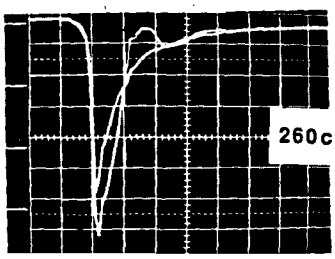
? What is the gain in the dead time, and time measurement.

? How can we decide if the terminator is needed?
Beam test.

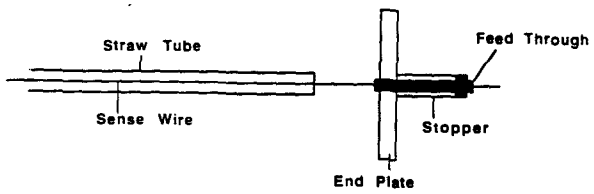
Source (Sr90) 1213



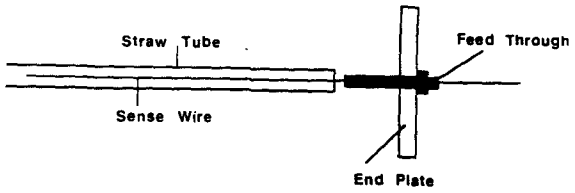




1214



Tension in the Wire.



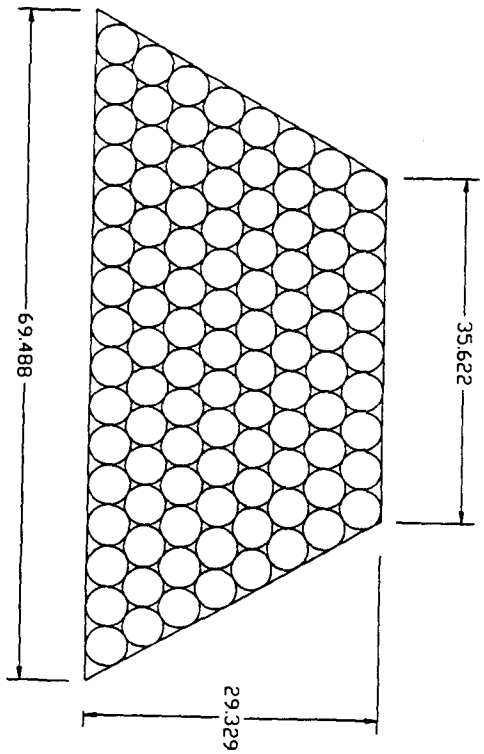
Tension is relieved.

1215

Advantage of the Shell-less module.

1. Reduction of material by about 35%.
2. Shell-less module is rigid enough to be handled, but flexibility enough to be aligned while being placed on the cylindrical base.
3. Cost less.
4. Can be made to 7-8 meter long module.
5. Sense wire breakage will be none during the transportation.

1216



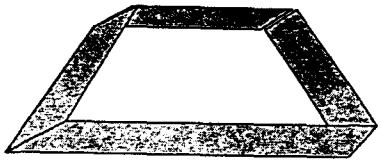


Fig. 1.10b Trapozoid shape band around tube stack

R&D in 1992

*Continue the evaluation of the 7 meter long straw cells.

*Determine the necessity of the terminator.

*Instrument and evaluate the shell-less 100 channel 3 meter module.

*Construct a shell-less trigger module.

*Feasibility study of a 7 meter long shell-less module

*Evaluation of Penn and KEK electronics.

*Preparation of the prototype super-layer consisting of about 1000 channels.

Conclusion

** There are no intrinsic problems with the straw tracker. We believe all the major problems are solved or are well underway to solutions.
We should be ready to start the prototype construction in the middle of 92.

Straw/Fiber Tracker

S. Reucroft(Northeastern)

Steve Revcroft

1221

Straw / Fiber Tracker

- Rationale, basic idea, etc.
- Current Design.
- Performance.
- Cost.
- Concluding Comments.

1222

Straw / Fiber Tracker Rationale

Match intrinsic advantages of straw and fiber techniques.

Precision: S is easier and probably better than F.

Stereo: F is better and probably easier than S.

Occupancy: F has better occupancy characteristics than S.

Basic Idea

Straws for precision ϕ measurement for $R \gtrsim 1$ m.

Fibers for stereo.

Fibers for ϕ measurement for $R < 1$ m.

The Rest is Optimisation

Current Design

Stereo fibers at large R. Large (1.5mm) diameter fibers

Plenty of light (relaxed R/O requirements)

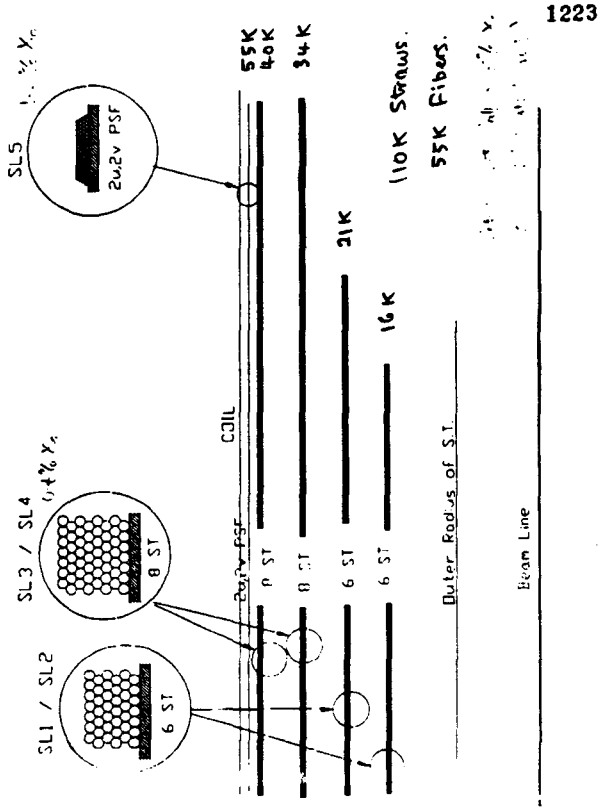
Few channels (~55K)

Axial straws; natural configuration (2 solutions: Modules or Single straws)

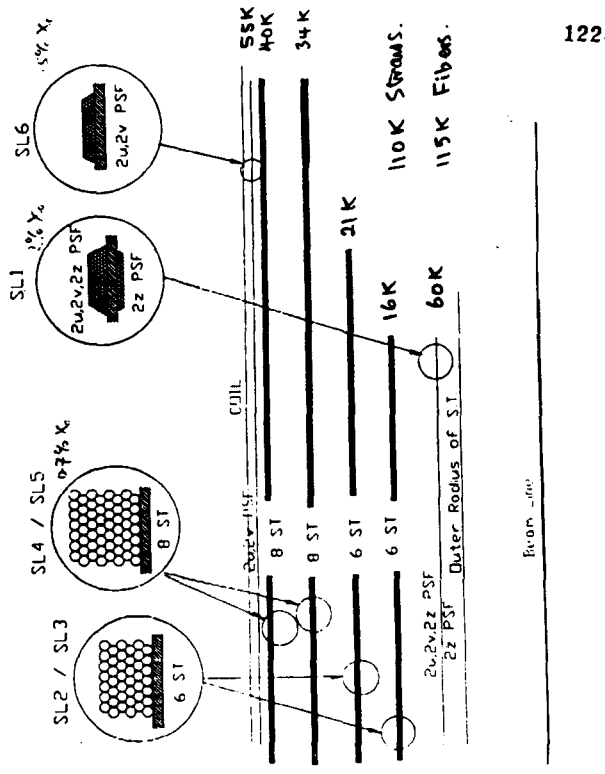
Small amount of material

Natural staging to high $\mathcal{L}$ NECESSARY & IMPORTANT

1223

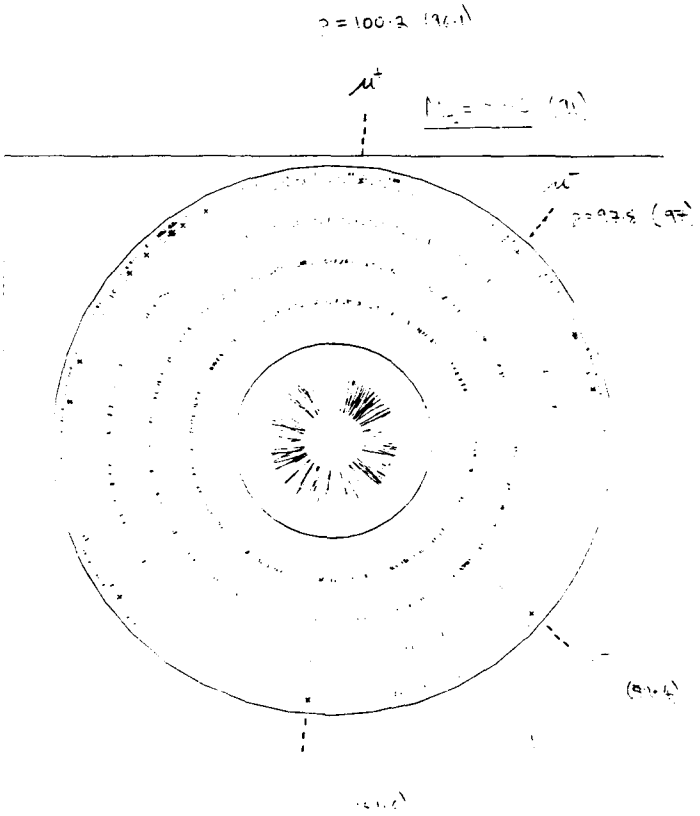


1224



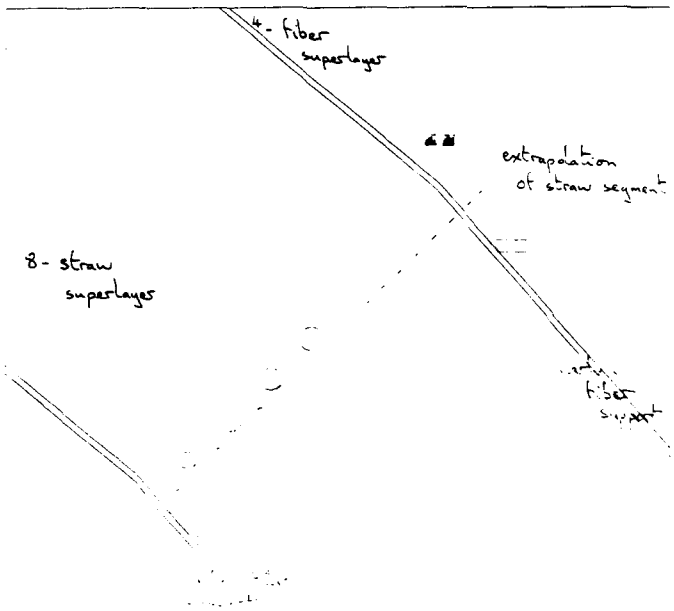
$M_H = 391\ (399)$

1225

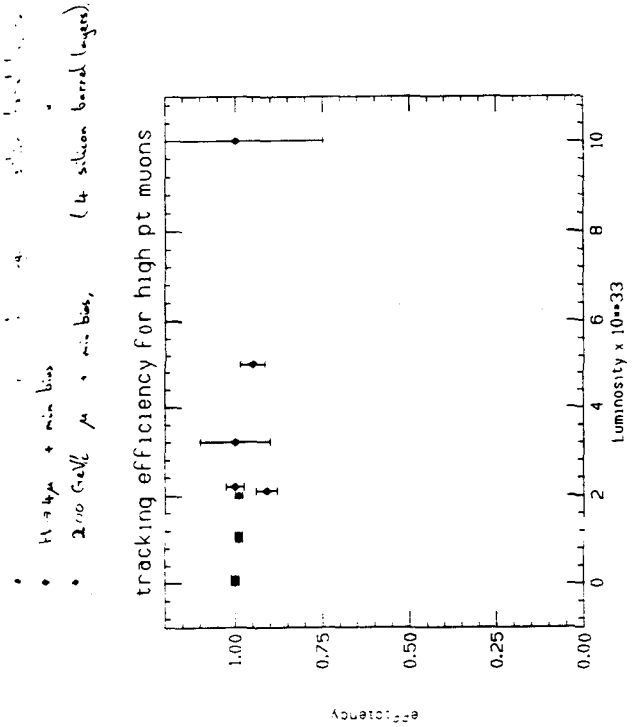


1226

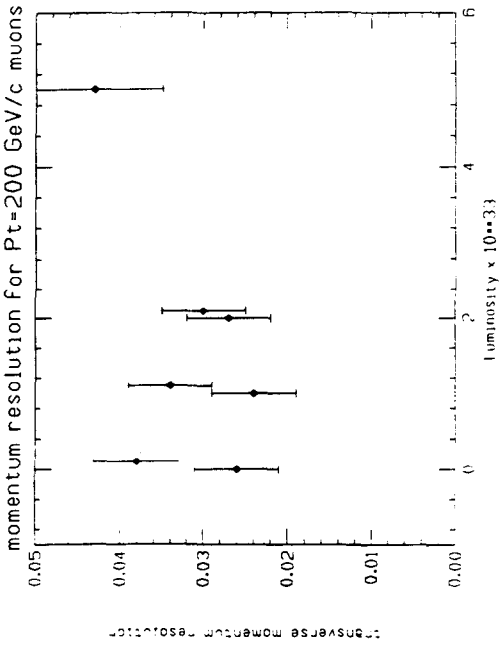
Hybrid Superlayer



1227



1228



1229

Cost Issues

- Neither technique is being pushed far beyond present level of expertise.
- This helps keep costs to a minimum.

  - No precision fiber alignment required
  - Few fiber channels (R/O cost not a critical issue)
  - Single straw approach costs less than modular
  - Purchase (rather than manufacture) ribbons
  - APD vs. VLPC (Competition!)

WBS (with ORNL)

Current design < $30M

Staging adds ~$5M

1230

Conclusions, etc.

Assumptions: Long, ≥ 1mm ϕ fibers work (incl. R/O)
Long, 4 mm ϕ straws work

Honesty: True VLPC doesn't yet exist
APD performance not yet proven
Long straws not yet operated at desired HV

Proof-of-principle doesn't yet exist for either technique.

Optimised Straw/Fiber outer tracker is affordable and feasible and provides the desired physics performance.

1231

Straw / Fiber Tracker

Conceptual Design Report

Organisation Meeting

8 AM Saturday 28th Room 1

— Everybody Welcome —

Progress in Simulating Combined Silicon and Straw Tube Tracking System

F. Luehring(Indiana)

PROGRESS IN SIMULATING COMBINED SILICON AND STRAW TUBE TRACKING SYSTEM

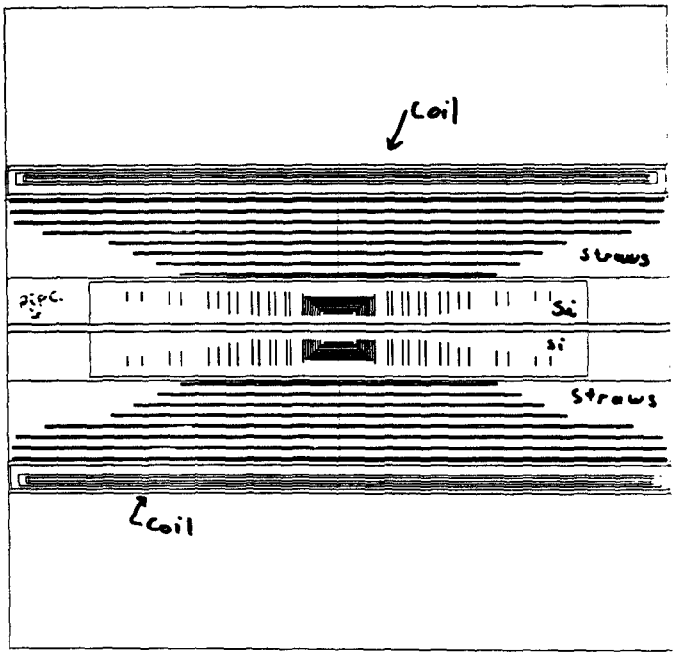
F. Luehring
Indiana University
26-Sep-91

INTRODUCTION

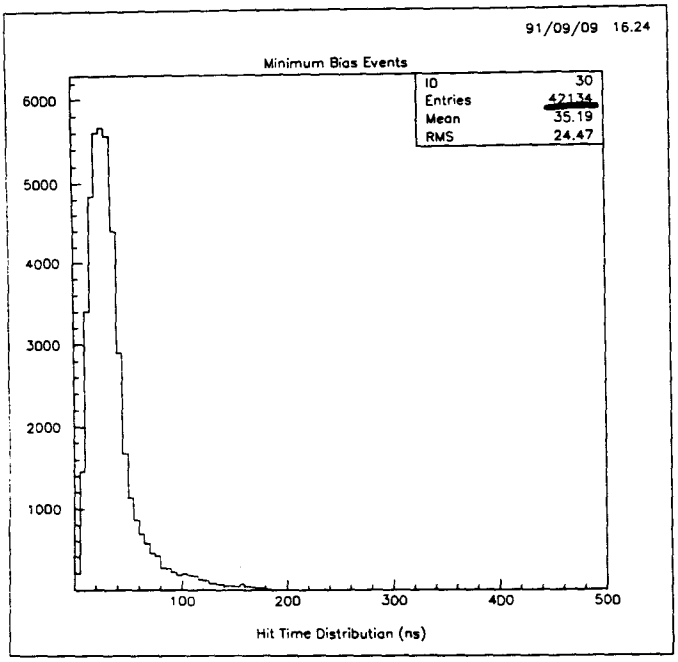
- Previous results
- New Segment Linking Algorithm
- Conclusions / Future Plans

STRAW TUBE OCCUPANCY REVIEW

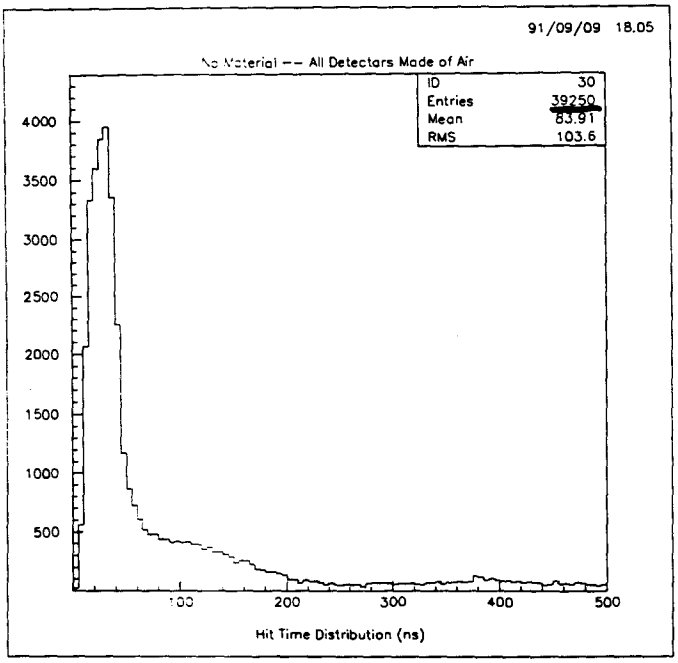
- Simulation conditions:
  - Beam pipe included.
  - Full silicon geometry (except pixels).
  - Full 8 superlayer straw tube system.
  - Magnet coil (with a uniform magnetic field over its entire thickness) included.
  - All parts of the detector have reasonable material allowances.
  - Minimum bias events are generated using Pythia version 5.4 and Jetset version 7.3.
  - Full accounting for flight time, drift time, and propagation time.
  - Events generated over the time range from -20 to +4 beam crossings. Hits from earlier tracks can shadow out later hits.



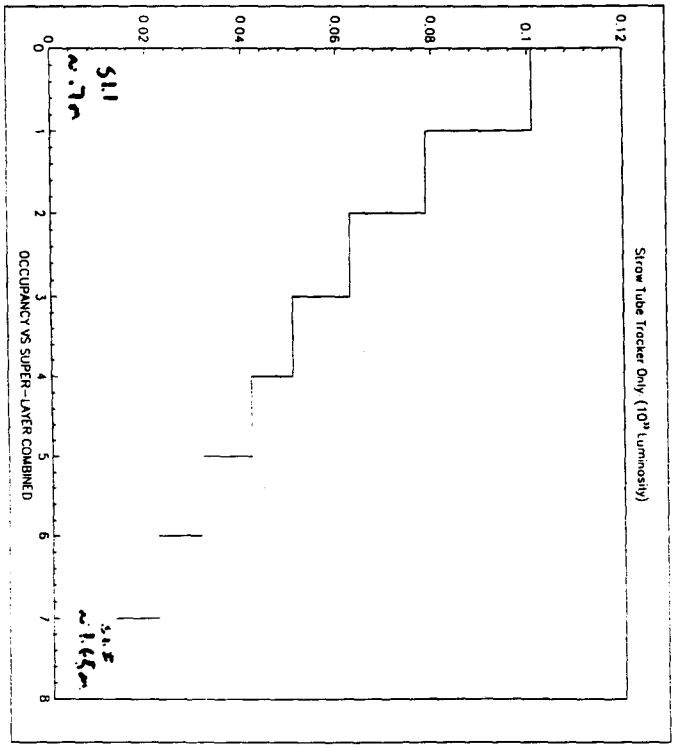
1237



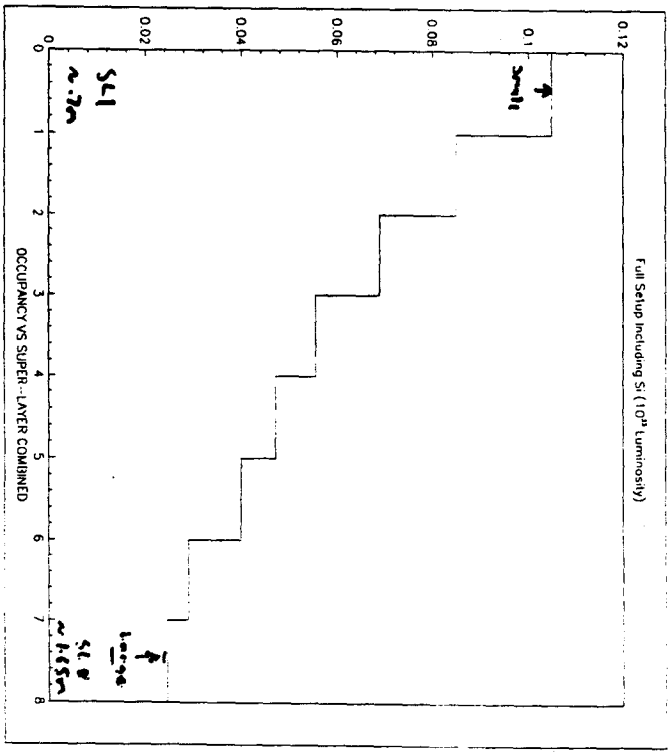
1238



1239



1240

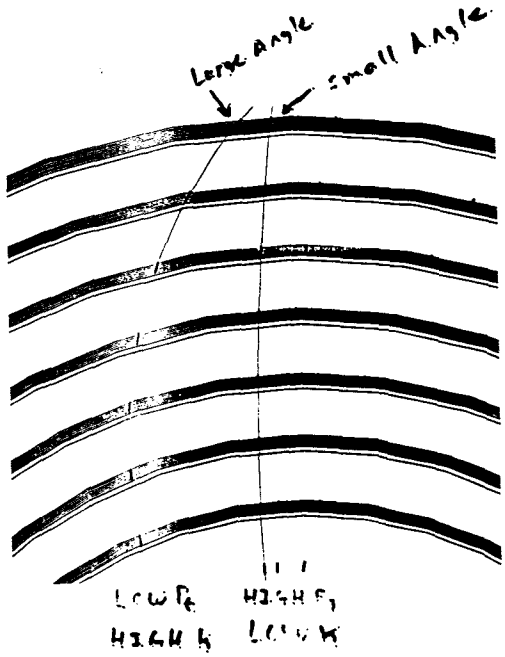


NEW SEGMENT LINKING ALGORITHM

1241

- **Algorithm Requirements**
  - Links previousiy found silicon and straw tube segments without requiring either system to anchor the track. The algorithm should treat both systems equally. In particular, we didn't want an algorithm that extrapolated a track from one system into the other.
  - The algorithm should not require any particular superlayer to have a hit to avoid losing tracks.
  - The algorithm must be able to work when the segment finding algorithm fails to find all of the segments on the track. Segments can be lost for a variety of reasons, both hardware and software.
  - The algorithm should take advantage of the curvature and Z information associated with segments to aid in the pattern recognition process.

1242



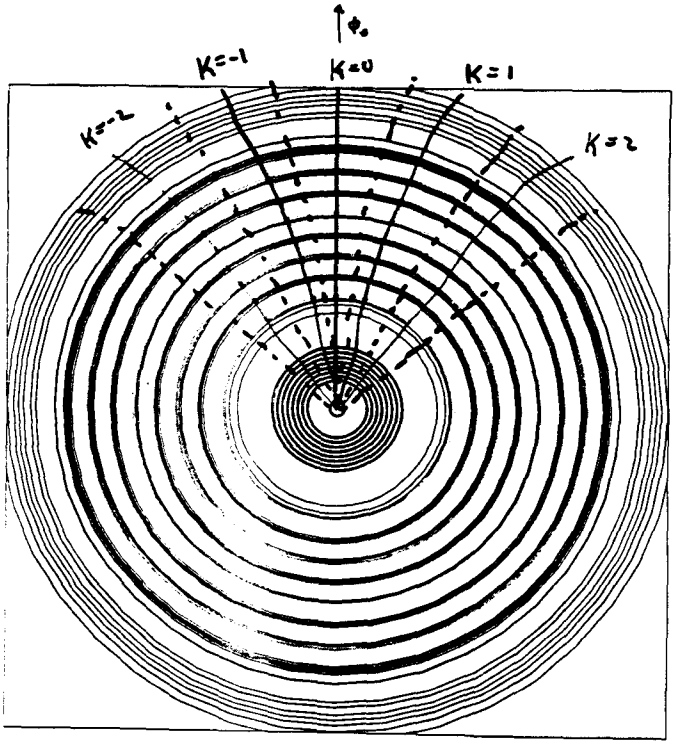
NEW ALGORITHM DESCRIPTION

1243

- Looks for hits along phi/curvature zones. The number of these zones is finite (a few thousand). These zones are trial tracks.
- Uses roads based on Φ_0 (Φ at the origin). For stiff tracks these zones look somewhat like a pizza pie. The zone edges are curved for lower P_t tracks.
- All superlayers are examined for segments that fall within the zones. Both forward and barrel silicon segments are considered when looking for segments within the zones.
- Z is considered in recognizing tracks. The Z matching algorithm uses stereo information for the straw superlayers and Z information from the silicon segments.
- If a segment is found within a zone, its <u>locally measured curvature</u> is compared with the zone curvature. If the segment passes this comparison, it is recorded as part of a potential track.
- If enough superlayers are struck, the potential track is recorded. A segment is allowed to be on any number of potential tracks.
- A second pass routine eliminates potential tracks that contain a large fraction of segments found on other tracks. When two potential tracks contain mostly the same segments, the one with segments linked in a larger number of superlayers is kept.

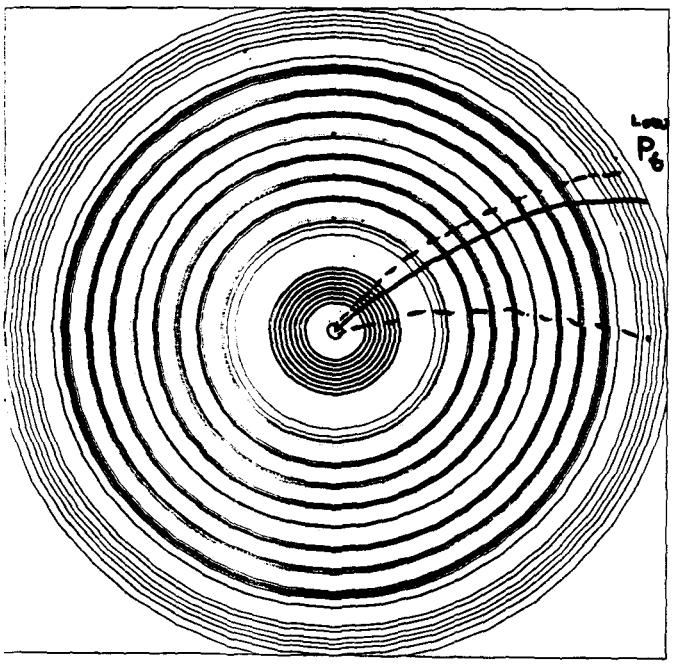
CURVATURE ZONES FOR ONE ϕ_0

1244



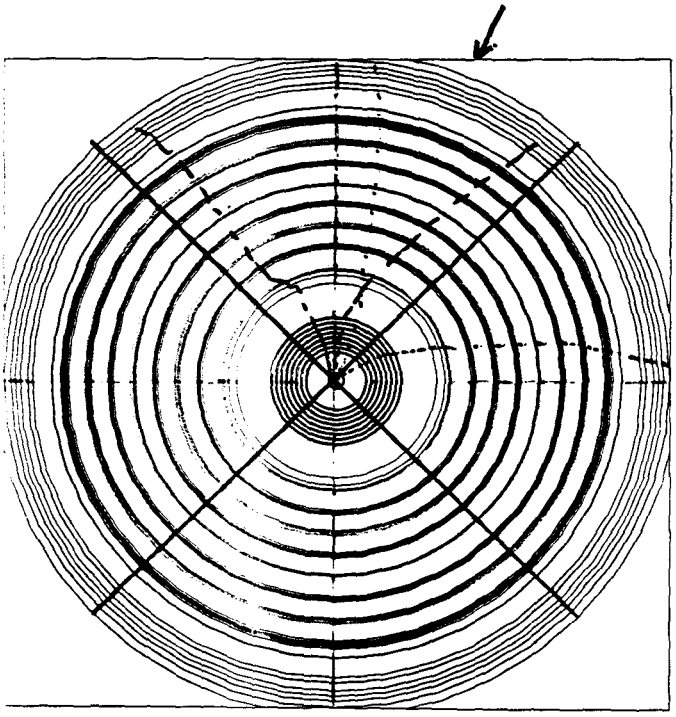
1245

HIGH VS. LOW P_t ZONES



1246

ϕ ZONES OVERLAP FOR A CURVATURE



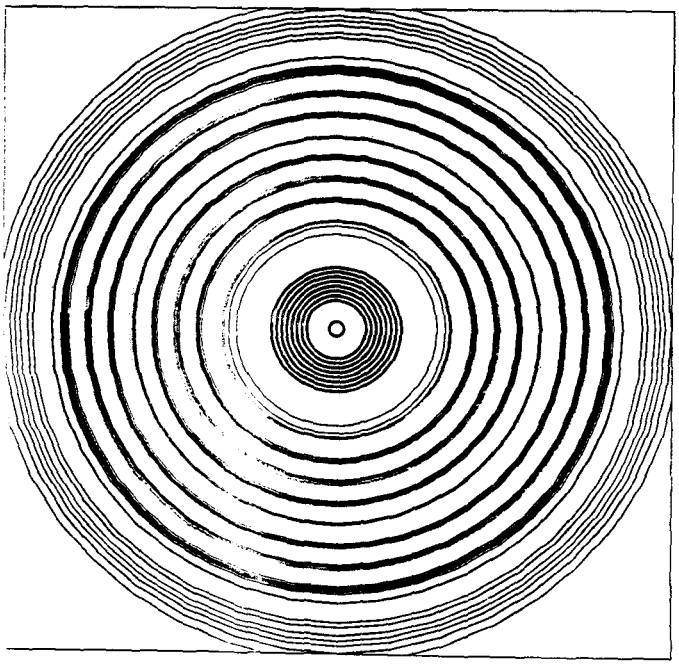
DETECTOR END VIEW

FIRST TEST OF NEW ALGORITHM

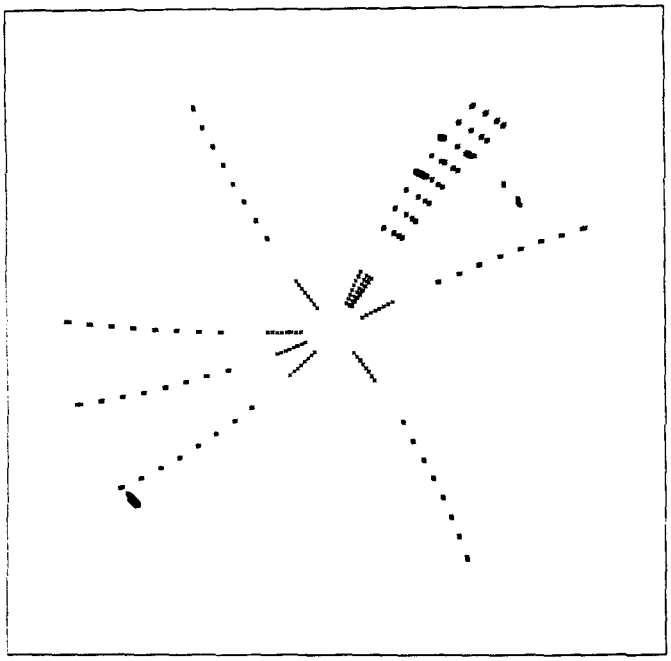
1247

- Types of Tests:
  - One track event (track stiff).
  - Two track event (tracks stiff).
  - Ten track event (tracks stiff).
  - The usual Higgs event (no minimum bias background).
- System Tested:
  - Full set of silicon strips (8 double-sided layers).
  - Full set of straws (7 superlayers of 6 straw layers and an 8th outer superlayer of 8 straw layers).
  - No pixels (but including pixel segments once they exist is in principle easy).
- General Observations from Tests:
  - The algorithm found the reasonably stiff tracks once it had been tuned up (even in the Higgs case).
  - The algorithm found extra tracks where the track densities were high. The part of the algorithm to remove the extra tracks removed some of these tracks but not all. Additional work remains on this point.
  - The CPU time consumption is higher than other segment finding algorithms but the time consumption is not totally unreasonable and much could be done to reduce it.
  - The shell is now usable for this kind of work because all of this was done within the shell.

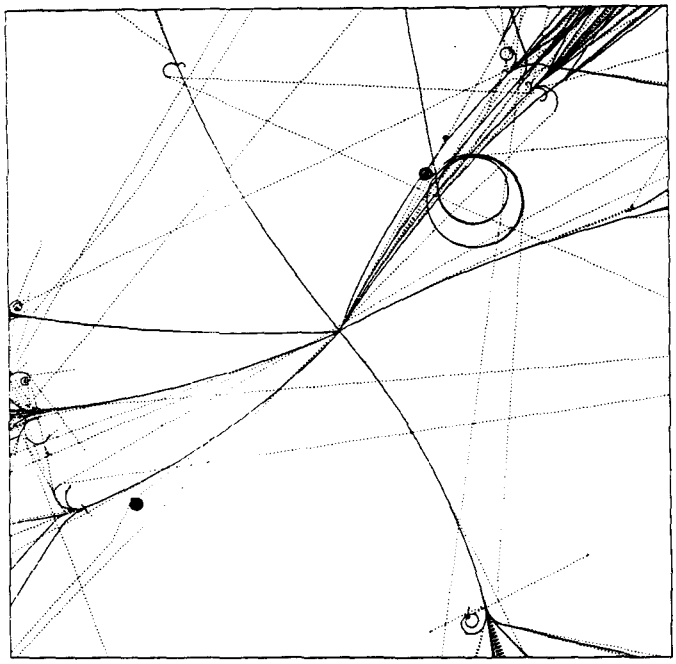
1248



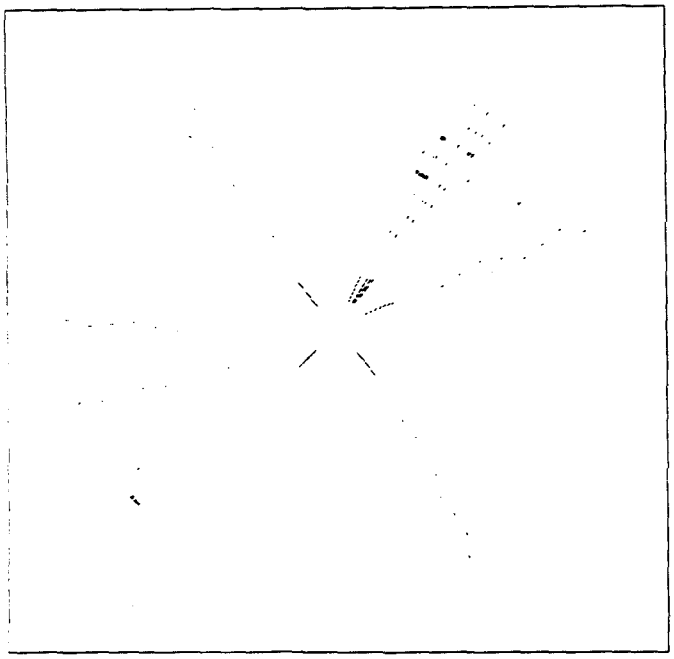
RAW HITS - 10 TRACK EVENT



RAW TRACKS - 10 TRACK EVENT



FOUND SEGMENT - 10 TRACK EVENT

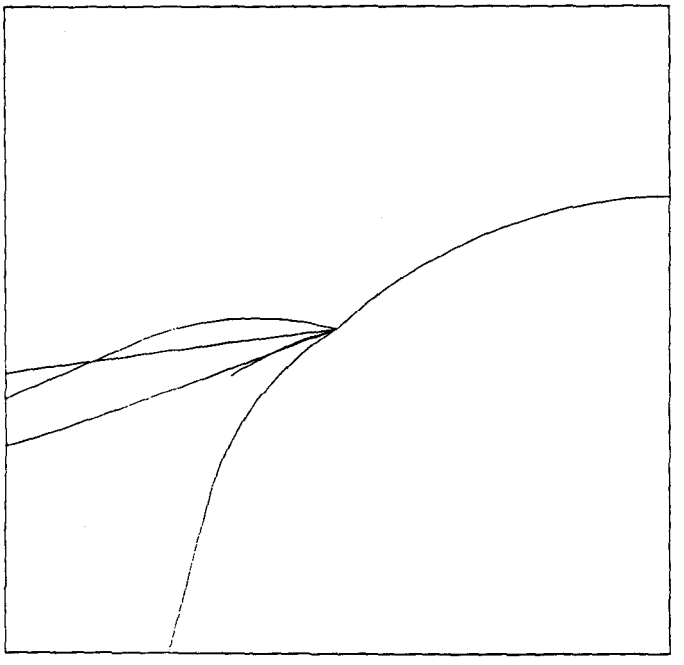


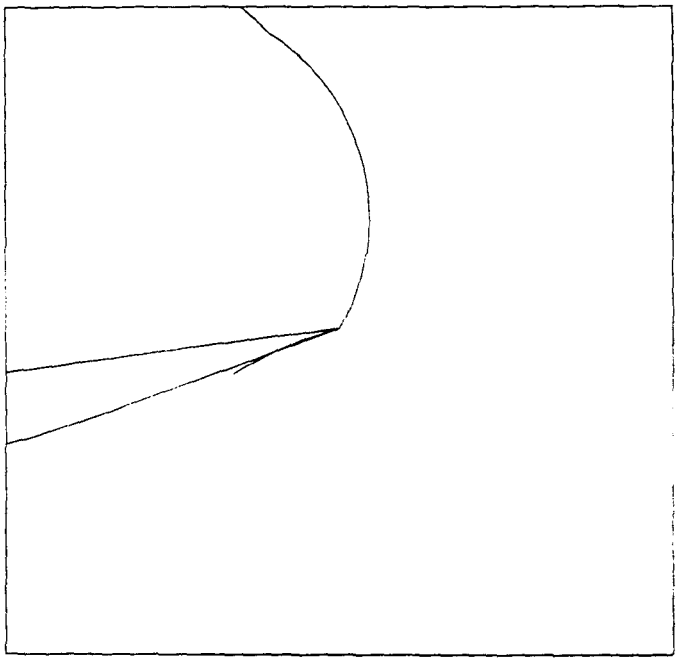
CONCLUSIONS / FUTURE PLANS

- Occupancy
  - Material increases the number of loopers but decreases the average looper track length and time in the system.
  - The occupancy is 10% on the innermost layers at the design luminosity.
  - The occupancy is 2% on the outer layer at the design luminosity (may be slightly overstated).
  - The Si tracker has a small effect on the straw tube occupancy.
  - The magnet coil has a much larger effect on the straw tube occupancy.
- New Segment Linking Algorithm
  - The algorithm is very promising and works in the test cases tried so far. More complicated types of events (Higgs + Min Bias, Jets) remain to be tried.
  - Trial descoped systems can be tested easily because the algorithm does not require a certain geometry (other than the existence of superlayers).
  - The track finding algorithm must be extended to fit the found tracks.
  - See Y'all in Dallas this November...

1253

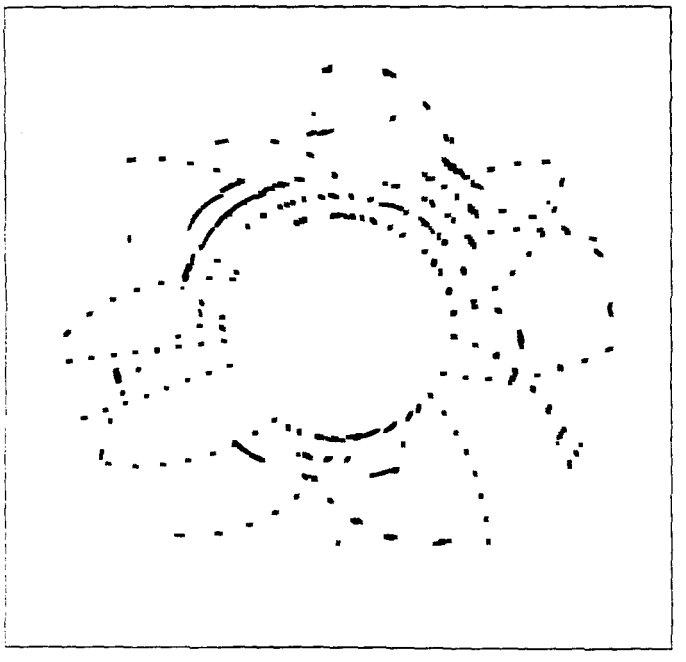
1254

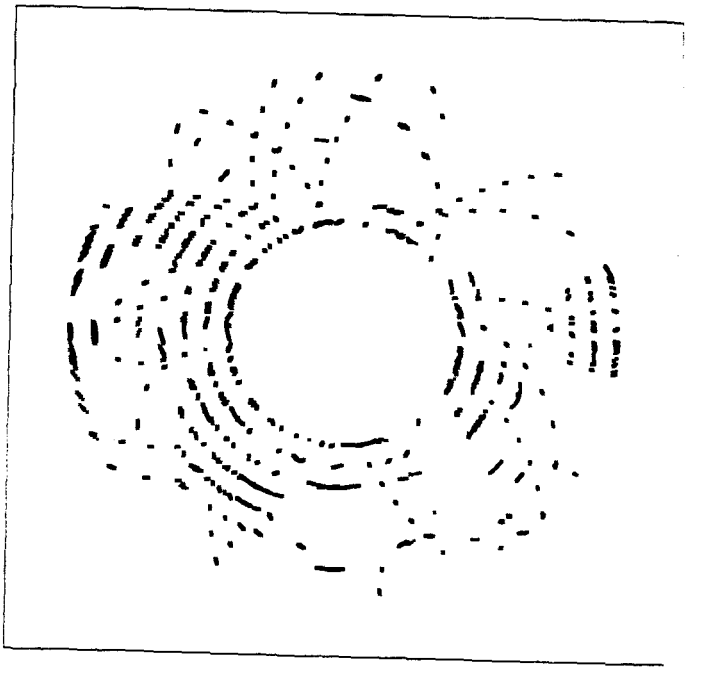




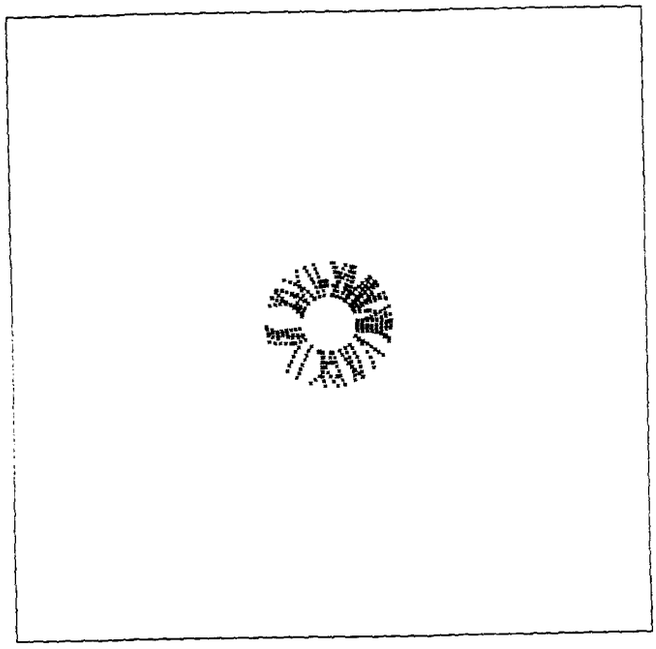
1255

1256

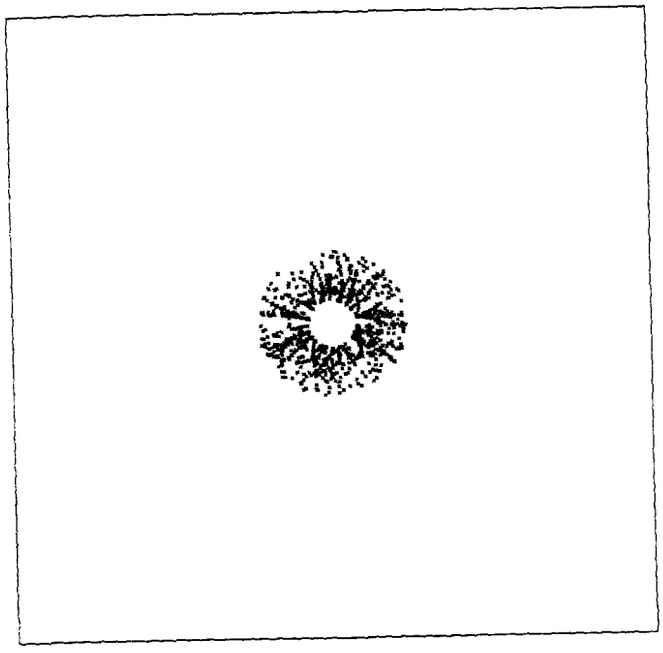




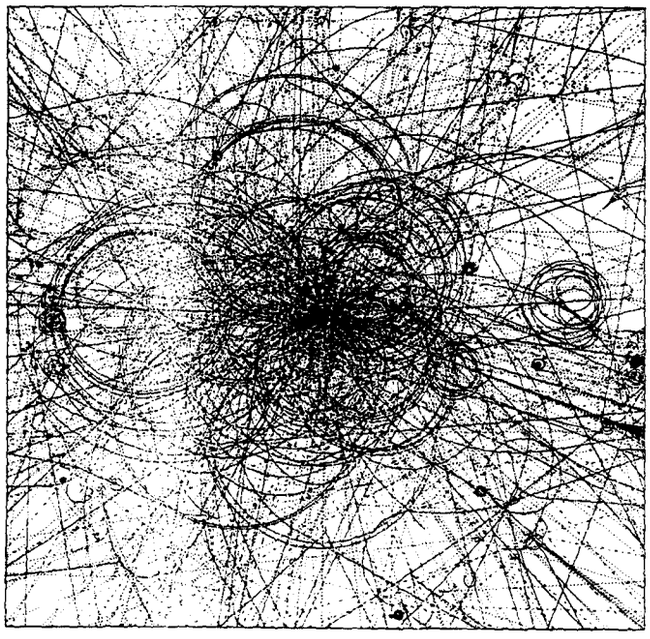
1257



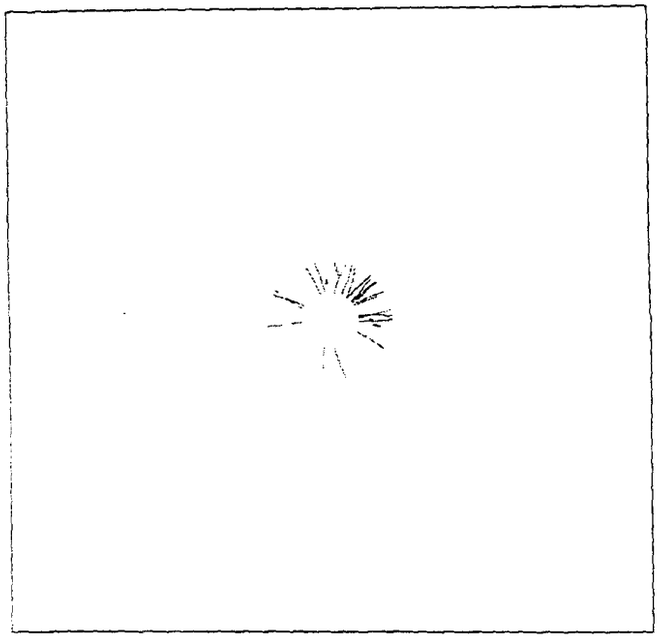
1258

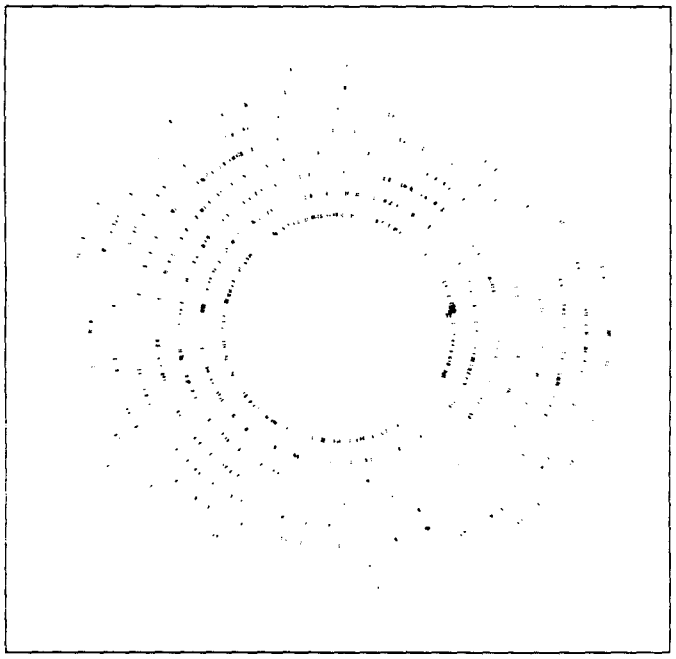


1259



1260





Pulse Attenuation in Straw Tubes

D. Rust(Indiana)

Pulse Attenuation in Straw Tubes

$V=V_0\exp(-\alpha z)$ where $\alpha=R_l/2Z_0$

z is the length along the tube
α is the attenuation constant
R_l is the sum of the of the cathode and the anode resistance per unit length
Z_0 is the characteristic impedance.

Z_0=304 ohms for a 25.4 μm wire in a 4 mm tube
=279 " " " 38.0 " " " " " " "
=262 " " " 51.0 " " " " " " "

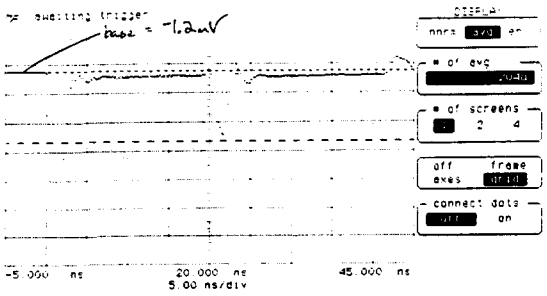
Resistance of 25.4 μm gold plated tungsten wire is 116±4 ohms/meter.

Resistance of 51. μm gold plated molybdenum wire is 30±1 ohms/meter

Resistivity of 0.2-0.25 μm aluminum coating is about 0.3 ohms/square

Resistivity of 0.15 μm copper coating is about 0.12 ohms/square

Mar 6, 91
CF_4 / Iso 80/20 Fe55
2519 V
2 mil 3 meter unterminated



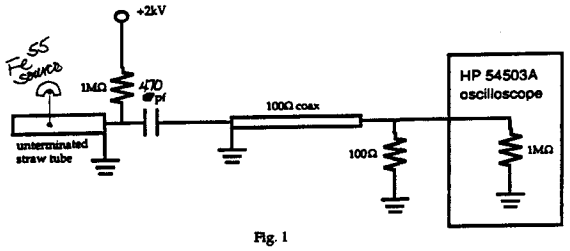


Fig. 1

Skin depth at 160 MHz for W/Mo is 10 μm:
No correction to the cathode resistance
~10% correction to R_l for 25.4 μm wire
~50% " " " " 51. " " .

Measurements:

25.4 μm wire, 0.25 μm Al cathode, α=0.26/m(calc.)
=0.26/m(meas.)

51 μm wire, 0.25 μm Al cathode, α=0.14/m(calc)
=0.14/m(meas)

Estimates:

38 μm wire, 0.15 μm Cu cathode, α=0.14/m

51 μm wire, 0.15 μm Cu cathode, α=0.11/m.

Amount of material:

0.25 μm aluminum ≈ 2.8×10^{-6} R.L.
0.15 " copper ≈ 10.5×10^{-6} "
35. " mylar ≈ $122.\times10^{-6}$ "

For a total of 34 layers, copper ≈ 0.1% R.L.

Conclusion: attenuation length is 7 m; a tolerable attenuation over 4 m. (44%)

Straw Tube Operation in High Radiation

Charged Particle Induced Integrated Current in straw tube:

Using £ = $10^{33}/cm^2/sec$
1 yr = 10^7 sec
tube length = 3m
tube radius = 0.4 cm
tube gain = 2×10^4
ionization in CF_4 = 180 e/cm

radius	Occupancy(50 ns)	Integrated Charge
69 cm	0.116	13.3 mC/cm/yr
82	0.088	10.1
95	0.070	8.0
108	0.052	6.0
122	0.040	4.6
135	0.024	2.8
148	0.018	2.1
161	0.011	1.3

Neutron Induced Intgrated Current in Straw Tube:

Using:
Neutron kinetic energy = 1MeV
Neutron fluence = $3\times10^{11}/cm^2/yr$
20% isobutane in gas
5% hydrogen in straw wall
Neutron cross section = 4.5 barns on hydrogen

Interaction rate = 1.2/cm/sec in gas
Integrated current = 0.8 mC/cm/yr from gas collisions

Interaction rate in tube wall = 15/sec/cm
assume 1/4 pass into the gas and deposit 1/2 the ave kinetic energy:
Integrated current = 1.2 mC/cm/yr from wall

More than half the current in outer layers from neutrons.

Limitations on the lifetime of straw tubes operated in a high radiation flux.

No problem at wire using CF_4 and isobutane.
No whisker growth; but there is a small gain change at levels of ~1mC/cm.

Possible limits of the cathode:

Ablation appears to occur at a rate not exceeding .1 μm/C/cm; or .01 μm in 10 years at 70 cm. Assumes no breakdown currents.

Measured from resistance change of an irradiated strip.

Alteration of an aluminum coating which causes breakdown.
After an extended exposure to radiation, a tube with an aluminum coating will breakdown at high gain in a high radiation flux.
Problems at the level of twice the dose, five times the gain and ten times the radiation level, for example, is a fair estimate.

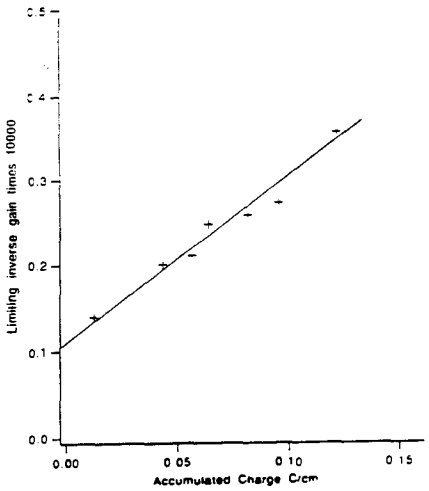


Fig. II-4. The dependence of the limiting inverse gain on the total exposure at a level of radiation 300 times the level expected at design luminosity for a tube 70 cm from the beam.

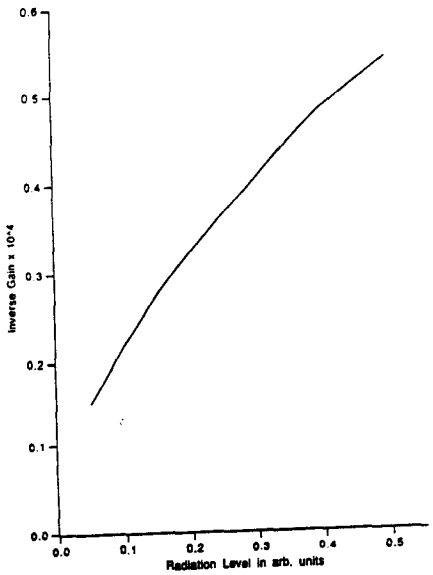


Fig. II-3. The limiting inverse gain vs. radiation level for a straw after exposure resulting in 0.2 C/cm of charge deposited on the wire. Full scale is 500 times the radiation level at design luminosity for a tube 70 cm from the beam.

Bypass the problem. Use copper coated tubes.
No breakdowns.

Besides better stability with respect to radiation they have better and more predictable conductivity.
Minor drawback: .1% R.L. vs. .03% R.L. for 34 layers.

Polycarbonate base material is inferior to mylar or kapton. Dimensional stability, adhesion.

Conclusion: Straw tubes of mylar or kapton with copper coating will endure many times the radiation levels anticipated at the SSC.

Straw Electronics and Interconnections

W. Ford(Colorado)

Straw Electronics & Interconnections

1272

Goal: Multi-crossing detector tests of straws with custom front-end electronics (high-sensitivity)

- low gas-gain operation
- efficiency
- resolution
- long detector performance
- trigger circuit performance

Detector prototypes at DAS, Colorado, Duke, Indiana, Michigan

A-5 chips in single channel packages: early '91

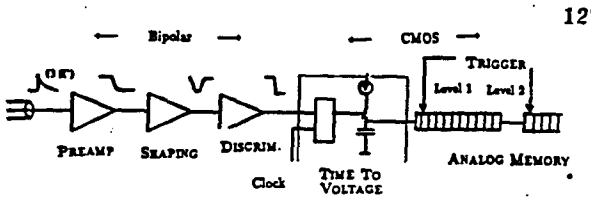
CM 16-channel boards compatible with all test setups
- board fabrication: 1st 3 in hand
- partially-loaded (4-chan) due for bench tests at Penn: next week
- sets for 64 chan. to each institution: mid-November

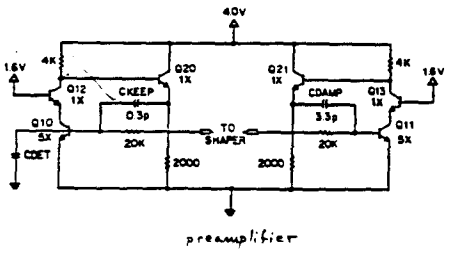
A-7 chips in 8-channel packages:
- submission in time for next Tektronix run (June)
- Delivery Dec'91 - Feb '92

7-bit chip w/ [illegible]
- built to MOSIS and ~~set~~ fit
- Delivery: early '92

[illegible]: mid Nov '91
- [illegible]
- High density ~~for~~ toward long range design
- Multi-[illegible] tubes

1273





preamplifier

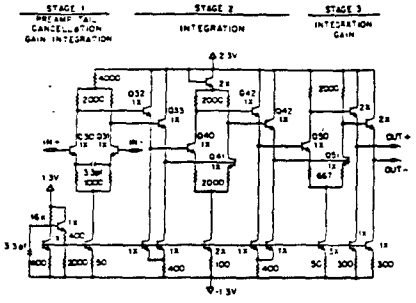
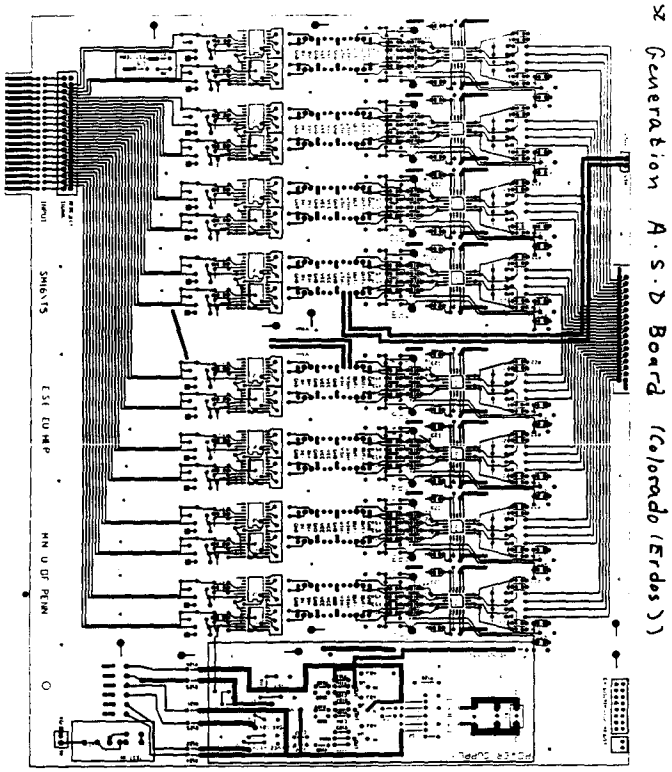


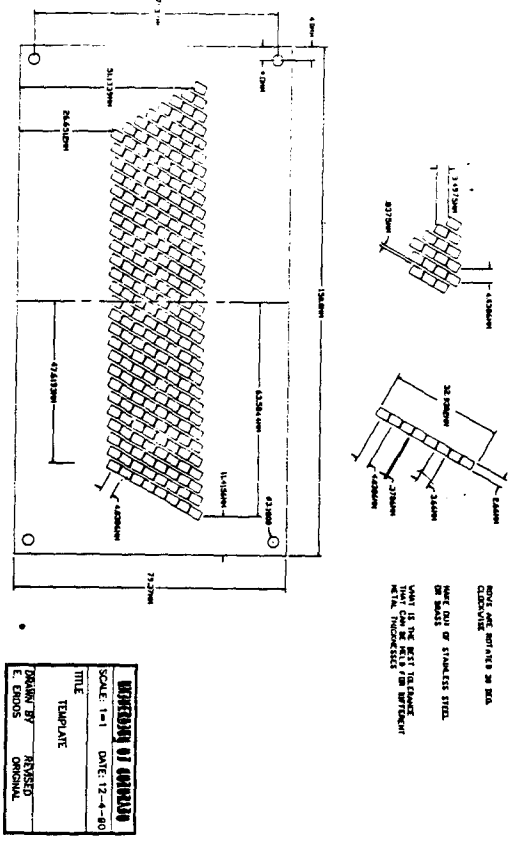
Figure 6 Schematic for prototype shaper

1274

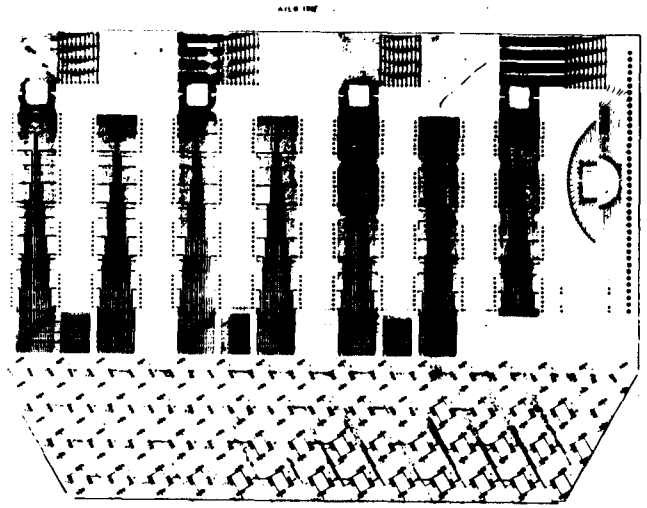


1x Generation A.S.D Board (Colorado (Erdos))

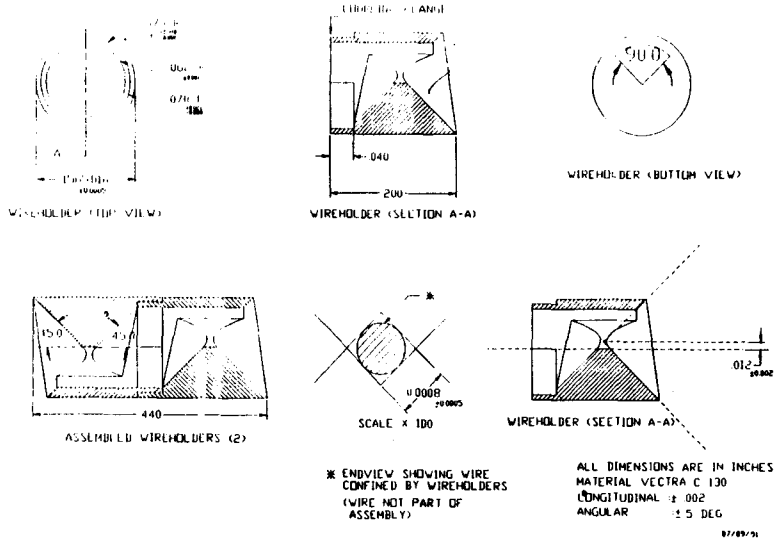
1275



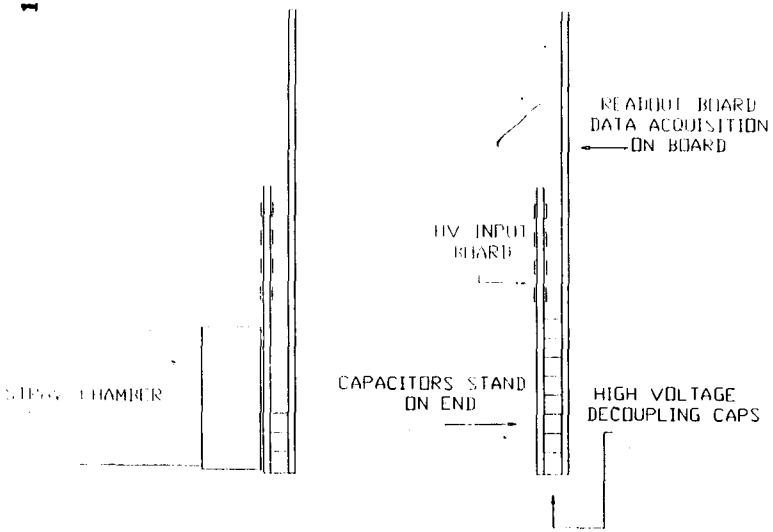
1277



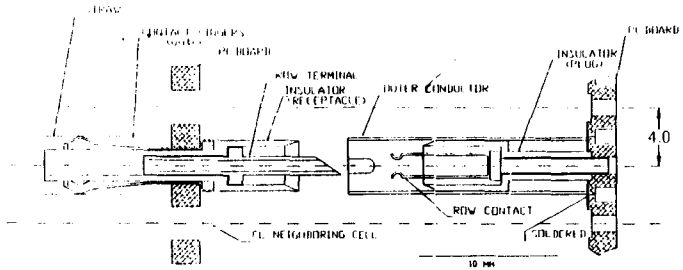
1279 (D. Alexander)



1276



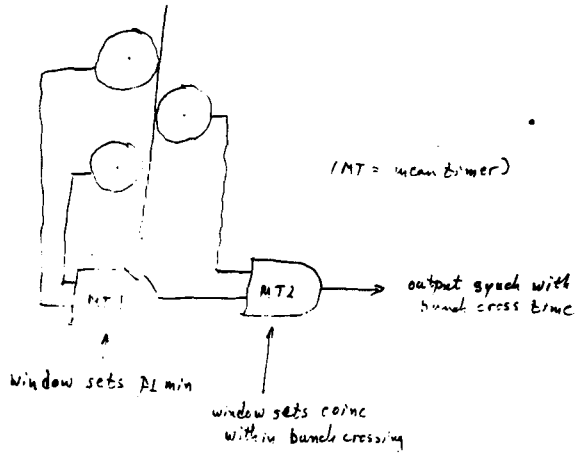
1278 (G. Schulte)



COAXIAL CONNECTOR STRAW CHAMBER
CROSS SECTIONAL VIEW

Straw Superlayer Trigger Circuit
(Chapman, Michigan)

1280



analog ... digital ... tested
simulation ... results
... Monte Carlo

1281

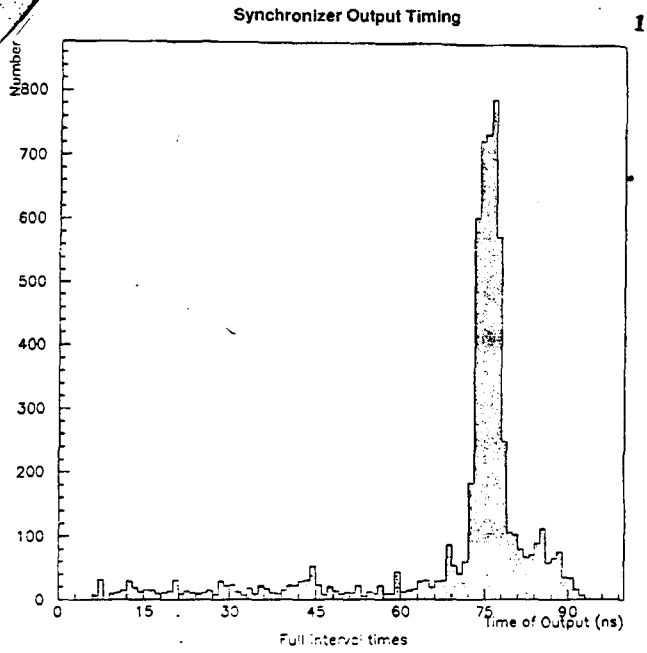


FIG. 1 Pulse timing for the GEANT simulation of tracks in the outer layer of the SDC detector instrumented with mean timer circuits that produce an output time displaced from the particle passing time by a fixed value, ≈45ns. An additional 30ns delay is seen in the plot due to the particle flight time to the superlayer and the propagation time of the signal to the end of the straw. This particle and signal flight time varies over a range of about 8ns and is therefore the major contributor to the spread in the arrival times.

1282

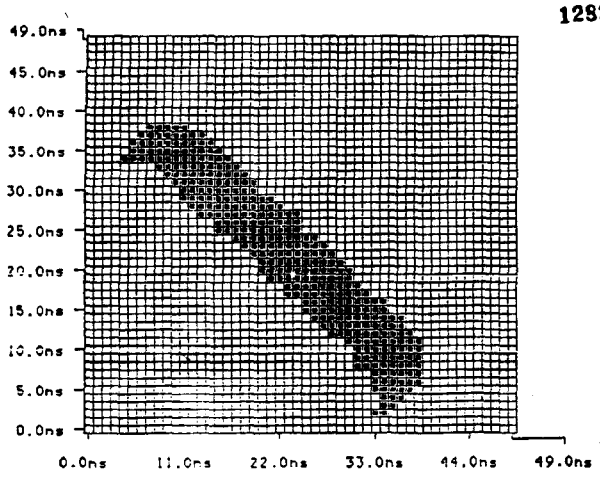


FIG. 2 A test plot of the P_t cut portion of the mean timer IC. The axis are the times of the aligned wire inputs and the plotted points are those values of the axis coordinates for which an output was generated at a predetermined value. A falling 45° is expected for ... straddling of the input times. The cutoff of the line at large coordinate differences is due to the time difference restriction (momentum cut).

Trigger Algorithm Simulation

We have ... trigger simulation in the framework of GEANT, a fast ... of a stiff ... and with a ... global trigger being simulated at Chicago. The ... stiff track signal for electron identification has been ... strons can

1283

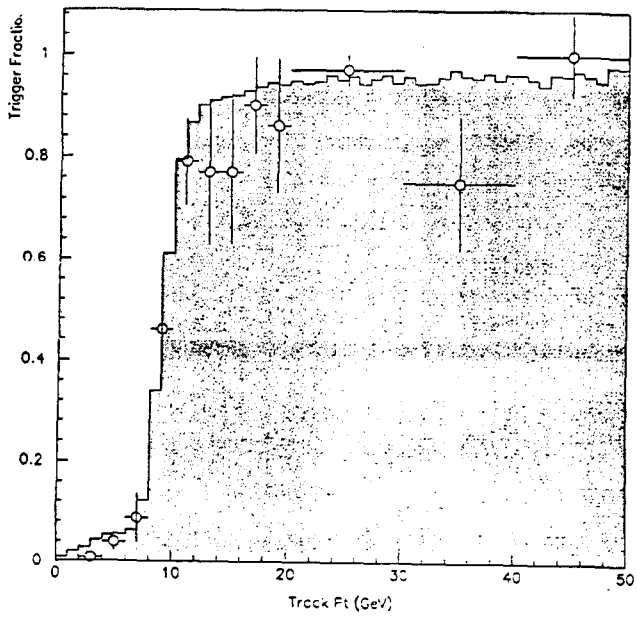


FIG. 3 The efficiency as a function of P_t for a digital mean timer based trigger operating on signals from an 8 tube deep superlayer of packed straw cells. The points are from a GEANT simulation of Higgs → ZZ events at 10^{33} luminosity and the shaded histogram is for a fast parameterized simulation tuned to match the GEANT points.

be effected) and the stiff track ... approximately 15% or

(includes some electronics)

We consider proof-of-principle to include the following:

1. Fabrication of a 4-meter long module shell; measurements to show that it meets tolerances for straightness, rigidity, dimensional stability, upper limit on number of radiation lengths, etc. Placement of straws and wire supports, and measurements showing that their position accuracy is within tolerances. Assessment of costs showing that they are within budget.

1a. The backup for this is demonstration of a technique for reproducibly placing straws directly onto precision cylinders; measurements showing that position accuracy of straws and wire supports is within tolerances. Assessment of costs showing that they are within budget.

2. Performance measurements with custom amplifier/shaper chips showing good straw chamber efficiency and resolution at gas gain levels low enough for operation at SSC design luminosity.

2a. Development of crosstalk-free connection from wire to electronics.

3. Continued radiation damage tests covering options for cathode conductor materials, thicknesses.

4. Bench test 8-channel A-S-D chip. (in Electronics budget)

5. Bench test TVC/AMU. (in Electronics budget)

6. Test A-S-D chip operation on same board as TVC/AMU to investigate crosstalk between digital and low-level analog lines. (in Electronics budget)

Next are long lead-time issues where important questions are outstanding:

1. Conceptual design of basic structure to support modules and attach them.

2. High-density packaging of custom readout chips directly on substrate. (in Electronics budget)

3. Low mass straw termination resistor/capacitor assembly.

4. Fo current spark protection for HV circuit.

5. Short isolation for HV circuit.

Good progress on the remaining items in the original R&D plan including system prototype fabrication for test beam run the following year is required to stay on the SDC construction schedule.

Overview of Fiber Tracking System Design

D. Koltick(Purdue)

Overview of Fiber Tracking System Design

1286

D. Koltick
Sept. 27
ORNL

University of California at Los Angeles
Fermi National Accelerator Laboratory
University of Illinois at Chicago
• Indiana University Purdue University at Indianapolis
• Massachusetts College of Pharmacy and Applied Health Sciences
• Northeastern University
University of Notre Dame
Oak Ridge National Laboratory
Pennsylvania State University
• Philadelphia College of Pharmacy and Science
Purdue University
Rice University
University of Texas at Dallas
Tsukuba University

• NEW Group This YEAR

September 24, 1991

STARTED Discussions with
Duke
INDIANA
⋮

Goals of The Scintillating Fiber Central Tracker

1287

I. First Level, FAST charged Particle Trigger $P_\perp$ measurement upto $L \sim 10^{31}\ cm^{-2}\ sec^{-1}$

II. Momentum Measurement

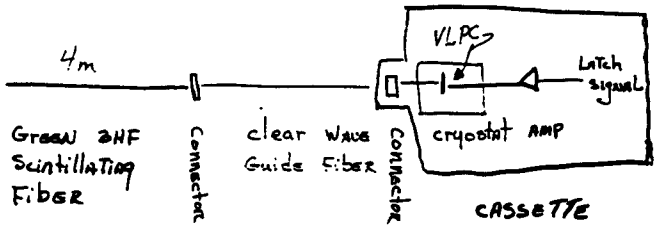
$$\frac{\delta P_\perp}{P_\perp} \sim 25\% \cdot P_\perp (TeV)$$

$\eta \lesssim 1.5$ upto $L \simeq 10^{31}$ (startup)

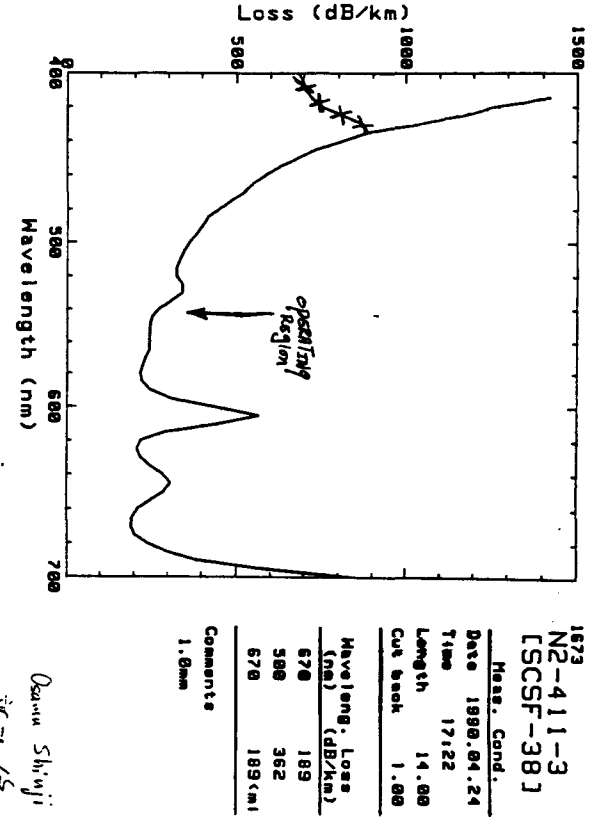
III. Excellent tracking efficiency for High $P_\perp$ tracks because of fine granularity + low occupancy.

Scintillating Fiber System

1288



1289



1673
N2-411-3
[SCSF-38]

Meas. Cond.	
Date	1990.04.24
Time	17:22
Length	14.00
Cut back	1.00

Wavelength (nm)	Loss (dB/km)
670	189
588	362
670	189(ml

Comments
1.0mm

Osamu Shiyji

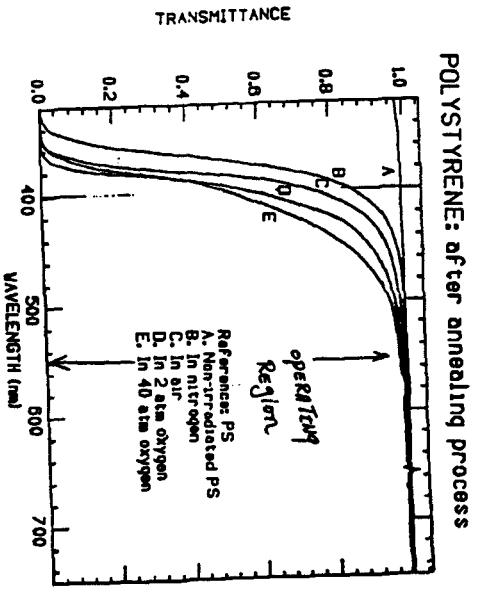


Figure D2. Irradiation and annealing of polystyrene in various atmospheres.

AT $L = 10^{34}\ cm^{-2}\ sec^{-1}$ dose ≈ 1 Mrad in 10 years

Table D1.

Light yield before and after 10 Mrad radiation dose from ^{60}Co source (in arbitrary units).

SCINTILLATOR[a]	λ^b (nm)	Light yield Before	After	After 13 d[c]	After 53 d[c]	Ratio[d]
MOPOM	420	0.79	0.04	0.42	0.49	0.62
MOPOM+0.01%BBQ	470	0.95	0.13	0.63	0.71	0.75
MOPOM+0.02%BBQ	470	0.96	0.16	0.69	0.76	0.79
MOPOM+0.01%K27	500	0.95	0.27	0.75	0.83	0.87
MOPOM+0.02%K27	500	0.95	0.27	0.75	0.84	0.88
O415A	415	0.92	0.49	0.79	0.88	0.96
O415A+0.01%BBQ	470	1.01	0.42	0.88	0.97	0.96
O415A+0.02%BBQ	470	1.02	0.34	0.89	0.99	0.97
O415A+0.01%K27	500	0.97	0.57	0.87	0.96	0.99
O415A+0.02%K27	500	0.99	0.53	0.86	0.98	0.99
O408	410	0.88	0.48	0.76	0.83	0.94
O408+0.02%BBQ	470	1.02	0.34	0.87	0.99	0.97
O408+0.02%K27	500	0.97	0.57	0.89	0.98	1.01
DAT	375	0.73	0.16	0.66	0.47	0.64
DAT+0.01%DMPOPOP	430	0.88	0.31	0.76	0.75	0.97
DAT+0.01%3HF	530	0.88	0.40	0.83	0.69	0.81
pT	360	0.84	0.21	0.41	0.42	0.50
pT+0.01%DMPOPOP	430	0.89	0.51	0.71		

[a]Fluor concentrations are by weight, the concentrations of primaries are 1% (1.25% for DAT and pT). [b]Wavelength of peak emission. [c]First 10 days in oxygen and the rest in the air. [d]After 53 d/Before.

81%

We have at least a factor 10 safety factor.

Key Points in the operation of the System.

1. VLPC's have ~85% Q.E. in the region $\lambda \approx .3 - 1\ \mu m$

   ⇒ good operation @ $\lambda \sim 550$ nm

2. Polystyrene has excellent transmission in the range $\lambda \sim 500 - 600$ nm

   ⇒ clear fibers with attenuation lengths of >10 meter are being made by several companies.

3. Radiation Damage to light out put and attenuation Length is small in the region $\lambda > 600$ nm

   ⇒ Scintillating fibers will perform well at the SSC.

Radiation at SSC will not be a Problem.

Nonetheless Experiment T-851 will check Radiation Damage with fibers in various environments in the FermiLab Tevatron

1294

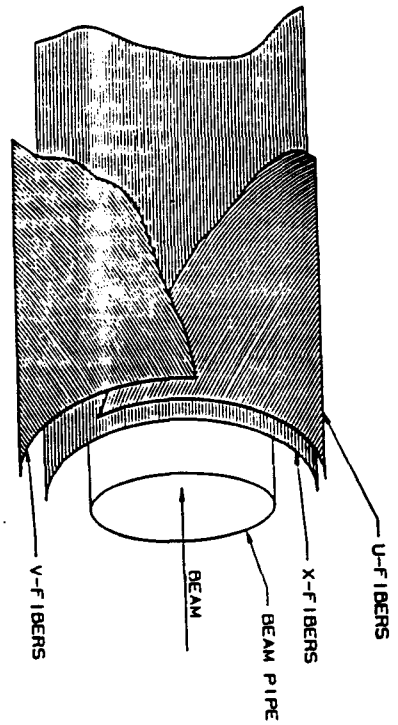


FIG. 1

FIBERS ARE FLEXABLE ⇒ STEREO IS EASY

850 μm DIAMETER

1295

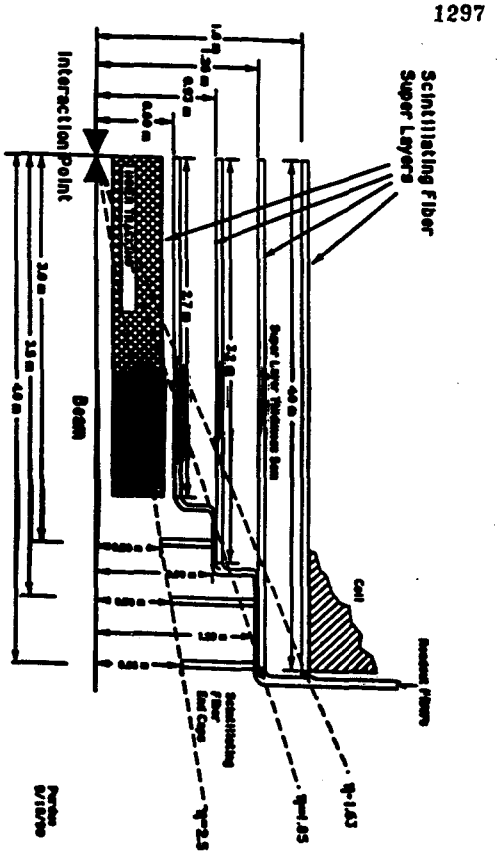
ADVANTAGES of A FIBER TRACKER

- Low Occupancy $< 1\%$ @ 10^{33}
  ⇒ CAN Operate well @ $L = 10^{34}$
- Electronics = 1 Latch/Fiber
  ⇒ Simple ⇒ Signals already digitized
- Two Track Resolution < 1 mm
- PASSIVE System Within Tracking Volume.
  - INSENSITIVE to R.F. NOISE/BEAM Pickup
  - INSENSITIVE to Magnetic Field
  - No High VoltAge
  - No HEAT dissipation
  - No Flammable gas

1296

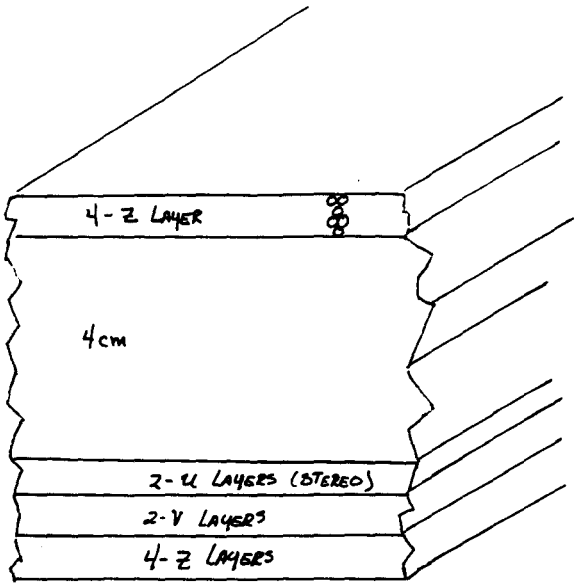
- SCINTILLATOR has an INTRINSICALLY prompt RESPONSE
  ⇒ SINGLE-crossing time resolution
- Flexibility of FIBERS + FIBER RIBBONS
  ⇒ Implementation of STEREO FIBERS Is Simple
- Good resistance to radiation DAMAGE IN our WORKING λ region
- All ELECTRONICS outside The TRACKING VOLUME FOR EASY ACCESS.
- VLPC ⇒ High Rate Capability

1297



Cross-Section of a SuperLayer

1298

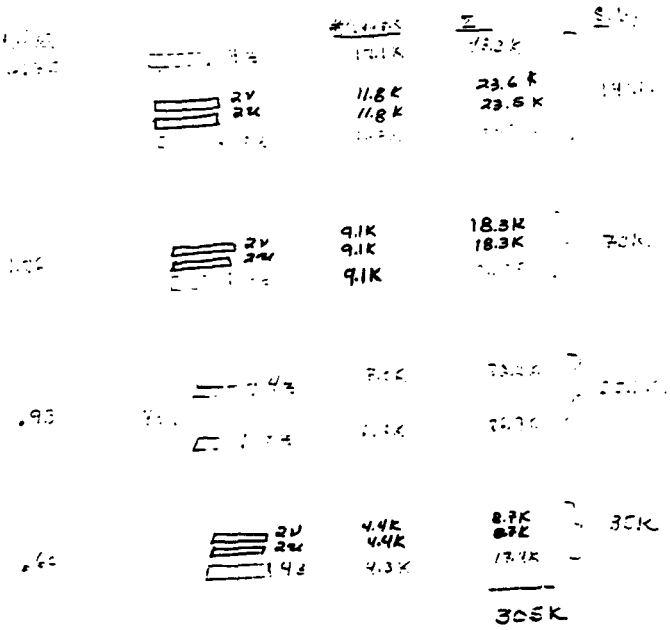


Vector LAYER

Fibers 830μm diameter

SuperLayer Structure

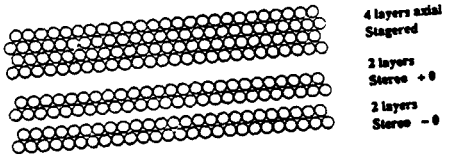
1299



TOTAL SYSTEM 610K Fibers IN the Central TRACKING Region.

1300

Scintillating Fiber Super layer



TOTAL # of FIBERS IN The CENTRAL Region 610K

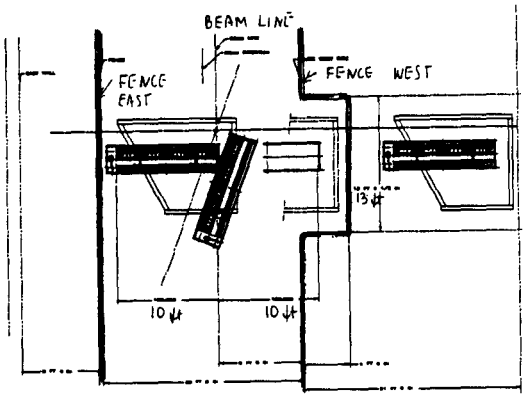
TOTAL # of FIBERS IN The INTERMEDIATE Region
= define 200K

Cost of Central Region tracking
$37.1M
with 36% Contingency $5CM.

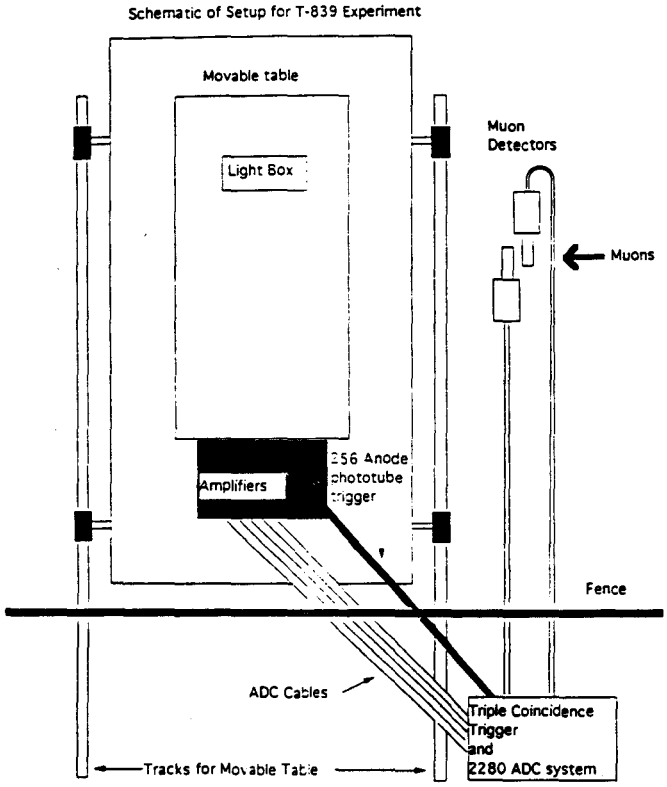
Cost of The Intermediate tracker
$11M.
with 36% contingency $1.5M.

1301

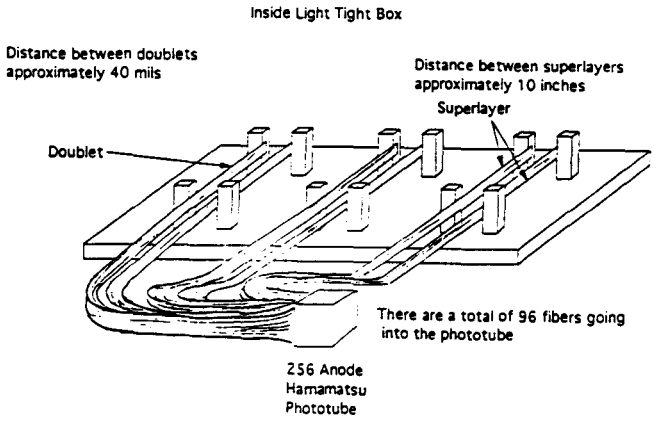
New Muon AT FERMI LAB



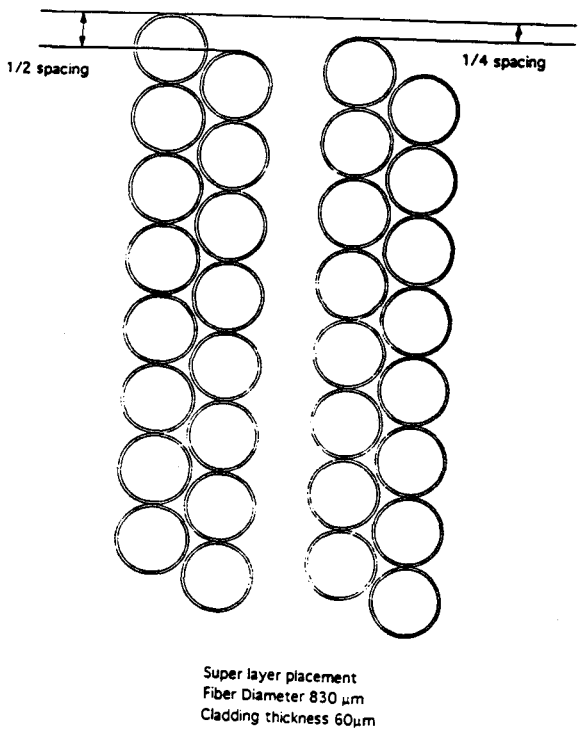
1302



1303



1304



1305

Fiber Ribbons made at Purdue.

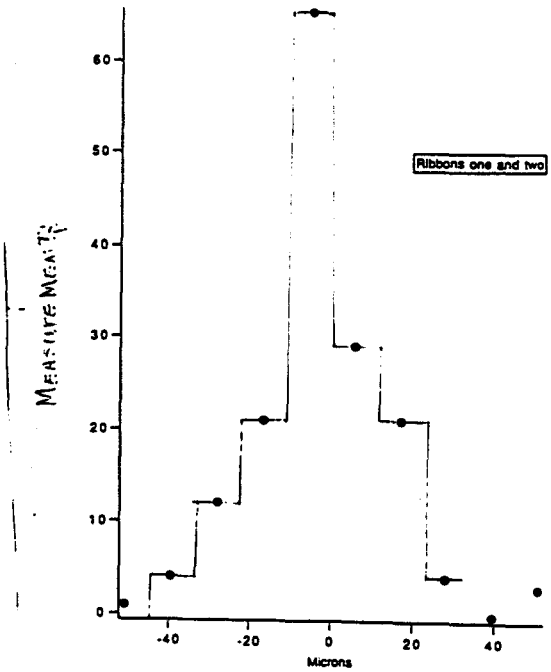
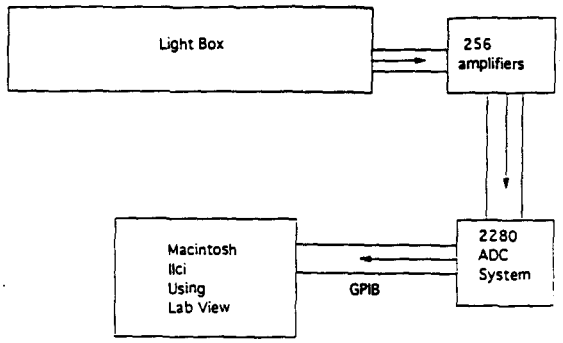
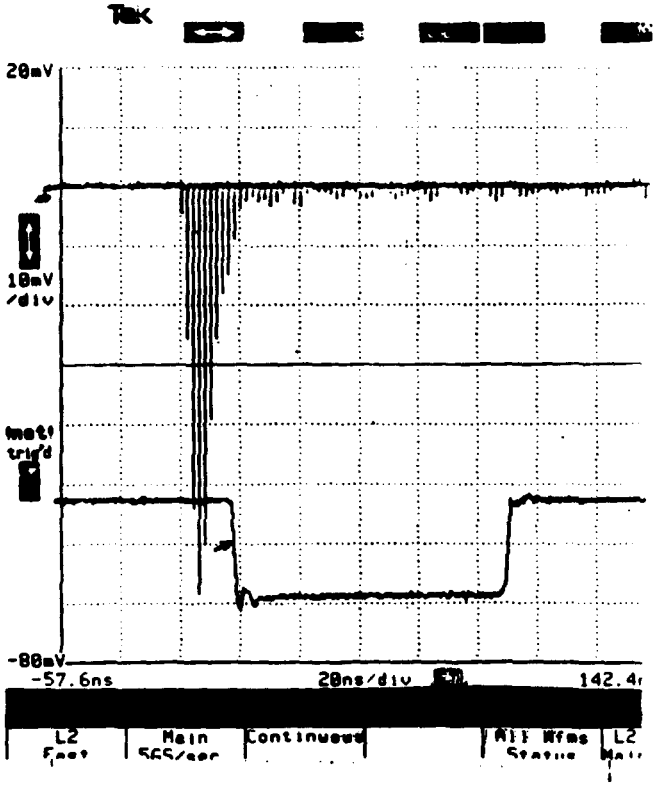


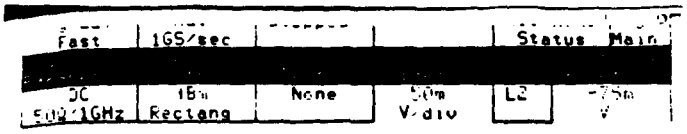
Figure F5. Registry of fiber ribbon fabricated at Purdue.

Schematic of Experiment

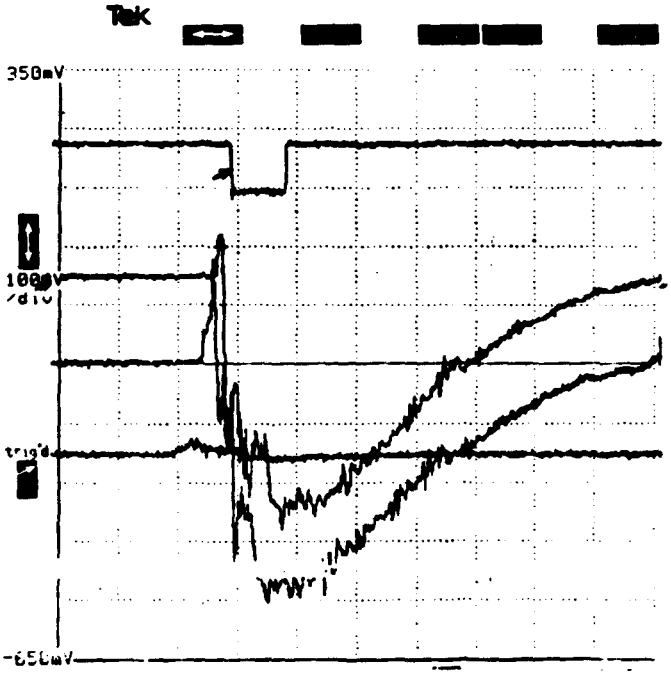


Typical Cosmic Trigger Line





Real hits on the fibers?



R+D goals

1991 - Establish proof of Principle tracking detector elements.

- VLPC
- Photon yield for fiber
- Photo-electron yield
- Clear wave guild atten. Length.
- Resolution

1992 Proof of Principle of the system

1024 channel test.

Key Points About Construction Schedule

1. Management of Project 7 years (1992-1999)

   1 - Engineer 1 Physicist
   + business manager
   + Secretary

2. NIF's are not on the critical Path
   - must appear in 1996

   There is time to complete
   - R&D
   - Excellent Concept + prototyping

3. Engineering design must start for
   - Cylinders
   - Support structures

   Complete design by 10/92

4. Fabrication + Testing R&D must start to start production

5. Fabrication construction must be complete in 2 years
   - need 4 firm companies
   - Bisson
   - Kvaerner

Simulation Studies for a Scintillating Fiber Tracker Trigger

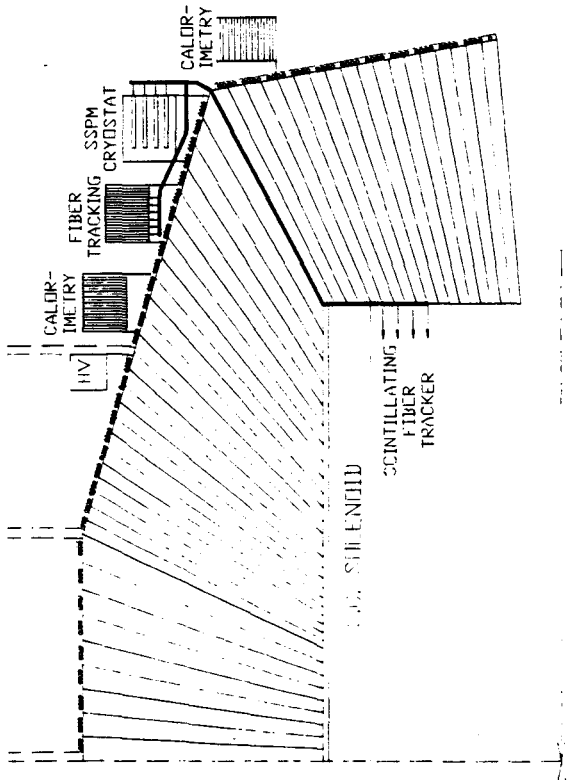
R. Lewis(Penn State)

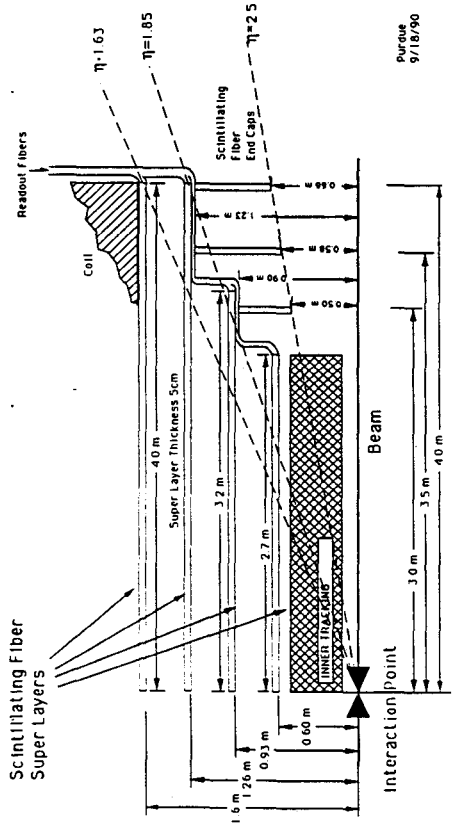
SIMULATION STUDIES FOR A SCINTILLATING FIBER TRACKER TRIGGER

B. Abbott[h], D. Adams[i], M. Atac[a,b], G. Anway[a], A.E. Baumbaugh[b], B. Baumbaugh[d], P. Berge[b], M. Binkley[b], J. Bishop[d], N. Biswas[d], A.D. Bross[b], C. Buchanan[a], N. Cason[d], R. Chaney[j], D. Chrisman[a], A. Clark[b], D. Cline[a], H. Cohn[e], M. Corcoran[i], R. Davies[h], J. Elias[b], E. Fenyves[j], D. Finley[b], G. Foster[b], J.M. Gaillard[b], J. Godfrey[d], H. Goldberg[c], H. Hammack[j], J. Jaques[d], V. Kenney[d], R. Kephart[b], D. Koltick[h], J. Kolonko[a], K. Kondo[k], R.A. Lewis[g], J. Marchant[d], R. McIlwain[h], S. Margulies[c], H. Miettenen[i], G.S. Mitchell[g], R.S. Moore[g], R.J. Mountain[d], T. Okusawa[f], J. Piekarz[d], R. Ruchti[d], R. Scalise[g], W. Shephard[d], E. Shibata[h], G.A. Smith[g], J. Solomon[c], K. Takikawa[k], S. Tkaczyk[b] and R. Wagner[b]

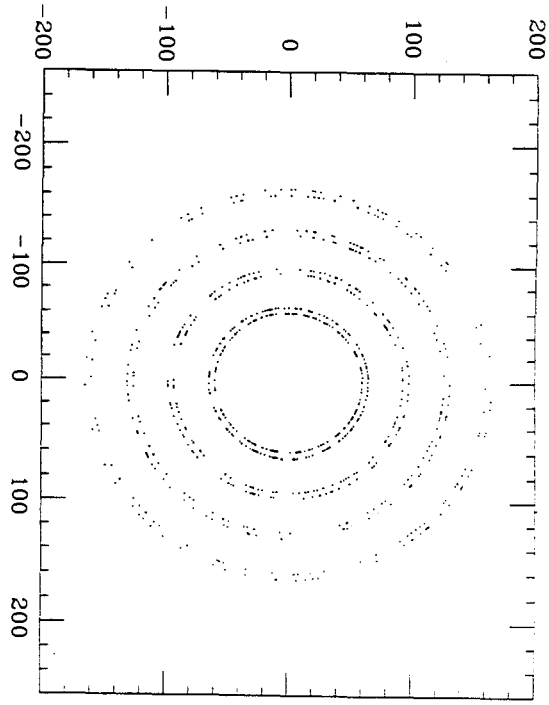
University of California at Los Angeles[a]
Fermi National Accelerator Laboratory[b]
University of Illinois at Chicago[c]
University of Notre Dame[d]
Oak Ridge National Laboratory[e]
Osaka City University[f]
Pennsylvania State University[g]
Purdue University[h]
Rice University[i]
University of Texas at Dallas[j]
Tsukuba University[k]

Presented by
Raymond A. Lewis
Pennsylvania State University

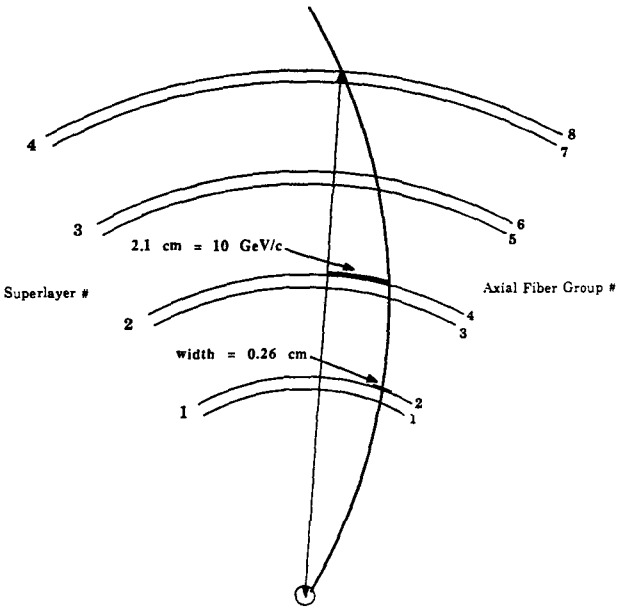


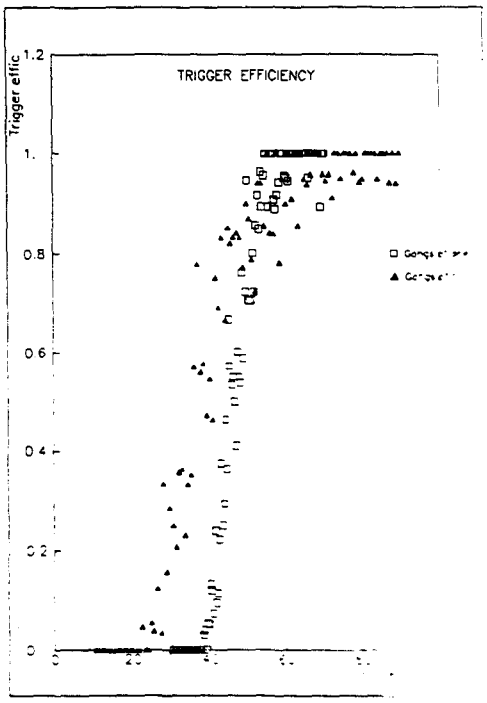


3 SUPERIMPOSED MIN BIAS EVENTS



Level 1 Central Tracking Scheme





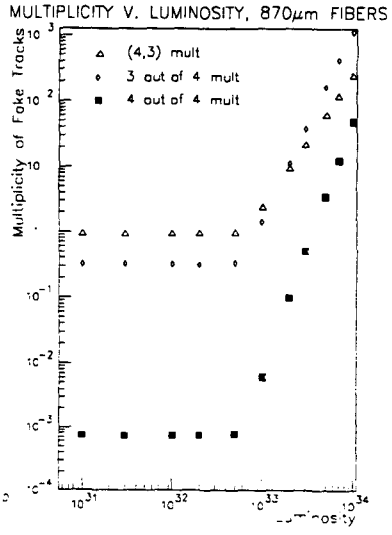
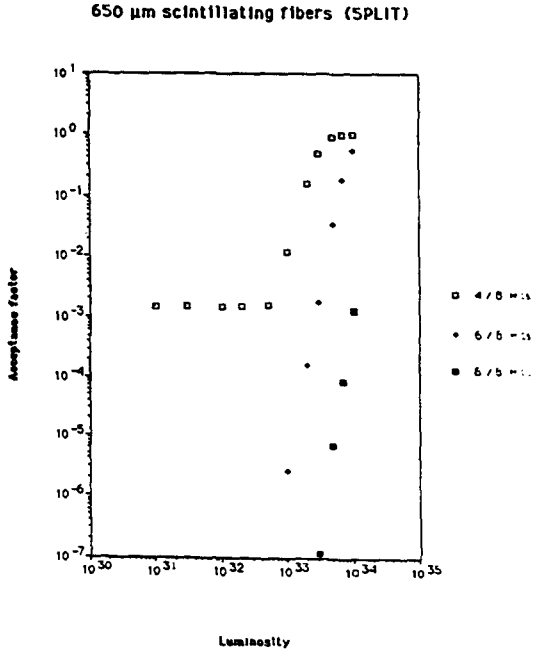
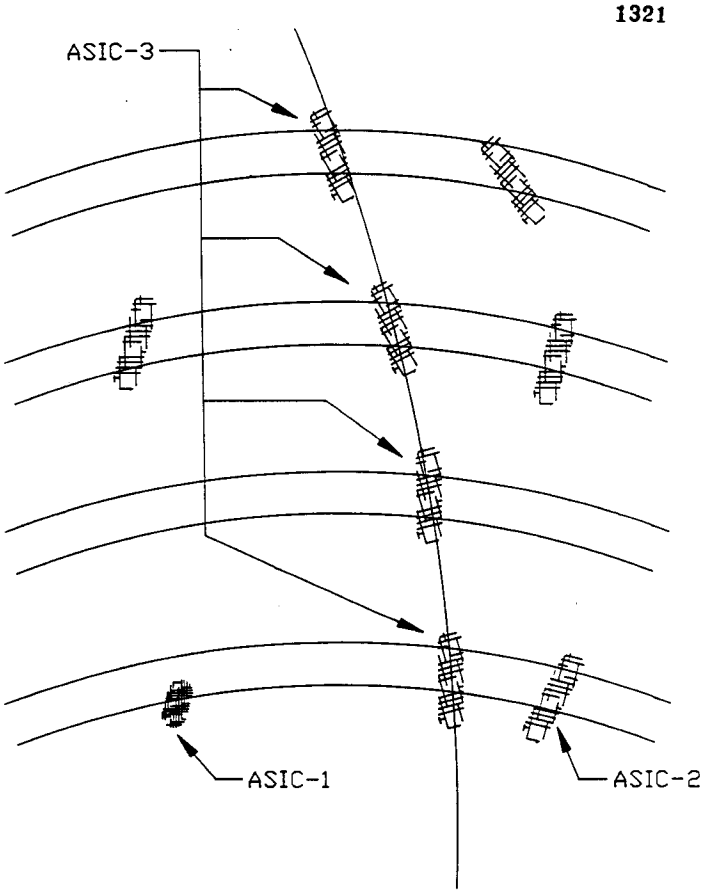


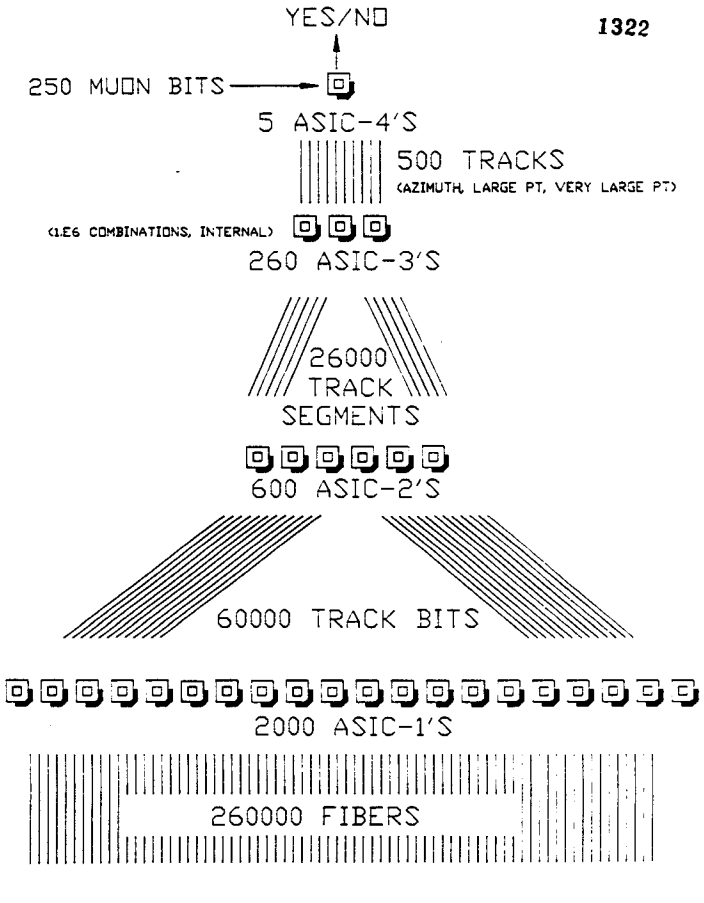
Figure 8



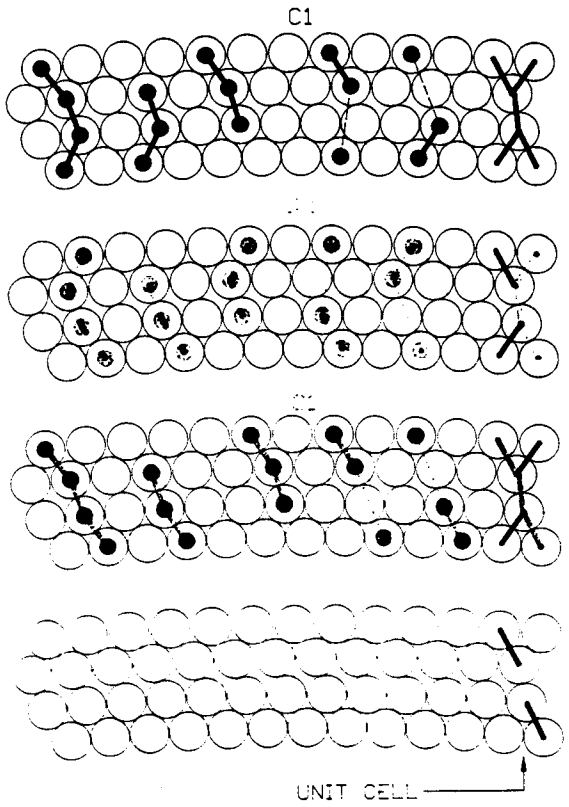
1321



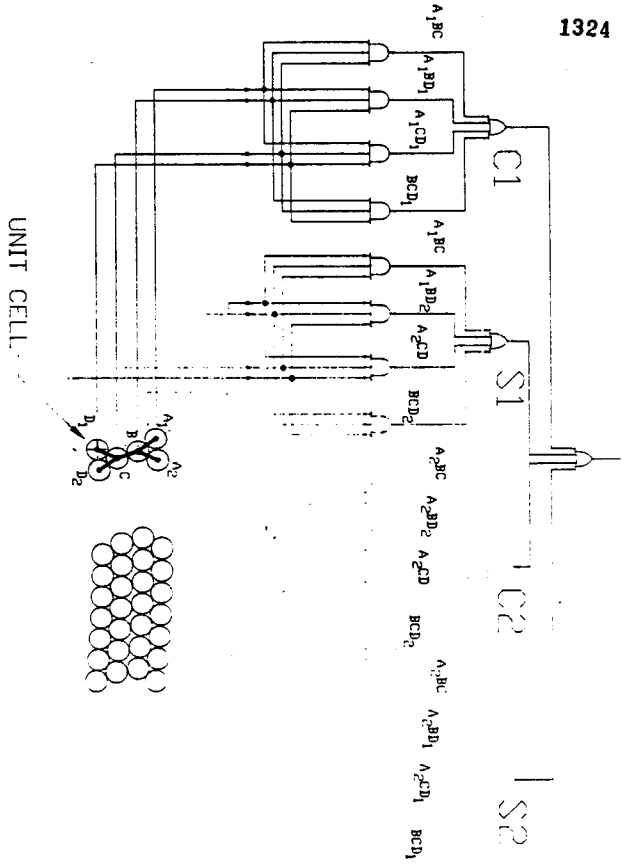
1322

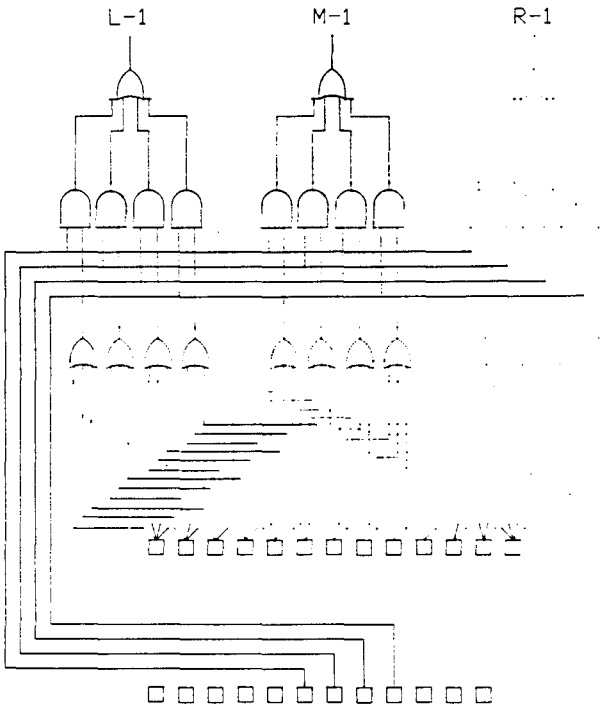


1323



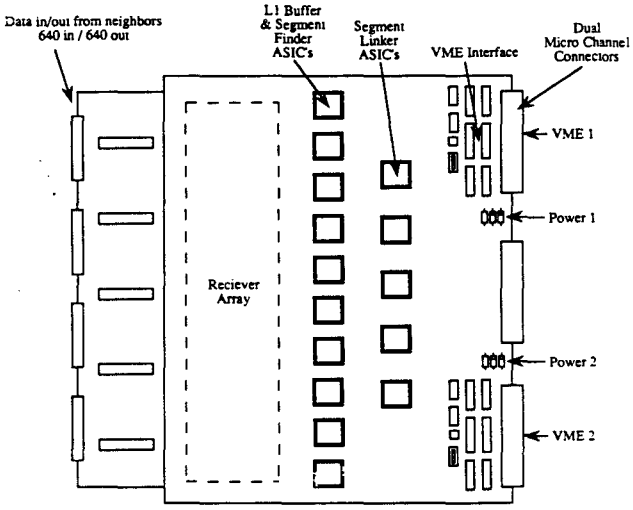
1324

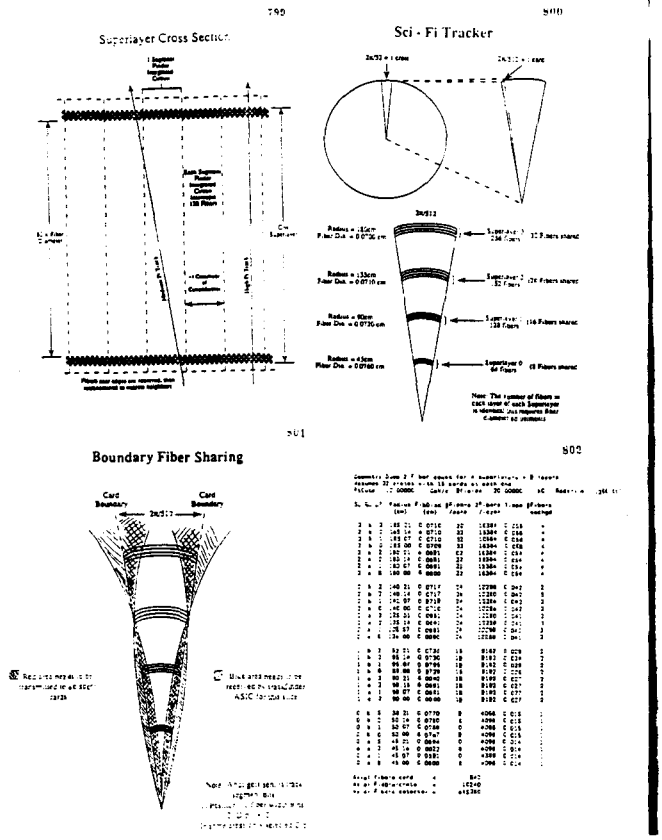




SDC Fiber Tracker
Reciever Board

9 U x 400mm (14.437" x 15.750") Printed Circuit Board





VLPC Status/Plans

P. Besser(Rockwell)

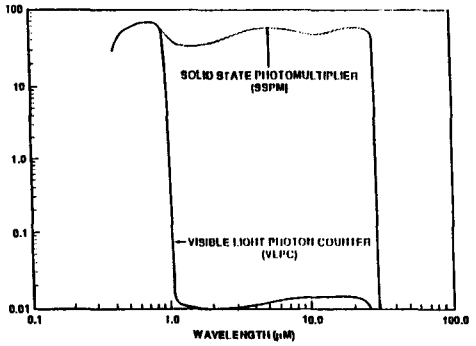
VLPC STATUS/PLANS

P. J. BESSER

ROCKWELL INTERNATIONAL
SCIENCE CENTER

VISIBLE LIGHT PHOTON COUNTER (VLPC)

CALCULATED SPECTRAL QUANTUM EFFICIENCY



- IMPURITY BAND CONDUCTION DEVICE
- ULTRA-SENSITIVE PHOTON DETECTOR IN VISIBLE SPECTRUM
- PRACTICALLY BLIND IN INFRARED SPECTRUM (> 1.1 μm)
- APPLICABLE TO

  ASTRONOMY
  HIGH ENERGY PHYSICS
  MEDICINE

OPENS DOOR TO IBC DETECTOR
APPLICATIONS TO HIGH ENERGY PHYSICS.

Rockwell International Science Center

HISTORY OF VLPC DEVELOPMENT

AUGUST 1987	–	APPLIED PHYSICS LETTER ON SSPM
SEPTEMBER 1987	–	CONTACT BY M. ATAC, FERMILAB
APRIL 1988	–	EXPERIMENTS BY PETROFF AND ATAC USING FIBERS AND WITH SSPM
NOVEMBER 1988	–	PRESENTATIONS BY PETROFF (IEEE) AND ATAC (SSC WORKSHOP) OF EXPERIMENT RESULTS
JANUARY 1989	–	HISTE PROPOSAL SUBMITTED (SSPM)
SUMMER 1989	–	VLPC DIFFERENTIATED FROM SSPM (PETROFF)
JULY 1990	–	PURCHASE ORDER FROM UCLA TO RI FOR HISTE
APRIL 1991	–	VLPC CONCEPT DEMONSTRATED

Rockwell International Science Center

HISTE

PERIOD OF PERFORMANCE: JULY 30, 1990 – DECEMBER 31, 1991

VALUE: $435K

GOALS:

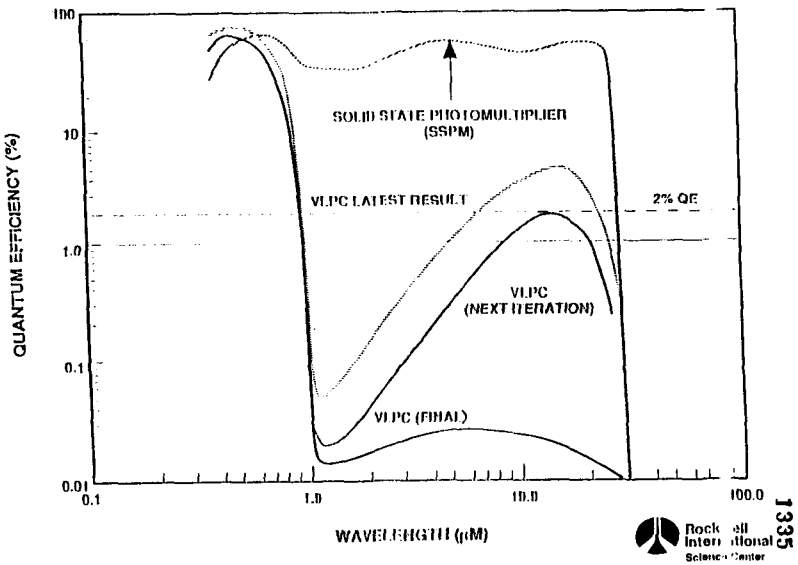
- PROVIDE DETECTORS FOR FIBER TRACKING EXPERIMENTS (SSPM/VLPC)
- DEMONSTRATE VLPC OPERATION
- IMPROVE VLPC PERFORMANCE

TASKS:

- MASK DESIGN AND FABRICATION
- MATERIAL GROWTH AND DEVICE FABRICATION
- DEVICE CHARACTERIZATION
- DELIVERY OF 200 DEVICES
- TECHNICAL SUPPORT

Rockwell International Science Center

VLPC SPECTRAL QUANTUM EFFICIENCY



Rockwell International Science Center

1335

HISTE STATUS

- PRELIMINARY WORK ON ROCKWELL IR&D
  - DEFINE TARGET MATERIAL PROPERTIES
  - FABRICATE DEVICES WITH SSPM MASK SET
- TWO LOTS OF VLPC MATERIAL GROWN
  - VLPC 1
  - VLPC 2
- FIRST DEVICE LOT FABRICATED AND TESTED
  - VLPC CONCEPT DEMONSTRATED
  - FURTHER IR SUPPRESSION REQUIRED
- SECOND DEVICE LOT COMPLETED SEPTEMBER 24
- DEVICE CHARACTERIZATION UNDERWAY
  - VERIFY VISIBLE PERFORMANCE, IR SUPPRESSION
  - EXPECT UNRESTRICTED DEVICES
- DEVICE DELIVERIES
  - PROVIDE DEVICES FOR FIBER TRACKING EXPERIMENTS
  - LATE OCTOBER, NOVEMBER

1337

Rockwell International Science Center

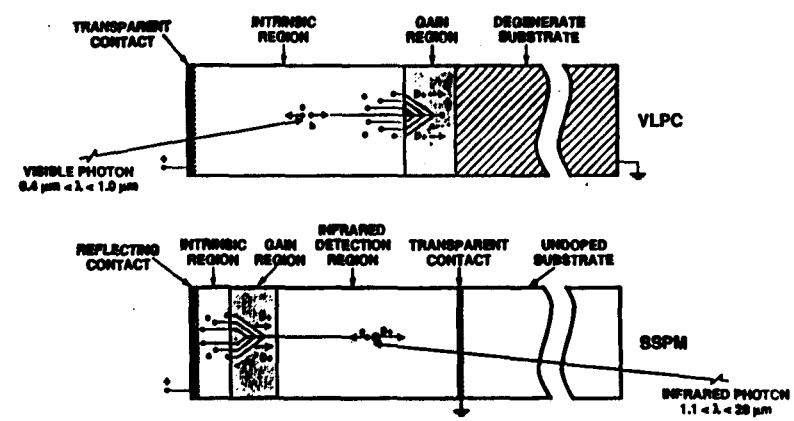
VLPC ACCOMPLISHMENTS

- DEVICES PROVIDED FOR FIBER TRACKING EXPERIMENTS
  - RADIOACTIVE SOURCES
  - COSMIC RAY TEST
- < 10 ns RISETIME DEMONSTRATED (REDUCED CONTACT RESISTANCE)
- MEASURED QE OF 85% AT λ = 500 nm (AR COATING)
- SIGNIFICANT PROGRESS IN IR SUPPRESSION
- ADDITIONAL EFFORT REQUIRED TO MEET SSC REQUIREMENTS

1336

Rockwell International Science Center

SCHEMATIC CROSS-SECTIONS OF VISIBLE LIGHT PHOTON COUNTER (VLPC) AND SOLID STATE PHOTOMULTIPLIER (SSPM)



1334

Rockwell International Science Center

VLPC DEVELOPMENT - FUTURE PLANS

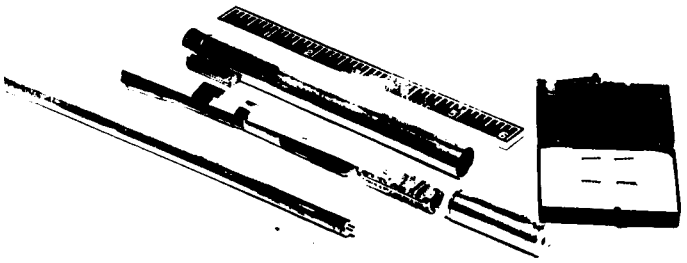
- DESIGN AND FABRICATE NEW MASK SET (FY'91 FUNDING)
  - CASSETTE APPROACH
- HIGHER IMPLANT DOSE FOR TRANSPARENT CONTACT
  - REDUCED CONTACT RESISTANCE
  - LWIR FILTER
- IMPROVED AR COATING
  - INCREASE QE
- MAXIMIZE RESPONSE AT FIBER SCINTILLATION WAVELENGTH
- FABIRCATE REFINED VLPC LOT
- CHARACTERIZATION/TESTING
- SCREENING, PACKAGING, DELIVERY OF 1024 DEVICES
- CHARACTERIZE EFFECTS OF NEUTRON AND GAMMA RADIATION
- TECHNICAL SUPPORT

Rockwell International Science Center

ROCKWELL VLPC IR&D ACTIVITY

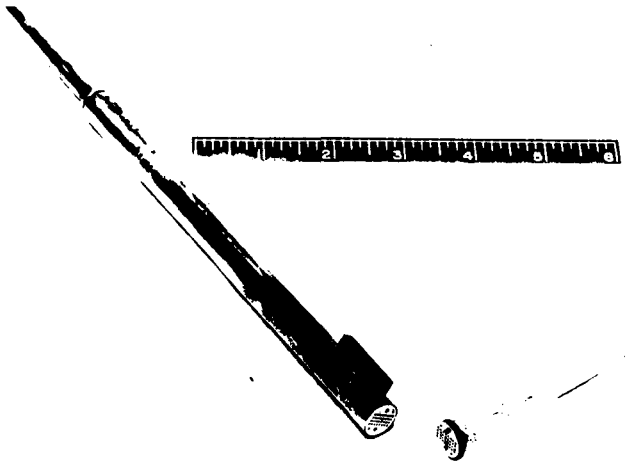
- DEVICE MODELLING
- CASSETTE DESIGN/FABRICATION/TEST
- MATERIAL IMPROVEMENT/CONTROL
- PROCESS DEVELOPMENT

Rockwell International Science Center



32 CHANNEL VLPC CASSETTE

Rockwell International Science Center



32 CHANNEL VLPC CASSETTE

Rockwell International Science Center

1341

1342

Cosmic Ray Tracking Using Scintillating Fiber Ribbons and VLPCs

M. Atac(FNAL/UCLA)

Presented by M.ATAC FNAL/UCLA

ORNL, Sept. 27, 91

Fiber Tracking Group

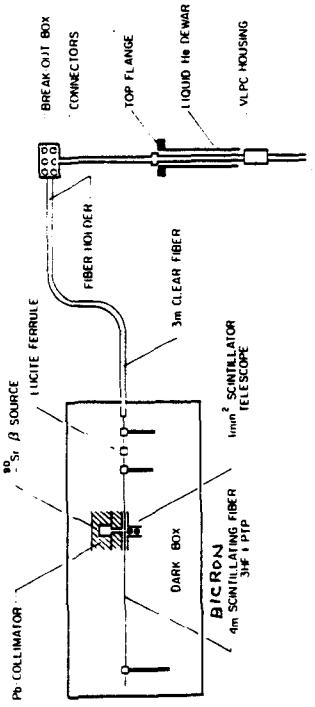
B. Abbott[a], D. Adams[f], E. Anderson[c], M. Atac[a,b], C. Anway[a], A. Baumbaugh[b,g], P. Berge[b], P. Besser[b], R. Bharat[c], M. Binkley[b], J. Bishop[b], N. Biswas[d], A.D. Bross[b], C. Buchanan[a], N. Cason[d], R. Cbaney[a], D. Carisman[a], A. Clark[b], D. Cline[a], H. Conn[a], M. Corcoran[i], R. Davis[b], J. Elias[b], E. Fenyves[g], D. Finley[b], G.W. Foster[b], J.-M. Gaillard[a], J. Godfrey[d], H. Goldberg[c], H. Hammack[g], X. Huang[d], J. Jacques[d], V. Kenney[d], R. Kephart[b], D. Koltick[h], J. Koionko[g], K. Kondo[j], R.A. Lewis[f], J. Marchant[d], R. McIlwain[h], S. Margulies[c], H. Mettenen[i], R. Moore[g], R.J. Mountain[d], T. Okusawa[j], J. Park[a], M. Petroff[a], J. Piekarz[g], A. PlaDalman[b], R. Ruchti[d], R. Sealise[g], W. Shepard[d], E. Shibata[b], G.A. Smith[g], J. Solomon[b], K. Takikawa[j], S. Tkaczyk[b] and R. Wagner[b]

M. MISHINA, KEK/FNAL

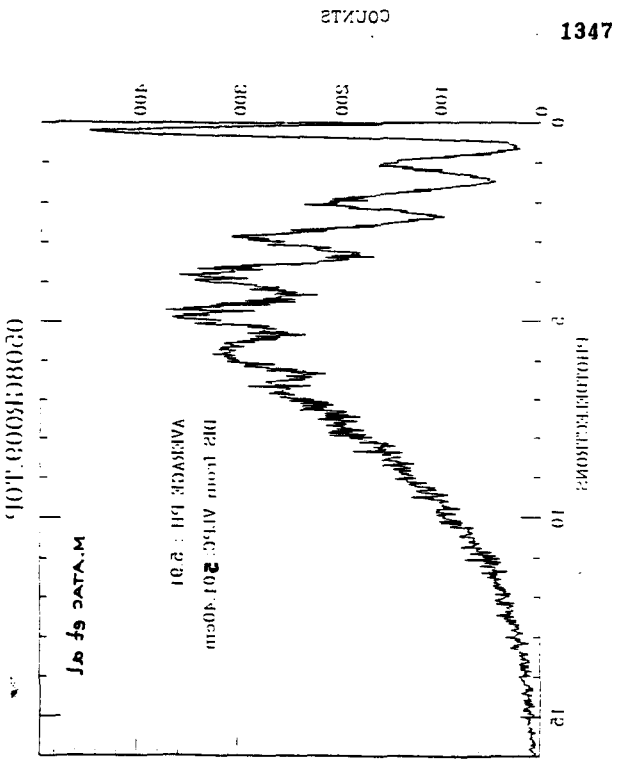
[a]University of California at Los Angeles
[b]Fermi National Accelerator Laboratory
[c]University of Illinois at Chicago
[d]University of Notre Dame
[e]Oak Ridge National Laboratory
[f]Osaka City University
[g]Pennsylvania State University
[h]Purdue University
[i]Rice University
[j]Rockwell International
[k]University of Texas at Dallas
[l]Tsukuba University

M. ATAC, J. PARK, M. PETROFF
AND D. CHRISMAN
AT UCLA

EXPERIMENTAL ARRANGEMENT

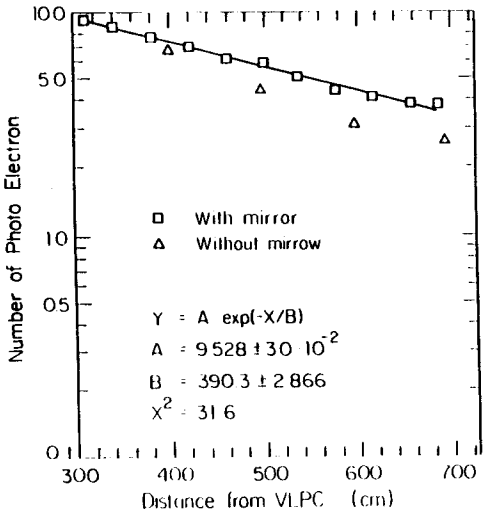


Experimental arrangement for measuring detected photon by a VLPC using a 4 meter length of scintillating fiber of 0.8 mm core (3HF+ PTP in polystyrene). The scintillating fiber is spliced to a 3 meter long optical clear fiber that carries the photons to the VLPC.



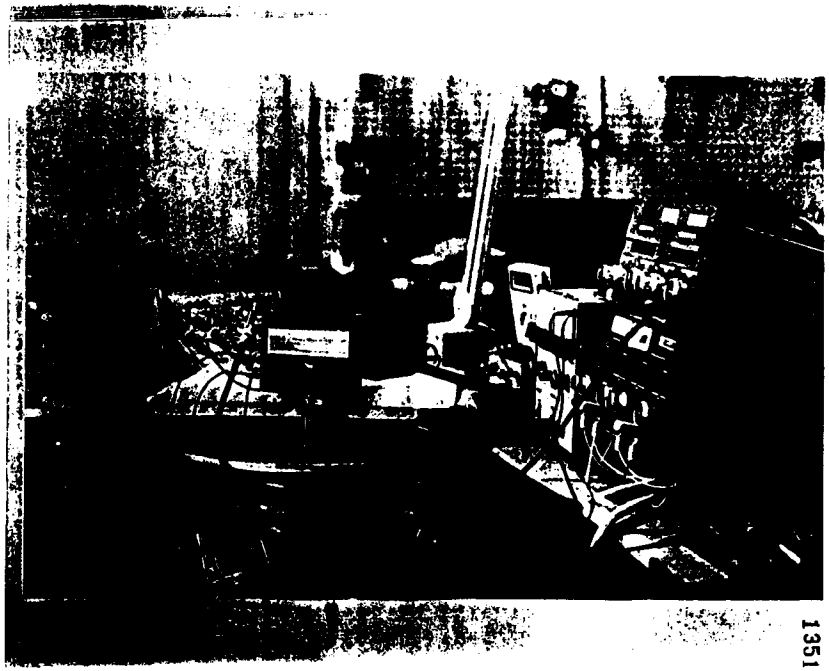


1350



Detected number of photons as a function of source positions from the VLPC are indicated with and without a mirror at the end of the scintillating fiber

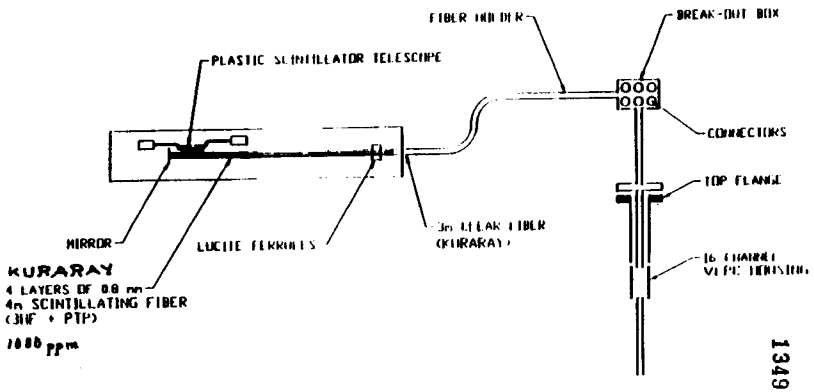
1348



1351

M.Atac, J. Park and D. Chrisman
UCLA
H. Fenker and K. Morgan
SSCL

UCLA COSMIC-RAY TEST

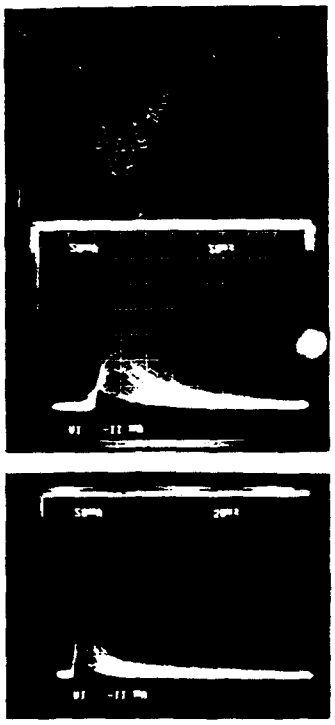


1349

1352

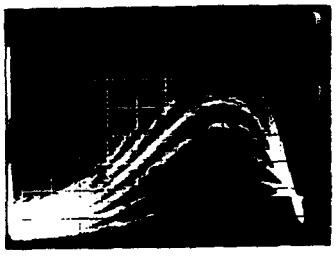


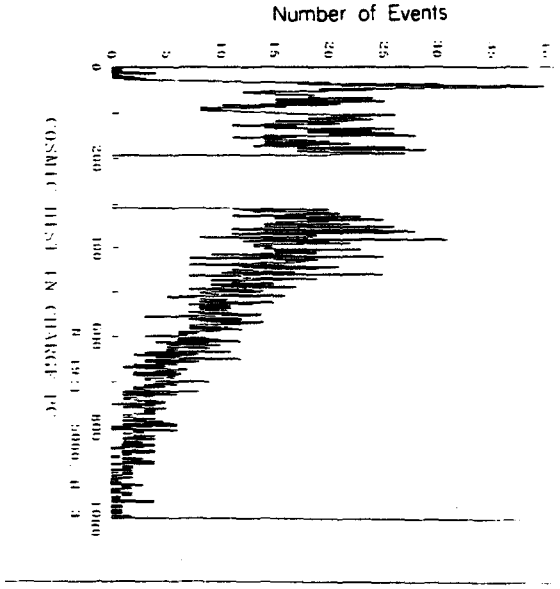
1353



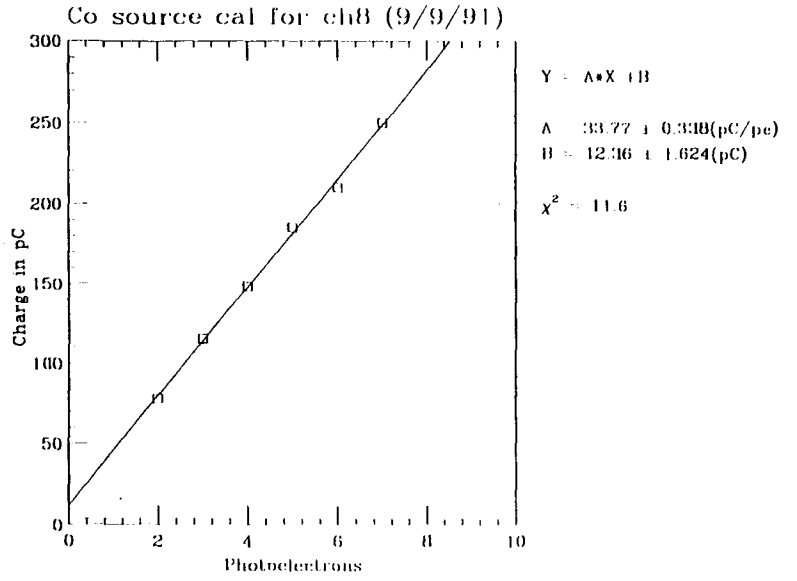
1354

1355

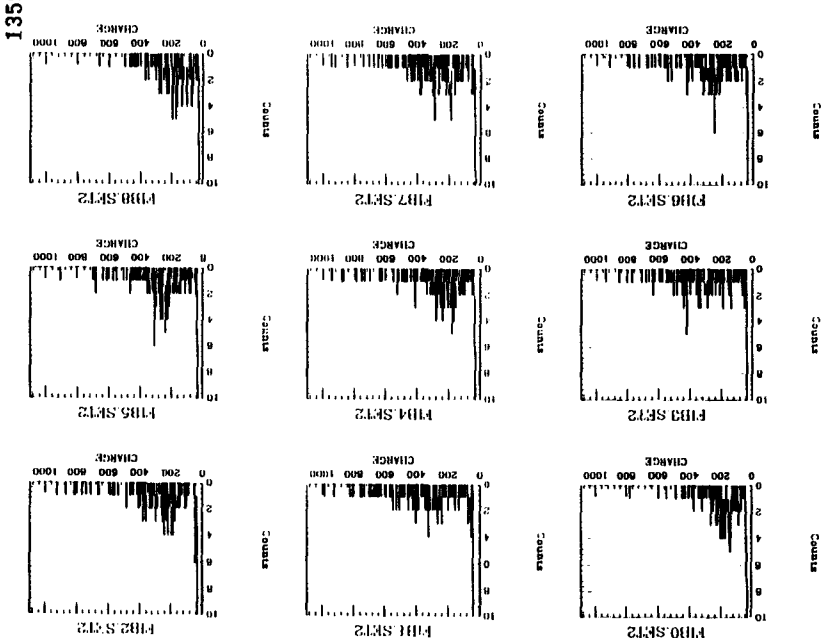




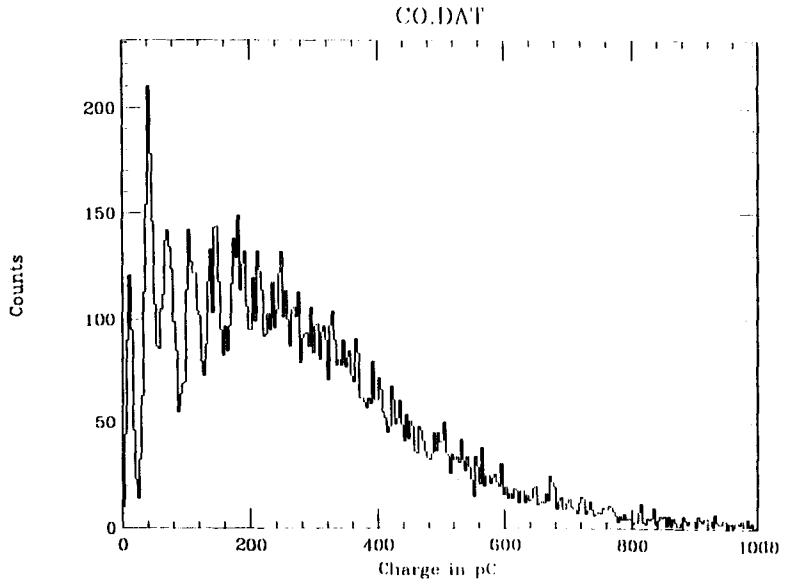
1357



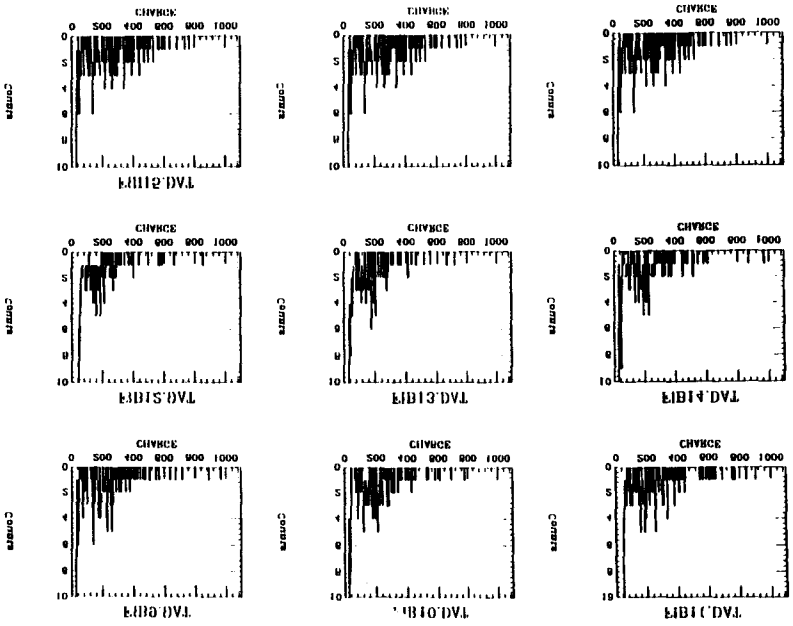
1359



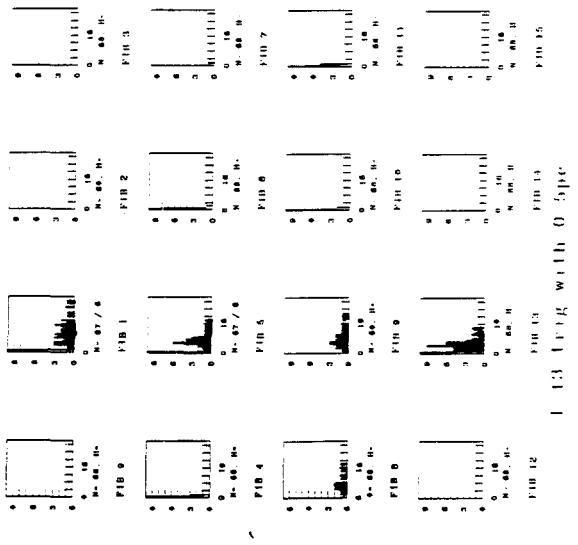
1356



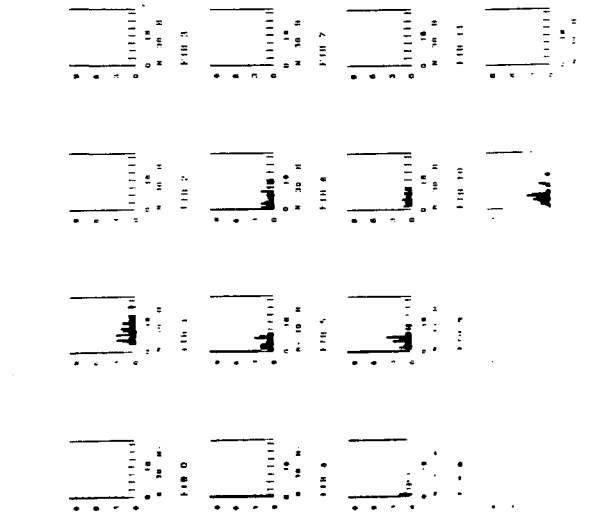
1358



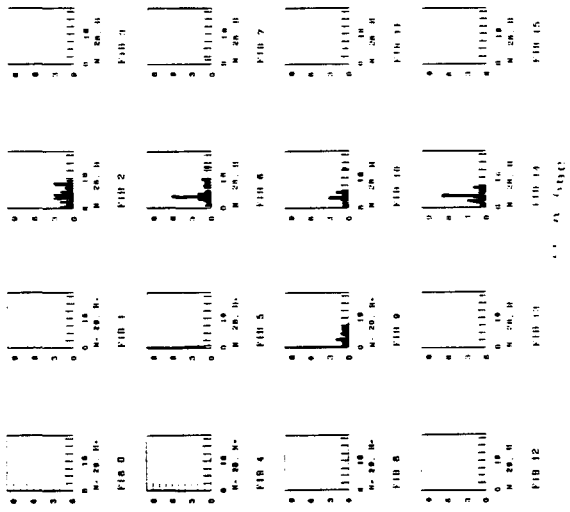
1360

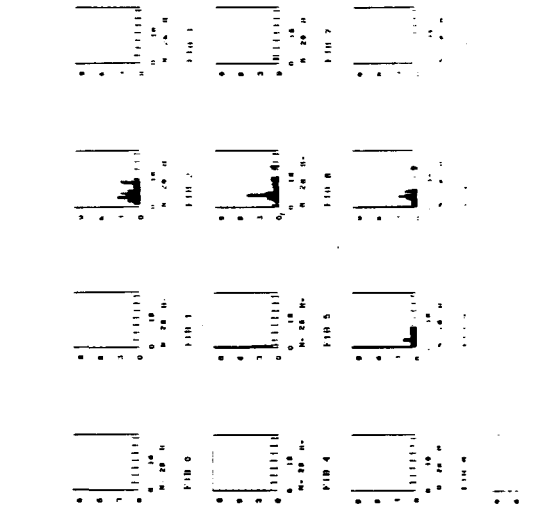


1361



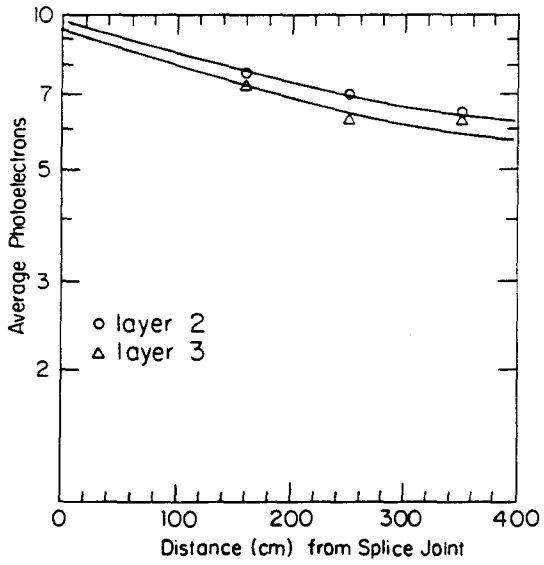
1362



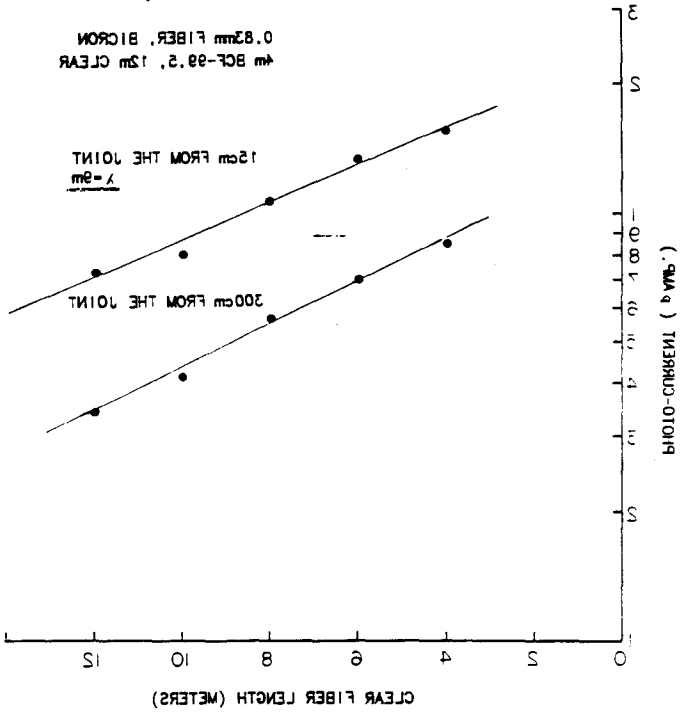


MAKING SCINTILLATING FIBER RIBBONS.
— PHOTON-REFLECTIVE GLUE WAS USED IN
SCINTILLATING FIBER RIBBONS FROM
KURARAY [M. MISHINA], K. KONDO.
— UCLA HAD RECEIVED HIGH QUALITY
SCINTILLATING FIBERS AND CLEAR FIBERS.
— IMPROVED OPTICAL COUPLER BETWEEN
THIS COSMIC-RAY EXPERIMENT
TO FURTHER INCREASE IN PHOTON YIELD WITH
THREE FACTORS MAY HAVE CONTRIBUTED

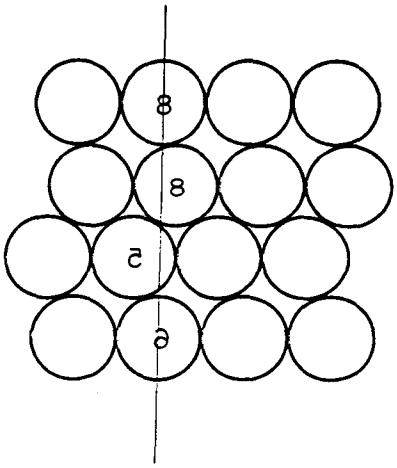
1368



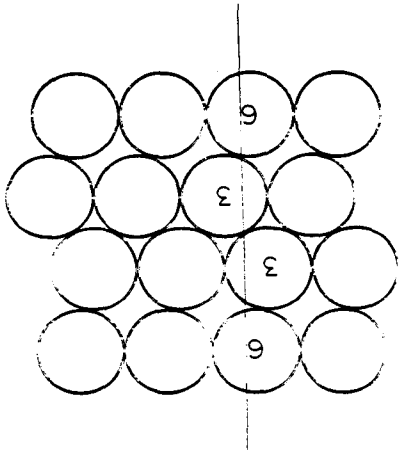
1369



1370



1371



1372

1373

1374

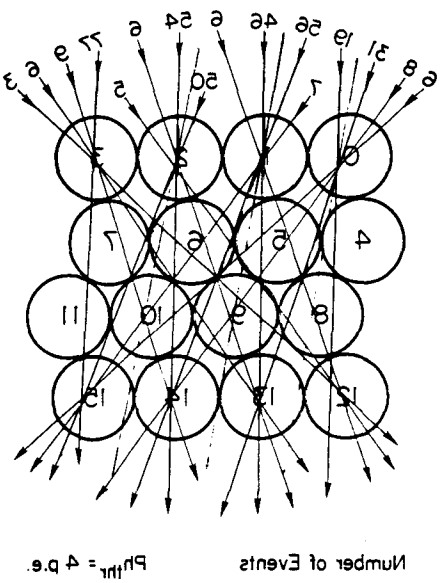
1375

1376

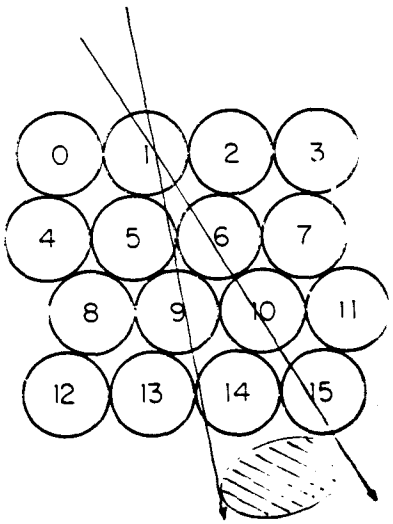
1377

1378

1379



Number of Events P_{thr} = 4 p.e.



90% OF COSMIC-RAY TRACKS ARE WITHIN THIS SOLID ANGLE

FUTURE PLANS

- COMLETED A NEW 32 CHANNEL CRYOSTAT AND PLAN TO TAKE COSMIC-RAY DATA AT UCLA.
- HOPING TO GET IR INSENSITIVE VLPCs FROM ROCKWELL WITHIN A MONTH
- REPLACE THE VLPC I CHIPS WITH VLPC II CHIPS IN THE PRESENT CRYOSTATS AND DO BEAM TESTS HOPEFULLY AT FERMILAB. IF WE ARE LATE WE WILL DO THE TEST AT BNL.

Summary Report of the Fiber Tracking Group

SUMMARY REPORT OF THE FIBER TRACKING GROUP (FTG)

FY 91 PROGRESS REPORT
FY92 PLANS*

University of California at Los Angeles
Fermi National Accelerator Laboratory
University of Illinois at Chicago
Indiana University Purdue University at Indianapolis
Massachusetts College of Pharmacy and Applied Health Sciences
Northeastern University
University of Notre Dame
Oak Ridge National Laboratory
Pennsylvania State University
Philadelphia College of Pharmacy and Science
Purdue University
Rice University
University of Texas at Dallas
Tsukuba University

September 24, 1991

ABSTRACT

The Fiber Tracking Group (FTG) is developing a high-rate tracking subsystem appropriate for SSC experiments based on scintillating fiber technology. The use of scintillating fibers as the detection medium affords the prospect for tracking particles with high resolution, low occupancy, and very short resolving time. These characteristics are being exploited in the development of a central tracking detector for the Solenoid Detector Collaboration (SDC) in which: (1) superlayer structures of scintillating fibers are used to provide a first level trigger for event selection on the basis of particle transverse momentum, and (2) excellent granularity allows track recognition and pattern recognition with resolution sufficient to measure particle momenta up to 1 TeV/c. This document reviews the latest developments and results obtained from the second year (FY91) of the subsystem program, and details the objectives and tasks for physical year FY92.

*BUDGET REQUEST WILL BE MADE SEPARATELY THROUGH SDC

TABLE OF CONTENTS

I. Collaboration Institutions and Personnel 3

II. Progress Report on FY91 Research and Development 6

A. Executive Summary 6
B. Review of Progress on Milestones for FY91 9
C. Review of Progress Toward Proof-of-Principle for Fiber Tracking 27

III. Research and Development Program for FY92 38

A. Overview 38
B. Description of the Development Plan 42
C. Milestones for FY92 47

IV. Progress Reports from Collaborating Institutions on FY91 R and D 48

A. UCLA /Rockwell 48
B. Fermilab
C. University of Illinois at Chicago
D. University of Notre Dame
E. Pennsylvania State University
F. Purdue University
G. Rice University
H. University of Texas at Dallas

V. Appendix

Memorandum of Understanding between the Fiber Tracking Group (FTG) and the SSC laboratory.

I. COLLABORATION INSTITUTIONS AND PERSONNEL

The participating institutions and participants in the Fiber Tracking Group (FTG) include:

- **University of California at Los Angeles**
  - M. Atac (Contact Person)
  - C. Buchanan
  - D. Chrisman
  - D. Cline
  - J. Kolonko
  - J. Kubic
  - J. Park
- **Fermi National Accelerator Laboratory**
  - M. Atac
  - A. Baumbaugh
  - M. Binkley
  - A. Bross
  - J. Elias (Contact Person)
  - D. Finley
  - G. Foster
  - R. Kephart
  - S. Tkaczyk
  - R. Wagner
- **University of Illinois at Chicago**
  - M. Adams
  - H. Goldberg
  - S. Margulies
  - J. Solomon
- **University of Illinois at Chicago**
  - F. Meiere
  - H. Paik
  - K. Vasavada

- **Massachusetts College of Pharmacy and Applied Health Sciences**
  - C. Kelly
- **Northeastern University (*)**
  - C. Linkis
  - I. Leedom
  - S. Reucroft
  - T. Yasuda

* Northeastern University has become a full participant in FTG in Spring 1991. However FY91 funding for this group was derived from the Hybrid Tracking Group, and their FY91 R and D is reported through that collaboration.

- **University of Notre Dame**
  - B. Baumbaugh
  - J. Bishop
  - N. Biswas
  - N. Cason
  - R. Kehoe
  - M. Kelly
  - J. Jaques
  - V. Kenney
  - J. LoSecco
  - R. Mountain
  - J. Piekarz
  - R. Ruchti (Contact Person)
  - W. Shephard
  - Balamurali V.
  - M. Wayne
- **Oak Ridge National Laboratory**
  - D. Vandergriff
- **Pennsylvania State University**
  - T. Armstrong
  - A. Hasan

S. Heppelmann
R. Lewis
R. Moore
B. Oh
J. Passaneau
R. Scalise
G. Smith
W. Toothacker
J. Whitmore

- **Philadelphia College of Pharmacy and Science**
  J. Kauffman

- **Purdue University**
  B. Abbott
  R. Davies
  D. Koltick
  E. Shibata
  R. McIlwain

- **Rice University**
  D. Adams
  M. Corcoran
  H. Miettenen
  J. Skeens

- **University of Texas at Dallas**
  R. Chaney
  E. Fenyves
  H. Hammack
  B. Lowery
  J. Orgeron

- **Tsukuba University**
  K. Kondo
  K. Takikawa

II. PROGRESS ON FY91 RESEARCH AND DEVELOPMENT

A. EXECUTIVE SUMMARY

The speed of response and high granularity (very low occupancy) of scintillating fibers make them an ideal choice for high resolution, charged particle tracking, for providing a fast, first-level trigger based on particle transverse momentum, and for operation at the highest luminosities expected at SSC. A tracking detector with these features would be an important element for many SSC experiments.

The goals of the Fiber Tracking Group (FTG) are to: (1) develop fiber tracking technology for general applications in SSC experimentation, and (2) to provide central tracking and first-level P_T triggering for the SDC experiment.

To realize the potential of fiber tracking technology, a challenging R & D program has been initiated which includes major developmental effort in the following areas: (1) high efficiency, low-loss, and radiation resistant fiber scintillators and waveguides; (2) high quantum efficiency, visible light sensitive photon counters (VLPCs) based upon the existing Rockwell Solid State Photomultiplier (SSPM) and incorporating associated front end electronics; (3) first-level trigger electronics based on ASIC (Application Specific Integration Ciruitry) technology; and (4) simulation packages capable of characterizing fiber tracking designs.

FTG has been pursuing these tasks, and FY91 has been productive. Specifically:

• A number of promising prototype fluorescent dyes which were synthesized in FY90 funding year have now been incorporated into scintillating fibers for studies of fiber efficiency and attenuation length and for manufacture of prototype fiber ribbons. When read out with Visible Light Photon Counters (VLPC-I), these fibers and ribbons provide excellent photon yields. Additional new fluorescent materials have been developed during FY91, and their incorporation into polystyrene have indicated high scintillation efficiency and excellent radiation resistance characteristics. We expect that the avenues opened by these new prototypes will yield further improvements.

• The development of the Visible Light Photon Counter (VLPC) has been underway at Rockwell International Science Center. This device is an evolutionary version of the Solid State Photomultiplier (SSPM), but optimized for visible wavelengths and higher rate capability, and desensitized for infrared response. The development has

proceeded in two steps. In Step 1 we have optimized the devices for visible wavelength response. Such devices (designated VLPC-I) have been successfully produced with a measured quantum efficiency of ~85% at a wavelength of 565nm, have been produced in linear arrays, and have been delivered in significant quantities (hundred channels) to the UCLA group. Highly successful preliminary studies have been performed with these devices coupled to individual fiber elements or to 16 element arrays of fiber ribbons. Step 2 is to optimize the devices for speed and to minimize the infrared response. Fabrication of the first lot of these new devices (VLPC-II) is in progress, with initial characterization and testing during late FY91 and early FY92.

• A study of cryogenic preamplifiers for use with VLPC/SSPM devices has been initiated in consultation with Honeywell, and studies continue within the FTG collaboration on the development and use of the room temperature preamplifier option.

• Monte Carlo simulations continue to be carried out by several of our collaborating institutions directed toward design and implementation of superlayers of fibers for triggering, pattern recognition, and momentum analysis. As part of this effort, the simulation package SFTSIM has been developed which provides a GEANT-based simulation of a scintillating fiber tracking system, as well as the associated track-finding code TRF. Additionally, the group has participated in the development of the SDC global simulation "shell", SDCSIM, of which the SFTSIM and TRF programs are now components. In a complementary effort, tracking simulation studies are underway to optimize a powerful transverse momentum trigger algorithm appropriate for incorporation into a fast Level-1 electronic trigger built in ASIC (application specific integrated circuitry).

Simulations of fiber waveguide structures, scintillation efficiency, and optical transport using our OPTICKS code are being continued.

• Limited engineering studies sufficient for a preliminary fiber tracking system costing have been carried out in collaboration with Oak Ridge National Laboratory. A work-baseline structure (WBS) has been developed in order to assess costs and schedules and critical path issues in the development, fabrication, and assembly of this detector. Essential engineering conceptual design studies could not be implemented in FY91 because of funding limitations.

• A beam test facility (T839) has been developed at Fermilab in the New Muon laboratory, equipped with a remotely operable transporter to position fiber ribbons and

superlayers at various angles relative to the beam. Initial beam studies are beginning now (end of FY91) using fiber ribbons and multianode phototubes for light detection, until such time as VLPC-II devices are available for beam tests.

• A radiation test facility (T851) is being developed at the C0 intersection region at Fermilab to test the effects of realistic levels of ionizing radiation on fibers and ribbons maintained under different ambient conditions.

• Highly successful initial tests of individual scintillating fibers and waveguides and arrays of ribbons of these structures have been performed using VLPC-I as the photodetectors in laboratory-based tests performed by the FTG group at UCLA. The fibers and ribbons have been tested with radioactive sources and cosmic rays. Fibers and waveguides are of 830μm diameter, with scintillator lengths of 4m and waveguide lengths of 3m or 4m depending upon the test configuration. When spliced together to form actual fiber detection elements, the total fiber lengths are 7-8m. The mean detected photo-electron yield at the VLPC when the far end of the scintillation fiber is excited by cosmic rays (7m - 8m from the VLPC) is remarkably good, and has been observed to be ~6 photoelectrons when the far end of the fiber is mirrored. Since 2.5 detected photoelectrons is the minimum acceptable level to establish an efficient double layer of fibers, our result shows that the fiber tracking concept is sound, and that the technique works and works well.

We now review the progress on our FY91 milestones as stated in the Memorandum of Understanding with the SSC Laboratory. It should be noted that agreement on this memorandum was reached in April, 1991, and that several groups have only recently received funding. This circumstance, as well as the overall limited available resources for SSC related R and D, have substantially slowed (and in some cases impeded) the progress we hoped to have achieved in FY91 as outlined in our Summary Report to the SSC Laboratory for the last fiscal year, dated September 1, 1991.

Following the review of FY91 milestones are two sections. The first outlines our FY92 R & D plan, funding for which will be requested within the R & D budget for the SDC experiment. The second section contains progress reports from individual institutions for FY91.

B. REVIEW OF PROGRESS ON FY91 MILESTONES:

Milestones for Scintillating Fiber Tracking Research during FY91 as listed on Pages 7-8 of the MOU '91 agreement (see Appendix A attached) are presented in this section. Institutions contributing to the R & D on a given task are listed alphabetically at the head of each section.

Task 1: Scintillator
(Fermilab, MCPAHS, Notre Dame, PCPS)

Substantial effort has been applied to refinements in the composition of scintillators for use in fiber detectors. These efforts have included:

The development of several new primary dyes at PCPS: including a sexiphenyl and two octiphenyl compounds having very high molar extinction coefficient (greater than twice that of p-Terphenyl) for short range of energy transfer and fast fluorescence decay and which are soluble in concentrations of 1% in polystyrene. These materials have been found to produce, in one step, scintillators of comparable efficiency to two step scintillation standards such as polystyrene with pTerphenyl and dimethyl-POPOP. Additionally, these materials have longer wavelength emission, in the 425nm-435nm range, allowing for the incorporation of new alternatives for secondary dyes.

The development of several new secondary dyes based on intra-molecular proton transfer to minimize self absorption and to provide long-wavelength emission. One series of these involves several variants of the well-known dye 3-hydroxyflavone (3HF) produced at PCPS, with substitutions for longer wavelength response or improved photostability. Another series involves a significant new developement in a group of dyes called hydroxybenzothiazoles (HBTs). Previous pioneering work by Fermilab and others had produced dyes in this family of roughly half the efficiency of 3HF at best. New work by MCPAHS has produced a candidate dye which, upon purification, yields performance comparable to 3HF. Because of differing chemical structure, dyes based on this prototype may afford better long-term photostability and improved fluorescence efficiency. Figure 1 shows the fluorescence emission and absorption for this new dye.

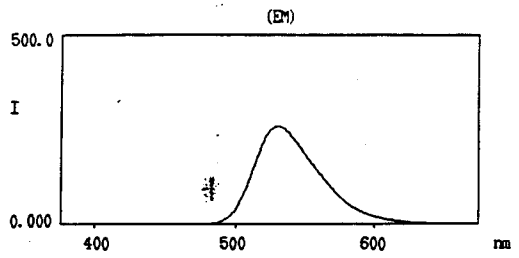


Figure 1a. Fluorescence emission of 3HF.

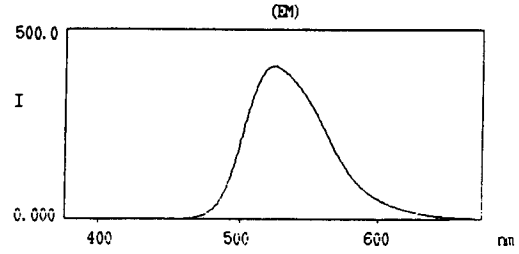


Figure 1b. Fluorescence emission of the new MCPAHS dye.

Task 2: Waveguide Development
(UCLA, Fermilab, Notre Dame)

Given the relatively short period of time for R & D to demonstrate proof-of-principle for fiber tracking, we have elected to concentrate on scintillating and non-scintillating fiber waveguides having polystyrene cores and some form of acrylic or polymeric cladding. Currently we are concentrating on PMMA (polymethylmethacrylate). Fibers have been successfully produced by several commercial houses using these materials. Other interesting options (such as PVT core) have not been developed to the same degree. We are pursuing initiatives in the study of cladding materials: (1) the incorporation of primary dyes to allow the full volume of the scintillating fiber to be efficient, and materials of lower refractive index than PMMA (n=1.49), of which there are several possibilities in the 1.3-1.4 range. Current fibers have diameters of 830μm and cladding thicknesses of ≤ 30μm. Studies have shown that the best of the clear fiber waveguides yield optical attenuation lengths of ~10m in the wavelength range of interest (centered around 530nm), and attenuation lengths for the best scintillating fibers are ~8m when viewed through a 4m length of clear fiber waveguide.

Task 3: Splicing Techniques for Fibers and Ribbons
(UCLA, Notre Dame)

Several coupling techniques for the splicing of fibers and waveguides have been proposed, including permanent connections such as thermal fusion, chemical melting, and glues, and quick-disconnect options based on optical couplants such as optical greases and gels and mineral oils. For a variety of reasons, we now favor the quick disconnect option because of its convenience and because of the simplicity it affords during detector construction and testing. Several different connector options have been explored, which have produced good results for optical transmission and low light loss. These are based on drilling precise holes in small acrylic blocks into which fibers and waveguides may be inserted. The registration is maintained by alignment pins. These initial ideas must now be developed for larger scale fiber systems.

Task 4: Ribbon Fabrication
(UCLA, Fermilab, Purdue, Notre Dame, UTDallas)

Figure 2 provides a schematic representation of fiber ribbons, and their arrangement into layers. Several methodologies have been developed for ribbon fabrication

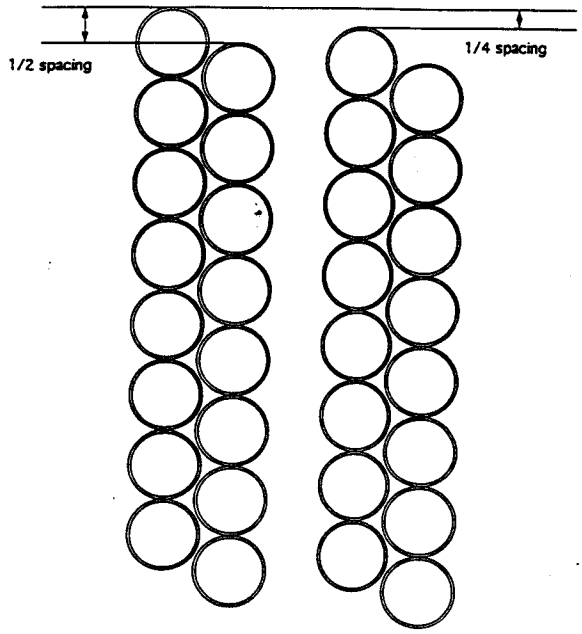


Figure 2. Schematic of a superlayer of fibers, composed of two double-layer ribbons offset by 1/4 spacing. Fibers are of 830micron diameter on 870 micron center-to-center spacing.

depending upon whether or not the fibers are scintillators or waveguides. In the scintillating fiber case, the waveguides must be precisely positioned relative to one another in the ribbons so that this spatial registry can be maintained on support structures such as stable base cylinders. However in the case of clear fiber waveguides, registry is only required at the connectors, and the fibers may in fact be loose (unregistered) between the ends. Registered scintillating fiber ribbons have been produced at Bicron Corp and at Kurraray. The ribbons at Bicron were produced using a registered drum, and fibers could be produced in single and double layers in lengths up to 3 meters (drum diameter was 1m), and in widths of up to hundreds of fibers. The Kurraray ribbon manufacturing procedure is not known, but the single-layer ribbons received are of high quality. Typically, fibers at Bicron or Kurraray have a diameter tolerance of <1% and center-to-center registry within the ribbons is good to an accuracy of σ ~25μm. Figure 3 indicates the measured registry of a single-layer Bicron fiber ribbon with fibers placed at 820μm pitch; Figure 4 for a single-layer ribbon fabricated at Purdue at 870μm pitch.

Task 5: VLPC and Preamp Development:
(UCLA, Rockwell, UTDallas)

Development of the photodetector optimized for fiber tracking has proceeded significantly in FY91, but, because of funding delays, at a pace 6 months behind where we should be. The VLPC development is taking place at the Rockwell International Science Center and has been divided, operationally, into two evolutionary steps from the original solid state photomultiplier SSPM invented at Rockwell. Step I is to develop linear arrays of devices optimized for visible wavelength response. Step II is to refine the structure for improved device speed and minimization of infrared response. Devices produced at each step are designated VLPC-I and VLPC-II in an obvious notation. Fig. 5 shows a schematic of SSPM and VLPC structures.

To date, VLPC-I devices have been successfully produced and several hundred channels have been delivered to UCLA. These devices have been demonstrated to have ~85% quantum efficiency at a wavelength λ ~565nm (which is optimal for the large Stokes' Shift dyes reported under Task I above). Hence, VLPC-I arrays have been used to demonstrate proof-of-principle of the fiber tracking concept in studies using individual fibers and waveguides and in structures of fiber ribbons excited by radioactive sources and cosmic rays. These results are presented in Section IIC below which summarizes these important measurements. The VLPC-I devices (like SSPMs) are restricted under ITAR

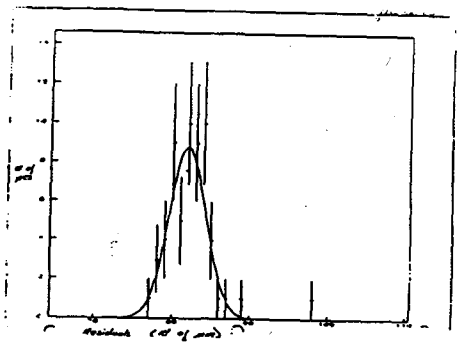


Figure 3. Registry of a ribbon fabricated by Notre Dame at Bicron. Mean is at 820μm with σ ~ 25μm.

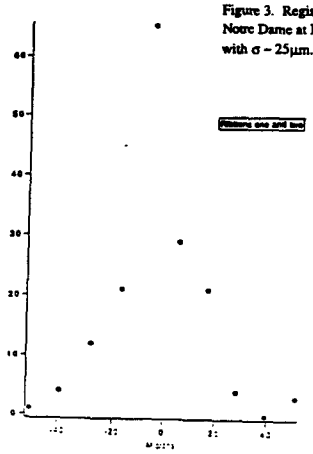


Figure 4. Registry of a ribbon fabricated at Purdue.

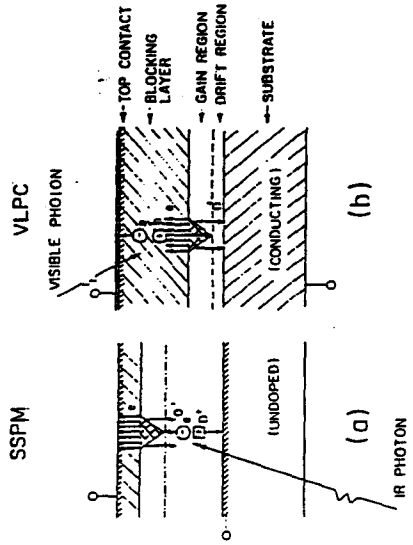


Figure 5. Operation principles of the SSPM and VLPC are indicated.

(International Trafficking in Arms Regulations) because of the IR sensitivity, and are not permitted for use in beam tests at Fermilab as directed by laboratory policy. However, since UCLA, Notre Dame, and Purdue are authorized to use these devices, tests using sources, cosmic rays, or in a beam at a controlled access laboratory are possible, assuming that one or more of these groups assumes responsibility. At this date, all of the VLPC-I devices delivered to FTG (with the exception of a 5-element array assigned to Purdue) are in the hands of the UCLA group which has exercised exclusive control over their distribution. The 5-element array has been used collaboratively by Purdue and Notre Dame to optimize the performance of 32 channels of transimpedance amplifiers which are being used in the cosmic ray tests.

The VLPC-II device fabrication is underway at Rockwell. A first attempt failed to produce useful detectors because of an impurity contamination during the production process. A second attempt is now in progress, with results expected by the end of September or early October 1991. When successful, the VLPC-II should maintain the high visible light quantum efficiency of the VLPC-I, but have improved device speed and markedly reduced sensitivity to IR for improved immunity to thermal noise. Additionally, the VLPC-II should be free of the ITAR restrictions, and will be available to the Fiber Tracking Group for open use in beam tests at Fermilab or elsewhere.

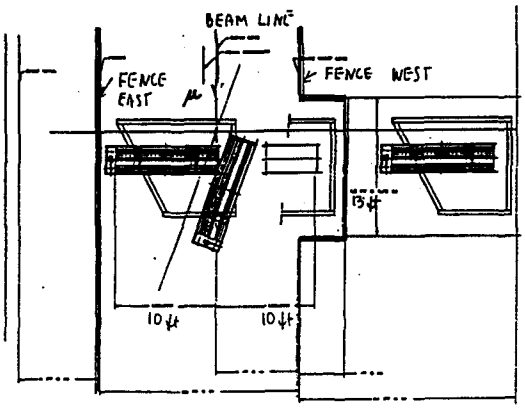
The cryogenic preamplifier option is being explored by UTDallas in collaboration with Honeywell Research Center, using GaAs technology. If successful, the fastest possible operation of the VLPCs could be realized by this approach. Tests of prototype preamplifier components have been made at liquid nitrogen and liquid helium temperatures.

Task 6: Test Beam/Source/Cosmic Ray Studies of Fibers and VLPC
(UCLA, Fermilab, UIChicago, Northeastern, Notre Dame, Penn State, Purdue, Rice, UTDallas)

A main goal of FTG for this fiscal year was a beam test of up to 256 channels of fibers and VLPC at Fermilab. This objective has not been realized in FY91. To date 16 channels of fibers and VLPC have been tested at UCLA on two occasions (July 1991 and September 1991).

However a beam test facility has been developed and located in the New Muon Laboratory at Fermilab for fiber studies and the tests have been officially designated T839. For these tests, a custom, remotely-operable transporter has been built onto which full-

length fiber structures can be mounted and positioned in any orientation relative to the beam (see Figure 6).



.Experimental setup in NM.

Figure 6. The transporter system in the New Muon Beam at Fermilab for T839.

Currently, tests of >96 fiber channels are underway at the facility by Purdue using a multianode PMT and fibers with blue emission (BCF10) appropriate to the vacuum photocathode of the tube. The goal of these tests is to verify the spatial resolution of ribbons of fibers arranged in superlayers for studies of correlated registry between the various layers. These tests are being pursued with the PMT option and blue fibers because of the unavailability as yet of VPLC-II for beam tests.

Task 7: Studies of Radiation Damage and Environmental Aspects of Scintillating Fiber and Waveguide Performance
(Fermilab, UIChicago, Notre Dame)

Initial activity on this task has been confined to studies of radiation damage effects on the optical properties of scintillators in small boules of 1cm diameter and in lengths of 1-10cm. Based on these measurements, a number of different scintillation materials have shown good performance at doses of 1Mrad or greater, and therefore will survive for at least 100 years at SSC design luminosity. Based on these important successes in bulk material, significant activity is now in progress to establish a test facility at the C0 interaction region at the Fermilab Tevatron collider at which scintillating fibers and ribbons can be subjected to realistic doses and dose rates of ionizing radiation under different ambient conditions. Stainless steel pipes fabricated by UI Chicago are to be positioned at C0 which contain scintillating fibers and waveguide fibers, individually and in ribbons, in nitrogen, air, oxygen, and argon atmospheres as well as vacuum. Optical and mechanical properties of the irradiated samples will be compared with unirradiated samples maintained in similar atmospheres, but well away from ionizing radiation. Based upon these comparisons, fiber/ribbon degradation and annealing will be studied as a function of time and atmosphere.

Task 8: Simulations
(IUPUI, Notre Dame, Penn State, Purdue, Rice)

Monte Carlo simulations continue to be carried out by several of our collaborating institutions directed toward design and implementation of superlayers of fibers for tracking, triggering, pattern recognition, and momentum analysis.

The first objective has been to build a simulation and pattern recognition program for an all-fiber tracker in the barrel region of the central detector ($|\eta| < 1.6$). The SFTSIM/TRF software package now exists and allows detailed studies of: superlayer

structure, stereo-angle for measurement of longitudinal coordinate, two-dimensional reconstruction ($r\phi$ measurements), three-dimensional reconstruction (combining $r\phi$ and narrow angle stereo measurements), pattern recognition and trigger options. These important studies are continuing. An example of a reconstructed event containing a Higgs decay to four leptons is shown in Figure 7. How well such algorithms function in a realistic SSC environment depends upon pileup effects from minimum-bias events. Figures 8 and 9 show the reconstruction efficiency and the ratio of false to true tracks as a function of the number of events in a crossing. Clearly the efficiency for true tracks stays high, but the false track rates increase significantly as the number of events per crossing is increased.

The second objective has been to incorporate fiber tracking algorithms into a global sofiware shell (SDCSIM) for studies of combined systems such as a silicon tracker at inner radii ($r < 50$cm and a fiber tracker at outer radii ($70\text{cm} < r < 170\text{cm}$), and for studies of performance with other detector components such as calorimetry and muon systems. Important recent progress has been achieved in this area, and global simulation studies by our group and others is underway. We expect that the incorporation of silicon layers into the pattern recognition study described above will eliminate most of the false tracks which appear in an analysis of fiber-only tracking information.

The third objective has been to incorporate tracking detectors at intermediate angles ($1.6 < |\eta| < 2.5$). Topologically, the detector structures are expected to be different in this region, for example planar disks, rather than the concentric shell configuration of the central region. Examples of candidate superlayer structures are shown in Figures 10 and 11. This work is directed specifically toward first level trigger formation (see Task 9 below) and development of algorithms is in progress.

The fourth objective has been to optimize a powerful transverse momentum trigger algorithm appropriate for incorporation into a fast Level-1 electronic trigger built in ASIC technology. Figures 12 and 13 show the trigger efficiency for single muons and electrons at $\eta = 0.5$ in one analysis (Rice/UTDallas) as a function of P_T for a fiber tracker in the currently favored configuration with superlayers at radii of 70,100,130 and 160 cm. The trigger threshold shows a clear, sharp onset, and effects of bremsstrahlung should be noted in the electron case, Fig 13. Fermilab and Penn State groups are working to translate such tracking algorithms (and others) directly into trigger electronics with implementation in ASIC. (Again see Task 9.)

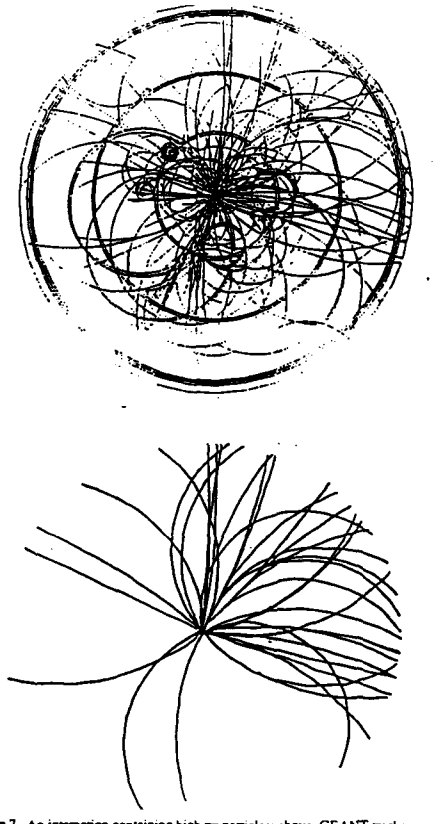


Figure 7. An interaction containing high p_T particles: above, GEANT tracks; below, reconstruction of tracks of p_T above a minimum threshold.

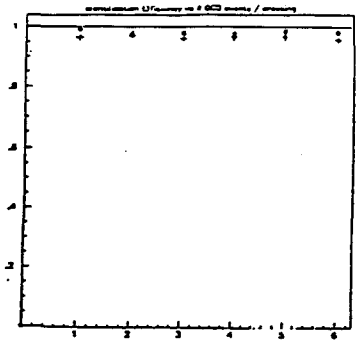


Figure 8. Track-finding efficiency vs the number of events/crossing for selected tracks. The crosses are for 3 degree stereo, the circles for 8-13 degrees.

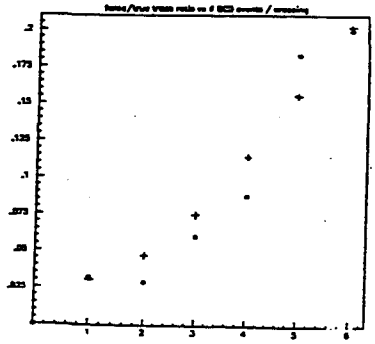


Figure 9. Ratio of false tracks to candidate tracks as a function of the number of events in a crossing. The crosses are for 3 degree stereo, the circles for 8-13 degrees.

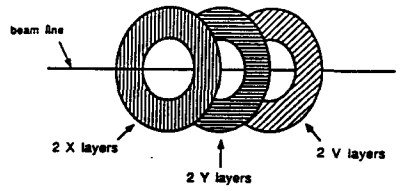


Figure 10. Superlayer option for the intermediate region. XUV configuration.

Curved Fiber Sublayer Construction

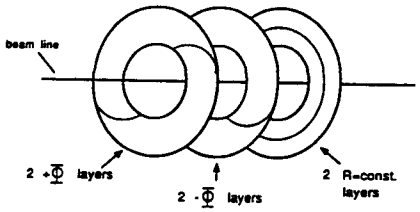


Figure 11. Superlayer option for the intermediate region. Spiral configuration.

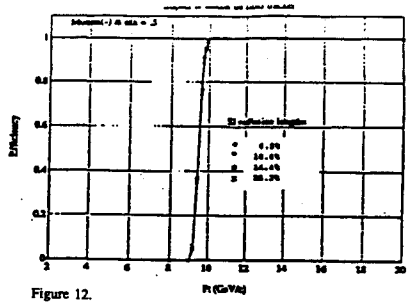


Figure 12.

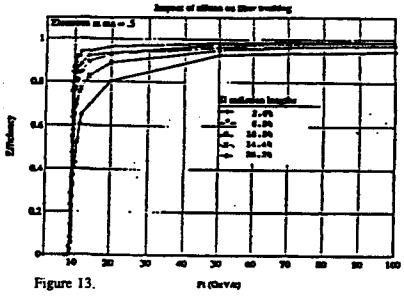


Figure 13.

The fifth objective has been the continued development of fiber waveguide simulation using the OPTICKS software package developed by Notre Dame. This work has focused attention on several important issues, including the effects of cladding and extramural materials (coatings and adhesives on the outside wall of the fibers). The efficiency of scintillation light production and collection in the scintillating fiber, at the site of the energy deposition by ionizing radiation, depends significantly on these characteristics and will have a significant influence on the selection of dyes and adhesives used in the fiber and ribbon manufacture. The other significant area of study has been optical transport within the fibers and waveguides, particularly the understanding of reflections at core and cladding interfaces, and of bulk absorption within the materials. This work is ongoing.

Task 9: Trigger Development
(Fermilab, Penn State)

A level-1 trigger is under development, based on recognizing high P_T tracks in the scintillating fiber tracker. The efforts this year have been concentrated on translating the basic trigger algorithms into trigger electronics using Verilog programs to demonstrate that the (ASIC) electronics can perform the appropriate pipeline logic. Three important issues have influenced the study: physics performance, detector granularity and segmentation, and descoping/staging issues. The first two issues affect trigger efficiency and the suppression of background pileup from minimum-bias events. The final issue has influence on the development of trigger strategy. Figure 14 shows schematically an arrangement of four fiber superlayers measuring $r\phi$ coordinate (i.e. directly measuring P_T). Also shown are clusters of hits in the fiber layers. Note that track position and angle are provided within a superlayer. Figures 14 and 15 together provide a diagram of the operation of three ASICs which are used to analyze the pattern. ASIC-1 finds radially continuous sets of hits within a superlayer; ASIC-2 forms track stubs with centroid and angle within the superlayer; and ASIC-3 links stubs among the superlayers to form tracks. The system is initially being designed and prototyped using discrete technology. Actual ASIC development is expected to begin in FY92.

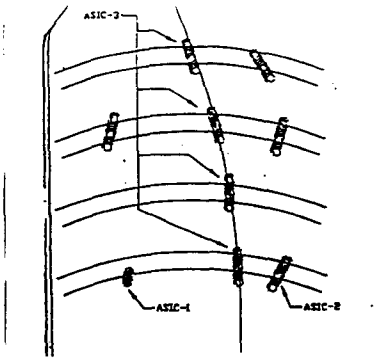


Figure 14. Superlayer structure indicating domain of ASIC usage.

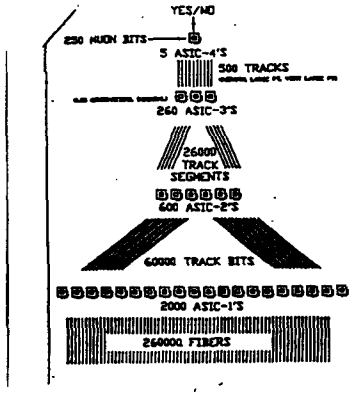


Figure 15. Cartoon indicating information sparsification through the ASIC trigger pipeline.

Task 10: Mechanical Engineering
(Purdue, ORNL)

Limited engineering studies sufficient for a preliminary fiber tracking system costing have been carried out in collaboration with Oak Ridge National Laboratory. A work-baseline structure (WBS) has been developed in order to assess costs and schedules and critical path issues in the development, fabrication, and assembly of a fiber tracking detector. This effort was assembled by Purdue and ORNL into a document presented to the SDC collaboration at the collaboration meeting held at LBL in August 1991 [1]. Essential engineering conceptual design studies could not be implemented in FY91 because of funding limitations. We are gravely concerned that, unless this situation is corrected in FY92, important initiatives in system development will be seriously delayed. Section III below outlines these initiatives.

References:

[1] D. Koltick and D. Vandergriff, "Scintillating Fiber Tracker Baseline Costing, Schedules and Construction Concepts", SDC Report, August 1991.

C. PROGRESS REPORT ON ACHIEVING PROOF-OF-PRINCIPLE FOR FIBER TRACKING

The principle aims of the Fiber Tracking Group are to demonstrate proof-of-principle of the fiber tracking technique, to develop and build a 1024 channel prototype, and ultimately to build a fiber tracking detector for SDC. During FY91, our program has achieved several impressive successes, and proof-of-principle has been established.

Polystyrene doped with scintillation dyes and clad with polymethylmethacrylate (PMMA) has been drawn into fibers of varying diameters from 1mm down to 250μm by several commercial vendors for studies by our group. For a variety of reasons including fiber efficiency, light collection and transmission, and total system cost for a fiber tracker, we are working with 830μm diameter fibers. This diameter value may change in response to further R and D results and studies of system costs. As has been observed by ourselves and others [1], radiation resistance of optical transmission in polystyrene is impressively better for wavelengths $\lambda > 500$nm and general optical transmission is best in unirradiated polystyrene for wavelengths peaked in the visible portion of the spectrum $500\text{nm} < \lambda < 650\text{nm}$ [2]. By operating in this wavelength range, less than 1% transmission loss is observed for polystyrene maintained in a nitrogen atmosphere during irradiation to 10 Mrad, and annealed in oxygen (see Fig. 16). For the present design of the fiber tracker for SDC, 10Mrad corresponds to the integrated dose expected for 100 years of operation at SSC design luminosity. These results give us confidence that optical transmission of an SDC fiber tracker will not be impaired over its working lifetime by radiation damage effects.

Candidate scintillators have been produced and drawn into fibers and ribbons of fibers for further study with sources, cosmic rays, and in beam tests. An example is polystyrene doped with p-terphenyl (PTP) and 3-hydroxyflavone (3HF) which has fluorescence emission peaked near 530nm, good radiation stability to several 10Mrad, and reasonable speed (5-7ns). Figure 17 shows the fluorescence emission spectrum of this scintillator. Several other candidates with improved characteristics for photostability and quantum yield are under study.

To detect light at 530nm is difficult and impractical with conventional vacuum photocathodes and is properly the domain of solid state materials (silicon and GaAs). The problem is to combine good quantum efficiency with high enough gain to do single-photon counting, which is invariably the circumstance for fiber tracking detectors attempting to record the presence of minimum ionizing particles. Possible conventional options include

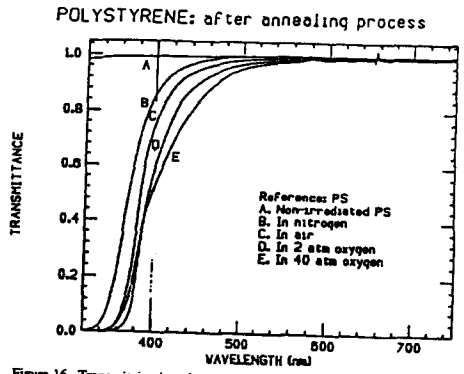


Figure 16. Transmission in polystyrene under various conditions during irradiation.

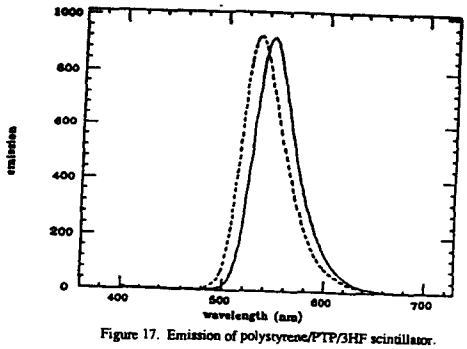


Figure 17. Emission of polystyrene/PTP/3HF scintillator.

Fluorescence emission for 3-HF (dashed curve) and a variant BC447 (solid curve) which has red-shifted emission. The new dye appears as a strong yellow, whereas 3-HF appears yellow-green.

image intensifiers, multianode photomultipliers, avalanche photodiodes (APDs), solid state photomultipliers (SSPMs), and a variant of the SSPM optimized for visible light sensitivity only (designated VLPC for visible light photon counter). VLPCs are the best of these alternatives, having a demonstrated quantum efficiency of 85% at 565nm and the capability of successful operation at an SSC luminosity of $L = 10^{34} cm^{-2} s^{-1}$. Note that the VLPC quantum efficiency is a factor 10 better than good phototubes in this wavelength range, and it is the combination of high QE and high rate performance which makes the fiber tracking technique viable and powerful.

For SDC, the basic detection element is an active fiber scintillator of ≤ 4m length, coupled by a 4m-to-6m long clear fiber waveguide to a high-rate photodetector. In recent tests (first at Fermilab and more recently at UCLA), a polystyrene/PTP/3HF scintillating fiber of 830μm diameter and 4m length was optically spliced to a clear fiber waveguide of 830μm diameter and 3m length, and read out with a Visible Light Photon Counter (VLPC). The VLPC has a quantum efficiency of ~85%, an electron gain of ~30K, and excellent signal to noise characteristics. Figure 18 provides a diagram of the experimental arrangement. The scintillator was excited by positioning a collimated beta source (^{90}Sr) near the fiber element and data is recorded into a QVT (ADC) using a telescope of scintillation counters to provide a coincidence gate. Observed photoelectron yields for several source positions along the scintillating fiber are shown in Figure 19. It should be noted that clear peaks are discernable in these figures for up to 6 (or more) simultaneously detected photoelectrons, and demonstrate clearly that the VLPC is a superb single photon-counting device. The mean detected photoelectron yield as a function of position along the scintillating fiber is shown in Figure 20 for two cases: fiber with mirrored end and unmirrored end. As the figure shows, we have detected ~3.8 photoelectrons when the source is placed at the far end of a scintillating fiber in the case of a mirrored end, and an attenuation length of 3.9m was deduced from this set of measurements. However, even these excellent photoelectron yields have been exceeded by a factor of 1.5 in our most recent tests described below.

Since the single-fiber measurements were performed and reported in Spring 1991 [3], further improvements have been made in the fiber scintillator and waveguide fabrication, and in the optical coupling technique between the scintillator and waveguide fibers. These have resulted in significant further (50%) improvement in detected photon yield. The fibers are now fabricated into fiber-ribbons with well-registered center-to-center spacing (pitch) between adjacent elements. [Arrays of fiber ribbons arranged in

EXPERIMENTAL ARRANGEMENT

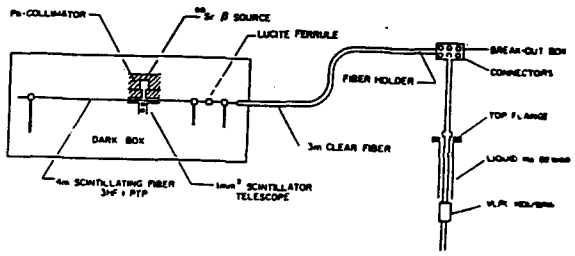


Figure 18. Experimental arrangement for measuring detected photon by a V.L.P.C. using a 4 meter length of scintillating fiber of 0.8 mm core (3HF + PTP in polystyrene). The scintillating fiber is spliced to a 3 meter long optical clear fiber that carries the photons to the VLPC.

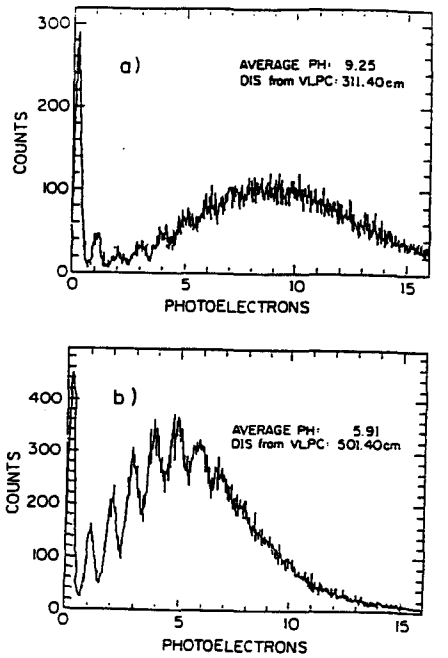


Figure 19. samples of pulse height spectra obtained at the indicated sources positions. The weighted average number of detected photons are given on the figures.

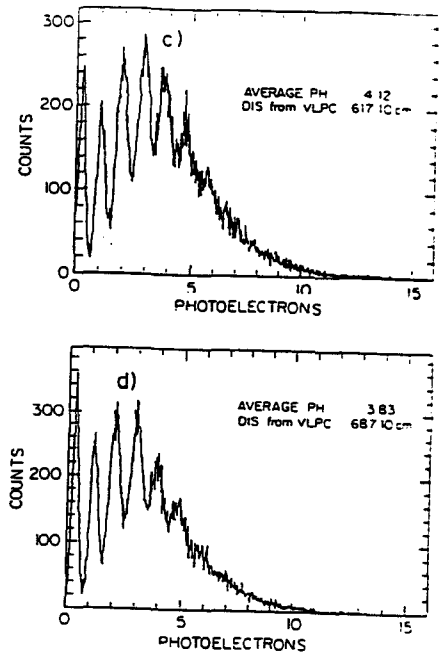


Figure 19 continued. samples of pulse height spectra obtained at the indicated sources positions. The weighted average number of detected photons are given on the figures.

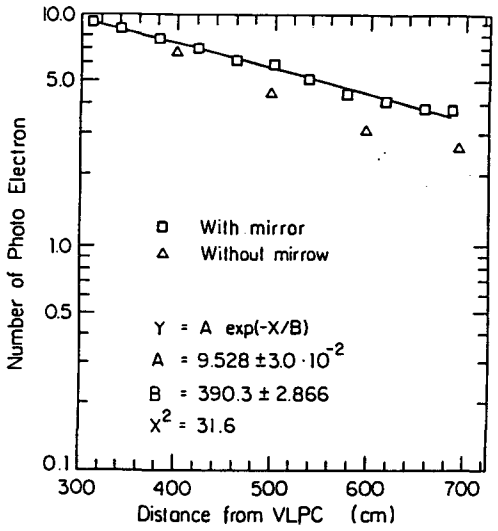


Figure 20. Detected number of photons as a function of source positions from the VLPC are indicated with and without a mirror at the end of the scintillating fiber.

superlayer structures represent the basic elements from which a fiber tracker is expected to be built.] Ribbons have been fabricated at several commerical houses including Bicron and Kuraray and several of our own groups have developed fiber fabrication techniques at their home institutions. The current configuration is 830μm fibers registered at 870μm pitch (see Fig. 2 above). Double layers are formed by placing a second layer of fibers in the gap between the fibers of the first layer, and a typical SDC superlayer lattice is comprised on two such double layers for measurement of the rφ coordinate. Multilayer lattices of fiber ribbons are now being tested with cosmic rays and in the Fermilab beam in the New Muon Laboratory. The beam studies which use multianode PMTs to read out fiber ribbons are directed toward spatial resolution of the fiber lattice. The cosmic ray tests utilize VLPC-1 devices for readout, and are focusing on the question of photostatistics and efficiency of the fiber lattice. It is this laner work which we now describe.

The test arrangement is basically of the same configuration as indicated in Figure 19. However, now a lattice of 16 fibers is under test, with the lattice composed of a stack of 4 ribbons containing 4 fibers each (see Figure 21). The fibers are of 830μm diameter and close packed in center-to-center spacing. Each scintillating fiber is optically coupled to its own waveguide fiber of identical diameter, and the fiber/waveguide elements are read out individually by VLPC-1 photodetectors. The VLPC signals are amplified by transimpedance amplifiers operated at room temperature. Data is recorded into Fastbus ADCs (LRS1882 and 1885) when a coincidence is recorded in a two-counter scintillation telescope signaling the presence of a cosmic ray.

Figure 22 indicates cosmic ray events in the 16 element lattice used during tests in July 1991 at UCLA. The pulse height in each active fiber is shown in photoelectron equivalents. Several thousand events of this kind have been recorded during July and September 1991, and we are analyzing these data for evidence of delta rays, cross talk and fiber layer efficiency. In the most recent tests (September 1991), new scintillator ribbons and waveguides from Kuraray are being tested. The quality of the ribbons is very high and we are observing substantially improved photoelectron yields. Figure 23 shows the detected photoelectron yield from the far end of fiber ribbon 3 (layer 3 in the lattice) when a software trigger is imposed, requiring at least 0.5 photoelectrons in each of fiber layers 1 and 4. We observe a mean detected yield of ~6 photoelectrons. Geometric effects such as gaps between fibers and cladding thickness which lead to inefficiency in the layers appear as the peak below 2 photoelectrons in the figure. Since a minimum of 2.5 detected photoelectrons is required to assure an efficient double layer of fibers, our result of 6

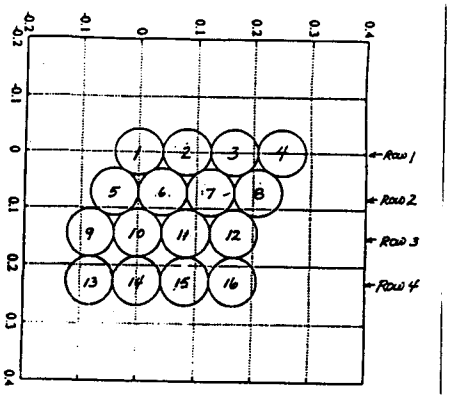


Figure 21. Schematic of the fiber lattice used in cosmic ray tests, July 1991 at UCLA.

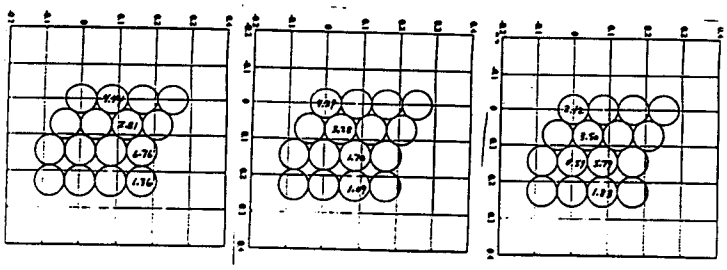


Figure 22. Sample cosmic ray tracks in the fiber lattice.

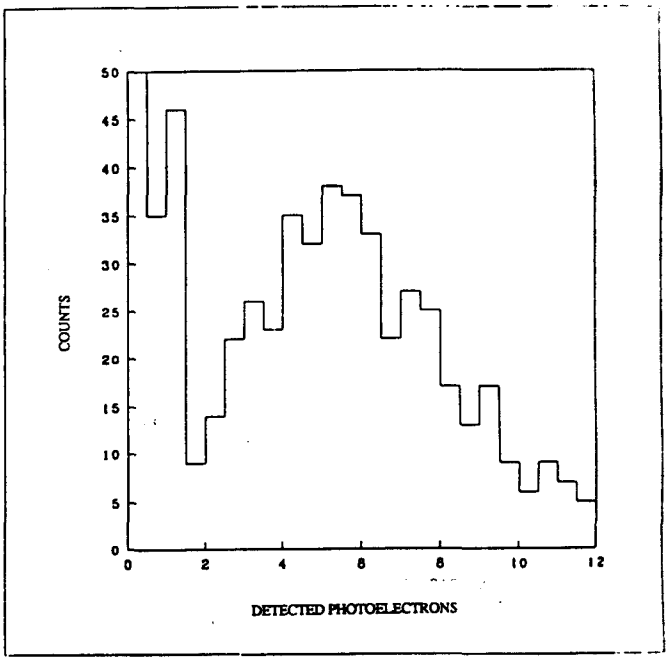


Figure 23. Detected photoelectron yield in layer 3 of a four-layer stack from cosmic rays with excitation at the far end of the scintillating fiber (7m from the photodetector)

photoelectrons shows that the fiber tracking concept is sound, and that proof-of-principle has been established. Indeed, these results establish a new standard of performance and give us confidence that we are well on the way to achieving our performance goals for SDC.

It is now essential to concentrate on system development and to produce a conceptual engineering design for fabrication of the basic elements of a fiber tracker and for construction of the overall detector. Clearly necessary are continued refinements of the basic detection elements: scintillator, waveguide, splicing, VLPCs and amplifiers. However, we must now design and fabricate at least one working prototype system containing 1024 fiber and VLPC elements to validate the concepts. And, a conceptual engineering design must be begun! These tasks will require substantial support for R and D and engineering in FY92.

References:

[1] A. Bross and A. Pla-Dalmau, American Chemical Society Symposium Series, October, 1990 and Fermilab/PUB 90-224.

[2] J. Alliti, et al, IEEE Transactions on Nuclear Science, Vol.36, No.1 (1989), 29-34.

[3] M. Atac, et al, "Scintillating Fiber Tracking at the SSC Using Visible Light Photon Counters", Fifth International Pisa Conference on Advanced Detectors, May, 1991. To be published in Nuclear Instruments and Methods.

III. RESEARCH PROGRAM FOR FY92

A. OVERVIEW

The physics goals of SDC include studies of electroweak symmetry breaking, properties of the top quark, searches for new physics, including heavier gauge bosons, evidence of compositeness, new particles implied by supersymmetry, and totally new and unexpected phenomena.

To meet the challenges implicit in these goals, SDC is proposing a general purpose detector (see Figure 24) with central tracking in a solenoidal magnetic field, hermetic calorimetry, identification and energy measurement for electrons and muons, and high resolution vertex detection. These capabilities will provide power and a level of redundancy essential for the understanding of new phenomena at the SSC. It is the intention of the SDC collaboration to design a detector whose subsystems are fully functional at the design luminosity of $10^{33}cm^{-2}s^{-1}$, and which can address more specialized physics issues at substantially higher luminosity with somewhat reduced functionality. The general characteristics of the SDC experiment are well summarized in the EOI and LOI documents. Here we limit our discussion to issues of central tracking and the scintillating fiber tracking option, which are two aspects of the detector in which the Fiber Tracking Group is making significant contribution.

The tracking system plays a major role in exploratory physics, lepton and heavy quark identification, mass reconstruction, and in the formation of the trigger. SDC has placed emphasis on reliable pattern recognition and precise momentum and vertex resolution over the pseudorapidity range $|\eta| < 2.5$ required for SSC physics. As stated in the LOI, the basic goals of the SDC tracking include: pattern recognition capability within jets of p_T up to 1 TeV/c; high resolution vertex detection capable of identifying jets containing b hadrons with good efficiency; capability of providing level 1 or 2 trigger information to identify tracks of p_T greater than 10 GeV/c; and functionality of at least part of the tracking system at luminosities significantly above the SSC design value.

In order of increasing radius, the central tracking system (Figure 25) consists of: two dimensional pixel silicon detectors to aid the pattern recognition and detect secondary vertices from heavy quark decay; an array of silicon strip detectors to provide pattern

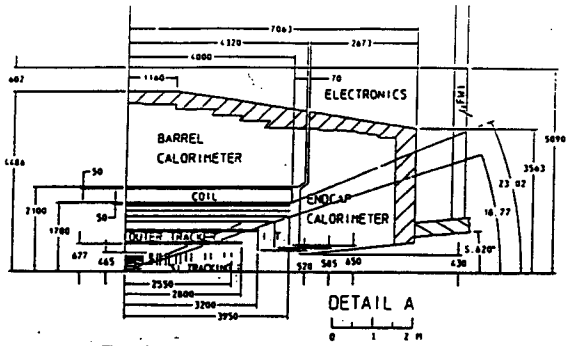


Figure 24. Layout of the SDC Detector (excerned from the SDC LOI).. One Quadrant is shown.

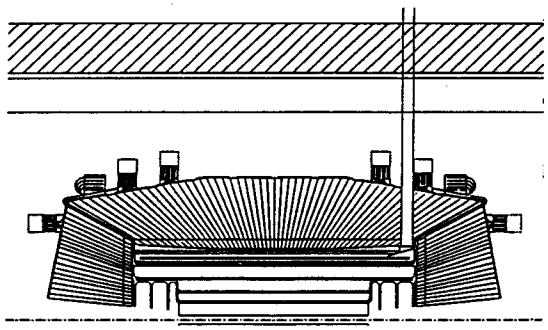


Figure 25. Schematic of the central tracker exhibiting the all-fiber outer tracking option.

recognition and momentum measurement in the range $|\eta| < 2.5$; and a straw-tube or scintillating fiber system to provide the curvature determination needed for high precision momentum and vertex measurements and trigger information for high p_T particles over the same range $|\eta| < 2.5$.

Scintillating fiber detectors are an attractive choice for meeting the challenge of central tracking at high luminosity and have the following features:

[i] Good tracking precision. Multilayer structures of 830μm diameter fibers can result in a measurement resolution of ≤ 150μm per double-fiber layer, ~100μm per quadruple-fiber layer, and provide good two track resolution.

[ii] Fine granularity. For fibers of 830μm diameter placed at radii r ≥ 70cm, the occupancy from all sources is expected to be ≤ 1% per fiber, per bunch crossing.

[iii] Single-crossing time resolution. Scintillator has an intrinsically prompt response.

[iv] Insensitivity to magnetic fields and to RF noise.

[v] Simple electronics as a binary (yes/no) readout is used.

[vi] No power dissipation or electronics in the tracking volume.

[vii] The implementation of stereo fiber layers is relatively straightforward because of the flexibility of the fibers and fiber ribbons.

[viii] Good resistance to radiation damage.

Now with proof-of-principle for the technique established, the Fiber Tracking Group intends to move forward with refinements of the detector elements, the development of system concepts, and a conceptual design for the fiber tracking detector.

B. DESCRIPTION OF THE DEVELOPMENT PLAN

Research and Development is focused toward system concepts and the development of a conceptual engineering design for fabrication of the basic elements of a fiber tracker and construction of the tracking detector. In support of this plan, R & D to refine of the basic detection elements will be continued in FY92, a working prototype system containing 1024 fiber and VLPC elements is to be built to validate system concepts, and a conceptual engineering design is to be initiated.

i. Scintillating Fiber and Waveguide R & D:
(Fermilab, UI Chicago, MCPAHS, Northeastern, Notre Dame, Purdue, PCPS)

Optimization of scintillating fiber characteristics for the SSC/SDC environment focuses on light yield, robustness, radiation hardness, and time response. The principal areas of development concern fluorescent dyes, claddings, and extramural coatings. The goal is selection of the final scintillating material and claddings on the basis of well understood and well demonstrated properties and performance characteristics.

Dyes - We plan to continue our systematic studies of large Stokes' Shift dyes in polystyrene using various multi-step combinations and concentrations. A portion of this work will be done in collaboration with industry as evidenced by the excellent light yield and attenuation length obtained this year with BCF99-05 (PTP/3HF) scintillating fiber spliced to clear BCF98 waveguides and similar results obtained with Kuraray fibers. The most promising scintillators will be fabricated into preforms and drawn into fiber for complete characterization measurements and radiation hardness evaluation.

Waveguides - Waveguide R & D to date has resulted in reasonably low-loss clear fibers with attenuation lengths in the range of 8-9 meters for light already collimated by a long scintillating fiber (as it is in our case). We will work to improve this further by concentrating on material purity and the care and cleanliness in preform preparation and fiber pulling. However, the current results are already adequate for the SDC application.

Cladding - A systematic evaluation is planned for the set of low refractive index claddings available. Use of such materials can improve overall light collection efficiency by trapping more of the scintillation light, provided that this is accompanied by an improved reflection coefficient between the core and cladding - large trapping angle implies more "bounces" as the photons propagate down the fiber waveguide. In addition, we will

be testing the option of incorporating primary scintillation dye into the cladding material, in order to render the full volume of fiber sensitive to ionizing radiation.

Extramural Coatings - Measurements of the performance characteristics of scintillating fiber arrays using a variety of extramural coatings is planned. The issues are reduction of optical cross talk, reduction of background illumination, and possible improvement in the light yield. Among the coatings to be studied are polysiloxane and opaque adhesives, TiO_2 and vacuum deposition of aluminum.

Waveguide Simulations - Initial work on waveguide simulations will be extended with studies of core/cladding interfaces, UV absorption, cladding thickness, extramural absorbers, and optical attenuation length. Results of the simulations will be compared to measurements with VLPC detectors and CCD images of the spatial distribution of the emitted light and will help guide our choices of fiber profile, fiber spacing, and the mechanics of ribbon manufacture.

Radiation Damage and Environmental Issues - Controlled exposure studies are planned to investigate the impact of normal air versus oxygen-free environment. Previous work has indicated that oxygen can both aid annealing and increase permanent damage. Most of these results have come from very high exposure rate tests where doses of several Mrad are delivered in minutes. The planned effort will involve a moderate dose rate over a six month period. The goal is to determine whether an oxygen-free environment will be necessary at the SSC.

Splicing - The splicing of scintillating fibers to clear waveguide fibers has been successfully accomplished in the laboratory by thermal fusion, adhesives, solvent fusion, and optical grease in a tight-fitting sleeve. When carefully performed, all of these methods have shown transmission greater than 95%. For the fiber tracker, it is necessary to consider the requirements of both the large scale utilization and the organization of fibers into linear ribbons. The ideal solution would be a quick disconnect linear connector structure that joins several thousand fibers to their waveguides with the same 95% transmission as achieved in the lab. This is potentially realizable, as our best splices have been obtained with optical grease. The current R & D work is aimed at designing the splicing technique and sequence for joining barrel fiber ribbons to the clear waveguides.

ii. Readout Research & Development and Engineering:
(UCLA, EG&G Montreal, Fermilab, Northeastern, Rockwell, UT Dallas)

The leading candidate and basic element of the readout system for scintillating fibers is the visible light photon counter (VLPC) developed by Rockwell International Science Center in collaboration with the UCLA group of M. Atac. VLPC devices operate at 6K to 7K and therefore require a helium cryostat and special techniques for packaging, biasing and photocoupling in a cryogenic environment. In collaboration with Rockwell, FTG will continue to develop and optimize these devices for reduced IR sensitivity, high speed, quantum efficiency, and simplicity of cryogenic operation. This includes development of IR reflective coatings, reduction in the ohmic resistance at the VLPC output, and refinements of the interaction between the VLPC and preamplifier to prevent occasional latching.

During FY92 and 93, tests of 1K to 10K fibers, waveguides and associated VLPCs will be undertaken for system tests of stability, light yield, and overall performance. To implement these systems, a close interaction with industry is required. Engineering design effort and prototyping work is essential to benchmark engineering parameters and operating conditions as the design proceeds. The concept calls for a cryostat unit which contains 16 individual modules that can be independently removed or inserted. Each module would contain 1024 VLPC channels and provide an appropriate optical quick disconnect and multipin electrical connectors. In this design only the VLPCs will be cold, the amplifier/shaper/discriminator being operated warm. The conceptual design for this unit is being prepared by Rockwell under contract with Fermilab. Developement of cryogenic preamplifiers will be continued as an important alternative, since this configuration affords the fastest overall system response.

An alternative readout method is the avalanche photodiode (APD) which functions well at or near room temperature, but which must operated in a geiger mode to achieve a high quantum efficiency for single photon counting. To achieve the improved rate capability required for the SSC operating conditions, the APD must be operated in a fast-quench mode or in sub-geiger mode. These techniques and the associated electronic circuitry are under development at EG&G Montreal in association with Northeastern. Substantial numbers of fibers (96 channels) with APD readout will be tested, under similar conditions to the VLPC tests, so that appropriate comparisons can be made on the performance characteristics of the two devices.

iii. Engineering Issues for the Fiber Tracker:
(Fermilab, Northeastern, Notre Dame, ORNL, Purdue)

Fiber Engineering - The technique of fabrication is a very important factor in the production of scintillating fiber of adequate light yield and attenuation length. Diameter control is crucial to the final assembly into ribbons. The work planned is to carry out a systematic engineering study of the process variables including integration of quality assurance (Q/A) steps in an automated way to optimize yield and quality. Process variables include molecular weight profile of the polymer, fused versus non-fused preform cladding, preform temperature during drawing, drawing speed and tension, normal versus oxygen free environment and diameter of the takeup spool. A collaboration with industry is foreseen with preforms provided by SDC and pulling towers and quality assurance instrumentation provided by industry. During the study, a significant amount of fiber will be produced (up to 300km being envisioned).

Ribbon Manufacturing Engineering - Initial attempts to produce fiber ribbons of good quality by winding fibers under tension on a registered drum have been successful. This represents but one approach to ribbon manufacture. Other opproaches include winding fixtures similar to those used with wire chamber winding machines and placement on registered planar frames. The choice of technique may well influence other parameters such as the type of adhesive and the need for a backing layer.

Small scale engineering and prototype studies are planned for all techniques so that the best tecbniques can be selected by comparison of the results from several methods. Subsequently, a production design will be engineered appropriate to large-scale manufacture. Appropriate quality assurance issues will be addressed by the design as well.

Engineering for Placement of Scintillating Fibers into Superlayers - Currently underway in FY91 are the development of preliminary engineering concepts for fiber tracking in the central barrel region and in the intermediate angle region. In FY92 these ideas must be developed into a full conceptual design. A key element to be decided is the support structure (stable base cylinders for the barrel region is the current preferred choice). Subsequently, the next phase calls for the development of appropriate techniques for placing fibers or ribbons of fibers onto the supports with adequate registry. Tooling, fixturing, and automated procedures including real-time alignment instrumentation are included in the design effort. The principle design responsibility resides at present with

Oak Ridge National Laboratory (in the current SDC arrangement) with strong consultation from the FTG collaboration. Industrial affiliates such as Westinghouse or Rockwell may be considered as well.

For the barrel, a prototyping effort is planned which will place fibers on comparable (or actual prototype) cylinders to test methodology, accuracy, and technique. The unique features for the SDC application will be included: light tighting, the provision for the flow of dry nitrogen within and among the superlayers to assure an oxygen-free environment, and thermal control to minimize linear expansion in the long fiber assemblies.

The intermediate angle region uses a disk format to support fibers in a plane perpendicular to the beam. Both the pattern of fibers, radial or spiral, and the number of layers per disk present significant challenges in design, tooling, placement, and registration. It is essential to develop the conceptual design for disk superlayers and to build several prototype structures to validate the concepts.

iv. **First Level Trigger:**
(Fermilab, Penn State, Rice)

The goal of the fiber tracking group is to design a level 1 trigger based on the fiber superlayer structure, which for the central region of pseudorapidity reports the momenta of individual tracks in units of sagitta. Given the fiber diameter, spacing, and superlayer structure, the momentum resolution at level 1 is expected to be approximately $\sigma_{p_T}/p_T \sim .004 p_T$ (with p_T in GeV/c units) for a 2 Tesla magnetic field and 1.7 meter tracking radius.

Goals of the R & D program include: simulation studies for the optimization of required channel count and superlayer structure to achieve the desired momentum resolution for the level 1 trigger; the implementation of a prototype trigger system based on discrete circuitry for validation of the trigger concept during beam tests of the fiber tracking system; and the design, fabrication and test of the ASICs by which the actual experimental DAQ and triggering will be implemented. This will include prototype level 1 and 2 storage, a segment finder ASIC, and a segment-linker and track extrapolation ASIC. The engineering of the crate mechanics will be studied, including tests of crate-to-crate pipelined trigger interconnects, and selection of appropriate high density cabling. A logic design for a pipelined intermediate track trigger similar to the barrel tracker will also be determined. Finally, we will perform a reliability analysis of the fiber tracking trigger by

studying the effect on trigger efficiency and momentum determination of dead (missing) fiber channels, dead interconnects and logic channels, and determine the appropriate level of redundancy in track trigger components.

v. **Beam/Cosmic Ray/Source Tests:**
(UCLA, Fermilab, UIChicago, Northeastern, Notre Dame, Penn State, Purdue, Rice, UTDallas)

Essential to the systematic and successful study of fiber tracking elements are continued cosmic ray, source, and beam tests. Tests of fibers ribbons and superlayer structures are planned for Fall 1991. Subsequent tests will be performed as needed where test beam is available or with cosmic rays.

vi. **Simulations:**
(IUPUI, Notre Dame, Penn State, Purdue, Rice)

Substantial work is underway to simulate track reconstruction and triggering in the fiber central tracker and intermediate tracker. The goal of these studies is to refine the concept of the superlayer, and to determine the minimum number of required superlayers and their deployment in the barrel and intermediate regions.

C. MILESTONES FOR FY92

Here we tabulate the milestones and goals for FY92 and estimates for FY93.

	Milestone and Goal	Date
1.	Scintillator R & D	
	Characterization of candidates	8/92
2.	Waveguide R & D	
	Selection of waveguide composition	1/92
	Selection of cladding material	8/92
3.	Splicing R & D	
	Review of splicing techniques	1/92
	Prototype candidate techniques	6/92
	Selection of splicing technique and sequence	8/92
4.	Fiber Manufacturing Engineering	
	Optimization of fabrication process	9/92
	Development of automated Q/A apparatus	1/93
	Production of significant quantities of fiber	2/93
5.	Ribbon Manufacturing Engineering	
	Selection of ribbon fabrication technique	8/92
	Engineering design of production facility	1/93
	Determination of Q/A procedures and equipment	1/93
6.	Readout R & D	
	Further IR desensitization	1/92
	Reduction in ohmic contact resistance	5/92
	Latching/preamplifier issues	8/92
	Croygenic preamp studies	8/92
7.	Readout Engineering	
	Conceptual design for the readout system	12/91
	Engineering design for the readout system	6/92
	Fully functional pre-production prototype	12/92
	Operation of a 1K fiber/VLPC system	4/93
	Operation of a 10K fiber/VLPC system	1/94
8.	Ribbon Placement onto Superlayers	
	Stable-base cylinder prototype development	9/92
	and construction	1/93
	Engineering placement concept	9/92
	Construction of placement jigs and fixtures	6/93
	Placement of fibers superlayers onto prototype cylinder	9/93
9.	Trigger/ASIC Development	
	Discrete technology prototype	6/92
	ASIC Development	9/92

IV. REPORTS FROM COLLABORATING INSTITUTIONS ON FY91 R AND D

A. UCLA /ROCKWELL

The UCLA fiber tracking group has made very good progress toward realization of scintillating fiber tracking for the SSCL notwithstanding the long delays in receiving funding. The results given in the presentation at the Pisa Conference [1] clearly indicate the accomplishments. The UCLA group has worked on the following projects:

SSPM and VLPC Development: Presently Rockwell and UCLA are developing the visible light version of the Solid State Photomultiplier (SSPM) called the VLPC. The VLPCs and SSPMs need to be cryogenically cooled, since the bandgap energy of the extrinsic semiconductor is about 0.046eV. The optimum operating temperature is around 7K. For the VLPC, sensitivity to infrared photons will be greatly reduced, the count rate capability will be increased, and time resolution and quantum efficiency will be improved. The quantum efficiency of the VLPCs has been optimized for wavelengths of ~565 nanometers by anti-reflective (AR) coating, to spectrally match the emission of the scintillator. Figure A1 depicts these quantum efficiency tests, and a QE of ~ 85% was obtained. Initial concerns that polystyrene fiber waveguides which transmit the photons to the VLPCs might be intolerant of cryogenic temperatures and temperature gradients have proved unfounded. Repeated tests have shown that the fibers are unaffected by careful, thermal cycling.

VLPC Characterization: Working together with Dr. M. Petroff of Rockwell International Science Center, we have measured device characteristics of VLPCs such as quantum efficiency as a function of temperature and bias voltage at each step of the VLPC R&D. Figure A2 indicates the results of several of these important measurements, and has allowed us to determine the effective operating point for the device.

Covar Cassettes: These are small housings that hold VLPC chips of 8-elements and rigidly hold clear optical fibers with provision to align them against the VLPCs to a few micron precision. Repeated tests showed that the cassette design was successful in operating at the required cryogenic temperatures. The thermal expansion coefficient of covar and silicon (VLPC substrate) are well matched

Cryostats: We have built several dip-stick cryostats containing the above described cassettes that can hold up to 16 channels of VLPCs and fibers. We have performed many experiments successfully in measuring the VLPC characteristics. These prototype cryostats performed well, achieving very small heat loss. We have also been developing a large-scale cryostat concept, in collaboration with Rockwell Science Center. Figure A3 shows a schematic of one approach.

Cabling: We have tested three types of low heat conductivity, small cross-talk cables, and working with our *UTD* collaborators, have developed an excellent ribbon cable with a low capacitance (6 pF/ft) and very low heat loss.

Fiber Tests: We have tested several scintillating and optical clear fibers that are commercially available and have measured photon yields and attenuation lengths. Jointly with the Notre Dame and Purdue groups we have performed cosmic ray tests at UCLA, a number of details from which are presented in Sections IIC above. Measurements with radioactive sources have been presented at the Pisa Conference [1].

General Applications: Because of their high quantum efficiency, high rate capability and excellent time resolution (better than 1 nanosecond), the VLPCs can also greatly advance particle astrophysics and medical imaging. Part of the slow experimental progress in these two fields is due to the low quantum efficiency of vacuum photomultiplier tubes. A factor of 4-5 increase in quantum efficiency will improve energy and position resolution for x-rays, gamma-rays, and high energy particles. We strongly believe that the advancement of science will greatly benefit from the research and development of the VLPCs not only for applications in high luminosity colliders such as the SSC but in other fields as well. The success of tests performed at UCLA help to strengthen our conviction.

References:

[1] M. Atac, et al, "Scintillating Fiber Tracking at the SSC Using Visible Light Photon Counters", Fifth International Pisa Conference on Advanced Detectors, May, 1991. To be published in Nuclear Instruments and Methods.

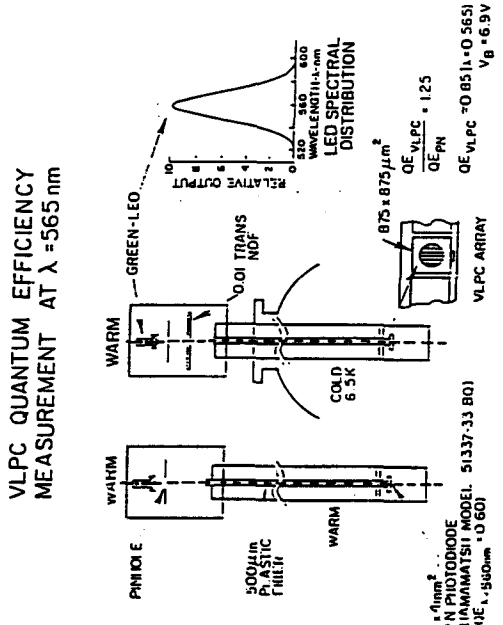


Figure A1. Schematic presentation of VLPC quantum efficiency measurement.

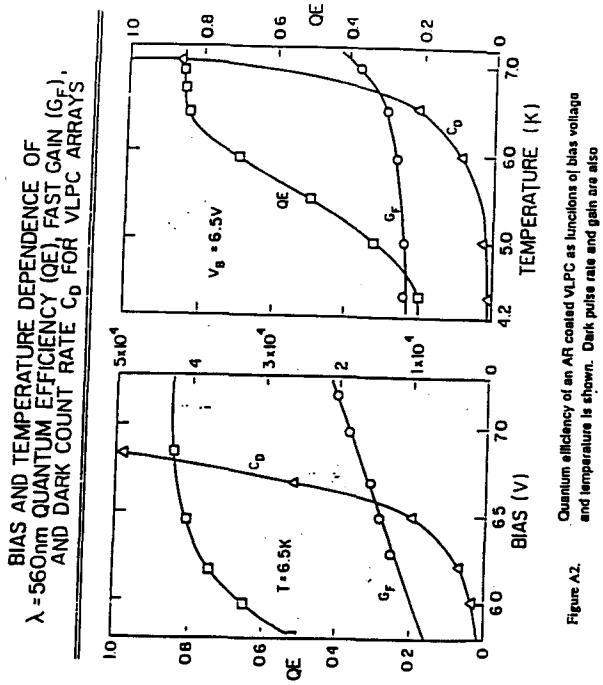


Figure A2. Quantum efficiency of an AR coated VLPC as functions of bias voltage and temperature is shown. Dark pulse rate and gain are also

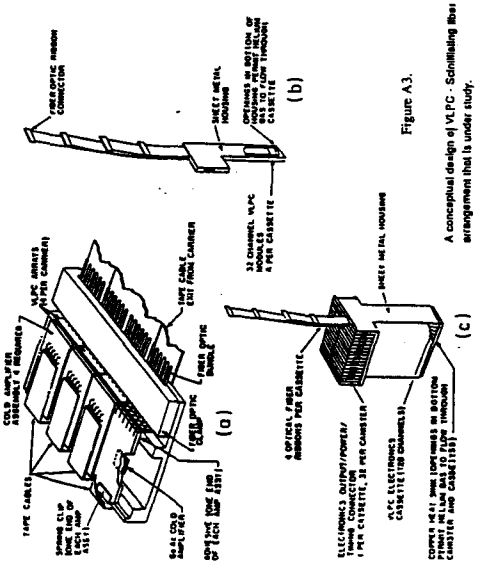


Figure A3.

A conceptual design of VLPC - Scintillating fiber - crystal arrangement that is under study.

B. FERMILAB

Research and development has been focused on the areas of scintillator development, radiation damage studies of scintillation materials, development of a fiber ribbon transporter system for beam tests (T839) and engineering support for these tests, and the development of electronics for a level-1 p_T trigger based on fiber tracking. Additionally a contract has been signed with Rockwell for the development of a conceptual design for a VLPC cassette cryostat capable of supporting up to 16K channels

Scintillator Development and Radiation Damage Studies: A number of studies were performed to investigate various effects on polystyrene-based scintillator. Since 3HF scintillator has shown much promise regarding light output and attenuation, we have irradiated a number of samples. Fig. B1 shows the results for a 10 Mrad exposure of polystyrene doped with 0.1% 3HF. As can be seen in the figure, even at this dose, the sample shows very little induced absorption (after annealing) in the region of fluorescence 525-600 nm.

We also investigated reports that scintillator that had been thermally cycled before irradiation showed more damage than scintillator that had not been. Three test scintillators, pT + DMPOPOP, 3HF, and BBQ, in addition to pure polystyrene, were tested. All samples where placed in containers and completely degassed. Then the containers were back-filled with nitrogen. One set of samples was heated to 90°C before the irradiation. After the irradiation (10 Mrad) the samples were annealed in oxygen and measured for induced absorption. No difference was found between the heated and unheated samples.

A study to measure the effects of oxygen during irradiation was also performed. Four samples of pure polystyrene were placed in containers and then degassed. One container was back-filled with nitrogen at 15 psig, one with dry air (also at 15 psig), one with pure oxygen at 30 psig, and one with pure oxygen at 600 psig. All samples where left in their respective environments for two weeks before they were irradiated. All the samples were irradiated to a total dose of 10 Mrad at a rate of 1 Mrad/hr. Fig B2 shows that after the irradiation (and annealing for the nitrogen and air samples, the two pure oxygen samples "self-annealed") the samples showed progressively more damage for increased partial pressure of oxygen. Obviously, the presence of oxygen during irradiation causes

significant damage, especially if sufficient oxygen is present in the bulk to keep up with the ionization rate.

Previously, it was reported that the oxygen annealing of irradiated polystyrene did not seem to be mediated by diffusion of oxygen into the sample. However, we have measured the rate at which the annealing volume changes as a function of the time that an irradiated sample has been in oxygen, and observe that the rate at which the annealing penetrates the bulk follows a simple square root law, Fig. B3. In all cases which were studied: annealing in air, pure oxygen, and in 300 psig of oxygen, we measured a square root dependence.

Additional fundamental work has been performed collaboratively with Notre Dame, MCPAHS, and PCPS groups. An example of this effort is the continued search for efficient, fast, highly stable scintillators. Examples are indicated in Table D1 below. Fermilab has considerable facilities for (1)the preparation of small test samples, and (2) for the fabrication of large preforms from which fiber may be drawn.

Engineering Support for Beam Tests: The Physics Section and the Research Division at Fermilab have provided resources to install T839, Scintillating Fiber Tracking Studies, in the New Muon hall. Commissioning has been completed on a darkbox and its transporter (see Fig.6 above), which has been designed to scan parallel arrays of 3 m long fiber ribbons across the beam and rotate the ribbons through 70 degrees to simulate inclined tracks. Mechanical mounts and the electronics required to operate a 64 channel photomultiplier tube have also been prepared, and the detector assembly has been connected to the T839 data acquisition system. Orders have been placed for a second phototube, which has a fiber optic faceplate to reduce optical crosstalk.

The transporter includes a fiber ribbon suspension system which provides stability of ±25μm in relative alignment of four layers of ribbons. It has remote motion control via stepping motors, and position and angle readback have been provided with local displays and analog voltages to be sent to the data acquisition system. The darkbox has been made to accomodate three types of detectors for reading out the fibers: (1) Visible Light Photon Counters, (2) multichannel photomultiplier tubes and (3) avalanche photodiodes. The transporter was recently modified to accomodate a separate darkbox brought from Purdue University.

A high voltage divider, 64 channels of analog amplifiers and delay cabling were built for the multichannel phototube. A mechanical mount for the tube and electronics incorporates an adjustable interface plate for aligning the optical fibers with respect to the tube pixels. Noise spectra have been recorded for all 64 channels of the system. Detailed studies with a radioactive source have demonstrated the single photoelectron resolution capability of the tube.

Trigger and Data Acquisition Electronics R & D: The data acquisition and trigger system for the fiber tracker is shown schematically in Figure B4, and currently several elements of this system are under development. These include:

(1) A tracking readout board which incorporates level 1 pipeline data storage and track segment and linking algorithms. The results of the segment linking are also stored in a pipeline on the board. Algorithms are implemented in electrically erasable PALs.

(2) A test data transmitter board which can be programmably loaded with data patterns to test the tracking board.

(3) A conceptual design for the level 1 storage ASIC-1 and ASIC-2 which associate clusters of hits in a fiber superlayer.

(4) A conceptual design for the track linker ASIC-3. This design is being developed in association with the Penn State group, and depends strongly on the superlayer structure of the fiber tracker.

(5) In collaboration with the SDC Trigger Group (W.Smith, et al), interfaces to the trigger system. These include signal protocols and p_T and ϕ bits generated by the tracker and sent to the trigger system, and conversely tracker electronics responses to a trigger signal initiated elsewhere in the SDC detector.

(6) A conceptual design of the readout crate and readout boards. Among the problems under consideration are: interconnects, data rates, power and cooling requirements, crate occupancy, clock timing, and trigger distribution.

This system is expected to evolve tactically, as the fiber superlayer architecture is established and trigger algorithms are refined, and technically, as the ASIC development proceeds.

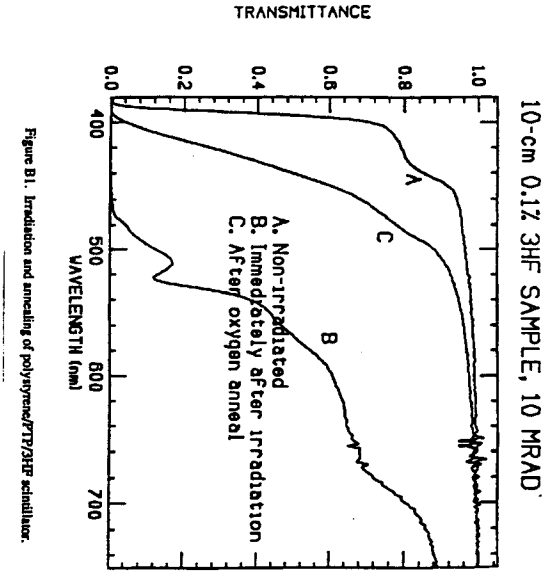


Figure B1. Irradiation and annealing of polystyrene/PTP/3HF scintillator.

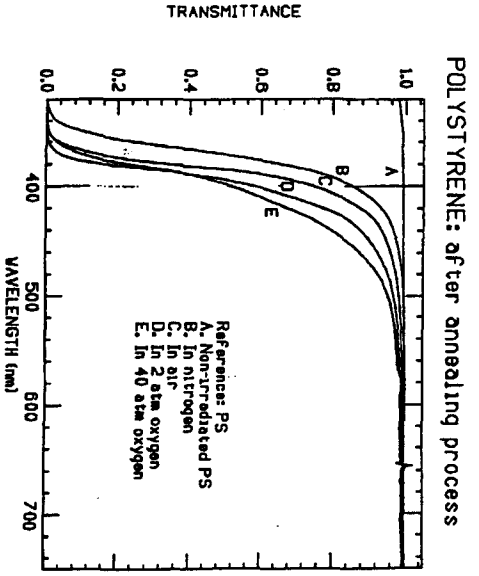


Figure B2. Irradiation and annealing of polystyrene in various atmospheres.

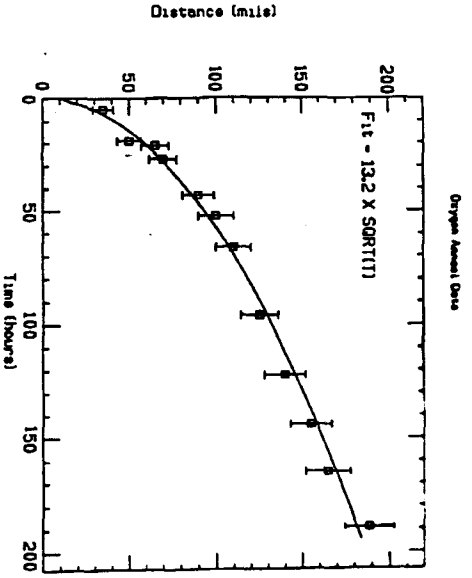


Figure B3. Annealing penetration as a function of time.

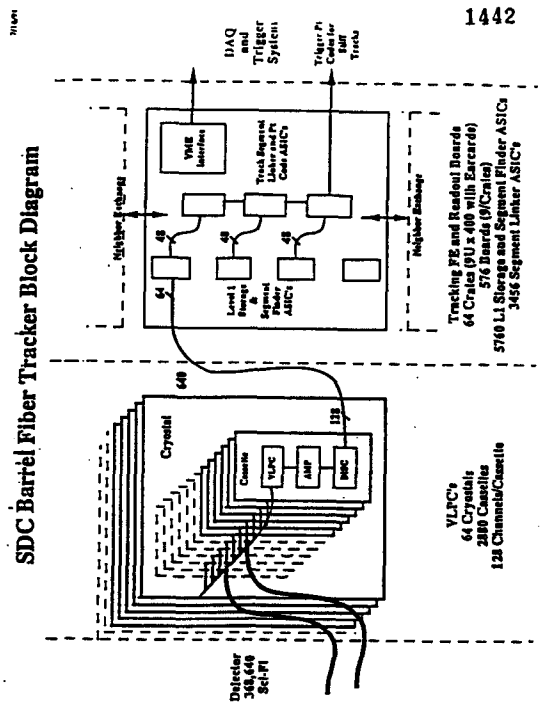


Figure B4. Block diagram of fiber tracker electronics for trigger and data acquisition.

C. UNIVERSITY OF ILLINOIS AT CHICAGO

UIChicago has been responsible for coordinating the beam tests at Fermilab (T839) and for development of facilities to understand in a controlled way the radiation damage and annealing of fibers and ribbons. Our work on this project has been supported by SSCL/DOE and the Texas National Research Laboratory Commission (TNRLC). Indeed without the supplementary funding from TNRLC, most of the work described below could not have been accomplished.

Radiation hardness of scintillating and clear wave-guide fibers. Two systems to measure fiber properties are being constructed. The first allows scintillating fibers up to 4.5 m long to be excited at predetermined positions by either ultraviolet light or monoenergetic conversion electrons from ^{207}Bi. Fiber light output is detected by an 8852 Quantacon PMT whose spectral response is appropriate to the scintillating fibers under test. This system operates under microcomputer control.

The *second* system excites scintillating fibers at *predetermined* positions with ultraviolet light and employs a scanning spectrometer system to measure the resulting fluorescence spectrum. This system is also capable of measuring the transmission spectrum of clear wave-guide fibers by introducing light from a broad-band source into one end and measuring the output with the spectrometer. Both modes of operation are controlled by a microcomputer.

The systems described above will be used to measure fiber properties before and after irradiation. A variety of scintillating and clear wave-guide fibers, and ribbons, will be irradiated at the C0 region at Fermilab (test T851) where acceleration losses and aborts provide a realistic radiation environment. Samples will be irradiated at various rates to a variety of maximum doses in atmospheres of air, dry nitrogen, oxygen, and argon, and unirradiated control samples will be maintained in these atmospheres are well. Thirty one inch-diameter by 4.3-m-long stainless-steel tubes for holding fiber samples are being constructed, along with four 1.5-inch-dia. by 4.3-m-long tubes to hold ribbons. The irradiation tubes are expected to be placed in the C0 region on about 1 Oct. Measurements of fiber properties before and after irradiation will be made both at Fermilab and UIC.

Beam tests at Fermilab: UIC, together with J. Pickarz of Notre Dame, has coordinated the development of a fiber beam-test facility at Fermilab (test T839). The facility, located in the New Muon Laboratory, contains a remotely controlled transporter

which allows fiber structures such as ribbons and superlayers to be exposed at various positions and orientations to a muon beam.

We have also written an off-line analysis program for these tests which finds tracks, computes efficiencies, and plots various histograms. This program contains a simulation section which allows fake tracks to be generated as input to the track-finding section, thereby allowing tests of various detector geometries.

Various Studies: Preliminary studies of the heat loads presented to the VLPC cryogenics systems have been performed. Under most conservative worst-case conditions, the load at a luminosity of 10^{34} cm^{-2} s^{-1} is expected to be less that 150 W. For comparison, a Fermilab Tevatron ring magnet uses 10 W of refrigeration.

The above calculations have required a measurement of the infrared transmission spectrum of polystyrene, which has been performed at UIC with the assistance of our colleagues in solid-state physics.

Studies have also been made of the background counting rate expected from the neutron albedo existing in the detector cavity. This background is due principally to (n,p) and (n,C) elastic scattering with the constituents of the polystyrene-core fibers. The results indicate that this background should not be troublesome.

Finally, we have examined the pulse-height spectrum and the photon distribution expected from a scintillator of circular cross-section in order to help understand results of measurements of photon yield from circular scintillating fibers.

Publications and reports:

1. H. Goldberg, S. Margulies, and J. Solomon, "Cryogenic Issues for Solid-State Photomultiplier Operation", proceedings of the Symposium on Detector Research for the Superconducting Super Collider, Ft. Worth, TX, 15-18 Oct. 1990, p. 300.
2. H. Goldberg, S. Margulies, and J. Solomon, "Transmission of Infrared Radiation Through Polystyrenes and Consequences for VLPC Cryogenics", UIC-3/91-1, 19 March 1991.
3. S. Margulies, "Neutron Interactions in Scintillating-Fiber Central Trackers for SDC and D-Zero", UIC-4/91-1, 22 April 1991.
4. S. Margulies, "Pulse-Height Distributions from Scintillators of Various Cross-Sectional Shapes", UIC-4/91-2, 26 April 1991.

5. S. Margulies, "The Shape of the VLPC Photoelectron Spectrum from a Scintillating Fiber of Circular Cross-Section", UIC-5/91-1, 15 May 1991.
6. S. Margulies, "Interactions of Albedo Neutrons with Scintillating Fibers", UIC-7/91-2, 29 June 1991.
7. Julius Solomon, "VAX Analysis Program for the July 1991 Fiber Test Run", UIC-7/91-1, 16 July 1991.

D. NOTRE DAME

The research and development program for FY91 has included several tasks. These include: scintillator development, studies of radiation damage, fiber waveguide development and waveguide simulation studies, splicing techniques, ribbon manufacturing techniques, studies with fibers and VLPCs, and participation in source, cosmic ray, and beam tests.

Scintillator and Waveguide Studies: Substantial effort has been applied to refinements in the composition of scintillators for use in fiber detectors. These efforts have included:

Studies of the photostability of polystyrene/pTerphenyl/3HF scintillator. These materials form the basis for the current best scintillating fiber. Therefore it is clearly important to understand the effects of environment on the stability of such materials, such as ambient atmosphere, effects of ionizing radiation, and photosensitivity. The optical properties of this material are very stable against radiation damage because of the long emission wavelength (530nm), particularly if the material is maintained in an ambient nitrogen atmosphere and annealed periodically with air or oxygen. The material, though, does lose efficiency when exposed to UV or fluorescent light by becoming optically absorbing in the 400-500nm range. However, we have found that the material remains stable when kept in a dark environment, and in general we store the material in dark containers slowly flushed with nitrogen gas at atmospheric pressure. Long term effects must be considered, and these studies are continuing. In collaboration with PCPS, several new variations of the dye 3HF have been synthesized, and polymerized with polystyrene and pTerphenyl. These compositions are under study for quantum efficiency, fluorescence emission and decay time, and also photostability properties.

The development of several new primary dyes at PCPS: including a sexiphenyl and two octiphenyl compounds having very high molar extinction coefficient (greater than twice that of p-Terphenyl) for short range of energy transfer and fast fluorescence decay and which are soluble in concentrations of 1% in polystyrene. These materials have been found to produce, in one step, scintillators of comparable efficiency to two step scintillation standards such as polystyrene with pTerphenyl and dimethyl-POPOP. Additionally, these materials have longer wavelength emission, in the 425nm-435nm range, allowing for the

incorporation of new alternatives for secondary dyes, prospects for which are currently under discussion.

The development of several new secondary dyes based on intra-molecular proton transfer to minimize self absorption and to provide long-wavelength emission. This series involves a significant new development in a group of dyes called hydroxybenzothiazoles (HBTs). Previous pioneering work by Fermilab and others had produced dyes in this family of roughly half the efficiency of 3HF at best. Discussions with PCPS and MCPAHS has led to new work by MCPAHS which has produced a candidate dye which, upon purification, yields performance comparable to 3HF. Because of differing chemical structure, dyes based on this prototype may afford better long-term photostability and improved fluorescence efficiency. The fluorescence emission and absorption for this new dye are shown in Fig. 1 above. Since the molar extinction coefficient of this material is also comparable to or greater than that of 3HF, it is expected that its fluorescence decay time of this family of materials will be at least as rapid as that of 3HF and perhaps slightly faster (5-6ns).

Studies of radiation damage effects on the optical properties of scintillators in the form of small boules of 1cm diameter and in lengths of 1-10cm have been performed in collaboration with Fermilab. Based on these measurements, a number of different scintillation materials have shown good performance at doses of 1Mrad or greater, and therefore will survive for at least 100 years at SSC design luminosity. Table D1 provides a partial listing of these measurements, which are ongoing

It should be noted that the effective development of these scintillation materials has been based on a strong collaborative effort between Notre Dame, Fermilab, PCPS, MCPAHS, and Bicron.

Given the relatively short period of time for R & D to demonstrate proof-of-principle for fiber tracking, we have elected to concentrate on scintillating and non-scintillating fiber waveguides having polystyrene cores and some form of acrylic or polymeric cladding. Currently we are concentrating on PMMA (polymethylmethacrylate). Fibers have been successfully produced by several commercial houses using these materials, and other interesting options (such as PVT core) have not been developed to the same degree. However, we are pursuing initiatives in the study of cladding materials: (1) the incorporation of primary dyes to allow the full volume of the scintillating fiber to be efficient, and (2) materials of lower refractive index than PMMA (n=1.49), of which there

are several possibilities in the 1.3-1.4 range. Current fibers have diameters of 830μm and cladding thicknesses of ≤ 30μm. Studies have shown that the best of the clear fiber waveguides yield optical attenuation lengths of ~10m in the wavelength range of interest (centered around 530nm), and attenuation lengths for the best scintillating fibers are ~8m when viewed through a 4m length of clear fiber waveguide.

Splicing: Several coupling techniques for the splicing of fibers and waveguides have been proposed, including permanent connections such as thermal fusion, chemical melting, and glues, and quick-disconnect options based on optical couplants such as optical greases and gels and mineral oils. For a variety of reasons, we now favor the quick disconnect option because of its convenience and because of the simplicity it affords during detector construction and testing. Several different connector options have been explored by both UCLA and Notre Dame groups, which have produced good results for optical transmission and low light loss. These are based on drilling precise holes in small acrylic blocks into which fibers and waveguides may be inserted. The registration is maintained by alignment pins. These initial ideas must now be developed for larger scale fiber systems.

Waveguide Simulation: As a part of our waveguide investigations we have continued the development of a fiber waveguide simulation package OPTICKS[1]. This work has focused attention on several important issues, particularly the effects of cladding and extramural materials (coatings and adhesives on the outside wall of the fibers). The efficiency of scintillation light production and collection in the scintillating fiber, at the site of the energy deposition by ionizing radiation, depends significantly on these characteristics and will have an important influence on the selection of dyes and adhesives used in the fiber and ribbon manufacture. The other significant area of study has been optical transport within the fibers and waveguides, including the understanding of reflections at core and cladding interfaces, and in bulk absorption within the materials.

Ribbon Development: Several methodologies have been developed for ribbon fabrication depending upon whether or not the fibers are scintillators or waveguides. In the scintillating fiber case, the waveguides must be precisely positioned relative to one another in the ribbons so that this spatial registry can be maintained on support structures such as stable base cylinders. Registered scintillating fiber ribbons have been produced by the Notre Dame group using facilities available at Bicron Corporation. Fibers have been produced in single and double layers in lengths of over 3 meters and in widths up to 128

fiber elements. However in the case of clear fiber waveguides, registry is only required at the connectors, and the fibers may in fact be loose (unregistered) between the ends. Unregistered waveguide ribbons of this form have been produced in facilities located at Notre Dame. Typically, fibers at Bicron or Kuraray have a diameter tolerance of <1% and center-to-center registry within the ribbons is good to an accuracy of σ ~25μm (see Fig. 2 above).

Beam and Source Tests: Notre Dame has been a participant in the development of the test facilities necessary to study the performance of scintillating fibers with VLPCs. This includes coordination of the test beam effort T839 at Fermilab. [J.Pieksarz has been one of two contact persons; S. Margulies of UIChicago is the other.] We have also participated in development and fabrication of 36 channels of transimpedance amplifiers in support of the VLPC/fiber array studies carried out at UCLA, the study and characterization of other room temperature amplifiers for use with VLPCs, and the study and characterization of fiber materials and splicing techniques. [B. Baumbaugh has coordinated our electronics initiatives.] These efforts were performed, in part, with strong collaboration from Purdue, and with consultation from Rockwell and UCLA.

References:

[1] R.J. Mountain, "Monte Carlo Simulations of Scintillating Fiber Optic Waveguides", Symposium on Research and Development for the Superconducting Super Collider, T. Dombeck, V. Kelly and J. P. Yost eds., (1990), 278-280.

[2] J. Pieksarz, "Measurements of Fluorescence Efficiency of Scintillators Before and After Irradiation", Symposium on Research and Development for the Superconducting Super Collider, T. Dombeck, V. Kelly and G.P.Yost, eds., (1990), 281-283.

Table D1.

Light yield before and after 10 Mrad radiation dose from ^{60}Co source (in arbitrary units).

SCINTILLATOR[a]	λ[b] (nm)	Light yield Before	After	After 13 d[c]	After 53 d[c]	Ratio[d]
MOPOM	420	0.79	0.04	0.42	0.49	0.62
MOPOM+0.01%BBQ	470	0.95	0.13	0.63	0.71	0.75
MOPOM+0.02%BBQ	470	0.96	0.16	0.69	0.78	0.79
MOPOM+0.01%K27	500	0.95	0.27	0.75	0.83	0.87
MOPOM+0.02%K27	500	0.95	0.27	0.75	0.84	0.88
O415A	415	0.92	0.49	0.79	0.88	0.96
O415A+0.01%BBQ	470	1.01	0.42	0.86	0.97	0.96
O415A+0.02%BBQ	470	1.02	0.34	0.89	0.99	0.97
O415A+0.01%K27	500	0.97	0.57	0.87	0.96	0.99
O415A+0.02%K27	500	0.99	0.53	0.88	0.98	0.99
O408	410	0.88	0.48	0.76	0.83	0.84
O408+0.02%BBQ	470	1.02	0.34	0.87	0.99	0.97
O408+0.02%K27	500	0.97	0.57	0.89	0.98	1.01
DAT	375	0.73	0.16	0.46	0.47	0.84
DAT+0.01%DMPOPOP	430	0.86	0.31	0.70	0.75	0.87
DAT+0.01%3HF	530	0.85	0.40	0.83	0.89	0.81
pT	360	0.04	0.21	0.41	0.42	0.50
pT+0.01%DMPOPOP	430	0.88	0.51	0.71		

[a]Floor concentrations are by weight, the concentrations of primaries are 1% (1.25% for DAT and pT). [b]Wavelength of peak emission. [c]First 10 days in oxygen and the rest in the air. [d]After 53 d/Before.

E. PENNSYLVANIA STATE UNIVERSITY

In FY91, Penn State has been concentrating on the development of level 1 trigger algorithms and, in collaboration with Fermilab, the development of the appropriate electronics implementation of the trigger. Specifically, an algorithm for recognizing high p_T tracks in the SciFi tracker has been described in ref. [1]. The simulation efforts this year have been concentrated on translating the basic algorithm into trigger electronics using Verilog programs to demonstrate that ASIC electronics can perform the pipeline logic.

1. Granularity Issues: The main challenge for the trigger electronics is to compare SciFi hit information from widely separated areas of the detector. The number of interconnects required increases with the fineness of the granularity chosen to extract the azimuth and p_T of tracks from the data. On the other hand, the resolution improves with finer granularity.

The logic for recognizing and linking track stubs is illustrated in Fig. E1. The first level of logic, ASIC-1, recognizes radially continuous sets of at least 3 out of 4 monolayers hit by a stiff track. Track stubs are formed by ASIC-2, passing on information about track position and angle within a superlayer. The track stubs are linked in ASIC 3, which determines the azimuthal angles of tracks which pass various p_T cuts.

Two choices of granularity, dubbed "gangs of one" and "gangs of four", have been evaluated. The following table describes the granularity parameters for the two choices.

		gangs of one	gangs of four
ASIC-1		1 fiber diameter	1 fiber diameter
ASIC-2	angles	left, middle,right	left, middle,right
	position	1 diameter	4 diameters
ASIC-3	p_T cuts	10, 50 GeV/c	10, 50 GeV/c
	azimuth angles	128	128.

The only difference in the two granularities occurs in ASIC-2, in which logic signals are ganged after the angle combinations are formed.

The multiplicities of signals which must be ported between levels of the logic (external ASIC connections) is depicted in Fig. E2, for the gangs of 4 logic, for the $\eta > 0$ half of the central tracker. Without ganging signals, ASIC-2 would produce 100,000 track

segments, which is more than the 60,000 available inputs. Ganging into groups of 4 reduces the number of outputs.

The importance of reducing ASIC to ASIC connections is due to physical limitations on I/O ports. A single ASIC could have 64 (or maybe 128) I/O ports, and a 9U VME card could handle 640 input channels.

2. Physics Performance: Two criteria are used to judge the physics performance, for a choice of granularity in the logic: trigger efficiency, and pileup background suppression. Figure E3 shows the trigger efficiency versus p_T for the following:

squares: gangs of one, cut nominal p_T>10 GeV/c
triangles: gangs of 4, cut at 10 GeV/c
diamonds: gangs of one, cut at 50 GeV/c,
circles: gangs of 4, cut at 50 GeV/c.

The resolution for both the 10 and 50 GeV cut is noticeably poorer with the gangs of 4, making such a signal less effective in the trigger. The effectiveness of the gangs-of-4 logic in rejecting background is currently being evaluated.

3. Descoped Tracker : Another item which was simulated at PSU was a descoped version of the fiber tracker. The super-layers were reduced from double sublayers to single sublayers. The background rejection versus luminosity curves for the descoped tracker is shown in Fig. E4. The conclusions are similar to those derived in ref. [1]: at a luminosity of $L = 10^{33}cm^{-2}s^{-1}$, four tracking layers are adequate to achieve background rates below the physics level. More redundancy is required to achieve a superb trigger rejection at $L = 10^{34}cm^{-2}s^{-1}$.

References:

* Work supported by DOE and TNLRC

[1] "Simulation Studies for a Scintillating Fiber Tracker," R.A. Lewis et al, Proceedings of the Symposium on Detector Research and Development for the Superconducting Super Collider, eds. T. Dombeck, V. Kelly and G.P. Yost, World Scientific, Singapore (1991), p. 275.

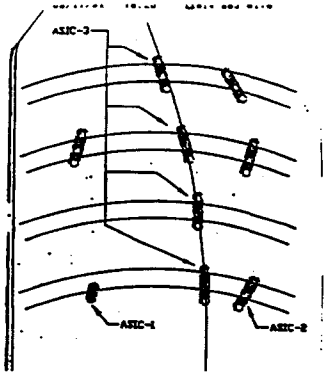


Figure E1. Superlayer structure indicating domain of ASIC usage.

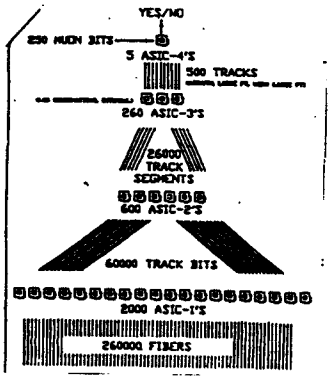


Figure E2. Cartoon indicating information sparsification through the ASIC trigger pipeline.

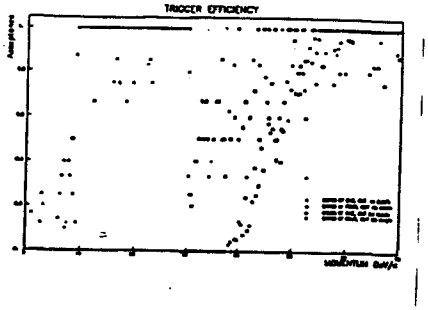


Figure E3. Trigger efficiency versus pT. (see text)

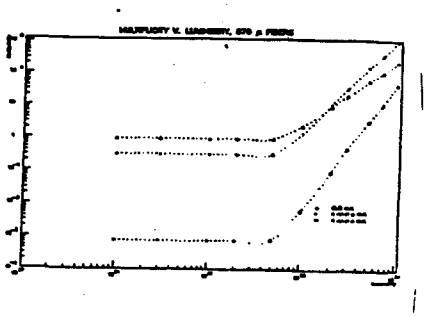


Figure E4. Background rejection versus luminosity.

F. PURDUE UNIVERSITY

In FY91, Purdue has concentrated on several essential FTG tasks including: coordination of engineering issues in collaboration with ORNL, the development of cryostable cassette structures for registered mounting of fibers and VLPCs in dip cryostats, the development of the data acquisition system for the beam tests at Fermilab (T839), and the construction and operation of a 96-channel fiber system for beam measurements of the resolution of fiber superlayers.

Engineering Coordination: Purdue has served as the engineering contact for the fiber tracking group. We have been working closely with Oak Ridge National Laboratory to develop the cost and schedule for the outer and intermediate angle scintillating fiber trackers. In order to develop the cost and schedule it was required to develop and outline the methods of construction, testing and management for the 7-year duration of the tracking construction program. This work has resulted in the writing of a cost, schedule, concept and management report which will serve as the foundation for refinements of the overall construction concept. The effort has also had the effect of more accurately determining when the critical milestones must occur in the project.

Cryogenics R & D: Purdue has also been actively involved in the testing and instrumenting of the solid state photon detectors that will be used to transduce the light produced in the fibers. We have designed and produced precision Covar cassettes that hold the fibers accurately on the surface of the photon detectors. The design of these cassettes is based on the use of computer controlled milling machines. Each array of solid state photon detectors is carefully measured using a scanning microscope. This information is then transferred to the computer controlled milling machine and a unique cassette is quickly made for each array.

This procedure yields a very simple cassette design and a large cost savings. The cost saving comes from not having delicate parts to adjust in order to align the fibers onto the cassette and a manpower saving in the time to align the fiber onto the cassettes. We feel that this design concept will have an important impact on the final design of the transducer system. In the test we have proformed with the transducers the cassette worked very well. Purdue has done its best to contribute to all the light yield tests and cosmic ray tests done using the solid state photon transducers.

Purdue has also produced an alternate cryostat design and has build a prototype to test its functioning. Our design is based on immersing the housing of the photo-transducer directly into the liquid helium and then using a small heating element, raising the temperature of the transducer to the desired 6.5K operating temperature. Our test results show that this technique provides an extremely stable operating environment. Further refinements and tests will be carried out.

Test Beam Measurements: In order to measure the resolution given by a scintillating fiber tracking system, the Purdue group is testing a precisely aligned array of three scintillating fiber superlayers in a test beam at Fermilab. This run is part of test beam experiment T839. A light tight box containing a total of 96 fibers has been placed just below the center of the muon beam in the New Muon Lab. The arrangement in the test beam is shown in Figure F1.

As shown in Figure F2, each superlayer consists of two doublets of ribbons, where a doublet is made by gluing two ribbons together with a half-cell offset in position. In addition, the two doublets in a superlayer are offset with respect to each other by a quarter-cell. Since we are using ribbons of eight fibers each, one of our superlayers contains 32 fibers and the whole test array of three superlayers consists of 96 fibers. The superlayers are separated by about 10 inches. The arrangement inside the box is shown in Figure F3. The light from the fibers is sensed by a Hamamatsu 256-channel multianode photomultiplier tube, whose outputs are amplified by transimpedance amplifiers designed and built by Purdue, and fed into a LeCroy 2285 analog-to-digital (ADC) system. Two scintillation counters are used to define the muon beam and are put in coincidence with each other and with an anode signal from the photomultiplier tube. The light tight box is mounted on a movable table.

Purdue has been responsible for providing the data acquisition computer and the necessary software for the T839 beam tests. The data acquisition set-up is shown in Figure F4. An Apple Macintosh IIci microcomputer with a GPIB (General Purpose Interface Bus) card has been set up for this purpose. The data acquisition software has been written within the framework of the National Instruments LabVIEW programming package.

High precision scintillating fiber ribbons are the key for achieving high momentum resolution in SSC experiments with a practical method of assembly and without a large number of calibration constants. Channel-by-channel assembly methods are costly in both

time and money. A goal is to find a way to manufacture ribbons of up 1024 fibers, which can be joined to clear fiberoptics using mass termination techniques and have enough precision to know the location of all the fibers in a ribbon if the position information is known for one fiber in the ribbon. The ribbons for this test beam experiment were made by positioning fibers on a precisely milled metal plate and then gluing them together as a ribbon. Figure F5 shows the measured placement accuracy of fibers in two of our ribbons. The goal was to achieve a placement accuracy of about 20 microns, and this has been achieved. For wider ribbons the milled plate method of fiber placement appears to be impractical, so we are building a wire bed system with very precisely drawn wires.

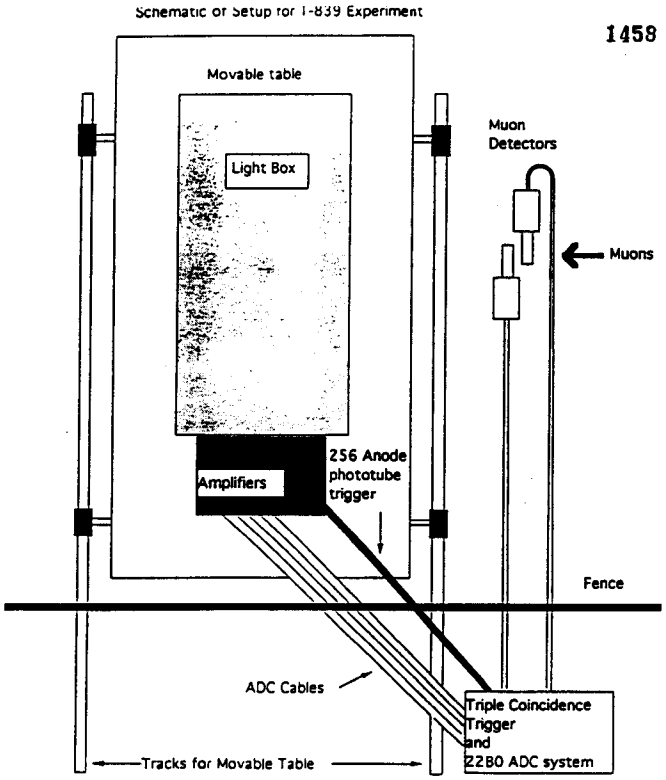


Figure F1. Schematic of the beam test arrangement for fibers with multianode PMT readout.

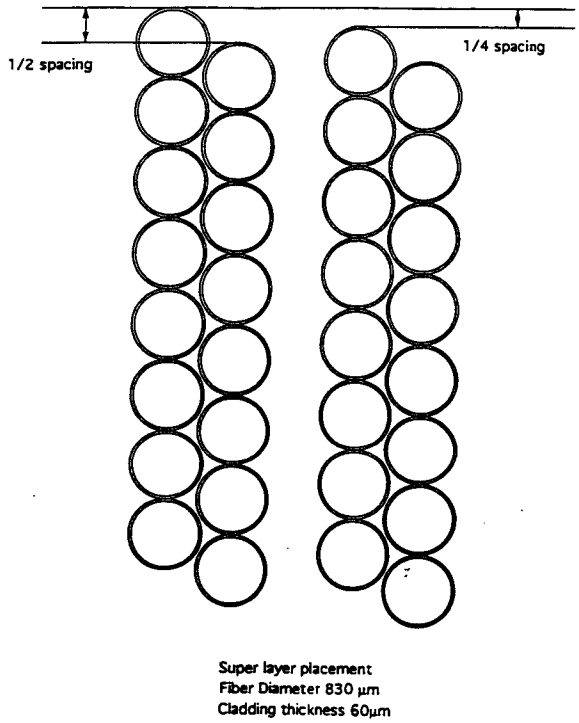


Figure F2. Schematic of a superlayer of fibers, composed of two double-layer ribbons offset by 1/4 spacing. Fibers are of 830micron diameter on 870 micron center-to-center spacing.

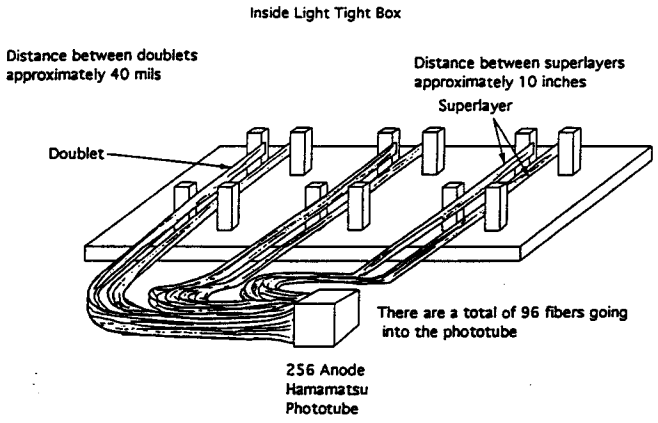


Figure F3. Arrangement of apparatus within the light tight box for beam tests.

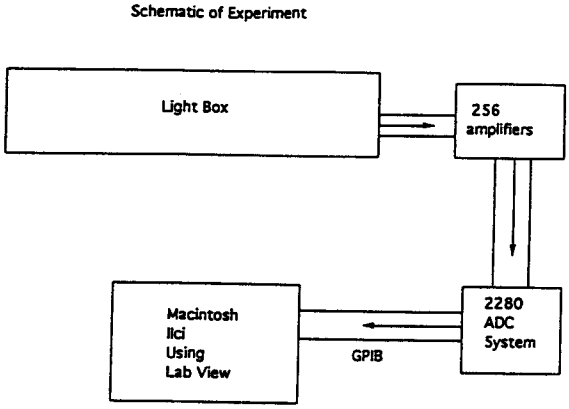


Figure F4. Readout and DAQ schematic for beam tests.

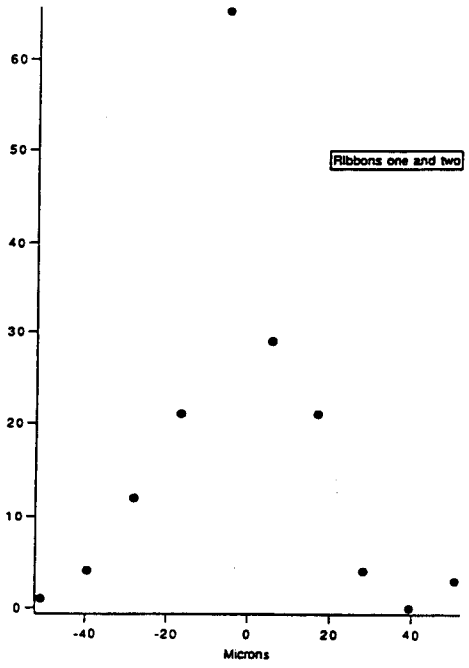


Figure F5. Registry of fiber ribbon fabricated at Purdue.

G. RICE UNIVERSITY

During the past year, the Bonner Lab group has focused on simulation as its contribution to the FTG. We have continued development of the package SFTSIM which provides a GEANT-based simulation of a scintillating fiber tracking system and have devoted considerable effort to the track-finding code TRF. We also participated in the development of the SDC global simulation shell SDCSIM and then expended effort moving SFTSIM and TRF into that framework. Here we briefly describe the status of these efforts and discuss several studies that were presented at the SDC meeting last August.

Software Development for Simulation and Pattern Recognition: The fiber simulation package SFTSIM is described in reference 1. During the last year we have made some small additions to the code. One change was to allow the user to redefine the fiber and readout characteristics (brightness, attenuation length, quantum efficiency, etc.) in the standard input file. One of our major efforts during the last year was to move this code in the SDC simulation shell. This work was done in collaboration with UT Dallas. The digitizations (i.e., the simulated response of the detector) are now put into the SDC data structure so that they are easily available to other parts of the SDC shell.

The track-finding package TRF is also described briefly in reference 1. It has two major pieces: clustering and track finding. In the clustering stage, hit fibers within a layer are combined to form clusters and then nearby layers are combined to form 2D superclusters. One of our additions during the past year has been to add code so that the 2D superclusters from different orientations can be combined to form 3D superclusters (space points). The track finding has been modified so that it can make either 2D or 3D superclusters or a combination of the two. Although the clustering is specific to the fibers, we intend to generalize the track-finding to include the silicon and possibly the gas-based detectors proposed for the SDC. The program makes use of road-following techniques which are CPU-intensive but inherently very efficient in finding tracks. We feel that this method will allow us to get the maximum information out of tracking systems with a small number of layers. This is very relevant to the SDC where cost and material concerns significantly constrain the number of layers.

Trigger Studies: In collaboration with UTD, we looked at triggering efficiency as a function of pT for a scifi tracking trigger with superlayers at 70, 100, 130 and 160 cm. The trigger makes use of four closely-packed layers of fibers in each superlayer. The

trigger threshold was chosen to be around 10 GeV. The efficiency for muons is shown in Figure G1 where the "turn-on" is seen to be very sharp, with negligible efficiency below 9 GeV/c and full efficiency at 10 GeV/c. Figure G2 shows the same efficiency for electrons with different amounts of material inside the scifi tracking system. Note the significant degradation in efficiency due to bremsstrahlung. This degradation is one of the material concerns mentioned above.

Pattern Recognition Issues: We have looked at the stand-alone pattern recognition capability of our proposed scifi tracker as a first step in understanding the capabilities of a combined silicon and fiber system. In our first study involving 3D reconstruction, we piled up different numbers of Pythia QCD inelastic events and measured track-finding efficiencies and false track rates. The detector again had four superlayers, each with four axial layers, two stereo layers in one direction and two stereo layers with equal angle in the opposite direction. Two cases were considered: 3 degree stereo in all superlayers and a constant pitch with the stereo angle varying from 8 degrees in the innermost superlayer to 18 degrees in the outermost.

The track-finding efficiency is measured with a subset of tracks which have $p_T >$ 0.5 GeV/c and do not scatter significantly in the tracking detector. We also require that these candidate tracks pass through all layers of the scifi tracking system which implies $|\eta| < 1.7$. Each reconstructed track is assigned the candidate track responsible for the plurality of its superclusters. If two reconstructed tracks are assigned to a single candidate track, then the least consistent one is declared a false track. Figures G3 and G4 show the efficiency and false/true track rates as a function of the number of events in a crossing. We see that the efficiency remains high but that the false track rates are increasing significantly as the number of events/crossing is increased. We expect that information from a few silicon layers will be able to eliminate most of these false tracks. Figure G5 shows the average CPU time on an IBM RS6000/530 (34.9 MIPS) required to track and reconstruct a crossing. There is a significant rise as the number of events/crossing increases especially for the larger stereo angles. For reference, note that the occupancy from an interesting event such as H --> ZZ --> 4 mu is 2-3 times that from the QCD inelastic events considered here.

We expect to be reconstructing events using both silicon and fiber detectors in the very near future so that these and other studies can be carried out with a more holistic view. We are also very active in the physics and detector performance group and plan to emphasize processes that provide an evaluation of the performance of the tracking system.

Another high priority is to complete those parts of TRF that deal with disk shaped detectors so our coverage can be extended larger eta. We would also like to improve the CPU performance, i.e. reduce the CPU time/event.

References

[1] D. Adams et al., "Symposium on Detector Research and Development for the Superconducting Super Collider", World Scientific (1990) p. 271.

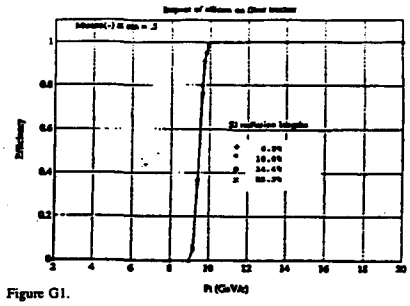


Figure G1.

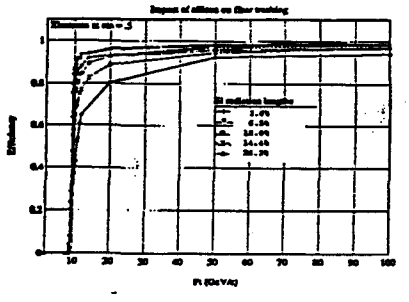


Figure G2.

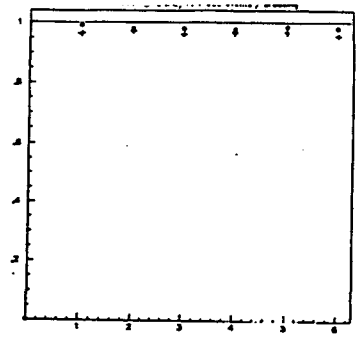


Figure G3.

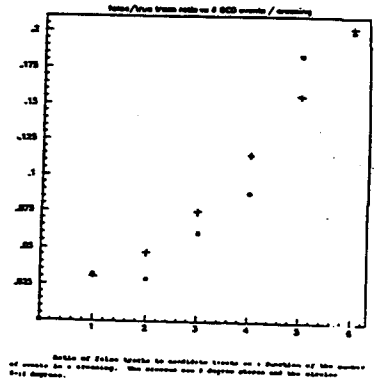
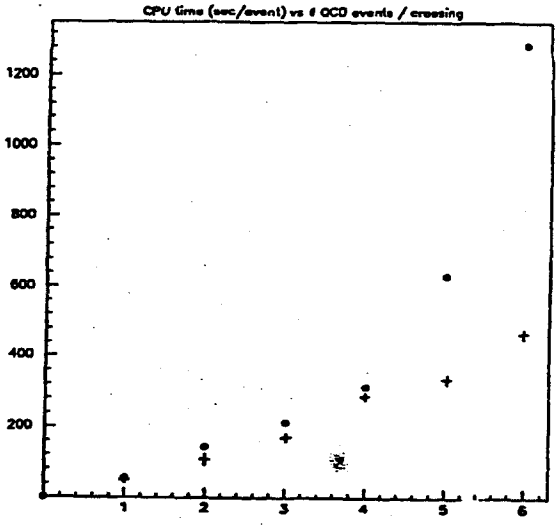


Figure G4.



CPU time required to track and reconstruct a crossing vs the number of events/crossing. The CPU was an IBM 3081600 rated at 24.9 MIPS.

Figure G5.

UT Dallas has been involved in several important aspects of the readout electronics for the VLPCs. The first of these is the development of a cryogenic preamplifier, capable of operation at liquid helium temperature, the function of which is to amplify the VLPC signals in situ in the cryostat. If successful, the fastest possible operation of the VLPC will be realized by this approach. The second aspect is the development of low heat-loss, low-capacitance cable for signal propagation out of the cryostat system.

Cryogenic Preamp Development: Honeywell Research Center, Bloomington, MN has considerable experience with cryogenic preamps based on GaAs technology and for initial studies, UTD has been testing some Honeywell GaAs preamplifier components at liquid nitrogen temperatures. Additionally, a testing device for liquid helium temperatures has been developed and constructed in our laboratory (Fig. H1). Recently, tests of the GaAs preamplifier components were initiated at liquid helium temperatures using the above-developed testing device. Improvement of the design of the preamplifier components will be based on the results of these tests, and contractual arrangements have been made with Honeywell Systems and Research Center for the production of the improved prototype GaAs preamplifiers which will be tested and studied at liquid helium temperatures at 4 °K.

Low Loss Cable Development: Excellent success has been obtained in the development of low-loss flat cable, and 20 units of 3 mil teflon-insulated copper-shielded cables have been received from Gore Co., which are now used in support of the VLPC/fiber tests (Fig. H2). This cable is of high quality and has very low capacitance (6pF/ft).

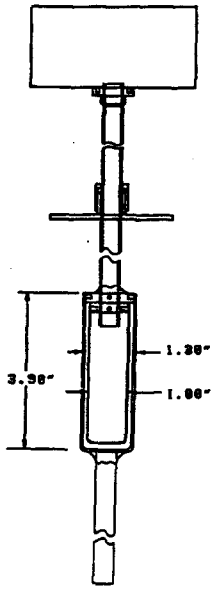


Figure H1. Cryogenic test facility for preamplifier studies.

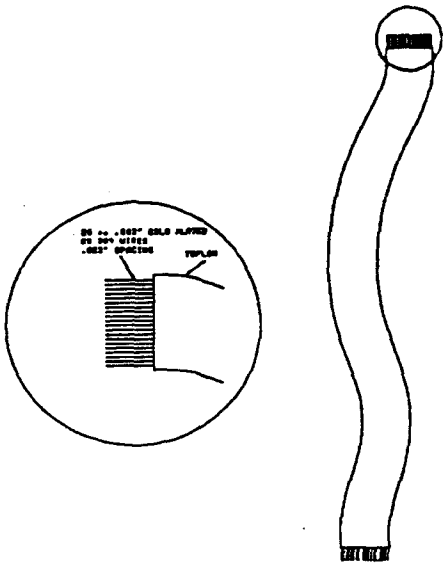


Figure H2. Low heat-loss, low capacitance cable for VLPC readout.

APPENDIX A.

MEMORANDUM OF UNDERSTANDING FOR FY91 BETWEEN THE
FIBER TRACKING GROUP (FTG)
AND
THE SSC LABORATORY

MEMORANDUM OF UNDERSTANDING FOR FY 1991

between

THE SCINTILLATING FIBER TRACKING COLLABORATION

and

THE SUPERCONDUCTING SUPER COLLIDER LABORATORY

This memorandum of understanding between the Fiber Tracking Group (FTG) and the Superconducting Super Collider Laboratory (SSCL) is intended solely for the purpose of providing a budget estimate and a work breakdown for the SSC Laboratory, the funding agencies, and the participating institutions. It is an agreement that is currently satisfactory to the parties. However, it is recognized and anticipated that changing circumstances of this evolving research and development program may necessitate revisions. The parties agree to negotiate amendments to this memorandum that will state such required adjustments. A short summary describing the research objectives of this experiment is given in Appendix I.

A. Personnel

The list of participating institutions, the names of the people in each (identifying the contact person and overall manager), and the percent of their time which will be dedicated to the project are listed below:

Overall Managers of the Project are:

Dr. Muzaffer Atac
Department of Physics
University of California at Los Angeles
Los Angeles, CA 90024
and
Fermi National Accelerator Laboratory
PO Box 500, MS223
Batavia, Illinois 60510
(708)840-3960

Dr. John Elias
Fermi National Accelerator Laboratory
PO Box 500, MS318
Batavia, Illinois 60510
(708)840-4135

Dr. Randy Ruchti
Department of Physics
University of Notre Dame
Notre Dame, Indiana 46556
(219)239-7143

The participating institutions, contact person for each institution, dedicated personnel, and percentage of time are indicated below:

UCLA:	M. Atac (Contact Person)	
	K. Ankoviak	20%
	M. Atac	50%
	D. Chrisman	20%
Fermilab:	J. Elias (Contact Person)	
	M. Atac	25%
	A. E. Baumbaugh	100%
	M. Binkley	20%
	A. D. Bross	20%
	J. E. Elias	20%
	D. Finley	20%
	G.W. Foster	10%
	J. Hylen	50%
	R. Kephart	10%

	S. Tkaczyk	5%
	R. Wagner	5%
UIChicago	S. Margulies (Contact Person)	
	H. Goldberg	15%
	S. Margulies	50%
	H. Mendez	50%
	J. Solomon	25%
Notre Dame	R. Ruchti (Contact Person)	
	B. Baumbaugh	100%
	J. Bishop	20%
	N. Biswas	20%
	J. Godfrey	20%
	J. Jaques	20%
	R. Kehoe	20%
	V. Kenney	10%
	Q. Lu	50%
	J. Marchant	100%
	R. Mountain	20%
	J. Pickarz	40%
	R. Ruchti	60%
Penn State	R. Lewis (Contact Person)	
	T. Armstrong	20%
	R. Lewis	30%
	R. Moore	20%
	R. Scalise	20%
	G. Smith	20%
Purdue	D.Koltick (Contact Person)	
	B. Abbott	50%
	R. Davies	50%
	D. Koltick	60%
	R. McIlwain	20%
	E. Shibata	20%
Rice	D. Adams (Contact Person)	
	D. Adams	30%
	H. Mientenen	20%
Rockwell	E. Anderson (Contact Person)	

E. Anderson
M. Petroff

UTDallas E. Fenyves (Contact Person)

R. Chaney 20%
E. Fenyves 20%
H. Hammack 20%

SSC Liaison Person Dr. Willi Chinowsky
Physics Research Division
M/S 2001
SSC Laboratory
2550 Beckleymeade Avenue
Dallas, Texas 75237

B. Responsibilities for Research Tasks

In this section we give a brief overview of our R&D program for FY91. Any modifications from our original Fiber Tracking Group Subsystem proposal were made to adjust to different constraints and to accommodate suggestions given us from the SSC Laboratory. The long-term goals of our detector development project are summarized in Appendix I.

Task 1: Scintillator Development: Coordinated through Notre Dame and Fermilab

Given our recent successful measurement of significant photoelectron yield from scintillation fiber, Bicron Type E, used in conjunction with clear waveguides, and visible light photon counters VLPC developed by Rockwell, we are encouraged to continue with a strong effort on scintillator development during FY92. We will be pursuing several avenues of R and D, but our principal focus will continue to be scintillator and scintillating fiber development directed toward high-efficiency, fast, yellow emiters which are resistive to radiation damage. Particular parameters of interest include: (a) for scintillator, the quantum yield, fluorescence emission wavelength, molar extinction coefficient, and radiation resistance; (b) for scintillating fibers, the attenuation length, effects of varying cladding thicknesses, cladding refractive index, the inclusion of extramural absorbers, and the effects of radiation damage on these structures.

Task 2 Waveguide Development: Coordinated through Notre Dame

Fiber-optic waveguides of polystyrene with various cladding materials, cladding thicknesses and refractive indices will be developed and studied for opomal light transmission between scintillation fibers and photodetectors.

Task 3 Splicing Techniques for Fibers and Ribbons. Coordinated by Purdue and Fermilab

Here we will review splicing options and techniques for mating scintillating fibers and waveguides. Possibilities include thermal fusion techniques for example by laser-induced local heating or fiber connectors with optical grease coupiant. A simple form of this latter procedure was used in our successful fiber tests in March 1991.

Task 4 Ribbon Fabrication. Coordinated by Notre Dame and Fermilab

Here we will review and develop options form ribbon manufacture for fibers, in which fiber diameter tolerance is controlled to ≤ 1% and fiber-to-fiber registry is maintained to ~ 25 μm. This includes studies of ribbon backing materials, adhesives, and mechanical structures, and procedures for placement of ribbons on supporting surfaces to the required precision.

Task 5 VLPC and Preamp Development. Coordinated by UCLA, Rockwell Science Center, and UT Dallas.

VLPC development will continue expeditiously. We expect to have VLPC chips available to us during this period and important operational characteristics such as gain as a function of temperature and bias voltage, quantum efficiency, rate dependence and noise will be measured. Development of monolithic cryogenic preamps, discrete cryogenic preamps and room temperature preamps (as a fall back) will be pursued. Room temperature preamps are already in use by UCLA-Fermilab and Notre Dame groups, and which preamps will be used depends upon the development programs and the timing of beam tests.

Task 6 Test Beam Studies of Fibers and VLPC. Coordinated by UI Chicago-Fermilab Notre Dame, and Purdue, with strong participation from all groups in the FTG Collaboration.

Tests of the fiber tracking concept will be undertaken in a Fermilab beam. This effort has been assigned the Fermilab designation T839, and FTG is setting up in the M6 beam for running, expected to begin in summer 1991. Systematic measurements will be performed on fibers, waveguides, and VLPCs, including: studies of efficiency, attenuation length, spatial resolution, multi-track resolvability, and superlayer structures. Up to 256 fiber and VLPC channels will be utilized in the tests.

Task 7 Studies of Radiation Damage and Environmental Aspects of Scintillating Fiber and Waveuide Performance. Coordinated by UI Chicago and Fermilab

Radiation damage studies to scintillation materials, scintillating fibers, and fiber waveguides will continue to be carried out. In particular we are [illegible] environmental effects on fiber annealing and scinnillation stability - for example, should the fibers be maintained in a nitrogen or air environment; should the fiber be maintained in a dark environment after manufacture, etc. What effects do such environments have in the presence of radiation and independent of radiation.

Task 8 Simulations. Coordinated by Rice, Penn State, Purdue and [illegible]

Simulation studies will continue for both central [illegible] ($|\eta| < 2.5$) tracking. These studies will emphasize momentum [illegible] occupancy. Intermediate tracking and prototype fiber tracker [illegible] special consideration during this year. Fibers may well play a [illegible]

of occupancy and trigger issues, and in part because the short magnet coil option has been selected by SDC - a choice which makes operation of gas/wire radial chambers more difficult because of field variation.

Simulation studies of scintillation light trapping and optical transport in fiber waveguides will be continued.

Task 9 Trigger Development. Coordinated by Fermilab and Penn State

A digital pipeline is being produced to develop a first level trigger based on track information in the fibers. It is an FTG goal to give these concepts an airing during beam tests. Based on these tests an ASIC pipeline architecture will be developed. The ultimate objective of this program is to exploit the high granularity and low occupancy of fiber tracker superlayers, and the resultant excellent spatial and angular resolution, to provide a first level P_T trigger for the SDC experiment. Issues of algorithm development for clusters of fiber hits, linking between layers, and the deployment of fibers in superlayers all bear on these studies.

Task 10 Mechanical Engineering. Coordinated by Purdue

Mechanical engineering of support cylinders and disks using composite materials of very low mass, and the mounting and registry of fibers and/or fiber ribbons and waveguides to such structures will be undertaken with funding and coordination with the Hybrid Subsystem Collaboration and the Modular Subsystem Collaboration. [Funding for this work is provided by SSCL through these other two collaborations.]

C. Test Beam Requirements

We will require a high energy, charged particle beam for tests of fiber ribbon and superlayer structures, and for prototype trigger tests. Currently we are scheduled for the Fermilab NM Beam (in the Muon Laboratory) for tests designated T839, and are scheduled for the current fixed target run at Fermilab. Additional test beam time may be required later in FY92, and we may need time at BNL or LANL for such studies if they are deemed necessary.

For radiation damage and environmental studies of fibers and waveguides, we intend to request permission to place materials on a temporary basis in the Fermilab accelerator tunnel, perhaps at C0 or some other location. We will approach Fermilab informally to request such access, as needed.

D. Special Considerations

- The contact persons for the Fiber Tracking Group (FTG), M. Atac, J. Elias, and R. Ruchti agree to be responsible for equipment borrowed by our collaboration and will insure its timely return.
- We understand that funding for this project will be provided in allocations of a single year, with successive year's funding dependent on successful progress to date and available funds as determined by an appropriate review process.

E. Milestones

Milestones for Scintillating Fiber Tracking research during FY91 are presented in this section. This R&D, if successful, will lead to the development of a powerful outer tracking system for SDC based, in part or in toto, on scintillating fiber technology and incorporating solid state photodetectors for the optical readout. Such a tracker is intrinsically fast and low in occupancy, and is capable of providing a powerful, first level trigger. Such a tracker holds promise for successful operation to the highest luminosities expected at the SSC.

Task 1: Scintillator: (Notre Dame and Fermilab)
The refinements of scintillator composition will be made in this fiscal year. Final selection will be made in FY92.

Task 2 Waveguide Development: (Notre Dame and Fermilab)
Refinements of core, cladding, and extramural absorber materials will be made in this fiscal year. Final selection will be made in FY92.

Task 3 Splicing Techniques for Fibers and Ribbons (Purdue, Fermilab, Notre Dame, UCLA)
Methodologies for splicing of individual fibers and fiber ribbons will be identified.

Task 4 Ribbon Fabrication. (Notre Dame, Purdue, Fermilab, UT Dallas)
Methodologies for ribbon fabrication will be identified and prototypes produced.

Task 5 VLPC and Preamp Development.(UCLA, Rockwell Science Center, UT Dallas)
IR desensitized, High QE, fast-response VLPC will be produced. Up to 256 channels will be delivered to UCLA. Additional VLPC channels will be provided to UCLA, Notre Dame, and Purdue, for bench tests of scintillating fibers, waveguides, splices and ribbons.

Task 6 Test Beam Studies of Fibers and VLPC. (All FTG groups)
A beam test of up to 256 channels of scintillating fibers and VLPC channels will be undertaken at Fermilab during the fixed target run. The test is designated T839, and contact persons are S. Margulies (UI Chicago) and J. Piekarz (Notre Dame).

Task 7 Studies of Radiation Damage and Environmental Aspects of Scintillating Fiber and Waveguide Performance. (UI Chicago and Fermilab)
Studies will be pursued vigorously. No specific milestone in FY9.

Task 8 Simulations. (Rice, Penn State, Purdue, and Notre Dame)
Studies will be pursued vigorously for refining fiber tracker design for the SDC proposal for central and intermediate tracking. The design must be ready by the end of FY91, in order to be incorporated in the SDC proposal.

Task 9 Trigger Development. (Fermilab and Penn State)
A hardware trigger scheme based on discrete circuit elements will be fabricated for inclusion with the beam tests.

Task 10 Mechanical Engineering. (Purdue, Fermilab, Notre Dame, ORNL, WSTC)
Development of a conceptual design for scintillating fiber tracking in central and intermediate tracking regions.

F. Reporting

The collaboration will provide the SSC Laboratory with copies of all talks and publications resulting from this R&D project. A short interim progress report will be provided to SSCL by April 1991 and a detailed written report will be provided SSCL by September 1, 1991. Proposals for continued support with a budget for FY1992 are to be presented to the SSCL together with the report.

G. Funding

- In this section we specify the allocation of funds by institution and by research task as defined in Section B.

Table I
Sources of Research Funds ($K)

	SSCL	Other
Capital equipment	383	0
Operating funds	302	400
Total	685	400

Table II
Distribution of Funds by Institution ($K)

	Capital Equipment (SSCL)	Operating Funds (SSCL)
UCLA	10	90
Fermilab	70	20
UIChicago	25	0
Notre Dame	30	40
ORNL	0	0
Penn State	0	25
Purdue	0	70
Rice	0	25
Rockwell	248	0
UTDallas	0	32
Total	383	302

Table III
Expenditures by Research Task ($K)

	Capital Equipment	Operating Funds
TASK I SCINTILLATOR	20	35
Task II WAVEGUIDE	10	15
Task III SPLICING	10	25
Task IV RIBBONS	20	10
TASK V VLPC AND PREAMPS	258	112
Task VI TEST BEAM	25	45
Task VII RADIATION AND ENVIRONMENTAL	25	0
TASK VIII SIMULATIONS	0	35
Task IX TRIGGER	15	25
Task X MECHANICAL ENGINEERING	0	0
TOTALS	383	302

The SSC Laboratory has identified and selected the Scintillating Fiber Tracking project for funding. It is expected that the DOE/OSSC will provide the Scintillating Fiber Tracking Collaboration with $302K of operating funds and $383K in equipment funds in FY 1991 for the above described detector R&D project.

H. Signatures

The undersigned have agreed to fulfill to the best of their abilities the terms of this Memorandum of Understanding between the Scintillating Fiber Tracking Collaboration and the Superconducting Super Collider Laboratory.

AGREED

Scintillating Fiber Tracking Collaboration Contact Person(s) and Institutions	Date
M. Atac, UCLA	4-16-91
J. Elias, Fermilab	April 16, 1991
R. Rucha, Notre Dame	April 11, 1991
R. Schwitters, Director Superconducting Super Collider Laboratory	

IN CONCURRENCE

	date
R. Diebold, DOE OSSC	
J. O'Fallon, DOE OHEP	

Appendix I Physics Goals and Motivation

The speed of response and high granularity (very low occupancy) of scintillating fibers make them an ideal choice for high resolution, charged particle tracking, for providing a fast, first-level trigger based on particle transverse momentum, and for operation at the highest luminosities expected at SSC. A tracking detector with these features would be an important element for many SSC experiments.

The goals of the Fiber Tracking Group (FTG) are to: (1) develop fiber tracking technology for general applications in SSC experimentation, and (2) to provide central tracking and first-level P_T triggering for the SDC experiment.

Discussion

An important challenge for any SSC experiment is the provision of an effective tracking detector. Because of the high luminosity environment and the short bunch separation at the SSC, any tracking detector must have fast response, low occupancy, good spatial resolution, and good resistance to radiation damage.

A central tracking system should be capable of reconstructing low-mass states such as the Z^0 with a precision of 1-2%, and should enable cross-checks of the electromagnetic and hadronic calorimeter calibration over a wide momentum range. Further, expected topologies such as the Higgs boson, detected via the decay $H \rightarrow Z^0Z^0 \rightarrow qq\,l\,l$ and the decay $H \rightarrow Z^0Z^0 \rightarrow$ 4 leptons, should be identifiable, with at least a 3σ charge sign determination for tracks of $p_T \leq 1$ TeV/c.

At an SSC detector operating at machine luminosities $L = 10^{33}$ cm^{-2} sec^{-1}, any viable tracking device must operate reliably in a high radiation environment (typically 10^5 rad/yr at a radius r = 50 cm from the interaction region due to beam interactions and neutron albedo). The tracking system, which must have low material thickness, should be capable of reconstructing all tracks, have good rejection against spurious tracks, and should be capable of separating tracks resulting from multiple interactions in a bunch crossing. At small radii (typically r < 50 cm) silicon-strip detectors and/or pixel detectors are being considered for track reconstruction. At larger radii, the possibility of a stand-alone scintillating fiber tracker is potentially very attractive. It should be noted that the advantages of these two detector types are complementary.

Since the first successful use of fiber tracking in a collider environment [1], significant progress has been made [2,3]. Fiber trackers have the following attractive features:

[i] good tracking precision: multilayer structures of 830μm diameter fibers can result in a measurement resolution of ≤ 150μm per double-fiber layer, ~ 100μm per quadrupole-fiber layer, and provide good two track resolution.

[ii] fine granularity: for fibers of 830μm diameter placed at radii r ≥ 60cm, the occupancy from all sources is expected to be ≤ 1% per fiber, per bunch crossing.

[iii] good time resolution: an intrinsically prompt response.

[iv] insensitivity to magnetic fields and to RF noise.

[v] simple electronics if a binary (yes/no) readout is used.

and [vi] no power dissipation in the tracking volume.

For SDC, the basic detection element is an active scintillator fiber of ≤ 4m length, coupled by a 4m-to-6m long, clear fiber waveguide to a high-rate photodetector. In recent tests of BCF99-05 scintillating fiber of 830μm diameter and 4m length, optically spliced to clear fiber waveguide of 830μm diameter and 4m length, and readout with a Visible Light Photon Counter (VLPC) having quantum efficiency of 80%, we have measured >5 detected photoelectrons when a radioactive (beta) source is placed at the far end of the scintillating fiber (i.e. source location is 8 meters from the photodetector). We are the first group to achieve such a result, and the measurement clearly establishes a new standard of performance. This important measurement gives us confidence that we will achieve our performance goals in SDC: the detection of minimum ionizing particles resulting from a beam-beam collision with an efficiency exceeding 95% per layer; the determination of the longitudinal coordinate and impact parameter to 1mm for each track; unambiguous assignment of each track to a beam crossing (16 nsec spacing); momentum resolution sufficient to reconstruct the mass of the 2^0 to < 2% in a leptonic decay; momentum resolution sufficient to make a 3σ determination of the charge of a 1 TeV/c particle; and radiation resistance adequate for all components to survive for several years of beam without significant degradation of capabilities.

It is essential that this program be pursued vigorously and with strong and enthusiastic support from SSCL in order for: (1) fiber tracking to be included effectively in the proposal preparation for SDC in 1991-2, and (2) the development of conceptual engineering design, fabrication, and construction of the detectors to be completed in a timely fashion for installation of fiber tracking in the SDC detector by 1998.

[1] J. Allitti, et al, IEEE Transactions on Nuclear Science, Vol. 36, No. 1(1989)

[2] For a comprehensive review of the field and progress prior to FY 90 see: The Proceedings of the Workshop on Scintillating Fiber Detectors for the SSC, Fermilab, November 14-16, 1988, S. Reucroft and R. Rucinski, eds.

[3] For a comprehensive review of work in the field over the last year, see: The Proceedings of the Fort Worth Meeting on Detector Development for the SSC, Fort Worth, Texas, October, 1990.

Tracking System Requirements for the ITD

A. Sill(Rochester)

A. Seiden
for ITD group

Tracking System Requirements for the ITD

Preliminary list of responses to questions raised for inclusion in the tracking system requirements document.

Work still in progress, but enough information exists to reply to most of these questions now.

Conclusions:

- Rate of level 1 triggers is approximately understood for a three-superlayer tracker, on the order of a few hundred kHz.

- Higher level triggers may be possible with the use of stereo layers or coupling to information from calorimeter and/or silicon.

- Basic resolution driven by total integral Bx dl, intrinsic resolution, and placement; adequate over most of the region (1.4 to 1.6) < eta < 2.5.

Layout needs to be studied further to optimize integral B x dl (or B dl**2, to be studied.)

Requirements for Tracking

(1) $|\eta|$ coverage out to $|\eta| \leq 2.5$, implying $H^0 \rightarrow 4$ charged lepton geometrical efficiency $\gtrsim 60\%$ for $m_H \geq 200$ GeV.

(2) Reconstruction efficiency $\geq 90\%$ (for $|\eta| < 2.5$) for $H^0 \rightarrow 4$ charged leptons, for each lepton having $P_\perp \geq 5$ GeV, at design luminosity, but assuming twice the occupancy calculated by GEANT (exclusive of lepton identification and trigger cuts).

(3) Reconstruction efficiency for same as in (2) $\geq 75\%$ at $4 \times$ design luminosity.

(4) Reconstructed (as opposed to parametric) vertex constrained momentum resolution of $\sigma_{P_\perp/P_\perp^2} < 15\%$ (TeV^{-1}) for $|\eta| \leq 2$ (leaves room still for a contribution from misalignments) for $H^0 \rightarrow 4$ charged leptons.

(5) Efficiency contribution from lepton identification of $\geq 85\%$ for electrons with $P_\perp \geq 10$ GeV and $\geq 95\%$ for muons with $P_\perp \geq 10$ GeV.

(6) Position resolution at the calorimeter of ≤ 2.5 mm in $r-\phi$ or z (want error $\lesssim \sigma/2$ of calorimeter position accuracy).

(7) No special position resolution requirements at the muon system. Achievable numbers ≤ 1 cm.

(8) B single tagging efficiency $\geq 30\%$ for 125 GeV $\leq m_{top} \leq$ 250 GeV.

(9) First level trigger with momentum resolution $\sigma_{P_\perp/P_\perp^2} \leq 10$ (TeV^{-1}) – implies a 10% error for a 10 GeV lepton.

(10) Second-level trigger with momentum resolution $\sigma_{P_\perp/P_\perp^2} =$ 2.5 (TeV^{-1}). Gives a 10% error for a 40 GeV lepton for triggering on $Z \rightarrow e^+e^-$, $W \rightarrow e\nu$ – needed for calorimeter calibration.

(11) Discovery potential – hard to quantify. In general want maximum capabilities from detector. Based on history highest priority (other than isolated lepton of Higgs case above) would be reconstruction and impact parameter measurement of leptons within jets up to the largest jet $P_\perp$ possible (at least ≥ 500 GeV). Desired reconstruction efficiency $\geq 50\%$.

(12) Measurement of jet fragmentation at modest luminosity for QCD studies and for modelling backgrounds from jets.

(13) Survivability at standard $\mathcal{L}$ for ≥ 10 years.

(14) Allows a natural path for upgrading to a system with survivability of ≥ 10 years at $10\times$ standard $\mathcal{L}$ with emphasis (e.g. momentum resolution, pattern recognition, isolated track efficiency) to be decided based on what is learned during initial running.

Req. (1), (2), (3):
abs(eta) < 2.5 for Higgs --> 4 leptons:

- Luminosity not a problem (see transparencies on occupancy from S. Maxfield, Liverpool.
- Pattern recognition and reconstruction efficiency adequate (HJ Trost, S Maxfield transparencies).
- Factor of two to go from eta = 1.5 to eta = 2.5 (K. Einsweiler, July SSC lab meeting.)

Req. (5), (6):
lepton identification & match to calorimeter:

- r-phi resolution of <100 microns per layer (<50 microns per superlayer) for 3 to 4 superlayers should be adequate to separate closely spaced tracks (needs further study).
- radial coordinate resolution from small angle stereo is presently understood to be <2 mm per pair (<1.5 mm per superlayer).
- track matching to endcap calorimeter should not be a problem.

SDC Intermediate Tracking

Req. (9, 10):

Trigger threshold and resolution

- sigma(p_T)/(p_T**2) for 10 GeV p_T cut has sharp turn-on for most of the intermediate angle region but is probably not as good as 10 (TeV)**-1 with present layout.
- can be optimized with slight (~0.5 m) variations in placement for IT superlayers, worst at eta > 2.0
- favors projective eta boundary placement.

Req. (13), (14):

Survivablility at "standard" and elevated luminosity

- Strongest argument for microstrips. Not considered a problem at present, but aging studies, substrate performance need to be verified. (Preliminary results show radhard substrates can be found.)

Req. (11):

Discovery potential

- Hard to quantify. Impact parameter resolution provided mostly by silicon, but intermediate tracking does provide trigger, improved pattern recognition, and does contribute to separation of charged particles within jets. Improved lepton ID via matches to calorimeter, muon system.

Req. (4):

Momentum resolution

- p_T resolution limited by total available B field, favors longer tracking length (4.0 m l/2) and best possible B field without re-entrant endcap EM.
- varies approximately linearly from eta=1.4 to eta=2.5, decreasing contribution according to integral B dl**2. Still useful up to at least eta=2.0. Negatively affected by shortening of the tracking length.

SDC Intermediate Tracking

Further work in progress.

Simulation Studies of Microstrip ITD

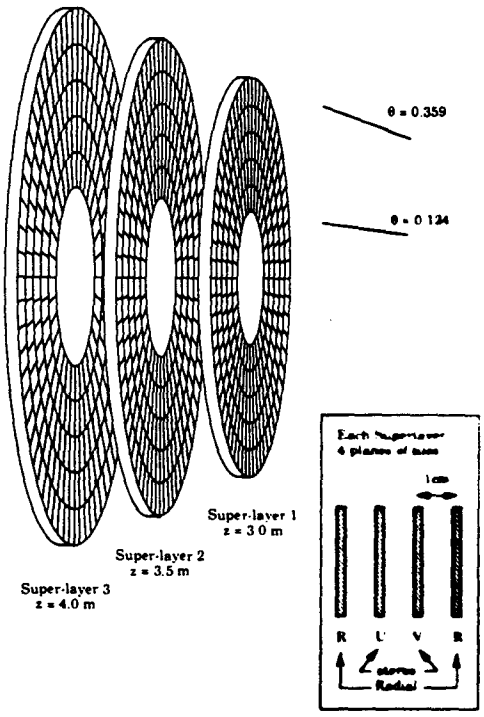
S. Maxfield(Liverpool)

SIMULATION STUDIES OF MICROSTRIP ITD

- Geometry of ITD
- Event generation
- Detector 'simulation'
- Simulation of a track trigger
- A few comments about reconstruction
- Conclusions

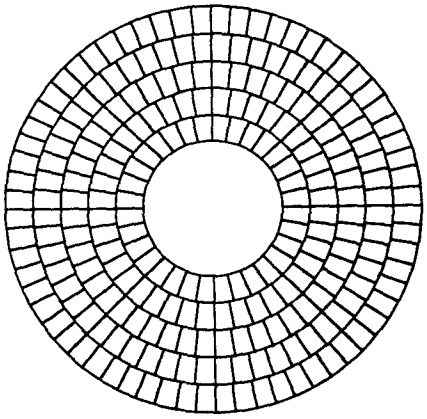
N.B. This simulation is not yet incorporated in the SDC shell!

ITD



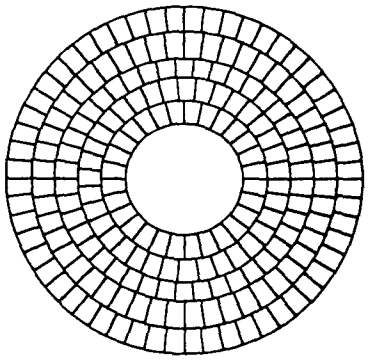
R-TILES at Z = ±4.0 m, ±4.03m.

Ring 1	0.500 - 0.700 m	32 tiles	10752 strips
Ring 2	0.700 - 0.900 m	40 tiles	12600 strips
Ring 3	0.900 - 1.100 m	48 tiles	18144 strips
Ring 4	1.100 - 1.300 m	56 tiles	18816 strips
Ring 5	1.300 - 1.500 m	64 tiles	21504 strips



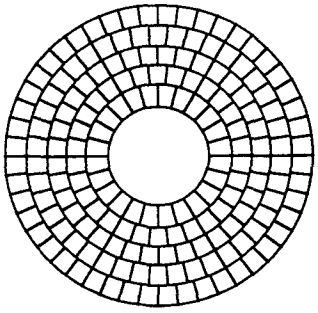
R-TILES at Z = ±3.5 m, ±3.53m.

Ring 1	0.4375 - 0.6125 m	28 tiles	10752 strips
Ring 2	0.6125 - 0.7875 m	35 tiles	12600 strips
Ring 3	0.7875 - 0.9625 m	42 tiles	18144 strips
Ring 4	0.9625 - 1.1375 m	48 tiles	18816 strips
Ring 5	1.1375 - 1.3125 m	56 tiles	21504 strips



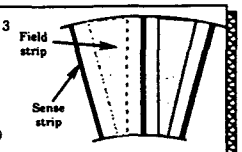
R-TILES at Z = ±3.0 m, ±3.03m.

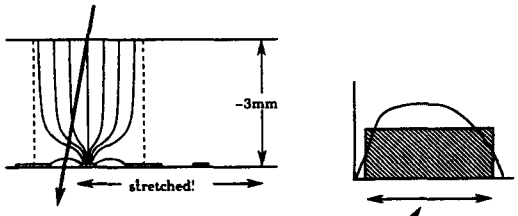
Ring 1	0.3750 - 0.5250 m	24 tiles	10752 strips
Ring 2	0.5250 - 0.6750 m	30 tiles	12600 strips
Ring 3	0.6750 - 0.8250 m	36tiles	18144 strips
Ring 4	0.8250 - 0.9750 m	42 tiles	18816 strips
Ring 5	0.9750 - 1.1250 m	48 tiles	21504 strips



'TYPICAL RADIAL TILE' z = 3.5 , Ring 3
Rmin = 78.75 cms Rmax = 96.25cms
432 anodes strips) $\Delta\Phi = 0.01984^{\circ}$ (between
$\Delta\Phi$ (of plate) = 8.5714°
Sense-sense pitch = 272.708μ (at inner radius)
= 333.309μ (at outer radius)

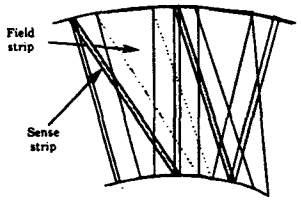
Sense (anode) strips constant width (10μ) and Sense-Field constant gap (90μ) - same for all tiles.

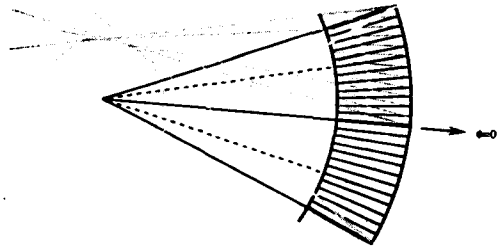




- Fast rise time
- For drift velocity ~ 70-75 μ/ns,
  time to sweep electrons from cell ~ 45ns ~ 3 bunch crossings

'STEREO' LAYERS





For definiteness, we define U and V tiles as follows:-

- At the outer radius of the tiles, the U and V strips are located at the same Φ points as the R tiles.
- At the inner radius, U-tile and V-tile strips have their endpoints displaced by angles $+n\Delta\phi$, and $-n\Delta\phi$ respectively.
- The number n determines the granularity of the system in radius: number of crossings of R and U-strips (or R and V-strips) is just (n-1)
- Properties:-
  - The angle between successive U or V strips is constant and the same as that between the corresponding R strips.
  - U and V strips are tangent to a common circle centred on the z axis.

These conditions determine s, the radius of the 'circle of tangents' . If R and r are the maximum and minimum radii of the tiles, then:

$s = R\sin\psi$,
where $\tan\psi$ is given by $R\sin(n\Delta\phi) / (R - r\cos(n\Delta\phi))$

EVENT GENERATION

Use PYTHIA Higgs + minimum bias background

Higgs mass 200 GeV, 300 GeV
Higgs decay → HH → 4μ
→ 4 jets
→ 2 jets + 2μ

NOTE : minimum bias includes elastic scattering, sundry diffractive processes etc. -> total cross-section ~196 nb (about 1/2 is elastic)

For ITD simulation, require (see later) events from 2 bunch-crossings before to 3 bunch-crossings after the event of interest.
- generate minimum bias events in each bunch-crossing - number according to Poisson distribution with mean determined by above X-sec and Luminosity (10**33, *3x10**33*)
- superimpose a Higgs event in bunch-crossing zero.

*For Luminosity 10**33, each 'event' typically contains 18 minimum bias and one Higgs 'sub-events'*

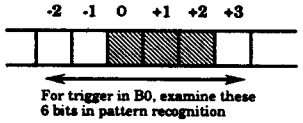
Subprocess	Sigma (nb)
f + f' -> f + f'	1.006E+00
f + fb -> f' + fb'	0.000E+00
f + fb -> g + g	0.000E+00
f + g -> f + g	1.493E+01
g + g -> f + fb	1.853E+00
g + g -> g + g	7.747E+01
Elastic scattering	7.088E+01
Single diffractive	2.569E+01
Double diffractive	3.104E+00
Low-pT scattering	1.165E+00
All included subprocesses	1.961E+02

DETECTOR 'SIMULATION'

- Simple propagation of tracks along helices.
- Generate hits in microstrips.
- Digitize hits by generating 'latch' settings (6 bits per hit strip). (see later)
- No material but we conservatively approximate the effects of additional tracks from conversions etc. by 'replacing' each neutral with a charged track of same momentum (random sign).
- Tracking was done in a uniform Field of 1.8 Tesla. *To estimate the effect of Field non-uniformities, we also tracked the events through a field reduced to 50% (10%) of its full value in the region between 3.5 and 4.0 meters from the interaction point (keeping it axial).*
- The tracks include 'loopers', but 'large radius' loopers which achieved their maximum excursion from the z-axis before reaching the ITD were assumed to be absorbed elsewhere in the detector and so not generate hits in the ITD.

'DIGITISATION'

- Precise read-out method to be decided. For definiteness assume the following in this simulation:
- Microstrip cell takes 3 bunch-crossings (45 ns) to 'clear'.
- Each microstrip produces a string of bits, one per bunch-crossing.
- A track passing through cell sets the bit in its bunch-crossing and those for the next two.
- We concentrate on reconstruction and triggering on one particular bunch crossing (labelled '0').
- The pattern of 6 bits ranging from B-2 to B+3 then provides information about the presence of hits coming from B0:-



- In the *trigger simulation,* we look at the bits in *one bunch-crossing only.*
- For track reconstruction, we can use the bits set in previous and later bunch-crossings. If the trigger was produced in bunch-crossing 0, the above pattern of 6 bits would *guarantee* a hit produced by a track from the triggering event.
- Other patterns *may* contain such a track:

e.g. hits from bunch-crossings -1 and +2 would yield:

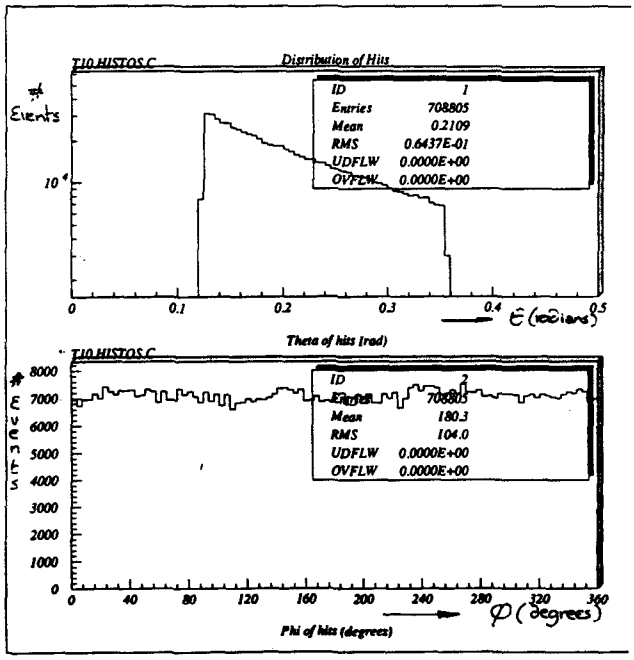


a hit from bunch zero may or may not be present too

- In practice, such bit-patterns might be generated by up-dating discriminators. It provides 'maximum' information for track reconstruction purposes. It has the disadvantage that the B0 bit is set by tracks from the previous two crossings and so these contaminate the trigger (for which we only look at the B0 bit) and contribute to the 'fake' rate.

- Alternatively, the fast rising edge of the pulses could be used to set a single bit, and a dead-time imposed for the next two crossings.
Although the latter would suppress some hits completely, *the cell-occupancy is so low that almost no loss of hits occurs*. Furthermore, we would eliminate contamination by tracks from previous crossings and reduce the fake trigger rate accordingly.

- In this study, the 'up-dating' discriminator case was simulated. The effect on the trigger-rates of imposing dead-time was simulated by choosing hits with B0 set but not B-2 or B-2.



OCCUPANCY

Number of hits/event/plane. ~150

'Event' means the composite consisting of 6 bunch-crossings worth of minimum bias events + 1 Higgs event →

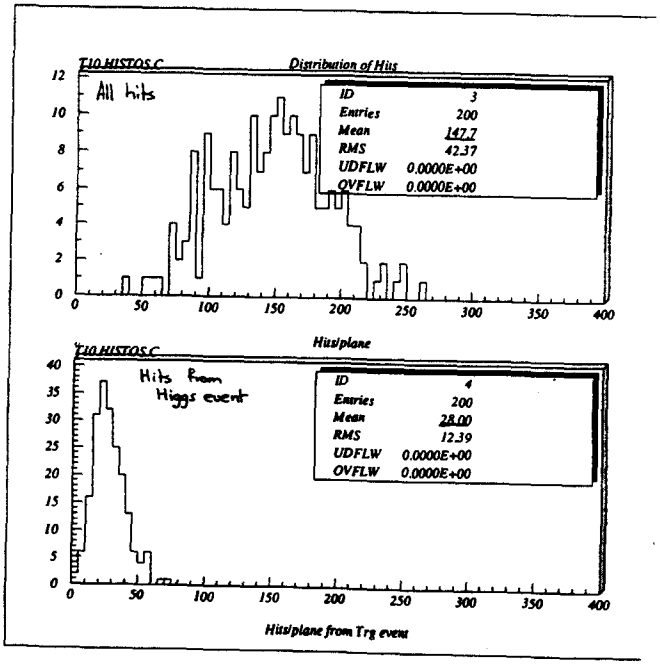
Mean number of hits / plane / bunch-crossing: ~20

Maximum ~33

Define occupancy as: $\frac{\#\text{ hits/plane}(\textit{ring})/\text{crossing}}{\#\ \mu\text{strips/plane}(\textit{ring})}$

Ring	Mean occupancy(%)	Max occupancy(%)
1	.047	.078
2	.035	.059
3	.02	.036
4	.018	.031
5	.014	.023
Mean	*.029*	*.049*

Low occupancy ⇒ low probability of 'masking' of hits by events from other bunch-crossings



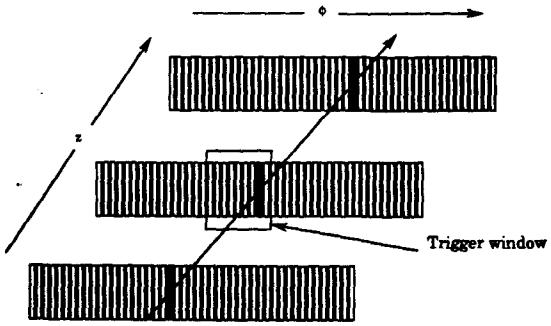
ITD TRIGGER

1510

- Exploit projective geometry:
- Tracks are straight lines in ϕ vs. z and approximate straight lines in r vs. z.

  $\Rightarrow$ tracks stay in one ring.

  The slope in ϕ measures Pt
- Form trigger using one R-layer (these measure ϕ) from superlayers 1 and 2:-
- For each hit in superlayer 1, look for hits in superlayer 2 within $\pm\Delta$I strip (in the same ring).



1511

TRIGGER SETTINGS FOR Pt 10GeV/c:-			
	ΔI	$\delta\phi_{track}$	$\delta\Phi_{ring}$
Ring 1	3	0.0020251680	0.0005843735
Ring 2	5	0.0026926502	0.0004986654
Ring 3	10	0.0033730555	0.0003462954
Ring 4	12	0.0040405833	0.0003339277
Ring 5	16	0.0047267745	0.0002921868

Size of trigger 'window' (±)

angle between μ-strips

Change in ϕ between superlayers for track with Pt=10GeV/c

1512

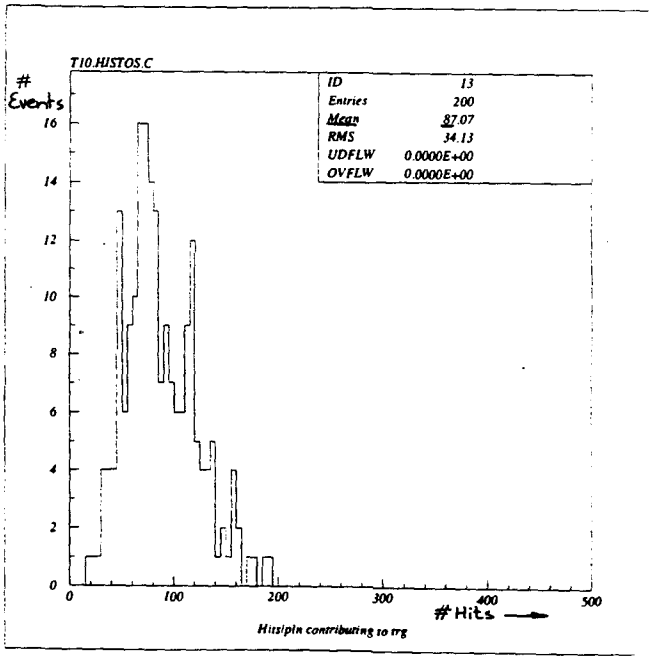
- The two-plane 'telescope' has a high accidental rate (~4 per event for 10GeV trigger)
- Use R-layer from third superlayer to verify trigger:

  For genuine tracks,

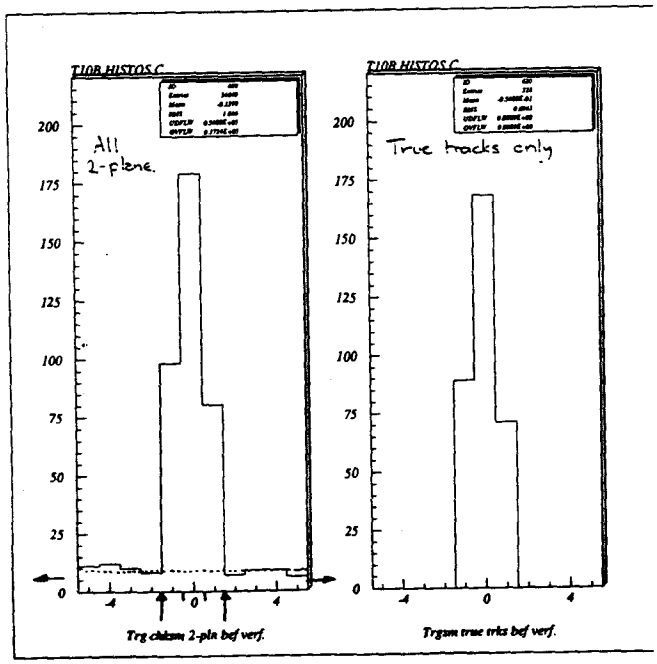
  $I_2 - (1/2)(I_1 + I_3) = 0 \pm 1$

  (straight line in ϕ)
- This successfully reduces the accidental rate to acceptable levels (see later).

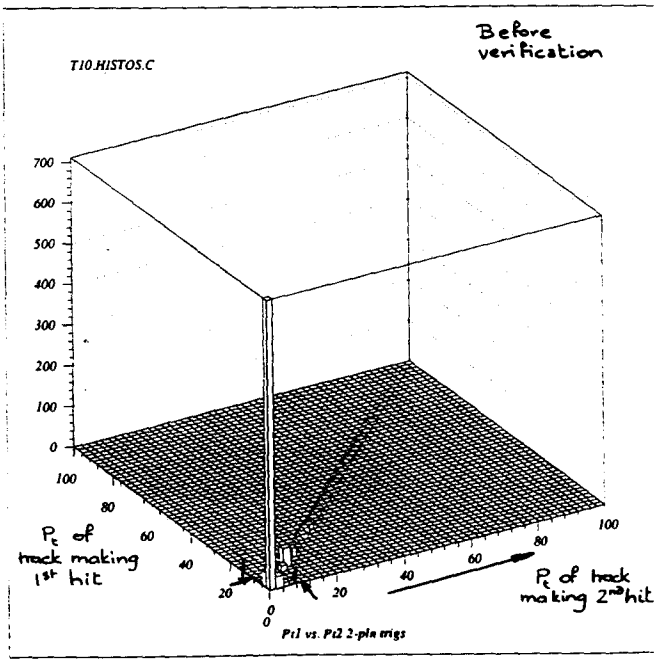
1513



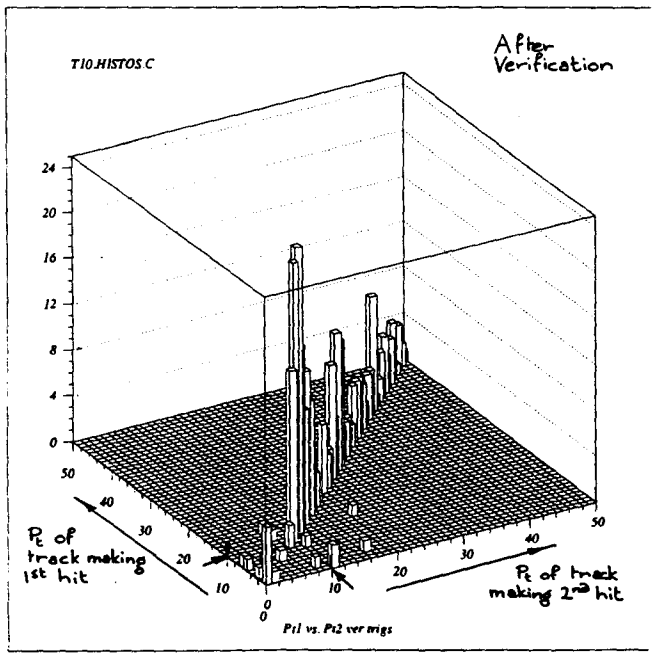
1514



1515



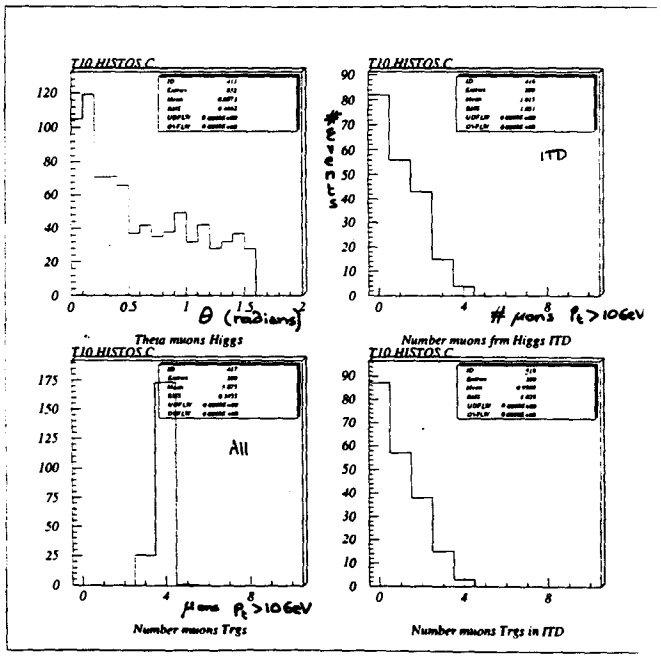
1516



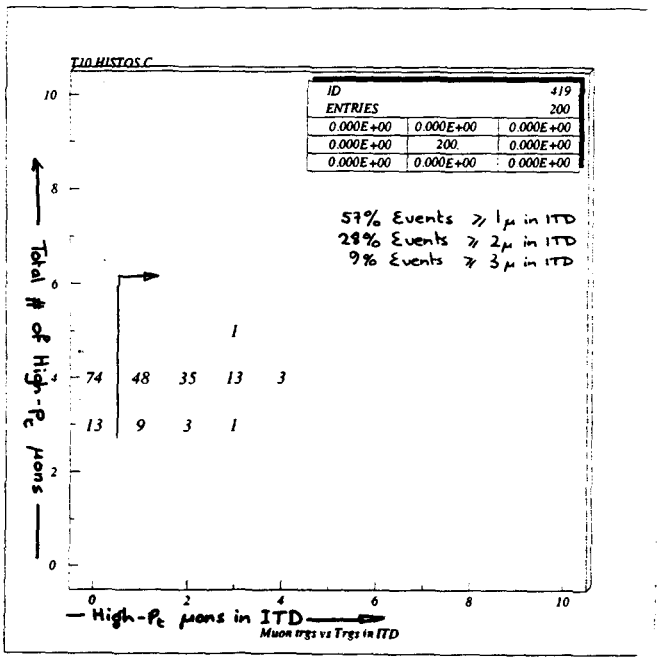
1517

Distribution of High P_t μons in $H \rightarrow 4\mu$ even

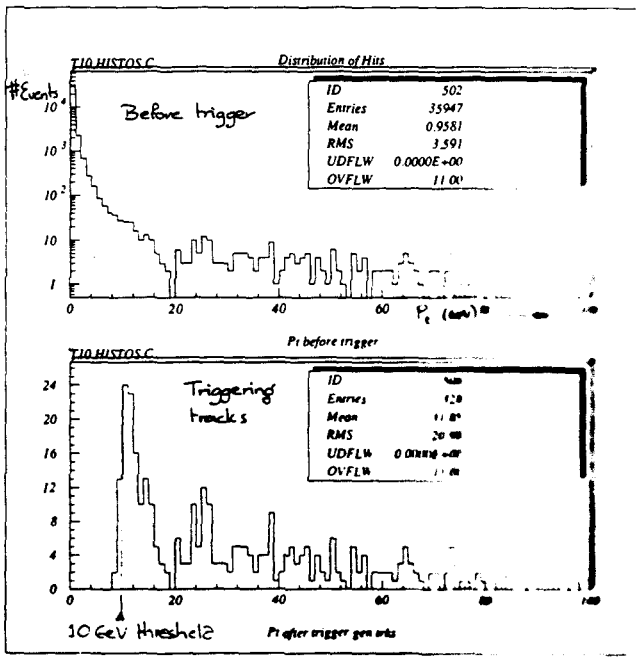
(200 GeV Higgs)



1518

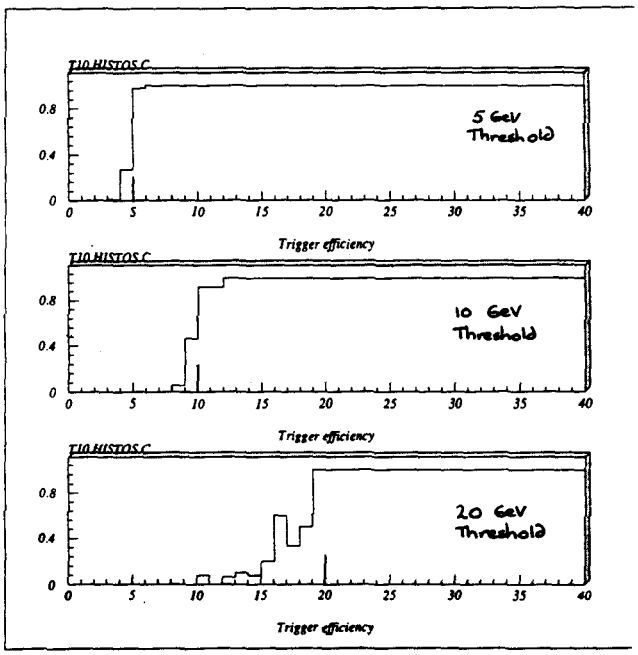


1519



1520

Broadening of trigger edge
– finite resolution in $\Delta\phi$
$\Delta p \sim \frac{1}{P_t}$



Steve Manfield

1521

TRIGGER STATISTICS FOR UNIFORM FIELD.

200 'events' containing Higgs (mass 200 GeV)

Pt threshold (GeV/c)	20	10	5
Two-plane 'telescopes'.	756	1194	2408
Verified triggers.	236	357	661
...coming from genuine tracks.	219	328	606
... with Pt > thresh.	207	313	561
Triggerable tracks.	207	317	563
Triggered events.	120	141	160
Triggerable events.	114	141	156
Events triggered by Higgs trk.	114	140	153
Events triggerable by Higgs trk.	114	140	153
Trigger 'efficiency' (per track)	100%	98.7%	99.6%

TRIGGER STATISTICS FOR UNIFORM FIELD.

200 'events' containing Higgs (mass 300 GeV)
H → 4 jets

Pt threshold (GeV/c)	10	5
Two-plane 'telescopes'.	2187	4537
Verified triggers.	684	1581
...coming from genuine tracks.	537	1262
... with Pt > thresh.	498	1169
Triggerable tracks.	517	1190
Triggered events.	119	161
Triggerable events.	119	153
Events triggered by Higgs trk.	118	146
Events triggerable by Higgs trk.	119	148
Trigger 'efficiency' (per track)	96%	98%

TRIGGER STATISTICS FOR UNIFORM FIELD.

200 'events' containing Higgs (mass 300 GeV)
H → 4 jets. Luminosity 3 x 1033**

Pt threshold (GeV/c)	10
Two-plane 'telescopes'.	5548
Verified triggers.	814
...coming from genuine tracks.	552
... with Pt > thresh.	509
Triggerable tracks.	526
Triggered events.	141
Triggerable events.	122
Events triggered by Higgs trk.	118
Events triggerable by Higgs trk.	119
Trigger 'efficiency' (per track)	97%

Steve Maxfield 9/9

1524

EFFECT OF NON-UNIFORM FIELD on TRIGGER

- Full field out to second super-layer of ITD.
- Field reduced to 50% (10%) of full value between super-layers 2 and 3

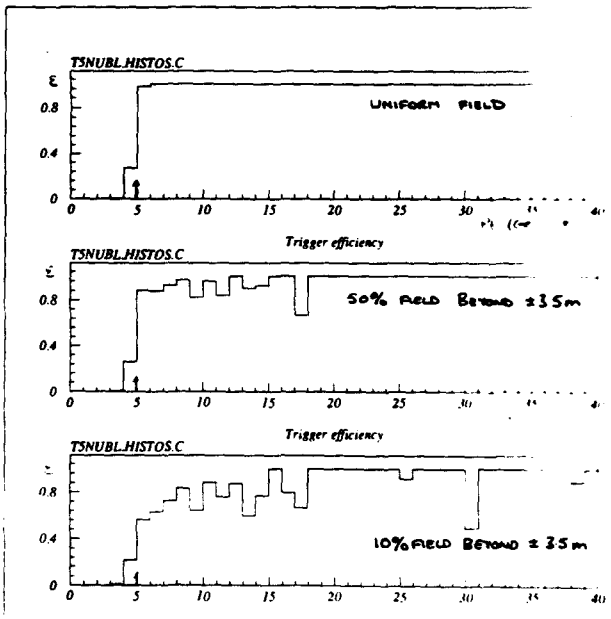
Field reduction factor	50%	50%	10%
Pt threshold (GeV/c)	10	5	5
Two-plane 'telescopes'.	1194	2408	2408
Verified triggers.	348	632	544
...coming from genuine tracks.	321	572	490
... with Pt > thresh.	307	529	453
Triggerable tracks.	317	563	563
Triggered events.	142	162	157
Triggerable events.	141	156	156
Events triggered by Higgs trk.	140	152	148
Events triggerable by Higgs trk.	140	153	153
Trigger 'efficiency' (per track)	97%	94%	81%

Steve Maxfield 9/91

1525

EFFECT OF NON-UNIFORM FIELD ON TRIGGER EFFICIENCY

NO ATTEMPT TO 'FIX UP' TRIGGER CONDITION (5 GeV Threshold)



TRIGGER STATISTICS FOR UNIFORM FIELD.

100 'events' containing Higgs (mass 200 GeV)
H → 2 jets+ 2 leptons Luminosity 1033**

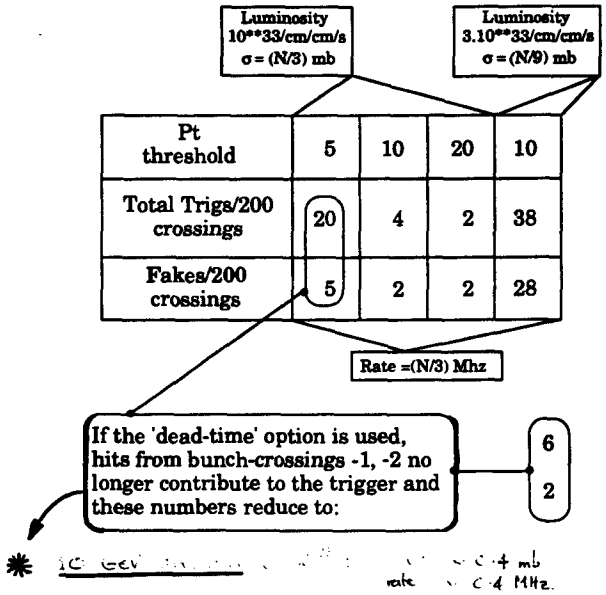
Pt threshold (GeV/c)	10
Two-plane 'telescopes'.	457
Verified triggers.	175
...coming from genuine tracks.	150
... with Pt > thresh.	136
Triggerable tracks.	142
Triggered events.	59
Triggerable events.	57
Events triggered by Higgs trk.	55
Events triggerable by Higgs trk.	57
Trigger 'efficiency' (per track)	96%
Evts triggered by Higgs lepton	12 *

* i.e. for about 1/4 of the 'triggerable' Higgs.
Relevant for combination with muon chambers, say.

'BACKGROUND' TRIGGER RATES.

The background trigger rate arises from genuine high Pt tracks from the underlying minimum bias events and 'fake' triggers arising from chance combinations of hits.

For minimum bias events with the 'up-dating discriminator' option:



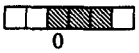
* 10 GeV ... c·4 mb
rate ... c·4 MHz.

Steve Maxfield

PATTERN RECOGNITION.

For pattern recognition purposes, the pattern of 6 bits can be used to reduce background from tracks produced in neighbouring bunch-crossings:-

A hit with a track in bunch-crossing zero must contain the following pattern of 6 bits:-



'Hard' selection: Hits with precisely the B0 pattern

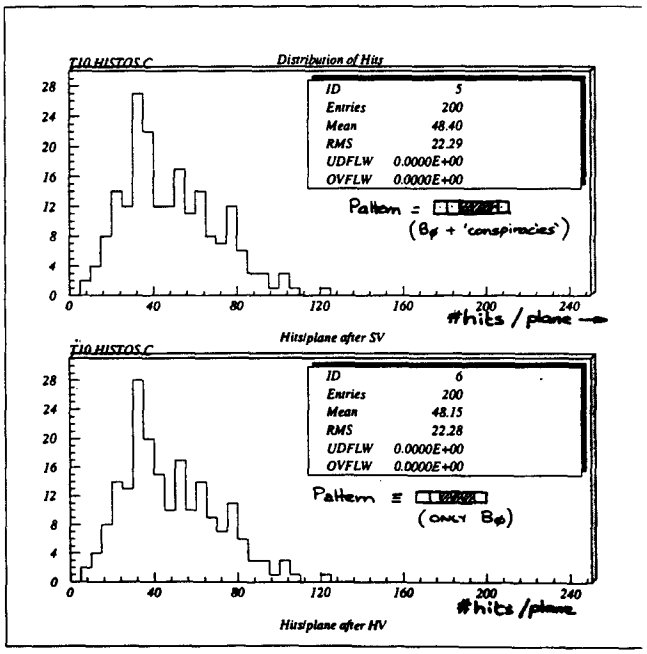
Only hits from bunch 0 survive,
but not all B0 survive.

'Soft' selection: Hits containing the B0 pattern:

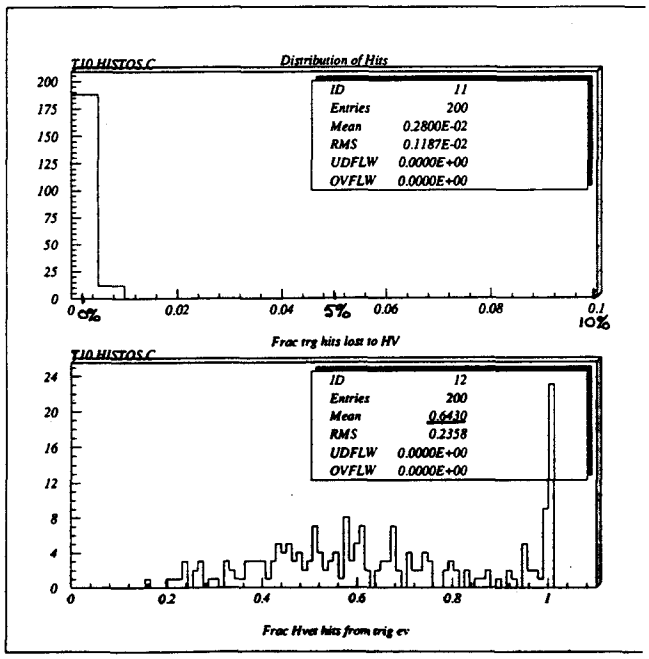
All B0 survive,
+ some others.

A slightly looser 'hard' selection is possible:-
Require:

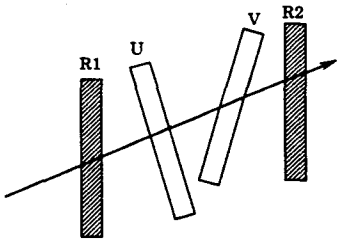




< ⅓ % real hits lost (just reflects low occupancy)
– almost always none



MAKING SPACE-POINTS

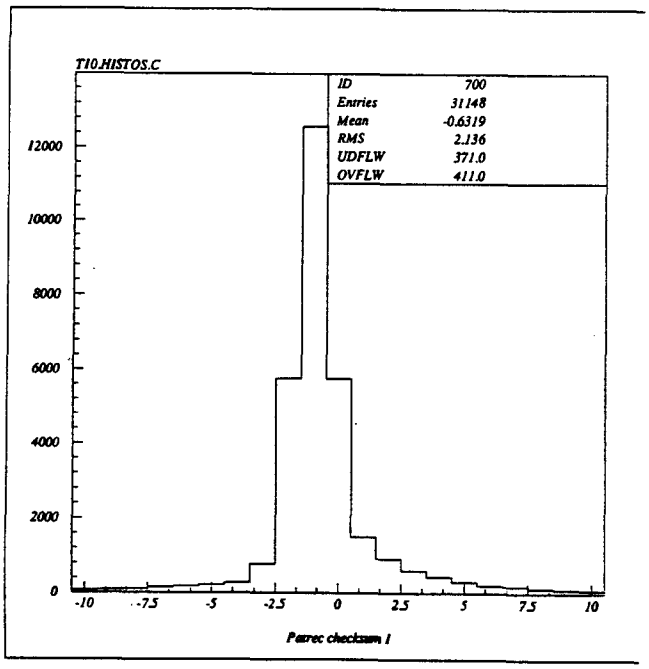


- For hits produced by genuine tracks, there are simple relationships between the numbers of the hit strips in the 4 layers:-

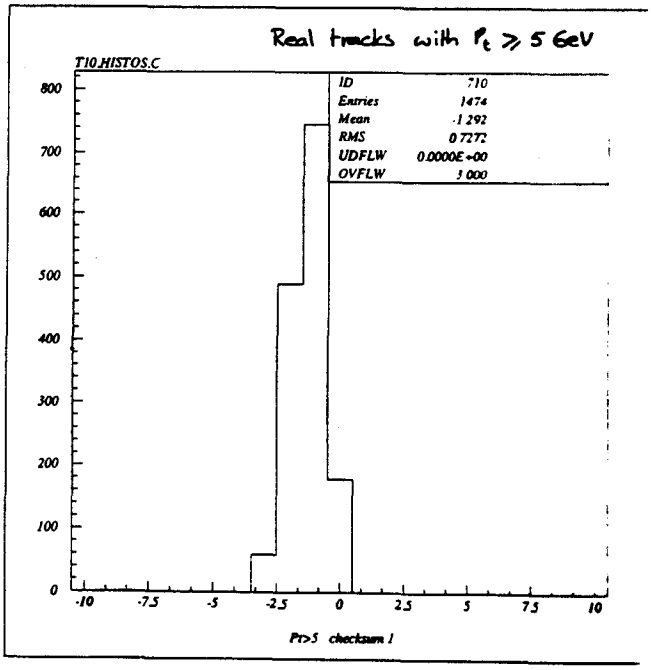
$$(I\phi_{R1} + I\phi_{R2}) - (I\phi_U + I\phi_V) = I\delta$$

- $I\delta$ is zero in the approximation that the track has the same radius at the U and V layers. It is < 0 for tracks with increasing radius (stiff tracks from interaction region) ->
- A cut on the value of $I\delta$ can be used to select hit combinations from real tracks
- The radius of the track at the mid-plane of the superlayer can be deduced from other linear combinations of the 4 strip numbers

'Check sum' for associating hits in 4 layers of a super-layer
– Distribution produced by REAL tracks

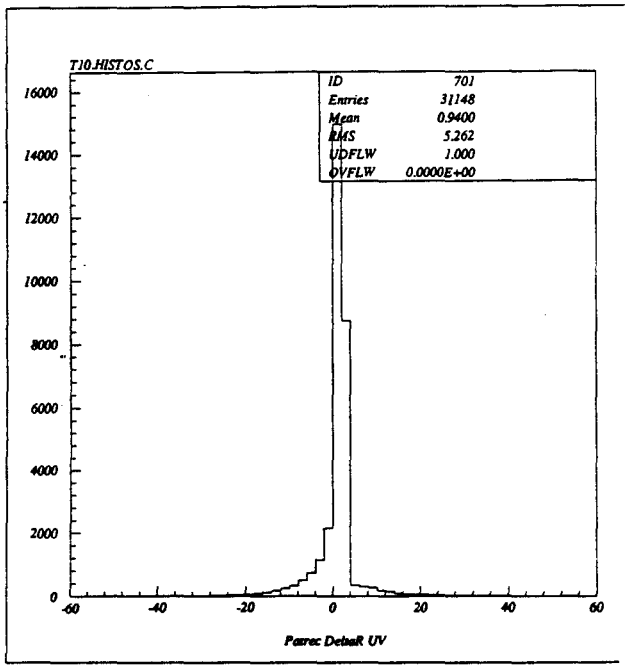


Real tracks with $P_t \geq 5$ GeV

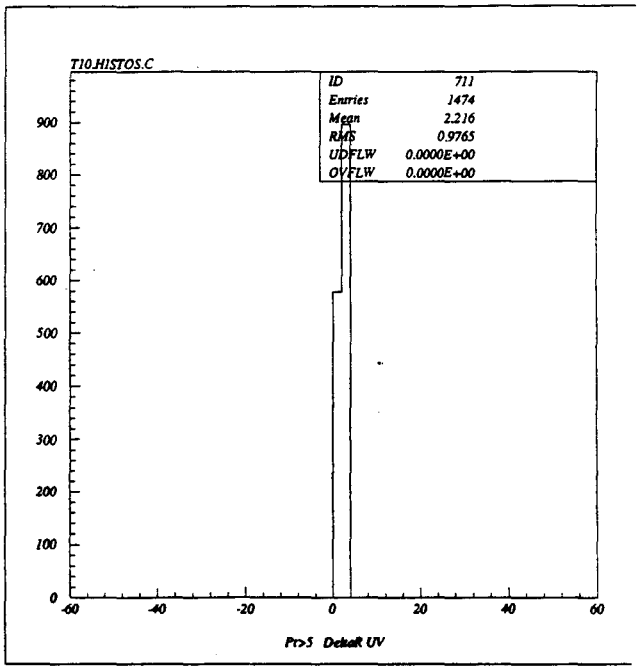


1534

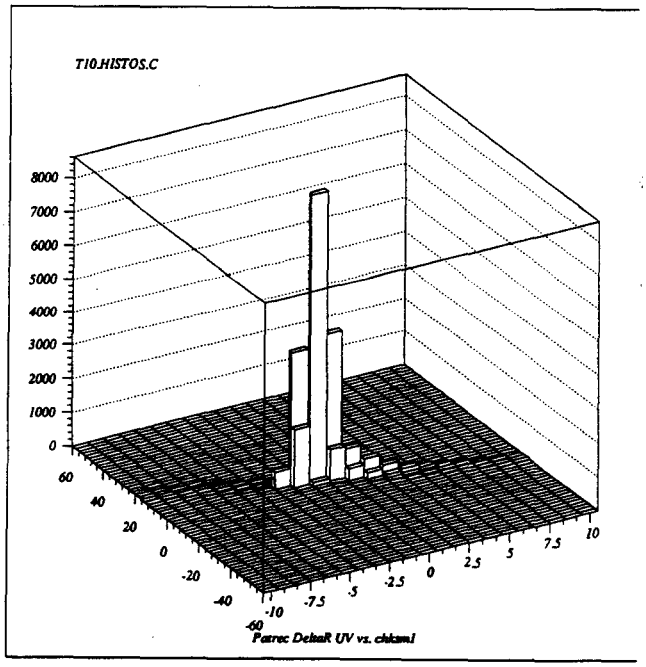
Difference in radial coordinates of real tracks at U and V layers



1535



1536



1537

INCORPORATION INTO SDC SHELL

- Gas-microstrip ITD has been put into SDC-shell (at least the geometry - M. Edwards design)

* Penny Estabrooks Ottawa
* Gene Baracsch Texas A&M

→ more realistic treatment of material, B-field etc.
→ Integration of ITD with other detector components

1538

TILE_WITH_ELECTRONICS

CRPP, Ottawa, Canada

Sept 23, 1991

xy slice through middle of z=-350 cm showing tracks with p>1 GeV, hits from all tracks (4 out of 4 layers of microstrips)

1539

1540

xy slice through middle of z=-350 cm showing tracks with p>1 GeV, hits from all tracks (4 out of 4 layers of microstrips)

1541

CRPP, Ottawa, Canada

Sept 23, 1991

TILE_WITH_ELECTRONICS

CONCLUSIONS

- The projective geometry and fine granularity in ϕ of the ITD microstrips enable it to provide both tracking and contribute to a level 1 trigger.

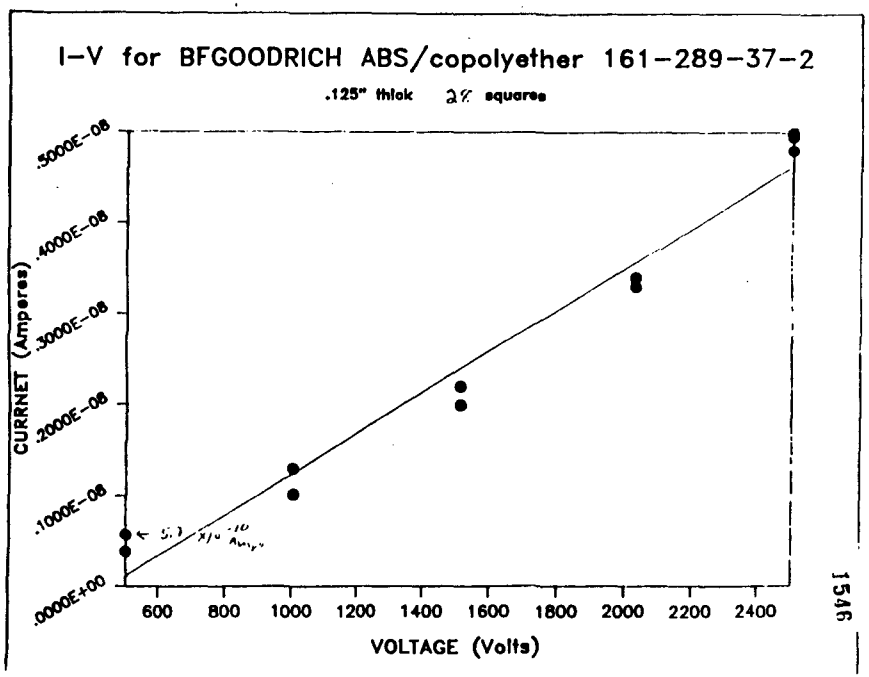
- Low occupancy (~0.03%) ⇒ hits from particular bunch-crossing can be isolated for pattern recognition.

- The ITD contribution to the level 1 trigger can be:-

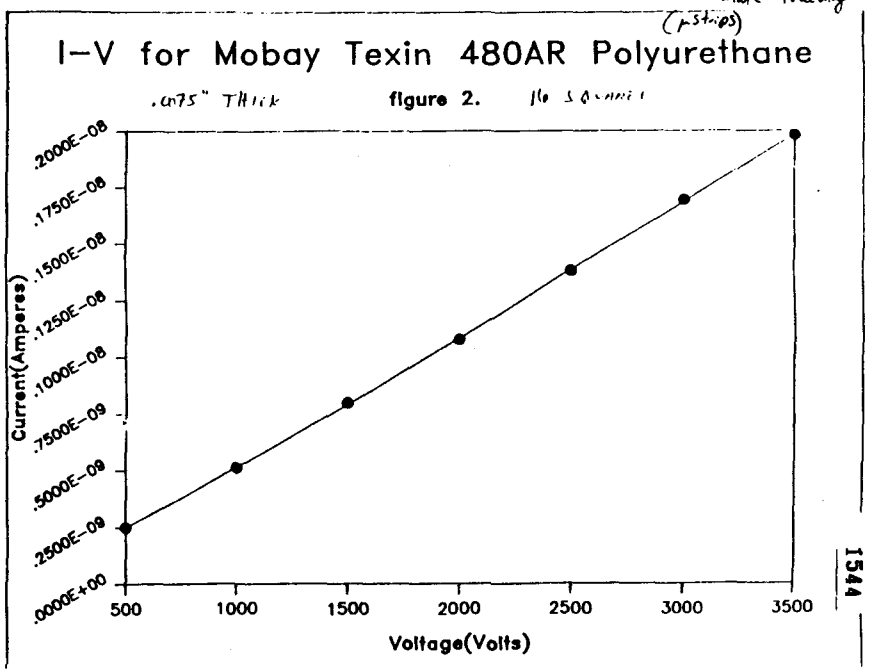
    - Close to 100% efficient at triggering on high Pt tracks.
    - Between 50% and 75% of Higgs events provide such a high Pt track.
    - The 'background' rate is typically between 1/3 and 1 MHz for L=10**33. - must be supplemented.

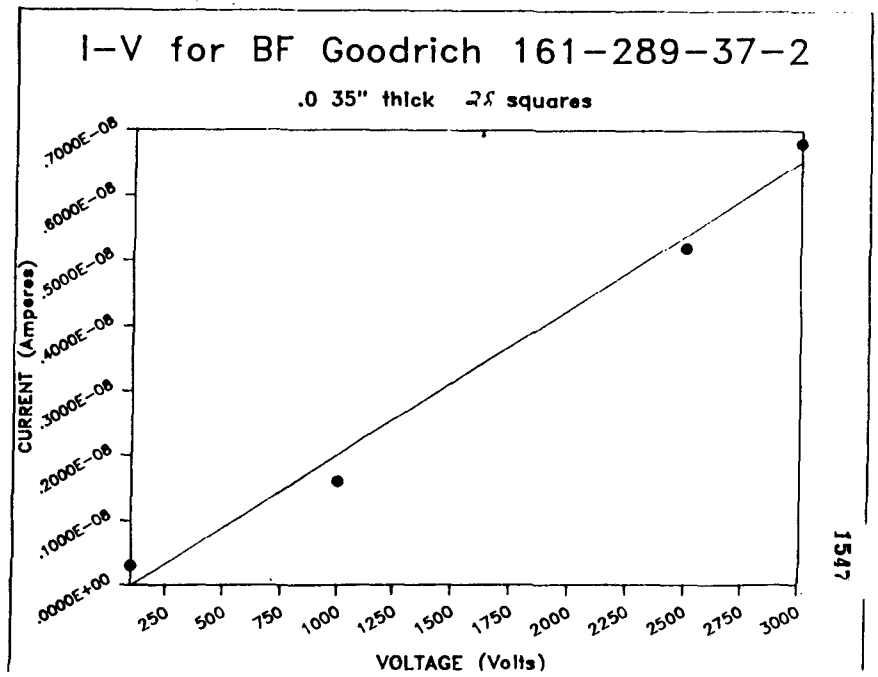
Test Results

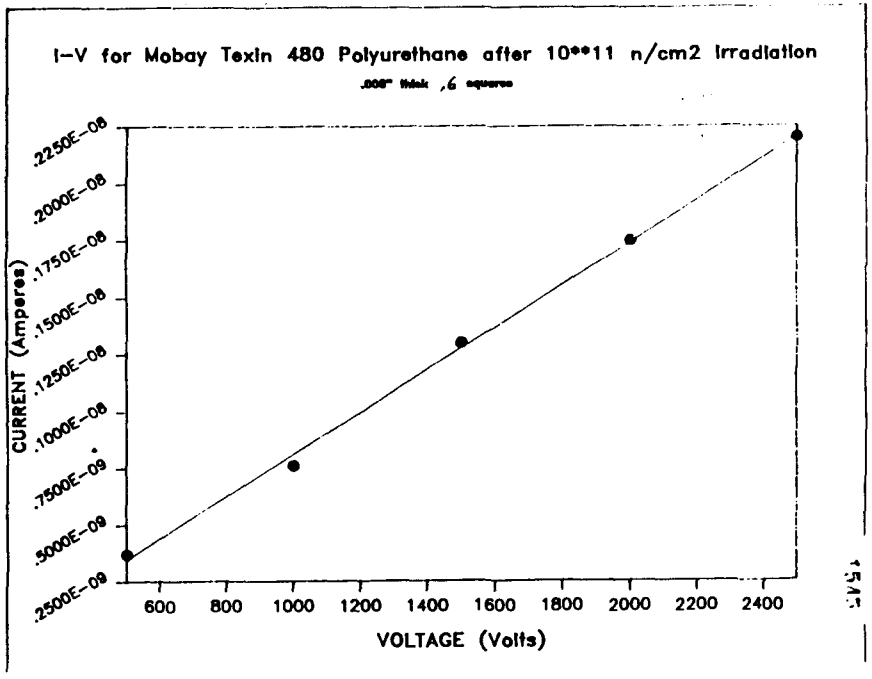
E. Barasch(TX A&M)

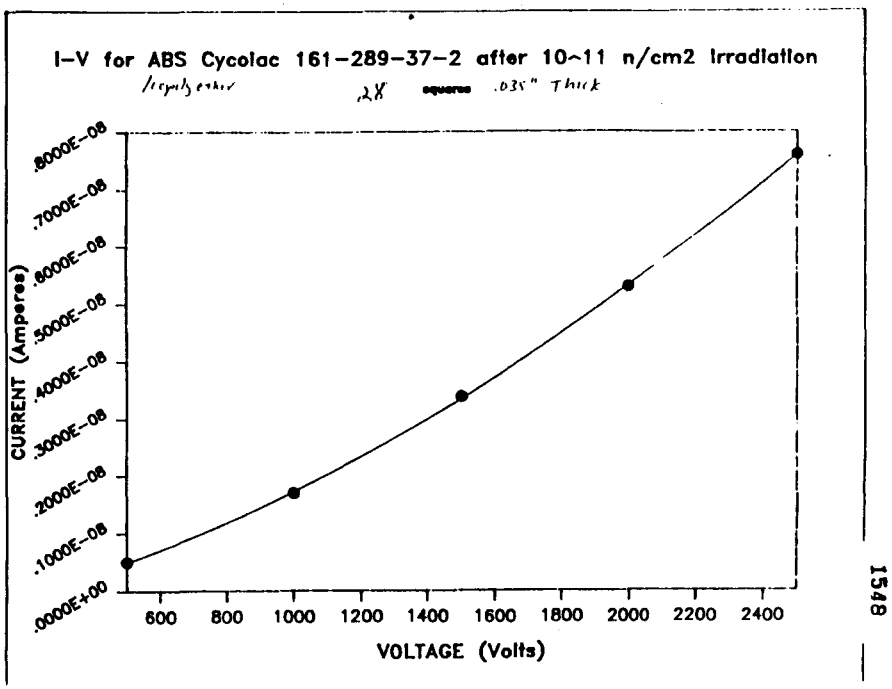


Gene Barnock
Intermediate Tracking
(μstrips)








I-V for ABS Cycolac 161-289-37-2 after 10~11 n/cm2 Irradiation
2" square .035" Thick
CURRENT (Amperes)
.8000E-08
.7000E-08
.6000E-08
.5000E-08
.4000E-08
.3000E-08
.2000E-08
.1000E-08
.0000E+00
600
800
1000
1200
1400
1600
1800
2000
2200
2400
VOLTAGE (Volts)

Gas Microstrip Chambers - Device Status

M. Dixit(Carleton)

National Research Council Canada / Conseil national de recherches Canada

FILE NO / DOSSIER NO

DATE

M. S. Dixit
27 Sept. 1991

1550

TO
A

Intermediate Tracking
Gas Microstrip Chambers - Device Status

Gaseous charged particle drift chambers with anode sense wires are severally limited in high rate environments

Maximum count rates limited by space charge effects
Also radiation damage causes aging (loss of pulse height)

In a gas μstrip chamber, the wire electrodes are replaced by alternating narrow anode strips and wider field electrode (cathode) strips printed on a near insulating substrate. Intense field at anodes causes gas multiplication.

a) Small spacing between anodes (~200μ) compared to ordinary wire chambers (~mm) results in higher precision, low occupancy.

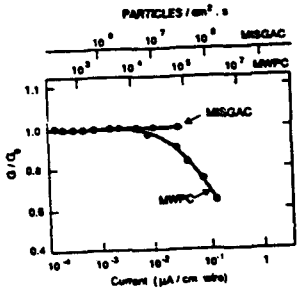
b) Very high rate capabilities without space charge limits (ions are collected at the nearby field electrodes)

c) Expected to be much less susceptible to aging and radiation damage (charge collected per unit length of electrodes is smaller due to closely spaced anode traces)

d) Electronics similar to Si μstrips. Gas gain. Cheap
First papers published Oed et al (1988) NIM
Angelini et al (1989) NIM

47 (1 8 71)

1551



gas gain vs input flux for HISGAC and standard HWPC

National Research Council Canada / Conseil national de recherches Canada

FILE NO / DOSSIER NO

DATE

1552

TO
A

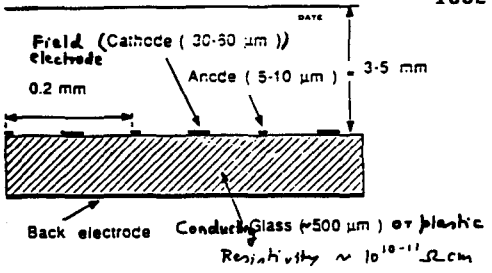


Fig. 6

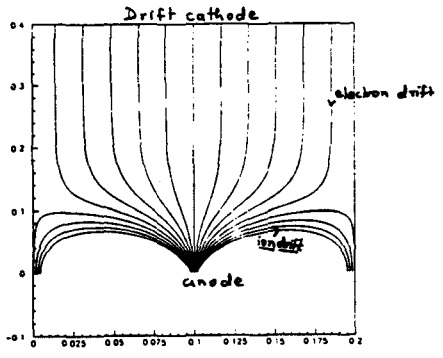


Fig. 7

National Research Council Canada / Conseil national de recherches Canada

FILE NO / DOSSIER NO

DATE

1553

TO
A

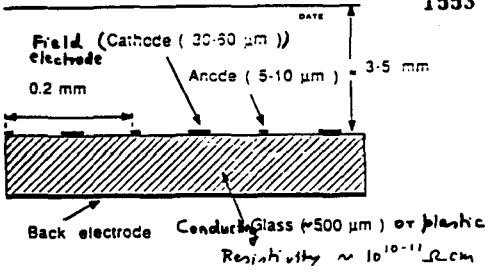


Fig. 6

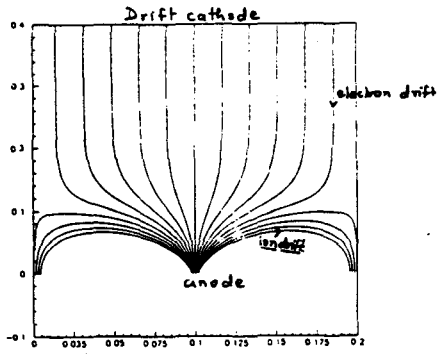


Fig. 7

TO A

Early chambers on glass and alumina showed instability due to charging of the substrate which destroys the field needed for gas multiplication

Substrates with bulk resistivity $\sim 10^{10\text{-}11}\ \Omega$cm (surface resistivity of $\sim 10^{13}\ \Omega/\square$) can dissipate stray charges landing in the gap between anode and field strip and not overheat.

Motivation for plastic substrates

i) Low mass and multiple scattering

ii) Small γ conversion

iii) can cover non planar areas or "wallpaper" large areas.

Extremely active field of research worldwide to solve the many problems in making practical large scale devices.

Lab	Recent activities
PISA (Bellazzini)	Ion implanted quartz substrate. 1100 channels at NAIR CERN – transparencies
NIKHEF (Udo)	Schot glass substrate appears to work well July 91 CERN beam tests. Study of gases for small Lorentz angle and high drift speed Xe/DME/CO_2, DME/CO_2
CERN (Sauli)	Plastic + glass chambers, rate tests – transparencies electronics (X rays)
KEK (Tanamori)	Beautiful results on Kapton on silicon with Toshiba

SDC collaborators

USA { Texas A and M, Rochester } transparencies

UK { RAL, Liverpool } transparencies

Canada { CRPP/Carleton, Montreal } transparencies

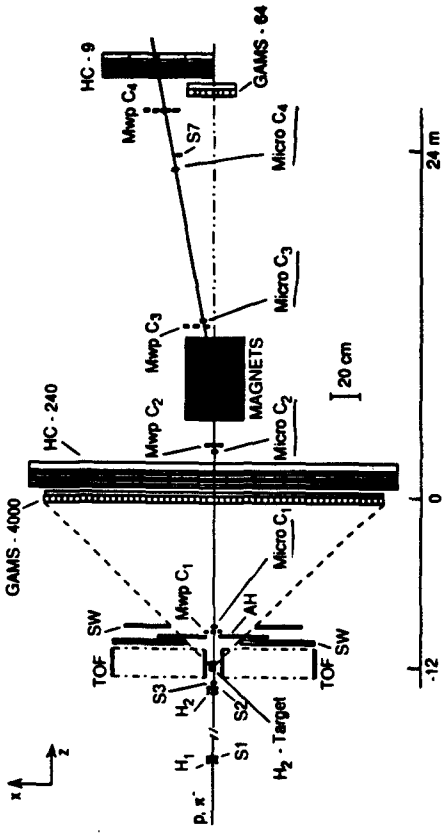


Fig. 4) Angelini et al CERN PPE/91-122

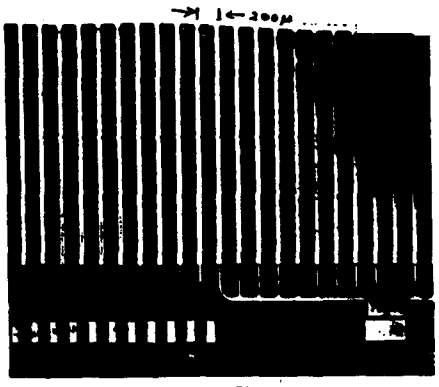


Fig. 5)

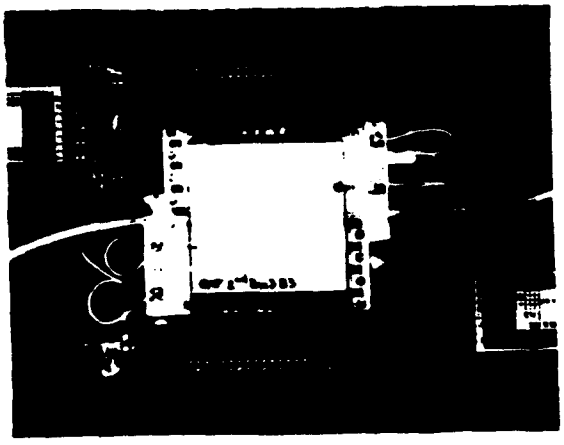
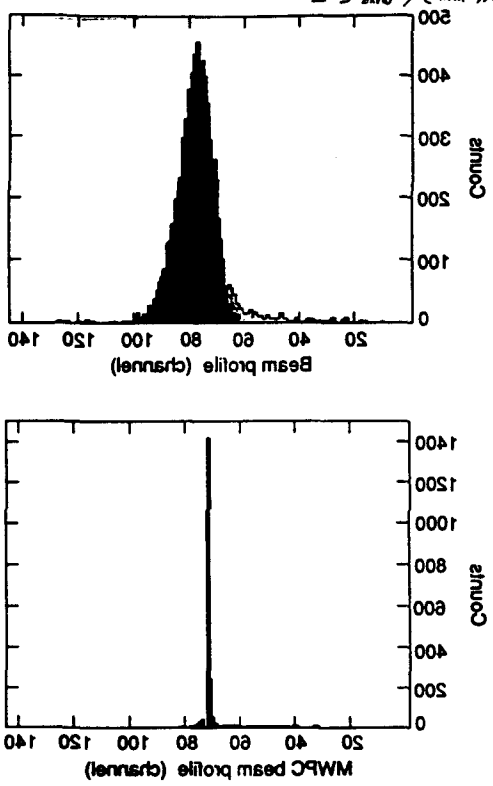


Fig. 6)

National Research Council Canada / Conseil national de recherches Canada

CERN NA12 beam test at 5×10^6/spill (2×2 mm) = 5×10^5/(mm²/sec)

1558



National Research Council Canada / Conseil national de recherches Canada

FILE NO / DOSSIER NO / DATE

1559

TO
A

CERN Tedlar chamber rate tests

Bouclier, Florent et al PPE/91-108

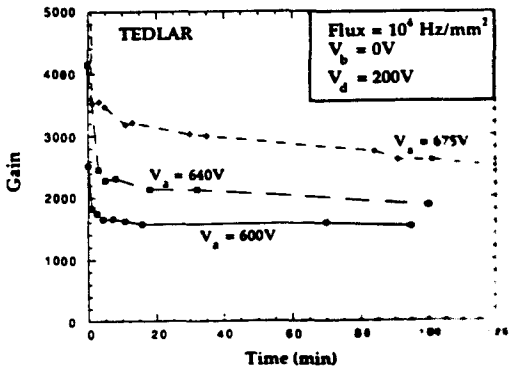
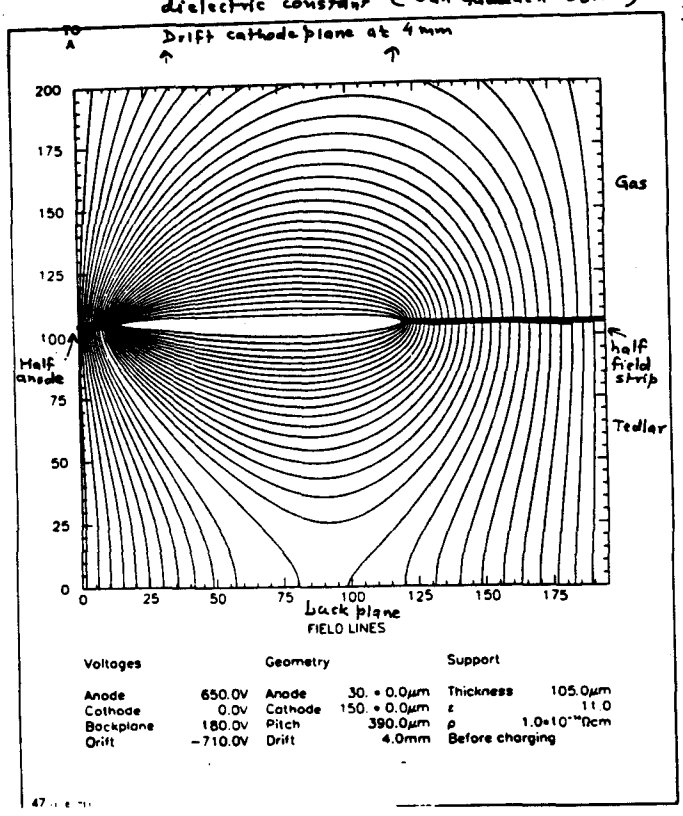


Fig. 9

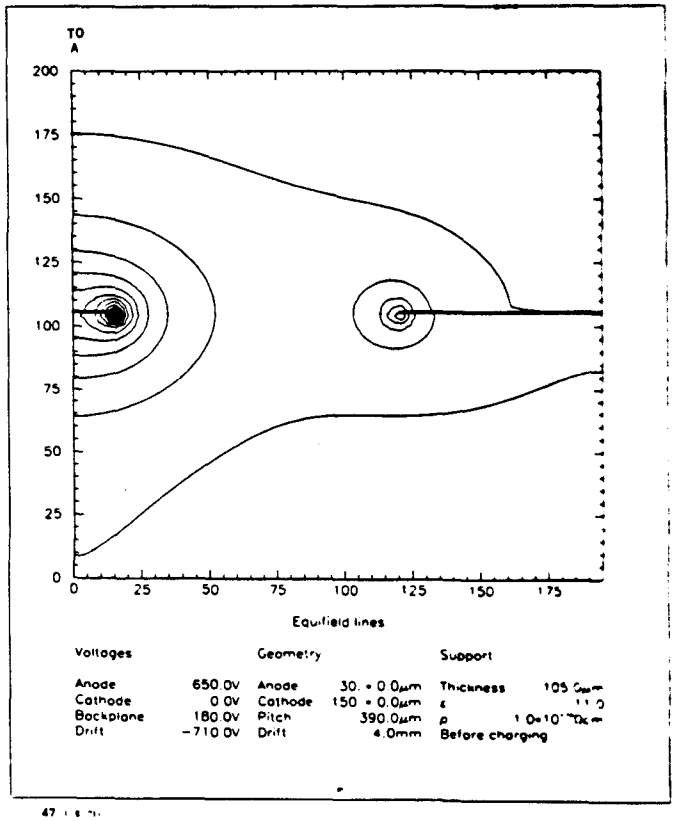
Electrostatics with finite conductivity and dielectric constant (Jan Gaudaen CERN)

1560



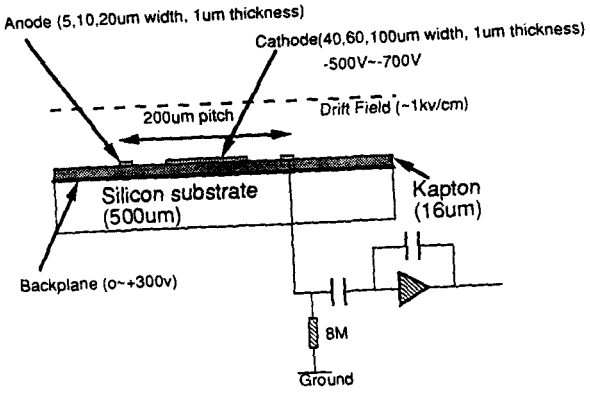
Equi-electric field lines - Tedlar chamber (Gaudaen)

1561



T. I. T. Gas Microstrip Detector

T.Tanimori



Size of Silicon Wafer , 5 inch
Material of anode, cathode Gold
Gas Argon 90%, Ethane 10%, etc.

National Research Council Canada / Conseil national de recherches Canada

TEXAS A&M UNIVERSITY

TO A

GAS MICROSTRIP CHAMBER R&D HIGHLIGHTS

1. PLASTIC SUBSTRATES

EXCELLENT PLASTIC IDENTIFIED:
- BF GOODRICH CO POLY ETHER ABS
- NO SURFACE CHARGING, OHMIC BEHAVIOR
- NO TIME CONSTANTS
- RAD-HARD

SUBSTRATE FABRICATED
- EXCELLENT METH. ADHESION

LARGE-AREA LITHOGRAPHY (300 μm ANODE PITCH)
- ~m² CHAMBERS

2. HIGH RESOLUTION CHAMBERS

75 μm PITCH PILLAR GEOMETRY (SI)
IMMUNE TO SURFACE BREAKDOWN, DIELECTRIC EFFECTS

3. READOUT ELECTRONICS

CMOS SYNCHRONOUS-BUFFERED FRONT END
- READ, HSPICE COMPLETE
- 2-CLOCK CYCLE RECOVERY
- MOSIS RUN THIS FALL

National Research Council Canada / Conseil national de recherches Canada

Plastic Texas A&M

MPI Radiation-Cured Coating on various plastics

TO A

Material

Ω/□

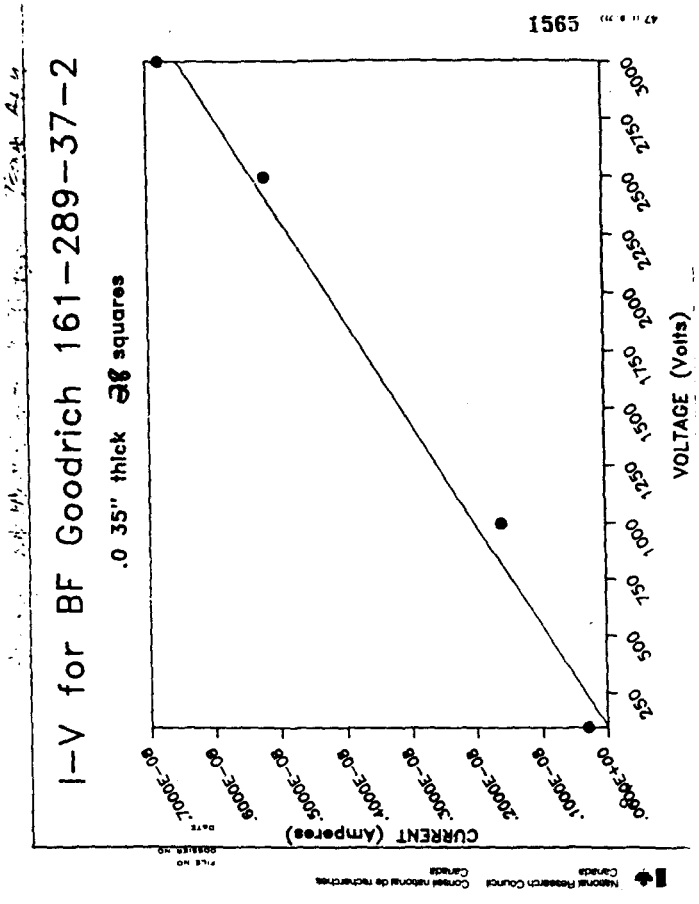
Material		Gage-Mils	Mode	Ohms/Sq @ 100V
Ionomer		4	Coated	6.0 x 10⁹ ~ 10⁹
			Back	6.0 x 10⁹ ~ 10⁹
		7.5	Coated	6.0 x 10¹⁰ ~ 10¹⁰
			Back	1.0 x 10¹² ~ 10¹²
Vinyl	Vinyl	6	Coated (1)	2.1 x 10¹¹ ~ 10¹¹
			Back	3.2 x 10¹¹ ~ 10¹¹
	Vinyl	7.5	Coated (1)	5.0 x 10⁹ ~ 10⁹
			Back	5.7 x 10¹⁰ ~ 10¹⁰
	Vinyl	10	Coated (1)	1.4 x 10¹⁰ ~ 10¹⁰
			Back	9.4 x 10¹⁰ ~ 10¹⁰
Polyimide	Polyimide	1	Coated (2)	2.3 x 10¹⁰ (3) ~ 10¹⁰
			Back	5.0 x 10¹¹ ~ 10¹¹
Low Density Polyethylene	LLDPE	4	Coated	3.3 x 10⁹ (3) ~ 10⁹
			Back	6.6 x 10¹⁰ ~ 10¹⁰
	LDPE	10	Coated	6.0 x 10¹⁰ (3) ~ 10¹⁰
			Back	3.5 x 10¹¹ ~ 10¹¹
Linear LDPE	LLDPE	4	Coated	1.0 x 10⁹ ~ 10⁹
			Back	4.2 x 10⁹ ~ 10⁹
Polyester	Polyester	0.5	Coated (2)	1.0 x 10¹⁰ (4) ~ 10¹⁰
			Back	8.3 x 10¹¹ ~ 10¹¹
	Polyester	3	Coated (2)	5.4 x 10¹⁰ ~ 10¹⁰
			Back	2.7 x 10¹² ~ 10¹²

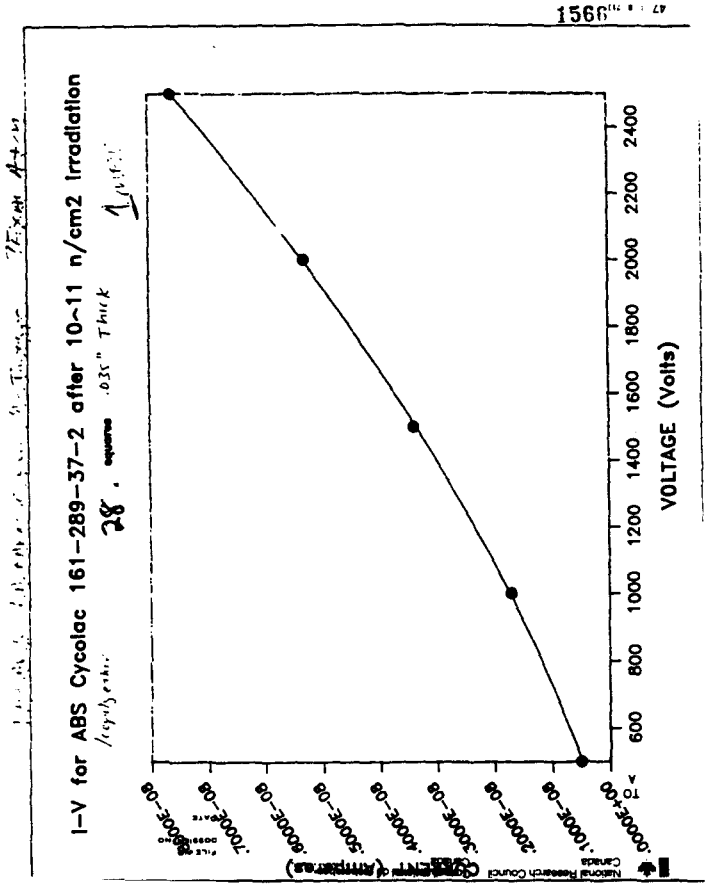
(1) Flexibilized coating
(2) Reduced anti-stat concentration
(3) After 48 hours at 12 percent RH
(4) After 24 hours at 8 percent RH

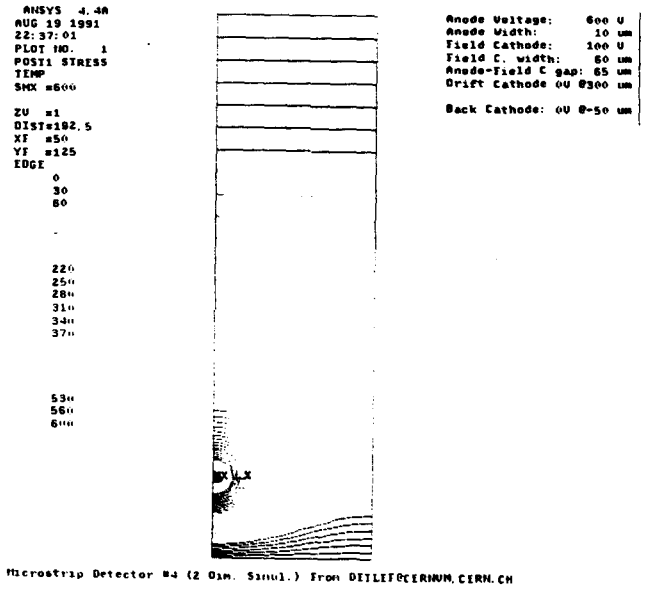
Table 2. EB Static Dissipative Coatings on Clear Plastic Films.

Nominal ~ 10^{11} Ω/□ , 100μm - 200μm thickness

(range from 10^{8} - 10^{12} ...)







National Research Council Canada

U.K.

TO A

RAL μstrip R and D

6 cm x1 cm working devices on tempex glass

bussed anodes and cathodes

300μ pitch

Stable gain 2 hours from turn on

No dependence of gain on rates seen

Cosmic ray tests with CF_4 based gases in progress

Working toward 20 x15 cm devices

Liverpool

Silicon based devices

Emphasis on built inline limiting resistors, built in electronics

Next RAL 300μ pitch chambers will be tested at Liverpool with individual anode readout.

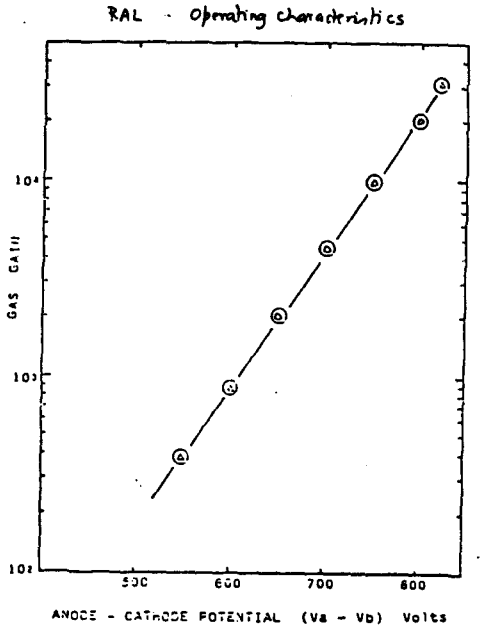
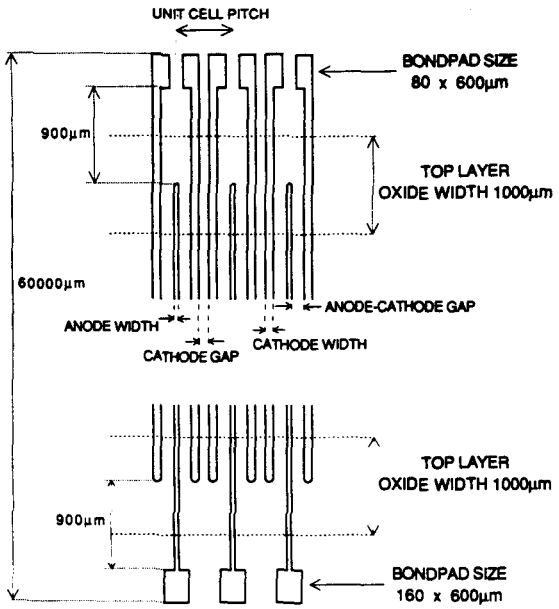


Figure 4

Gas gain curve measured in the test detector with a gas filling of argon + 23% isobutane (Vc = 500V, Vb = 0V).

It will be noted that gas gains greater than 10000 are achieved.

CATHODE READOUT END.



ANODE READOUT END.

	1	2	3	4	5
unit cell pitch	200µm	200µm	200µm	200µm	100µm
cathode gap	10µm	10µm	10µm	8µm	-----
cathode width	30µm	30µm	30µm	35µm	26µm
anode width	10µm	8µm	6µm	8µm	6µm
anode-cathode gap	60µm	61µm	62µm	57µm	34µm

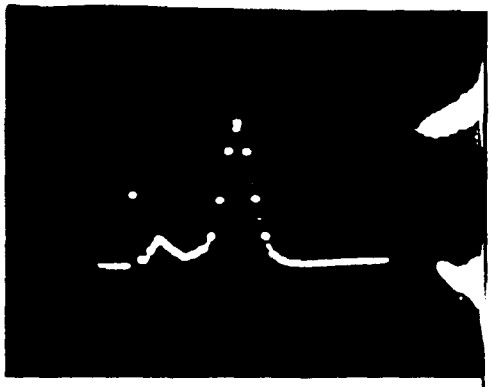
NB LHC dimensions!

National Research Council Canada / Conseil national de recherches Canada

Oct. 13, 1991
Ottawa

TO
A

Tedlar 400µ chamber Fe^{55} test



Fe^{55} Argon escape peak at 2.95 keV and at 5.9 keV are seen.

Peak	Energy (keV)	Peak A Channel number
Escape Peak	2.95	
Fe^{55}	5.9	

National Research Council Canada / Conseil national de recherches Canada

FILE NO / DOSSIER NO

Microstrip Work in Ottawa DATE

TO
A

1) CERN design tedlar chambers operational. Fe^{55} tests systematic study to follow.

2) Precision lithography on plastic comparable to that available for silicon and glass. Development project with PPM, Montreal (in collaboration with Sauli group at CERN) - In progress

3) Electrostatics of keystone µstrip geometry (Garfield - no dielectrics)

Field strip width	70µ	105µ	140µ
Anode field (kV/cm)	171.9	172.9	173.8

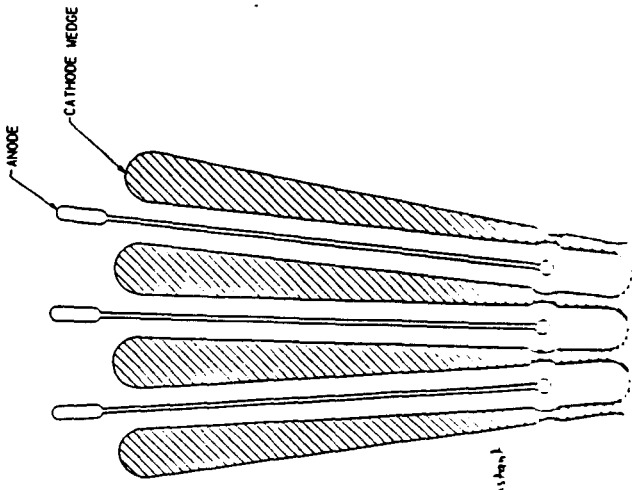
~1% change in surface field for 100% change in field strip width.

Other issues of interest

Individual anodes
Wire bonding
Electronics
Rate tests
Radiation damage — In collaboration with TRIUMF, Canada

University of Montreal

Interest in silicon based gas µstrip chamber substrates



ARRANGEMENT FOR RADIAL DETECTOR

Keystone geometry
Anode = constant width
ap (anode-field strip) constant
Variable width field strip
Anode fan radially

DATE
ON REQUEST
ON DEMANDE

National Research Council Canada / Conseil national de recherches Canada

11

Summary

TO
A

Working devices at many labs RAL, NIKHEF, INFN, CERN, OTTAWA and others

1100 channel HEP experiment at CERN (NA11) uses ion implanted quartz and appears to run reliably to rates ~ $5 \times 10^5/(mm^2\ sec)$

However, rate effects not understood for all substrates
Search for suitable substrates in plastics/other materials continues. Substrate search mainly by Texas A&M and Rochester. Radiation damage to substrate
Electrostatics and optimized operating points need to be better understood

Individual anode read out, wire bonding not understood for all substrates
Choice of metallization (gold - versus aluminum)
Choice of gas, aging studies all need to be done

Printing on plastics accurately, construction of large devices all need added effort.
Detailed layout of realistic devices
Much progress has been made, but much remains to be done.

TO
A

Gas Microstrip Chambers - Device Status

Gaseous charged particle drift chambers with anode sense wires are severally limited in high rate environments

Maximum count rates limited by space charge effects
Also radiation damage causes aging (loss of pulse height)

In a gas μstrip chamber, the wire electrodes are replaced by alternating narrow anode strips and wider field electrode (cathode) strips printed on a near insulating substrate. Intense field at anodes causes gas multiplication.

a) Small spacing between anodes (~ 200μ) compared to ordinary wire chambers (~ mm) results in higher precision, low occupancy.

b) Very high rate capabilities without space charge limits (ions are collected at the nearby field electrodes)

c) Expected to be much less susceptible to aging and radiation damage (charge collected per unit length of electrodes is smaller due to closely spaced anode traces)

d) Electronics similar to Si μstrips. Gas gain. Cheap
First papers published Oed et al (1988) NIM
Angelini et al (1989) NIM

Layout, Material, and Tracking Length Considerations for the Intermediate Angle Region

A. Sill(Rochester)

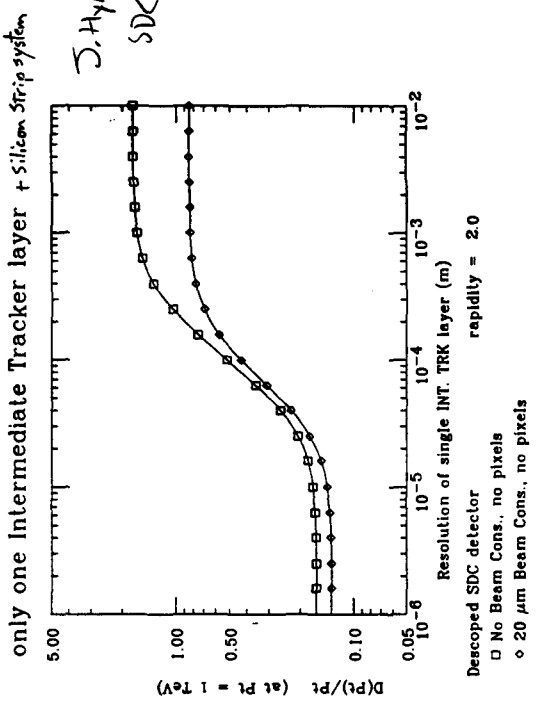
1577

Layout, Material, and Tracking Length Considerations for the Intermediate Angle Region.

A. Sill, U. of Rochester
Oak Ridge SDC Meeting
27 Sept 91
Tracking Review Session

1578

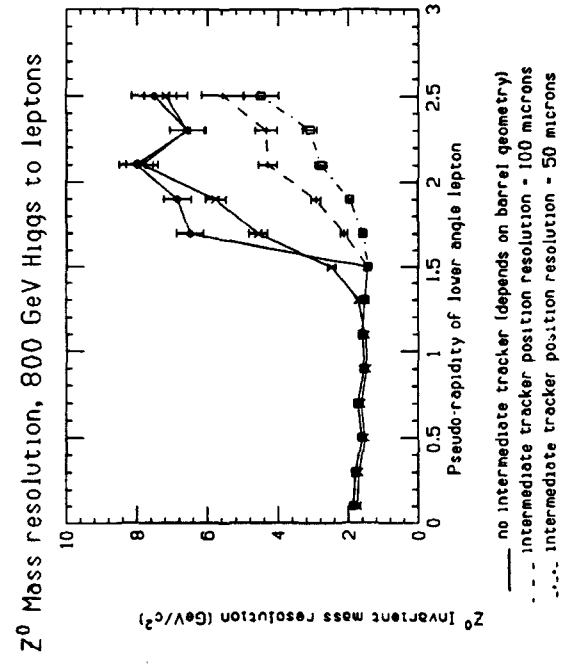
J. Hylen SDC



FEB-10-'91 19:42 ID:FERMILAB-CIF TEL NO:708-840-2968 #466 P02

1579

J. Hylen SDC



J. Hylen SDC

1580

CONCLUSIONS: (Generic)

- Intermediate angle tracker should have superlayer position resolution ~ 50 μm to match silicon strip system.
- With said intermediate angle tracker, $\sigma_{M_{4\ell}}$ is close to the natural limit from the Z^0 width for 300 GeV Higgs → ZZ → llll
- Should intermediate angle tracker measure R as well as φ? Not necessary for best momentum resolution, but useful for invariant mass resolution.
- Bremsstrahlung imparts long tail on tracking resolution for electrons.

J. Mathews (SDC) Need [illegible] good $P_\perp$ cut [illegible] trigger. Need to measure φ well & more cavalierly.

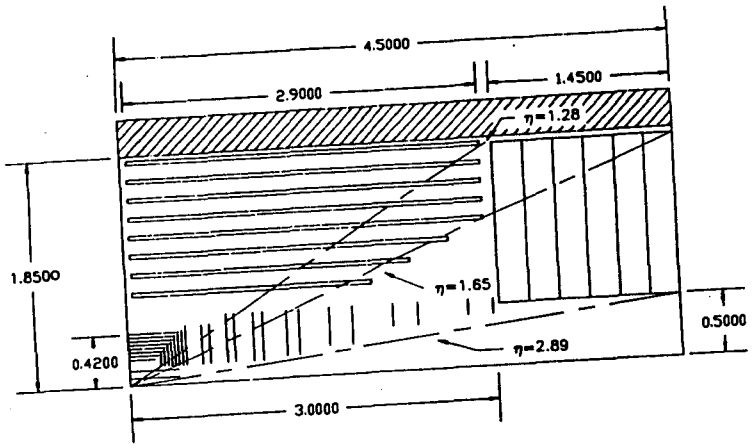
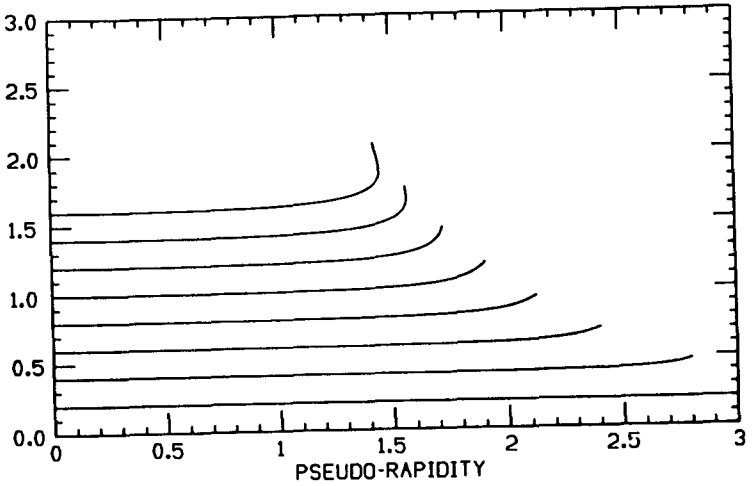


Fig. 1. Conceptual design for a pixel, silicon strip, and wire chamber tracking system for a solenoidal detector.

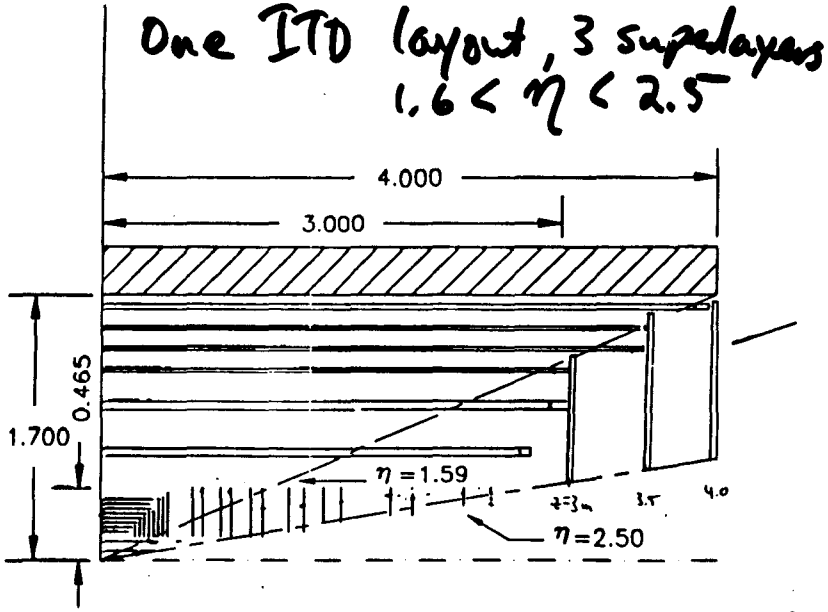
LOI 4 radial wire ITD

1553



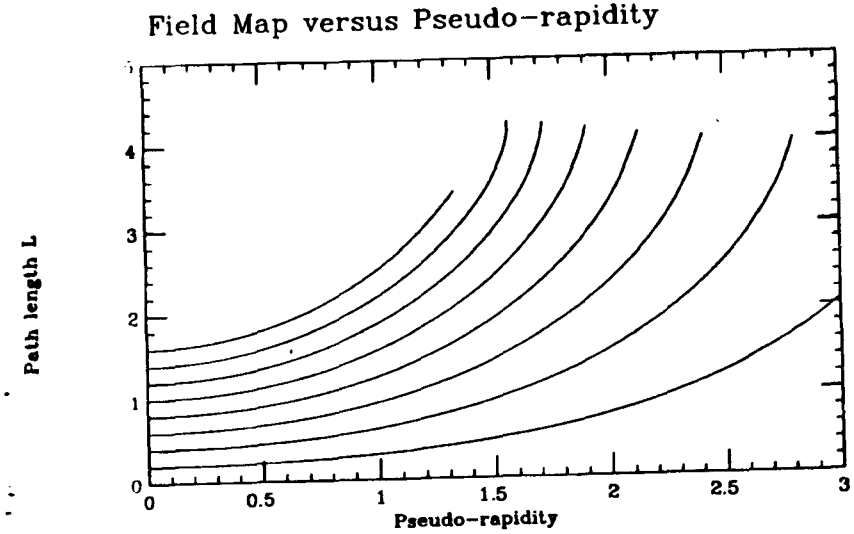
1591

One ITD layout, 3 superlayers
$1.6 < \eta < 2.5$

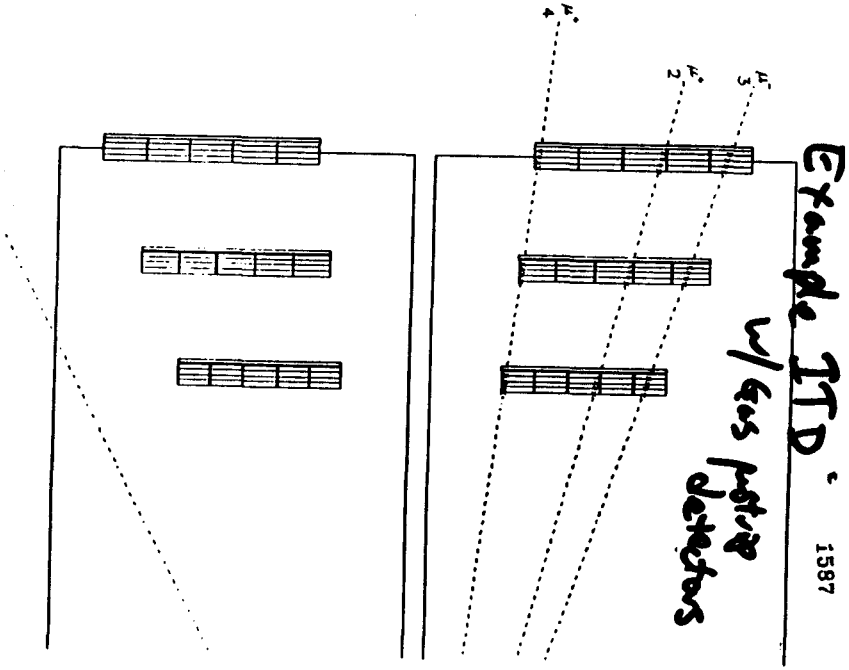


1584

(LBL meeting example)

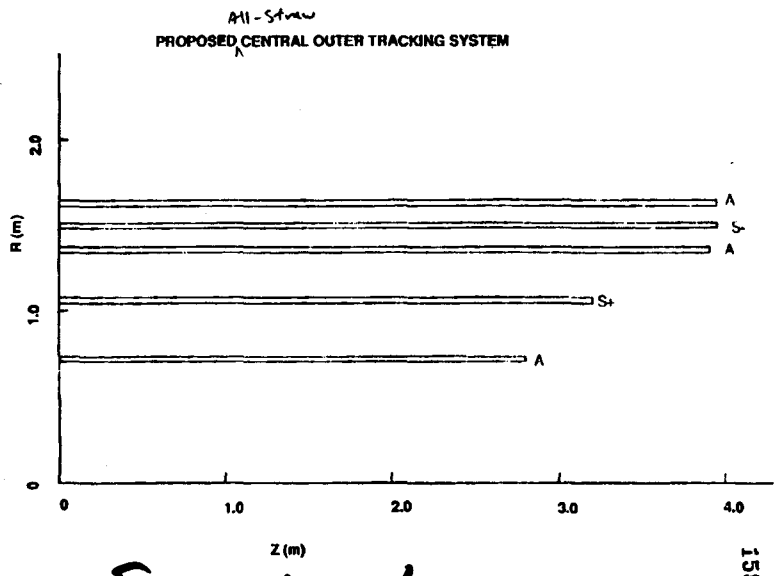


1582



Example ITD w/ Gas tube detectors

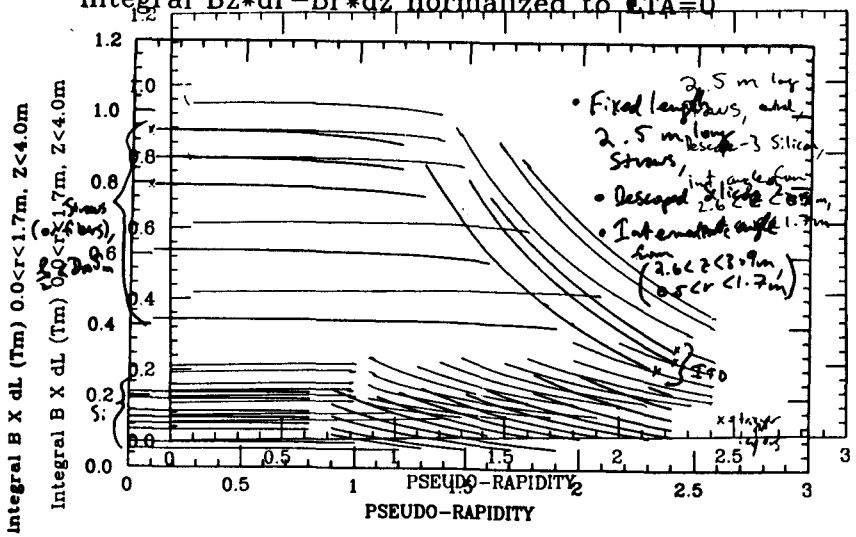
1587



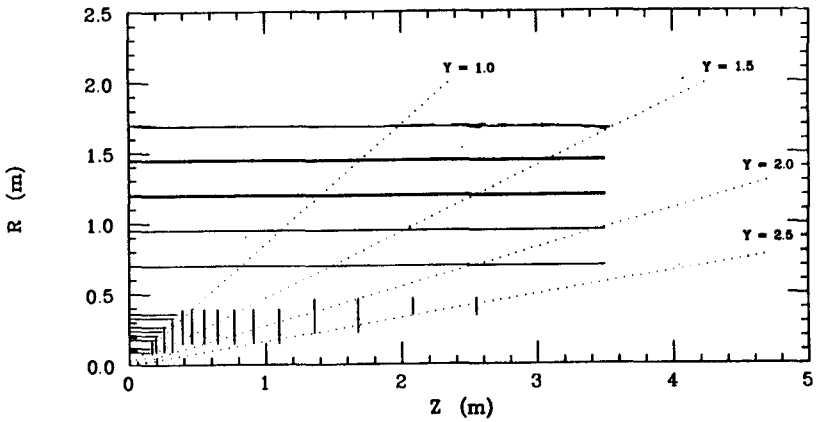
Example S:/All-straw barrel

1585

"Log like" layout



1588



Example S:/Sci-fi

1586

"Example" w/ η_{barrel} = 1.1

```
C     SSC Solenoid path MAP
      OPEN(unit=29,file='path2.THP',status='NEW')
      CALL MAP              ! PLOT field LINES versus path length

C
C     Call to plot integral path length is for (rmin, rmax, zmin, zmax):
C     First call to set normalizations over full range of interest
C     (always do this, even though it doesn't plot anything!!
C
      CALL path(0.0,1.7,0.0,4.0) ! INTEGRAL PATH for full region 1.7m at eta=0

C     Now call PATH for the components of the detector of interest:
C     Note subroutine PATH always integrates from the origin in this version!

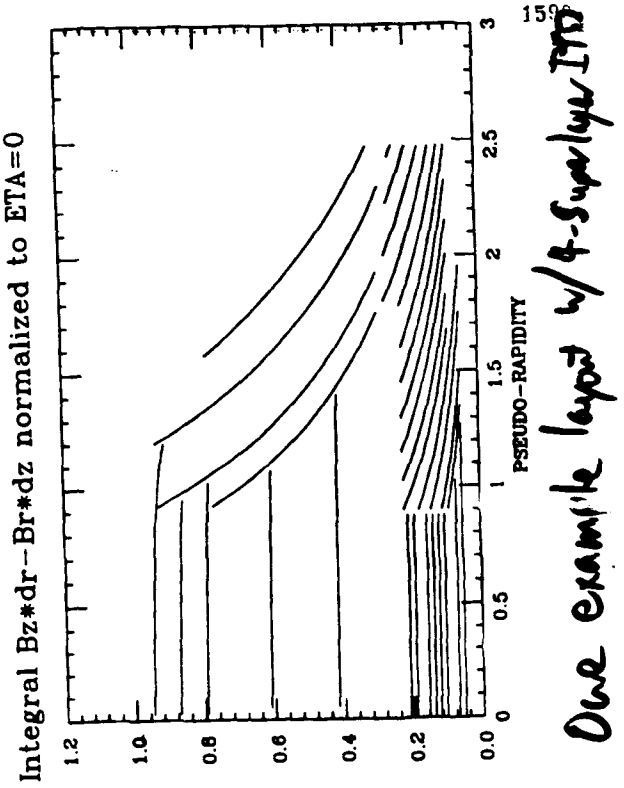
      CALL path(0.09,0.09,0.0,0.15) ! INTEGRAL PATH for silicon barrel layer 1
      CALL path(0.12,0.12,0.0,0.15) ! INTEGRAL PATH for silicon barrel layer 2
      CALL path(0.18,0.18,0.0,0.18) ! INTEGRAL PATH for silicon barrel layer 3
      CALL path(0.21,0.21,0.0,0.21) ! INTEGRAL PATH for silicon barrel layer 4
      CALL path(0.24,0.24,0.0,0.24) ! INTEGRAL PATH for silicon barrel layer 5
      CALL path(0.27,0.27,0.0,0.27) ! INTEGRAL PATH for silicon barrel layer 6
      CALL path(0.33,0.33,0.0,0.33) ! INTEGRAL PATH for silicon barrel layer 7
      CALL path(0.36,0.36,0.0,0.36) ! INTEGRAL PATH for silicon barrel layer 8

      CALL path(0.09,0.165,0.165,0.165) ! INTEGRAL PATH for silicon disk layer 1
      CALL path(0.09,0.195,0.195,0.195) ! INTEGRAL PATH for silicon disk layer 2
      CALL path(0.09,0.255,0.255,0.255) ! INTEGRAL PATH for silicon disk layer 3
      CALL path(0.08,0.315,0.315,0.315) ! INTEGRAL PATH for silicon disk layer 4
      CALL path(0.15,0.390,0.390,0.390) ! INTEGRAL PATH for silicon disk layer 5
      CALL path(0.15,0.390,0.460,0.460) ! INTEGRAL PATH for silicon disk layer 6
      CALL path(0.15,0.390,0.550,0.550) ! INTEGRAL PATH for silicon disk layer 7
      CALL path(0.15,0.390,0.650,0.650) ! INTEGRAL PATH for silicon disk layer 8
      CALL path(0.15,0.390,0.770,0.770) ! INTEGRAL PATH for silicon disk layer 9
      CALL path(0.15,0.390,0.910,0.91) ! INTEGRAL PATH for silicon disk layer 10
      CALL path(0.15,0.390,1.10,1.10)  ! INTEGRAL PATH for silicon disk layer 11
      CALL path(0.225,0.465,1.36,1.36) ! INTEGRAL PATH for silicon disk layer 12
      CALL path(0.225,0.465,1.68,1.68) ! INTEGRAL PATH for silicon disk layer 13
      CALL path(0.225,0.465,2.08,2.08) ! INTEGRAL PATH for silicon disk layer 14
      CALL path(0.225,0.465,2.55,2.55) ! INTEGRAL PATH for silicon disk layer 15

      CALL path(0.708,0.711,0.03,1.35) ! INTEGRAL PATH for central straw layer 1
      CALL path(1.040,1.043,0.03,1.35) ! INTEGRAL PATH for central straw layer 2
      CALL path(1.350,1.354,0.03,1.65) ! INTEGRAL PATH for central straw layer 3
      CALL path(1.480,1.483,0.03,1.65) ! INTEGRAL PATH for central straw layer 4
      CALL path(1.610,1.614,0.03,2.45) ! INTEGRAL PATH for central straw layer 5

!     CALL path(0.5,0.7,0.72,0.73)  !INTEGRAL PATH for intermediate ustrip lyr 1
      CALL path(0.5,1.345,1.4,1.41) !INTEGRAL PATH for intermediate ustrip lyr 2
      CALL path(0.5,1.600,1.7,1.71) !INTEGRAL PATH for intermediate ustrip lyr 3
      CALL path(0.5,1.700,2.5,2.51) !INTEGRAL PATH for intermediate ustrip lyr 4
      CALL path(0.5,1.600,3.9,3.91) !INTEGRAL PATH for intermediate ustrip lyr 5
```

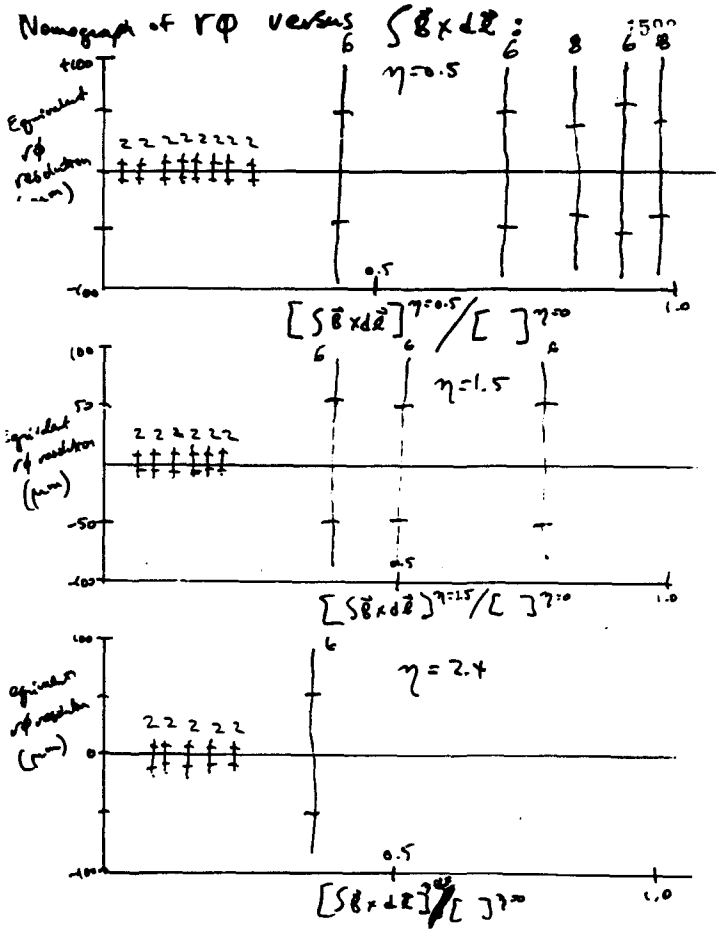
1.7m



Our example layout w/4-superlayer ITD

Integral B X dL (Tm) 0.0<r<1.7m, Z<4.0m

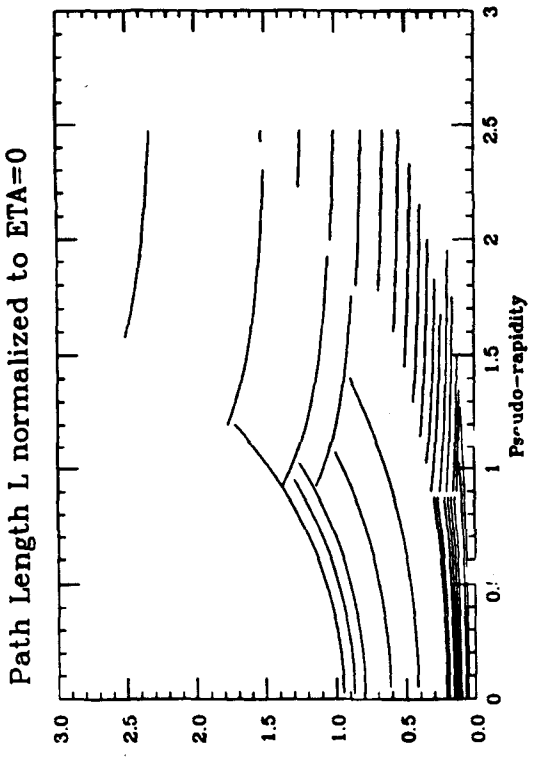
Nomograph of rφ versus $\int B \times dL$:



$[\int B \times dL]^{\eta=0.5} / [\ ]^{\eta=\infty}$

$[\int B \times dL]^{\eta=1.5} / [\ ]^{\eta=\infty}$

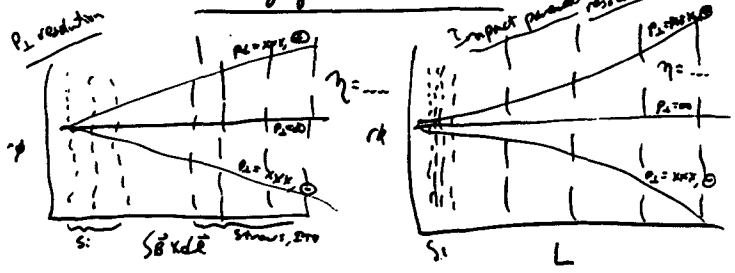
$[\int B \times dL] / [\ ]^{\eta=\infty}$



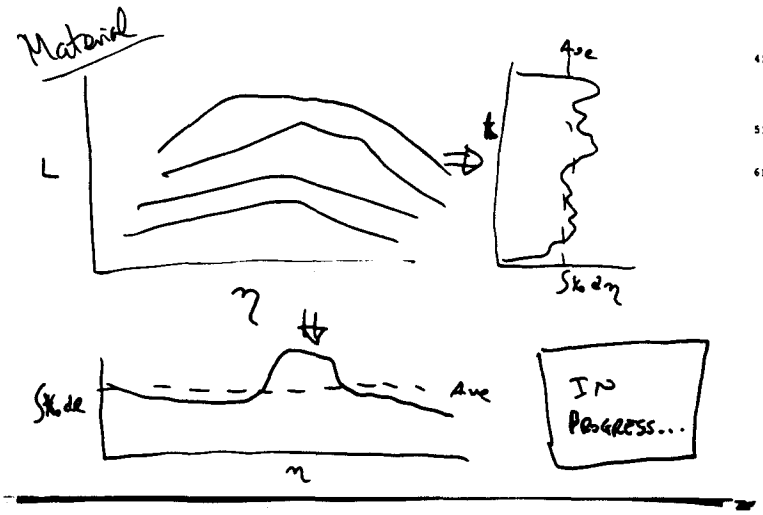
Path length L for 0.0<r<1.7m, z<4.0m

our particular (example) design

Nomographs to make:



... Also Plots to make:



1593

Material:

1594

From: F2UVAX::UNMB::LA[illegible]::MATTHEWS "John A.J. Matthews/Univ. of New Mexico - LANL" 29-Al
To: UNMB::1226::47454::ALANSILL
CC: MATTHEWS
Subj: RE: talk at Oak Ridge

Alan,

Here was a naieve model for tracking material; with the 1.7m radius "decided" the outer tracking material should probably extend to 165 cm, the coil should be at a slightly larger radius etc.

Cheers, John

Task Force on Impact of Material in Tracking Volume

As the tracking system will descope from the "engineering baseline design", an estimate of the material in a possible "descoped" tracker is:

1)	"internal bremsstrahlung"	r = 0 cm	all eta	δX_0 = 2.5%
2)	"beam pipe"	r = 5 cm	all eta	δX_0 = 0.2%/sin(theta)
3)	"silicon"	r = 10 - 45 cm	theta > pi/4 theta < pi/4	δX_0 = 5.0%/sin(theta) δX_0 = 5.0%/cos(theta)
	"outer shell"	r = 60 cm	all eta	δX_0 = 0.5%/sin(theta)
4)	"outer tracker"	r = 70 - 155 cm	eta < 1.5 eta > 1.5	δX_0 = 6.0%/sin(theta) δX_0 = [illegible]
5)	"coil center"	r = 180 cm	(use B = 2 T to this radius)	
6)	"EM Color front"	r = 205 cm	(for e/gamma match at central rapidity)	

B-Field Considerations:

1595

From: FNAL::FNALD::KEPHART 20-SEP-1991 18:10:29.07
To: FNAL::URHEP::ALANSILL
CC:
Subj: RE: Field map for SDC solenoid

Alan,

We have assumed a 4 m half length for tracking. For calorimeter designs with flat endwalls (ie non uniform fields) 3.87 m is a reasonable guess as to how long we can make the superconducting current sheet. Moreover, we have not been able to come up with a plausible scheme for raising the field integrals in the region of the intermediate tracker for such a design....eg we looked at extra windings near the end, graded current sheets, and various trim coil options....if one puts enough current in these to be effective, then nasty things happen to the coil forces, field uniformity, and the amount of material near the end of the coil. Solutions with reentrant steel look much better in terms of field integral in this region since one can raise the field to 2 T essentially everywhere in the tracking volume. However, in this case either one must lengthen the calorimeter by about half a meter or shorten the tracking half length by this amount. The calorimeter guys say the .5 m length increase is not all that expensive since the actual volume of calorimeter doesn't change all that much and the tower count doesn't change at all. The muon guys like this design since it give them more integral Bdl. As far as the actual construction cost of the coil is concerned, the costs scale linearly with the length. However, since a significant part of the cost is engineering, refrigeration systems, transfer lines, etc and these costs are roughly independent of length, the actual cost dependence is slower than linear. Bottom line is that coil cost vs length for small changes +/- 0.5 M is not an issue.

Hope this helps,
Bob

1596

SDC Intermediate Tracking

Conclusions:

ETA COVERAGE:

- Material optimizes at 45 degrees (eta = 0.86)
- Track considerations push optimum breakpoint slightly further out to perhaps 60 degrees
- Best eta break point in the range near eta=1.2 to 1.4

TRIGGER:

- Trigger possible over most of the natural intermediate tracking range from eta=1.4 to eta=2.5
- Integral B x dl tapers off in rapidity due to available tracking volume length
- Beyond eta=2, performance is limited.
- Performance is best with 4 superlayers.

TRACKING LENGTH:

- **4.0 meters minimum length recommended (non-reentrant endcaps). Performance is definitely compromised below this value!!!**

Conclusions cont'd:

- $\int \vec{B} \times d\vec{l}$, path length, resolution can be studied w/ analytical methods to give useful input into the process of placement & # of superlayers both central & intermediate.
- Shorter straws, fibers ⇒ lower occupancy (1.4 → 3.2 m for $\eta_{max\ point} = 1.4$)
- Use limited # of lengths to give inputs to the material budget from the ends of the central outer tracker that are the least possible (⇒ lower η) and that do not line up on equal-η boundaries. (Neither do they spread out too far over η, since they occur in "lumps"). Further details to be studied.

Work on ITD

J. Dainton(Liverpool)

Work on ITD

1599

J. B. Dainton
Liverpool

μstrip devices	Liverpool RAL	Canada	Texas	Rochester New Mexico
radial/tilted radial wires	✓			
μstrip manufacture				
substrate	Si glass	plastic (CERN)	Si plastic	plastic glass
electrodes	Al	Al (CERN)	✓	
connections	✓	✓ (CERN)	✓	
lithography	EBL Keystone SDC file	✓	✓	
μstrip testing				
Fe^{55} + comic	✓	✓	✓	
ageing	✓	✓		
rate	✓	✓	✓	
gas	✓	✓	✓	
μstrip operation + simul^n	✓	✓	✓	✓

→ SDC-ITD-μstrip-proof-of-principle ≤ fall 1992
+ i/p to design concept document → TP

1600

SDC ITD μstrips	Liverpool RAL	Canada	Texas	Rochester New Mexico
SDC μstrip ITD				
layout + physics simul^n	✓	✓	✓	
layout engineering	✓	✓		
production engineering	✓	✓		
assembly (incl tests)				
precision				
gas				
cables				✓ tech transfer + $s LANL
FE electronics	✓ + Oxf?	✓	✓	
bigger electronics	✓ + Oxf?	✓		

→ TP
development + production + construction

Costings (a bed of nails)^3

1601

	ITD costing US		ITD costing UK
	$ US	Canada	£ UK
tiles (5000)	3.0 M$		1.8M
labor + manag^t	4M		MYs
FE electronics (2M ch) (det. dependt)	1M		0.6M
read-out (det. dependt)	0.8M		0.5M
mechanical support	6.2M		1.8M + MYs
(trigger)	(1.5M)		(0.6M + MYs
(DAQ electronics)	(? M)		(? M)
	15M		4.7M
	(+ 1.5M + ?)		(+ 0.6M + m + MYs)

Speculative! MYs ≡ lab + univ man years

1602

Funding

	bid	answer
Canada $? M	Oct. 92	April 93 KAON?
UK $? M	≥ April 93	≥ April 93 LHC?
US $?		

NB all funding is very unclear and speculative

0 ≤ get ≤ request

Time Scales

i/p : Canada + RAL + Liverpool
still to be really evaluated
preliminary (very)
funding + MY dependent

strip device proof of principle	≥ fall 1992
full scale prototypes	1993 - 1995
full scale engineering design	1991 →
production engineering	1991 →
construction	1995 → 1998
installation	1998

M. EDWARDS RAL (2)

SDC ITD Workshop

Friday Oct 25th

Saturday Oct 26th

Sunday Oct 27th

Cosener's House, Abingdon, England

Contact Mike Edwards @ RAL

ME @ UK.AC.RL.IB (JANET)

ALL WELCOME

PLANS

FALL 1991

1/ FOUND mass ✓ STABLE, THIN ! SUBSTRATES →
2/ CHOSEN OPTIMUM METALISATION THICKNESS.
3/ DEVELOPED BONDING TECHNIQUE. → ✓
4/ FIRST LARGE AREA (200 x 150 MM) PLATES →
5/ FIRST PULSE SHAPE FROM MIN. I. PARTICLES → ✓
6/ FIRST MEASUREMENTS OF EFFICIENCY beg Oct
7/ FIRST LAYOUT DRAWINGS. →

SUMMER 1992

"PROOF OF PRINCIPLE"

1/ DEMONSTRATED RAD. HARDNESS & AGEING.
2/ CHOSEN OPTIMUM METALISATION METAL AND GAS
3/ WORKING LARGE AREA, THIN DETECTORS →
4/ DETAILED LAYOUT →
5/ PRELIMINARY COST ESTIMATE →
6/ PULSE SHAPE V. GAS, VOLTAGE, DRIFT GAP. →
7/ EFFICIENCY, RESOLUTION, RATE IN TEST BEAM. →
8/ PROTOTYPE ELECTRONICS AND ASIC DESIGN.

TIME FOR PROTOTYPES - ENGINEERING DESIGN - CONSTRUCTION. INSTALLATION 1993 - 1998. (6 YEARS).

Sept 91 : → = ongoing begun
→ ✓ = done

Outer Tracker
Mechanical Engineering Aspects

SDC Outer Tracking System: Scope of Work and Program Planning	D. Hackworth (Westinghouse)
SDC Outer Tracking-ORNL/ORDC	T. Gabriel(ORNL)
Central and Forward Tracking Subsystem	R. Swensrud (Westinghouse)
Central Tracking Chamber Assembly Proposal	D. Vandergriff(ORNL)
Radiation Length Study	R. Leitch(ORNL)

LPBautz:11/4/91

SDC Outer Tracking System

SUCCESSFUL PROJECT MANAGEMENT CAN BE DEFINED AS HAVING ACHIEVED THE PROJECT OBJECTIVES:

- Within Schedule
- Within Cost
- At the Desired Performance/Technology Level
- While Utilizing the Assigned Resources Effectively and Efficiently

These Objectives Are Obtained by Proper Project Planning and Project Monitoring.

SDC OUTER TRACKING SYSTEM

SCOPE OF WORK
AND
PROGRAM PLANNING

DONALD T. HACKWORTH

September 26, 1991

SDC Outer Tracking System

PROJECT PLANNING INVOLVES:

- Definition of Work Requirements
- Definition of Quantity of Work
- Definition of Resources Needed

PROJECT MONITORING INVOLVES:

- Tracking Progress
- Comparing Actual to Predicted
- Analyzing Impact
- Making Adjustments

SDC Outer Tracking System

WHAT IS A PROJECT?

SERIES OF ACTIVITIES AND TASKS THAT:

- Have a Specific Objective to Be Completed Within Certain Specifications
- Have Defined Start and End Dates
- Have Funding Limits (Total Project, Yearly)
- Consumes Resource (Money, People, Equipment)

SDC Outer Tracking System

PLANNING → DETERMINING WHAT NEEDS TO BE DONE,
BY WHOM, AND BY WHEN,
IN ORDER TO FULFILL ONE'S ASSIGNED RESPONSIBILITIES.

THERE ARE NINE MAJOR COMPONENTS:

- Objectives
- Program
- Schedule
- Budget
- Forecast
- Organization
- Policy
- Procedure
- Standard

Westinghouse
Science & Technology Center

SDC Outer Tracking System

POTENTIAL BENEFITS FROM PROJECT PLANNING/MANAGEMENT

- Identification of Function Responsibilities to Ensure That All Activities Are Accounted For, Regardless of Personnel Turnover
- Minimizing the Need for Continuous Reporting
- Identification of Time Limits for Scheduling
- Identification of Methodology for Tradeoff Analysis
- Measurement of Accomplishment Against Plan
- Early Identification of Problems So That Corrective Action May Follow
- Improved Estimating Capability for Future Planning
- Knowing When Objectives Cannot Be Met or Will Be Exceeded

Westinghouse
Science & Technology Center

SDC Outer Tracking System

PROJECT PLANNING

EFFECTIVE TOTAL PROGRAM PLANNING CANNOT BE ACCOMPLISHED UNLESS ALL OF THE NECESSARY INFORMATION BECOMES AVAILABLE AT PROJECT INITIATION.

THE INFORMATION REQUIREMENTS ARE:

- Statement of Work (SOW)
- Project Specifications
- Milestone Schedule
- Work Breakdown Structure

Westinghouse
Science & Technology Center

SDC Outer Tracking System

PROJECT PLANNING MUST BE:

1. Systematic
2. Flexible Enough to Handle Unique Activities
3. Disciplined Through Reviews and Controls
4. Capable of Accepting Multifunctional Inputs

Westinghouse
Science & Technology Center

SDC Outer Tracking System

SDC STRAW MODULE CENTRAL TRACKER
PROGRAM PLANNING INFORMATION

RESOURCE AND COST PROFILES BY QUARTER 1992 THROUGH 1999

- Engineering and Drafting Manpower
- Technician and Labor Manpower
- Total Manpower and Material Costs
- Summary of Costs

COST DETAILS

- Summary List to Level 3 Without Contingency
- Summary List to Level 5 Without Contingency
- Spreadsheet of Estimates and Evaluation Data
- Spreadsheet of Contingency Calculations

Viewgraph 11
DTH
9.21.91

Westinghouse
Science & Technology Center

1617

SDC Outer Tracking System

SDC STRAW MODULE CENTRAL TRACKER
PROGRAM PLANNING INFORMATION

WBS CHARTS

1.2	Central Tracker
1.2.1	Modules
1.2.2	Support Structure
1.2.3	Superlayer (S/L) Subassembly
1.2.4	Tracker (S/L) to (S/L) Assembly
1.2.5	Equipment Tooling & Fixtures
1.2.6	Final Factory Assembly
1.2.7	Final Factory Testing
1.2.8	Tracker Transportation System
1.2.9	Erection at Super Collider Site
1.2.10	Facilities
1.2.11	Program Management
1.2.12	R&D Efforts

CONTRACT WBS

This List Identifies All WBS Legs to Level 8.

WBS DICTIONARY

This Dictionary is Written From Level 1 Through Level 4 or 5.

Viewgraph 9
DTH
9.21.91

Westinghouse
Science & Technology Center

1615

WBS 1.2 CENTRAL TRACKER

WBS

CHARTS

1618

SDC Outer Tracking System

SDC STRAW MODULE CENTRAL TRACKER
PROGRAM PLANNING INFORMATION

BAR CHARTS

Bar Charts Provided in Various Sorts and Rollups as Identified Below:

- Summary Chart Identifying Functional Detail at Level 4
- Activity Details in Order by WBS

NETWORK/TIME LOGIC DIAGRAMS

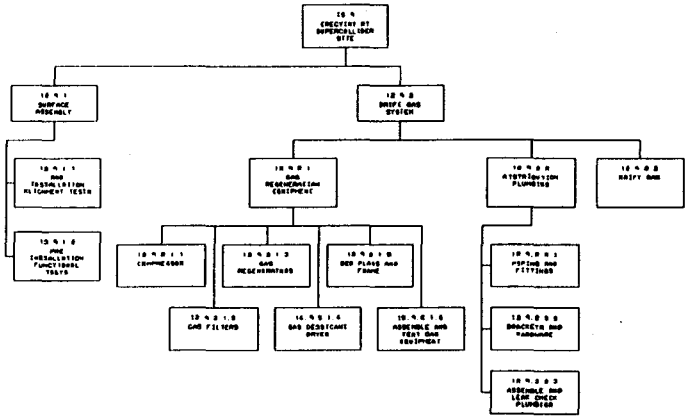
Selected Logic Diagrams Are Provided for Various Work Efforts:

- Critical Path
- Design Activities of Straw Tube Modules
- Design Activities of Support Structure
- Fab. & Assy Activities for Straw Tube Modules
- Fab. & Assy Activities for Support Structure
- Fab. & Assy Activities for Subassy Tooling
- Final Factory Assy & Test
- Site Assy & Test

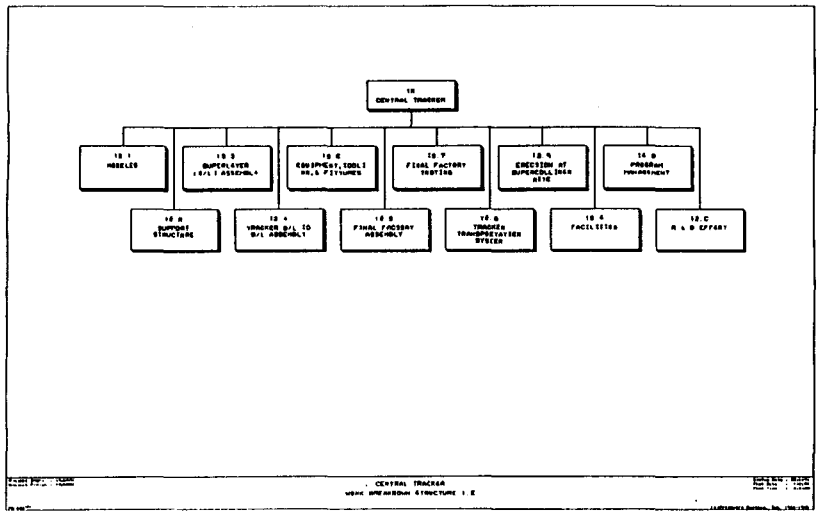
Viewgraph 10
DTH
9.21.91

Westinghouse
Science & Technology Center

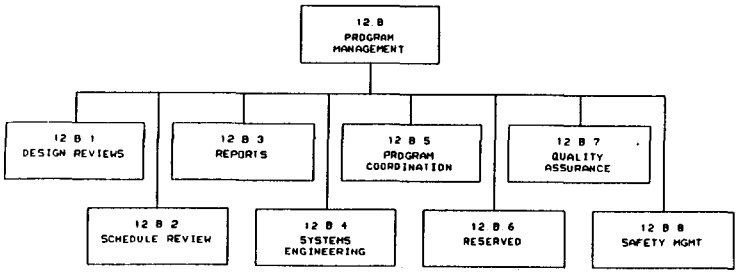
1616



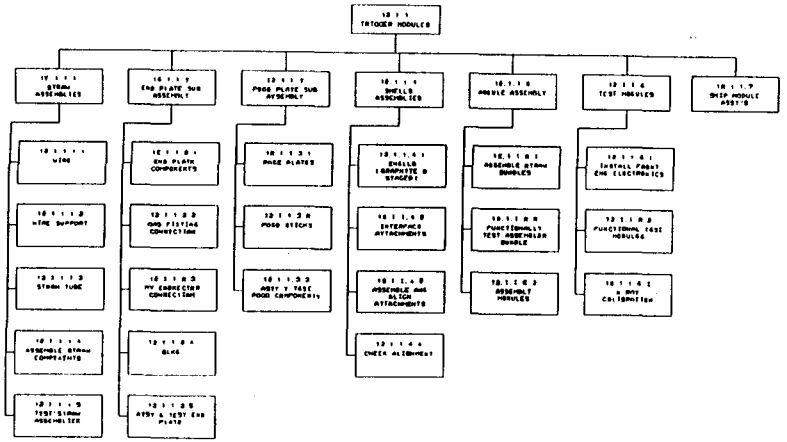
1621



1619

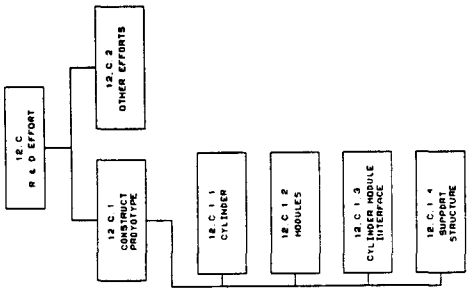


1622



1620

WBS 1.2 CENTRAL TRACKER



CONTRACT WORK BREAKDOWN STRUCTURE

WBS 1.2 CENTRAL TRACKER

WBS DICTIONARY

WORK BREAKDOWN STRUCTURE REV. 1

WBS	TITLE
	REVISED: JULY 30, 1991
1.2	CENTRAL TRACKER (Average Rating)
1.2.1	MODULES
1.2.1.1	TRIGGER MODULES
1.2.1.1.1	STRAW ASSEMBLIES
1.2.1.1.1.1	WIRE
1.2.1.1.1.2	WIRE SUPPORT
1.2.1.1.1.3	STRAW TUBE
1.2.1.1.1.3.1	METALIZED WRAPPER MATERIAL
1.2.1.1.1.3.2	WIND STRAWS
1.2.1.1.1.4	ASSEMBLE STRAW COMPONENTS
1.2.1.1.1.5	TEST STRAW ASSEMBLIES
1.2.1.1.2	END PLATE SUB ASSEMBLY
1.2.1.1.2.1	END PLATE COMPONENTS
1.2.1.1.2.1.1	WIRE TENSION PLATE
1.2.1.1.2.1.2	SOLDER CUP
1.2.1.1.2.1.3	RESISTOR TERMINATION
1.2.1.1.2.2	GAS FITTING CONNECTION
1.2.1.1.2.3	HV CONNECTOR CONNECTION
1.2.1.1.2.4	GLUE
1.2.1.1.2.5	ASSY & TEST END PLATE
1.2.1.1.3	POGO PLATE SUB ASSEMBLY
1.2.1.1.3.1	POGO PLATES
1.2.1.1.3.2	POGO STICKS
1.2.1.1.3.3	ASSY & TEST POGO COMPONENTS
1.2.1.1.4	SHELLS ASSEMBLIES
1.2.1.1.4.1	SHELLS (GRAPHITE B STAGED)
1.2.1.1.4.1.1	TRIGGER UP
1.2.1.1.4.1.2	TRIGGER DOWN
1.2.1.1.4.2	INTERFACE ATTACHMENTS
1.2.1.1.4.2.1	TRIGGER UP
1.2.1.1.4.2.2	TRIGGER DOWN
1.2.1.1.4.3	ASSEMBLE AND ALIGN ATTACHMENTS
1.2.1.1.4.4	CHECK ALIGNMENT
1.2.1.1.5	MODULE ASSEMBLY
1.2.1.1.5.1	ASSEMBLE STRAW BUNDLES
1.2.1.1.5.2	FUNCTIONALLY TEST ASSEMBLED BUNDLE
1.2.1.1.5.5	ASSEMBLE MODULES
1.2.1.1.6	TEST MODULES
1.2.1.1.6.1	INSTALL FRONT END ELECTRONICS
1.2.1.1.6.2	FUNCTIONAL TEST MODULES
1.2.1.1.6.2.1	LEAK TEST MODULE
1.2.1.1.6.2.2	ELECTRICALLY TEST MODULE
1.2.1.1.6.3	X RAY CALIBRATION
1.2.1.1.7	SHIP MODULE ASSY'S
1.2.1.2	AXIAL/STEREO MODULES

WBS DICTIONARY

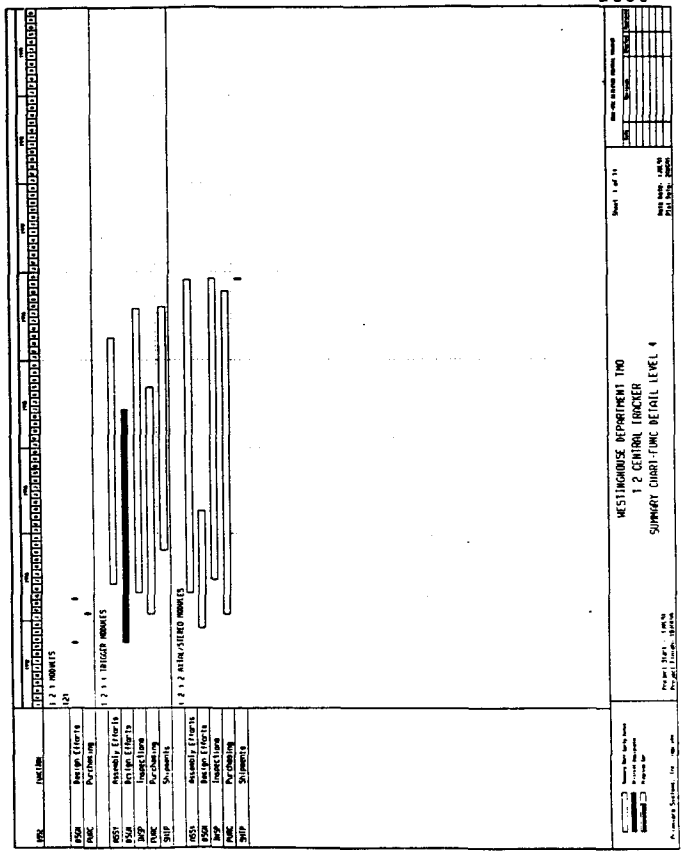
WBS #	TITLE	SCOPE – REVISED: 05-Aug-91
1.2	CENTRAL TRACKER	The Central Tracker is a construction of four concentric superlayers of alternating modules. The modules are attached to support cylinders with shim rings. The module arrangment of the superlayers are aligned axially for layers six and four, layers five and three are called stereo layers and their modules are arranged plus and minus three degrees to the beam axis. The outermost layer, superlayer number six is also the trigger layer.
1.2.1	MODULES	Modules are groups of straws that are arranged as trapazoidal bundles, thes trapazoids are covered with a thin graphite/epoxy wrapper that provides mechanical protection and structrual support for the straws. Modules in the same superlayer are standard sized units that are interchangeable and replaceable.
1.2.1.1	TRIGGER MODULES	Trigger modules are modules that contain extra layers of straws and have curved tops and bottoms. Two styles of these modules are needed since the modules are arranged as alternating trapezoids.
1.2.1.1.1	STRAW ASSEMBLIES	Straw Assembly components are the straw tube, spacers and the anode wire. The straw tube is spiral wound from a metalized material, the spacers are two piece insulating bushing that support the anode wire in the center of the tube and allow for drift gas passage. The anode wire is a tungsten wire, centrally supported that provides the trigger potential.
1.2.1.1.1.1	WIRE	The wire is the anode electrode for the straw assembly providing potential for triggering.
1.2.1.1.1.2	WIRE SUPPORT	Wire supports are snap together insulators that are spaced about every eighty(80) cm over the length of the straw. The wire supports center the wire and provide drift gas flow passages.
1.2.1.1.1.3	STRAW TUBE	Straw tubes are Spiral wound tubes wound from metalized material that is sealed to be gas tight over it's length. This tube is the cathode of the straw tube assembly.
1.2.1.1.2	END PLATE SUB ASSEMBLY	The end plate assembly fits on the ends of the straw tube modules and provides the interface between the straw tubes and the electrical signals and connections for drift gas. It is comprised of a wire tension plate, solder clips, resistor terminations and gas & HV connectors.
1.2.1.1.2.1	END PLATE COMPONENTS	
1.2.1.1.2.1.1	WIRE TENSION PLATE	
1.2.1.1.2.1.2	SOLDER CLIP	
1.2.1.1.2.1.3	RESISTOR TERMINATION	
1.2.1.1.2.2	GAS FITTING CONNECTION	
1.2.1.1.2.3	HV CONNECTOR CONNECTION	
1.2.1.1.2.4	GLUE	
1.2.1.1.2.5	ASSY & TEST END PLATE	
1.2.1.1.3	POGO PLATE SUB ASSEMBLY	
1.2.1.1.3.1	POGO PLATES	
1.2.1.1.3.2	POGO STICKS	
1.2.1.1.4	SHELLS ASSEMBLIES	

WBS 1.2 CENTRAL TRACKER

BAR CHARTS

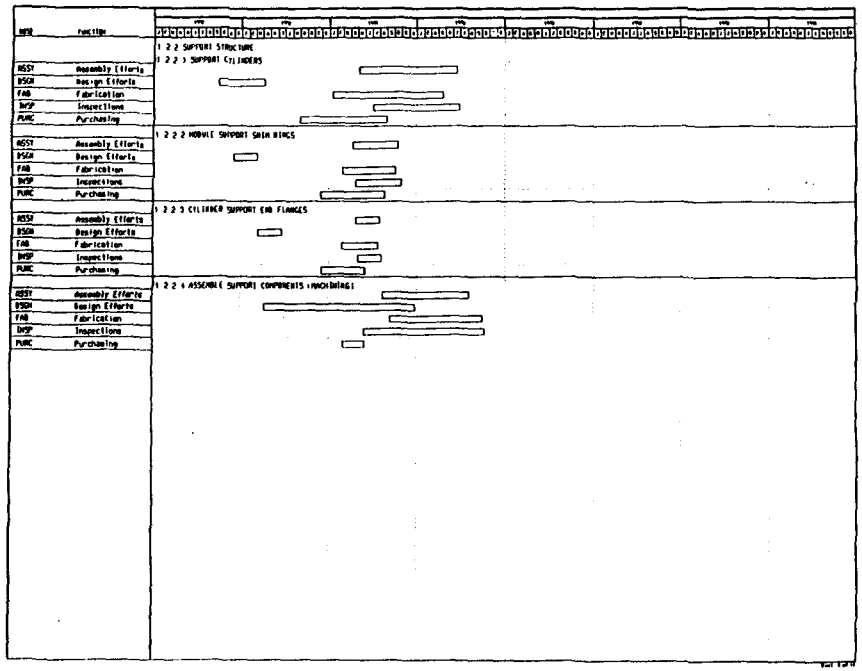
WBS 1.2 CENTRAL TRACKER

SUMMARY BAR CHART IDENTIFYING FUNCTIONAL DETAIL TO WBS LEVEL 4 (i.e. 1.2.1.1)

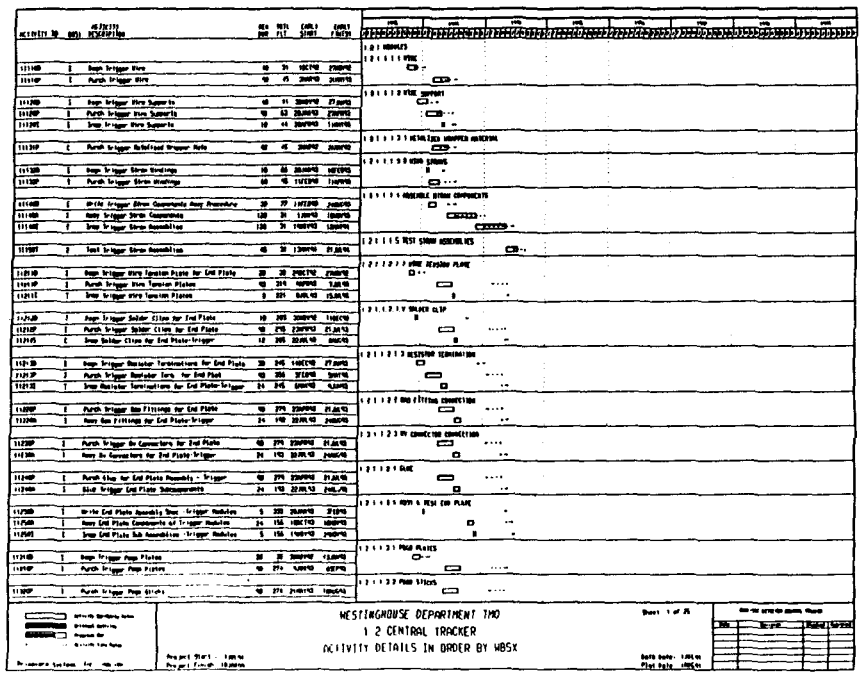


WBS 1.2 CENTRAL TRACKER

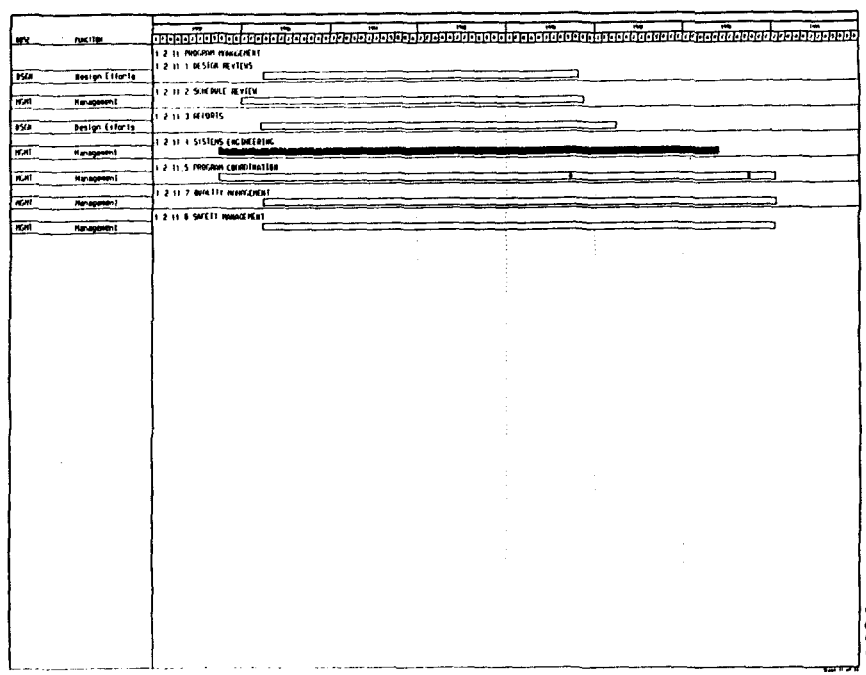
ACTIVITY DETAILS
IN ORDER BY WBS



1631



1633

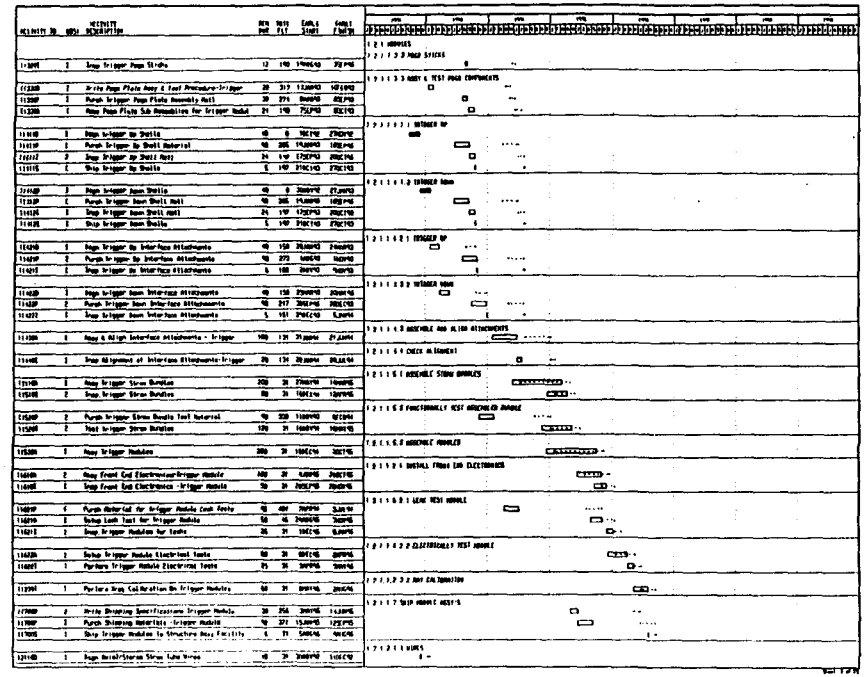


1632

1634

WBS 1.2 CENTRAL TRACKER

NETWORK DIAGRAMS

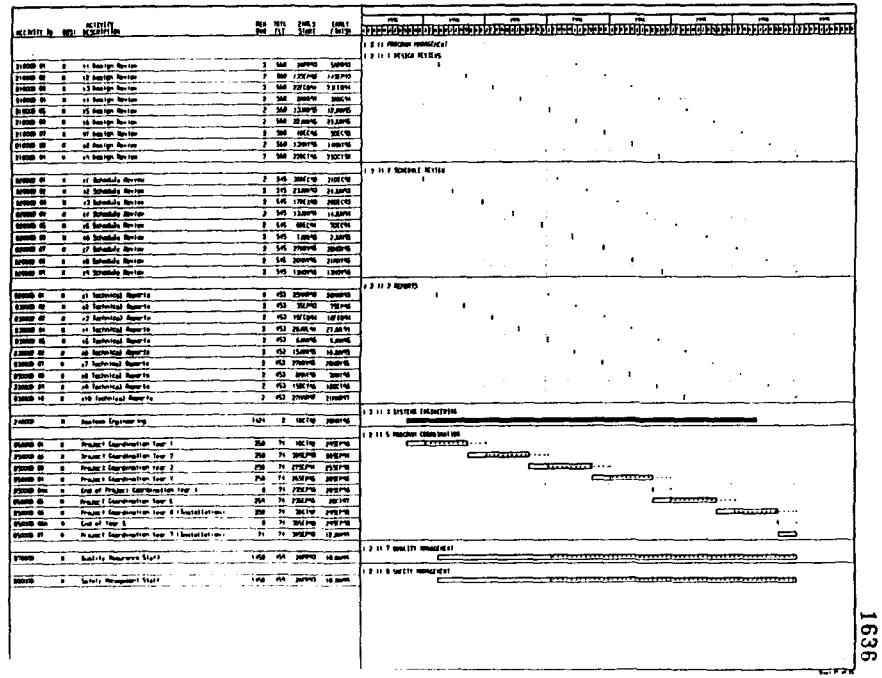


1635

1637

WBS. 1.2 CENTRAL TRACKER

CRITICAL PATH NETWORK

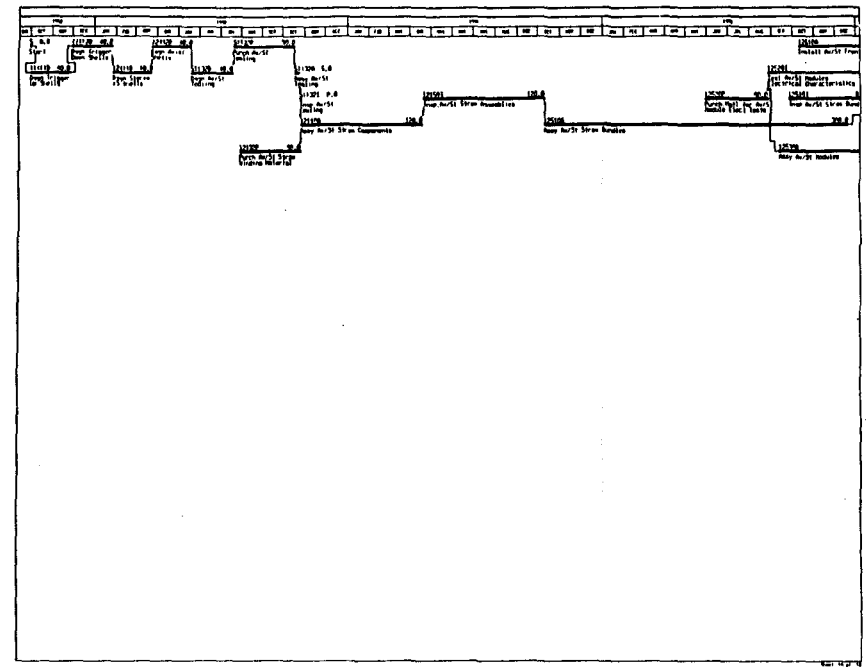


1636

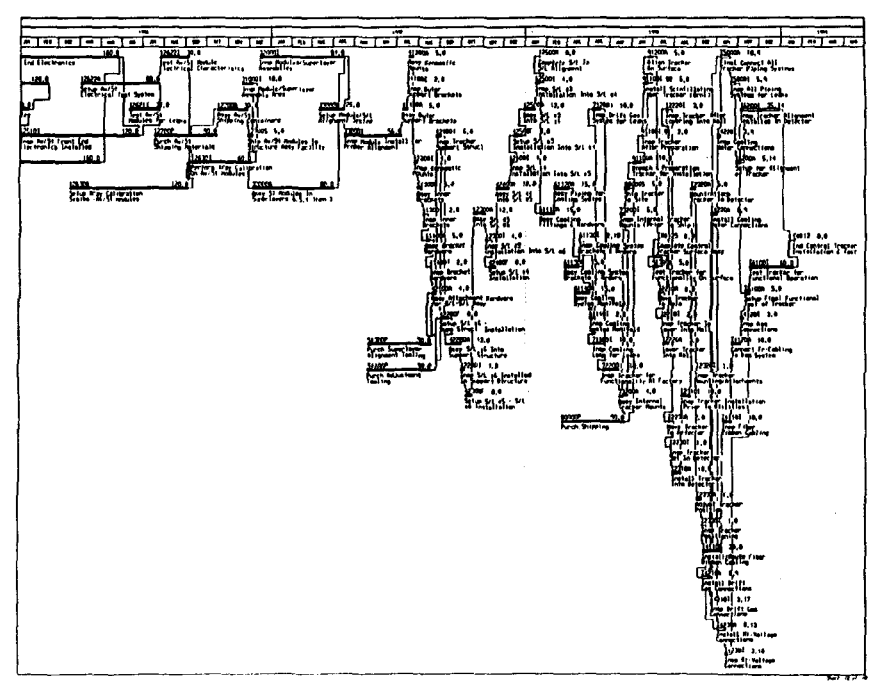
1638

WBS 1.2 CENTRAL TRACKER

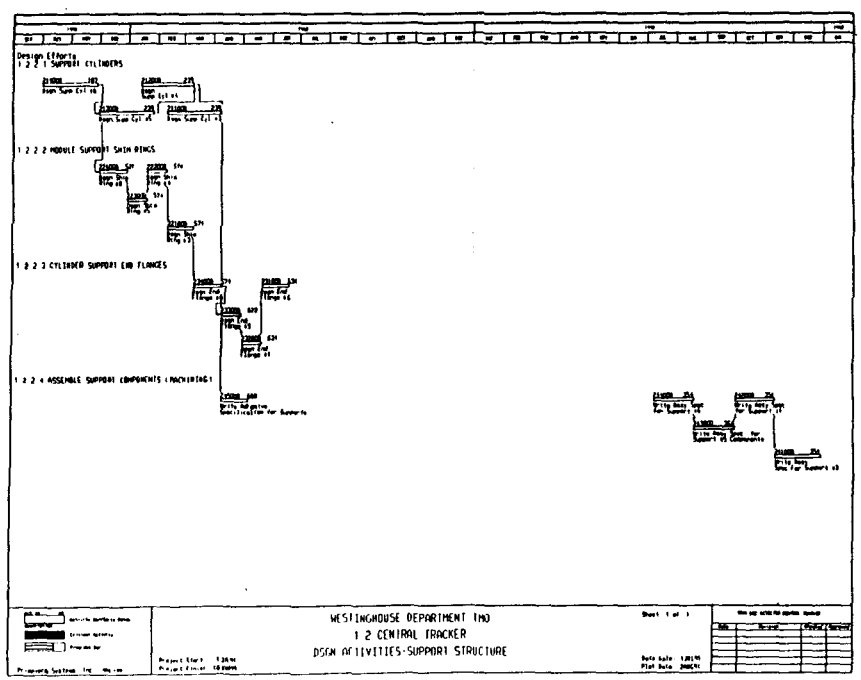
DESIGN
ACTIVITIES OF
SUPPORT STRUCTURE



1639



1640



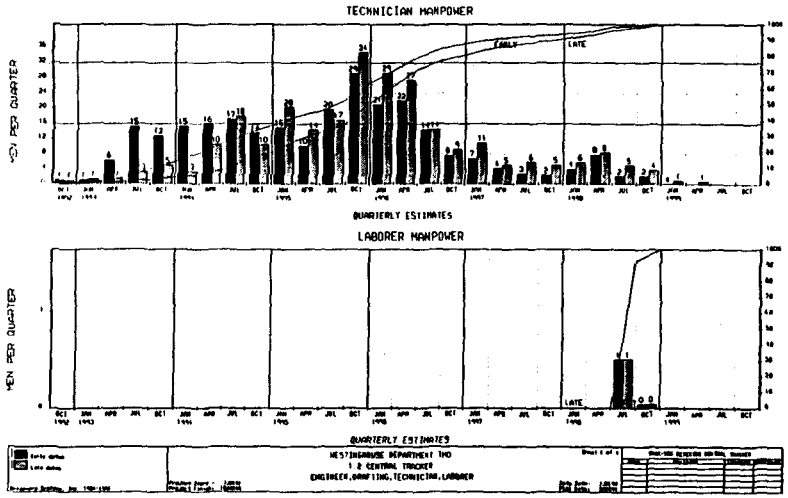
1642

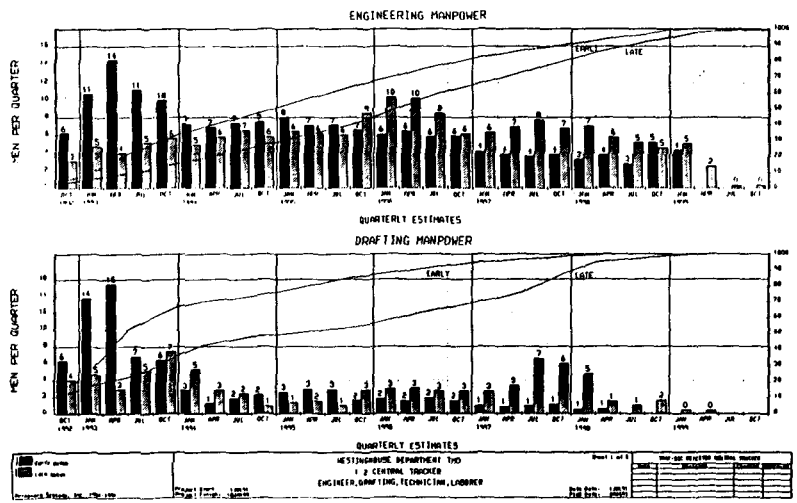
1641

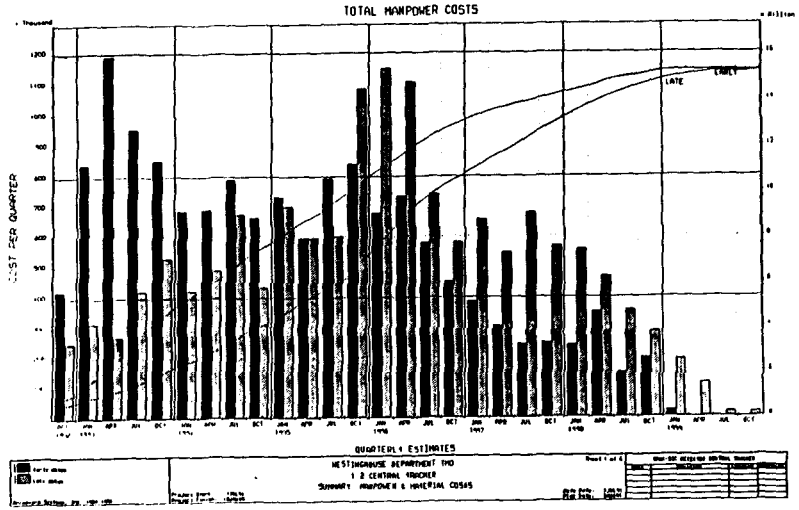
WBS 1.2 CENTRAL TRACKER

RESOURCE & COST PROFILES

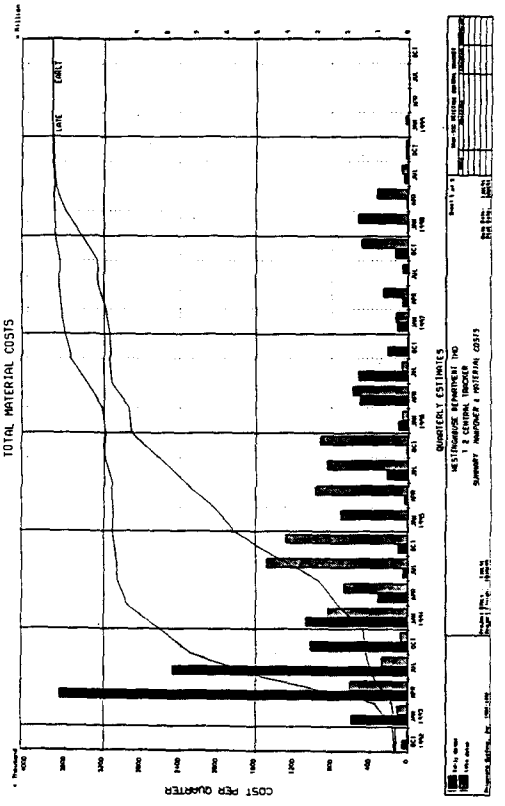
- MANPOWER
  - ENGR
  - DRAFT
  - TECH
  - LABOR
- COSTS
  - MANPOWER
  - MATL
  - SUMMARY OF COSTS



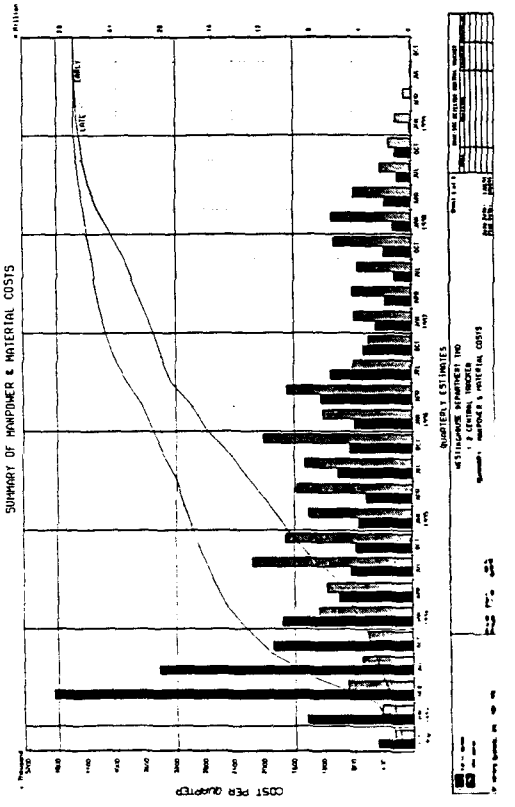




1647



1648



1649

WBS 1.2 CENTRAL TRACKER

- SUMMARY LIST OF COSTS TO LEVEL 3 (1.2.1)
- SUMMARY LIST OF COSTS TO LEVEL 5
- SPREADSHEET CALCULATIONS
- CONTINGENCY CALCULATIONS

1650

WESTINGHOUSE DEPARTMENT TMO — PRIMAVERA PROJECT PLANNER — 1.2 CENTRAL TRACKER

REPORT DATE 14JUL91 14:17 — RUN NO. 16 — TRAK-SSC DETECTOR CENTRAL TRACKER — START DATE 1JUL91 — FIN DATE 18JAN99

1.2 Summary of Budgets without Contingency — DATA DATE 1JUL91 — PAGE NO

	DUR	%	SUMMARY DESCRIPTION	BUDGET	EARNED	SCHEDULED START	SCHEDULED FINISH
121	1527	0	1.2.1 MODULES	6557797.00	.00	10CT92	30EC96
122	1107	0	1.2.2 SUPPORT STRUCTURE	3548016.71	.00	10CT92	12OCT95
123	823	0	1.2.3 SUPERLAYER (S/L) ASSEMBLY	858654.10	.00	29DEC94	8JUL97
124	1748	0	1.2.4 TRACKER S/L TO S/L ASSEMBLY	579613.80	.00	9APR93	29JAN98
125	1784	0	1.2.5 EQUIPMENT,TOOLING,& FIXTURES	6458542.11	.00	10CT92	19AUG97
126	1836	0	1.2.6 FINAL FACTORY ASSEMBLY	836835.01	.00	25MAR93	3APR98
127	1884	0	1.2.7 FINAL FACTORY TESTING	277010.01	.00	25MAR93	21MAY98
128	1016	0	1.2.8 TRACKER TRANSPORTATION SYSTEM	32404.50	.00	10AUG95	21MAY98
129	1875	0	1.2.9 SURFACE ASST AT SUPERCOLLIDER SITE	722391.20	.00	21MAY93	8JUL98
12A	1879	0	1.2.10 FACILITIES	2772141.00	.00	30NOV92	20JAN98
12B	1583	0	1.2.11 PROGRAM MANAGEMENT	2668973.42	.00	10CT92	18JAN99
12C	900	0	1.2.12 R & D EFFORT	1312299.60	.00	15JUL91	30DEC93
821	1268	0	8.2.1 SUBSYSTEM INSTALLATION IN HALL	335295.48	.00	28OCT93	9NOV98
822	835	0	8.2.2 SUBSYSTEM AND SYSTEM TEST IN HALL	103304.20	.00	27JUN95	18JAN99
REPORT TOTAL				27163278.22	.00		

1651

WESTINGHOUSE DEPARTMENT TMO — PRIMAVERA PROJECT PLANNER — 1.2 CENTRAL TRACKER

RE[illegible] DATE 1AUG91 14:19 RUN NO. 17 — TRAK-SSC DETECTOR CENTRAL TRACKER — START DATE 1JUL91 FIN DATE 18JAN99

Wb[illegible] Summary of Budgets without Contingency — DATA DATE 1JUL91 PAGE NO. 1

1.2.1 MODULES

	DUR	%		SUMMARY DESCRIPTION	BUDGET	EARNED	SCHEDULED START	FINISH
1.2.1.1 TRIGGER MODULES								
12111	659	D		STRAW ASSEMBLIES	392881.00	.00	10CT92	21JUL94
12112	397	D		END PLATE SUB ASSEMBLY	211912.80	.00	29OCT92	29NOV93
12113	313	D		POGO PLATE SUB ASSEMBLY	84136.00	.00	30NOV92	80CT93
12114	658	D		SHELLS ASSEMBLIES	776738.00	.00	10CT92	20JUL94
12115	692	D		MODULE ASSEMBLY	421297.00	.00	11NOV93	30CT95
12116	849	D		TEST MODULES	300737.00	.00	7APR94	2AUG96
12117	465	D		SHIP MODULE ASSY'S	29110.00	.00	3MAY95	9AUG96
LINE TOTAL			1211		2218811.00	.00		
1.2.1.2 AXIAL/STEREO MODULES								
12121	680	D		ASSEMBLE STRAW COMPONENTS	641120.00	.00	30NOV92	10OCT94
12122	380	D		END PLATE SUB ASSEMBLY	374351.00	.00	14JAN93	28JAN94
12123	336	R		POGO PLATE SUB ASSEMBLY	98599.00	.00	25MAR93	23FE094
12124	650	D		SHELLS ASSEMBLIES	1553826.00	.00	28JAN93	8NOv94
12125	567	D		MODULE ASSEMBLY	814675.00	.00	11OCT94	29APR96
12126	554	D		TEST MODULES	788705.00	.00	30MAY95	30EC96
12127	1016	D		SHIP MODULE ASSEMBLES	67710.00	.00	24FEB94	5DEC96
LINE TOTAL			1212		4338966.00	.00		
SUBTOTAL			121		6557797.00	.00		

1652

WESTINGHOUSE DEPARTMENT TMO — PRIMAVERA PROJECT PLANNER — 1.2 CENTRAL TRACKER

RE[illegible] DATE 1AUG91 14:19 RUN NO. 17 — TRAK-SSC DETECTOR CENTRAL TRACKER — START DATE 1JUL91 FIN DATE 18JAN99

[illegible] Summary of Budgets without Contingency — DATA DATE 1JUL91 PAGE NO. 14

1.2.11 PROGRAM MANAGEMENT

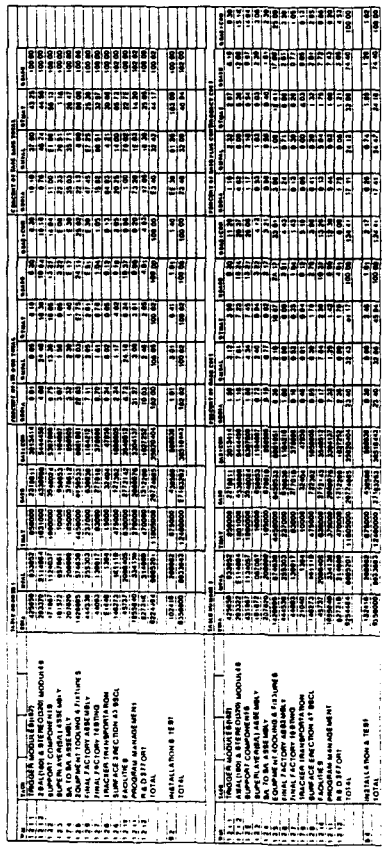
	DUR	%		SUMMARY DESCRIPTION	BUDGET	EARNED	SCHEDULED START	FINISH
1.2.11.1 DESIGN REVIEWS								
1281	898	0		1281	47700.36	.00	2APR93	23OCT96
LINE TOTAL			1281		47700.36	.00		
1.2.11.2 SCHEDULE REVIEW								
12R2	97R	0		1282	47700.36	.00	30DEC92	13NOV96
LINE TOTAL			1282		47700.36	.00		
1.2.11.3 REPORTS								
1283	1010	0		1283	76668.00	.00	25MAR93	31MAR97
LINE TOTAL			1283		76668.00	.00		
1.2.11.4 SYSTEMS ENGINEERING								
1284	1424	0		1284	783524.70	.00	10CT92	28MAT98
LINE TOTAL			12R4		783524.70	.00		
1.2.11.5 PROGRAM COORDINATION								
1285	1583	0		1285	1379245.00	.00	10CT92	16JAN99
LINE TOTAL			1285		1379245.00	.00		
1.2.11.7 QUALITY MANAGEMENT								
12D7	1458	0		12R7	167067.50	.00	2APR93	18JAN99
LINE TOTAL			1287		167067.50	.00		
1.2.11.8 SAFETY MANAGEMENT								
1286	1458	D		1286	167067.50	.00	2APR93	16JAN99
LINE TOTAL			1286		167067.50	.00		
SUBTOTAL			12R		2668973.42	.00		

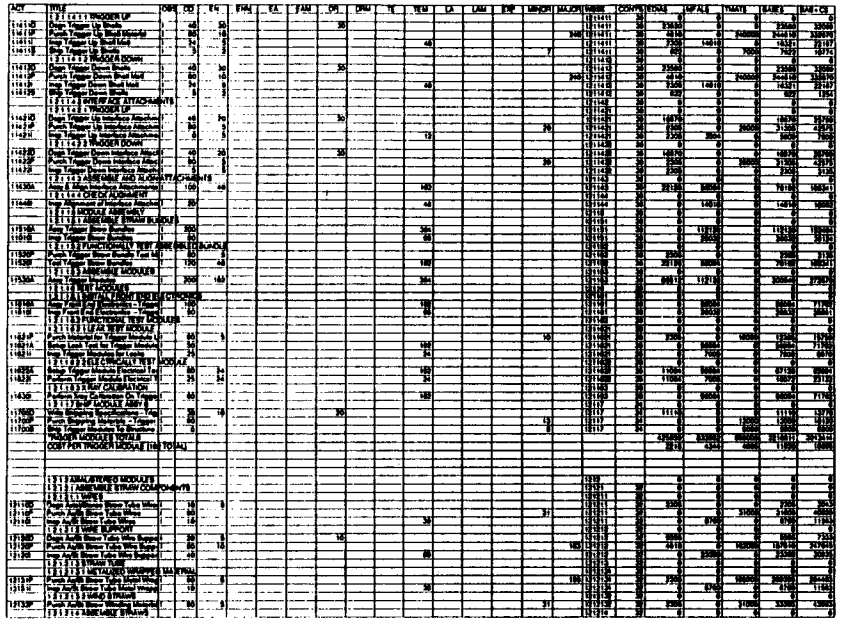
WBS 1.2 CENTRAL TRACKER

SPREADSHEET CALCULATIONS

1653

1654





1.3 CENTRAL TRACKER

1657

TABLE NUMBER 3

WBS	TASK	EDIA	MFAL	TMAT	BASE	BAS+CON
1.2.1.1	TRIGGER MODULES(192)	425859	833952	959000	2218811	3013414
1.2.1.2	AXIAL(160) & STEREO(320) MODULES	293322	2114684	1631000	4338986	5444456
1.2.2	SUPPORT COMPONENTS	421007	1134037	1990000	3546024	5367800
1.2.3	SUPERLAYER(S/L) ASSEMBLY	181972	857681	10000	859653	1104987
1.2.4	S/L TO S/L ASSEMBLY	207620	206998	165000	579016	898355
1.2.5	EQUIPMENT,TOOLING,& FIXTURES	1428695	574638	4450000	6459333	8961861
1.2.6	FINAL FACTORY ASSEMBLY	444536	255303	237800	836839	1184219
1.2.7	FINAL FACTORY TESTING	47058	41083	139917	93000	277010
1.2.8	TRACKER TRANSPORTATION	21040	1364	10000	32404	47958
1.2.9	SURFACE ERECTION AT SSCL	146273	181119	475000	722382	1056605
1.2.10	FACILITIES	45737	2066406	630000	2772142	3548512
1.2.11	PROGRAM MANADEMENT	1955840	334136	378000	2688978	3304137
1.2.12	R & D EFFORT	627318	214899	470000	1312299	1627252
8.2	INSTALLATION & TEST	102416	269682	875000	438598	580036
	SUBTOTAL	6356900	8933883	12480000	27163283	36510443

TABLE NUMBER 4
STRAW TUBE CENTRAL TRACKER
SCALING CONSTANTS INCLUDING CONTINGENCY

	FIXED COSTS	(K$)
1.2.5	EQUIPMENT,TOOLING,& FIXTURES	8962
1.2.7	FINAL FACTORY TESTING	379
1.2.8	TRACKER TRANSPORTATION SYST	48
1.2.9	ERECTION AT SUPERCOLLIDER SI	1059
1.2.10	FACILITIES	3549
1.2.11	PROGRAM MANAGEMENT	3304
1.2.12	R & D EFFORT	1627
8.2	INSTALLATION & TEST	586
	TOTAL:	19537
	SUPPORT STRUCTURE COSTS	
1.2.3	SUPPORT STRUCTURE	6368
1.2.3	SUPERLAYER (S/L) ASSEMBLY	1105
1.2.4	TRACKER SUB ASSEMBLY	859
1.2.6	FINAL FACTORY ASSEMBLY	1184
	FOUR SUPERLAYER SUPPORTS	8515
	ONE SUPERLAYER SUPPORT:	2129
	TRIGGER MODULES COSTS	
1.2.1.1	192 TRIGGER MODULES	3013
	ONE TRIGGER MODULE	15.695
	STEREO OR AXIAL MODULE COSTS	
1.2.1.2	480 AXIAL OR STEREO MODULES	5444
	ONE AXIAL OR STEREO MODULE	11.343
	CHECK	
	ZERO BASELINE DESIGN	36510

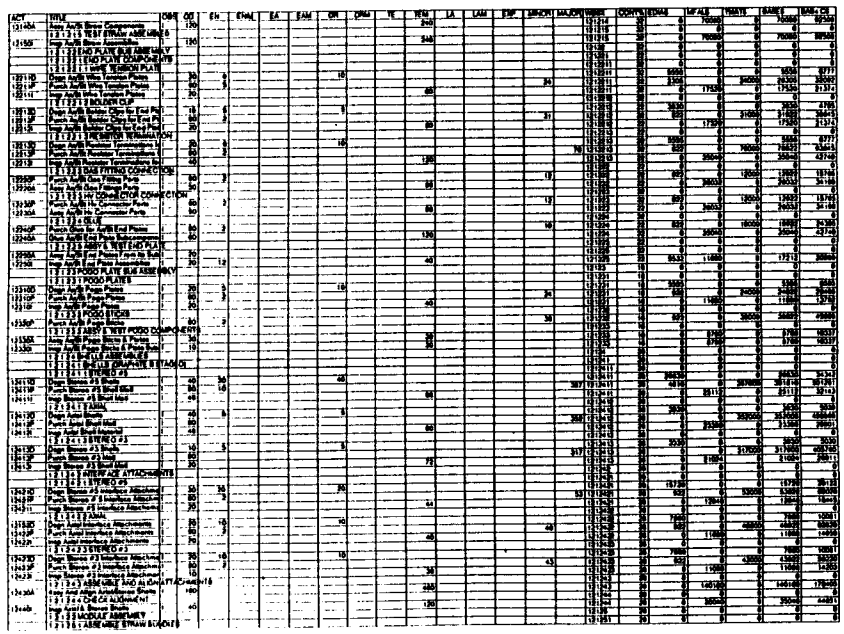
TABLE NUMBER 5
SCALING TABLE FOR NUMBER OF MODULES VS. SUPERLAYER DIAMETER (REF 1.7 M DIA. DESIGN)

DIA IN METERS	NO. REQUIRED
1.81	192.00
1.46	176.00
1.34	160.00
1.22	144.00

TABLE NUMBER 6
SCALING TABLE FOR COST VS. TRACKER LENGTH (REF 1.7 M DIA. DESIGN)(683K$*1.3CONT/LAYER)

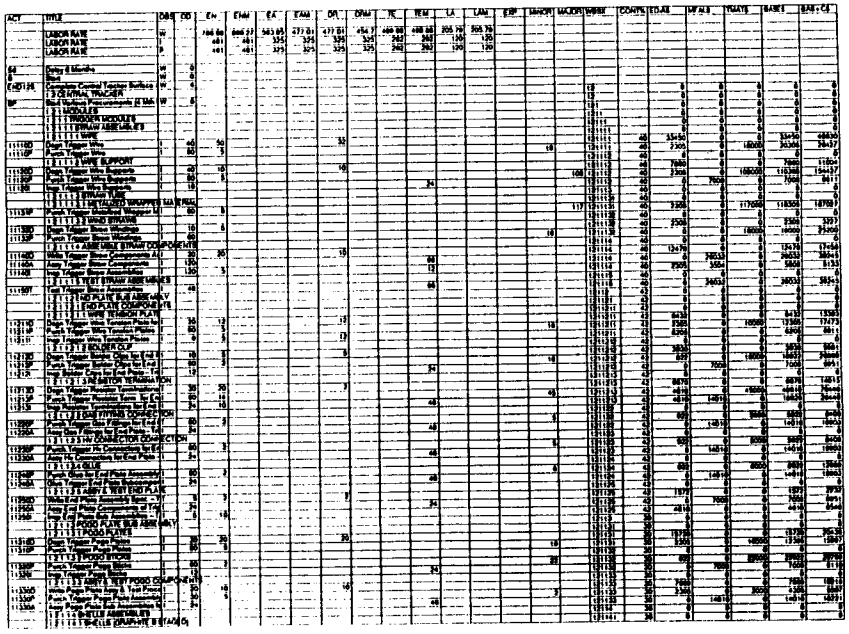
LENGTH IN METERS	COST (K$)
8	36510
7	35623
6	34735
5	33847

1655



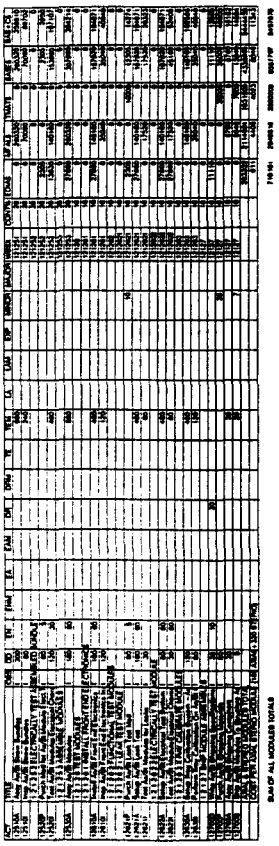
1.2 CENTRAL TRACKER

1658



1.2 CENTRAL TRACKER

1656



WBS 1.2 CENTRAL TRACKER

CONTINGENCY CALCULATIONS

CONTINGENCY TABLE

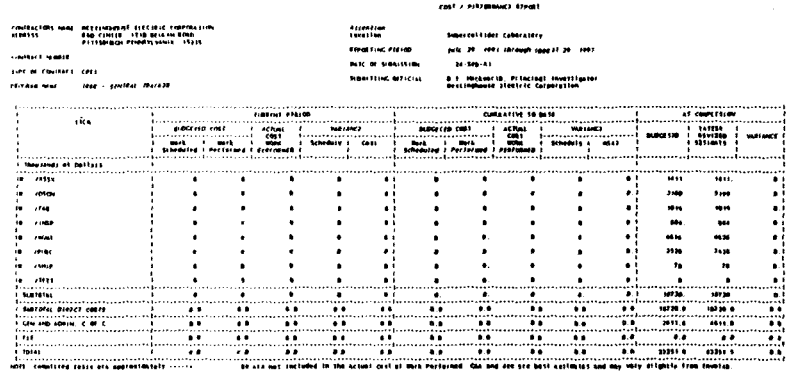
ACT		RISK FACTOR			WBS FACTORS			CONTIN.
	REVISED: JULY 30, 1991	TR	CR	SR	TR	CR	SR	%
1.2	CENTRAL TRACKER (Average Rating)	5.9	4.6	5.0	3.4	1.9	1.8	34
1.2.1	MODULES							
1.2.1.1	TRIGGER MODULES							
1.2.1.1	STRAW ASSEMBLIES	8	2	4	4	2	1	40
1.2.1.1.1	WIRE							
1.2.1.1.2	WIRE SUPPORT							
1.2.1.1.3	STRAW TUBE							
1.2.1.1.3.1	METALIZED WRAPPER MATERIAL							
1.2.1.1.3.2	WIND STRAWS							
1.2.1.1.4	ASSEMBLE STRAW COMPONENTS							
1.2.1.1.5	TEST STRAW ASSEMBLIES							
1.2.1.2	END PLATE SUB ASSEMBLY	8	3	4	4	2	1	42
1.2.1.2.1	END PLATE COMPONENTS							
1.2.1.2.1.1	WIRE TENSION PLATE							
1.2.1.2.1.2	SOLDER CLIP							
1.2.1.2.1.3	RESISTOR TERMINATION							
1.2.1.2.2	GAS FITTING CONNECTION							
1.2.1.2.3	HV CONNECTOR CONNECTION							
1.2.1.2.4	GLUE							
1.2.1.2.5	ASSY & TEST END PLATE							
1.2.1.3	POGO PLATE SUB ASSEMBLY	8	3	8	2	2	1	30
1.2.1.3.1	POGO PLATES							
1.2.1.3.2	POGO STICKS							
1.2.1.3.3	ASSY & TEST POGO COMPONENTS							
1.2.1.4	SHELLS ASSEMBLIES	18	6	4	2	2	1	34
1.2.1.4.1	SHELLS (GRAPHITE B STAGED)							
1.2.1.4.1.1	TRIGGER UP							
1.2.1.4.1.2	TRIGGER DOWN							
1.2.1.4.2	INTERFACE ATTACHMENTS							
1.2.1.4.2.1	TRIGGER UP							
1.2.1.4.2.2	TRIGGER DOWN							
1.2.1.4.3	ASSEMBLE AND ALIGN ATTACHMENTS							
1.2.1.4.4	CHECK ALIGNMENT							
1.2.1.5	MODULE ASSEMBLY	4	6	8	4	2	1	36
1.2.1.5.1	ASSEMBLE STRAW BUNDLES							
1.2.1.5.2	FUNCTIONALLY TEST ASSEMBLED BUNDLE							
1.2.1.5.3	ASSEMBLE MODULES							
1.2.1.6	TEST MODULES	3	4	8	4	2	1	28
1.2.1.6.1	INSTALL FRONT END ELECTRONICS							
1.2.1.6.2	FUNCTIONAL TEST MODULES							
1.2.1.6.2.1	LEAK TEST MODULE							
1.2.1.6.2.2	ELECTRICALLY TEST MODULE							
1.2.1.6.3	X RAY CALIBRATION							
1.2.1.7	SHIP MODULE ASSY'S	2	4	8	4	2	1	24
1.2.1.2	AXIAL/STEREO MODULES							

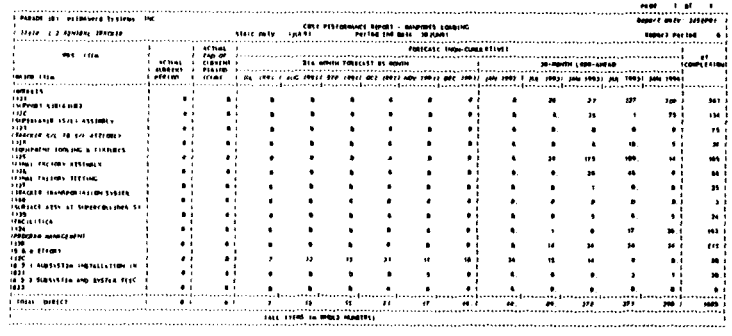
CONTINGENCY TABLE

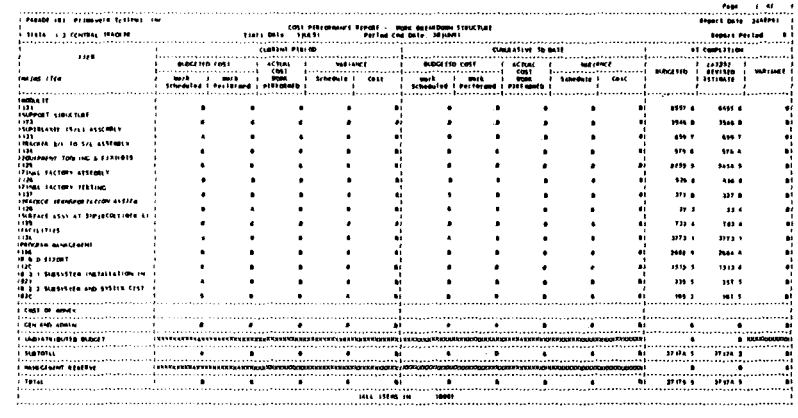
ACT		RISK FACTOR			WBS FACTORS			CONTIN.
	REVISED: JULY 30, 1991	TR	CR	SR	TR	CR	SR	%
1.2.1.2.1	ASSEMBLE STRAW COMPONENTS	8	6	4	2	2	1	32
1.2.1.2.1.1	WIRES							
1.2.1.2.1.2	WIRE SUPPORT							
1.2.1.2.1.3	STRAW TUBE							
1.2.1.2.1.3.1	METALIZED WRAPPER MATERIAL							
1.2.1.2.1.3.2	WIND STRAWS							
1.2.1.2.1.4	ASSEMBLE STRAWS							
1.2.1.2.1.5	TEST STRAW ASSEMBLIES							
1.2.1.2.2	END PLATE SUB ASSEMBLY	4	6	2	2	2	1	32
1.2.1.2.2.1	END PLATE COMPONENTS							
1.2.1.2.2.1.1	WIRE TENSION PLATE							
1.2.1.2.2.1.2	SOLDER CLIP							
1.2.1.2.2.1.3	RESISTOR TERMINATION							
1.2.1.2.2.2	GAS FITTING CONNECTION							
1.2.1.2.2.3	HV CONNECTOR CONNECTION							
1.2.1.2.2.4	GLUE							
1.2.1.2.2.5	ASSY & TEST END PLATE							
1.2.1.2.3	POGO PLATE SUB ASSEMBLY	4	4	2	2	2	1	18
1.2.1.2.3.1	POGO PLATES							
1.2.1.2.3.2	POGO STICKS							
1.2.1.2.3.3	ASSY & TEST POGO COMPONENTS							
1.2.1.2.4	SHELLS ASSEMBLIES	8	4	4	2	2	1	28
1.2.1.2.4.1	SHELLS (GRAPHITE B STAGED)							
1.2.1.2.4.1.1	STEREO #5							
1.2.1.2.4.1.2	AXIAL							
1.2.1.2.4.1.3	STEREO #3							
1.2.1.2.4.2	INTERFACE ATTACHMENTS							
1.2.1.2.4.2.1	STEREO #5							
1.2.1.2.4.2.2	AXIAL							
1.2.1.2.4.2.3	STEREO #3							
1.2.1.2.4.3	ASSEMBLE AND ALIGN ATTACHMENTS							
1.2.1.2.4.4	CHECK ALIGNMENT							
1.2.1.2.5	MODULE ASSEMBLY	8	4	4	2	2	1	28
1.2.1.2.5.1	ASSEMBLE STRAW BUNDLES							
1.2.1.2.5.2	ELECTRICALLY TEST ASSEMBLED BUNDLE							
1.2.1.2.5.3	ASSEMBLE MODULES							
1.2.1.2.6	TEST MODULES	2	2	8	2	2	1	14
1.2.1.2.6.1	INSTALL FRONT END ELECTRONICS							
1.2.1.2.6.2	FUNCTIONAL TEST MODULES							
1.2.1.2.6.2.1	LEAK TEST MODULE							
1.2.1.2.6.2.2	ELECTRICALLY TEST MODULE							
1.2.1.2.6.3	X RAY CALIBRATE MODULES							
1.2.1.2.7	SHIP MODULE ASSEMBLES	2	2	8	2	2	1	16
1.2.2	SUPPORT STRUCTURE							
1.2.2.1	SUPPORT CYLINDERS	8	8	8	4	2	1	56

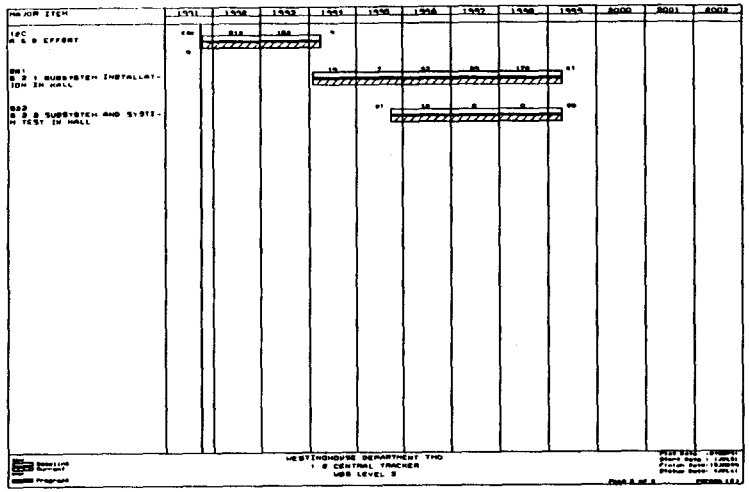
WBS 1.2 CENTRAL TRACKER

COST PERFORMANCE REPORTS

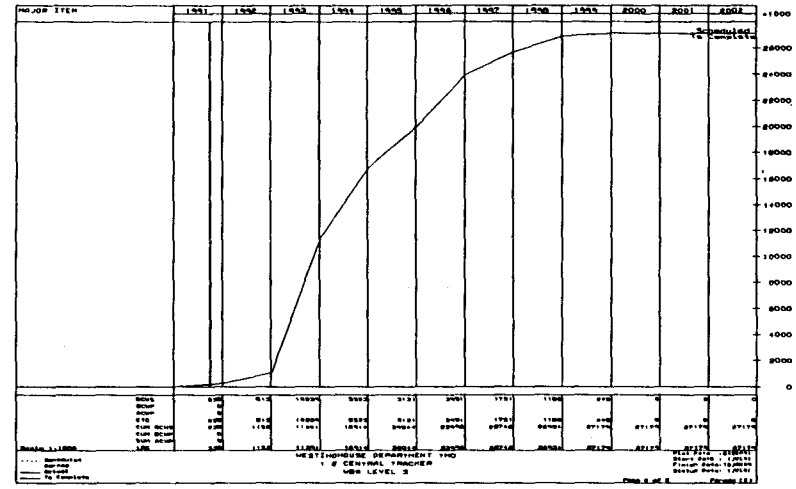








1669



1667

SDC Outer Tracking System

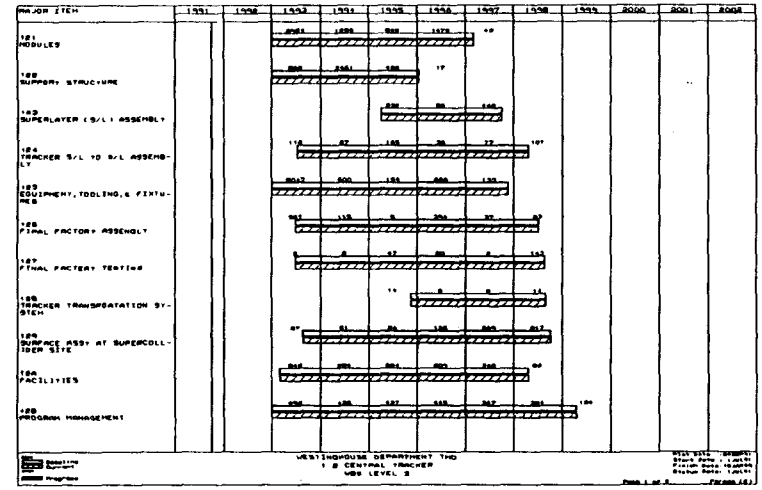
SUMMARY

- A Statement of Work (SOW) is Available But Not Finalized for Module Straw Tracker
- A Work Breakdown Structure (WBS) (Based Primarily Hardware) is Available
- Milestone Schedule Has Been Developed
- Project Specification as Specified in the SOW and WBS Dictionary
- The WBS Has Been Scheduled, Resource Loaded and Budgeted
- A Procedure for Maintaining the Plan and Forecasting Changes is Available

Viewgraph 12
DTH
9.23.91

Westinghouse
Science & Technology Center

1670



1668

SDC OUTER TRACKING
ORNL/ORDC

Tony A. Gabriel - Co-ordinator

Lead Mechanical Engineer
Ted L. Ryan

Lead Electrical Engineer
Gary T. Alley

Lead Material Engineer
John Shaffer

During the next 7 - 9 months ORNL will provide 3 - 4 full time mechanical engineers, 1 electrical engineer, 1 material engineer, and 1 high energy physicist to start the detailed engineering necessary for the development of the outer central tracker as well as the overall integration of the central tracking system.

ORNL PLANNED MECHANICAL AND MATERIAL ENGINEERING ACTIVITIES FOR FY 92

- Continue analysis, design, and fabrication of modules to determine feasibility and cost.
- Continue analysis and design of stable base cylinder and supporting structure (modules, fibers, or single straws).
- Electronic cooling, piping, and detector gas system
- Development plan: costing and scheduling for various options.
- System integration

ORNL PLANNED ELECTRONICS ACTIVITIES FOR FY 92

- Design a printed circuit board assembly prototype for large (100 channel) strawtube array readout.
- Investigate critical issues such as packaging density, crosstalk, voltage distribution, mechanical alignment, and cooling.
- Develop 100 channel readout system utilizing the new 8-channel Penn ASD chip and advanced packaging techniques.
- Successful completion of this work will be a working demonstration of the packaging, cooling, and readout density necessary for the full-scale strawtube tracking system.

1676

ORNL IS WELL QUALIFIED TO DEVELOP, DESIGN AND BUILD THE CENTRAL TRACKER

- National Laboratories historically develop, construct, and coordinate large DOE projects.
- High energy physicists on staff at ORNL
- Have in depth capabilities
  - graphite composite design development and fabrication
  - engineering of high technology equipment (mechanical, electrical, and developmental)
  - fabrication of large high precision equipment and developmental electronics
  - high accuracy testing and QA assembly
  - available facilities to house assembly

1675

ORNL WANTS RESPONSIBILITY FOR THE FOLLOWING ON THE SDC CENTRAL TRACKER WITH TRACKING GROUP OVERSITE

Task	How Accomplished
Coordination with the central tracking task force and the physics community to define detail design requirements and monitor the engineering.	ORNL staff physicists and visiting scientist
Hardware integration with silicon tracker, intermediate tracker and remainder of detector	ORNL Engineering
Coordination with silicon and intermediate tracker designers	ORNL Engineering
Conceptual design of outer tracker	ORNL Engineering
Software integration/development	ORNL/other Labs and Universities/Industry
Construction of outer tracker (mechanical and electrical)	ORNL/Industry/Other Labs and Universities
Assembly of outer tracker	ORNL/Industry/SSCL
Test and Checkout	ORNL/SSC
Installation support	ORNL/SSC
Operational support (if required)	ORNL/SSC

1678

OBSERVATIONS

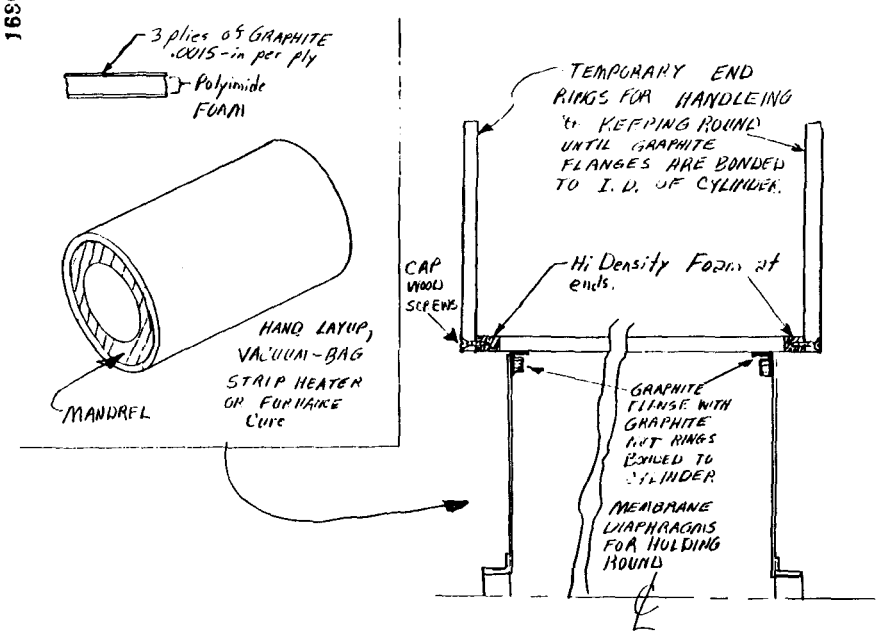
- ORNL cannot dictate and does not intent to dictate physics design aspects.
- Only a best guess can be made for the physics design until the simulations models have been completed and the analysis completed. This may be 18 months in the future.
- Also the design requirements cannot be finalized and must encompass a broad range of options.
- R&D is still required for both straws and fibers and demonstration of operation in a beam before either can be assured of meeting tracker requirements.
- R&D is still required for straw electronics and fiber detectors.

1677

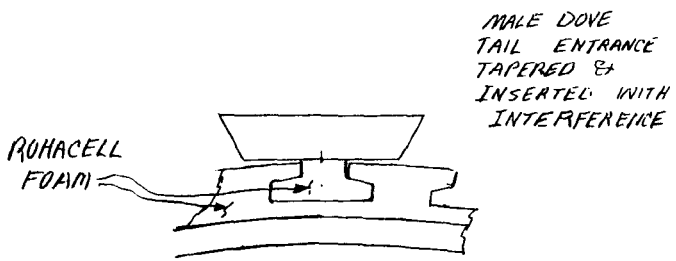
ORNL IS WELL QUALIFIED TO DEVELOP, DESIGN AND BUILD THE CENTRAL TRACKER (cont'd)

- ORNL has made major contributions to all tracker concepts
  - stable base cylinder
  - analysis, design, and fabrication of modules
  - structure support concepts
  - electronics design/development/packaging

1650



1652

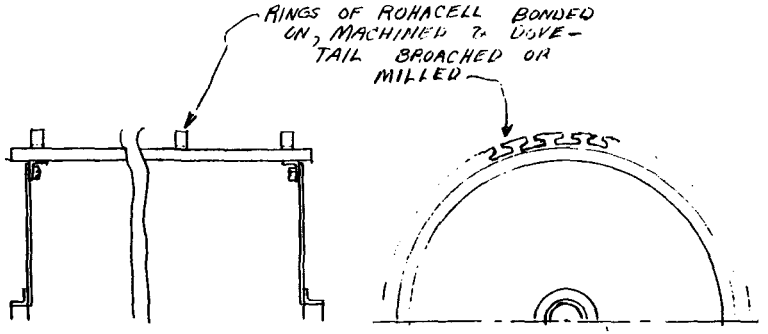


1670

RECOMMENDATIONS

- **Pick a base line physics design now**
- **Continue straw and fiber R&D**
- **Develop a flexible mechanical/structural design which will support both straws and fibers and be adaptable to phasing/staging/upgrading of tracker.**
- **Finalize physics and mechanical design when the simulation results are available.**

1651



CENTRAL AND FORWARD TRACKING SUBSYSTEM
ORNL COLLABORATION MEETING REPORT
SEPTEMBER 25 1991

PROJECT # 9TM3-IUTDB

COVERING MAY 1991 TO SEPTEMBER 1991

WESTINGHOUSE ELECTRIC CORPORATION

(W)STC

PITTSBURGH, PA

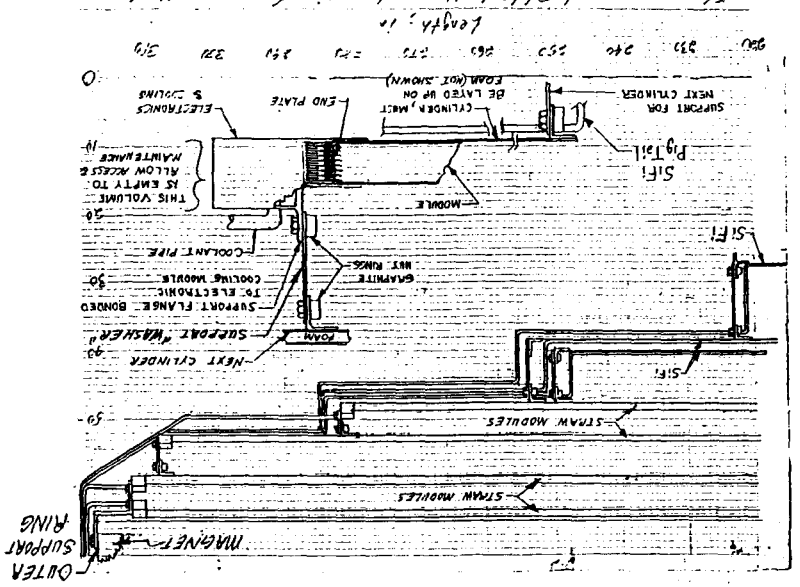
R.L.SWENSRUD (ROGER)

D.T.HACKWORTH (DON)

Viewgraph 1
RLS
09.26.91

Westinghouse
Science & Technology Center

1685



If you can not attach the outer ring (the ring that provides overall support) to the magnet (or any other structure) except in a few radial points, then beef up the outer ring only. You need no other rings.

1663

CENTRAL AND FORWARD TRACKING SUBSYSTEM

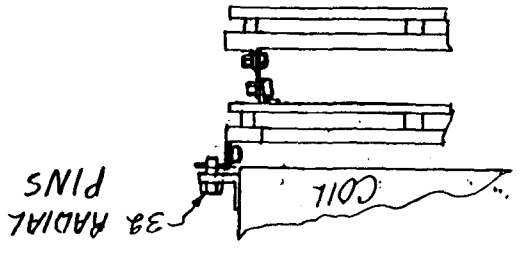
TABLE OF CONTENTS

	Introduction
1	Support Structure Overview
	Requirements
	Alignment Required
2	Materials Available
*	Component Radiation Lengths
	Support Component Design, Manufacturing, and Costing
3	Spaceframe End Support
4	Support Structure Analysis
5	Support Cylinders
6	Shim Rings
7	Mandrel Analysis
	Support Component Assembly
	Module Attachment

Viewgraph 3
RLS
09.26.91

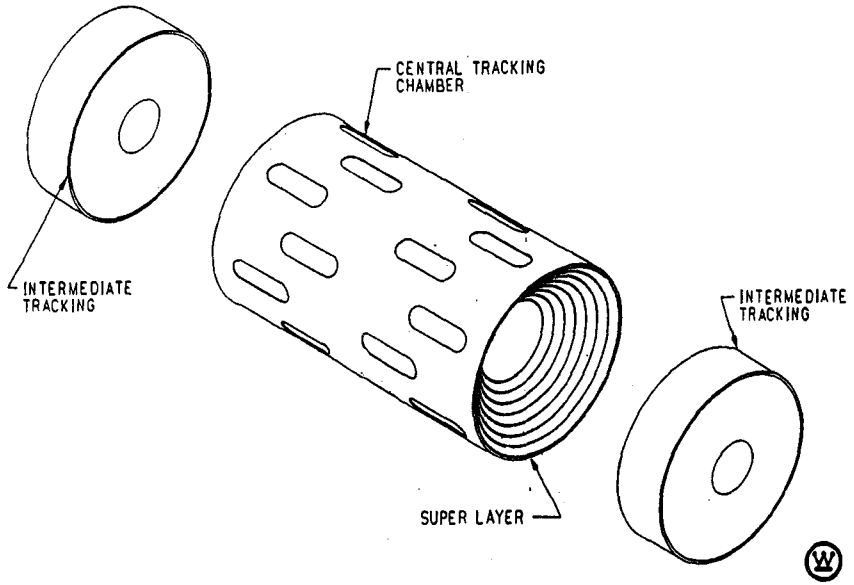
Westinghouse
Science & Technology Center

1686



1654

MODULAR STRAW TUBE TRACKING SYSTEM
EXPLODED VIEW



0.389.4136A44.RI
KEPES 12-4-90

1689

CENTRAL AND FORWARD TRACKING SUBSYSTEM

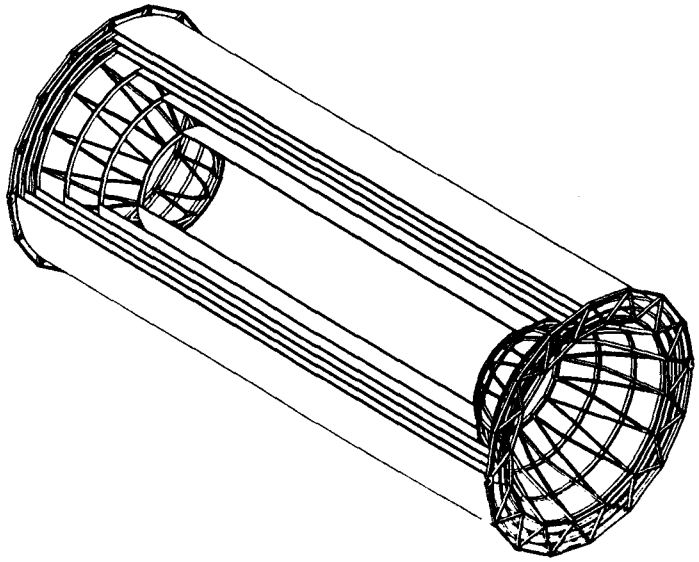
1 **SUPPORT STRUCTURE OVERVIEW**

Viewgraph 6
RLS

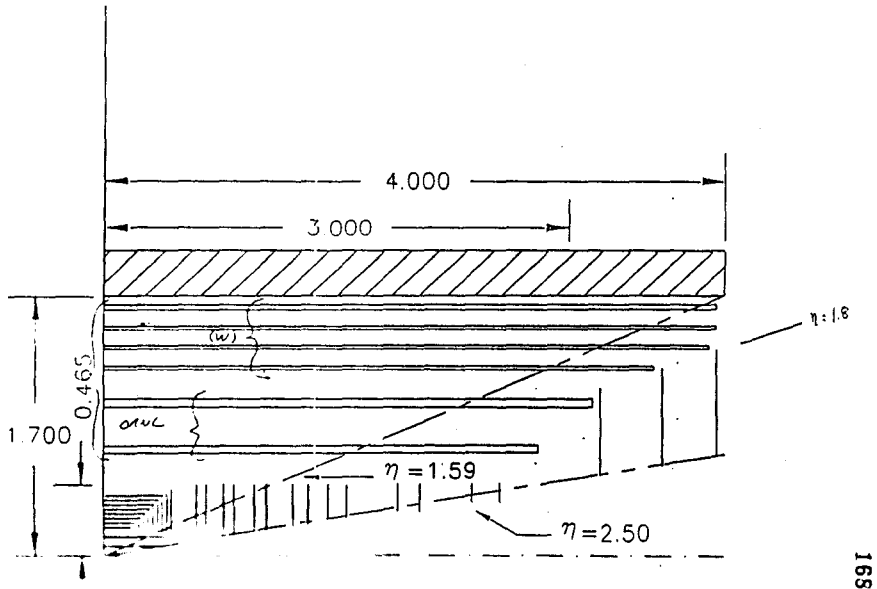
Westinghouse
Science & Technology Center

1687

CENTRAL TRACKER SUPPORT STRUCTURE



1690



1688

SILICON TRACKING SYSTEM

Candidate	(1) Elastic Modulus E - GP_a	Thermal Strain ppm @ - 20°C ΔT	Moisture Elongation ppm @ max H_2O Absorption	(2) Water Absorption % by Weight
Epoxy Matrix				
IM6/3501-6	78.1	-28.70	610	1.9
AS4/3501-6	54.6	-48.24	684	1.9
UHM/3501-6	95.8	- 3.77	446	1.9
P75/3501-6	107.8	+10.10	349	1.9
GY70/930	113.9	+ 0.99		
P75/PR500			45	
P75/ ERL 1962			110	
P100/ERL 1962			47	
Cyanate Ester Matrix				
P75/954-3			10	

(1) Quasi-isotropic
(2) Butane absorption unknown, expected % less than H_2O

Los Alamos

1693

CENTRAL AND FORWARD TRACKING SUBSYSTEM

TABLE 1 - SUMMARY TABLE OF RADIATION LENGTH CALCULATIONS

	Support Cylinder				Modules				
	Graphite TK/Layer	Foam		Shim Ring	Graphite TK/Layer	Foam		Module Edge	Percent Radiation
Table #	Inches	Type	TK Inches	Effects	Inches	Type	TK Inches	Effects	Length/Layer
2	0.0045	51WF	1	No	0.006	51WF	0.14	No	0.98
	0.0045	311G	1	No	0.006	51WF	0.14	No	1.15
3	0.0045	311G	1	No	0.006	51WF	0.14	No	0.92
4	0.0045	311G	1	No	0.0045	51WF	0.14	No	0.87
5	0.0045	311G	1	No	0.0045	311G	0.14	No	0.98
6	0.0045	311G	0.59	No	0.0045	51WF	0.14	No	0.82
7	0.0045	311G	0.59	No	0.0045	311G	0.14	No	0.76
8	0.0045	311G	0.59	No	0.0045	311G	0.14	Yes	0.78
9	0.0045	311G	0.59	Yes	0.0045	311G	0.14	Yes	0.79
9	(Same as above except EDA = 1.64)								2.12
10	(Spaceframe end disk spread radiation length calculation)								0.24
	0.24 rad lg is equivalent to				0.008 inch thick aluminum sheet)				
					0.024 inch thick graphite sheet)				

1691

CENTRAL AND FORWARD TRACKING SUBSYSTEM

SUPPORT STRUCTURE COMPONENT DESIGN, MANUFACTURING, AND COSTS

3 Spaceframe End Support
4 Support Structure Analysis
5 Support Cylinders
6 Shim Rings
7 Mandrel Analysis
Support Component Assembly
Module Attachment

Viewgraph 10
RLS
09.26.91

Westinghouse Science & Technology Center

1694

CENTRAL AND FORWARD TRACKING SUBSYSTEM

2 MATERIAL AVAILABLE

MATERIAL	Elastic Modulus E-Msi	Density ρ (lb/in³)	CTE α ppm/F	Tensile Yield Strength Ksi	Compressing Strength Ksi	Volume Change 50% Humidity Percent	Effective Radiation Length L-cm
MATERIAL CANDIDATES							
Graphite & Epoxy**	40.00	0.0571	0.06	32.0	7.0	0.2(est.)	25.7
Carbon-Carbon**	16.00	0.0600	-0.11	40.0	40.0	0.0	18.8
Al-MMC sub f*	53.97	0.0907	0.60	100.0	40.0	0.0	11.8
Al-MMC sub p***	15.07	0.1000	5.00	75.0	75.0	0.0	9.0
Rohacell 31 lg	0.005	0.0012	2.05	0.142	0.057	0.2	936.6
51 WF	0.011	0.0019	1.83	0.232	0.116	0.2	576.4
300 WF	0.052	0.0109	?	1.450	2.320	0.2	99.9
REFERENCE MATERIALS							
Aluminum	10.40	0.1012	12.89	40.0	40.0	0.0	8.9
Beryllium	42.05	0.0665	6.44	27.0	27.0	0.0	35.4
Copper	16.99	0.3219	9.39	10.8	10.0	0.0	0.8

*Graphite Fiber (P-110) MMC-Metal Matrix Composite, uni-directional properties
**Uni-directional properties
***Particle Reinforced MMC-Metal Matrix Composite, machineable, brazable

Viewgraph 9
RLS
09.26.91

Westinghouse Science & Technology Center

1692

CENTRAL AND FORWARD TRACKING SUBSYSTEM

MANDREL FEA ANALYSIS

7 "CATENARY TYPE SUPPORT" MANDREL

THE DESIGN GOALS:

1) Machining On The Mandrel Requires The Mandrel To Be Round And Straight
2) Design Mandrel To Have Minimum Sag or Bending Deflection
   - o Goal of Sag Less Than .005 Inches
   - o Goal of Roundness Within .005 Inches
3) Without Bending Isolation FEA Predicts .020 inches Sag

Viewgraph 21
RLS
09.26.91

Westinghouse Science & Technology Center

1697

CENTRAL AND FORWARD TRACKING SUBSYSTEM

5 SUPPORT CYLINDERS

THE DESIGN USES:

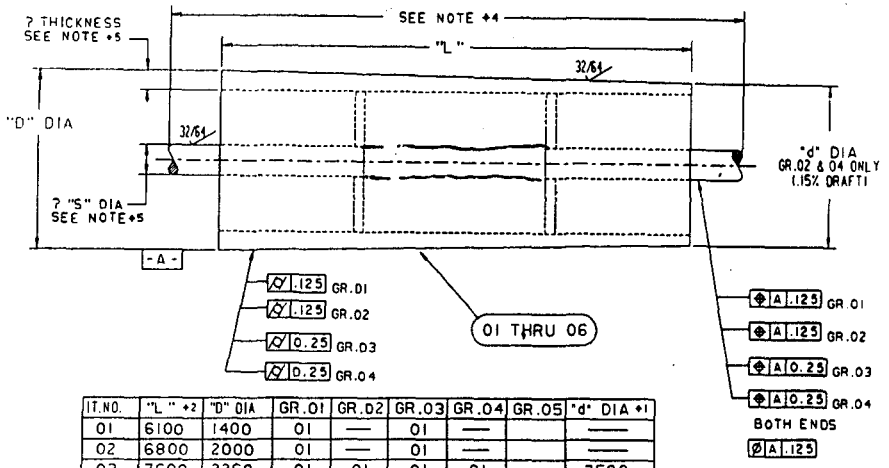
1) Graphite Lamina With Foam Core Composite Cylinders On Which The Detectors Are Mounted
2) Need At Least Two 0.0045 Inch 3 Ply Layups with 15 Milimeter (.59) Inch Thick Rohacell 31IG Core
3) Meets Radiation Length Requirements

Viewgraph 15
RLS
09.26.91

Westinghouse Science & Technology Center

1695

CENTRAL AND FORWARD TRACKING SUPPORT CYLINDER TAPE LAYUP MANDREL

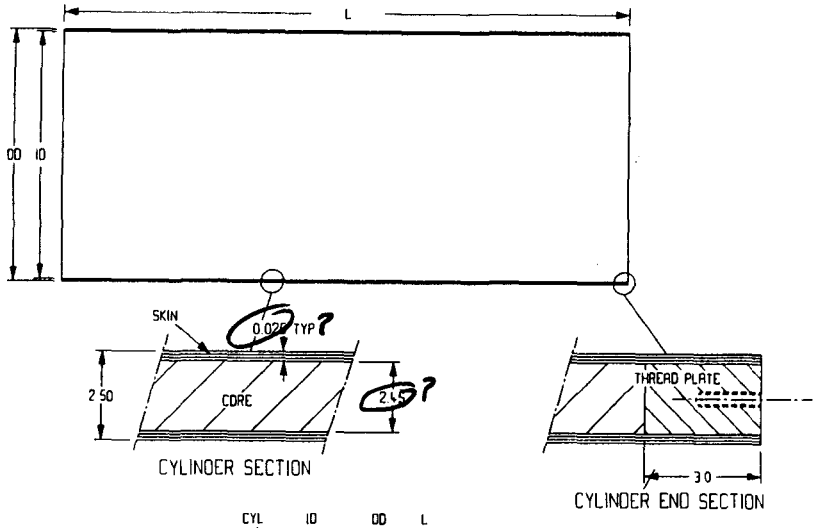


IT.NO.	"L" +2	"D" DIA	GR.01	GR.02	GR.03	GR.04	GR.05	"d" DIA +1
01	6100	1400	01	—	01	—		—
02	6800	2000	01	—	01	—		—
03	7600	2268	01	01	01	01		7589
04	8300	2532	01	01	01	01		8288
05	8400	2790	01	01	01	01		8387
06	8400	3064	01	01	01	01		8387

+1· USE .15% TO CALCULATE ACTUAL DIAMETER AT "d" END
+2· "L" INCREASED BY .5 m FOR "AIR FLANGE" AND TEST COUPONS
+3· INCLUDE ONE SET SHAFT AND BEARING SEPARATE QUOTE
+4· SUPPLY BEARING CENTERLINE AND TOTAL SHAFT LENGTH
+5· SUPPLY SHAFT DIA AND SHELL THICKNESS
+6· ALL ITEMS TO BE BALANCED

D.389.4136A84.R1
DIMS. IN MILLIMETERS
KEPES 5-10-91

1698



CYL	ID	OD	L
1	--	--	--
2	--	--	--
3	232.0	237.0	820
4	258.6	263.6	820
5	284.8	289.8	820
6	311.2	316.2	820

SUPPORT CYLINDER DIMENSIONS WESTINGHOUSE STC

ALL DIMENSIONS ARE IN CM
DM 8-15-91 AS PER CENTAK1A

1696

CENTRAL AND FORWARD TRACKING SUBSYSTEM

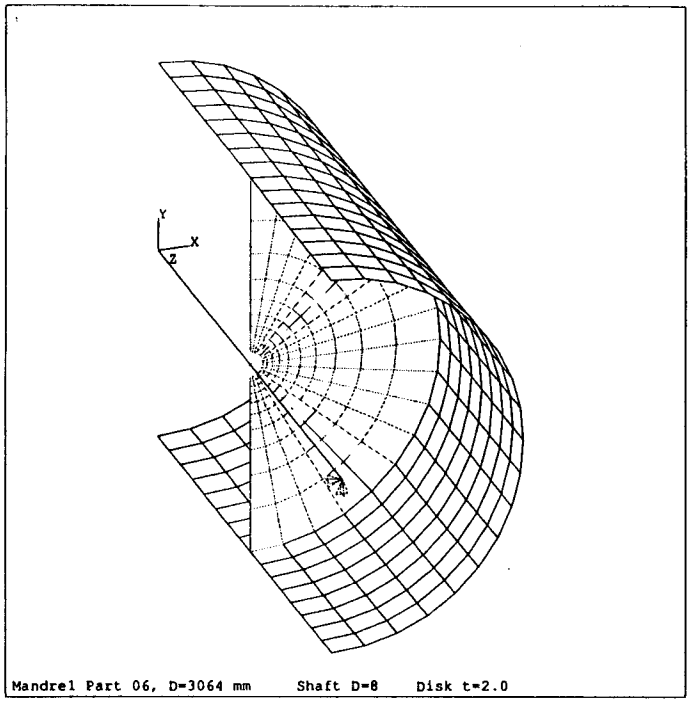
7 MANDREL STRESSES & DISPLACEMENTS FROM FINITE ELEMENT ANALYSIS

Shaft Dia in.	Disk Tk in.	Disk Nom. kips -in.	Disk Slope	Disk σ_θ ksi	Disk σ_r ksi	Displacement Inches Place	Cyl End	Disk	Cyl Midpt	Local Max.	Local Min.
8.0	1.0	170.	0.0186	74.5	83.7	T/B	2.32452	2.32413	2.32464	2.3250	2.3226
						Side	2.32448	2.32441	2.32463		
						Shaft		2.32377			
8.0	2.0	642.	0.0092	67.0	75.1	T/B	1.61647	1.61655	1.61710	1.6196	1.6137
						Side	1.61642	1.61672	1.61715		
						Shaft		1.61634			
10.	1.0	93.	0.0091	34.1	38.2	T/B	1.11005	1.10961	1.11011	1.1107	1.088
						Side	1.11001	1.10988	1.11009		
						Shaft		1.10929			
10.	2.0	404.	0.0062	41.4	46.5	T/B	0.89374	0.89371	0.89422	0.8960	0.8916
						Side	0.89369	0.89388	0.89425		
						Shaft		0.89352			
12.0	1.0	63.	0.0051	17.8	10.9	T/B	0.60024	0.59978	0.60027	0.6005	0.5994
						Side	0.60020	0.60005	0.60024		
						Shaft		0.59948			

Viewgraph 22
RLS
09.26.91

Westinghouse Science & Technology Center

1701



Mandrel Part 06, D=3064 mm Shaft D=8 Disk t=2.0

ANSYS 4.4A
SEP 5 1991
15:49:16
PLOT NO. 1
POST1 ELEMENTS
TYPE NUM

XV =-1
YV =-1.4
ZV =-3
*DIST=101.549
*XF =29.97
*ZF =87.677
PRECISE HIDDEN

POST1 NODES
TDIS

XV =-1
YV =-1.4
ZV =-3
*DIST=101.549
*XF =29.97
*ZF =87.677

1699

CENTRAL AND FORWARD TRACKING SUBSYSTEM

3 SPACEFRAME END CYLINDER SUPPORTS

THE DESIGN USES:

1) Selected Simple Spaceframe Which Utilizes Commercially Available Technology (Kaiser Aerotech, Oakland Calf.)
   - o High Stiffness Graphite Fiber Struts
   - o Molded Graphite Joints

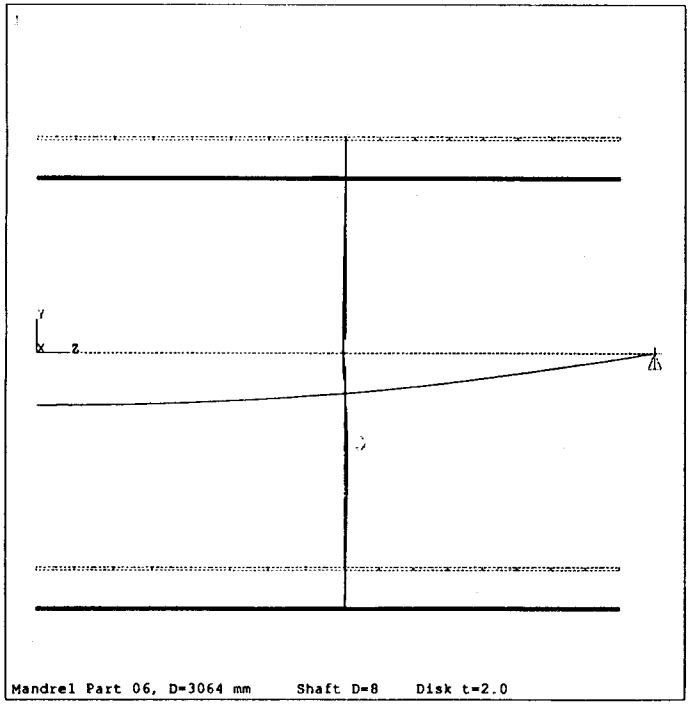
2) Advocate Graphite Bolts For Cylinder Spaceframe Interface which Are Commercially Available (K-Karb from Kaiser AeroSpace)

3) Kaiser Issued Written Quoted Estimate on Material Costs (09-19-91)

Viewgraph 11
RLS
09.26.91

Westinghouse Science & Technology Center

1702



Mandrel Part 06, D=3064 mm Shaft D=8 Disk t=2.0

ANSYS 4.4A
SEP 5 1991
15:57:49
PLOT NO. 1
POST1 DISPL.
STEP=1
ITER=1
DMX =1.453
ERPC=0

*DSCA=10
XV =-1
DIST=96.445
XF =5.998
ZF =87.677

POST1 NODES
TDIS

XV =-1
*DIST=96.445
*XF =5.998
*ZF =87.677

1700

SPACE FRAME

WESTINGHOUSE STC

DM 9-13-91

1703

SPACE FRAME
WITH CYLINDER RINGS

WESTINGHOUSE STC

DM 9-13-91

1704

STRUCTURAL TUBING QUANITIES FOR TWO SUPPORT FRAMES

TUBE #	L.CM	QUAN-FRAME	TOTAL
1	43.45	16	32
2	54.36	2	4
3	53.19	2	4
4	55.92	28	32
5	58.91	2	4
6	61.91	2	4
7	64.55	12	24
		TOTAL	128 PCS.

MATERIAL GRAPHITE - EPOXY COMPOSITE

ALL DIMENSIONS IN CM.

SUPPORT FRAME STRUCTURAL TUBING WESTINGHOUSE STC

DM 8-2-91

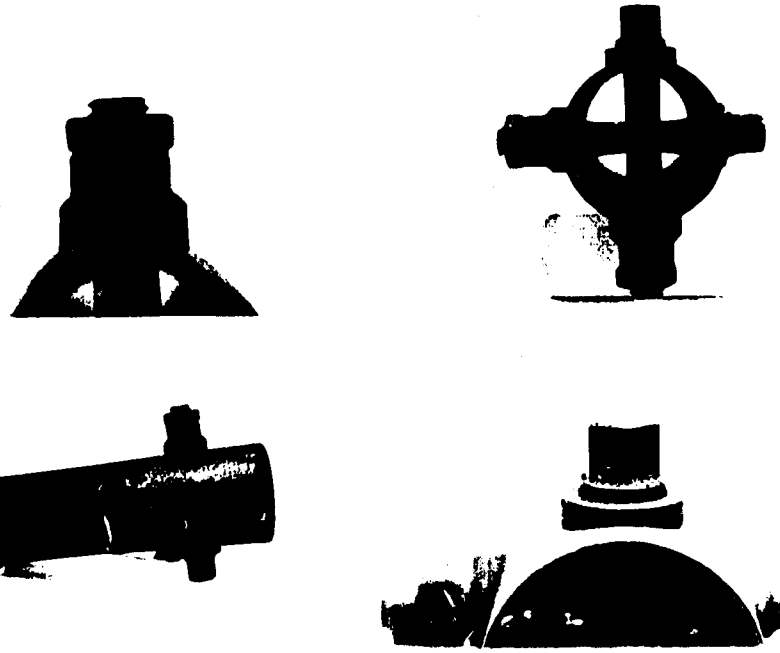
1706

SPACE FRAME OUTSIDE STRUT CONNECTOR

WESTINGHOUSE STC

DM 9-20-91

1705



1709

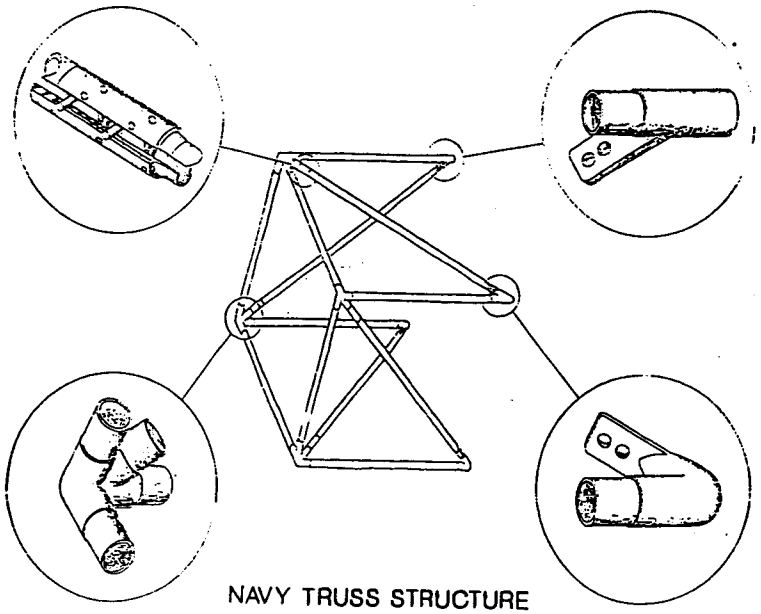
KAISER AEROSPACE & ELECTRONICS

- ORIGIN: Kaiser Industries (Aluminum, Steel, Cement, Gypsum, Engineers, Permanente)
- CURRENT SALES: $300 Million
- 2,000 Employees
- 30 Years Ablative and Carbon-Carbon Production
- 25,000 Rocket Nozzles to Date
- Free World's Largest Producer of Structural Carbon-Carbon

KAISER AEROTECH
A KAISER AEROSPACE & ELECTRONICS COMPANY
FORM SL-230A

February 1991

1707



NAVY TRUSS STRUCTURE

1710

KAISER AEROTECH

- Carbon-Carbon Rocket Nozzles
- Carbon-Phenolic Ablatives
- Industrial-grade Carbon-Carbon
- Advanced Ceramics
- High Temperature Fasteners and Joining (3-D Braiding)
- Space Structures and Tubing (Thin Wall)
- 3-D Fabric Weaving and Densification (Cylinder and Nose Cones)
- Carbon-Carbon and Composite Tooling
- Coatings for Carbon-Carbon and Ceramics
- Carbon-Carbon and Titanium Complex Machining
- Carbon-Carbon Honeycomb and Graphite Foam Panels
- Sandwich Panels: Graphite Foam, Honeycomb
- Deployable Space Structures
- Broad Thermal, Mechanical, Physical, Surface Properties Data Base

KAISER AEROTECH
A KAISER AEROSPACE

February 1991

1708

1711

KAISER AEROTECH

KAISER AEROTECH
[illegible]
MAIL ADDRESS P.O. BOX 1678
SAN LEANDRO, CALIFORNIA 94577-0867 · (415) 562-2456
FAX (415) 568-8420 / TWX 910-366-7014 (KAISER AEROSLN)

KA91-081-RLB-001
September 19, 1991

Westinghouse
Science and Technology Center
1310 Beulah Road
Pittsburgh, PA 15236

Attention: Mr. Robert Swensrud

Subject: Budgetary Estimate to
Fabricate Superconductor Super Collider Support Tubing

Gentlemen:

Below are budgetary prices for graphite/epoxy Support Frame Structural Tubing and Connectors. For the Tubing, we used three different moduli graphite fibers yielding 17, 40, and 50 million modulus Tubing. All Connectors have 17 million modulus material.

We expect that the coefficient of thermal expansion will be between -1 and 0 x 10^{-6} in/in/°F.

As we discussed, the wall thickness of the highest modulus Tubing could be reduced, which would lower the price since these high modulus fibers are very costly. We can address this as you get closer to your final design.

The prices are based on a total of 470 feet of Tubing, cut to roughly two-foot lengths, with 160 Connectors. We will ship these components unassembled. Fasteners and any adhesives are not included, and we have given you separate prices on our K-Karb bolts and nuts.

Total Budgetary Price for Support Frame Structural Tubing, 470 feet, with 160 Connectors:

1712

	17 MILLION MODULUS TUBING	40 MILLION MODULUS TUBING	50 MILLION MODULUS TUBING
3 cm OD Round Tubing	$180,000	$250,000	$300,000
4 cm OD Round Tubing	220,000	310,000	350,000
2 x 4 cm Rectangular Tubing, with 0.5 cm Radius	190,000	260,000	300,000

If you should have any questions, please contact the undersigned at (510) 562-2456, extension 238 or Wade Brown at extension 251.

Sincerely,

KAISER AEROTECH

Ronald L. Bauer
Vice President of Marketing
and Business Development

WHB:pg

1713

CENTRAL AND FORWARD TRACKING SUBSYSTEM

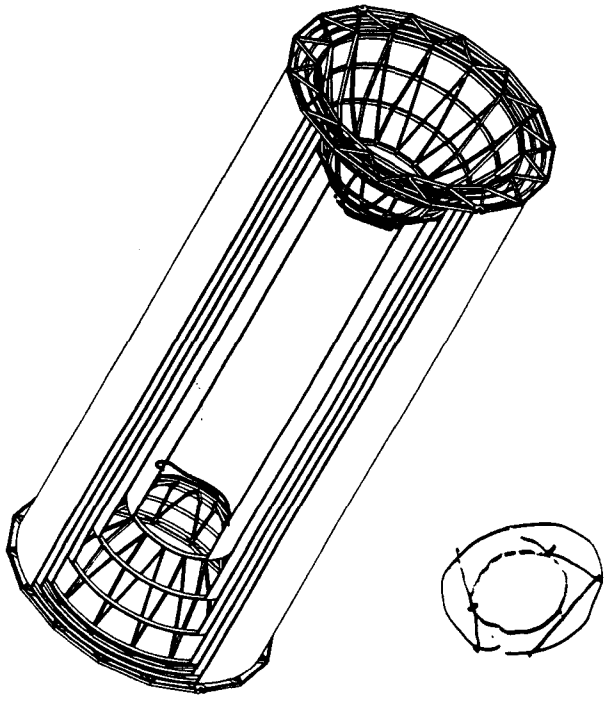
K-KARB® CARBON-CARBON AND GRAPHITE EPOXY BOLTS BY KAISER AEROTECH

Fabricated Bolt Material Properties:

Bolt	Size	Tap Drill Inches	Thread Shear Psi SS Ult @ 1.5 o.d.	Pounds
A) Alum	1/4-20	0.204	36000	7060
B) Steel	1/4-20	0.204	32000	6276
C) K-Karb	1/4-20	0.204	3640	714
D) K-Karb	3/8-16	0.316	2640	1242
E) K-Karb	1/2-13	0.422	1970	1653

1714

CENTRAL TRACKER SUPPORT STRUCTURE

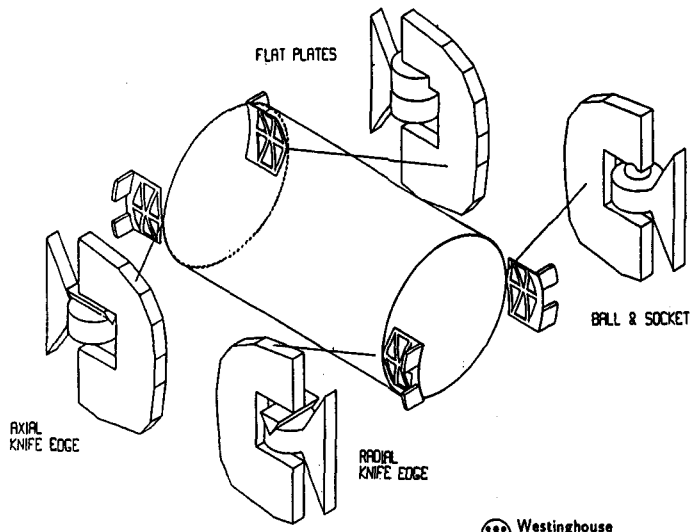


DM 9-20-91

WESTINGHOUSE STC

CENTRAL AND FORWARD TRACKING SUBSYSTEM

CENTRAL TRACKER MOUNTING



Westinghouse
Science & Technology Center

1717

CENTRAL AND FORWARD TRACKING SUBSYSTEM

4

DEFLECTION FEA ANALYSIS
SPACEFRAME AND CYLINDER STRUCTURE

TABLE NUMBER 1
COMPONENT PROPERTY MODEL IN FEA

Cylinders			P-75		Spaceframe		
	Foam Core		Graphite	Composit		Struts	
Foam Core	Thickness	Lamina	Thickness	Thicknes	Modulus	Size	Wall Tk
31 IG	.59 IN.	0/60/60	.0045 IN.	15mm	40 MSI	2 X 4 cm	2.5 mm

TABLE NUMBER 2
MASS SUMMARY OF MODEL FROM COMPUTER

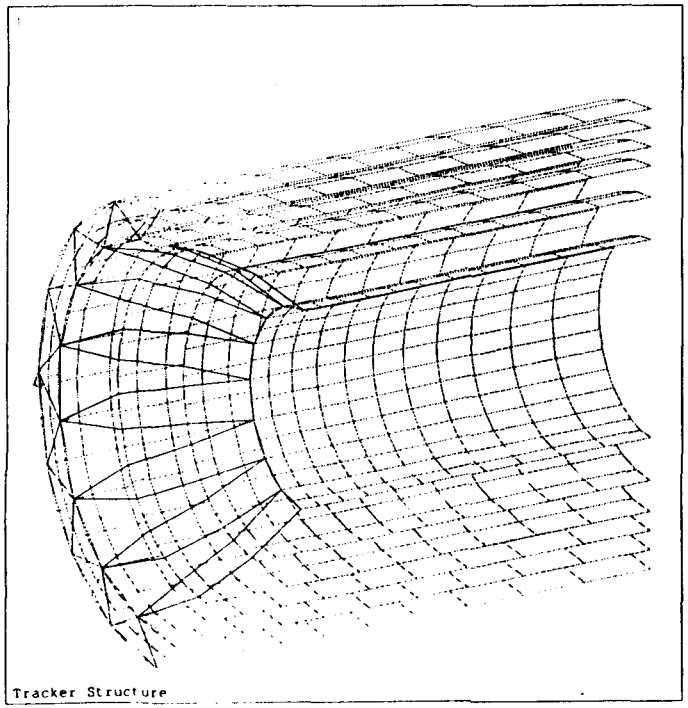
	All Straws Layer1,2,3,4,5,6		Mixed System Straws 3,4,5,6 SiFi 1,2	
Item	Mass Kg	Pound	Mass Kg	Pounds
Cyls With/Modules	1015.5	2239.2	828.4	1826.2
Cyls With/SiFi	0	0 *	613.8	1353.5
Struts & Joints	70.9	156.3	70.9	156.3
Rings	29.3	64.6	29.3	64.6
Pigtails	0.0	0.0	254.0	560.1
TOTAL	1115.7	2460.1	1796.4	3960.7

*(940.5 lbs is 42% less wt for modules)

Viewgraph 13
RLS
09.26.91

Westinghouse
Science & Technology Center

1715




```
 ANSYS  4.4A
 SEP 22 1991
 18:30:27
 PLOT NO.   1
 PREP7 ELEMENTS
 REAL NUM

 XV  =-1
 YV  =0.4
 ZV  =-0.6
*DIST=2320
*XF  =807.5
*ZF  =1975
 PRECISE HIDDEN

 PREP7 ELEMENTS
 REAL NUM

 XV  =-1
 YV  =0.4
 ZV  =-0.6
*DIST=2320
*XF  =807.5
*ZF  =1975

 PREP7 NODES
 TDLS

 XV  =-1
 YV  =0.4
 ZV  =-0.6
*DIST=2320
*XF  =807.5
```

1718

```
COMPOSITE MATERIAL PROPERTIES

MATERIALS:
   FIBER - HERCULES CARBON FIBER Type URM
           MODULUS 44.5 Mpsi

           RESIN - HERCULES 3501-6 (present system)
                   HERCULES 55x-3 (proposed for low moisture
                                   absorption)
           CORE - ROHACELL FOAM

MECHANICAL PROPERTIES FOR FIBER / RESIN LAYUP [ 0 , +/- 60 ]sym

ELASTIC MODULUS                    POISSON RATIO

Ex (axial) = 16.6 Mpsi             MUxy = .317
Ey (hoop)  = 16.6 Mpsi             MUyz = .337    MUzy = .018
Ez (radial) = 1.67 Mpsi            MUxz = .337    MUzx = .018

SHEAR MODULUS

Gxy = 5.45 Mpsi
Gyz = .5   Mpsi
Gxz = .5   Mpsi

COMPOSITE CONSTRUCTION VALUES

                                   .059 inches
   INNER COMPOSITE PLY             .236 inches
   FOAM CORE                       .059 inches
   OUTER COMPOSITE PLY             .354 inches
                          TOTAL
```

1716

CENTRAL AND FORWARD TRACKING SUBSYSTEM

4

DEFLECTION FEA ANALYSIS
SPACEFRAME AND CYLINDER STRUCTURE
TABLE NUMBER 3
DEFLECTION RESULTS

Case No.	Model Descriptions	Vertical Support Conditions	Strut Modulus MSI	Results Deflections Microns
1	1 Spaceframe End Only (Fully Loaded With All Straws)	2 @180 Deg	17.0	61.3
2	(Same As Case 1 Above)	2 @90 Deg	17.0	158.0
3	(Same As 1 Above) With Triangles	2 @180 Deg	17.0	38.8 / 23.3
4	(Same As Case 1) No Triangles	2 @180 Deg	40.0	[redacted]
5	Complete All Straw 1,2,3,4,5,6	2 @180 Deg	40.0	[redacted]
6	Straw 3,4,5,6 SIFI 1,2	2 @180 Deg	40.0	[redacted]
7	(Same as 6 Above) With Triangles	2 @180 Deg	40.0	[redacted]

Westinghouse Science & Technology Center

1719

Tracker Support Frame

1720

Tracker Support Frame Supported at 45-deg points

1721

CYLINDER MATRIX

CAP ENDS

0 90 0 [0 +60 -60 0 +60 0]

CORE 2 EX

GRAPHITE

COMPOSITE TRACKER FEA PANEL MESH

MAX DEFLECTIONS - MICRONS - [redacted]

STRAWS | STRAWS & LAYERS | STRAWS & LAYERS

ONLY | SIFI & LAYERS | SIFI & LAYERS

SPACEFRAME | STRAIGHT | STRAIGHT TRIANGLE

[0 90 0 3 LAYERS] | 393 | - | 365

GRAPHITE .0045"EX | | |

CORE 15MM (.59") — REAL-EX ROLL-BUT W/O S

[0 +60 -60 +60 0] | 57 | 126 | 93

GRAPHITE .009 EX | | |

CORE 25MM (1.00"EX) — REAL BUT W/O ROLL

[0 +60 -60 +60 0] | 136 | 317 | 268

GRAPHITE .0045"EX | | |

CORE 15MM (.59") — NOT REAL-EX ROLL

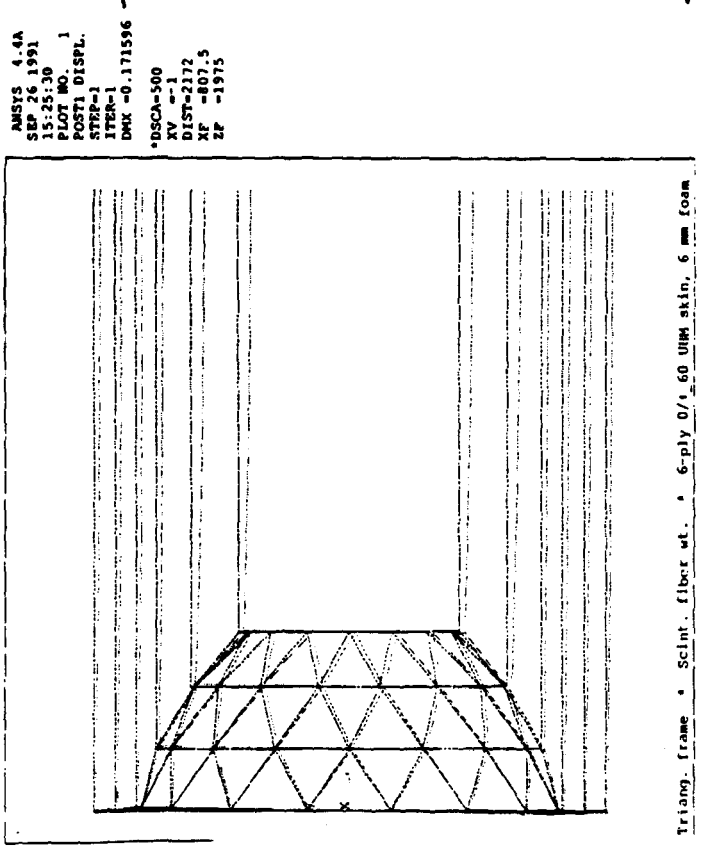
[0 +60 -60 +60 0] | 91 | - | 173

GRAPHITE .009 EX | | |

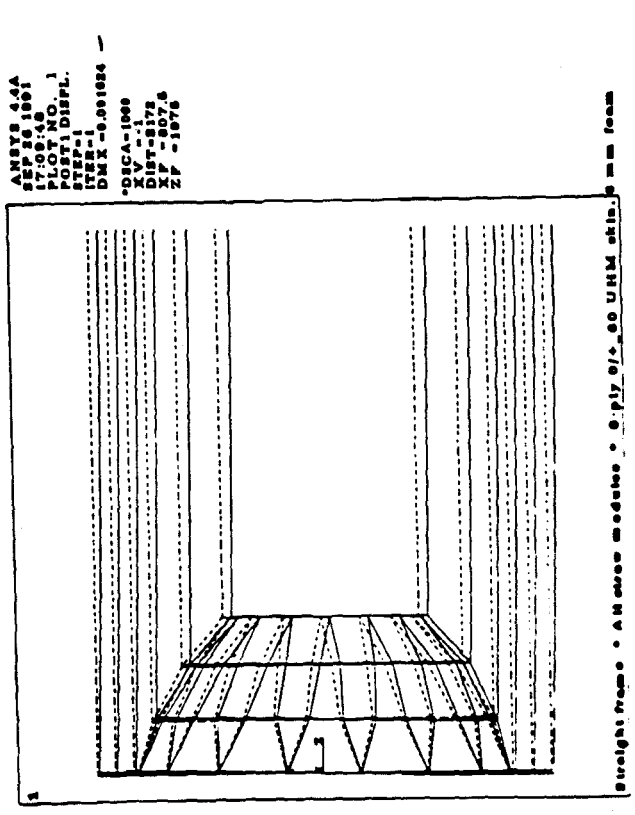
CORE 6MM (.236") — REAL - EX ROLL

1722

1723



1724



1725

CENTRAL TRACKING CHAMBER ASSEMBLY PROPOSAL

DAVID H. VANDERGRIFF

OAK RIDGE NATIONAL LABORATORY

SEPTEMBER 26, 1991

MM-ES

1726

CENTRAL TRACKING CHAMBER ASSEMBLY PROPOSAL OAK RIDGE NATIONAL LABORATORY

This proposal outlines the steps required to fabricate the Solenoidal Detector Collaboration (SDC) Central Tracking Chamber (CTC) at the Oak Ridge National Laboratory (ORNL). The process described utilizes existing ORNL facilities and equipment. The major assumption in this proposal is that the carbon composite support cylinders will be fabricated at ORNL and all other major tooling and equipment will be procured.

The fabrication of the support cylinders and assembly of components will be performed at the K-25 site. This site contains facilities that have been used extensively for the fabrication of composite cylindrical shells. The K-1200 complex will be used in the manufacture of the carbon composite cylinders required for use in the CTC. This facility will also be used for the intermediate and final assembly phases. It provides sufficient head room and crane capacities for the overall assembly and handling of the CTC. The K-1401 shop facility will provide machine shop and autoclaves resources that will be used in the manufacture of the cylinders.

Assembly of the CTC will be performed in two separate areas of the K-1200 complex. The superlayer assembly will be performed in the center bay, where there is sufficient floor space and accommodations for a clean room environment for assembly. The final assembly steps will be performed in the high bay area. This portion of the facility has sufficient size to allow for either horizontal or vertical assembly of the CTC. It is important to have both options available to allow for flexibility in this critical assembly phase.

The overall assembly stand that is proposed will be designed for operation in either the horizontal or vertical position, dependant on design constraints. An outer shell and a central shaft of the fixture will serve as locators for the outer superlayer. The outer shell may also be used as a shipping container. The superlayers will be loaded into the shell or onto the shaft and attached to one another. Upon completion of assembly, the entire unit will be positioned and prepared for shipment.

OBJECTIVES

- DEPICT FABRICATION AND ASSEMBLY STEPS
- DETAIL THE SUPPORT STRUCTURE
- DESCRIBE FACILITIES AND EQUIPMENT AVAILABLE AT ORNL

ASSEMBLY PROPOSAL

- SUPPORT CYLINDER FABRICATION AND ASSEMBLY
- SUPERLAYER ASSEMBLY AND TESTING
- CTC ASSEMBLY AND TESTING
- SHIPPING PREPARATION

SUPPORT CYLINDER FABRICATION (K-1200)

- MODIFY WINDING MACHINE (FOR HEAVIER MANDRELS)
- PROCURE MANDRELS
- PROCURE CARBON FIBERS AND EPOXY
- WIND INNER CARBON LAYER
- INITIAL CURE (K-1400)
- ADD "FOAM" CORE
- MACHINE CORE TO O.D. (K-1400)
- WIND OUTER LAYER
- FINAL CURE (K-1400)
- ADD END PLATES
- REMOVE TO ASSEMBLY AREA

FABRICATION/ASSEMBLY OUTLINE

1. CYLINDER FABRICATION (K1200)
   - A. Procure Mandrels
   - B. Procure Carbon Fibers and Epoxy
   - C. Modify Winding Machine (For heavier Mandrels)
   - D. Wind Cylinder
   - E. Initial Cure - K1400
   - F. Add "Foam" Core
   - G. Machine Core - K1400
   - H. Wind Outer Layer
   - I. Final Cure
   - J. Remove to Assembly Area
2. SUPERLAYER ASSEMBLY (K1200)
   - A. Procure Pretested Straws/Fibers
   - B. Procure Assembly/Alignment Fixtures
   - C. Set up Cylinder in Assembly Fixture (Horizontal)
   - D. Assemble Tracking Elements onto Cylinders (Horizontal)
   - E. S.P.C. Alignment Checking
   - F. Move Unit to Inspection/Testing Area
   - G. Test and Certify Superlayer
3. CTC ASSEMBLY (K1200 HIGH BAY)
   - A. Procure Overall Assembly Stand (Horizontal/Vertical)
   - B. Procure Superlayer Assembly Components
   - C. Attach Outer Superlayer to Assembly Support
   - D. Position Subsequent Superlayer to Outer
   - E. Attach Superlayers to each Other
   - F. Repeat for other Superlayers
   - G. Rotate Unit to Horizontal Position (If Vertical)
4. SHIPPING PREPARATION (K1200)
   - A. Attach End Plates to Fixture
   - B. Evacuate and Fill with Nitrogen
   - C. Remove Complete Unit from Stand
   - D. Place Complete Unit on Transporter

1731

SUPERLAYER ASSEMBLY (K-1200)

- PROCURE PRETESTED TRACKING ELEMENTS
- PROCURE/FABRICATE ASSEMBLY/ALIGNMENT FIXTURES
- REMOVE MANDREL FROM CYLINDER
- INSTALL ROUNDING RINGS TO CYLINDER
- PLACE CYLINDER IN ASSEMBLY FIXTURE
- ASSEMBLE TRACKING ELEMENTS ONTO CYLINDER
- ALIGNMENT CHECKING
- ELECTRONICS ASSEMBLY (IF REQUIRED)
- MOVE SUPERLAYER TO INSPECTION/TESTING AREA
- TEST AND CERTIFY SUPERLAYER

1732

A. INSIDE - OUT ASSEMBLY SEQUENCE (Horizontal or Vertical)

1. Fabricate Cylinders
2. Remove mandrels
3. Insert rounding rings/fixtures onto cylinders
4. Attach tracking elements and inspect
5. Fabricate assembly stand
6. Load inner s/l on positioner cart
7. Move inner s/l into position on stand
8. Align inner s/l and secure to assembly stand shaft
9. Load second s/l onto positioner cart
10. Move second s/l into position on stand
11. Align second s/l relative to inner s/l and secure to assy stand
12. Attach second s/l to inner s/l using support struts
13. Repeat procedure for subsequent s/l's
14. Recheck alignment of all s/l's
15. Move shipping shell into position over CTC
16. Secure end plates of shipping shell
17. Evacuate shell and fill with nitrogen
18. Remove complete unit from stand
19. Load complete unit onto transporter
20. Ship to SSCL site

Assumptions:

Rounding rings keep the cylinders round during s/l assembly and handling
Assembly stand shaft provides sufficient stability to maintain alignment
Cylinder alignment is done relative to locator fiducial

A1. PREPARATION AND ASSEMBLY AT SSCL

a. Complete unit arrives at SSCL
b. Nitrogen is exhausted
c. Shipping shell is removed
d. Alignment of cylinders checked and adjusted if necessary
e. On-site tracking element check-out performed
f. Unit lowered to assembly hall
g. Unit placed onto final assembly track
h. Unit moved into position in the detector
i. CTC attached to the calorimeter supports
j. Rounding rings/fixtures removed from CTC
k. Final alignment and check-out performed

1733

A. OUTSIDE - IN ASSEMBLY SEQUENCE (Vertical)

1. Fabricate Cylinders
2. Remove mandrels
3. Insert rounding rings/fixtures onto cylinders
4. Attach tracking elements and inspect
5. Fabricate assembly stand
6. Load outer s/l on positioner fixture
7. Move outer s/l into position on stand
8. Align outer s/l and secure to assembly stand shell
9. Load second s/l onto positioner fixture
10. Move second s/l into position within inner s/l
11. Align second s/l relative to outer s/l
12. Attach second s/l to outer s/l using support struts
13. Repeat procedure for subsequent s/l's
14. Recheck alignment of all s/l's
15. Rotate assembly to horizontal position
16. Secure end plates to assembly stand shell
17. Evacuate shell and fill with nitrogen
18. Remove complete unit from stand
19. Load complete unit onto transporter
20. Ship to SSCL site

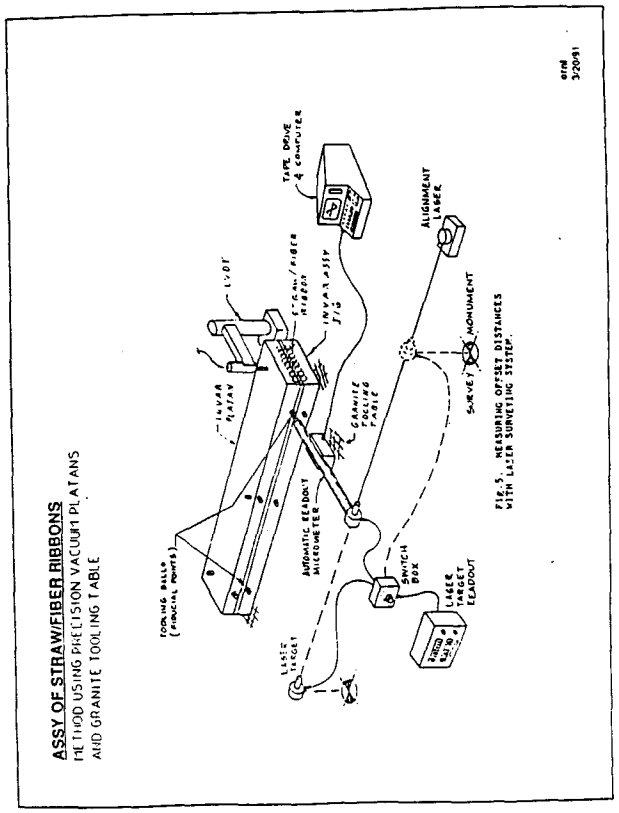
Assumptions:

Rounding rings keep the cylinders round during s/l assembly and handling
Assembly stand shell provides sufficient stability to maintain alignment
Cylinder alignment is done relative to locator fiducial

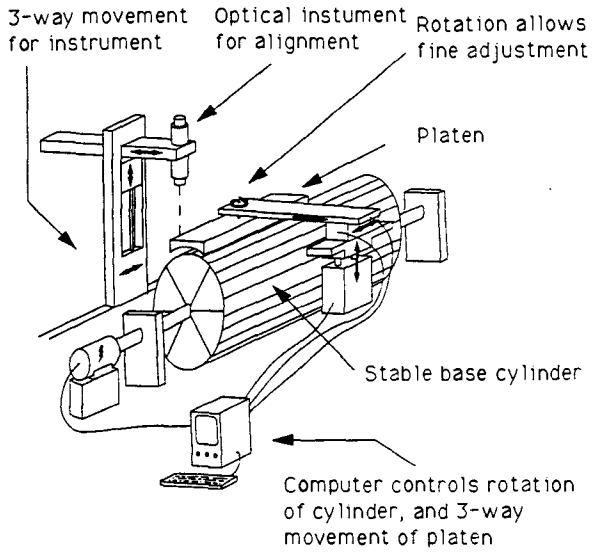
A1. PREPARATION AND ASSEMBLY AT SSCL

a. Complete unit arrives at SSCL
b. Nitrogen is exhausted
c. Shipping shell is removed
d. Alignment of cylinders checked and adjusted if necessary
e. On-site tracking element check-out performed
f. Unit lowered to assembly hall
g. Unit placed onto final assembly track
h. Unit moved into position in the detector
i. CTC attached to the calorimeter supports
j. Rounding rings/fixtures removed from CTC
k. Final alignment and check-out performed

1734



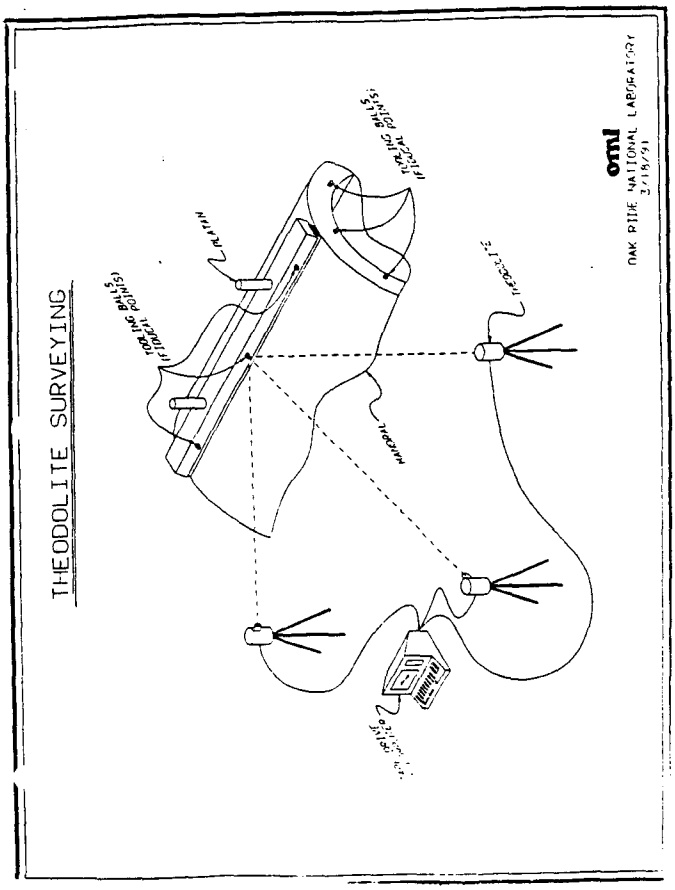
1735



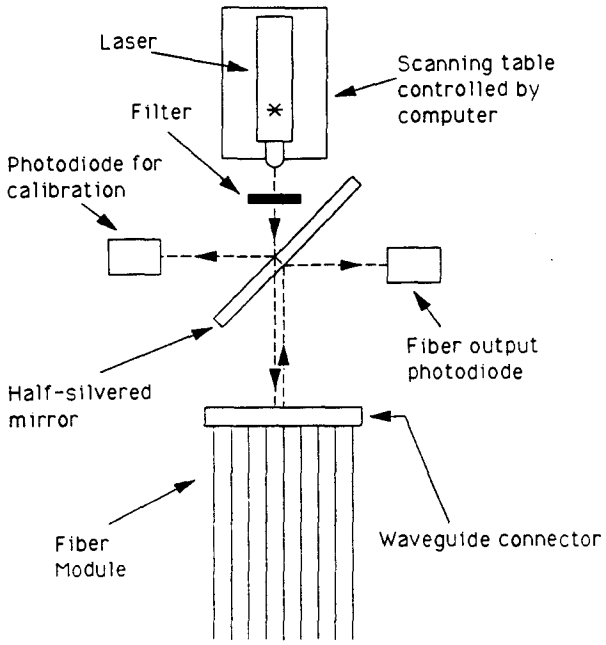
Fiber ribbon placement

Attaching the ribbons will require a large, stable, computer controlled arm for placement. The cylinder is indexed. An optical instrument is used to check the alignment.

1736



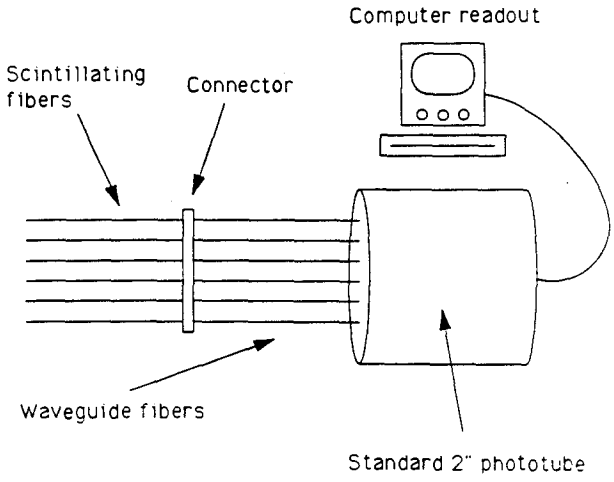
1737



Setup for testing of individual fibers

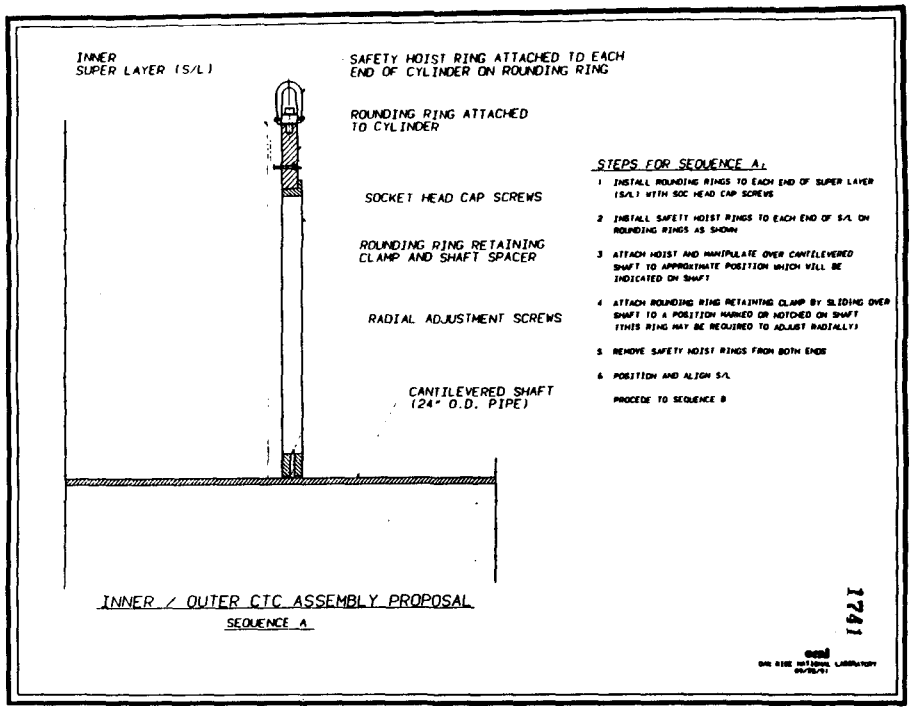
The performance of individual fibers in a module is tested by aiming a laser beam into the fiber. The beam reflects and returns. The measured output is then compared to that of the laser.

1738



Setup for checking screening of background light

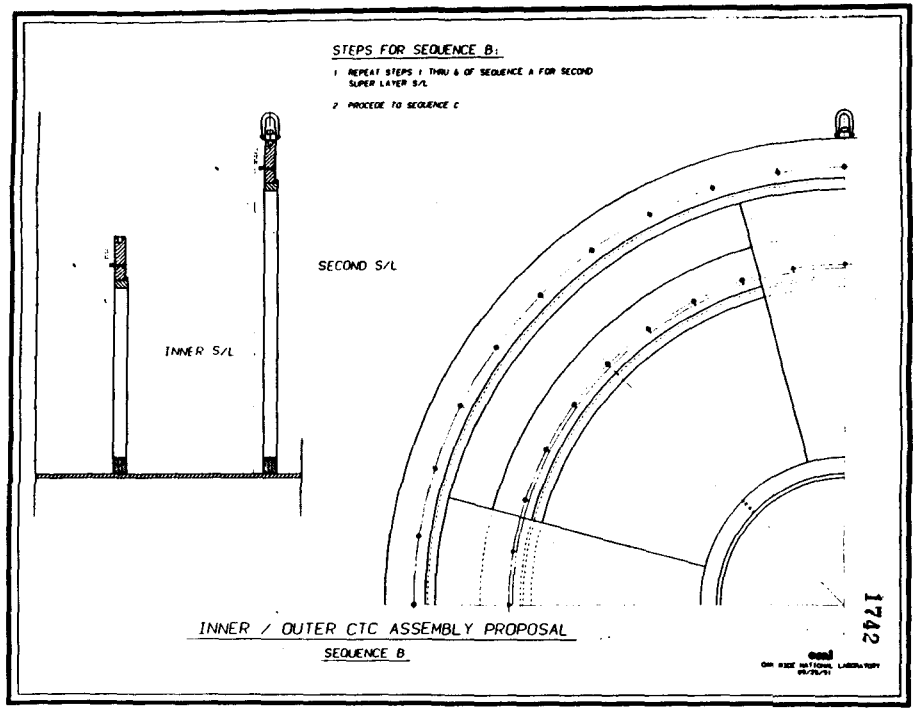
To check that the fiber modules are "light tight", the entire bundle of 1024 fibers is connected with a phototube. Any significant activity indicates a light leak

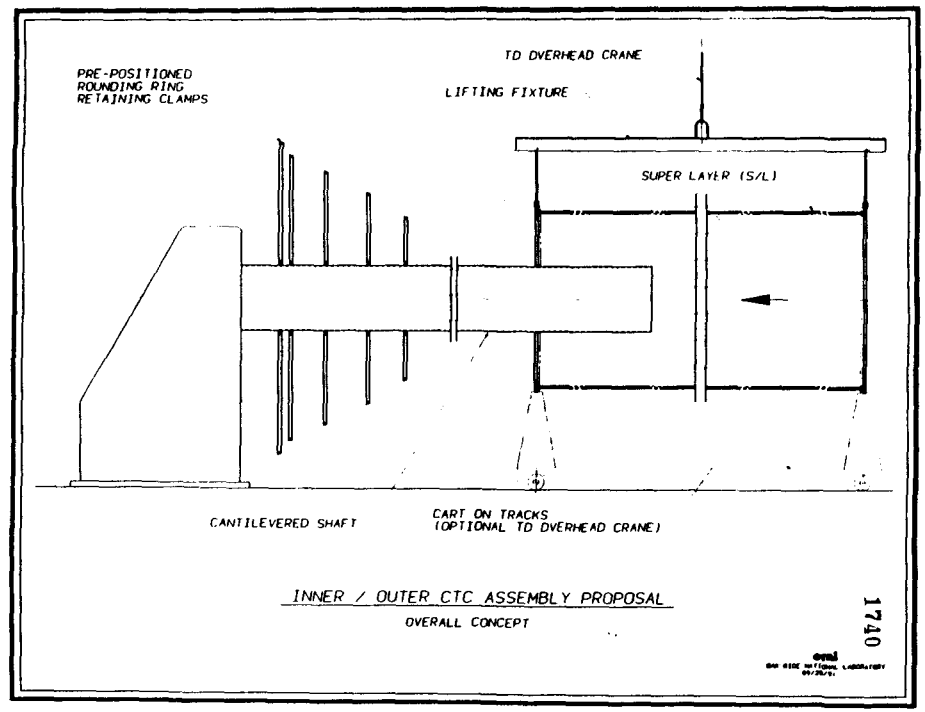


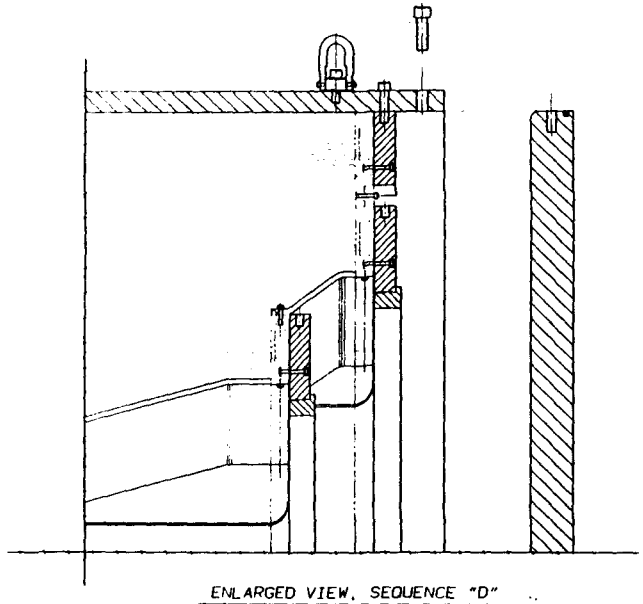
CTC ASSEMBLY (K-1200 HIGH BAY)

- PROCURE/FABRICATE CTC ASSEMBLY STAND
- PROCURE/FABRICATE CTC ASSEMBLY COMPONENTS
- POSITION INNER SUPERLAYER ON ASSEMBLY STAND
- ALIGN AND SECURE INNER SUPERLAYER
- POSITION SUBSEQUENT SUPERLAYERS ON ASSEMBLY STAND
- ALIGN AND ATTACH SUPERLAYERS TO ONE ANOTHER
- VERIFY OVERALL ALIGNMENT OF CTC
- MOVE SHIPPING SHELL INTO POSITION OVER CTC AND SECURE

1739



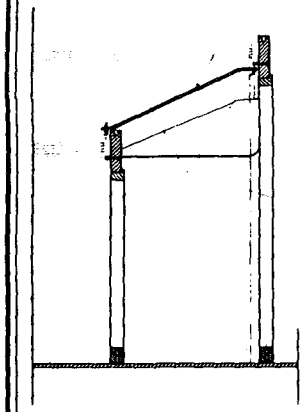




ENLARGED VIEW, SEQUENCE "D"

1745

ornl



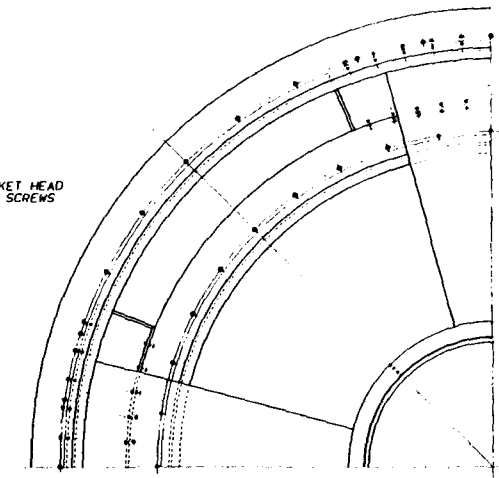
SEGMENTED SHROUD
(FOUR SEGMENTS EACH END)

STEPS FOR SEQUENCE C:

1 AFTER INNER AND SECOND S/L'S ARE POSITIONED AND ALIGNED ATTACH SEGMENTED SHROUDS (FOUR EACH END) WITH SOCKET HEAD CAP SCREWS

2 PROCEED TO SEQUENCE D

SOCKET HEAD CAP SCREWS

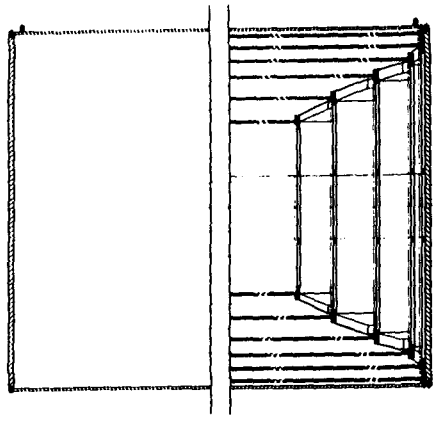


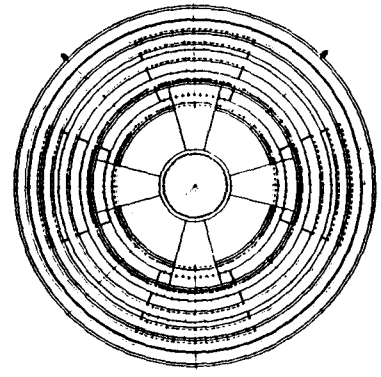
INNER / OUTER CTC ASSEMBLY PROPOSAL

SEQUENCE C

1743

ornl





INNER / OUTER CTC ASSEMBLY PROPOSAL

PARTIAL OVERALL ASSEMBLY

1746

ornl

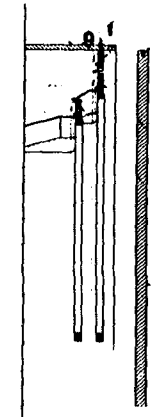
SOCKET HEAD CAP SCREWS
ATTACHED THRU OUTER CONTAINER
INTO OUTER S/L

SHIPPING SHELL
FOR TRANSPORT

SOCKET HEAD CAP SCREWS
FOR END PLATE ATTACHMENT

OUTER S/L ROUNDING RING

O-RING OR GASKET



FIFTH S/L ROUNDING RING
(S/L SHALL BE NOTCHED
TO ACCOMODATE OUTER S/L)

FOURTH S/L ROUNDING RING

SHIPPING SHELL
END PLATES

STEPS FOR SEQUENCE D

1 CONTINUE WORKING OUTWARD THRU FIFTH S/L REPEATING SEQUENCE A, B AND C

2 ATTACH SAFETY HOIST RING TO OUTER S/L AND MANIPULATE INTO POSITION SLIDING ONTO NOTCHES WHICH ARE CUT CIRCUMFERENTIALLY AROUND FIFTH AND OUTER S/L'S AND ATTACH THESE S/L'S TOGETHER

3 MANIPULATE SHIPPING SHELL INTO POSITION AND SECURE TO OUTER S/L ROUNDING RING USING SOCKET HEAD CAP SCREWS

4 WHILE HOIST IS ATTACHED TO SHIPPING SHELL REMOVE COMPLETE UNIT FROM CANTILEVERED SHAFT BY LOOSENING RADIAL ADJUSTMENT SCREWS ON ROUNDING RING RETAINING CLAMPS

5 INSTALL SHIPPING SHELL END PLATES USING SOCKET HEAD CAP SCREWS

6 EVACUATE SHIPPING SHELL AND FILL WITH NITROGEN

7 LOAD SHIPPING SHELL ONTO TRANSPORTER

8 SHIP TO SSCL SITE

INNER / OUTER CTC ASSEMBLY PROPOSAL

SEQUENCE D

1744

ornl

RADIATION LENGTH STUDY

ROB LEITCH

SOLENOIDAL DETECTOR COLLABORATION MEETING
OAK RIDGE NATIONAL LABORATORY
9/27/91

1749

SHIPPING PREPARATION (K-1200)

- SUPPORT CTC ASSEMBLY/SHIPPING SHELL ON PREPARATION STAND
- ATTACH END PLATES TO SHIPPING SHELL
- EVACUATE AND FILL WITH NITROGEN
- REMOVE COMPLETE UNIT FROM STAND
- PLACE UNIT ON TRANSPORTER

1747

3 CONCEPTS

MODULES

5 SUPERLAYERS

8, 6, 6, 6, 6

SCINTILLATING FIBERS

4 SUPERLAYERS

12, 4, 12, 4

HYBRID

3 STRAW SUPERLAYERS
8, 6, 6

2 FIBER SUPERLAYERS

4, 4

ornl
RML
9/27/91

1750

CONCLUSION

- LARGE SCALE PROJECT EXPERIENCE IS REQUIRED
- MULTI-DISCIPLINE DESIGN CAPABILITIES ARE ESSENTIAL
- THE EXPERTISE NECESSARY TO FABRICATE AND ASSEMBLE THE CYLINDERS IS AVAILABLE
- THE FACILITIES NEEDED TO ASSEMBLE AND TEST THE COMPONENTS EXIST

1748

ASSUMPTIONS

AVERAGE LENGTH THROUGH A FIBER = $\frac{\pi D}{4}$

Where: D = Fiber Diameter

AVERAGE LENGTH THROUGH A STRAW = πt

Where: t = Straw thickness

AVERAGE LENGTH THROUGH A WIRE IN A STRAW = $\frac{\pi d^2}{4D}$

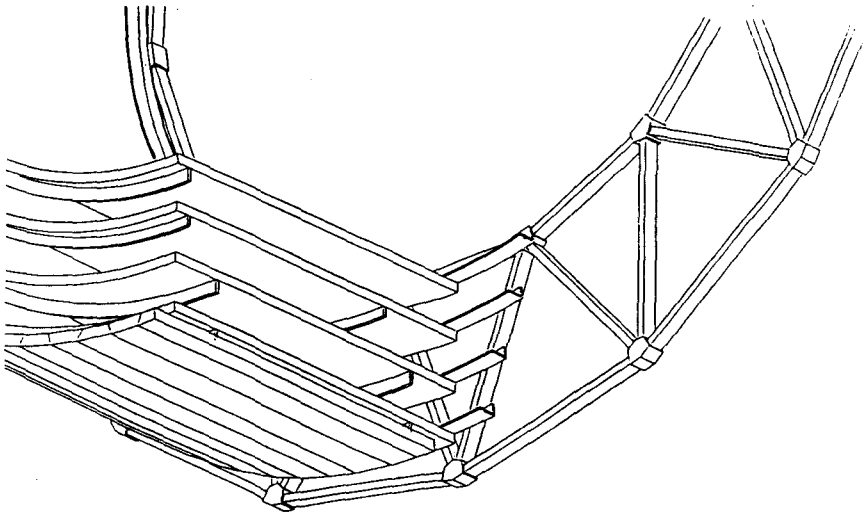
Where: d = Wire Diameter

D = Straw Diameter

OUTERMOST SUPERLAYER IS NOT INCLUDED IN THE RADIATION LENGTH CALCULATIONS

ASSUMPTIONS (CONT.)

SCINTILLATING FIBER	d = 0.84 mm
HYBRID FIBERS	d = 1.5 mm
STRAWS	d = 4 mm t = 0.037 mm
TUNGSTEN WIRE	d = 0.025 mm
MODULES	3 ply Face Sheet - Rohacell Core - 3 ply Face Sheet 0.038 mm/ply 1 mm
MODULE SUPPORT RINGS	40 mm x 2.5 mm



WESTINGHOUSE MODULAR DESIGN CONCEPT

CENTRAL TRACKER MATERIALS

	Radiation Length (cm)	Density (g/cc)	Comments
*Aluminum	8.9	2.7	
Alumina Oxide	8.2	3.9	Based on mass weighted average of Aluminum (2) and Oxygen (3)
*Copper	1.43	8.96	
*G-10	19.4	1.7	
*Glass (Borosilicate)	12.7	2.23	Used as a passivator in electronics
‡Graphite Epoxy	25	1.68	
*Lucite	34.4	1.18	Used as connector for fiber optics
†Straws	24		Combination of Mylar, epoxy, and polycarbonate
* Polystyrene	42.4	1.032	
Rohacell	875	0.048	Scaled by density from Graphite Epoxy
*Silicon	9.36	2.33	
*Tungsten	0.35	19.3	

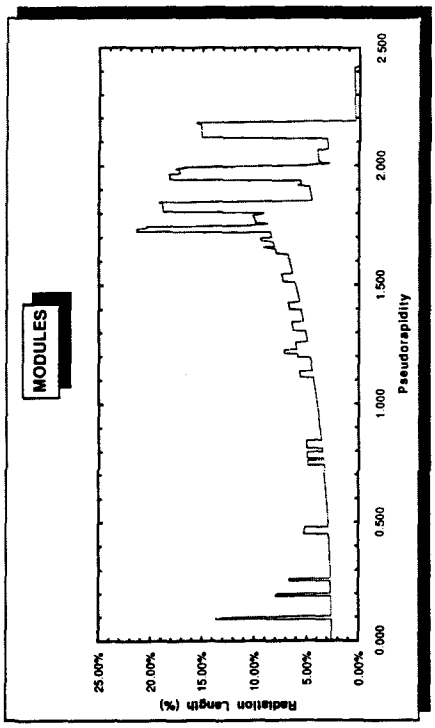
*"Reviews in Modern Physics", Volume 56, Number 2, Part II, April 1984, Page S53

†"Straw Tube Superlayer Design Concepts", Prepared for SDC Tracker Review, May 20, 1991 University of Colorado, Duke University, Indiana University, ORNL, and WSTC Section 4.5 "Materials in the Particle Path", Pages 30-32

‡"Superconducting Super Collider, Silicon Tracking Subsystem, Research and Development" Los Alamos National Laboratory, LA-12029, Table 3-2, Page 17

HERMITICITY FOR MODULES

1759



ornl
RML
9/27/91

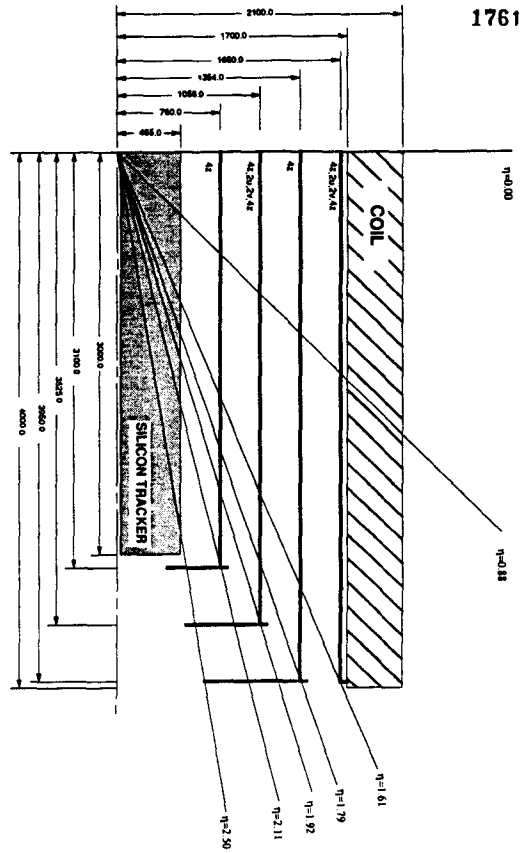
1760

MODULES

	η=0.00	η=0.88	η=1.60	η=1.75	η=1.85	η=1.95	η=2.15
Straws Mylar et. al. (Xo=24 cm) Tungsten (Xo=0.35 cm)	1.36%	1.93%	3.52%	4.02%	3.33%	2.44%	1.48%
Modules Graphite Epoxy (Xo=25 cm) Rohacell Foam (Xo=875 cm)	0.87%	1.23%	2.17%	2.56%	2.12%	1.56%	0.94%
Support Cylinder Graphite Epoxy (Xo=25 cm) Rohacell Foam (Xo=875 cm)	0.37%	0.52%	0.94%	1.08%	0.89%	0.66%	0.40%
End Plates Graphite Epoxy (Xo=25 cm)	0.00%	0.00%	0.00%	4.25%	4.20%	4.17%	4.11%
Pogo Holder Graphite Epoxy (Xo=25 cm)	0.00%	0.00%	0.00%	4.25%	4.20%	4.17%	4.11%
Capacitor Substrate G-10 (Xo=19.4 cm)	0.00%	0.00%	0.00%	0.70%	0.69%	0.68%	0.67%
Capacitor Alumina Oxide (Xo=6.2 cm)	0.00%	0.00%	0.00%	2.18%	2.15%	2.13%	2.10%
Silicon Substrate G-10 (Xo=19.4 cm)	0.00%	0.00%	0.00%	0.70%	0.69%	0.68%	0.67%
Electronics Silicon (Xo=9.36 cm)	0.00%	0.00%	0.00%	0.41%	0.41%	0.41%	0.41%
Passivator Glass (Xo=12.7 cm)	0.00%	0.00%	0.00%	0.08%	0.08%	0.08%	0.08%
Copper (Xo=1.43 cm)	0.00%	0.00%	0.00%	0.19%	0.18%	0.18%	0.18%
Structural Supports Graphite Epoxy (Xo=25 cm)	0.00%	0.00%	0.00%	0.00%	0.30%	0.29%	0.28%
TOTAL	2.60%	3.67%	6.63%	20.42%	19.24%	16.16%	14.86%

ornl
RML
9/27/91

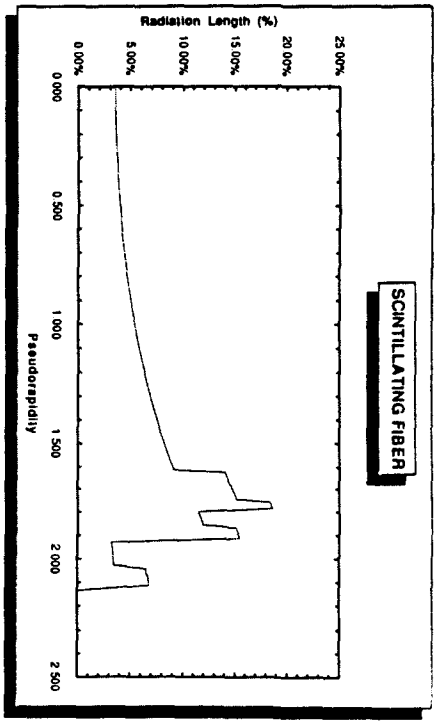
1761



SCINTILLATING FIBERS BASELINE CONCEPT

ornl
RML
9/27/91

1762



ornl
RML
9/27/91

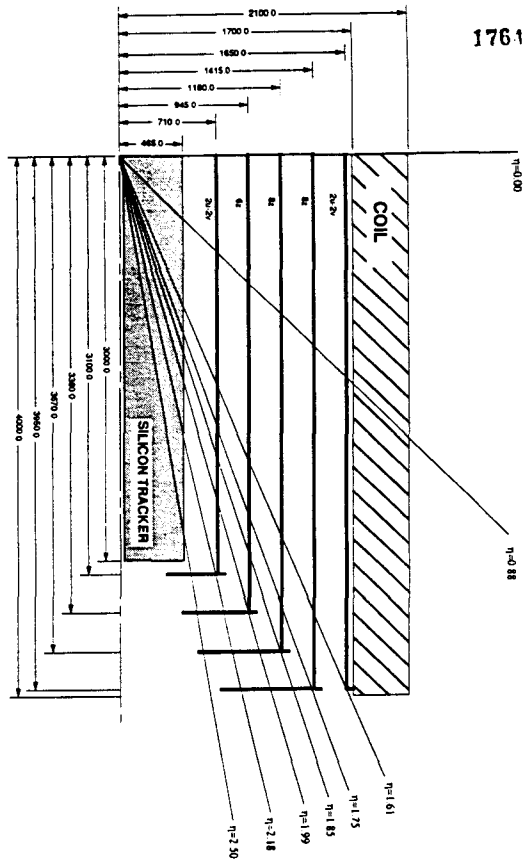
1763

SCINTILLATING FIBERS

	η=0.00	η=0.88	η=1.60	η=1.77	η=1.90	η=2.10
Scintillating Fiber Polystyrene (Xo=42.4 cm)	3.11%	4.40%	8.05%	14.05%	11.12%	3.21%
Support Cylinder Graphite Epoxy (Xo=25 cm)	0.27%	0.39%	0.71%	0.83%	0.63%	0.38%
Fiber Feedthroughs Lucite (Xo=34.4 cm)	0.00%	0.00%	0.00%	3.00%	3.04%	3.00%
Structural Support Graphite Epoxy (Xo=25 cm) Rohacell (Xo=875 cm)	0.00%	0.00%	0.00%	0.19%	0.19%	0.19%
Foam Separator Rohacell (Xo=875 cm)	0.11%	0.16%	0.30%	0.35%	0.39%	0.00%
TOTAL	3.50%	4.95%	9.05%	18.51%	15.37%	6.78%

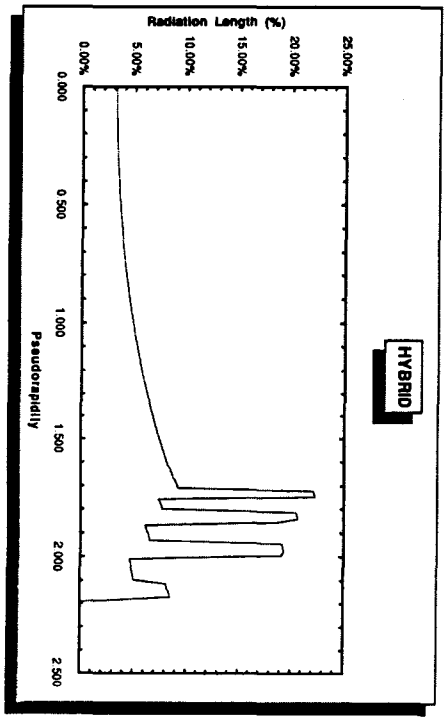
ornl
RML
9/27/91

1761



ornl
RML
9/27/91

1765



ornl
RML
9/27/91

1766

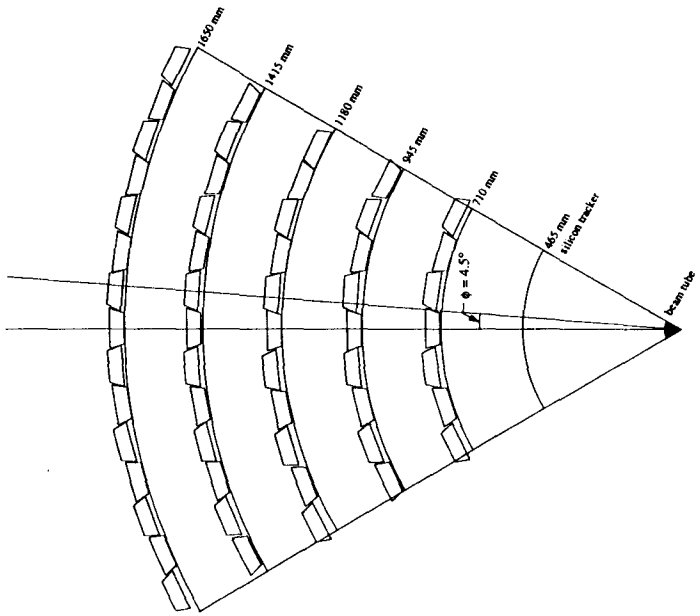
HYBRID

	η=0.00	η=0.88	η=1.60	η=1.75	η=1.85	η=1.95	η=2.15
Straws Mylar et. al. (Xo=24 cm) Tungsten (Xo=0.35 cm)	1.14%	1.61%	2.94%	3.36%	1.12%	1.22%	0.00%
Modules Graphite Epoxy (Xo=25 cm) Rohacell Foam (Xo=875 cm)	0.55%	0.78%	1.42%	1.62%	0.60%	0.65%	0.00%
Fibers Polystyrene (Xo=42.4 cm)	1.11%	1.57%	2.87%	3.29%	3.65%	3.97%	4.85%
Support Cylinder Graphite Epoxy (Xo=25 cm) Rohacell Foam (Xo=875 cm)	0.37%	0.52%	0.95%	1.00%	0.60%	0.65%	0.40%
Fiber Feedthroughs Lucite (Xo=34.4 cm)	0.00%	0.00%	0.00%	0.00%	0.00%	0.00%	2.99%
End Plates Graphite Epoxy (Xo=25 cm)	0.00%	0.00%	0.00%	4.25%	4.20%	4.17%	0.00%
Pogo Holder Graphite Epoxy (Xo=25 cm)	0.00%	0.00%	0.00%	4.25%	4.20%	4.17%	0.00%
Capacitor Substrate G-10 (Xo=19.4 cm)	0.00%	0.00%	0.00%	0.70%	0.69%	0.68%	0.00%
Capacitor Alumina Oxide (Xo=6.2 cm)	0.00%	0.00%	0.00%	2.16%	2.15%	2.13%	0.00%
Silicon Substrate G-10 (Xo=19.4 cm)	0.00%	0.00%	0.00%	0.70%	0.69%	0.68%	0.00%
Electronics Silicon (Xo=9.35 cm)	0.00%	0.00%	0.00%	0.41%	0.41%	0.41%	0.00%
Copper (Xo=1.43 cm)	0.00%	0.00%	0.00%	0.19%	0.18%	0.18%	0.00%
Passivator Glass (Xo=12.7 cm)	0.00%	0.00%	0.00%	0.00%	0.06%	0.00%	0.00%
Structural Supports Graphite Epoxy (Xo=25 cm)	0.00%	0.00%	0.10%	0.19%	0.19%	0.19%	0.19%
TOTAL	3.16%	4.47%	8.27%	22.26%	18.75%	19.19%	8.42%

ornl
RML
9/27/91

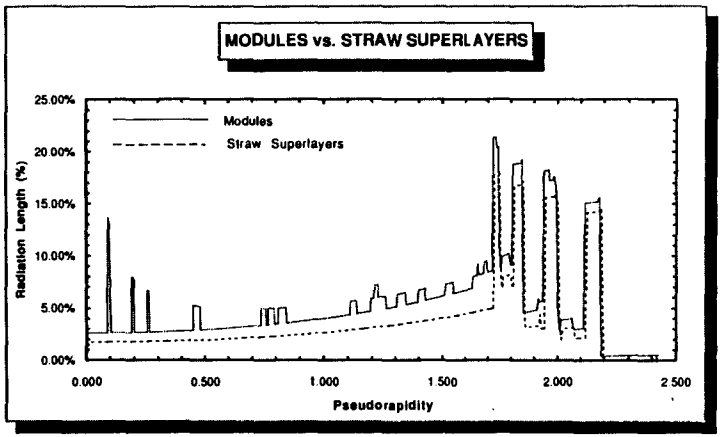
1768

END VIEW OF MODULAR DESIGN



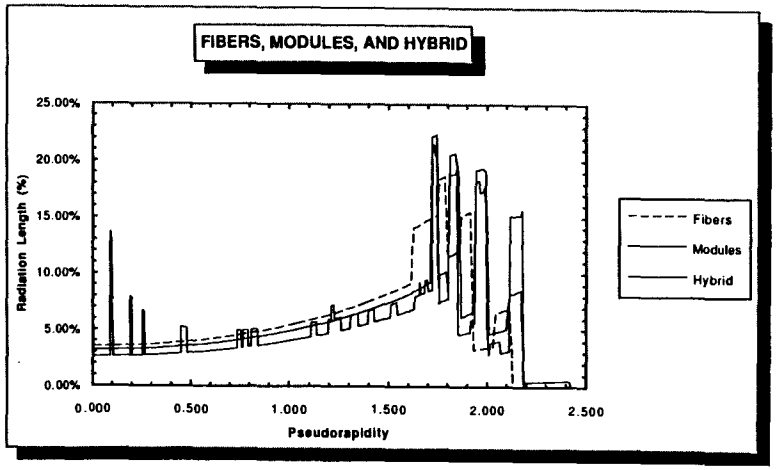
ornl
RML
9/27/91

1770



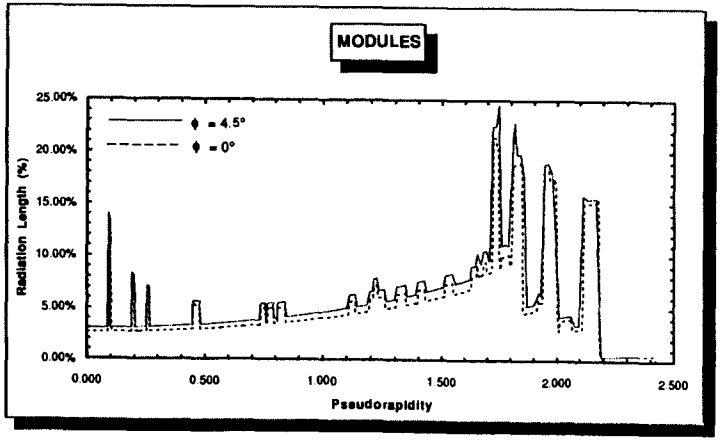
ornl
RML
9/27/91

1767

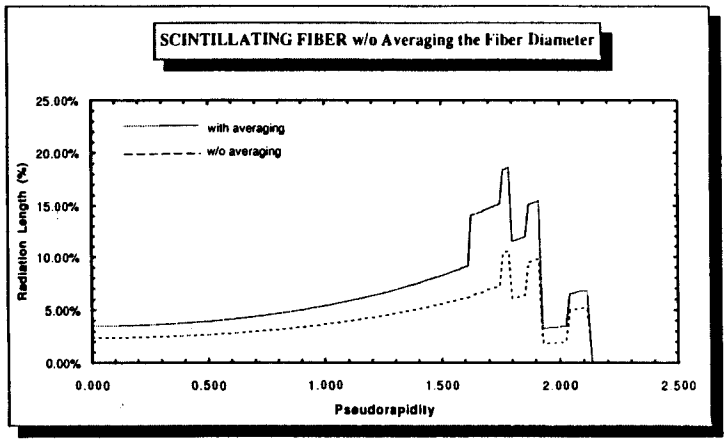


ornl
RML
9/27/91

1769

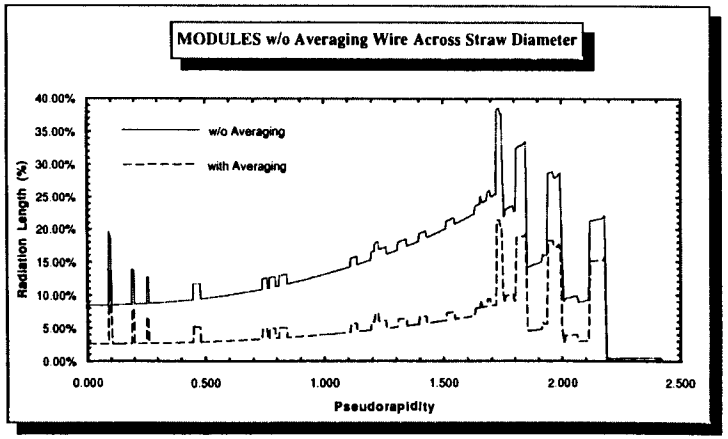


ornl
RML
9/27/91



ornl

RML
9/27/91



ornl

RML
9/27/91

FUTURE WORK

WORK WITH EACH COLLABORATION TO VERIFY AND MODIFY ASSUMPTIONS

EMPLOY AS A DESIGN CRITERIA

UPDATE AS DESIGN EVOLVES

INCREASE FIDELITY AS DESIGN CONCEPTS MATURE

ornl

RML
9/27/91

Appendix

List of Participants

Gerald S. Abrams
Lawrence Berkeley Laboratory
1 Cyclotron Road
Mail Station 50A/2160
Berkeley, CA 94720

David Adams
Rice University
Bonner Nulcer Laboratory
Houston, TX 77251-1892

Angie Alford
Oak Ridge National Laboratory
P. O. Box 2008
Oak Ridge, Tennessee 37831-6363

Gary T. Alley
Oak Ridge National Laboratory
P. O. Box 2008
Oak Ridge, TN 37831-6006

F. S. Alsmiller
Oak Ridge National Laboratory
P. O. Box 2008
Oak Ridge, TN 37831-6364

R. G. Alsmiller, Jr.
Oak Ridge National Laboratory
P. O. Box 2008
Oak Ridge, TN 37831-6364

Katsuya Amako
1-1 Ohi
Tsubkuba-shi
Ibaraki-ken 305 JAPAN

Salvator R. Amendolia
University and INFN - Pisa
Via Livornese 582
S. Piero A Grado
Pisa
1-56020 ITALY

Bill R. Appleton
Oak Ridge National Laboratory
P. O. Box 2008
Oak Ridge, TN 37831-6240

Muzaffer Atac
Fermilab/UCLA
Mail Station 223
P. O. Box 500
Batavia, Illinois 60510

Andrew Baden
University of Maryland
HEP Laboratory
Department of Physics & Astronomy
College Park, MD 20742

Jon A. Bakken
Martin Marietta - Science Systems
P. O. Box 201
M. S. DC 6069
Denver, CO 80201

Eugene A. Barasch
Texas A&M University
Physics Department
College Station, TX 77843

Larry Bartoszck
FERMILAB
P. O. box 500, M. S. 221
Batavia, Illinois 60510

Martin Bauer
Oak Ridge National Laboratory
P. O. Box 2008
Oak Ridge, TN 37831-6006

Alan Baumbaugh
FERMILAB
M. S. 222, WH14SW
P. O. Box 500
Batavia, IL 60510

Laura P. Bautz
Lawrence Berkeley Laboratory
Mail Station 2160
Berkeley, CA 94720

Chris Bebek
Lawrence Berkeley Laboratory
1 Cyclotron Road
Room 50A/2160
Berkeley, CA 94720

P. J. Besser
Rockwell Int. Corp.
3370 Miraloma Avenue
Mail Stop 031-BC16
Anaheim, CA 92803

Fred Bird
Superconducting Super Collider
Laboratory
2550 Beckleymeade Avenue
M. S. 2000
Dallas, TX 75237

Barbara Bishop
Oak Ridge National Laboratory
P. O. Box 2008
Oak Ridge, TN 37831-6364

Barry Blumenfeld
Johns Hopkins University
Department of Physics
Baltimore, MD 21218

Hugh Brashear
Oak Ridge National Laboratory
P. O. Box 2008
Oak Ridge, TN 37831-6006

Roy C. Chaney
University Texas - Dallas
M. S. FO 23
Richardson, Texas 75083-0688

Duncan Carlsmith
University of Wisconsin
Physics Department
High Energy Group
1150 University Avenue
Madison, WI 53706

Masami Chiba
Toyko Metropolitan University
1-1 Minamiohsawa Hachioji-shi
Tokyo,
192-03 JAPAN

Charles Collins
Superconducting Super
Collider Laboratory
2550 Beckeleymeade Avenue
Dallas, Texas 75237

Martyn Corden, Jr.
Florida State University
289 Hawkbill Court
Tallahassee, FL 32312

David Coupal
Superconducting Super
Collider Laboratory
2550 Beckeleymeade Avenue
Mail Station 2000
Dallas, TX 75237

John Dainton
University of Liverpool
Department of Physics
P. O. Box 147
Liverpool, L693BX
United Kingdom

Colin H. Daley
University of Washington
Mechanical Engineering Department
M. S. FU-10
Seattle, WA 98195

Richard Davisson
University of Washington
Physics Department
M. S. FM-15
Seattle, WA 98195

Frank Derosier
University of Maryland
Physics Department
College Park, MD 20742-4111

Madhu Sudan Dixit
Center for Research in Particle Physics
Carleton University
Ottawa, CANADA KJ5B6

Paul A. Draper
FERMILAB
Mail Station 357
Batavia, IL 60510

Andy Dubois
Superconducting Super
Collider Laboratory
2550 Beckeleymeade Avenue
Mail Station 2000
Dallas, Texas 75237

William Dunn
Quantum Research Services
Alston Technical Park, Suite 109
100 Capitola Drive
Durham, NC 27713-4411

Dave Eartly
FERMILAB
P. O. Box 500
M.S. 357
Batavia, IL 60510

Tony Elam
IBM-Federal Systems
3700 Bay Area Boulevard
M. S. 5600
Houston, Texas 77058

John Elias
FERMILAB
Mail Station 318
P. O. Box 500
Batavia, IL 60510

Mike Emery
Oak Ridge National Laboratory
P. O. Box 2008
Oak Ridge, TN 37831-6006

Bob Ennis
IBM- Federal Systems
3700 Bay Area Boulevard
M. S. 5600
Houston, Texas 77058

Steven Errede
University of Illinois
1110 W. Green Street
Urbana, IL 61801

Gary Feldman
Harvard University
Lyman Laboratory
Cambridge, MA 02138

Bill Ford
University of Colorado
P. O. Box 390
Boulder, CO 80409-0390

Soren G. Frederiksen
Superconducting Super Collider
Laboratory
2550 Beckeleymeade Avenue
M. S. 1011
Dallas, Texas 75237

William R. Frisken
York University/LBL
Building 50A/2160
1 Cyclotron Road
Berkeley, CA 94720

Alan Fry
Superconducting Super Collider
Laboratory
2550 Beckleymeade
Dallas, Texas 75237

Hirofumi Fujii
National Laboratory for High
Energy Physics (KEK)
1-1 Oho
Tsukuba,
Ibaraki, 305, JAPAN

Tony A. Gabriel
Oak Ridge National Laboratory
P. O. Box 2008
Oak Ridge, TN 37831-6364

Irwin Gaines
FERMILAB
Mail Station 127
P. O. Box 500
Batavia, IL 60510

Murdock Gilchriese
Lawrence Berkeley Laboratory
Mail Station 50A/2160
Berkeley, CA 94720

Michael J. Glaubman
Northeastern University
Physics Department
Boston, MA 02115

Chuck Glover
Oak Ridge National Laboratory
P. O. Box 2008
Oak Ridge, TN 37831-6360

Alfred T. Goshaw
Duke University
Physics Department
Durham, North Carolina 27706

Stephen A. Gourlay
FERMILAB
P. O. Box 500
Mail Station 316
Batavia, IL 60510

Daniel R. Green
FERMILAB
Mail Station 205
P. O. Box 500
Batavia, IL 60510

Donald T. Hackworth
Westinghouse - STC
1310 Beulah Road
Pittsubrgh, PA 15235

Vasken Hagopian
Florida State University
Physics Department
Mail Stop B-159
Tallahassee, FL 32306

Tom Handler
University of Tennessee
Department of Physics
401 Physics Building
Knoxville, Tennessee 37996-1200

Gail H. Hanson
Indiana University
Physics Department
Bloomington, IN 47405

Mike Harris
Superconducting Super Collider
Laboratory
2550 Beckeleymeade Avenue
Suite 400
M/S 2000
Dallas, Texas 75237

Christopher Hearty
Lawrence Berkeley Laboratory
1 Cyclotron Road
Berkeley, CA 94720

Kenneth Heller
University of Minnesota
School of Physics and Astronomy
Minneapolis, MN 55455

Hiroyuki Iwasaki
National Laboratory for
High Energy Physics (KEK)
1-1, Oho, Tsukuba-shi
Ibaraki-ken, 305
JAPAN

Ann Jordan
Oak Ridge National Laboratory
P. O. Box 2008
Oak Ridge, TN 37831-6364

Tom Kirk
Argonne National Laboratory
High Energy Physics
Argonne, Illinois 60439

Libby Kittrell
SAHEP/ORAU
Administration Building
Room 031A
Oak Ridge, Tennessee 37831

David Koltick
Purdue University
Physics Department
West Lafayette, IN 47907

Takahiko Konda
KEK
3-536 Namiki
Tsukuba-shi
Japan, 305

Glen Kubena
IBM - Federal Systems
3700 Bay Area Boulevard
M. S. 5600
Houston, Texas 77058

Alexei V. Kulik
Inst. of High Energy Physics
Protvino, Moscow
USSR 142284

Shuichi Kunoir
University of Maryland
Mail Stop 221
FERMILAB
P. O. Box 500
Batavia, IL 60510

Leonoid Landsberg
Institute of High Energy Physics
Protvino, Moscow Region
Moscow, USSR 142284

Ruth Lawson
Oak Ridge National Laboratory
P. O. Box 2008
Oak Ridge, TN 37831-6363

Patrick LeDu
Saclay CEA
CEN Saclay
91191 Gif Sur Yvette Cedex
FRANCE

Mark Levi
Lawrence Berkeley Laboratory
1 Cyclotron Road
M. S. 50A/2160
Berkeley, CA 94720

Raymond A. Lewis
Pennsylvania State University
303 Osmond Laboratory
University Park, PA 16802

Kenneth Liao
IBM - Federal Systems
3700 Bay Area Boulevard
M. S. 5600
Houston, Texas 77058

William Lockman
University of Ca. - Santa Cruz
SCIPP
Santa Cruz, CA 95064

Henry J. Lubatti
University of Washington
Physics Department FM-15
Seattle, WA 98195

Frederick Luehring
Indiana University
Swain Hall 117
Physics Depattment
Bloomington, IN 47405

Christopher Lyndon
Louisiana State University
Department of Physics and Astronomy
102 Nicholson Hall
Baton Rouge, LA 70803-4001

Paul Mantsch
FERMILAB
P. O. Box 500
MS-136
Batavia, IL 60510

Lilliam Mashburn
Assistant to Dean of Engineering
University of Tennessee
College of Engineering
Industrial Relations
Knoxville, TN 37996-2000

John A. Matthews
University of New Mexico
Physics Department
800 Yale Boulevard NE
Albuquerque, NM 87131

Stephen J. Maxfeld
University of Liverpool
Department of Physics
P. O. Box 147
Liverpool, L693BX,
United Kingdom

John Mayhall
Martin Marietta Energy Systems, Inc.
Engineering Division
Oak Ridge, TN 37831-8053

Peter McIntyre
Texas A&M
Physics Department
College Station, TX 77843

David Harry Miller
Purdue University
Physics Department
West Lafayette, IN 47907

William Miller
Los Alamos National Laboratory
MEE-12 Group, M. S. E-533
P. O. Box 1663
Los Alamos, NM 87545

Hitoshi Miyata
Niigata University
8050 2-No-Cho, Ikarashi
Niigata 950-21
JAPAN

Luke W. Mo
Virginia Polytechnic Institute
and State University
Physics Department
315 Robeson Hall
Blacksburg, Virginia 24061-0435

Thomas L. Moore
Lawrence Livermore National Lab.
P. O. Box 808, L-280
Livermore, CA 94550

Mike Murbach
University of Maryland
Physics Department
College Park, MD 20742-4111

Mitchell Newcomer
University of Pennsylvania
Department of Physics
209 S. 33rd Street
Philadelphia, PA 19104

David Nygren
Lawrence Berkeley Laboratory
1 Cyclotron Road
Mail Station 50B-6222
Berekeley, CA 94720

Kathy F. O'Shaughnessy
University of CA - Santa Cruz
SCIPP, Natural Sciences II
Santa Cruz, CA 95064

Eugene F. Oberst
Lawrence Livermore National
Laboratory
P. O. Box 808, L-280
Livermore, CA 94550

Harold Ogren
Indiana University
Physics Department
Bloomington, IN 47405

Andrea Palouneu
Los Alamos National Laboratory
M. S. D-456
Los Alamos, NM 87545

Jun Park
UCLA
Physics Department
405 Highland Avenue
Los Angeles, CA 90024

Sherwood Parker
University of Hawii
Department of Physics
2505 Correa Road
Honolulu, HI 96822

David Pellett
University of CA - Davis
Department of Physics
Davis, CA 95616

John Piles
Superconducting Super
Collider Laboratory
2550 Beckeleymeade Avenue
Mail Station 2001
Dallas, Texas 75237

Frank Plasil
Oak Ridge National Laboratory
P. O. Box 2008
Oak Ridge, TN 378316372

Joe Pohlen
Martin Marietta - Science Systems
P. O. Box 179
M. S. DC6069
Denver, CO 80201

Larry Price
Argonne National Laboratory
High Energy Physics Division
Argonne, IL 60439

Jim Reidy
University of Mississippi
2207 Lee Loop
Oxford, MS 38655

Stephen Reucroft
Northeastern University
360 Huntington Avenue
Boston, MA 02115

Randy Ruchti
University of Notre Dame
Department of Physics
Notre Dame, IN 46556

David R. Rust
Indiana University
Physics Department
Swain Hall W117
Bloomington, IN 47401

Ted Ryan
Martin Marietta Energy Systems, Inc.
Engineering Division
Oak Ridge, TN 37831-8055

Vladimir Rykalin
Institute of High Energy Physics
Protvino, Moscow Region
Moscow, USSR 142284

Hartmut Sadrozinski
University of CA - Santa Cruz
62 Churchill Avenue
Palo Alto, CA 94306

Abraham Seiden
University of CA - Santa Cruz
Santa Cruz Institute for Particle Physics
Santa Cruz, CA 95064

Edward I. Shibata
Purdue University
Department of Physics
1396 Physics Building
West Lafayette, IN 47907-1396

Alan Sill
University of Rochester
Department of Physics and Astronomy
River Campus
Rochester, N. Y 14627-0011

Patrick Skubic
University of Oklahoma
Department of Physics
Norman, OK 73019

Adris Skuja
University of Maryland
7711 Lake Glen Road
Glen Dale, Maryland 20769

Wesley Smith
University of Wisconsin
Physics Department
1150 University Avenue
Madison, WI 53706

Mark W. Strovink
University of CA - Berkeley
Mail Station 50-341
Berekeley, CA 94720

Roger L. Swensrud
Westinghouse - STC
1310 Beulah Road
Mail Stop 501-3W62
Pittsburgh, PA 15235

Carrick Talmadge
Purdue University
West Lafayette, IN 47907-1396

Susuma Terada
KEK - Physics Department
Takasai, 3068-5
Shimotsuma-shi
Ibaraki-ken, 304 JAPAN

Rudolph Thun
University of Wisconsin
Physics Department
High Energy Group
1150 University Avenue
Madison, WI 53706

Tim Thurston
Superconducting Super Collider
Laboratory
2550 Beckeleymeade Avenue
M. S. 2001
Dallas, Texas 75237

George Trilling
Lawrence Berkeley Laboratory
Building 50A, Room 2160
Berkeley, CA 94720

Hans-Jochen Trost
Argonne National Laboratory
585 Eric Way
Bolingway, IL 60440

Roman Turkevich
Superconducting Super
Collider Laboratory
2550 Beckeleymeade Avenue
Mail Station 2000
Dallas, TX 75237

David Vandergriff
Martin Marietta Energy Systems, Inc.
P. O. Box 2003
Oak Ridge, Tennessee 37831-7520

David Veal
Superconducting Super
Collider Laboratory
2550 Beckeleymeade Avenue
Dallas, Texas 75237

James King Walker
University of Florida
Physics Department
Gainesville, FL 32611

Elsworth A. Wente IV
Indiana University
117 Swain West
Bloomington, IN 47405

Andrew White
University of Texas - Arlington
Physics Department
P. O. Box 19059
Arlington, TX 76019

Hugh H. Williams
University of Pennsylvania
Physics Department
Philadelphia, PA 19104

Suzanne Willis
Northern Illinois University
Physics Department
Dekalb, IL 60115

Dong Xiao
Florida State University
Supercomputer Computations
Research Institute
Tallahassee, FL 32306-4052

Takahiro Yasuda
Northeastern University
360 Huntington Avenue
Boston, MA 02115

Tianchi Zhao
FERMILAB
Mail Station 223
P. O. Box 500
Batavia, IL 60510